LABORATORY AND FIELD TESTS OF MULTIPLE CORROSION PROTECTION SYSTEMS FOR REINFORCED CONCRETE BRIDGE COMPONENTS AND 2205 PICKLED STAINLESS STEEL

By

Guohui Guo

David Darwin

JoAnn P. Browning

Carl E. Locke, Jr.

A Report on Research Sponsored by

FEDERAL HIGHWAY ADMINISTRATION
Contract No. DTFH61-03-C-00131

KANSAS DEPARTMENT OF TRANSPORTATION
Contract Nos. C1131 and C1281

Structural Engineering and Engineering Materials
SM Report No. 85

THE UNIVERSITY OF KANSAS CENTER FOR RESEARCH, INC.

LAWRENCE, KANSAS

June 2006

ABSTRACT

Multiple corrosion protection systems for reinforcing steel in concrete and the laboratory and field test methods used to compare these systems are evaluated. The systems include conventional steel, epoxy-coated reinforcement (ECR), ECR with a primer containing microencapsulated calcium nitrite, multiple coated reinforcement with a zinc layer underlying DuPont 8-2739 epoxy, ECR with a chromate pretreatment to improve adhesion between the epoxy and the steel, two types of ECR with high adhesion coatings produced by DuPont and Valspar, 2205 pickled stainless steel, concrete with water-cement ratios of 0.45 and 0.35, and three corrosion inhibitors (DCI-S, Rheocrete 222+, and Hycrete). The rapid macrocell test, three bench-scale tests (Southern Exposure, cracked beam, and ASTM G 109 tests), and a field test are used to evaluate the corrosion protection systems. The linear polarization resistance test is used to determine microcell corrosion activity. An economic analysis is performed to find the most cost-effective corrosion protection system. Corrosion performance of 2205 pickled stainless steel is evaluated for two bridges, the Doniphan County Bridge and Mission Creek Bridge in Kansas. The degree of correlation between results obtained with the Southern Exposure, cracked beam, and rapid macrocell tests is determined based on the results from a study by Balma et al. (2005).

In uncracked mortar and concrete containing corrosion inhibitors, total corrosion losses are lower than observed at the same water-cement ratios in concrete with no inhibitors. In cracked concrete, however, the presence of corrosion inhibitors provides no or, at best, very limited protection to reinforcing steel. In uncracked concrete with a water-cement ratio of 0.35, corrosion losses are generally lower than observed at a water-cement ratio of 0.45. In cracked concrete, a lower water-cement ratio provides only limited or no additional corrosion protection.

Compared to conventional ECR, ECR with a primer containing microencapsulated

calcium nitrite shows improvement in corrosion resistance in uncracked concrete with a *w*/*c* ratio of 0.35. At a higher *w*/*c* ratio (0.45), however, the primer provides corrosion protection for only a limited time.

The three types of ECR with increased adhesion show no consistent improvement in corrosion resistance when compared to conventional ECR. The multiple coated reinforcement exhibits total corrosion losses between 1.09 and 14.5 times of the losses for conventional ECR. Corrosion potentials, however, show that the zinc provides protection to the underlying steel. A full evaluation of the system must await the end of the tests when the bars can be examined.

Microcell corrosion losses measured with the linear polarization resistance test shows good correlation with macrocell corrosion losses obtained with the Southern Exposure and cracked beam tests.

An economic analysis shows that, for the systems evaluated in the laboratory, the lowest cost option is provided by a 230-mm concrete deck reinforced with the following steels (all have the same cost): conventional ECR, ECR with a primer containing calcium nitrite, multiple coated reinforcement, or any of the three types of ECR with increased adhesion.

Corrosion potential mapping results show that no corrosion activity is observed for either bridge deck. To date, the 2205p stainless steel has exhibited excellent corrosion performance.

Total corrosion losses in the Southern Exposure and cracked beam tests at either 70 or 96 weeks are appropriate to evaluate the corrosion performance of corrosion protection systems. For the current comparisons, the rapid macrocell test was better at identifying differences between corrosion protection systems than either of the bench-scale tests.

Key words: chlorides, concrete, corrosion, corrosion inhibitor, epoxy-coated reinforcement, linear polarization resistance, multiple corrosion protection systems, potential, stainless steel reinforcement

ACKNOWLEDGEMENTS

This report is based on a thesis submitted by Guohui Guo in partial fulfillment of the requirements of the Ph.D. degree. Major funding and material support for this research was provided by the United States Department of Transportation Federal Highway Administration under Contract No. DTFH61-03-C-00131, with technical oversight by Yash Paul Virmani, and the Kansas Department of Transportation under Contract Nos. C1131 and C1281, with technical oversight by Dan Scherschligt and Don Whisler. Additional support for this project was provided by the Concrete Steel Reinforcing Institute, DuPont Powder Coatings, 3M Corporation, Valspar Corporation, Degussa Construction Chemicals (now BASF Construction Chemicals), W. R. Grace & Co., Broadview Technologies, Inc., Western Coating, Inc., and LRM Industries.

TABLE OF CONTENTS

LIST OF TABLES

LIST OF FIGURES

CHAPTER 1

INTRODUCTION

1.8 GENERAL

Deterioration problems with reinforced concrete structures and bridge components have been recognized for decades. One of the major worldwide durability problems for reinforced concrete structures is chloride-induced steel corrosion. Corrosion can impair not only the serviceability of structures but their safety as well.

According to Yunovich et al. (2002), approximately 15 percent of the bridges in the United States are defined as structurally deficient, primarily due to the corrosion of structural steel and reinforcing bars. The annual direct cost of corrosion for highway bridges is estimated to be $8.3 billion and the indirect cost due to traffic delays and lost productivity is estimated at more than 10 times the direct cost of corrosion maintenance, repair, and rehabilitation.

For concrete bridge decks, the dominant damage mechanism is chloride-induced corrosion of reinforcing steel, which accounts for approximately 40% of the current backlog of highway bridge repair and rehabilitation costs (Weyers et al. 1993).

Due to the use of deicing salts since the early 1960s, concrete bridges and parking garages are now deteriorating at alarming rates due to chloride-induced corrosion (Berke, Pfeifer, and Weil 1988). Marine structures, such as bridges and offshore structures, are also susceptible to severe corrosion due to chloride ingress, especially substructures (Sagües 1994).

Alternate deicing chemicals, such as magnesium chloride, calcium chloride, and calcium magnesium acetate (CMA), can be used to keep highways and bridge decks

clear of snow and ice. Magnesium chloride and calcium chloride are more effective than rock salt at low temperatures and, thus, could presumably reduce chloride exposure to some extent. However, a study carried out by Cody et al. (1996) indicates that magnesium chloride can cause severe deterioration to concrete and is the most destructive deicing chemical, followed by calcium chloride. Among several deicing chemicals, pure CMA is the only deicer that significantly inhibits the corrosion of steel embedded in concrete (Callahan 1989). However, CMA needs a much higher application rate and can cost 10 times more than deicing salts (Roberge 2000). Moreover, tests performed by Ge et al. (2004) showed that CMA can cause severe concrete surface deterioration, even though it can reduce the corrosion rate significantly. Because of its low cost, sodium chloride remains the primary deicing chemical for use on highways. The use of deicing salts in the snow belt rose from 0.6 million tons in 1950 to 10.5 million tons in 1988 (Roberge 2000).

Different corrosion protection systems have been developed to protect reinforcing bars from corrosion. These systems include epoxy-coated reinforcement (ECR), increased concrete cover, lower permeability concrete, corrosion inhibiting admixtures, pretreating sealers, galvanized reinforcing steel, alternative metallic or alloyed steel, and combinations of these systems. For existing structures, cathodic protection, re-alkalization, and electrochemical removal of chlorides can be used as remedial measures (Smith and Tullman 1999). A detailed description of corrosion protection systems related to this research is given in Section 1.6.

1.9 MECHANISM OF STEEL CORROSION IN CONCRETE

Corrosion can be defined as the destructive result of chemical reactions between a metal or metal alloy and its environment (Jones 1996). There are four

essential components involved in a basic corrosion cell: an anode, a cathode, an electrolyte, and an electrical conductor. The removal of any one of these components will stop the corrosion.

The corrosion process starts with the oxidation of iron at the anode. Ferrous ions dissolve in the concrete pore solution and electrons are released [Eq. (1.1)]. At the cathode, hydroxyl ions are generated when water and oxygen are present [Eq. (1.2)].

$$Fe \rightarrow Fe^{2+} + 2e^{-} \tag{1.1}$$

$$H_2O + {}^{1}/_{2}O_2 + 2e^{-} \rightarrow 2OH^{-} \tag{1.2}$$

These reactions are just the first steps in the process of producing rust. The anodic product Fe^{2+} reacts with hydroxyl ions to form ferrous hydroxide [Eq. (1.3)]. Ferrous hydroxide can be oxidized to hydrated ferric oxide, also known as ordinary red-brown rust [Eq. (1.4)] and hydrated magnetite [Eq. (1.5)], which is green in color. The hydrated corrosion products can dehydrate to form what is commonly referred to as rust, ferric oxide Fe_2O_3 and black magnetite Fe_3O_4.

$$Fe^{2+} + 2OH^{-} \rightarrow Fe(OH)_2 \tag{1.3}$$

$$4Fe(OH)_2 + O_2 \rightarrow 2Fe_2O_3 \cdot H_2O + 2H_2O \tag{1.4}$$

$$6Fe(OH)_2 + O_2 \rightarrow 2Fe_3O_4 \cdot H_2O + 4H_2O \tag{1.5}$$

Typically, concrete pore solution maintains a high pH value, from 12.5 to 13.6, the result of the highly alkaline environment in cement paste. Reinforcing steel in concrete is normally passive due to the formation of a gamma ferric oxyhydroxide film [Eq. (1.6)], which is impermeable and strongly adherent to the steel surface. As long as the pH of the concrete pore solution stays above 11.5, the protective film on

the steel surface tends to be stable in the absence of chloride ions (Metha and Monteiro 1993).

$$2Fe(OH)_2 + {}^1/_2O_2 \rightarrow 2\gamma\text{-}FeOOH + H_2O \qquad (1.6)$$

Concrete cover provides a physical barrier to limit the corrosion of reinforcing steel in harsh environments. However, the ingress of aggressive species can cause the breakdown of the passive film by migrating through the porous structure of concrete and existing microcracks. The two most common causes of film depassivation are the ingress of chloride ions and neutralization of the concrete pore solution by atmospheric carbonation.

Once the passive film breaks down, steel in concrete will start corroding and corrosion products will form on the concrete-steel interface. The volume of the oxidation products may be more than six times the original volume occupied by metallic iron (Mansfeld 1981). As the steel corrodes, expansive forces can develop within concrete and eventually crack the surrounding concrete.

In concrete bridge decks, it is generally believed that the macrocell corrosion between the top and bottom mats of reinforcing bars is the primary cause of early age bridge deck deterioration, and that the microcell corrosion that occurs locally is less important (Virmani 1990). The ingress of chloride ions from deicing salts used on bridge decks makes the potential of the bars in the top mat more negative than those in the bottom mat, and thus the top mat bars serve as the anode. The potential difference between mats results in the formation of a galvanic cell that drives the current flow between the top anode and the bottom cathode. The electronic conductor is usually provided by tie wires, bar chairs, truss bars, expansion dams and/or scuppers (Virmani, Clear, and Pasko 1983).

The corrosion of reinforcing steel can cause serious deterioration of structural

concrete. The damage to concrete manifests in the form of expansion due to the formation of corrosion products, cracking, spalling, and the eventual loss of concrete cover. A literature review indicates that, for uniform corrosion, reinforcing bar skin thickness losses of about 25 μm (0.001 in., 1 mil) can cause concrete to crack (Pfeifer 2000). For localized corrosion in a small region, the quantity of corrosion products needed to crack concrete depends on anodic length and member dimensions, including concrete clear cover and reinforcing bar diameter. The required reinforcing bar thickness loss is between 30 and 270 μm (1.2 and 10.7 mils) (Torres-Acosta and Sagües 2004).

The consequences of steel corrosion include the reduction of the steel cross section, possible loss of steel ductility, and reduced concrete-steel bond strength (Andrade and Alonso 2001). All of these can result in serviceability problems or even lead to structural failure. For prestressed concrete structures, this is especially true because prestressing steel is more susceptible to stress corrosion and hydrogen embrittlement in aggressive environments than normal reinforcing steel.

1.2.1 Chloride Induced Corrosion

It is well known that chloride ions can lead to the corrosion of reinforcing steel in concrete in the presence of oxygen and moisture. Chloride-induced corrosion is the most prevalent cause of the corrosion of steel in reinforced concrete structures.

Chlorides may be introduced into concrete from an internal or external source. They can be mixed into concrete (internal chlorides) if the concrete-making materials are contaminated with chlorides or concrete admixtures contain chlorides. They can also diffuse into concrete (external chlorides) through deicing salt application, sea salt spray, and direct seawater wetting.

Chloride ions reach steel via the concrete pore solution and through cracks. They can penetrate the protective film and react with ferrous ions to form soluble iron-chloride complex ions [Eq. (1.7)] (Smith and Virmani 2000). The soluble iron-chloride complex ions diffuse away from the anode to an area with a higher pH and concentration of oxygen to react with hydroxyl ions [Eq. (1.8)]. The formation of ferrous hydroxide lowers the pH of the concrete pore solution, which in turn destroys the passive film and promotes the corrosion process. The chloride ions are not consumed during the process and remain available to sustain the corrosion process.

$$Fe^{2+} + Cl^{-} \rightarrow [FeCl\,Complex]^{+} \tag{1.7}$$

$$[FeCl\ complex]^{+} + 2OH^{-} \rightarrow Fe(OH)_2 + Cl^{-} \tag{1.8}$$

In the case of chloride attack, anodes and cathodes are usually well separated, resulting in corrosion at a macrocell level.

To initiate corrosion, the chloride concentration at the surface of the reinforcing bar needs to be above a given value, which is a function of such variables as the hydroxyl ion concentration and the tricalcium aluminate (C_3A) content of the cement. For steel reinforcement in concrete, this is referred to as the chloride corrosion threshold, discussed at greater length in Section 1.5.

1.2.2 Carbonation Induced Corrosion

Carbonation is the process of the interaction of CO_2 in the atmosphere with the alkaline hydroxides in the concrete. Carbon dioxide dissolves in water to form carbonic acid [Eq. (1.9)], neutralizes the alkalis in the concrete pore solution, and combines with calcium hydroxide to form calcium carbonate [Eq. (1.10)].

$$CO_2 + H_2O \rightarrow H_2CO_3 \tag{1.9}$$

$$Ca(OH)_2 + H_2CO_3 \rightarrow CaCO_3 + 2H_2O \quad (1.10)$$

Carbonation induces the corrosion of reinforcing steel by lowering the pH of the concrete pore solution and causing the protective film covering the steel surface to dissolve.

Many factors influence the carbonation rate, such as cement type, water-cement (*w/c*) ratio, cement content, relative humidity, concrete pore structure, and the degree of saturation of the concrete. In complete dry or saturated concrete, the carbonation rate stays at a very low level.

Compared to the macrocell corrosion under chloride attack, corrosion under carbonation usually occurs at a microcell level with apparently continuous corrosion along reinforcing bars.

1.10 CORROSION MONITORING METHODS

Methods frequently used to evaluate the corrosion of reinforcing steel in concrete include monitoring the corrosion potential, measuring the macrocell corrosion rate, determining the linear polarization resistance, and using electrochemical impedance spectroscopy. The first three methods will be described in this section.

1.3.3 Corrosion Potential

Monitoring the corrosion potential of reinforcing bars has widespread application in corrosion studies for reinforced concrete structures. The corrosion potential of a metal is a basic indicator of its electrochemical status and a measure of its tendency to corrode. On its own, corrosion potential does not provide any information on corrosion rate. It is, however, qualitatively associated with the

corrosion of steel in concrete.

The corrosion potential of reinforcing steel is measured with respect to a reference electrode. The reaction in the standard hydrogen electrode (SHE) is chosen to represent "zero potential." The SHE, however, is not convenient to use to monitor the corrosion potential of reinforcing steel. The two most common reference electrodes are the copper-copper sulfate electrode (CSE) and the saturated calomel electrode (SCE). Their potentials with respect to the SHE are 0.318 V and 0.241 V, respectively.

ASTM C 876 provides general guidelines for evaluating the corrosion of uncoated reinforcing steel in reinforced concrete structures, as shown in Table 1.1.

Table 1.1 – Corrosion interpretations according to half-cell potential readings

Half-cell Potential Reading (V)		**Corrosion Activity**
CSE	**SCE**	
> –0.200	> –0.125	Greater than 90% probability of no corrosion
–0.200 to –0.350	–0.125 to –0.275	An increasing probability of corrosion
< –0.350	< –0.275	Greater than 90% probability of corrosion

Practically, when interpreting half-cell potential data, a number of factors such as concrete resistance, carbonation, oxygen and chloride concentration, the use of corrosion inhibitors, and the use of epoxy-coated and galvanized reinforcing steel, have to be considered because they have a significant influence on the readings. Gu and Beaudoin (1998) discussed these factors and their effects on the potential readings. They concluded that only corrosion conditions related to carbonation, chloride ingress, and the use of anodic corrosion inhibitors could be evaluated using ASTM C 876.

Because of its simplicity, the measurement of corrosion potential is the method

most frequently used in field studies. An electrical connection is made to a reinforcing bar in the concrete and a copper-copper sulfate electrode is placed on a well-wetted concrete surface. The potential difference between the electrode and the reinforcing bar is the corrosion potential, which can be measured using a high impedance voltmeter. For reinforced concrete structures, however, the measured potentials depend on the moisture content of concrete, concrete admixtures, surface treatment, cement characteristics, etc. (Marquardt 1991).

In research applications, the corrosion potential technique has been used to identify corrosion in large concrete slabs [1829 × 610 × 152 mm (72 × 24 × 6 in.)] using a 51 × 51 mm (2 × 2 in.) grid (Gaidis and Rosenberg 1987). Potential measurements on these simulated bridge decks were in agreement with the corrosion current measurements on concrete cylinders and visual observations on bare bars in simulated solutions.

To determine if reinforcing steel was actively corroding, corrosion potentials were recorded over a concrete surface using a 152 × 152 mm (6 × 6 in.) grid on bridge decks (Marquardt 1991). Efficient measuring equipment that consisted of 112 CSE electrodes was developed to assess corrosion zones on large concrete surfaces. The author pointed out that high potential gradients in a small area might be symptomatic for corrosion.

In 1998, Marquardt used potential measurements to locate steel corrosion in concrete walls. In this study, the influences of several parameters on corrosion potentials were evaluated, such as the concrete cover thickness, temperature, paints or coatings on the wall, and the use of galvanized reinforcement. The study indicated that it is very difficult, if not impossible, to detect corrosion in concrete walls containing galvanized steel, and that thick concrete cover makes it difficult to find

small corrosion areas. The results also showed that areas undergoing corrosion could be determined with more certainty using the relative potential measurement technique than by the classical potential measurement method.

1.3.4 Corrosion Rate

The corrosion potential of reinforcing bars in concrete only provides information concerning the tendency of corrosion to occur. It is the corrosion rate that represents how fast reinforcing bars in concrete are corroding.

In reinforced concrete members where a macrocell forms, some reinforcing bars, such as top bars in a bridge deck, serve as the anode, while other bars, such as the bottom bars in a bridge deck, serve as the cathode. The top and bottom bars are electrically connected by other steel in the deck, which provides an electrical path, and the pore solution within the concrete, which provides an ionic path. The potential difference between the anode and cathode provides the driving force for current to flow in the closed circuit. In the laboratory, this behavior can be represented by appropriately designed tests that include a resistor in the electrical connection between the anode and cathode. The corrosion current is determined by measuring the voltage drop across the resistor, and the macrocell corrosion rate of the anode can be determined using Faraday's Law

$$r = \frac{ia}{nDF} \tag{1.11}$$

where r is the corrosion rate in terms of thickness loss per unit time, i is the corrosion current density in terms of amps per unit area, a is the atomic weight, n is the number of equivalents exchanged, D is the density of metal, and F is Faraday's constant (96,500 coulombs/equivalent).

1.3.5 Linear Polarization Resistance Test

The linear polarization resistance technique provides rapid nondestructive corrosion rate measurements. It involves the potentiostatic measurement of the voltage-current curve in the immediate vicinity of the open circuit potential E_{oc}. Measurement of the slope of this curve yields polarization resistance R_P, allowing the calculation of the microcell corrosion rate. The polarization resistance can be defined as

$$R_p = \left(\frac{\Delta E}{\Delta i} \right)_{\Delta E \to 0} \tag{1.12}$$

where ΔE is the potential difference between the applied potential and E_{oc}, and Δi is the corresponding current change.

The linear polarization resistance is related to the instantaneous corrosion current density through the Stern-Geary equation

$$i_{corr} = \frac{(\beta_a \beta_c)}{2.3 R_p (\beta_a + \beta_c)} = \frac{B}{R_p} \tag{1.13}$$

where β_a is the anodic Tafel coefficient, β_c is the cathodic Tafel coefficient, and B is the Stern-Geary constant given by

$$B = \frac{(\beta_a \beta_c)}{2.3(\beta_a + \beta_c)} \tag{1.14}$$

The Stern-Geary constant B may vary from 13 to 52 mV for a wide range of metal-electrolyte systems (Stern and Weisert 1958). For the case of the reinforcing steel in concrete, Andrade and González (1978) suggested using 26 mV for bare steel in the active state and for galvanized steel, and 52 mV for bare steel in the passive state. A value of 26 mV is usually taken as the constant B for reinforcing steel in concrete (Lambert, Page, and Vassie 1991, McDonald, Pfeifer, and Sherman 1998),

along with values of 120 mV for both the anodic and cathodic Tafel coefficients.

The linear polarization resistance technique has been used extensively to measure the microcell corrosion current density of reinforcing steel in the laboratory. The main difficulty involved with using this technique on-site is the definition of area over which the applied current is acting. Another issue related to on-site testing is the fact that the corrosion current is weather dependent. A method involving taking several measurements over a 12-month period was suggested by Andrade and Alonso (2001) to take into account the different weather seasons.

1.11 TESTING METHODS

One rapid macrocell test, three bench-scale tests and one field test are used to evaluate the corrosion performance of different corrosion protection systems in the current study. The rapid macrocell test provides corrosion results in 15 weeks. Bench-scale tests are used to simulate the long-term performance of reinforcing steel in concrete bridge decks with a test period of 2 years. The field test aims to simulate more realistic conditions for bridge decks exposed to deicing salts and is expected to provide useful results in 5 to 10 years. A brief discussion of the previous work related to these test methods is given in this section, and all of the test methods are described in detail in Chapter 2.

1.4.1 Rapid Macrocell Test

For the rapid macrocell test, specimens are placed in two containers, one with concrete pore solution (cathode) and the other with pore solution containing a deicer (anode). The solution covers a portion of the test specimens, which are placed vertically in the containers. The anode and cathode are electrically connected across a

resistor and the solutions are ionically connected by a salt bridge. Both bare steel and steel encased in mortar have been used in the test. The history of the development of the rapid macrocell test is shown in Table 1.2.

The steel in both specimen types is 127 mm (5 in.) long. All of the mortar specimens in Table 1.2 have a diameter of 30 mm (1.2 in.) that provides a mortar cover thickness of 7 mm (0.287 in.) for No. 16 (No. 5) bars, and 9 mm (0.35 in.) for No. 13 (No. 4) bars.

Martinez et al. (1990) developed a rapid macrocell test and a corrosion potential test to investigate the effects of different deicers on the corrosion of reinforcing steel cast in mortar. The specimen configuration is listed in Table 1.2. The specimen, referred to as a lollipop specimen because the steel is partly embedded in the mortar, was placed in a covered plastic container. A 15-mm (0.6-in.) wide band of epoxy was applied around the bar at the steel-mortar interface to prevent crevice corrosion. A 100,000-ohm resistor was used in the rapid macrocell test. Macrocell current and open circuit corrosion potential are recorded daily for the rapid macrocell and corrosion potential tests, respectively. More consistent results were observed for the corrosion potential test than the macrocell test because the high resistance connecting the specimens in the macrocell test limited the corrosion current. A lower resistance was recommended for future tests. The mortar specimens used in the rapid macrocell tests were based on work performed by Yonezawa, Ashworth, and Procter (1988), which used two different mortar specimen configurations to study the effects of concrete pore solution composition and chloride on the corrosion of steel in concrete.

Table 1.2 – Development of the rapid macrocell test

References	Bar Size*	Mortar Specimens		Resistor (ohm)	Specimen Number		Deicers	Test Period
		Mortar Length	Bar Embedment		Anode	Cathode		
Martinez et al. (1990)	No. 13 (No. 4)	102 mm (4 in.)	76-mm (3-in.) bar in mortar	100,000	1	1	NaCl, $CaCl_2$, CMA	56 days
Smith, Darwin, and Locke (1995)	No. 16 (No. 5)	102 mm (4 in.)	76-mm (3-in.) bar in mortar	10	3	3	NaCl	100 days
Schwensen, Darwin, and Locke (1995)	No. 16 (No. 5)	102 mm (4 in.)	76-mm (3-in.) bar in mortar	10	1	2	$CaCl_2$, CMA	130 days
					2	4	NaCl	100 days
Darwin et al. (2002), Gong et al. (2002)	No. 16 (No. 5)	152 mm (6 in.)	Completely in mortar	10	1	2	NaCl	105 days

* length = 127 mm (5 in.)

The corrosion performance of four different types of reinforcing steel was evaluated by Smith, Darwin, and Locke (1995). A No. 16 (No. 5) bar was used to reduce the mortar cover and, therefore, lower the time to corrosion initiation. As recommended by Martinez et al. (1990), a 10-ohm resistor was used in place of the 100,000-ohm resistor. To prevent oxygen depletion, compressed air was bubbled into the cathode after passing it through saturated NaOH solution to remove carbon dioxide.

The open circuit corrosion potentials at the anode and cathode in the macrocell were recorded once a week by Schwensen, Darwin, and Locke (1995). The specimen configuration used by Smith et al. (1995) was adopted. The authors concluded that the separate corrosion potential test could be discontinued because the open circuit potentials in the macrocell test provided the same information.

The corrosion performance of bars clad with 304 stainless steel was evaluated using the corrosion potential and rapid macrocell tests (Darwin et al. 1999, Kahrs, Darwin, and Locke 2001). The mortar specimens used by Smith et al. (1995) were adopted. In addition, bare bar specimens with a length of 127 mm (5 in.) were introduced in this study to provide a harsher test environment. The bare bar specimens were evaluated in the same manner as the mortar-wrapped specimens. Test results showed that bare bar specimens exhibited a higher corrosion rate than mortar specimens with the same reinforcing steel.

The rapid macrocell test was used by Ge et al. (2004) to evaluate the corrosion performance of several corrosion protection systems for conventional steel. Both corrosion rates and open circuit corrosion potentials were recorded daily for the first week, and then once a week. The test results showed that higher corrosion rates generally correlate with more negative corrosion potentials. During the tests,

corrosion products were observed on the exposed steel in the lollipop specimens above solution due to the high humidity in the covered container.

The corrosion performance of MMFX steel was evaluated by Darwin et al. (2002) and Gong et al. (2002) using the rapid macrocell test. During these studies, additional modifications were made to the test. The mortar specimen was modified so that the No. 16 (No. 5) bars were completely enclosed in the mortar (specimens were now referred to as mortar-wrapped specimens). In addition, the bare bar specimens were evaluated in the same manner as the mortar-wrapped specimens. For both bare bar and mortar-wrapped specimens, the lid was placed just above the level of the solution to prevent corrosion on the portion of the specimens above the solution.

1.4.2 Bench-Scale Tests

The bench-scale test specimens consist of concrete slabs with two mats of reinforcing steel. The Southern Exposure (SE) test is used to simulate an uncracked bridge deck, while the cracked beam (CB) test simulates a bridge deck with cracks over the top reinforcing bars. The SE and CB test specimens are subjected to alternate ponding and drying cycles with a 15% salt solution. The ASTM G 109 test was developed in 1992 to determine the effects of chemical admixtures on the corrosion of reinforcing bars in concrete in a chloride environment. The test includes ponding and drying with a 3% salt solution.

The severe corrosion environment provided by the SE and CB tests is generally believed to simulate 15 to 20 years of exposure for marine structures under tropical conditions and 30 to 40 years of exposure for bridges within a 48-week test period (Perenchio 1992). The environment provided by the ASTM G 109 test is significantly milder.

In 1981, Pfeifer and Scali developed the SE test to evaluate concrete sealers for bridge protection. The aim of this accelerated test is to simulate the alternate wet and dry environment in southern climatic regions where periodic seawater splash is very common, but no freezing is observed. The test slabs were 305 × 305 × 127 mm (12 × 12 × 5 in.) with one mat of reinforcing bars and cracks intentionally placed across the bars at midlength. The total test period was 24 weeks. The weekly test cycle consisted of ponding the specimens continuously for 100 hours with a 15% salt solution and drying them in a heat chamber at 100˚F for 68 hours using heat lamps. A dike with a height of 25 mm (1 in.) was attached to the specimen top surface to hold the salt solution. The corrosion potential of the steel was recorded every week for the first six weeks and then every other week. Visual inspections were made during the test and photographs were taken for each test condition. A good correlation was observed between corrosion potential readings and the amount and degree of corrosion products found on the bar when the test was completed.

The SE test was modified by Pfeifer, Landgren, and Zoob in 1987 to evaluate the corrosion performance of 11 corrosion protection systems. All of the SE specimens had two mats of reinforcing bars, electrically connected across a 10-ohm resistor. The height of specimens varied with the concrete clear cover to keep a constant thickness of concrete between top and bottom bars. The ponding and drying cycle used by Pfeifer and Scali (1981) was adopted for a total test period of 48 weeks. Corrosion current was recorded weekly and corrosion potentials were measured with respect to a copper-copper sulfate electrode monthly. Also, concrete electrical resistance between the top and bottom steel mats was measured each month. The results demonstrated the benefits of deep concrete cover and lower *w/c* ratios.

Cracked beam specimens [762 × 152 × 152 mm (30 × 6 × 6 in.)] were used to

evaluate the performance of corrosion inhibitors in concrete with cracks (Tourney and Berke 1993). A crack was made to each beam specimen using flexural load bearing techniques so that it extended down to the top bar. The crack was shimmed to a width of 0.25 mm (0.01 in.) to provide a consistent crack size during the test. The cracked beam specimens were ponded with a 3% salt solution for two weeks and then dried for two weeks. At the end of the 15-month test period, an autopsy was conducted to confirm the test results based on macrocell current measurements.

In 1994, the SE test was used by Nmai, Bury, and Farzam to evaluate the effectiveness of a sodium thiocyanate-based admixture in concrete. Each slab specimen [305 × 305 × 178 mm (12 × 12 × 7 in.)] had two mats of reinforcing bars, top and bottom, electrically connected across a resistor. The specimens were ponded for four days, followed by three days of air-drying. The macrocell current and corrosion potential of the top layer of steel were recorded on a weekly basis. An autopsy of the specimens was performed at the end of a 52-week test period to check the top reinforcing bars. The test results showed that the average time to corrosion initiation indicated by the corrosion potential measurements and macrocell current data follow similar trends.

The corrosion resistance of microalloyed reinforcing steel was evaluated by Senecal, Darwin, and Locke (1995) using SE and CB tests, as well as the rapid macrocell test. Each SE specimen [305 × 305 × 178 mm (12 × 12 × 7 in.)] consisted of six 457-mm (18-in.) long reinforcing bars, extending 76 mm (3 in.) from both sides of the slab. The CB test specimens were only half the width of the SE specimen, with a load-induced transverse crack placed in the concrete through to the top mat of steel. The top and bottom reinforcing bars are electrically connected across a 10-ohm resistor. An epoxy-coated wood dam was placed around the top of the specimen to

hold the salt solution, and the dam was sealed with silicone caulking material. The weekly test cycle used by Pfeifer and Scali (1981) was repeated 48 times to complete the tests. Every week, macrocell current, half-cell potential, and mat-to-mat resistance were recorded. The following recommendations were made at the end of the tests: a) a two-year test period should be used to better observe how the corrosion products affected the concrete; b) the concrete dam should be cast monolithically with the specimen to prevent leakage during the test; c) to provide more realistic conditions, a 3 or 4 percent salt solution should be used instead of the 15 percent solution; d) the effects of a longitudinal crack along the length of the top reinforcing bar should be investigated. Moreover, the linear polarization resistance test should be performed monthly to provide more information about microcell corrosion. The latter recommendation on crack orientation was based on the observation that cracks in bridge decks are almost always parallel to and directly over top reinforcing bars (Schmitt and Darwin 1995).

The corrosion resistance of 12 bar types, including epoxy-coated, metallic-clad, and solid metallic reinforcing bars, was evaluated using the SE and CB tests by McDonald et al. (1998). Each specimen consisted of six 305-mm (12-in.) long reinforcing bars embedded in a concrete slab [305 × 305 × 178 mm (12 × 12 × 7 in.)]. The CB test specimen had two 152-mm (6-in.) long longitudinal cracks over the two top reinforcing bars. Simulated cracks were made using a 0.3 mm (12-mil) stainless steel shim, cast into the concrete to the depth of the top bars. A 10-ohm resistor was used to connect one top and two bottom reinforcing bars together. A 24-week test cycle was used, which included 12 weeks with four days of ponding with a 15% salt solution and three days of drying at 100˚F, and 12 weeks of continuous ponding. The test period was 96 weeks. Over the 96-week test period, almost all specimens showed

corrosion rates that were relatively uniform, indicating that corrosion occurred gradually. It was concluded that the tests were sufficient to evaluate the corrosion resistance of different reinforcing bars.

The corrosion performance of MMFX microcomposite steel was evaluated using SE and CB tests (Darwin et al. 2002, Gong et al. 2002). The specimen configuration and ponding cycles used by McDonald et al. (1998) were adopted with some modifications. The CB specimen was only half the width of the SE specimen and the top and bottom mat bars were electrically connected across a 10-ohm resistor. In addition, a concrete dam with a height of 19 mm ($^3/_4$ in.) was cast monolithically with the specimen to prevent leakage during ponding, as recommended by Senecal et al. (1995). The test results showed that MMFX steel exhibited a corrosion rate between one-third and two-thirds that of conventional reinforcing bars.

The SE test was used by Civjan et al. (2003) to evaluate the corrosion performance of several corrosion inhibiting admixtures, including calcium nitrite, silica fume, fly ash, slag, and Hycrete. The specimen configuration and ponding cycles used by McDonald et al. (1998) were adopted. Each corrosion protection system was evaluated with three specimens and one specimen was fabricated with two longitudinal cracks. The test results showed that corrosion is significantly reduced through the use of triple admixture combinations of calcium nitrite, silica fume, and either fly ash or slag, the combination of calcium nitrite and slag, or Hycrete.

The SE and CB tests used by Darwin et al. (2002) were adopted by Ge et al. (2004) to evaluate the corrosion performance of corrosion inhibitors and conventional steel in concrete with *w/c* ratios of 0.45 and 0.35.

In 2005, Balma et al. used the SE, CB, and ASTM G 109 tests to compare the

corrosion performance of different corrosion protection systems, including concrete with a low *w/c* ratio, two corrosion inhibitors, one conventional Thermex-treated steel, three microalloyed Thermex-treated steels, MMFX microcomposite steel, epoxy-coated reinforcement, and two duplex steels (2101 and 2205, pickled and nonpickled). The authors concluded that the CB test should not be used to evaluate the effect of concrete properties on the corrosion protection of steel. Pickled 2101 and 2205 duplex stainless steels were recommended for use in reinforced concrete bridge decks based on both corrosion performance and economic analyses.

1.4.3 Field Test

Usually, the field tests are large-scale and carried out outdoors to study the long-term corrosion performance of reinforcing bars in concrete structures.

Virmani et al. (1983) used thirty-one large concrete slabs [610 × 1524 × 152 mm (24 × 60 × 6 in.)] to evaluate the corrosion resistance of epoxy-coated reinforcement and conventional steel in concrete with calcium nitrite. The slabs were tested at the FHWA (Federal Highway Administration) outdoor exposure site. The specimens were continuously ponded with a 3% salt solution until corrosion was induced in a control slab with conventional reinforcing bars. After the ponding was discontinued, the slabs were exposed to the natural environment near Washington, D.C. Compared with the control, both protection systems provided more than an order of magnitude reduction in corrosion rate.

Gaidis and Rosenberg (1987) used concrete slabs [1829 × 610 × 152 mm (72 × 24 × 6 in.)] to evaluate the effectiveness of calcium nitrite in bridge decks. Corrosion potentials were recorded on a 51 × 51 mm (2 × 2 in.) grid during a 60-month test period. To calculate a weighted corrosion rate for each specimen, a weight factor was

given for each test point, 1 for potentials between –0.35 and –0.40 V, 2 for potentials between –0.40 and –0.45 V, 4 for potentials between –0.45 and –0.50 V, and so on geometrically. Potentials more positive than –0.35 V were considered to be noncorroding. The number of test points undergoing corrosion were multiplied by the appropriate weight factor and then summed to give the weighted corrosion rate. The results showed that the use of calcium nitrite at a dosage of 2% by weight of cement could reduce corrosion significantly.

To evaluate the corrosion performance of reinforcing bars, Rasheeduzzafar et al. (1992) conducted outdoor exposure tests using prismatic concrete specimens with conventional, galvanized, epoxy-coated reinforcement, and stainless clad reinforcing bars in a 7-year exposure site program. The specimens were exposed to an environment characterized by seawater splash and spray, intense heat, often associated with high humidity, and strong, persistent drying winds. The corrosion evaluation methods included the onset and propagation of concrete cracking, the weight loss of steel, and the condition of steel based on the percentage of rust covering the bar surface.

Liu and Weyers (1998) used 1180 × 1180 × 216 mm (46.5 × 46.5 × 8 in.) concrete slabs to simulate the performance of typical concrete bridge decks. Forty-four specimens were exposed to the elements, and 16 were placed indoors to maintain a near constant moisture content and temperature. It was observed that most surface cracks were located directly above and parallel to the top reinforcing bars. A time to corrosion cracking model was proposed and the test results showed that the experimentally observed time to cracking was in good agreement with the model predicted time to cracking.

1.12 CHLORIDE THRESHOLD

The critical chloride threshold is defined as the concentration of chlorides necessary to break down the protective passive film on the reinforcing steel surface and initiate corrosion (Daigle, Lounis, and Cusson 2004).

Funahashi (1990) reported that the chloride threshold was likely to vary widely between different concretes. Therefore, the adoption of a single value for the purpose of specification or service life prediction is inappropriate. As a result, no specific threshold value for steel corrosion in concrete is universally accepted (Thomas 1996).

Many researchers have reported different chloride thresholds corresponding to the corrosion initiation of reinforcing steel. Alonso et al. (2000) attributed the lack of agreement to variations in concrete mix design, cement type and alkalinity, C_3A content of cement, blended materials, concrete *w/c* ratio, temperature, relative humidity, steel surface conditions and source of chloride contamination (internal or external). Another reason for this lack of agreement can be related to the definition of the threshold itself, that is, how corrosion initiation is identified (Alonso et al. 2000).

In this section, the chloride threshold is discussed in terms of the ratio of chloride to hydroxyl ion concentrations and the total chloride content.

1.5.1 Corrosion Initiation

Various methods have been used to identify the onset of corrosion and, thus, the threshold level for samples exposed to an external source of chloride contamination. A significant rise in macrocell corrosion current is used most commonly to identify the onset of corrosion. Corrosion initiation is also identified using polarization resistance methods, AC impedance methods, and time-dependent changes in corrosion potential.

Glass and Buenfeld (1997) stated that corrosion rates were considered to be significant for reinforcing steel when they exceeded values of 0.1 to 0.2 μA/cm^2. These values correspond to corrosion rates of 1.16 to 2.32 μm/yr (0.05 to 0.09 mil/yr).

A surge in corrosion current measured between the top and bottom mat bars in concrete slabs is also used to define the chloride threshold (Pfeifer et al. 1987).

The linear polarization resistance method has been used to identify the onset of corrosion of steel in concrete slab specimens. The passive condition of steel in concrete is characterized by corrosion current density values substantially lower than 0.1 μA/cm^2 (Lambert et al. 1991).

Allyn and Frantz (2001a) defined corrosion initiation based on a significant increase in the $1/R_P$ value in linear polarization resistance tests in a study to evaluate the effectiveness of different corrosion inhibitors. Similarly, Trejo and Monteiro (2005) used this technique to determine the chloride thresholds for ASTM A 615 conventional steel and ASTM A 706 low alloy steel. Their test results showed that ASTM A 706 low alloy steel has an average chloride threshold of 0.19 kg/m^3 (0.32 lbs/yd^3), much lower than that for conventional steel, 0.87 kg/m^3 (1.46 lbs/yd^3).

Active corrosion has been defined for reinforcing steel as a corrosion current density greater than 0.1 μA/cm^2, as determined by the linear polarization resistance test (Alonso et al. 2000).

In a study performed by Trépanier, Hope, and Hansson (2001), a combination of corrosion potential and AC impedance tests was used to define the corrosion initiation.

Clemeña (2003) identified the onset of corrosion as occurring when a rise in the positive macrocell current in the concrete block occurred along with rapid shifts of potential measurements toward more negative values.

1.5.2 Cl^-/OH^- Ratio

It has been reported that the protective film that provides passive protection to reinforcing steel in concrete may be destroyed even at pH values considerably above 11.5. In 1967, Hausmann tested over 400 bare steel rods in pure and chloride-contaminated alkaline solutions with pH values from 11.6 to 13.2. The test results indicate that the threshold value for Cl^-/OH^- is 0.6 for steel in aqueous solutions simulating concrete.

For steel in concrete containing internal chlorides, Lambert et al. (1991) reported that the threshold Cl^-/OH^- ratio necessary to initiate corrosion was somewhere between 0.3 and 0.6, close to that observed for steel immersed in aqueous solutions. When steel in concrete was exposed to external chlorides, however, the threshold Cl^-/OH^- ratio was approximately 3, markedly higher than the threshold observed for steel in aqueous solutions or in concrete containing internal chlorides. The threshold difference is probably due to the formation of a passive film and the buffering effect of a layer of cement hydration products deposited in intimate contact with the passive film on the embedded steel in concrete.

In 1997, Glass and Buenfeld performed a literature review on chloride threshold values. The threshold Cl^-/OH^- ratios determined in the pore solution expressed from concrete, mortar, and cement paste specimens varied widely from 0.22 to 40. It was suggested that the use of Cl^-/OH^- ratios to represent chloride threshold levels offered no advantages over the use of total chloride contents. Expressing the threshold level in terms of Cl^-/OH^- ratios ignores the potentially important inhibitive effects of other factors. These include the barrier properties of a relatively dense layer at the steel surface and the effective buffering capacity of precipitated $Ca(OH)_2$, which prevents the pH from falling below 12.6.

1.5.3 Chloride Content

As mentioned earlier, chlorides can be classified into internal and external chlorides. For the internal chlorides, the calcium aluminate (C_3A) within cement paste can react with the chlorides and chemically bind them to form calcium chloroaluminate. The bound chlorides are insoluble in concrete pore solution. It is generally believed that only freely dissolved chloride ions in the pore solution are available for the corrosion reactions. The total chloride content, however, may be taken as the total aggressive ion content and the bound chlorides present a potential corrosion risk by serving as a reservoir for the locally available chlorides at the steel-concrete interface.

The total chloride content can be expressed in terms of weight of chloride ions per volume of concrete or as a percentage of the weight of cement.

For typical concrete used in reinforced concrete structures, the total chloride threshold has been reported to be in the range of 0.6 to 0.9 kg/m^3 (1.0 to 1.5 lb/yd^3) (Metha and Monteiro 1993).

A wide range in the total chloride threshold level, from 0.17 to 2.5% by weight of cement, was reported in a literature review by Glass and Buenfeld (1997). The large variation in the chloride threshold can be attributed to a number of possible influential factors, such as *w/c* ratio, length of curing period, $CaCl_2$ content, bar condition, and the definition of corrosion initiation. A chloride threshold value as low as 0.097% by weight of cement was reported by Hope and Ip (1987).

1.13 CORROSION PROTECTION SYSTEMS

A variety of corrosion protection systems have been developed to protect reinforcing bars in concrete from corrosion, especially in marine structures and bridge decks. Several of the most commonly used strategies are discussed in this section.

Different models have been used to predict the service lives of reinforced concrete structures. Typically, service life is divided into two distinct phases: corrosion initiation and corrosion propagation, also known as the initiation-propagation model. The corrosion initiation phase can be defined as the time for chloride ions to penetrate the concrete cover and depassivate the protection film on the steel surface. The corrosion propagation phase can be taken as the time elapsed from initiation until structures reach their useful service life or repair becomes mandatory. Each corrosion protection system provides corrosion protection for reinforcing steel in concrete either by increasing the time to corrosion initiation or by reducing the corrosion rate to lengthen the corrosion period, or both.

1.6.1 Epoxy-Coated Reinforcement (ECR)

Epoxy-coated reinforcement (ECR) was developed and first implemented in the 1970s to minimize chloride-induced corrosion damage and to extend the useful life of highway structures. ASTM A 775 and A 934 are the specifications that govern the quality of epoxy-coated bars.

Early FHWA studies indicated that ECR was highly corrosion resistant and therefore was able to prevent early deterioration of reinforced concrete structures in chloride environments (Pike et al. 1973). ECR was first used in a four-span bridge over the Schuylkill River near Philadelphia in 1973 and the application of ECR in bridge structures grew rapidly in the 1970s. By 1977, the use of ECR was adopted as

a standard construction procedure by 17 states. By 1989, there were 17 coating applicators in the United States and Canada, and the market was dominated by Scotchkote 213, produced by 3M Company (Manning 1996).

In the late 1970s, most bridge decks were cast with top ECR and bottom conventional steel. In 1980, an outdoor exposure study was initiated to investigate the corrosion performance of ECR (Virmani et al. 1983). Concrete slabs [610 × 1524 × 152 mm (24 × 60 × 6 in.)] were fabricated in two lifts with a *w/c* ratio of 0.53. The top lift consisted of the top mat bars in concrete mixed with a specific amount of NaCl and the bottom lift consisted of the bottom mat bars in chloride-free concrete. All specimens were ponded with a 3% salt solution for the first 46 days and then subjected to natural weathering only. ECR used in the study had excessive holidays and surface damage and did not pass the coating flexibility test. The test results indicated that even poor quality ECR is very effective in reducing corrosion of reinforcing bars in concrete, especially when ECR is used in both mats. The excellent performance of ECR is attributed to the barrier provided by the epoxy coating that prevents chloride and oxygen from reaching the steel surface and provides the high electrical resistance between neighboring bars. Some of the test specimens were continued and their results were summarized in a C-SHRP (Canadian Strategic Highway Research Program) interim report (Clear 1992). In contrast to the early findings, all of the slabs containing ECR experienced corrosion-induced distress and were badly cracked by 1989. Significant corrosion of top epoxy-coated bars and undercutting of the epoxy coating were observed in the autopsy after the test. A deliquescent liquid of low pH was present under the epoxy coating of the corroded bars.

A 1981 FHWA study indicated that macrocell corrosion is dominant in bridge

decks and is the primary cause of early age bridge deck deterioration (Clear 1981). A direct electrical contact between top and bottom mats is available in bridge decks with conventional steel, while for bridge decks with top ECR and bottom conventional steel, partial contact is the most common condition. In the latter case, bottom bars provide large steel surface area to serve as oxygen-reducing cathode and a corrosion macrocell of significant magnitude can develop.

An FHWA study performed by Wiss, Janney, and Elstner (Pfeifer et al. 1987) involved two laboratory test methods to investigate the corrosion performance of ECR. At the end of the tests, no detectable corrosion activity was observed for specimens containing ECR either in the top mat only or in both mats. The authors concluded that ECR was greatly superior to conventional steel in minimizing corrosion.

In 1986, six years after reconstruction using ECR, the Florida Keys Bridges showed signs of corrosion, especially in the substructures. Field bridge surveys (Sagües 1994) revealed that a dramatic reduction in adhesion bond between the epoxy coating and the underlying metal had occurred independent of the chloride levels at the reinforcement, even in chloride free concrete. This observation was further confirmed in the laboratory tests. In 1992, the Florida Department of Transportation discontinued the use of ECR in all construction (Manning 1996).

In September 1982, an outdoor exposure study was initiated by CRSI (Concrete Reinforcing Steel Institute) to evaluate the long-term performance of ECR (Scannell and Clear 1990, Clear 1994). Concrete slabs [305 × 610 × 152 mm (12 × 24 × 6 in.)] with a *w/c* ratio of 0.42 were fabricated with conventional-conventional, epoxy-epoxy, and epoxy-conventional steel in the top and bottom mats, respectively. The tests started in November 1982, and slabs with conventional steel in both mats exhibited

corrosion-induced cracks in 0.9 to 1.5 years. In June 1991, after 8.5 years of salt exposure, slabs containing ECR had not experienced any cracking, as indicated by corrosion rate and corrosion potential results. However, in November 1991, after 9 years of exposure, all of the slabs containing ECR exhibited cracks. The authors concluded that ECR was many times more resistant to chloride-induced corrosion than conventional steel. An autopsy indicated that significant corrosion had developed under the epoxy coating. An adhesion loss of the epoxy coating was observed and the pH beneath the epoxy coating was between 4.5 and 6.0.

Epoxy-coated bars from 12 coaters, seven jobsites, and over 130 cores from 19 field structures were evaluated by Clear (1994) using visual examination, microscopic examination, coating hardness and adhesion tests, anchor patterns on the steel substrate, and coating electrical property tests. A failure mechanism was identified involving the progressive loss of coating adhesion and underfilm corrosion. Clear concluded that the life of ECR structures would exceed that of structures with conventional steel by only three to six years in marine or deicing salt environments in Canada and the northern U.S. He also concluded that the fusion-bonded epoxy coatings would not be able to provide long-term (50 years or more) corrosion protection in chloride-contaminated concrete.

Six concrete beams [0.2 × 0.2 × 6.1 m (7.9 × 7.9 × 240 in.)] were used to evaluate the corrosion performance of ECR (Griffith and Laylor 1999). In 1980, the beams were attached to a concrete dolphin, with the lower section of the beam in water, the upper section of the beam exposed in air, and the middle section of the beam in the tidal zone between the low and high tide levels of Yaquina Bay in Newport, Oregon. Two beams were removed from Yaquina Bay, one in 1989 and the other in 1998. A visual inspection of the beams and ECR bars, corrosion potential

measurement, and chloride content test were performed for each beam. Significant corrosion and adhesion loss were observed for both beams, especially within the tidal zone. The authors concluded that the use of ECR for long-term protection against corrosion in coastal bridges in Oregon should be discontinued.

Five different epoxy-coated bars, as well as conventional, metal-clad, and stainless steel reinforcing bars, were evaluated in an FHWA study by McDonald et al. (1998). In all cases, ECR performed better than conventional reinforcing bars and the results support the continued use of ECR as an effective corrosion protection system. McDonald et al. concluded that, when used, ECR should be used in both the top and bottom mats in bridge decks. Otherwise, bottom conventional steel can accelerate the corrosion rate through macrocell action because bare areas on top coated bars are relatively small, causing macrocell current densities on the exposed surface to be very high. From September 1998 to December 2002, 31 SE test slabs that had not been autopsied during the 1993-1998 FHWA study were subjected to long-term natural weathering exposure tests (Lee and Krauss 2004). These slabs were autopsied and analyzed upon termination of the test program. The research further confirmed the conclusion that ECR should be used in both top and bottom mats. The use of ECR in the top mat alone reduced the corrosion susceptibility by at least 50% in comparison to conventional bars. When ECR was used in both mats, the mean macrocell current density approached the corrosion resistant level exhibited by stainless steel. Autopsies were performed when the tests ended, after about seven years. For ECR slabs with negligible macrocell current densities, the extracted ECR specimens showed no sign of corrosion. For ECR specimens with high macrocell current densities, severe coating deterioration due to corrosion was observed and the extracted ECR specimens exhibited numerous hairline cracks and/or blisters in conjunction with adhesion loss,

coating disbondment, and underlying steel corrosion. No consistent relationship, however, was found between the extent of adhesion loss and the level of macrocell corrosion current density exhibited by the test specimens.

The performance of ECR in bridge decks was investigated in an FHWA study (Smith and Virmani 1996) that included 92 bridge decks, two bridge barrier rails, and one noise barrier rail. The structures had been in service for 3 to 20 years at the time of the investigation. The investigation included the overall condition of structures, concrete cover, chloride content at the level of reinforcing bars, epoxy coating thickness and holidays, and visual inspection of 202 extracted ECR segments from the bridge decks. Overall, the bridge decks were found to be in good condition. Very few spalls or delaminations were found and generally not related to the corrosion of ECR Approximately 81% of the extracted ECR segments were corrosion free. The other 19% exhibited evidence of corrosion, but only four ECR segments (2%) exhibited significant corrosion. The ECR segments exhibited higher corrosion when extracted from locations of heavy cracking, shallow concrete cover, high concrete permeability, and high chloride concentration.

In 1996, a field investigation that included the piles in three marine structures and three bridge decks in Virginia indicated that the loss of adhesive bond between the epoxy coating and the steel surface could occur in 6 years in marine structures and in 15 years in bridge decks (Weyers et al. 1998). Later, another study was performed to determine the physical condition of ECR in concrete bridge decks in Virginia (Pyc et al. 2000). ECR segments were extracted from 18 bridge decks constructed between 1977 and 1995 and 94% of the samples exhibited adhesion reduction to complete coating disbondment. The test results showed that adhesion reduction could happen in as little as 4 years and long before chlorides arrive at the level of reinforcing bars in

concrete. As described by Weyers et al. (1998), the adhesion reduction was related to water penetrating the coating and oxidation of the underlying steel, rather than the presence of the chloride ions or excessive coating damage.

Laboratory research and field studies over the past 30 years have produced mixed results on the effectiveness of epoxy coatings, from satisfactory corrosion protection performance to the conclusion that ECR will not provide long-term corrosion protection for structures in a chloride-contaminated environment.

1.6.2 Stainless Steel or Stainless Steel Clad Reinforcement

Stainless steels contain a minimum of 12% chromium and are resistant to staining and corrosion. Compared to conventional steel, stainless steel offers a number of advantages, as discussed by Smith and Tullman (1999). For a number of years, the three types of stainless steel most commonly used for reinforcing bars were types 304, 316, and 316LN, although 2205 appears to be the current stainless steel of choice (Magee 2005).

Previous research and field investigations of solid stainless steel and stainless steel clad reinforcing bars were reviewed by McDonald et al. (1995). Generally, both types of reinforcing bar have exhibited excellent corrosion performance in chloride-contaminated environments. In all of the studies reviewed, no cracks were observed in concrete as a result of the corrosion of stainless steel bars. McDonald et al. concluded that the use of stainless steel may be warranted when guaranteed long-term corrosion resistance is required.

Concrete cylinder specimens with different amount of pre-mixed chlorides were used to evaluate the corrosion performance of stainless steel (Gu 1996). In chloride-contaminated concrete, stainless steel corroded at a rate that was less than 2% of that

exhibited by conventional reinforcing steel.

In 1993, an FHWA study was initiated to find reinforcing materials to achieve a 75 to 100-year design life using the SE test. In that study, McDonald et al. (1998) concluded that Type 316 stainless steel would be able to provide 75 to 100 years of crack free design life. This conclusion was based on the fact that Type 316 stainless steel corroded at a rate of 1/800 of that exhibited by conventional steel under the same exposure conditions. Type 304 stainless steel provided excellent corrosion protection when it was used in both mats. However, Type 304 stainless steel was not recommended because moderate corrosion was observed when it was used with a conventional steel cathode in precracked concrete.

Along with conventional steel, reinforcing bars clad with Type 304 stainless steel were evaluated based on corrosion potential tests and rapid macrocell tests by Darwin et al. (1999) and Kahrs et al. (2001). For bars not encased in mortar, the clad bars corroded at a rate of about 1/100 of the value observed for conventional reinforcing bars. For mortar specimens, the corrosion rate was about 1/20 to 1/50 of the value observed for conventional bars. The results in the study showed that the 304 stainless steel clad bars exhibited significant improvement in corrosion performance compared to conventional reinforcing bars.

The corrosion resistance of 316L stainless steel clad bars was investigated by Clemeña and Virmani (2002), along with conventional reinforcing bars and three types of solid stainless steel (316LN, 304, and 2205). Concrete slabs [254 × 229 × 184 mm (10 × 9 × 7.25 in.)] were used to evaluate corrosion resistance based on the macrocell current, corrosion rate from linear polarization resistance tests, and open circuit corrosion potential. Overall, the clad bars provided virtually the same corrosion resistance as the three types of solid stainless steel. Chloride content test

results indicated that the three solid stainless steel bars and the clad bars can tolerate at least 15 times more chloride than conventional reinforcing bars.

In search of metallic reinforcing bars that are not only more durable and corrosion resistant than ECR, but also economical, several new metallic bars were evaluated by Clemeña (2003). They included 316L clad bars, bars made of MMFX-2 "microcomposite" steel, nonpickled 2101 LDX, a carbon steel coated with a 0.05-mm (2-mil) layer of arc-sprayed zinc and then epoxy (Zn/EC), Type 304 and 316LN solid stainless steel bars. Based on the estimated times to corrosion, the chloride thresholds for 2101 LDX and microcomposite steel bars are 2.6 to 3.7 times and 4.6 to 6.4 times that observed for conventional reinforcing bars, respectively. The two solid stainless steel bars, 316L clad bars, and the Zn/EC bars were still in passive state after three years. Their chloride threshold is at least 9 times greater than that measured for conventional reinforcing bars.

Three microalloyed steels, one conventional thermex-treated steel, MMFX microcomposite steel, and two duplex stainless steels (2101 and 2205, pickled and nonpickled), were tested using the rapid macrocell test and bench-scale tests by Balma et al. (2005). Compared with conventional steel, the three microalloyed steels and conventional thermex-treated steel showed no improvement in corrosion resistance. The MMFX steel had a higher chloride threshold, but exhibited corrosion losses between 26 and 60% of those observed for conventional steel. The corrosion potential results indicated that MMFX and conventional steel have a similar tendency to corrode. Two stainless steels, pickled 2101 and 2205, exhibited the best corrosion resistance, with the average corrosion losses ranging from 0.3% to 1.8% of that exhibited by conventional reinforcing steel.

1.6.3 Corrosion Inhibitors

Corrosion inhibitors are chemical admixtures that are added to concrete to prevent or minimize the corrosion of reinforcing steel without significantly changing the properties of the concrete. They are considered as cost-effective solutions to the widespread problem of corrosion in reinforced concrete structures and have been used increasingly in both new and existing reinforced concrete bridges over the past 15 years (Daigle et al. 2004).

Corrosion inhibitors can protect steel in concrete by performing one or more of the following functions (Hansson, Mammolitu, and Hope 1998): a) increase the resistance of the passive film on the steel surface to break down by chlorides, b) create a barrier film on the steel, c) block the ingress of chlorides, d) increase the degree of chloride binding in concrete, e) scavenge the oxygen dissolved in the concrete pore solution, and f) block the ingress of oxygen.

Corrosion inhibitors usually can be divided into three types, inorganic, organic, or vapor-phase corrosion inhibitors or be classified as anodic, cathodic, or mixed corrosion inhibitors, depending on how they affect the corrosion process.

Anodic inhibitors act by forming an oxide film barrier on anodic surfaces of the reinforcing steel or by promoting the stabilization of the natural passivating layer of the steel, thereby delaying corrosion initiation and controlling the rate of corrosion. The most commonly used anodic inhibitor is calcium nitrite, commercially available as Darex Corrosion Inhibitor (DCI or DCI-S). Cathodic inhibitors will simply reduce the rate of cathodic reaction by forming insoluble films on cathodic surfaces (Daigle et al. 2004). Mixed corrosion inhibitors form a corrosion resistant film that adheres to the metal surface physically and/or chemically to block both the anodic and the cathodic reactions (Nmai, Farrington, and Bobrowski 1992).

DCI (for Darex Corrosion Inhibitor) is an inorganic corrosion inhibitor containing 30% calcium nitrite and 70% water. It provides protection to reinforcing bars in concrete through the formation of a passive protective film [Eq. (1.15)].

$$Fe^{2+} + OH^- + NO_2^- \rightarrow NO(g) + \gamma\text{-}FeOOH \quad (1.15)$$

As shown in Eq. (1.11), nitrite ions are consumed as they provide corrosion protection for steel in concrete. Test results show that there is no loss of nitrite ions in the absence of corrosion and that the rate of nitrite ion consumption is dependent on the corrosion rate of reinforcing steel (Pyke and Cohen 1948).

In a field exposure program, the corrosion performance of calcium nitrite was evaluated using concrete cylinders with a *w/c* ratio of 0.60 (Burke 1994). Four No. 13 (No. 4) bars were embedded in concrete cylinders [152 × 610 mm (6 × 24 in., diameter × length)] with varying amounts of concrete cover. During this 76-month study, the specimens were suspended in nylon mesh nets in the intertidal zone at the Naval Air Station Trumbo Point Annex, Key West, Florida. The test results showed that the corrosion of reinforcing bars with 50 mm (2 in.) of cover was reduced by 57% in the presence of calcium nitrite. The loss of nitrite at the end of 76 months was determined to be 23, 20, and 7% at depths of 25, 50, and 75 mm (1, 2, and 3 in.), respectively. The author attributed the loss of nitrite ions to the leaching process in porous concrete.

The SE test was used to investigate the corrosion performance of calcium nitrite in concrete with different *w/c* ratios (0.50, 0.40, and 0.32) and different clear covers [25, 51, and 76 mm (1, 2, and 3 in.)] (Pfeifer et al. 1987). The investigation showed that calcium nitrite can reduce the corrosion rate significantly, but cannot delay corrosion initiation. The test results indicated that as the quality of concrete improves, the corrosion inhibition benefits provided by calcium nitrite increase significantly.

The test results from an accelerated corrosion study that included 1,200 samples, 15 mix designs, and three dosage rates of calcium nitrite showed that calcium nitrite can delay corrosion initiation and reduce the corrosion rate of reinforcing steel significantly (Berke et al. 1988). The test results showed that the more calcium nitrite is used, the more protective benefits are provided. When the dosage rate of calcium nitrite increases from 10 to 30 L/m^3 (2 to 6 gal/yd^3), the chloride threshold increases from 3.56 to 9.50 kg/m^3 (6 to 16 lb/yd^3).

When calcium nitrite is used, it is believed that chloride, nitrite, and hydroxyl ions engage in a competition for Fe^{2+} at flaws in the protective oxide layer. Nitrite and hydroxyl ions inhibit corrosion by reacting with Fe^{2+} to form a protective film and chloride ions promote corrosion by producing soluble iron-chloride complex ions. Therefore, the chloride-to-nitrite ratio determines the level of nitrite required for protection of reinforcing bars.

A study conducted by the South Dakota Department of Transportation (1984) used concrete cylinders with and without admixed chloride to determine the critical chloride-to-nitrite ratio. The linear polarization resistance test was used to measure the corrosion rate of reinforcing bars. The test results showed that calcium nitrite prevented corrosion at chloride-to-nitrite ratios of 1.6 to 2.2 for chloride levels above 10.7 kg/m^3 (18 lb/yd^3).

Concrete cylinders [152 × 305 mm (6 × 12 in.)] and large concrete slabs [1829 × 610 × 152 mm (72 × 24 × 6 in.)] were used to evaluate the critical chloride-to-nitrite ratio (Gaidis and Rosenberg 1987). The cylinders were fabricated with calcium nitrite at a constant rate of 2% by weight of cement, and with mixed chloride at several different dosages. The cylinder test results showed that corrosion could be controlled if the chloride-to-nitrite ratio is below 1.5. The slab specimens were cast

with calcium nitrite at different dosages and they were salted daily. In contrast to the earlier report by the South Dakota Department of Transportation (1984), the slab specimen test results indicated that ratios of chloride to nitrite higher 1.6 would result in the corrosion of reinforcing steel in concrete.

An FHWA study including 18 large concrete slabs [610 × 1524 × 152 mm (24 × 60 × 6 in.)] was carried out to investigate the effectiveness of calcium nitrite in preventing the corrosion of reinforcing steel (Virmani et al. 1983, and Virmani 1990). The slabs were fabricated in two lifts and the top lift was mixed with NaCl. The results showed that calcium nitrite reduced the corrosion rate of reinforcing steel by a factor of 10 in poor quality chloride-contaminated concrete at a chloride-to-nitrite ratio below 0.9, and by at least a factor of two for chloride-to-nitrite ratios of up to 2.5. It was shown that for chloride-to-nitrite ratios less than 1.5, calcium nitrite was able to inhibit corrosion. The conclusion was based on both periodic measurements over seven years and a visual survey at the end of the test.

Conventional reinforcing bars were submerged in oxygenated limewater with added calcium chloride to study the corrosion performance of calcium nitrite (Hope and Ip 1989). The chloride threshold value in terms of chloride-to-nitrite ratios was estimated to be between 11 and 14. It was observed that calcium nitrite could repassivate the reinforcing steel even after corrosion had been initiated by calcium chloride.

Lollipop and beam specimens were used to evaluate the corrosion resistance of ECR and calcium nitrite in an eight-year study by Berke (1998). ECR with and without 2% damage to the epoxy coating, along with conventional reinforcing bars, were evaluated with and without calcium nitrite. The lollipop specimen results showed that calcium nitrite alone significantly outperforms ECR with 2% damage to

the epoxy coating and is equivalent to ECR without damage alone. The lollipop specimens containing ECR with flaws and calcium nitrite showed corrosion activity between 5 and 7 years due to high chloride content. The autopsy and resistivity results for those specimens demonstrated that calcium nitrite had not prevented coating disbondment or corrosion underneath the coating. For the beam tests, no corrosion was observed for samples containing calcium nitrite. In general, calcium nitrite improved the performance of all types of steel. The combination of ECR without damage and calcium nitrite gave the best results.

Two calcium nitrite-based corrosion inhibitors and two organic compounds were tested in synthetic pore solution by Mammolitu, Hansson, and Hope (1999). The results showed that corrosion inhibitors were ineffective in preventing the corrosion of steel in synthetic pore solutions and did not increase the chloride threshold of reinforcing steel. The effectiveness of these four corrosion inhibitors was further investigated using lollipop and mortar specimens by Trépanier et al. (2001). The results showed that all corrosion inhibitors delay the onset of corrosion to varying degrees. However, once corrosion has been initiated, the inhibitors have little detectable effect on the corrosion rate of the embedded steel.

Three corrosion inhibitors, DCI, Rheocrete 222, and Armatec 2000 were evaluated by Pyc et al. (1999) using bare bars in a simulated pore solution, and by Zemajtis, Weyers, and Sprinkel (1999) using concrete specimens. Both Rheocrete 222 and Armatec 2000 are water based organic corrosion inhibitors consisting of amines and esters, and they appeared to provide little or no corrosion inhibition. The corrosion inhibitor DCI-S increased the chloride threshold of reinforcing steel in concrete. In addition, chloride content and rapid concrete chloride permeability tests indicated no significant difference either in the rate of chloride ingress or in the

diffusion coefficients for concretes with and without corrosion inhibitors.

Cracked beam tests were used to evaluate the performance of calcium nitrite and an organic corrosion inhibitor in cracked concrete (Nmai et al. 1992). The results showed that both corrosion inhibitors can delay corrosion initiation and reduce the corrosion rate, but that the organic corrosion inhibitor is more effective than calcium nitrite. The authors concluded that the organic corrosion inhibitor protected reinforcing steel from corrosion by a two-fold mechanism, reducing chloride ions ingress and forming a protective film on the steel surface.

Conventional reinforcing bars were evaluated in concrete with two corrosion inhibitors, DCI-S and Rheocrete 222+, using rapid macrocell and bench-scale tests (Balma et al. 2005). The concrete used in the tests had *w/c* ratios of 0.35 and 0.45. In uncracked mortar and concrete, the results showed that both corrosion inhibitors can reduce the corrosion rate and corrosion losses by at least 50%. However, only Rheocrete 222+ can improve the corrosion protection of reinforcing steel in concrete with cracks, primarily due to its ability to lower concrete permeability.

The corrosion performance of three corrosion inhibitors, Hycrete (alkali metal and ammonium salt of an alkenyl-substituted succinic acid), calcium nitrite, and an organic corrosion inhibitor, were evaluated using lollipop and concrete slab specimens by Allyn and Franz (2001a). The tests were performed at 1% and 2% Hycrete concentration by weight of cement. The linear polarization resistance was recorded every week. The test results showed that Hycrete can prevent the corrosion initiation in intact specimens and prevent or reduce corrosion significantly in cracked specimens. The authors concluded that Hycrete provided dual protection against corrosion of reinforcing steel by reducing permeability and inhibiting corrosion. Calcium nitrite and the organic corrosion inhibitor delayed the corrosion initiation

and reduced corrosion for uncracked concrete, but were not effective in precracked concrete.

Southern Exposure test specimens both with and without cracks were used to evaluate the performance of DCI-S and Hycrete (Civjan et al. 2003). Civjan et al. concluded that calcium nitrite provided excellent protection in uncracked concrete, but was not effective in cracked concrete. Hycrete protected reinforcing steel from corrosion in both cracked and uncracked concrete.

A review of corrosion inhibitors (Berke 1989, Berke and Rosenberg 1989) indicated that calcium nitrite is not detrimental to concrete properties.

Concrete property tests revealed that Rheocrete has little effect on slump and setting time, but its use in concrete may require increasing the amount of air-entraining agent and extending mixing to achieve a given air content (Nmai et al. 1992). The use of Rheocrete in concrete can reduce chloride content as compared to the concrete without Rheocrete. The test results also showed that this organic corrosion inhibitor reduces concrete compressive strength marginally, and has no effects on concrete-steel bond strength or freeze-thaw resistance.

Strength and durability properties were investigated for concrete containing Hycrete, DCI-S or Rheocrete (Allyn and Frantz 2001b). Compared with concrete cast with DCI-S or Rheocrete, concrete containing Hycrete had a lower resistance to freezing and thawing, but still satisfied high-performance concrete requirements. Absorption for concrete with Hycrete is at least 50% lower than concrete cast with and without DCI-S or Rheocrete. Hycrete, however, can reduce concrete compressive strength by up to 18% and 27% for concrete with and without a defoaming agent, respectively.

Civjan et al. (2003) recommended an optimum dosage of corrosion inhibitors

based on a literature review of the use of durability enhancing admixtures in concrete:

1) Calcium nitrite: 15 to 25 L/m^3 (3 to 5 gal/yd^3) with a *w/c* ratio less than 0.50,
2) Rheocrete 222: 5 L/m^3 (1 gal/yd^3) with a *w/c* of 0.50, and
3) Hycrete: $^1/_2$ to 1% addition by weight of cement.

1.6.4 Low Permeability Concrete

Quality concrete with sufficient concrete cover is the first line of defense against the chloride-induced corrosion of reinforcing steel in concrete. Quality concrete with low *w/c* ratios can increase the concrete electrical resistivity and slow down the penetration of aggressive chloride ions, moisture, and oxygen. ACI 318R-05 *Building Code Requirements for Structural Concrete* states that a maximum *w/c* ratio of 0.40 should be used for corrosion protection of reinforcement in concrete exposed to chlorides.

Both concrete and cement paste cylinders at three different *w/c* ratios (0.61, 0.45, and 0.37) were used for chloride permeability tests by Ost and Monfore (1974). The authors found that, after 12 months of soaking in a 8% calcium chloride solution, the chloride content at 51 mm (2 in.) depth was reduced by 50 times when the *w/c* ratio was decreased from 0.61 to 0.37. They also found that chlorides more readily penetrated the concrete than the cement paste.

Three *w/c* ratios (0.51, 0.40, and 0.28) were used in an FHWA study (Pfeifer et al. 1987) to evaluate the corrosion performance of 11 different corrosion protection systems, including corrosion inhibitors, different concrete covers, epoxy-coated reinforcement, galvanized bars, and pretreating sealers. The SE test was used, and the cyclic ponding used by Pfeifer and Scali (1981) was adopted. After 44 weeks of cyclic testing, chloride profile results from the study showed that the *w/c* ratio is the

most dominant factor in reducing concrete permeability. When the *w/c* ratio was reduced from 0.51 to 0.40, the chloride content was reduced by 80% at a depth of 25 mm (1 in.). When the *w/c* ratio was reduced further to 0.28, the chloride content was reduced by 95%. The chloride profile results are similar to those presented by Clear (1976).

Another laboratory study (Sherman, McDonald, and Pfeifer 1996) indicated that when the *w/c* ratio was reduced from 0.46 to 0.32, the chloride content was reduced by 94% at a depth of 25 mm (1 in.) after severe salt water exposure testing.

Macrocell and bench-scale tests were used to evaluate the effect of *w/c* ratio on corrosion protection (Ge et al. 2004). Three different *w/c* ratios, 0.50, 0.45, and 0.35 were used for the macrocell test and two *w/c* ratios, 0.45 and 0.35, were used for the bench-scale tests. Overall, the specimens with a lower *w/c* ratio exhibited lower corrosion rates and more positive corrosion potentials. The results from cracked beam tests, however, indicated that corrosion rate is largely independent of *w/c* ratio.

1.14 OBJECTIVE AND SCOPE

The principal objectives of this research are to: 1) evaluate the corrosion resistance of 2205 pickled stainless steel in Kansas bridge decks, and 2) study techniques for making epoxy-coated reinforcement (ECR) more corrosion resistant by using multiple corrosion protection strategies in bridge decks, as well as bridge members in a marine environment.

The corrosion protection systems evaluated in this study include:

1) 2205 pickled stainless steel,

2) ECR embedded in concrete with corrosion inhibitor DCI-S (calcium nitrite), Rheocrete 222+ (a combination of esters and amines), or Hycrete (alkali metal

and ammonium salts of an alkenyl-substituted succinic acid) with *w/c* ratios of 0.45 and 0.35,

3) ECR with a primer containing calcium nitrite with *w/c* ratios of 0.45 and 0.35,

4) Multiple coated reinforcement with a zinc layer (containing 98% zinc and 2% aluminum) underlying the DuPont 8-2739 epoxy (flex west blue). The zinc layer has a nominal thickness of approximately 0.05 mm (2 mils).

5) ECR with the epoxy coating applied after pretreatment of the steel bar with zinc chromate and ECR using improved adhesion epoxy coatings developed by DuPont and Valspar, and

6) The three types of ECR described in item 5 cast in concrete containing the corrosion inhibitor DCI-S.

The regular epoxy coating on the conventional ECR, ECR with the chromate pretreatment, and ECR with a primer containing encapsulated calcium nitrite is 3M™ Scotchkote™ 413 Fusion Bonded Epoxy.

The first objective is achieved by recording corrosion potentials on bridge decks every six months, and monitoring accompanying bench-scale and field test specimens. Conventional steel and normal ECR are evaluated as control specimens. The rapid macrocell test, bench-scale tests, and field test are used to evaluate multiple corrosion protection systems.

The testing techniques used in this study are described in Chapter 2. Macrocell current and open circuit corrosion potential are measured for the rapid macrocell test. Macrocell current, mat-to-mat resistance, and open circuit corrosion potential are recorded for both the bench-scale and field tests. For each of the corrosion protection systems, one bench-scale test specimen is evaluated using the linear polarization

resistance test.

Chapter 3 covers the test results for both objectives.

Chapter 4 presents the results of the linear polarization resistance test.

A life-cycle cost analysis is performed in Chapter 5 to compare the cost effectiveness of different corrosion protection systems for bridge decks over a 75-year economic life.

The comparisons between the results of the rapid macrocell and bench-scale tests are presented in Chapter 6. The corrosion rates and total corrosion losses are used to determine the degree of correlation between the tests. The comparisons are performed based on the results in the study carried out by Balma et al. (2005).

Conclusions and recommendations are presented in Chapter 7.

CHAPTER 2

EXPERIMENTAL WORK

The rapid macrocell test, three bench-scale tests, and a field test are used to evaluate the multiple corrosion protection systems included in this study. This chapter provides a description of the test specimens, test procedures, specimen preparation, and equipment and materials used for each test method.

The multiple corrosion protection systems in this study include epoxy-coated reinforcement (ECR), ECR with zinc chromate pretreatment, two types of ECR with increased adhesion coatings produced by DuPont and Valspar, multiple coated reinforcement (with a zinc layer containing 98% zinc and 2% aluminum underlying a conventional epoxy coating), ECR with a primer containing encapsulated calcium nitrite, three corrosion inhibitors (DCI-S, Rheocrete 222+, and Hycrete), concrete with water-cement (*w/c*) ratios of 0.45 and 0.35, and combinations of these systems.

Two bridges with 2205 pickled stainless steel are included in the current study, the Doniphan County Bridge (DCB) located in Doniphan County, Kansas and the Mission Creek Bridge (MCB) located in Shawnee County, Kansas. They are the first two bridges constructed using stainless steel reinforcement in Kansas. The type of steel was selected based on the results of a study performed at the University of Kansas. Two duplex stainless steels, 2101 and 2205 (pickled and non-pickled), were evaluated by Balma et al. (2005) using rapid macrocell and bench-scale tests. An economic analysis showed that decks containing pickled 2101 or 2205 stainless steel are more cost effective than decks with ECR or conventional reinforcing steel. The results also show that decks with 2101 pickled steel are more cost effective than decks with 2205 pickled steel. However, only 2205 pickled stainless steel was recommended for use in reinforced concrete bridge decks because some of the 2101

pickled bars showed some corrosion activity.

The corrosion performance of stainless steel in the bridge decks is monitored using the corrosion potential mapping technique. In addition, accompanying field and bench-scale test specimens were cast using the same reinforcing steel and concrete as those used in the bridge decks. All of the experimental work related to the two bridges is also presented in this report.

2.1 CORROSION PROTECTION SYSTEMS

The corrosion protection systems evaluated in this study include nonstandard types of steel and coatings, plus corrosion inhibiting admixtures. A detailed description of the systems is provided below.

- **Reinforcing Bars**

  2205p – 2205 pickled stainless steel for both the DCB and MCB bridges,

  Conv. – Conventional steel,

  ECR – Conventional epoxy-coated reinforcement,

  ECR(Chromate) – ECR with chemical pretreatment of the steel bar with zinc chromate prior to application of the epoxy coating,

  ECR(DuPont) – ECR with increased adhesion by DuPont,

  ECR(primer/Ca(NO$_2$)$_2$) – ECR with a primer containing encapsulated calcium nitrite,

  ECR(Valspar) – ECR with increased adhesion by Valspar, and

  MC – Multiple coated reinforcement with a zinc layer underlying DuPont 8-2739 epoxy (flex west blue). The zinc layer contains 98% zinc and 2% aluminum and has a nominal thickness of approximately 0.05 mm (2 mils).

The regular epoxy coating on the conventional ECR, ECR(Chromate) and ECR(Primer/Ca(NO$_2$)$_2$) bars is 3M™ Scotchkote™ 413 Fusion Bonded Epoxy.

- **Corrosion Inhibitors**

  DCI – Darex Corrosion Inhibitor (DCI-S) manufactured by W. R. Grace, used at a dosage rate of 15 L/m^3 (3 gal/yd^3) in concrete, and 23.87 L/m^3 (4.82 gal/yd^3) in mortar,

  Rheocrete – Rheocrete 222+ manufactured by Master Builders, Inc., used at a dosage rate of 5 L/m^3 (1 gal/yd^3) in concrete, and 7.96 L/m^3 (1.61 gal/yd^3) in mortar, and

  Hycrete – Hycrete DSS manufactured by Broadview Technologies, used at a dosage rate of 2.25% by weight of cement.

ECR, ECR cast in concrete with corrosion inhibitor DCI, Rheocrete or Hycrete, and ECR with a primer containing encapsulated calcium nitrite are evaluated in concrete with *w/c* ratios of 0.45 and 0.35.

The reinforcing bars used in the Doniphan County Bridge are 2205 stainless steel that is hot rolled, shot blasted, and pickled. The pickling procedure involved blasting the bars to a near white finish with stainless steel grit and then placing them in a solution of 25% nitric acid and 3% to 6% hydrofluoric acid at 110 to 130 ºF for 40 to 50 minutes. The steel used in the Mission Creek Bridge is 2205 duplex with hot finish and unannealed pickling. The steel was blast-cleaned with stainless steel shot and then cleaned in an aqueous solution containing 2 to 3% hydrofluoric acid and 7.5 to 12% sulfuric acid for 15 to 20 minutes and water-rinsed at a temperature of 105º F (maximum). The steel was then cleaned in a 10 to 12% nitric acid solution for 5 minutes and water-rinsed at room temperature.

The chemical and physical properties of 2205 pickled stainless steel for both bridges are presented in Tables 2.1 and 2.2, respectively, as well as those for conventional steel. Only No. 16 (No. 5) bars are used in the accompanying field and bench-scale tests for both bridges.

Table 2.1 – Chemical properties of 2205p stainless steel and conventional steel as provided by manufacturers

Steel[a]	Bar No.	Heat No.	C	Mn	Si	P	S	CR	Ni	Mo	Cu	N	B
DCB-2205p	16 (5)	150694	0.02	1.72	0.41	0.021	0.001	21.53	4.85	2.60	0.19	0.16	-
DCB-2205p	13 (4)	150692	0.02	1.80	0.47	0.023	0.004	21.30	4.67	2.65	0.22	0.16	-
MCB-2205p	16 (5)	150876	0.02	1.75	0.47	0.024	0.003	21.55	4.75	2.59	0.26	0.16	0.0025
MCB-2205p	13 (4)	150863	0.02	1.73	0.42	0.027	0.003	21.54	4.72	2.59	0.22	0.18	0.0027
Conv.	16 (5)	231159	0.43	0.95	0.21	0.014	0.046	0.200	0.17	0.038	0.49	-	0.0005

[a] DCB-2205p = 2205 pickled stainless steel for the Doniphan County Bridge.
MCB-2205p = 2205 pickled stainless steel for the Mission Creek Bridge.
Conv. = conventional steel.

Table 2.2 – Physical properties of 2205p stainless steel and conventional steel as provided by manufacturers

Stee[a]	Bar No.	Heat No.	Yield Strength		Tensile Strength		Elongation (%)
			(MPa)	(ksi)	(MPa)	(ksi)	in 203 mm (8 in.)
DCB-2205p	16 (5)	150694	632	91.5	1255	182.0	28.0
DCB-2205p	13 (4)	150692	655	95.0	848	123.0	25.0
MCB-2205p	16 (5)	150876	627	91.0	848	123.0	25.0
MCB-2205p	13 (4)	150863	717	104.0	883	128.0	25.0
Conv.	16 (5)	231159	442.7	64.2	713.6	103.5	15.0

[a] DCB-2205p = 2205 pickled stainless steel for the Doniphan County Bridge.
MCB-2205p = 2205 pickled stainless steel for the Mission Creek Bridge.
Conv. = conventional steel.

2.2 RAPID MACROCELL TEST

The rapid macrocell test evaluates the corrosion performance of different corrosion protection systems within a 15-week time frame, as discussed in this section. Both bare bar and mortar-wrapped specimens are used in the test.

The rapid macrocell test requires two containers, one with two specimens in simulated concrete pore solution (cathode), and the other with one specimen in pore solution containing a specific concentration of sodium chloride (anode). The anode and cathode are electrically connected across a 10-ohm resistor and ionically by a salt bridge, as shown in Figure 2.1 for the bare bar specimens, and Figure 2.2 for the mortar-wrapped specimens. Crushed mortar fill, which consists of the same mixture as used in the test specimens, is added to the containers with mortar-wrapped

specimens. Compressed air, scrubbed to remove carbon dioxide, is bubbled into the cathode solution to provide an adequate supply of oxygen for the cathodic reaction.

Previous versions of the rapid macrocell test setup placed the lid at some distance above the liquid solution. In these tests, corrosion products tended to form in the humid environment between the lid and the liquid surface. In the current test configuration, the lids in the containers are placed just above the level of the solution for both the bare bar and mortar-wrapped specimens.

The voltage drop across a 10-ohm resistor and open circuit corrosion potential are recorded to evaluate the corrosion performance of the reinforcing steel. The corrosion rate can be determined using Faraday's Law, as described in Chapter 1. The corrosion rate (in μm/yr) can be calculated from the voltage drop using the following equation:

$$r = 11.59i = \frac{11590V}{AR} \tag{2.1}$$

where, r = corrosion rate in μm/yr,

i = corrosion current density in μA/cm^2,

V = voltage drop of the resistor in mV,

R = resistance of the resistor in Ω, and

A = area of the reinforcing bars at the anode in cm^2.

For specimens with both layers penetrated, zinc exists only around the perimeter of the drilled holes (A). In this report, however, the whole damaged area was used as the effective area to calculate corrosion rates and total corrosion losses based on exposed area. The corrosion loss is then obtained by integrating the corrosion rate.

In this study, the corrosion rate is considered "positive" when the reinforcement that is exposed to chlorides (in salt solution for the rapid macrocell test, or top bars in the bench-scale tests) has a more negative potential than the bars separated from chlorides (in pore solution for the rapid macrocell test, or bottom bars in the bench-

scale tests) so that the current flows from the latter to the former bars. Conversely, when current flows in the opposite direction, this corrosion rate is referred to as "negative corrosion" in this study.

In this study, 1.6 m ion concentration of NaCl is used in the anodic solution to evaluate all of the corrosion protection systems.

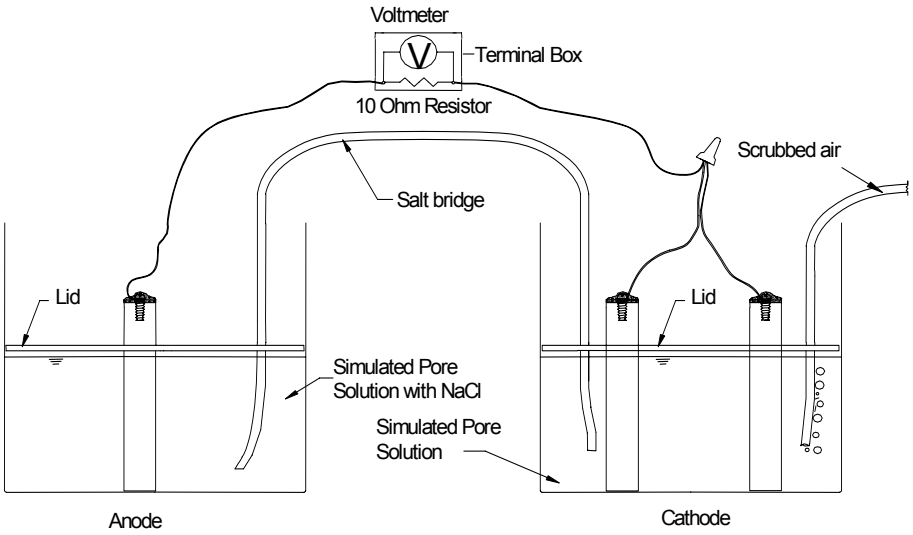

Figure 2.1 – Macrocell test with bare bar specimens

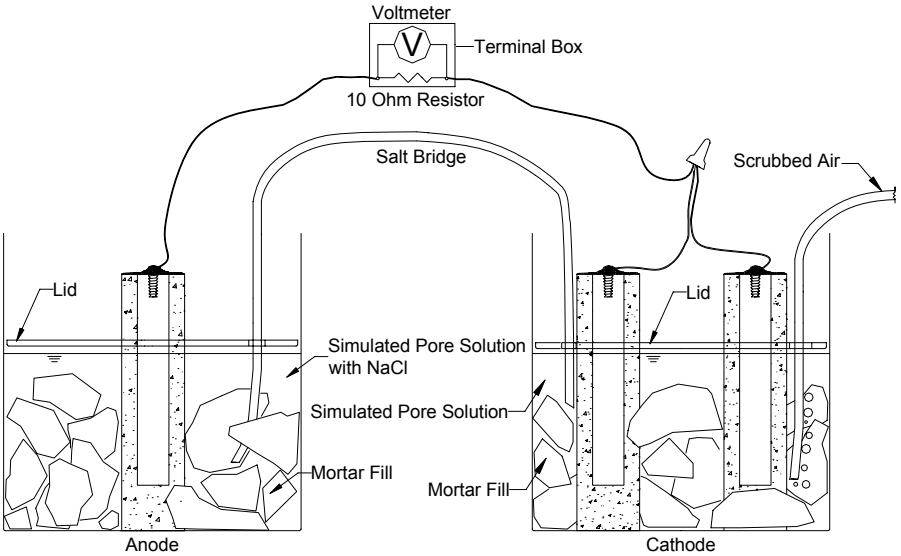

Figure 2.2 – Macrocell test with mortar-wrapped specimens

2.2.1 Equipment and Materials

The equipment and materials used in the rapid macrocell test are described as follows:

- *Voltmeter* – Hewlett Packard digital voltmeter, Model 3455A, with a resolution of 0.001 mV and an impedance of 2 MΩ. Used to measure the voltage drop across the 10-ohm resistor and the corrosion potential of the anode and cathode.
- *Saturated Calomel Electrode (SCE)* – Fisher Scientific Catalog No. 13-620-52. All corrosion potentials are measured with respect to an SCE.
- *Resistor* – A 10-ohm resistor connects the anode and cathode and is used to measure the corrosion current.
- *Mixer* – Hobart mixer, Model N-50. The mixer is used to mix mortar for mortar-wrapped specimens and complies with ASTM C 305.
- *Container* – Plastic container with a diameter of 178 mm (7 in.) and a height of 191 mm (7.5 in.).
- *Wire* – 16-gage insulated copper wire is used to provide electrical connection for reinforcing bars at the anode and cathode in the rapid macrocell test.
- *Terminal Box* – A project box with six pairs of binding posts. Each pair contains a red and a black post, which are connected by a 10-ohm resistor. The anode is wired to a red post and the cathode to a black post. When an open circuit is required, the anode is disconnected from the red post.
- *Mortar* – The mortar has a water-cement (*w/c*) ratio of 0.50 and a sand-cement ratio of 2.0 by weight. The mortar is made with Type I/II portland cement, ASTM C 778 graded Ottawa sand, and distilled water. When a corrosion inhibitor is used, the mix water is adjusted to account for the water in the corrosion inhibitor. The mortar mix designs are shown in Table 2.3.

Table 2.3 – Mortar mix designs

Mortar Mix	Water g (lb)	Cement g (lb)	Fine Aggregate g (lb)	DCI (mL)	Hycrete g (lb)	Rheocrete (mL)
1	400 (0.88)	800 (1.76)	1600 (3.53)	-	-	-
2	374 (0.82)	800 (1.76)	1600 (3.53)	31	-	-
3	386.5 (0.85)	800 (1.76)	1600 (3.53)	-	18 (0.04)	-
4	391 (0.86)	800 (1.76)	1600 (3.53)	-	-	10.3

- *Mortar Fill* – Mortar fill is cast on a 25 mm (1 in.) deep metal baking sheet using the same materials and mixing procedures as the mortar used in the specimens. No corrosion inhibitor is used to make the mortar fill. The mortar is broken into pieces within 24 hours of casting and stored until the time of the test.
- *Pore Solution* – The content of the simulated concrete pore solution is prepared based on the analysis by Fazammehr (1985), but without the small chloride content obtained in the analysis. One liter of the concrete pore solution contains 974.8 g of distilled water, 18.81 g of KOH, and 17.87 g of NaOH. The pH of the simulated concrete pore solution is 13.4.
- *Pore Solution Containing NaCl* – A 1.6 molal ion concentration of sodium chloride is used in this study. The solution is prepared by adding 45.6 g of NaCl to one liter of the simulated concrete pore solution.
- *Air Scrubber* – An air scrubber is used to remove carbon dioxide from compressed air. Compressed air is bubbled into the scrubber and out to the simulated pore solution at the cathode through latex tubing, which provides an adequate supply of oxygen for the cathodic reaction. A 19-liter (5-gallon) plastic container with 1M NaOH solution serves as the air scrubber. A pH value of 12.5 is maintained by adding NaOH as needed. The procedure for preparing

the air scrubber is described as follows [Adapted from Balma et al. (2005)]:

1) Two barbed fittings are inserted on the top of the container.
2) A 1.5 m (5 ft) piece of plastic tubing is cut. On one end of the tubing, 1.2 m (4 ft) is perforated with a knife, making hundreds of holes to allow the air to produce small bubbles. The end of the tubing closest to the holes is sealed with a clamp.
3) The end with the holes is coiled at the bottom of the container and trap rock is used to hold down the tubing. The other end of the tubing is connected to the inside part of one of the barbed fittings.
4) The other side of the barbed fitting is connected to a plastic tube, which is connected to the compressed air outlet.
5) Another piece of plastic tubing is connected to the outside of the other barbed fitting. The air is distributed to the solution surrounding the cathodes using 0.3 m (1 ft) lengths of latex tubing and polypropylene T-shaped connectors.
6) Screw clamps are placed on the tubing to regulate the amount of air bubbled into each container.

Distilled water is periodically added to the container to replace water that is lost due to evaporation. The pH of the solution is checked every two months.

- *Salt Bridge* – A salt bridge provides an ionic path between the anode and cathode. It consists of a conductive gel in a flexible latex tube, and is produced as described by Steinbach and King (1950). The gel is prepared with 4.5 g (0.16 oz) of agar, 30 g (1.06 oz) of potassium chloride (KCl), and 100 g (3.53 oz) of distilled water. The mixture is heated over a burner or hotplate for about one minute or until it starts to congeal. The mixture is then poured into four latex

tubes with a length of 0.6 m (2 ft) each. The ends of the tubes are fastened with rubber bands to prevent any leakage. The salt bridges are placed in boiling water for one hour and then allowed to cool until firm. The ends of the salt bridges, along with the rubber bands, are cut off before use. To provide a good ionic path between the anode and cathode, the gel in the salt bridge must be continuous, without any air bubbles.

- *Epoxy* – 3M Scotchkote™ Brush Grade Rebar Patch Kit, and ThoRoc™ Sewer Guard HBS 100 Epoxy Liner, from ChemRex, Inc.
- *Agar* – Agar high gel strength [9002-18-0], manufactured by Sigma Chemical Co.
- *KOH* – Used to make simulated concrete pore solution, from Fisher Scientific.
- *NaOH* – Used to make simulated concrete pore solution, from Fisher Scientific.
- *NaCl* – Used to make anodic solution, from Fisher Scientific.

2.2.2 Test Specimen Preparation

The procedures for fabricating bare bar specimens are described as follows:

1) Reinforcing bars are cut to 127 mm (5 in.) in length and then the sharp edges on the ends of the bars are removed with a grinder.
2) The bars are drilled and tapped at one end to a depth of 13 mm (0.5 in.) to receive a 10-24 threaded bolt.
3) Conventional bars are cleaned with acetone to remove dust and grease. The epoxy-coated bars are cleaned with soap and warm water, and then air dried.
4) The coating on some of the epoxy-coated bars is penetrated with four 3-mm ($^1/_8$-in.) diameter holes to simulate damage to the epoxy coating. A 3-mm ($^1/_8$-in.) diameter four flute drill bit mounted on a drill press is used to create

holes with a depth of 0.4 mm (15 mils). Two holes are made on each side of the bar, 25 mm (1 in.) and 51 mm (2 in.), respectively, away from the unthreaded end.

5) For some of the multiple coated bars, the epoxy coating is penetrated just slightly but not deep enough to expose the zinc layer. A soldering gun is then used to burn off the remaining epoxy coating and expose the underlying zinc. The temperature of the soldering gun is set to be 400°C (752°F), which is below the zinc melting temperature 420°C (787°F). The debris is then removed with acetone, leaving an undamaged, shiny zinc surface.
6) The unthreaded ends of all epoxy-coated bars are protected by plastic caps that are half-filled with 3M Rebar Patch epoxy.

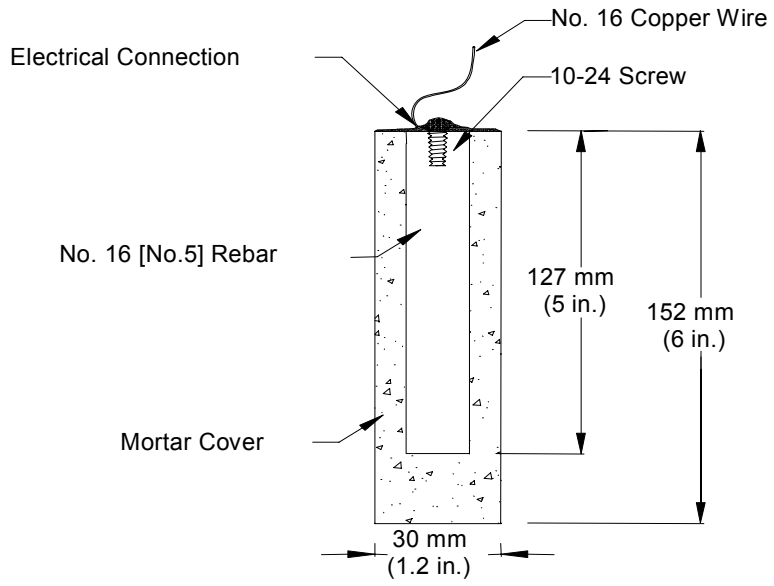

Figure 2.3 – Mortar-wrapped specimen

The mortar-wrapped specimen consists of a 127-mm (5-in.) long No. 16 (No. 5)

reinforcing bar embedded in mortar, as shown in Figure 2.3. The mortar cylinder [30 × 152 mm (1.2 × 6 in., diameter × height)] provides a mortar cover thickness of 7 mm (0.28 in.). The bars for the mortar wrapped specimens are prepared the same as those for the bare bar specimens. The preparation of the mold and mortar are described in the following sections.

- **Mold Design**

The mold for the mortar-wrapped specimens was designed by Martinez et al. (1990) and it consists of the following materials, as shown in Figure 2.4:

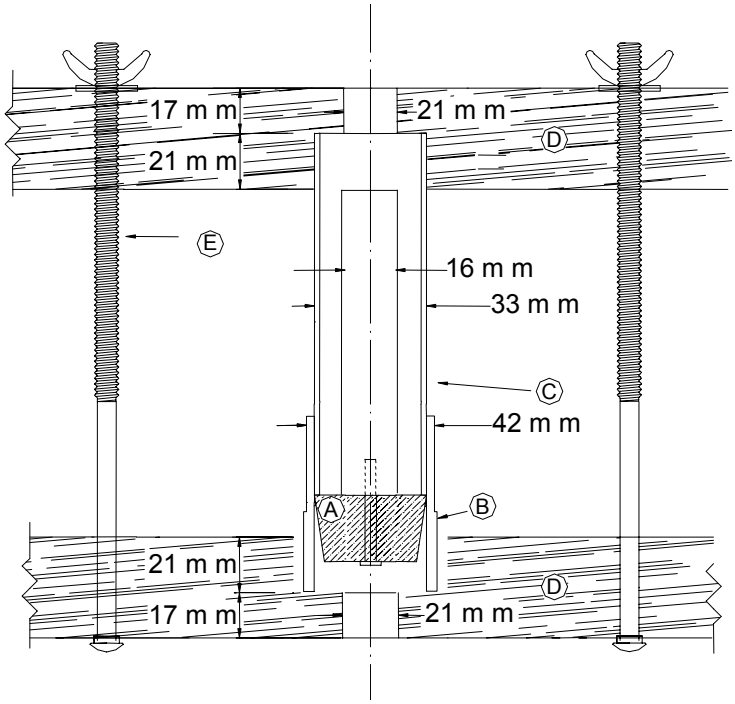

Figure 2.4 – Mold for mortar-wrapped specimens

1) One laboratory grade No. 6.5 rubber stopper, **A** (identified in Figure 2.4), with a centered 4 mm ($^1/_6$ in.) diameter hole.

2) One ASTM D 2466 32 mm (1.25 in.) to 32 mm (1.25 in.) PVC fitting, **B**, 42 mm (1.65 in.) external diameter, shortened by 14 mm (0.55 in.) on one end.
3) One ASTM D 2241 SDR 21 25.4 mm (1 in.) PVC pipe, **C**, with an internal diameter of 30 mm (1.18 in.) and a length of 152 mm (6 in.). The pipe is sliced longitudinally to facilitate the removal of the specimen. To prevent the mortar from leaking, the slice is covered with masking tape during casting.
4) Two pieces of 38 × 203 × 381 mm (1.5 × 8 × 15 in.) pressure treated lumber, **D**. Holes and recesses are bored into the flat surfaces to hold the specimen molds in position.
5) Six threaded rods, **E**, 6 × 305 mm (0.25 × 12 in.), are inserted between the two pieces of lumber, three on each side.

- **Mold Assembly**

The mold is assembled using the following procedures (as shown in Figure 2.4):

1) The rubber stopper **A** is inserted in the machined end of the PVC fitting **B**. The wider end of the rubber stopper is placed in contact with the internal surface of the PVC fitting.
2) A 10-24 × 38 mm (1.5 in.) threaded bolt is inserted into the hole centered in the rubber stopper. The tapped end of the reinforcing bar is then attached to the bolt.
3) Masking tape is used to cover the longitudinal slice along the side of the PVC pipe **C**. The pipe is then inserted in the free end of the PVC fitting.
4) The assembled mold is placed between the two pieces of lumber **D** in the holes and recesses as provided. The threaded rods **E** are then inserted

between the two pieces of lumber to hold the molds together. The reinforcing bars are centered by tightening or loosening the wing nuts on the rods.

- **Specimen Fabrication**

  Mortar-wrapped specimens are fabricated as follows:

  1) Using the mix designs from Table 2.3 (Section 2.2.1), the mortar is mixed following the procedures outlined in ASTM C 305.
  2) The specimens are cast in four equal layers and each layer is rodded 25 times using a rod [2 × 305 mm (0.08 × 12 in., diameter × length)]. The rod is allowed to penetrate the previous layer. After rodding, each layer is consolidated on a vibrating table with an amplitude of 0.15 mm (0.006 in.) at a frequency of 60 Hz for 30 seconds.
  3) The specimens are removed from the molds within 24 hours of casting and then cured in lime-saturated water for 13 days at room temperature. After curing, the specimens are dried with compressed air. The anode specimens are hand picked based on minimum visible cracks on the surface and vacuum dried for one day.

A 16-gage insulated copper wire is attached to the tapped end of each specimen with a 10-24 threaded bolt. The electrical connection is covered with two coats of 3M Rebar Patch epoxy for the bare bar specimens and two coats of Degussa epoxy for the mortar-wrapped specimens to prevent crevice corrosion. The epoxy is allowed to dry for at least four hours after each application.

2.2.3 Test Procedure

The voltage drop and open circuit corrosion potential of the specimens are recorded every day for the first week and once a week after that.

The voltage drop across a 10-ohm resistor is measured using a voltmeter and the circuit is then opened about two hours before measuring the corrosion potential. The corrosion potentials of the anode and cathode are measured with respect to a saturated calomel electrode.

Both the anodic and cathodic solutions are changed every five weeks to maintain the pH of the solution at 13.4.

2.2.4 Test Program

A total of 57 macrocell tests with bare bar specimens and 111 macrocell tests with mortar-wrapped specimens were performed in this study using a 1.6 m ion NaCl concentration with simulated pore solution at the anode. The macrocell test programs for the bare bar and mortar-wrapped specimens are summarized in Tables 2.4 and 2.5, respectively.

Table 2.4 – Test program for the rapid macrocell test with bare bar specimens

Bare Bar Specimens		
Steel Designation[a]	**Number of tests**	**Notes**
Control		
Conv.	6	
ECR	6	w/ 4 drilled holes
ECR-no holes	3	w/o holes
Multiple Coated Bars		
MC(both layers penetrated)	6	w/ 4 drilled holes
MC(only epoxy penetrated)	6	w/ 4 holes
MC-no holes	3	w/o holes
Increased Adhesion		
ECR(DuPont)	6	w/ 4 drilled holes
ECR(Chromate)	6	w/ 4 drilled holes
ECR(Valspar)	6	w/ 4 drilled holes
ECR(DuPont)-no holes	3	w/o holes
ECR(Chromate)-no holes	3	w/o holes
ECR(Valspar)-no holes	3	w/o holes

[a] Conv. = conventional steel. ECR = conventional epoxy-coated reinforcement.

MC = multiple coated bars. ECR(Chromate) = ECR with the chromate pretreatment.

ECR(DuPont) = ECR with high adhesion DuPont coating.

ECR(Valspar) = ECR with high adhesion Valspar coating.

MC(both layers penetrated) = multiple coated bars with both the zinc and epoxy layers penetrated.

MC(only epoxy penetrated) = multiple coated bars with only the epoxy layer penetrated.

Table 2.5 – Test program for the rapid macrocell test with mortar-wrapped specimens

Mortar-wrapped Specimens		
Steel Designation[a]	**Number of tests**	**Notes**
Control		
Conv.	6	
ECR	6	w/ 4 drilled holes
ECR-no holes	3	w/o holes
Corrosion Inhibitors		
ECR(Rheocrete)	6	w/ 4 drilled holes
ECR(DCI)	6	w/ 4 drilled holes
ECR(Hycrete)	6	w/ 4 drilled holes
ECR(primer/$Ca(NO_2)_2$)	6	w/ 4 drilled holes
ECR(Rheocrete)-no holes	3	w/o holes
ECR(DCI)-no holes	3	w/o holes
ECR(Hycrete)-no holes	3	w/o holes
ECR(primer/$Ca(NO_2)_2$)-no holes	3	w/o holes
Multiple Coated Bars		
MC(both layers penetrated)	6	w/ 4 drilled holes
MC(only epoxy penetrated)	6	w/ 4 holes
MC-no holes	3	w/o holes
Increased Adhesion		
ECR(DuPont)	6	w/ 4 drilled holes
ECR(Chromate)	6	w/ 4 drilled holes
ECR(Valspar)	6	w/ 4 drilled holes
ECR(DuPont)-no holes	3	w/o holes
ECR(Chromate)-no holes	3	w/o holes
ECR(Valspar)-no holes	3	w/o holes
ECR(DuPont)-DCI	6	w/ 4 drilled holes
ECR(Chromate)-DCI	6	w/ 4 drilled holes
ECR(Valspar)-DCI	6	w/ 4 drilled holes

[a] Conv. = conventional steel. ECR = conventional epoxy-coated reinforcement.

MC = multiple coated bars. ECR(Chromate) = ECR with the chromate pretreatment.

ECR(DuPont) = ECR with high adhesion DuPont coating.

ECR(Valspar) = ECR with high adhesion Valspar coating.

ECR(DCI) = ECR in concrete with DCI inhibitor.

ECR(Hycrete) = ECR in concrete with Hycrete inhibitor.

ECR(Rheocrete) = ECR in concrete with Rheocrete inhibitor.

ECR(primer/$Ca(NO_2)_2$) = ECR with a primer containing calcium nitrite.

MC(both layers penetrated) = multiple coated bars with both the zinc and epoxy layers penetrated.

MC(only epoxy penetrated) = multiple coated bars with only the epoxy layer penetrated.

2.3 BENCH-SCALE TESTS

Three bench-scale tests are used in the current study, the Southern Exposure (SE), the cracked beam (CB), and the ASTM G 109 tests.

The SE test specimen consists of a concrete slab [305 × 305 × 178 mm (12 × 12 × 7 in.)] with six 305-mm (12-in.) long bars, two top and four bottom bars, as shown in Figure 2.5. The top and bottom concrete clear cover is 25 mm (1 in.). The top and bottom mat bars are electrically connected across a 10-ohm resistor. A concrete dam is cast monolithically around the top surface of the specimen to hold the salt solution.

The CB test specimen has dimensions of 305 × 152 × 178 mm (12 × 6 × 7 in.) and is half the size of the SE test specimen, as shown in Figure 2.6. One top and two bottom bars are electrically connected across a 10-ohm resistor. A 152-mm (6 in.) long, 25 mm (1 in.) deep simulated crack is made in the concrete directly above and parallel to the top bar using a 0.3 mm (12 mil) stainless steel shim.

Figure 2.7 shows the ASTM G 109 test specimen [279 × 152 × 114 mm (11 × 6 × 4.5 in.)]. The concrete cover is 25 mm (1 in.) for both the top and bottom bars. The specimen contains one top and two bottom bars, electrically connected across a 100-ohm resistor. A plexiglass dam [150 × 75 mm (6 × 3 in.)] is placed on the specimen top surface to facilitate the ponding.

The test period for both the SE and CB tests is 96 weeks. The ASTM G 109 test is continued until the average macrocell current reaches 10 μA and at least half of the specimens have a current greater than 10 μA.

The voltage drop across a resistor, open circuit corrosion potential, and mat-to-mat resistance are recorded weekly. Linear polarization resistance tests are performed for selected bench-scale test specimens every four weeks throughout the test period.

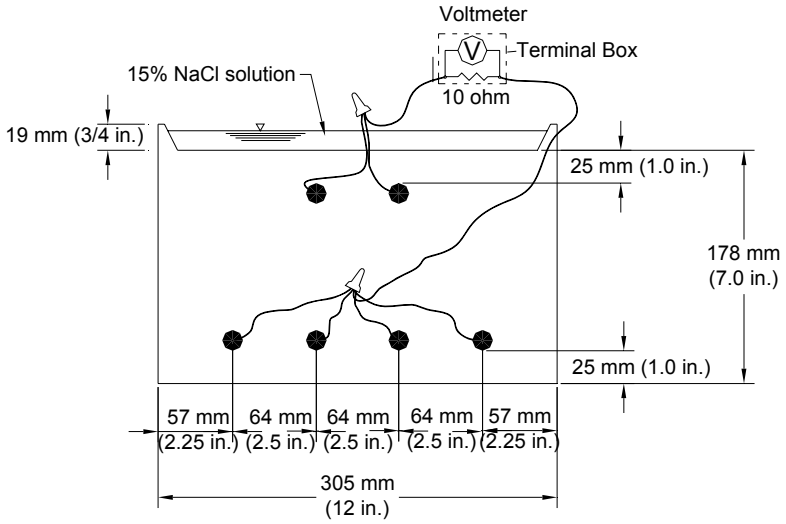

Figure 2.5 – Southern Exposure test specimen

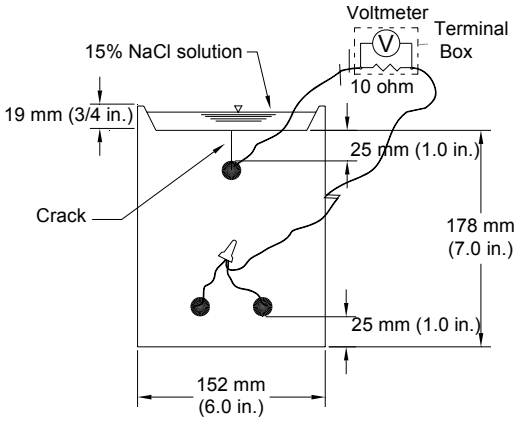

Figure 2.6 – Cracked beam test specimen

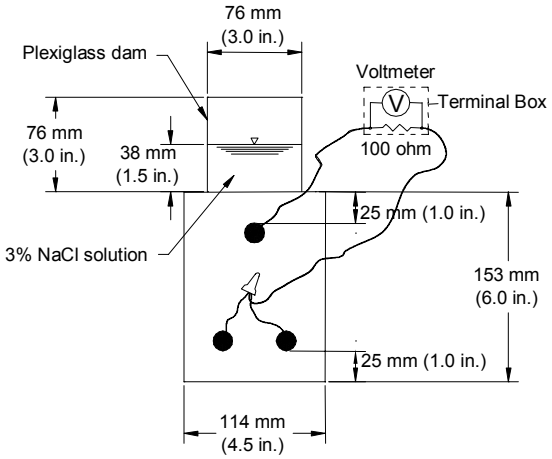

Figure 2.7 – ASTM G 109 test specimen

2.3.1 Equipment and Materials

The equipment and materials used in the bench-scale tests are described as follows:

- *Voltmeter* – Hewlett Packard digital voltmeter, Model 3455A, with a resolution of 0.001 mV and an impedance of 2 MΩ. Used to measure the voltage drop across the 10-ohm resistor and the corrosion potential of both top and bottom mat bars.
- *Ohmmeter* – Hewlett Packard digital AC milliohmmeter, Model 4338A.
- *Copper-Copper Sulfate Electrode (CSE)* – MC Miller Co. Electrode Model RE-5. Used to measure corrosion potentials during the ponding and drying cycle.
- *Saturated Calomel Electrode (SCE)* – Fisher Scientific Catalog No. 13-620-52. Used to measure corrosion potentials during the continuous ponding cycle.
- *Resistor* – A 10-ohm resistor connects the top and bottom mat bars for the SE and CB specimens, and a 100-ohm resistor is used for the ASTM G 109 specimens. It is used to measure the corrosion current.
- *Wire* – 16-gage insulated copper wire is used to provide electrical connection for reinforcing bars in bench-scale test specimens.
- *Shop vacuum cleaner* – Used to vacuum salt solution for bench-scale specimens during the ponding and drying cycle.
- *Terminal Box* – Each terminal box consists of a project box with six sets of three binding posts, red, black, and red/black mix. The red and the red/black mix binding posts are connected by 10-ohm resistors. The top bars are wired to the red posts and the bottom bars to the red/black mix posts. When the open circuit is required, the bottom bars are connected to the black binding posts.
- *Concrete Mixer* – Lancaster Counter Current Batch Mixer with a capacity of

0.06 m^3 (2 ft^3), manufactured by Lancaster Iron Works Inc. The mixer complies with ASTM C 192.

- *Salt Solution* – 15% NaCl by mass dissolved in distilled water for the SE and CB specimens, 3% NaCl by mass dissolved in distilled water for the ASTM G 109 specimens.
- *Epoxy* – ThoRoc™ Sewer Guard HBS 100 Epoxy Liner, from ChemRex, Inc.
- *Silicon Caulk* – The 100% silicon caulk, manufactured by Macklenburg-Duncan.
- *NaCl* – Used to make the salt solution, from Fisher Scientific.
- *Rheobuild 1000* – High range water reducer, manufactured by Degussa Admixtures, Inc.
- *Concrete* – The concrete has a water-cement (*w/c*) ratio of 0.45 or 0.35, with 6 ± 1% entrained air, and 76 ± 13 mm (3 ± 0.5 in.) slump. The concrete mix designs are shown in Table 2.6. The materials used in concrete include:

  Cement: Type I/II portland cement.

  Coarse Aggregate: Crushed limestone from Fogle Quarry with 19 mm (¾ in.) nominal maximum size, bulk specific gravity (SSD) = 2.58, absorption = 2.27 %, and unit weight of 1536 kg/m^3 (95.9 lb/ft^3).

  Fine Aggregate: Kansas River sand with bulk specific gravity (SSD) = 2.62, absorption = 0.78%, fineness modulus = 2.51.

  Air-entraining Agent: Daravair 1400, from W. R. Grace, Inc.

  Water: Tap water. When a corrosion inhibitor is used, the mix water is adjusted to account for the water in the corrosion inhibitor.

Table 2.6 – Concrete mix designs for the bench-scale tests

w/c	Water	Cement	Coarse Aggregate	Fine Aggregate	Air-entraining Agent	DCI	Hycrete	Rheocrete	S.P.[a]
	kg/m^3 (lb/yd^3)	kg/m^3 (lb/yd^3)	kg/m^3 (lb/yd^3)	kg/m^3 (lb/yd^3)	mL/m^3 (oz/yd^3)	L/m^3 (gal/yd^3)	kg/m^3 (lb/yd^3)	L/m^3 (gal/yd^3)	L/m^3 (gal/yd^3)
0.45	160 (269)	355 (598)	881 (1484)	852 (1435)	90 (2.33)	-	-	-	-
	147.4 (248.2)	355 (598)	881 (1484)	852 (1435)	140 (3.62)	15 (3.03)	-	-	-
	154.0 (259.4)	355 (598)	881 (1484)	852 (1435)	35 (1.18)	-	8.0 (13.5)	-	-
	155.7 (262.2)	355 (598)	881 (1484)	852 (1435)	300 (7.74)	-	-	5 (1.01)	-
0.35	153 (258)	438 (738)	862 (1452)	764 (1287)	355 (9.16)	-	-	-	2.12 (0.43)
	140.4 (236.4)	438 (738)	862 (1452)	764 (1287)	740 (19.1)	15 (3.03)	-	-	2.12 (0.43)
	145.6 (245.2)	438 (738)	862 (1452)	764 (1287)	330 (8.52)	-	9.9 (16.7)	-	2.25 (0.45)
	148.7 (250.4)	438 (738)	862 (1452)	764 (1287)	1480 (38.2)	-	-	5 (1.01)	2.25 (0.45)

[a] S.P. = superplasticizer, Rheobuild 1000.

2.3.2 Test Specimen Preparation

The reinforcing bars used for the bench-scale test specimens are prepared as follows:

1) Reinforcing bars are cut to a length of 305 mm (12 in.) for the SE and CB test specimens, and 279 mm (11 in.) for the G 109 test specimens. The sharp edges on the ends of the bars are removed with a grinder.
2) Both ends of the bars are drilled and tapped to receive a 10-24 threaded bolt with a depth of 13 mm (0.5 in.).
3) Conventional bars are cleaned with acetone to remove dust and grease. Epoxy-coated bars are cleaned with soap and warm water, and then air dried.
4) The coating on the epoxy-coated bars is penetrated with four or ten 3-mm ($^1/_8$-in.) diameter holes to simulate damage to the epoxy coating. A 3-mm ($^1/_8$-in.) diameter four flute drill bit mounted on a drill press is used to create holes with a depth of 0.4 mm (15 mils). Two or five holes are made on each

side of the epoxy-coated bars with four or ten holes, respectively. The holes are distributed evenly along the length of the bars.

5) For some of the multiple coated bars, the epoxy coating is penetrated just slightly but not deep enough to expose the zinc layer. A soldering gun is then used to burn off the remaining epoxy coating and expose the underlying zinc. The temperature of the soldering gun is set to be 400°C (752°F), which is below the zinc melting temperature 420°C (787°F). The debris is then removed with acetone, leaving an undamaged, shiny zinc surface.

The bench-scale test specimens are fabricated using the following procedures:

1) The form consists of four side pieces and one bottom piece made of plywood with a thickness of 19 mm ($^3/_4$ in.). Small holes are provided in the two side pieces to hold the reinforcing bars in the form.
2) Mineral oil is applied to the wooden forms and clay is used to seal the inside corners to prevent concrete from leaking.
3) A 0.3-mm (12-mil) thick stainless steel shim is attached to the bottom slab for the CB test specimens. The bars are then bolted into the forms.
4) The concrete is mixed according to ASTM C 192. The specimens are cast in two equal layers and each layer is consolidated for 30 seconds on a vibrating table with an amplitude of 0.15 mm (0.006 in.) at a frequency of 60 Hz. The upper surface of the specimens is then finished using a wooden float.
5) The SE and CB test specimens are cast upside down to monolithically create a dam on the specimen top surface. The ASTM G 109 test specimens

are also cast upside down to obtain a smooth top surface to attach the plexiglass dams.

The bench-scale test specimens are cured and set up as follows:

1) The specimens are covered with a plastic sheet and cured for 24 hours at room temperature. The stainless steel shims are taken out from the CB test specimens between 8 and 12 hours after casting. The forms are removed 24 hours after casting.
2) The SE and CB test specimens are cured for two days in a plastic bag with distilled water. They are then removed from the bags and cured in air for 25 days.
3) The G 109 test specimens are cured for 28 days in a curing room with a temperature of 23 ± 2°C (73.4 ± 3.6°F) and a relative humidity above 95%. The specimens are then allowed to dry for two weeks in 50% relative humidity environment in room temperature.
4) Before a test starts, 16-gage insulated copper wires are attached to the bars using 10-24 threaded bolts. The four sides of the specimens are coated with two layers of epoxy (see Section 2.3.1). The epoxy on the sides of the specimens serves two functions: protects the electrical connections and prevents the salt solution from exiting through the sides of the specimen.
5) The specimen top surface is lightly sanded. The plexiglass dams are attached to the top of the G 109 test specimens using superglue. Silicon caulk is used to seal the joints.
6) The 16-gage copper wires from the top mat bars are connected to the red binding posts, while the wires from the bottom mat bars are connected to the red/black mix binding posts.

2.3.3 Test Procedures

The test procedures used for the SE and CB tests and the ASTM G 109 test are described below:

- **SE and CB Tests**

  The SE and CB tests follow the same test procedure.

  1) The specimens are ponded with 600 ml (0.16 gal) 15% salt solution for four days at room temperature. A plastic sheet is used to cover the specimens to reduce evaporation.
  2) The voltage drop across a 10-ohm resistor is recorded for each specimen using a voltmeter. The circuit is then opened and the mat-to-mat resistance is measured using an ohmmeter. About two hours after taking the mat-to-mat resistance, the salt solution is removed using a shop vacuum. The corrosion potentials of the top and bottom mat bars are measured with respect to a copper-copper sulfate electrode (CSE).
  3) The specimens are covered by a heating tent for three days, which maintains a temperature of 38 ± 1.5°C (100 ± 3°F). This weekly ponding-drying cycle is repeated for 12 weeks.
  4) The specimens are then continuously ponded with a 15% NaCl solution for 12 weeks at room temperature. On the fourth day of each week, the voltage drop and mat-to-mat resistance are recorded. The corrosion potentials of the top and bottom mat bars are measured with respect to a saturated calomel electrode (SCE).
  5) The 24-week cyclic ponding is repeated three more times to complete 96 weeks of testing.

- **ASTM G 109 Test**

The ASTM G 109 test uses different ponding and drying cycles from those used for the SE and CB tests.

1) The specimens are ponded with 300 ml (0.08 gal) 3% NaCl solution for two weeks at room temperature. At the end of each week, the voltage drop across a 100-ohm resistor is recorded using a voltmeter. The circuit is then opened and the mat-to-mat resistance is measured using an ohmmeter. The circuit remains open for approximately two hours, after which the corrosion potentials of the top and bottom mat bars are measured. At the end of the first week, the corrosion potentials are taken with respect to an SCE. At the end of the second week, the salt solution is removed with a shop vacuum and the corrosion potentials are recorded with respect to a CSE.
2) The specimens are then allowed to dry for two weeks. Only the voltage drop and mat-to-mat resistance are recorded weekly during this period.
3) The 4-week ponding and drying cycle is repeated throughout the test period.

2.3.4 Test Program

Tables 2.7 and 2.8 summarize the test programs for the SE and CB tests. A summary of the test program for the ASTM G 109 test is presented in Table 2.9.

The linear polarization resistance (LPR) test is used to determine the microcell corrosion rate for some of the bench-scale test specimens. The number of the specimen is given as "LPR Test Specimen No." in Tables 2.7 to 2.9. The linear polarization resistance test is described in Section 2.7.

Table 2.7 – Test program for the Southern Exposure test

Steel Designation[a]	Number of Tests	LPR Test Specimen No.
Control		
Conv.	6	6
Conv.-35	3	3
ECR	6	6
ECR-10h	3	3
ECR-10h-35	3	3
Corrosion Inhibitors		
ECR(DCI)	3	3
ECR(DCI)-10h	3	3
ECR(DCI)-10h-35	3	3
ECR(Rheocrete)	3	3
ECR(Rheocrete)-10h	3	3
ECR(Rheocrete)-10h-35	3	3
ECR(Hycrete)	3	3
ECR(Hycrete)-10h	3	3
ECR(Hycrete)-10h-35	3	3
ECR(primer/$Ca(NO_2)_2$)	3	3
ECR(primer/$Ca(NO_2)_2$)-10h	3	3
ECR(primer/$Ca(NO_2)_2$)-10h-35	3	3
Multiple Coated Bars		
MC(both layers penetrated)	3	3
MC(both layers penetrated)-10h	3	3
MC(only epoxy penetrated)	3	3
MC(only epoxy penetrated)-10h	3	3
Increased Adhesion		
ECR(Chromate)	3	1
ECR(Chromate)-10h	3	1
ECR(DuPont)	3	1
ECR(DuPont)-10h	3	1
ECR(Valspar)	3	1
ECR(Valspar)-10h	3	1
Increased Adhesion with Corrosion Inhibitor DCI		
ECR(Chromate)-DCI	3	1
ECR(DuPont)-DCI	3	1
ECR(Valspar)-DCI	3	1

[a] Conv. = conventional steel. ECR = conventional epoxy-coated reinforcement.
ECR(Chromate) = ECR with the chromate pretreatment.
ECR(DuPont) = ECR with high adhesion DuPont coating.
ECR(Valspar) = ECR with high adhesion Valspar coating.
ECR(DCI) = ECR in concrete with DCI inhibitor.
ECR(Hycrete) = ECR in concrete with Hycrete inhibitor.
ECR(Rheocrete) = ECR in concrete with Rheocrete inhibitor.
ECR(primer/$Ca(NO_2)_2$) = ECR with a primer containing calcium nitrite.
MC(both layers penetrated) = multiple coated bars with both the zinc and epoxy layers penetrated.
MC(only epoxy penetrated) = mutiple coated bars with only the epoxy layer penetrated.
10h = epoxy-coated bars with 10 holes, otherwise four 3-mm ($^1/_8$-in.) diameter holes.
35 = concrete w/c =0.35, otherwise w/c =0.45.

Table 2.8 – Test program for the cracked beam test

Steel Designation[a]	Number of Tests	LPR Test Specimen No.
Control		
Conv.	6	6
Conv.-35	3	3
ECR	6	6
ECR-10h	3	3
ECR-10h-35	3	3
Corrosion Inhibitors		
ECR(DCI)	3	3
ECR(DCI)-10h	3	3
ECR(DCI)-10h-35	3	3
ECR(Rheocrete)	3	3
ECR(Rheocrete)-10h	3	3
ECR(Rheocrete)-10h-35	3	3
ECR(Hycrete)	3	3
ECR(Hycrete)-10h	3	3
ECR(Hycrete)-10h-35	3	3
ECR(primer/$Ca(NO_2)_2$)	3	3
ECR(primer/$Ca(NO_2)_2$)-10h	3	3
ECR(primer/$Ca(NO_2)_2$)-10h-35	3	3
Multiple Coated Bars		
MC(both layers penetrated)	3	3
MC(both layers penetrated)-10h	3	3
MC(only epoxy penetrated)	3	3
MC(only epoxy penetrated)-10h	3	3
Increased Adhesion		
ECR(Chromate)	3	1
ECR(Chromate)-10h	3	1
ECR(DuPont)	3	1
ECR(DuPont)-10h	3	1
ECR(Valspar)	3	1
ECR(Valspar)-10h	3	1

[a] Conv. = conventional steel. ECR = conventional epoxy-coated reinforcement.
ECR(Chromate) = ECR with the chromate pretreatment.
ECR(DuPont) = ECR with high adhesion DuPont coating.
ECR(Valspar) = ECR with high adhesion Valspar coating.
ECR(DCI) = ECR in concrete with DCI inhibitor.
ECR(Hycrete) = ECR in concrete with Hycrete inhibitor.
ECR(Rheocrete) = ECR in concrete with Rheocrete inhibitor.
ECR(primer/$Ca(NO_2)_2$) = ECR with a primer containing calcium nitrite.
MC(both layers penetrated) = multiple coated bars with both the zinc and epoxy layers penetrated.
MC(only epoxy penetrated) = mutiple coated bars with only the epoxy layer penetrated.
10h = epoxy-coated bars with 10 holes, otherwise four 3-mm ($^1/_8$-in.) diameter holes.
35 = concrete w/c=0.35, otherwise w/c=0.45.

Table 2.9 – Test program for the ASTM G 109 test

Steel Designation[a]	Number of Tests	LPR Test Specimen No.
Control		
Conv.	6	6
ECR	3	6
ECR-10h	3	3
Multiple Coated Bars		
MC(both layers penetrated)	3	3
MC(both layers penetrated)-10h	3	3
MC(only epoxy penetrated)	3	3
MC(only epoxy penetrated)-10h	3	3

[a] Conv. = conventional steel. ECR = conventional epoxy-coated reinforcement.
MC(both layers penetrated) = multiple coated bars with both the zinc and epoxy layers penetrated.
MC(only epoxy penetrated) = mutiple coated bars with only the epoxy layer penetrated.
10h = epoxy-coated bars with 10 holes, otherwise four 3-mm ($^1/_8$-in.) diameter holes.

2.4 FIELD TEST

A field test specimen consists of a concrete slab [1219 × 1219 × 165 (48 × 48 × 6.5 in.)] with two mats of No. 16 (No. 5) reinforcing bars. Each mat contains seven bars in both the longitudinal and transverse direction, as shown in Figures 2.8(a) and 2.8(c). Each bar is 1067 mm (42 in.) long and all of the epoxy-coated bars have 16 3-mm ($^1/_8$-in.) diameter holes, representing damage to 0.24% of the epoxy coating. Each bar is totally embedded in concrete with the top and bottom concrete cover of 25 mm (1 in.) and an end cover of 76 mm (3 in.). A dam is made by attaching weather striping to the top concrete surface to hold the salt solution.

As shown in the front view of Figure 2.8(d), bars numbered 1, 3, 5, and 7 are selected as test bars. One top and one bottom bar form a pair that is electrically connected across a 10-ohm resistor, providing four test points for each field test specimen. In early test specimens, only bars 3 and 5 were selected as test bars,

providing only two test points for those specimens.

Field test specimens are evaluated by recording the voltage drop across the 10-ohm resistors, open circuit corrosion potential, and mat-to-mat resistance every four weeks. The voltage drop allows the calculation of the macrocell corrosion rate.

- **Simulated Cracks**

The simulated crack length was determined using data collected from bridge deck crack surveys (Lindquist, Darwin, and Browning 2005) in Kansas. From 1993 to 2004, 77 bridges were surveyed, including 30 bridges with silica fume overlay decks, 30 bridges with conventional overlay decks, and 17 bridges with monolithic decks. At the time of the crack surveys, the bridges had been in service from several months to 20 years. The test results show that for the majority of bridge decks, the crack densities typically ranged from 0.2 to 0.8 m/m^2 (0.061 to 0.244 ft/ft^2), regardless of the type of bridge deck.

Each field specimen has an area of 1.486 m^2 (16 ft^2) and the corresponding crack lengths based on the observed range of crack densities would be 0.3 to 1.19 m (0.98 to 3.90 ft). A total crack length of 1.22 m (4 ft) is selected to allow the simulated cracks in the field test specimens to correspond to the upper level of crack densities observed in the surveys

For each corrosion protection system, two specimens have no cracks and two have four 305-mm (12-in.) long simulated cracks with a depth of 25 mm (1 in.). The cracks are placed directly above and parallel to the top test bars numbered 1, 3, 5, and 7 using 0.3 mm (12 mil) stainless steel shims at the center of the bar length, as shown in Figure 2.8(b).

- **Salt Exposure**

The exposure program for the field test specimens was developed to reflect actual conditions in Kansas. Deicing salts are used to clear roads covered by snow and ice during winter seasons to improve driving conditions. The *KDOT Maintenance Manual* (2001) provides general guidelines for applying salts during the snow season. The typical salt application rate in Kansas is in the range of 28 to 85 kilograms per kilometer of driving lane (100 to 300 lb/lane-mile). Overall, KDOT uses an average application rate of 85 kg/lane-km (300 lb/lane-mile) for rock salt and 283 kg/lane-km (1000 lb/lane-mile) for salt-sand mixtures. Salt brine is applied weekly on bridge decks when frost is present or when snow or ice is forecast and the temperature is between -9° and 0° C (15° and 32 °F). The salt brine pretreatment consists of 23% sodium chloride by weight and is applied at a rate of 94 to 118 liters per kilometer of driving lane (40 to 50 gallons per lane-mile).

Table 2.10 shows the salt usage in Kansas from 1998 to 2002. The total length of all driving lanes is 33,742 kilometers (20,967 miles). As shown in Table 2.10, the yearly average salt application on roads is 0.66 kg/m^2 (0.13 lb/ft^2), with an average lane width of 3.7 m (12 ft). For each field test specimen, the corresponding yearly average salt usage, based on area, would be 0.98 kg (2.15 lb).

Table 2.10 – KDOT salt usage history

Fiscal Year	Rock Salt Totals		Average Application Rate	
	(Tons)	(Metric Tons)	(kg/m^2)	(lb/ft^2)
1998	95,374	86,507	0.71	0.14
1999	70,840	64,254	0.52	0.11
2000	64,588	58,583	0.48	0.10
2001	137,392	124,619	1.02	0.21
2002	74,609	67,673	0.55	0.11
Average	88,561	80,327	0.66	0.13

Compared with regular pavements, bridge decks usually freeze quicker, and therefore, they are subjected to heavier salt application. Detwiler, Kojundic, and Fidjestol (1997) indicated that bridge decks in Illinois could receive 10 times the salt of the adjacent pavement, or in excess o f 31 kg/m^2 (6.3 lb/ft^2) annually.

Additional information was gathered from KDOT Lawrence Maintenance Office. According to Daniel (2004), it is estimated that bridge decks can receive four to five times the salt of the adjacent pavement and the additional salt may come from the following sources:

1) Compared to regular pavement, the maintenance operators usually increase salt application on bridge decks. For a salt/sand mix, the application rate may increase from 113-170 to 425 kg/lane-km (400-600 to 1500 lb/lane-mile). If only salt is used, the increase is from 57-85 to 170-226 kg/lane-km (200-300 to 600-800 lb/lane-mile). This means that the salt application rate on bridge decks is approximately three times as much as that on the adjacent pavement.
2) Salt brine is applied weekly only on bridge decks, as mentioned earlier. The application season is from late November to March, a period of about four months. The salt from weekly salt brine is approximately 0.101 to 0.126 kg/m^2 (0.021 to 0.025 lb/ft^2).
3) Because maintenance operators cannot simply blow snow off bridge decks, and also because the bridge decks have a lower temperature than the adjacent pavement, bridge decks have to be salted more times than the adjacent pavement.

Based on the above information, an application rate equal to four times the

yearly average salt application in Kansas is used for the field test specimens, equal to 2.64 kg/m^2 (0.52 lb/ft^2), or 3.92 kg (8.32 lb) per specimen.

The field test specimens are serviced every four weeks, based on the fact that the field test is a long-term exposure test. According to the above calculations, the salt application at four-week intervals should be 0.30 kg (0.66 lb). A 10% rock salt solution is used to pond the field test specimens every four weeks. The solution is allowed to dry, and natural exposure to precipitation and sun light create the environmental testing conditions. The rock salt used for the field test specimens is obtained from the KDOT Lawrence Maintenance Office.

Corrosion potential measurements are made at potential test points on the specimen top surface, as shown in Figure 2.9. For specimens with conventional steel, there are two test bars and 12 potential test points [Figure 2.9(a)]. For the specimens with ECR, potentials are measured directly above the test bars, providing 12 test points for specimens with four test bars [Figure 2.9(b)] and six test points for specimens with two test bars [Figure 2.9(c)]. The configuration of potential test points shown in Figure 2.9 applies to specimens with and without simulated cracks. The potential test points for each specimen are listed in Table 2.12 (Section 2.4.4).

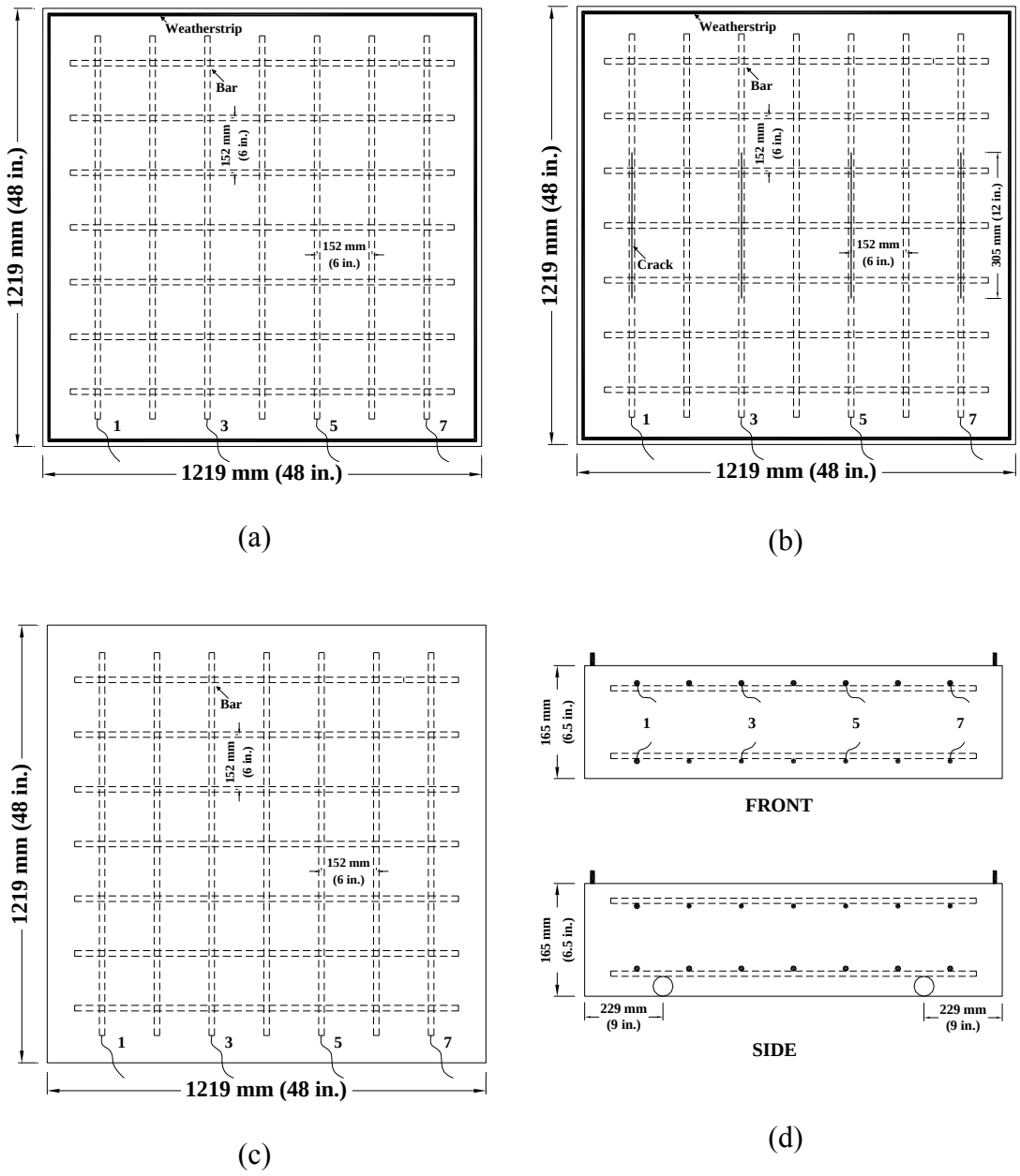

Figure 2.8 – Field test specimens (a) top slab (without cracks), (b) top slab (with cracks), (c) bottom slab, and (d) front and side views

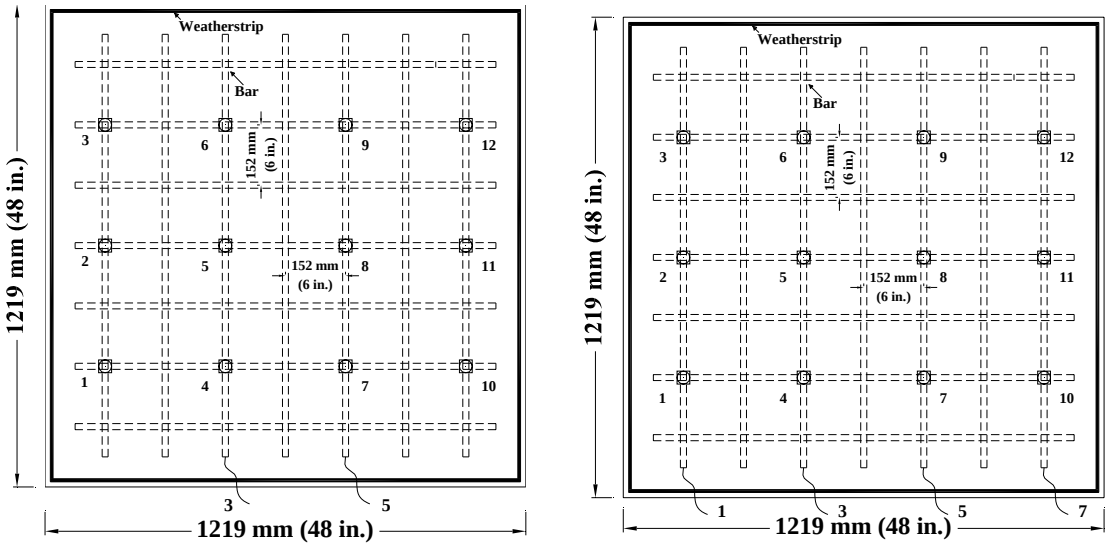

Figure 2.9 – Potential test points for field test specimens (a) conventional steel, (b) epoxy-coated bar with four test bars, and (c) epoxy-coated bar with two test bars

2.4.1 Equipment and Materials

The equipment and materials used in the field test are described as follows:

- *Voltmeter* – Hewlett Packard digital voltmeter, Model 3455A, with a resolution of 0.001 mV and an impedance of 2 MΩ. It is used to measure the voltage drop and the corrosion potentials.
- *Ohmmeter* – Hewlett Packard digital AC milliohmmeter, Model 4338A.
- *Copper-Copper Sulfate Electrode (CSE)* – MC Miller Co. Electrode Model RE-5. All corrosion potentials are measured with respect to a CSE.
- *Resistor* – A 10-ohm resistor connects the top and bottom mat bars and is used to measure the corrosion current.
- *Wire* – 14-gage insulated copper wire is used to provide electrical connection for reinforcing bars in the field test specimens.
- *Terminal Box* – Each specimen has one terminal box that consists of a project box with either two or four pairs of binding posts, red and black in color. When the open circuit is required, the top test bars are disconnected.
- *Ponding Solution* – 10% rock salt by weight dissolved in tap water.
- *Epoxy* – 3M Scotchkote™ Brush Grade Rebar Patch Kit.
- *Silicon Caulk* – GE MAX3500 siliconized acrylic caulk.
- *Weatherstrip* – Marine & Automotive weatherstrip tape with a thickness of 9.5 mm (0.375 in.) and a width of 12.7 mm (0.5 in.), manufactured by MD Specialty.
- *Heat Shrinkable Tube* – Polyvinyl Chloride (PVC) tubing from McMASTER-CARR, with expanded inner diameter 19 mm ($^3/_4$ in.) and shrunk inner diameter 9.5 mm (0.375 in.).
- *PVC Pipe* – PVC pipe with a length of 1372 mm (54 in.), an outside diameter

of 25 mm (1 in.), and an inside diameter of 19 mm ($^3/_4$ in.).

- *Form Braces* – Made of two pieces of 51 × 102 mm (2 × 4 in.) lumber with a length of 1524-mm (5-ft) and two 1829-mm (6-ft) long all-threaded rods. Two holes are created with a spacing of 114 mm (4.5 ft) for each piece of lumber and the rods are placed through the holes. Washers and bolts are used to attach it to the specimen form.
- *Concrete* – The concrete has a water-cement (*w/c*) ratio of 0.45, with 6 ± 1% entrained air and 3 ± 0.5 in. slump. The concrete mix designs are shown in Table 2.11. The materials used in concrete include:

  Cement: Type I/II portland cement.

  Coarse Aggregate: Crushed limestone from Fogle Quarry with 19 mm ($^3/_4$ in.) nominal maximum size, bulk specific gravity (SSD) = 2.58, absorption = 2.27 %, and unit weight of 1536 kg/m^3 (95.9 lb/ft^3).

  Fine Aggregate: Kansas River sand with bulk specific gravity (SSD) = 2.62, absorption = 0.78%, fineness modulus = 2.51.

  Air-entraining Agent: Daravair 1400, from W. R. Grace, Inc.

  Water: Tap water. When a corrosion inhibitor is used, the mix water is adjusted to account for the water in the corrosion inhibitor.

Table 2.11 – Concrete mix designs for the field test specimens

Water	Cement	Coarse Aggregate	Fine Aggregate	Air-entraining Agent	DCI	Hycrete	Rheocrete
kg/m^3 (lb/yd^3)	kg/m^3 (lb/yd^3)	kg/m^3 (lb/yd^3)	kg/m^3 (lb/yd^3)	mL/m^3 (oz/yd^3)	L/m^3 (gal/yd^3)	kg/m^3 (lb/yd^3)	L/m^3 (gal/yd^3)
160 (269)	355 (598)	881 (1484)	852 (1435)	90 (2.33)	-	-	-
147.4 (248.2)	355 (598)	881 (1484)	852 (1435)	140 (3.62)	15 (3.03)	-	-
154.0 (259.4)	355 (598)	881 (1484)	852 (1435)	35 (1.18)	-	8.0 (13.5)	-
155.7 (262.2)	355 (598)	881 (1484)	852 (1435)	300 (7.74)	-	-	5 (1.01)

2.4.2 Test Specimen Preparation

The reinforcing bars used for the field test specimens are prepared as follows:

1) Reinforcing bars are cut to a length of 1067 mm (42 in.), and the sharp edges on the ends of the bars are removed with a grinder.
2) The test bars are drilled and tapped to receive a 10-24 threaded bolt with a depth of 13 mm (0.5 in.) at one end.
3) Conventional bars are cleaned with acetone to remove dust and grease. Epoxy-coated bars are cleaned with soap and warm water, and then air dried.
4) The coating on the epoxy-coated bars is penetrated with 16 3-mm ($^1/_8$ -in.) diameter holes to simulate the damage to the epoxy coating. A 3-mm ($^1/_8$-in.) diameter four flute drill bit mounted on a drill press is used to create holes with a depth of 0.4 mm (15 mils). Eight holes are made on each side and evenly distributed along the length of the bars.
5) For multiple coated bars, all of the 16 3-mm ($^1/_8$ -in.) diameter holes are drilled through both the epoxy and the zinc layers.
6) Both ends of the epoxy-coated bars are patched with 3M Rebar Patch epoxy. For the test bars, only the unthreaded ends are patched.

7) For the test bars, a 914 mm (36 in.) long 14-gage insulated copper wire is attached to the tapped end with a 10-24 × 10 mm ($^3/_8$ in.) threaded bolt. The electrical connection is coated with epoxy to prevent crevice corrosion. The epoxy is allowed to dry for one day and then a 76-mm (3-in.) long heat shrinkable tube is used to anchor the copper wire along the length of the test bars. Epoxy is used to fill the interface between the shrinkable tube and the tapped end.

The reinforcing bar cage is prepared using the following procedures:

1) The field test specimen form consists of four side pieces and one bottom pieces that are made of plywood with a thickness of 19 mm ($^3/_4$ in.). The form is prepared by connecting the five pieces together using wood screws.
2) The inside of the form is cleaned thoroughly with clothe rags and the form corners are sealed with clay. The inside of the form is then coated with mineral oil prior to placing the bars.
3) As shown in the side view of Figure 2.8(d), two side pieces have two 25 mm (1 in.) diameter holes that are 229 mm (9 in.) away from the specimen side. Two 1.37-m (4.5-ft) long PVC pipes are installed all the way through the holes on the two side pieces. Two 1.83-m (6-ft) long No. 16 (No. 5) conventional bars are put into the PVC pipes so that they can be used to lift the concrete slabs.
4) Eight plastic chairs, two chairs for each test bar, with a height of 25 mm (1 in.) are placed underneath the bottom test bars. The two layers of bottom mat bars are then connected using conventional tie wire for conventional bars and plastic tie wire for epoxy-coated bars.

5) Six plastic chairs, two chairs for each bar, with a height of 108 mm (4.25 in.) are placed under the top mat bars to support the top mat. The use of plastic chairs prevents the electrical connection between the top and bottom mat bars in the concrete.
6) Stainless steel tie wire is used to attach both the top and bottom mat bars separately to the sides of the form. This helps keep the reinforcing bar cage in place during transportation of the forms and casting of the concrete. There is no internal electrical connection between the top and bottom mat bars.
7) Two form braces are attached to the specimen form to make the form stable during concrete casting.
8) When appropriate, a shim holder is then attached to the form to create simulated cracks. The details of the shim holder are given next.

A shim holder is used to create simulated cracks in the test specimens by positioning stainless steel shims immediately over selected reinforcing bars as follows:

1) The shim holder consists of seven pieces of plywood, each with a thickness of 19 mm ($^3/_4$ in.), as shown in Figure 2.10.
2) Pieces of sheet metal are connected to four vertical pieces of plywood on the shim holder, and then stainless steel shims with a thickness of 0.3 mm (12 mils) are attached to each piece of sheet metal. The stainless steel shims are parallel to and directly above the top test bars. The combination of sheet metal and stainless steel shim allows more room to screed and finish the concrete.

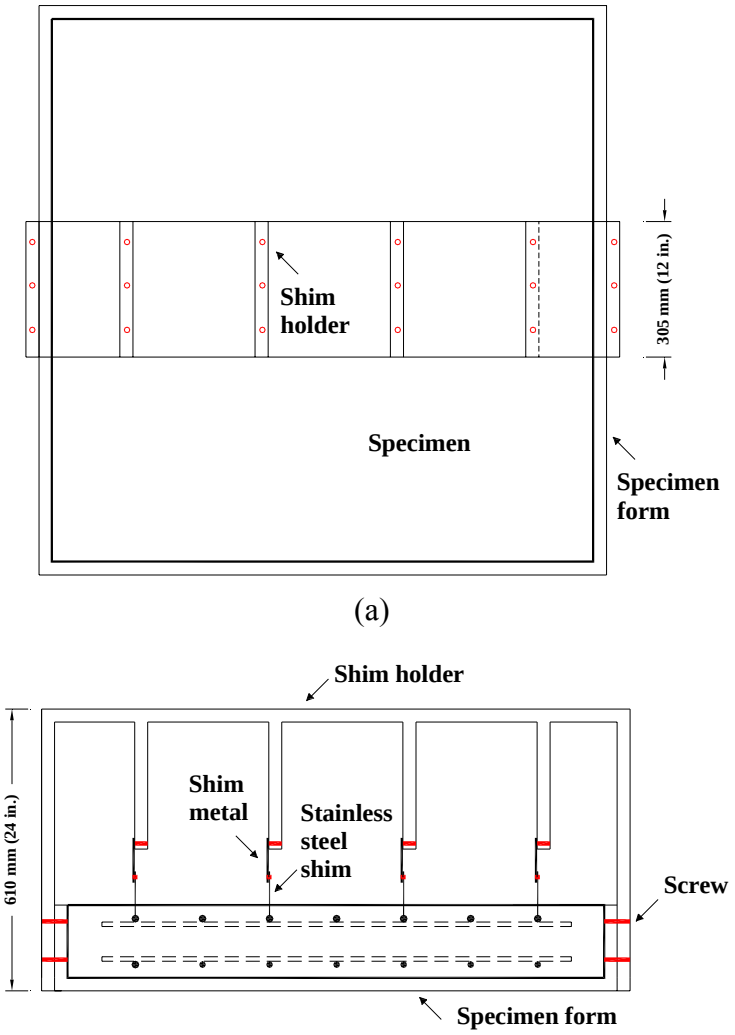

Figure 2.10 – Schematic diagram of shim holder (a) top view, (b) front view, and (c) side view

The field test specimens are fabricated as follows:

1) Concrete is ordered from a local ready mix (Lawrence Ready Mix) plant. The mix designs used for the field test specimens are given in Table 2.11 (Section 2.4.1). The concrete properties are described in Tables 2.14 and 2.15 (Section 2.4.5).
2) The concrete is placed directly into the form from the mixing truck chute. For the specimens with cracks, however, the concrete is first placed into a mixing pan so that two people can lift the pan and carefully place the concrete into the form. This prevents the displacement of the stainless steel shims or excessive movement of the shim holder.
3) An electric vibrator with a 33-mm ($1^3/_8$ in.) diameter head is used to consolidate the concrete. For epoxy-coated bars, care must be taken during vibration to avoid damage to the epoxy coating.
4) One 51 × 152 mm (2 × 6 in.) piece of lumber is used to screed the concrete. The top surface of the specimen is then finished using a bullfloat. For the field test specimens with cracks, a wooden float is used in place of the bullfloat.
5) Within 12 hours of casting, the shim holder is removed and the stainless steel shims are removed to form the simulated cracks.
6) The specimens are covered with wet burlap and plastic and kept continuously wet for seven days in accordance with the *Kansas Standard Specifications for State Road and Bridge Construction* (1990). The specimen form is then removed.
7) The specimens are then moved out of the lab and cured in air for three months.

The final preparation of the field test specimens is as follows:

1) Several days before the initiation of the tests, the specimens are moved to the Corrosion Field Test Facility at the Adams Campus of the University of Kansas.
2) Each field test specimen is supported by six concrete blocks [203 × 203 × 406 mm (8 × 8 × 16 in.)]. The specimens are kept at a height of 203 mm (8 in.) to allow air to flow underneath. The spacing between the field test specimens in each direction is 914 mm (3 ft).
3) Weatherstriping is used to make a dam around the specimen top surface. Silicon caulk seals the corners to prevent leakage of the solution.
4) The top test bars are connected to the red binding posts on the terminal box, while the bottom bars are connected to the black binding posts.

2.4.3 Test Procedure

The specimens are stored at the Adams Campus of the University of Kansas and exposed to the weather.

The test cycle is four weeks. The specimens are ponded on the first day with 3.3 L (0.87 gal) 10% rock salt solution, and corrosion related readings are recorded on the 14^{th} day. When readings are taken, the voltage drop across the 10-ohm resistors is measured using a voltmeter. The circuits are then opened and the mat-to-mat resistance is recorded using a ohmmeter. About two hours after opening the circuits, a copper-copper sulfate electrode is used to measure the corrosion potentials of the top and bottom mat test bars.

The test cycle is repeated every four weeks.

The moisture content in concrete can affect all of the corrosion measurements,

the voltage drop, mat-to-mat resistance, and corrosion potential. The lower the moisture content or the drier the concrete, the lower the voltage drop, the higher the mat-to-mat resistance, and the more positive the corrosion potential. To obtain uniform measurements, an appropriate amount of water is added to each specimen according to the weather conditions (temperature, wind speed, and moisture content of concrete) when the readings are taken. Usually, an hour before taking the voltage drop, about 1.5-liter water is added to each specimen when the ambient temperature is around 22°C (70°F). More water is used when the specimens are very dry.

2.4.4 Test Program

A total of 42 field test specimens were fabricated and the test program is summarized in Table 2.12. For each corrosion protection system, there are four field test specimens, two without simulated cracks and two with four 305-mm (12-in.) long simulated cracks directly above the test bars.

Table 2.12 – Test program for the field test

Without Cracks			With Cracks		
Steel Designation[a]	**Number of Tests[b]**	**Number of Potential Test Points**	**Steel Designation[a]**	**Number of Tests[b]**	**Number of Potential Test Points**
Control					
Conv. (1)	2	12	Conv. (1)	2	12
Conv. (2)	2	12	Conv. (2)	2	12
ECR (1)	2	6	ECR (1)	2	6
ECR (2)	4	12	ECR (2)	4	12
Corrosion Inhibitors					
ECR(primer/$Ca(NO_2)_2$) (1)	4	12	ECR(primer/$Ca(NO_2)_2$) (1)	4	12
ECR(primer/$Ca(NO_2)_2$) (2)	4	12	ECR(primer/$Ca(NO_2)_2$) (2)	4	12
ECR(DCI) (1)	4	12	ECR(DCI) (1)	4	12
ECR(DCI) (2)	4	12	ECR(DCI) (2)	4	12
ECR(DCI) (3)	4	12	ECR(DCI) (3)	4	12
ECR(Rheocrete) (1)	4	12	ECR(Rheocrete) (1)	4	12
ECR(Rheocrete) (2)	4	12	ECR(Rheocrete) (2)	4	12
ECR(Hycrete) (1)	4	12	ECR(Hycrete) (1)	4	12
ECR(Hycrete) (2)	4	12	ECR(Hycrete) (2)	4	12
Multiple Coated Bars					
MC (1)	2	6	MC (1)	2	6
MC (2)	4	12	MC (2)	4	12
Increased Adhesion					
ECR(Valspar) (1)	2	6	ECR(Valspar) (1)	2	6
ECR(Valspar) (2)	4	12	ECR(Valspar) (2)	4	12
ECR(DuPont) (1)	2	6	ECR(DuPont) (1)	2	6
ECR(DuPont) (2)	4	12	ECR(DuPont) (2)	4	12
ECR(Chromate) (1)	2	6	ECR(Chromate) (1)	2	6
ECR(Chromate) (2)	4	12	ECR(Chromate) (2)	4	12

[a] Conv. = conventional steel. ECR = conventional epoxy-coated reinforcement. All epoxy-coated bars are penetrated with 16 surface holes.
MC = multiple coated bars. Multiple coated bars have both the zinc and epoxy layers penetrated.
ECR(Chromate) = ECR with the chromate pre-treatment.
ECR(DuPont) = ECR with high adhesion DuPont coating. ECR(Valspar) = ECR with high adhesion Valspar coating.
ECR(DCI) = ECR in concrete with DCI inhibitor. ECR(Hycrete) = ECR in concrete with Hycrete inhibitor.
ECR(Rheocrete) = ECR in concrete with Rheocrete inhibitor.
ECR(primer/Ca(NO2)2) = ECR with a primer containing calcium nitrite.

[b] This is the total number of tests in each field test specimen.

2.4.5 Concrete Properties

Table 2.13 summarizes the corrosion protection systems and number of specimens in each concrete batch. It should be noted that Batch No. 6 with the corrosion inhibitor DCI-S had a very high slump [201 mm (8.25 in.)]. Therefore, two

additional field test specimens with DCI-S were cast in Batch No. 7.

Table 2.13 – Concrete batches for the field test specimens

Batch No.	Steel Designation[a]	Number of Specimens	Total Number of Specimens
1	Conv.	2	6
	ECR	2	
	ECR(Valspar)	2	
2	ECR(DuPont)	2	6
	ECR(Chromate)	2	
	MC	2	
3	ECR(primer/Ca$(NO_2)_2$)	2	6
	Conv.	2	
	ECR	2	
4	ECR(Valspar)	2	6
	ECR(DuPont)	2	
	ECR(Chromate)	2	
5	MC	2	4
	ECR(primer/Ca$(NO_2)_2$)	2	
6	ECR(DCI)	4	4
7	ECR(DCI)	2	2
8	ECR(Rheocrete)	4	4
9	ECR(Hycrete)	4	4

[a] Conv. = conventional steel. ECR = conventional epoxy-coated reinforcement. All epoxy-coated bars are penetrated with 16 surface holes.
MC = multiple coated bars. Multiple coated bars have both the zinc and epoxy layers penetrated.
ECR(Chromate) = ECR with the chromate pre-treatment.
ECR(DuPont) = ECR with high adhesion DuPont coating. ECR(Valspar) = ECR with high adhesion Valspar coating.
ECR(DCI) = ECR in concrete with DCI inhibitor. ECR(Hycrete) = ECR in concrete with Hycrete inhibitor.
ECR(Rheocrete) = ECR in concrete with Rheocrete inhibitor.
ECR(primer/Ca(NO2)2) = ECR with a primer containing calcium nitrite.

For each batch, a concrete sample is obtained during discharge of the middle portion of the batch. Slump, air content, temperature, unit weight, and 28-day concrete compressive strength were recorded. Tables 2.14 and 2.15 summarize the test results. As shown in Table 2.14, the concrete unit weight and air content using the pressure method were not available for Batch No. 7 because the concrete was very stiff [25 mm (1 in.) slump] and a vibrator was not used. The concrete air content was obtained using the volumetric method for Batch No. 9.

Table 2.14 – Concrete properties for the field test specimens

Batch No.	*w/c*	Slump mm (in.)	Temp. °C (°F)	Unit Weight kg/m^3 (lb/ft^3)	Air content (%)	
					(Pressure)	(Volumetric)
1	0.39	100 (4)	19 (66)	2219 (138.4)	7.00	6.25
2	0.43	100 (4)	19 (67)	2319 (144.7)	6.20	5.00
3	0.41	50 (2)	28 (82)	2307 (143.9)	5.30	4.00
4	0.42	125 (5)	24 (75)	2296 (143.2)	7.80	5.75
5	0.44	110 (4.25)	23 (73)	2291 (142.9)	6.40	5.25
6	0.48	210 (8.25)	22 (72)	2255 (140.7)	11.00	7.25
7	0.40	25 (1)[a]	21 (70)	-	-	5.50
8	0.44	165 (6.5)	23 (73)	2295 (143.2)	7.00	5.50
9	0.41	185 (7.25)	16 (61)	2216 (138.2)	-	5.65

[a] A slump of 150 mm (6 in.) slump was obtained at the Lawrence Ready Mix Plant before transporting concrete to the lab.

Table 2.15 – Concrete compressive strength for the field test specimens

Batch No.	Average Concrete Compressive Strength[a] MPa (psi)		
	Curing Tank	Curing Room	With Specimens
1	-	28.4 (4110)	30.6 (4440)
2	-	35.7 (5180)	37.4 (5430)
3	-	34.4 (4990)	36.9 (5350)
4	-	32.5 (4710)	32.9 (4780)
5	32.8 (4760)	32.6 (4730)	33.2 (4810)
6	35.3 (5110)	30.9 (4480)	29.6 (4290)
7	36.8 (5340)	35.9 (5210)	-
8	29.1 (4220)	28.5 (4130)	28.1 (4080)
9	15.0 (2170)	13.5 (1960)	13.1 (1900)

[a] Average of three cylinders.

From batches No. 1 to 4, six cylinders were made for each batch. Three of them were cured in the curing room and three stayed with the field test specimens. Beginning with Batch No. 5, three additional cylinders were made and cured in a curing tank containing lime saturated water. The solution in the curing tank consists of saturated calcium hydroxide and has a pH of 12.4. For Batch No. 7, the three

cylinders cured adjacent to the specimens had very rough ends because a vibrator was not used and they were tested without cutting off the ends using a masonry saw. Therefore, concrete compressive strength for cylinders with specimens was not available, as shown in Table 2.15.

As shown in Table 2.15, for batches No. 5 to 9, cylinders cured in the curing tank have a slightly higher compressive strength than those cured in the curing room. The differences in compressive strength between the two curing methods are between 0.2 to 1.5 MPa (30 to 210 psi) for all batches except for Batch No. 6, which had a difference of 4.3 MPa (630 psi).

For the first five batches, cylinders cured adjacent to the field test specimens had a higher compressive strength than those cured in the curing room, with differences between 0.5 and 2.5 MPa (70 and 360 psi). For batches No. 6, 8, and 9, cylinders cured in the curing room had a compressive strength 0.3 to 1.3 MPa (50 to 190 psi) higher than those cured adjacent to the specimens. The difference in compressive strength between the two curing methods can be explained by the curing temperature. In general, for the first five batches, a higher curing temperature was observed for cylinders cured adjacent to the specimens because they were cast from April to late August. The remaining batches were made from late September to early December, representing a lower curing temperature for cylinders cured adjacent to the specimens.

For the first eight batches, the compressive strength of cylinders ranges from 28.4 to 35.9 MPa (4110 to 5210 psi). The results indicate that the corrosion inhibitor Hycrete (Batch No. 9) reduced the concrete compressive strength by at least 50%.

2.5 KDOT BRIDGE PROJECTS

This report covers the test results of two bridge decks with 2205p stainless steel, the Doniphan County Bridge (DCB) and Mission Creek Bridge (MCB). The reinforcing steel for both bridges is Grade 420 stainless steel produced under ASTM A 955, *Standard Specification for Deformed and Plain Stainless Steel Bars for Concrete Reinforcement* that also met the Kansas specification. Corrosion potential mapping is used to evaluate the corrosion performance of 2205p stainless steel in both bridge decks every six months. Accompanying bench-scale and field test specimens were made for the bridges, as described in Sections 2.5.4 and 2.5.5.

The Doniphan County Bridge (Bridge No. 7-22-18.21(004)) is located on K-7 over the Wolf River in the Northeast region of Kansas. The bridge structure is a three span continuous composite steel beam with a total length of 75.8 m (249 ft). The bridge deck was replaced on February 26, 2004 due to the severe corrosion problems of reinforcing steel in the old bridge deck. The superstructure concrete was bid as Concrete (Grade 30)(AE)(SA), that is, air entrained structural concrete with select coarse aggregate for wear and absorption.

The Mission Creek Bridge (Bridge No. 4-89-4.58(281)) is located on K-4 over the Mission Creek. The bridge structure consists of one-span with composite steel girder construction and with a total length of 27.45 m (90 ft). The bridge deck was cast on August 25, 2004. The concrete used for the superstructure is Concrete (Grade 30)(AE)(SW), that is, air entrained structural concrete with select coarse aggregate for wear.

2.5.1 Bridge Description

Table 2.16 lists the bridge component descriptions. In Kansas, bridge decks

usually have overlays to provide additional corrosion protection for the reinforcing bars in concrete. In this case, an overlay is not used for the decks because 2205p stainless steel is corrosion resistant.

Table 2.16 – Basic bridge configurations

Bridge	DCB	MCB
Bridge No.	7-22-18.21 (004)	4-89-4.58 (281)
Type of Girder	Steel composite	Steel composite
Number of Spans	3	1
Abutment	Integral	Integral
Length m (ft)	75.8 (249)	27.45 (90)
Roadway m (ft)	8 (26)	11 (36)
Number of Steel Girders	5	6
Deck Type	Monolithlic	Monolithlic
Deck Depth mm (in.)	210 (8.3)	210 (8.3)
Top Clear Cover mm (in.)	65 (2.6)	65 (2.6)
Bottom Clear Cover mm (in.)	30 (1.2)	30 (1.2)

Table 2.17 – Reinforcing steel distribution at sections near midspan

Direction	Position	Bar No.	Spacing mm (in.)	
			DCB	MCB
Longitudinal	Top	16 (5)	290 (11.4)	300 (11.8)
	Bottom	16 (5)	260 (10.2)	250 (9.8)
Transverse	Top	16 (5)	170 (6.7)	170 (6.7)
	Bottom	16 (5) / 13 (4)*	170 (6.7)	170 (6.7)

* No. 16 (No. 5) and No. 13 (No. 4) bars are used alternately in the bottom mat

Table 2.17 lists the reinforcing steel distribution at the sections near midspan. At the sections at piers, longitudinal reinforcing bars at the top mat have a spacing that is only half of those at the sections near midspan. The field test specimens were fabricated with the similar geometry, reinforcing steel, and concrete at sections near

midspan for both bridges because 2205p stainless steel was not adequate. The details of the field test specimens are given in Section 2.5.4.

2.5.2 Monitoring of Reinforcement for Corrosion

To monitor the corrosion activity of the stainless steel in the bridge decks, test bars were installed in both decks next to transverse reinforcing bars before the concrete was cast. After the bridge deck was cast, the test bars remained in the bridge decks for long-term monitoring.

All of the test bars are prepared in the same manner as the test bars for the field test specimens (Section 2.4) with the exception that the test bars in the bridge decks have different lengths, as discussed below.

Tables 2.18 and 2.19 summarize the number and distribution of the test bars in both bridge decks. The wires attached to the test bars have different colors for easy identification.

Table 2.18 – Test bars in the Doniphan County Bridge

Position	Location	No.	Wire Color	Bar Length cm (ft)	Bar Location
Pier #2	Top	1	Blue	183 (6)	East
		2	Blue	183 (6)	Center
		3	Blue	183 (6)	West
	Bottom	4	Black	46 (1.5)	East
		5	White	46 (1.5)	West
Midspan	Top	6	Yellow	183 (6)	East
		7	Green	183 (6)	Center
		8	Black	183 (6)	West
	Bottom	9	White	46 (1.5)	East
		10	Black	46 (1.5)	West

Ten test bars were used for the Doniphan County Bridge: five at the Pier #2 and

five at midspan between Pier # 2 and the east abutment, as shown in Figure 2.11. These two locations are 23.01 m (75.5 ft) and 11.51 m (37.75 ft) away from the east abutment, respectively.

Table 2.19 – Test bars in the Mission Creek Bridge

Position	Location	No.	Wire Color	Bar Length cm (ft)	Bar Location
About 3 m (10 ft) away from the east abutment	Top	1	Black	91 (3)	West
		2	Black	91 (3)	Center
		3	Black	91 (3)	East
	Bottom	4	Yellow	91 (3)	West
		5	Yellow	91 (3)	Center
		6	Yellow	91 (3)	East

There are six test bars in the Mission Creek Bridge deck, placed 3 m (9.84 ft) away from the east abutment, as shown in Figure 2.12.

The test bars were embedded in the bridge decks to have direct contact with the transverse reinforcing bars. A 14-gage insulated wire was attached to each test bar to provide an electrical connection to the reinforcing steel in the bridge decks for recording corrosion potentials. The test bars are prepared as follows:

1) All of the test bars were prepared in the lab in the same manner as the test bars for the field test specimens in Section 2.4. A 14-gage insulated copper wire was attached to each test bar. According to the location of the test bars in bridge decks, each 14-gage insulated wire has a different length.

2) The test bars were tied to the transverse reinforcing bars using stainless steel tie wire. For both the top and bottom mats, the spacing between the test bars was two times the spacing of the reinforcing bars in the transverse direction in both decks.

3) The 14-gage insulated copper wire was run along the longitudinal

reinforcing bars to the east abutment for both bridges. For the Doniphan County Bridge, plastic zip ties were used to attach copper wires directly to the longitudinal reinforcing bars. For the Mission Creek Bridge, all of the copper wires were included in a PVC pipe to protect the wires from potential damage during construction, most notably from the concrete consolidation process. The PVC pipe was then tied to the longitudinal reinforcing bars using plastic zip ties.

4) A hole was drilled in the bottom formwork about 1 m (3.28 ft) away from the east abutment, as shown in Figures 2.11 and 2.12. The copper wires were threaded through the hole and were collected together close to the outside steel girder. Foam sealant was used to seal the holes to prevent concrete from leaking during casting.

Table 2.20 lists the concrete mix designs for the bridges, including the design *w/c*, design slump, design air content, and design unit weight.

Table 2.20 – Concrete mix design for the DCB and MCB

Bridge		**DCB**	**MCB**
Water	kg/m^3 (lb/yd^3)	143 (241)	129 (217)
Cement	kg/m^3 (lb/yd^3)	357 (602)	357 (602)
CA	kg/m^3 (lb/yd^3)	883 (1487)	893 (1504)
FA	kg/m^3 (lb/yd^3)	883 (1487)	893 (1504)
AE	mL/m3 (oz/yd^3)	290 (7.5)	154 (4)
Design *w/c*		0.40	0.36
Design Slump	mm (in.)	75 (2.95)	55 (2.25)
Design Air Content	(%)	6.5	6.5
Design Unit Weight	kg/m^3 (lb/ft^3)	2267 (141.37)	2272 (141.70)

The concrete test results for both bridges were provided by KDOT and are summarized in Tables 2.21 and 2.22. For the Doniphan County Bridge, cylinders were made for Tests No. 1 to 4 and the compressive strengths are between 35.6 and 41.9 MPa (5160 and 6080 psi). For the Mission Creek Bridge, cylinders were made for bridge deck Tests No. 1 and 2. The compressive strengths are 42.7 and 42.1 MPa (6190 and 6110 psi) for Test No. 1 and 2, respectively.

Table 2.21 – Concrete test results for the DCB

Test No.	Sample Location	Slump mm (in.)	Unit Weight kg/m^3 (lb/ft^3)	Air Content[a] (%)	Air Temp. °C (°F)	Conc Temp. °C (°F)	Compressive Strength[b] Mpa (psi)
Test #1	Pump	90 (3.5)	2313 (144.26)	2.5	7 (45)	11 (52)	41.9 (6080)
Test #2	Pump	100 (4)	2333 (145.28)	2	9 (49)	16 (60)	41.0 (5950)
Test #3	Pump	90 (3.5)	2321 (144.74)	1	12 (53)	21 (70)	40.8 (5920)
Test #4	Deck	90 (3.5)	2177 (135.78)	8	12 (53)	21 (70)	35.6 (5160)
Test #5	Deck	75 (3.0)	2174 (135.59)	9	12 (53)	21 (70)	-
Test #6	Deck	75 (3.0)	2200(137.22)	6.5	12 (53)	21 (70)	-
Test #7	Deck	75 (3.0)	2171 (135.41)	8	12 (53)	21 (70)	-
Test #8	Deck	75 (3.0)	2170 (135.41)	8	12 (53)	21 (70)	-
Test #9	Deck	75 (3.0)	2177 (135.78)	8	12 (53)	21 (70)	-

[a] Pressure method was used to test concrete air content.

[b] Average of three cylinders.

Table 2.22 – Concrete test results for the MCB

Sample Location	Slump mm (in.)	Unit Weight kg/m^3 (lb/ft^3)	Air Content[a] (%)	Air Temp. oC (°F)	Conc. Temp. oC (°F)	Compressive Strength[b] Mpa (psi)
East Abutment	100 (4.0)	2269 (141.52)	6.1	27 (81)	31 (88)	-
West Abutment	90 (3.5)	2253 (140.52)	5.25	25 (77)	34 (92)	-
Bridge Deck Test #1	75 (3.0)	204 (143.70)	4.25	28 (82)	32 (89)	42.7 (6190)
Bridge Deck Test #2	50 (2.0)	2293 (143.00)	5.0	25 (77)	33 (91)	42.1 (6110)
Bridge Deck Test #3	65 (2.5)	2264 (141.19)	6.0	25 (77)	35 (94)	-
North Handrail	50 (2.0)	2294 (143.11)	5.5	25 (77)	30 (86)	-
South Handrail	145 (5.75)	2253 (140.52)	5.0	18 (64)	28 (82)	-

[a] Pressure method was used to test concrete air content.

[b] Average of three cylinders.

2.5.3 Bridge Potential Mapping

In a bridge deck with conventional uncoated bars, an electrical connection between the top and bottom mat bars is normally provided by truss bars, tie wires, bar chairs, expansion dams, and/or scuppers (Clear et al. 1990). Although plastic chairs were used in both the bridges, the resistance between the top and bottom test bars equals zero, which indicates that a direct electrical connection exists between the top and bottom mat bars in both bridge decks. Therefore, to monitor the long-term corrosion performance of the 2205p stainless steel in the bridge decks, corrosion potentials, rather than corrosion current, are measured. Measurements are taken every six months on a fixed grid.

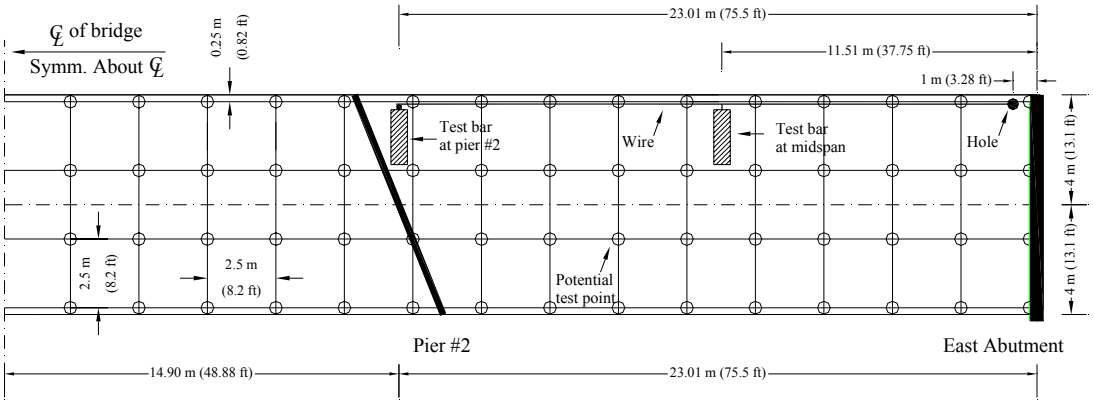

Figure 2.11 – Potential test points for the Doniphan County Bridge

For the Doniphan County Bridge, corrosion potential measurements are taken on a 2.5 × 2.5 m (8.2 × 8.2 ft) grid across the full bridge length, as shown in Figure 2.11. The corrosion potential measurements are recorded starting at the east abutment. There are a total of 124 test points.

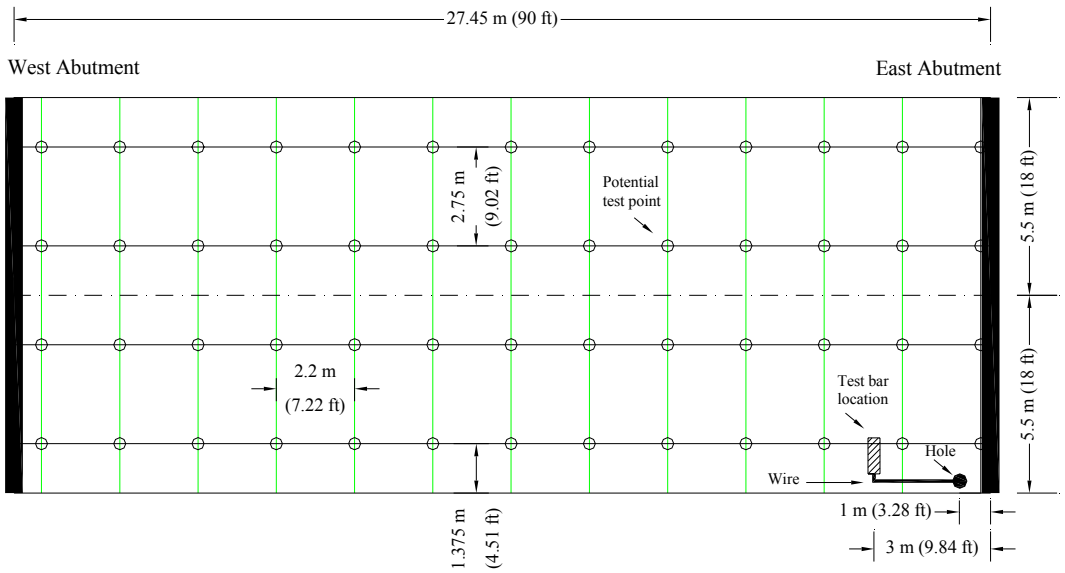

Figure 2.12 – Potential test points for the Mission Creek Bridge

Figure 2.12 shows the corrosion potential measuring grid [2.75 × 2.2 m (9.0 × 7.2 ft)] for the Mission Creek Bridge. The corrosion potential readings are recorded starting at the east abutment. There are a total of 52 test points.

Corrosion potentials are measured using the following procedures:

1) Several weeks before the corrosion potential measurements are recorded, contact is made with KDOT to coordinate traffic control during the test.
2) One hour before testing the bridge, water is sprayed on the bridge decks at a rate of approximately 6.3 L/m^2 (1.4 gal/yd^2) to obtain stable corrosion potentials. A 1600 gallon potable water tank with a water pump that is mounted in a maintenance dump truck is used for this purpose.
3) On the day of the test, a lumber crayon is used to mark the test points on the bridge deck. Potential readings are recorded in one lane as traffic passes in the free lane. Then the other lane is surveyed as traffic is switched to the first lane.

4) The generator and voltmeter are placed at the east abutment for both bridges.
5) The wires from the test bars are connected to the positive terminal of the voltmeter. A copper-copper sulfate electrode is connected to the negative terminal of the voltmeter through a large spool of wire.
6) The copper-copper sulfate electrode is placed on a wet sponge to measure corrosion potentials. Good contact between the electrode and concrete helps to maintain stable corrosion potential readings.

The equipment and materials used in the potential measurement are listed below:

- *Voltmeter* – Hewlett Packard digital voltmeter, Model 3455A, with an impedance of 2 MΩ. Used to measure the corrosion potential of reinforcing bars in bridge decks.
- *Copper-Copper Sulfate Electrode (CSE)* – MC Miller Co. Electrode Model RE-5.
- *Generator* – A generator is usually provided by KDOT to provide power for the voltmeter.
- *Nylon Cord* – Used to identify corrosion potential test points on the bridge decks. Marked with black dots at the appropriate spacing.
- *Lumber Crayon* – Used to mark the potential test points on the bridge decks.
- *Spool of Wire* – Used to measure corrosion potentials. Must be long enough to cover the entire bridge length.

2.5.4 Field Tests

Six field test specimens were made for each bridge, including two specimens

with conventional steel, two with 2205p stainless steel, and two with epoxy-coated reinforcement. The specimens were cast using the geometry and concrete used in the bridge decks, with some modifications. The specimen has a depth of 165 mm (6.5 in.) with the top and bottom concrete cover of 25 mm (1 in.), compared with the top concrete cover of 65 mm (2.6 in.) in both bridge decks, to accelerate the tests. The bottom mat in the transverse direction contains only No. 16 (No. 5) reinforcing bars. Concrete from a trial-batch at the ready mix plant was used to cast the field test specimens.

Figures 2.13 and 2.14 illustrate the field test specimens for the Doniphan County and Mission Creek bridges, respectively.

The field test specimens for the Doniphan County Bridge do not contain simulated cracks. Bars numbered 2 and 6 serve as the test bars for these specimens, as shown in Figure 2.13. The coating has no intentional damage for the two specimens with epoxy-coated reinforcement.

Of the six field test specimens made for the Mission Creek Bridge, half of them have four 305-mm (12-in.) long simulated cracks with a depth of 25 mm (1 in.). The simulated cracks are created directly above the top test bars numbered 1, 3, 5, and 7 using 0.3 mm (12 mil) stainless steel shims. For specimens with stainless steel or conventional steel, bars numbered 2 and 6 are selected as the test bars, as shown in Figure 2.14. For specimens with ECR, there are four test bars selected similar to the regular field test specimens (Section 2.4). The coating on all of the epoxy-coated bars is penetrated with 16 3-mm ($^1/_8$-in.) diameter holes, representing damage to 0.24% of the epoxy coating.

Stainless steel tie wire was used to fabricate the specimens containing stainless steel reinforcing bars.

The forms and reinforcement for the field test specimens were prepared in the lab and then transported to concrete ready-mix plants. The concrete from a trial-batch for the bridge project was used to cast the field test specimens. Concrete was left in the mixing truck to simulate the haul time from the plant to the jobsite, 55 minutes for the DCB and 35 minutes for the MCB. For both bridges, the field test specimens were cast 41 days earlier than the cast of the bridge deck. The specimens for the Doniphan County Bridge were cast at Builders Choice Concrete (St. Joseph, MO) on January 16, 2004. For the Mission Creek Bridge, the specimens were cast at Meier's Ready Mix, Inc. (Topeka, KS) on July 15, 2004.

The specimens were covered with burlap and plastic and continuously wet-cured for seven days. The specimens for the Doniphan County Bridge were also protected with heat insulation blankets during the curing period. The specimen forms were then removed and the specimens were transported to the Corrosion Field Test Facility at the University of Kansas.

Table 2.23 summarizes the properties of the concrete used for both field test specimen groups.

Table 2.23 – Concrete properties for the field test specimens for the DCB and MCB

Bridge	Simulated Haul Time (min.)	Slump mm (in.)	Air Content (%)	Concrete Temp. ^{o}C (^{o}F)	Unit Weight kg/m^3 (lb/ft^3)
DCB	55	55 (2.25)	5[a]	20 (68)	2292 (142.96)
MCB	30	50 (2)	5.25[b]	27 (80)	2261 (141.04)

[a] Pressure method was used to test concrete air content for the Doniphan County Bridge.

[b] Volumetric method was used to test concrete air content for the Mission Creek Bridge.

As shown in Table 2.23, the concrete slump was 55 mm (2.25 in.) and 50 mm (2 in.) for the DCB and MCB, respectively. The field test specimens for the DCB

were cast successfully with an ambient temperature of approximately 7°C (45°F). For the Mission Creek Bridge, the ambient temperature was approximately 35°C (95°F) and the concrete set very fast. The three field test specimens without cracks were cast first and a very smooth top surface was obtained. The three specimens with simulated cracks, however, had a very rough finished surface.

Six cylinders were made for each batch of specimens. Three were cured in the curing room and three remained with the field test specimens. The average concrete compressive strength calculated using the cylinders cast with specimens from both bridges is presented in Table 2.24. For the DCB, the field test specimens were cast in January 2004. The cylinders cured in the curing room have a higher compressive strength than those cured adjacent to the field test specimens. In the case of the MCB, the concrete was cast in July 2004 and a higher compressive strength was observed for the cylinders cured adjacent to the field test specimens.

Table 2.24 – Average concrete compressive strength for the DCB and MCB

Bridge	**Average Concrete Compressive Strength[a] MPa (psi)**	
	Curing Room	**With Field Test Specimens**
DCB	32.8 (4750)	28.9 (4190)
MCB	35.4 (5140)	38.2 (5540)

[a] Average of three cylinders.

The test procedures described in Section 2.4 are also used for the field test specimens for the bridges, except for different potential test points on the specimen top surface, as shown in Figures 2.15 and 2.16.

Table 2.25 summarizes the number of potential test points for the field test specimens for both bridges.

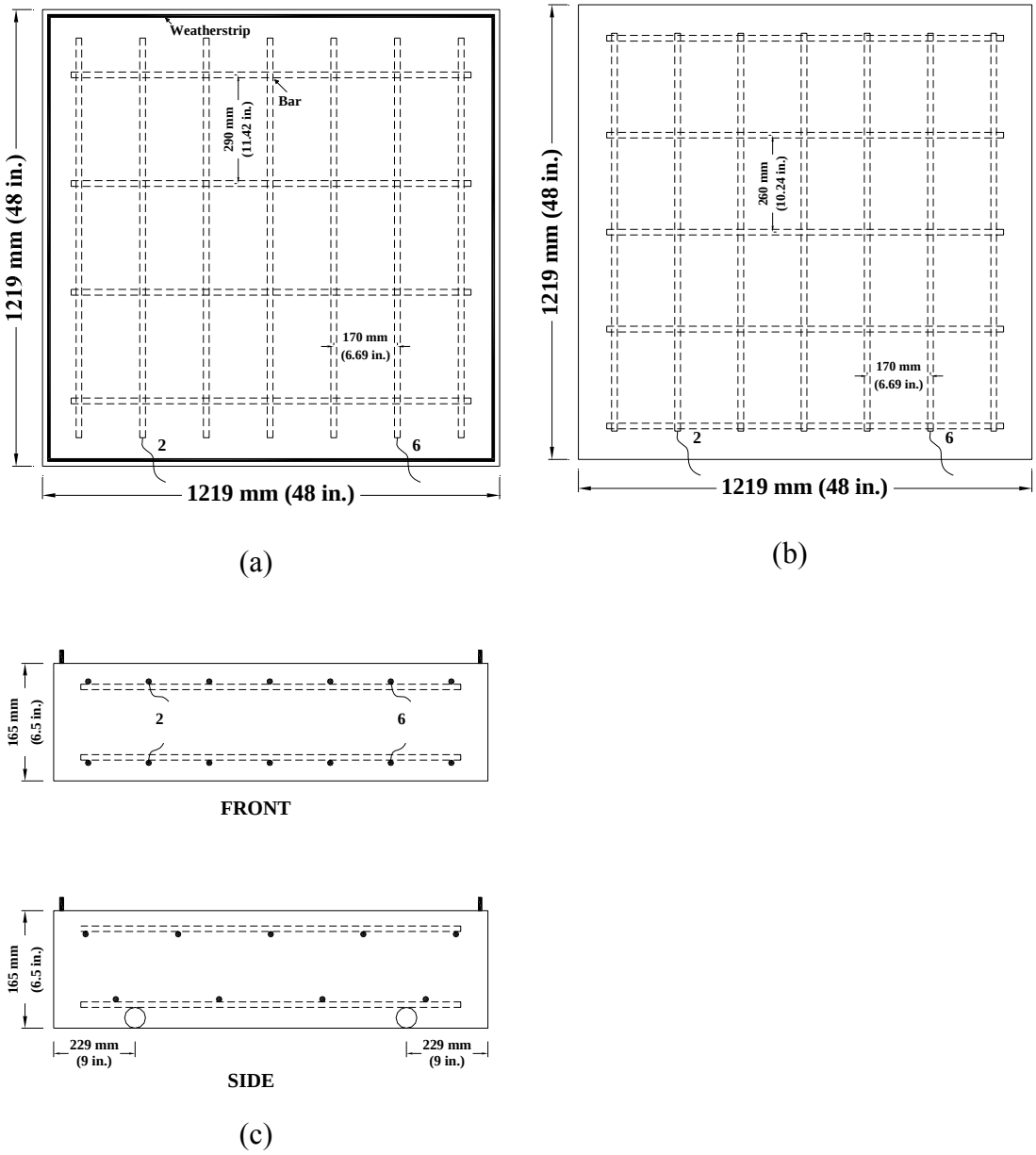

Figure 2.13 – Field test specimens for the Doniphan County Bridge (a) top slab, (b) bottom slab, and (c) front and side views

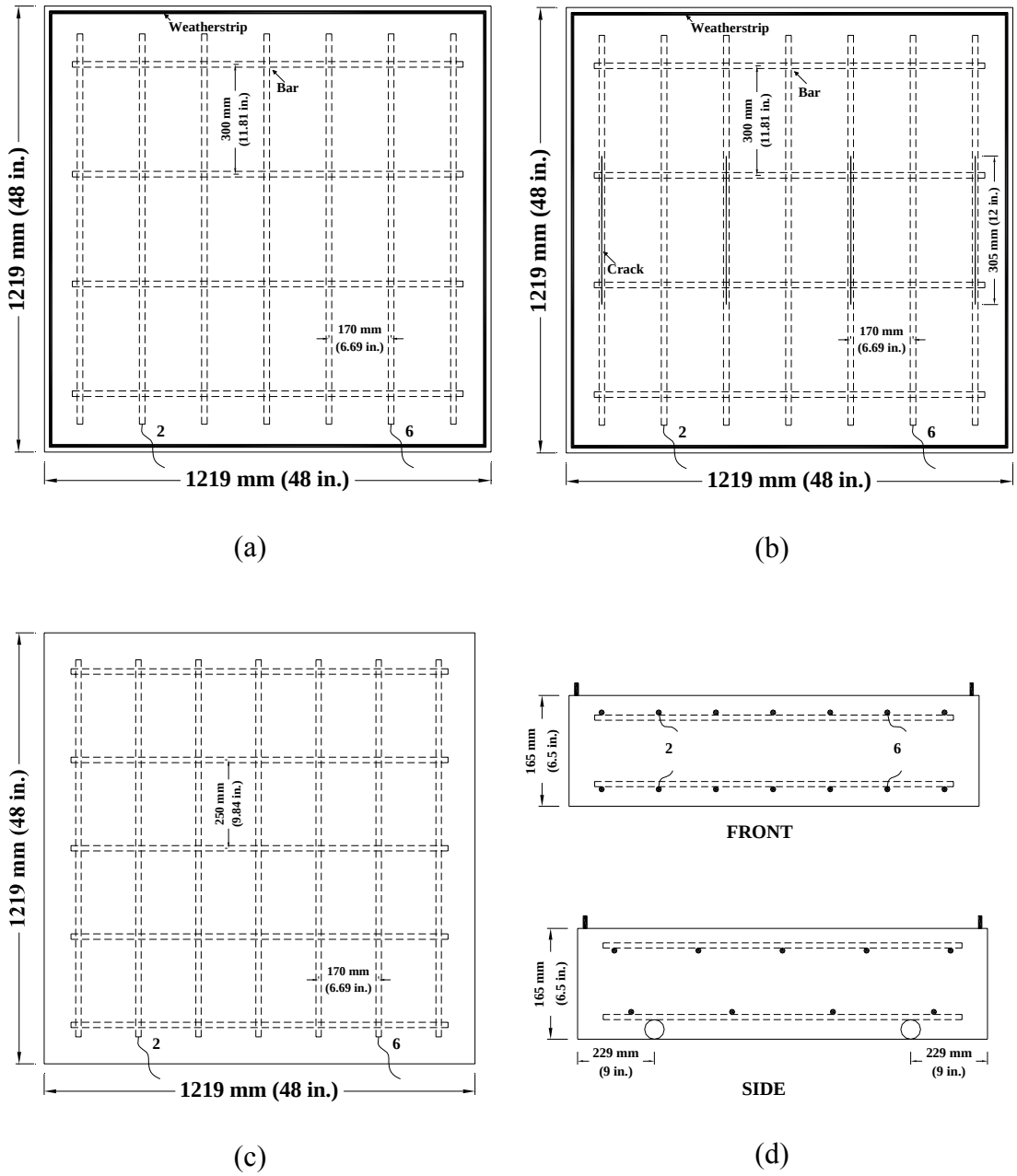

Figure 2.14 – Field test specimens for the Mission Creek Bridge (a) top slab (without cracks), (b) top slab (with cracks), (c) bottom slab, and (d) front and side views

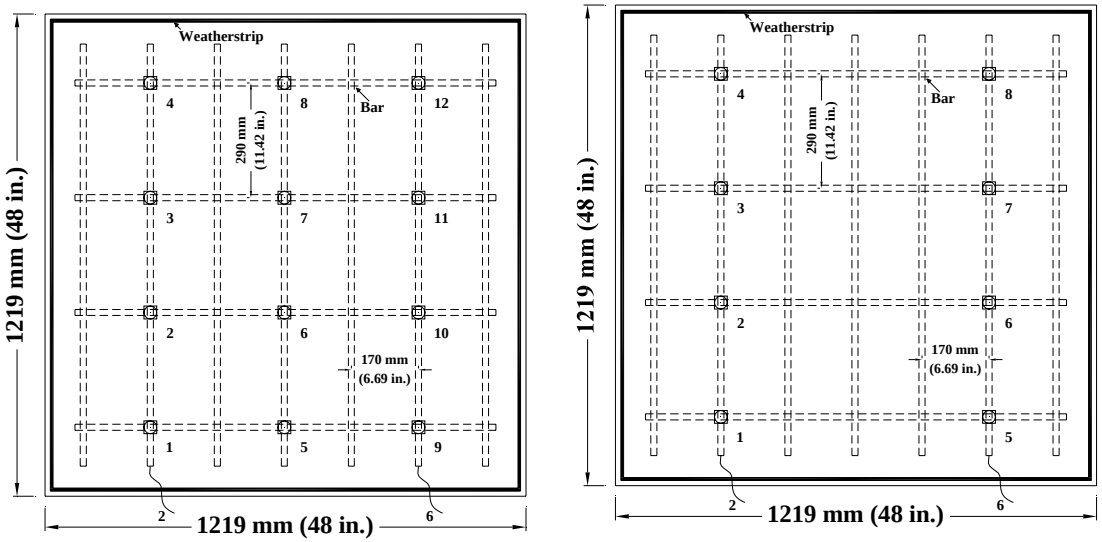

(a) (b)

Figure 2.15 – Potential test points for the field test specimen for the Doniphan County Bridge (a) conventional or stainless steel, and (b) epoxy-coated reinforcement

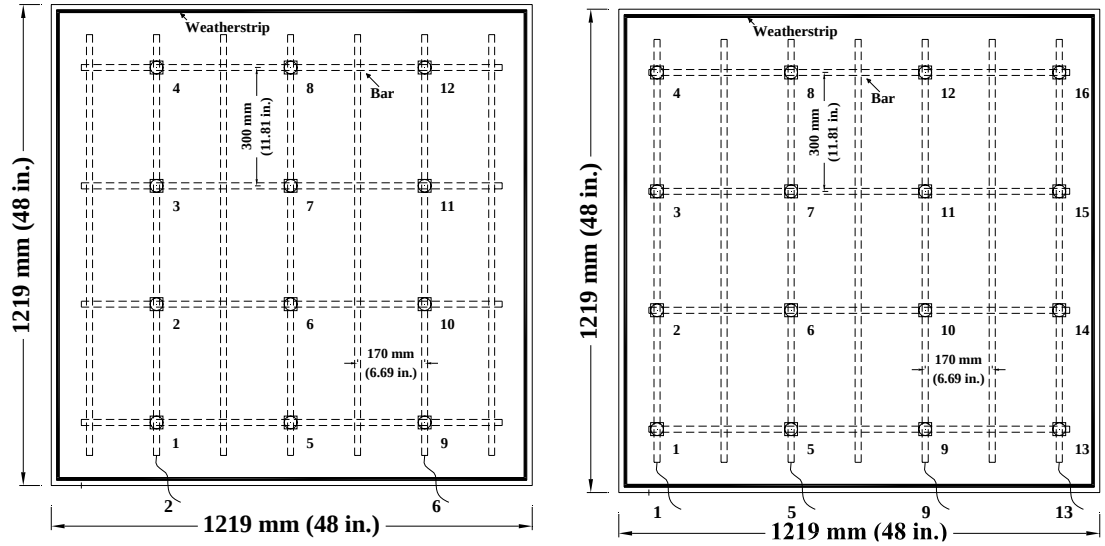

(a) (b)

Figure 2.16 – Potential test points for the field test specimen for the Mission Creek Bridge (a) conventional or stainless steel, and (b) epoxy-coated reinforcement

2.5.5 Test Program

- **Field Test**

There are a total of six field test specimens for each bridge. A summary of the test program is presented in Table 2.25. The number of tests in Table 2.25 represents the number of test bars in each specimen. For specimens with ECR for the Mission Creek Bridge, all ECR bars have 16 holes through the epoxy.

Table 2.25 – Test program for the field tests for the DCB and MCB

Bridge	Steel Designation[a]	Number of Test Bars	Potential Test Points	Notes
DCB	Conv. (1)	2	12	
	Conv. (2)	2	12	
	ECR (1)	2	8	
	ECR (2)	2	8	
	2205p (1)	2	12	
	2205p (2)	2	12	
MCB	Conv. (1)	2	12	
	Conv. (2)	2	12	with cracks
	ECR (1)	4	16	with 16 drilled holes
	ECR (2)	4	16	with cracks and 16 drilled holes
	2205p (1)	2	12	
	2205p (2)	2	12	with cracks

[a] Conv. = conventional steel.
ECR = conventional epoxy-coated reinforcement.
2205p = 2205 pickled stainless steel used in the bridge decks.

- **Bench-scale Tests**

Only stainless steel reinforcing bars are used in the bench-scale tests to evaluate the corrosion performance of the stainless steel in the DCB and MCB bridges. The test program is summarized in Table 2.26.

The forms and reinforcement in the bench-scale test specimens were prepared in the lab, and the specimens were cast with the field test specimens. An internal

electric vibrator with a diameter of 19 mm ($^3/_4$ in.) was used instead of a vibrating table to consolidate the concrete. The number of bench-scale test specimens is shown in Table 2.26 for each bridge.

Table 2.26 – Test program for the bench-scale test specimens

Bridge	Steel Designation[a]	Number of Test Specimens
Southern Exposure (SE) Test		
DCB	SE-2205p	6
MCB	SE-2205p	5
Cracked Beam (CB) Test		
DCB	CB-2205p	3
MCB	CB-2205p	6

[a] 2205p = 2205 pickled stainless steel used in the bridge decks.

2.6 CATHODIC DISBONDMENT TEST

The cathodic disbondment test is performed in accordance with ASTM G 8 and ASTM A 775. Cathodic disbondment can be defined as the destruction of adhesion between a coating and its substrate by products of a cathodic reaction. The test provides accelerated conditions for a reduction in adhesion and, therefore, measures the resistance of epoxy coatings to this type of action. As described in ASTM G 8, the ability to resist disbondment is a desired quality on a comparative basis, but disbondment is not necessarily an adverse indication.

The equipment and materials used in the cathodic disbondment tests are listed below:

- *Potentiostat* – PGS151 Potentiostat/Galvanostat, manufactured by Intertech Systems Inc.
- *Platinum Plated Electrode* – A 150-mm (6-in.) long platinum clad electrode with a nominal diameter of 3 mm ($^1/_8$ in.), manufactured by Anomet Inc.

- *Saturated Calomel Electrode (SCE)* – Fisher Scientific Catalog No. 13-620-52.
- *Container* – Plastic container with a diameter of 178 mm (7 in.) and a height of 191 mm (7.5 in.).
- *Electrolyte* – 3% NaCl by mass dissolved in distilled water.
- *Epoxy* – 3M Scotchkote^{TM} Brush Grade Rebar Patch Kit.

The ECR test specimens used for the cathodic disbondment test are prepared as follows:

1) ECR bars are cut to a length of 250 mm (10 in.) and the sharp edges on the ends of the bars are removed with a grinder.
2) The test bar is drilled and tapped to receive a 10-24 threaded bolt with a depth of 13 mm (0.5 in.) at one end.
3) The test bar is cleaned with soap and warm water, and then air dried.
4) The unthreaded end of the bar is protected with a plastic caps that is half-filled with 3M Rebar Patch epoxy.
5) The epoxy coating is penetrated with a drill bit to provide one 3-mm ($^{1}/_{8}$-in.) diameter hole approximately 50 mm (2 in.) from the unthreaded end of the test bar centered between the longitudinal and transverse ribs.
6) A 14-gage insulated copper wire is attached to the tapped end of the test bar with a 10-24 threaded bolt. The electrical connection is protected with two coats of 3M Rebar Patch epoxy.
7) The SCE electrode, test bar, and platinum electrode are placed in the test container and connected to the PGS151 Potentiostat according to the configuration in ASTM A 775. The container contains a 3% NaCl solution with a depth of 100 mm (4 in.).

To perform the cathodic disbondment test, a potential of –1.5 V measured with respect to a copper-copper sulfate electrode is applied for a total test period of 168 hours. The test bar is then removed from the container and allowed to cool for 1 ± 0.25 h prior to evaluation. Radial 45° cuts are made through the coating intersecting at the center of the hole with a utility knife, and the knife is used to peel the epoxy coating around the hole. The total disbonded coating area (not including the original hole) is recorded in accordance with ASTM G 8. In addition, in accordance with ASTM A 775, four radial measurements from the original hole are taken at 0°, 90°, 180°, and 270°, and the values averaged. The cathodic disbondment test results are reported in terms of both the area of the disbonded coating and the average coating disbondment radius.

The cathodic disbondment test is performed for the conventional ECR used in this study, conventional ECR from a previous batch, ECR with zinc chromate pretreatment, two types of ECR with increased adhesion coatings produced by DuPont and Valspar, ECR with a primer containing calcium nitrite, and multiple coated reinforcement.

2.7 LINEAR POLARIZATION RESISTANCE (LPR) TEST

The LPR test is a rapid, non-destructive test method for measuring the microcell corrosion rate of reinforcing bars in concrete. The tests are performed on the bench-scale test specimens included in this study. For each specimen, both the top and bottom mat bars are tested every four weeks and the connected mats are tested every eight weeks.

The tests are performed using a PCI4/750 Potentiostat and DC105 DC Corrosion Measurement Software from Gamry Instruments. The LPR data are

collected using the DC105 data acquisition system and analyzed using the polarization resistance data analysis macro POLRES, part of the DC105 corrosion data analysis package.

2.7.1 Data Acquisition

PCI4/750 Potentiostat is a three-electrode Potentiostat, with connections to the working electrode, reference electrode, and counter electrode. The bars in the bench-scale test specimens serve as the working electrode and a saturated Calomel electrode is used as the reference electrode. The counter electrode is a platinum electrode immersed in the 15% NaCl solution that is ponded on the upper surface of specimens.

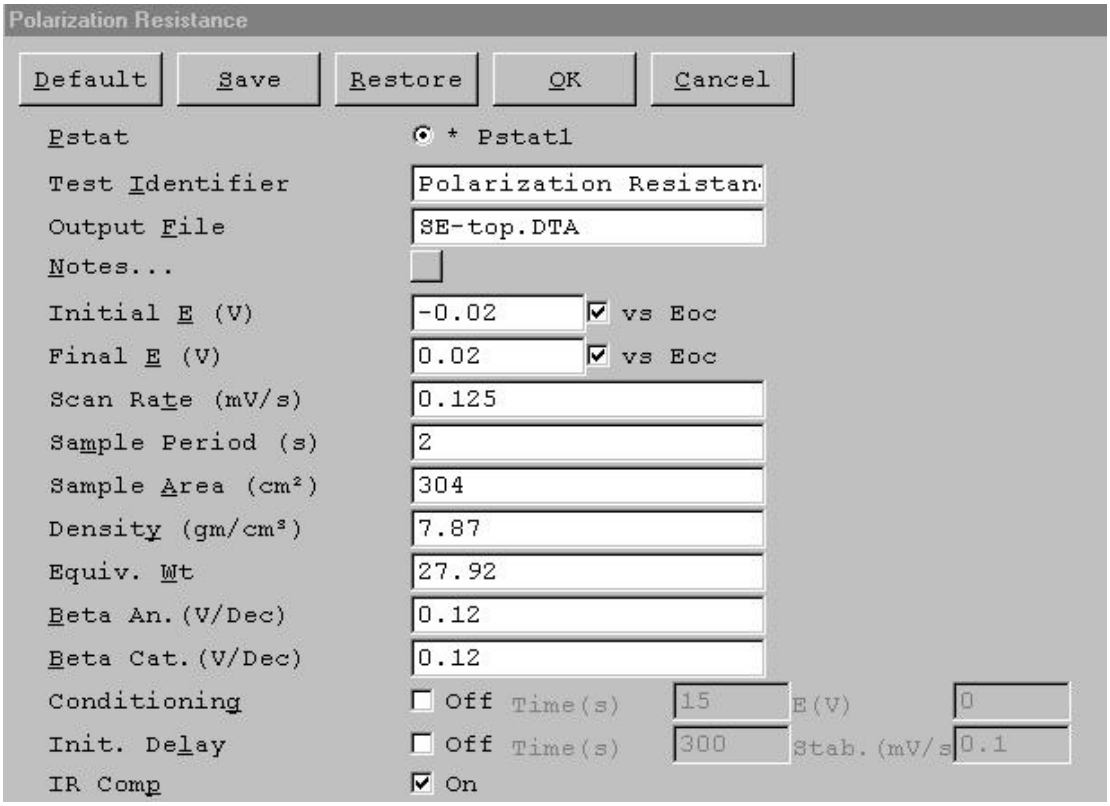

Figure 2.17 – Setup window for the LPR test

Figure 2.17 shows the setup window for the LPR test. The *Default* button is used to restore all the parameters on the screen to their default values. The *Save* button can save the current parameter set and the *Restore* button can recover a parameter set. This feature is useful for repetitive tests. The parameters are described as follows:

- *Initial and Final E* – The *Initial E* and *Final E* define the starting and ending points for the potential scan range during data acquisition.
- *Scan Rate* – The scan rate defines the speed of the potential sweep in mV/s. ASTM G 59 stipulates 0.167 mV/s for the analysis of corroding systems.
- *Sample Period* – The sample period determines the spacing between data points.
- *Sample Area* – The surface area of reinforcing steel in cm^2 in concrete.
- *Density* – The density of steel in g/cm^3.
- *Equiv. Wt* – The equivalent weight of steel (atomic weight of an element divided by its valence).
- *Beta An*. – The anodic Tafel constant in V/Dec.
- *Beta Cat.* – The cathodic Tafel constant in V/Dec.
- *Conditioning* – Used to insure the metal has a known surface condition at the start of the test. *Conditioning E* and *Conditioning Time* are the potential applied during the conditioning phase of the experiment and the length of time it is applied, respectively. It is set off during the test.
- *Init. Delay*. – When the *Init. Delay* is set to ON, it allows E_{oc} (open circuit corrosion potential of the sample) to stabilize before the scan. Time in seconds defines the time that the cell is held at open circuit before starting the scan. The delay is stopped if the value for Stab. is reached before the Time is reached. During the test, no *Init. Delay* is specified and this step only lasts long enough

for E_{oc} to be measured.

- *IR Comp.* – When current flows in an electrochemical cell, the solution resistance creates a voltage drop along the current path. As a three-electrode Potentiostat, the Gamry Instruments PC4 measures and controls the potential difference between the non-current carrying reference electrode and the current carrying working electrode.

The parameters used in the study are shown in Figure 2.17. The sample area is modified according to the sample being evaluated, as shown in Table 2.27 in different mats for bench-scale test specimens. The current density readings are taken during a short, slow sweep of the potential. The sweep is from –20 to +20 mV relative to E_{oc}. If ΔE is defined as the potential difference between the applied potential and E_{oc}, the potential of the sample is swept from ΔE = –20 mV to ΔE = +20 mV at a scan rate of 0.125 mV/s, that is, a total of 320 seconds for each test. Current density readings are taken every 2 seconds during the sweep without operator intervention. A plot of current versus potential is displayed during the scan.

Table 2.27 – The steel surface area in cm^2 ($in.^2$) for bench-scale test specimens

Steel Location	Southern Exposure Test	Cracked Beam Test	ASTM G 109 Test
Top Mat	304 (47.1)	152 (23.6)	139 (21.6)
Bottom Mat	608 (94.2)	304 (47.1)	278 (43.2)
Connected Mat	912 (141.4)	456 (70.7)	418 (64.8)

2.7.2 Data Analysis

The polarization resistance data are analyzed by the POLRES as follows:

1) Use the *New Graph* command to load a curve. When a curve is loaded, the

selected region defaults to the entire curve.

2) Before the polarization resistance calculation, use the *Set Select Region* command to select the potential region, which is from –10 to +10 mV relative to E_{oc}. The program then performs the linear least square fit over this region.

3) Select the *Polarization Resistance* command to perform the analysis. In the polarization resistance setup window, enter the Tafel constants as 0.12 V for both the anodic and cathodic Tafel constants. A linear least squares fit of the current versus voltage curve over the selected region yields an estimate of the polarization resistance R_P. R_P is then used to calculate the corrosion rate using the Stern-Geary equation

$$r = 11.59 i_{corr} = 11590 \frac{B}{R_p} \tag{2.2}$$

Where

r = microcell corrosion rate in μm/yr,

i_{corr} = corrosion current density in μA/cm^2,

R_p = polarization resistance in ohm.cm^2,

B = the Stern-Geary constant, 26 mV.

For each of the corrosion protection systems, one bench-scale test specimen of each type in the test is evaluated using the linear polarization resistance test. The specimen number is given as “LPR Test Specimen No.” in Tables 2.7 to 2.9 for the bench-scale test specimens (Section 2.3).

CHAPTER 3

RESULTS AND EVALUATION

This chapter presents the test results of the rapid macrocell test, three bench-scale tests, and the field test. The macrocell test includes both bare bar and mortar-wrapped specimens. The bench-scale tests include the Southern Exposure (SE), cracked beam (CB), and ASTM G 109 tests. Specimens with and without cracks are used in the field test. The test results for two bridges with 2205 pickled stainless steel, the Doniphan County Bridge (DCB) and Mission Creek Bridge (MCB), are also presented, as are three rounds of cathodic disbondment tests.

For the rapid macrocell test, the reported results include the corrosion rate, total corrosion loss, and corrosion potentials of the anode and cathode with respect to a saturated calomel electrode. For the bench-scale and field tests, the results include the corrosion rate, total corrosion loss, mat-to-mat resistance, and corrosion potentials of the top and bottom mats of steel with respect to a copper-copper sulfate electrode. For the two bridges with 2205p stainless steel, the results include the corrosion potential maps obtained at six month intervals, along with the results of accompanying bench-scale and field test specimens. The test specimens in the cathodic disbondment tests include conventional ECR, conventional ECR from a previous batch, multiple coated reinforcement, ECR with the chromate pretreatment, two types of ECR with high adhesion epoxy coatings produced by DuPont and Valspar, and ECR with a primer containing calcium nitrite.

For the rapid macrocell test, epoxy-coated reinforcement (ECR) was evaluated in two different conditions: with four holes penetrating the epoxy and without holes (or in the as-delivered condition). For the bench-scale tests, the ECR bars were evaluated with either four or 10 holes. All ECR bars in the field test were drilled with

16 holes. In this chapter, the average corrosion rates and total corrosion losses are reported based on both the total area of the bars exposed to chlorides (the exposed area below the liquid for macrocell specimens and full area of the bars for other specimens) and the exposed area of the steel at the holes.

In the tables and figures included in this report, an asterisk (*) is added to the steel designation to identify the corrosion rates or total corrosion losses based on the exposed area of the steel. Table 3.1 shows the total bar area, the exposed area at the holes in the epoxy, and the ratios of the corrosion rates and total corrosion losses based on the exposed and total area of the steel for the tests included in this report.

Table 3.1 – Bar areas, exposed areas at holes in epoxy, and ratios of corrosion rates, and total corrosion losses between the results based on the exposed area and total area of the steel

Test Method		Bench-scale Tests			Rapid	Field
		SE	CB	ASTM G 109	Macrocell Test	Test
Number of Bars		2	1	1	1	1
Bar Length cm (in.)		30.5 (12)	30.5 (12)	27.9 (11)	6.4 (2.5)[d]	99.1 (39.5)[e]
Total Area cm^2 ($in.^2$)		304 (47.1)	152 (23.6)	139 (21.6)	32 (4.9)	494 (76.6)
with 4 holes	Exposed Area cm^2 ($in.^2$)	0.63 (0.10)	0.32 (0.05)	0.32 (0.05)	0.32 (0.05)	-
	Ratio[a]	480	480	440	100	-
with 10 holes	Exposed Area cm^2 ($in.^2$)	1.59 (0.25)	0.79 (0.12)	0.79 (0.12)	-	-
	Ratio[b]	192	192	176	-	-
with 16 holes	Exposed Area cm^2 ($in.^2$)	-	-	-	-	1.27 (0.20)
	Ratio[c]	-	-	-	-	390

[a] Ratio for specimens with four holes. [b] Ratio for specimens with 10 holes.

[c] Ratio for field test specimens with 16 holes.

[d] The test bar is 7.6 cm (3 in.) in solution with a 1.3-cm (0.5-in.) long cap at the unthreaded end.

[e] The test bar is 106.7 cm (42 in.) long with a 7.6-cm (3-in.) long heat shrinkable tube at the threaded end.

The voltage meter used in this study features a 0.001 mV resolution. As pointed out in Chapter 2, it was observed that the voltage drop could fluctuate between -0.003 and 0.003 mV when the voltage drop was close to zero. The voltage drop readings in this region will not represent the actual condition and, therefore, they are filtered out for the individual specimens in this study. Voltage drop readings beyond this region are used to evaluate the corrosion performance of different corrosion protection

systems. As noted in Chapter 2, “negative corrosion” occurs when the current flows from the is exposed to chlorides (in salt solution for the rapid macrocell test, or top bars in the bench-scale tests) has a more positive potential than the bars separated from chlorides (in pore solution for the rapid macrocell test, or bottom bars in the bench-scale tests), so that the current flows from the former to the latter bars.

The individual test results are presented in Appendices A and B. Corrosion rates and total corrosion losses based on the total area of the steel and corrosion potentials are shown in Appendix A. The corrosion rates and total corrosion losses based on the exposed area of the steel can be obtained by multiplying the corrosion rates and losses by the appropriate ratios from Table 3.1. Appendix B shows the mat-to-mat resistances for the individual bench-scale and field tests.

In this report, the test results are compared at week 15 for the rapid macrocell test, at week 40 for the Southern Exposure and cracked beam tests, at week 60 for the ASTM G 109 test, and at week 32 for the field tests, respectively. Conventional steel and epoxy-coated reinforcement (ECR) are evaluated as control specimens, and their results are presented in Section 3.1. Section 3.2 presents the results for specimens with ECR with a primer containing calcium nitrite and ECR cast with corrosion inhibitors DCI-S, Rheocrete 222+, and Hycrete. The test results for the multiple coated reinforcement are described in Section 3.3. Section 3.4 presents the results of ECR with increased adhesion, including ECR with the zinc chromate pretreatment and the two types of ECR with improved adhesion epoxy produced by DuPont and Valspar. Section 3.5 gives the results of three types of ECR with increased adhesion cast in mortar or concrete with the corrosion inhibitor DCI-S. Section 3.6 provides the corrosion potential mapping results of the two bridges built with 2205 pickled stainless steel (DCB and MCB), as well as the test results of the accompanying bench-scale and field test specimens. Section 3.7 discusses the cathodic disbondment test results. The test results are summarized in Section 3.8.

3.1 CONVENTIONAL STEEL AND EPOXY-COATED REINFORCEMENT

This section presents the results of the rapid macrocell, bench-scale, and field tests for specimens with conventional steel and epoxy-coated reinforcement (ECR).

3.1.1 Rapid Macrocell Test

Both bare bar and mortar-wrapped specimens were used to evaluate conventional steel and ECR in 1.6 m ion NaCl and simulated concrete pore solution. A water-cement (*w/c*) ratio of 0.50 was used for the mortar-wrapped specimens. The tests included six tests each for conventional steel and ECR with four drilled holes, and three tests for ECR without holes in the as-delivered condition.

3.1.1.1 Bare Bar Specimens

The test results are presented in Figures 3.1 through 3.5 for the rapid macrocell test with bare bar specimens. The total corrosion losses at week 15 are summarized in Table 3.2.

Based on total area, conventional steel had the highest corrosion rate during the test period, with values as high as 43.0 μm/yr at day 5, as shown in Figure 3.1(a). Figure 3.1(b) shows that the corrosion rates exhibited by ECR with four drilled holes were below 1.6 μm/yr. Conventional ECR without holes did not show corrosion rates except at week 12, when a corrosion rate of 0.06 μm/yr occurred due to a jump in one of the three specimens. Based on exposed area, the average corrosion rates of ECR with four holes were much higher than those observed for conventional steel, with the highest value equal to 149 μm/yr at day 5, as shown in Figure 3.2.

The average total corrosion losses versus time are shown in Figures 3.3 and 3.4 and the results at week 15 are summarized in Table 3.2. Conventional steel exhibited the highest corrosion loss, 6.03 μm, followed by ECR with four holes at 0.34 μm

based on total area (5.6% of the total corrosion loss of conventional steel). ECR specimens without holes had a total corrosion loss of less than 0.005 μm, as indicated by the symbol β. These results demonstrate the high corrosion resistance provided by an undamaged epoxy coating. Based on exposed area, ECR with four holes had a total corrosion loss of 33.6 μm, 5.56 times the corrosion loss of conventional steel, indicating that very high corrosion activity can occur at localized areas.

Table 3.2 – Average corrosion losses (μm) at week 15 as measured in the macrocell test for bare bar specimens with conventional steel and ECR

Steel Designation[a]	Specimen						Average	Standard Deviation
	1	2	3	4	5	6		
Bare Bar Specimens								
Conv.	7.05	5.25	4.70	7.43	6.49	5.24	6.03	1.12
ECR	0.26	0.65	0.22	0.38	0.49	0.02	0.34	0.22
ECR*	25.62	64.89	21.53	38.07	49.40	1.81	33.55	22.22
ECR-no holes	0.000	β	0.000				β	β

[a] Conv. = conventional steel. ECR = conventional epoxy-coated reinforcement.
no holes = epoxy-coated bars without holes, otherwise four 3-mm ($^1/_8$-in.) diameter holes.

* Epoxy-coated bars, calculations based on exposed area of four 3-mm ($^1/_8$-in.) diameter holes.

β Corrosion loss (absolute value) less than 0.005 μm.

The average corrosion potentials of the anode and cathode with respect to a saturated calomel electrode are shown in Figure 3.5. According to ASTM C 876, corrosion potentials more negative than –0.275 V with respect to a saturated calomel electrode indicate active corrosion. At the anodes, conventional ECR with four holes had more negative corrosion potentials than conventional steel. Throughout the test period, the anode corrosion potentials remained more negative than –0.500 V for ECR with four holes, and between –0.350 and –0.500 V for conventional steel, indicating active corrosion. Both steels had cathode corrosion potentials more positive than –0.275 V, indicating that there was a low probability of corrosion. Because of the insulative properties of the epoxy coating, stable corrosion potentials at the anode and cathode were not obtained for conventional ECR without holes.

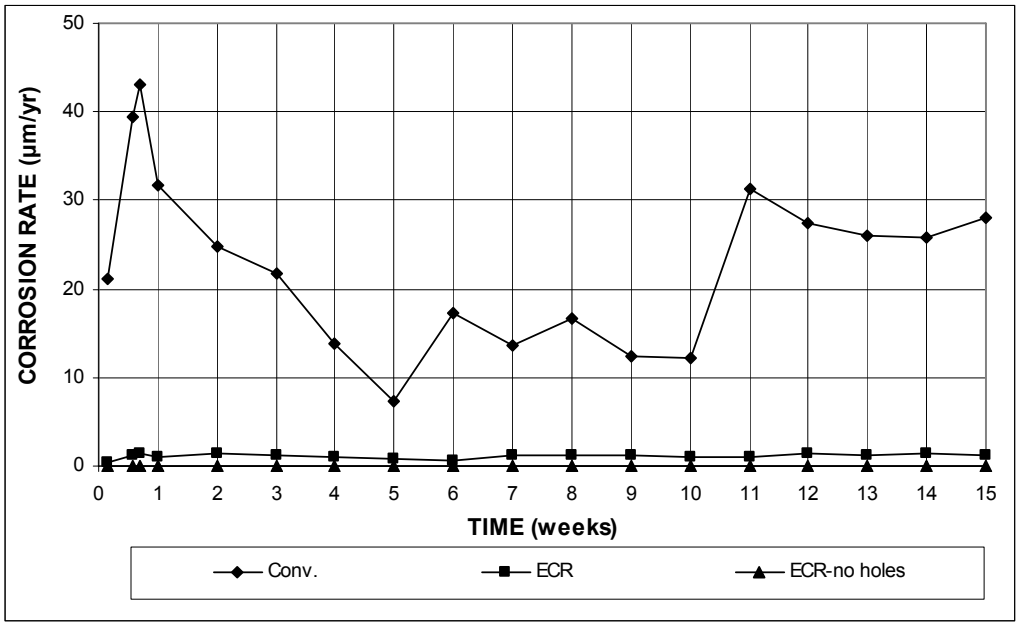

Figure 3.1 (a) – Average corrosion rates as measured in the rapid macrocell test for bare bar specimens with conventional steel and ECR (ECR bars have four holes).

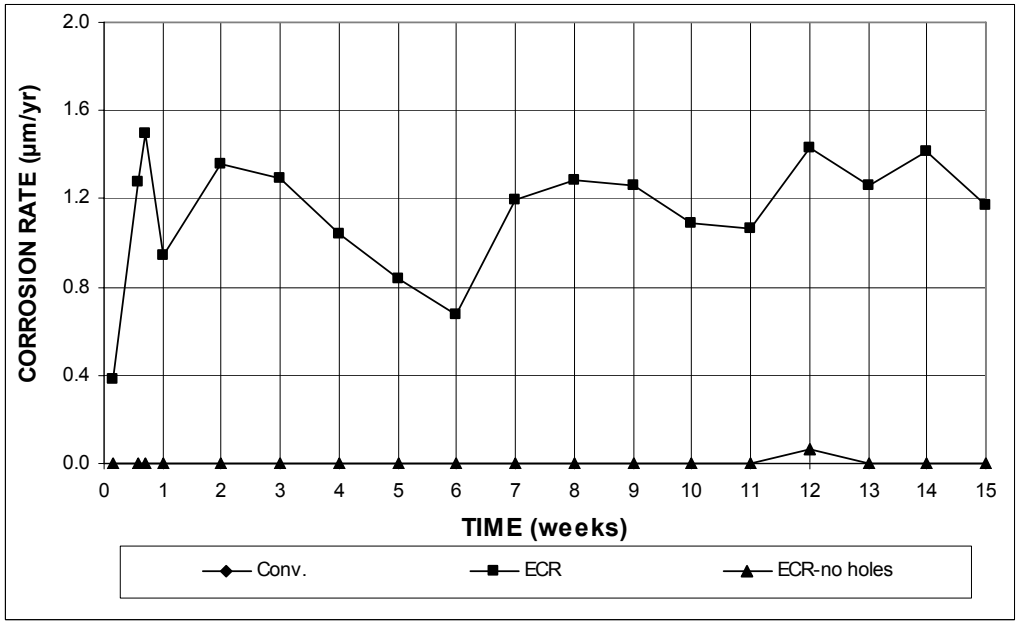

Figure 3.1 (b) – Average corrosion rates as measured in the rapid macrocell test for bare bar specimens with conventional steel and ECR (ECR bars have four holes).

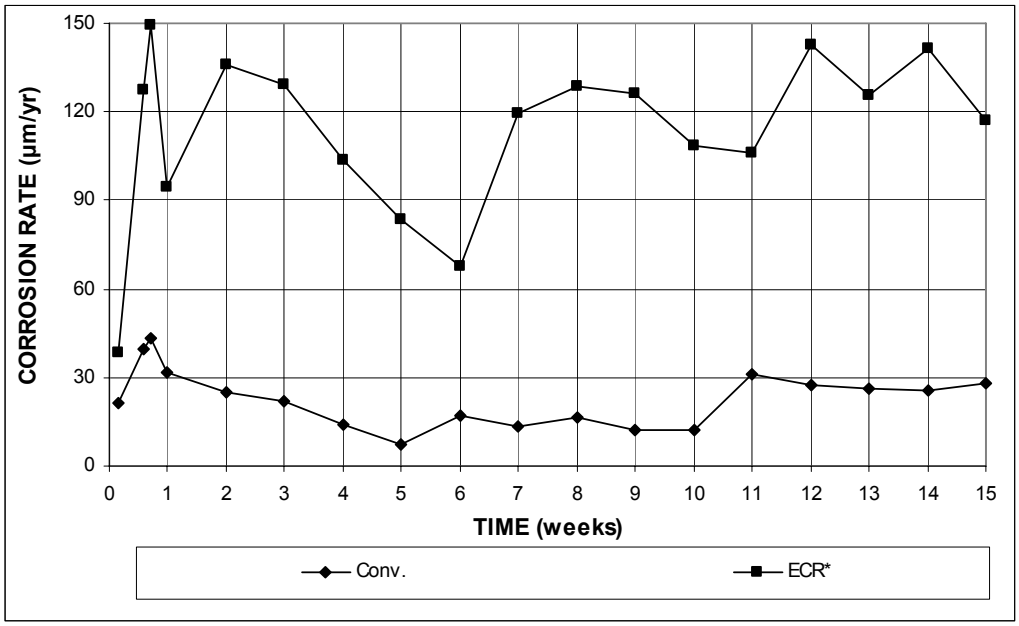

Figure 3.2 – Average corrosion rates as measured in the rapid macrocell test for bare bar specimens with conventional steel and ECR. * Based on exposed area (ECR bars have four holes).

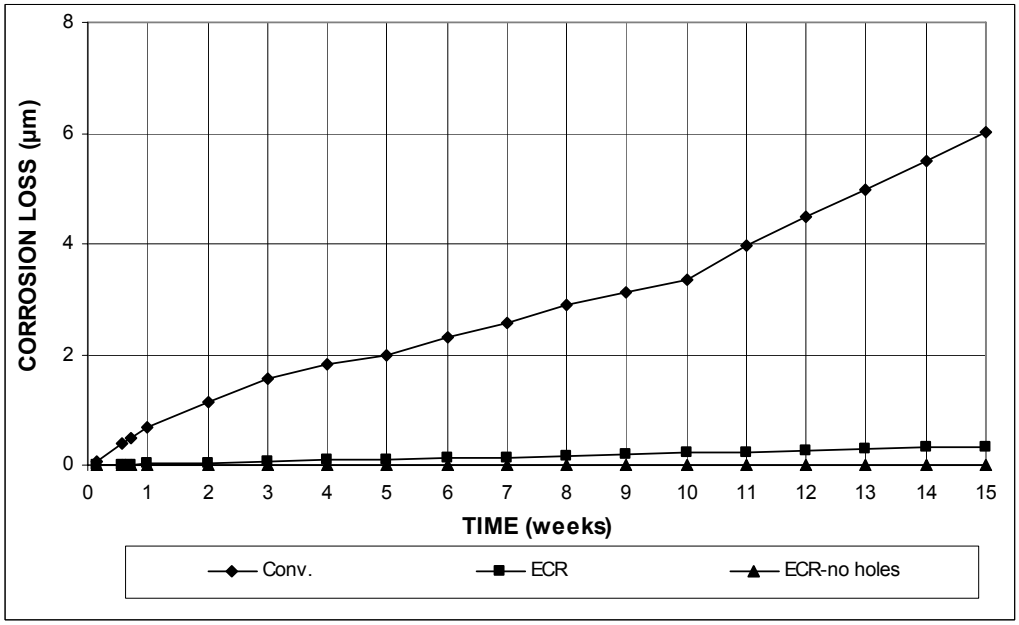

Figure 3.3 (a) – Average corrosion losses as measured in the rapid macrocell test for bare bar specimens with conventional steel and ECR (ECR bars have four holes).

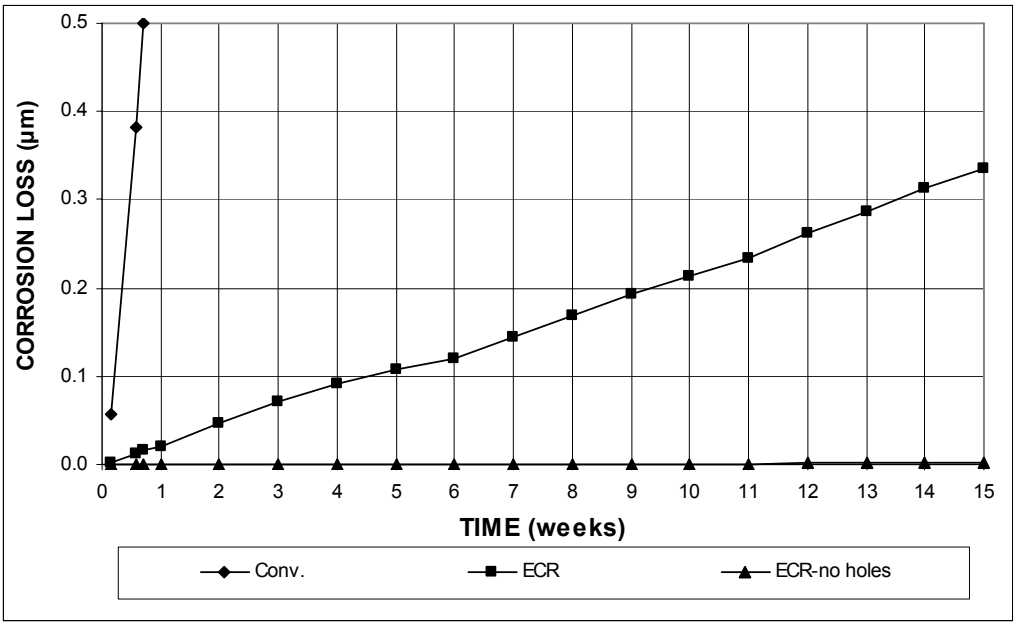

Figure 3.3 (b) – Average corrosion losses as measured in the rapid macrocell test for bare bar specimens with conventional steel and ECR (ECR bars have four holes).

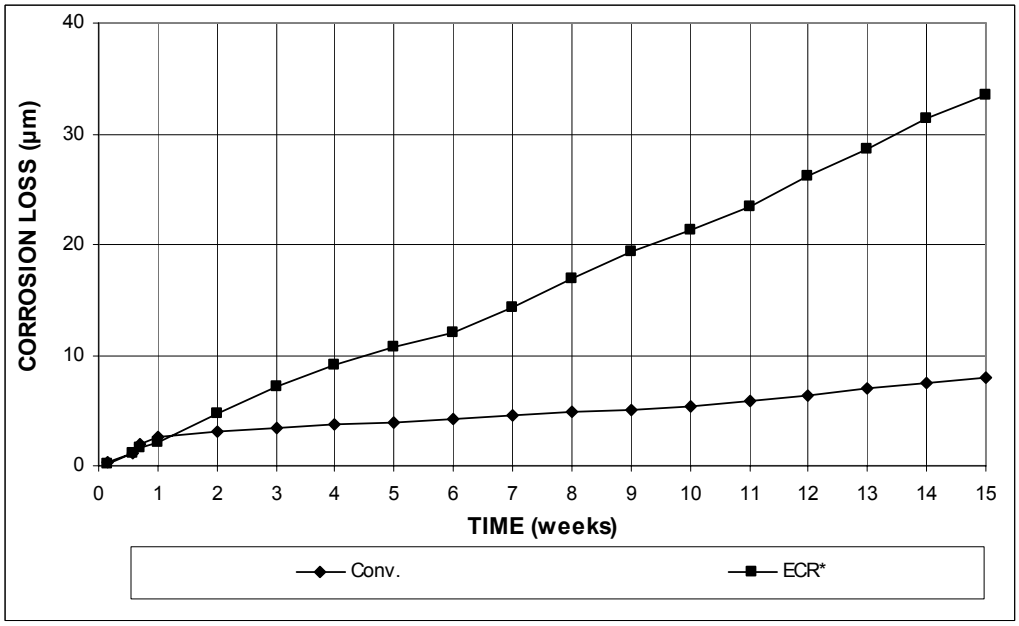

Figure 3.4 – Average corrosion losses as measured in the rapid macrocell test for bare bar specimens with conventional steel and ECR. * Based on exposed area (ECR bars have four holes).

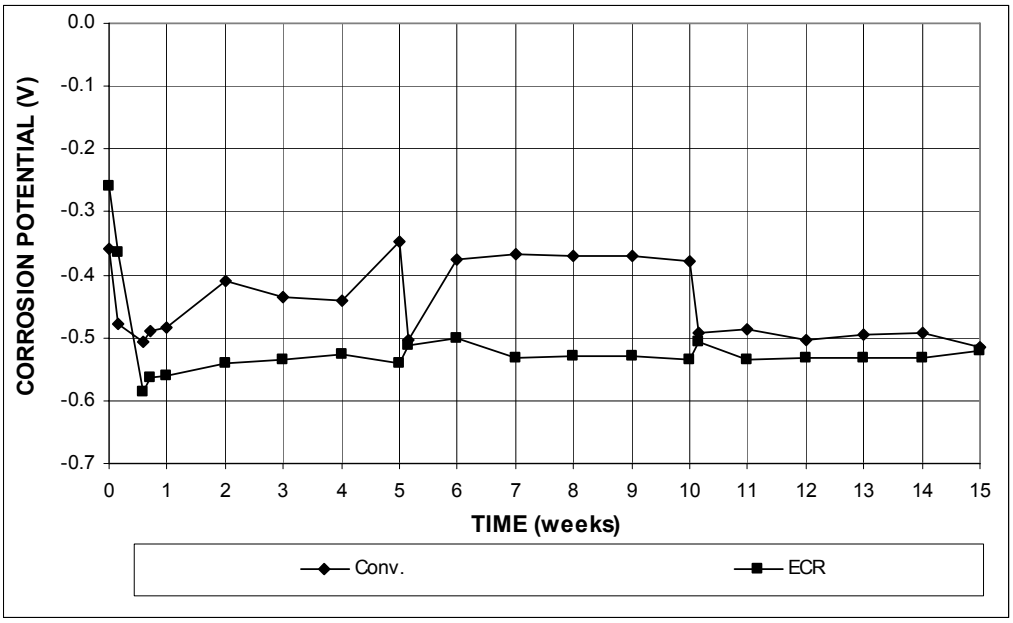

Figure 3.5 (a) – Average anode corrosion potentials, with respect to a saturated calomel electrode as measured in the rapid macrocell test for bare bar specimens with conventional steel and ECR (ECR bars have four holes).

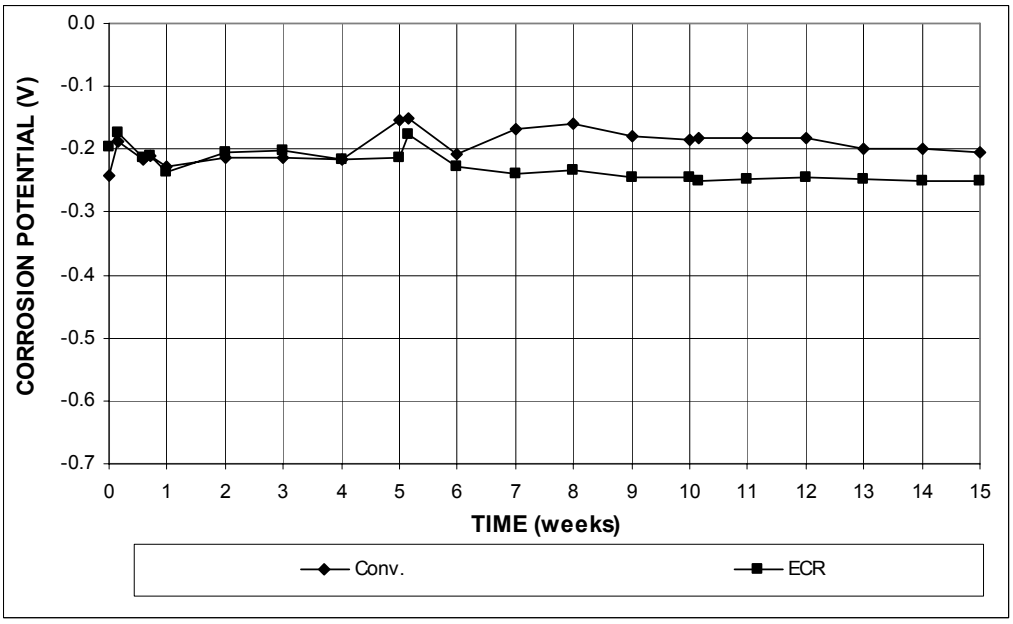

Figure 3.5 (b) – Average cathode corrosion potentials, with respect to a saturated calomel electrode as measured in the rapid macrocell test for bare bar specimens with conventional steel and ECR (ECR bars have four holes).

After the 15-week test period, the specimens were visually inspected for corrosion products. As shown in Figure 3.6, corrosion products were observed on conventional anode bars below the surface of the solution. For some bars, such as shown in Figure 3.7, corrosion products were formed at the surface of the solution between the bar and the plastic lid. Figure 3.8 shows an epoxy-coated anode bar with corrosion products formed at the drilled holes.

Figure 3.6 – Bare bar specimen. Conventional steel anode bar showing corrosion products that formed below the surface of the solution at week 15.

Figure 3.7 – Bare bar specimen. Conventional steel anode bar showing corrosion products that formed at the surface of the solution at week 15.

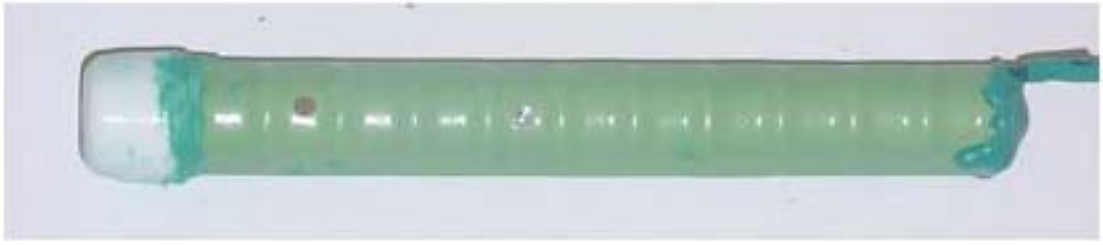

Figure 3.8 – Bare bar specimen. ECR anode bar showing corrosion products that formed at drilled holes at week 15.

3.1.1.2 Mortar-Wrapped Specimens

The test results for mortar-wrapped specimens are presented in Figures 3.9 through 3.13 for the rapid macrocell test. The total corrosion losses at week 15 are summarized in Tables 3.3.

As shown in Figure 3.9(a), conventional steel had the highest corrosion rates during the test period, with values above 11 μm/yr after week 2 and above 18 μm/yr after week 8. Figure 3.9(b) shows that conventional ECR with four holes did not show corrosion rates, except at week 9, when a corrosion rate of –0.03 μm/yr occurred. The negative corrosion rate at week 9 was caused by one of the three specimens, which had a corrosion rate of –0.18 μm/yr based on total area. This negative corrosion rate at week 9, however, was not accompanied by a more negative corrosion potential at cathode than at anode and in all likelihood is an aberrant reading. As shown in Figure 3.9(b), no corrosion activity was observed for conventional ECR without holes. Based on exposed area, conventional ECR with four holes did not show corrosion rates except at week 9 (–3.05 μm/yr based on the single specimen just discussed). The corrosion rates, based on exposed area, are shown in Figure 3.10.

The average total corrosion losses versus time are presented in Figures 3.11 and 3.12. Table 3.3 summarizes the total corrosion losses for these specimens at week 15. Conventional steel exhibited the highest total corrosion loss at week 15, 4.82 μm. Conventional ECR with four holes had a total corrosion loss (absolute value) of less than 0.005 μm based on total area and –0.06 μm based on exposed area, indicating that no corrosion occurred for the anode bars during the 15-week test period. This is in agreement with the corrosion potentials of the anode, which remained more positive than -0.275 V with respect to a saturated calomel electrode. No corrosion

activity was observed for conventional ECR without holes.

Table 3.3 – Average corrosion losses (μm) at week 15 as measured in the macrocell test for mortar-wrapped specimens with conventional steel and ECR

Steel Designation[a]	Specimen						Average	Standard Deviation
	1	2	3	4	5	6		
Mortar-wrapped Specimens								
Conv.	5.81	6.68	3.46	3.80	3.76	5.40	4.82	1.33
ECR	0.00	0.00	0.00	0.00	β	0.00	β	β
ECR*	0.00	0.00	0.00	0.00	-0.35	0.00	-0.06	0.14
ECR-no holes	0.00	0.00	0.00				0.00	0.00

[a] Conv. = conventional steel. ECR = conventional epoxy-coated reinforcement.
no holes = epoxy-coated bars without holes, otherwise four 3-mm ($^1/_8$-in.) diameter holes.

* Epoxy-coated bars, calculations based on exposed area of four 3-mm ($^1/_8$-in.) diameter holes.

β Corrosion loss (absolute value) less than 0.005 μm.

As shown in Tables 3.2 and 3.3, conventional steel had a total corrosion loss equal to 80% of the corrosion loss of the corresponding specimens without mortar. Conventional ECR with four holes had a total corrosion loss of 0.39 μm in the rapid macrocell test with bare bar specimens and showed no corrosion activity in the test with mortar-wrapped specimens. The reasons for the lack of corrosion activity for conventional ECR with four holes in the latter case include a lower concentration of chlorides at the anodes, additional passive protection provided by the cement hydration products, and a lower rate of diffusion of oxygen and moisture to the bars at the cathodes. In addition, a variation in the chloride content at the steel-mortar interface due to the non-homogeneous nature of chloride diffusion in mortar could result in a locally low chloride content at the exposed areas on ECR bar with holes. This point is supported by (1) the fact that both conventional ECR with four holes and ECR without holes did not show corrosion activity and (2) the corrosion potential measurements.

Figure 3.13 shows the average corrosion potentials of the anode and cathode

with respect to a saturated calomel electrode. At the anodes, conventional steel exhibited much more negative corrosion potentials than ECR with four holes. The anode corrosion potentials for conventional steel became more negative than –0.275 V during the first week, indicating active corrosion. The anode corrosion potentials continued to drop and then remained between –0.500 and –0.600 V after week 7. In contrast, ECR specimens with four holes had anode corrosion potentials that remained more positive than –0.275 V, indicating a low probability of corrosion. Conventional steel had cathode potentials more positive than –0.275 V, while ECR with four holes had cathode potentials above –0.200 V, indicating a passive condition. As discussed in Section 3.1.1.1, stable corrosion potentials of the anode and cathode were not available for ECR specimens without holes.

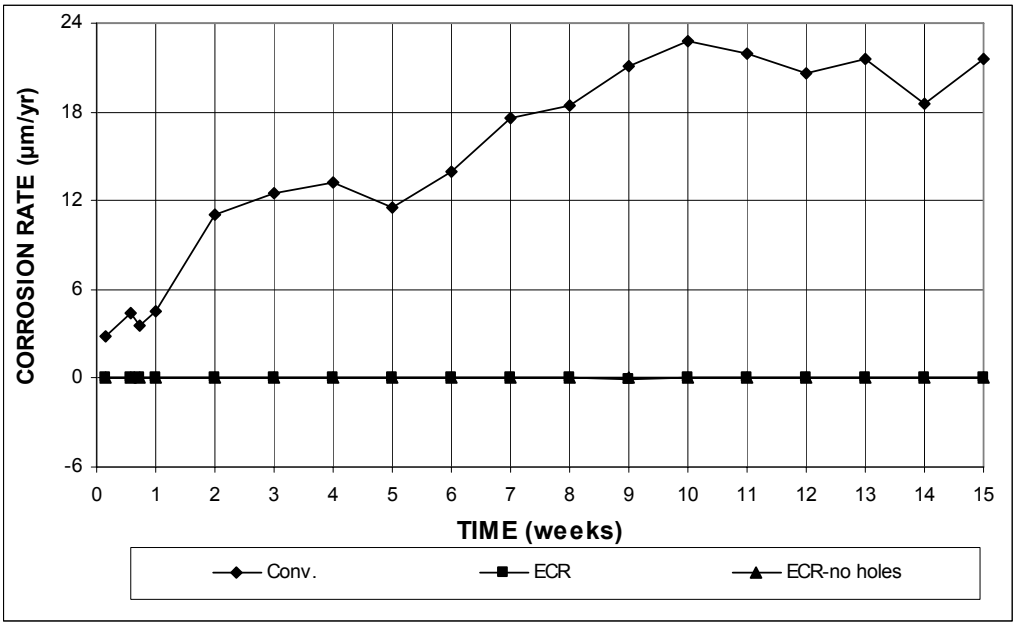

Figure 3.9 (a) – Average corrosion rates as measured in the rapid macrocell test for mortar-wrapped specimens with conventional steel and ECR (ECR bars have four holes).

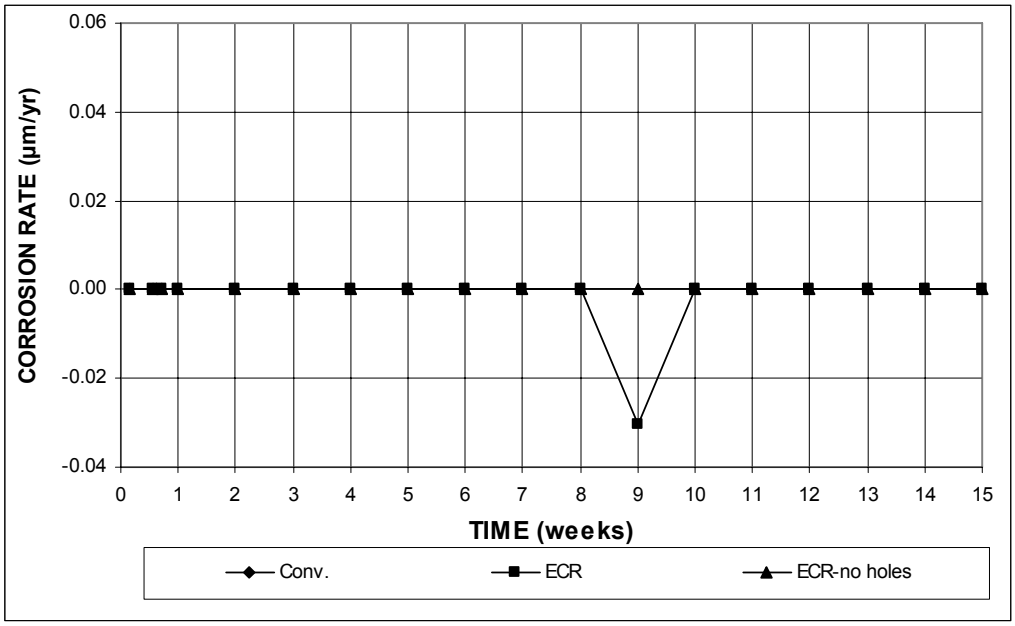

Figure 3.9 (b) – Average corrosion rates as measured in the rapid macrocell test for mortar-wrapped specimens with conventional steel and ECR (ECR bars have four holes).

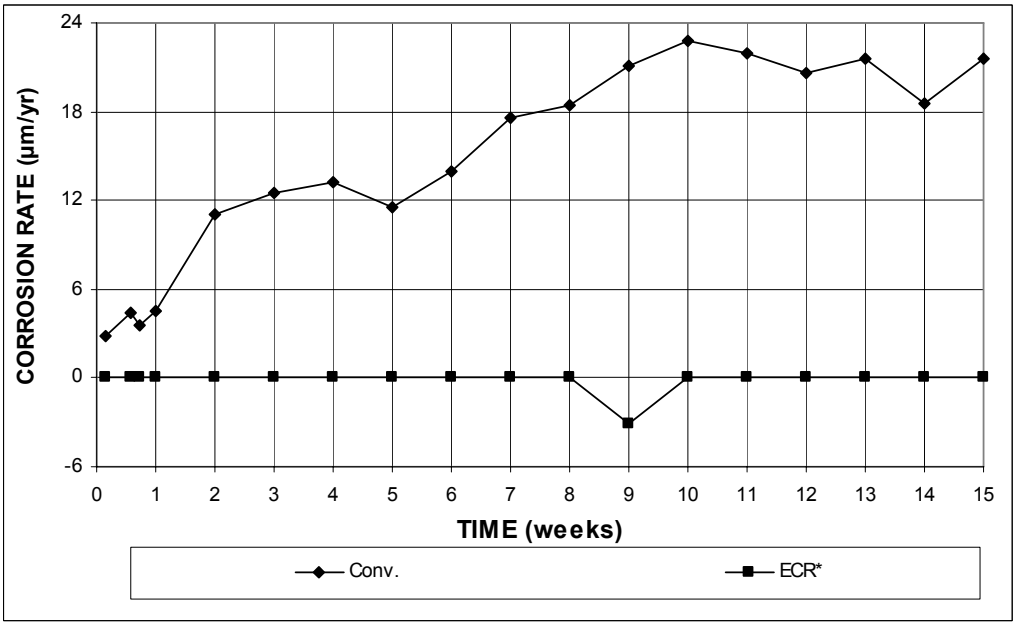

Figure 3.10 – Average corrosion rates as measured in the rapid macrocell test for mortar-wrapped specimens with conventional steel and ECR. * Based on exposed area (ECR bars have four holes).

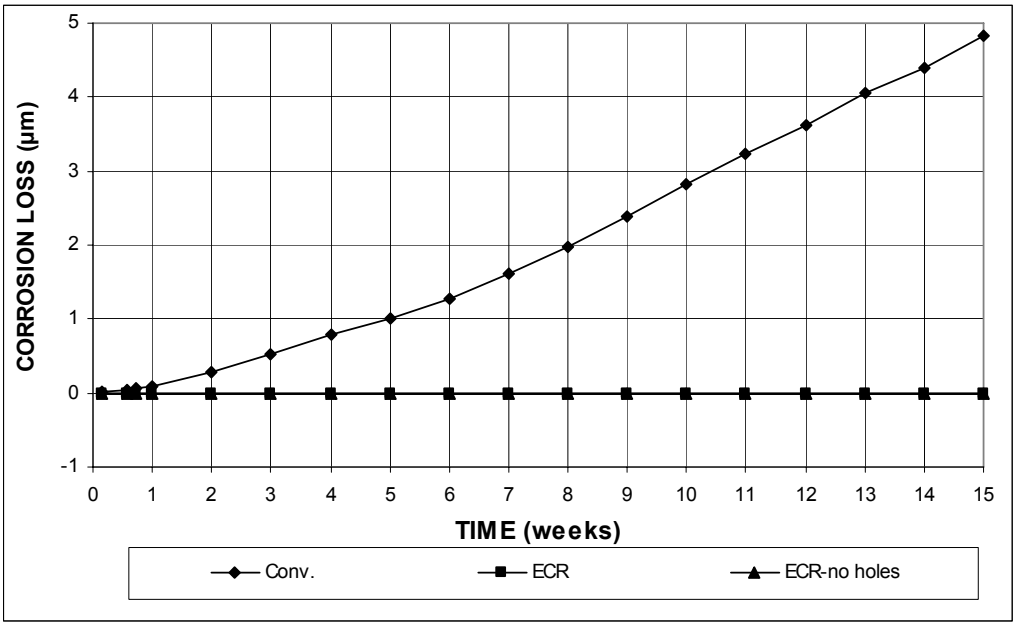

Figure 3.11 (a) – Average corrosion losses as measured in the rapid macrocell test for mortar-wrapped specimens with conventional steel and ECR (ECR bars have four holes).

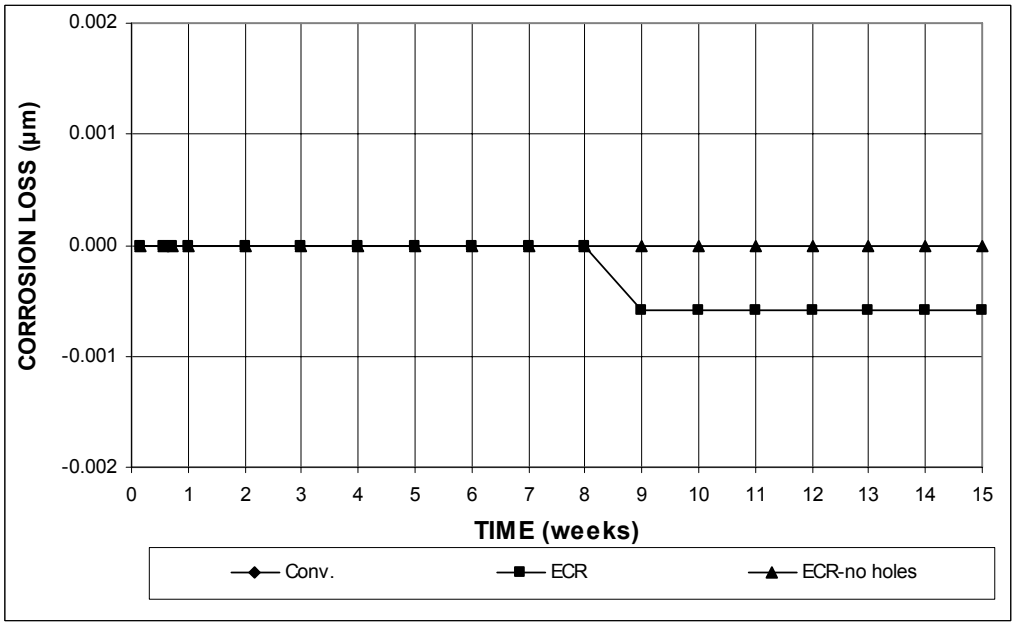

Figure 3.11 (b) – Average corrosion losses as measured in the rapid macrocell test for mortar-wrapped specimens with conventional steel and ECR (ECR bars have four holes).

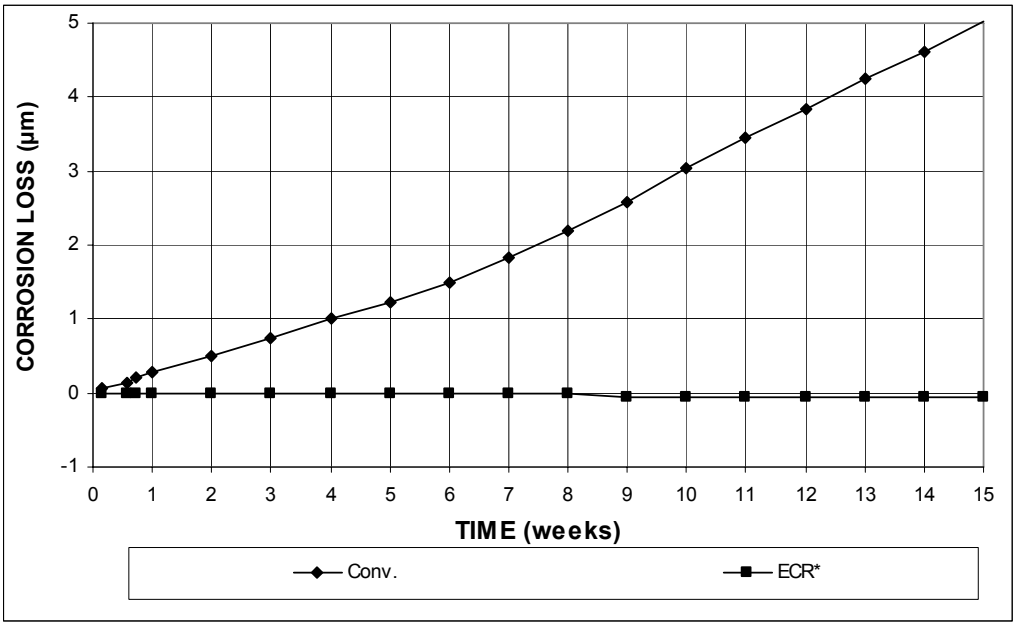

Figure 3.12 – Average corrosion losses as measured in the rapid macrocell test for mortar-wrapped specimens with conventional steel and ECR. * Based on exposed area (ECR bars have four holes).

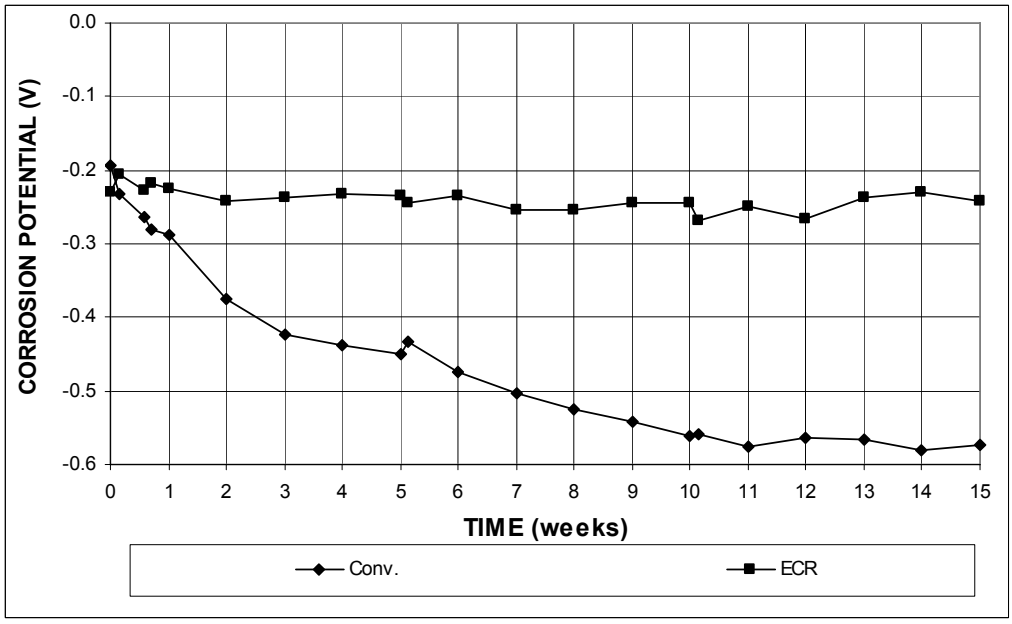

Figure 3.13 (a) – Average anode corrosion potentials, with respect to a saturated calomel electrode as measured in the rapid macrocell test for mortar-wrapped specimens with conventional steel and ECR (ECR bars have four holes).

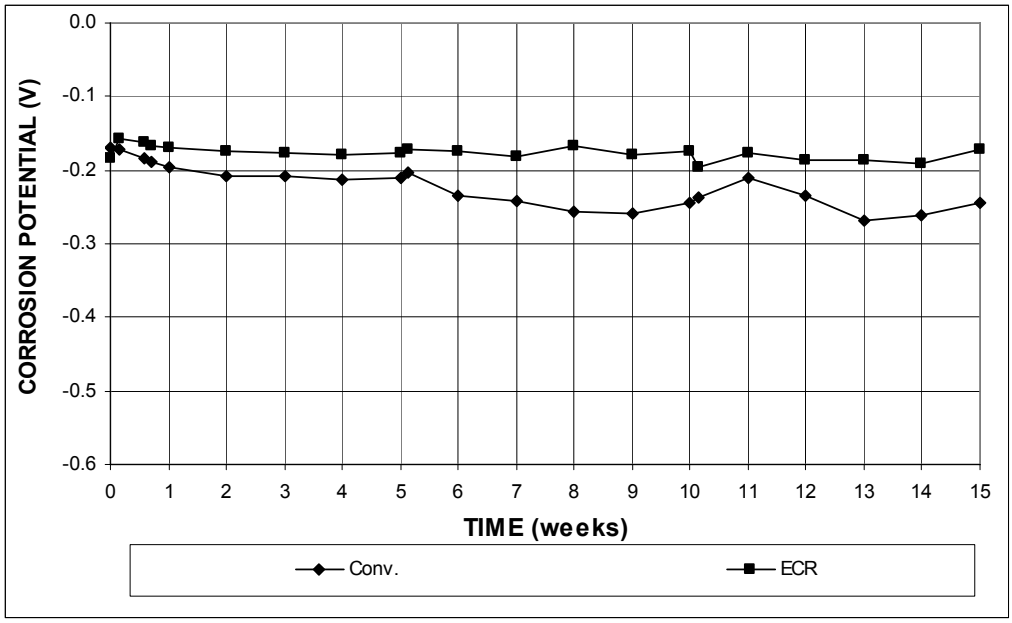

Figure 3.13 (b) – Average cathode corrosion potentials, with respect to a saturated calomel electrode as measured in the rapid macrocell test for mortar-wrapped specimens with conventional steel and ECR (ECR bars have four holes).

After 15 weeks, the mortar cover was removed and the specimens were visually inspected. Corrosion products were observed for conventional anode bars below the surface of the solution, as shown in Figure 3.14. No corrosion products were found on any of the mortar-wrapped specimens with ECR, in agreement with the anode corrosion potentials, which were more positive than –0.275 V.

Figure 3.14 – Mortar-wrapped specimen. Conventional steel anode bar showing corrosion products after removal of mortar cover at week 15.

3.1.2 Bench-Scale Tests

The Southern Exposure (SE), cracked beam (CB), and ASTM G 109 tests were used to evaluate conventional steel and ECR. The SE and CB tests included six tests each for conventional steel and ECR with four holes at a *w/c* ratio of 0.45, and three tests each for conventional steel at a *w/c* ratio of 0.35 and ECR with 10 holes at *w/c* ratios of 0.45 and 0.35. The ASTM G 109 test included six tests for conventional steel and three tests each for ECR with four and 10 holes at a *w/c* ratio of 0.45. The results are presented at week 40 for the SE and CB tests, and at week 60 for the ASTM G 109 test.

3.1.2.1 Southern Exposure Test

The test results are shown in Figures 3.15 through 3.20 and the total corrosion losses at week 40 are summarized in Table 3.4. It should be noted that the resistance meter was not functional for several weeks before the data cut-off date and, therefore, average mat-to-mat resistances are not reported for the same weeks as the corrosion rates, total corrosion losses, and corrosion potentials.

Figures 3.15 and 3.16 show the average corrosion rates for specimens with conventional steel and ECR. Conventional steel had the highest corrosion rates, with values as high as 2.00 μm/yr at week 72, followed by conventional steel with a *w/c* ratio of 0.35 (Conv.-35). Specimens with epoxy-coated reinforcement had the lowest average corrosion rates. Conventional steel started showing obvious corrosion at week 15, with an average corrosion rate of 0.08 μm/yr. Between weeks 18 and 22, conventional steel showed negative corrosion rates, with the highest value of –0.21 μm/yr at week 20. As shown in Figure A.37(a), four out of the six test specimens with conventional steel showed negative corrosion rates (specimen No. 3 between weeks

18 and 37, specimen No. 4 between weeks 18 and 23, and specimen No. 5 between weeks 20 and 49). These negative corrosion rates were all characterized by more negative corrosion potentials in the bottom mat than in the top mat of the steel. The corrosion rates then remained between 0.40 and 0.80 μm/yr between weeks 23 and 50, and between 0.80 and 2.00 μm/yr between weeks 50 and 74. As shown in Figure 3.15(a), Conv.-35 showed negative corrosion rates between weeks 19 and 35, with the most negative value equal to –0.09 μm/yr at week 23. As shown in Figure A.41(a), between weeks 19 and 38, one of the three conventional steel specimens with a *w*/*c* ratio of 0.35 exhibited negative corrosion rates, which were characterized by the more negative corrosion potentials in the bottom mat than in the top mat of the steel. Conv.-35 started showing observable corrosion around week 40 and after week 50 it showed similar corrosion rates to conventional steel, with a high corrosion rate of 1.50 μm/yr at week 59, as shown in Figure 3.15(a). As shown in Figures 3.15(b) and 3.16, all specimens with ECR exhibited similar corrosion rates, with values less than 0.03 μm/yr based on total area and less than 8 μm/yr based on exposed area. Negative corrosion rates were observed for conventional ECR (four holes) at weeks 60 and 61 and for conventional ECR with 10 holes (ECR-10h) at week 29, due to the negative corrosion rates in one of the six or three test specimens, as shown in Figures A.47(a) and A.51(a). These negative corrosion rates for these specimens, however, were not characterized by more negative corrosion potentials in the bottom mat than in the top mat.

Figures 3.17 and 3.18 show the average total corrosion losses for specimens with conventional steel and ECR. As shown in Figure 3.17(a), conventional steel had the highest total corrosion loss, followed by Conv.-35. Figure 3.17(a) also demonstrates the benefit of a lower w/c ratio of 0.35, which delayed the corrosion

initiation by about 25 weeks. As shown in Figure 3.17(b), Conv.-35 had negative total corrosion losses between weeks 26 and 40, with a most negative value of –0.005 μm (out of range on the plot). Figure 3.17(b) also shows that specimens with ECR had similar corrosion losses, with values less than 0.005 μm based on total area. Based on exposed area (Figure 3.18), conventional ECR with four holes showed the highest corrosion loss, followed by ECR-10h and ECR-10h-35, respectively.

Table 3.4 – Average corrosion losses (μm) at week 40 as measured in the Southern Exposure test for specimens with conventional steel and ECR

Steel Designation[a]	Specimen						Average	Standard Deviation
	1	2	3	4	5	6		
Southern Exposure Test								
Conv.	β	1.09	-0.08	0.15	-0.16	0.05	0.17	0.46
Conv.-35	β	-0.03	0.01				β	0.02
ECR	β	β	β	β	β	β	β	β
ECR*	0.77	1.20	1.55	0.53	2.07	2.25	1.40	0.69
ECR-10h	β	β	β				β	β
ECR-10h*	0.65	0.66	0.52				0.61	0.08
ECR-10h-35	β	β	β				β	β
ECR-10h-35*	0.51	0.60	0.38				0.50	0.11

[a] Conv. = conventional steel. ECR = conventionl epoxy-coated reinforcement.
10h = epoxy-coated bars with 10 holes, otherwise four 3-mm ($^1/_8$-in.) diameter holes.
35 = concrete *w/c* =0.35, otherwise *w/c* = 0.45.

* Epoxy-coated bars, calculations based on exposed area of four or 10 3-mm ($^1/_8$-in.) diameter holes.

β Corrosion loss (absolute value) less than 0.005 μm.

Table 3.4 summarizes the average total corrosion losses at week 40, the shortest duration of any of the bench-scale tests described in this report. Conventional steel had the highest corrosion loss, 0.17 μm, and Conv.-35 had a negative total corrosion loss of –0.003 μm. As shown in Figure 3.17(a), however, the total corrosion loss for Conv.-35 showed a rapid increase after week 40. By week 63, Conv.-35 had an average corrosion loss of 0.27 μm, equal to 45% of that observed for conventional steel (0.60 μm at week 63). Based on total area, all specimens with ECR had total corrosion losses of less than 0.005 μm, as indicated by the symbol β in Table 3.4.

Based on exposed area, ECR had the highest corrosion loss, 1.40 μm, followed by ECR-10h and ECR-10h-35 at 0.61 and 0.50 μm, respectively, as shown in Table 3.4. The ECR-10h-35 specimens had a total corrosion loss equal to 82% of the value for conventional ECR cast in concrete with a *w*/*c* ratio of 0.45 and 10 holes.

The average corrosion potentials of the top and bottom mats of steel with respect to a copper-copper sulfate electrode are shown in Figure 3.19. According to ASTM C 876, corrosion potentials below –0.350 V with respect to a copper-copper sulfate electrode indicate active corrosion. The top mat corrosion potentials dropped to values more negative than –0.350 V at week 42 for conventional steel, at week 49 for ECR-10h, and at week 52 for Conv.-35, respectively. ECR specimens with four holes had average top mat corrosion potentials above –0.275 V except at week 70, when the potential dropped to –0.320 V, rebounding to –0.200 V the following week. The top mat corrosion potentials for ECR-10h-35 remained above –0.214 V, indicating a low probability of corrosion. The average corrosion potentials of the bottom mat steel remained more positive than –0.350 V for all specimens, with the exception of ECR-10h, which exhibited active corrosion after week 56.

Figure 3.20 shows that the average mat-to-mat resistances increased with time for specimens with conventional steel and ECR, primarily due to the formation of corrosion products on the surface of the bars. Conventional steel had the lowest mat-to-mat resistance, with values below 600 ohms. For specimens with epoxy-coated reinforcement, ECR with four holes showed the highest mat-to-mat resistance, followed by ECR-10h and ECR-10h-35, respectively. The average mat-to-mat resistance started around 1,980 ohms for ECR, and remained around 10,000 ohms after week 40. ECR-10h and ECR-10h-35 had mat-to-mat resistances of approximately 800 ohms at the beginning of the test, and showed similar values as the

test progressed. The mat-to-mat resistances were around 4,500 ohms for ECR-10h at week 62 and 4,300 ohms for ECR-10h-35 at week 59, respectively. The resistance difference between ECR with four and 10 holes can be attributed to the fact that the exposed area of the steel for ECR with 10 holes is 2.5 times that for ECR with four holes.

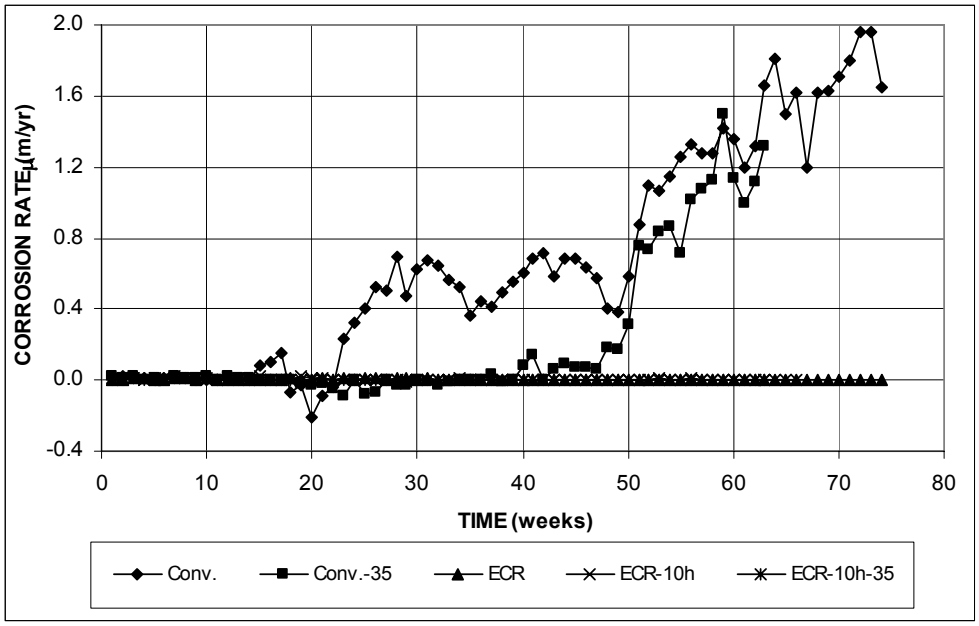

Figure 3.15 (a) – Average corrosion rates as measured in the Southern Exposure test for specimens with conventional steel and ECR (ECR have four holes and ECR-10h have 10 holes).

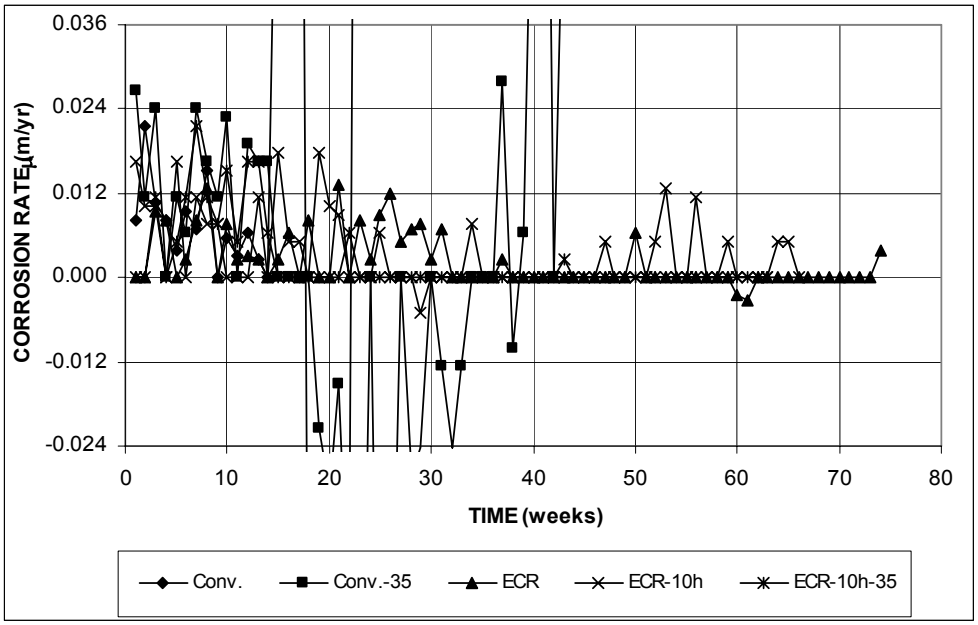

Figure 3.15 (b) – Average corrosion rates as measured in the Southern Exposure test for specimens with conventional steel and ECR (ECR have four holes and ECR-10h have 10 holes).

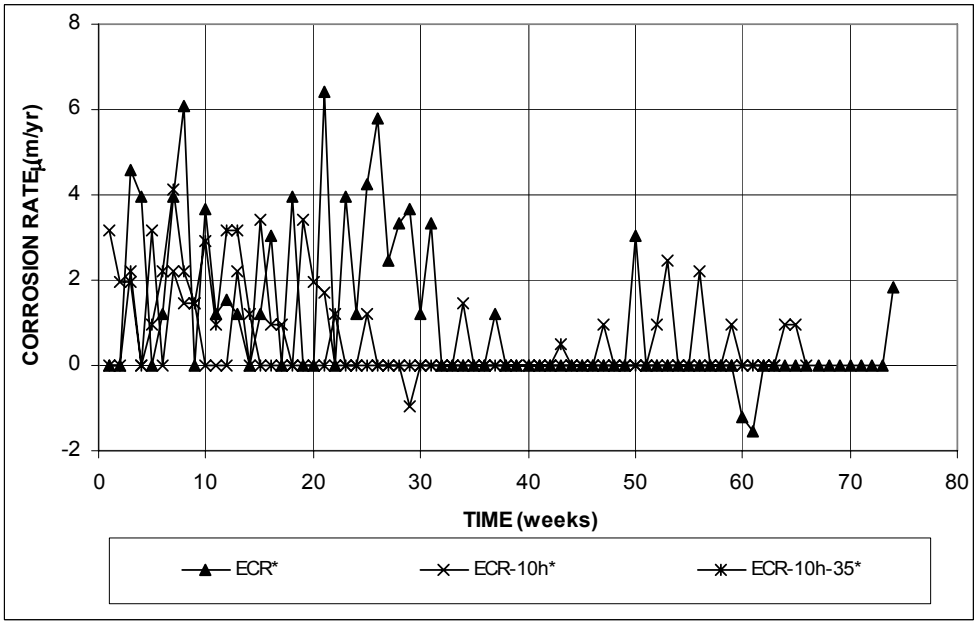

Figure 3.16 – Average corrosion rates as measured in the Southern Exposure test for specimens with ECR. * Based on exposed area (ECR have four holes and ECR-10h have 10 holes).

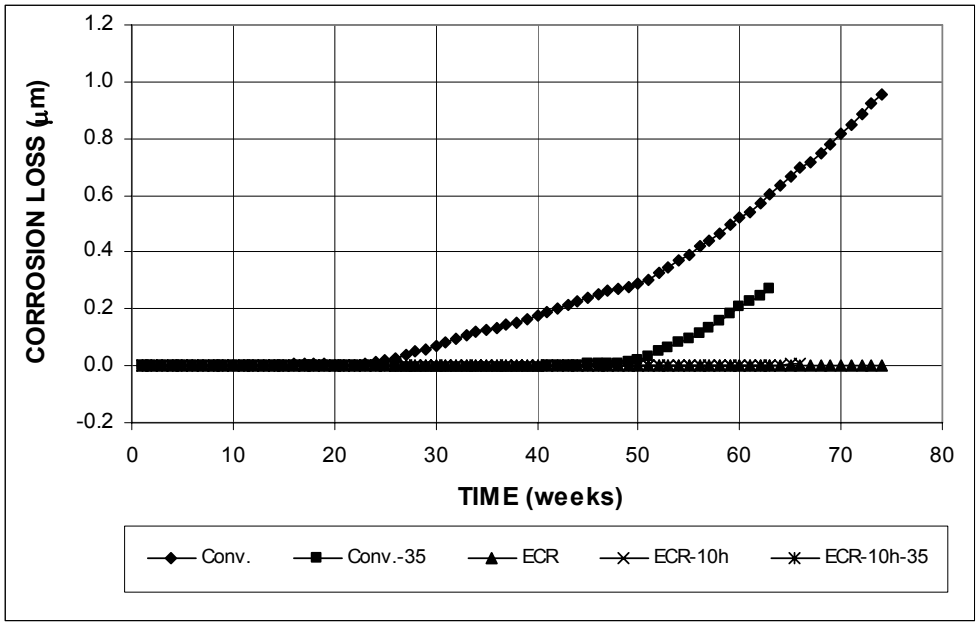

Figure 3.17 (a) – Average corrosion losses as measured in the Southern Exposure test for specimens with conventional steel and ECR (ECR have four holes and ECR-10h have 10 holes).

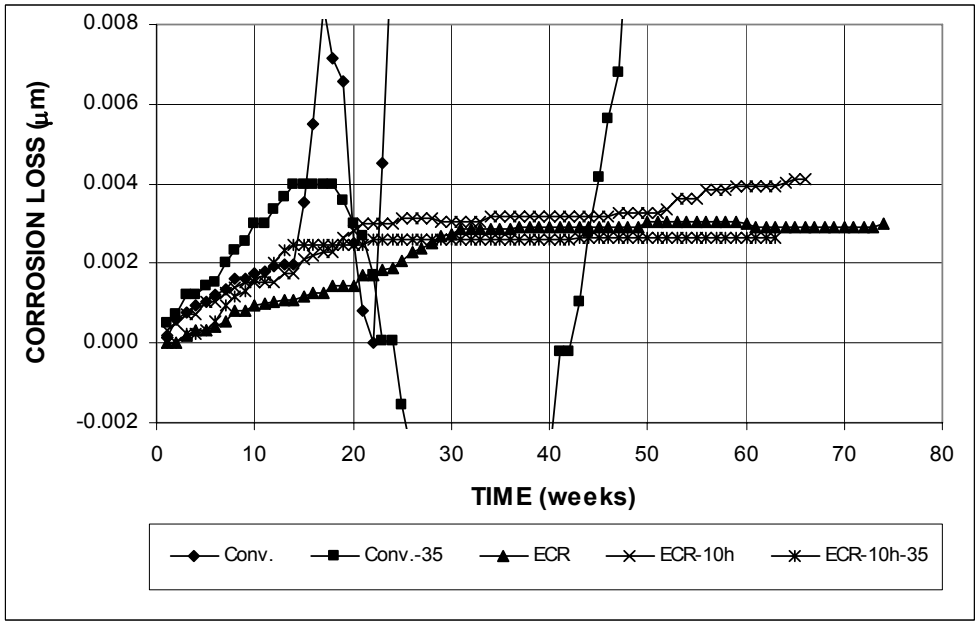

Figure 3.17 (b) – Average corrosion losses as measured in the Southern Exposure test for specimens with conventional steel and ECR (ECR have four holes and ECR-10h have 10 holes).

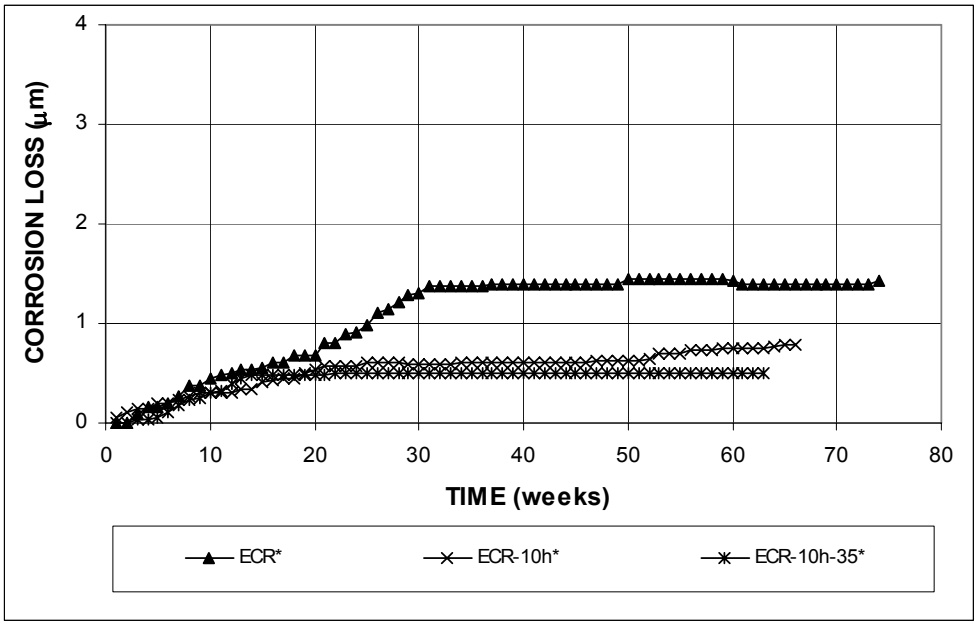

Figure 3.18 – Average corrosion losses as measured in the Southern Exposure test for specimens with ECR. * Based on exposed area (ECR have four holes and ECR-10h have 10 holes).

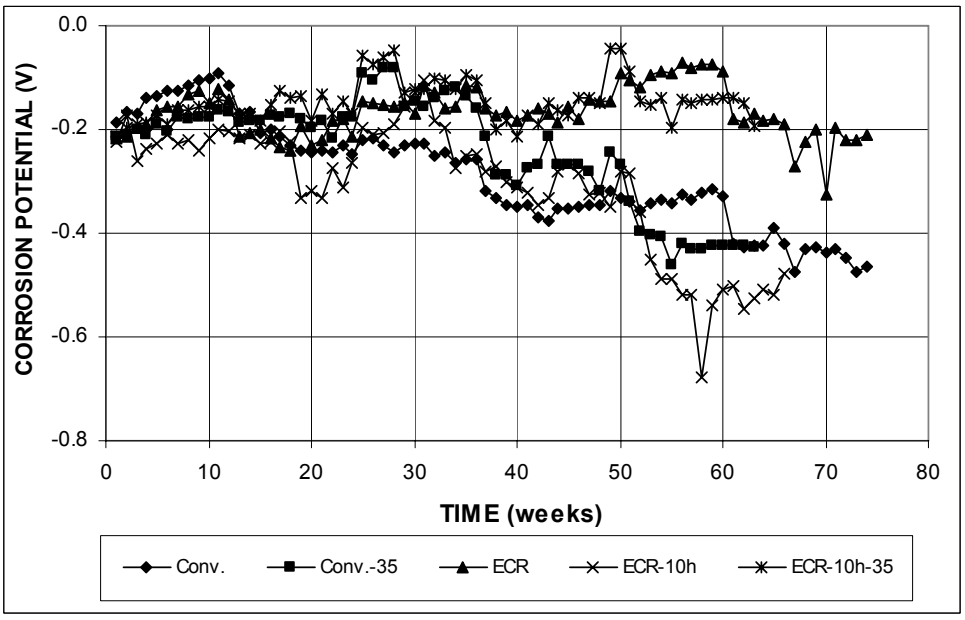

Figure 3.19 (a) – Average top mat corrosion potentials, with respect to a copper-copper sulfate electrode as measured in the Southern Exposure test for specimens with conventional steel and ECR (ECR have four holes and ECR-10h have 10 holes).

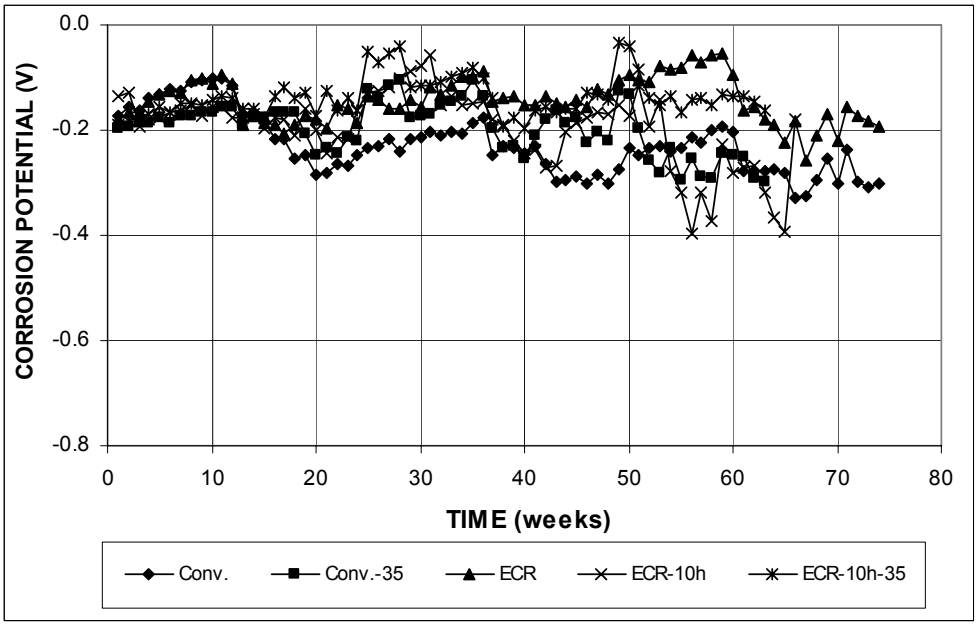

Figure 3.19 (b) – Average bottom mat corrosion potentials, with respect to a copper-copper sulfate electrode as measured in the Southern Exposure test for specimens with conventional steel and ECR (ECR have four holes and ECR-10h have 10 holes).

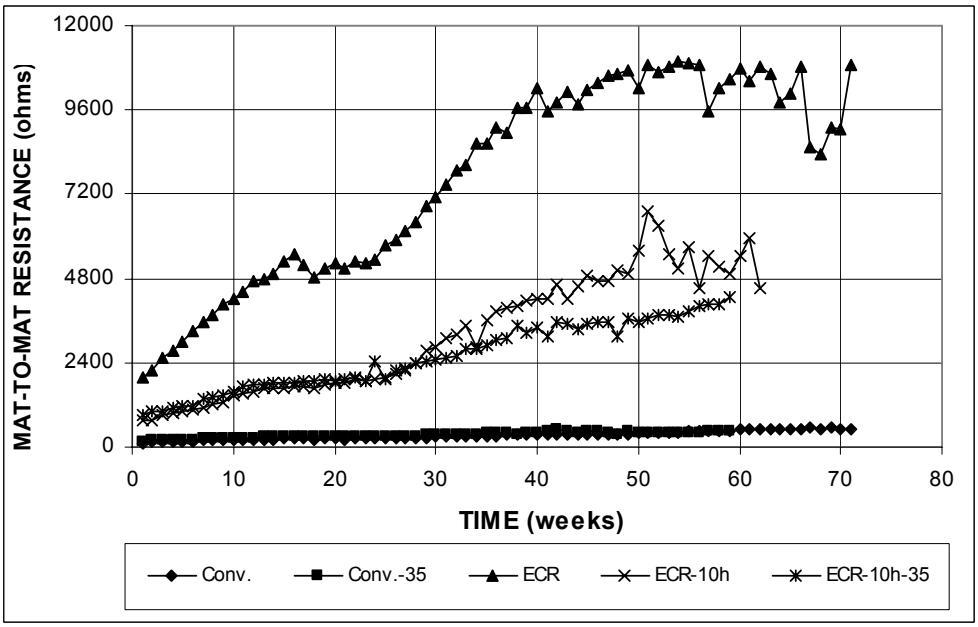

Figure 3.20 – Average mat-to-mat resistances as measured in the Southern Exposure test for specimens with conventional steel and ECR (ECR have four holes and ECR-10h have 10 holes).

3.1.2.2 Cracked Beam Test

The test results for the cracked beam tests are shown in Figures 3.21 through 3.26. The total corrosion losses at week 40 are summarized in Table 3.5.

Figures 3.21 and 3.22 show the average corrosion rates for specimens with conventional steel and ECR. Conventional steel had the highest corrosion rates, followed by Conv.-35, as shown in Figure 3.21(a). Conventional steel had corrosion rates above 9 μm/yr during the first five weeks and then remained between 3 and 9 μm/yr. Conv.-35 had corrosion rates above 6 μm/yr for the first six weeks and then stayed between 2 and 6 μm/yr. As discussed by Balma et al. (2005), high corrosion rates during the initial weeks are observed for conventional steel because the cracks in the specimens provide a direct path for the chlorides to the steel. The formation of corrosion products can seal the crack and limit the ingress of chlorides and oxygen, in turn slowing the rate of corrosion with time. For specimens with epoxy-coated reinforcement, ECR-10h-35 generally showed the highest corrosion rates based on total area, with values as high as 0.27 μm/yr at week 5. ECR and ECR-10h had average corrosion rates less than 0.15 μm/yr based on total area, as shown in Figure 3.21(b). Figure 3.22 shows that all specimens with epoxy-coated reinforcement had similar corrosion rates based on exposed area.

Table 3.5 – Average corrosion losses (μm) at week 40 as measured in the cracked beam test for specimens with conventional steel and ECR

Steel Designation[a]	Specimen						Average	Standard Deviation
	1	2	3	4	5	6		
Ceacked Beam Test								
Conv.	8.19	4.19	4.49	6.15	4.93	3.41	5.23	1.71
Conv.-35	4.28	2.10	2.91				3.10	1.10
ECR	0.03	0.03	0.01	0.04	0.03	0.01	0.02	0.01
ECR*	12.52	12.45	5.56	19.98	12.94	4.85	11.38	5.57
ECR-10h	0.02	0.05	0.03				0.03	0.02
ECR-10h*	4.19	9.96	5.26				6.47	3.07
ECR-10h-35	0.07	0.08	0.08				0.08	0.01
ECR-10h-35*	13.05	14.88	15.70				14.55	1.35

[a] Conv. = conventional steel. ECR = conventional epoxy-coated reinforcement.
10h = epoxy-coated bars with 10 holes, otherwise four 3-mm ($^1/_8$-in.) diameter holes.
35 = concrete w/c =0.35, otherwise w/c = 0.45.

* Epoxy-coated bars, calculations based on exposed area of four or 10 3-mm ($^1/_8$-in.) diameter holes.

Figures 3.23 and 3.24 show the average total corrosion losses for specimens with conventional steel and ECR. As shown in Figure 3.23(a), conventional steel had the highest total corrosion losses, followed by Conv.-35. The low corrosion losses for Conv.-35 are presumably due to reduced access of oxygen and moisture to the lower bars, which serve as the cathode, due to the lower *w/c* ratio. Figure 3.23(b) shows that among all specimens with epoxy-coated reinforcement, ECR-10h-35 had the highest corrosion loss, followed by ECR-10h and ECR with four holes, respectively. Based on exposed area, ECR-10h-35 had the highest total corrosion losses, and ECR-10h had the lowest corrosion losses. The average total corrosion losses at week 40 are summarized in Table 3.5. Conventional steel had the highest corrosion loss, 5.23 μm, followed by Conv.-35 at 3.10 μm, equal to 59% of the corrosion loss of conventional steel. Among specimens with epoxy-coated reinforcement, ECR-10h-35 showed the highest corrosion loss of 0.08 μm, followed by ECR-10h and ECR with four holes at 0.03 and 0.02 μm, respectively. These values are equal to less than 3% of the total corrosion loss of conventional steel. Based on exposed area, the total corrosion losses at 40 weeks were 11.4, 6.47, and 14.6 μm for ECR with four holes, ECR-10h, and

ECR-10h-35, respectively. At the low corrosion currents observed for the epoxy-coated bar specimens, the impact of the low *w/c* ratio is not observable as it is for the conventional steel specimens.

The average corrosion potentials of the top mat and bottom mats of steel with respect to a copper-copper sulfate electrode are shown in Figure 3.25. Conventional steel with *w/c* ratios of 0.45 and 0.35 had corrosion potentials of the top mat more negative than –0.500 V in the first week and then remained between –0.450 V and –0.670 V, indicating active corrosion. ECR specimens had corrosion potentials of the top mat around –0.200 V at the beginning of the test, dropping to values between –0.400 and –0.700 V after week 4. In the bottom mat, conventional steel showed corrosion potentials of the bottom mat more negative than –0.400 V after week 61, indicating that chlorides had reached the reinforcing bars in the bottom mat. The corrosion potentials of the bottom mat for ECR-10h-35 remained above –0.270 V, indicating a low probability of corrosion. Conventional ECR with four and 10 holes at a *w/c* ratio of 0.45 occasionally exhibited bottom mat corrosion potentials below –0.350 V.

Figure 3.26 shows that the average mat-to-mat resistances increased with time for specimens with conventional steel and ECR. Specimens with conventional steel had the lowest mat-to-mat resistances, with values below 1,800 ohms. ECR showed the highest mat-to-mat resistance during the first 45 weeks, and after that, it showed similar mat-to-mat resistances to ECR specimens with 10 holes, with values between 8,000 and 18,000 ohms. ECR-10h and ECR-10h-35 showed similar mat-to-mat resistances to each other.

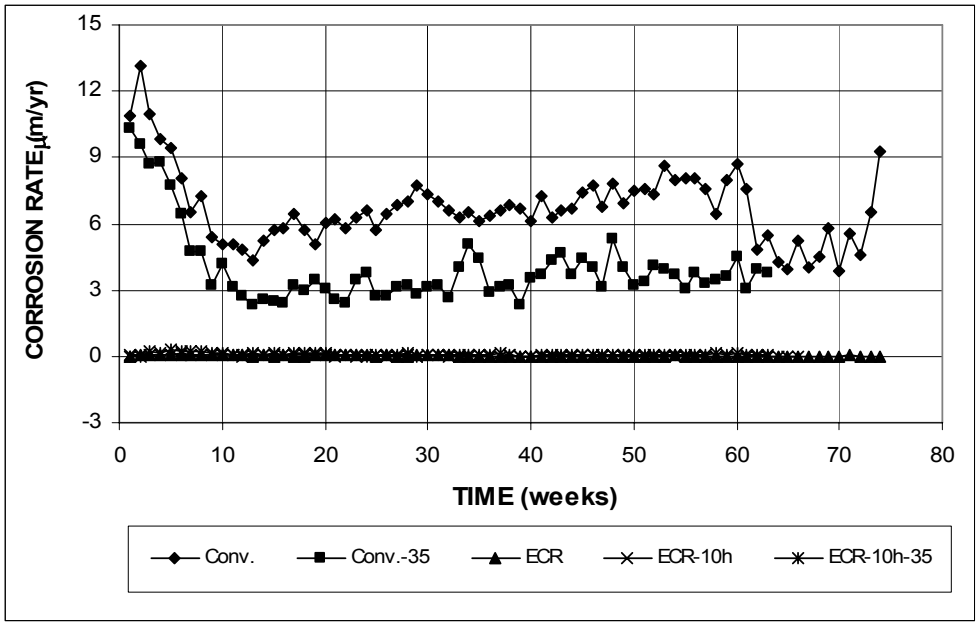

Figure 3.21 (a) – Average corrosion rates as measured in the cracked beam test for specimens with conventional steel and ECR (ECR have four holes and ECR-10h have 10 holes).

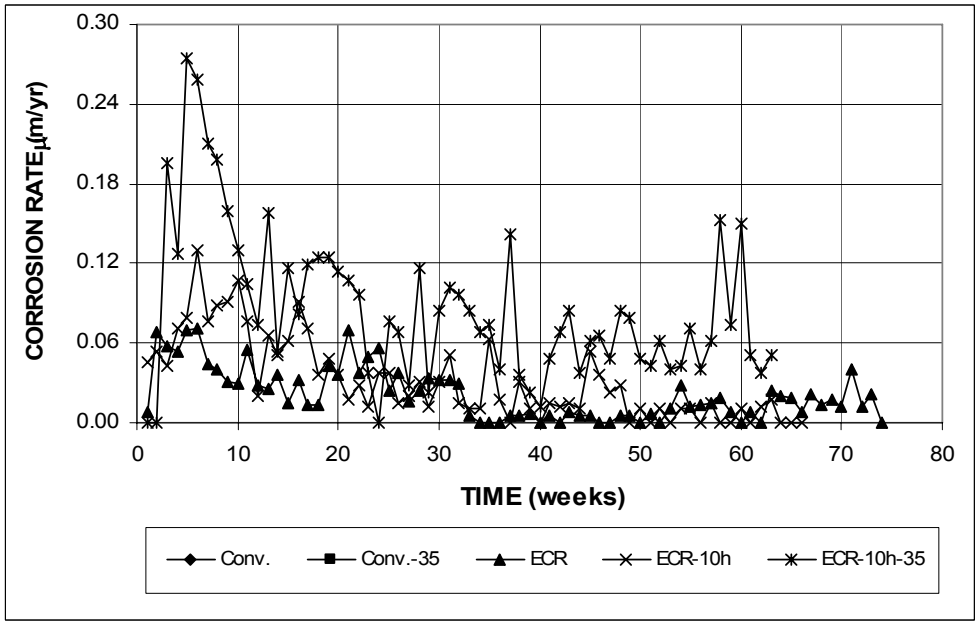

Figure 3.21 (b) – Average corrosion rates as measured in the cracked beam test for specimens with conventional steel and ECR (ECR have four holes and ECR-10h have 10 holes).

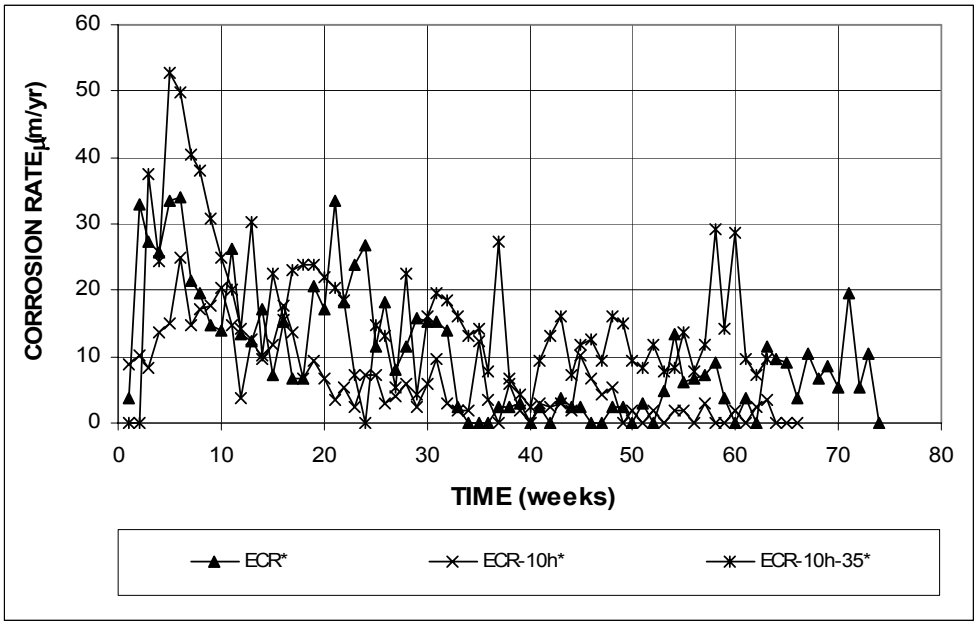

Figure 3.22 – Average corrosion rates as measured in the cracked beam test for specimens with conventional steel and ECR. * Based on exposed area (ECR have four holes and ECR-10h have 10 holes).

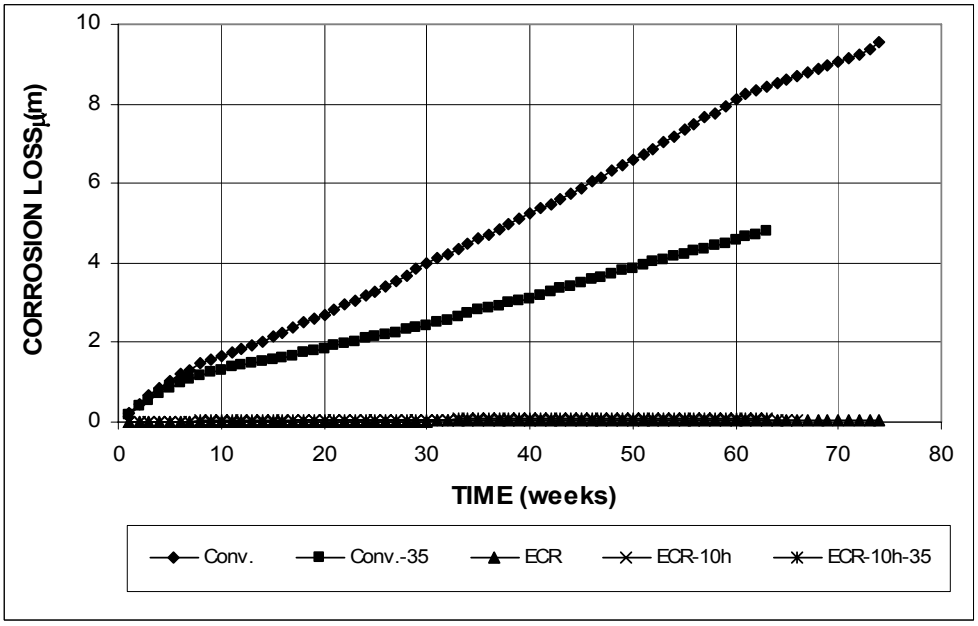

Figure 3.23 (a) – Average corrosion losses as measured in the cracked beam test for specimens with conventional steel and ECR (ECR have four holes and ECR-10h have 10 holes).

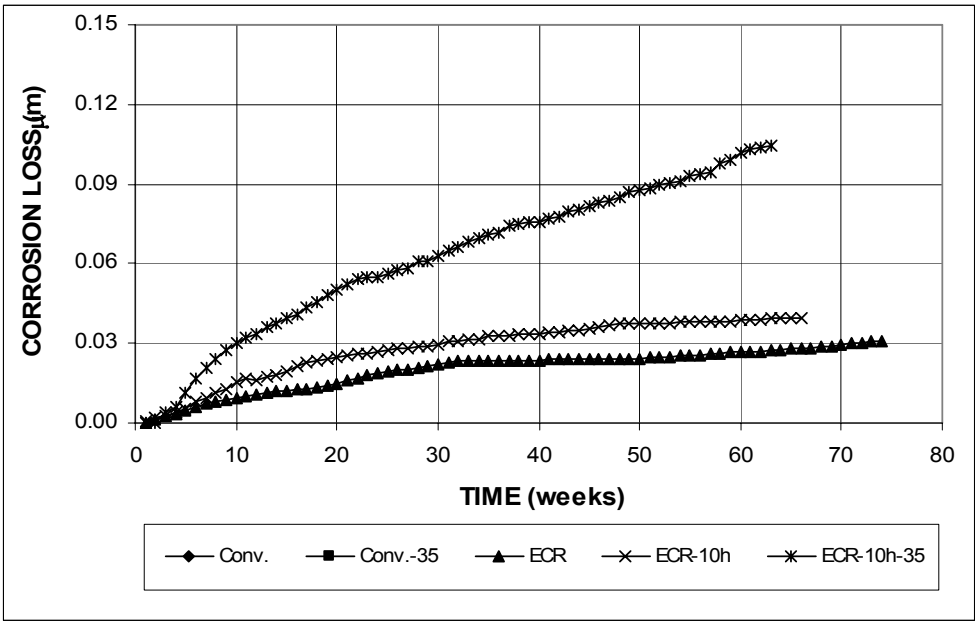

Figure 3.23 (b) – Average corrosion losses as measured in the cracked beam test for specimens with conventional steel and ECR (ECR have four holes and ECR-10h have 10 holes).

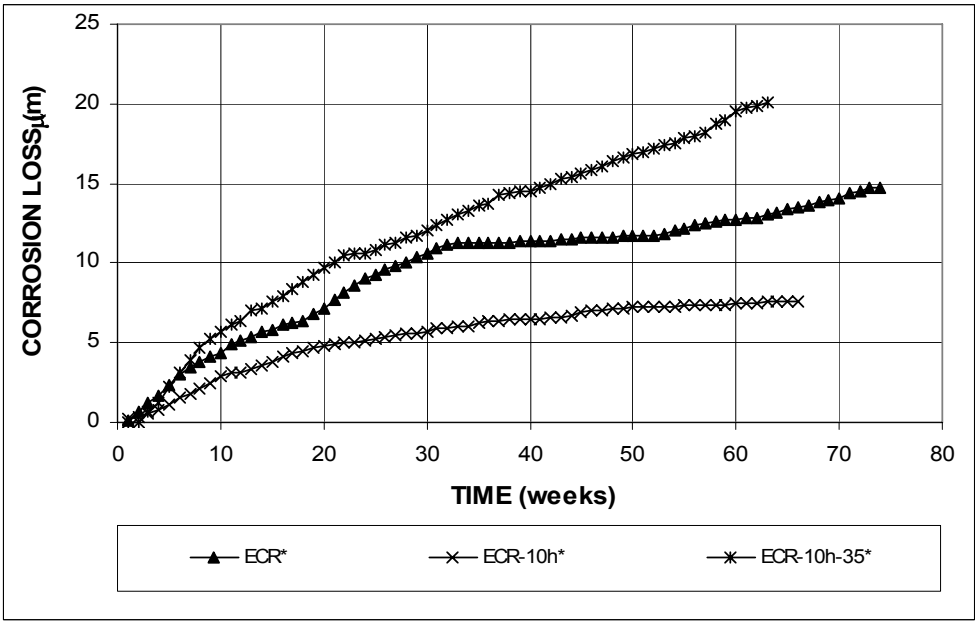

Figure 3.24 – Average corrosion losses as measured in the cracked beam test for specimens with conventional steel and ECR. * Based on exposed area (ECR have four holes and ECR-10h have 10 holes).

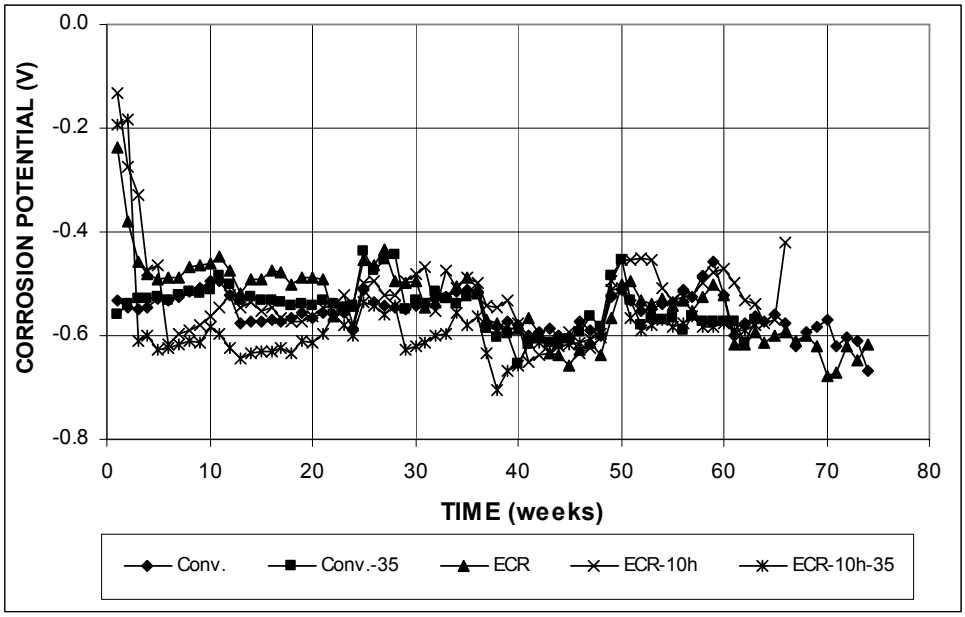

Figure 3.25 (a) – Average top mat corrosion potentials, with respect to a copper-copper sulfate electrode as measured in the cracked beam test for specimens with conventional steel and ECR (ECR have four holes and ECR-10h have 10 holes).

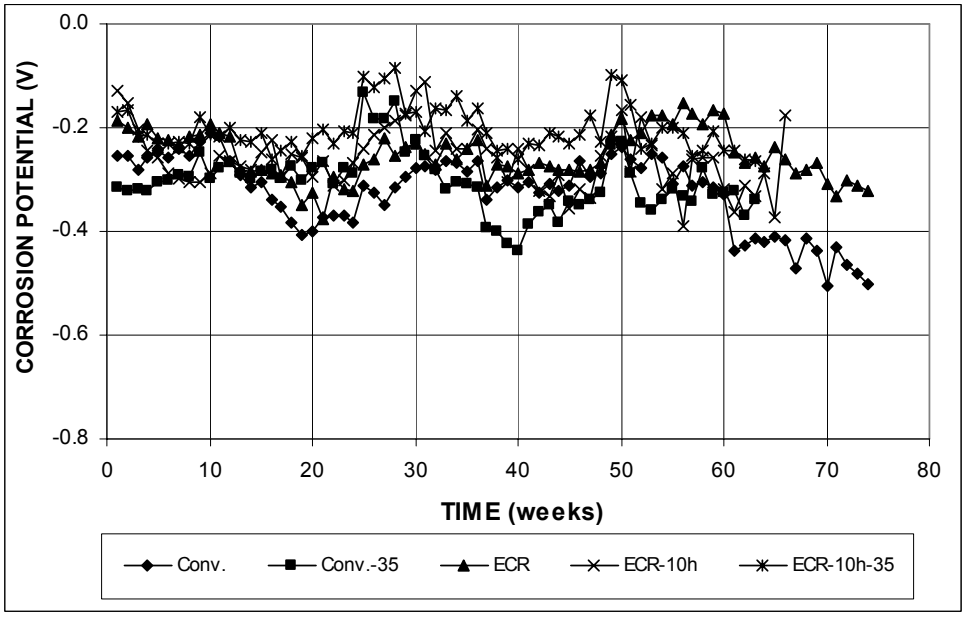

Figure 3.25 (b) – Average bottom mat corrosion potentials, with respect to a copper-copper sulfate electrode as measured in the cracked beam test for specimens with conventional steel and ECR (ECR have four holes and ECR-10h have 10 holes).

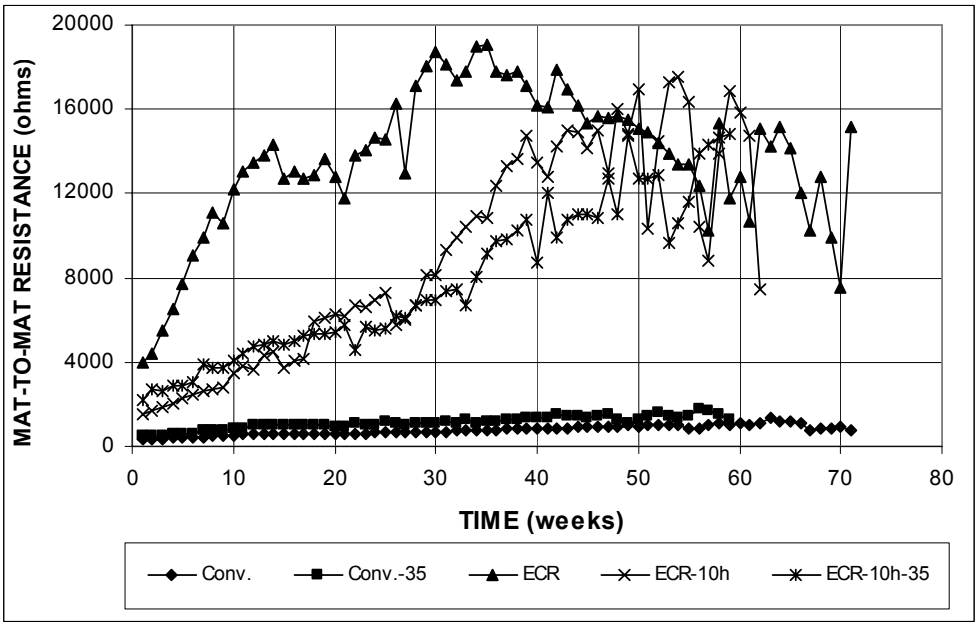

Figure 3.26 – Average mat-to-mat resistances as measured in the cracked beam test for specimens with conventional steel and ECR (ECR have four holes and ECR-10h have 10 holes).

3.1.2.3 ASTM G 109 Test

The ASTM G 109 test provides a much milder testing environment than the Southern Exposure test, including a lower salt concentration of the ponding solution and the less aggressive ponding and drying cycle. As a result, chloride penetration rate and corrosion activity are much lower in the ASTM G 109 test than in the SE test.

The test results are shown in Figures 3.27 through 3.31 for the ASTM G 109 tests. The total corrosion losses at week 60 are summarized in Table 3.6.

Figures 3.27 and 3.28 show the average corrosion rates for specimens with conventional steel and ECR. As shown in Figure 3.27(a), very low corrosion activity was observed for all specimens before week 57. After week 57, conventional steel showed significant corrosion, with a high (and increasing) corrosion rate of 0.43 μm/yr at week 77. Specimens with epoxy-coated reinforcement had average corrosion

rates less than 0.03 μm/yr, with, in general, ECR-10h specimens showing higher corrosion rates than ECR specimens with four holes, as shown in Figure 3.27(b). Based on exposed area, ECR and ECR-10h specimens showed corrosion rates below 6 and 2 μm/yr, respectively, as shown in Figure 3.28.

Table 3.6 – Average corrosion losses (μm) at week 60 as measured in the ASTM G 109 test for specimens with conventional steel and ECR

Steel Designation[a]	Specimen						Average	Standard Deviation
	1	2	3	4	5	6		
Southern Exposure Test								
Conv.	0.03	β	β	β	β	β	0.01	0.01
ECR	β	β	β				β	β
ECR*	0.56	0.44	0.51				0.50	0.06
ECR-10h	β	0.01	β				β	0.01
ECR-10h*	0.13	2.24	0.15				0.84	1.21

[a] Conv. = conventional steel. ECR = conventional epoxy-coated reinforcement.
10h = epoxy-coated bars with 10 holes, otherwise four 3-mm ($^1/_8$-in.) diameter holes.
* Epoxy-coated bars, calculations based on exposed area of four or 10 3-mm ($^1/_8$-in.) diameter holes.
β Corrosion loss (absolute value) less than 0.005 μm.

The average total corrosion losses for all specimens were very low, as shown in Figures 3.29 and 3.30. As shown in Figure 3.29, ECR with 10 holes (ECR-10h) had the highest total corrosion loss during the first 58 weeks, but after 58 weeks conventional steel had the highest total corrosion losses. Conventional steel had a total corrosion loss of approximately 0.04 μm at week 77, while ECR specimens had losses below 0.005 μm. Based on exposed area, ECR-10h had a total corrosion loss close to 0.74 μm at week 68, and ECR had a loss of approximately 0.23 μm at week 78. The average total corrosion losses at week 60 are summarized in Table 3.6. At week 60, conventional steel had a total corrosion loss of approximately 0.01 μm, equal to 1.0% of the corrosion loss of conventional steel in the SE test (0.52 μm). ECR specimens had total corrosion losses less than 0.005 μm based on total area. Based on exposed area, conventional ECR with four holes had a total corrosion loss of 0.21 μm, equal to 35% of the corrosion loss of conventional ECR in the SE test.

Conventional ECR with 10 holes had a total corrosion loss of 0.84 μm, compared with 0.76 μm for conventional ECR with 10 holes in the SE test.

The average corrosion potentials of the top mat and bottom mats of steel with respect to a copper-copper sulfate electrode are shown in Figure 3.31. On June 21, 2005, the copper-copper sulfate electrode used to take corrosion potential readings for the ASTM G 109 specimens was found to be out of calibration. Therefore, for all of the corrosion potentials taken before June 21, 2005, only the data obtained with respect to a saturated calomel electrode are included for analysis. The results, however, are presented in terms of a copper-copper sulfate electrode. As shown in Figure 3.31, before week 66, ECR-10h exhibited the most negative top mat corrosion potentials, followed by ECR and conventional steel, respectively. The top mat corrosion potentials were more positive than –0.200, –0.250, and –0.300 V for conventional steel, ECR, and ECR-10h, respectively, indicating a low probability of corrosion. After week 66, all specimens had corrosion potentials of the top mat more positive than –0.300 V, with the exception of conventional steel, which had a top mat corrosion potential of –0.440 V at week 78. In the bottom mat, ECR-10h had bottom mat corrosion potentials more positive than –0.300 V. Specimens with ECR and conventional steel showed values more positive than –0.230 V, indicating a lower probability of corrosion.

Figure 3.32 shows that the average mat-to-mat resistances increased with time for specimens with conventional steel and ECR. Specimens with conventional steel had the lowest mat-to-mat resistances, with values below 1,550 ohms. As in the other tests, due to the smaller exposed area of the steel, ECR with four holes showed the highest mat-to-mat resistance, starting at 4,300 ohms and increasing to 23,000 ohms after week 60. ECR-10h had a mat-to-mat resistance of 1,800 ohms at the beginning of the test, increasing to 3,300 ohms at week 63.

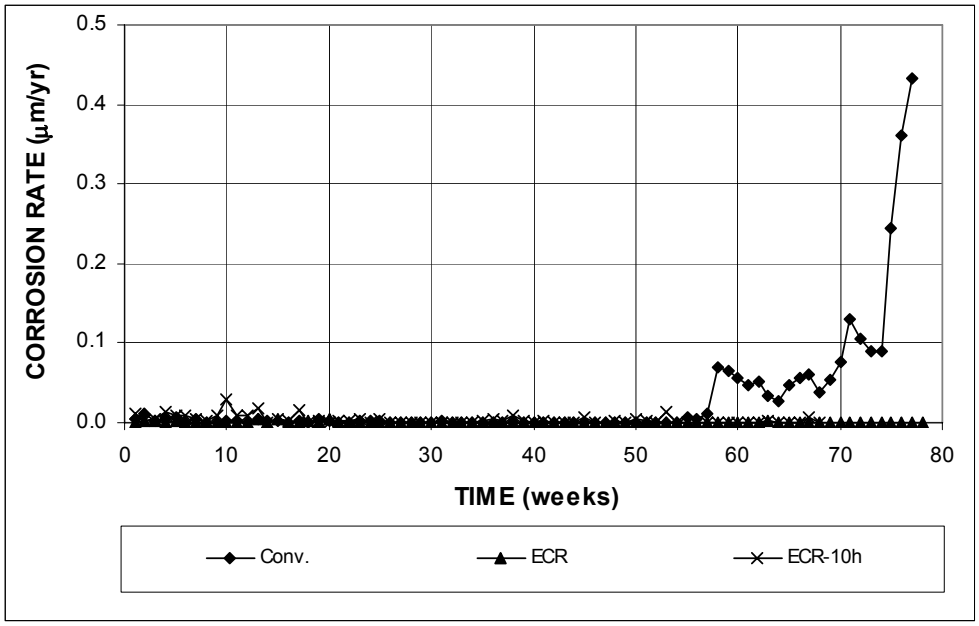

Figure 3.27 (a) – Average corrosion rates as measured in the ASTM G 109 test for specimens with conventional steel and ECR (ECR have four holes and ECR-10h have 10 holes).

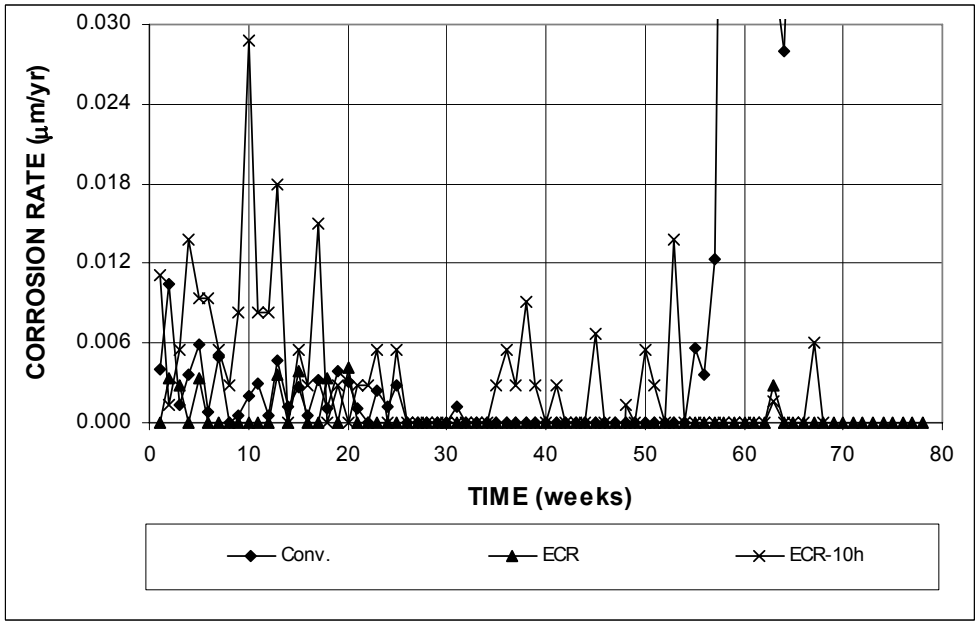

Figure 3.27 (b) – Average corrosion rates as measured in the ASTM G 109 test for specimens with conventional steel and ECR (ECR have four holes and ECR-10h have 10 holes).

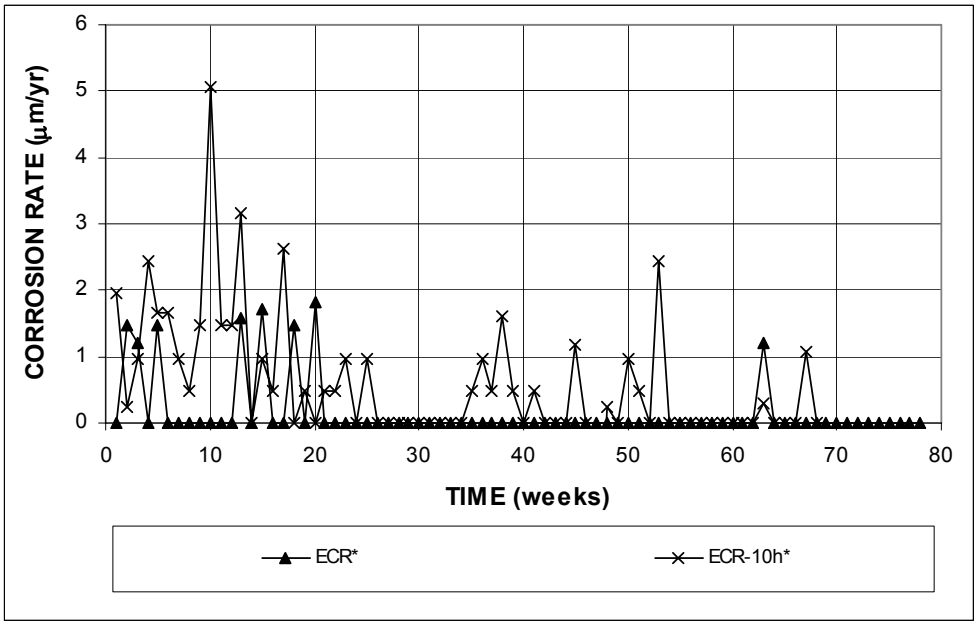

Figure 3.28 – Average corrosion rates as measured in the ASTM G 109 test for specimens with ECR. * Based on exposed area (ECR have four holes and ECR-10h have 10 holes).

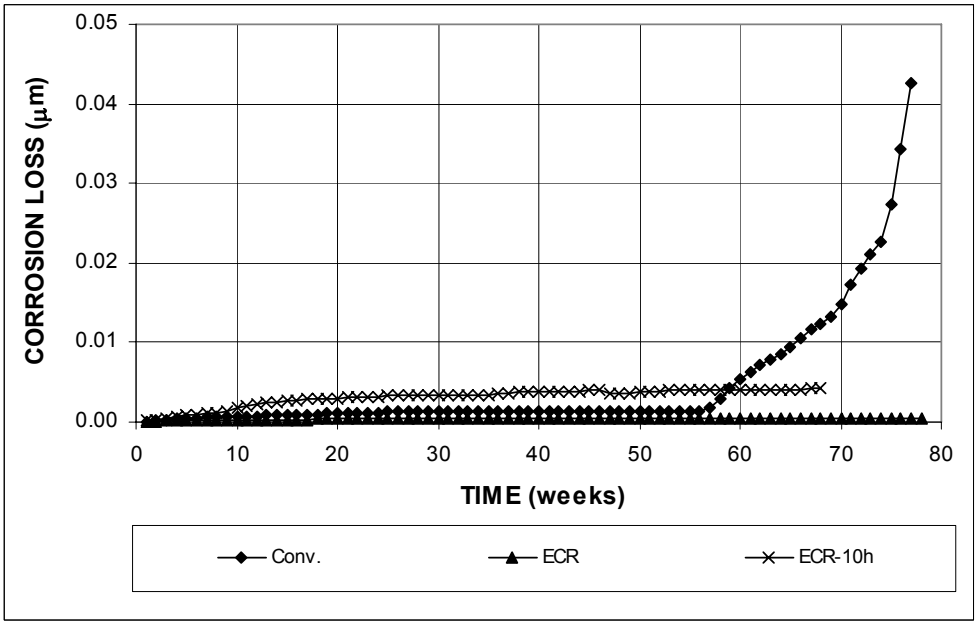

Figure 3.29 – Average corrosion losses as measured in the ASTM G 109 test for specimens with conventional steel and ECR (ECR have four holes and ECR-10h have 10 holes).

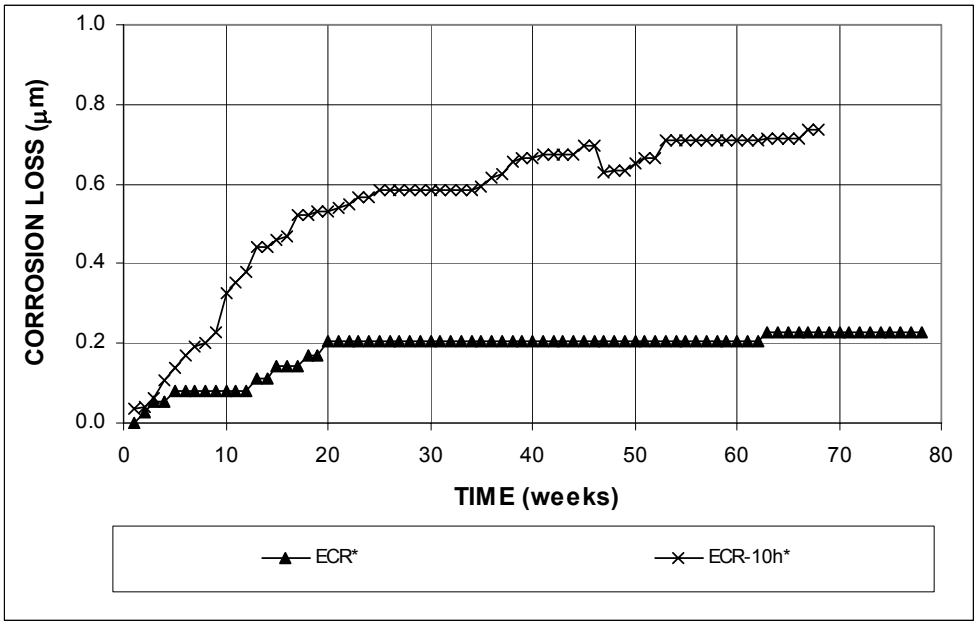

Figure 3.30 – Average corrosion losses as measured in the ASTM G 109 test for specimens with ECR. * Based on exposed area (ECR have four holes and ECR-10h have 10 holes).

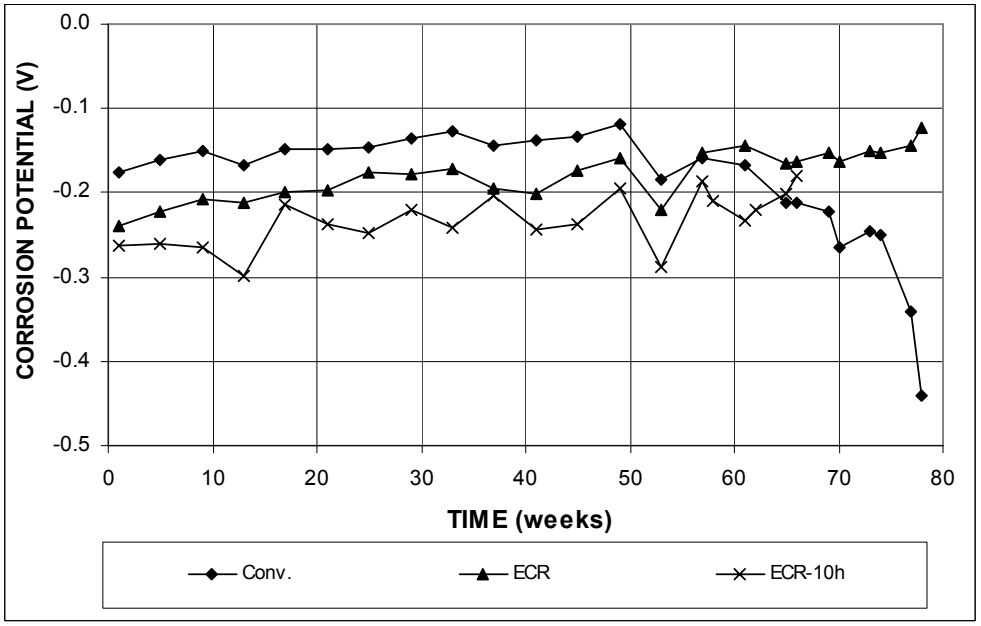

Figure 3.31 (a) – Average top mat corrosion potentials, with respect to a copper-copper sulfate electrode as measured in the ASTM G 109 test for specimens with conventional steel and ECR (ECR have four holes and ECR-10h have 10 holes).

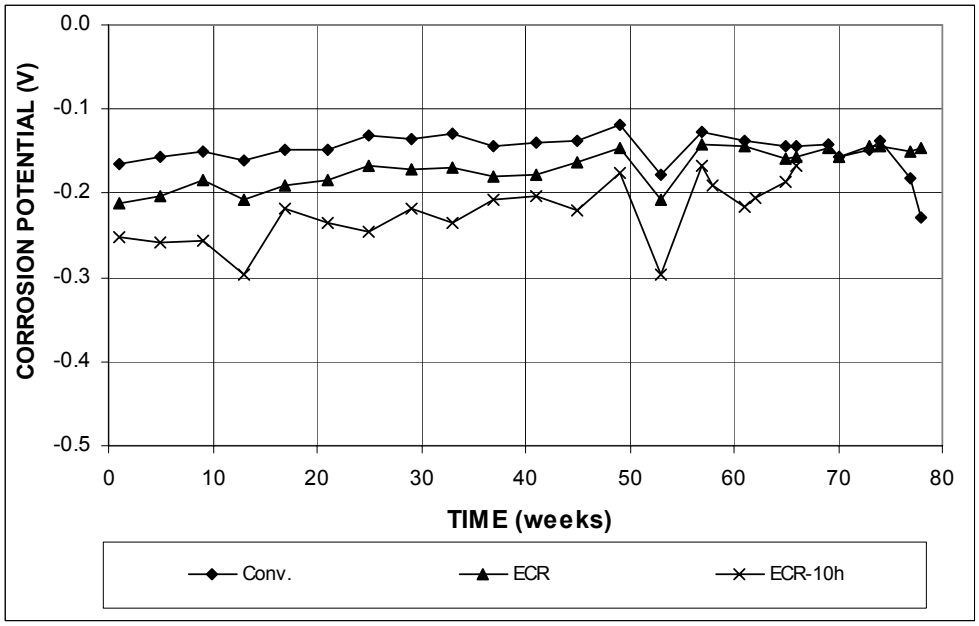

Figure 3.31 (b) – Average bottom mat corrosion potentials, with respect to a copper-copper sulfate electrode as measured in the ASTM G 109 test for specimens with conventional steel and ECR (ECR have four holes and ECR-10h have 10 holes).

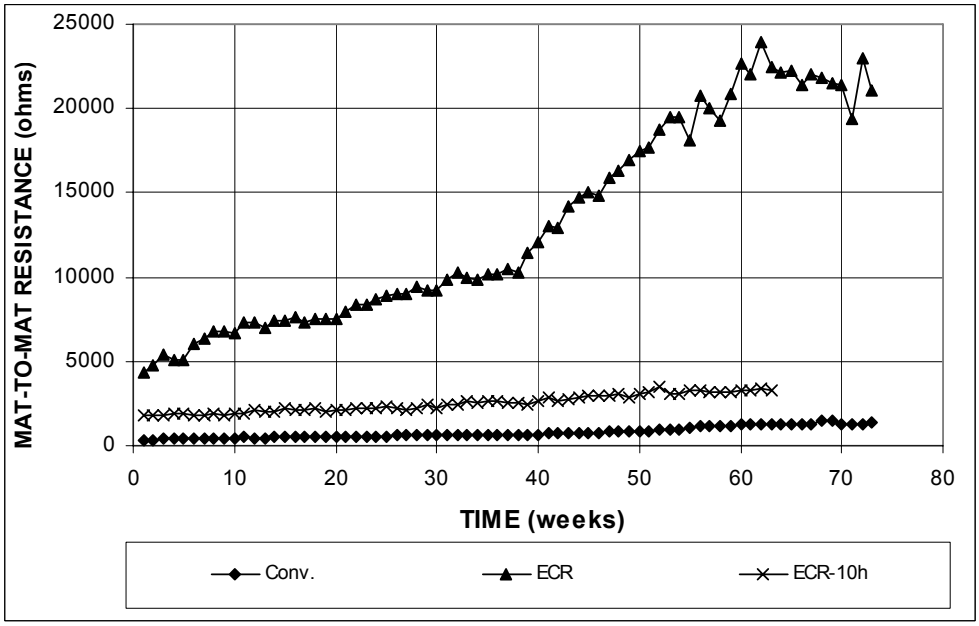

Figure 3.32 – Average mat-to-mat resistances as measured in the ASTM G 109 test for specimens with conventional steel and ECR (ECR have four holes and ECR-10h have 10 holes).

3.1.3 Field Test

This section describes the test results for specimens with conventional steel and epoxy-coated reinforcement. The coating on the epoxy-coated bars was penetrated with 16 holes. In the tables and figures, a number in parentheses following the steel designation is the specimen number. For example, Conv. (1) means specimen No. 1 with conventional steel.

3.1.3.1 Field Test Specimens Without Cracks

The test results are shown in Figures 3.33 through 3.38 for specimens without simulated cracks in the field test. The total corrosion losses at week 32, the lowest time period for any specimen, are summarized in Table 3.7.

Figures 3.33 and 3.34 show the average corrosion rates for specimens with conventional steel and ECR. As shown in Figure 3.33, all specimens had corrosion rates less than 0.02 μm/yr based on total area, with the exception of Conv. (2), which had rates of 0.16 and 0.14 μm/yr at weeks 40 and 44, respectively, and dropped to values close to zero after week 48. Figure 3.34, based on the exposed area, shows that corrosion rates as high as 5.95 and 1.14 μm/yr occurred at localized areas for ECR (1) and ECR (2), respectively.

The average total corrosion losses for specimens with conventional steel and ECR are shown in Figures 3.35 and 3.36. Figure 3.35 shows that Conv. (2) had the highest corrosion loss, but the value was only 0.024 μm at week 56. The remaining specimens had total corrosion losses less than 0.005 μm. As shown in Figure 3.36, ECR (1) showed a higher total corrosion loss than ECR (2) based on exposed area. Table 3.7 summarizes the average total corrosion losses for conventional steel and ECR at week 32. All specimens showed total corrosion losses less than 0.005 μm based on total area, as indicated by the symbol β in the table. Total corrosion losses

were 0.81 and 0.18 μm for ECR (1) and ECR (2), respectively, based on exposed area.

Table 3.7 – Average corrosion losses (μm) at week 32 as measured in the field test for specimens with conventional steel and ECR, without cracks

Steel Designation[a]	Test Bar				Average	Standard Deviation
	1	2	3	4		
without cracks						
Conv. (1)	β	β			β	β
Conv. (2)	β	β			β	β
ECR (1)	β	β			β	β
ECR* (1)	0.77	0.85			0.81	0.05
ECR (2)	β	0.00	β	0.00	β	β
ECR* (2)	0.35	0.00	0.35	0.00	0.18	0.20

[a] Conv. = conventional steel. ECR = conventionl epoxy-coated reinforcement.

* Epoxy-coated bars, calculations based on exposed area of 16 3-mm ($^1/_8$-in.) diameter holes.

β Corrosion loss (absolute value) less than 0.005 μm.

The average corrosion potentials of the top mat and bottom mats of steel with respect to a copper-copper sulfate electrode are shown in Figure 3.37. According to ASTM C 876, the potential of the saturated copper-copper sulfate half cell with respect to the standard hydrogen electrode is –0.316 V at 22.2 °C (72 °F). To report corrosion potentials at 22.2 °C (72 °F), actual potentials measured in the field increase 0.0009 V per °C (0.0005 V per °F) for the temperature range from 0 to 22.2 °C (32 to 72 °F) and decrease 0.0009 V per °C (0.0005 V per °F) for the temperature between 22.2 to 49 °C (72 to 120 °F). As shown in Figure 3.37(a), all specimens had corrosion potentials in the top mat more positive than –0.320 V, with the exception of Conv. (1), which had top mat corrosion potentials below –0.350 V after week 60. As shown in Figure 3.37(b), all specimens had bottom mat corrosion potentials more positive than –0.260 V, indicating a low probability of corrosion.

Figure 3.38 shows the average mat-to-mat resistances for specimens with conventional steel and ECR. ECR specimens had mat-to-mat resistances between 600 and 2,600 ohms, while specimens with conventional steel had values between 4 and

20 ohms, which are two orders in magnitude lower than those for ECR specimens. For both conventional steel and ECR, lower mat-to-mat resistances are observed for field test specimens than for bench-scale test specimens, primarily due to the larger exposed area of the steel in field test specimens. In the field, the temperature and moisture content of concrete for the field test specimens change from time to time. As a result, average mat-to-mat resistances for specimens in the field test (Figure 3.38) did not show a clear trend of increasing with time, as did for the specimens in the bench-scale tests.

3.1.3.2 Field Test Specimens With Cracks

The test results are shown in Figures 3.39 through 3.44 for field test specimens with cracks. The total corrosion losses at week 32 are summarized in Table 3.8.

Figures 3.39 and 3.40 show the average corrosion rates for specimens with conventional steel and ECR. As shown in Figure 3.39, specimens with conventional steel had much higher corrosion rates than the ECR specimens, with values as high as 1.49 and 1.97 μm/yr for Conv. (1) and Conv. (2), respectively. The corrosion rates were highly variable, due largely to changes in moisture content in concrete. ECR specimens exhibited corrosion rates less than 0.02 and 6 μm/yr based on total area and exposed area, respectively.

The average total corrosion losses for specimens with conventional steel and ECR are shown in Figures 3.41 and 3.42. Figure 3.41 shows that Conv. (2) had the highest corrosion loss, followed by Conv. (1). As shown in Figures 3.41(b) and 3.42, ECR specimens had total corrosion losses less than 0.005 and 1.5 μm based on total area and exposed area, respectively. Table 3.8 summarizes the average total corrosion losses for conventional steel and ECR at week 32. All specimens showed total

corrosion losses less than 0.005 μm based on total area, with the exception of Conv. (2), which had a value of 0.29 μm. Based on exposed area, the total corrosion losses were 1.06 for ECR (1). The ECR (2) specimen showed no corrosion activity.

Table 3.8 – Average corrosion losses (μm) at week 32 as measured in the field test for specimens with conventional steel and ECR, with cracks

Steel Designation[a]	Test Bar 1	2	3	4	Average	Standard Deviation
with cracks						
Conv. (1)	β	β			β	β
Conv. (2)	0.28	0.30			0.29	0.01
ECR (1)	β	β			β	β
ECR* (1)	1.76	0.35			1.06	1.00
ECR (2)	0.00	0.00	0.00	0.00	0.00	0.00
ECR* (2)	0.00	0.00	0.00	0.00	0.00	0.00

[a] Conv. = conventional steel. ECR = conventionl epoxy-coated reinforcement.

* Epoxy-coated bars, calculations based on exposed area of 16 3-mm ($^1/_8$-in.) diameter holes.

β Corrosion loss (absolute value) less than 0.005 μm.

The average corrosion potentials of the top mat and bottom mats of steel with respect to a copper-copper sulfate electrode are shown in Figure 3.43. Specimens with conventional steel had top mat corrosion potentials between –0.350 and –0.500 V after week 12. Specimens with ECR showed top mat corrosion potentials more positive than –0.350 V, with the exception of ECR (1), which had values below –0.350 V between weeks 24 and 28 and at week 68. All specimens showed similar bottom mat corrosion potentials, with values above –0.350 V, except for Conv. (1) at week 64, which dropped to –0.520 V before rebounding to –0.320 V at week 68.

Figure 3.44 shows the average mat-to-mat resistances for specimens with conventional steel and ECR. Specimens with ECR had average mat-to-mat resistances between 600 and 2,500 ohms, while specimens with conventional steel had values between 4 and 20 ohms.

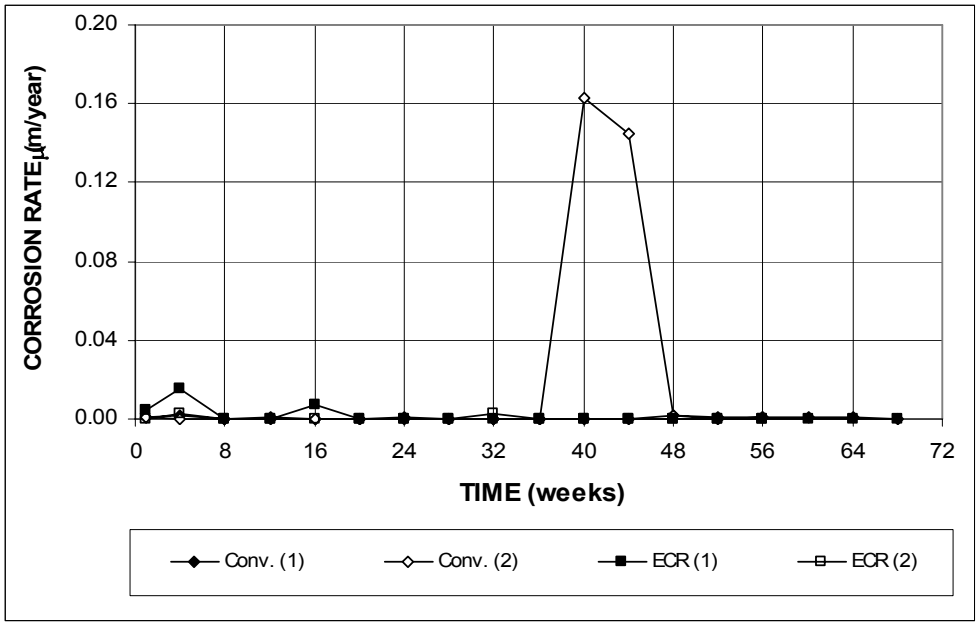

Figure 3.33 (a) – Average corrosion rates as measured in the field test for specimens with conventional steel and ECR, without cracks (ECR bars have 16 holes).

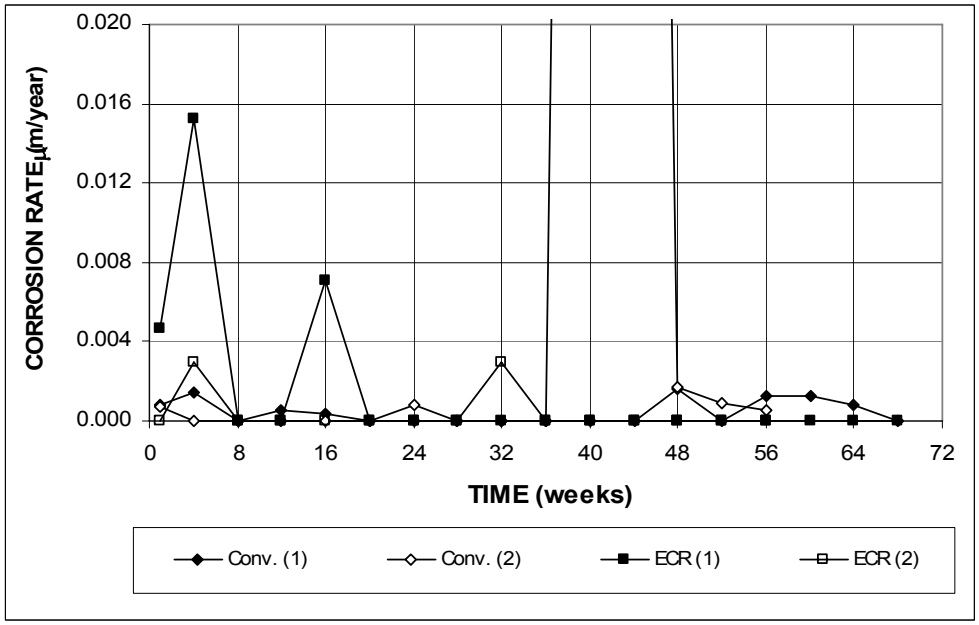

Figure 3.33 (b) – Average corrosion rates as measured in the field test for specimens with conventional steel and ECR, without cracks (ECR bars have 16 holes).

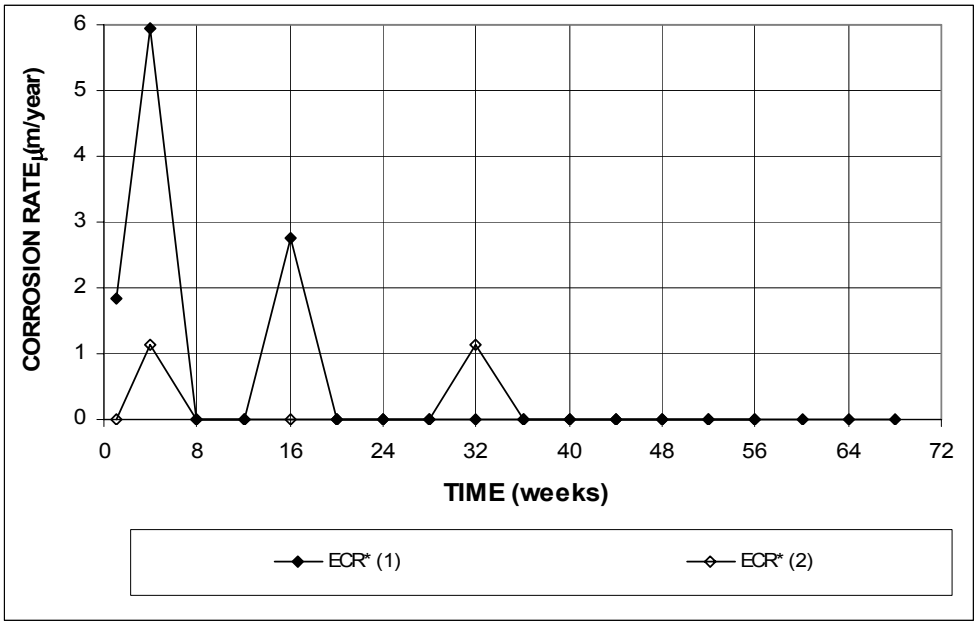

Figure 3.34 – Average corrosion rates as measured in the field test for specimens with ECR, without cracks. * Based on exposed area (ECR bars have 16 holes).

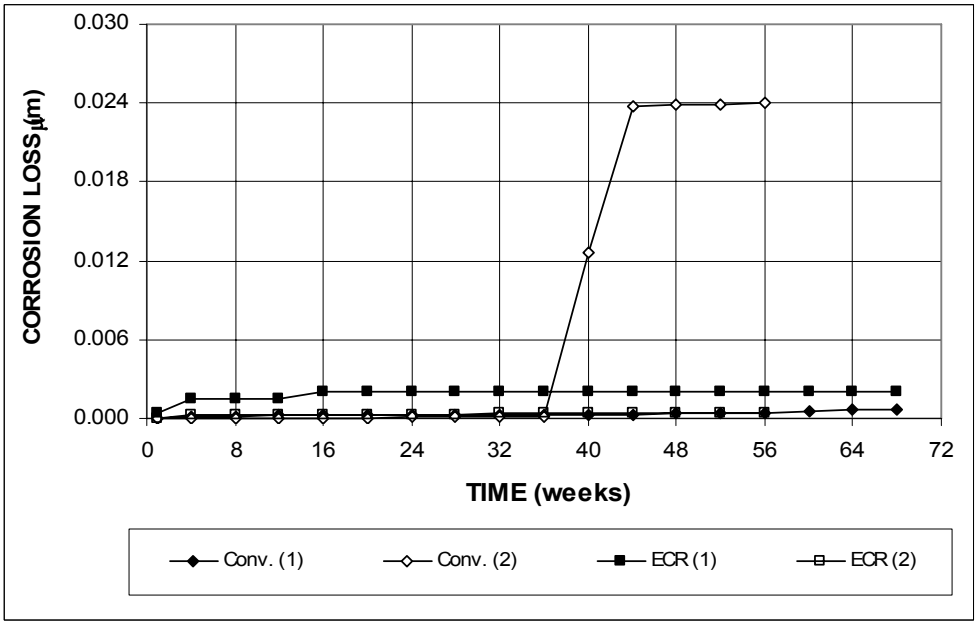

Figure 3.35 – Average corrosion losses as measured in the field test for specimens with conventional steel and ECR, without cracks (ECR bars have 16 holes).

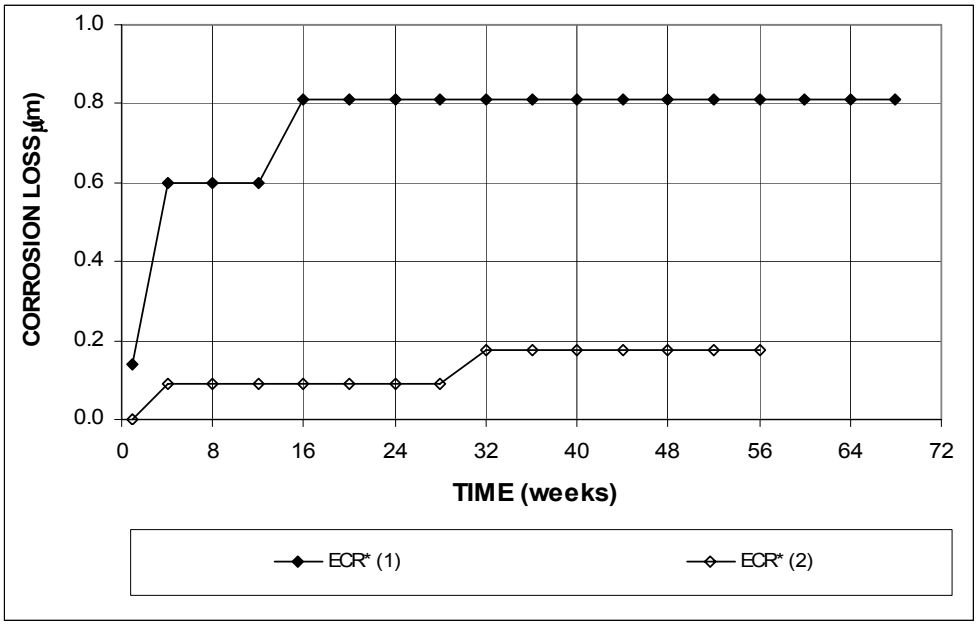

Figure 3.36 – Average corrosion losses as measured in the field test for specimens with ECR, without cracks. * Based on exposed area (ECR bars have 16 holes).

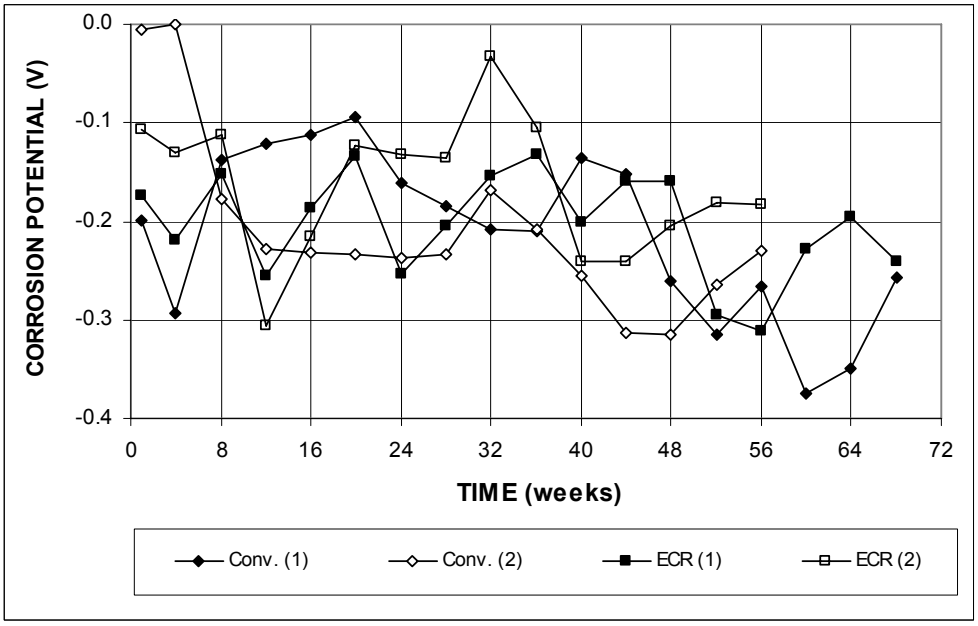

Figure 3.37 (a) – Average top mat corrosion potentials, with respect to a copper-copper sulfate electrode as measured in the field test for specimens with conventional steel and ECR, without cracks (ECR bars have 16 holes).

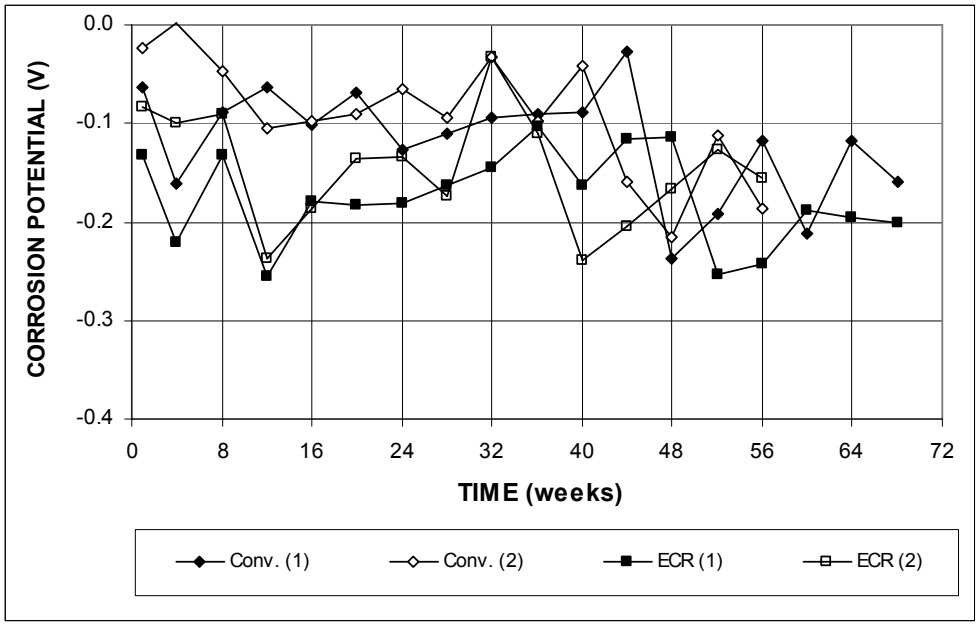

Figure 3.37 (b) – Average bottom mat corrosion potentials, with respect to a copper-copper sulfate electrode as measured in the field test for specimens with conventional steel and ECR, without cracks (ECR bars have 16 holes).

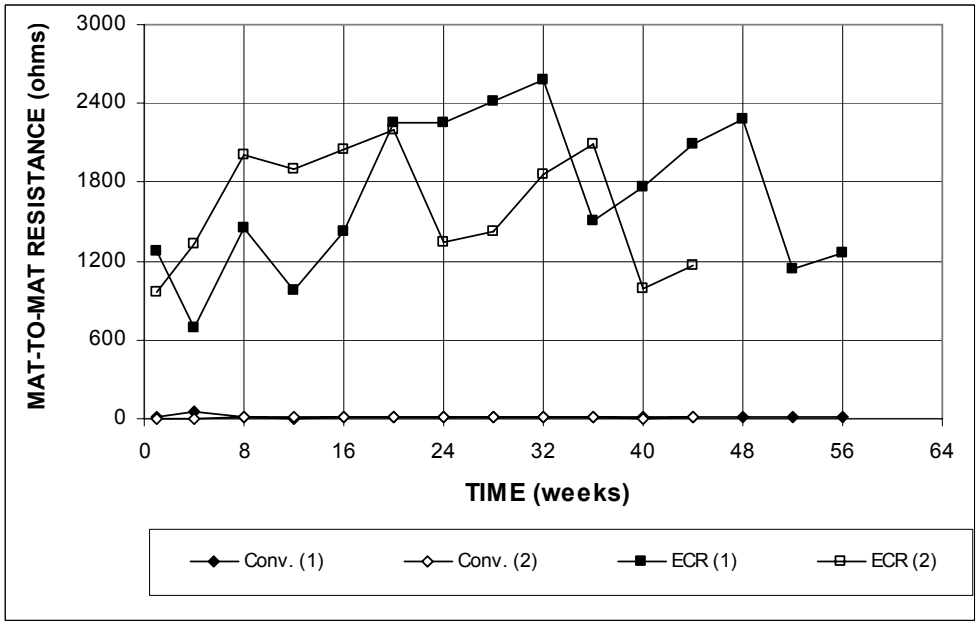

Figure 3.38 (a) – Average mat-to-mat resistances as measured in the field test for specimens with conventional steel and ECR, without cracks (ECR bars have 16 holes).

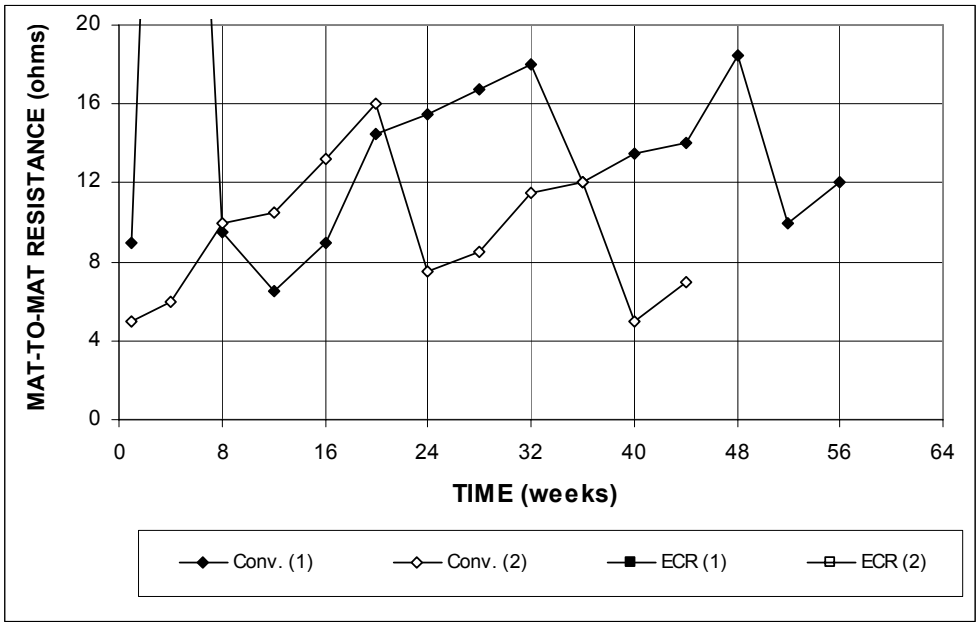

Figure 3.38 (b) – Average mat-to-mat resistances as measured in the field test for specimens with conventional steel and ECR, without cracks (ECR bars have 16 holes).

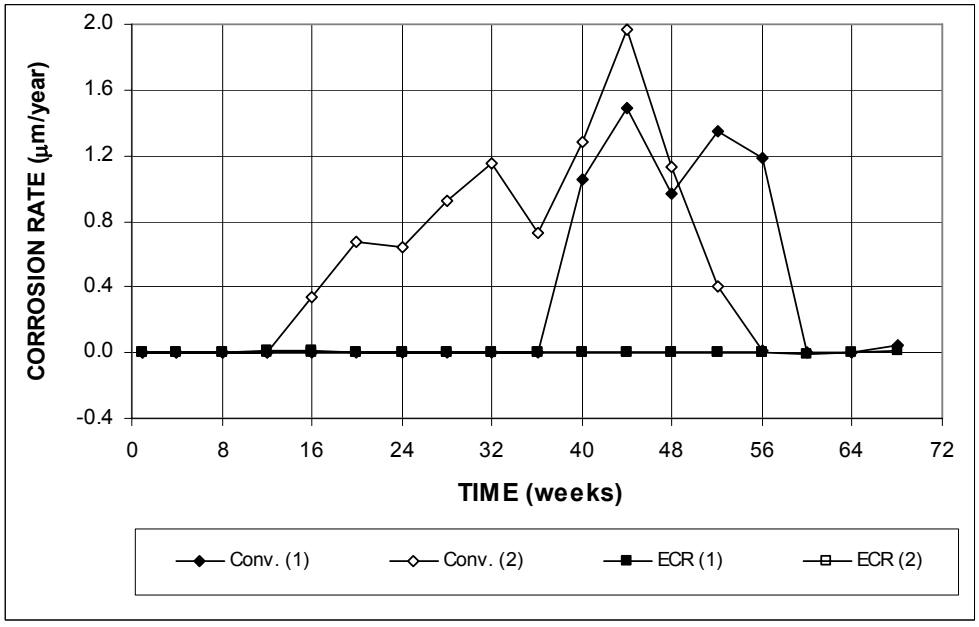

Figure 3.39 (a) – Average corrosion rates as measured in the field test for specimens with conventional steel and ECR, with cracks (ECR bars have 16 holes).

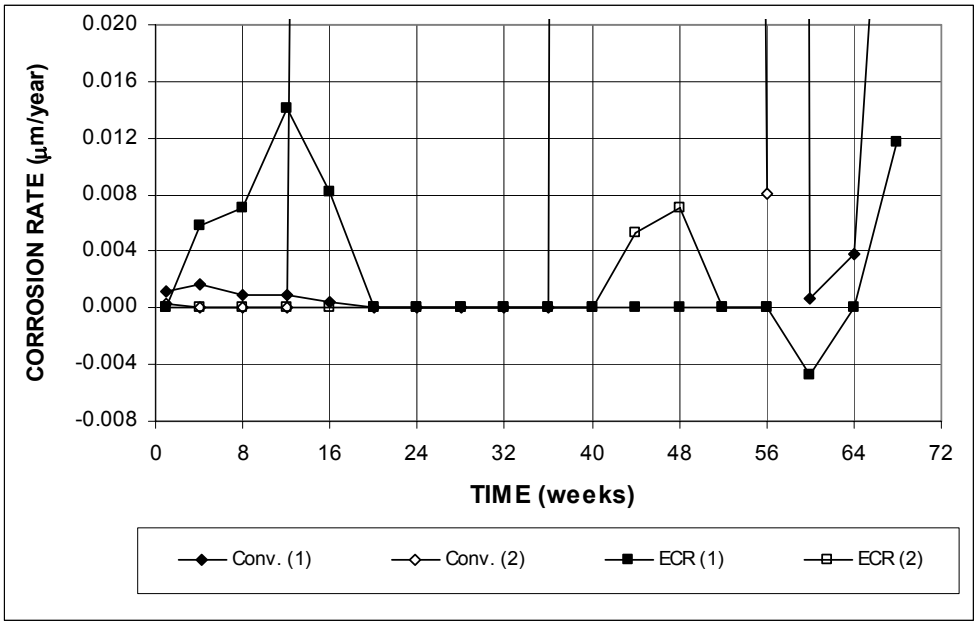

Figure 3.39 (b) – Average corrosion rates as measured in the field test for specimens with conventional steel and ECR, with cracks (ECR bars have 16 holes).

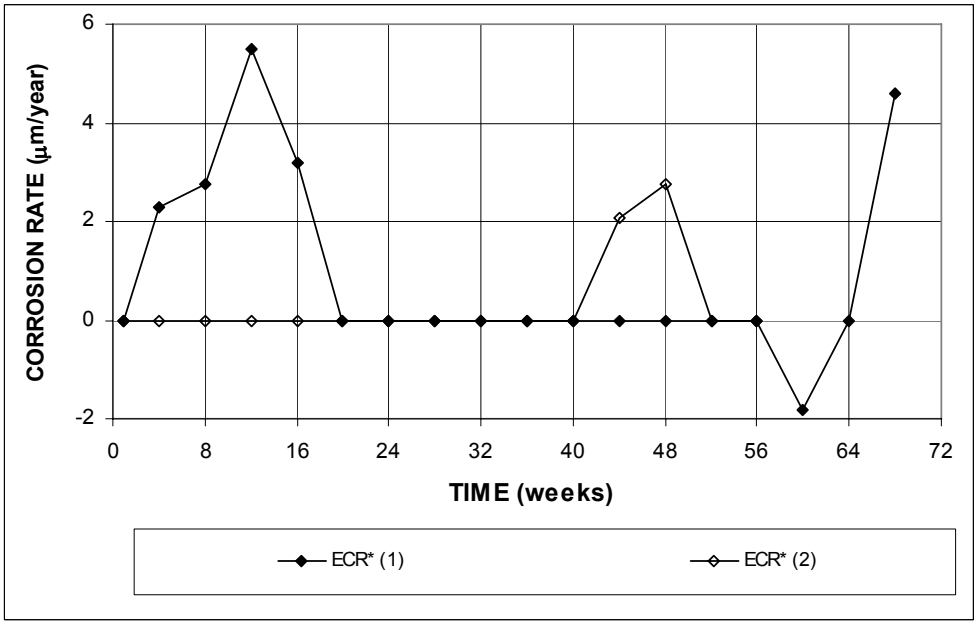

Figure 3.40 – Average corrosion rates as measured in the field test for specimens with ECR, with cracks. * Based on exposed area (ECR bars have 16 holes).

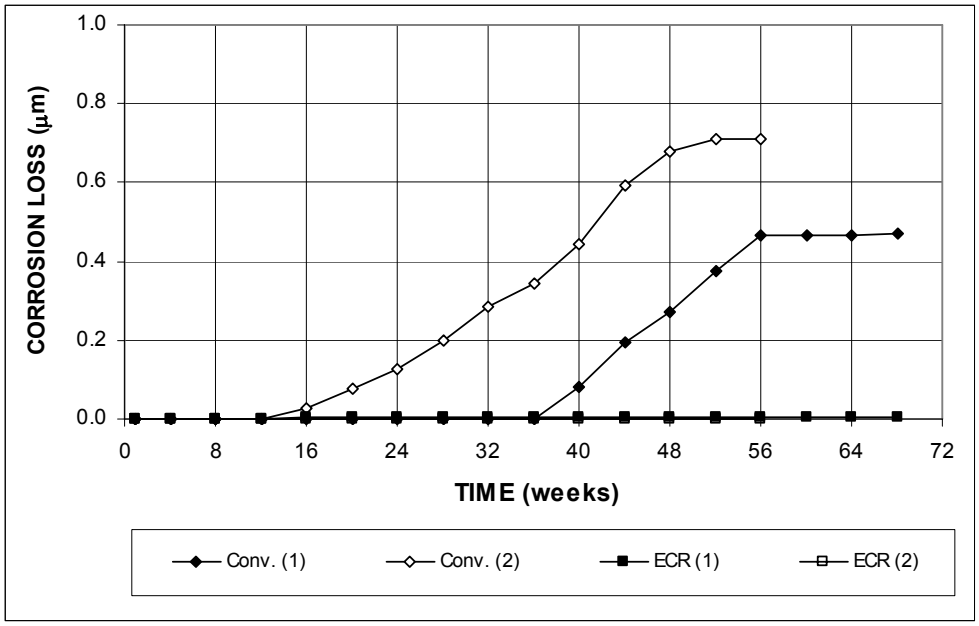

Figure 3.41 (a) – Average corrosion losses as measured in the field test for specimens with conventional steel and ECR, with cracks (ECR bars have 16 holes).

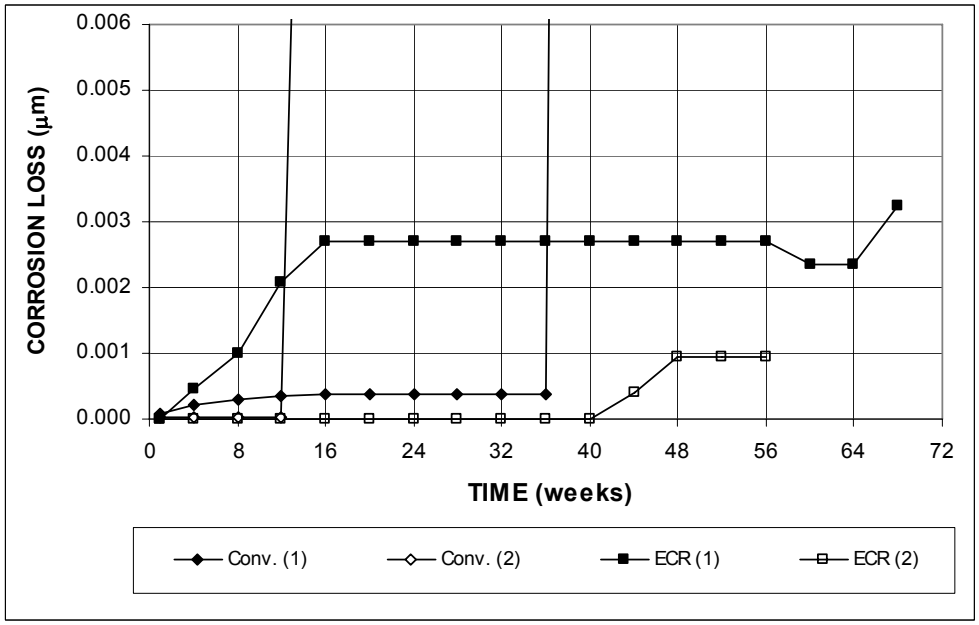

Figure 3.41 (b) – Average corrosion losses as measured in the field test for specimens with conventional steel and ECR, with cracks (ECR bars have 16 holes).

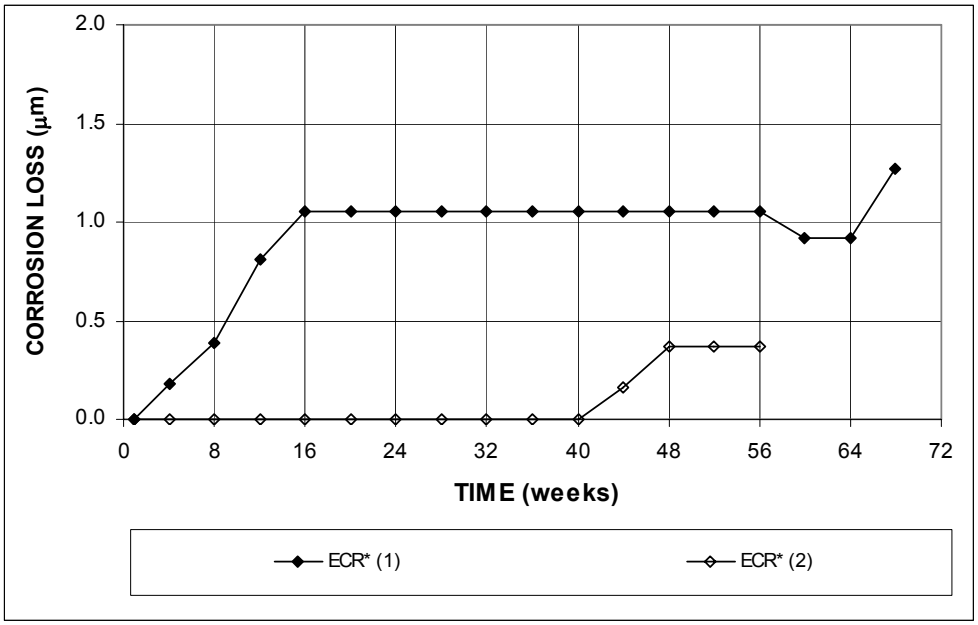

Figure 3.42 – Average corrosion losses as measured in the field test for specimens with ECR, with cracks. * Based on exposed area (ECR bars have 16 holes).

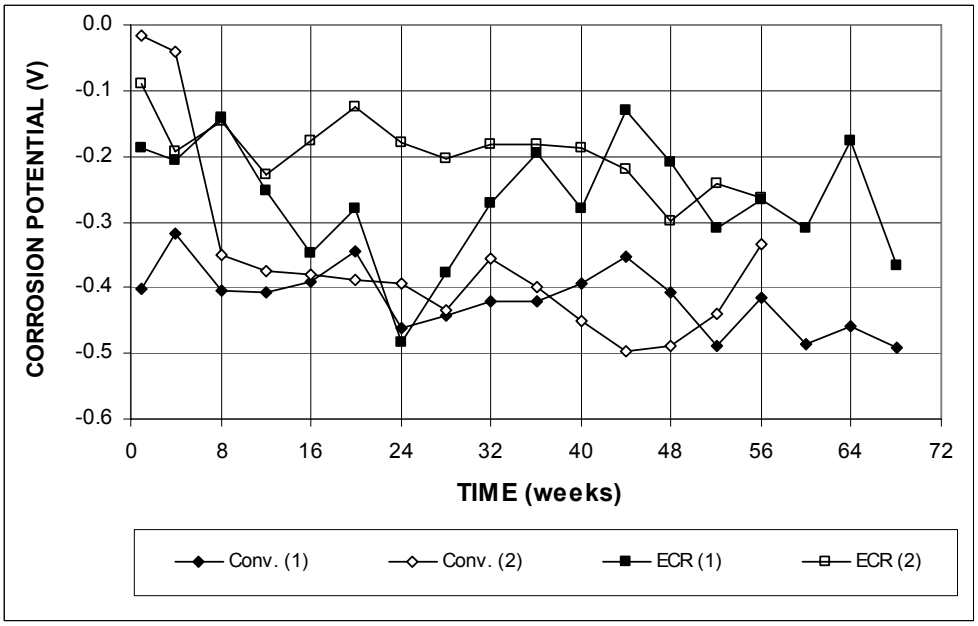

Figure 3.43 (a) – Average top mat corrosion potentials, with respect to a copper-copper sulfate electrode as measured in the field test for specimens with conventional steel and ECR, with cracks (ECR bars have 16 holes).

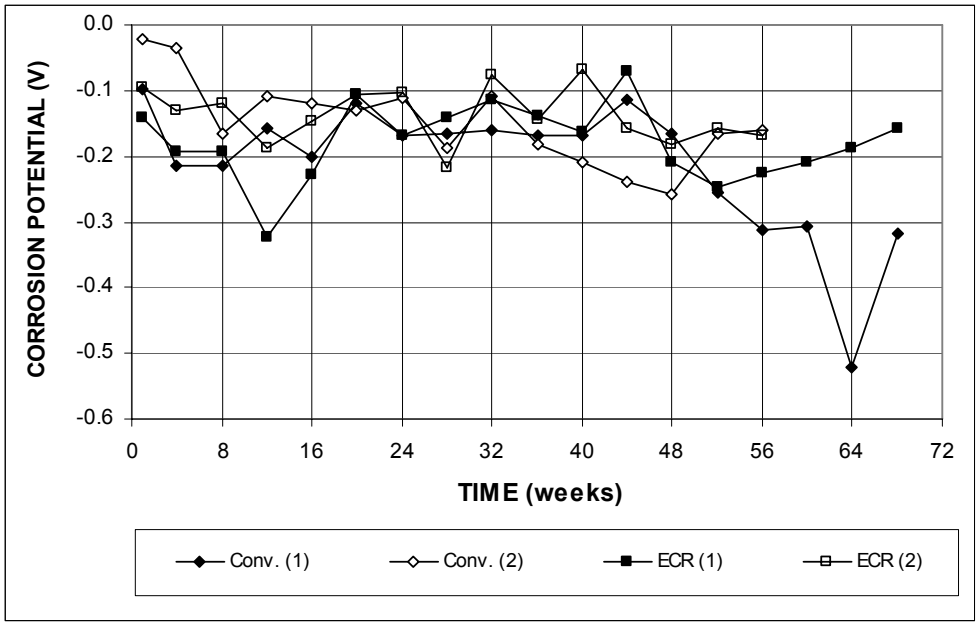

Figure 3.43 (b) – Average bottom mat corrosion potentials, with respect to a copper-copper sulfate electrode as measured in the field test for specimens with conventional steel and ECR, with cracks (ECR bars have 16 holes).

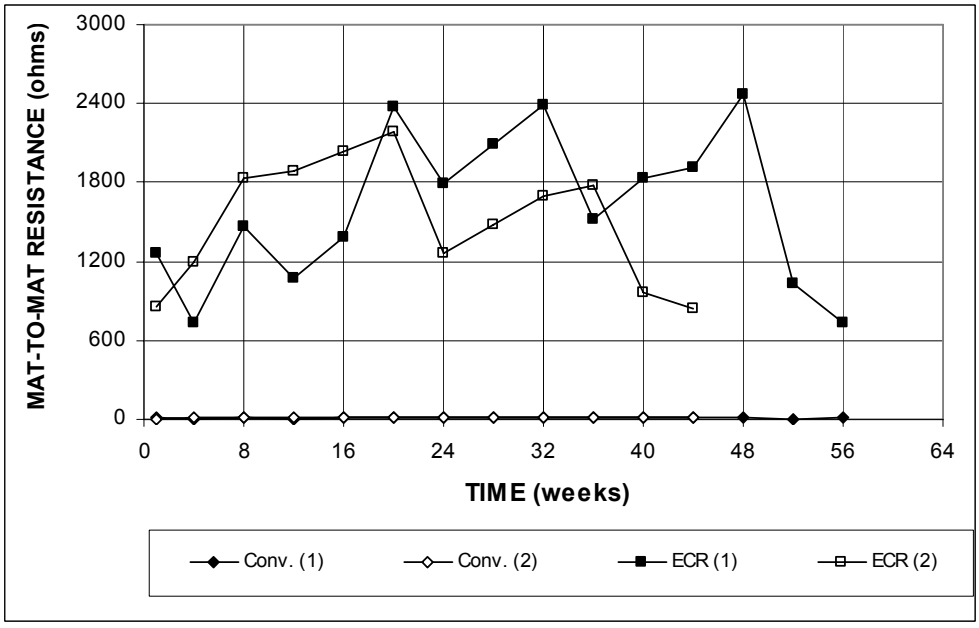

Figure 3.44 (a) – Average mat-to-mat resistances as measured in the field test for specimens with conventional steel and ECR, with cracks (ECR bars have 16 holes).

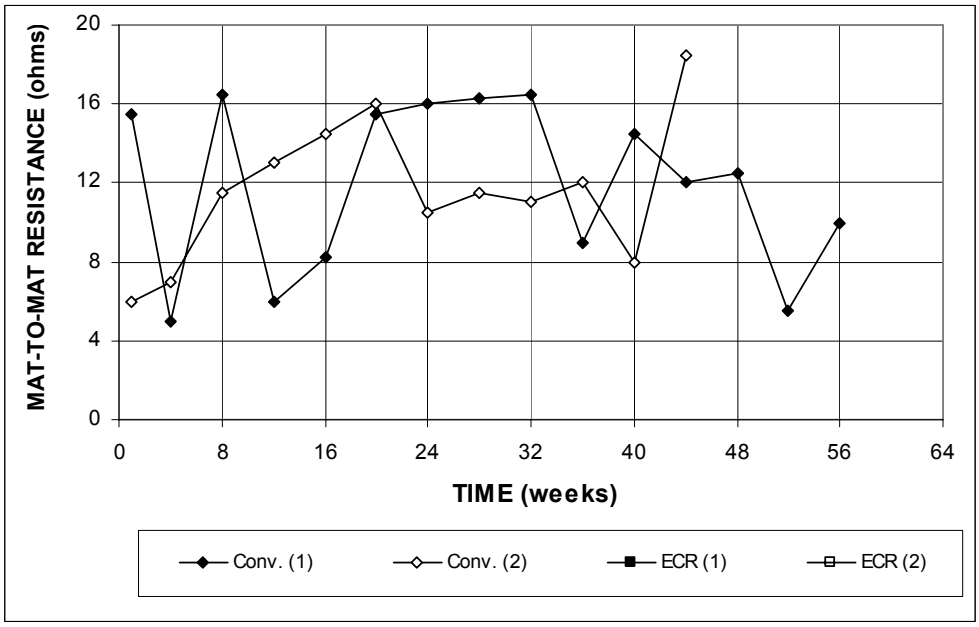

Figure 3.44 (b) – Average mat-to-mat resistances as measured in the field test for specimens with conventional steel and ECR, with cracks (ECR bars have 16 holes).

3.2 CORROSION INHIBITORS AND LOW WATER-CEMENT RATIOS

This section presents the results of the rapid macrocell, bench-scale, and field tests for specimens containing ECR with a calcium nitrite primer, and ECR cast with corrosion inhibitors DCI-S, Rheocrete and Hycrete. In the Southern Exposure (SE) and cracked beam (CB) tests, *w/c* ratios of 0.45 and 0.35 were used. In this and in following sections, the figures included the results for conventional steel and conventional ECR from Section 3.1 for purpose of comparison. The tables include only the new information presented in the section.

3.2.1 Rapid Macrocell Test

ECR with a primer containing calcium nitrite and ECR cast in mortar with corrosion inhibitors were evaluated in the rapid macrocell test with mortar-wrapped

specimens in 1.6 m ion NaCl and simulated concrete pore solution. The mortar had a *w/c* ratio of 0.50. The tests included six tests each for ECR with four drilled holes and three tests each for ECR in the as-delivered condition.

The test results are presented in Figures 3.45 through 3.51 for the rapid macrocell test with mortar-wrapped specimens. The total corrosion losses at week 15 are summarized in Tables 3.9.

Based on the total area exposed to the solution (below the liquid surface), conventional steel exhibited the highest corrosion rates during the test period, as discussed in Section 3.1. As shown in Figure 3.45(b), of the ECR specimens, ECR(primer/$Ca(NO_2)_2$) showed the highest corrosion rates, accompanied by the most negative anode corrosion potentials (Figure 3.51). ECR(primer/$Ca(NO_2)_2$) had the highest corrosion rate of approximately 0.07 μm/yr based on total area and 7 μm/yr based on exposed area at week 13 (Figure 3.47). The ECR(DCI) specimens showed no corrosion activity except at week 3, when then had a negative corrosion rate of –0.02 μm/yr caused by one of the three specimens. This negative corrosion rate, however, in all likelihood is an aberrant reading because it was not accompanied by a more negative corrosion potential at cathode than at anode. The ECR(Hycrete) and ECR(Rheocrete) specimens showed no corrosion activity during the 15-week test period. Figure 3.46 shows that all specimens without holes showed no corrosion activity, with the exception of ECR(Hycrete) without holes, which showed a corrosion rate of –0.05 μm/yr based on exposed area at week 5. As shown in Figures 3.45(b) and 3.46, little corrosion was observed for conventional ECR cast in mortar containing corrosion inhibitors with or without four holes. It can be concluded that chlorides might not have reached the steel-mortar interface, or a locally low chloride content at the exposed area existed due to the non-homogeneous nature of chloride

diffusion in mortar. The test results indicate that the current rapid macrocell test procedure should be modified to better evaluate different corrosion protection systems in this study. The action may include a longer test period, a higher salt concentration, and using ECR specimens with more coating damage.

Table 3.9 – Average corrosion losses (μm) at week 15 as measured in the macrocell test for mortar-wrapped specimens with ECR with a primer containing calcium nitrite and ECR cast with corrosion inhibitors

Steel Designation[a]	Specimen						Average	Standard Deviation
	1	2	3	4	5	6		
Mortar-wrapped Specimens								
ECR(DCI)	0.00	β	0.00	0.00	0.00	0.00	β	β
ECR(DCI)*	0.00	-0.28	0.00	0.00	0.00	0.00	-0.05	0.11
ECR(DCI)-no holes	0.00	0.00	0.00				0.00	0.00
ECR(Hycrete)	0.00	0.00	0.00	0.00	0.00	0.00	0.00	0.00
ECR(Hycrete)*	0.00	0.00	0.00	0.00	0.00	0.00	0.00	0.00
ECR(Hycrete)-no holes	0.00	0.00	0.00				0.00	0.00
ECR(Rheocrete)	0.00	0.00	0.00	0.00	0.00	0.00	0.00	0.00
ECR(Rheocrete)*	0.00	0.00	0.00	0.00	0.00	0.00	0.00	0.00
ECR(Rheocrete)-no holes	0.00	0.00	β				β	β
ECR(primer/$Ca(NO_2)_2$)	0.00	0.00	0.00	0.00	0.01	0.01	β	β
ECR(primer/$Ca(NO_2)_2$)*	0.00	0.00	0.00	0.00	0.77	0.92	0.28	0.44
ECR(primer/$Ca(NO_2)_2$)-no holes	0.00	0.00	0.00				0.00	0.00

[a] ECR = conventional epoxy-coated reinforcement. ECR(DCI) = ECR in mortar with DCI.
ECR(Hycrete) = ECR in mortar with Hycrete. ECR(Rheocrete) = ECR in mortar with Rheocrete.
ECR(primer/$Ca(NO_2)_2$) = ECR with primer containing calcium nitrite.
no holes = epoxy-coated bars without holes, otherwise four 3-mm ($^1/_8$-in.) diameter holes.

* Epoxy-coated bars, calculations based on exposed area of four 3-mm ($^1/_8$-in.) diameter holes.

β Corrosion loss (absolute value) less than 0.005 μm.

The average total corrosion losses versus time are presented in Figures 3.48 through 3.50 and the results at week 15 are summarized in Table 3.9. As shown in Tables 3.48(b) and 3.50, the ECR(primer/$Ca(NO_2)_2$) had the highest total corrosion loss of approximately 0.003 μm based on total area and 0.28 μm based on exposed area. The remaining specimens did not show total corrosion losses, with the exception of ECR(DCI), which had total corrosion losses of –0.05 μm based on exposed area based on measured corrosion one time on one specimen (Figures 3.47 and A.23). The

ECR(Hycrete) and ECR(Rheocrete) showed no corrosion losses at week 15. For specimens without holes (Figure 3.49), ECR(Rheocrete) had total corrosion losses (absolute value) of less than 0.005 μm, as indicated by the symbol β in Table 3.9. The ECR(DCI) and ECR(Hycrete) specimens exhibited no corrosion loss.

The average anode and cathode corrosion potentials with respect to a saturated calomel electrode are shown in Figure 3.51. At the anodes, conventional steel exhibited the most negative potential, followed by ECR(primer/$Ca(NO_2)_2$) with values between –0.300 and –0.400 V after week 2. Two specimens with ECR containing a calcium nitrite primer, specimens No. 5 and 6, had the most negative corrosion potentials, with values more negative than –0.490 V after week 6 (Figure A.22). This is in good agreement with the fact that these two specimens showed corrosion activity, as shown in Table 3.9. ECR(Rheocrete) had anode corrosion potentials more negative than –0.275 V at weeks 6 and 7, indicating active corrosion. ECR(DCI) and ECR(Hycrete) had anode potentials more positive than –0.240 V during the test period, indicating a low probability of corrosion. At the cathodes, ECR(primer/$Ca(NO_2)_2$) exhibited the most negative corrosion potentials, with values between –0.261 and –0.313 V from week 9 to 15. The remaining specimens had cathode potentials more positive than –0.270 V throughout the test period, indicating a low probability of corrosion. Unstable corrosion potentials were obtained for intact ECR in mortar with corrosion inhibitors and ECR with a calcium nitrite primer, primarily due to the insulative properties of the epoxy coating.

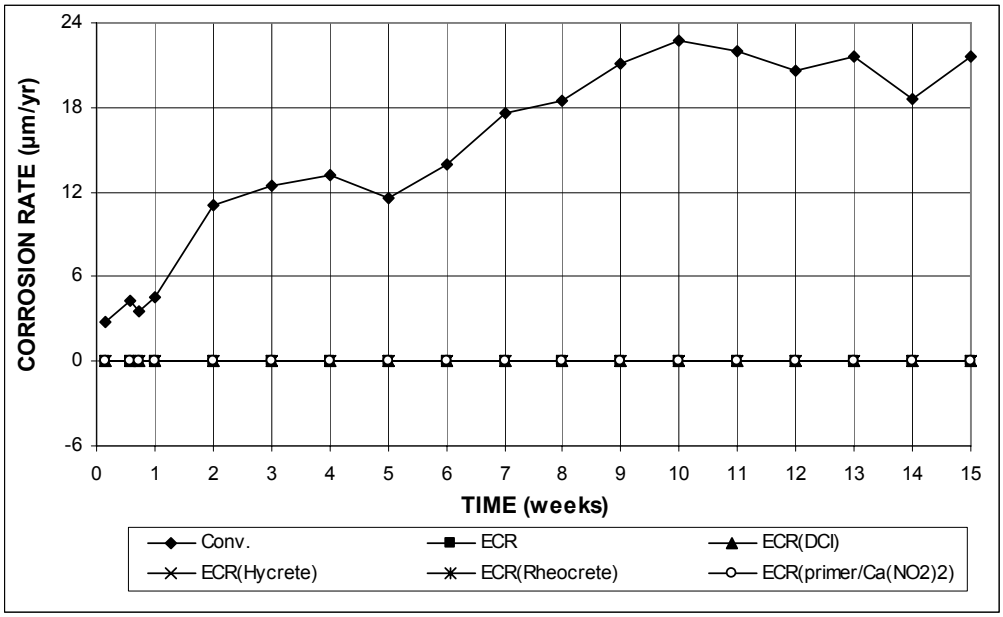

Figure 3.45 (a) – Average corrosion rates as measured in the rapid macrocell test for mortar-wrapped specimens with conventional steel, ECR, ECR cast with corrosion inhibitors, and ECR with a primer containing calcium nitrite (ECR bars have four holes).

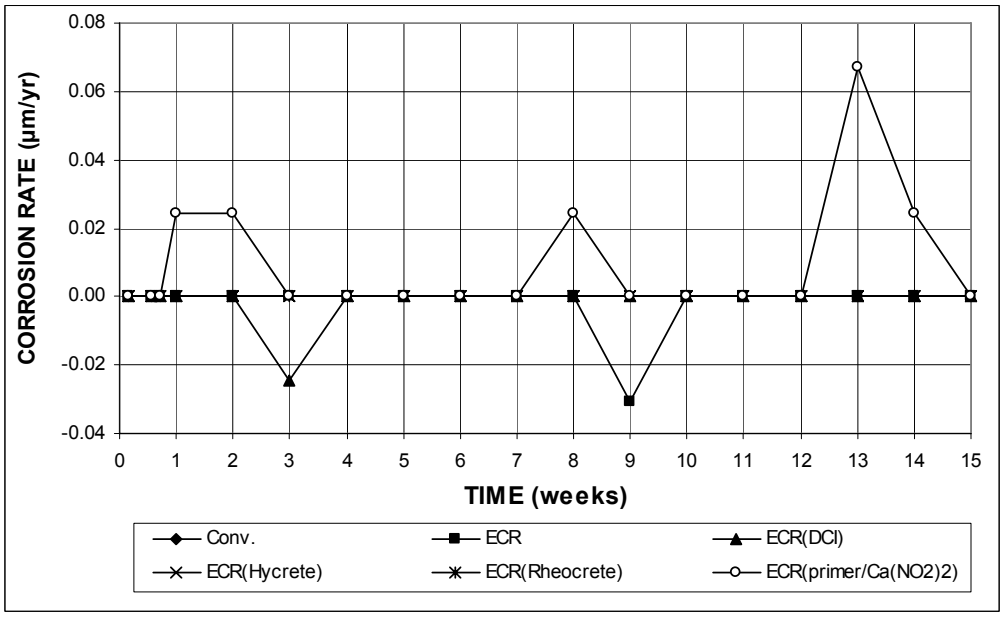

Figure 3.45 (b) – Average corrosion rates as measured in the rapid macrocell test for mortar-wrapped specimens with conventional steel, ECR, ECR cast with corrosion inhibitors, and ECR with a primer containing calcium nitrite (ECR bars have four holes).

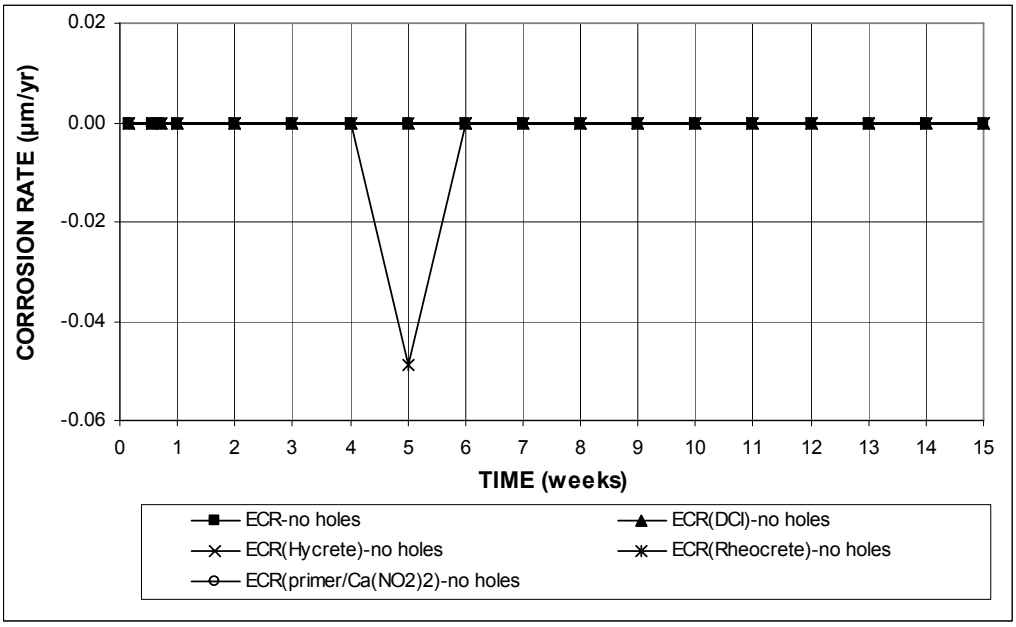

Figure 3.46 – Average corrosion rates as measured in the rapid macrocell test for mortar-wrapped specimens with ECR, ECR cast with corrosion inhibitors, and ECR with a primer containing calcium nitrite, without holes.

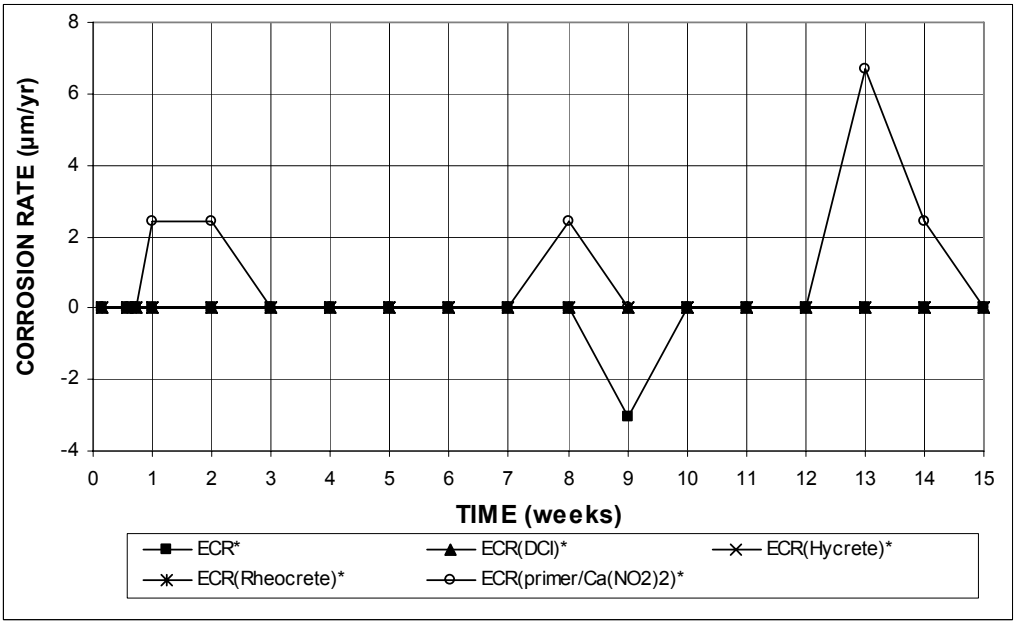

Figure 3.47 – Average corrosion rates as measured in the rapid macrocell test for mortar-wrapped specimens with ECR, ECR cast with corrosion inhibitors, and ECR with a primer containing calcium nitrite. * Based on exposed area (ECR bars have four holes).

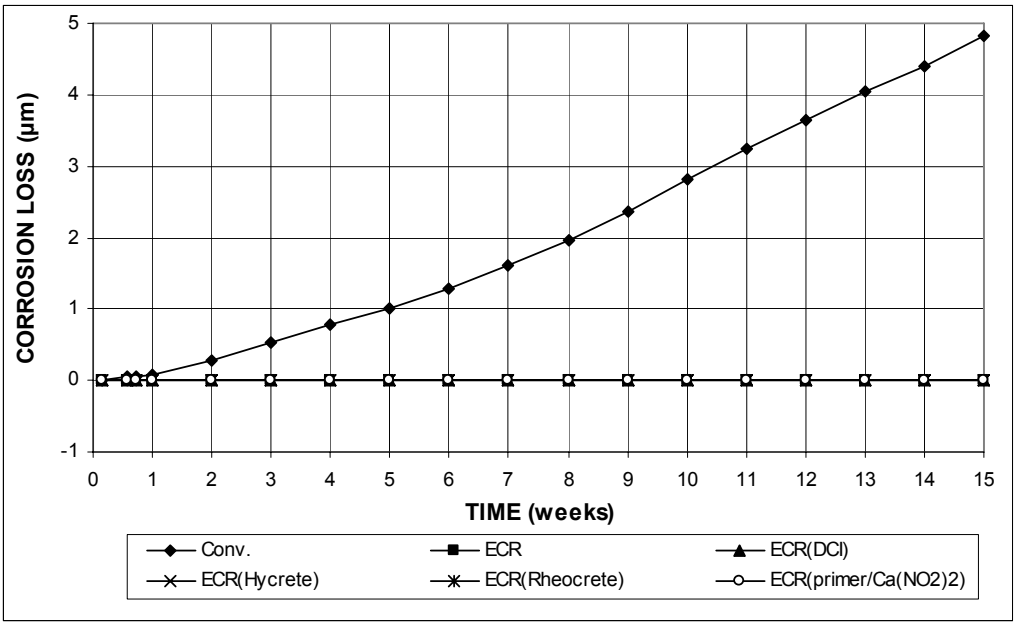

Figure 3.48 (a) – Average corrosion losses as measured in the rapid macrocell test for mortar-wrapped specimens with conventional steel, ECR, ECR cast with corrosion inhibitors, and ECR with a primer containing calcium nitrite (ECR bars have four holes).

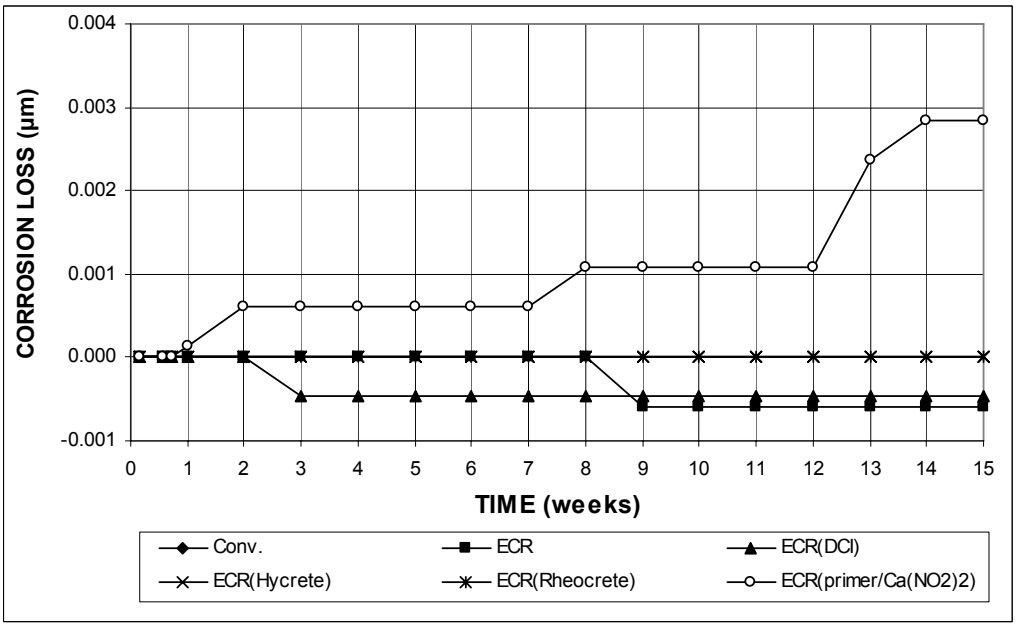

Figure 3.48 (b) – Average corrosion losses as measured in the rapid macrocell test for mortar-wrapped specimens with conventional steel, ECR, ECR cast with corrosion inhibitors, and ECR with a primer containing calcium nitrite (ECR bars have four holes).

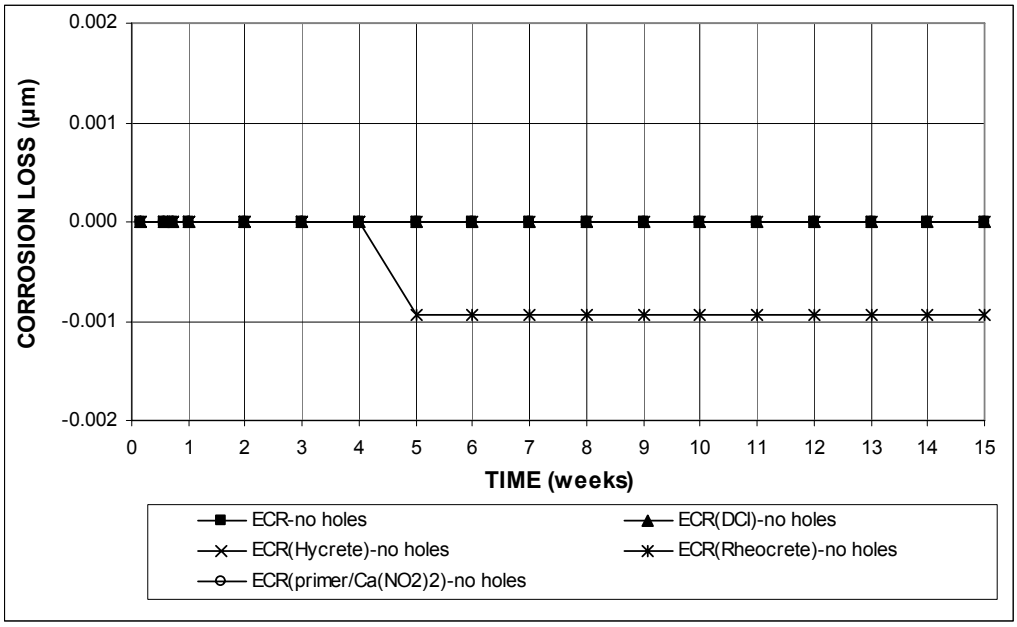

Figure 3.49 – Average corrosion losses as measured in the rapid macrocell test for mortar-wrapped specimens with ECR, ECR cast with corrosion inhibitors, and ECR with a primer containing calcium nitrite, without holes.

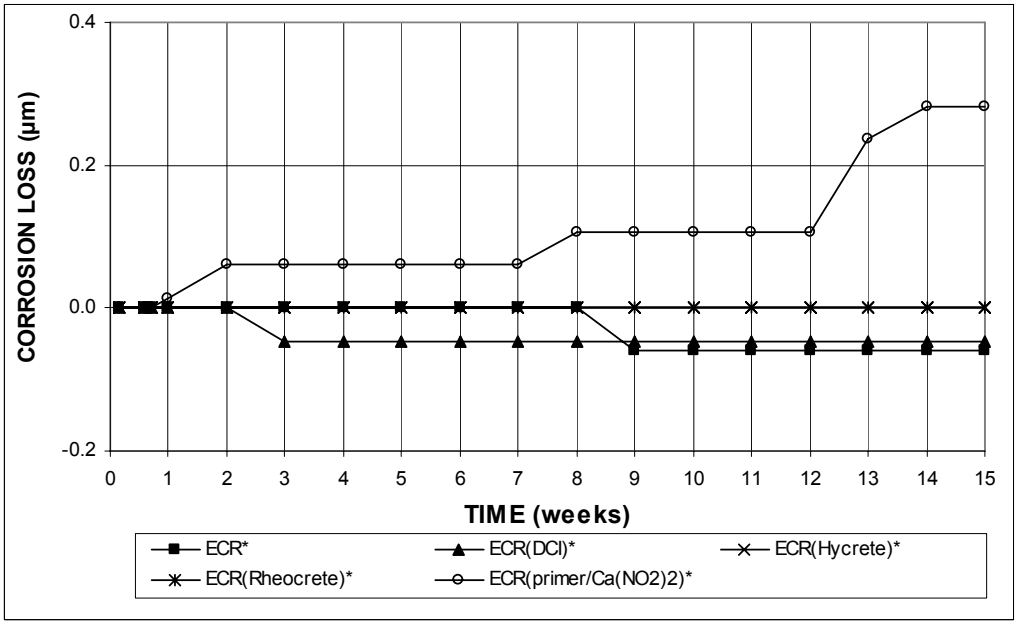

Figure 3.50 – Average corrosion losses as measured in the rapid macrocell test for mortar-wrapped specimens with ECR, ECR cast with corrosion inhibitors, and ECR with a primer containing calcium nitrite. * Based on exposed area (ECR bars have four holes).

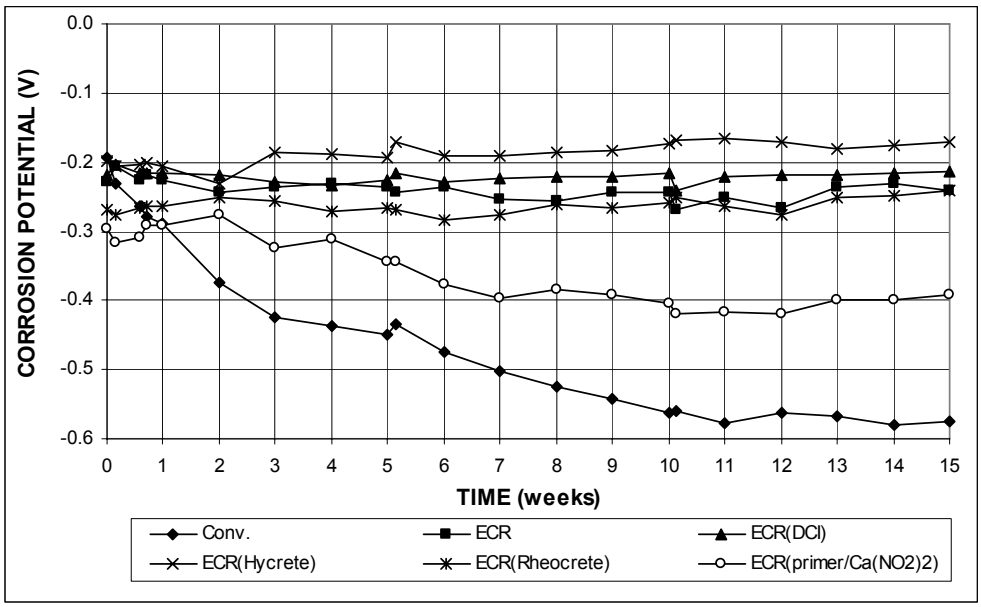

Figure 3.51 (a) – Average anode corrosion potentials, with respect to a saturated calomel electrode as measured in the rapid macrocell test for mortar-wrapped specimens with conventional steel, ECR, ECR cast with corrosion inhibitors, and ECR with a primer containing calcium nitrite (ECR bars have four holes).

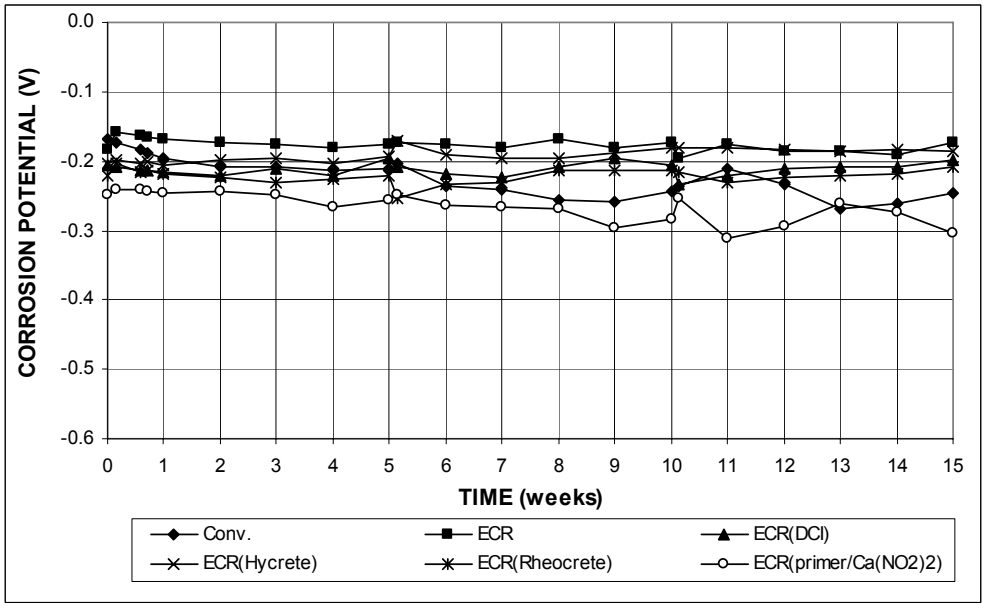

Figure 3.51 (b) – Average cathode corrosion potentials, with respect to a saturated calomel electrode as measured in the rapid macrocell test for mortar-wrapped specimens with conventional steel, ECR, ECR cast with corrosion inhibitors, and ECR with a primer containing calcium nitrite (ECR bars have four holes).

At the end of the test period, the mortar cover was removed and the specimens were visually inspected for corrosion products. None of the mortar-wrapped specimens, including the ECR(primer/($Ca(NO_2)_2$) specimens, showed corrosion products.

3.2.2 Bench-Scale Tests

The Southern Exposure and cracked beam tests were used to evaluate conventional ECR cast in concrete with corrosion inhibitors DCI, Rheocrete, or Hycrete, and ECR with a primer containing calcium nitrite. The SE and CB tests included three tests each of ECR with four holes cast in concrete with corrosion inhibitor at a *w/c* ratio of 0.45, and three tests each of ECR with 10 holes cast in concrete with corrosion inhibitor at *w/c* ratios of 0.45 and 0.35.

3.2.2.1 Southern Exposure Test

The test results are shown in Figures 3.52 through 3.69 for the Southern Exposure tests. The total corrosion losses at week 40 are summarized in Table 3.10.

Figures 3.52 and 3.53 show the average corrosion rates for specimens cast in concrete with a *w/c* ratio of 0.45 and four holes. Figure 3.52(a) shows that conventional steel had the highest corrosion rates, as discussed in Section 3.1.2.1. For the specimens with epoxy-coated reinforcement shown in Figures 3.52(b) and 3.53, conventional ECR had the highest corrosion rates between weeks 10 and 31 and ECR(primer/$Ca(NO_2)_2$) showed the highest corrosion rates between weeks 45 and 56. The ECR(DCI), ECR(Hycrete), and ECR(Rheocrete) specimens occasionally showed negative corrosion rates between weeks 26 and 46, with values between –0.014 and –0.005 μm/yr based on total area and between –6.71 and –2.44 μm/yr based on exposed area. These negative corrosion rates are generally not accompanied by more

negative corrosion potentials at cathode than at anode, and in all likelihood are aberrant readings. Overall, ECR specimens with four holes had average corrosion rates between –0.02 and 0.03 μm/yr based on total area and between –8 and 12 μm/yr based on exposed area, respectively, with the exception of ECR(DCI), which had a rate slightly above 0.03 μm/yr based on total area at week 32.

Figures 3.54 and 3.55 show the average corrosion rates for specimens cast in concrete with a *w*/*c* ratio of 0.45 and 10 holes. Of the epoxy-coated bars, ECR(primer/$Ca(NO_2)_2$)-10h generally had the highest corrosion rates between weeks 39 and 56. This specimen, however, showed negative corrosion rates from week 17 to 21, and between weeks 29 and 33, with rates between –0.020 and –0.005 μm/yr based on total area and between –3.88 and –1.05 μm/yr based on exposed area. These negative corrosion rates were caused by one of the three test specimens, and were accompanied by more negative corrosion potentials at cathode than at anode. Negative corrosion rates between –0.008 and –0.003 μm/yr based on total area were observed for ECR(DCI)-10h at week 34, for ECR(Hycrete)-10h at week 28, and for ECR(Rheocrete)-10h at week 26, respectively. These negative corrosion rates, however, were not accompanied by more negative corrosion potentials at cathode than at anode. As shown in Figures 3.54(b) and 3.55, ECR specimens with 10 holes had average corrosion rates between –0.02 and 0.03 μm/yr based on total area and between –4 and 5 μm/yr based on exposed area, respectively, with the exception of ECR(DCI)-10h, which spiked to 0.06 μm/yr (11 μm/yr based on exposed area) at week 48, and ECR(primer/$Ca(NO_2)_2$)-10h, which had corrosion rates between 0.03 and 0.08 μm/yr (between 6 and 16 μm/yr based on exposed area) between weeks 39 and 56.

Figures 3.56 and 3.57 show the average corrosion rates for specimens cast in concrete with a *w/c* ratio of 0.35 and 10 holes. As shown in Figures 3.56(b) and 3.57,

ECR specimens with a *w/c* ratio of 0.35 and 10 holes had average corrosion rates below 0.02 and 4 μm/yr based on total area and exposed area, respectively, with the exception of ECR(Rheocrete)-10h-35, which spiked to 0.024 μm/yr (4.6 μm/yr based on exposed area) at week 32, and ECR(primer/$Ca(NO_2)_2$)-10h-35 and ECR(Rheocrete)-10h-35, which spiked to 0.10 and 0.06 μm/yr (19 and 11 μm/yr based on exposed area), respectively, at week 39. Some specimens occasionally showed negative corrosion rates, including ECR(Hycrete)-10h-35 at week 24, ECR(Rheocrete)-10h-35 at weeks 25 and 41, and ECR(primer/$Ca(NO_2)_2$)-10h-35 at week 25, with values between –0.024 and –0.006 μm/yr based on total area, as shown in Figure 3.56(b). These isolated negative rates sometimes were accompanied by more negative corrosion potentials at cathode than at anode, and sometimes not.

Figures 3.58 and 3.59 show the average total corrosion losses for specimens cast in concrete with a *w/c* ratio of 0.45 and four holes. In plots for total corrosion losses, a plateau indicates very little or no corrosion activity and a steep slope means active corrosion. As shown in Figure 3.58(b), conventional steel had the highest corrosion losses (as discussed in Section 3.1.2.1), followed by conventional ECR, which showed steady corrosion up to 32 weeks and very little corrosion after that. ECR specimens cast in concrete with corrosion inhibitors exhibited lower total corrosion losses than conventional ECR. The ECR(Hycrete) and ECR(Rheocrete) specimens showed negative corrosion losses after week 27. As shown in Figures 3.58 and 3.59, all specimens with corrosion inhibitors had total corrosion losses less than 0.003 and 1.63 μm based on total area and exposed area, respectively.

Figures 3.60 and 3.61 show the average total corrosion losses for specimens cast in concrete with a *w/c* ratio of 0.45 and 10 holes. As shown in Figure 3.61, all ECR specimens exhibited progressive corrosion, with the exception of ECR(primer/$Ca(NO_2)_2$)-10h, which had negative corrosion losses between weeks 29

and 38, and showed more active corrosion after week 41, as indicated by a steeper slope. Figure 3.60(b) shows that ECR-10h had higher total corrosion losses than all specimens with a corrosion inhibitor, with the exception of ECR(primer/$Ca(NO_2)_2$)-10h, which had higher corrosion losses than ECR-10h after 43 weeks. As shown in Figure 3.61, ECR specimens cast with corrosion inhibitors had corrosion losses less than 1.0 μm based on exposed area, with the exception of ECR(primer/$Ca(NO_2)_2$), which had a loss of approximately 3.7 μm at week 56.

Figures 3.62 and 3.63 show the average total corrosion losses for specimens cast in concrete with a *w/c* ratio of 0.35 and 10 holes. As shown in Figure 3.62(b), conventional steel took off after week 48 and showed significant corrosion. All ECR specimens cast with corrosion inhibitors had lower total corrosion losses than ECR-10h-35, with values below 0.003 μm. At week 39, ECR(primer/$Ca(NO_2)_2$)-10h-35 and ECR(Rheocrete)-10h-35 showed a large increase in the total corrosion losses due to a spike in corrosion rate at week 39. Due to negative corrosion rates, some specimens showed negative corrosion losses, including ECR(Hycrete)-10h-35 between weeks 24 and 40 and ECR(primer/$Ca(NO_2)_2$)-10h-35 between weeks 25 and 38. Based on exposed area, all specimens had total corrosion losses less than 0.51 μm, as shown in Figure 3.63.

The average corrosion losses at week 40 for all ECR specimens with corrosion inhibitors are summarized in Table 3.10. All specimens showed total corrosion losses less than 0.005 μm based on total area, as indicated by the symbol β. Based on exposed area, average total corrosion losses ranged between –0.22 and 0.62 μm. For specimens with four holes, ECR(DCI) had the highest corrosion loss based on exposed area, 0.62 μm, followed by ECR(primer/$Ca(NO_2)_2$) at 0.60 μm. These values equal 45% and 43% of the total corrosion losses for conventional ECR. The ECR(Hycrete) and ECR(Rheocrete) specimens had total corrosion losses of –0.22 and

–0.16 μm, respectively, indicating that macrocell corrosion losses were not observed for the reinforcing bars at the anode. Specimens with a *w/c* ratio of 0.45 and 10 holes had total corrosion losses between 0.10 and 0.17 μm (between 16% and 28% of the corrosion loss of ECR-10h). For specimens with a *w/c* ratio of 0.35 and 10 holes, the ECR(Hycrete)-10h-35 had a total corrosion loss of –0.02 μm, and the remaining specimens had total corrosion losses ranged from 0.07 to 0.45 μm (from 14% to 92% of the corrosion loss of ECR-10h-35). For specimens with different *w/c* ratios, ECR(DCI) with a *w/c* ratio of 0.35 had a total corrosion loss equal to 71 of the corrosion loss of the corresponding specimens with a *w/c* ratio of 0.45. The ECR(Rheocrete) and ECR(primer/$Ca(NO_2)_2$) specimens with a *w/c* ratio of 0.35 exhibited total corrosion losses that were, in fact, higher than those of the corresponding specimens with a *w/c* ratio of 0.45, by 3.46 and 2.75 times, respectively. ECR containing a calcium nitrite primer with a *w/c* ratio of 0.35, however, had a total corrosion loss at week 44, 0.36 μm, 40% of the corrosion loss for the corresponding specimens with a *w/c* ratio of 0.45.

As shown in Figures 3.59 and 3.61 for specimens cast in concrete with a *w/c* ratio of 0.45, the encapsulated calcium nitrite around drilled holes appeared to provide corrosion protection for the first 45 weeks and then, when it was consumed, total corrosion losses took off rapidly. This observation agrees with the fact that the specimens with a *w/c* ratio of 0.45 remained passive before week 45 and then showed active corrosion, with potentials more negative than –0.350 V (Figures 3.64 and 3.65). Compared to specimens with corrosion inhibitors DCI-S, Hycrete, and Rheocrete, ECR with a primer containing calcium nitrite performed better in concrete with a *w/c* ratio of 0.35 than in concrete with a *w/c* ratio of 0.45. This is probably due to the low chloride penetration rate in concrete with a *w/c* ratio of 0.35, lowering the demand for the encapsulated calcium nitrite. As shown in Figure 3.66, the ECR with a calcium

nitrite primer cast in concrete with a *w*/*c* ratio of 0.35 had top mat corrosion potentials more positive than –0.240 V, indicating a passive condition. As shown in Figures 3.59 and 3.61, ECR with a calcium nitrite primer eventually performed more poorly than conventional ECR at a *w*/*c* ratio of 0.45. This may be due to the lower quality of the epoxy as indicated by the higher number of holidays and the nonuniform coating color.

Table 3.10 – Average corrosion losses (μm) at week 40 as measured in the Southern Exposure test for specimens with ECR with a primer containing calcium nitrite and ECR cast in concrete with corrosion inhibitors

Steel Designation[a]	Specimen			Average	Standard Deviation
	1	2	3		
Southern Exposure Test					
ECR(DCI)	β	β	β	β	β
ECR(DCI)*	0.63	0.32	0.91	0.62	0.30
ECR(DCI)-10h	β	β	β	β	β
ECR(DCI)-10h*	0.07	0.10	0.13	0.10	0.03
ECR(DCI)-10h-35	β	β	0.00	β	β
ECR(DCI)-10h-35*	0.10	0.11	0.00	0.07	0.06
ECR(Hycrete)	β	β	0.00	β	β
ECR(Hycrete)*	-0.46	-0.21	0.00	-0.22	0.23
ECR(Hycrete)-10h	β	0.00	0.00	β	β
ECR(Hycrete)-10h*	0.51	0.00	0.00	0.17	0.29
ECR(Hycrete)-10h-35	0.00	0.00	β	β	β
ECR(Hycrete)-10h-35*	0.00	0.00	-0.07	-0.02	0.04
ECR(Rheocrete)	β	0.00	β	β	β
ECR(Rheocrete)*	-0.14	0.00	-0.35	-0.16	0.18
ECR(Rheocrete)-10h	β	β	β	β	β
ECR(Rheocrete)-10h*	0.07	0.13	0.20	0.13	0.06
ECR(Rheocrete)-10h-35	β	β	β	β	β
ECR(Rheocrete)-10h-35*	0.11	0.73	0.52	0.45	0.31
ECR(primer/$Ca(NO_2)_2$)	β	0.00	β	β	β
ECR(primer/$Ca(NO_2)_2$)*	0.77	0.00	1.02	0.60	0.53
ECR(primer/$Ca(NO_2)_2$)-10h	β	β	β	β	β
ECR(primer/$Ca(NO_2)_2$)-10h*	0.13	0.02	0.25	0.13	0.12
ECR(primer/$Ca(NO_2)_2$)-10h-35	β	β	β	β	β
ECR(primer/$Ca(NO_2)_2$)-10h-35*	0.77	0.04	0.27	0.36	0.37

[a] ECR = conventional epoxy-coated reinforcement. ECR(DCI) = ECR in concrete with DCI.
ECR(Hycrete) = ECR in concrete with Hycrete. ECR(Rheocrete) = ECR in concrete with Rheocrete.
ECR(primer/$Ca(NO_2)_2$) = ECR with a primer containing calcium nitrite.
10h = epoxy-coated bars with 10 holes, otherwise four 3-mm ($^1/_8$-in.) diameter holes.
35 = concrete *w*/*c* =0.35, otherwise *w*/*c* = 0.45.

* Epoxy-coated bars, calculations based on exposed area of four or 10 3-mm ($^1/_8$-in.) diameter holes.

β Corrosion loss (absolute value) less than 0.005 mm.

The average corrosion potentials of the top and bottom mats of steel with respect to a copper-copper sulfate electrode are shown in Figures 3.64 through 3.66. For specimens with four holes (Figure 3.64), active corrosion of the top mat of the steel, indicated by corrosion potentials below –0.350 V, was first observed for conventional steel at week 42, followed by ECR(primer/$Ca(NO_2)_2$) at week 45. Specimens with a corrosion inhibitor in the concrete exhibited top mat corrosion potentials similar to conventional ECR, with values more positive than –0.320 V, with the exception of ECR(primer/$Ca(NO_2)_2$), which showed potentials more negative than –0.350 V after week 45. Due to the lower quality of the epoxy, ECR with a calcium nitrite primer exhibited top mat corrosion potentials similar to those for conventional steel. As shown in Figure 3.64(b), the average corrosion potentials of the bottom mats were similar to those for ECR and remained more positive than –0.300 V for all specimens, indicating a low probability of corrosion.

As shown in Figure 3.65(a), in general, ECR specimens with corrosion inhibitors and 10 holes showed more positive corrosion potentials for the top mat than conventional ECR with 10 holes (ECR-10h). ECR(Hycrete)-10h had top mat corrosion potentials more positive than –0.330 V, indicating a low probability of corrosion. ECR(DCI)-10h showed active corrosion at week 47, with a top mat corrosion potential of –0.369 V. ECR(primer/$Ca(NO_2)_2$)-10h had a top mat corrosion potential of –0.359 V at week 47, and after that it had values below –0.400 V. The average corrosion potentials of the bottom mat for specimens with corrosion inhibitors were similar to those for ECR-10h, as shown in Figure 3.65(b). ECR(DCI)-10h and ECR(primer/$Ca(NO_2)_2$)-10h had bottom mat corrosion potentials more positive than –0.300 V, while ECR(Hycrete)-10h had values above –0.170 V, indicating a passive condition.

For specimens with a *w/c* ratio of 0.35 and 10 holes (Figure 3.66), all epoxy-

coated specimens showed top mat corrosion potentials more positive than –0.350 V, with the exception of ECR(Rheocrete)-10h-35 at week 33 and ECR(Hycrete)-10h-35 at week 36. ECR(DCI)-10h-35 and ECR(primer/$Ca(NO_2)_2$)-10h-35 had top mat corrosion potentials above –0.250 V, indicating a low probability of corrosion. As shown in Figure 3.66(b), the average corrosion potentials of the bottom mat for specimens with corrosion inhibitors were similar to those for ECR-10h-35 and remained more positive than –0.270 V for all specimens, indicating a low probability of corrosion.

The average mat-to-mat resistances are shown in Figure 3.67 for specimens with four holes, in Figure 3.68 for specimens with 10 holes, and in Figure 3.69 for specimens with a *w/c* ratio of 0.35 and 10 holes, respectively. Figure 3.67 shows that the average mat-to-mat resistances increased with time at a similar rate for all specimens with four holes. The average mat-to-mat resistances started with values between 1,600 and 2,750 ohms and increased to values between 5,900 and 10,100 ohms at week 40. ECR(Hycrete) showed slightly higher mat-to-mat resistance than the remaining specimens. As shown in Figure 3.68, the average mat-to-mat resistances for ECR specimens with a *w/c* ratio of 0.45 and 10 holes increased with time at a similar rate to ECR-10h. These specimens had average mat-to-mat resistances around 1,000 ohms at the beginning and increased to values between 3,700 and 6,800 ohms at week 40. Figure 3.69 shows that ECR specimens with a *w/c* ratio of 0.35 and 10 holes had lower mat-to-mat resistances than those for specimens with a *w/c* ratio of 0.45 and 10 holes. These specimens had average mat-to-mat resistances of approximately 1,000 ohms in the first week and increased to values around 3,500 ohms at week 39.

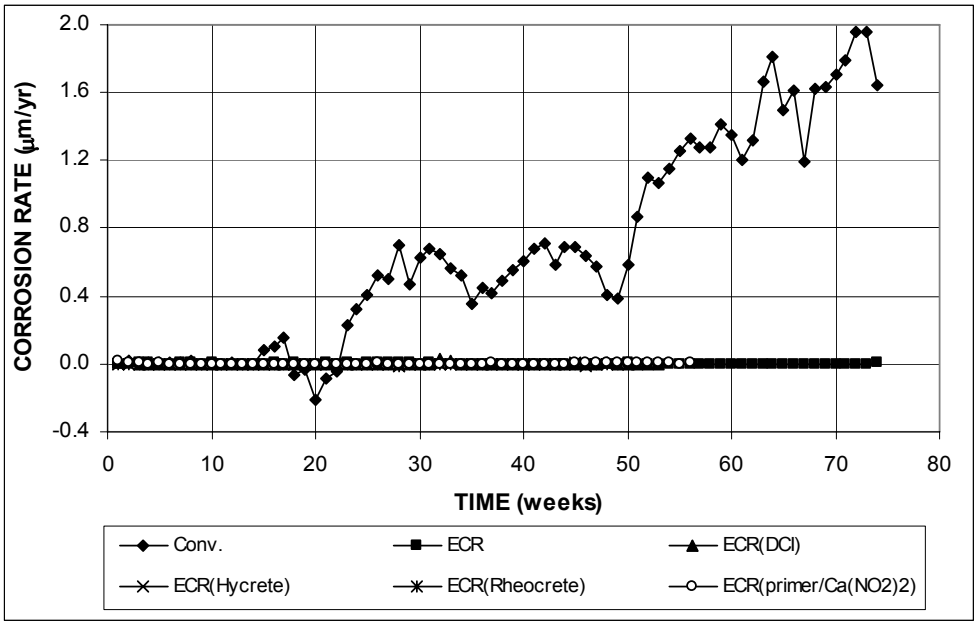

Figure 3.52 (a) – Average corrosion rates as measured in the Southern Exposure test for specimens with conventional steel, ECR, ECR in concrete with corrosion inhibitors, and ECR with a primer containing calcium nitrite (ECR bars have four holes).

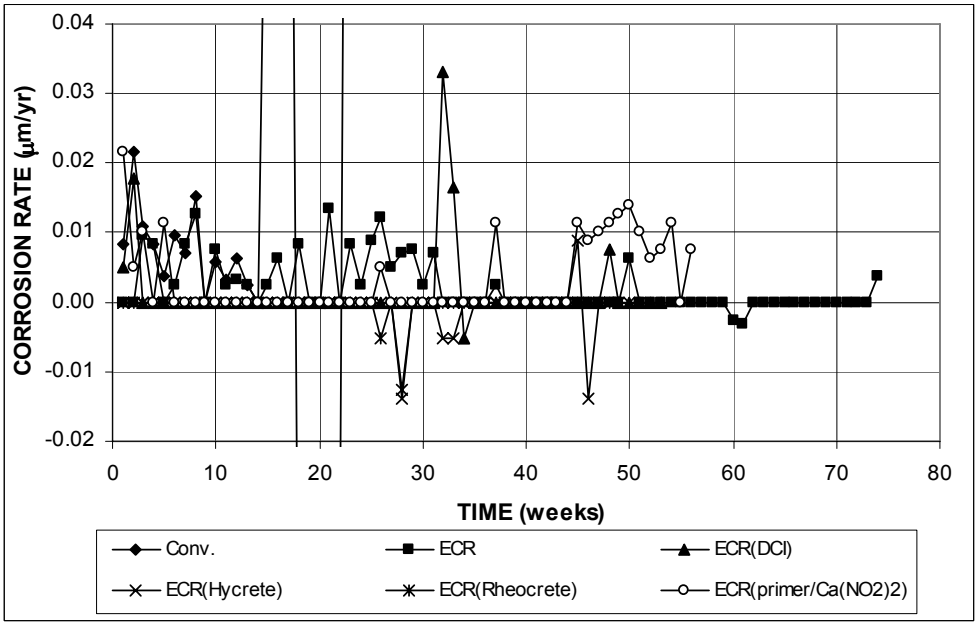

Figure 3.52 (b) – Average corrosion rates as measured in the Southern Exposure test for specimens with conventional steel, ECR, ECR in concrete with corrosion inhibitors, and ECR with a primer containing calcium nitrite (ECR bars have four holes).

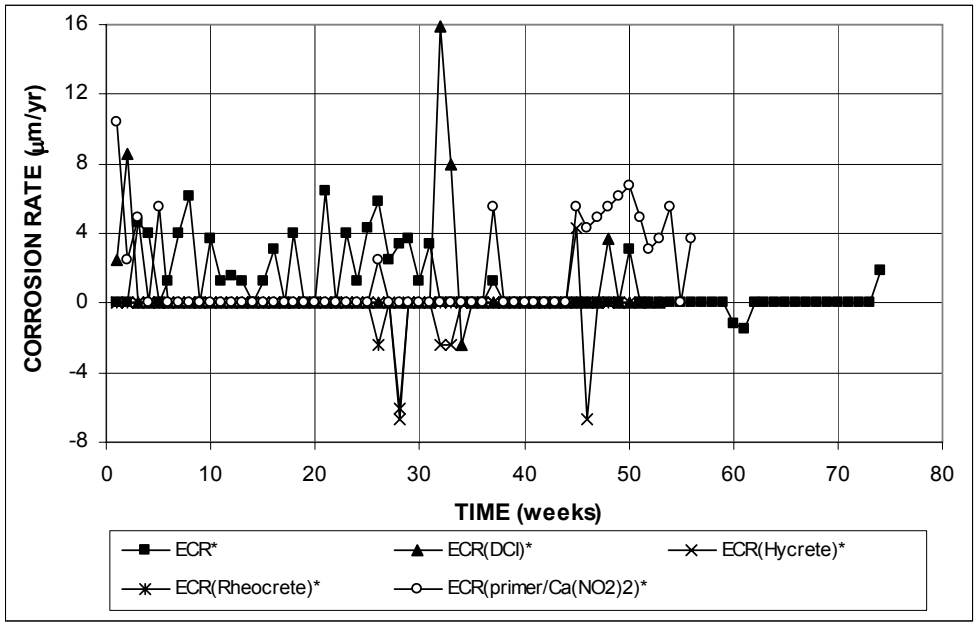

Figure 3.53 – Average corrosion rates as measured in the Southern Exposure test for specimens with ECR, ECR in concrete with corrosion inhibitors, and ECR with a primer containing calcium nitrite. * Based on exposed area (ECR bars have four holes).

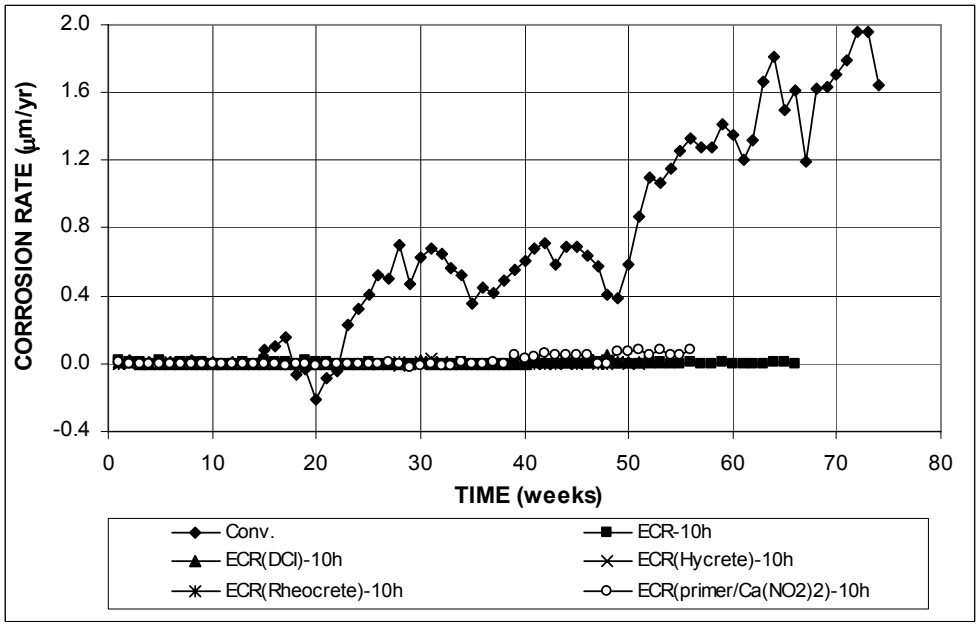

Figure 3.54 (a) – Average corrosion rates as measured in the Southern Exposure test for specimens with conventional steel, ECR, ECR in concrete with corrosion inhibitors, and ECR with a primer containing calcium nitrite (ECR bars have 10 holes).

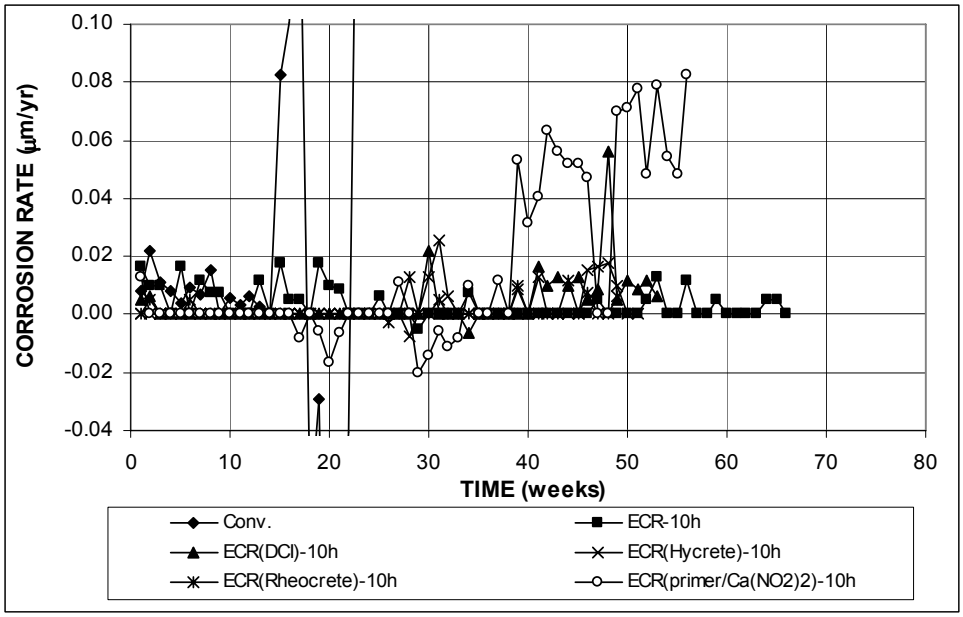

Figure 3.54 (b) – Average corrosion rates as measured in the Southern Exposure test for specimens with conventional steel, ECR, ECR in concrete with corrosion inhibitors, and ECR with a primer containing calcium nitrite (ECR bars have 10 holes).

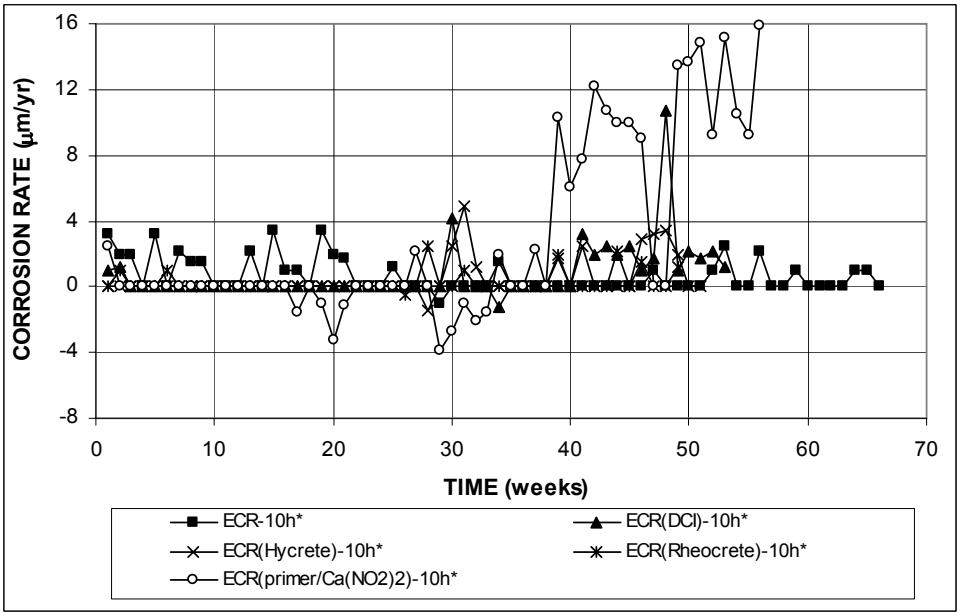

Figure 3.55 – Average corrosion rates as measured in the Southern Exposure test for specimens with ECR, ECR in concrete with corrosion inhibitors, and ECR with a primer containing calcium nitrite. * Based on exposed area (ECR bars have 10 holes).

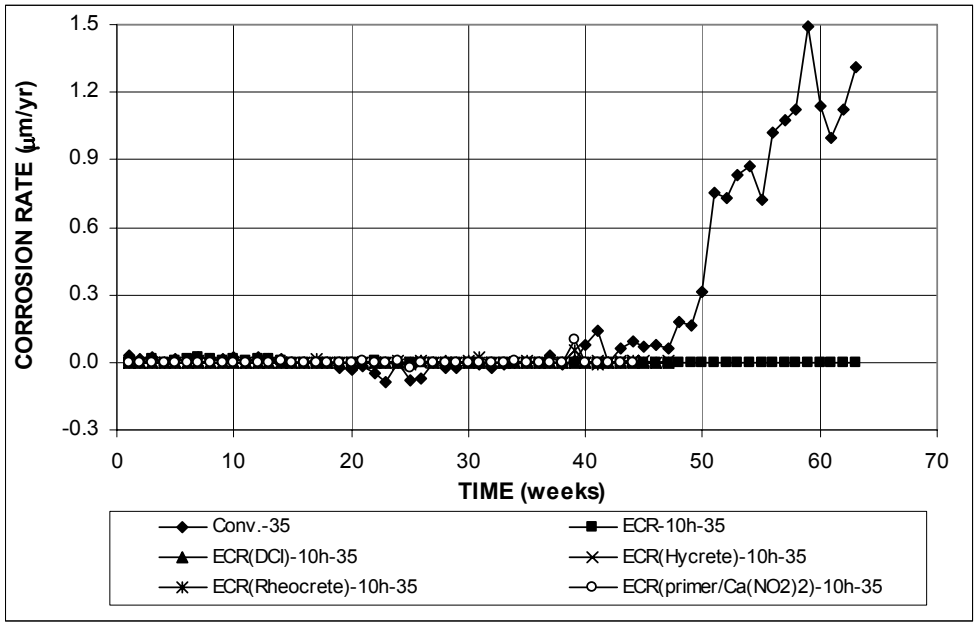

Figure 3.56 (a) – Average corrosion rates as measured in the Southern Exposure test for specimens with conventional steel, ECR, ECR in concrete with corrosion inhibitors, and ECR with a primer containing calcium nitrite, water-cement ratio = 0.35 (ECR bars have 10 holes).

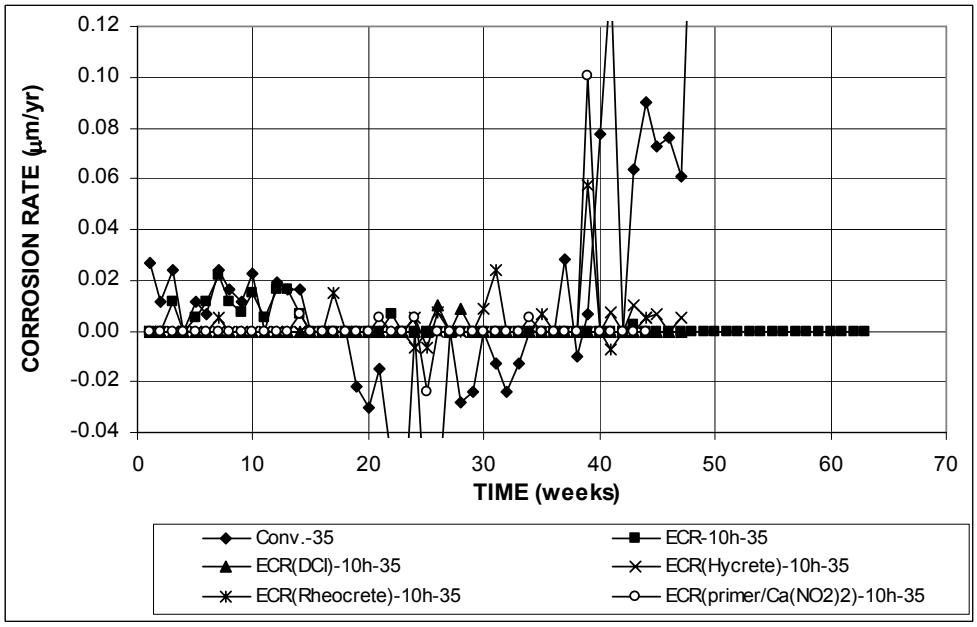

Figure 3.56 (b) – Average corrosion rates as measured in the Southern Exposure test for specimens with conventional steel, ECR, ECR in concrete with corrosion inhibitors, and ECR with a primer containing calcium nitrite, water-cement ratio = 0.35 (ECR bars have 10 holes).

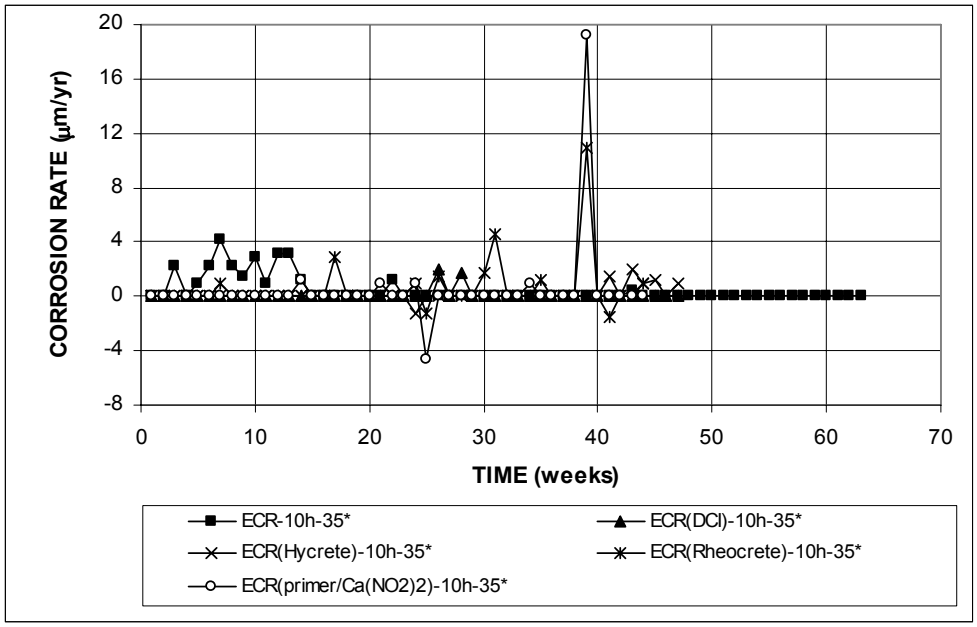

Figure 3.57 – Average corrosion rates as measured in the Southern Exposure test for specimens with ECR, ECR in concrete with corrosion inhibitors, and ECR with a primer containing calcium nitrite, water-cement ratio = 0.35. * Based on exposed area (ECR bars have 10 holes).

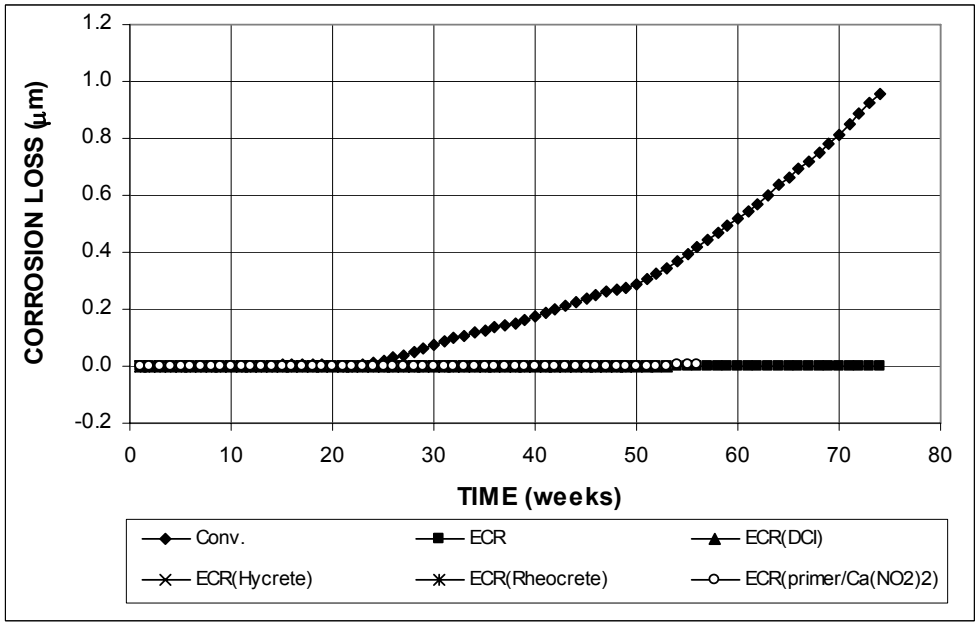

Figure 3.58 (a) – Average corrosion losses as measured in the Southern Exposure test for specimens with conventional steel, ECR, ECR in concrete with corrosion inhibitors, and ECR with a primer containing calcium nitrite (ECR bars have four holes).

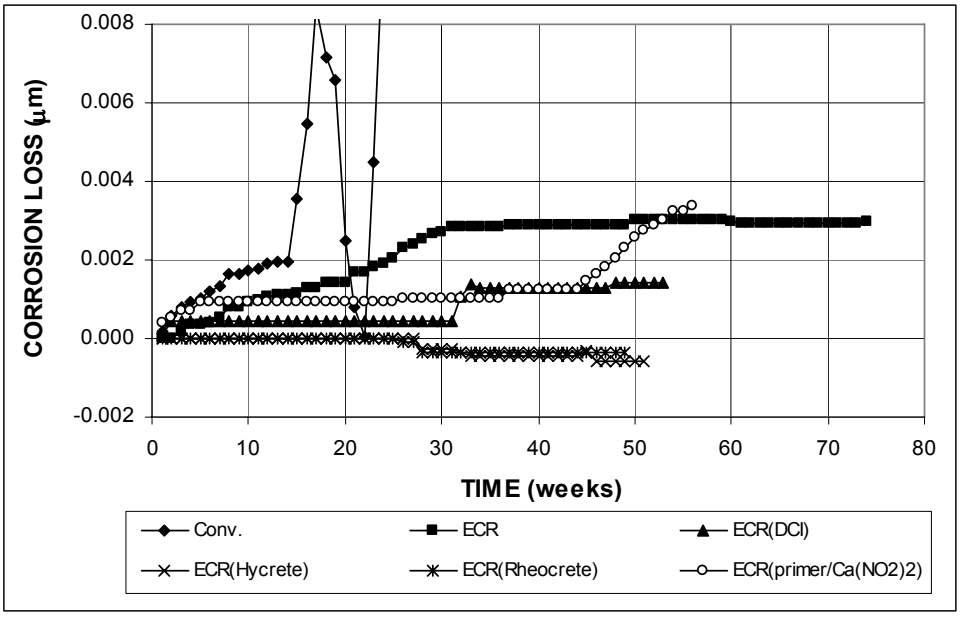

Figure 3.58 (b) – Average corrosion losses as measured in the Southern Exposure test for specimens with conventional steel, ECR, ECR in concrete with corrosion inhibitors, and ECR with a primer containing calcium nitrite (ECR bars have four holes).

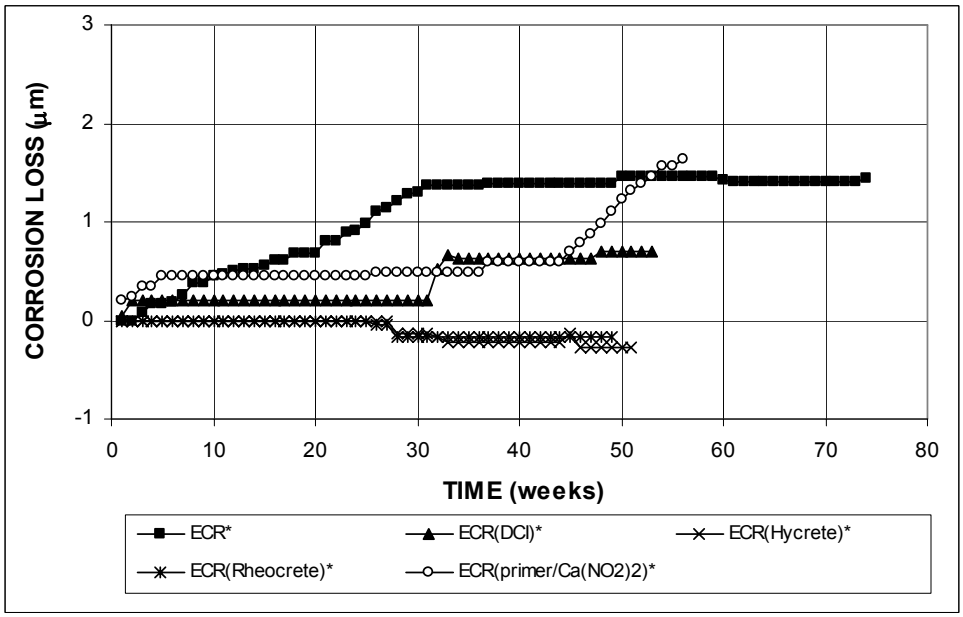

Figure 3.59 – Average corrosion losses as measured in the Southern Exposure test for specimens with ECR, ECR in concrete with corrosion inhibitors, and ECR with a primer containing calcium nitrite. * Based on exposed area (ECR bars have four holes).

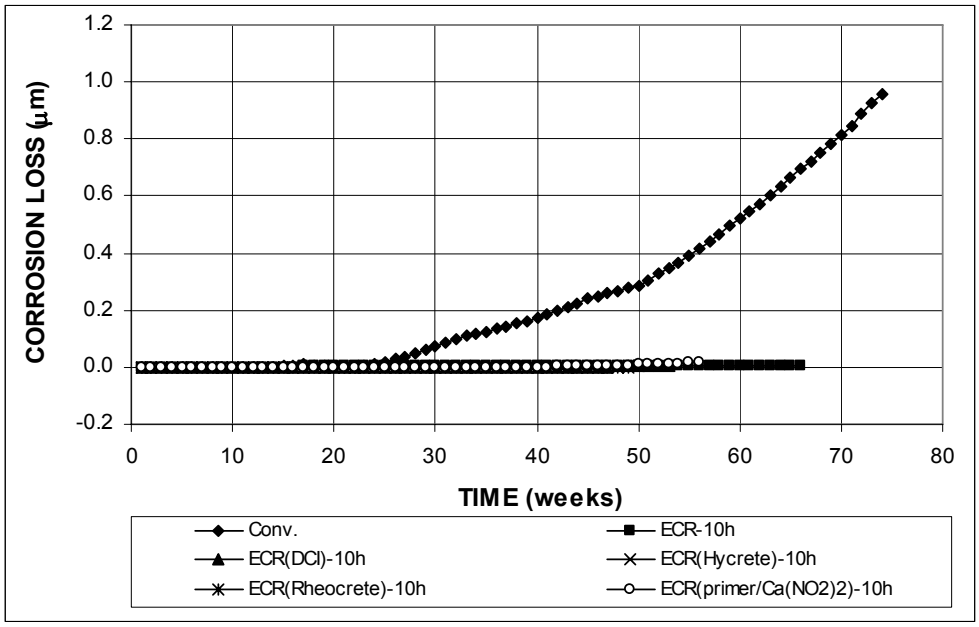

Figure 3.60 (a) – Average corrosion losses as measured in the Southern Exposure test for specimens with conventional steel, ECR, ECR in concrete with corrosion inhibitors, and ECR with a primer containing calcium nitrite (ECR bars have 10 holes).

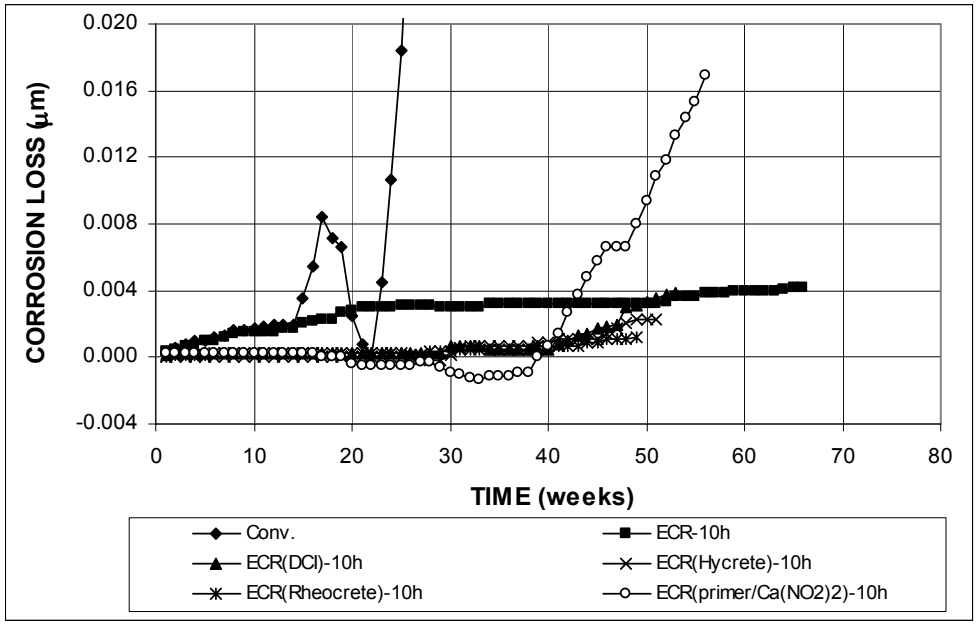

Figure 3.60 (b) – Average corrosion losses as measured in the Southern Exposure test for specimens with conventional steel, ECR, ECR in concrete with corrosion inhibitors, and ECR with a primer containing calcium nitrite (ECR bars have 10 holes).

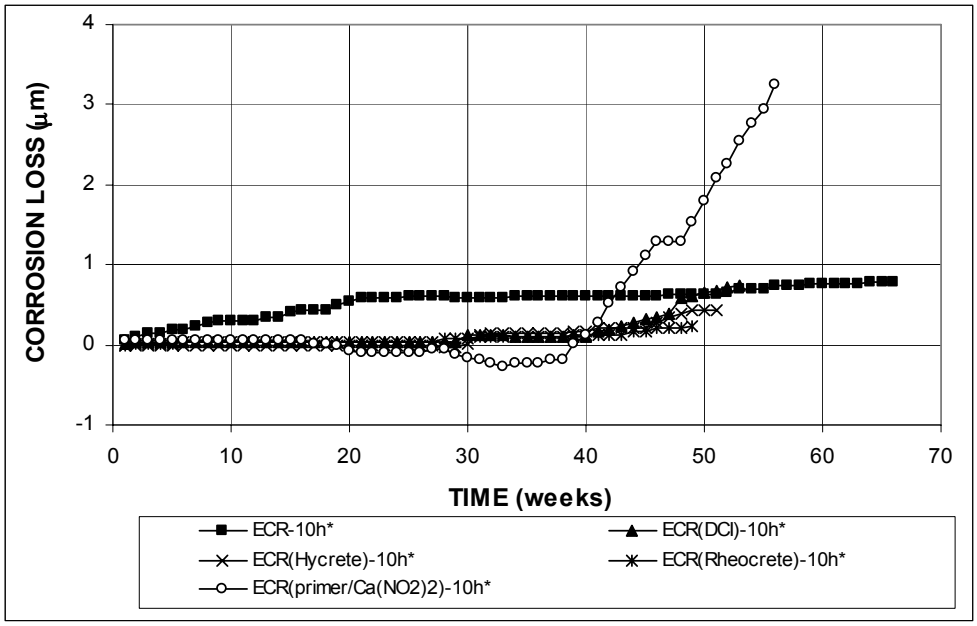

Figure 3.61 – Average corrosion losses as measured in the Southern Exposure test for specimens with ECR, ECR in concrete with corrosion inhibitors, and ECR with a primer containing calcium nitrite. * Based on exposed area (ECR bars have 10 holes).

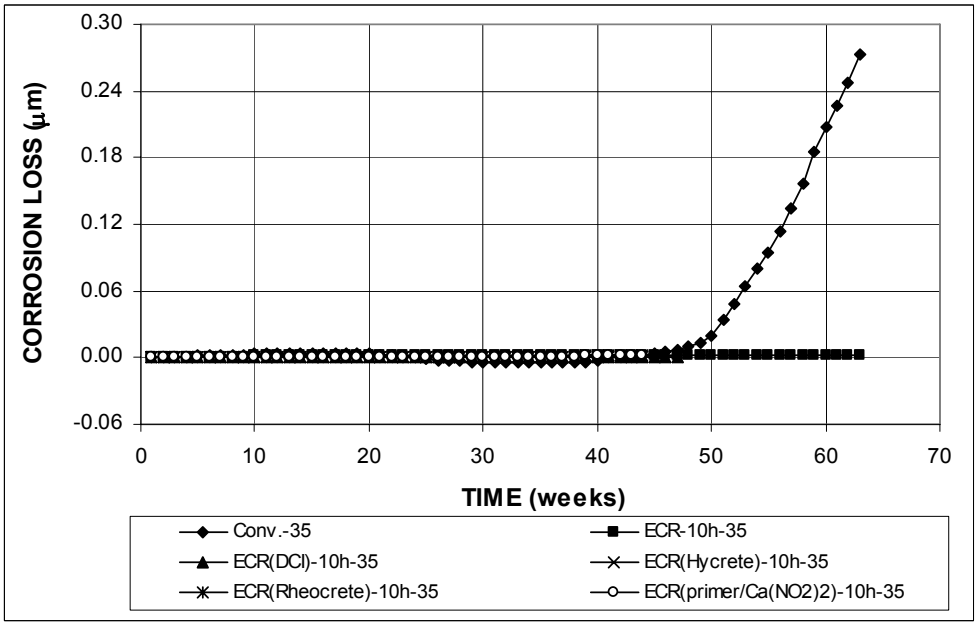

Figure 3.62 (a) – Average corrosion losses as measured in the Southern Exposure test for specimens with conventional steel, ECR, ECR in concrete with corrosion inhibitors, and ECR with a primer containing calcium nitrite, water-cement ratio = 0.35 (ECR bars have 10 holes).

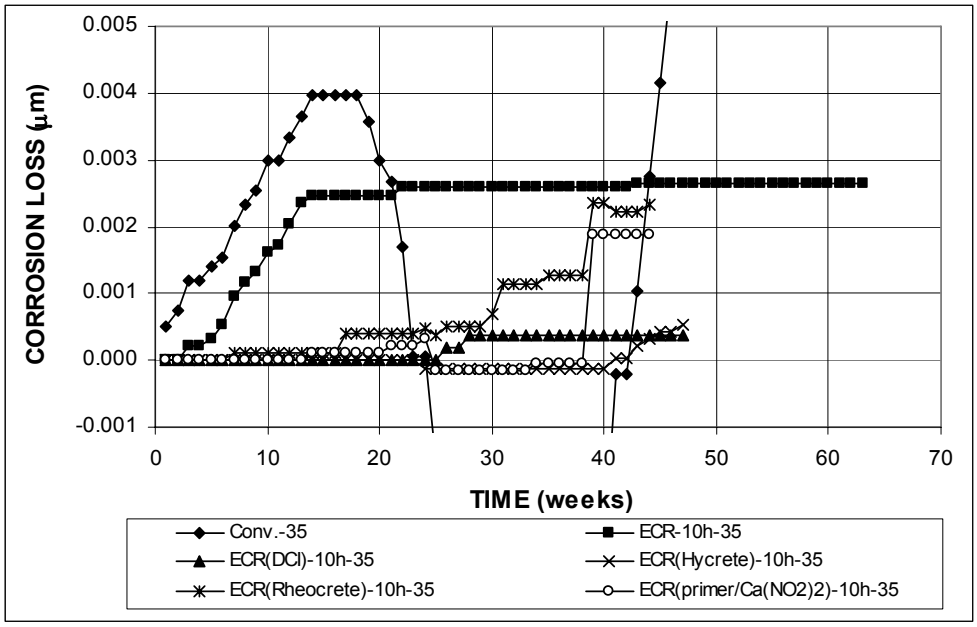

Figure 3.62 (b) – Average corrosion losses as measured in the Southern Exposure test for specimens with conventional steel, ECR, ECR in concrete with corrosion inhibitors, and ECR with a primer containing calcium nitrite, water-cement ratio = 0.35 (ECR bars have 10 holes).

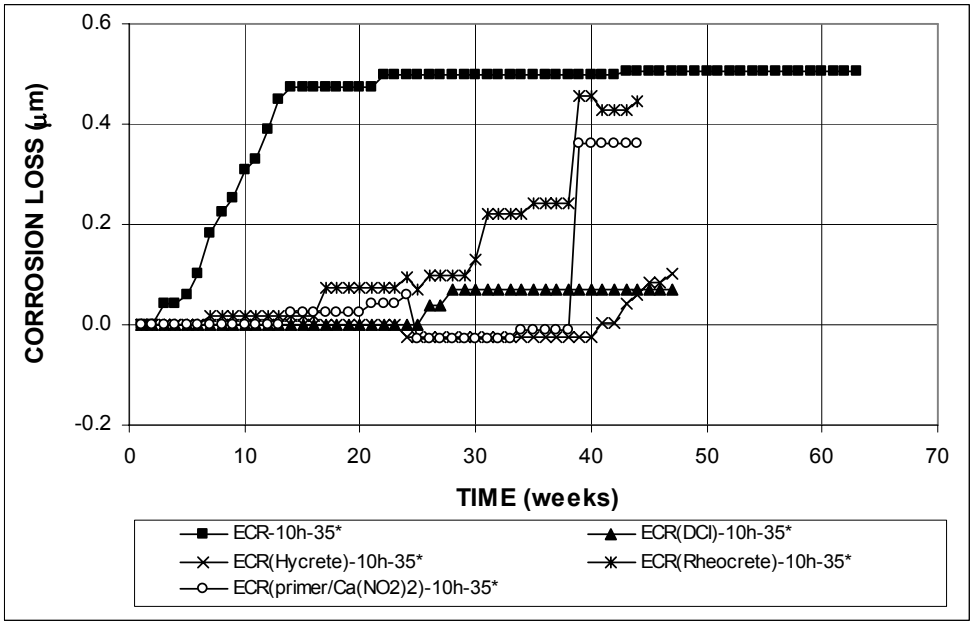

Figure 3.63 – Average corrosion losses as measured in the Southern Exposure test for specimens with ECR, ECR in concrete with corrosion inhibitors, and ECR with a primer containing calcium nitrite, water-cement ratio = 0.35. * Based on exposed area (ECR bars have 10 holes).

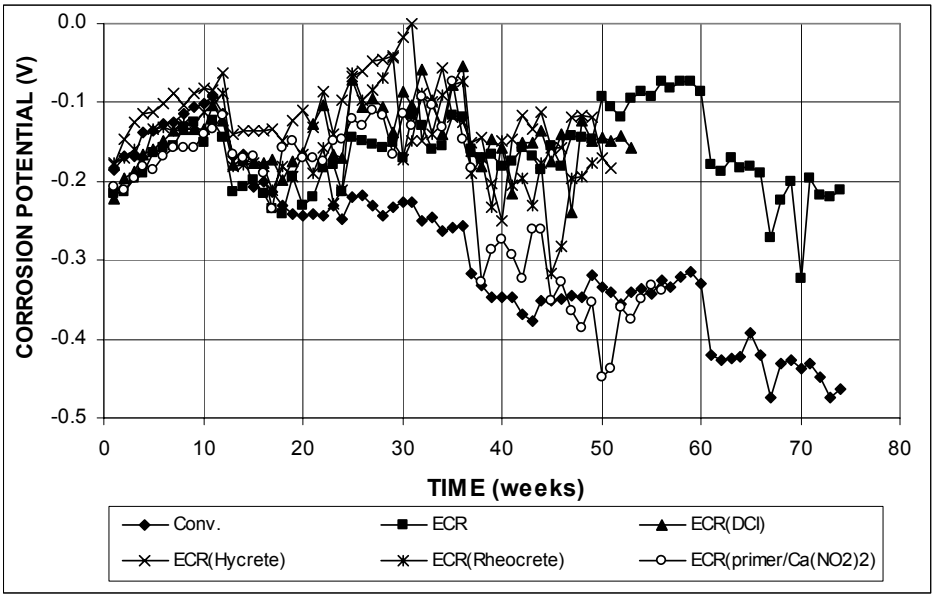

Figure 3.64 (a) – Average top mat corrosion potentials, with respect to a copper-copper sulfate electrode as measured in the Southern Exposure test for specimens with conventional steel, ECR, ECR in concrete with corrosion inhibitors, and ECR with a primer containing calcium nitrite (ECR bars have four holes).

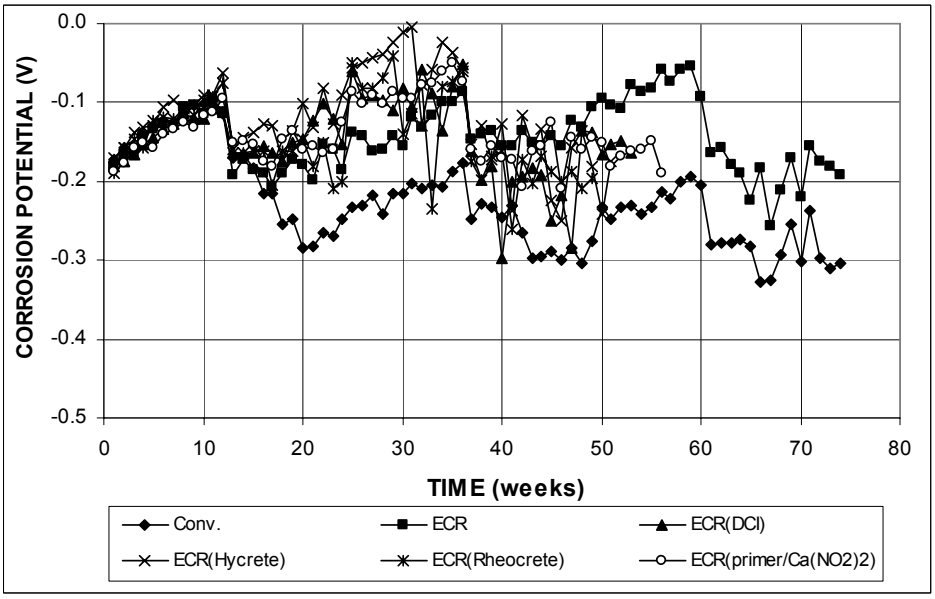

Figure 3.64 (b) – Average bottom mat corrosion potentials, with respect to a copper-copper sulfate electrode as measured in the Southern Exposure test for specimens with conventional steel, ECR, ECR in concrete with corrosion inhibitors, and ECR with a primer containing calcium nitrite (ECR bars have four holes).

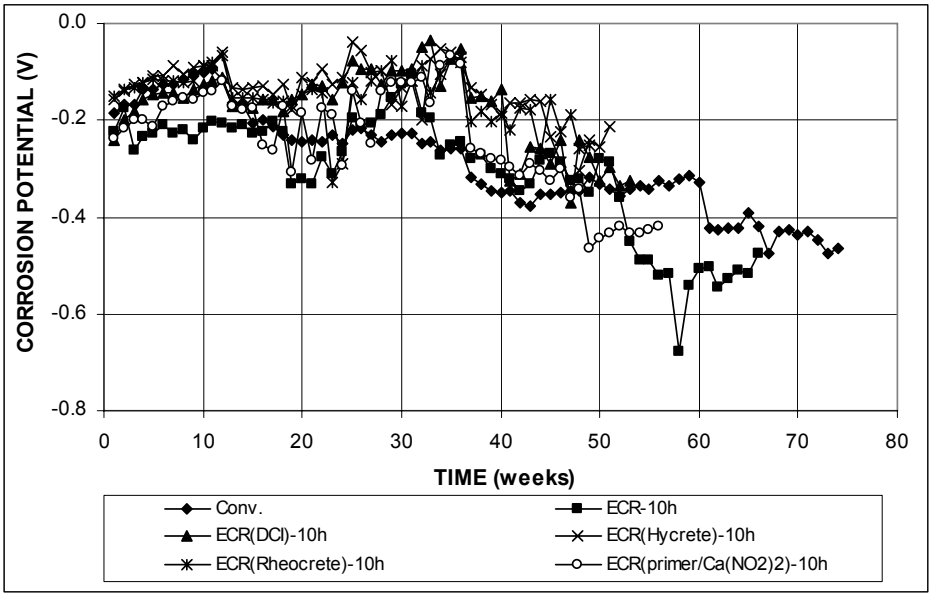

Figure 3.65 (a) – Average top mat corrosion potentials, with respect to a copper-copper sulfate electrode as measured in the Southern Exposure test for specimens with conventional steel, ECR, ECR in concrete with corrosion inhibitors, and ECR with a primer containing calcium nitrite (ECR bars have 10 holes).

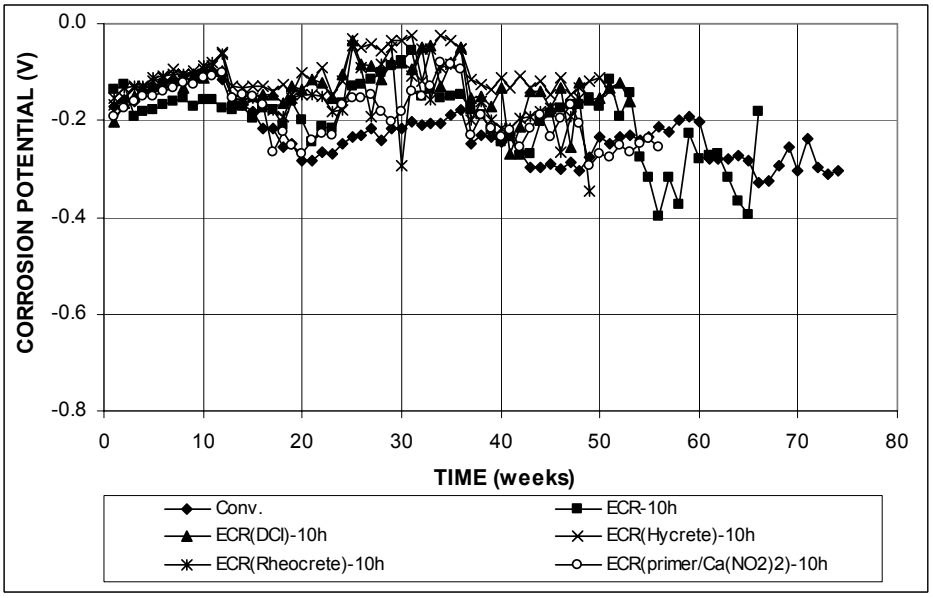

Figure 3.65 (b) – Average bottom mat corrosion potentials, with respect to a copper-copper sulfate electrode as measured in the Southern Exposure test for specimens with conventional steel, ECR, ECR in concrete with corrosion inhibitors, and ECR with a primer containing calcium nitrite (ECR bars have 10 holes).

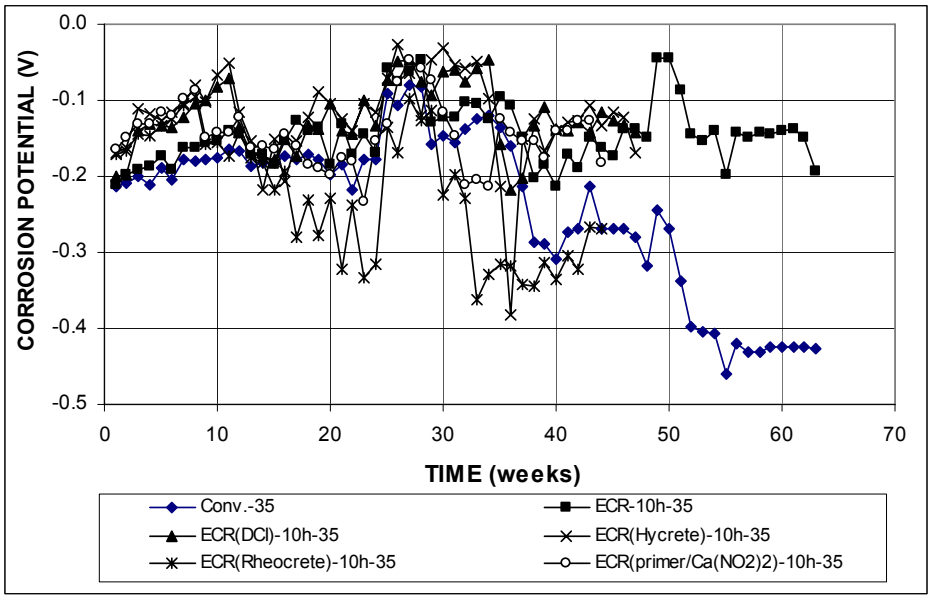

Figure 3.66 (a) – Average top mat corrosion potentials, with respect to a copper-copper sulfate electrode as measured in the Southern Exposure test for specimens with conventional steel, ECR, ECR in concrete with corrosion inhibitors, and ECR with a primer containing calcium nitrite, water-cement ratio = 0.35 (ECR bars have 10 holes).

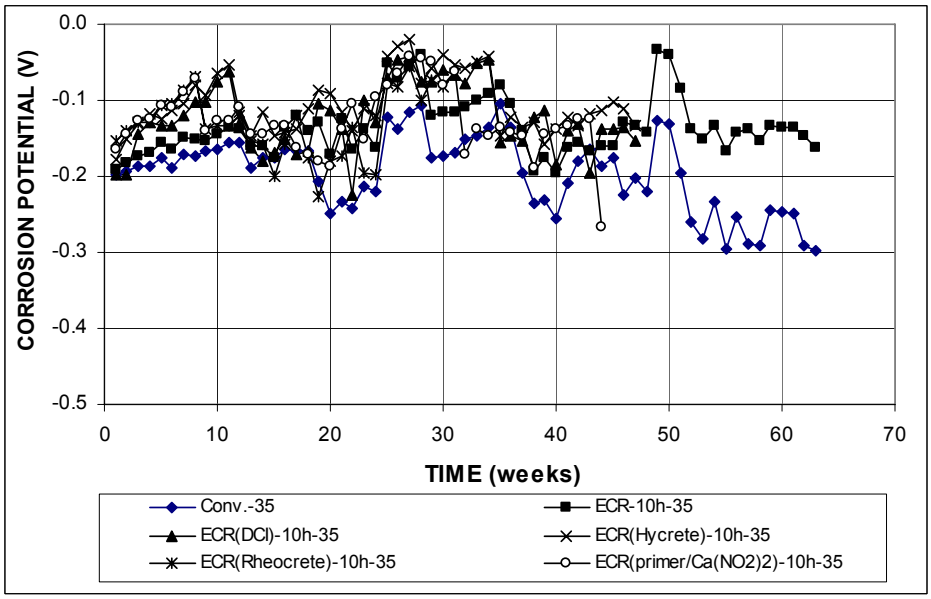

Figure 3.66 (b) – Average bottom mat corrosion potentials, with respect to a copper-copper sulfate electrode as measured in the Southern Exposure test for specimens with conventional steel, ECR, ECR in concrete with corrosion inhibitors, and ECR with a primer containing calcium nitrite, water-cement ratio = 0.35 (ECR bars have 10 holes).

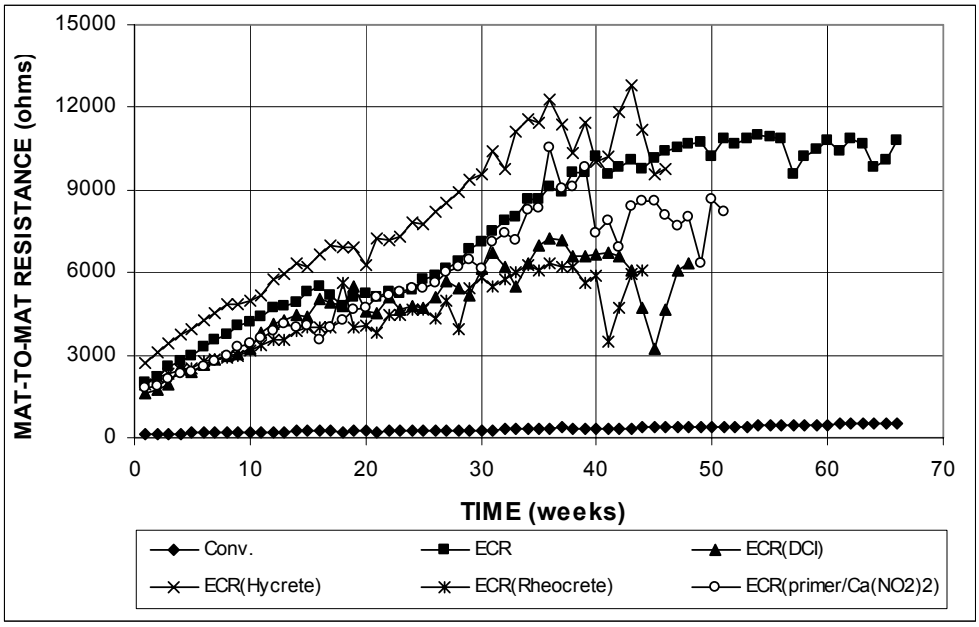

Figure 3.67 – Average mat-to-mat resistances as measured in the Southern Exposure test for specimens with conventional steel, ECR, ECR in concrete with corrosion inhibitors, and ECR with a primer containing calcium nitrite (ECR bars have four holes).

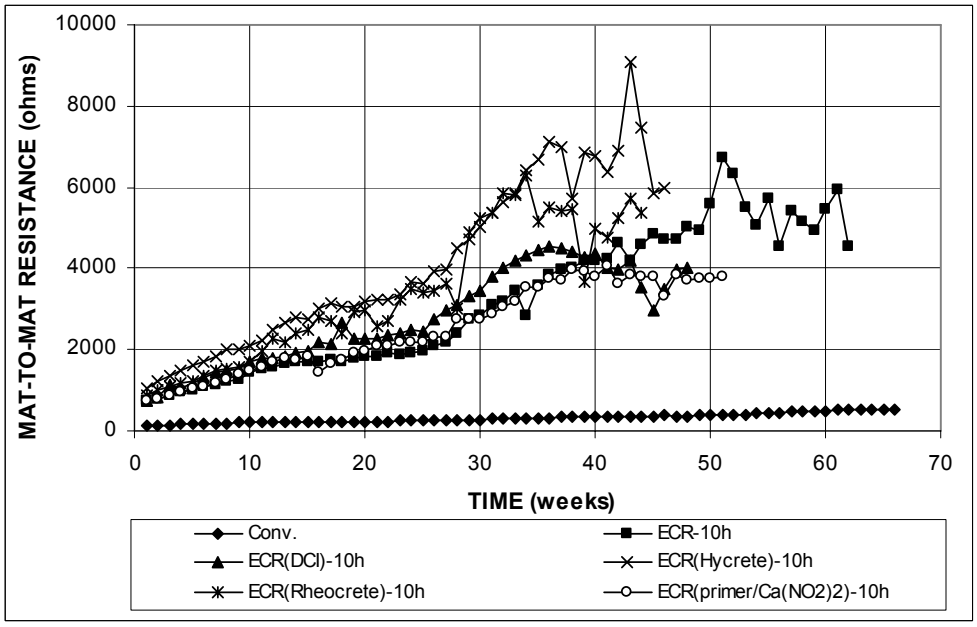

Figure 3.68 – Average mat-to-mat resistances as measured in the Southern Exposure test for specimens with conventional steel, ECR, ECR in concrete with corrosion inhibitors, and ECR with a primer containing calcium nitrite (ECR bars have 10 holes).

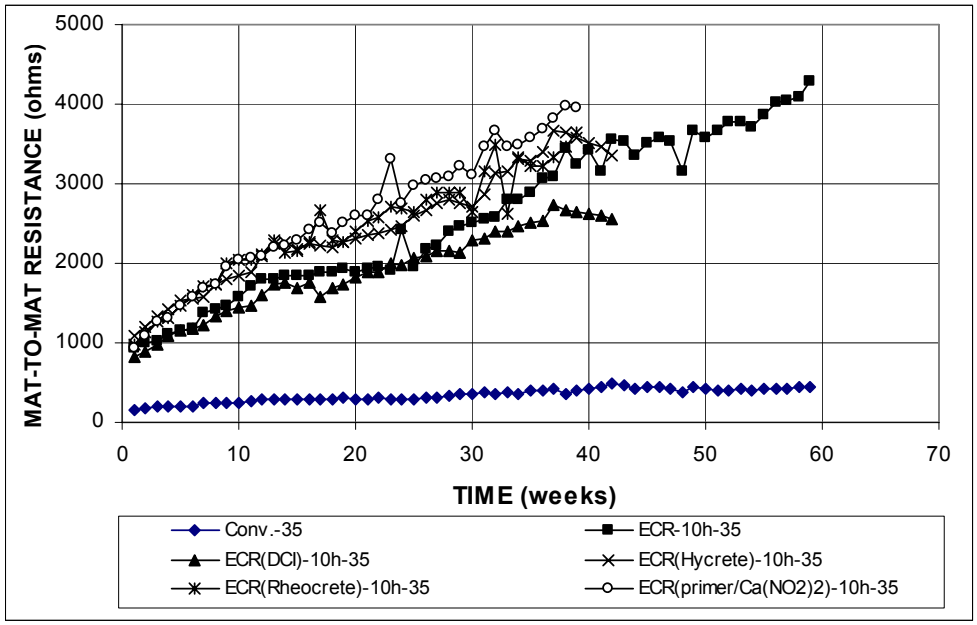

Figure 3.69 – Average mat-to-mat resistances as measured in the Southern Exposure test for specimens with conventional steel, ECR, ECR in concrete with corrosion inhibitors, and ECR with a primer containing calcium nitrite, water-cement ratio = 0.35 (ECR bars have 10 holes).

3.2.2.2 Cracked Beam Test

The test results are shown in Figures 3.70 through 3.87 for the cracked beam tests. The total corrosion losses at week 40 are summarized in Table 3.11.

The average corrosion rates are shown in Figures 3.70 through 3.75. Some specimens showed negative corrosion rates, including ECR(Hycrete) at week 28, ECR(primer/$Ca(NO_2)_2$) at weeks 40 and 45, ECR(DCI)-10h at weeks 30 and 34, ECR(Hycrete)-10h at week 26 and ECR(primer/$Ca(NO_2)_2$)-10h at week 45, with values between –0.003 and –0.043 μm/yr based on total area. These negative corrosion rates, however, in all likelihood represent aberrant readings and were not accompanied by more negative corrosion potentials at cathode than at anode. Figures 3.70 and 3.71 show the average corrosion rates for specimens cast in concrete with a *w*/*c* ratio of 0.45 and four holes. Figure 3.70(a) shows that conventional steel had the

highest corrosion rates, as discussed in Section 3.1.2.2. As shown in Figures 3.70(b) and 3.71, all specimens with four holes showed erratic behavior and had corrosion rates similar to conventional ECR. The corrosion rates for these specimens were less than 0.13 and 60 μm/yr based on total area and exposed area, respectively, with the exception of ECR(Rheocrete), which spiked to 0.20 μm/yr (95 μm/yr based on exposed area) at week 40. Figures 3.72 and 3.73 show the average corrosion rates for specimens cast in concrete with a *w*/*c* ratio of 0.45 and 10 holes. As shown in Figure 3.72(b), ECR(Rheocrete)-10h generally showed the highest corrosion rates between weeks 17 and 46. All ECR specimens with 10 holes had average corrosion rates less than 0.22 μm/yr based on total area and 41.9 μm/yr based on exposed area, respectively. Figures 3.74 and 3.75 show the average corrosion rates for specimens cast in concrete with a *w/c* ratio of 0.35 and 10 holes. Figure 3.74(b) shows that, in general, all specimens with a *w/c* ratio of 0.35 and 10 holes showed higher corrosion rates than conventional ECR, but with values below 0.47 and 91 μm/yr based on total and exposed area, respectively.

Figures 3.76 and 3.77 show the average total corrosion losses for specimens cast in concrete with a *w*/*c* ratio of 0.45 and four holes. As shown in Figure 3.76, conventional steel had, by far, the highest corrosion losses at week 74, approximately 10 μm. The remaining specimens had total corrosion losses below 0.036 and 17.2 μm based on total area and exposed area, respectively. The average total corrosion losses for specimens with a *w*/*c* ratio of 0.45 and 10 holes are shown in Figures 3.78 and 3.79. As shown in Figures 3.78(b) and 3.79, specimens with corrosion inhibitors exhibited higher total corrosion losses than conventional ECR (ECR-10h), with the exception of ECR(DCI)-10h, which was approximately the loss of conventional ECR by week 53. These specimens had total corrosion losses less than 0.093 μm based on total area and 18.0 μm based on exposed area. Figures 3.80 and 3.81 show the

average total corrosion losses for specimens with a *w/c* ratio of 0.35 and 10 holes. By week 40, all specimens had higher total corrosion losses than conventional ECR (ECR-10h-35), with total corrosion losses for these specimens less than 0.16 μm based on total area and 30.0 μm based on exposed area.

The average total corrosion losses at week 40 for ECR specimens with corrosion inhibitors are summarized in Table 3.11. Total corrosion losses between 0.01 and 0.14 μm based on total area were observed for all specimens. For specimens with a *w/c* ratio of 0.45 and four holes, ECR(primer/$Ca(NO_2)_2$) and ECR(Rheocrete) had average total corrosion losses of 0.03 and 0.02 μm, respectively, similar to the corrosion loss of conventional ECR (0.03 μm). The total corrosion losses were approximately 0.01 μm for ECR(DCI) and ECR(Hycrete). Based on exposed area, ECR(primer/$Ca(NO_2)_2$) had the highest total corrosion loss, 13.9 μm, followed by ECR(Rheocrete), ECR(Hycrete), and ECR(DCI) at 8.16, 6.68, and 2.84 μm, respectively. These values vary from 25% to 122% of the corrosion loss exhibited by conventional ECR. For specimens with a *w/c* ratio of 0.45 and 10 holes, the total corrosion losses were 0.02, 0.04, 0.07, and 0.06 μm for ECR(DCI), ECR(Hycrete), ECR(Rheocrete)-10h, and ECR(primer/Ca(NO2)2)-10h, respectively. Based on exposed area, the total corrosion losses ranged from 3.34 to 14.0 μm, equal to 52% to 216% of the corrosion loss of ECR-10h. Based on total area, ECR(Hycrete)-10h-35 and ECR(primer/Ca(NO2)2)-10h-35 each had a total corrosion loss of 0.14 μm, followed by ECR(DCI)-10h-35 at 0.13 μm and ECR(Rheocrete)-10h-35 at 0.09 μm. The total corrosion losses based on exposed area were between 11.4 and 26.7 μm, 1.13 to 1.83 times the corrosion loss of ECR-10h-35. For specimens with different *w/c* ratios, specimens with a *w/c* ratio of 0.35 showed total corrosion losses between 1.18 and 7.60 times the total corrosion losses for the corresponding specimens with a *w/c* ratio of 0.45. The reasons for the higher losses at the lower *w/c* ratio are not clear.

Table 3.11 – Average corrosion losses (μm) at week 40 as measured in the cracked beam test for specimens with ECR with a primer containing calcium nitrite and ECR cast with corrosion inhibitors

Steel Designation[a]	Specimen			Average	Standard Deviation
	1	2	3		
Cracked beam test					
ECR(DCI)	0.01	0.01	β	0.01	0.01
ECR(DCI)*	6.12	2.46	-0.07	2.84	3.11
ECR(DCI)-10h	0.02	0.01	0.02	0.02	0.01
ECR(DCI)-10h*	3.57	2.08	4.36	3.34	1.16
ECR(DCI)-10h-35	0.07	0.04	0.29	0.13	0.14
ECR(DCI)-10h-35*	13.05	6.81	56.21	25.36	26.90
ECR(Hycrete)	0.01	β	0.03	0.01	0.01
ECR(Hycrete)*	3.02	2.18	14.84	6.68	7.08
ECR(Hycrete)-10h	β	0.06	0.06	0.04	0.03
ECR(Hycrete)-10h*	0.70	12.13	11.39	8.07	6.39
ECR(Hycrete)-10h-35	0.10	0.07	0.24	0.14	0.09
ECR(Hycrete)-10h-35*	20.14	13.67	46.25	26.69	17.25
ECR(Rheocrete)	0.01	0.02	0.02	0.02	β
ECR(Rheocrete)*	6.61	10.06	7.81	8.16	1.75
ECR(Rheocrete)-10h	0.07	0.08	0.06	0.07	0.01
ECR(Rheocrete)-10h*	13.59	16.15	12.18	13.97	2.01
ECR(Rheocrete)-10h-35	0.07	0.13	0.06	0.09	0.04
ECR(Rheocrete)-10h-35*	12.66	25.63	11.20	16.50	7.94
ECR(primer/$Ca(NO_2)_2$)	0.05	0.01	0.03	0.03	0.02
ECR(primer/$Ca(NO_2)_2$)*	22.51	4.50	14.56	13.86	9.02
ECR(primer/$Ca(NO_2)_2$)-10h	0.09	0.04	0.05	0.06	0.03
ECR(primer/$Ca(NO_2)_2$)-10h*	17.24	7.84	9.06	11.38	5.11
ECR(primer/$Ca(NO_2)_2$)-10h-35	0.17	0.09	0.14	0.14	0.04
ECR(primer/$Ca(NO_2)_2$)-10h-35*	32.50	18.01	27.40	25.97	7.35

[a] ECR = conventional epoxy-coated reinforcement. ECR(DCI) = ECR in concrete with DCI.
ECR(Hycrete) = ECR in concrete with Hycrete. ECR(Rheocrete) = ECR in concrete with Rheocrete.
ECR(primer/$Ca(NO_2)_2$) = ECR with a primer containing calcium nitrite.
10h = epoxy-coated bars with 10 holes, otherwise four 3-mm ($^1/_8$-in.) diameter holes.
35 = concrete *w/c* =0.35, otherwise *w/c* = 0.45.

* Epoxy-coated bars, calculations based on exposed area of four or 10 3-mm ($^1/_8$-in.) diameter holes.

β Corrosion loss (absolute value) less than 0.005 mm.

The average corrosion potentials of the top and bottom mats of steel with respect to a copper-copper sulfate electrode are shown in Figures 3.82 through 3.84. All specimens exhibited top mat corrosion potentials around –0.200 V at the beginning of the test, except for ECR(Hycrete)-10h and ECR(primer/$Ca(NO_2)_2$)-10h-35, which had top mat corrosion potentials of –0.300 and –0.450 V, respectively. The top mat corrosion potentials quickly dropped to values more negative than –0.350 V, indicating active corrosion for all specimens. After week 10, the top mat corrosion

potentials for all specimens remained between –0.400 and –0.600 V. For specimens with four holes, ECR(Hycrete) and ECR(primer/$Ca(NO_2)_2$) had bottom mat corrosion potentials more positive than –0.300 V, indicating a low probability of corrosion. Active corrosion, indicated by corrosion potentials below –0.350 V, was observed for ECR(DCI) at week 46 and for ECR(Rheocrete) at weeks 37 and 41, respectively. Specimens with 10 holes had bottom mat corrosion potentials more positive than –0.320 V, indicating a low probability of corrosion. For specimens with a *w/c* ratio of 0.35 and 10 holes, ECR(primer/$Ca(NO_2)_2$)-10h-35 had bottom mat corrosion potentials between –0.215 and –0.541 V after week 18, indicating that chlorides had reached the bottom mat of steel. The remaining specimens had potentials more positive than –0.340 V, with the exception of ECR(DCI), which had a value of –0.389 V at week 39.

The average mat-to-mat resistances increased with time for all specimens, as shown in Figures 3.85 through 3.87. Figure 3.85 shows that for specimens with four holes, the average mat-to-mat resistances started with values between 2,600 and 4,100 ohms and increased to values around 13,000 ohms at week 40. As shown in Figure 3.86, the average mat-to-mat resistances for specimens with 10 holes increased with time at a rate similar to ECR-10h. These specimens had average mat-to-mat resistances around 1,500 ohms at the start of the test and increased to values around 9,000 ohms at week 40. Figure 3.87 shows that specimens with a *w/c* ratio of 0.35 and 10 holes had lower mat-to-mat resistances than those for specimens with a *w/c* ratio of 0.45 and 10 holes. These specimens had average mat-to-mat resistances of approximately 1,500 ohms in the first week and increased to values less than 6,000 ohms at week 39.

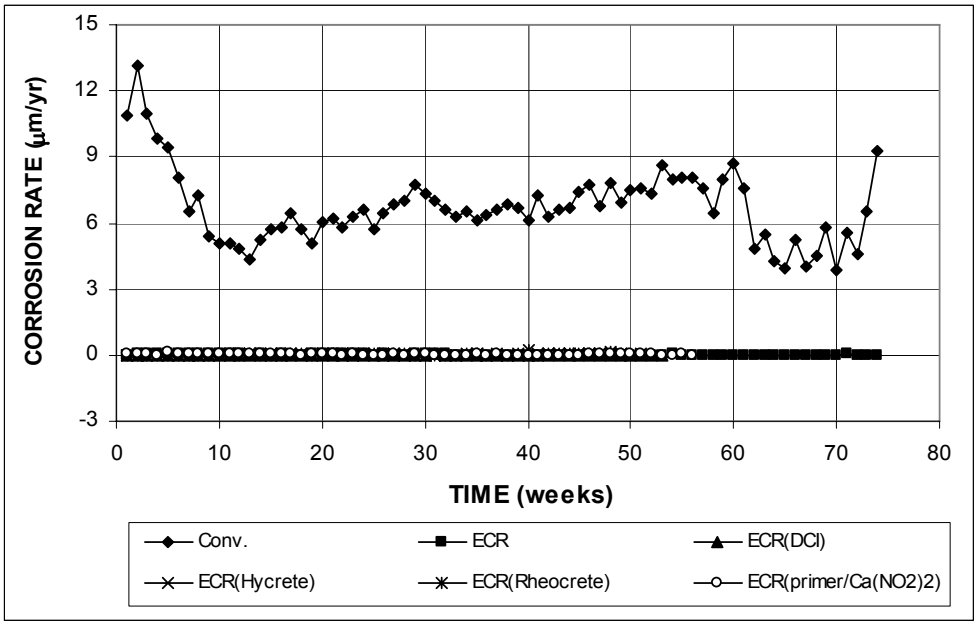

Figure 3.70 (a) – Average corrosion rates as measured in the cracked beam test for specimens with conventional steel, ECR, ECR in concrete with corrosion inhibitors, and ECR with a primer containing calcium nitrite (ECR bars have four holes).

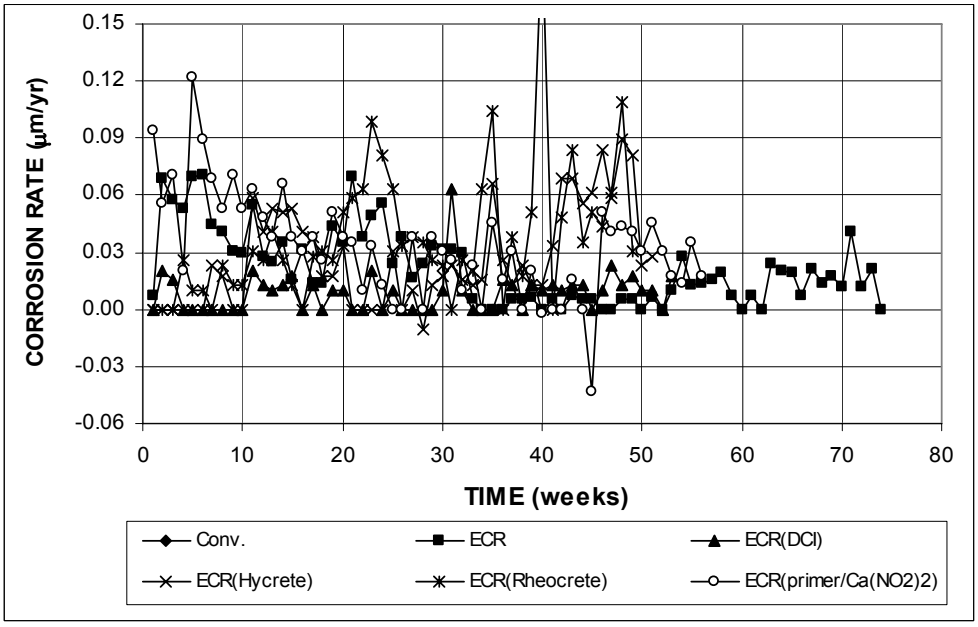

Figure 3.70 (b) – Average corrosion rates as measured in the cracked beam test for specimens with conventional steel, ECR, ECR in concrete with corrosion inhibitors, and ECR with a primer containing calcium nitrite (ECR bars have four holes).

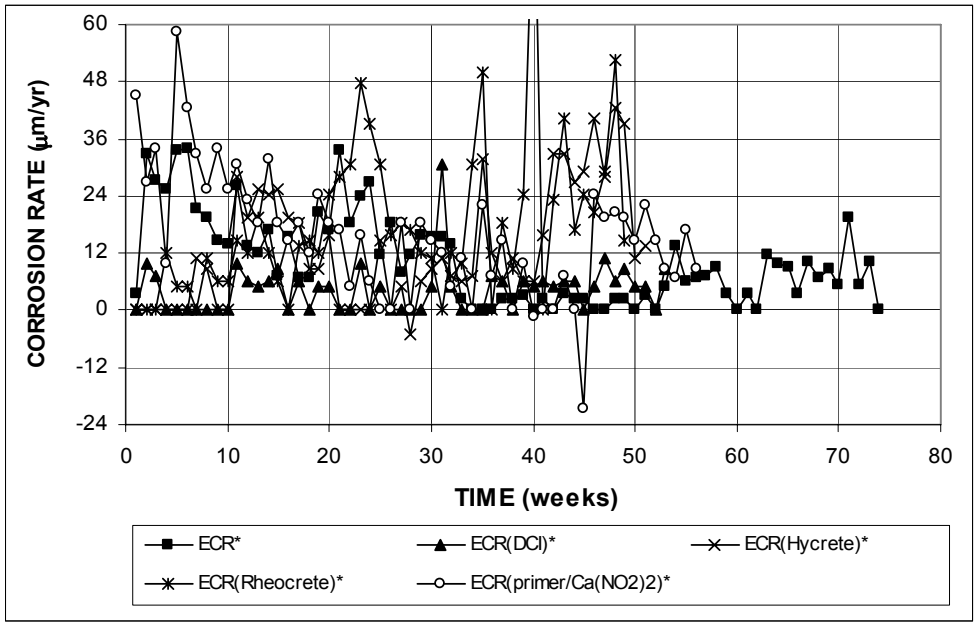

Figure 3.71 – Average corrosion rates as measured in the cracked beam test for specimens with ECR, ECR in concrete with corrosion inhibitors, and ECR with a primer containing calcium nitrite. * Based on exposed area (ECR bars have four holes).

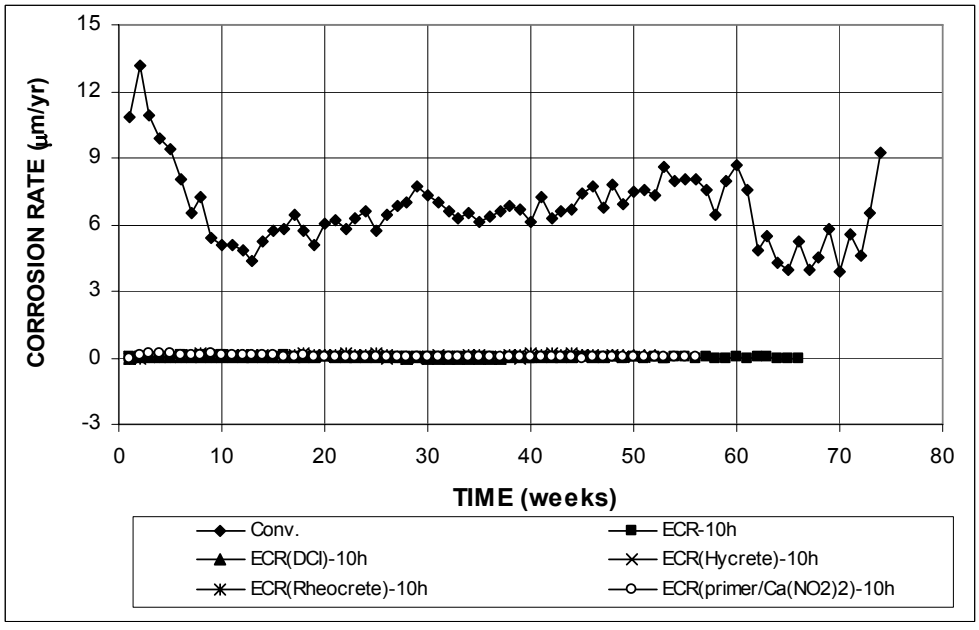

Figure 3.72 (a) – Average corrosion rates as measured in the cracked beam test for specimens with conventional steel, ECR, ECR in concrete with corrosion inhibitors, and ECR with a primer containing calcium nitrite (ECR bars have 10 holes).

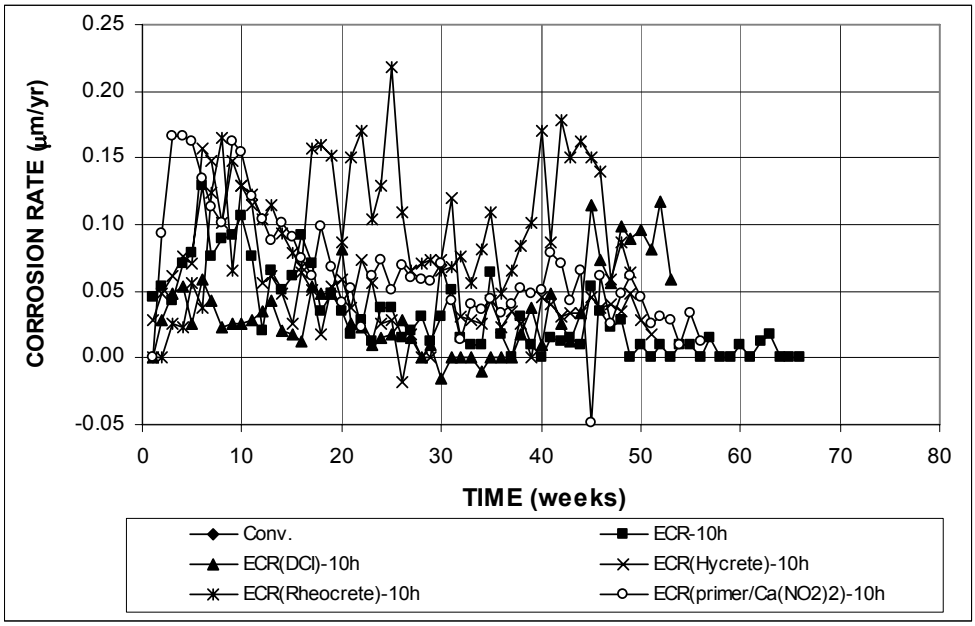

Figure 3.72 (b) – Average corrosion rates as measured in the cracked beam test for specimens with conventional steel, ECR, ECR in concrete with corrosion inhibitors, and ECR with a primer containing calcium nitrite (ECR bars have 10 holes).

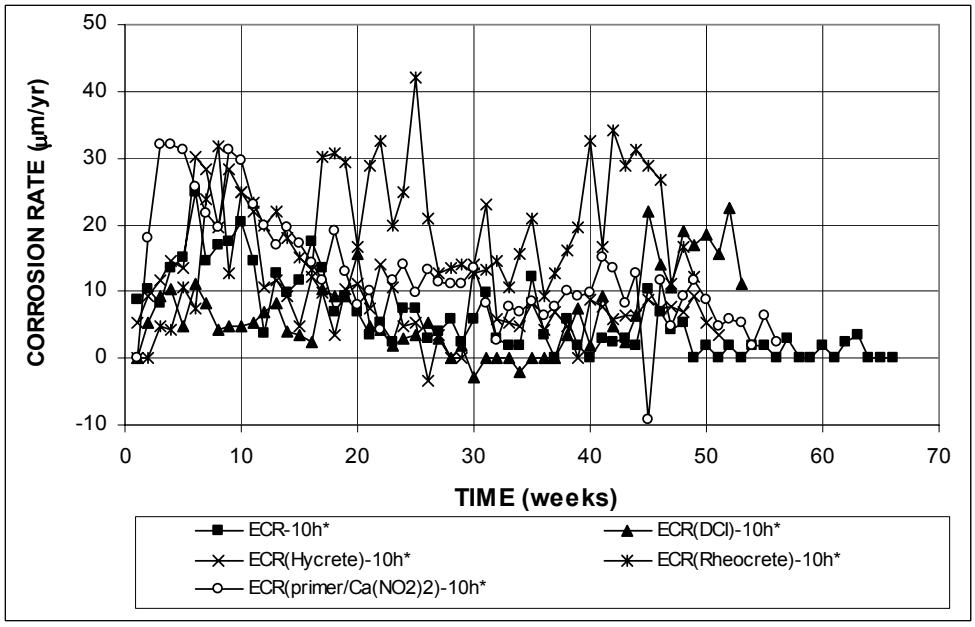

Figure 3.73 – Average corrosion rates as measured in the cracked beam test for specimens with ECR, ECR in concrete with corrosion inhibitors, and ECR with a primer containing calcium nitrite. * Based on exposed area (ECR bars have 10 holes).

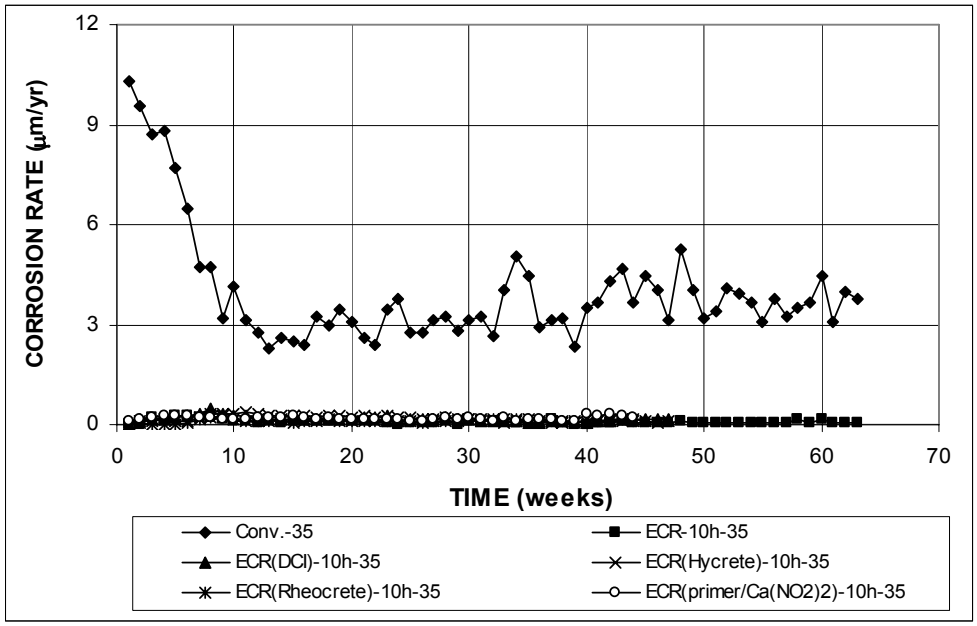

Figure 3.74 (a) – Average corrosion rates as measured in the cracked beam test for specimens with conventional steel, ECR, ECR in concrete with corrosion inhibitors, and ECR with a primer containing calcium nitrite, water-cement ratio = 0.35 (ECR bars have 10 holes).

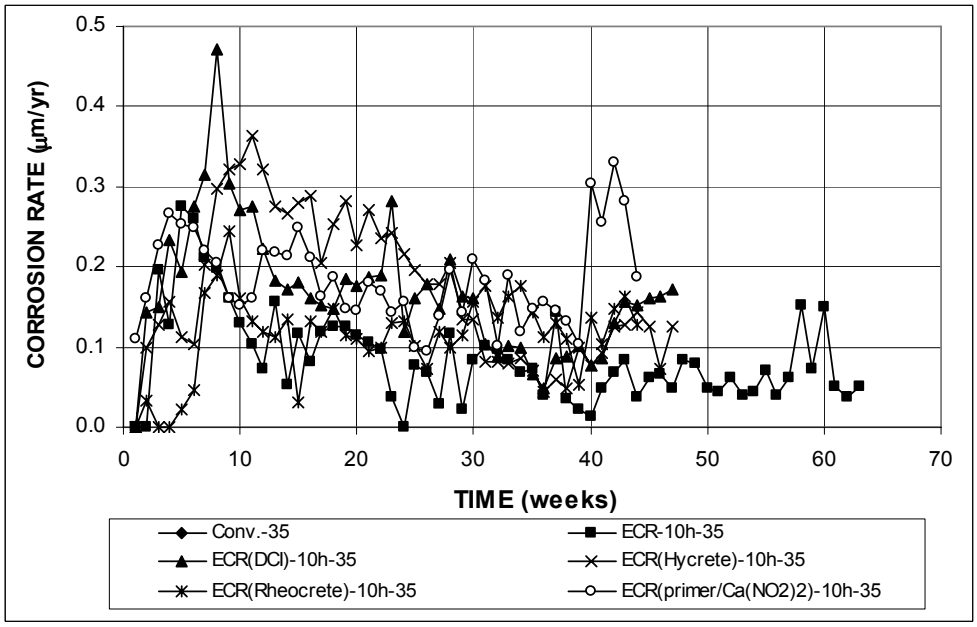

Figure 3.74 (b) – Average corrosion rates as measured in the cracked beam test for specimens with conventional steel, ECR, ECR in concrete with corrosion inhibitors, and ECR with a primer containing calcium nitrite, water-cement ratio = 0.35 (ECR bars have 10 holes).

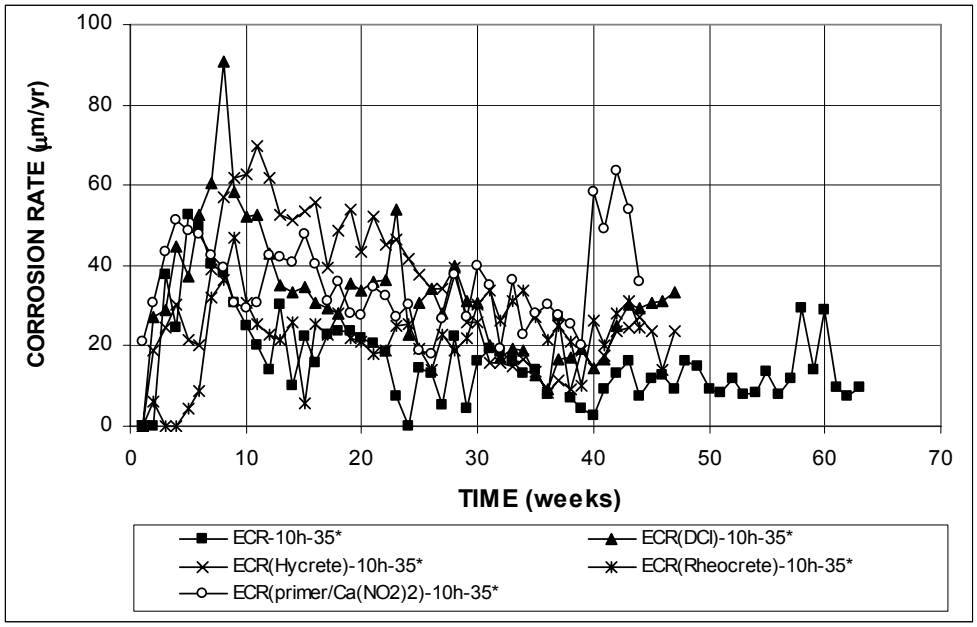

Figure 3.75 – Average corrosion rates as measured in the cracked beam test for specimens with ECR, ECR in concrete with corrosion inhibitors, and ECR with a primer containing calcium nitrite, water-cement ratio = 0.35. * Based on exposed area (ECR bars have 10 holes).

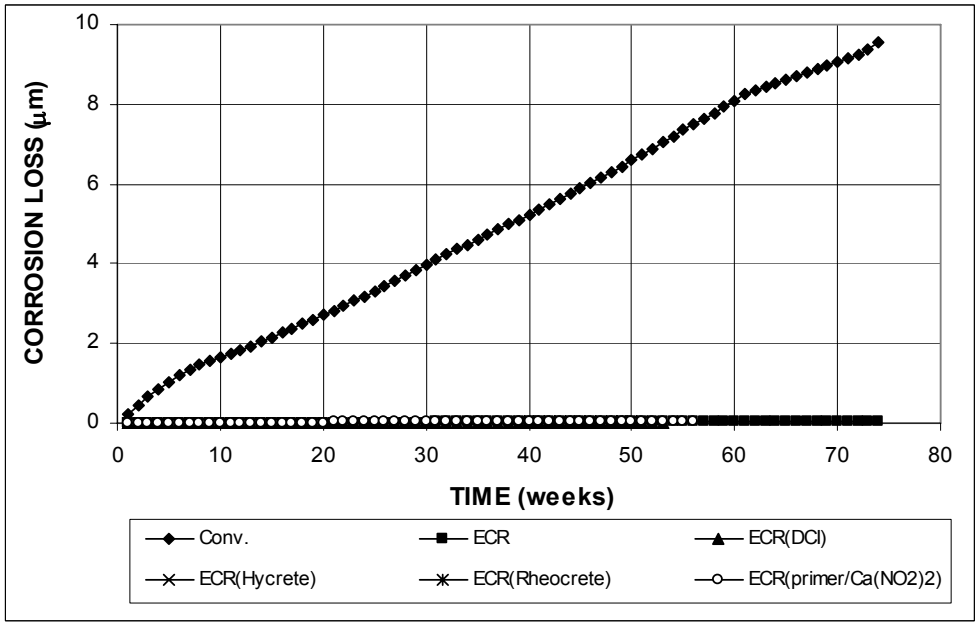

Figure 3.76 (a) – Average corrosion losses as measured in the cracked beam test for specimens with conventional steel, ECR, ECR in concrete with corrosion inhibitors, and ECR with a primer containing calcium nitrite (ECR bars have four holes).

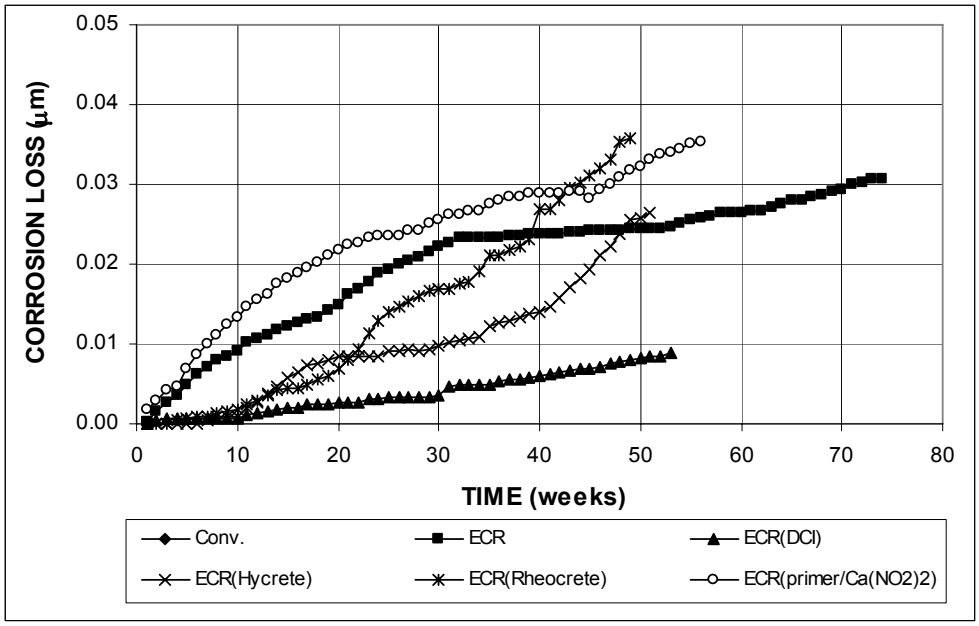

Figure 3.76 (b) – Average corrosion losses as measured in the cracked beam test for specimens with conventional steel, ECR, ECR in concrete with corrosion inhibitors, and ECR with a primer containing calcium nitrite (ECR bars have four holes).

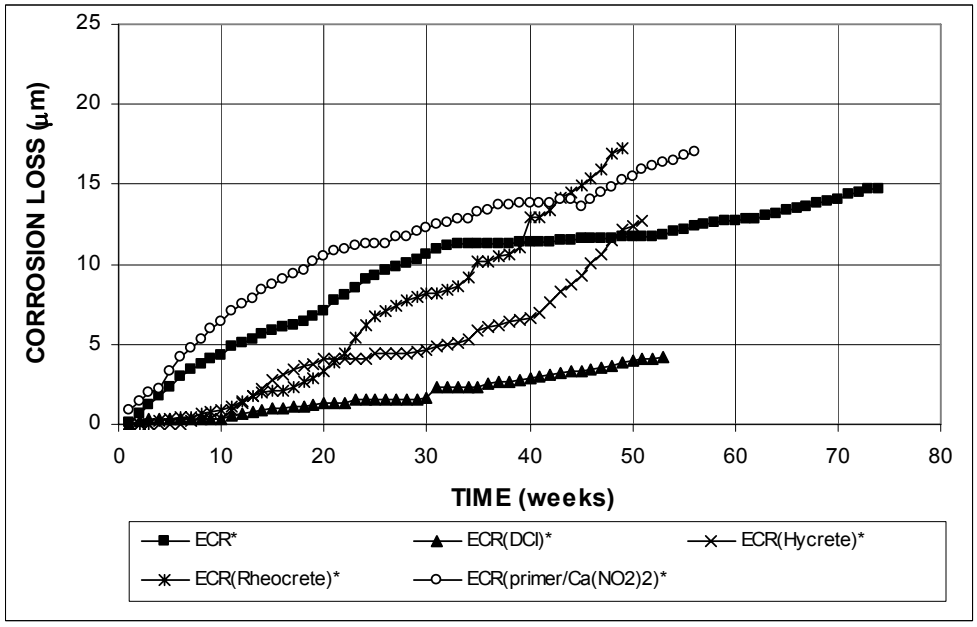

Figure 3.77 – Average corrosion losses as measured in the cracked beam test for specimens with ECR, ECR in concrete with corrosion inhibitors, and ECR with a primer containing calcium nitrite. * Based on exposed area (ECR bars have four holes).

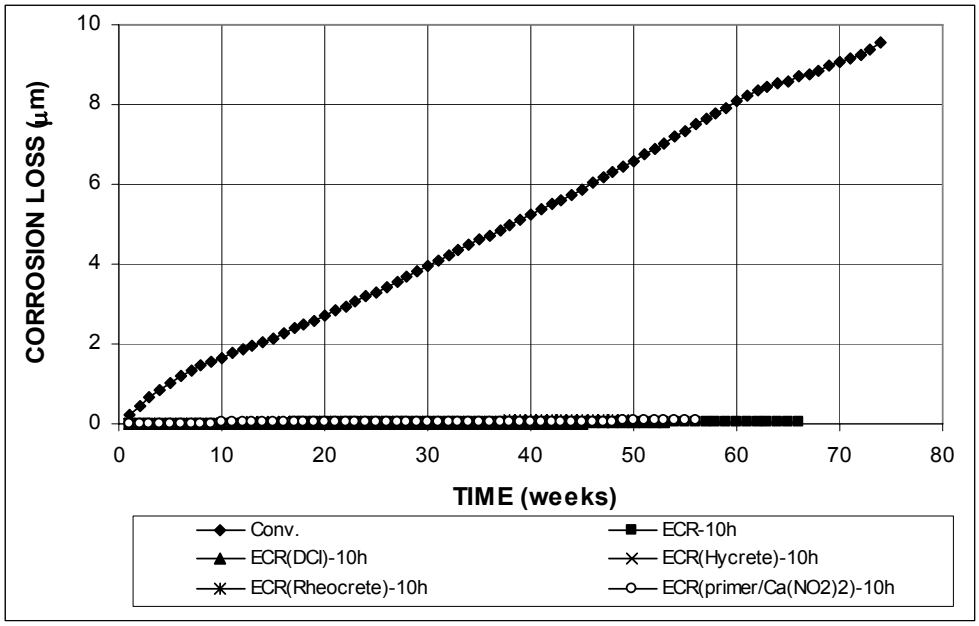

Figure 3.78 (a) – Average corrosion losses as measured in the cracked beam test for specimens with conventional steel, ECR, ECR in concrete with corrosion inhibitors, and ECR with a primer containing calcium nitrite (ECR bars have 10 holes).

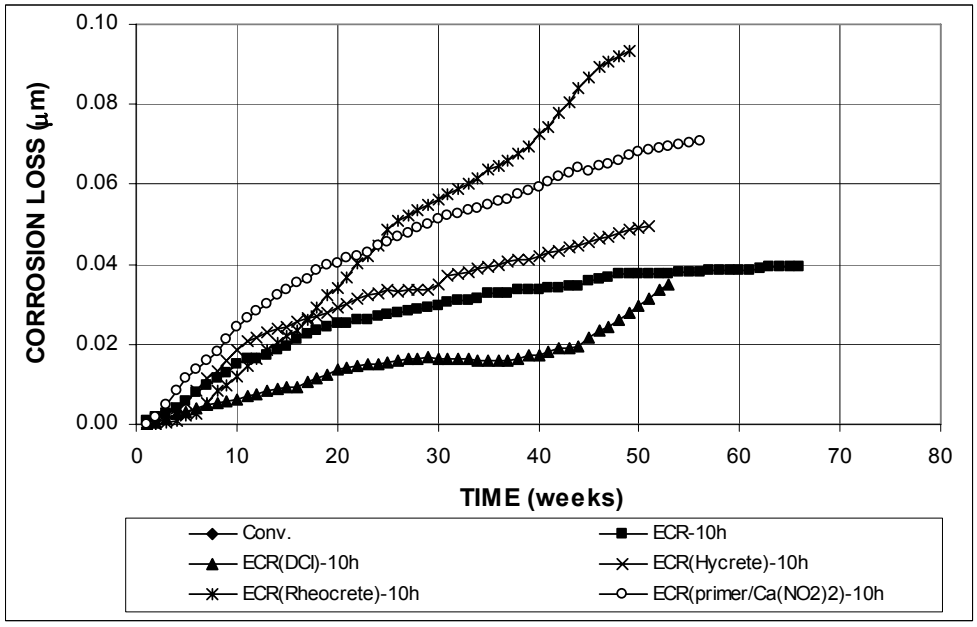

Figure 3.78 (b) – Average corrosion losses as measured in the cracked beam test for specimens with conventional steel, ECR, ECR in concrete with corrosion inhibitors, and ECR with a primer containing calcium nitrite (ECR bars have 10 holes).

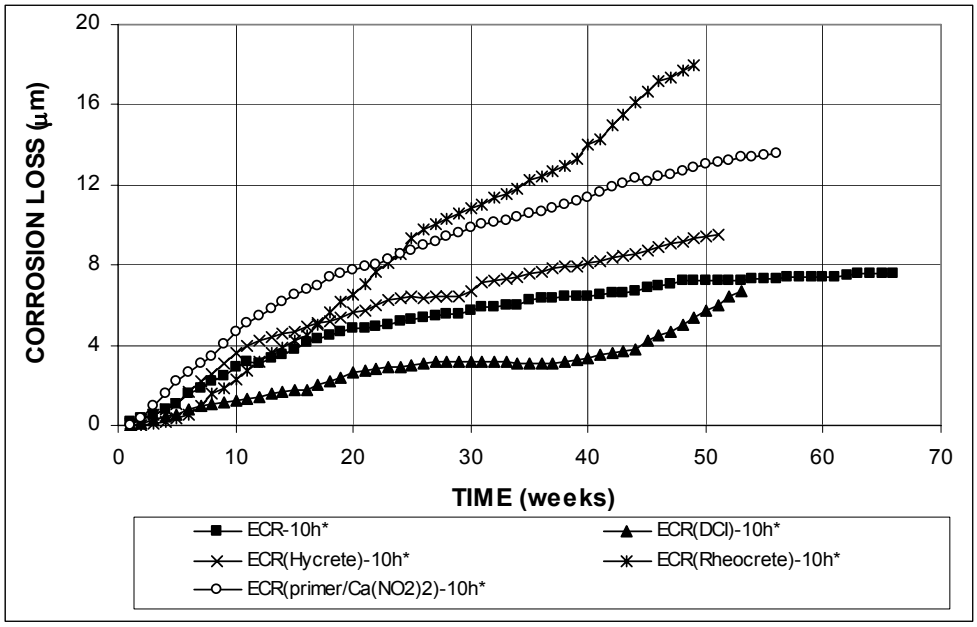

Figure 3.79 – Average corrosion losses as measured in the cracked beam test for specimens with ECR, ECR in concrete with corrosion inhibitors, and ECR with a primer containing calcium nitrite. * Based on exposed area (ECR bars have 10 holes).

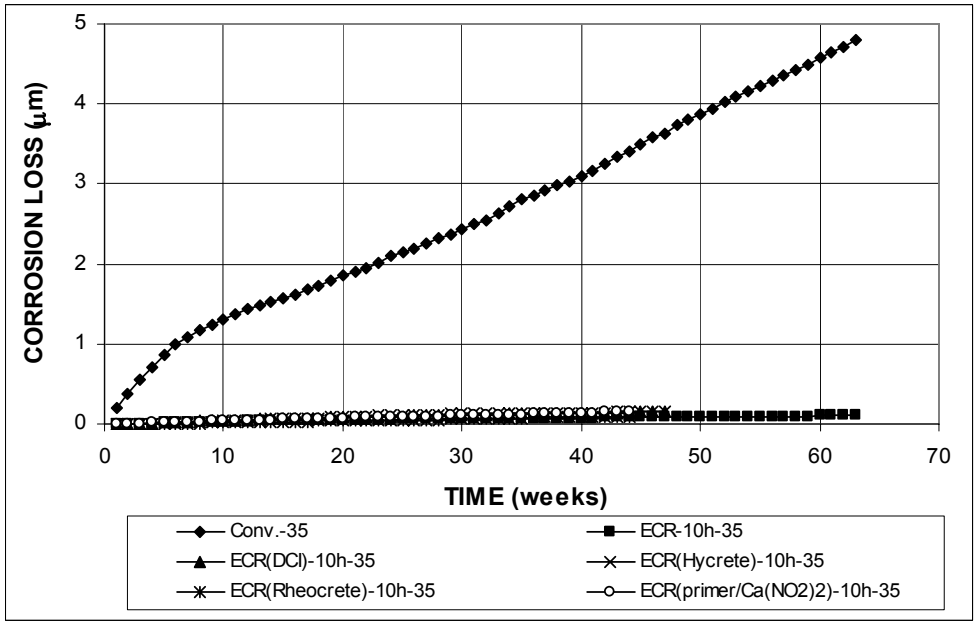

Figure 3.80 (a) – Average corrosion losses as measured in the cracked beam test for specimens with conventional steel, ECR, ECR in concrete with corrosion inhibitors, and ECR with a primer containing calcium nitrite, water-cement ratio = 0.35 (ECR bars have 10 holes).

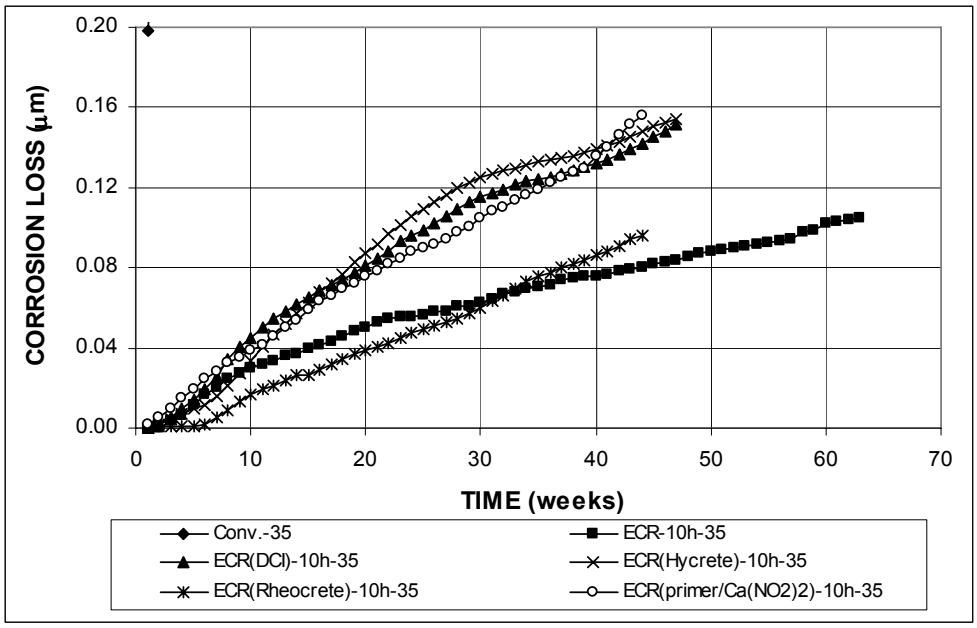

Figure 3.80 (b) – Average corrosion losses as measured in the cracked beam test for specimens with conventional steel, ECR, ECR in concrete with corrosion inhibitors, and ECR with a primer containing calcium nitrite, water-cement ratio = 0.35 (ECR bars have 10 holes).

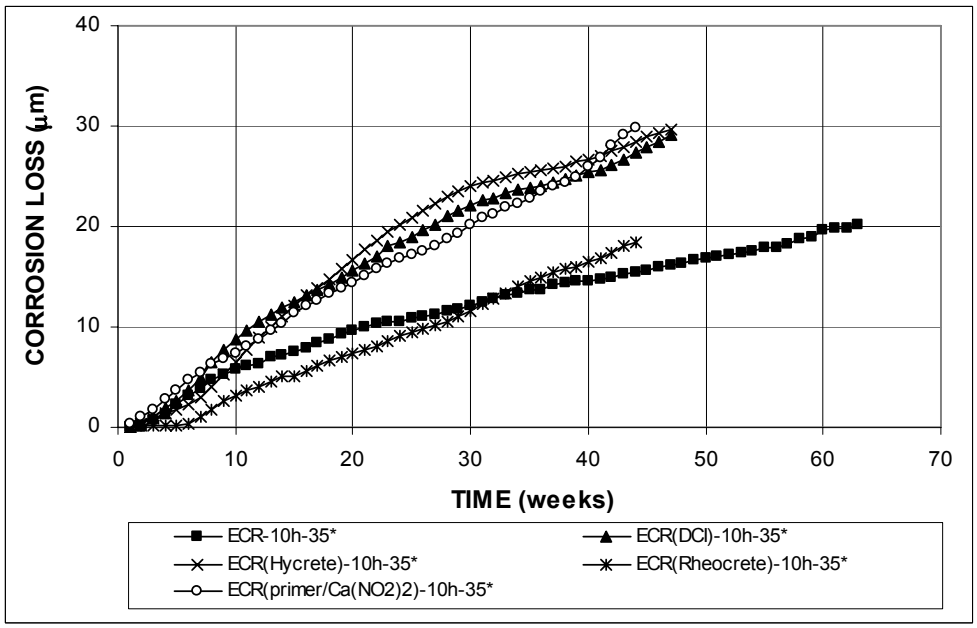

Figure 3.81 – Average corrosion losses as measured in the cracked beam test for specimens with ECR, ECR in concrete with corrosion inhibitors, and ECR with a primer containing calcium nitrite, water-cement ratio = 0.35.
* Based on exposed area (ECR bars with 10 holes).

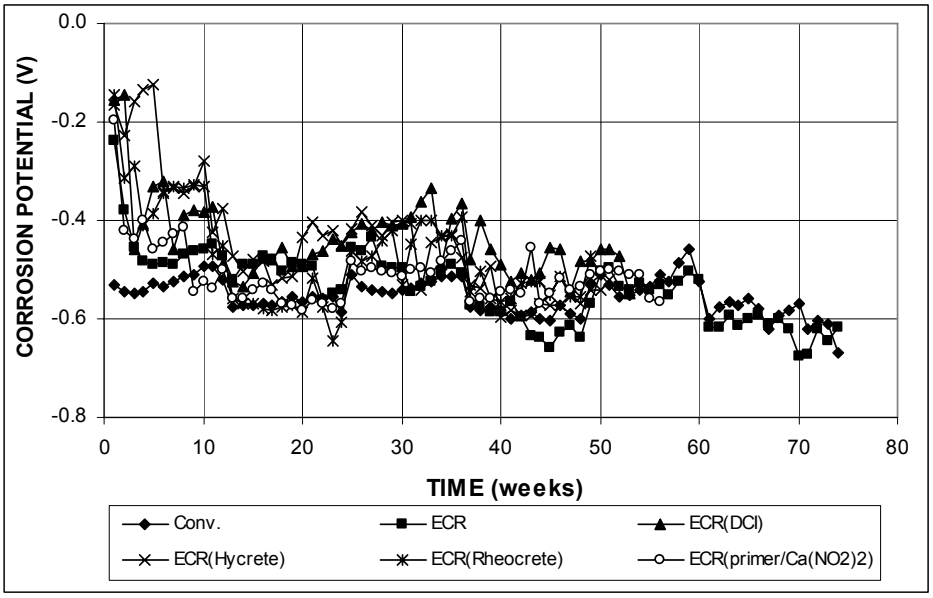

Figure 3.82 (a) – Average top mat corrosion potentials, with respect to a copper-copper sulfate electrode as measured in the cracked beam test for specimens with conventional steel, ECR, ECR in concrete with corrosion inhibitors, and ECR with a primer containing calcium nitrite (ECR bars have four holes).

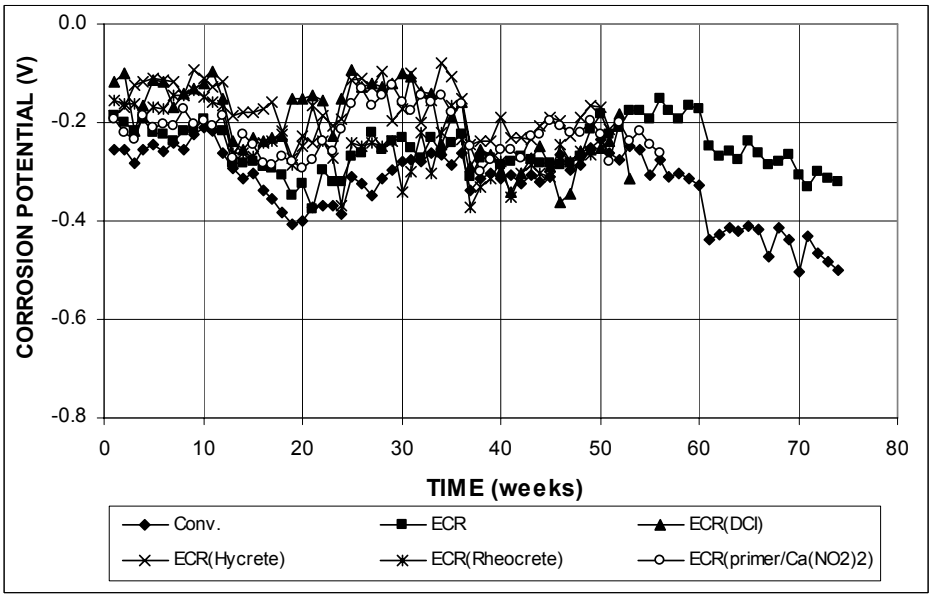

Figure 3.82 (b) – Average bottom mat corrosion potentials, with respect to a copper-copper sulfate electrode as measured in the cracked beam test for specimens with conventional steel, ECR, ECR in concrete with corrosion inhibitors, and ECR with a primer containing calcium nitrite (ECR bars have four holes).

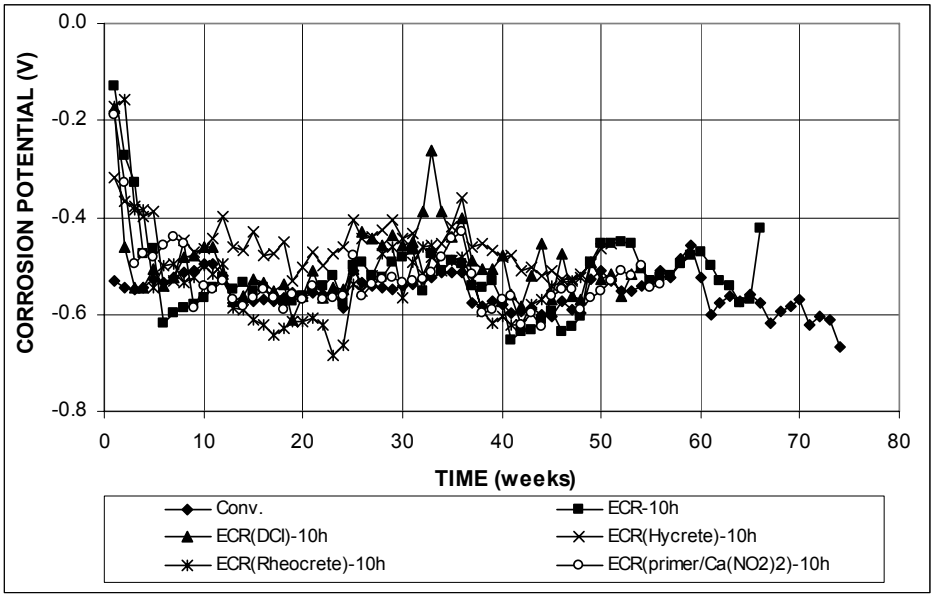

Figure 3.83 (a) – Average top mat corrosion potentials, with respect to a copper-copper sulfate electrode as measured in the cracked beam test for specimens with conventional steel, ECR, ECR in concrete with corrosion inhibitors, and ECR with a primer containing calcium nitrite (ECR bars have 10 holes).

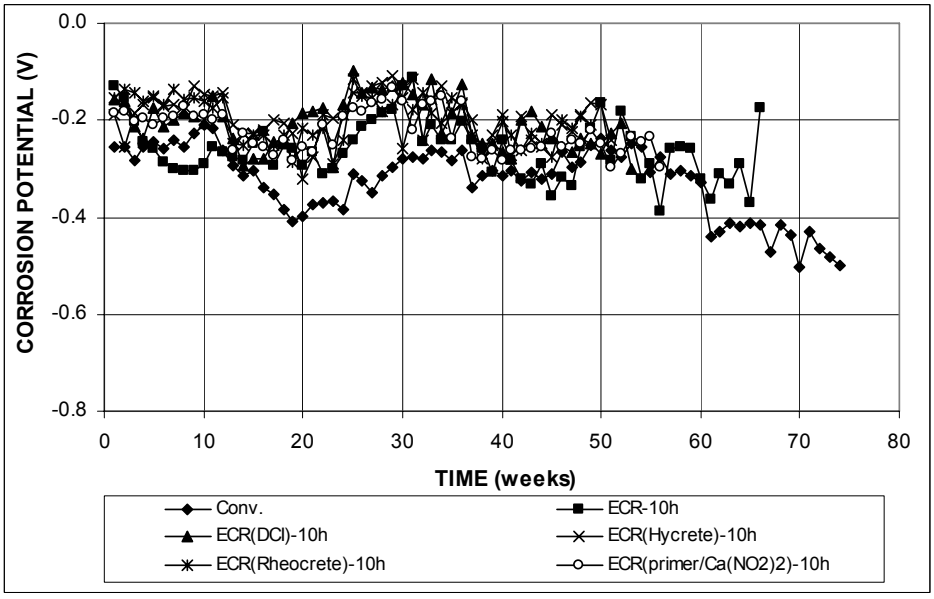

Figure 3.83 (b) – Average bottom mat corrosion potentials, with respect to a copper-copper sulfate electrode as measured in the cracked beam test for specimens with conventional steel, ECR, ECR in concrete with corrosion inhibitors, and ECR with a primer containing calcium nitrite (ECR bars have 10 holes).

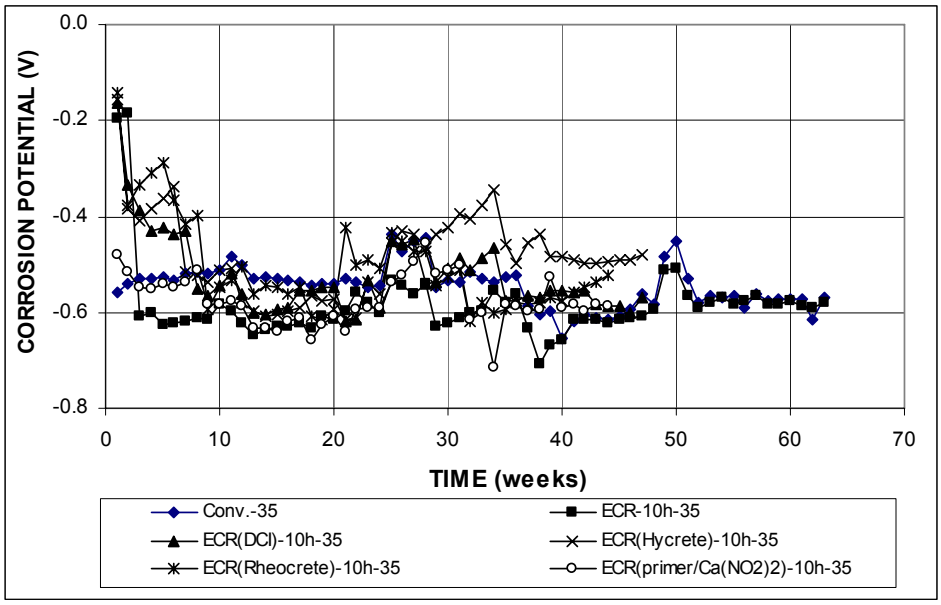

Figure 3.84 (a) – Average top mat corrosion potentials, with respect to a copper-copper sulfate electrode as measured in the cracked beam test for specimens with conventional steel, ECR, ECR in concrete with corrosion inhibitors, and ECR with a primer containing calcium nitrite, water-cement ratio = 0.35 (ECR bars have 10 holes),.

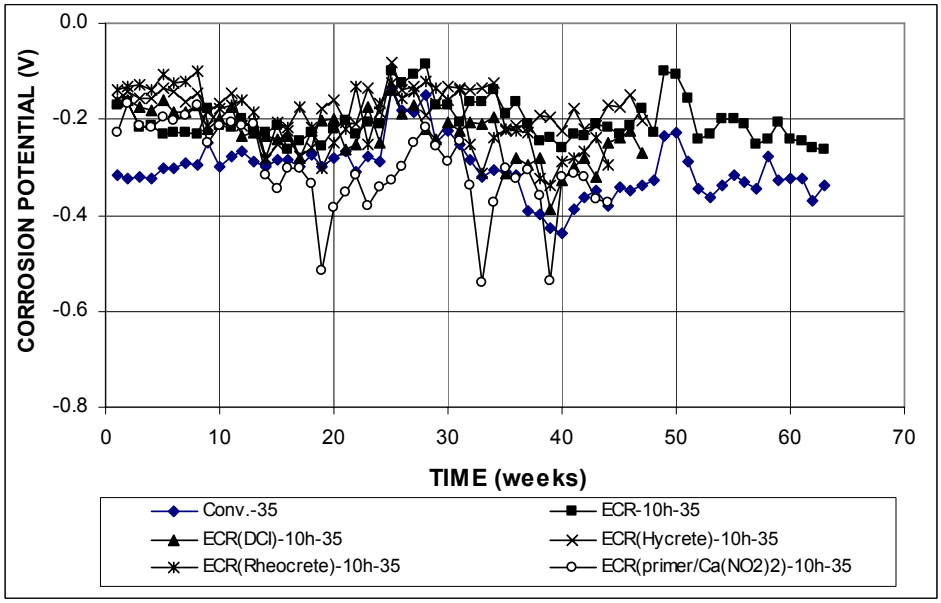

Figure 3.84 (b) – Average bottom mat corrosion potentials, with respect to a copper-copper sulfate electrode as measured in the cracked beam test for specimens with conventional steel, ECR, ECR in concrete with corrosion inhibitors, and ECR with a primer containing calcium nitrite, water-cement ratio = 0.35 (ECR bars have 10 holes).

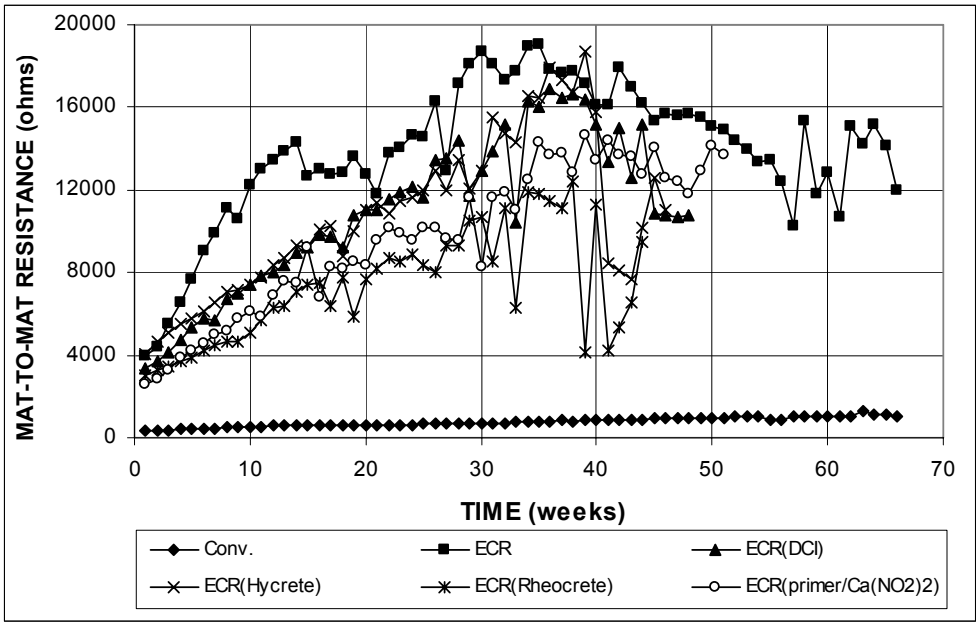

Figure 3.85 – Average mat-to-mat resistances as measured in the cracked beam test for specimens with conventional steel, ECR, ECR in concrete with corrosion inhibitors, and ECR with a primer containing calcium nitrite (ECR bars have four holes).

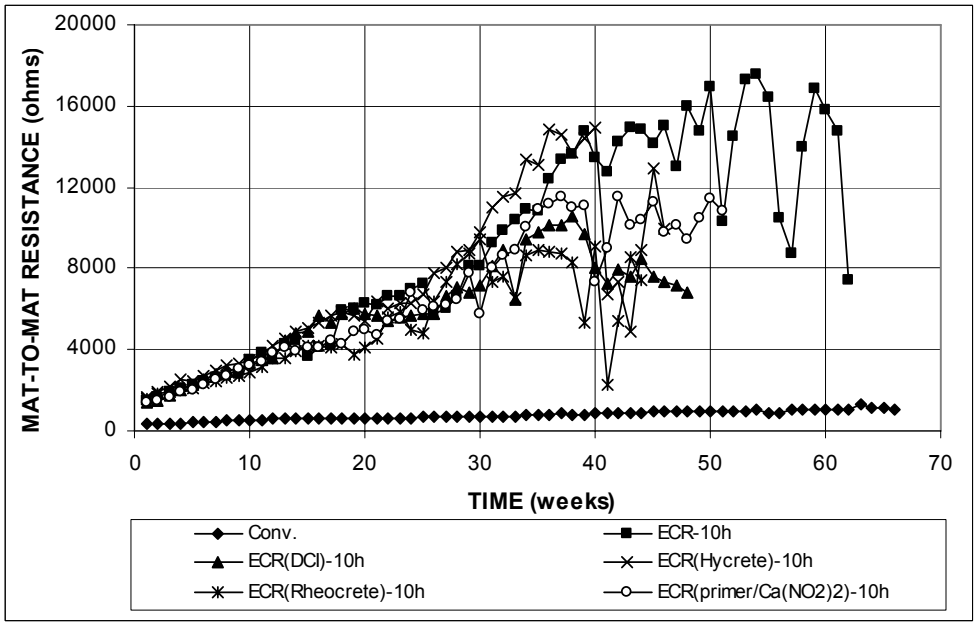

Figure 3.86 – Average mat-to-mat resistances as measured in the cracked beam test for specimens with conventional steel, ECR, ECR in concrete with corrosion inhibitors, and ECR with a primer containing calcium nitrite (ECR bars have 10 holes).

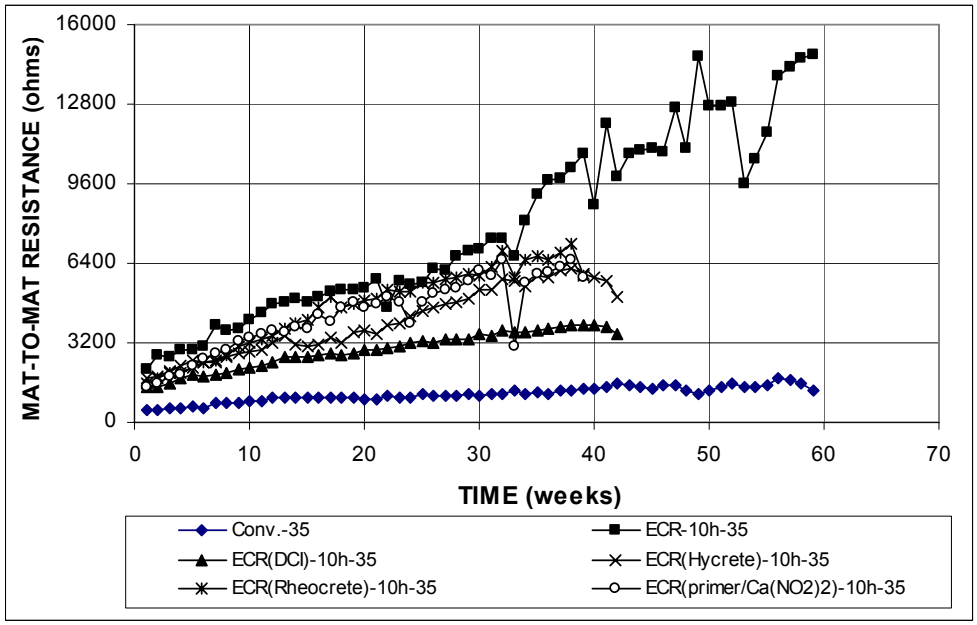

Figure 3.87 – Average mat-to-mat resistances as measured in the cracked beam test for specimens with conventional steel, ECR, ECR in concrete with corrosion inhibitors, and ECR with a primer containing calcium nitrite, water-cement ratio = 0.35 (ECR bars have 10 holes).

3.2.3 Field Test

This section shows the test results for specimens with ECR cast in concrete with corrosion inhibitor DCI, Rheocrete, or Hycrete, and ECR with a primer containing calcium nitrite. The coating on the epoxy-coated bars was penetrated with 16 holes.

3.2.3.1 Field Test Specimens Without Cracks

The test results for specimens without simulated cracks in the field test are shown in Figures 3.88 through 3.93. The total corrosion losses at week 32 are summarized in Table 3.12.

Figures 3.88 and 3.89 show the average corrosion rates for specimens with corrosion inhibitors, along with conventional ECR. As shown in Figure 3.88, all

specimens had similar corrosion rates. The corrosion rates were less than 0.01 and 3 μm/yr based on total area and exposed area, respectively, with the exception of ECR (1) and ECR(primer/$Ca(NO_2)_2$) (2) at week 4, which had corrosion rates of 0.011 and 0.015 μm/yr (4.3 and 6.0 μm/yr based on exposed area), respectively. Some specimens occasionally showed negative corrosion rates, as shown in Figure 3.88. Based on total area, ECR(Rheocrete) (1) had a corrosion rate of –0.001 μm/yr at week 28, and ECR(DCI) (3) had values of –0.005 and –0.002 μm/yr, respectively, at weeks 12 and 32. For ECR(Rheocrete) (1), the negative corrosion rate was not associated with more negative corrosion potentials at cathode than at anode, but for ECR(DCI) (3), more negative corrosion potentials at cathode than at anode were observed at weeks 12 and 32.

The average total corrosion losses for conventional ECR and ECR with corrosion inhibitors are shown in Figures 3.90 and 3.91. Figure 3.90 shows that ECR (1) had the highest corrosion losses, all of which occurred by week 16, followed by ECR(primer/$Ca(NO_2)_2$) (2) with a loss of 0.001 μm, all of which occurred by week 24. The remaining specimens had similar total corrosion losses, with values less than 0.001 μm based on total area and 10 μm based on exposed area. Table 3.12 summarizes the average total corrosion losses at week 32. ECR(DCI) (3) specimen had a negative total corrosion loss of –0.23 μm based on exposed area. The remaining specimens had total corrosion losses less than 0.005 μm (as indicated by the symbol β) based on total area and 0.42 μm based on exposed area, compared to values of 0.18 and 0.81 μm for conventional ECR based on exposed area.

Table 3.12 – Average corrosion losses (μm) at week 32 as measured in the field test for specimens with ECR with a primer containing calcium nitrite and ECR cast with corrosion inhibitors, without cracks

Steel Designation[a]	Test Bar				Average	Standard Deviation
	1	2	3	4		
without cracks						
ECR(DCI) (1)	0.00	0.00	β	β	β	β
ECR(DCI)* (1)	0.00	0.00	0.35	0.28	0.16	0.19
ECR(DCI) (2)	0.00	0.00	β	0.00	β	β
ECR(DCI)* (2)	0.00	0.00	0.42	0.00	0.11	0.21
ECR(DCI) (3)	β	β	0.00	β	β	β
ECR(DCI)* (3)	-0.28	-0.35	0.00	-0.28	-0.23	0.16
ECR(Hycrete) (1)	0.00	0.00	0.00	0.00	0.00	0.00
ECR(Hycrete)* (1)	0.00	0.00	0.00	0.00	0.00	0.00
ECR(Hycrete) (2)	0.00	0.00	0.00	0.00	0.00	0.00
ECR(Hycrete)* (2)	0.00	0.00	0.00	0.00	0.00	0.00
ECR(Rheocrete) (1)	0.00	0.00	β	β	β	β
ECR(Rheocrete)* (1)	0.00	0.00	0.56	-0.35	0.05	0.38
ECR(Rheocrete) (2)	β	β	0.00	0.00	β	β
ECR(Rheocrete)* (2)	0.35	0.28	0.00	0.00	0.16	0.19
ECR(primer/($Ca(NO_2)_2$) (1)	0.00	0.00	0.00	0.00	0.00	0.00
ECR(primer/($Ca(NO_2)_2$)* (1)	0.00	0.00	0.00	0.00	0.00	0.00
ECR(primer/($Ca(NO_2)_2$) (2)	β	β	β	β	β	β
ECR(primer/($Ca(NO_2)_2$)* (2)	0.35	0.70	0.28	0.35	0.42	0.19

[a] ECR = conventional epoxy-coated reinforcement. ECR(DCI) = ECR in concrete with DCI. ECR(Hycrete) = ECR in concrete with Hycrete. ECR(Rheocrete) = ECR in concrete with Rheocrete. ECR(primer/$Ca(NO_2)_2$) = ECR with a primer containing calcium nitrite.

* Epoxy-coated bars, calculations based on exposed area of 16 3-mm ($^1/_8$-in.) diameter holes.

β Corrosion loss (absolute value) less than 0.005 μm.

The average corrosion potentials of the top mat and bottom mats of steel with respect to a copper-copper sulfate electrode are shown in Figure 3.92. All specimens, in general, had corrosion potentials similar to each other in the top and bottom mats. As shown in Figure 3.92(a), all specimens had corrosion potentials of the top mat more positive than –0.330 V, indicating a low probability of corrosion. Figure 3.92(b) shows that all specimens had bottom mat corrosion potentials more positive than –0.290 V, with the exception of ECR (primer/Ca(NO2)2) (1) at week 12, indicating a lower probability of corrosion.

Figure 3.93 shows that all specimens had average mat-to-mat resistances

similar to those for specimens with ECR, with values between 450 and 2,200 ohms. As discussed in Section 3.1.3, variations of average mat-to-mat resistances over time are due to the changes in concrete moisture content for field test specimens.

3.2.3.2 Field Test Specimens With Cracks

The test results are shown in Figures 3.94 through 3.99 for specimens with simulated cracks in the field test. The total corrosion losses at week 32 are summarized in Table 3.13.

Figures 3.94 and 3.95 show the average corrosion rates for conventional ECR and ECR with corrosion inhibitors. As shown in Figure 3.94, the specimens had similar corrosion rates, with values less than 0.03 and 12 μm/yr based on total area and exposed area, respectively, with the exception of ECR(DCI) (2), which had corrosion rates above 0.02 μm/yr (8 μm/yr based on exposed area) at weeks 20 and 24. The ECR(Rheocrete) (1) had a negative corrosion rate of –0.002 μm/yr (–0.915 μm/yr based on exposed area), which was caused by one of the four test bars and accompanied by more negative potentials at the cathode than at the anode.

The average total corrosion losses for conventional ECR and ECR with corrosion inhibitors are shown in Figures 3.96 and 3.97. Figure 3.96 shows that ECR(DCI) (2) had the highest corrosion loss, followed by ECR(DCI) (1), with values of 0.010 and 0.008 μm, respectively, at week 40. The remaining specimens had lower total corrosion losses, with values below 0.004 μm. Based on exposed area, total corrosion losses less than 4 μm were observed for all specimens, as shown in Figure 3.97. Table 3.13 summarizes the average total corrosion losses for these specimens at week 32. ECR(DCI) (1) and ECR(DCI) (2) showed a measurable total corrosion loss of approximately 0.01 μm and the remaining specimens exhibited total corrosion

losses below 0.005 μm based on total area, as indicated by the symbol β in Table 3.13. Based on exposed area, the specimens had total corrosion losses between 0 and 3.63 μm, compared to values of 0 and 1.06 μm for conventional ECR based on exposed area.

Table 3.13 – Average corrosion losses (μm) at week 32 as measured in the field test for specimens with ECR with a primer containing calcium nitrite and ECR cast with corrosion inhibitors, with cracks

Steel Designation[a]	Test Bar				Average	Standard Deviation
	1	2	3	4		
with cracks						
ECR(DCI) (1)	0.01	0.01	β	0.00	0.01	0.01
ECR(DCI)* (1)	4.79	4.65	0.99	0.00	2.61	2.47
ECR(DCI) (2)	β	0.00	0.02	0.02	0.01	0.01
ECR(DCI)* (2)	0.35	0.00	7.04	7.11	3.63	3.99
ECR(DCI) (3)	β	0.01	β	0.00	β	β
ECR(DCI)* (3)	0.28	2.32	0.28	0.00	0.72	1.08
ECR(Hycrete) (1)	β	β	0.00	0.00	β	β
ECR(Hycrete)* (1)	0.92	0.28	0.00	0.00	0.30	0.43
ECR(Hycrete) (2)	0.00	β	0.00	0.00	β	β
ECR(Hycrete)* (2)	0.00	1.48	0.00	0.00	0.37	0.74
ECR(Rheocrete) (1)	0.00	0.00	0.00	β	β	β
ECR(Rheocrete)* (1)	0.00	0.00	0.00	1.41	0.35	0.70
ECR(Rheocrete) (2)	0.00	0.00	0.00	0.00	0.00	0.00
ECR(Rheocrete)* (2)	0.00	0.00	0.00	0.00	0.00	0.00
ECR(primer/($Ca(NO_2)_2$) (1)	0.00	0.00	β	β	β	β
ECR(primer/($Ca(NO_2)_2$)* (1)	0.00	0.00	0.49	1.06	0.39	0.50
ECR(primer/($Ca(NO_2)_2$) (2)	0.00	0.00	0.00	β	β	β
ECR(primer/($Ca(NO_2)_2$)* (2)	0.00	0.00	0.00	0.77	0.19	0.39

[a] ECR = conventional epoxy-coated reinforcement. ECR(DCI) = ECR in concrete with DCI. ECR(Hycrete) = ECR in concrete with Hycrete. ECR(Rheocrete) = ECR in concrete with Rheocrete. ECR(primer/$Ca(NO_2)_2$) = ECR with a primer containing calcium nitrite.

* Epoxy-coated bars, calculations based on exposed area of 16 3-mm ($^1/_8$-in.) diameter holes.

β Corrosion loss (absolute value) less than 0.005 μm.

The average corrosion potentials of the top and bottom mats of steel with respect to a copper-copper sulfate electrode are shown in Figure 3.98. In general, the specimens showed similar corrosion potentials. As shown in Figure 3.98(a), all specimens with corrosion inhibitors showed active corrosion between week 8 and 32,

with the exception of ECR(DCI) (3) and ECR(Rheocrete) (1). The top mat corrosion potentials for these two specimens remained above –0.320 V, indicating a low probability of corrosion. ECR(DCI) (1) had the most negative corrosion potentials at the top mat, with values between –0.400 and –0.630 V between weeks 8 and 40. As shown in Figure 3.98(b), all specimens had bottom mat corrosion potentials more positive than –0.330 V, indicating a lower probability of corrosion. As shown in Figures 3.92 and 3.98, specimens with cracks had top mat corrosion potentials more negative than those for specimens without cracks. Both types of specimens, however, showed similar bottom mat corrosion potentials.

Figure 3.99 shows that the specimens with corrosion inhibitors had average mat-to-mat resistances similar to those for specimens with ECR, with values between 600 and 2,000 ohms.

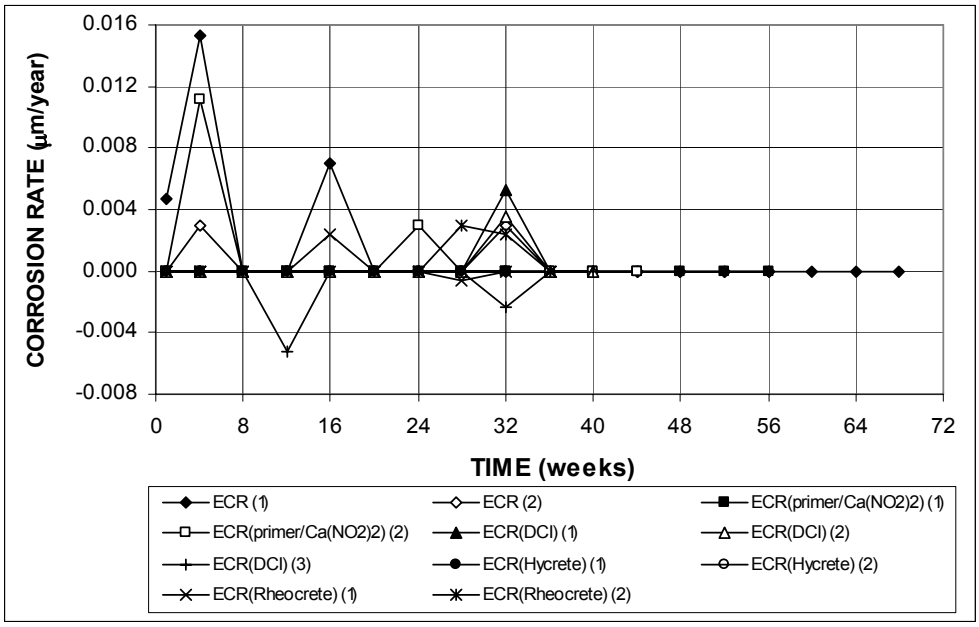

Figure 3.88 – Average corrosion rates as measured in the field test for specimens with ECR, ECR in concrete with corrosion inhibitors, and ECR with a primer containing calcium nitrite, without cracks (ECR bars have 16 holes).

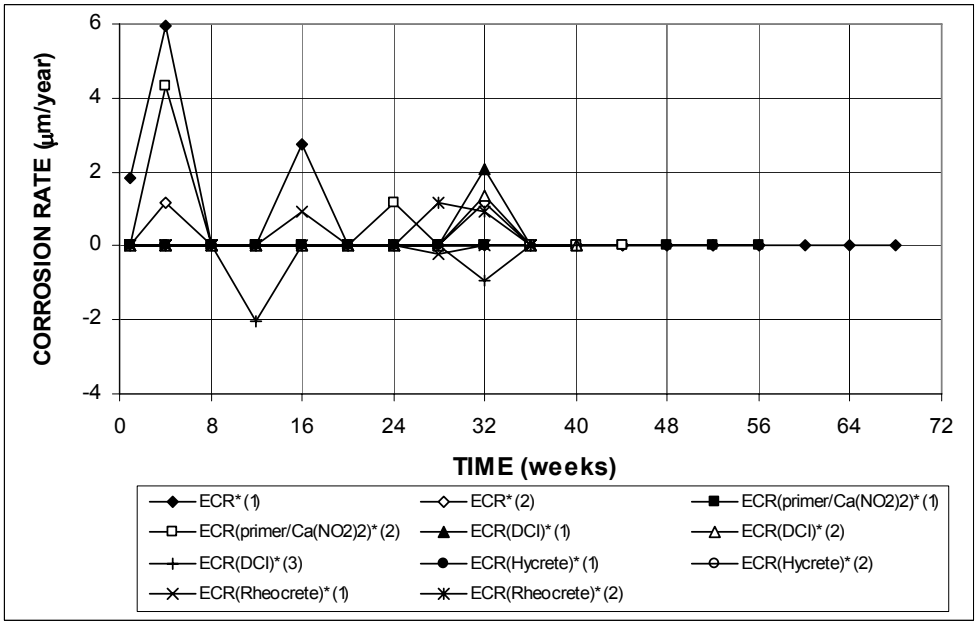

Figure 3.89 – Average corrosion rates as measured in the field test for specimens with ECR, ECR in concrete with corrosion inhibitors, and ECR with a primer containing calcium nitrite, without cracks. * Based on exposed area (ECR bars have 16 holes).

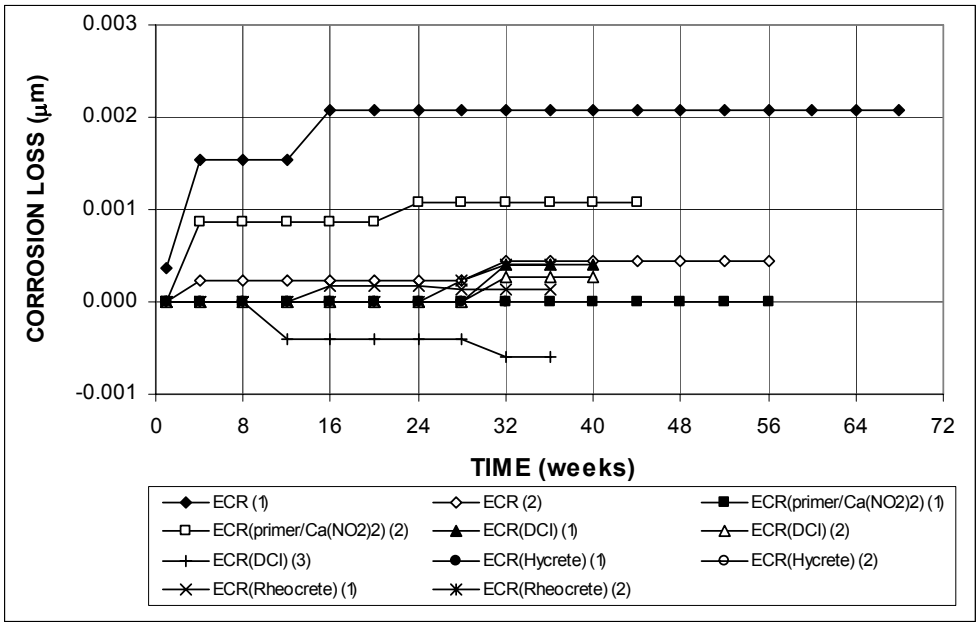

Figure 3.90 – Average corrosion losses as measured in the field test for specimens with ECR, ECR in concrete with corrosion inhibitors, and ECR with a primer containing calcium nitrite, without cracks (ECR bars have 16 holes).

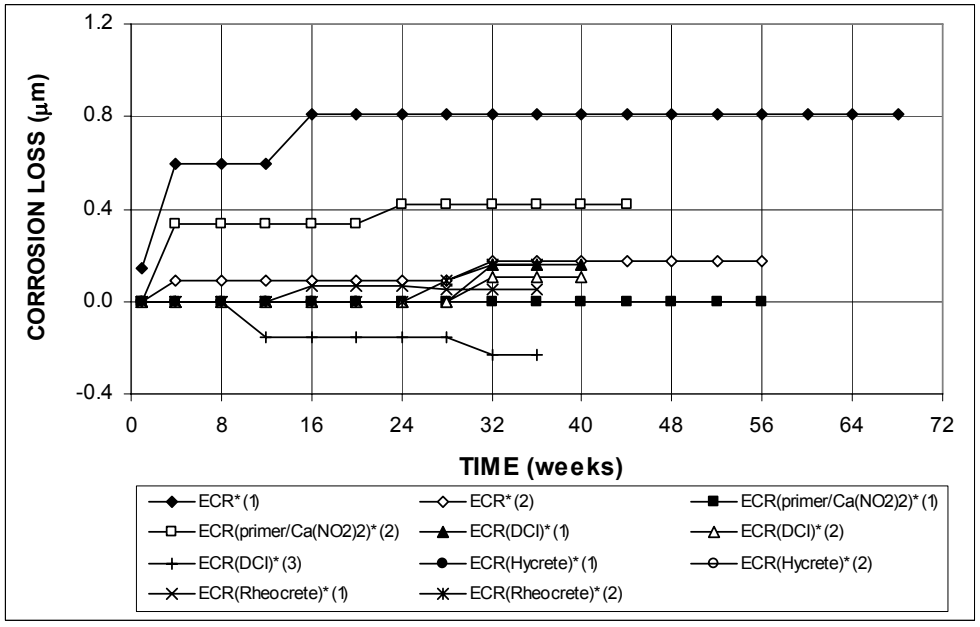

Figure 3.91 – Average corrosion losses as measured in the field test for specimens with ECR, ECR in concrete with corrosion inhibitors, and ECR with a primer containing calcium nitrite, without cracks. * Based on exposed area (ECR bars have 16 holes).

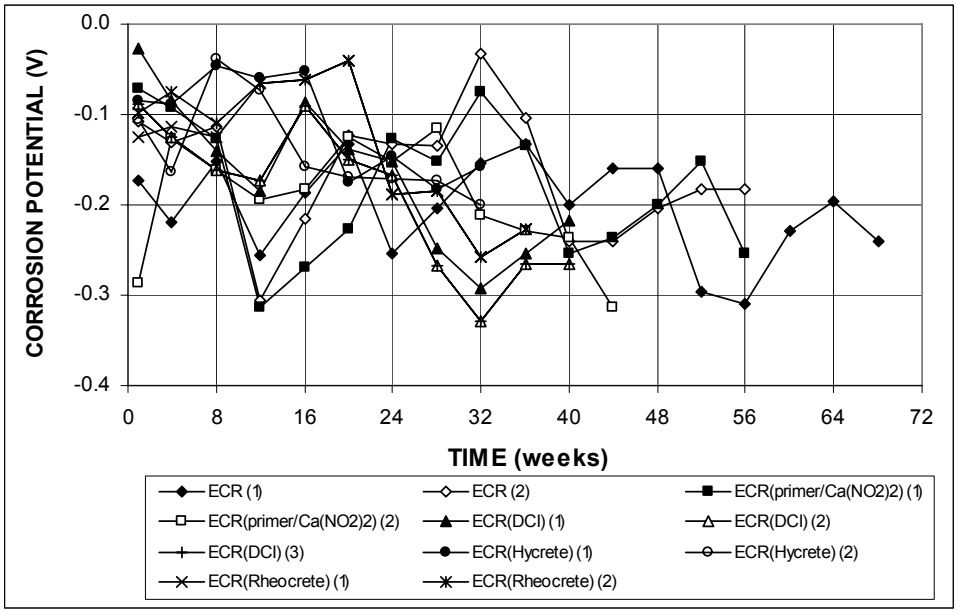

Figure 3.92 (a) – Average top mat corrosion potentials, with respect to a copper-copper sulfate electrode as measured in the field test for specimens with ECR, ECR in concrete with corrosion inhibitors, and ECR with a primer containing calcium nitrite, without cracks (ECR bars have 16 holes).

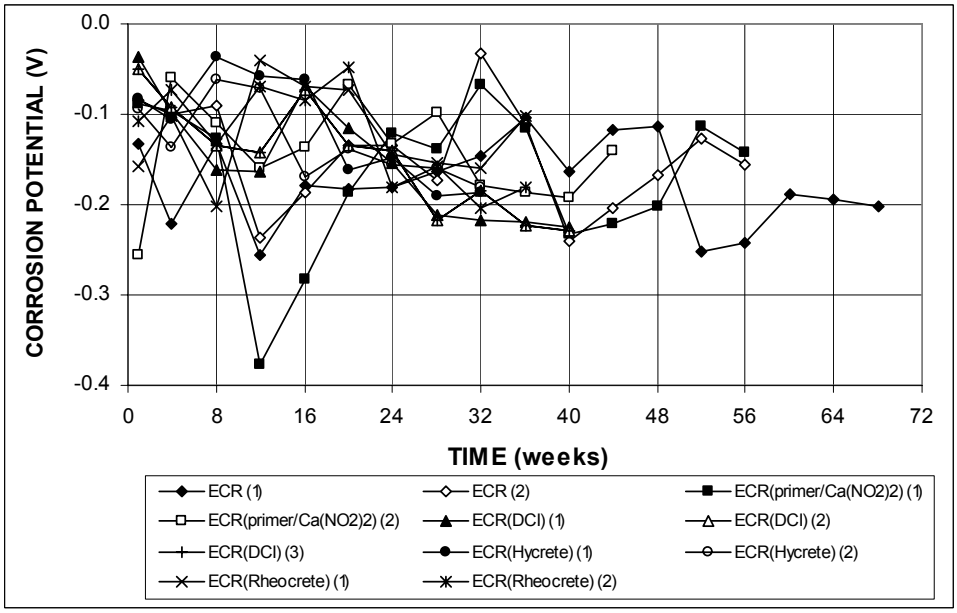

Figure 3.92 (b) – Average bottom mat corrosion potentials, with respect to a copper-copper sulfate electrode as measured in the field test for specimens with ECR, ECR in concrete with corrosion inhibitors, and ECR with a primer containing calcium nitrite, without cracks (ECR bars have 16 holes).

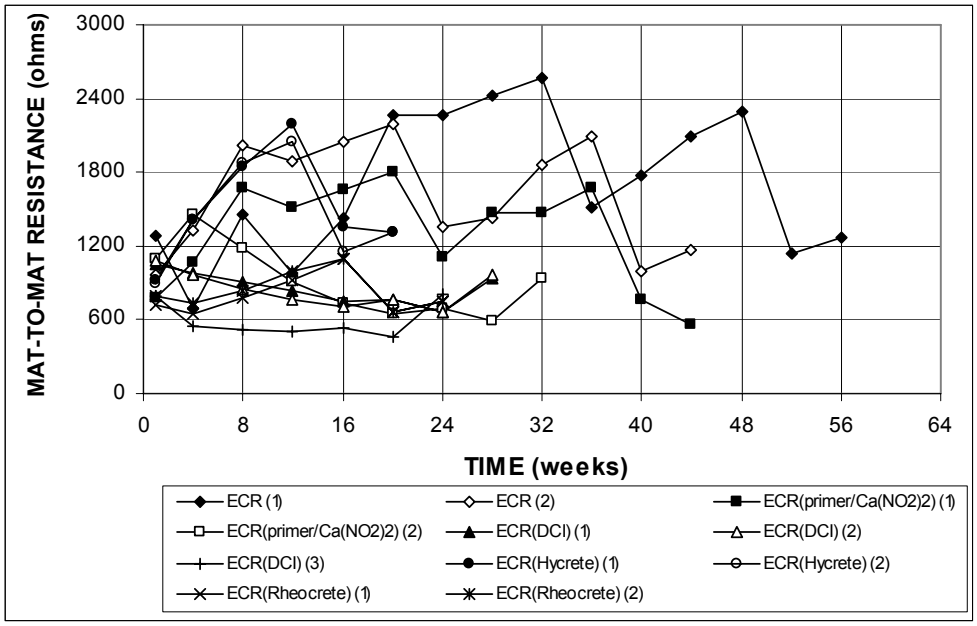

Figure 3.93 – Average mat-to-mat resistances as measured in the field test for specimens with ECR, ECR in concrete with corrosion inhibitors, and ECR with a primer containing calcium nitrite, without cracks (ECR bars have 16 holes).

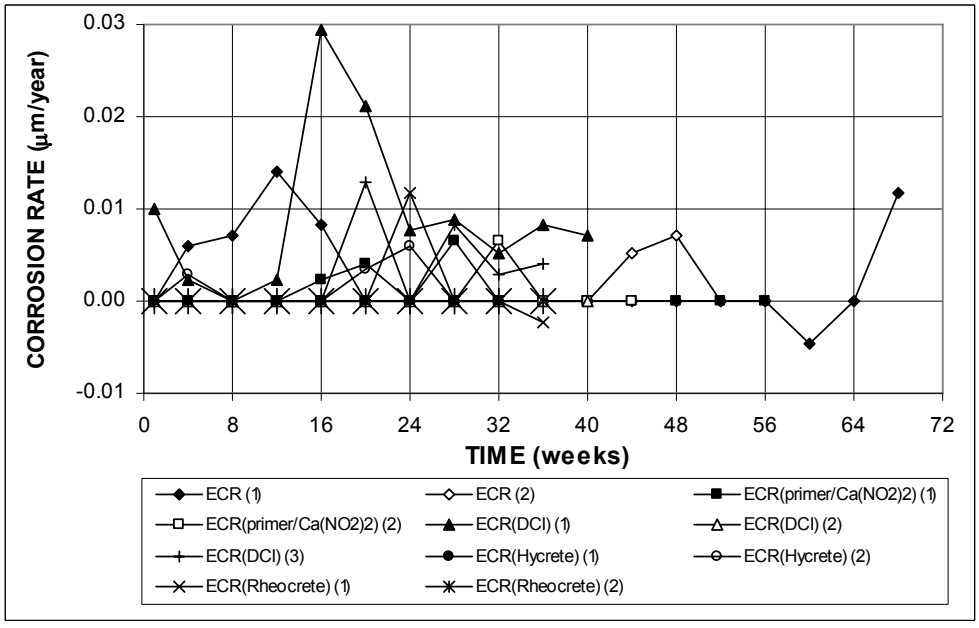

Figure 3.94 – Average corrosion rates as measured in the field test for specimens with ECR, ECR in concrete with corrosion inhibitors, and ECR with a primer containing calcium nitrite, with cracks (ECR bars have 16 holes).

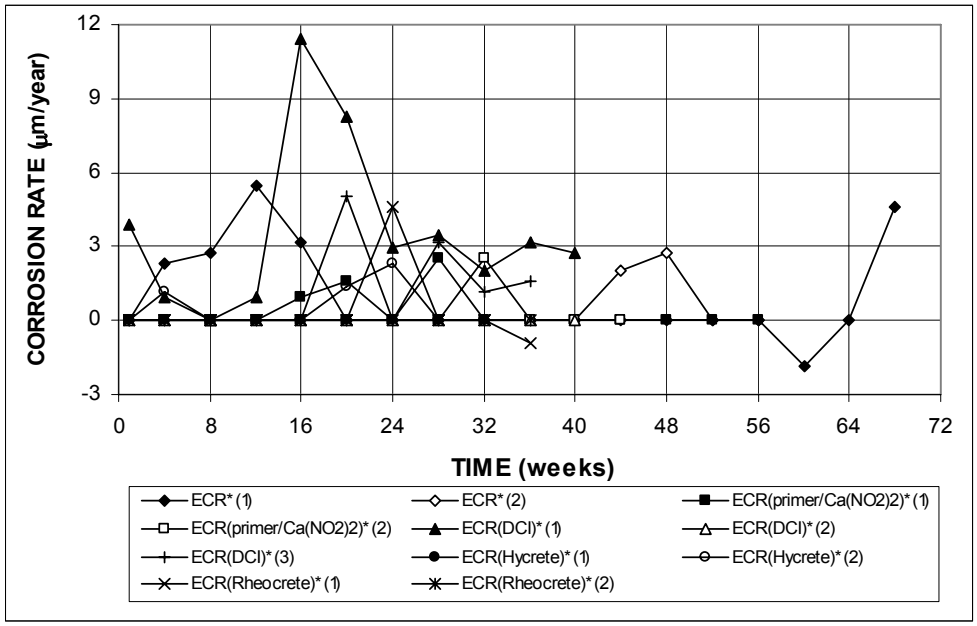

Figure 3.95 – Average corrosion rates as measured in the field test for specimens with ECR, ECR in concrete with corrosion inhibitors, and ECR with a primer containing calcium nitrite, with cracks. * Based on exposed area (ECR bars have 16 holes).

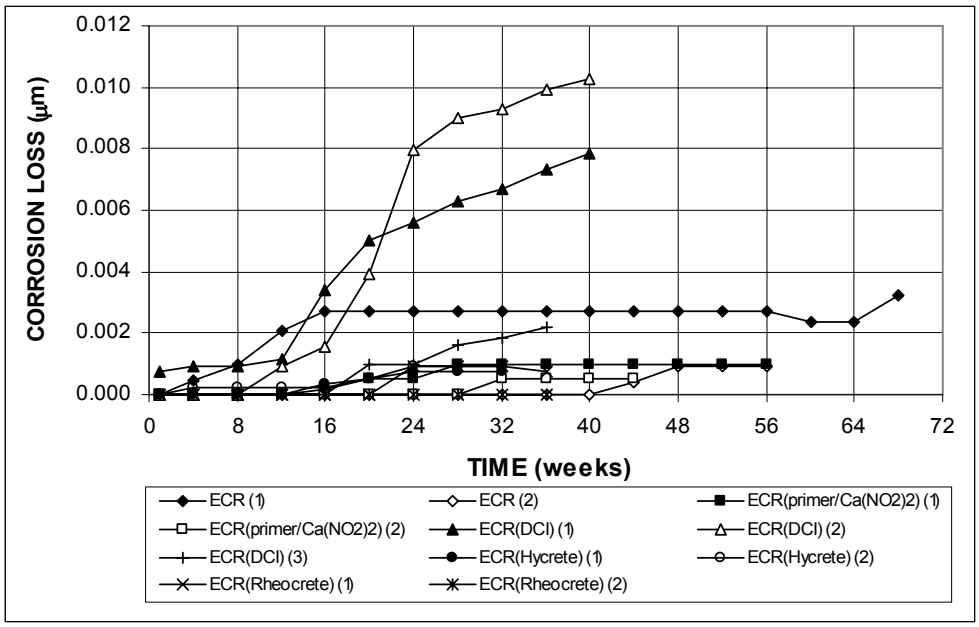

Figure 3.96 – Average corrosion losses as measured in the field test for specimens with ECR, ECR in concrete with corrosion inhibitors, and ECR with a primer containing calcium nitrite, with cracks (ECR bars have 16 holes).

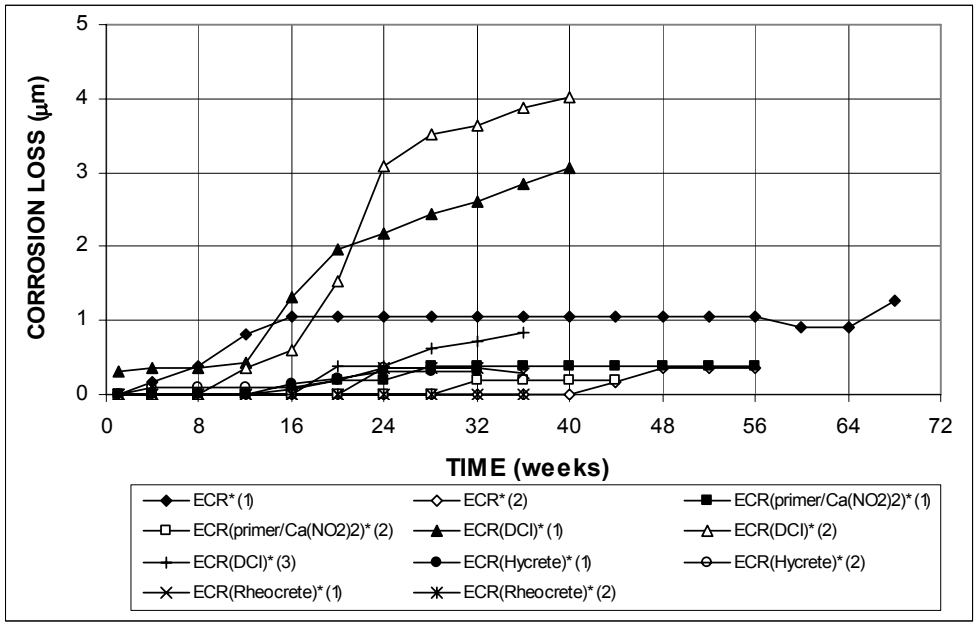

Figure 3.97 – Average corrosion losses as measured in the field test for specimens with ECR, ECR in concrete with corrosion inhibitors, and ECR with a primer containing calcium nitrite, with cracks. * Based on exposed area (ECR bars have 16 holes).

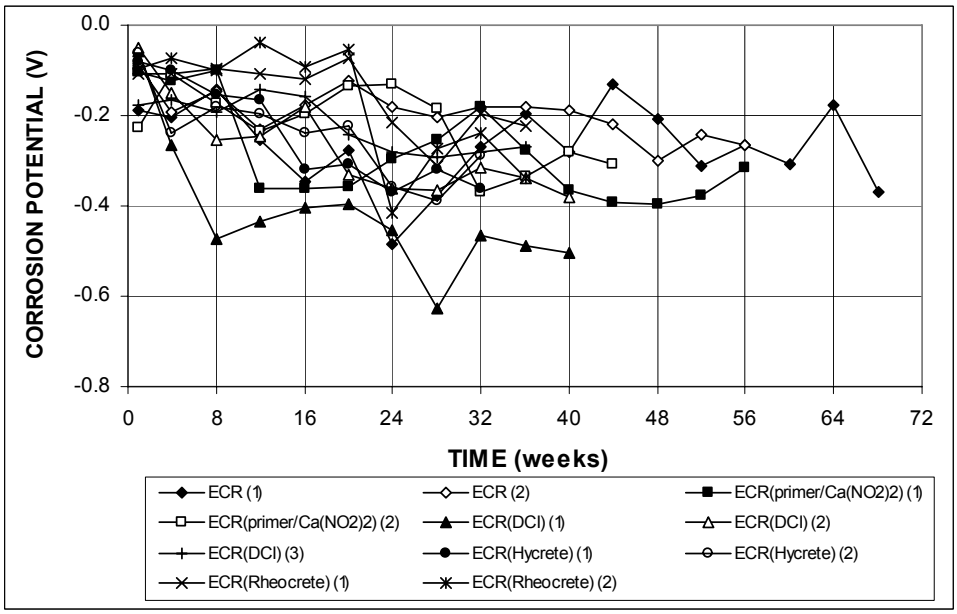

Figure 3.98 (a) – Average top mat corrosion potentials, with respect to a copper-copper sulfate electrode as measured in the field test for specimens with ECR, ECR in concrete with corrosion inhibitors, and ECR with a primer containing calcium nitrite, with cracks (ECR bars have 16 holes).

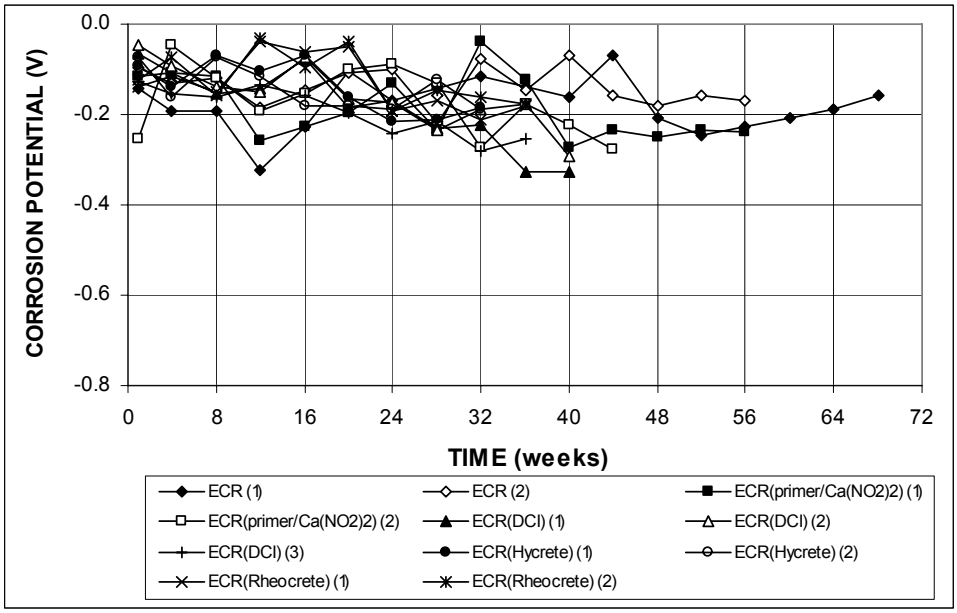

Figure 3.98 (b) – Average bottom mat corrosion potentials, with respect to a copper-copper sulfate electrode as measured in the field test for specimens with ECR, ECR in concrete with corrosion inhibitors, and ECR with a primer containing calcium nitrite, with cracks (ECR bars have 16 holes).

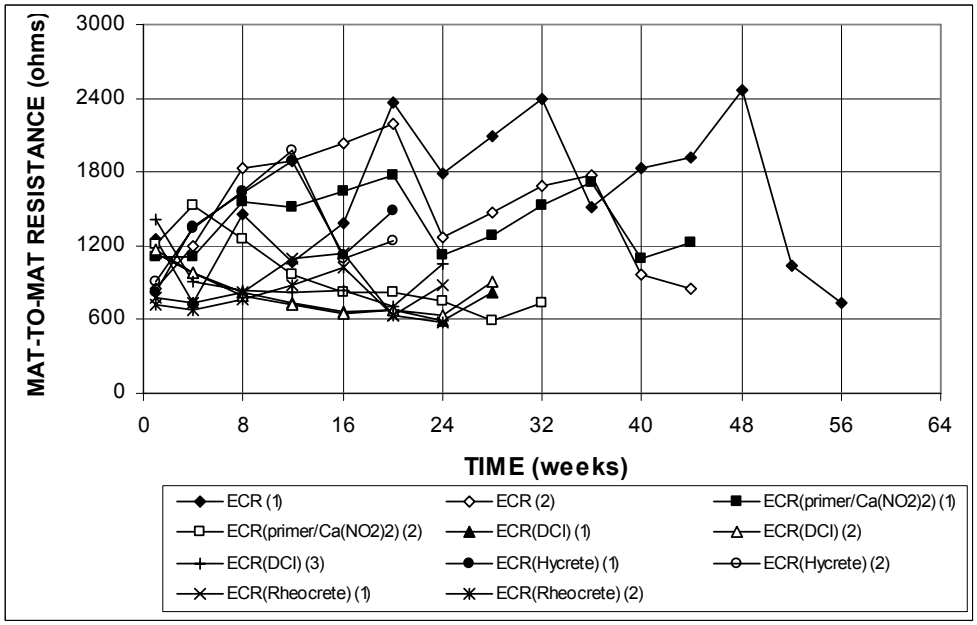

Figure 3.99 – Average mat-to-mat resistances as measured in the field test for specimens with ECR, ECR in concrete with corrosion inhibitors, and ECR with a primer containing calcium nitrite, with cracks (ECR bars have 16 holes).

3.3 MULTIPLE COATED REINFORCEMENT

This section presents the results of the rapid macrocell, bench-scale, and field tests for specimens containing multiple coated reinforcement with a zinc layer underlying the conventional epoxy coating. The zinc layer contains 98% zinc and 2% aluminum and has a nominal thickness of approximately 0.05 mm (2 mils).

In all of the tests, the multiple coated bars were evaluated in two ways: 1) with only the epoxy penetrated, and 2) with both the zinc and epoxy layers penetrated. The corrosion rates and total corrosion losses were calculated based on the properties of zinc for both specimens with only the epoxy penetrated and specimens with both layers penetrated. For specimens with both layers penetrated, zinc exists only around the perimeter of the drilled holes. As mentioned in Chapter 2, the whole damaged area was used as the effective area to calculate corrosion rates and total corrosion losses based on exposed area. For the rapid macrocell test, multiple coated bars were also evaluated in the as-delivered condition (without holes) using both bare bar and mortar-wrapped specimens; in this case, the corrosion rates and total corrosion losses were also obtained based on the properties of zinc.

3.3.1 Rapid Macrocell Test

Both the bare bar and mortar-wrapped specimens were used in the rapid macrocell test to evaluate multiple coated bars in 1.6 m ion NaCl and simulated concrete pore solution. The mortar had a *w/c* ratio of 0.50. For both types of specimens, the tests included six tests each for multiple coated bars penetrated with four holes through either the epoxy layer only or both the zinc and epoxy layers, and three tests with the bars in the as-delivered condition.

3.3.1.1 Bare Bar Specimens

The test results are shown in Figures 3.100 through 3.104 for the rapid macrocell test with multiple coated bare bar specimens. Table 3.14 summarizes the total corrosion losses at week 15.

Figure 3.100 shows the average corrosion rates for multiple coated bars with four holes. Based on the total area of the bar immersed in the solution, multiple coated bars had corrosion rates much lower than those for conventional steel, as shown in Figure 3.100(a). Figure 3.100(b) shows that except at week 11, multiple coated bars had corrosion rates below 0.4 μm/yr during the test period, which is one-half to one-third of the rate observed for conventional ECR with four holes. Multiple coated bars with both layers penetrated exhibited negative corrosion rates between week 5 and 10, indicating that the cathode bars were corroding. Due to its amphoteric nature, zinc can react with oxygen in the alkaline environment at the cathode, leading to "negative" corrosion. Multiple coated bars without holes showed no corrosion activity during the 15-week test period. Figure 3.101 shows that, based on the area exposed at the holes, multiple coated bars with only the epoxy layer penetrated had corrosion rates between 0 and 57.48 μm/yr, while multiple coated bars with both layers penetrated exhibited corrosion rates between –9.58 and 34.33 μm/yr.

The average total corrosion losses versus time are presented in Figures 3.102 through 3.103 and the values at week 15 are summarized in Table 3.14. Based on total area, the average total corrosion losses were 0.06 and 0.02 μm for specimens with only the epoxy penetrated and with both layers penetrated, respectively, at week 15. Based on exposed area, specimens with only the epoxy penetrated and both layers penetrated had total corrosion losses of 5.56 and 1.78 μm, respectively, equal to 17% and 5.3% of the corrosion loss of conventional ECR. For multiple coated bars with

only the epoxy penetrated, the average corrosion rate based on the exposed area over the 15-week test period is 0.37 μm/week, meaning that it should take 135 weeks for the zinc layer (with a thickness of 50 μm) to be lost.

Table 3.14 – Average corrosion losses (μm) at week 15 as measured in the macrocell test for bare bar specimens with multiple coated bars

Steel Designation[a]	Specimen						Average	Standard Deviation
	1	2	3	4	5	6		
Bare Bar Specimens								
MC(only epoxy penetrated)	0.06	0.02	0.10	0.05	0.04	0.05	0.06	0.03
MC(only epoxy penetrated)*	6.26	2.41	10.44	4.94	4.00	5.29	5.56	2.72
MC(both layers penetrated)	0.06	0.05	0.01	0.01	-0.05	0.03	0.02	0.04
MC(both layers penetrated)*	5.57	5.40	0.85	0.86	-4.99	2.98	1.78	3.91
MC-no holes	0.00	0.00	0.00				0.00	0.00

[a] MC = multiple coated bars.
MC(only epoxy penetrated) = multiple coated bars with only the epoxy layer penetrated.
MC(both layers penetrated) = multiple coated bars with both the zinc and epoxy layers penetrated.
no holes = epoxy-coated bars without holes, otherwise four 3-mm ($^1/_8$-in.) diameter holes.

* Epoxy-coated bars, calculations based on exposed area of four 3-mm ($^1/_8$-in.) diameter holes.

The average anode and cathode corrosion potentials with respect to a saturated calomel electrode are shown in Figure 3.104. According to Yeomans (1994), the corrosion potential of zinc with respect to a copper-copper sulfate electrode is –1.050 V when it is actively corroding and –0.650 V when it is passive. As will be shown in Section 3.3.2, multiple coated bars with only the epoxy penetrated showed bottom mat corrosion potentials generally between –0.200 and –0.500 V in the SE and ASTM G 109 tests. Therefore, it is reasonable to believe that zinc is passive when its potential is more positive –0.500 V. As shown in Figure 3.104(a), for specimens with both layers penetrated, the anode potentials started at –1.20 V, rising to –0.497 V at week 3, indicating that zinc around the holes served as a sacrificial anode and provided cathodic protection to the underlying steel during the first three weeks. Then the anode potentials remained around –0.450 V for the rest of the test period. The

anode potentials for specimens with only the epoxy penetrated started at –1.40 V and slowly increased to –0.658 V at week 15, indicating that zinc was corroding, but providing protection to the underlying steel throughout the test period. The cathode potentials behaved similarly to the anode potentials for specimens with only the epoxy penetrated and both layers penetrated, as shown in Figure 3.104(b). The cathode potentials were slightly more positive than the corresponding anode potentials. Stable corrosion potentials at both the anodes and cathodes were not available for intact specimens with multiple coated bars.

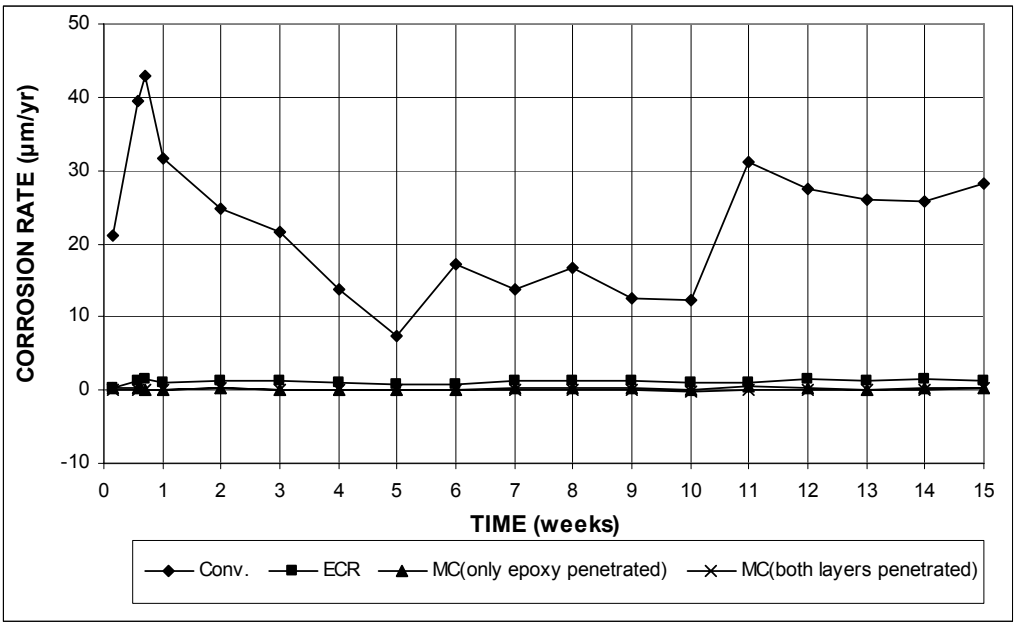

Figure 3.100 (a) – Average corrosion rates as measured in the rapid macrocell test for bare bar specimens with conventional steel, ECR, and multiple coated bars (ECR bars have four holes).

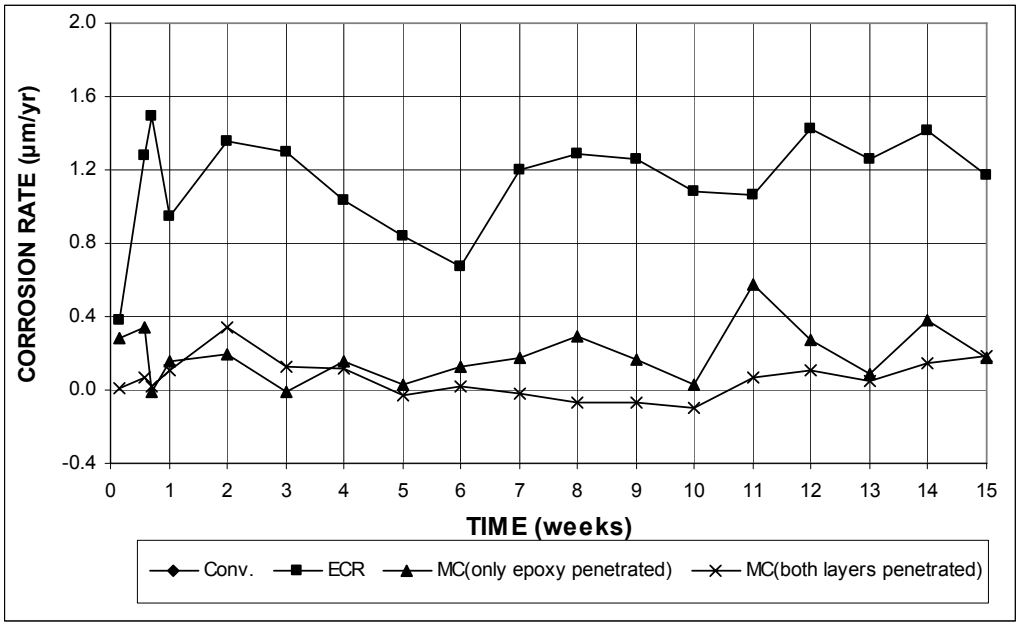

Figure 3.100 (b) – Average corrosion rates as measured in the rapid macrocell test for bare bar specimens with conventional steel, ECR, and multiple coated bars (ECR bars have four holes).

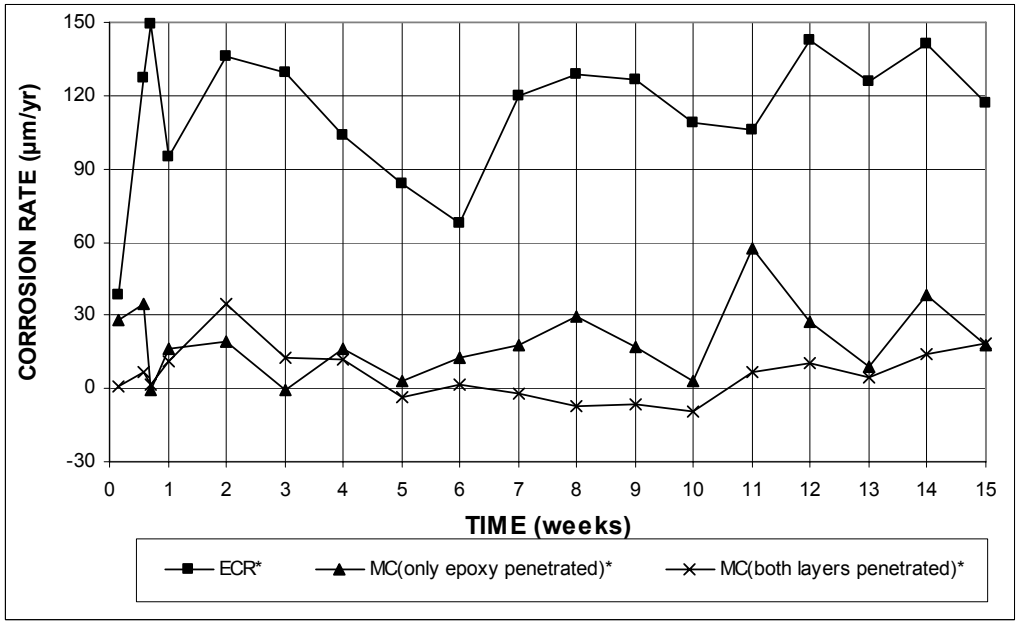

Figure 3.101 – Average corrosion rates as measured in the rapid macrocell test for bare bar specimens with ECR and multiple coated bars. * Based on exposed area (ECR bars have four holes).

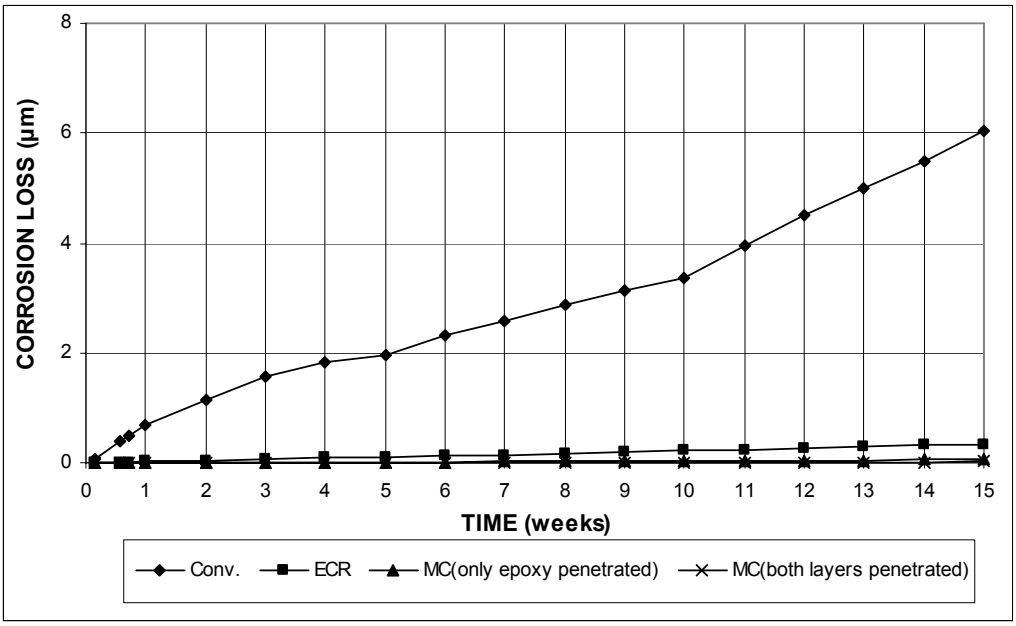

Figure 3.102 (a) – Average corrosion losses as measured in the rapid macrocell test for bare bar specimens with conventional steel, ECR, and multiple coated bars (ECR bars have four holes).

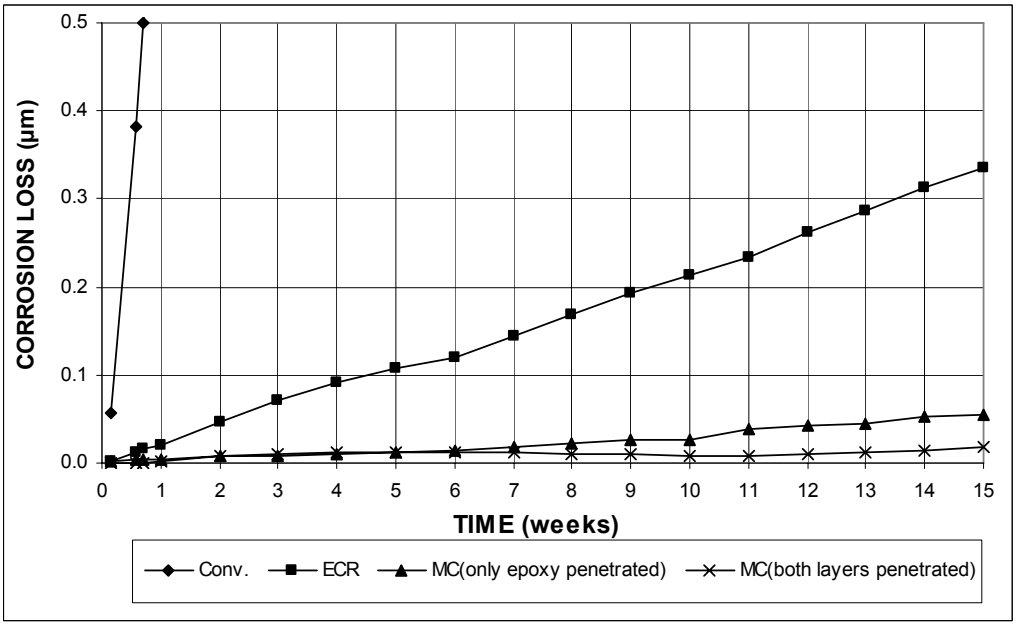

Figure 3.102 (b) – Average corrosion losses as measured in the rapid macrocell test for bare bar specimens with conventional steel, ECR, and multiple coated bars (ECR bars have four holes).

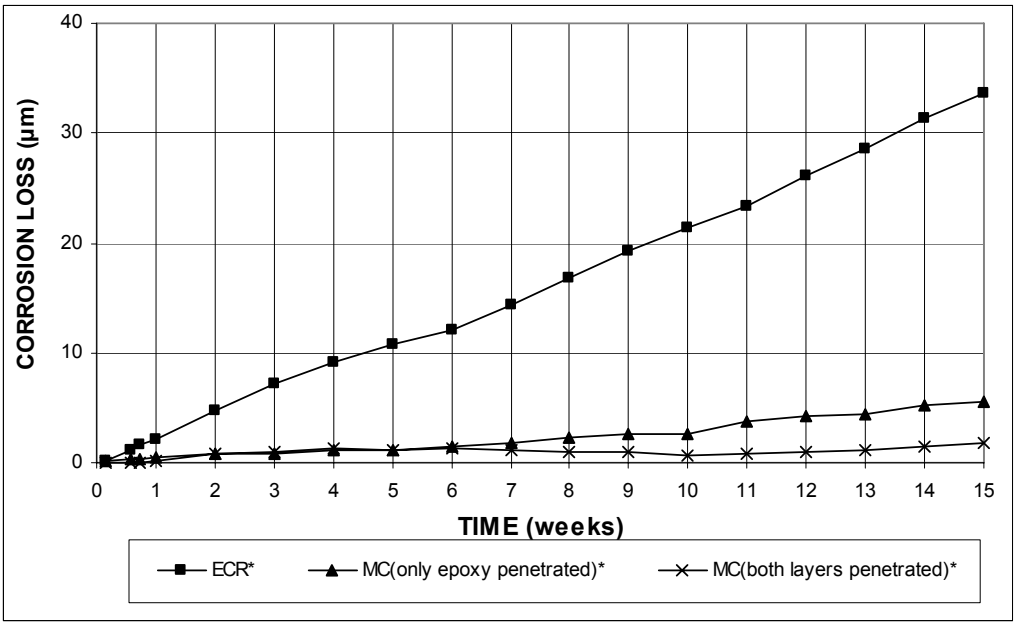

Figure 3.103 – Average corrosion losses as measured in the rapid macrocell test for bare bar specimens with ECR and multiple coated bars. * Based on exposed area (ECR bars have four holes).

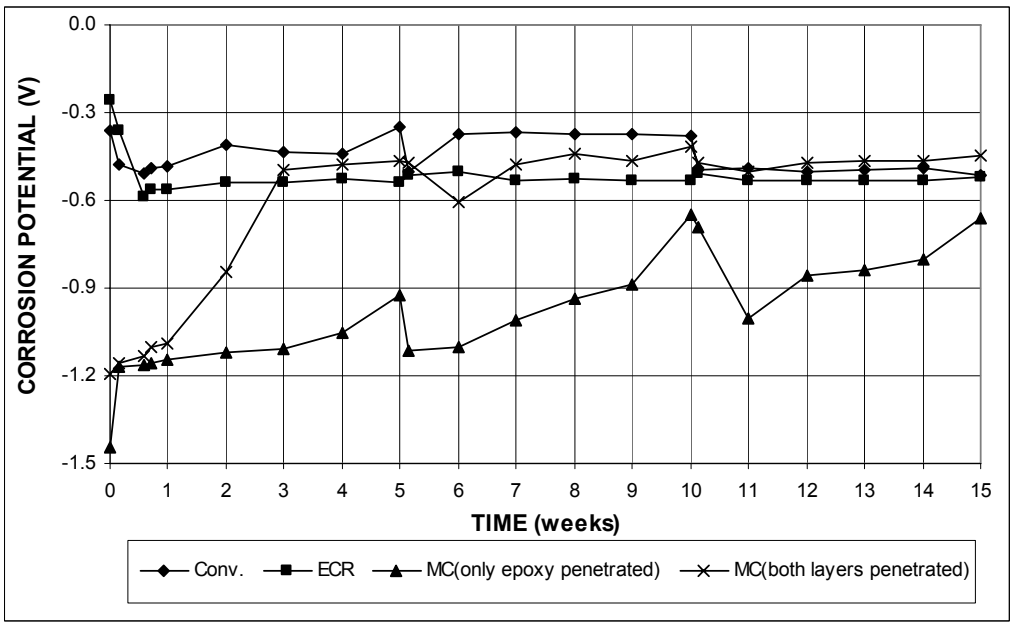

Figure 3.104 (a) – Average anode corrosion potentials, with respect to a saturated calomel electrode as measured in the rapid macrocell test for bare bar specimens with conventional steel, ECR, and multiple coated bars (ECR bars have four holes).

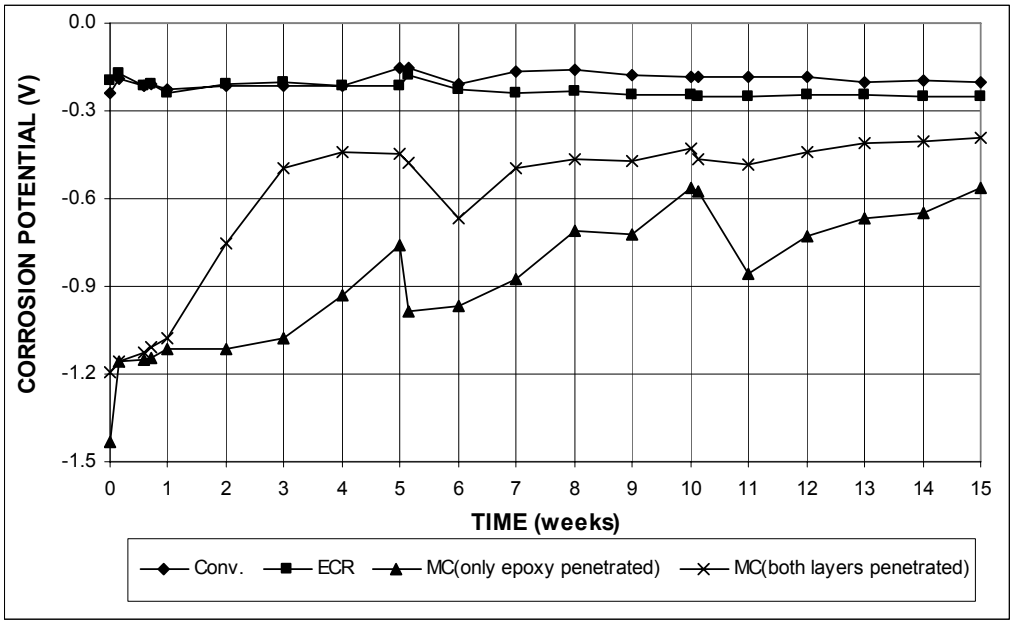

Figure 3.104 (b) – Average cathode corrosion potentials, with respect to a saturated calomel electrode as measured in the rapid macrocell test for bare bar specimens with conventional steel, ECR, and multiple coated bars (ECR bars have four holes).

After the 15-week test period, the specimens were visually inspected. Corrosion products were found at holes for specimens with only the epoxy penetrated and with both layers penetrated, as shown in Figures 3.105 and 3.106, respectively.

Figure 3.105 – Bare bar specimen. Multiple coated anode bar with only epoxy penetrated showing corrosion products that formed at holes at week 15.

Figure 3.106 – Bare bar specimen. Multiple coated anode bar with both layers penetrated showing corrosion products that formed at holes at week 15.

3.3.1.2 Mortar-Wrapped Specimens

The test results are presented in Figures 3.107 through 3.111 for the rapid macrocell test with mortar-wrapped multiple coated bar specimens. The total corrosion losses at week 15 are summarized in Table 3.15.

Figure 3.107 shows the average corrosion rates for multiple coated bars with four holes. Based on total area, multiple coated bars exhibited corrosion rates much lower than those for conventional steel, as shown in Figure 3.107(a). Figure 3.107(b) shows that multiple coated bars with only the epoxy penetrated showed relatively high corrosion rates during the first five weeks, with the highest corrosion rate of 0.359 μm/yr based on total area, and then showed no corrosion activity for the rest of the test period. For specimens with both layers penetrated, the average corrosion rates were between –0.056 and 0.032 μm/yr. As discussed in Section 3.3.1.1, negative corrosion rates are due to the amphoteric nature of zinc that allows it to be oxidized in the alkaline environment at the cathode. Multiple coated bars without holes showed no corrosion activity during the test period. Figure 3.108 shows that, based on the area exposed at the holes, multiple coated bars with only the epoxy layer penetrated had corrosion rates below 35.93 μm/yr, while specimens with both layers penetrated exhibited corrosion rates between –5.59 and 3.19 μm/yr.

Table 3.15 – Average corrosion losses (μm) at week 15 as measured in the macrocell test for mortar-wrapped specimens with multiple coated bars

Steel Designation[a]	Specimen						Average	Standard Deviation
	1	2	3	4	5	6		
Mortar-wrapped Specimens								
MC(only epoxy penetrated)	0.02	0.03	0.02	0.02	0.01	0.02	0.02	0.01
MC(only epoxy penetrated)*	1.86	3.00	1.66	2.28	0.60	2.04	1.91	0.79
MC(both layers penetrated)	β	β	β	0.00	-0.01	0.00	β	0.01
MC(both layers penetrated)*	-0.46	0.16	0.10	0.00	-1.38	0.00	-0.26	0.59
MC-no holes	0.00	0.00	0.00				0.00	0.00

[a] MC = multiple coated bars.

MC(only epoxy penetrated) = multiple coated bars with only the epoxy layer penetrated.

MC(both layers penetrated) = multiple coated bars with both the zinc and epoxy layers penetrated.

no holes = epoxy-coated bars without holes, otherwise four 3-mm ($^1/_8$-in.) diameter holes.

* Epoxy-coated bars, calculations based on exposed area of four 3-mm ($^1/_8$-in.) diameter holes.

β Corrosion loss (absolute value) less than 0.005 μm.

The average total corrosion losses versus time are presented in Figures 3.109 through 3.110 and the results at week 15 are summarized in Table 3.15. As shown in Figure 3.109(b), specimens with only the epoxy penetrated had much higher total corrosion losses than conventional ECR, while specimens with both layers penetrated had negative total corrosion losses, indicating that macrocell corrosion losses were not observed for the reinforcing bars at the anode. At week 15, specimens with only the epoxy penetrated had a total corrosion loss of 0.02 μm based on total area and 1.91 μm based on exposed area. Specimens with both layers penetrated had a total corrosion loss (absolute value) of less than 0.005 μm based on total area and –0.26 μm based on exposed area, compared to a value less than –0.06 μm for conventional ECR based on exposed area. Specimens without holes had a total corrosion loss less than 0.005 μm, as indicated by the symbol β in Table 3.15. For multiple coated bars with only the epoxy penetrated, the average corrosion rate over the 15-week test period was 0.13 μm/week, indicating that it will take approximately 390 weeks (7.5 years) for the zinc layer (with a thickness of 50 μm) to be lost.

The average anode and cathode corrosion potentials with respect to a saturated

calomel electrode are shown in Figure 3.111. As shown in Figure 3.111, at the beginning of the test, both types of specimens had anode corrosion potentials around –0.500 V, which is the corrosion potential when zinc is passive. For specimens with both layers penetrated, the anode potentials remained around –0.700 V after the first week, indicating that the zinc around the holes protected the steel during the test period. For specimens with only the epoxy penetrated, the anode potentials slowly decreased to –0.710 V at week 15, indicating that the zinc layer protected the steel throughout the test period. This is in agreement with the fact that during the 15-week test period, only 3.8% of the zinc layer was lost due to corrosion. The cathode potentials for specimens with only the epoxy penetrated started at –0.342 V, and then gradually dropped to –0.611 V at week 15. For specimens with both layers penetrated, the cathode potentials started at –0.493 V and slowly dropped to –0.796 V at week 15. Stable corrosion potentials at both the anodes and cathodes were not available for multiple coated bars without holes.

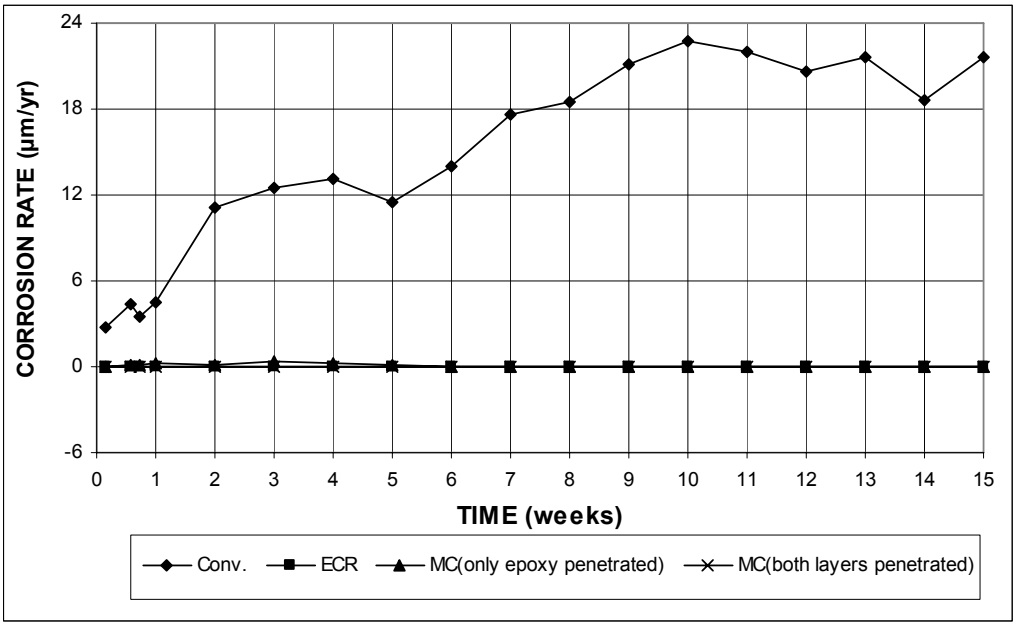

Figure 3.107 (a) – Average corrosion rates as measured in the rapid macrocell test for mortar-wrapped specimens with conventional steel, ECR, and multiple coated bars (ECR bars have four holes).

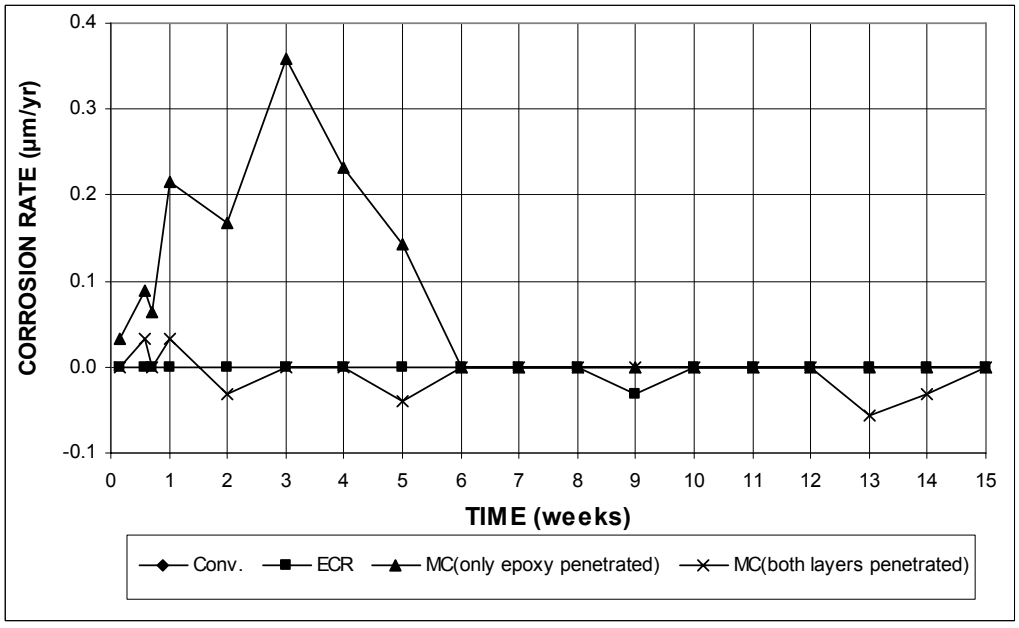

Figure 3.107 (b) – Average corrosion rates as measured in the rapid macrocell test for mortar-wrapped specimens with conventional steel, ECR, and multiple coated bars (ECR bars have four holes).

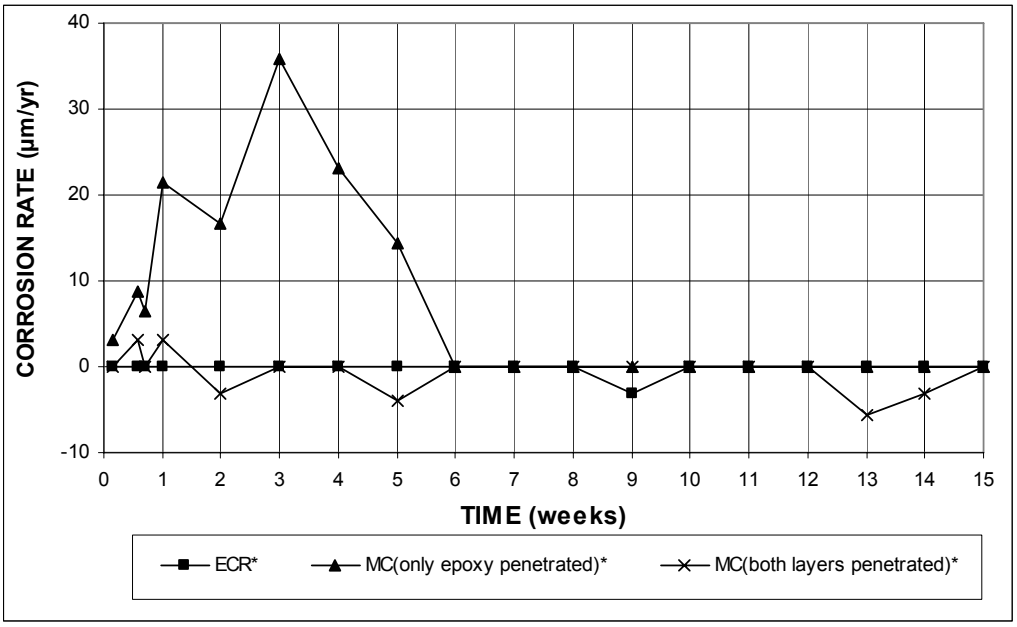

Figure 3.108 – Average corrosion rates as measured in the rapid macrocell test for mortar-wrapped specimens with ECR and multiple coated bars. * Based on exposed area (ECR bars have four holes).

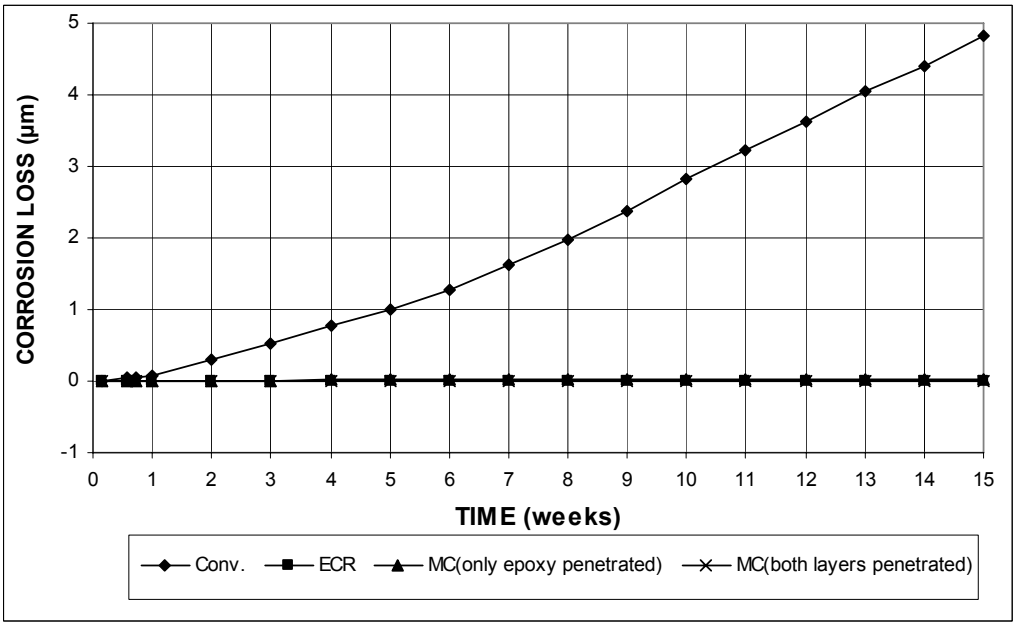

Figure 3.109 (a) – Average corrosion losses as measured in the rapid macrocell test for mortar-wrapped specimens with conventional steel, ECR, and multiple coated bars (ECR bars have four holes).

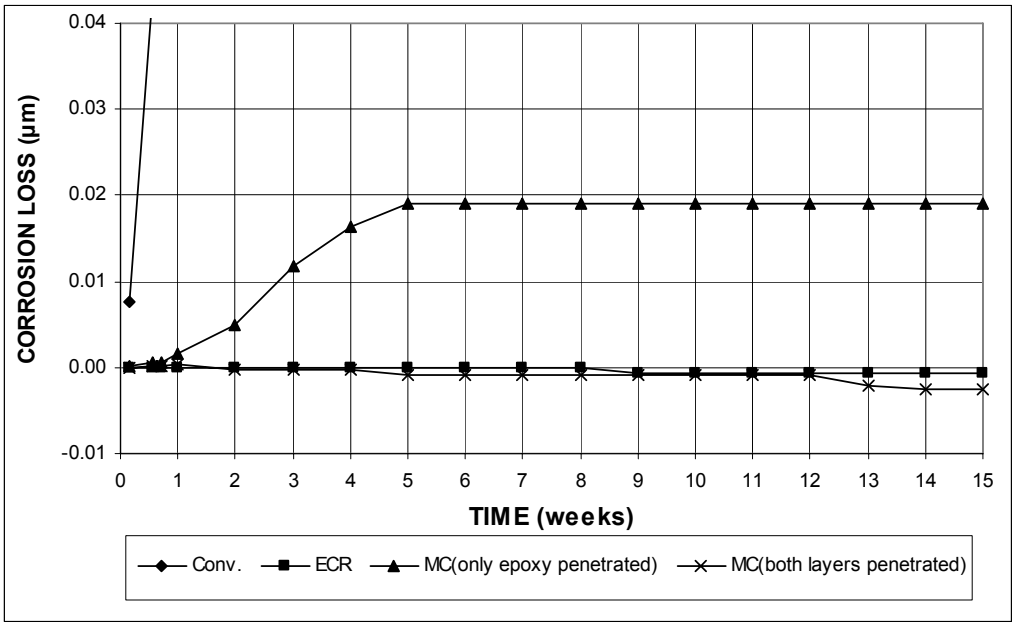

Figure 3.109 (b) – Average corrosion losses as measured in the rapid macrocell test for mortar-wrapped specimens with conventional steel, ECR, and multiple coated bars (ECR bars have four holes).

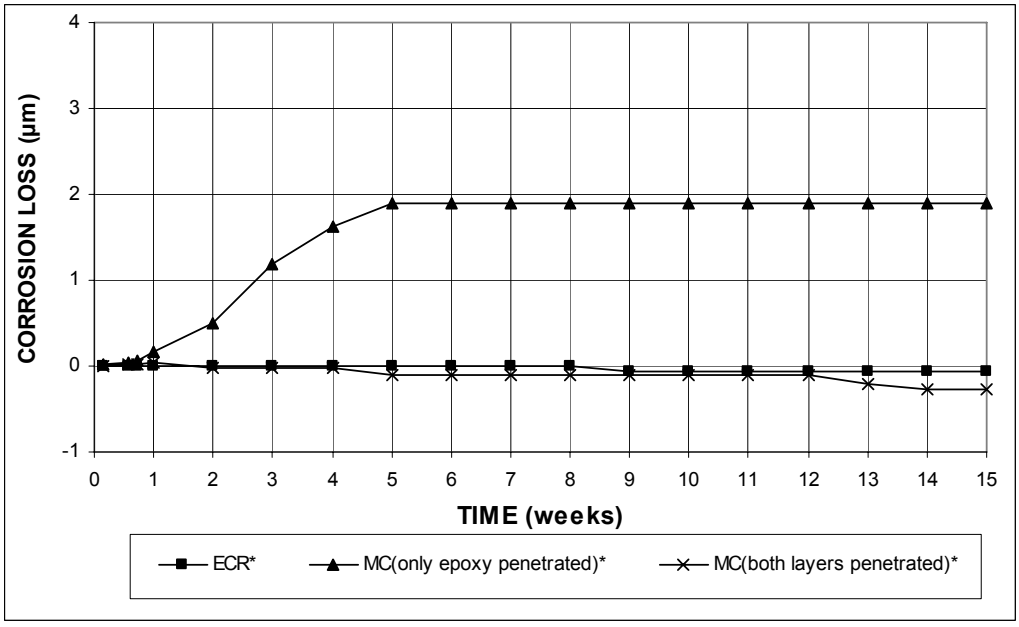

Figure 3.110 – Average corrosion losses as measured in the rapid macrocell test for mortar-wrapped specimens with ECR and multiple coated bars. * Based on exposed area (ECR bars have four holes).

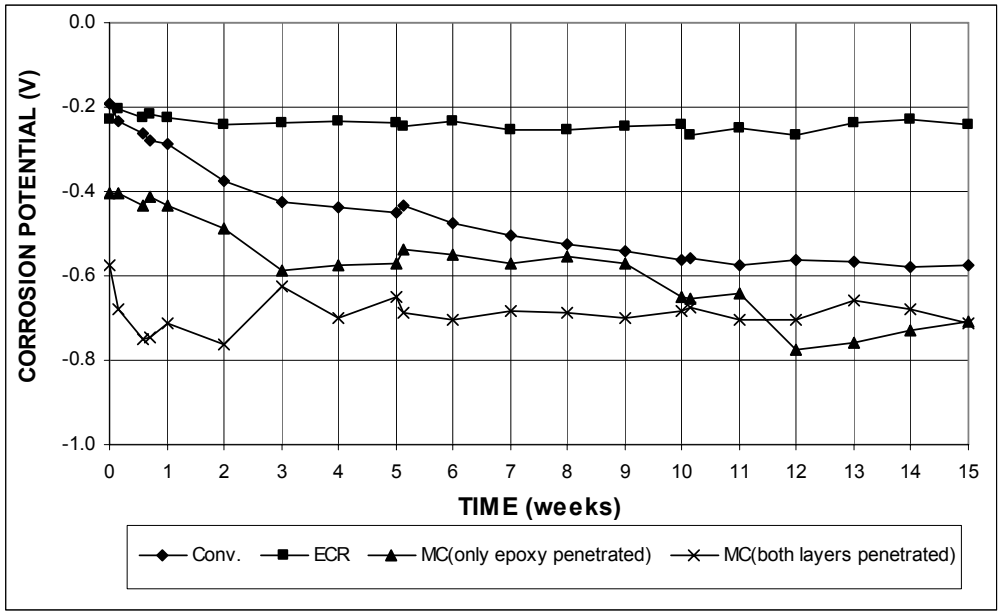

Figure 3.111 (a) – Average anode corrosion potentials, with respect to a saturated calomel electrode as measured in the rapid macrocell test for mortar-wrapped specimens with conventional steel, ECR, and multiple coated bars (ECR bars have four holes).

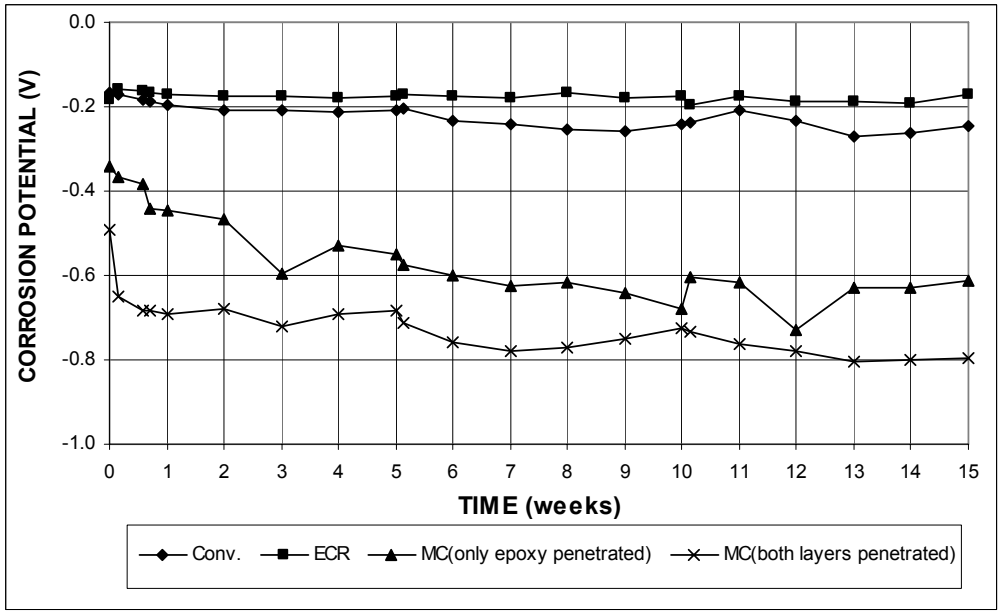

Figure 3.111 (b) – Average cathode corrosion potentials, with respect to a saturated calomel electrode as measured in the rapid macrocell test for mortar-wrapped specimens with conventional steel, ECR, and multiple coated bars (ECR bars have four holes).

At the end of the test period, the mortar was removed and the specimens were visually inspected. No corrosion products were found on mortar-wrapped specimens with multiple coated bars, as was the case for mortar-wrapped specimens containing conventional ECR, ECR with a calcium nitrite primer, and ECR cast in mortar with the corrosion inhibitors DCI-S, Rheocrete, and Hycrete.

3.3.2 Bench-Scale Tests

The Southern Exposure, cracked beam, and ASTM G 109 tests were used to evaluate multiple coated bars. The tests include three tests each for multiple coated bars with only the epoxy layer and both the zinc and epoxy layers penetrated with four or 10 holes.

3.3.2.1 Southern Exposure Test

The results for the Southern Exposure tests are shown in Figures 3.112 through 3.117, and the total corrosion losses at week 40 are summarized in Table 3.16.

Figures 3.112 and 3.113 show the average corrosion rates for multiple coated bars with only the epoxy layer and both the zinc and epoxy layers penetrated. As shown in Figure 3.112(b), MC(both layers penetrated)-10h showed corrosion rates less than 0.06 μm/yr before week 12 and then showed corrosion rates between 0.07 and 0.17 μm/yr between weeks 12 and 33. After week 33, the corrosion rates dropped below 0.08 μm/yr for MC(both layers penetrated)-10h. Based on total area, MC(both layers penetrated)-10h showed the highest corrosion rates, followed by MC(only epoxy penetrated)-10h. These two specimen types had average corrosion rates as high as 0.17 and 0.08 μm/yr, respectively. Multiple coated bars with four holes exhibited similar corrosion rates to specimens with conventional ECR, with values below 0.04

μm/yr. Negative corrosion rates between –0.005 and –0.012 μm/yr were observed for MC(both layers penetrated) at week 17, for MC(only epoxy penetrated) in the first two weeks and at week 17, and for MC(only epoxy penetrated)-10h at week 38, as shown in Figure 3.112(b). These negative corrosion rates, however, were not associated with more negative corrosion potentials at cathode than at anode, with the exception of specimens with only the epoxy penetrated with four holes in the first two weeks. Based on exposed area (Figure 3.113), all specimens had corrosion rates between –5.75 and 32.8 μm/yr.

The average total corrosion losses are shown in Figures 3.114 and 3.115 for multiple coated bars. As shown in Figure 3.114, all specimens showed little corrosion loss in the first 10 weeks and then showed progressive corrosion. MC(only epoxy penetrated)-10h showed very little corrosion after week 23. MC(both layers penetrated)-10h showed a steeper slope in total corrosion loss than the remaining specimens after week 12. As shown in Figure 3.115, multiple coated bars with only the epoxy penetrated with four holes exhibited negative corrosion loss before week 20, and then showed very little corrosion. Table 3.16 summarizes the average total corrosion losses for these specimens at week 40. By week 40, all specimens with multiple coated bars had higher total corrosion losses than the corresponding specimens with ECR, as shown in Figures 3.114(b) and 3.115. Based on total area, MC(both layers penetrated)-10h had the highest total corrosion loss of 0.06 μm, and MC(only epoxy penetrated) had the lowest total corrosion loss of less than 0.005 μm, as indicated by the symbol β in Table 3.16. The remaining two specimens, MC(both layers penetrated) and MC(only epoxy penetrated)-10h, had total corrosion losses of approximately 0.02 and 0.01 μm, respectively. Based on exposed area, the total corrosion losses equaled 1.51 and 7.21 μm for MC(only epoxy penetrated) and

MC(both layers penetrated), respectively, equal to 1.09 and 4.78 times the corrosion loss of conventional ECR with four holes. MC(only epoxy penetrated)-10h and MC(both layers penetrated)-10h had total corrosion losses of 2.23 and 11.8 μm, respectively. These values are, respectively, equal to 3.67 and 18.3 times the total corrosion loss of conventional ECR with 10 holes. The average corrosion rates during the first 40 weeks are 0.04 and 0.06 μm/week, respectively, for multiple coated bars with four and 10 holes penetrated with only the epoxy. Based on this calculation, it will take the zinc layer (with a thickness of 50 μm) 1320 and 900 weeks (25 and 17 years), respectively, to be consumed in these two specimens.

Table 3.16 – Average corrosion losses (μm) at week 40 as measured in the Southern Exposure test for specimens with multiple coated bars

Steel Designation[a]	Specimen			Average	Standard Deviation
	1	2	3		
Southern Exposure Test					
MC(only epoxy penetrated)	0.01	β	β	β	β
MC(only epoxy penetrated)*	3.22	2.32	-1.00	1.51	2.22
MC(only epoxy penetrated)-10h	β	0.01	0.02	0.01	0.01
MC(only epoxy penetrated)-10h*	0.15	2.00	4.56	2.23	2.22
MC(both layers penetrated)	0.03	β	0.01	0.02	0.01
MC(both layers penetrated)*	12.42	2.18	7.02	7.21	5.12
MC(both layers penetrated)-10h	0.03	0.07	0.08	0.06	0.03
MC(both layers penetrated)-10h*	5.77	13.50	15.97	11.75	5.32

[a] MC = multiple coated bars.
MC(only epoxy penetrated) = multiple coated bars with only the epoxy layer penetrated.
MC(both layers penetrated) = multiple coated bars with both the zinc and epoxy layers penetrated.
10h = epoxy-coated bars with 10 holes, otherwise four 3-mm ($^1/_8$-in.) diameter holes.

* Epoxy-coated bars, calculations based on exposed area of four or 10 3-mm ($^1/_8$-in.) diameter holes.

β Corrosion loss (absolute value) less than 0.005 mm.

The average corrosion potentials of the top and bottom mats of steel with respect to a copper-copper sulfate electrode are shown in Figure 3.116. All specimens had top mat corrosion potentials that were more negative than those for specimens with ECR. As shown in Figure 3.116(a), specimens with multiple coated bars had top

mat corrosion potentials between –0.310 and –0.480 V at the start of the test. After week 10, the top mat corrosion potentials for these specimens showed a slight decrease and, in general, remained between –0.400 and –0.600 V. MC(only epoxy penetrated)-10h occasionally exhibited a top mat corrosion potential more negative than –0.650 V, showing active corrosion. In the bottom mat, specimens with only the epoxy layer penetrated had more negative corrosion potentials than specimens with both layers penetrated, with values as low as –0.394 V and –0.478 V for MC(only epoxy penetrated) and MC(only epoxy penetrated)-10h, respectively. The corrosion potentials remained more positive than –0.300 V for specimens with both the zinc and epoxy layers penetrated.

Figure 3.117 shows the average mat-to-mat resistances for multiple coated bars. As mentioned in Section 3.1.2, average mat-to-mat resistances are not reported at the same week as other results because the resistance meter broke down several weeks before the data cut-off date. Multiple coated bars with four holes had average mat-to-mat resistances of approximately 2,100 ohms at the beginning of the test, increasing with time at a similar rate to conventional ECR. At week 35, the average mat-to-mat resistances were approximately 6,900 and 6,400 ohms for MC(only epoxy penetrated) and MC(both layers penetrated), respectively. Specimens with 10 holes had lower average mat-to-mat resistances at the beginning of the test, with values of approximately 800 ohms. The average mat-to-mat resistances increased with time at a rate similar to ECR-10h and were about 3,850 and 2,300 ohms at week 38 for MC(only epoxy penetrated)-10h and MC(both layers penetrated)-10h, respectively.

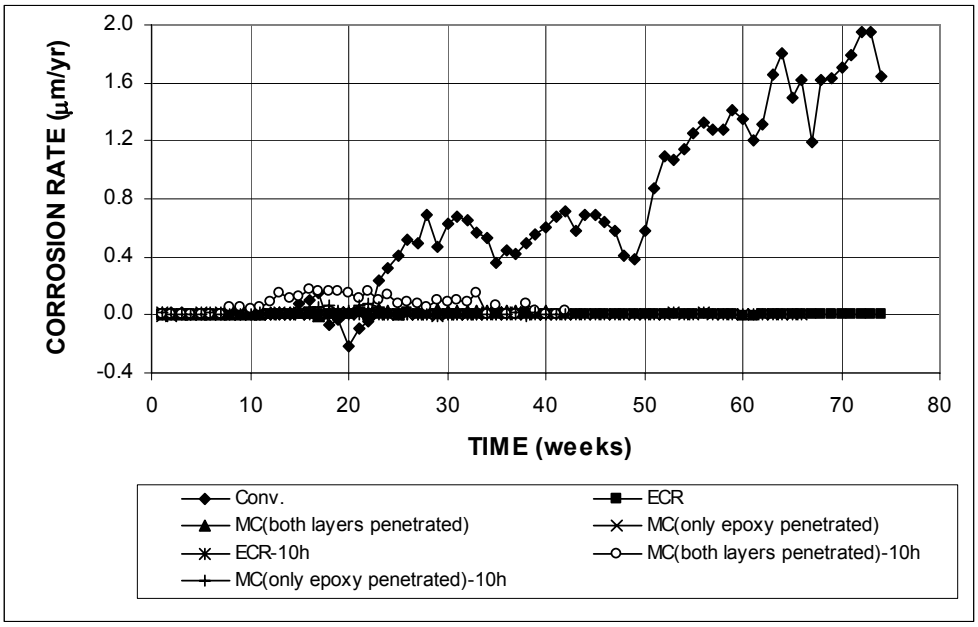

Figure 3.112 (a) – Average corrosion rates as measured in the Southern Exposure test for specimens with conventional steel, ECR, and multiple coated bars (ECR have four holes and ECR-10h have 10 holes).

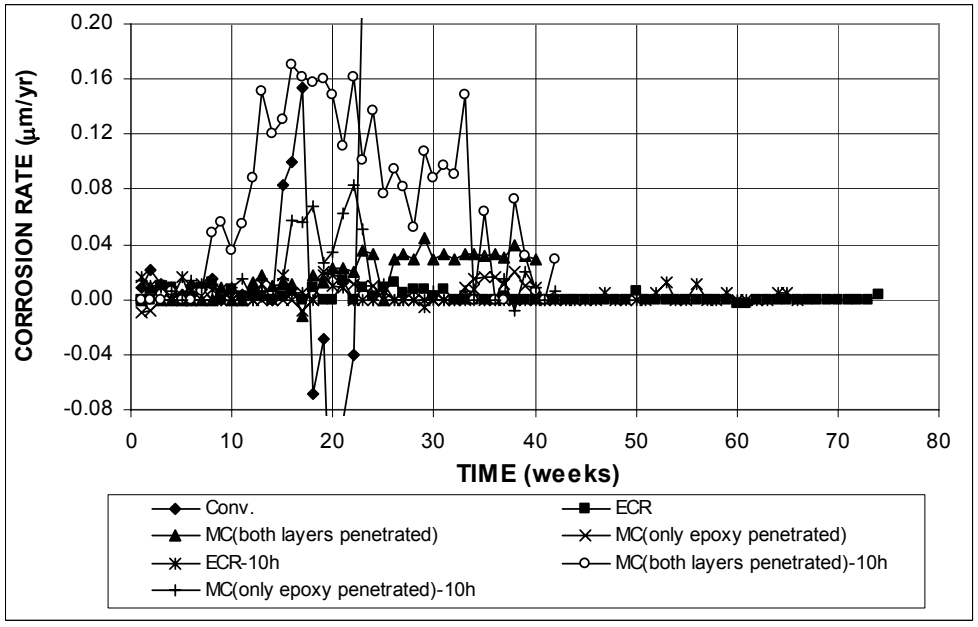

Figure 3.112 (b) – Average corrosion rates as measured in the Southern Exposure test for specimens with conventional steel, ECR, and multiple coated bars (ECR have four holes and ECR-10h have 10 holes).

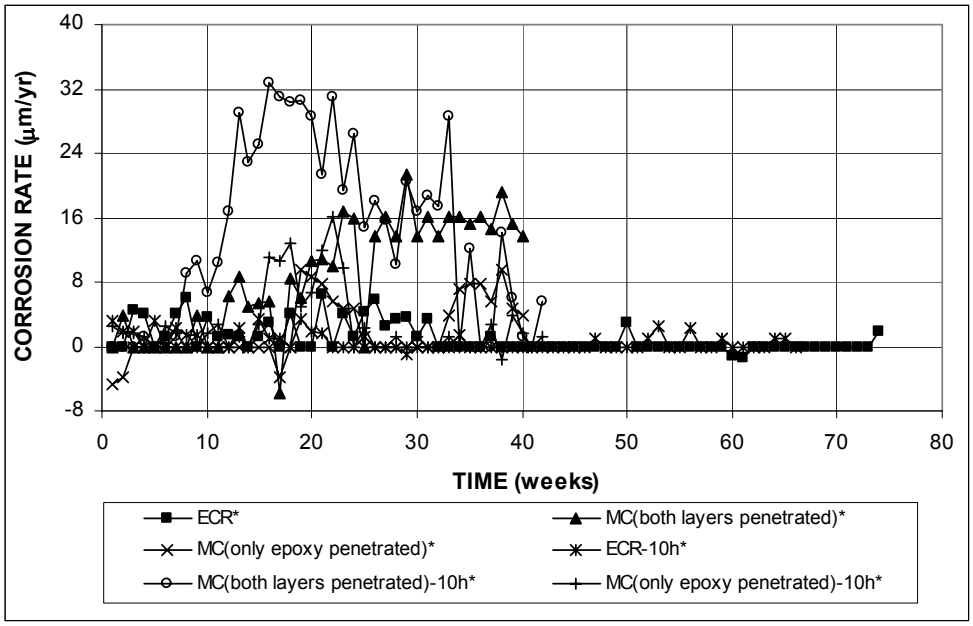

Figure 3.113 – Average corrosion rates as measured in the Southern Exposure test for specimens with ECR and multiple coated bars. * Based on exposed area (ECR have four holes and ECR-10h have 10 holes).

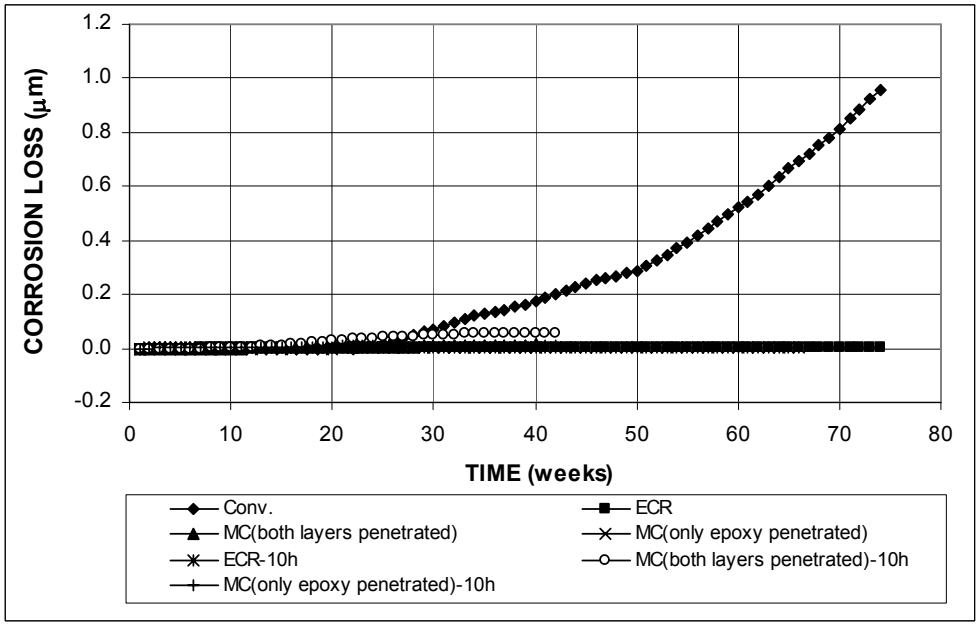

Figure 3.114 (a) – Average corrosion losses as measured in the Southern Exposure test for specimens with conventional steel, ECR, and multiple coated bars (ECR have four holes and ECR-10h have 10 holes).

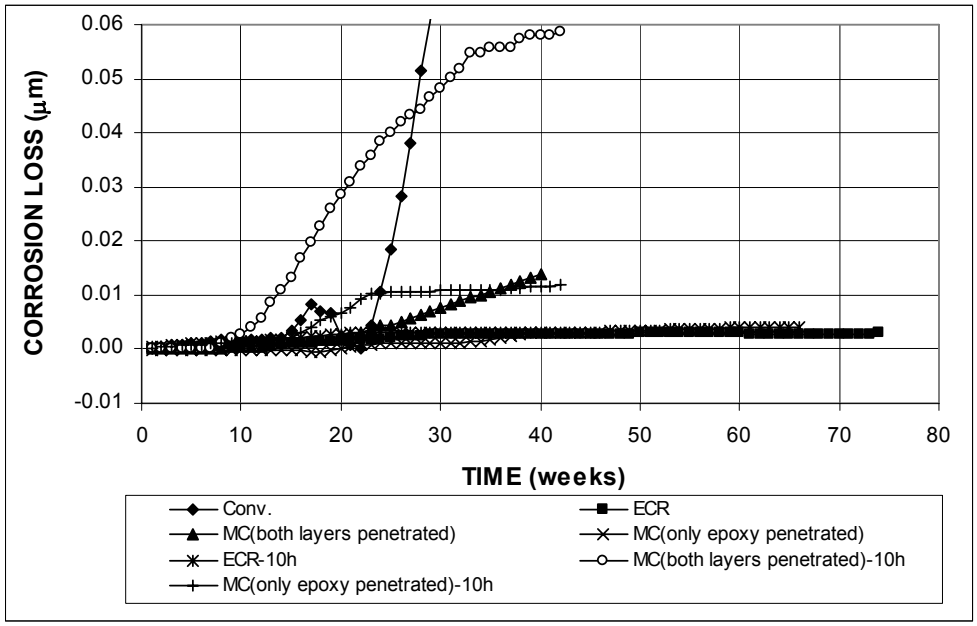

Figure 3.114 (b) – Average corrosion losses as measured in the Southern Exposure test for specimens with conventional steel, ECR, and multiple coated bars (ECR have four holes and ECR-10h have 10 holes).

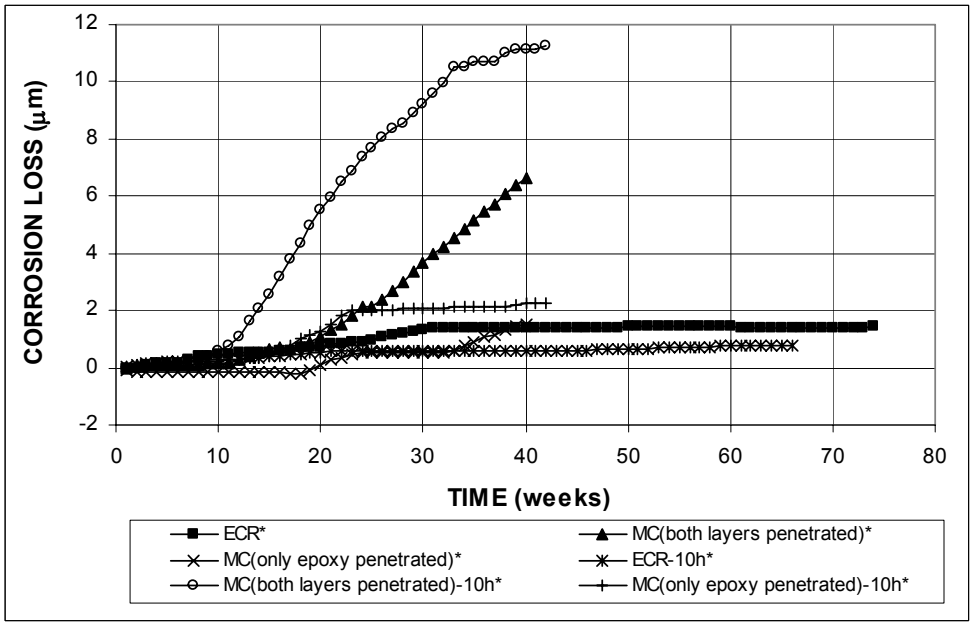

Figure 3.115 – Average corrosion losses as measured in the Southern Exposure test for specimens with ECR and multiple coated bars. * Based on exposed area (ECR have four holes and ECR-10h have 10 holes).

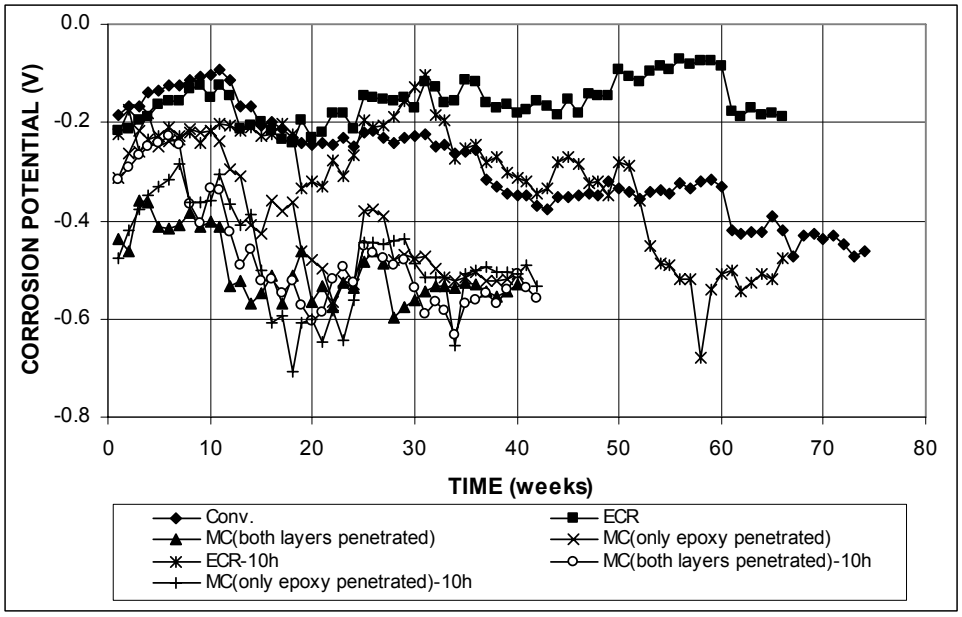

Figure 3.116 (a) – Average top mat corrosion potentials, with respect to a copper-copper sulfate electrode as measured in the Southern Exposure test for specimens with conventional steel, ECR, and multiple coated bars (ECR have four holes and ECR-10h have 10 holes).

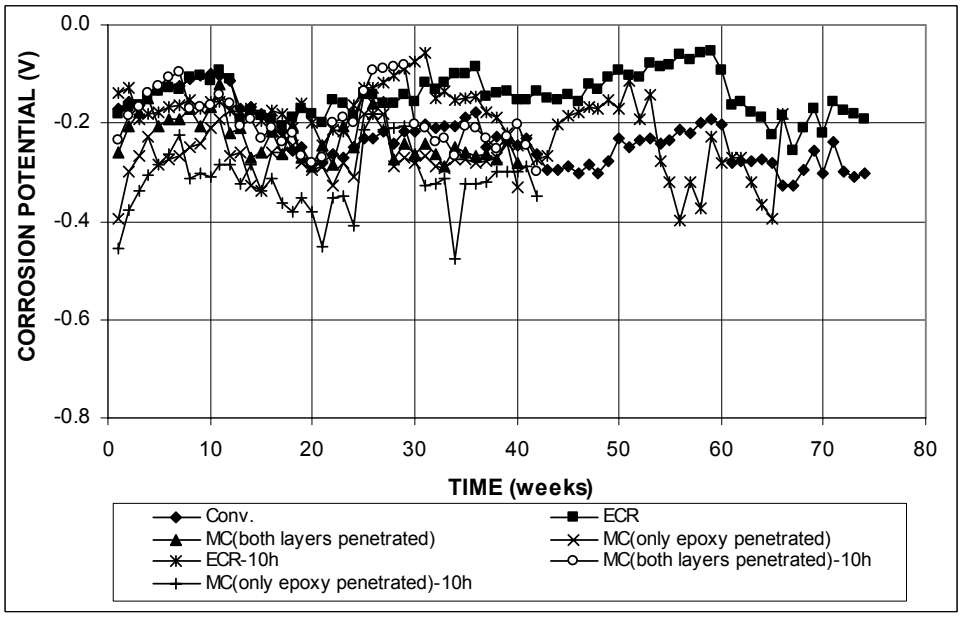

Figure 3.116 (b) – Average bottom mat corrosion potentials, with respect to a copper-copper sulfate electrode as measured in the Southern Exposure test for specimens with conventional steel, ECR, and multiple coated bars (ECR have four holes and ECR-10h have 10 holes).

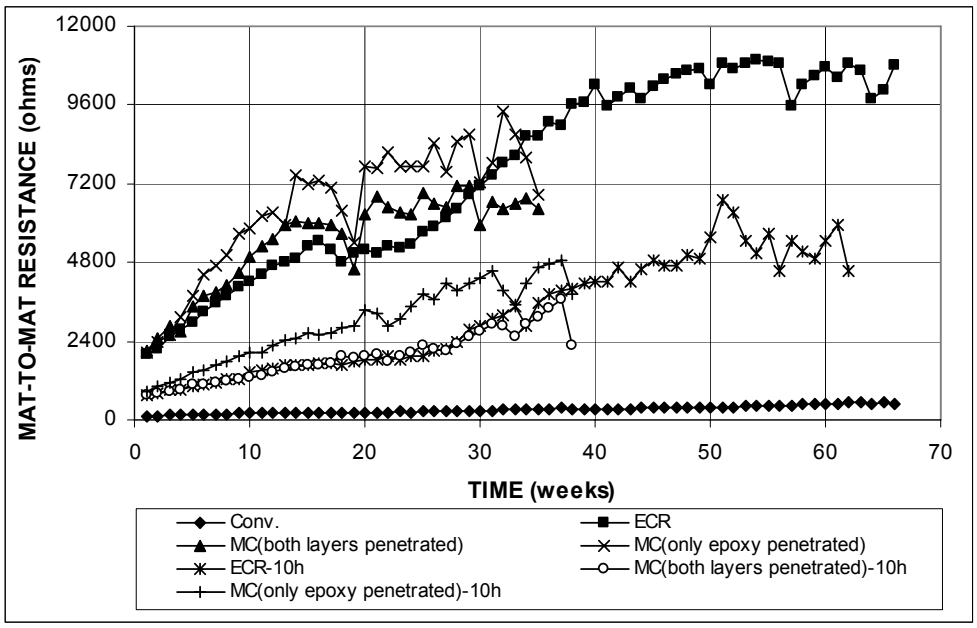

Figure 3.117 – Average mat-to-mat resistances as measured in the Southern Exposure test for specimens with conventional steel, ECR, and multiple coated bars (ECR have four holes and ECR-10h have 10 holes).

3.3.2.2 Cracked Beam Test

The results for the cracked beam tests are shown in Figures 3.118 through 3.123 and the total corrosion losses at week 40 are summarized in Table 3.17.

Figures 3.118 and 3.119 show the average corrosion rates for specimens with multiple coated bars. As shown in Figure 3.118(b), all specimens had high corrosion rates during the first five weeks, and then showed a decrease in corrosion rates. Specimens with multiple coated bars exhibited higher corrosion rates than conventional ECR. MC(both layers penetrated)-10h had the highest corrosion rates, with values as high as 0.64 μm/yr at week 2, and then remained between 0.19 and 0.58 μm/yr. The remaining specimens had corrosion rates below 0.30 μm/yr, with the exception of MC(only epoxy penetrated)-10h, which had a value of 0.32 μm/yr at week 6. Based on exposed area (Figure 3.119), specimens with multiple coated bars exhibited erratic corrosion rates over time, with values less than 125 μm/yr.

Table 3.17 – Average corrosion losses (μm) at week 40 as measured in the cracked beam test for specimens with multiple coated bars

Steel Designation[a]	Specimen			Average	Standard Deviation
	1	2	3		
Cracked beam test					
MC(only epoxy penetrated)	0.04	0.03	0.16	0.08	0.07
MC(only epoxy penetrated)*	18.46	15.55	74.56	36.19	33.26
MC(only epoxy penetrated)-10h	0.07	0.07	0.14	0.09	0.04
MC(only epoxy penetrated)-10h*	13.60	12.77	27.60	17.99	8.34
MC(both layers penetrated)	0.15	0.08	0.13	0.12	0.03
MC(both layers penetrated)*	71.69	39.76	63.69	58.38	16.62
MC(both layers penetrated)-10h	0.14	0.51	0.12	0.26	0.22
MC(both layers penetrated)-10h*	26.67	98.02	23.47	49.39	42.15

[a] MC = multiple coated bars.
MC(only epoxy penetrated) = multiple coated bars with only the epoxy layer penetrated.
MC(both layers penetrated) = multiple coated bars with both the zinc and epoxy layers penetrated.
10h = epoxy-coated bars with 10 holes, otherwise four 3-mm ($^1/_8$-in.) diameter holes.

* Epoxy-coated bars, calculations based on exposed area of four or 10 3-mm ($^1/_8$-in.) diameter holes.

The average total corrosion losses are shown in Figures 3.120 and 3.121 for multiple coated bars. Table 3.17 summarizes the average total corrosion losses for these specimens at week 40. As shown in Figures 3.120(b) and 3.121, all specimens with multiple coated bars experienced steady corrosion loss and had higher total corrosion losses than conventional ECR. Based on total area, MC(both layers penetrated)-10h had the highest total corrosion loss of 0.26 μm, and the remaining specimens had total corrosion losses less than 0.12 μm. Based on exposed area, the total corrosion losses were 36.2 and 58.4 μm for MC(only epoxy penetrated)and MC(both layers penetrated), respectively, equal to 3.18 and 5.09 times the corrosion loss of conventional ECR with four holes. MC(only epoxy penetrated)-10h and MC(both layers penetrated)-10h had total corrosion losses of 18.0 and 49.4 μm, respectively. These values, respectively, are equal to 2.78 and 7.63 times the total corrosion loss of conventional ECR with 10 holes. The average corrosion rates during the first 40 weeks are 0.90 and 0.45 μm/week, respectively, for multiple coated bars

with four and 10 holes with only the epoxy penetrated. Based on this calculation, it will take (with a thickness of 50 μm) approximately 55 and 110 weeks, respectively, to lose the zinc layer for these two specimens.

The average corrosion potentials of the top and bottom mats of steel with respect to a copper-copper sulfate electrode are shown in Figure 3.122. All specimens with multiple coated bars had top mat corrosion potentials similar to those for conventional ECR, except for in the first few weeks when conventional ECR showed potentials more positive than –0.400 V. As shown in Figure 3.122(a), all specimens with multiple coated bars had top mat corrosion potentials more negative than –0.500 V, indicating corrosion of the zinc. In the bottom mat, specimens with only the epoxy layer penetrated had bottom mat corrosion potentials above –0.340 V, with the exception of MC(only epoxy penetrated)-10h in the first week, which had a value of –0.370 V. MC(both layers penetrated) had bottom mat corrosion potentials more positive than –0.280 V, indicating a low probability of corrosion. The corrosion potentials of MC(both layers penetrated)-10h remained above –0.340 V except at week 39.

Figure 3.123 shows the average mat-to-mat resistances for multiple coated bars. Multiple coated bars with four or 10 holes had lower average mat-to-mat resistances than the corresponding specimens with ECR. As shown in Figure 3.123, The average mat-to-mat resistances started around 3,000 ohms for specimens with four holes and increased to values of approximately 8,000 ohms at week 35. For specimens with 10 holes, the average mat-to-mat resistances were approximately 1,400 ohms at the beginning and increased to 6,500 ohms at week 37.

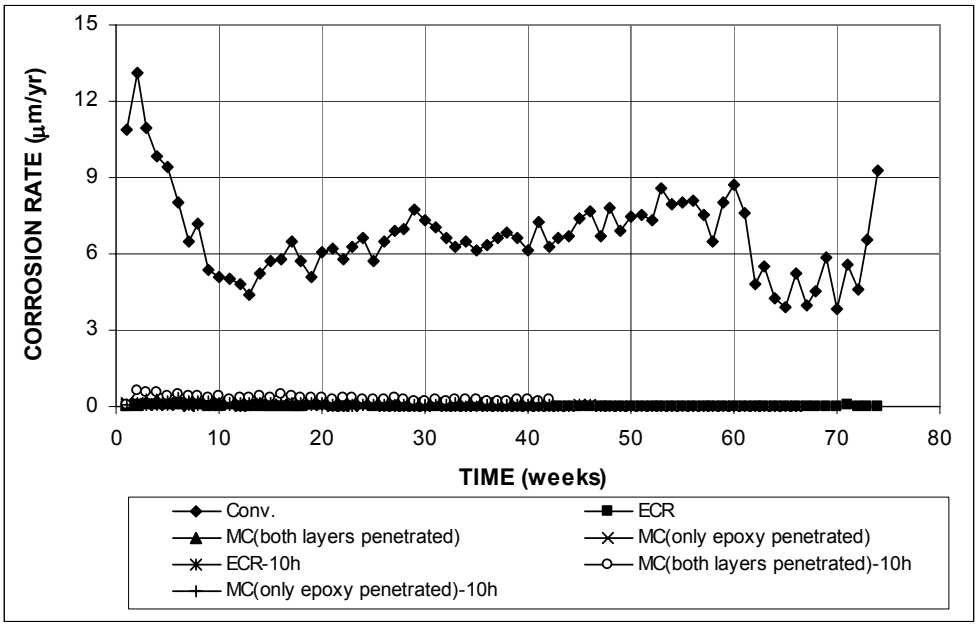

Figure 3.118 (a) – Average corrosion rates as measured in the cracked beam test for specimens with conventional steel, ECR, and multiple coated bars (ECR have four holes and ECR-10h have 10 holes).

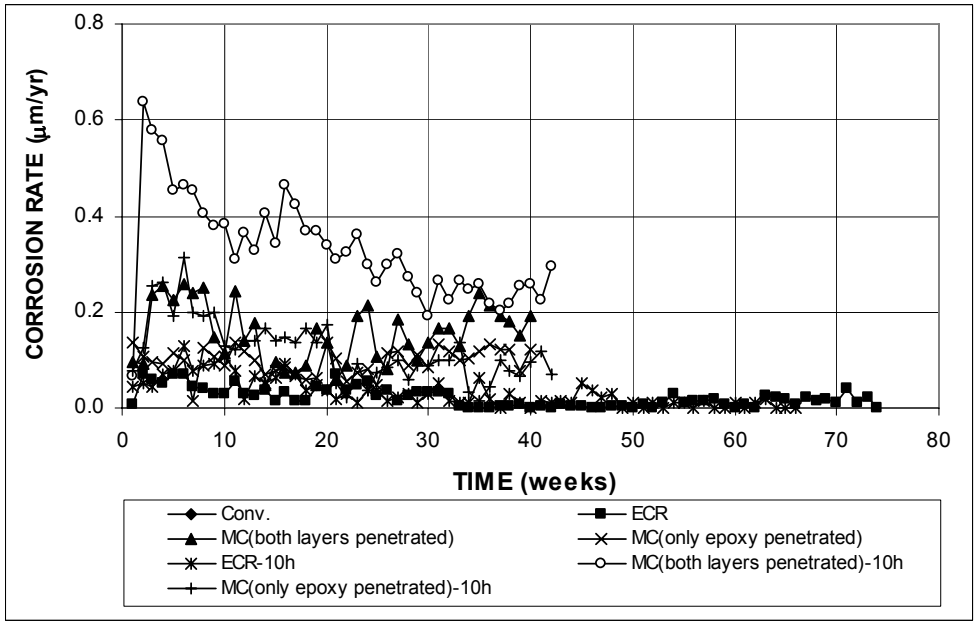

Figure 3.118 (b) – Average corrosion rates as measured in the cracked beam test for specimens with conventional steel, ECR, and multiple coated bars (ECR have four holes and ECR-10h have 10 holes).

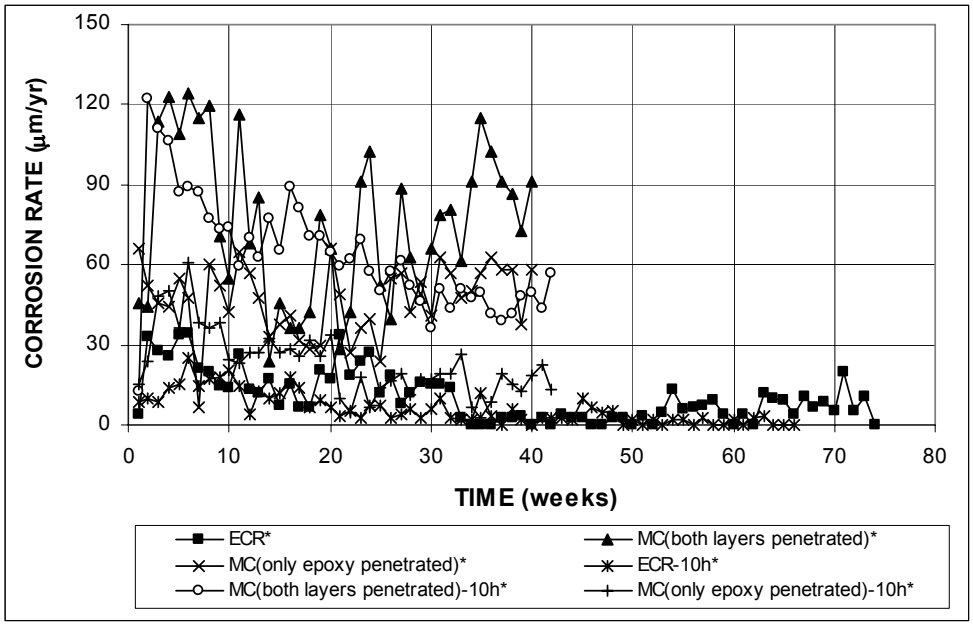

Figure 3.119 – Average corrosion rates as measured in the cracked beam test for specimens with ECR and multiple coated bars. * Based on exposed area (ECR have four holes and ECR-10h have 10 holes).

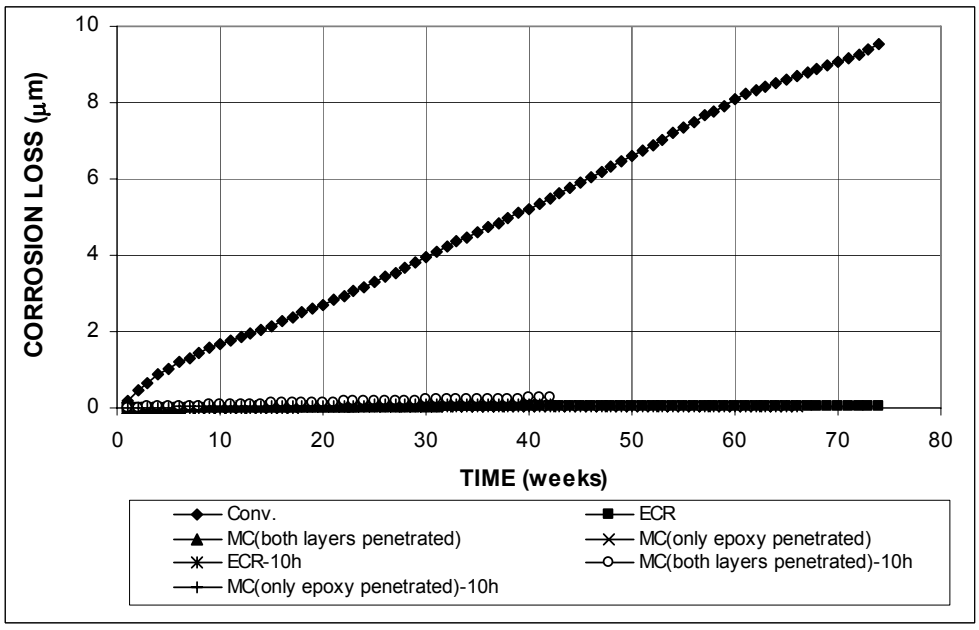

Figure 3.120 (a) – Average corrosion losses as measured in the cracked beam test for specimens with conventional steel, ECR, and multiple coated bars (ECR have four holes and ECR-10h have 10 holes).

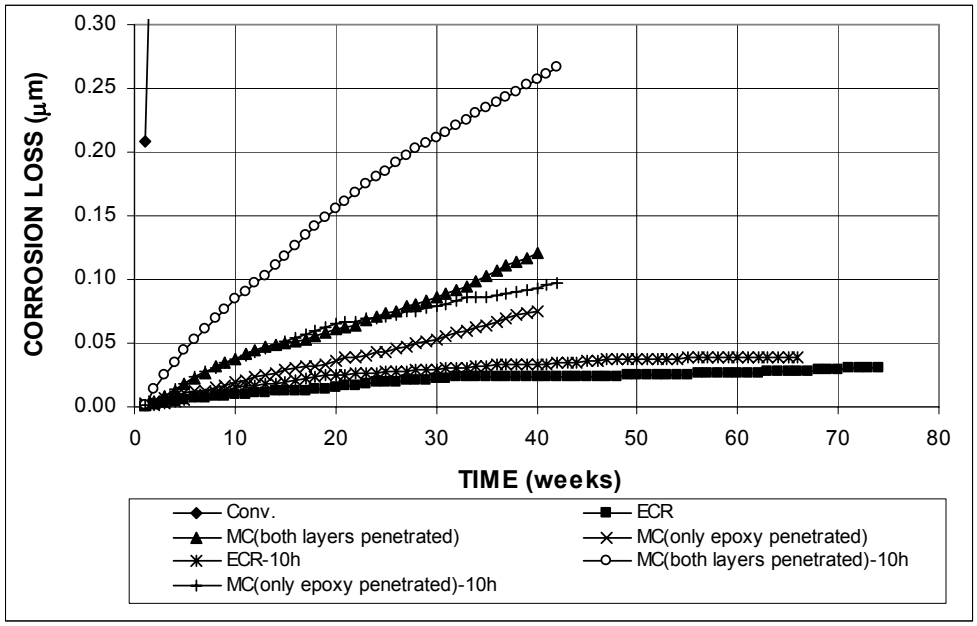

Figure 3.120 (b) – Average corrosion losses as measured in the cracked beam test for specimens with conventional steel, ECR, and multiple coated bars (ECR have four holes and ECR-10h have 10 holes).

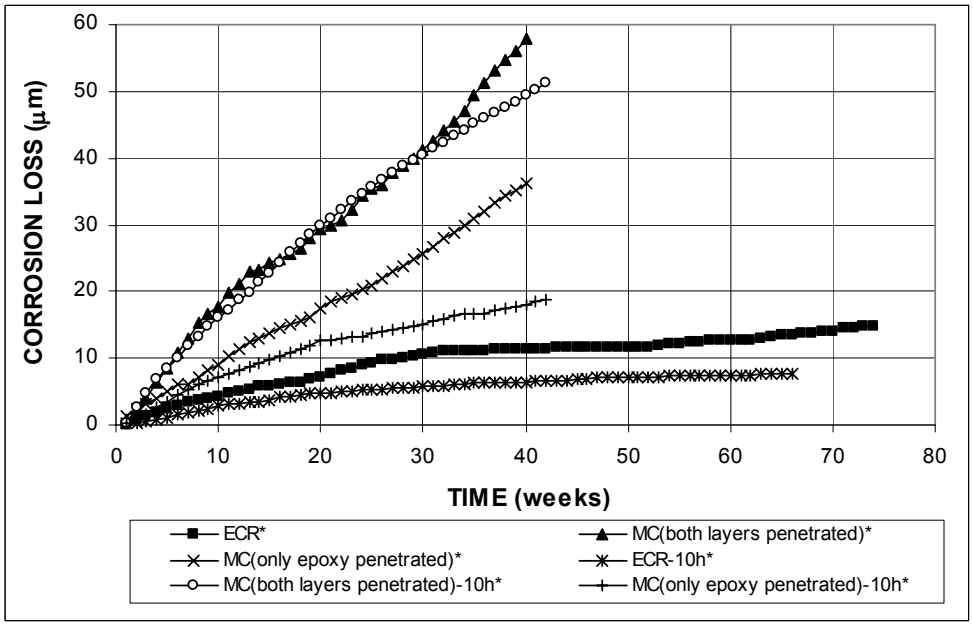

Figure 3.121 – Average corrosion losses as measured in the cracked beam test for specimens with ECR and multiple coated bars. * Based on exposed area (ECR have four holes and ECR-10h have 10 holes).

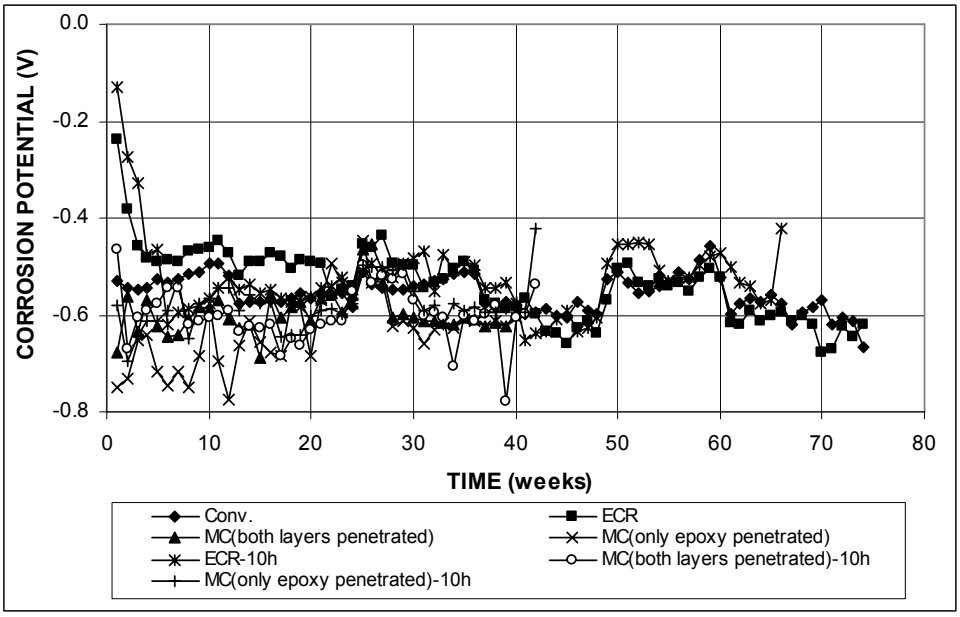

Figure 3.122 (a) – Average top mat corrosion potentials, with respect to a copper-copper sulfate electrode as measured in the cracked beam test for specimens with conventional steel, ECR, and multiple coated bars (ECR have four holes and ECR-10h have 10 holes).

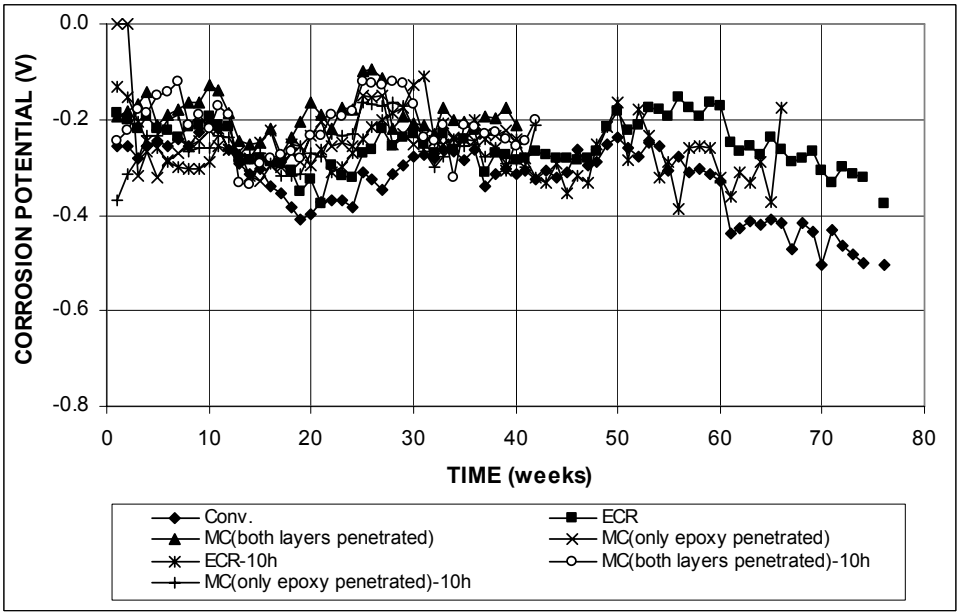

Figure 3.122 (b) – Average bottom mat corrosion potentials, with respect to a copper-copper sulfate electrode as measured in the cracked beam test for specimens with conventional steel, ECR, and multiple coated bars (ECR have four holes and ECR-10h have 10 holes).

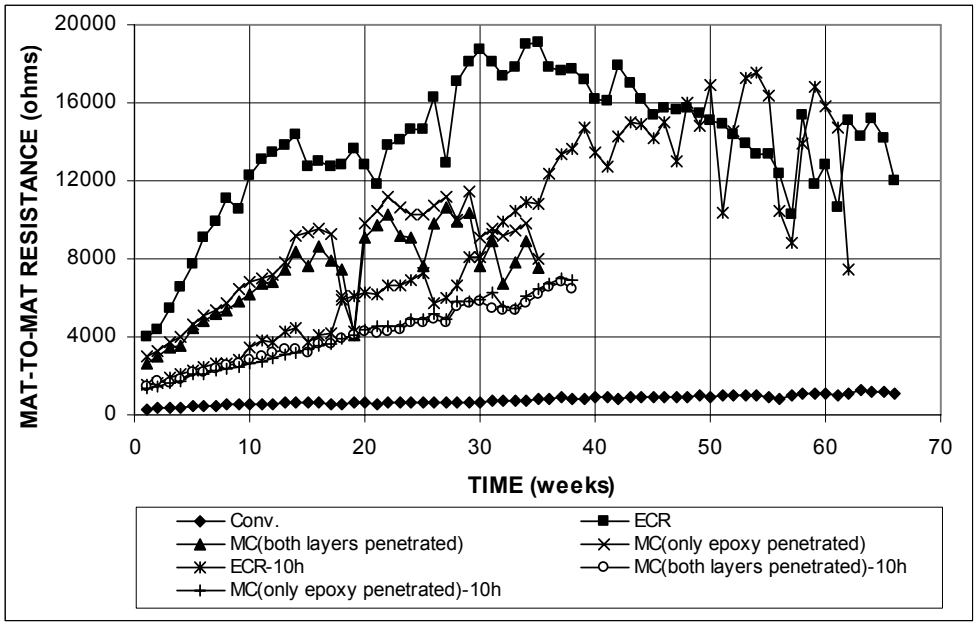

Figure 3.123 – Average mat-to-mat resistances as measured in the cracked beam test for specimens with conventional steel, ECR, and multiple coated bars (ECR have four holes and ECR-10h have 10 holes).

3.3.2.3 ASTM G 109 Test

The test results for specimens with multiple coated bars in the ASTM G 109 test are shown in Figures 3.124 through 3.129. The total corrosion losses at week 60 are summarized in Table 3.18.

Figures 3.124 and 3.125 show the average corrosion rates for specimens with multiple coated bars. Specimens with multiple coated bars exhibited corrosion rates similar to the corresponding specimens with ECR, with values less than 0.01 μm/yr based on total area. Much higher corrosion rates were obtained based on exposed area, as shown in Figure 3.125

The average total corrosion losses are shown in Figures 3.126 and 3.127 for multiple coated bars. As shown in Figures 3.126(b) and 3.127, all specimens with multiple coated bars experienced steady corrosion loss during the first 20 weeks and

then showed little corrosion. The total corrosion losses for conventional steel were similar to those for specimens with multiple coated bars and conventional ECR during the first 56 weeks, and then took off after week 56. Table 3.18 summarizes the average total corrosion losses for these specimens at week 60. As shown for corrosion rates in Figures 3.126(b) and 3.127, multiple coated bars with four holes had higher total corrosion losses than conventional ECR with four holes. Specimens with 10 holes had lower total corrosion losses than conventional ECR with 10 holes. Based on total area, all specimens showed total corrosion losses less than 0.005 μm, as indicated by the symbol β in Table 3.18. Based on exposed area, total corrosion losses were 1.16 and 0.98 μm for MC(only epoxy penetrated) and MC(both layers penetrated), respectively, equal to 3.87 and 2.87 times the corrosion loss of conventional ECR. MC(only epoxy penetrated)-10h and MC(both layers penetrated)-10h had total corrosion losses of 0.42 and 0.26 μm at week 60, which correspond to 35% and 10% of the corrosion loss of ECR-10h.

Table 3.18 – Average corrosion losses (μm) at week 60 as measured in the ASTM G 109 test for specimens with multiple coated bars

Steel Designation[a]	Specimen			Average	Standard Deviation
	1	2	3		
ASTM G 109 test					
MC(only epoxy penetrated)	β	β	β	β	β
MC(only epoxy penetrated)*	0.88	1.25	1.33	1.16	0.24
MC(only epoxy penetrated)-10h	β	β	β	β	β
MC(only epoxy penetrated)-10h*	0.39	0.31	0.55	0.42	0.12
MC(both layers penetrated)	β	β	β	β	β
MC(both layers penetrated)*	0.92	0.98	1.04	0.98	0.06
MC(both layers penetrated)-10h	β	β	β	β	β
MC(both layers penetrated)-10h*	0.27	0.31	0.19	0.26	0.06

[a] MC = multiple coated bars.
MC(only epoxy penetrated) = multiple coated bars with only the epoxy layer penetrated.
MC(both layers penetrated) = multiple coated bars with both the zinc and epoxy layers penetrated.
10h = epoxy-coated bars with 10 holes, otherwise four 3-mm ($^1/_8$-in.) diameter holes.

* Epoxy-coated bars, calculations based on exposed area of four or 10 3-mm ($^1/_8$-in.) diameter holes.

β Corrosion loss (absolute value) less than 0.005 mm.

The average corrosion potentials of the top and bottom mats of steel with respect to a copper-copper sulfate electrode are shown in Figure 3.128. In general, MC specimens with only the epoxy penetrated showed more negative potential than MC specimens with both layers penetrated, indicated that the zinc was functioning. The top mat corrosion potentials for specimens with only the epoxy layer penetrated started around –0.650 V, increasing with time. After week 20, the top mat potentials remained between –0.350 V and –0.500 V, indicating a passive condition of the zinc. Specimens with both layers penetrated had corrosion potentials of approximately –0.450 V at the start of the test, rising to around –0.200 V after week 45. In the bottom mat, the corrosion potentials for specimens with only the epoxy layer penetrated started around –0.550 V and slightly increased with time. After week 49, the average corrosion potentials stabilized around –0.320 V. Specimens with both layers penetrated had corrosion potentials of approximately –0.350 V at the beginning, which had risen to around –0.200 V after week 53.

Figure 3.129 shows the average mat-to-mat resistances for multiple coated bars. Multiple coated bars with four holes had average mat-to-mat resistances similar to specimens with conventional ECR, as shown in Figure 3.129. The average mat-to-mat resistances started around 5,000 ohms and increased to approximately 21,700 and 18,300 ohms at week 68 for MC(only epoxy penetrated) and MC(both layers penetrated), respectively. Multiple coated bars with 10 holes had higher average mat-to-mat resistances than ECR-10h. The average mat-to-mat resistances were approximately 2,500 ohms at the start of the test, increasing to about 9,500 ohms at week 66.

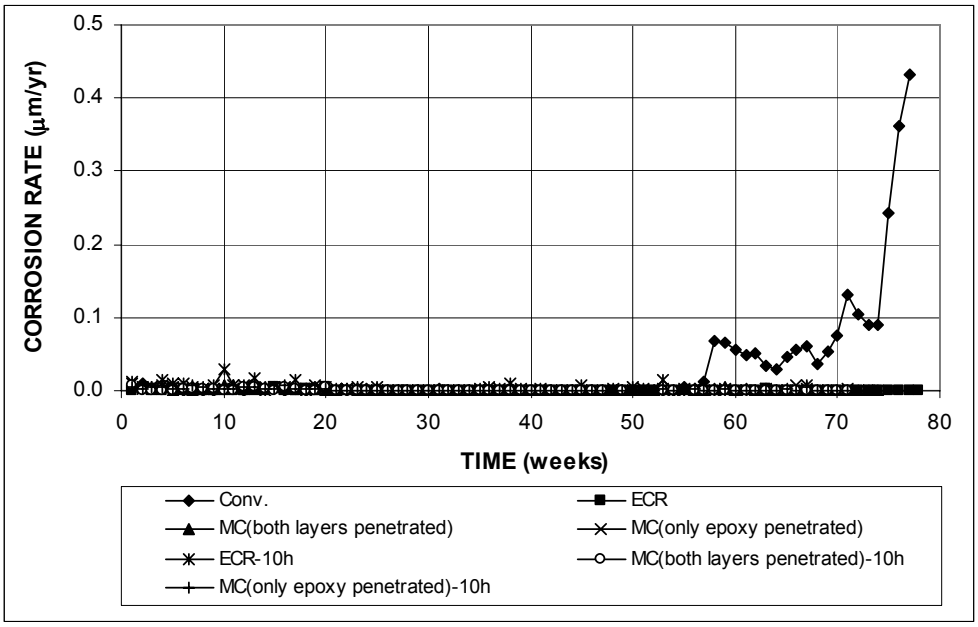

Figure 3.124 (a) – Average corrosion rates as measured in the ASTM G 109 test for specimens with conventional steel, ECR, and multiple coated bars (ECR have four holes and ECR-10h have 10 holes).

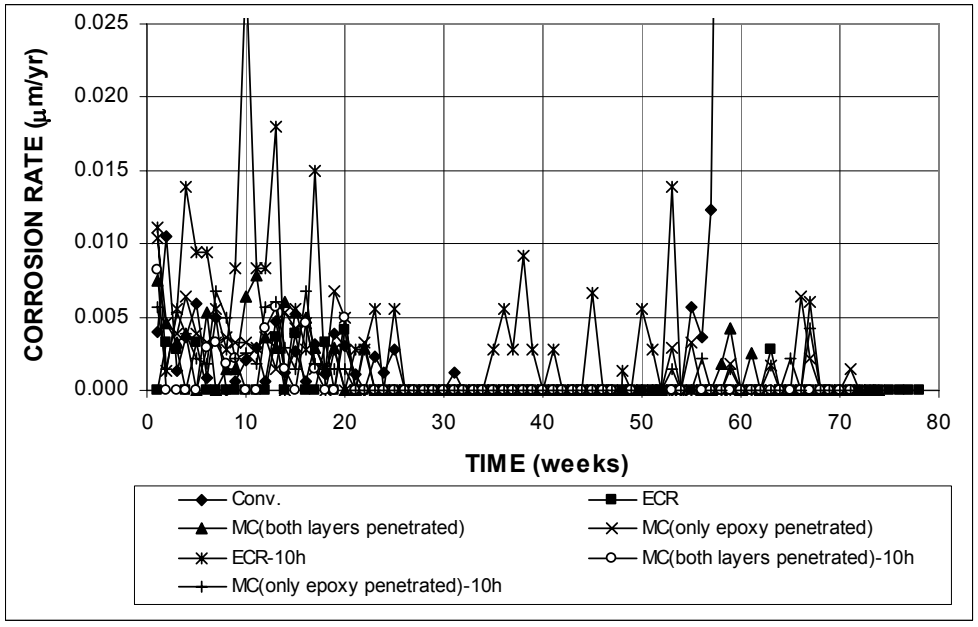

Figure 3.124 (b) – Average corrosion rates as measured in the ASTM G 109 test for specimens with conventional steel, ECR, and multiple coated bars (ECR have four holes and ECR-10h have 10 holes).

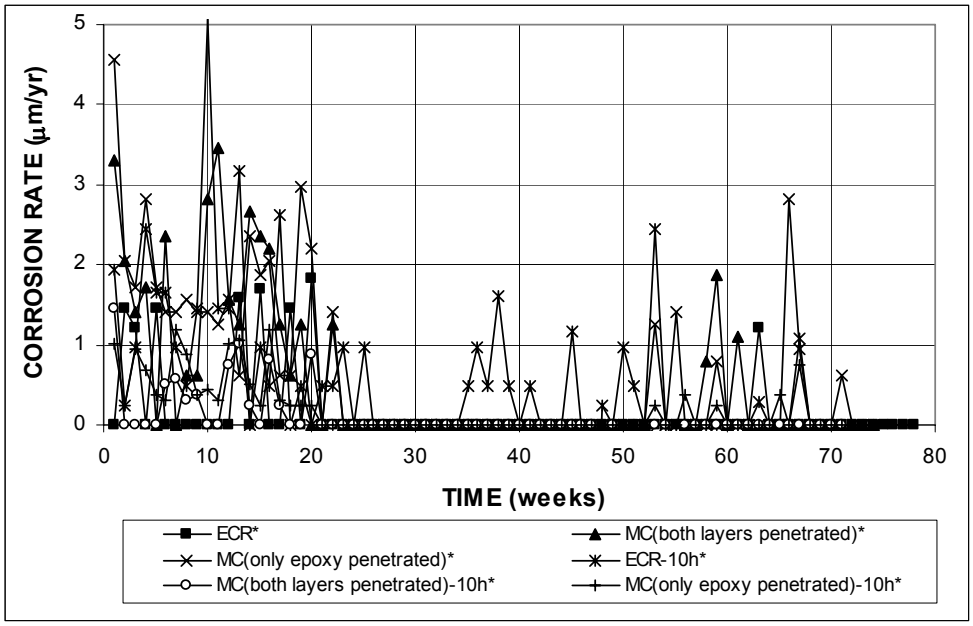

Figure 3.125 – Average corrosion rates as measured in the ASTM G 109 test for specimens with ECR and multiple coated bars. * Based on exposed area (ECR have four holes and ECR-10h have 10 holes).

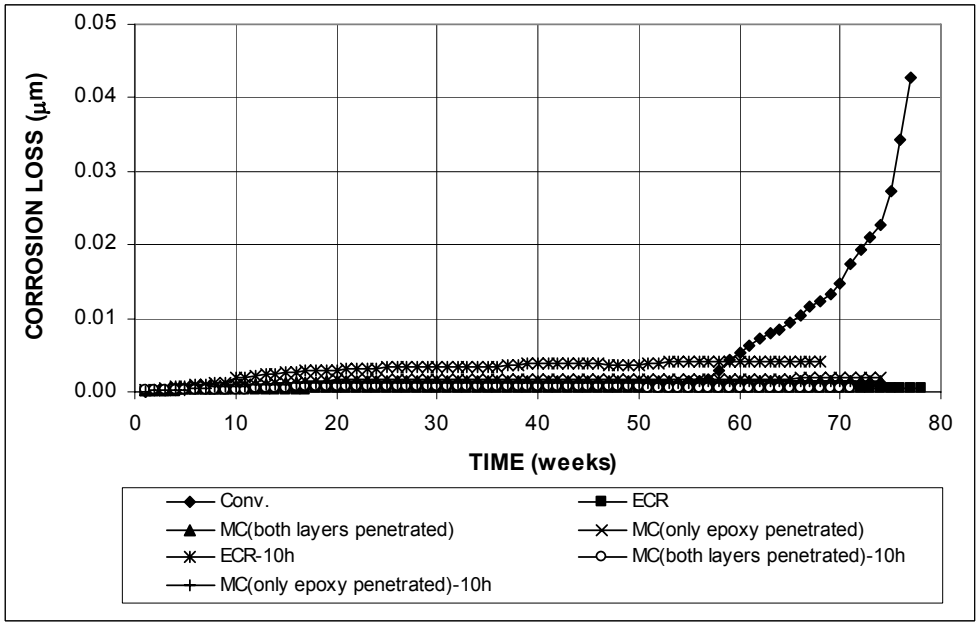

Figure 3.126 (a) – Average corrosion losses as measured in the ASTM G 109 test for specimens with conventional steel, ECR, and multiple coated bars (ECR have four holes and ECR-10h have 10 holes).

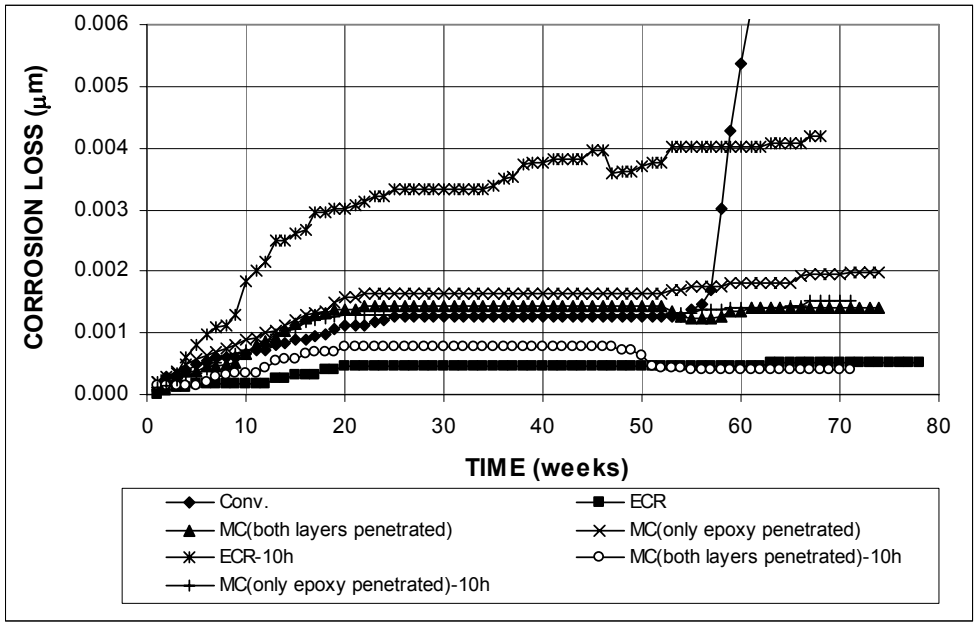

Figure 3.126 (b) – Average corrosion losses as measured in the ASTM G 109 test for specimens with conventional steel, ECR and multiple coated bars (ECR have four holes and ECR-10h have 10 holes).

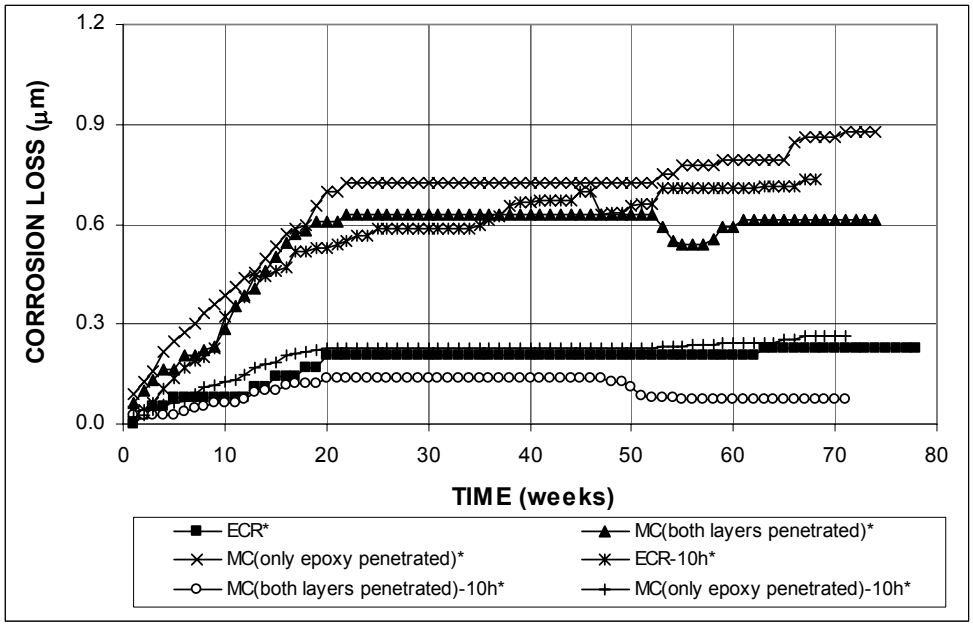

Figure 3.127 – Average corrosion losses as measured in the ASTM G 109 test for specimens with ECR and multiple coated bars. * Based on exposed area (ECR have four holes and ECR-10h have 10 holes).

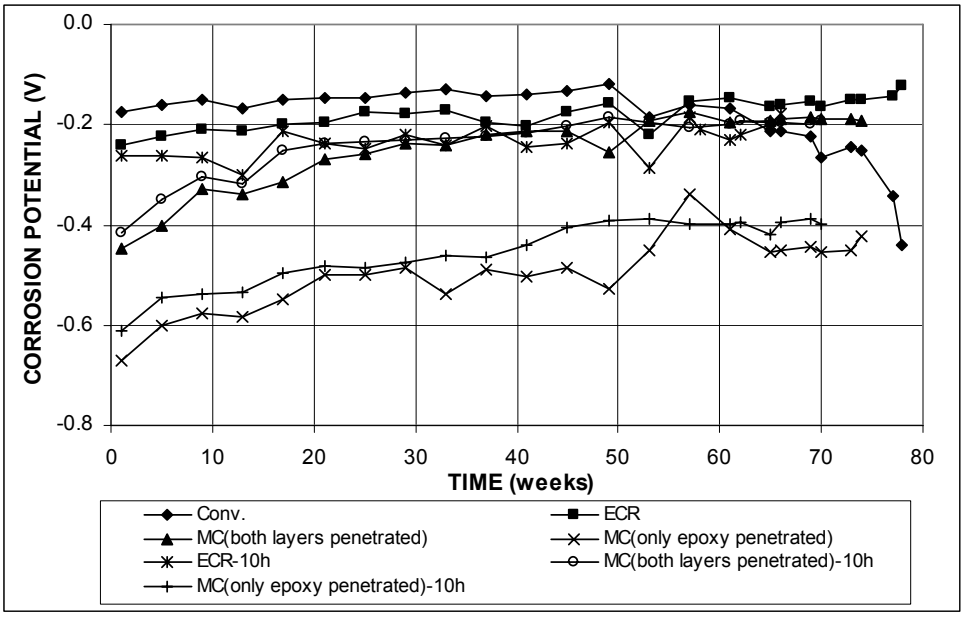

Figure 3.128 (a) – Average top mat corrosion potentials, with respect to a copper-copper sulfate electrode as measured in the ASTM G 109 test for specimens with conventional steel, ECR, and multiple coated bars (ECR have four holes and ECR-10h have 10 holes).

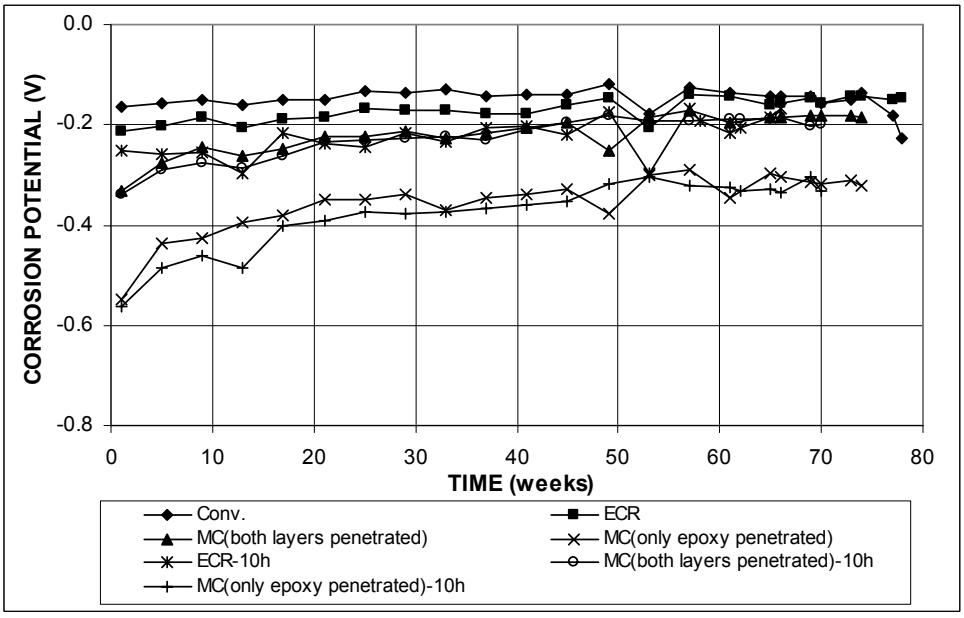

Figure 3.128 (b) – Average bottom mat corrosion potentials, with respect to a copper-copper sulfate electrode as measured in the ASTM G 109 test for specimens with conventional steel, ECR, and multiple coated bars (ECR have four holes and ECR-10h have 10 holes).

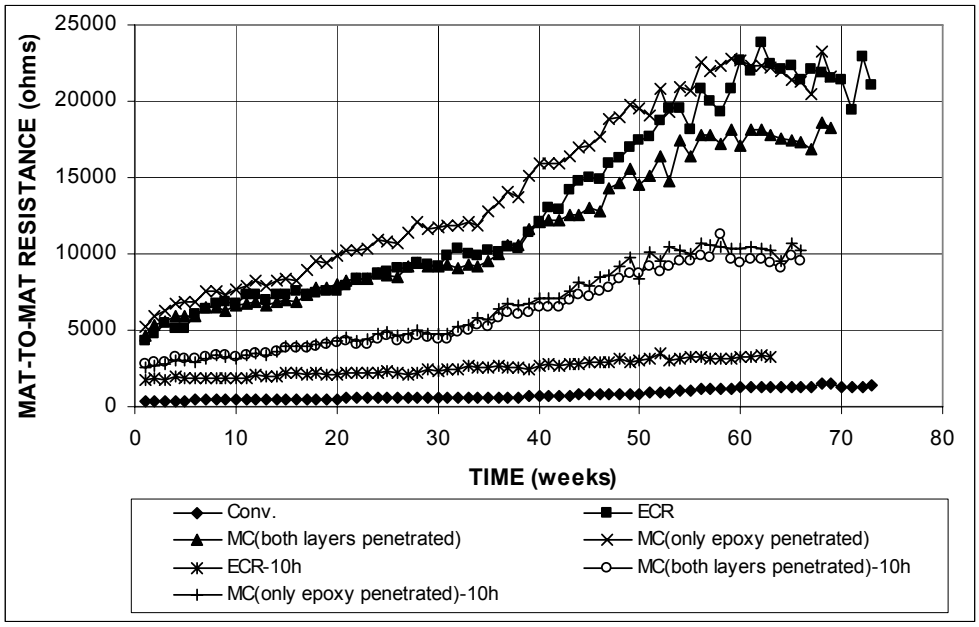

Figure 3.129 – Average mat-to-mat resistances as measured in the ASTM G 109 test for specimens with conventional steel, ECR, and multiple coated bars (ECR have four holes and ECR-10h have 10 holes).

3.3.3 Field Test

This section presents the results for the field test specimens with multiple coated bars. The coating on the epoxy-coated bars was penetrated with 16 holes.

3.3.3.1 Field Test Specimens Without Cracks

The results for field test specimens without simulated cracks are shown in Figures 3.130 through 3.135. The total corrosion losses at week 32 are summarized in Table 3.19.

Figures 3.130 and 3.131 show the average corrosion rates for the multiple coated bars. As shown in Figure 3.130, specimens with multiple coated bars had corrosion rates similar to specimens with ECR, with values less than 0.012 μm/yr, with the exception of MC (1) at week 4. Based on exposed area, the corrosion rates

were below 4.8 μm/yr for specimens with multiple coated bars except for MC (1) at week 4, which had a value of 13.6 μm/yr.

Table 3.19 – Average corrosion losses (μm) at week 32 as measured in the field test for specimens with multiple coated bars, without cracks

Steel Designation[a]	Test Bar				Average	Standard Deviation
	1	2	3	4		
without cracks						
MC (1)	β	β			β	β
MC* (1)	1.73	1.45			1.59	0.19
MC (2)	β	β	β	β	β	β
MC* (2)	0.73	0.91	1.00	0.73	0.84	0.14

[a] MC = multiple coated bars.

* Epoxy-coated bars, calculations based on exposed area of 16 3-mm ($^1/_8$-in.) diameter holes.

β Corrosion loss (absolute value) less than 0.005 μm.

The average total corrosion losses for specimens with multiple coated bars are shown in Figures 3.132 and 3.133. Specimens with multiple coated bars showed total corrosion losses similar to specimens with ECR. The total corrosion losses for specimens with multiple coated bars were less than 0.005 and 1.6 μm/yr based on total area and exposed area, respectively. Table 3.19 summarizes the average total corrosion losses for specimens with multiple coated bars at week 32. Specimens with multiple coated bars showed total corrosion losses less than 0.005 μm based on total area, as indicated by the symbol β. Based on exposed area, the total corrosion losses were 1.59 and 0.84 μm for MC (1) and MC (2), respectively, compared to values between 0.18 and 0.81 μm for conventional ECR without cracks.

The average corrosion potentials of the top mat and bottom mats of steel with respect to a copper-copper sulfate electrode are shown in Figure 3.134. Specimens with multiple coated bars had corrosion potentials between –0.300 and –0.490 V at the top mat, and between –0.230 and –0.400 V at the bottom mat.

Figure 3.135 shows that all specimens with multiple coated bars had average

mat-to-mat resistances similar to those for specimens with ECR, with values between 700 and 3,200 ohms.

3.3.3.2 Field Test Specimens With Cracks

The results for the field test specimens with simulated cracks are shown in Figures 3.136 through 3.141. The total corrosion losses at week 32 are summarized in Table 3.20.

Figures 3.136 and 3.137 show the average corrosion rates for multiple coated bars. As shown in Figure 3.136, specimens with multiple coated bars had corrosion rates similar to specimens with ECR, with values less than 0.014 μm/yr, with the exception of MC (1), which had a corrosion rate of 0.033 μm/yr at week 4. Based on total area, the corrosion rates were less than 6 μm/yr for specimens with multiple coated bars except for MC (1), which had a value of 13.0 μm/yr at week 4.

Table 3.20 – Average corrosion losses (μm) at week 32 as measured in the field test for specimens with multiple coated bars, with cracks

Steel Designation[a]	Test Bar				Average	Standard Deviation
	1	2	3	4		
with cracks						
MC (1)	0.01	β			β	β
MC* (1)	2.09	1.27			1.68	0.58
MC (2)	0.00	β	β	0.01	β	β
MC* (2)	0.00	0.91	0.36	2.64	0.98	1.17

[a] MC = multiple coated bars.

* Epoxy-coated bars, calculations based on exposed area of 16 3-mm ($^1/_8$-in.) diameter holes.

β Corrosion loss (absolute value) less than 0.005 μm.

The average total corrosion losses for specimens with multiple coated bars are shown in Figures 3.138 and 3.139. Specimens with multiple coated bars showed total corrosion losses similar to specimens with ECR, with values less than 0.006 μm based on total area and 2.1 μm based on exposed area, respectively. Table 3.20

summarizes the average total corrosion losses at week 32. Based on total area Specimens with multiple coated bars showed total corrosion losses less than 0.005 μm, as indicated by the symbol β in Table 3.20. Based on exposed area, the total corrosion losses were 1.68 and 0.98 μm for MC (1) and MC (2), respectively, compared to values between 1.59 and 0.84 μm for MC specimens without cracks.

Figure 3.140 shows the average corrosion potentials of the top mat and bottom mats of steel with respect to a copper-copper sulfate electrode. Specimens with multiple coated bars had corrosion potentials between –0.400 and –0.600 V at the top mat, and between –0.200 and –0.400 V at the bottom mat. The top mat corrosion potentials for MC specimens with cracks are more negative than those for MC specimens without cracks, which had top mat potentials between –0.300 and –0.490 V, as shown in Figure 3.134(a).

Figure 3.141 shows that all specimens with multiple coated bars had average mat-to-mat resistances similar to those for specimens with ECR, with values between 600 and 3,000 ohms.

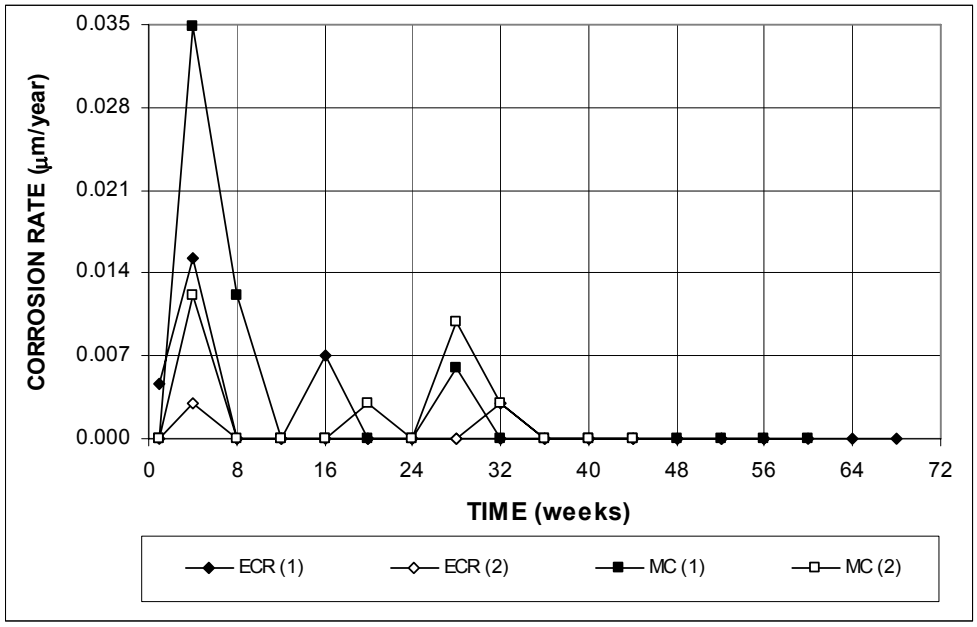

Figure 3.130 – Average corrosion rates as measured in the field test for specimens with ECR and multiple coated bars, without cracks (ECR bars have 16 holes).

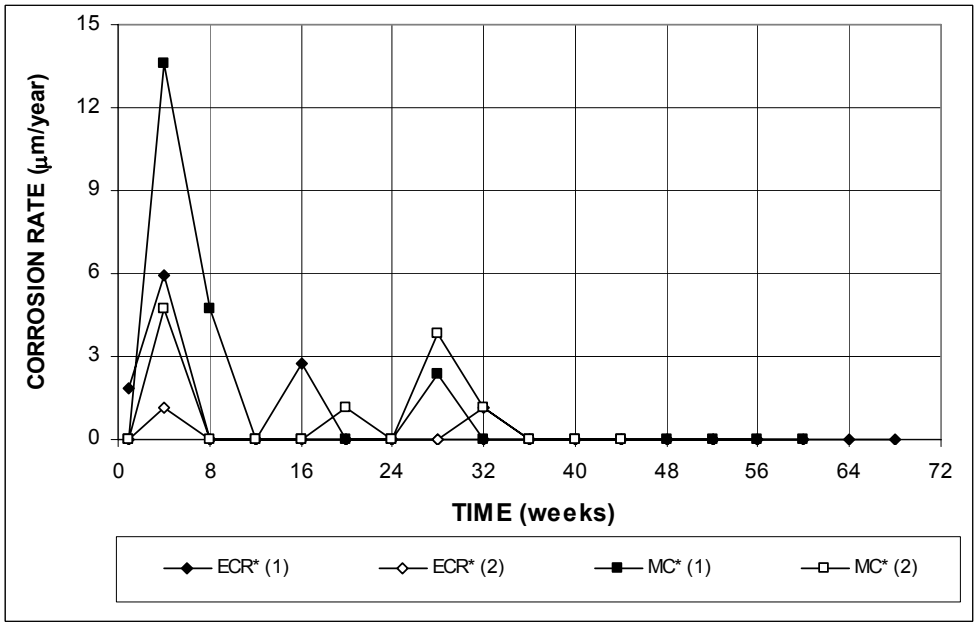

Figure 3.131 – Average corrosion rates as measured in the field test for specimens with ECR and multiple coated bars, without cracks. * Based on exposed area (ECR bars have 16 holes).

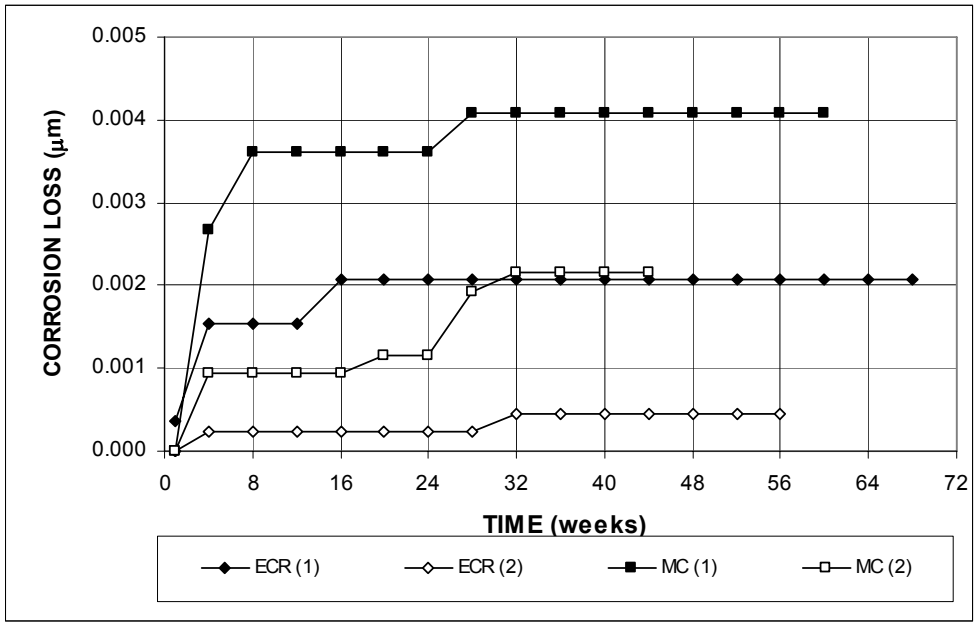

Figure 3.132 – Average corrosion losses as measured in the field test for specimens with ECR and multiple coated bars, without cracks (ECR bars have 16 holes).

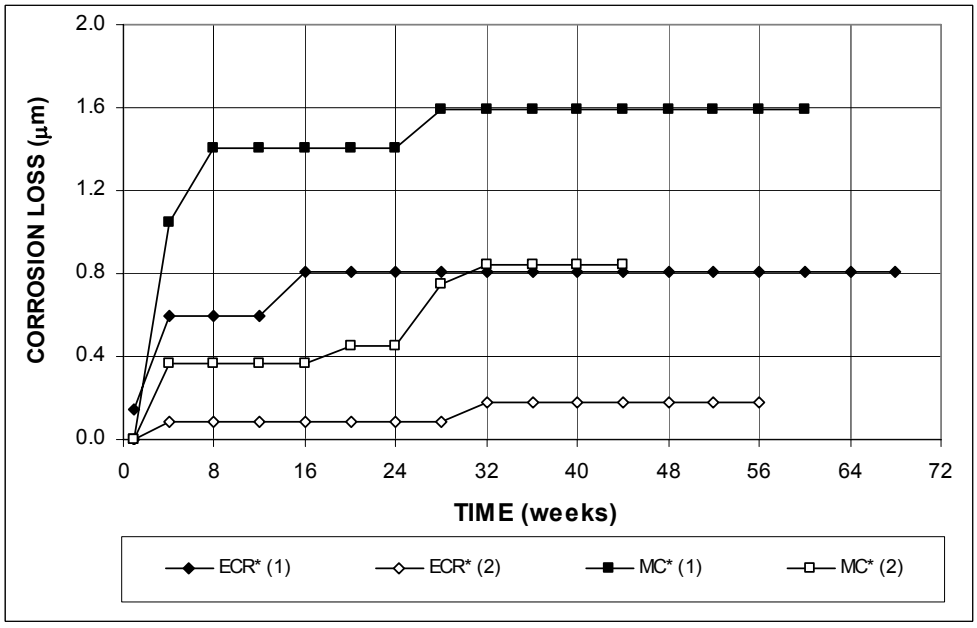

Figure 3.133 – Average corrosion losses as measured in the field test for specimens with ECR and multiple coated bars, without cracks. * Based on exposed area (ECR bars have 16 holes).

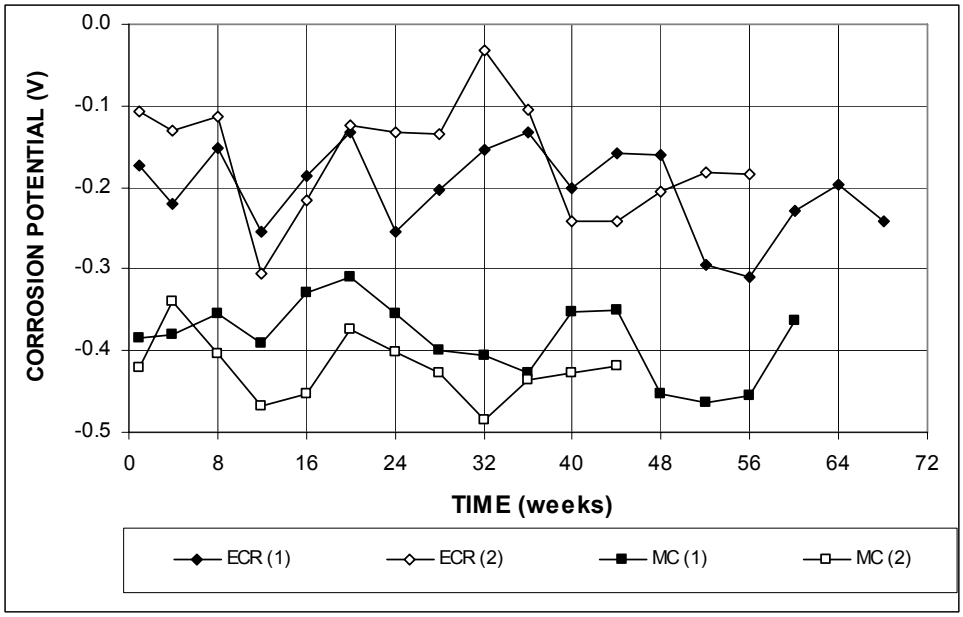

Figure 3.134 (a) – Average top mat corrosion potentials, with respect to a copper-copper sulfate electrode as measured in the field test for specimens with ECR and multiple coated bars, without cracks (ECR bars have 16 holes).

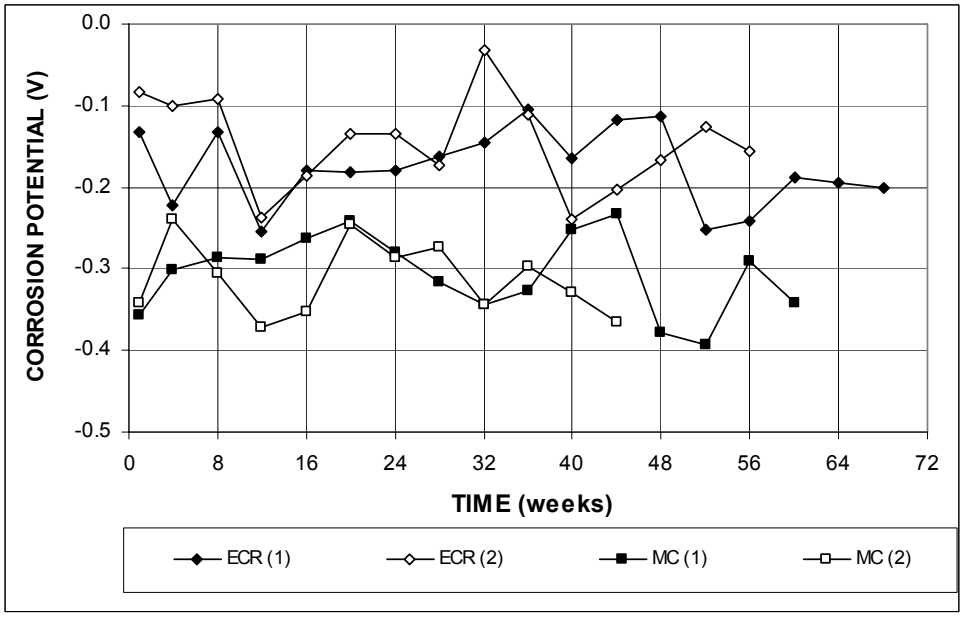

Figure 3.134 (b) – Average bottom mat corrosion potentials, with respect to a copper-copper sulfate electrode as measured in the field test for specimens with ECR and multiple coated bars, without cracks (ECR bars have 16 holes).

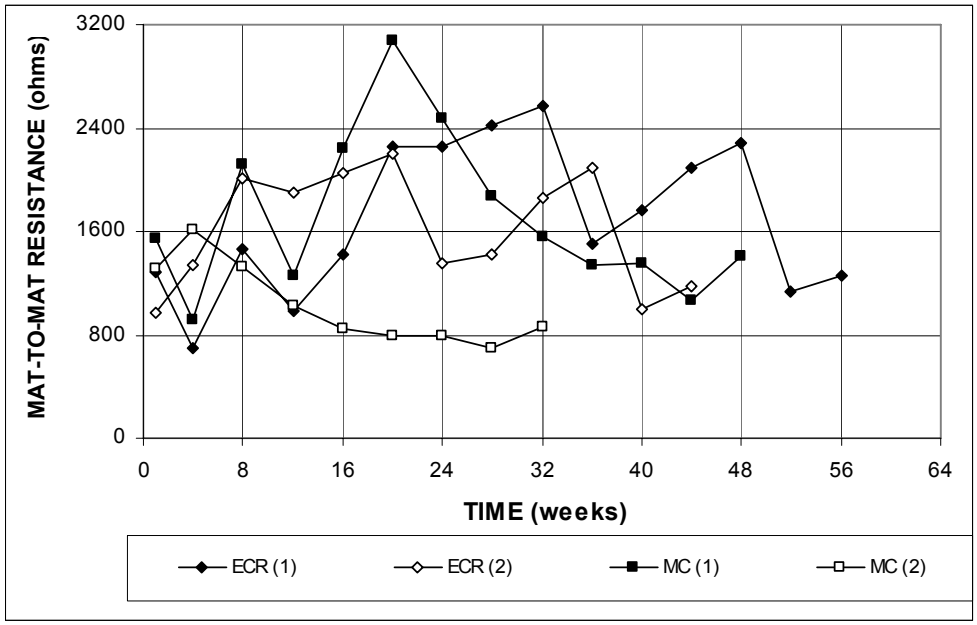

Figure 3.135 – Average mat-to-mat resistances as measured in the field test for specimens with ECR and multiple coated bars, without cracks (ECR bars have 16 holes).

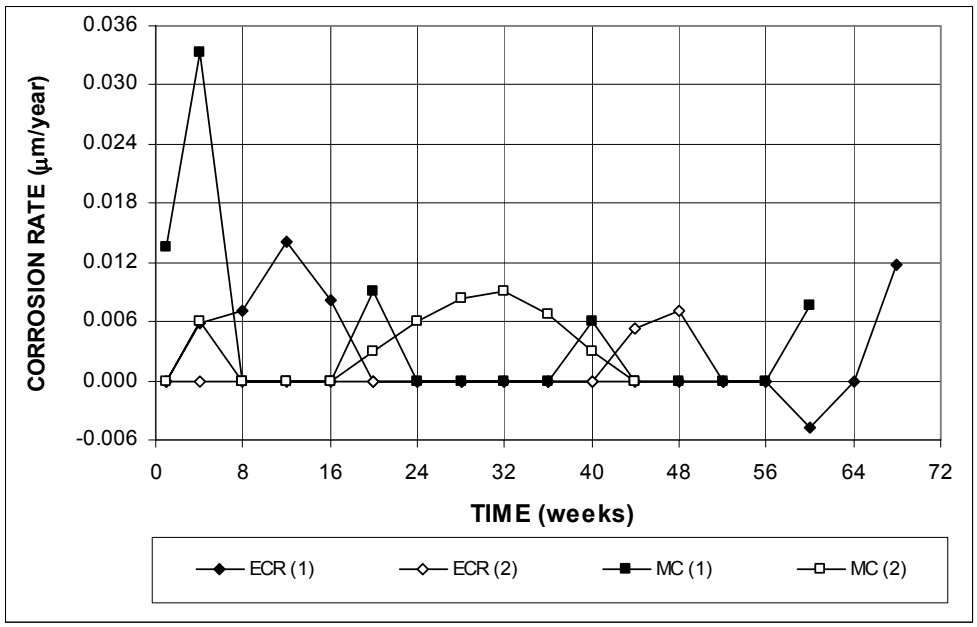

Figure 3.136 – Average corrosion rates as measured in the field test for specimens with ECR and multiple coated bars, with cracks (ECR bars have 16 holes).

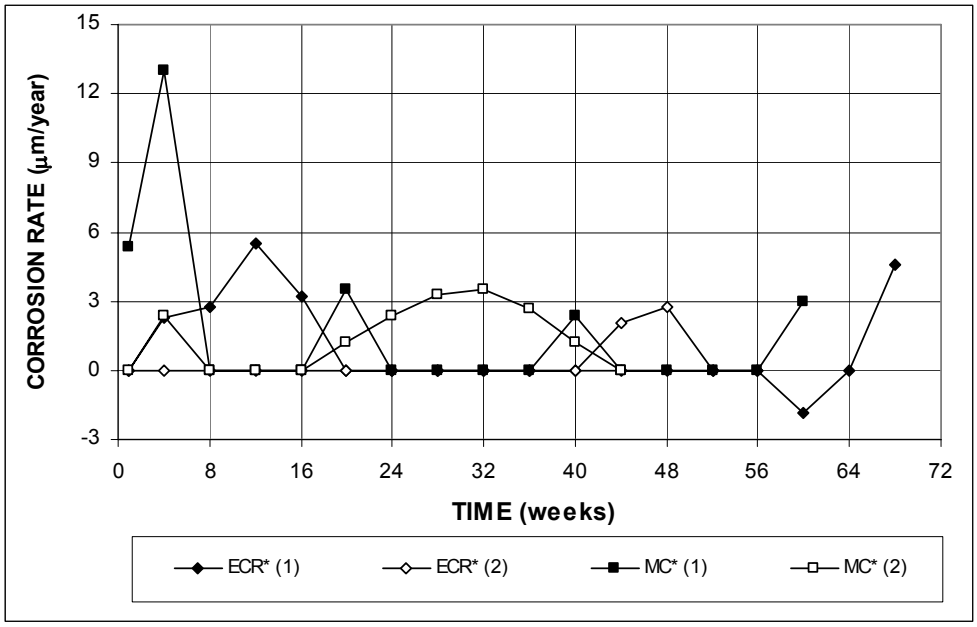

Figure 3.137 – Average corrosion rates as measured in the field test for specimens with ECR and multiple coated bars, with cracks. * Based on exposed area (ECR bars have 16 holes).

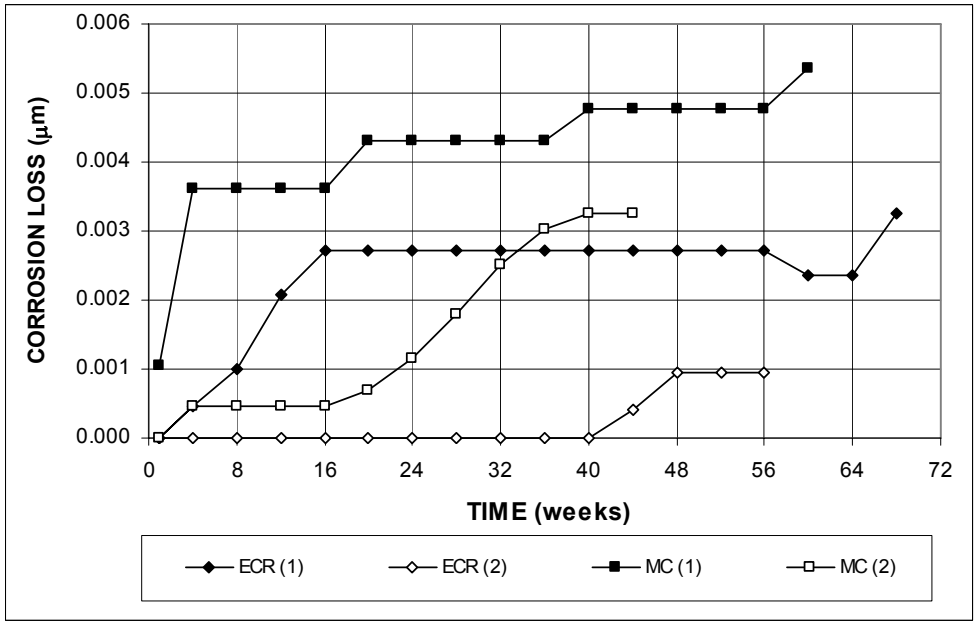

Figure 3.138 – Average corrosion losses as measured in the field test for specimens with ECR and multiple coated bars, with cracks (ECR bars have 16 holes).

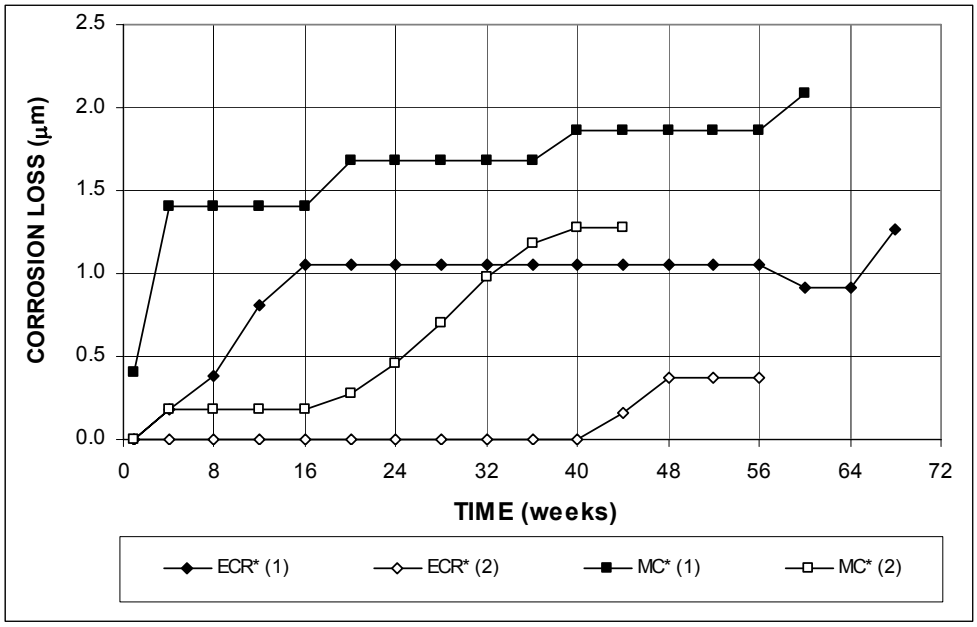

Figure 3.139 – Average corrosion losses as measured in the field test for specimens with ECR and multiple coated bars, with cracks. * Based on exposed area (ECR bars have 16 holes).

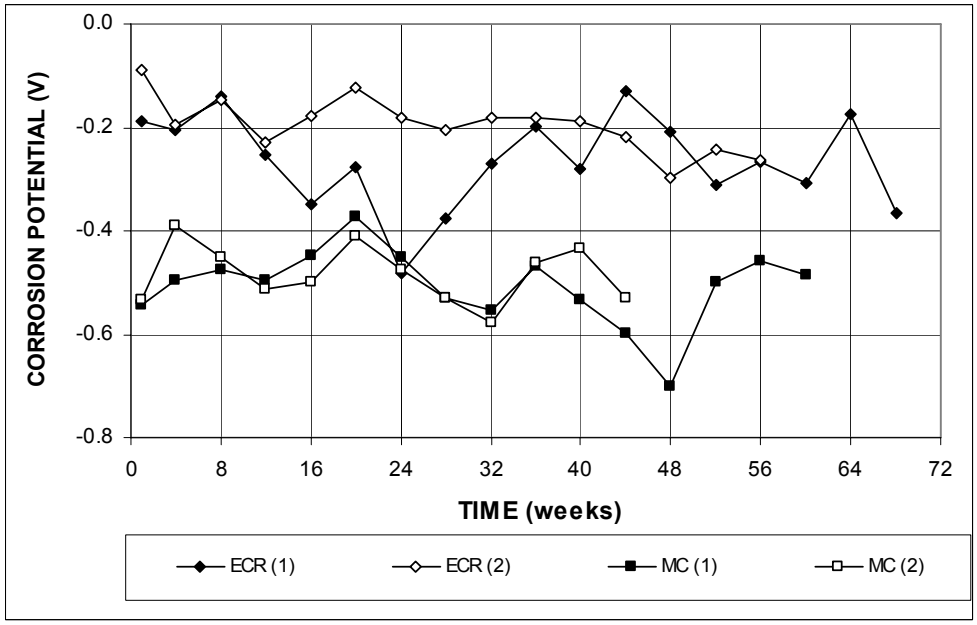

Figure 3.140 (a) – Average top mat corrosion potentials, with respect to a copper-copper sulfate electrode as measured in the field test for specimens with ECR and multiple coated bars, with cracks (ECR bars have 16 holes).

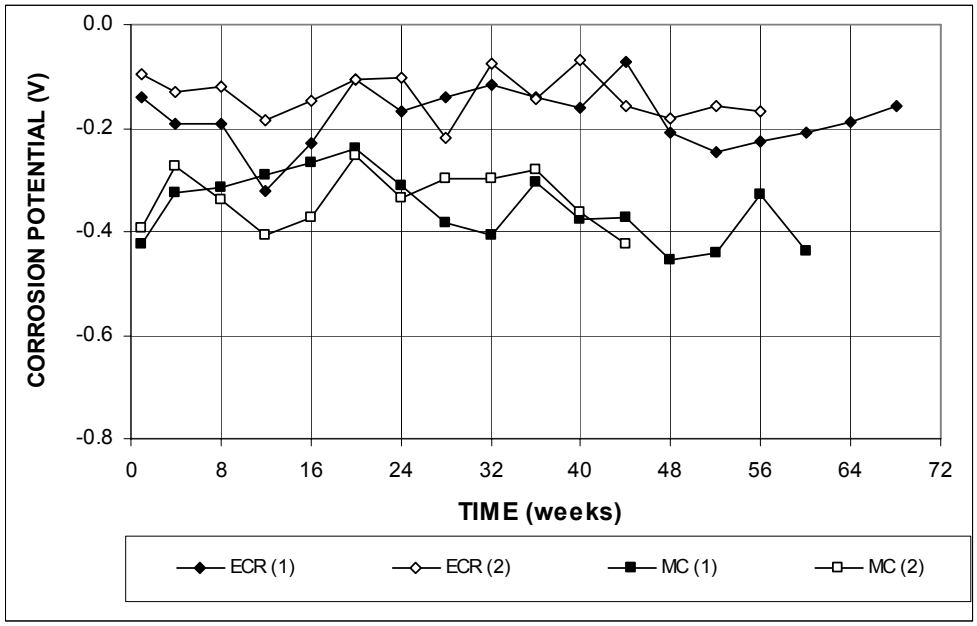

Figure 3.140 (b) – Average bottom mat corrosion potentials, with respect to a copper-copper sulfate electrode as measured in the field test for specimens with ECR and multiple coated bars, with cracks (ECR bars have 16 holes).

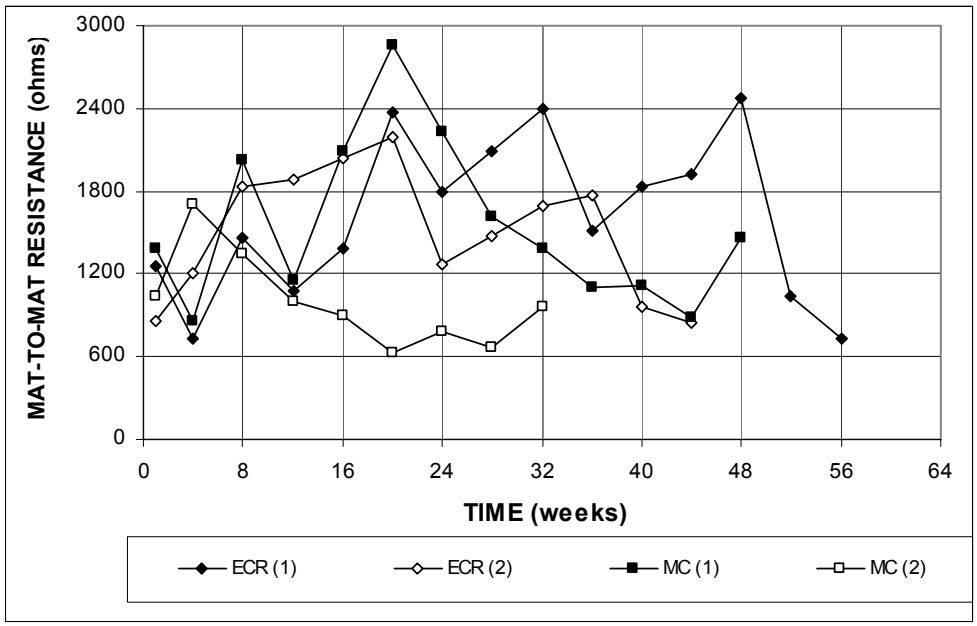

Figure 3.141 – Average mat-to-mat resistances as measured in the field test for specimens with ECR and multiple coated bars, with cracks (ECR bars have 16 holes).

3.4 ECR WITH INCREASED ADHESION

This section presents the results of the rapid macrocell, bench-scale, and field tests for high adhesion ECR bars, including ECR with the chromate pretreatment, and two types of ECR with improved adhesion coatings produced by DuPont and Valspar.

As described in Sections 2.6 and 3.7, cathodic disbondment tests were performed for all epoxy-coated bars in this study. Those tests show that the conventional ECR bars had the highest areas of disbonded coating, followed by high adhesion Valspar and DuPont bars, and ECR with the chromate pretreatment.

3.4.1 Rapid Macrocell Test

Both bare bar and mortar-wrapped specimens were used in the rapid macrocell test to evaluate high adhesion ECR bars in 1.6 m ion NaCl and simulated concrete pore solution. The mortar had a *w/c* ratio of 0.50. For both types of specimens, the study includes six tests each for bars with four drilled holes and three tests each for bars without holes or in the as-delivered condition.

3.4.1.1 Bare Bar Specimens

The test results for bare high adhesion epoxy-coated bars are presented in Figures 3.142 through 3.148, and the total corrosion losses at week 15 are summarized in Table 3.21.

Figure 3.142 shows the average corrosion rates for high adhesion ECR bars with four drilled holes. Based on total area, ECR(Chromate) exhibited the lowest corrosion rates, with values less than 0.32 μm/yr. ECR(DuPont) and ECR(Valspar) had corrosion rates similar to conventional ECR, with values between 0.80 and 1.60 μm/yr during the test period, as shown in Figure 3.142(b). ECR(Chromate) without holes (Figure 3.143) showed corrosion in the first week and then exhibited no

corrosion activity for the rest of the test period. No corrosion activity was observed for ECR(DuPont) and ECR(Valspar) without holes. Based on exposed area (Figure 3.144), ECR(Chromate) exhibited the lowest corrosion rates, with values below 32.3 μm/yr. The average corrosion rates for ECR (DuPont) and ECR(Valspar) were between 59 and 168 μm/yr, and between 32 and 143 μm/yr, respectively.

Table 3.21 – Average corrosion losses (μm) at week 15 as measured in the macrocell test for bare bar specimens with high adhesion ECR bars

Steel Designation[a]	Specimen						Average	Standard Deviation
	1	2	3	4	5	6		
Bare Bar Specimens								
ECR(Chromate)	0.10	0.00	0.00	0.00	β	0.05	0.03	0.04
ECR(Chromate)*	10.14	0.00	0.00	0.00	0.04	5.49	2.61	4.29
ECR(Chromate)-no holes	0.00	β	β				β	β
ECR(DuPont)	0.00	0.44	0.34	0.36	0.43	0.42	0.33	0.17
ECR(DuPont)*	0.00	43.85	33.65	36.12	42.53	41.80	32.99	16.64
ECR(DuPont)-no holes	0.00	0.00	0.00				0.00	0.00
ECR(Valspar)	0.27	0.39	0.60	0.08	0.06	0.50	0.32	0.22
ECR(Valspar)*	26.61	38.92	59.93	8.31	5.56	49.93	31.54	22.08
ECR(Valspar)-no holes	0.00	0.00	0.00				0.00	0.00

[a] ECR(Chromate) = ECR with the chromate pretreatment.
ECR(DuPont) = high adhesion DuPont bars. ECR(Valspar) = high adhesion Valspar bars.
no holes = epoxy-coated bars without holes, otherwise four 3-mm ($^1/_8$-in.) diameter holes.

* Epoxy-coated bars, calculations based on exposed area of four 3-mm ($^1/_8$-in.) diameter holes.

β Corrosion loss (absolute value) less than 0.005 μm.

The average total corrosion losses versus time are presented in Figures 3.145 through 3.147, and the average results at week 15 are summarized in Table 3.21. Based on total area, ECR(DuPont) exhibited the highest corrosion loss, 0.33 μm (98% of the corrosion loss of conventional ECR), followed by ECR(Valspar) and ECR(Chromate) at 0.32 and 0.03 μm (94% and 7.8% of the corrosion loss of conventional ECR), respectively. ECR(Chromate) without holes exhibited a total corrosion loss of less than 0.005 μm, as indicated by the symbol β in Table 3.21. The ECR(DuPont) and ECR(Valspar) specimens without holes showed no corrosion

activity. Based on exposed area, the total corrosion losses at week 15 were 2.61, 33.0, and 31.5 μm for ECR(Chromate), ECR(DuPont), and ECR(Valspar), respectively, compared with 33.6 μm for conventional ECR.

The average anode and cathode corrosion potentials with respect to a saturated calomel electrode are shown in Figure 3.148. As shown in Figure 3.148(a), ECR(DuPont) and ECR(Valspar) exhibited anode potentials similar to conventional ECR and conventional steel, with anode potentials between –0.400 and –0.600 V during the test period, indicating active corrosion. ECR(Chromate) had the most positive anode potentials, with values above –0.275 V throughout the test, indicating a low probability of corrosion. All of the cathode potentials were similar to each other and above –0.250 V, indicating that the cathode bars remained passive, as shown in Figure 3.148(b). High adhesion ECR bars without holes showed unstable corrosion potentials at both the anodes and cathodes.

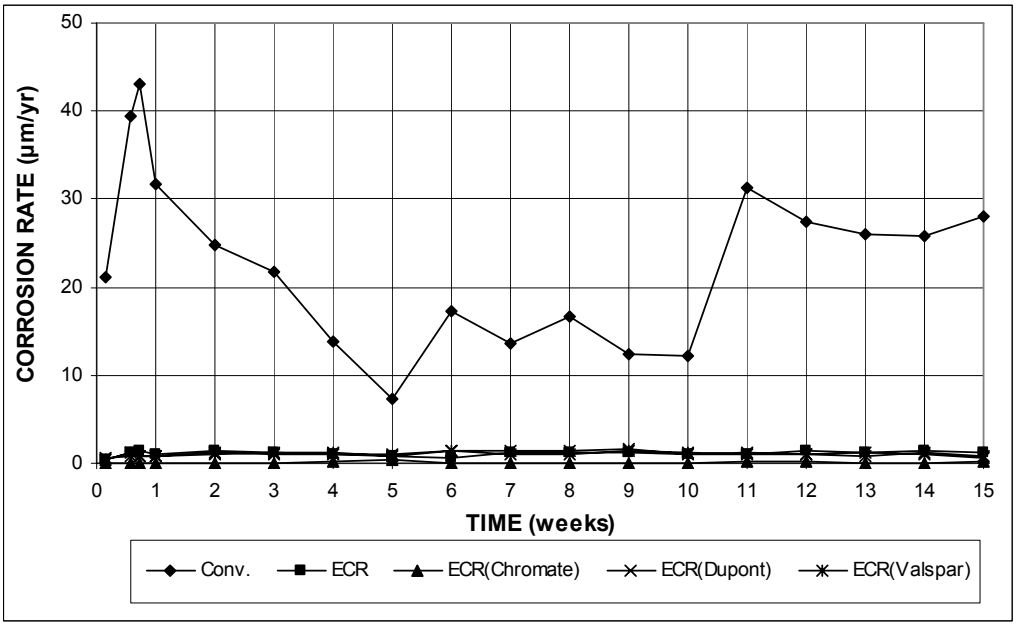

Figure 3.142 (a) – Average corrosion rates as measured in the rapid macrocell test for bare bar specimens with conventional steel, ECR, and high adhesion ECR bars (ECR bars have four holes).

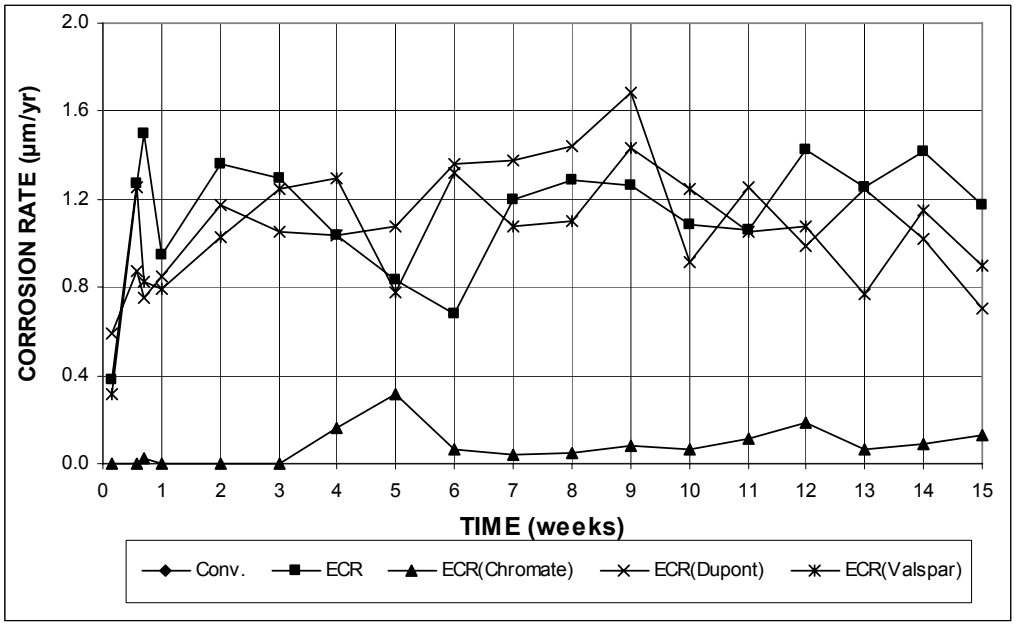

Figure 3.142 (b) – Average corrosion rates as measured in the rapid macrocell test for bare bar specimens with conventional steel, ECR, and high adhesion ECR bars (ECR bars have four holes).

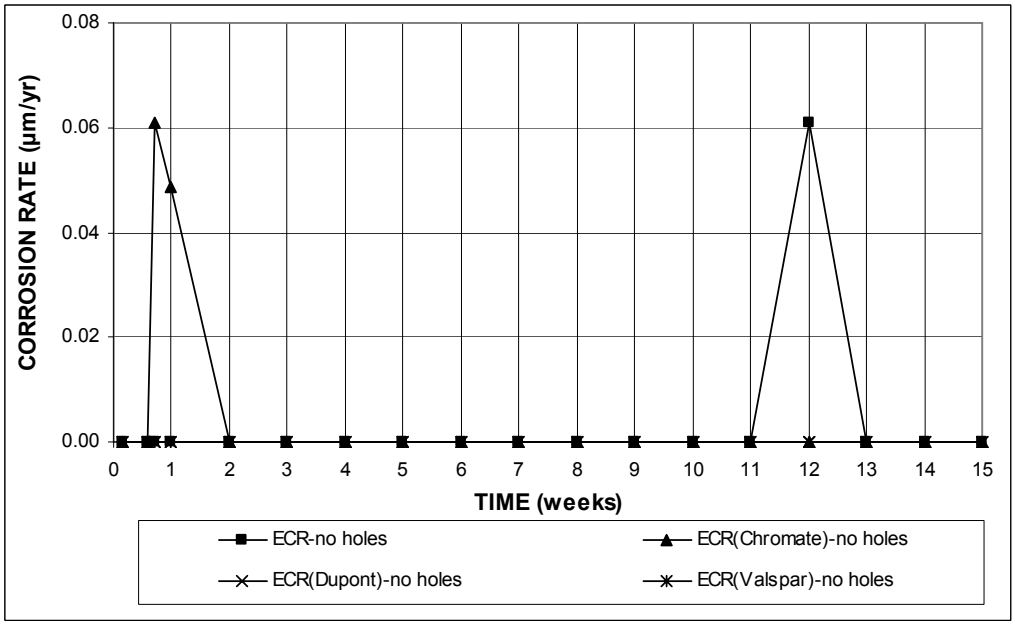

Figure 3.143 – Average corrosion rates as measured in the rapid macrocell test for bare bar specimens with ECR and high adhesion ECR bars, without holes.

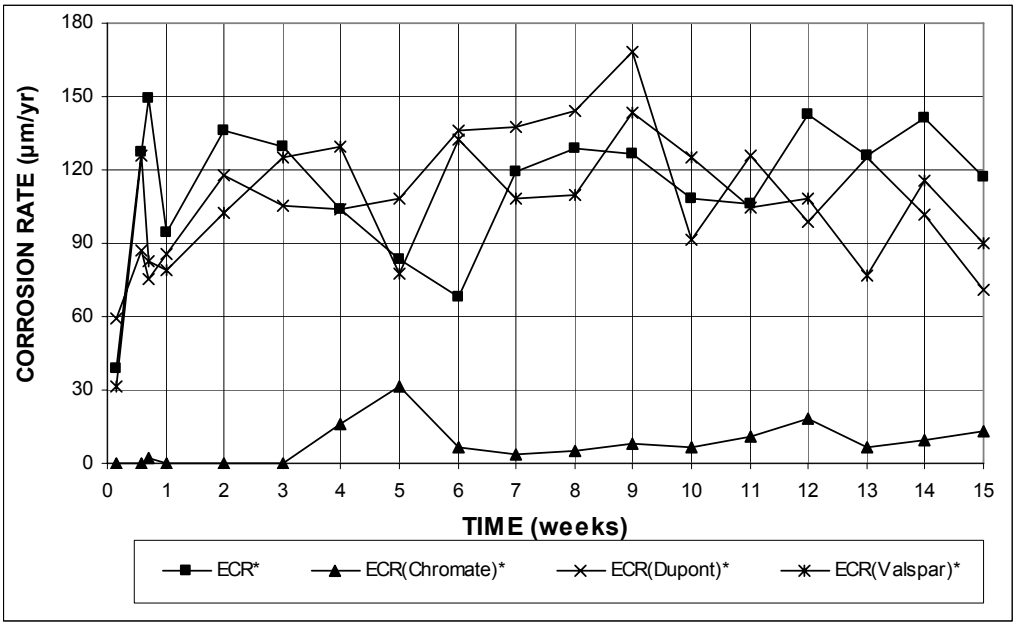

Figure 3.144 – Average corrosion rates as measured in the rapid macrocell test for bare bar specimens with ECR and high adhesion ECR bars. * Based on exposed area (ECR bars have four holes).

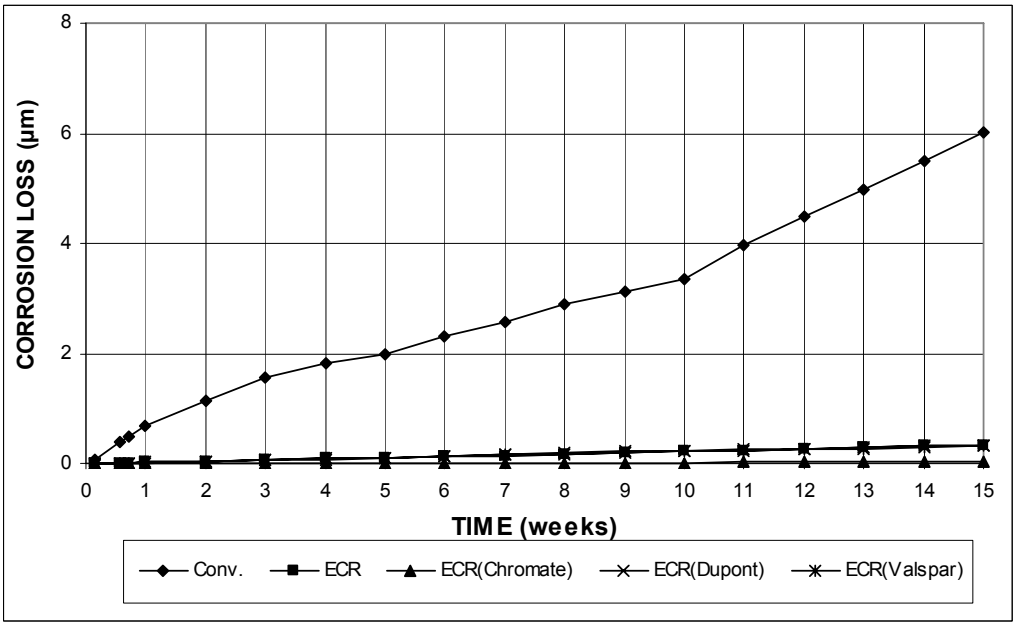

Figure 3.145 (a) – Average corrosion losses as measured in the rapid macrocell test for bare bar specimens with conventional steel, ECR, and high adhesion ECR bars (ECR bars have four holes).

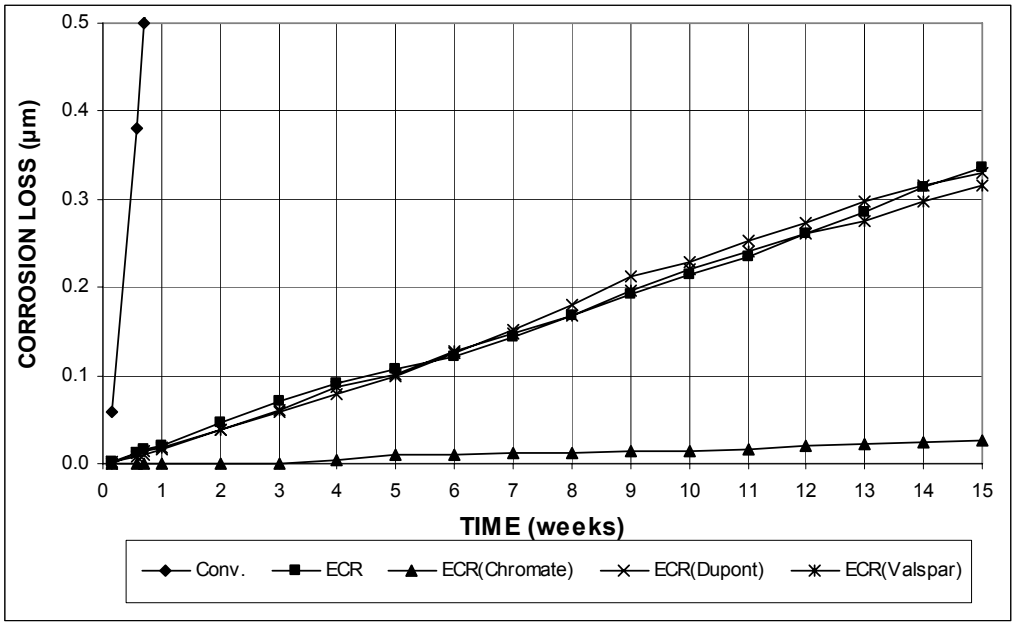

Figure 3.145 (b) – Average corrosion losses as measured in the rapid macrocell test for bare bar specimens with conventional steel, ECR, and high adhesion ECR bars (ECR bars have four holes).

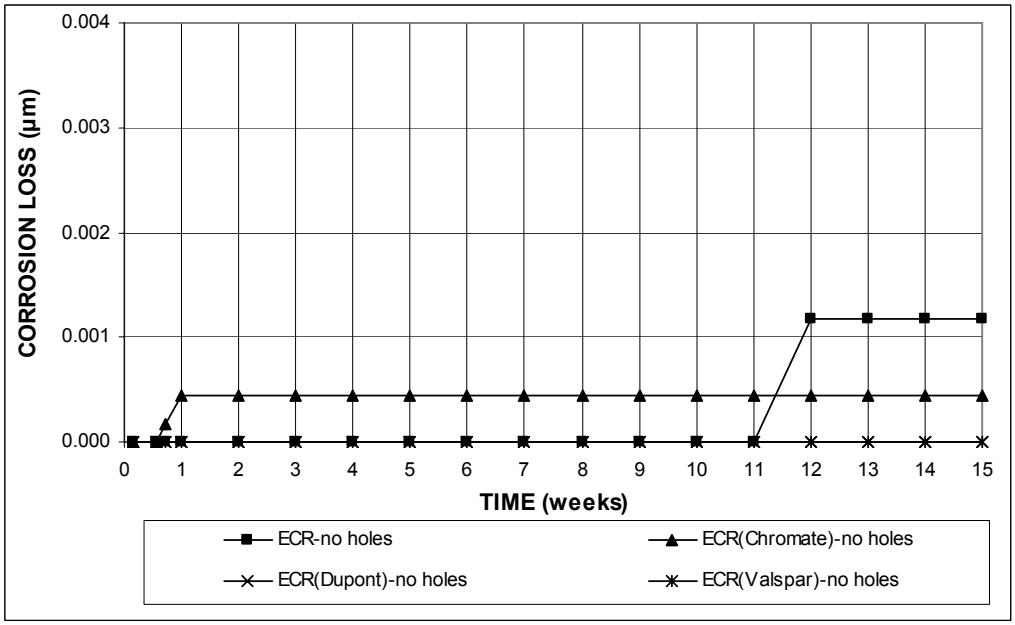

Figure 3.146 – Average corrosion losses as measured in the rapid macrocell test for bare bar specimens with ECR and high adhesion ECR bars, without holes.

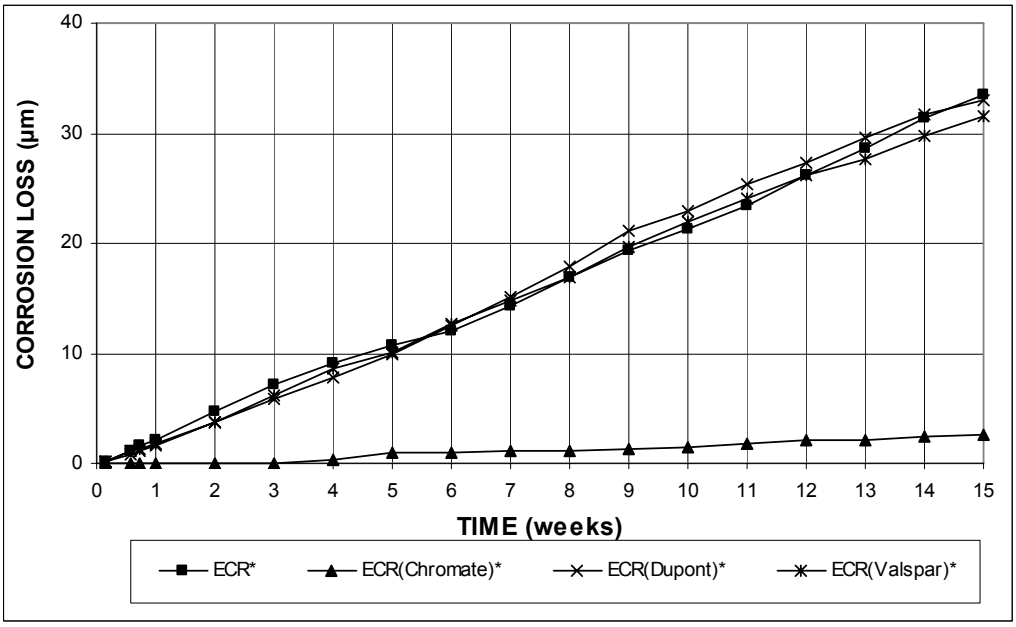

Figure 3.147 – Average corrosion losses as measured in the rapid macrocell test for bare bar specimens with ECR and high adhesion ECR bars. * Based on exposed area (ECR bars have four holes).

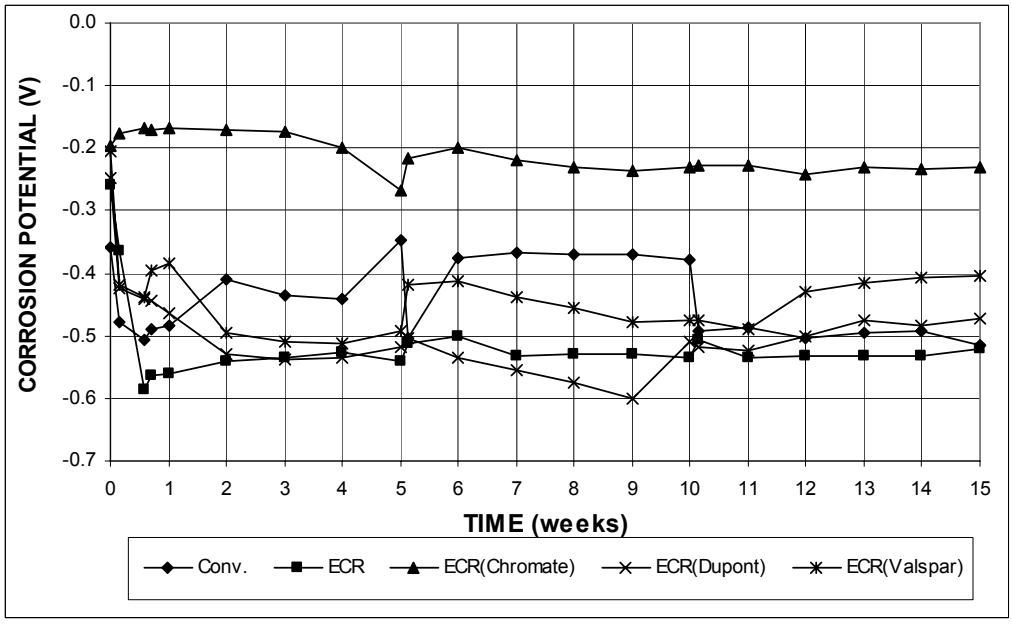

Figure 3.148 (a) – Average anode corrosion potentials, with respect to a saturated calomel electrode as measured in the rapid macrocell test for bare bar specimens with conventional steel, ECR, and high adhesion ECR bars (ECR bars have four holes).

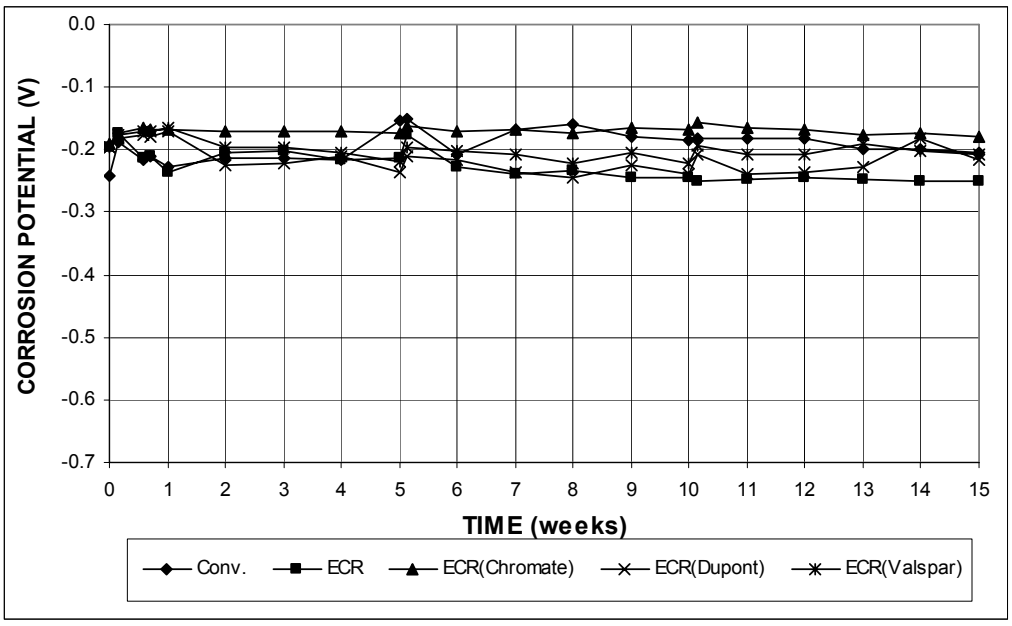

Figure 3.148 (b) – Average cathode corrosion potentials, with respect to a saturated calomel electrode as measured in the rapid macrocell test for bare bar specimens with conventional steel, ECR, and high adhesion ECR bars (ECR bars have four holes).

When the tests were finished, the specimens were visually inspected. For specimens with ECR(DuPont) and ECR(Valspar) with four drilled holes, corrosion products were found at the drilled holes, as shown in Figures 3.149 and 3.150, respectively. No corrosion products were observed for ECR(Chromate) with holes or for any type of the specimens without holes. The autopsy agreed with the corrosion test results, as ECR(DuPont) and ECR(Valspar) exhibited much higher corrosion rates and total corrosion losses than ECR(Chromate).

Figure 3.149 – Bare bar specimen. ECR(DuPont) anode bar showing corrosion products that formed at drilled holes at week 15.

Figure 3.150 – Bare bar specimen. ECR(Valspar) anode bar showing corrosion products that formed at drilled holes at week 15.

3.4.1.2 Mortar-Wrapped Specimens

The three types of high adhesion ECR bars showed no corrosion activity in the rapid macrocell test with mortar-wrapped specimens.

The average anode and cathode corrosion potentials with respect to a saturated calomel electrode are shown in Figure 3.151. At the anodes, all specimens exhibited nearly constant corrosion potentials more positive than –0.260 V during the test period, with the exception of ECR(DuPont), which had an anode potential of –0.280 V at week 11. The corrosion potentials at the anodes indicated that no corrosion activity was expected for high adhesion ECR bars. At the cathodes, all specimens had potentials more positive than –0.210 V, indicating a passive condition. Stable corrosion potentials at both the anodes and cathodes were not available for high adhesion ECR bars without holes.

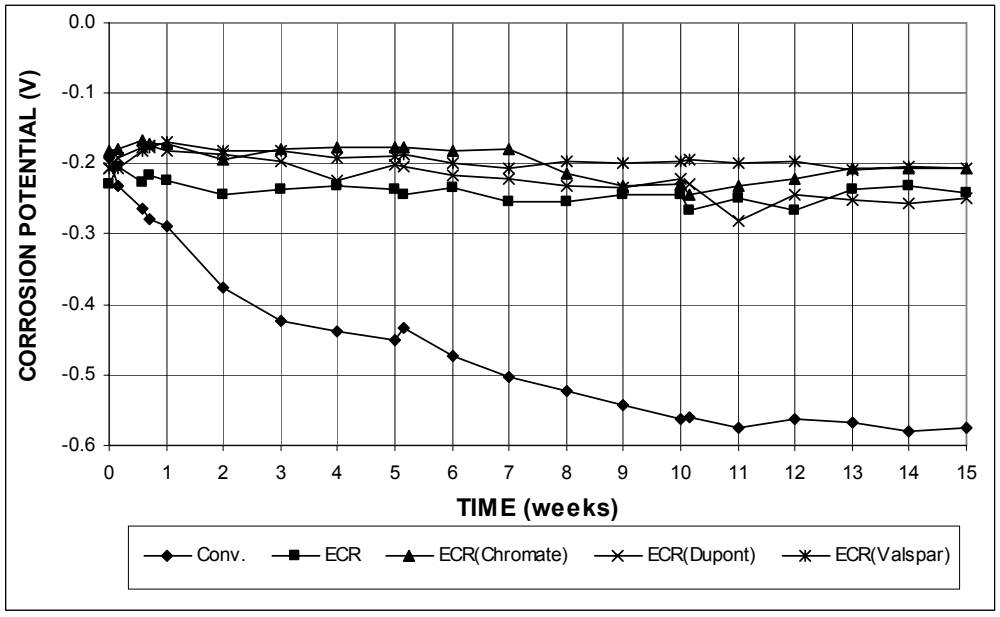

Figure 3.151 (a) – Average anode corrosion potentials, with respect to a saturated calomel electrode as measured in the rapid macrocell test for mortar-wrapped specimens with conventional steel, ECR, and high adhesion ECR bars (ECR bars have four holes).

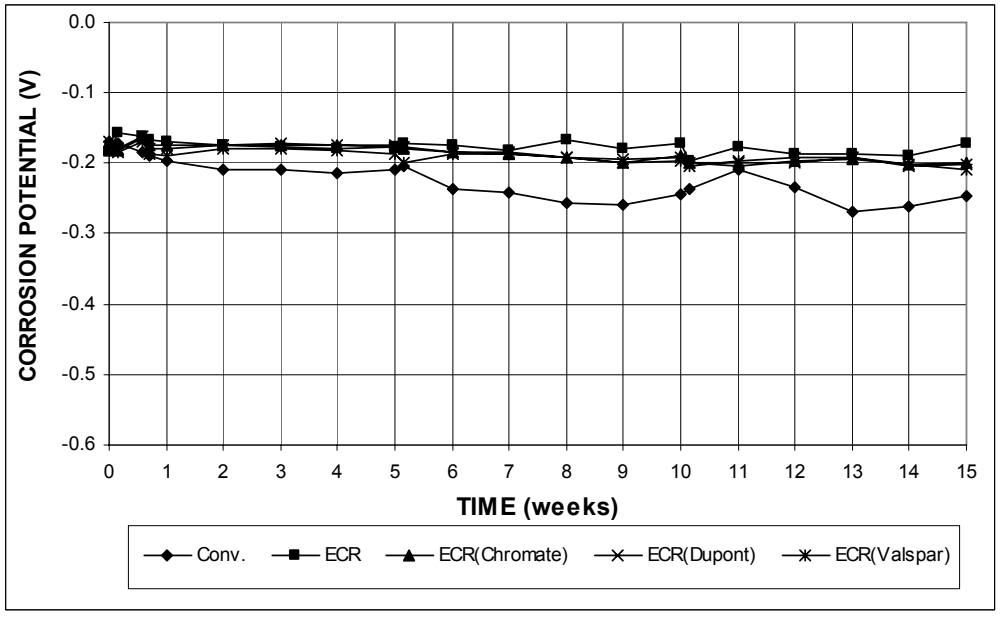

Figure 3.151 (b) – Average cathode corrosion potentials, with respect to a saturated calomel electrode as measured in the rapid macrocell test for mortar-wrapped specimens with conventional steel, ECR, and high adhesion ECR bars (ECR bars have four holes).

At the end of the test period, the mortar was removed and the specimens were visually inspected. No corrosion products were found for mortar-wrapped specimens with high adhesion ECR bars.

3.4.2 Bench-Scale Tests

The Southern Exposure and cracked beam tests were used to evaluate the high adhesion ECR bars. The tests included three tests each of ECR(Chromate), ECR(DuPont), and ECR(Valspar) penetrated with four or 10 holes.

3.4.2.1 Southern Exposure Test

The results for the Southern Exposure tests of the high adhesion bars are shown in Figures 3.152 through 3.163. The average total corrosion losses at week 40 are summarized in Table 3.22.

Figures 3.152 and 3.153 show the average corrosion rates for high adhesion ECR bars with four holes. Figure 3.152(b) shows that during the first 40 weeks, specimens with four holes had corrosion rates similar to conventional ECR, with values below 0.03 μm/yr based on total area. After week 40, specimens with four holes showed higher corrosion rates than conventional ECR. The ECR(DuPont) specimens had negative corrosion rates of –0.005 and –0.006 μm/yr, respectively, at weeks 48 and 57. These two average negative corrosion rates were caused by one of the three test specimens. The corrosion rate of –0.005 μm/yr at week 48 was not accompanied by more negative corrosion potentials at cathode than at anode, and in all likelihood was an aberrant reading. While the corrosion rate of rates –0.006 μm/yr at week 57 was associated with more negative corrosion potentials at cathode than at anode. Based on exposed area, shown in Figure 3.153, corrosion rates as high as 11.0, 7.93, and 17.1 μm/yr were observed for ECR(Chromate), ECR(DuPont), and

ECR(Valspar), respectively. Figures 3.154 and 3.155 show the average corrosion rates for high adhesion ECR bars with 10 holes. As shown in Figures 3.154(b) and 3.155, all specimens with 10 holes had similar corrosion rates to conventional ECR, with values below 0.03 and 5.4 μm/yr based on total area and exposed area, respectively, with the exception of ECR(Chromate)-10h between weeks 38 and 40, which had corrosion rates between 0.04 and 0.07 μm/yr (between 8 and 13 based on exposed area μm/yr).

Table 3.22 – Average corrosion losses (μm) at week 40 as measured in the Southern Exposure test for specimens with high adhesion ECR bars

Steel Designation[a]	Specimen			Average	Standard Deviation
	1	2	3		
Southern Exposure Test					
ECR(Chromate)	β	β	β	β	β
ECR(Chromate)*	0.88	1.79	1.20	1.29	0.46
ECR(Chromate)-10h	β	0.01	0.01	0.01	β
ECR(Chromate)-10h*	0.52	1.96	1.74	1.41	0.77
ECR(DuPont)	β	β	β	β	β
ECR(DuPont)*	0.77	0.60	1.30	0.89	0.37
ECR(DuPont)-10h	0.01	0.01	β	β	β
ECR(DuPont)-10h*	1.06	1.24	0.00	0.76	0.67
ECR(Valspar)	β	β	β	β	β
ECR(Valspar)*	0.14	0.67	0.39	0.40	0.26
ECR(Valspar)-10h	β	0.01	β	β	β
ECR(Valspar)-10h*	0.39	1.27	0.06	0.57	0.62

[a] ECR(Chromate) = ECR with the chromate pretreatment.
ECR(DuPont) = ECR with high adhesion DuPont coating.
ECR(Valspar) = ECR with high adhesion Valspar coating.
10h = epoxy-coated bars with 10 holes, otherwise four 3-mm ($^1/_8$-in.) diameter holes.

* Epoxy-coated bars, calculations based on exposed area of four or 10 3-mm ($^1/_8$-in.) diameter holes.

β Corrosion loss (absolute value) less than 0.005 mm.

The average total corrosion losses are shown in Figures 3.156 and 3.157 for specimens with four holes, and in Figures 3.158 and 3.159 for specimens with 10 holes, respectively. Table 3.22 summarizes the average total corrosion losses for these specimens at week 40. As shown in Figures 3.156(b) and 3.157, all ECR specimens showed progressive total corrosion losses during the first 12 weeks, and

between weeks 12 and 40, the total corrosion losses for specimens with four holes increased at a rate lower than that of conventional ECR. After week 40, the total corrosion losses for the ECR(Chromate) and ECR(Valspar) specimens increased at a higher rate than the corrosion loss of ECR. By week 46, the ECR(Chromate) and ECR(Valspar) exhibited a higher total corrosion loss than conventional ECR. At week 40, specimens with four holes showed total corrosion losses less than 0.005 μm based on total area, as indicated by the symbol β in Table 3.22. Based on exposed area, total corrosion losses of 1.29, 0.89, and 0.40 μm were observed for ECR(Chromate), ECR(DuPont), and ECR(Valspar), respectively. These values are equal to 92%, 64%, and 29% of the corrosion loss of conventional ECR, although the trend shown in Figures 3.156 and 3.157 indicates that the corrosion losses for the high adhesion bars will eventually exceed the losses for conventional ECR, as is clearly the case for ECR(Chromate) and ECR(Valspar). As shown in Figures 3.158(b) and 3.159, conventional ECR with 10 holes had a higher total corrosion loss than high adhesion ECR specimens with 10 holes before week 27. A total corrosion loss higher than the corrosion loss of conventional ECR with 10 holes was observed for ECR(Chromate)-10h by week 27 and for ECR(DuPont)-10h by week 38. At week 40, ECR(Chromate)-10h had a measurable corrosion loss of 0.01 μm based on total area. The ECR(DuPont)-10h and ECR(Valspar)-10h specimens had total corrosion losses less than 0.005 μm, as indicated by the symbol β in Table 3.22. Based on exposed area, ECR(Chromate)-10h had the highest corrosion loss, 1.41 μm, equal to 2.31 times the corrosion loss of conventional ECR with 10 holes (ECR-10h). ECR(DuPont)-10h had a total corrosion loss of 0.76 μm, similar to that of ECR-10h (0.61 μm). ECR(Valspar)-10h had the lowest corrosion loss, 0.57 μm, equal to 94% of the corrosion loss of ECR-10h.

The average corrosion potentials of the top and bottom mats of steel with

respect to a copper-copper sulfate electrode are shown in Figure 3.160 for specimens with four holes, and in Figure 3.161 for specimens with 10 holes. The top mat corrosion potentials for specimens with four holes, shown in Figure 3.160(a), remained above –0.300 V before week 40 and then quickly dropped below –0.350 V after week 40. Between weeks 40 and 60, ECR(Chromate) had top mat corrosion potentials around –0.350 V, and ECR(DuPont) and ECR(Valspar) had values of approximately –0.500 V. Figure 3.160(b) shows that specimens with four holes had bottom mat corrosion potentials above –0.280 V, indicating a low probability of corrosion. Figure 3.161(a) shows that during the first 20 weeks, specimens with 10 holes had top mat corrosion potentials more positive than –0.350 V. After week 20, the top mat corrosion potentials decreased to values below –0.350 V for all specimens with 10 holes and remained between –0.250 and –0.450 V. In the bottom mat, the corrosion potentials remained above –0.330 V for ECR(Valspar)-10h, indicating a low probability of corrosion. The bottom mat corrosion potentials were more positive than –0.250 V for ECR(Chromate)-10h and ECR(DuPont)-10h, indicating a lower probability of corrosion.

Figures 3.162 and 3.163 show the average mat-to-mat resistances for high adhesion ECR bars. As mentioned in Section 3.1.2, average mat-to-mat resistances are not reported at the same week as other results because the resistance meter broke several weeks before the data cut-off date. As shown in Figure 3.162, specimens with four holes had average mat-to-mat resistances of approximately 2,000 ohms at the start of the test period, which increased at a similar rate as conventional ECR to values around 7,200 ohms at week 40. For specimens with 10 holes, the average mat-to-mat resistances started around 900 ohms and increased to values of approximately 3,000 ohms at week 40.

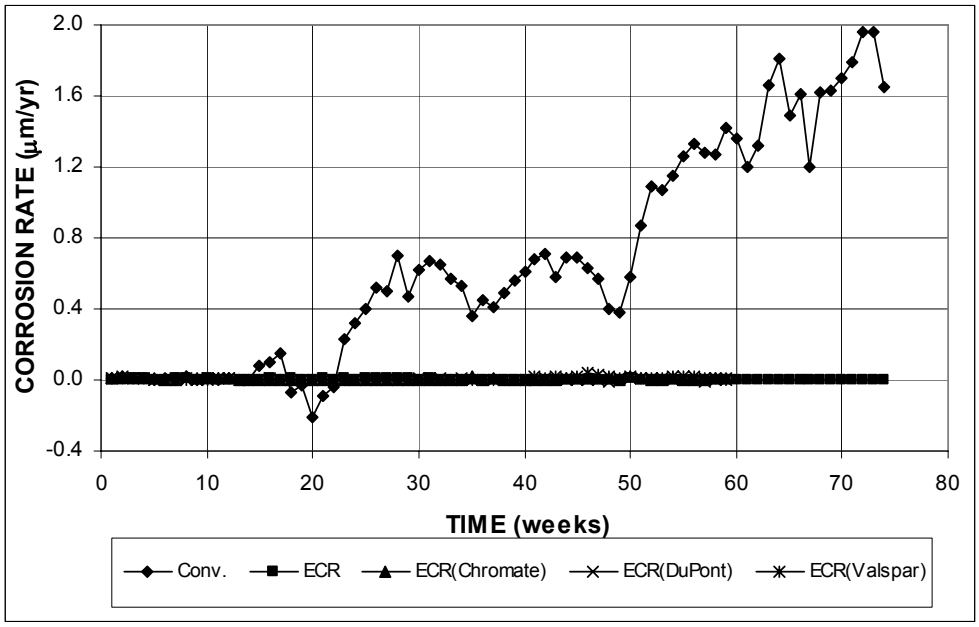

Figure 3.152 (a) – Average corrosion rates as measured in the Southern Exposure test for specimens with conventional steel, ECR, and high adhesion ECR bars (ECR bars have four holes).

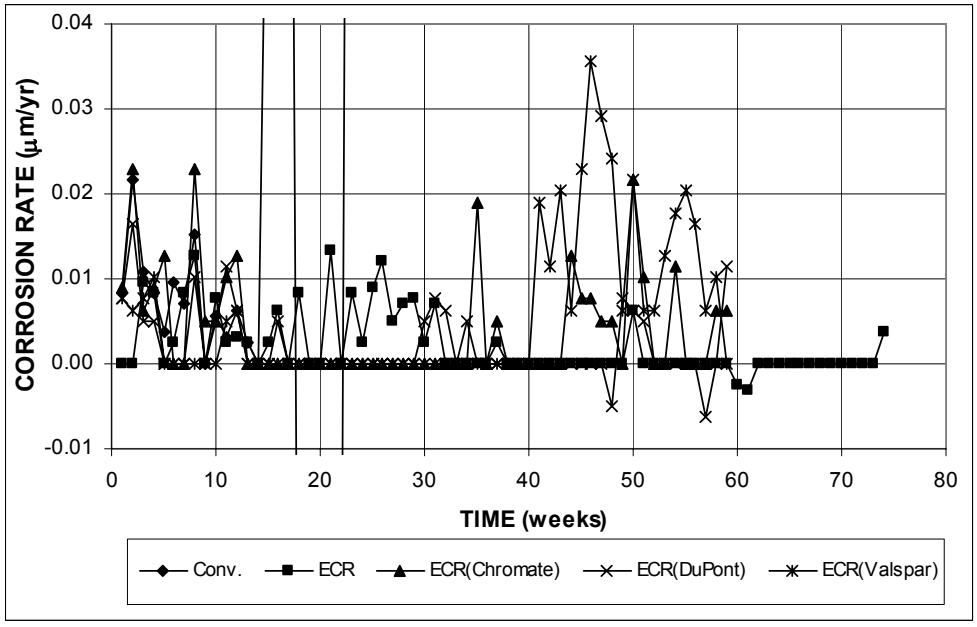

Figure 3.152 (b) – Average corrosion rates as measured in the Southern Exposure test for specimens with conventional steel, ECR, and high adhesion ECR bars (ECR bars have four holes).

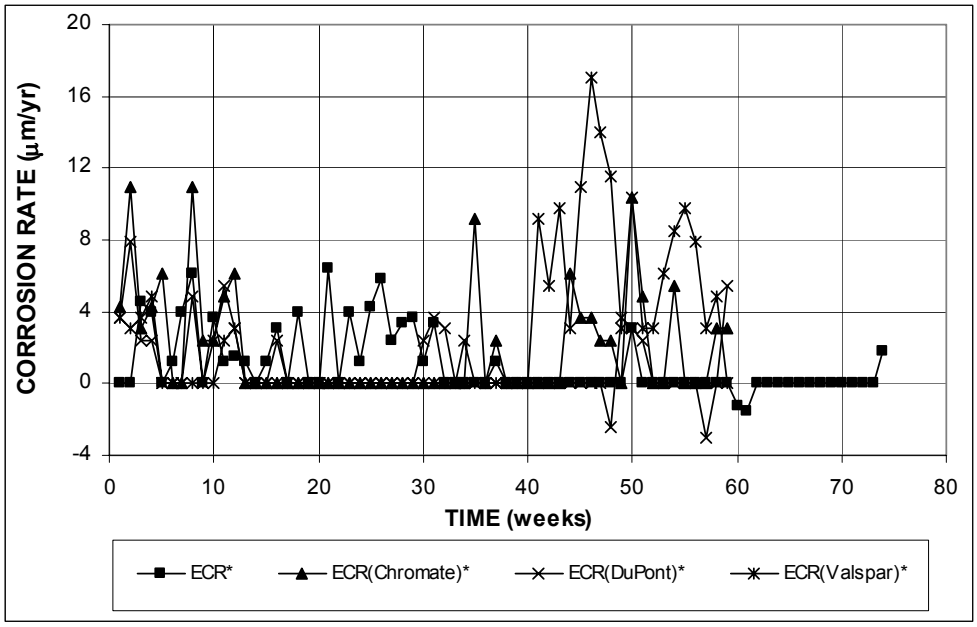

Figure 3.153 – Average corrosion rates as measured in the Southern Exposure test for specimens with ECR and high adhesion ECR bars. * Based on exposed area (ECR bars have four holes).

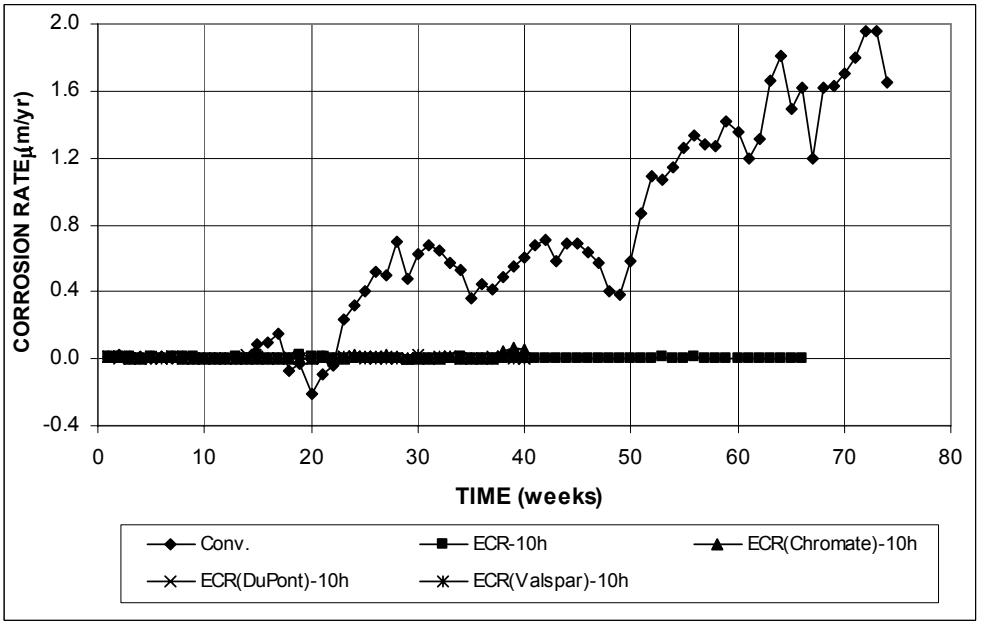

Figure 3.154 (a) – Average corrosion rates as measured in the Southern Exposure test for specimens with conventional steel, ECR, and high adhesion ECR bars (ECR bars have 10 holes).

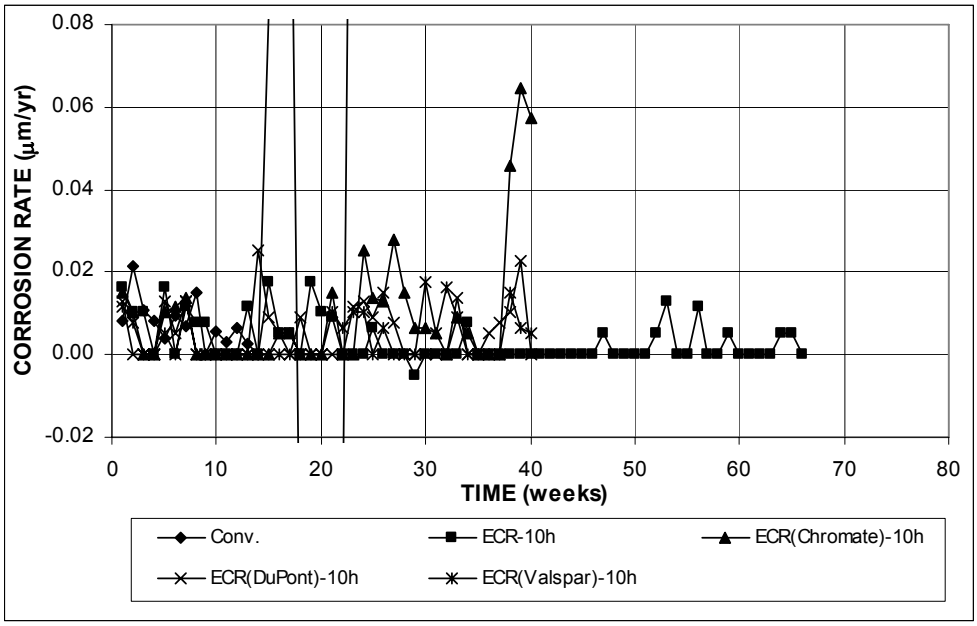

Figure 3.154 (b) – Average corrosion rates as measured in the Southern Exposure test for specimens with conventional steel, ECR, and high adhesion ECR bars (ECR bars have 10 holes).

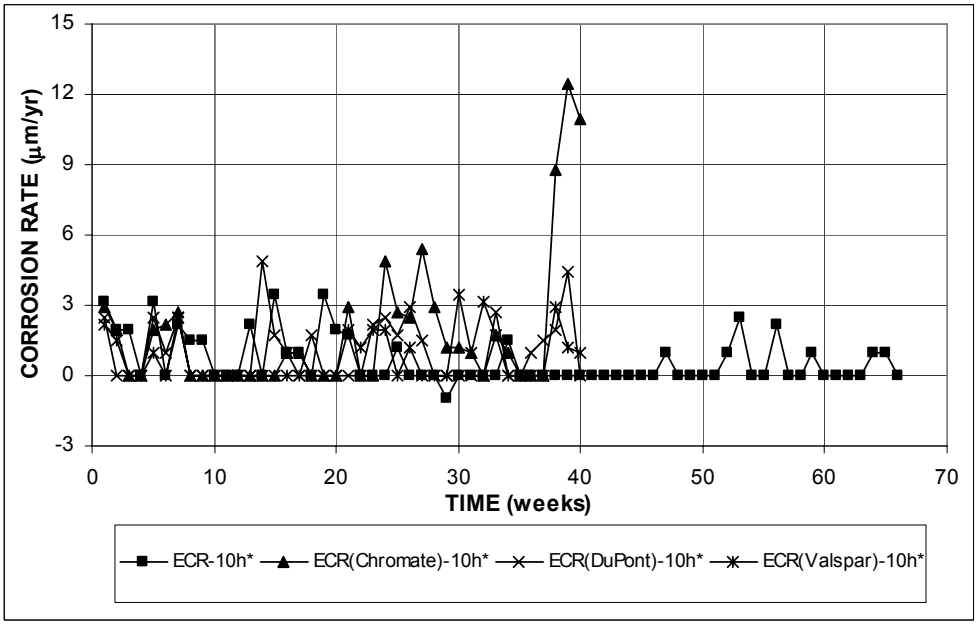

Figure 3.155 – Average corrosion rates as measured in the Southern Exposure test for specimens with ECR and high adhesion ECR bars. * Based on exposed area (ECR bars have 10 holes).

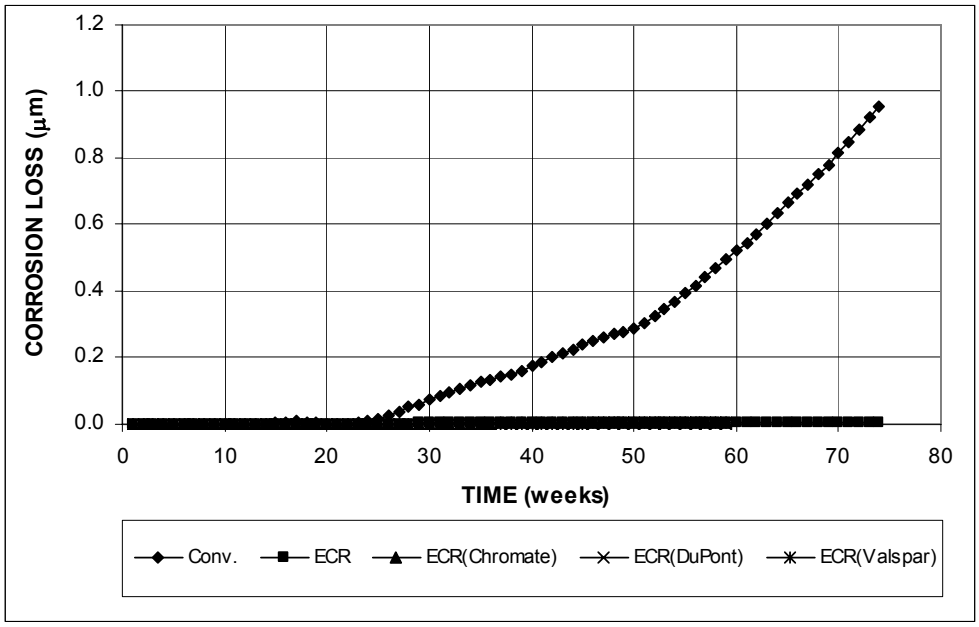

Figure 3.156 (a) – Average corrosion losses measured in the Southern Exposure test for specimens with conventional steel, ECR, and high adhesion ECR bars (ECR bars have four holes).

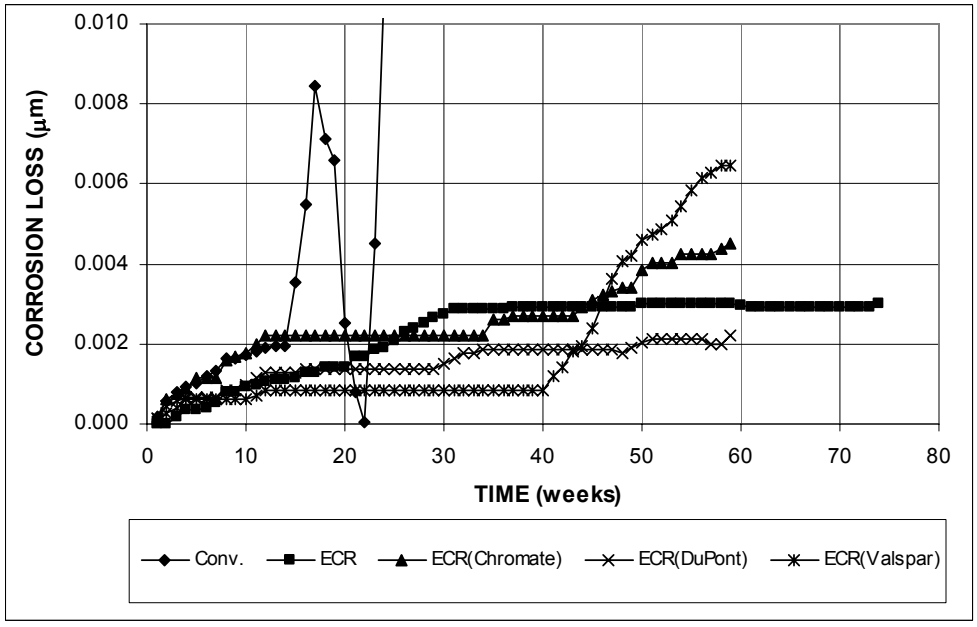

Figure 3.156 (b) – Average corrosion losses measured in the Southern Exposure test for specimens with conventional steel, ECR, and high adhesion ECR bars (ECR bars have four holes).

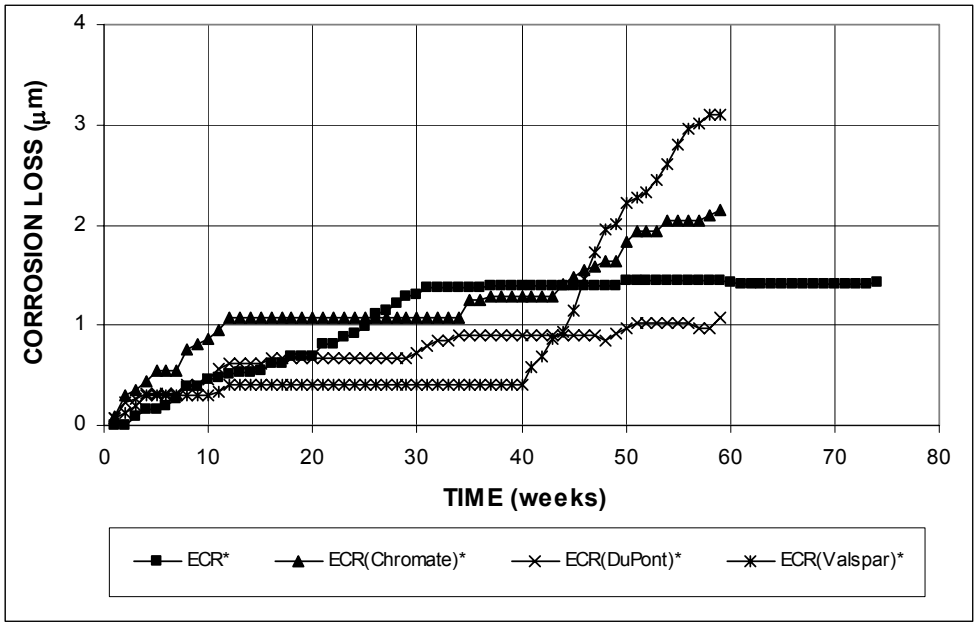

Figure 3.157 – Average corrosion losses measured in the Southern Exposure test for specimens with ECR and ECR high adhesion ECR bars. * Based on exposed area (ECR bars have four holes).

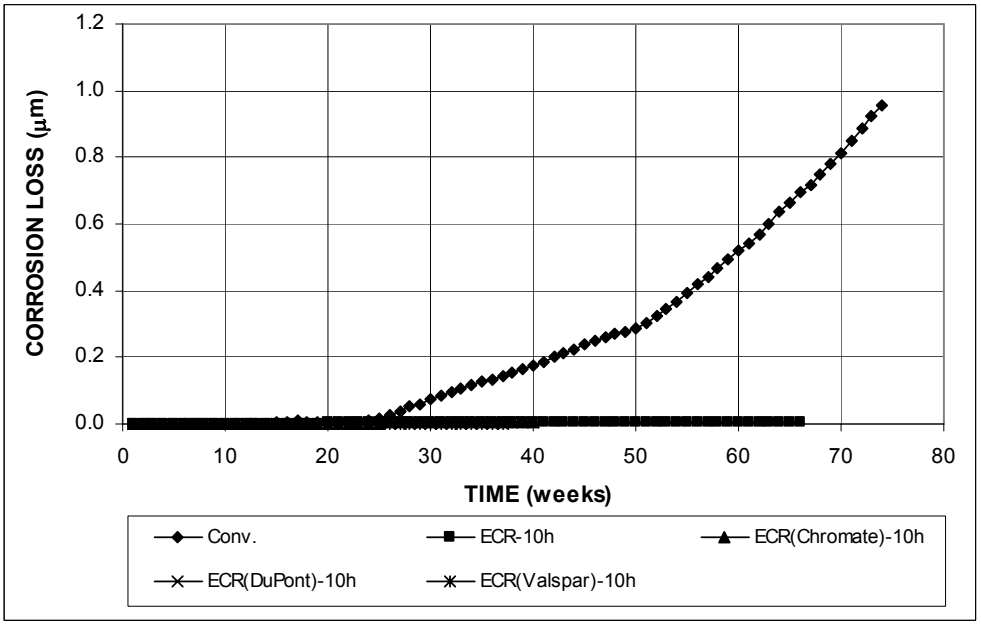

Figure 3.158 (a) – Average corrosion losses measured in the Southern Exposure test for specimens with conventional steel, ECR, and high adhesion ECR bars (ECR bars have 10 holes).

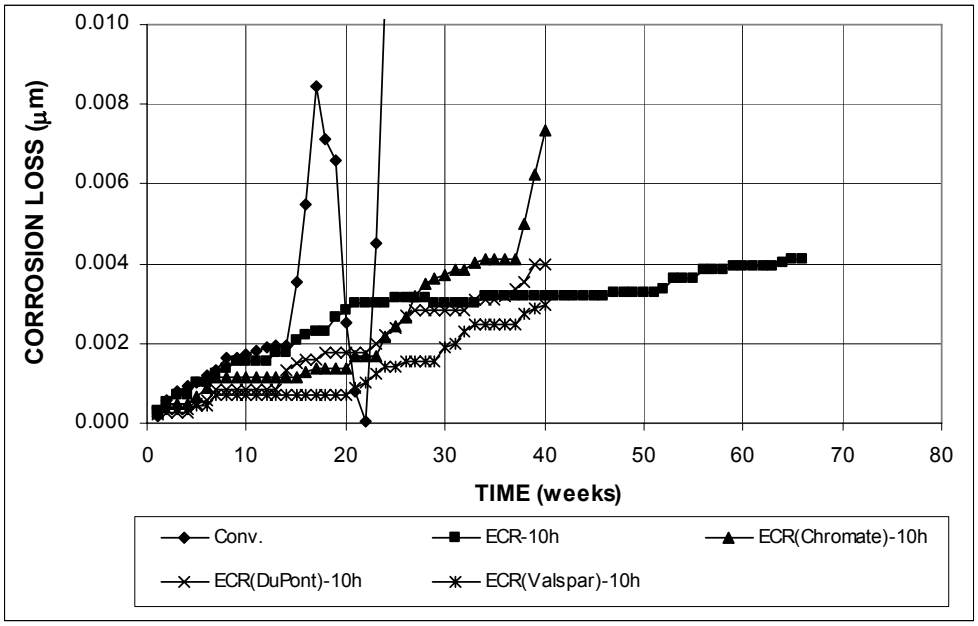

Figure 3.158 (b) – Average corrosion losses measured in the Southern Exposure test for specimens with conventional steel, ECR, and high adhesion ECR bars (ECR bars have 10 holes).

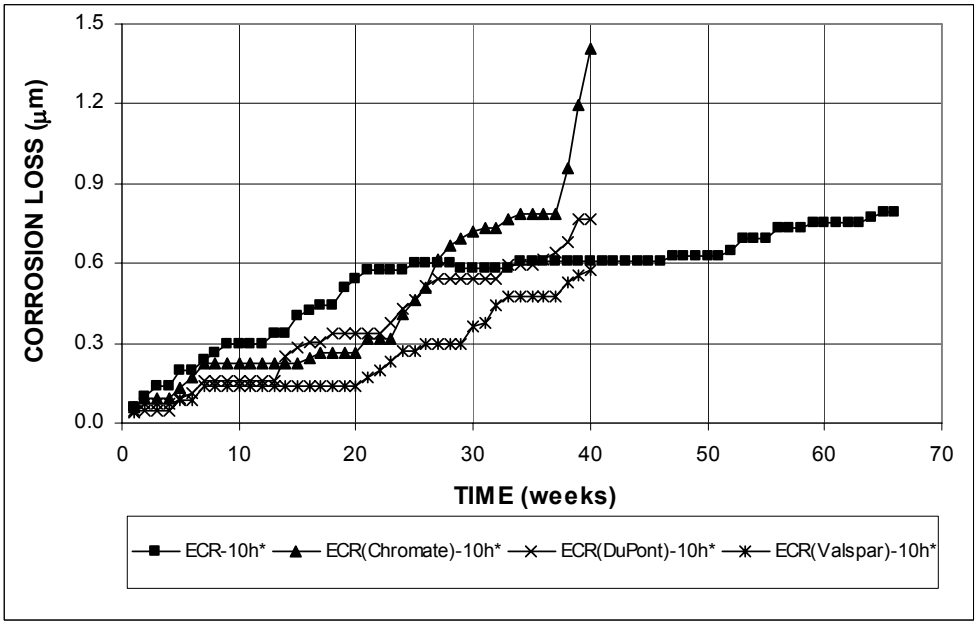

Figure 3.159 – Average corrosion losses measured in the Southern Exposure test for specimens with ECR and high adhesion ECR bars. * Based on exposed area (ECR bars have 10 holes).

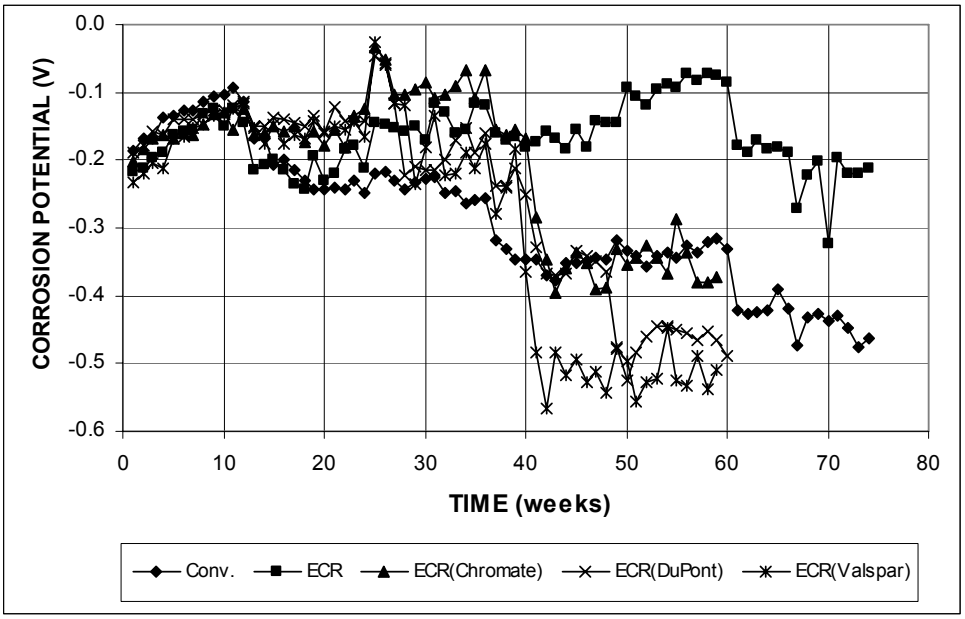

Figure 3.160 (a) – Average top mat corrosion potentials, with respect to a copper-copper sulfate electrode as measured in the Southern Exposure test for specimens with conventional steel, ECR, and high adhesion ECR bars (ECR bars have four holes).

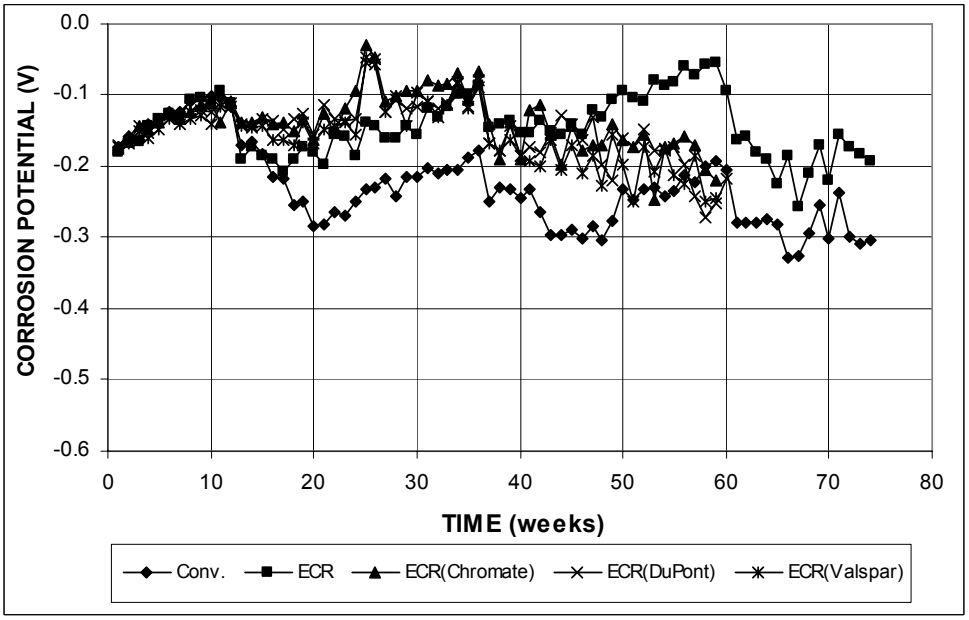

Figure 3.160 (b) – Average bottom mat corrosion potentials, with respect to a copper-copper sulfate electrode as measured in the Southern Exposure test for specimens with conventional steel, ECR, and high adhesion ECR bars (ECR bars have four holes).

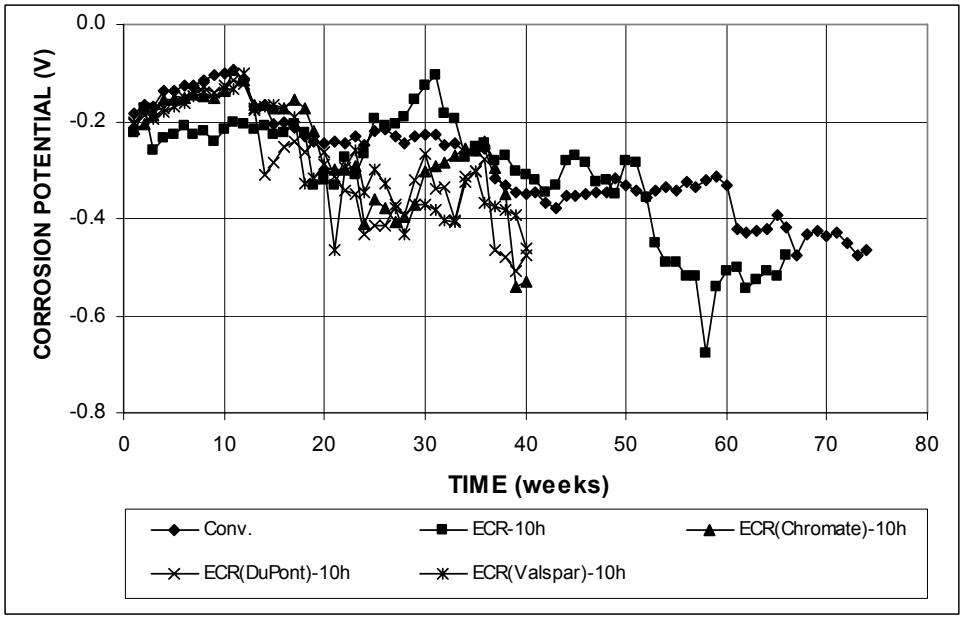

Figure 3.161 (a) – Average top mat corrosion potentials, with respect to a copper-copper sulfate electrode as measured in the Southern Exposure test for specimens with conventional steel, ECR, and high adhesion ECR bars (ECR bars have 10 holes).

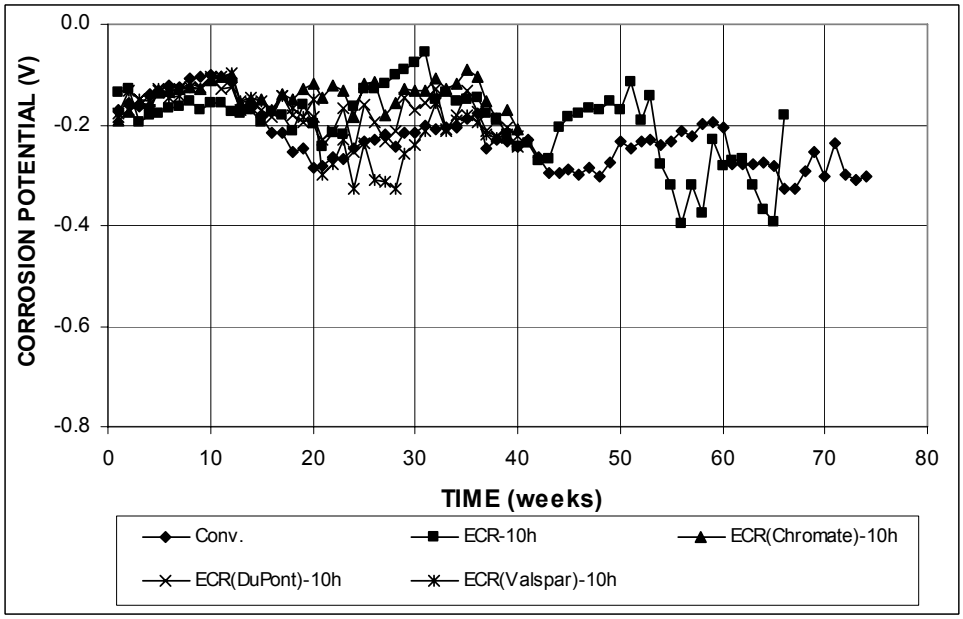

Figure 3.161 (b) – Average bottom mat corrosion potentials, with respect to a copper-copper sulfate electrode as measured in the Southern Exposure test for specimens with conventional steel, ECR, and high adhesion ECR bars (ECR bars have 10 holes).

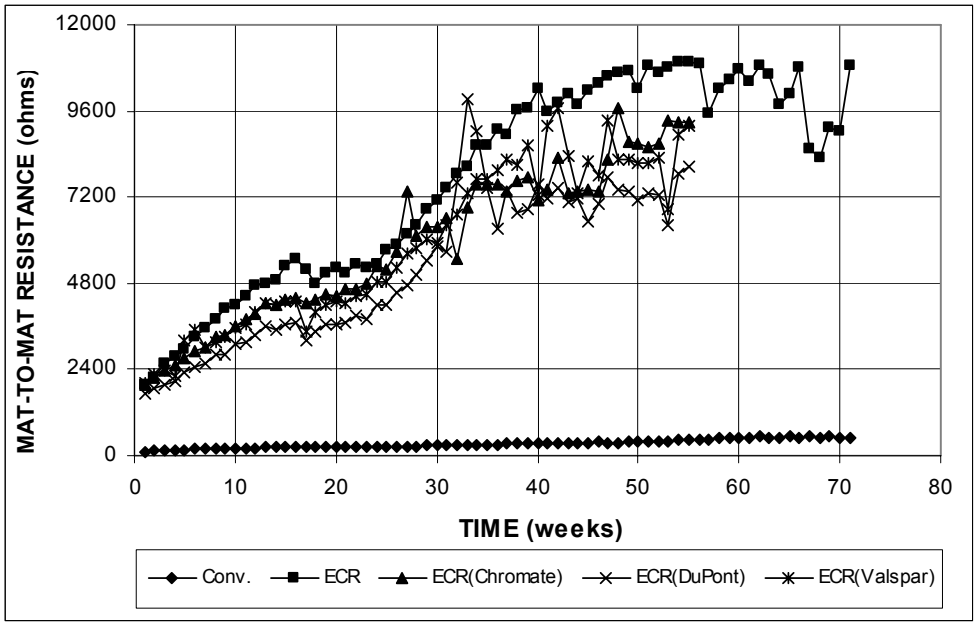

Figure 3.162 – Average mat-to-mat resistances as measured in the Southern Exposure test for specimens with conventional steel, ECR, and high adhesion ECR bars (ECR bars have four holes).

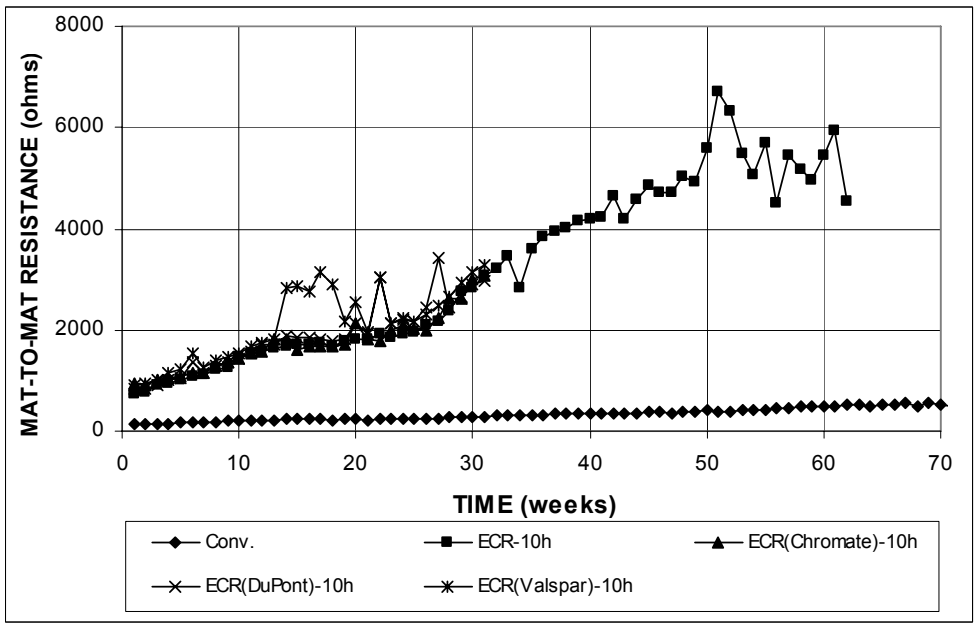

Figure 3.163 – Average mat-to-mat resistances as measured in the Southern Exposure test for specimens with conventional steel, ECR, and high adhesion ECR bars (ECR bars have 10 holes).

3.4.2.2 Cracked Beam Test

The results for the high adhesion bar cracked beam tests are shown in Figures 3.164 through 3.175. The total corrosion losses at week 40 are summarized in Table 3.23.

Figures 3.164 and 3.165 show the average corrosion rates for high adhesion ECR bars with four holes. Figure 3.164(b) shows that specimens with four holes had erratic corrosion rates, with values below 0.20 μm/yr, except for ECR(Valspar) at week 51, which had a value of 0.23 μm/yr. An average corrosion rate of –0.015 μm/yr was observed for ECR(Valspar) at week 39 and was caused by one of the three test specimens (the other specimens showed no corrosion). This corrosion rate was not accompanied by a more negative corrosion potential at the cathode than at the anode and in all likelihood was an aberrant reading. Based on exposed area, as shown in Figure 3.165, corrosion rates as high as 65.8, 67.1, and 110 μm/yr were obtained for ECR(Chromate), ECR(DuPont), and ECR(Valspar), respectively, compared to a maximum of 34.1 μm/yr for conventional ECR. Figures 3.166 and 3.167 show the average corrosion rates for high adhesion ECR bars with 10 holes. Similar to conventional ECR, all specimens with 10 holes [Figure 3.166(b)] exhibited erratic corrosion rates, with values below 0.25 μm/yr based on the total area of the top bars. Figure 3.167 shows that based on exposed area, corrosion rates were as high as 46 μm/yr for specimens with 10 holes.

The average total corrosion losses are shown in Figures 3.168 and 3.169 for specimens with four holes and in Figures 3.170 and 3.171 for specimens with 10 holes. Table 3.23 summarizes the average total corrosion losses for these specimens at week 40. As shown in Figures 3.168(b) and 3.169, specimens with four holes had higher total corrosion losses than conventional ECR. At week 40, specimens with four holes showed total corrosion losses between 0.04 and 0.06 μm based on total

area. Based on exposed area, total corrosion losses of 22.5, 18.9, and 28.8 μm were observed for ECR(Chromate), ECR(DuPont), and ECR(Valspar), respectively. These values are equal to 1.98, 1.66, and 2.53 times the corrosion loss of conventional ECR with four holes. As shown in Figures 3.170(b) and 3.171, specimens with 10 holes exhibited higher total corrosion losses than conventional ECR with 10 holes. At week 40, total corrosion losses based on total area between 0.06 and 0.08 μm were observed for specimens with 10 holes. Based on exposed area, the total corrosion losses were 16.2, 11.9, and 12.3 μm for ECR(Chromate)-10h, ECR(DuPont)-10h, and ECR(Valspar)-10h, respectively. These values are, respectively, equal to 2.50, 1.84, and 1.90 times the corrosion loss of conventional ECR with 10 holes.

Table 3.23 – Average corrosion losses (μm) at week 40 as measured in the cracked beam test for specimens with high adhesion ECR bars

Steel Designation[a]	Specimen			Average	Standard Deviation
	1	2	3		
Cracked beam test					
ECR(Chromate)	0.05	0.04	0.05	0.05	0.01
ECR(Chromate)*	25.39	20.33	21.73	22.48	2.61
ECR(Chromate)-10h	0.01	0.06	0.18	0.08	0.09
ECR(Chromate)-10h*	2.42	11.79	34.41	16.21	16.45
ECR(DuPont)	0.05	0.05	0.02	0.04	0.02
ECR(DuPont)*	24.06	23.21	9.57	18.94	8.13
ECR(DuPont)-10h	0.06	0.04	0.09	0.06	0.02
ECR(DuPont)-10h*	10.97	7.82	16.97	11.92	4.65
ECR(Valspar)	0.12	0.05	0.01	0.06	0.06
ECR(Valspar)*	57.82	24.34	4.29	28.82	27.04
ECR(Valspar)-10h	0.05	0.01	0.13	0.06	0.06
ECR(Valspar)-10h*	10.10	2.67	24.11	12.30	10.89

[a] ECR(Chromate) = ECR with the chromate pretreatment.
ECR(DuPont) = ECR with high adhesion DuPont coating.
ECR(Valspar) = ECR with high adhesion Valspar coating.
10h = epoxy-coated bars with 10 holes, otherwise four 3-mm ($^1/_8$-in.) diameter holes.

* Epoxy-coated bars, calculations based on exposed area of four or 10 3-mm ($^1/_8$-in.) diameter holes.

The average corrosion potentials of the top and bottom mats of steel with respect to a copper-copper sulfate electrode are shown in Figures 3.172 and 3.173 for high adhesion ECR bars with four and 10 holes, respectively. As shown in Figure

3.172(a), the top mat corrosion potentials were more positive than –0.350 V for ECR(Chromate) and ECR(Valspar) in the first week and for ECR(Chromate) in the first three weeks. After week 4, the top mat corrosion potentials for these specimens remained more negative than –0.350 V with the exception of ECR(DuPont), which had potentials above –0.350 V at weeks 25, 26, and 28. As shown in Figure 3.172(b), ECR(Chromate) and ECR(DuPont) had bottom mat corrosion potentials above –0.330 V, indicating a low probability of corrosion. ECR(Valspar) had bottom mat corrosion potentials more positive than –0.300 V, except at week 39 and between week 45 and 48, at which time the corrosion potentials were below –0.400 V. As shown in Figure 3.173(a), all specimens with 10 holes had top mat corrosion potentials more negative than –0.350 V by week 2. After week 10, specimens with 10 holes showed active corrosion, with corrosion potentials of the top mat between –0.500 and –0.600 V. The bottom mat corrosion potentials for the high adhesion bar specimens with 10 holes, shown in Figure 3.173(b), were more positive than –0.280 V, indicating a low probability of corrosion.

Figures 3.174 and 3.175 show the average mat-to-mat resistances for high adhesion ECR bars. As mentioned in Section 3.1.2.1, the resistance meter was not functional for several weeks before the data cut-off date and, therefore, average mat-to-mat resistances are not reported for the same time period as the other results. As shown in Figure 3.174, high adhesion ECR bars with four holes had average mat-to-mat resistances less than those for conventional ECR with four holes during the first 31 weeks and then showed similar values to each other. The average mat-to-mat resistances started around 3,200 ohms and increased at a rate similar to conventional ECR to values between 14,150 and 19,000 ohms at week 40. Specimens with 10 holes exhibited average mat-to-mat resistances similar to those for conventional ECR with 10 holes, with values between 1,550 and 1,800 ohms at the start of the test, increasing to values of approximately 7,500 ohms at week 31.

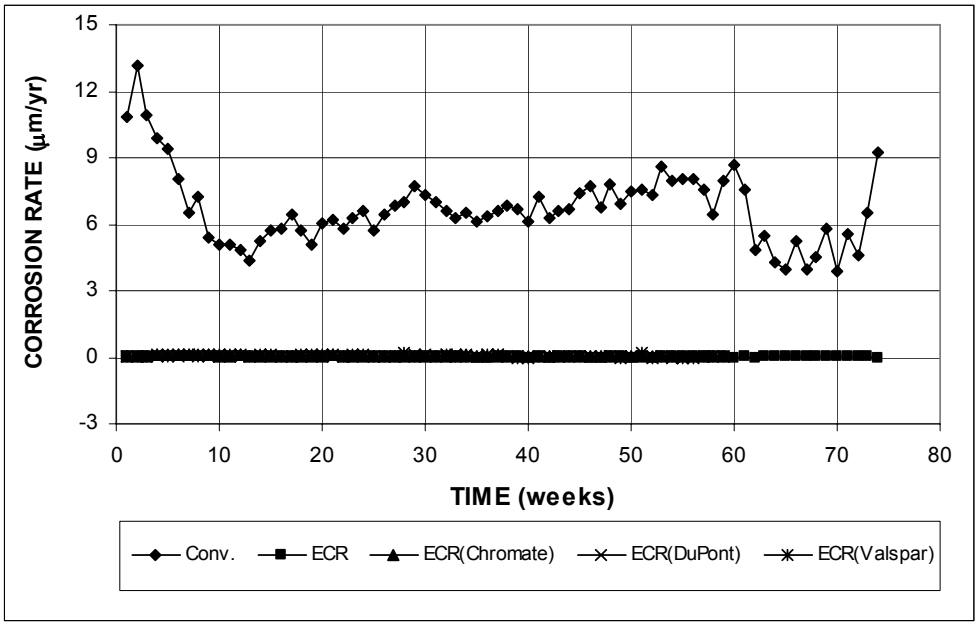

Figure 3.164 (a) – Average corrosion rates as measured in the cracked beam test for specimens with conventional steel, ECR, and high adhesion ECR bars (ECR bars have four holes).

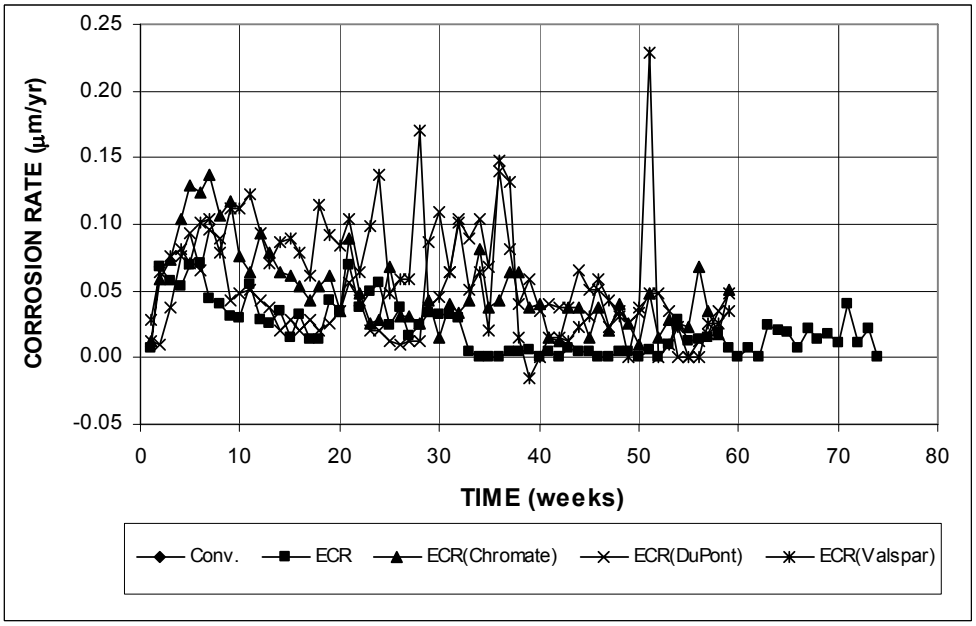

Figure 3.164 (b) – Average corrosion rates as measured in the cracked beam test for specimens with conventional steel, ECR, and high adhesion ECR bars (ECR bars have four holes).

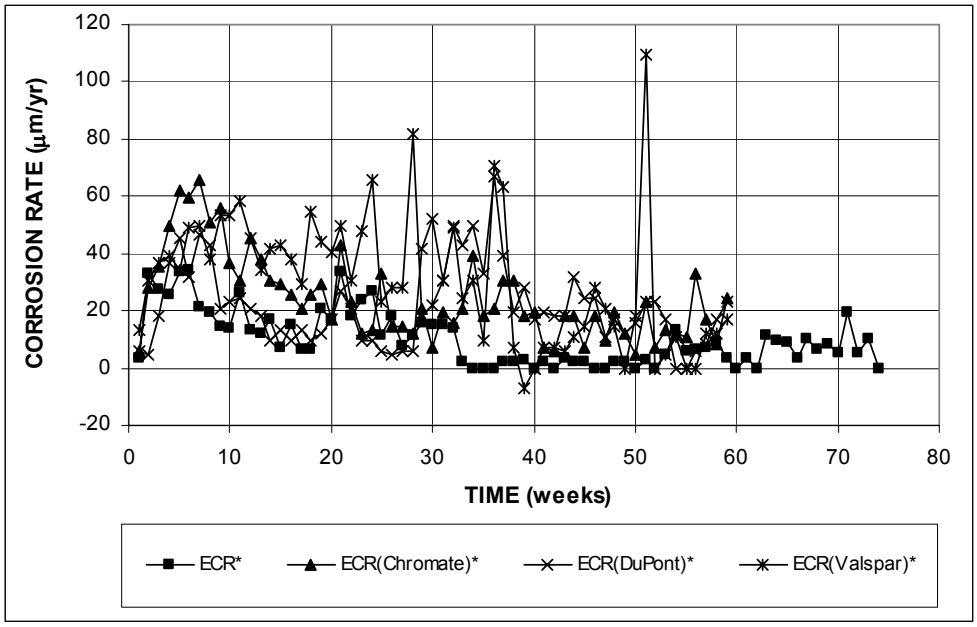

Figure 3.165 – Average corrosion rates as measured in the cracked beam test for specimens with ECR and high adhesion ECR bars. * Based on exposed area (ECR bars have four holes).

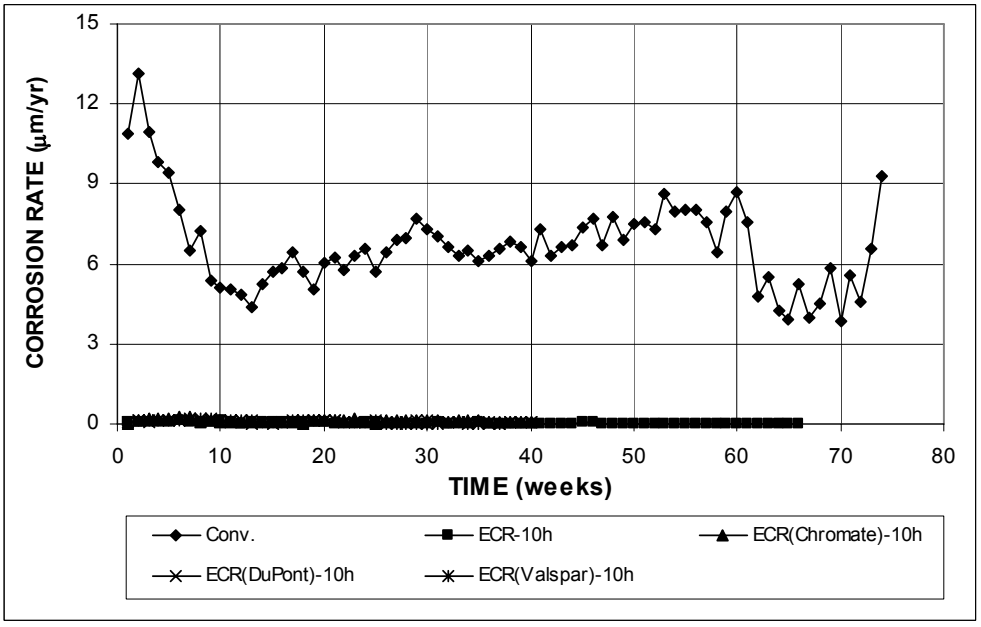

Figure 3.166 (a) – Average corrosion rates as measured in the cracked beam test for specimens with conventional steel, ECR, and high adhesion ECR bars (ECR bars have 10 holes).

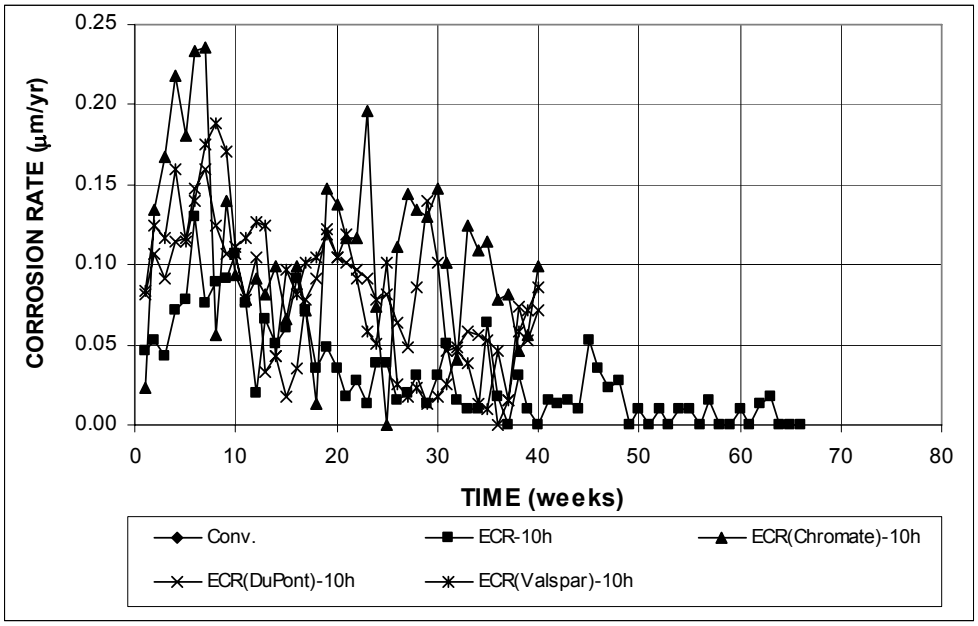

Figure 3.166 (b) – Average corrosion rates as measured in the cracked beam test for specimens with conventional steel, ECR, and high adhesion ECR bars (ECR bars have 10 holes).

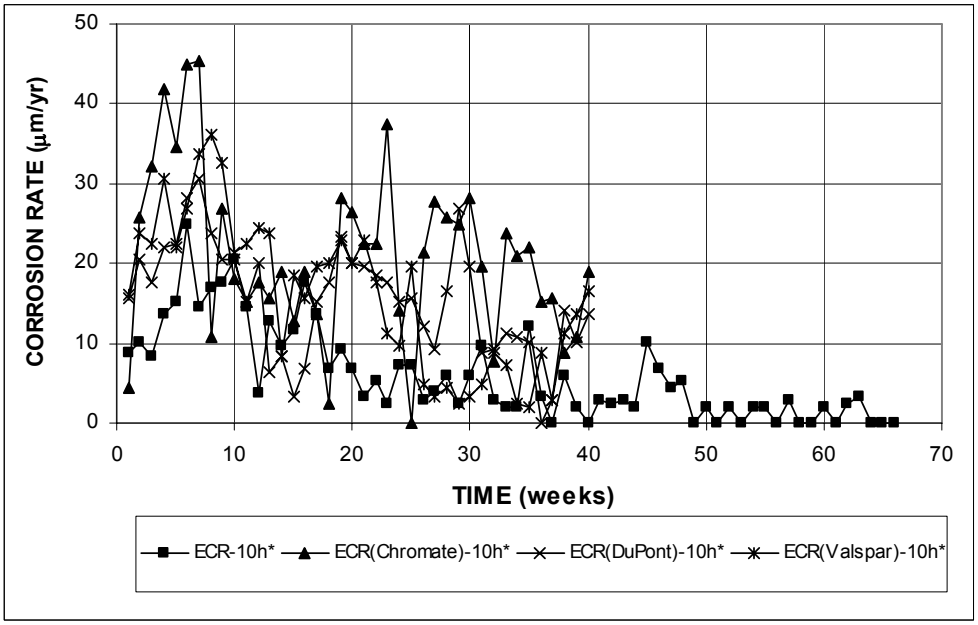

Figure 3.167 – Average corrosion rates as measured in the cracked beam test for specimens with ECR and high adhesion ECR bars. * Based on exposed area (ECR bars have 10 holes).

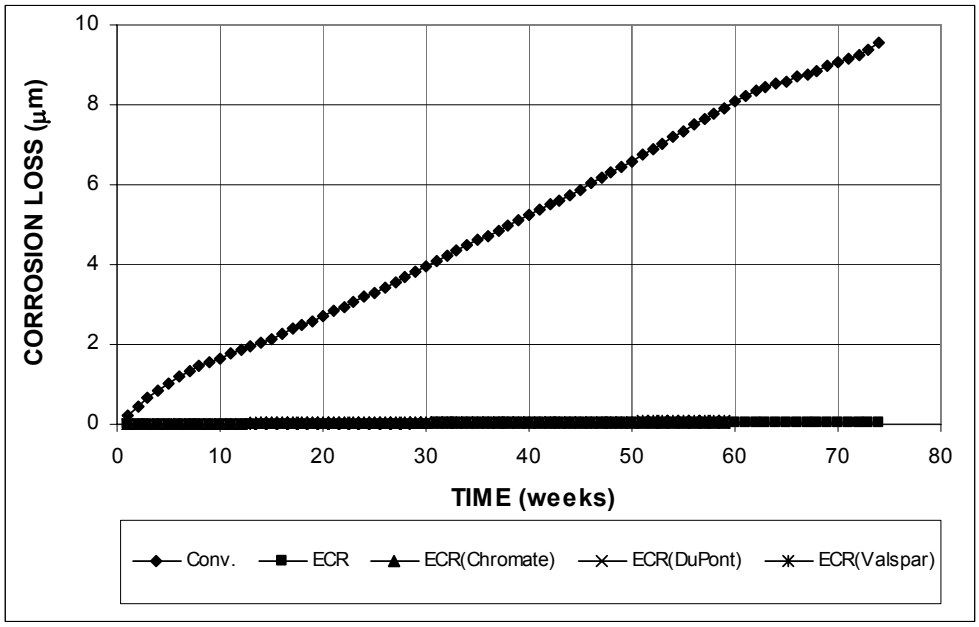

Figure 3.168 (a) – Average corrosion losses measured in the cracked beam test for specimens with conventional steel, ECR, and high adhesion ECR bars (ECR bars have four holes).

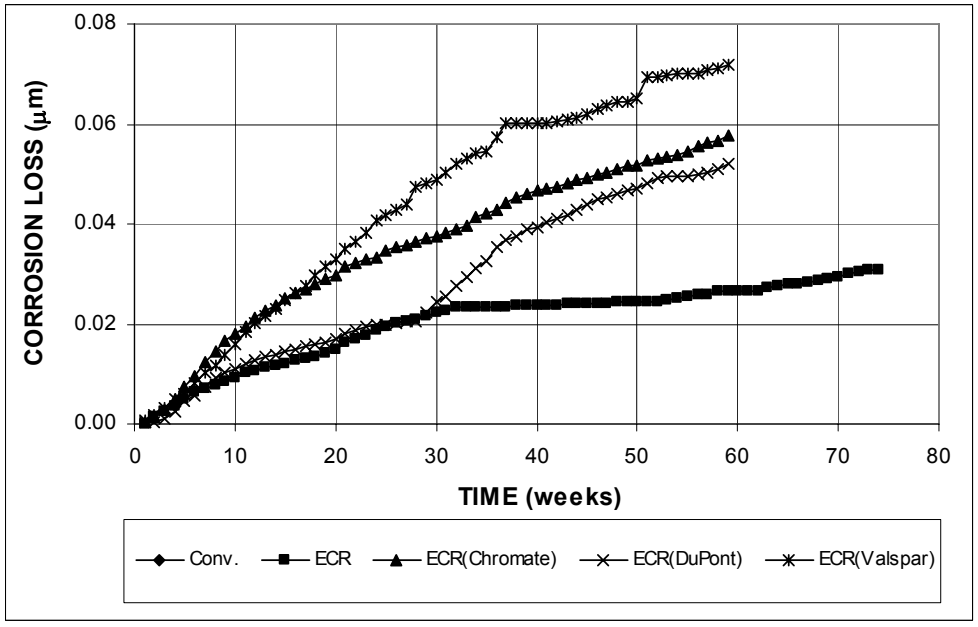

Figure 3.168 (b) – Average corrosion losses measured in the cracked beam test for specimens with conventional steel, ECR, and high adhesion ECR bars (ECR bars have four holes).

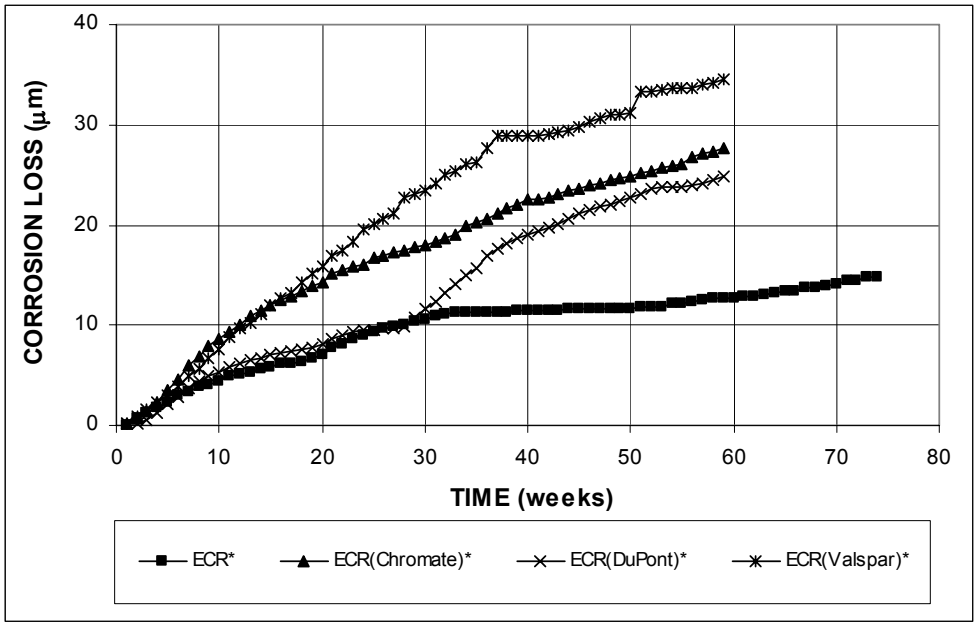

Figure 3.169 – Average corrosion losses measured in the cracked beam test for specimens with ECR and high adhesion ECR bars. * Based on exposed area (ECR bars have four holes).

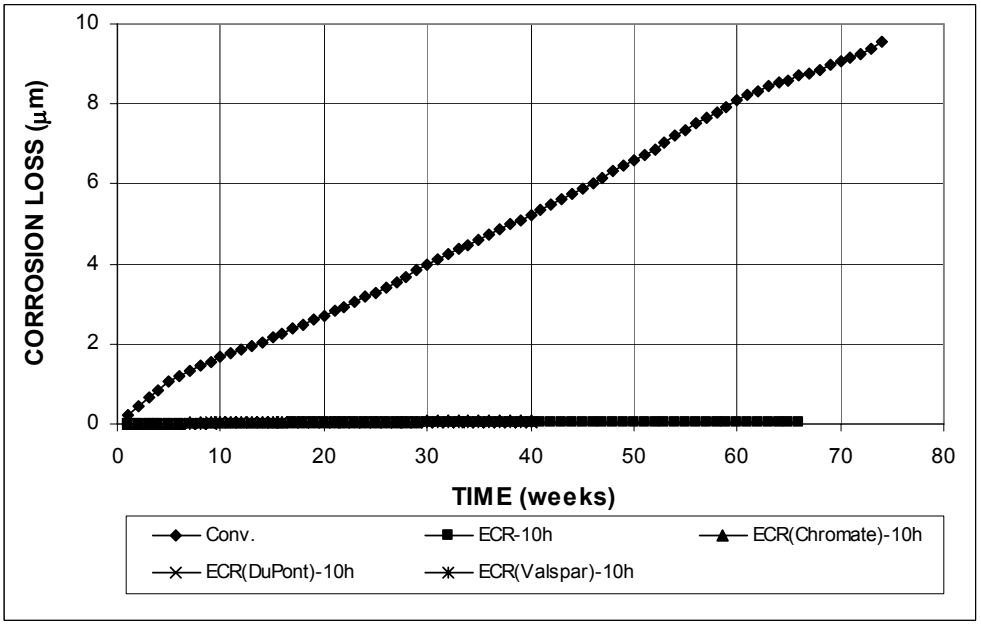

Figure 3.170 (a) – Average corrosion losses measured in the cracked beam test for specimens with conventional steel, ECR, and high adhesion ECR bars (ECR bars have 10 holes).

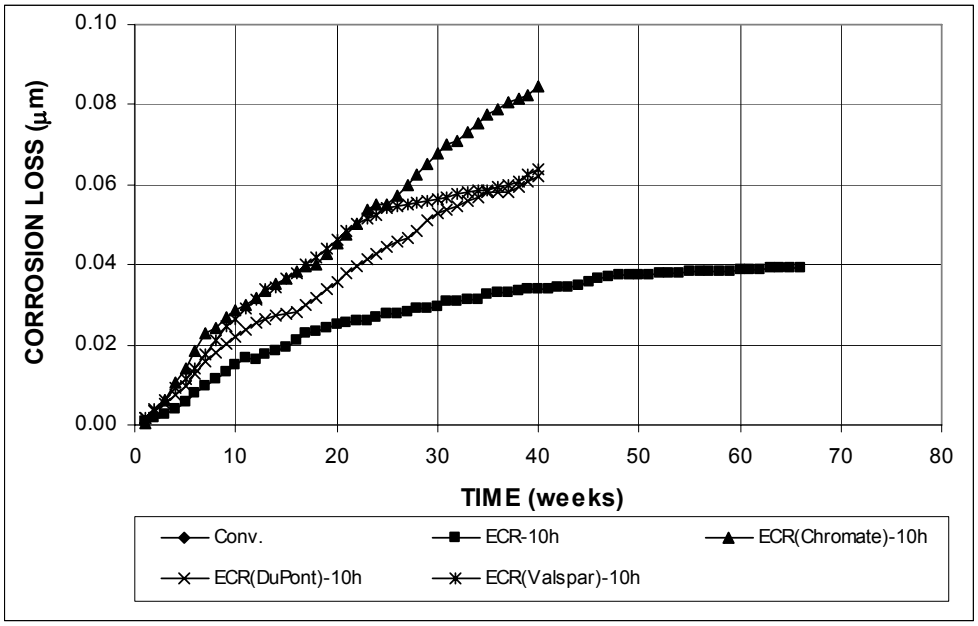

Figure 3.170 (b) – Average corrosion losses measured in the cracked beam test for specimens with conventional steel, ECR, and high adhesion ECR bars (ECR bars have 10 holes).

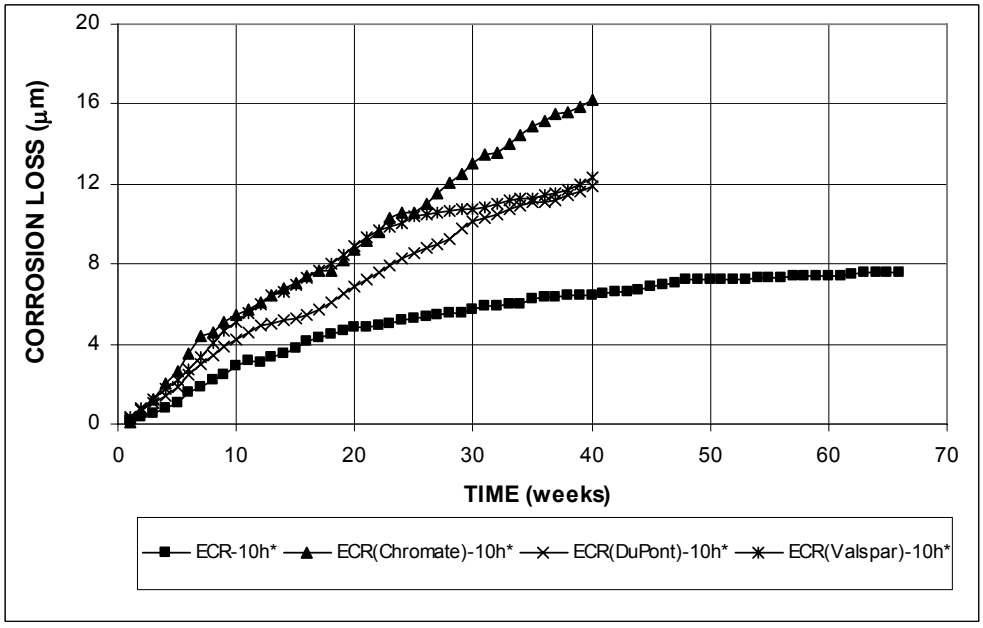

Figure 3.171 – Average corrosion losses measured in the cracked beam test for specimens with ECR and ECR high adhesion ECR bars. * Based on exposed area (ECR bars have 10 holes).

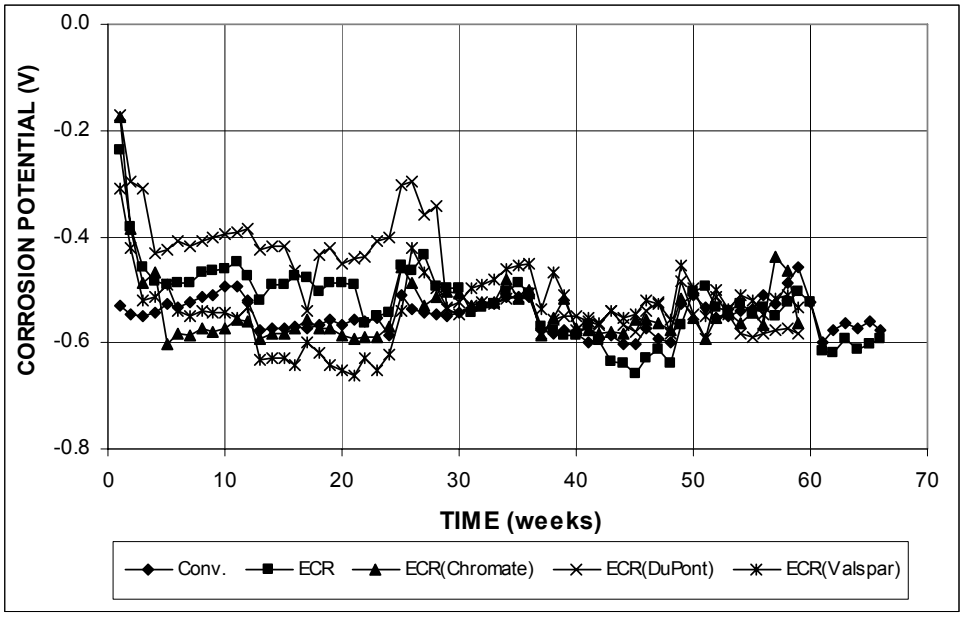

Figure 3.172 (a) – Average top mat corrosion potentials, with respect to a copper-copper sulfate electrode as measured in the cracked beam test for specimens with conventional steel, ECR, and high adhesion ECR bars (ECR bars have four holes).

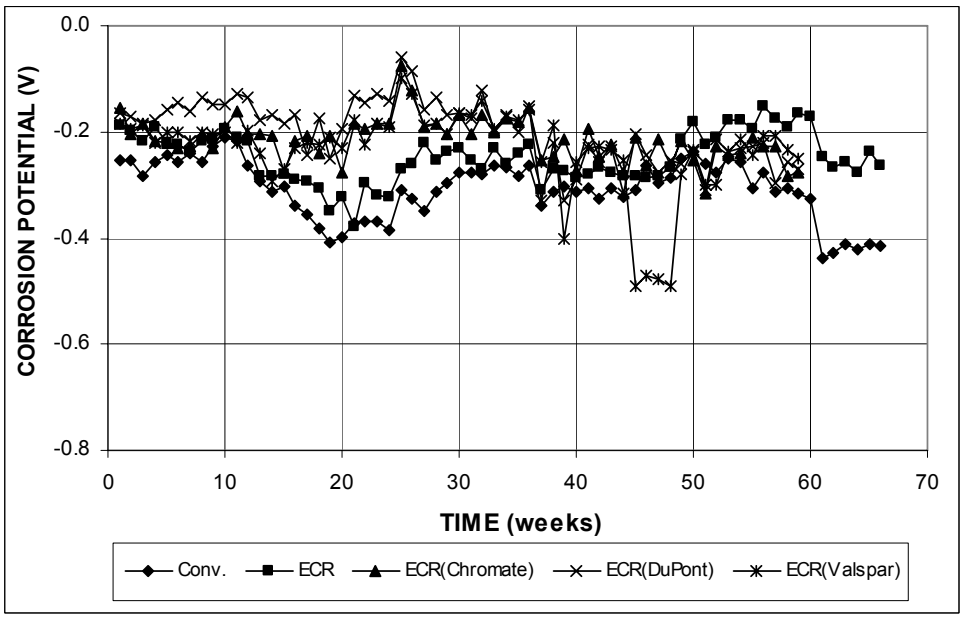

Figure 3.172 (b) – Average bottom mat corrosion potentials, with respect to a copper-copper sulfate electrode as measured in the cracked beam test for specimens with conventional steel, ECR, and high adhesion ECR bars (ECR bars have four holes).

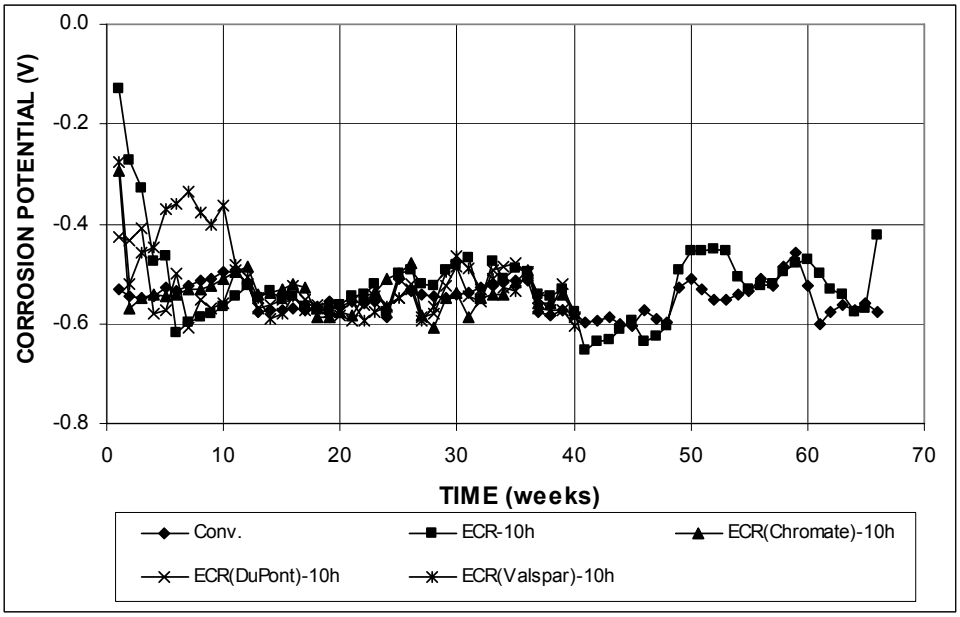

Figure 3.173 (a) – Average top mat corrosion potentials, with respect to a copper-copper sulfate electrode as measured in the cracked beam test for specimens with conventional steel, ECR, and high adhesion ECR bars (ECR bars have 10 holes).

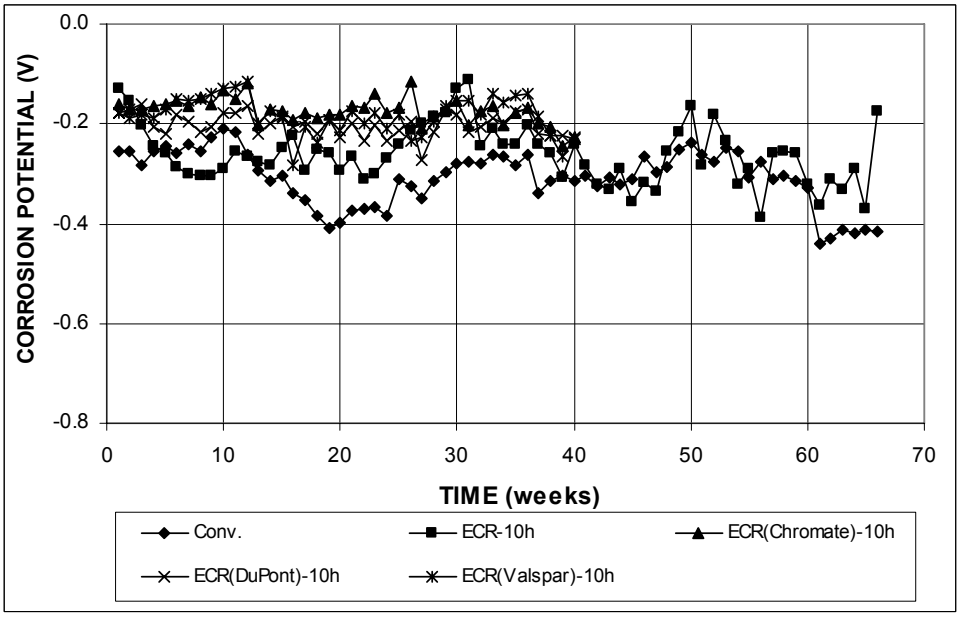

Figure 3.173 (b) – Average bottom mat corrosion potentials, with respect to a copper-copper sulfate electrode as measured in the cracked beam test for specimens with conventional steel, ECR, and high adhesion ECR bars (ECR bars have 10 holes).

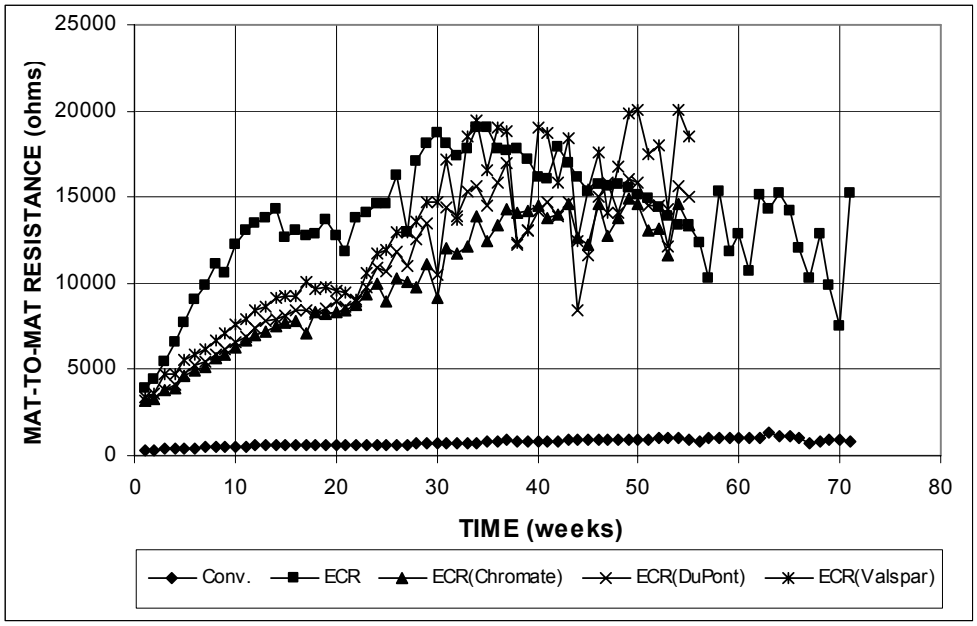

Figure 3.174 – Average mat-to-mat resistances as measured in the cracked beam test for specimens with conventional steel, ECR, and high adhesion ECR bars (ECR bars have four holes).

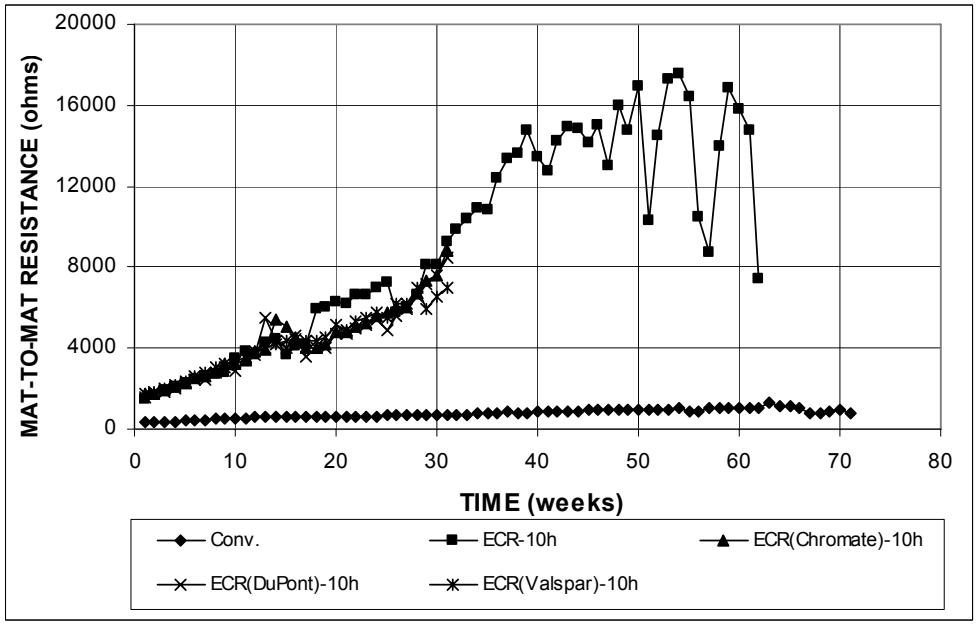

Figure 3.175 – Average mat-to-mat resistances as measured in the cracked beam test for specimens with conventional steel, ECR, and high adhesion ECR bars (ECR bars have 10 holes).

3.4.3 Field Test

This section presents the test results for specimens with high adhesion ECR bars. The coating on the epoxy-coated bars were penetrated with 16 holes.

3.4.3.1 Field Test Specimens Without Cracks

The results for the high adhesion bar specimens without simulated cracks are shown in Figures 3.176 through 3.181. The total corrosion losses at week 32 are summarized in Tables 3.24.

Figures 3.176 and 3.177 show the average corrosion rates for high adhesion ECR bars. As shown in Figure 3.176, specimens with high adhesion ECR bars had corrosion rates similar to conventional ECR. The corrosion rates were less than 0.02 and 7 μm/yr based on total area and exposed area, respectively, with the exception of ECR(DuPont) (1) and ECR(Valspar) (1). ECR(DuPont) (1) had a corrosion rate of 0.027 μm/yr at week 4 and ECR(Valspar) (1) had a corrosion rate of 0.023 μm/yr at week 16. Negative corrosion rates, between –0.003 and –0.006 μm/yr, were observed for ECR(Chromate) (2) at week 24, ECR(DuPont) (1) at week 28, and ECR(Valspar) (1) at week 32. These negative corrosion rates were not accompanied by more negative corrosion potentials at cathode than at anode and in all likelihood were aberrant readings.

The average total corrosion losses for specimens with high adhesion ECR bars are shown in Figures 3.178 and 3.179. Specimens with high adhesion ECR bars had total corrosion losses less than 0.006 μm based on total area. Table 3.24 summarizes the average total corrosion losses for high adhesion ECR bars at week 32. All specimens showed total corrosion losses less than 0.005 μm based on total area and ECR(DuPont) (2) showed no corrosion activity. Based on exposed area, the total corrosion losses were between 0 and 1.94 μm for all specimens, compared to 0.18 and

0.81 μm for conventional ECR.

Table 3.24 – Average corrosion losses (μm) at week 32 as measured in the field test for specimens with high adhesion ECR bars, without cracks

Steel Designation[a]	Test Bar				Average	Standard Deviation
	1	2	3	4		
without cracks						
ECR(Chromate) (1)	β	β			β	β
ECR(Chromate)* (1)	1.20	1.76			1.48	0.40
ECR(Chromate) (2)	β	0.00	β	0.00	β	β
ECR(Chromate)* (2)	-0.35	0.00	0.95	0.00	0.15	0.56
ECR(DuPont) (1)	β	β			β	β
ECR(DuPont)* (1)	1.06	0.84			0.95	0.15
ECR(DuPont) (2)	0.00	0.00	0.00	0.00	0.00	0.00
ECR(DuPont)* (2)	0.00	0.00	0.00	0.00	0.00	0.00
ECR(Valspar) (1)	β	0.01			β	β
ECR(Valspar)* (1)	1.55	2.32			1.94	0.55
ECR(Valspar) (2)	β	β	0.00	β	β	β
ECR(Valspar)* (2)	0.35	1.62	0.00	0.35	0.58	0.71

[a] ECR(Chromate) = ECR with the chromate pretreatment.
ECR(DuPont) = ECR with high adhesion DuPont coating.
ECR(Valspar) = ECR with high adhesion Valspar coating.

* Epoxy-coated bars, calculations based on exposed area of 16 3-mm ($^1/_8$-in.) diameter holes.

β Corrosion loss (absolute value) less than 0.005 μm.

The average corrosion potentials of the top mat and bottom mats of steel with respect to a copper-copper sulfate electrode are shown in Figure 3.180. All specimens had top mat corrosion potentials above –0.325 V, with the exception of ECR(DuPont) (1) and ECR(Chromate) (1). ECR(DuPont) (1) had a corrosion potential of –0.379 V at week 60 and ECR(Chromate) (1) exhibited corrosion potentials more negative than –0.360 V after week 56. In the bottom mat, all specimens had corrosion potentials above –0.350 V, indicating a low probability of corrosion.

Figure 3.181 shows the average mat-to-mat resistances for specimens with high adhesion ECR bars. Due to the changes in concrete moisture content, average mat-to-mat resistances for field test specimens were erratic and did not show an obvious

trend of increasing with time, as did for specimens in the bench-scale tests. These specimens exhibited average mat-to-mat resistances similar to those for conventional ECR, with values between 600 and 3,000 ohms.

3.4.3.2 Field Test Specimens With Cracks

The test results for the high adhesion bar specimens with simulated cracks are shown in Figures 3.182 through 3.187. The total corrosion losses at week 32 are summarized in Table 3.25.

Figures 3.182 and 3.183 show the average corrosion rates for high adhesion ECR bars. As shown in Figures 3.182 and 3.183, specimens with high adhesion ECR bars had corrosion rates similar to conventional ECR, with values less than 0.04 μm/yr based on total area and 12 μm/yr based on exposed area, respectively, with the exception of ECR(Valspar) (1), which spiked to 0.075 μm/yr (29.3 μm/yr based on exposed area) at week 52. ECR(DuPont) (2) had a corrosion rate of –0.002 μm/yr based on total area at week 12. This negative corrosion rate was not accompanied by more negative corrosion potentials at the cathode than at the anode and in all likelihood was an aberrant reading.

The average total corrosion losses for specimens with high adhesion ECR bars are shown in Figures 3.184 and 3.185. Based on total area, ECR(Valspar) (1) had the highest total corrosion loss at week 32, 0.01 μm, while the remaining specimens showed total corrosion losses similar to conventional ECR, with values below 0.008 μm. Table 3.25 summarizes the average total corrosion losses for high adhesion ECR bars at week 32. All high adhesion ECR bars had total corrosion losses less than 0.005 μm based on total area, with the exception of ECR(Valspar) (1), which had a total corrosion loss of 0.01 μm. Based on exposed area, total corrosion losses between 0.04 and 3.82 μm were observed for all specimens with high adhesion ECR bars,

compared to values between 0 and 1.06 μm for conventional ECR and between 0 and 1.94 μm for high adhesion specimens without cracks.

Table 3.25 – Average corrosion losses (μm) at week 32 as measured in the field test for specimens with high adhesion ECR bars, with cracks

Steel Designation[a]	Test Bar				Average	Standard Deviation
	1	2	3	4		
with cracks						
ECR(Chromate) (1)	β	β			β	β
ECR(Chromate)* (1)	1.65	-0.63			0.51	1.62
ECR(Chromate) (2)	β	0.00	β	β	β	β
ECR(Chromate)* (2)	0.35	0.00	0.77	0.42	0.39	0.32
ECR(DuPont) (1)	β	β			β	β
ECR(DuPont)* (1)	1.55	1.06			1.30	0.35
ECR(DuPont) (2)	0.00	β	0.00	β	β	β
ECR(DuPont)* (2)	0.00	0.42	0.00	-0.28	0.04	0.29
ECR(Valspar) (1)	0.01	0.01			0.01	β
ECR(Valspar)* (1)	4.82	2.82			3.82	1.42
ECR(Valspar) (2)	0.01	β	β	β	β	β
ECR(Valspar)* (2)	3.80	0.84	-0.28	1.62	1.50	1.72

[a] ECR(Chromate) = ECR with the chromate pretreatment.
ECR(DuPont) = ECR with high adhesion DuPont coating.
ECR(Valspar) = ECR with high adhesion Valspar coating.

* Epoxy-coated bars, calculations based on exposed area of 16 3-mm ($^1/_8$-in.) diameter holes.

β Corrosion loss (absolute value) less than 0.005 μm.

The average corrosion potentials of the top and bottom mats of steel with respect to a copper-copper sulfate electrode are shown in Figure 3.186. The specimens started showing active corrosion between weeks 8 and 44, with corrosion potentials of the top mat more negative than –0.350 V. In the bottom mat, all specimens had corrosion potentials above –0.330 V, with the exception of ECR(chromate) (1), which had potentials between –0.360 and –0.514 V starting week 48.

The average mat-to-mat resistances for high adhesion specimens with cracks are shown in Figure 3.187. As for specimens without cracks, high adhesion specimens with cracks exhibited erratic average mat-to-mat resistances and were similar to those for conventional ECR, with values between 600 and 2,700 ohms.

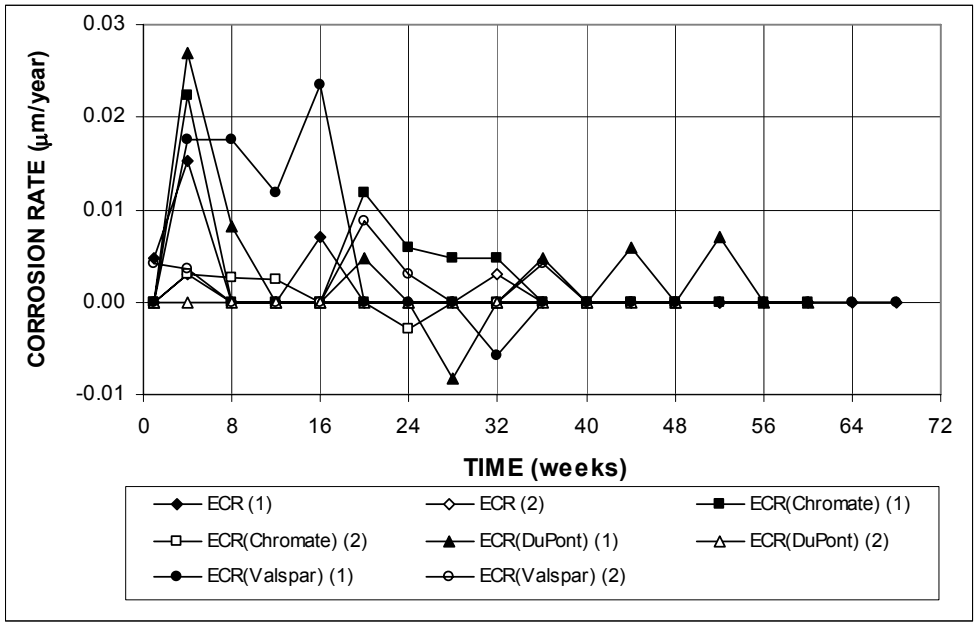

Figure 3.176 – Average corrosion rates as measured in the field test for specimens with ECR and high adhesion ECR bars, without cracks (ECR bars have 16 holes).

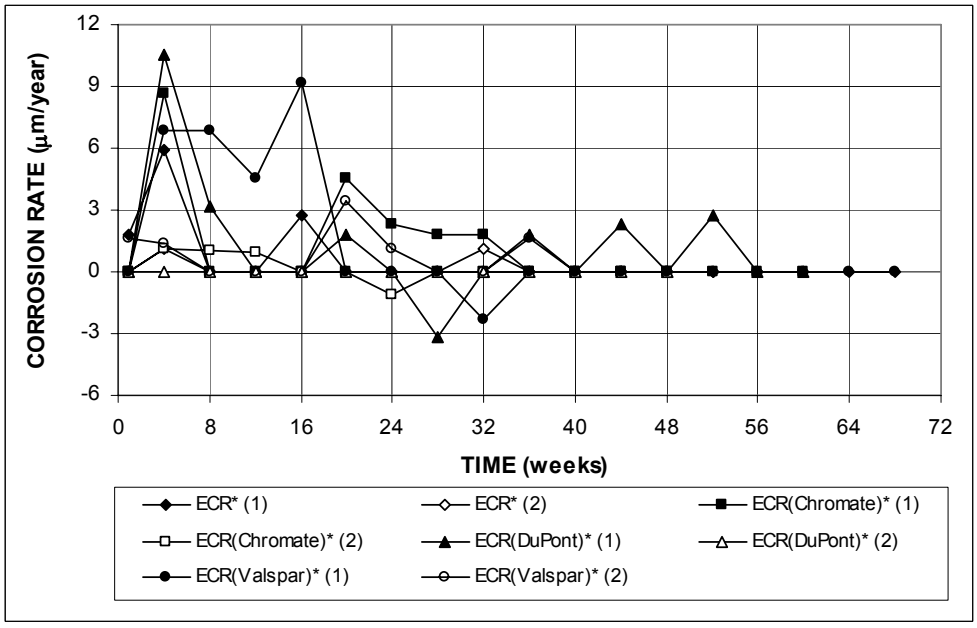

Figure 3.177 – Average corrosion rates as measured in the field test for specimens with ECR and high adhesion ECR bars, without cracks. * Based on exposed area (ECR bars have 16 holes).

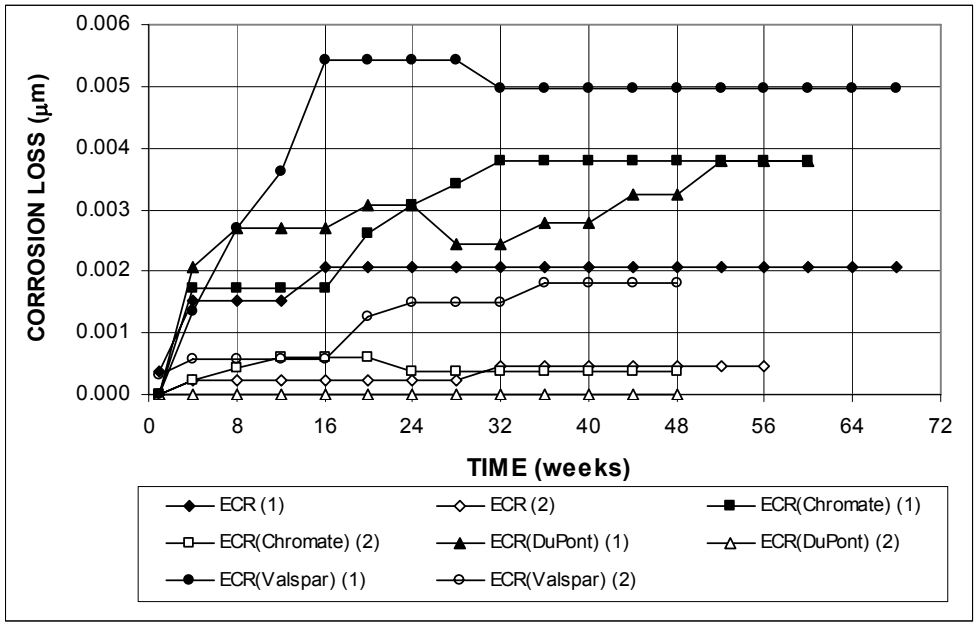

Figure 3.178 – Average corrosion losses as measured in the field test for specimens with ECR and high adhesion ECR bars, without cracks (ECR bars have 16 holes).

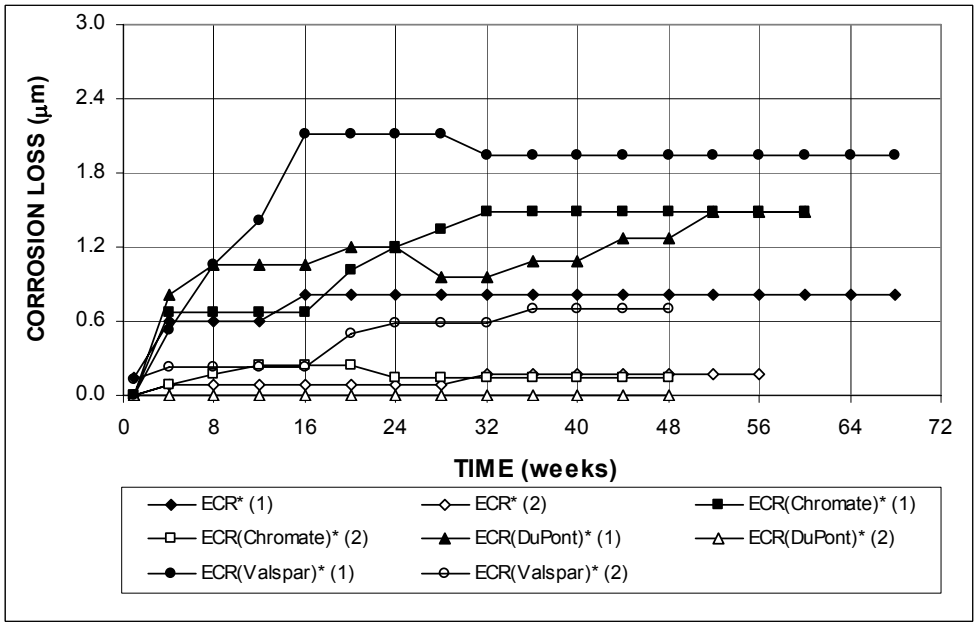

Figure 3.179 – Average corrosion losses as measured in the field test for specimens with ECR and high adhesion ECR bars, without cracks. * Based on exposed area (ECR bars have 16 holes).

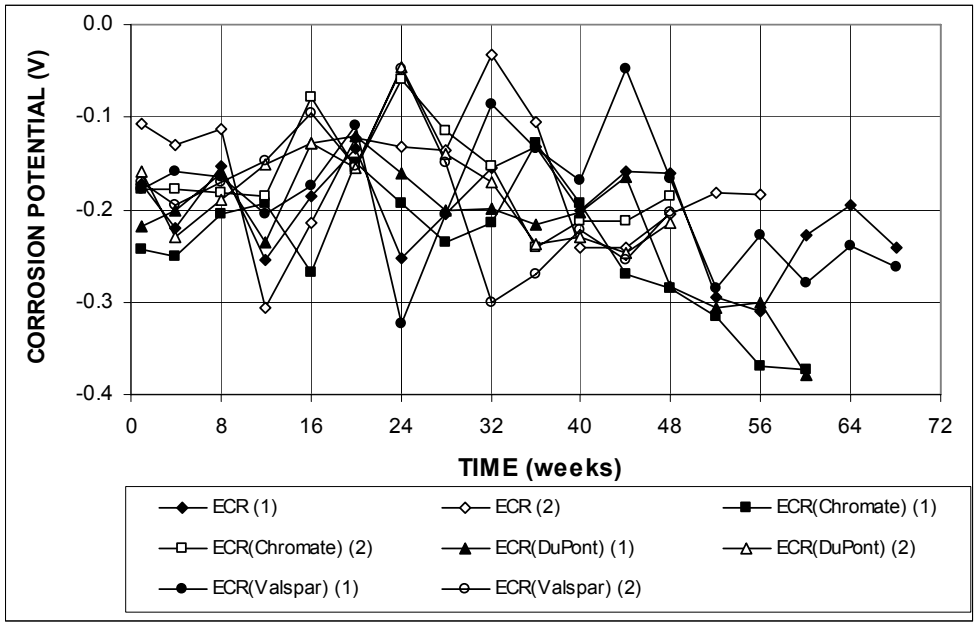

Figure 3.180 (a) – Average top mat corrosion potentials, with respect to a copper-copper sulfate electrode as measured in the field test for specimens with ECR and high adhesion ECR bars, without cracks (ECR bars have 16 holes).

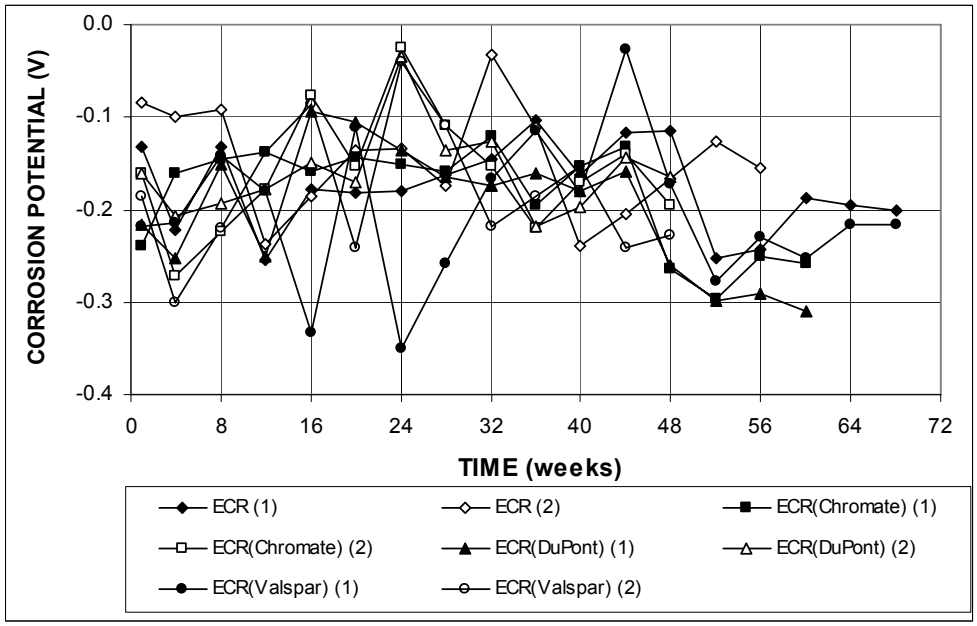

Figure 3.180 (b) – Average bottom mat corrosion potentials, with respect to a copper-copper sulfate electrode as measured in the field test for specimens with ECR and high adhesion ECR bars, without cracks (ECR bars have 16 holes).

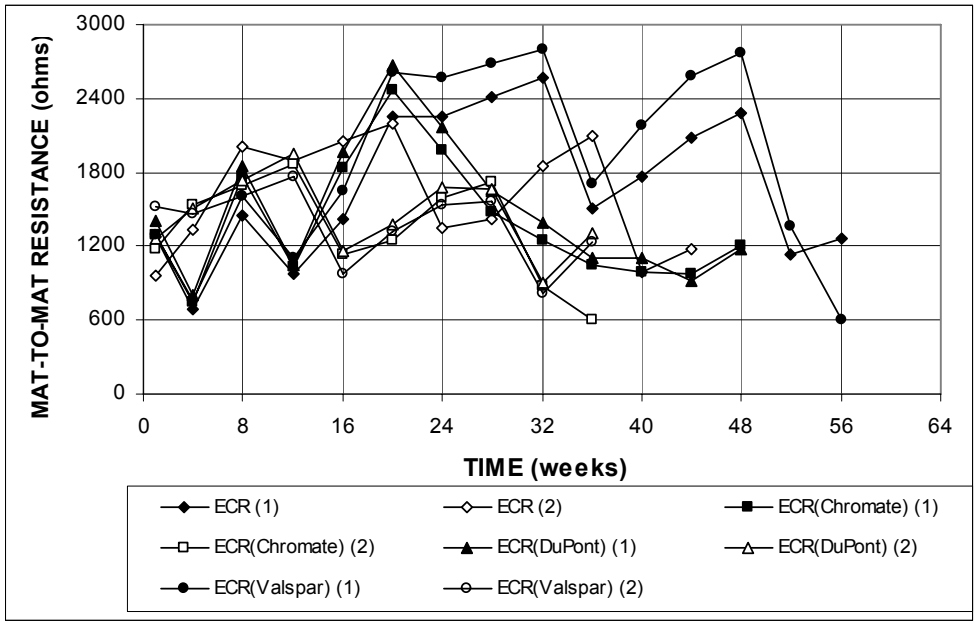

Figure 3.181 – Average mat-to-mat resistances as measured in the field test for specimens with ECR and high adhesion ECR bars, without cracks (ECR bars have 16 holes).

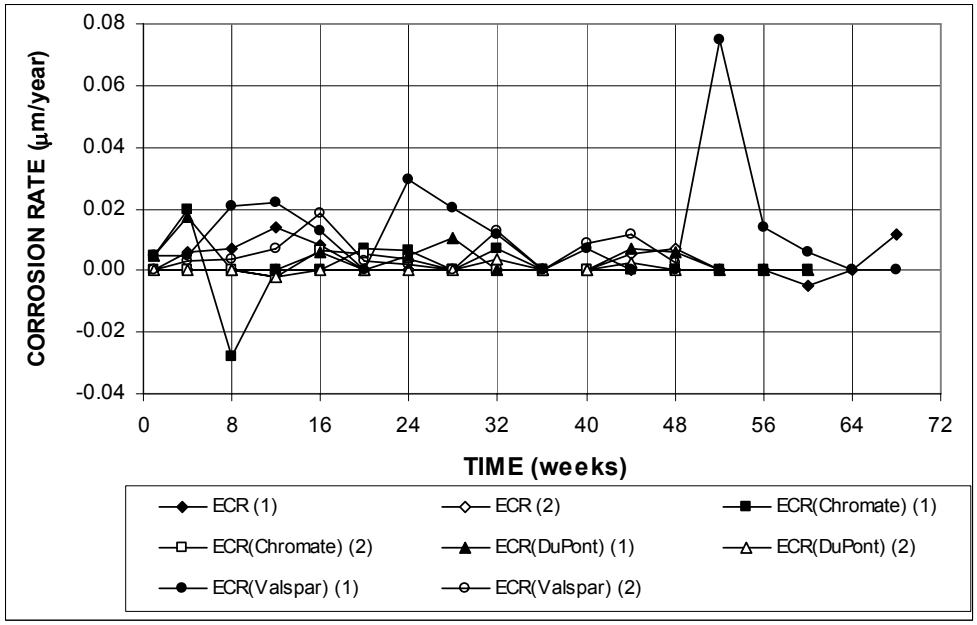

Figure 3.182 – Average corrosion rates as measured in the field test for specimens with ECR and high adhesion ECR bars, with cracks (ECR bars have 16 holes).

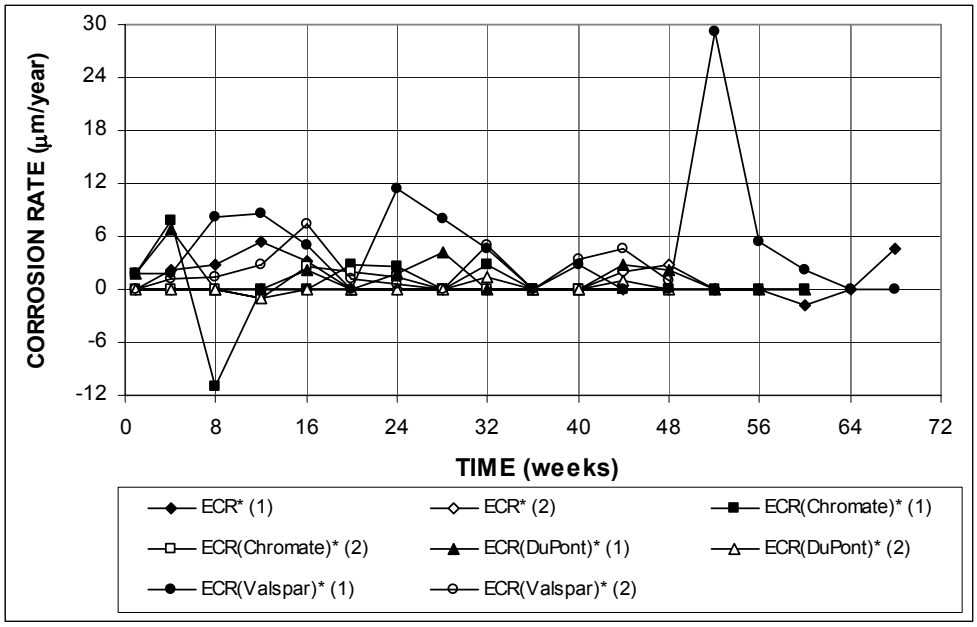

Figure 3.183 – Average corrosion rates as measured in the field test for specimens with ECR and high adhesion ECR bars, with cracks. * Based on exposed area (ECR bars have 16 holes).

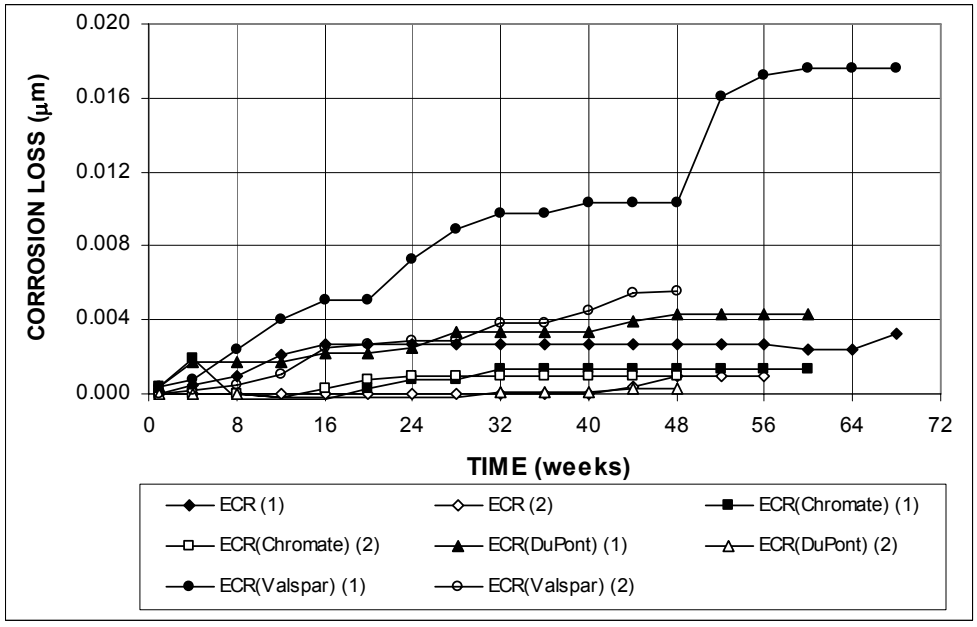

Figure 3.184 – Average corrosion losses as measured in the field test for specimens with ECR and high adhesion ECR bars, with cracks (ECR bars have 16 holes).

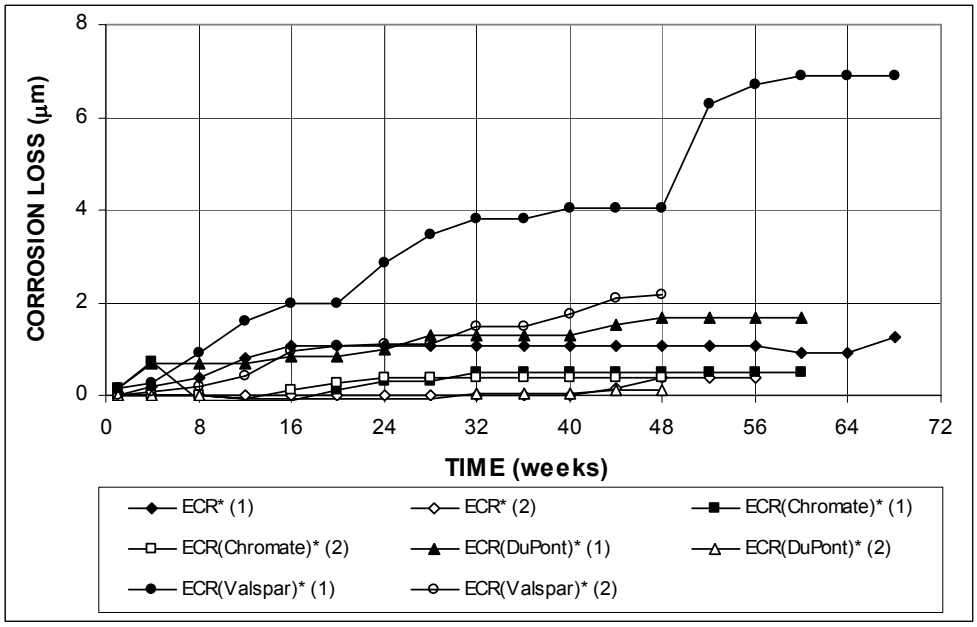

Figure 3.185 – Average corrosion losses as measured in the field test for specimens with ECR and high adhesion ECR bars, with cracks. * Based on exposed area (ECR bars have 16 holes).

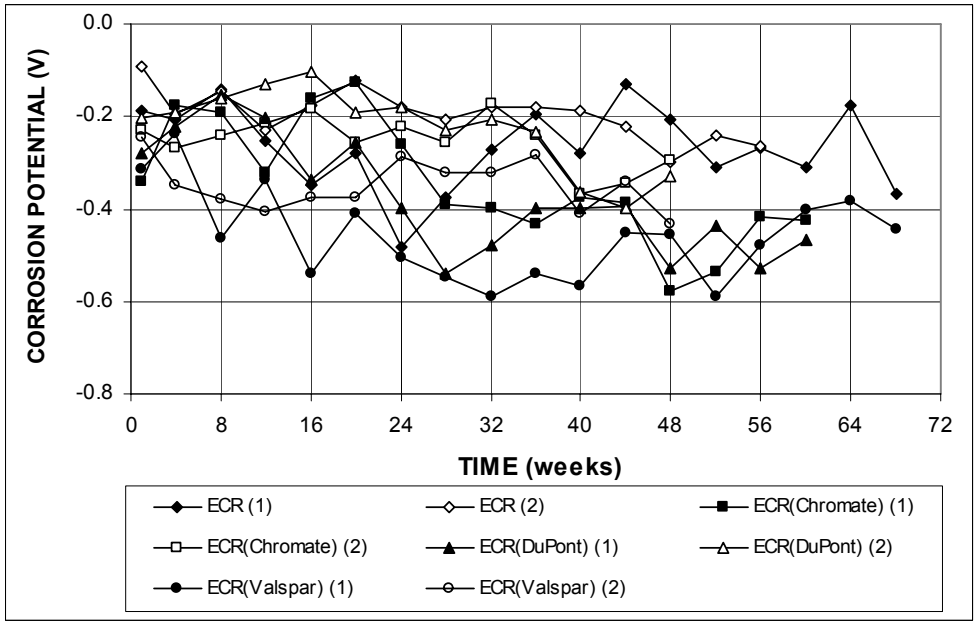

Figure 3.186 (a) – Average top mat corrosion potentials, with respect to a copper-copper sulfate electrode as measured in the field test for specimens with ECR and high adhesion ECR bars, with cracks (ECR bars have 16 holes).

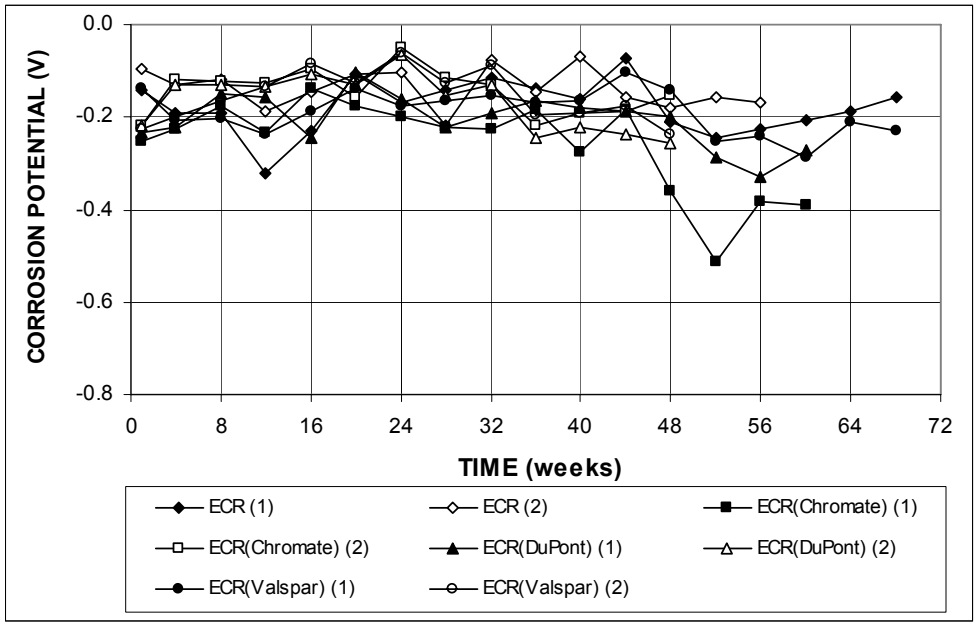

Figure 3.186 (b) – Average bottom mat corrosion potentials, with respect to a copper-copper sulfate electrode as measured in the field test for specimens with ECR and high adhesion ECR bars, with cracks (ECR bars have 16 holes).

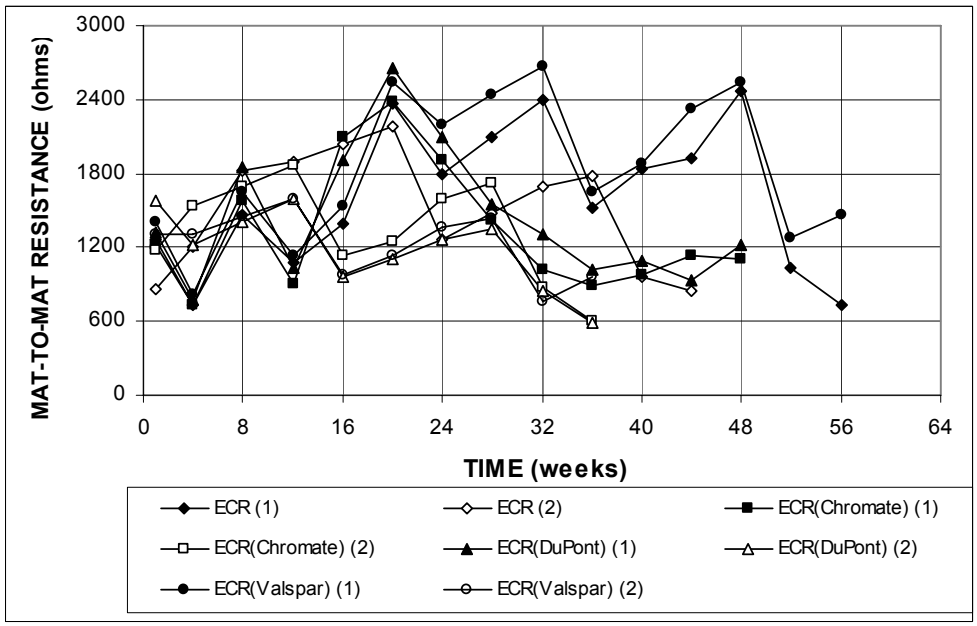

Figure 3.187 – Average mat-to-mat resistances as measured in the field test for specimens with ECR and ECR high adhesion ECR bars, with cracks (ECR bars have 16 holes).

3.5 ECR WITH INCREASED ADHESION EPOXY CAST IN MORTAR OR CONCRETE CONTAINING CALCIUM NITRITE

This section presents the results of the rapid macrocell and Southern Exposure tests for specimens containing high adhesion ECR bars cast in mortar or concrete with the corrosion inhibitor calcium nitrite (DCI-S).

3.5.1 Rapid Macrocell Test

Mortar-wrapped specimens were used in the rapid macrocell test to evaluate high adhesion ECR bars cast in mortar with the corrosion inhibitor DCI-S. The mortar had a *w/c* ratio of 0.50. The tests included six tests each of high adhesion ECR bars with four holes drilled through the epoxy.

The test results, presented in Figure 3.188 for the rapid macrocell test with mortar-wrapped specimens in 1.6 m ion NaCl and simulated concrete pore solution, are limited to corrosion potential because the three types of high adhesion ECR bars cast in mortar with DCI-S showed no corrosion activity.

The average anode and cathode corrosion potentials with respect to a saturated calomel electrode are shown in Figure 3.188. At the anodes, the most negative corrosion potentials for ECR(DuPont)-DCI and ECR(Valspar)-DCI were –0.275 V and –0.217 V, respectively, indicating a low probability of corrosion. ECR(Chromate)-DCI exhibited anode potentials between –0.275 and –0.284 V between week 12 and 15, indicating possible corrosion activity. Cathode potentials more positive than –0.250, –0.240, and –0.200 V were observed for ECR(Chromate)-DCI, ECR(DuPont)-DCI, and ECR(Valspar)-DCI, respectively, indicating a passive condition.

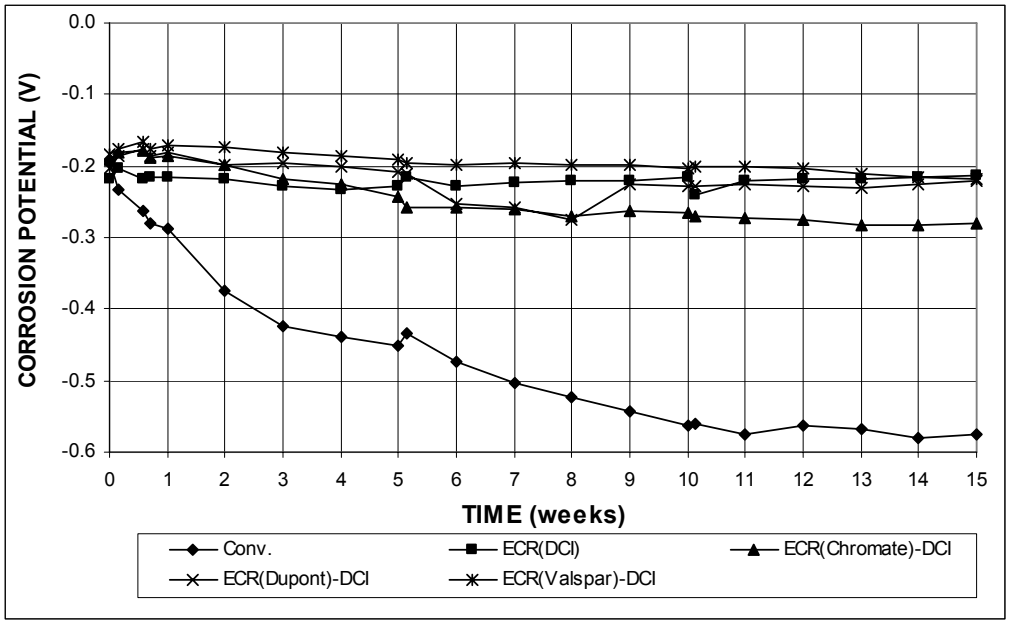

Figure 3.188 (a) – Average anode corrosion potentials, with respect to a saturated calomel electrode as measured in the rapid macrocell test for mortar-wrapped specimens with conventional steel, ECR, and high adhesion ECR bars in mortar with DCI (ECR bars have four holes).

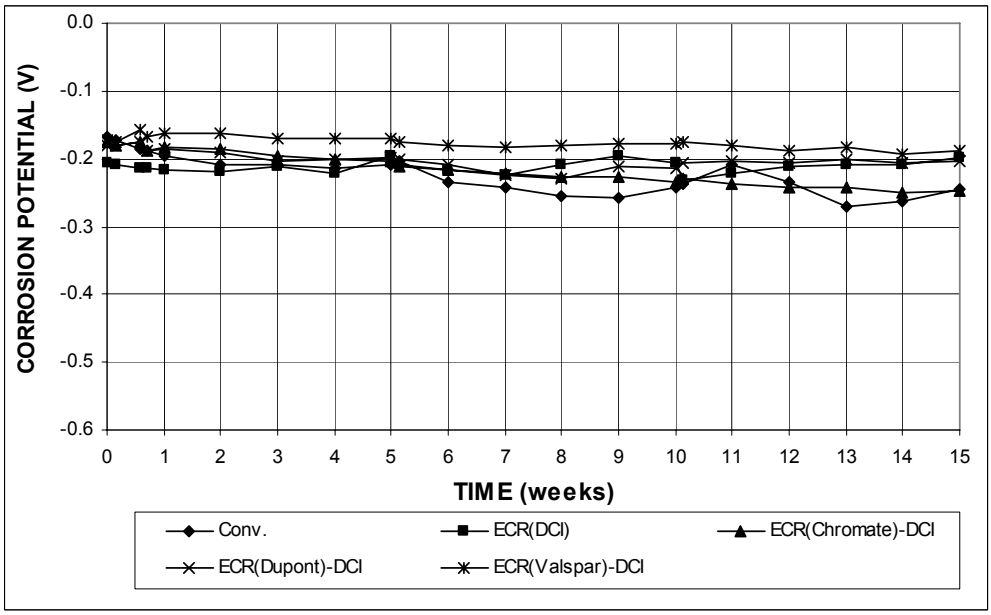

Figure 3.188 (b) – Average cathode corrosion potentials, with respect to a saturated calomel electrode as measured in the rapid macrocell test for mortar-wrapped specimens with conventional steel, ECR, and high adhesion ECR bars in mortar with DCI (ECR bars have four holes).

After 15 weeks, the mortar cover was removed and the specimens were visually inspected. No corrosion products were found at the drilled holes for any of the mortar-wrapped specimens.

3.5.2 Southern Exposure Test

The Southern Exposure test was used to evaluate high adhesion ECR bars cast in concrete with the corrosion inhibitor DCI. The tests included three tests each of ECR(Chromate), ECR(DuPont), and ECR(Valspar) bars with four holes cast in concrete with DCI.

The test results are shown in Figures 3.189 through 3.194, and the average total corrosion losses at week 40 are summarized in Table 3.26.

Figures 3.189 and 3.190 show the average corrosion rates. As shown in Figures 3.189(b) and 3.190, specimens with high adhesion ECR bars exhibited corrosion rates between –0.043 and 0.018 μm/yr based on total area and between –20.7 and 8.53 μm/yr based on exposed area. Negative corrosion rates between –0.001 and –0.043 μm/yr were observed for ECR(Chromate)-DCI at week 6 and weeks between 14 and 26, for ECR(DuPont)-DCI at weeks between 15 and 20, and for ECR(Valspar)-DCI at weeks 15, 23 and between 35 and 38. With the exception of the corrosion rates for ECR(Valspar)-DCI at weeks 15 and 23, these negative corrosion rates were accompanied by more negative corrosion potentials at cathode than at anode.

The average total corrosion losses are shown in Figures 3.191 and 3.192 for specimens with high adhesion ECR bars cast in concrete with DCI-S. Table 3.26 summarizes the total corrosion losses for these specimens at week 40. Figure 3.191(b) shows that all specimens with high adhesion ECR bars cast in concrete with DCI-S had negative total corrosion losses. All specimens showed total corrosion losses (absolute value) less than 0.005 μm based on total area, as indicated by the symbol β

in Table 3.26. Based on exposed area, the average total corrosion losses were –1.74, –0.25, –0.08 μm for ECR(Chromate)-DCI, ECR(DuPont)-DCI, and ECR(Valspar)-DCI, respectively, compared to 0.62 μm for ECR(DCI).

Table 3.26 – Average corrosion losses (μm) at week 40 as measured in the Southern Exposure test for specimens with high adhesion ECR bars in concrete with DCI-S

Steel Designation[a]	Specimen			Average	Standard Deviation
	1	2	3		
Southern Exposure Test					
ECR(Chromate)-DCI	β	β	-0.01	β	0.01
ECR(Chromate)-DCI*	0.53	-0.53	-5.21	-1.74	3.05
ECR(DuPont)-DCI	β	β	β	β	β
ECR(DuPont)-DCI*	-0.35	-0.67	0.28	-0.25	0.48
ECR(Valspar)-DCI	β	0.00	0.00	β	β
ECR(Valspar)-DCI*	-0.25	0.00	0.00	-0.08	0.14

[a] ECR(Chromate)-DCI = ECR with the chromate pretreatment in concrete with DCI.
ECR(DuPont)-DCI = ECR with high adhesion DuPont coating in concrete with DCI.
ECR(Valspar)-DCI = ECR with high adhesion Valspar coating in concrete with DCI.
All epoxy-coated bars are drilled with four 3-mm ($^1/_8$-in.) diameter holes.

* Epoxy-coated bars, calculations based on exposed area of four 3-mm ($^1/_8$-in.) diameter holes.

β Corrosion loss (absolute value) less than 0.005 mm.

The average corrosion potentials of the top and bottom mats of steel with respect to a copper-copper sulfate electrode are shown in Figure 3.193. All specimens had top mat corrosion potentials more positive than –0.310 V, with the exception of ECR(DuPont)-DCI, which had a top mat corrosion potential of –0.366 V at week 33. The bottom mat corrosion potentials for all specimens remained above –0.350 V, indicating a low probability of corrosion, as shown in Figure 3.193(b).

Figure 3.194 shows the average mat-to-mat resistances for specimens with high adhesion ECR bars cast in concrete with DCI. The average mat-to-mat resistances had values of approximately 2,100 ohms at the beginning and increased with time at a rate similar to ECR(DCI) for all specimens. As shown in Figure 3.194, these specimens had average mat-to-mat resistances between 4,900 and 6,200 ohms at week 31, compared to values between 5,600 and 6,600 ohms for high adhesion ECR bars cast in concrete without the corrosion inhibitor DCI-S.

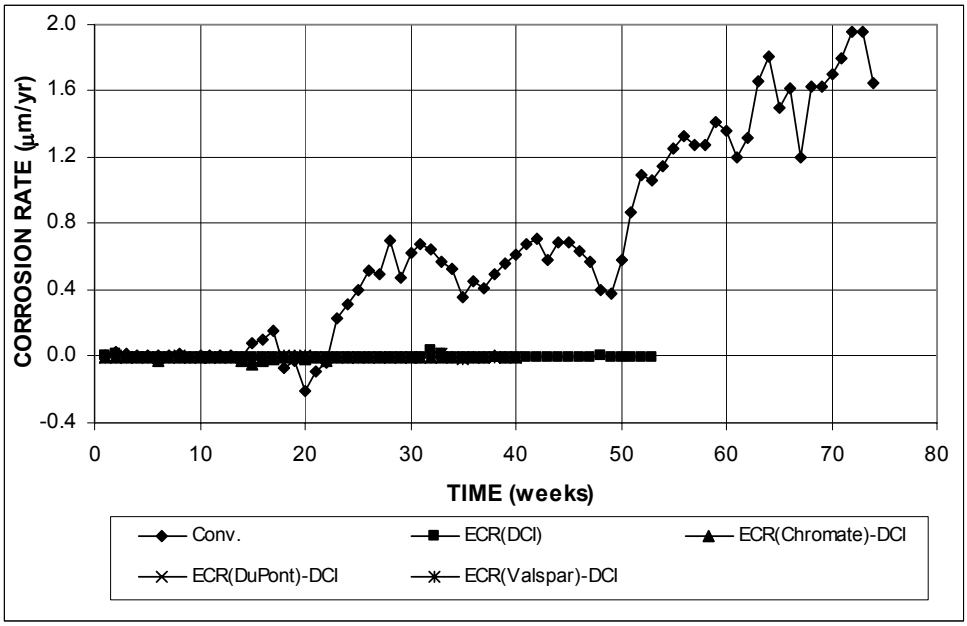

Figure 3.189 (a) – Average corrosion rates as measured in the Southern Exposure test for specimens with conventional steel, ECR, and high adhesion ECR bars in concrete with DCI-S (ECR bars have four holes).

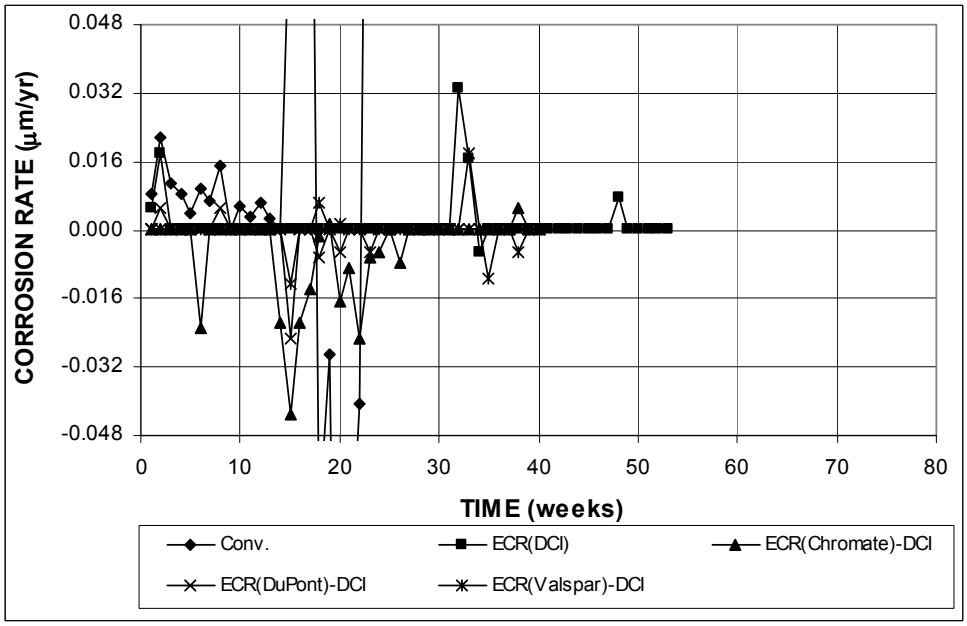

Figure 3.189 (b) – Average corrosion rates as measured in the Southern Exposure test for specimens with conventional steel, ECR, and high adhesion ECR bars in concrete with DCI-S (ECR bars have four holes).

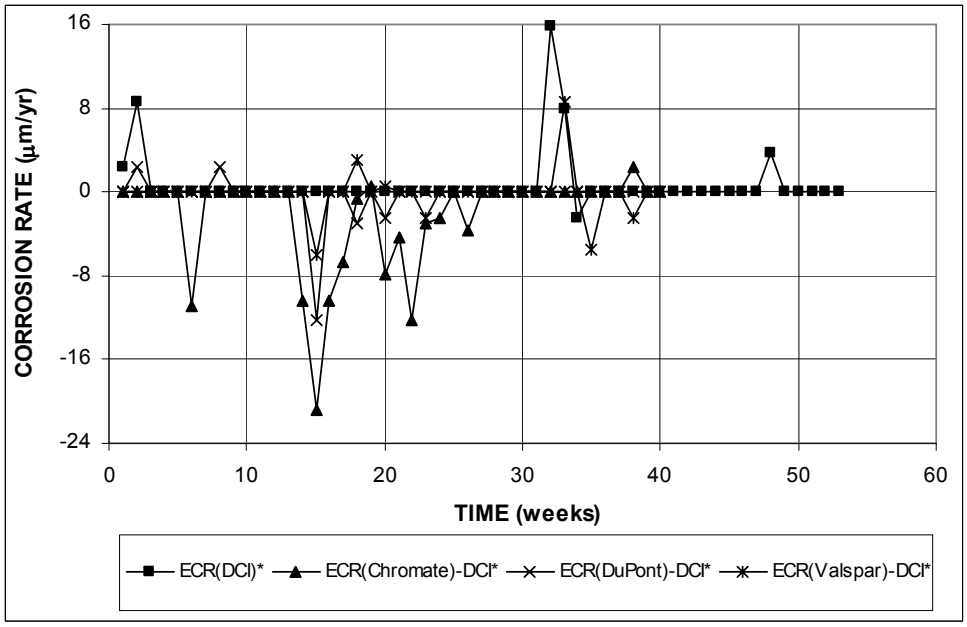

Figure 3.190 – Average corrosion rates as measured in the Southern Exposure test for specimens with ECR and high adhesion ECR bars in concrete with DCI-S. * Based on exposed area (ECR bars have four holes).

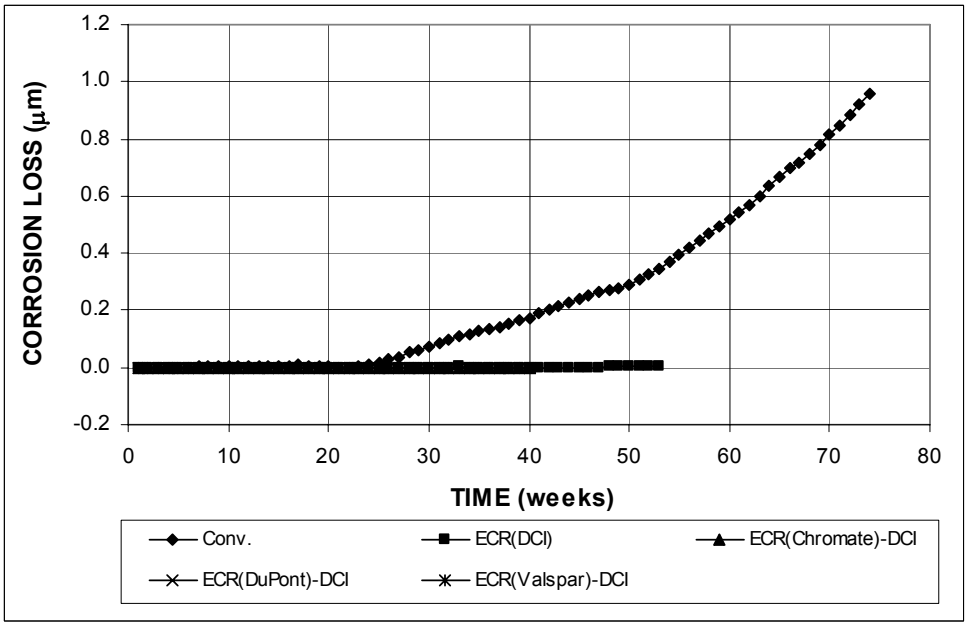

Figure 3.191 (a) – Average corrosion losses as measured in the Southern Exposure test for specimens with conventional steel, ECR, and high adhesion ECR bars in concrete with DCI-S (ECR bars have four holes).

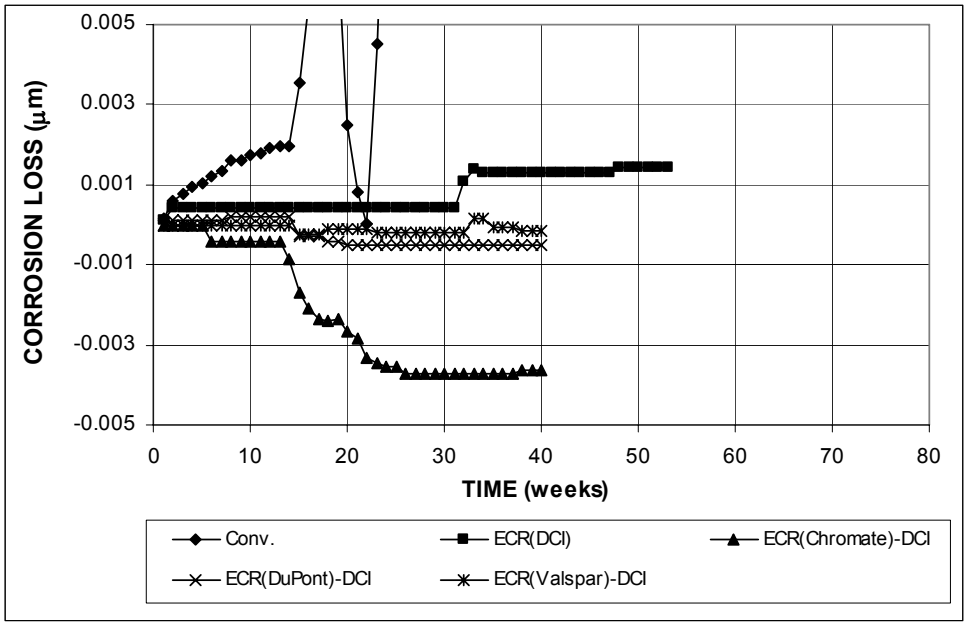

Figure 3.191 (b) – Average corrosion losses as measured in the Southern Exposure test for specimens with conventional steel, ECR, and high adhesion ECR bars in concrete with DCI-S (ECR bars have four holes).

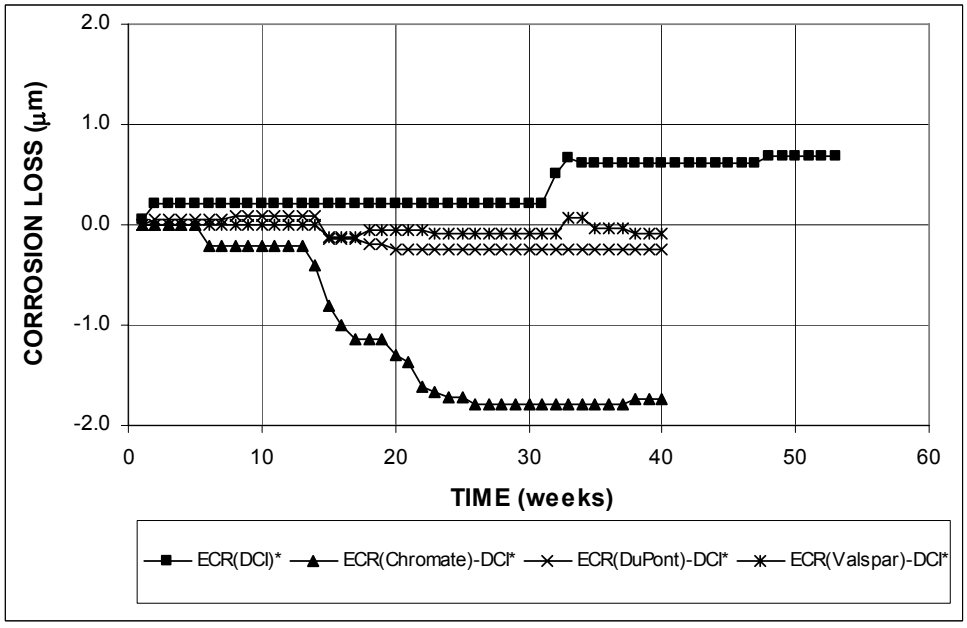

Figure 3.192 – Average corrosion losses as measured in the Southern Exposure test for specimens with ECR and high adhesion ECR bars in concrete with DCI-S. * Based on exposed area (ECR bars have four holes).

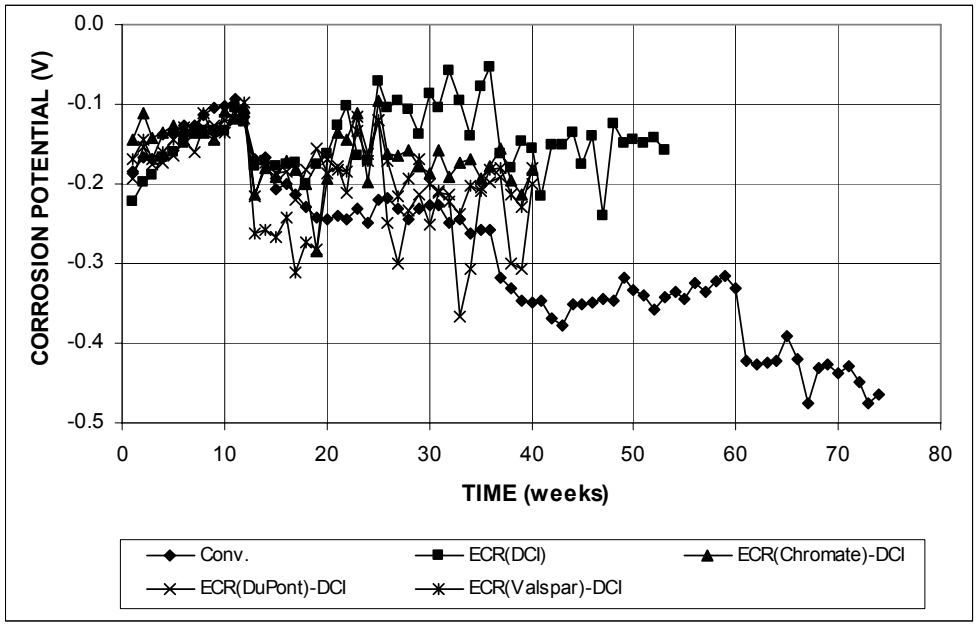

Figure 3.193 (a) – Average top mat corrosion potentials, with respect to a copper-copper sulfate electrode as measured in the Southern Exposure test for specimens with conventional steel, ECR, and high adhesion ECR bars in concrete with DCI-S (ECR bars have four holes).

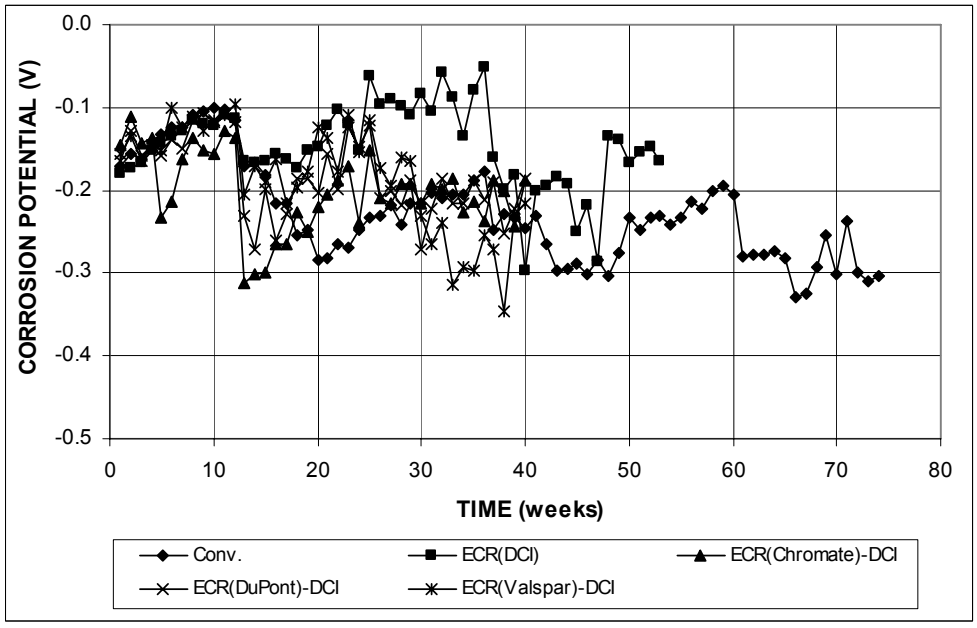

Figure 3.193 (b) – Average bottom mat corrosion potentials, with respect to a copper-copper sulfate electrode as measured in the Southern Exposure test for specimens with conventional steel, ECR, and high adhesion ECR bars in concrete with DCI-S (ECR bars have four holes).

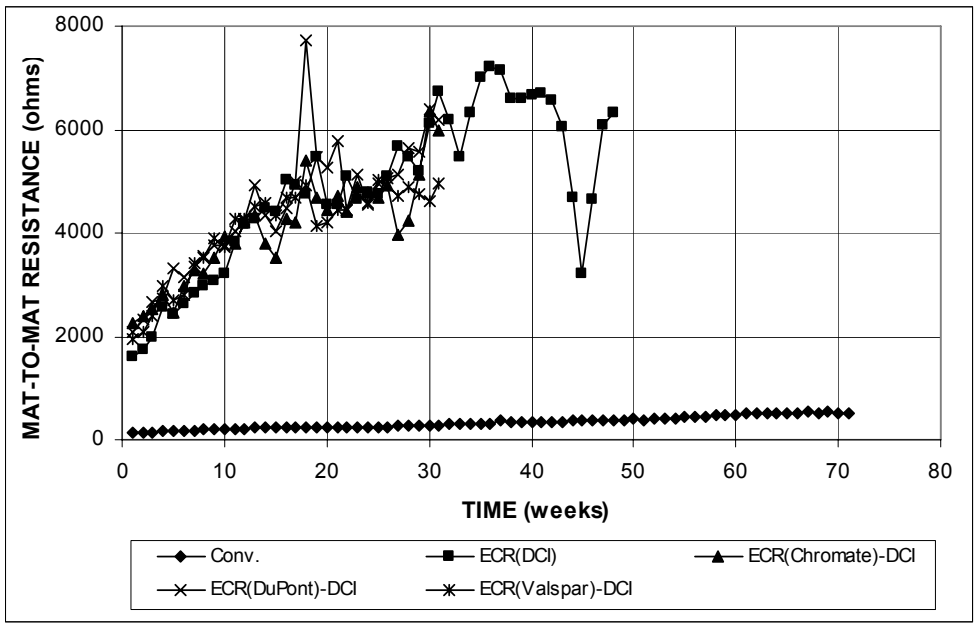

Figure 3.194 – Average mat-to-mat resistances as measured in the Southern Exposure test for specimens with conventional steel, ECR, and high adhesion ECR bars in concrete with DCI-S (ECR bars have four holes).

3.6 KDOT BRIDGE PROJECTS

This section presents the test results for the two bridges constructed with pickled 2205 stainless steel, the Doniphan County Bridge (DCB) and Mission Creek Bridge (MCB). The results include corrosion potential maps obtained at six month intervals, and the accompanying bench-scale and field tests.

For the steel used on the DCB, the pickling procedure involved blasting the bars to a near white finish with stainless steel grit and then placing them in a solution of 25% nitric acid and 3% to 6% hydrofluoric acid at 110 to 130 ºF for 40 to 50 minutes. The steel used in MCB was blast-cleaned with stainless steel shot and then cleaned in an aqueous solution containing 2 to 3% hydrofluoric acid and 7.5 to 12% sulfuric acid for 15 to 20 minutes and water-rinsed at a temperature of 105º F (maximum). The steel was then cleaned in a 10 to 12% nitric acid solution for 5 minutes and water-rinsed at room temperature.

3.6.1 Corrosion Potential Mapping

Electrical resistance between the top and bottom bars was measured and results showed that there was direct electrical contact between the top and bottom mat bars. Therefore, only corrosion potentials are measured to monitor the corrosion performance of 2205p stainless steel in both bridge decks. The corrosion potentials are recorded with respect to a copper-copper sulfate electrode.

3.6.1.1 Doniphan County Bridge

The Doniphan County Bridge (Bridge No. 7-22-18.21(004)) is located at K-7 over the Wolf River in Doniphan County, KS. The bridge is a three span continuous composite steel beam bridge with a total length of 75.8 m (249 ft). The bridge deck was replaced on February 26, 2004 due to severe corrosion problems in the old deck.

The first round of corrosion potential mapping was performed on September 17, 2004. About 1000 gallons of water were sprayed on the bridge deck to moisten concrete in the afternoon the day before the test. When concrete is dry, its resistance is high and corrosion potential readings are usually unstable, especially when a voltmeter does not have a high internal resistance. The purpose of the water is to lower the concrete resistance and obtain stable corrosion potentials. A contour of corrosion potential measurements over the DCB deck is shown in Figure 3.195. It shows that no corrosion activity can be observed on the bridge deck. Over most of the bridge deck, the corrosion potentials remained more positive than –0.150 V, indicating a passive condition. However, the corrosion potentials close to both abutments were somewhat more negative, but generally above –0.300 V, indicating a low probability of corrosion, corrosion that may have occurred on the mild steel form ties that were cast into the abutments.

On April 26, 2005, the second round of corrosion potential mapping for the DCB deck was conducted. This time, water was sprayed on the whole bridge deck about two hours before the corrosion potential measurements, rather than the day before. The corrosion potentials were much more stable than those obtained in the first round on September 17, 2004. The contour of corrosion potential measurements over the DCB deck is shown in Figure 3.196. Once again, the corrosion potential mapping shows that no corrosion activity is occurring in the bridge deck. For the majority of the deck surface, the corrosion potentials were more positive than –0.150 V, except for two small regions in the westbound (north) lane. In these two regions, the corrosion potentials were between –0.150 and –0.250 V. Similar to the first round of corrosion potential measurements, the test points close to both abutments had more negative corrosion potentials, but generally more positive than –0.300 V.

The third round of corrosion potential measurements was performed on October 14, 2005 using the same wetting procedures for the April 26, 2005 readings. The contour of corrosion potential measurements is shown in Figure 3.197. The corrosion potentials for the majority of the deck surface, shown in Figure 3.197, were above –0.200 V, indicating a high probability of no corrosion activity. The regions close to both abutments, however, showed more negative corrosion potentials. The west abutment region had corrosion potentials between –0.250 and –0.350 V. The corrosion potentials at the east abutment were more negative than –0.400 V, indicating active corrosion. This may be, as noted earlier, due to the use of mild steel form ties that were cast into both abutments, as shown in Figure 3.201 at the east abutment for the Mission Creek Bridge.

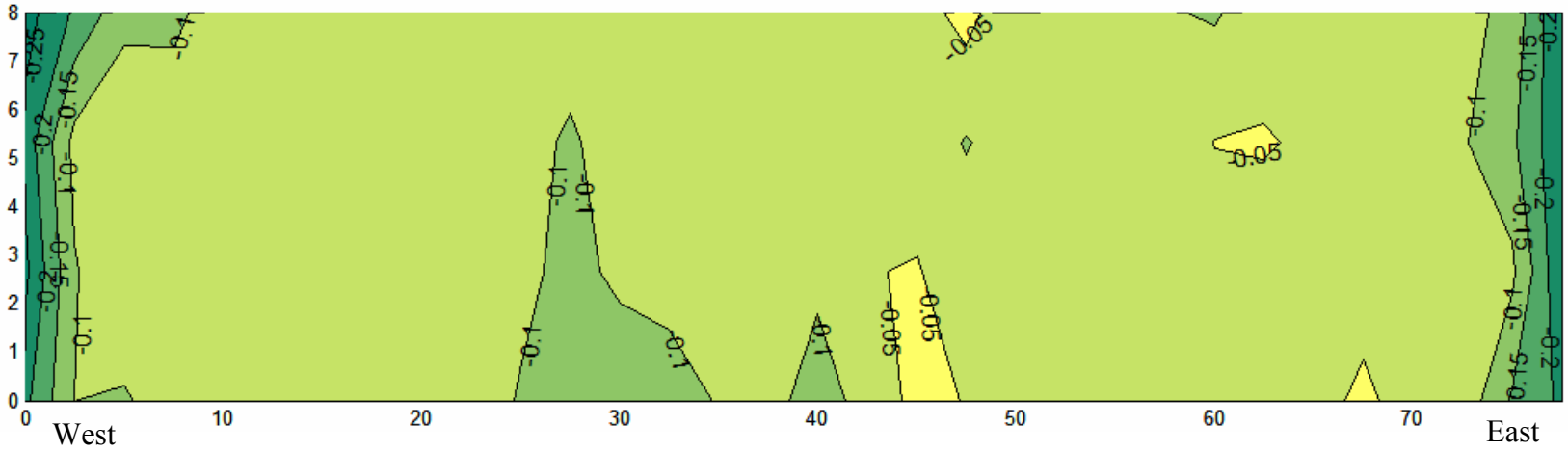

Figure 3.195 – Corrosion potential map for the Doniphan County Bridge (Sept. 17, 2004)

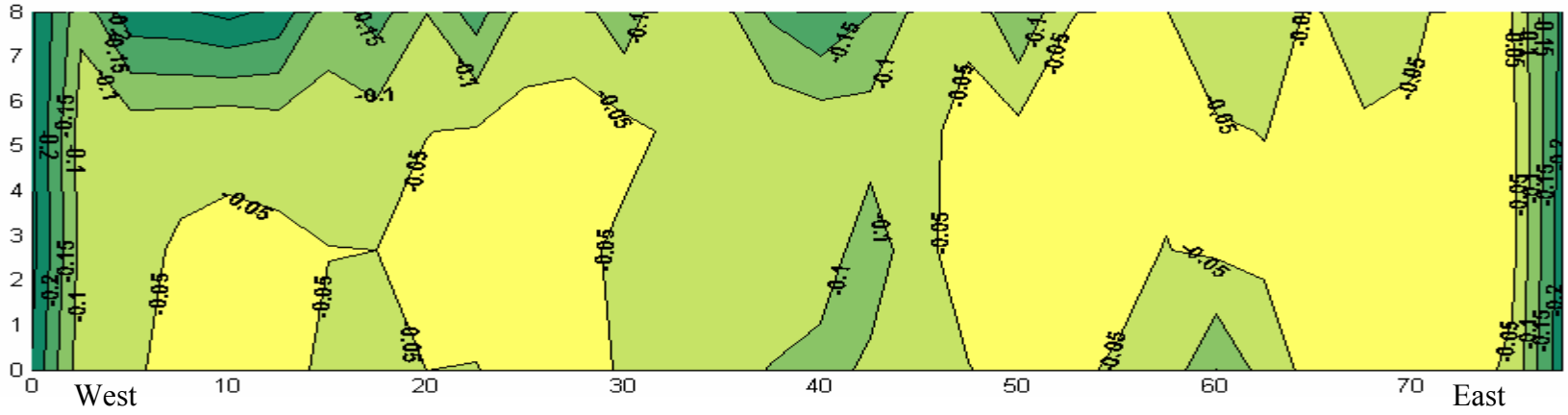

Figure 3.196 – Corrosion potential map for the Doniphan County Bridge (April 26, 2005)

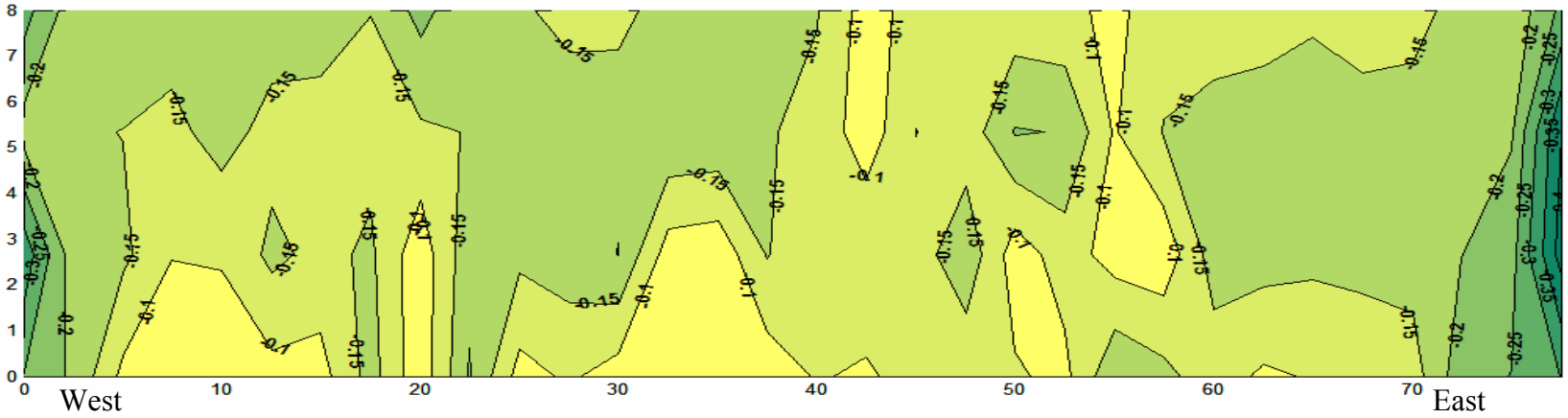

Figure 3.197 – Corrosion potential map for the Doniphan County Bridge (October 14, 2005)

3.6.1.2 Mission Creek Bridge

The Mission Creek Bridge (Bridge No. 4-89-4.58(281)) is located on K-4 over Mission Creek in Shawnee County, KS. The bridge is a single-span composite steel beam bridge with a total length of 27.45 m (90 ft). The bridge deck was cast on August 25, 2004.

The first round of corrosion potential measurements was performed on September 1, 2004, immediately after the seven-day wet curing of the new bridge deck. A contour of corrosion potential measurements for the MCB deck is shown in Figure 3.198. Due to the high temperature and strong wind, the bridge deck was very dry. A wet sponge was used to take the corrosion potentials, but it was still very hard to get stable readings. As a result, the corrosion potentials varied greatly over a small area, as shown in Figure 3.198. The corrosion potential map, however, shows that no corrosion activity is observed for the deck. All of the corrosion potentials were above –0.300 V, indicating a low probability of corrosion.

The second round of corrosion potential measurements for the MCB deck was conducted on April 1, 2005. About 500 gallons of water were sprayed on the bridge deck two hours before the test. The deck surface remained wet during the test and very stable corrosion potential readings were obtained. Figure 3.199 shows the contour map of corrosion potential measurements. For the majority of the deck surface, the corrosion potentials were more positive than –0.150 V, indicating a high probability of no corrosion activity. The west abutment region had corrosion potentials around –0.300 V, indicating a low probability of corrosion activity. The East abutment region, however, had corrosion potentials more negative than –0.350 V, indicating active corrosion.

On September 27, 2005, the third round of corrosion potential measurements was obtained for the MCB deck. Figure 3.200 shows the corrosion potential map.

Overall, corrosion potentials remained above –0.150 V for the middle section of the bridge deck, indicating a passive condition. The regions close to both abutments, however, had readings more negative than –0.400 V, indicating active corrosion. As with the DCB deck, the more negative corrosion potentials at both abutments may have been caused by corrosion of the mild steel form ties shown in Figure 3.201.

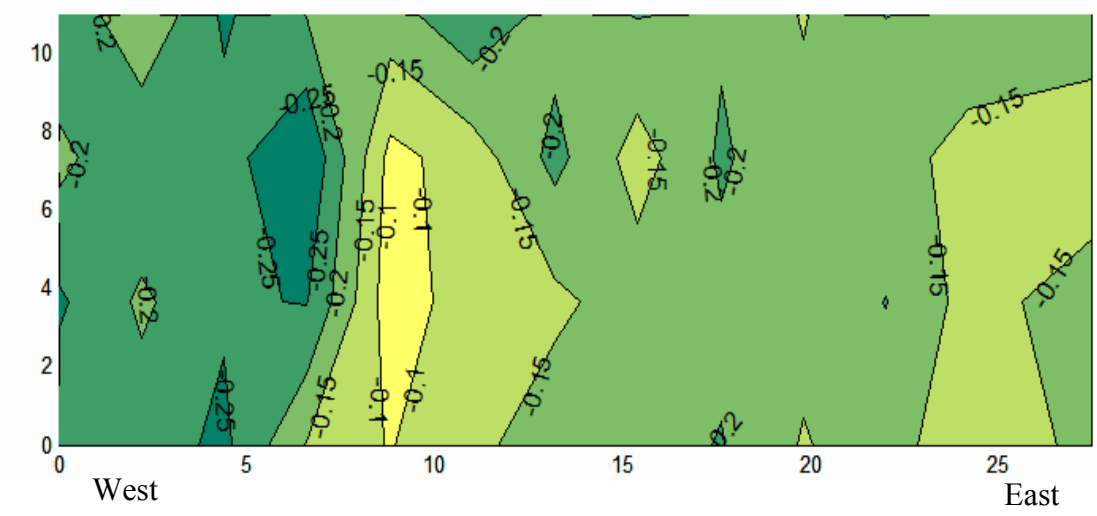

Figure 3.198 – Corrosion potential map for the Mission Creek Bridge (Sept. 1, 2004)

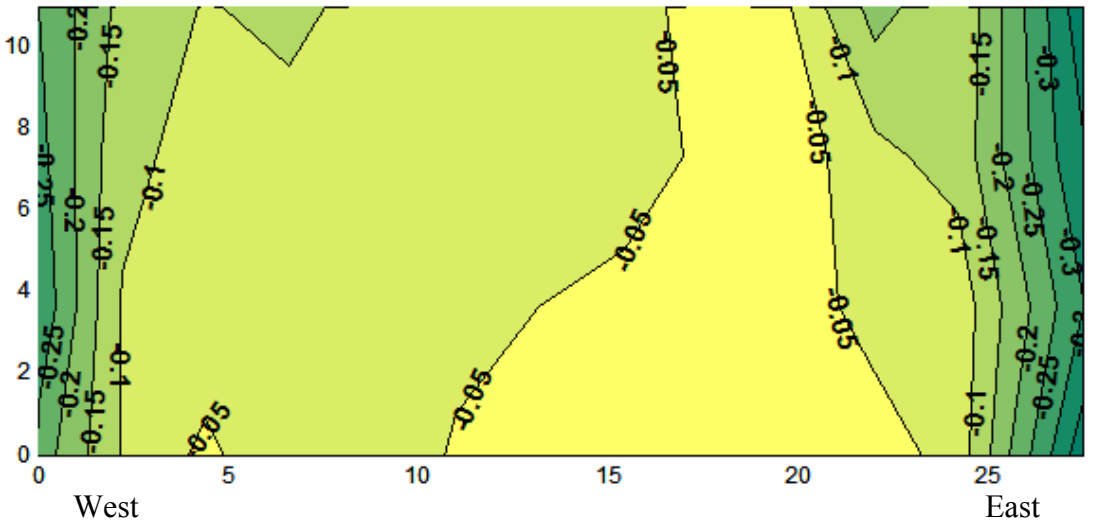

Figure 3.199 – Corrosion potential map for the Mission Creek Bridge (April 1, 2005)

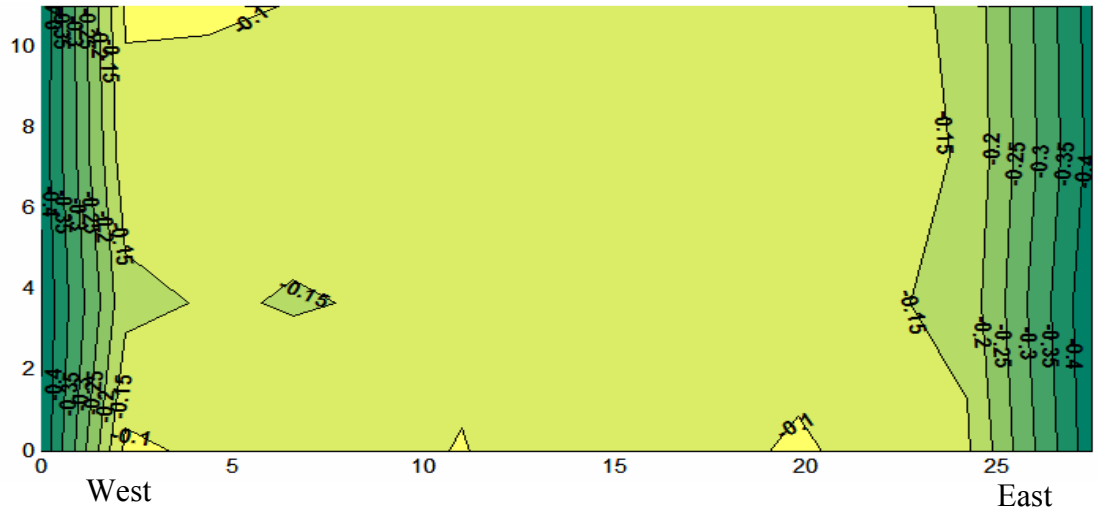

Figure 3.200 – Corrosion potential map for the Mission Creek Bridge (Sept. 27, 2005)

Figure 3.201 – Reinforcing bar cage at the east abutment for the Mission Creek Bridge

3.6.2 Bench-Scale Tests

Accompanying bench-scale and field test specimens were fabricated for the two bridges. This section presents the results of the Southern Exposure and cracked beam test specimens with 2205p stainless steel. The results of the field test specimens with conventional steel, 2205p stainless steel, and epoxy-coated reinforcement are reported in Section 3.6.3.

The specimens were fabricated using concrete in a trial batch for the two bridges. The concrete properties are presented in Chapter 2.

3.6.2.1 Southern Exposure Test

The test results are presented in Figures 3.202 through 3.205 for specimens in the Southern Exposure test, and the total corrosion losses at week 57 are summarized in Table 3.27. Figure 3.202 shows the average corrosion rates and Figure 3.203 shows the average total corrosion losses for specimens with 2205p stainless steel for both bridges. As shown in Figure 3.202, specimens with 2205p stainless steel had corrosion rates between –0.036 and 0.017 μm/yr for the DCB and between –0.041 and 0.027 μm/yr for the MCB. Negative corrosion rates were observed for specimens with 2205p stainless steel for both bridges. The negative corrosion rates observed for both specimens were sometimes accompanied by more negative corrosion potentials at cathode than at anode, but sometimes were not. As shown in Figure 3.203, DCB-2205p exhibited progressive total corrosion losses during the first 34 weeks and then showed little corrosion between weeks 34 and 60. After week 60, the total corrosion losses for DCB-2205p decreased with time, indicating that negative corrosion rates were occurring. MCB-2205p showed progressive corrosion losses during the first 8 weeks and then had total corrosion losses decreasing with time. As shown in Table 3.27, the total corrosion losses at week 57 were approximately 0.003 and –0.002 μm

(indicated by the symbol β) for DCB-2205p and MCB-2205p, respectively, compared to 0.51 μm for conventional steel at the same week. DCB-2205p, however, had a negative total corrosion loss after week 67. These results are in agreement with the test results from a previous study by Balma et al. (2005) in which 2205p stainless steel was evaluated in the Southern Exposure test as well. In that study, a total corrosion loss of approximately 0.01 μm was obtained at week 57.

Table 3.27 – Average corrosion losses (μm) as measured in the Southern Exposure test for specimens with 2205 pickled stainless steel for the DCB and MCB.

Steel Designation[a]	Age (weeks)	Specimen						Average	Standard Deviation
		1	2	3	4	5	6		
Southern Exposure Test									
DCB-2205p	57	0.01	β	β	β	β	β	β	β
MCB-2205p	57	-0.01	β	β	β	β		β	β

[a] 2205p = 2205 pickled stainless steel used in the bridge decks.
DCB = Doniphan County Bridge. MCB = Mission Creek Bridge.
β Corrosion loss less than 0.005 μm.

Figure 3.204 shows the average corrosion potentials of the top and bottom mats of steel with respect to a copper-copper sulfate electrode. Both DCB-2205p and MCB-2205p showed top and bottom corrosion potentials above –0.250 V, indicating a low probability of corrosion.

Figure 3.205 shows the average mat-to-mat resistances for both specimens. As mentioned in Section 3.1.2, average mat-to-mat resistances are not reported at the same week as other results because the resistance meter broke down several weeks before the data cut-off date. As shown in Figure 3.205, the average mat-to-mat resistance was about 130 ohms for DCB-2205p and 90 ohms for MCB-2205p, respectively, at the start of the test period. The average mat-to-mat resistances increased with time for both specimens, but at a much lower rate for MCB-2205p than for DCB-2205p. By week 52, the average mat-to-mat resistances were approximately 850 and 200 ohms for DCB-2205p and MCB-2205p, respectively.

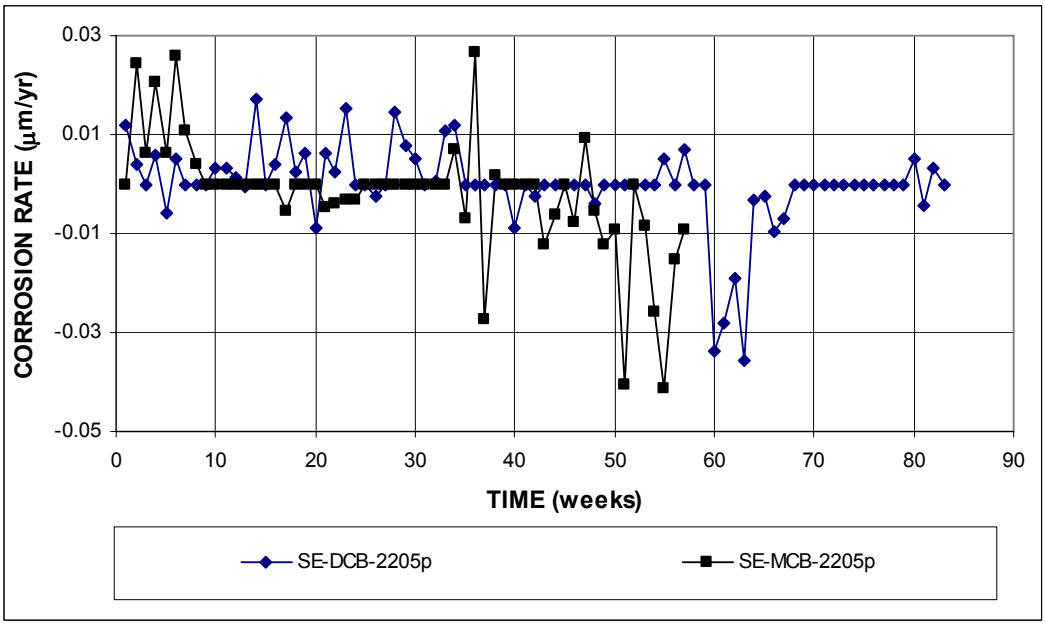

Figure 3.202 – Average corrosion rates as measured in the Southern Exposure test for specimens with 2205p stainless steel for the DCB and MCB.

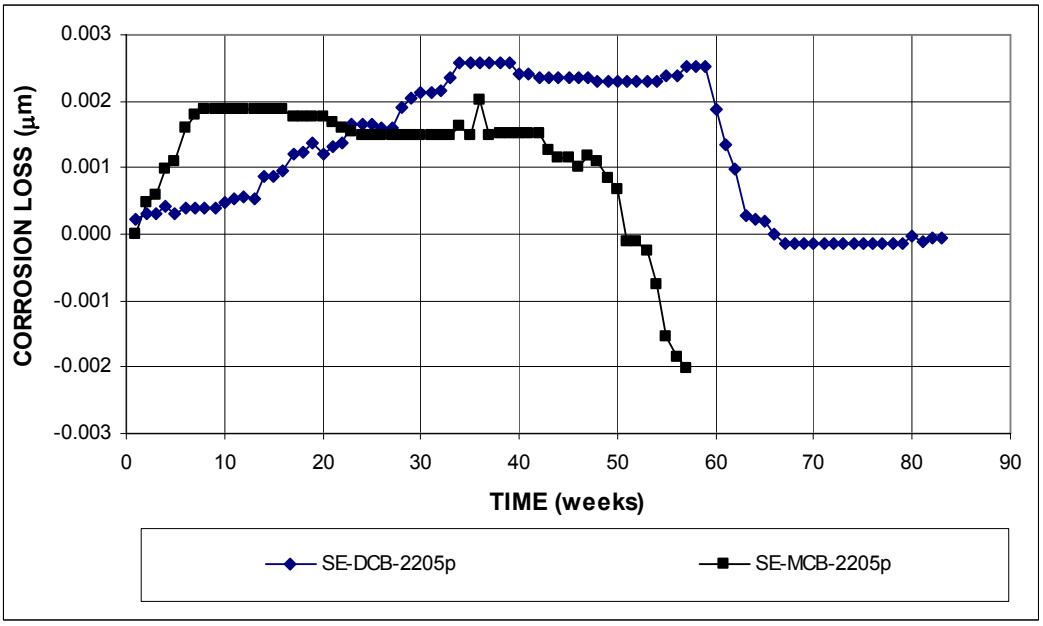

Figure 3.203 – Average corrosion losses as measured in the Southern Exposure test for specimens with 2205p stainless steel for the DCB and MCB.

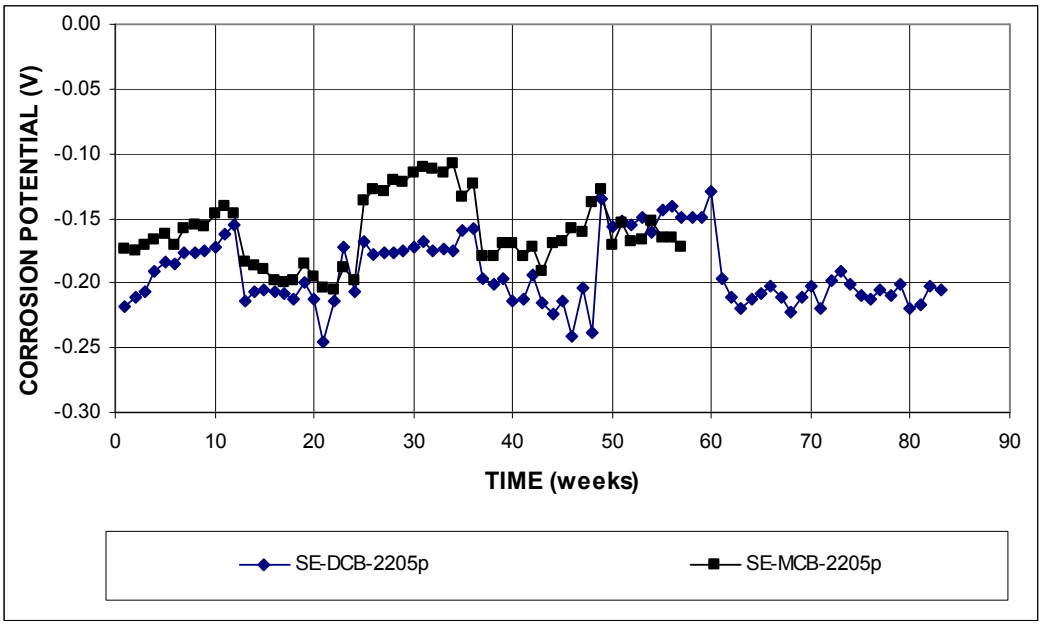

Figure 3.204 (a) – Average top mat corrosion potentials, with respect to a copper-copper sulfate electrode as measured in the Southern Exposure test for specimens with 2205p stainless steel for the DCB and MCB.

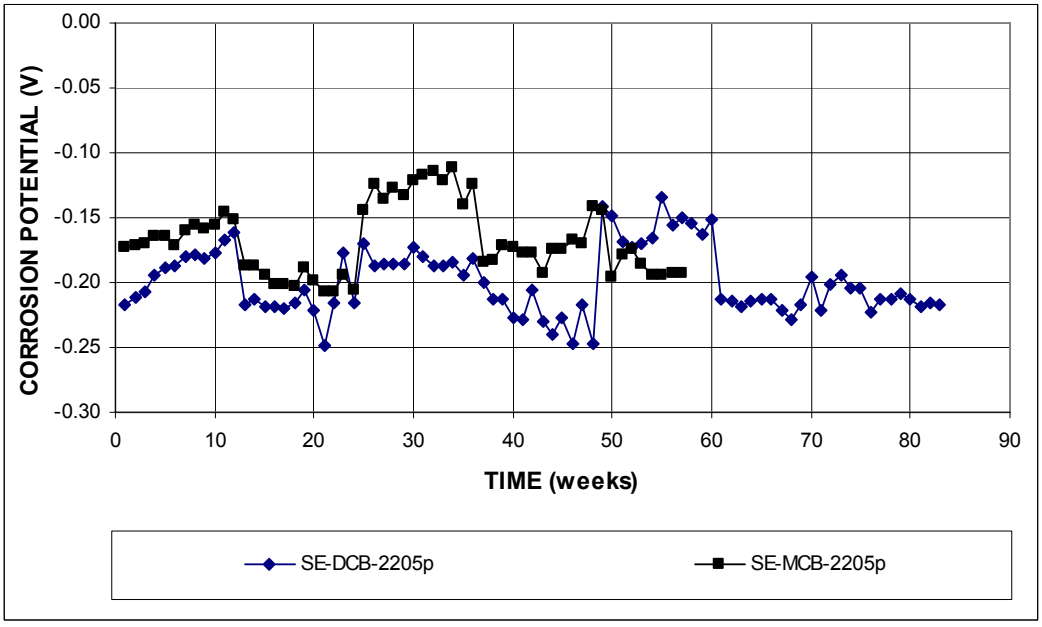

Figure 3.204 (b) – Average bottom mat corrosion potentials, with respect to a copper-copper sulfate electrode as measured in the Southern Exposure test for specimens with 2205 pickled stainless steel for the DCB and MCB.

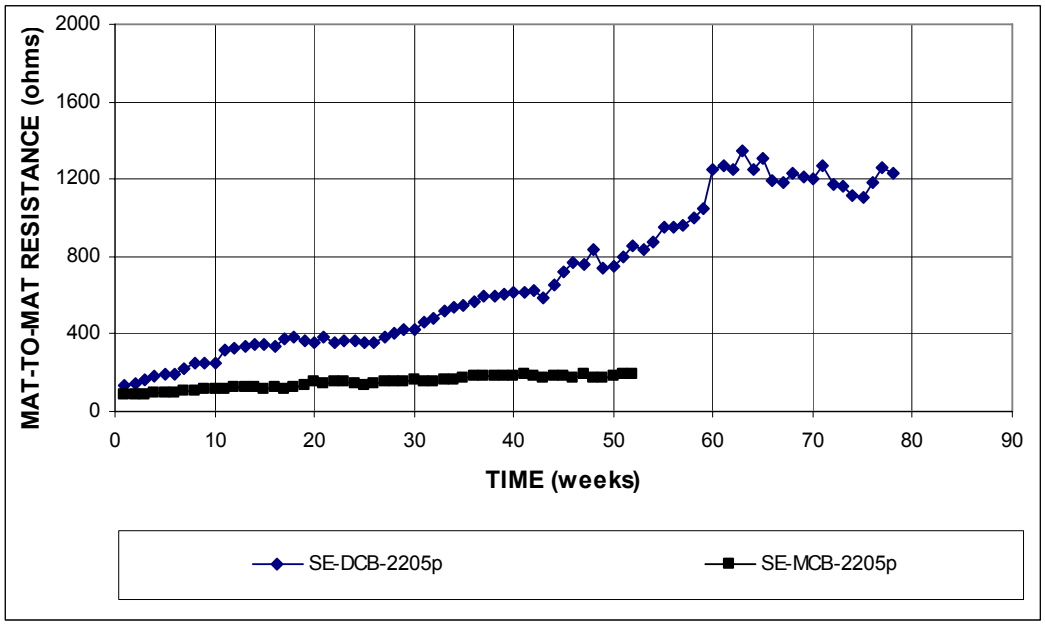

Figure 3.205 – Average mat-to-mat resistances as measured in the Southern Exposure test for specimens with 2205p stainless steel for the DCB and MCB.

3.6.2.2 Cracked Beam Test

The test results are presented in Figures 3.206 through 3.209 for specimens with 2205p stainless steel and the total corrosion losses at week 57 are summarized in Table 3.28.

Figure 3.206 shows the average corrosion rates and Figure 3.207 shows the average total corrosion losses for 2205p stainless steel for both bridges. As shown in Figure 3.206, 2205p stainless steel had corrosion rates between –0.025 and 0.069 μm/yr for the DCB and between –0.069 and 0.037 μm/yr for the MCB. Negative corrosion rates were observed for specimens with 2205p stainless steel for both bridges. The negative corrosion rates observed for both specimens were sometimes accompanied by more negative corrosion potentials at cathode than at anode, but sometimes were not. As shown in Figure 3.207, DCB-2205p exhibited progressive corrosion losses during the first 34 weeks and then had total corrosion losses

decreasing with time. MCB-2205p showed progressive corrosion losses during the first 10 weeks and had no corrosion between weeks 10 and 20. After week 20, the total corrosion losses for MCB-2205p decreased with time. As shown in Table 3.28, total corrosion losses of approximately 0.01 and –0.01 μm were observed for DCB-2205p and MCB-2205p at week 57, respectively, compared to 7.65 μm for conventional steel in the cracked beam test (shown in Figure 3.23). At week 57, a total corrosion loss of approximately 0.01 μm was obtained for 2205p steel in the previous study by Balma et al. (2005).

Table 3.28 – Average corrosion losses (μm) as measured in the cracked beam test for specimens with 2205 pickled stainless steel for DCB and MCB.

Steel Designation[a]	Age (weeks)	Specimen						Average	Standard Deviation
		1	2	3	4	5	6		
Cracked Beam Test									
DCB-2205p	57	0.02	0.01	0.01				0.01	β
MCB-2205p	57	β	0.01	-0.08	β	0.01	0.01	-0.01	0.04

[a] 2205p = 2205 pickled stainless steel used in the bridge decks.
DCB = Doniphan County Bridge. MCB = Mission Creek Bridge.
β Corrosion loss less than 0.005 μm.

The average corrosion potentials of the top and bottom mats of steel with respect to a copper-copper sulfate electrode are shown in Figure 3.208. Both DCB-2205p and MCB-2205p showed top and bottom corrosion potentials above –0.250 V, indicating a low probability of corrosion.

Figure 3.209 shows the average mat-to-mat resistances for both specimens. The mat-to-mat resistance was around 300 ohms for DCB-2205p and 230 ohms for MCB-2205p, respectively, at the start of the test period. The mat-to-mat resistance increased with time for both specimens, but as for the Southern Exposure specimens, MCB-2205p did so at a much lower rate. By week 52, the mat-to-mat resistances were approximately 2,600 and 600 ohms for DCB-2205p and MCB-2205p, respectively.

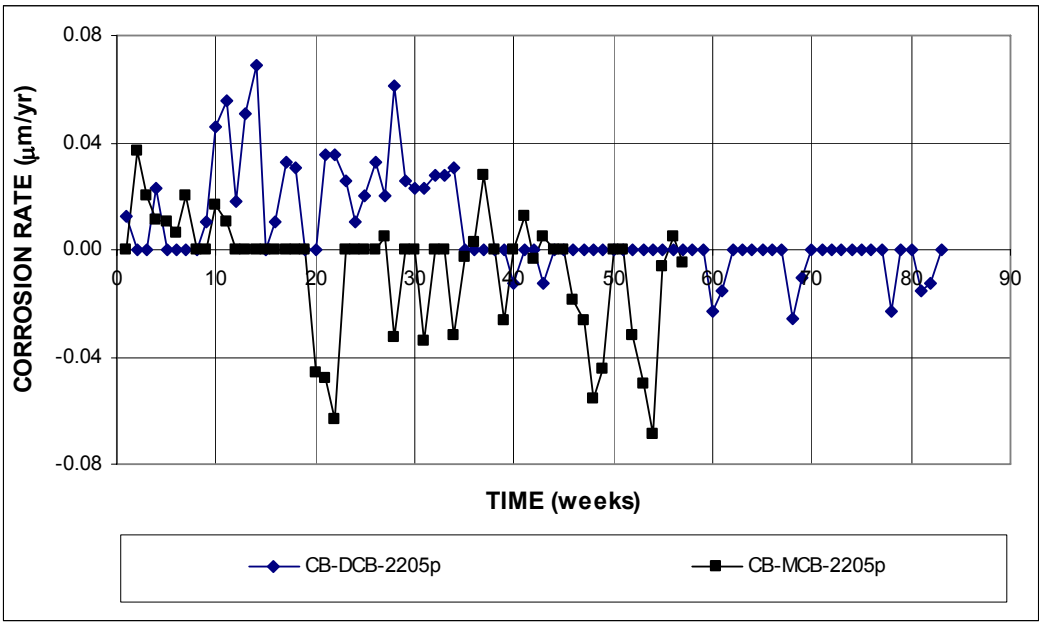

Figure 3.206 – Average corrosion rates as measured in the cracked beam test for specimens with 2205p stainless steel for the DCB and MCB.

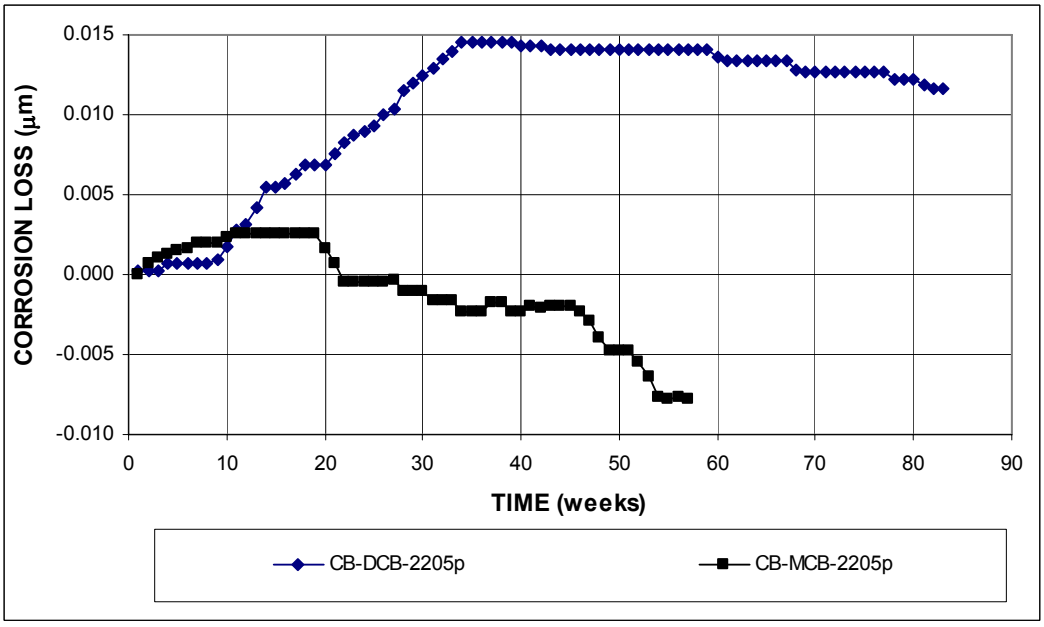

Figure 3.207 – Average corrosion losses as measured in the cracked beam test for specimens with 2205p stainless steel for the DCB and MCB.

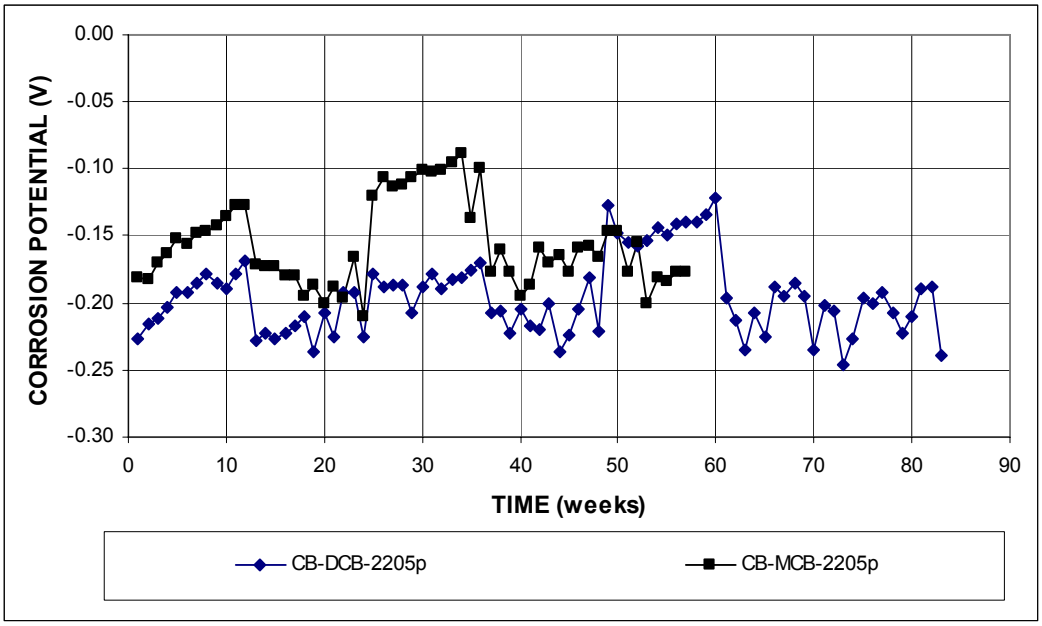

Figure 3.208 (a) – Average top mat corrosion potentials, with respect to a copper-copper sulfate electrode as measured in the cracked beam test for specimens with 2205p stainless steel for the DCB and MCB.

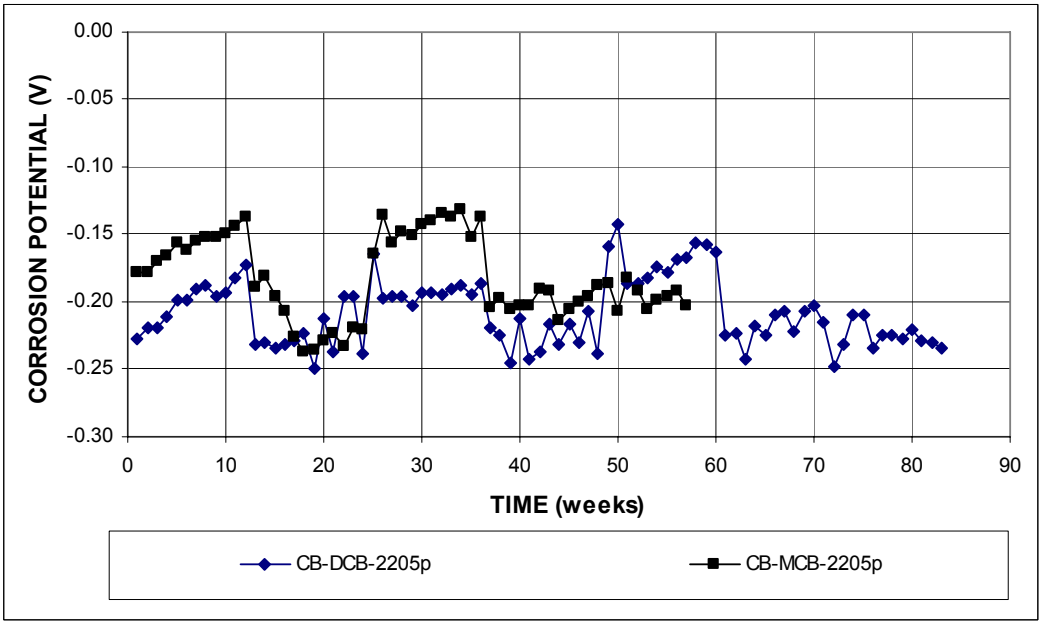

Figure 3.208 (b) – Average bottom mat corrosion potentials, with respect to a copper-copper sulfate electrode as measured in the cracked beam test for specimens with 2205p stainless steel for the DCB and MCB.

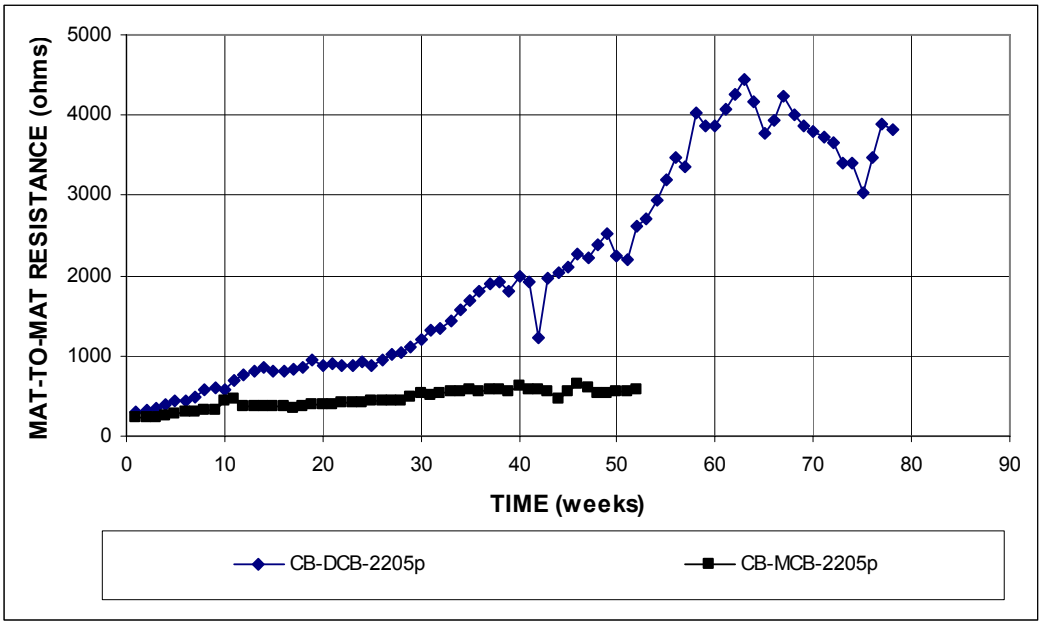

Figure 3.209 – Average mat-to-mat resistances as measured in the cracked beam test for specimens with 2205p stainless steel for the DCB and MCB.

3.6.3 Field Test

This section presents the results of field test specimens with conventional steel, 2205p stainless steel, and epoxy-coated reinforcement as conducted for the Doniphan County Bridge and Mission Creek Bridge comparisons.

For specimens with conventional steel and 2205p stainless steel, the total area of top mat bars is used to calculate the average corrosion rates and total corrosion losses. The epoxy coating was not penetrated with holes for the Doniphan County Bridge specimens, and the results are reported based on the total area of the bar only. The ECR bars for the Mission Creek Bridge specimens were penetrated with 16 3-mm ($^1/_8$-in.) diameter holes, and the results are reported based on both total area and exposed area of the bar. For Mission Creek Bridge specimens, one of the two specimens had four 305-mm (12-in.) long simulated cracks directly above top reinforcing bars numbered 1, 3, 5, and 7, as shown in Figure 2.14(b).

3.6.3.1 Doniphan County Bridge

The test results of specimens for the Doniphan County Bridge are presented in Figures 3.210 through 3.214. The total corrosion losses at week 72 are summarized in Table 3.29.

Figure 3.210 shows that specimens with conventional steel had the highest corrosion rates, with a high value of 0.93 μm/yr for DCB-Conv. (1) and 0.63 μm/yr for DCB-Conv. (2), respectively. Specimens with ECR showed corrosion rates less than 0.03 μm/yr, followed by specimens with 2205p stainless steels, with values below 0.01 μm/yr. DCB-ECR (1) showed negative corrosion rates of –0.027 and –0.006 μm/yr, respectively, at weeks 24 and 44. The negative corrosion rates were accompanied by more negative corrosion potentials at the cathode than at the anode.

Table 3.29 – Average corrosion losses (μm) as measured in the field test for specimens with conventional steel, 2205 pickled stainless steel, and ECR for the Doniphan County Bridge.

Steel Designation[a]	Age (weeks)	Test Bar		Average	Standard Deviation
		1	2		
DCB-Conv. (1)	72	0.28	0.57	0.43	0.21
DCB-Conv. (2)	72	0.02	0.12	0.07	0.07
DCB-2205p (1)	72	β	β	β	β
DCB-2205p (2)	72	β	β	β	β
DCB-ECR (1)	72	β	β	β	β
DCB-ECR (2)	72	0.01	β	0.01	β

[a] DCB = Doniphan County Bridge. Conv. = conventional steel.
2205p = 2205 pickled stainless steel used in the bridge decks. ECR = epoxy-coated reinforcement.

β Corrosion loss (absolute value) less than 0.005 mm.

Figure 3.211 shows that DCB-Conv. (1) had the highest total corrosion loss, followed by DCB-Conv. (2) and DCB-ECR (2), respectively. The specimen DCB-ECR (1) and specimens with 2205p stainless steel showed the lowest total corrosion losses. As shown in Table 3.29, DCB-Conv. (1) had a total corrosion loss of 0.43 μm at week 72, followed by DCB-Conv. (2) at 0.07 μm. These values equal 49% and

7.9% of the total corrosion loss of conventional steel in the SE test at the same week. Specimens with 2205p stainless steel had total corrosion losses of less than 0.005 μm, compared to a loss of less than 0 μm for 2205p stainless steel and 0.89 μm for conventional steel in the SE test. For specimens with conventional ECR, total corrosion losses of 0.003 and 0.006 μm were observed for DCB-ECR (1) and DCB-ECR (2), respectively, compared to a loss of 0.003 μm for conventional ECR with four holes in the SE test at the same week.

The average corrosion potentials of the top and bottom mats of steel with respect to a copper-copper sulfate electrode are shown in Figure 3.212. DCB-Conv. (1) showed active corrosion in the top mat after week 64 and the remaining specimens had top mat corrosion potentials more positive than –0.300 V, with the exception of DCB-ECR (1) at week 40, DCB-Conv. (2) at week 72, and DCB-2205p (1) at week 72, respectively. The bottom mat corrosion potentials remained above –0.350 V with the exception that DCB-Conv. (1) showed active corrosion at week 72, indicating that chlorides had reached the bottom mat of steel.

Figure 3.213 shows the mat-to-mat resistances for specimens with conventional steel and 2205p stainless steel and Figure 3.214 shows the results for specimens with ECR. For specimens with conventional steel and 2205p stainless steel, mat-to-mat resistances remained between 4 and 60 ohms. Figure 3.214 shows that specimens with ECR had mat-to-mat resistances between 2,300 and 13,600 ohms, with average values around 7,500 ohms. As mentioned earlier, variations of average mat-to-mat resistances over time are due to the changes in concrete moisture content in the field test specimens.

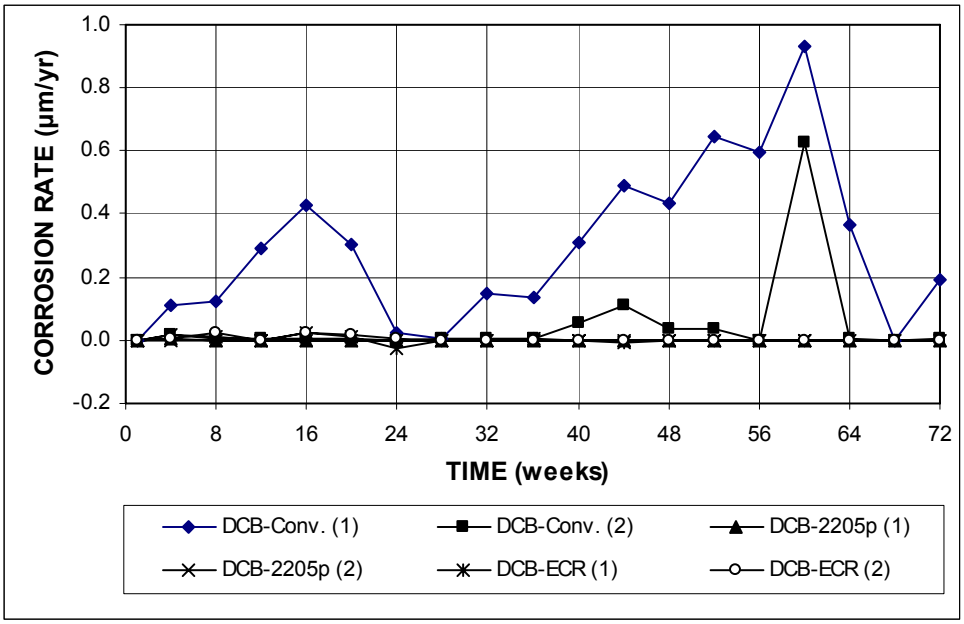

Figure 3.210 (a) – Average corrosion rates as measured in the field test for specimens with conventional steel, 2205p stainless steel, and ECR for the Doniphan County Bridge.

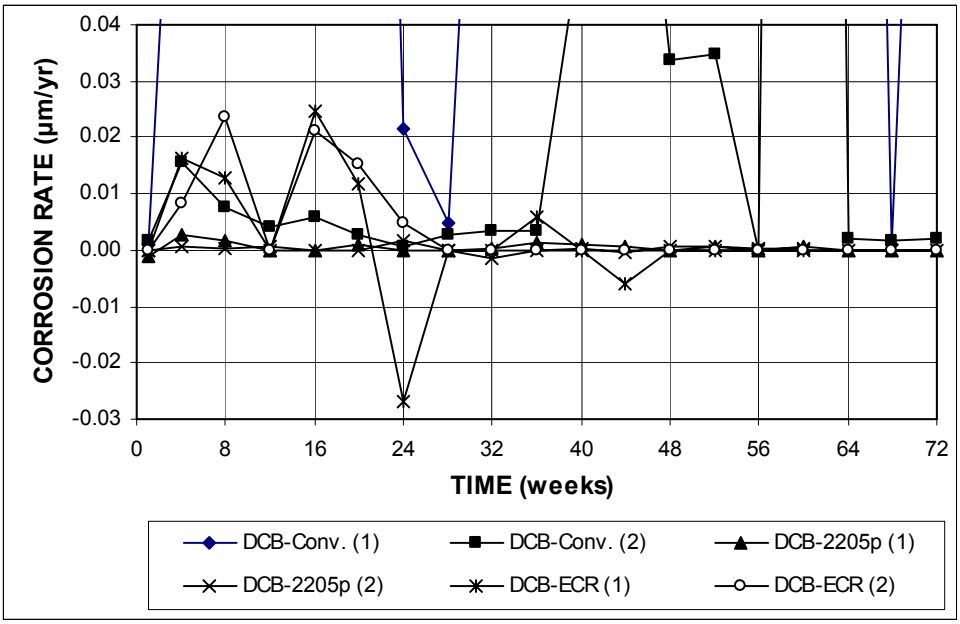

Figure 3.210 (b) – Average corrosion rates as measured in the field test for specimens with conventional steel, 2205p stainless steel, and ECR for the Doniphan County Bridge.

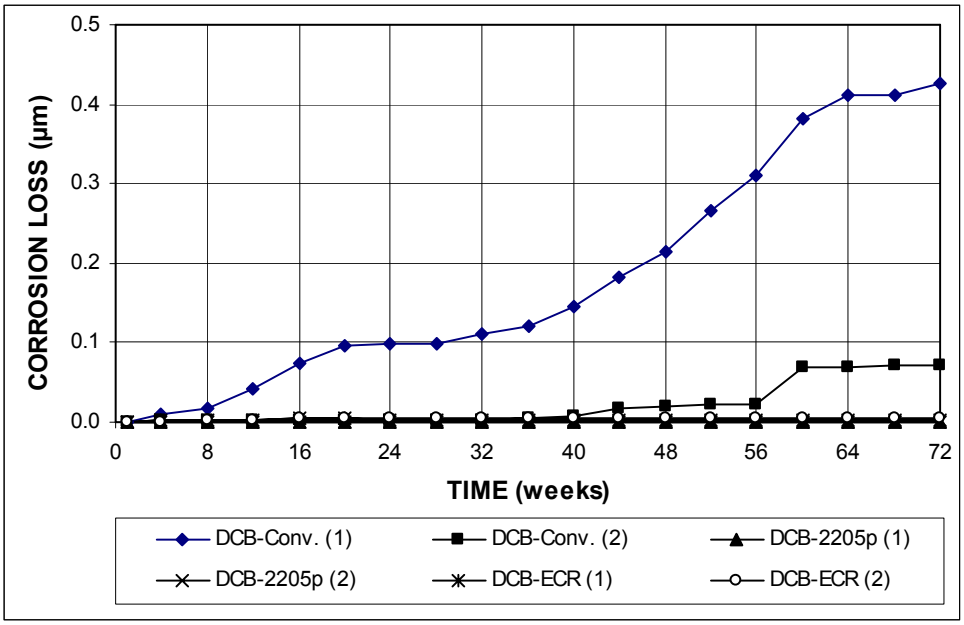

Figure 3.211 (a) – Average corrosion losses as measured in the field test for specimens with conventional steel, 2205p stainless steel, and ECR for the Doniphan County Bridge.

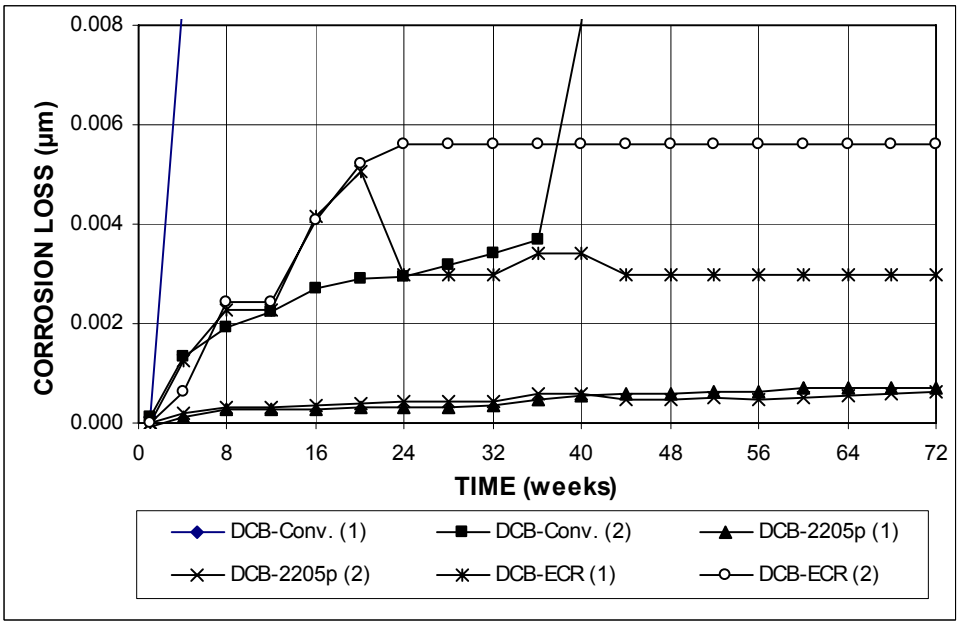

Figure 3.211 (b) – Average corrosion losses as measured in the field test for specimens with conventional steel, 2205p stainless steel, and ECR for the Doniphan County Bridge.

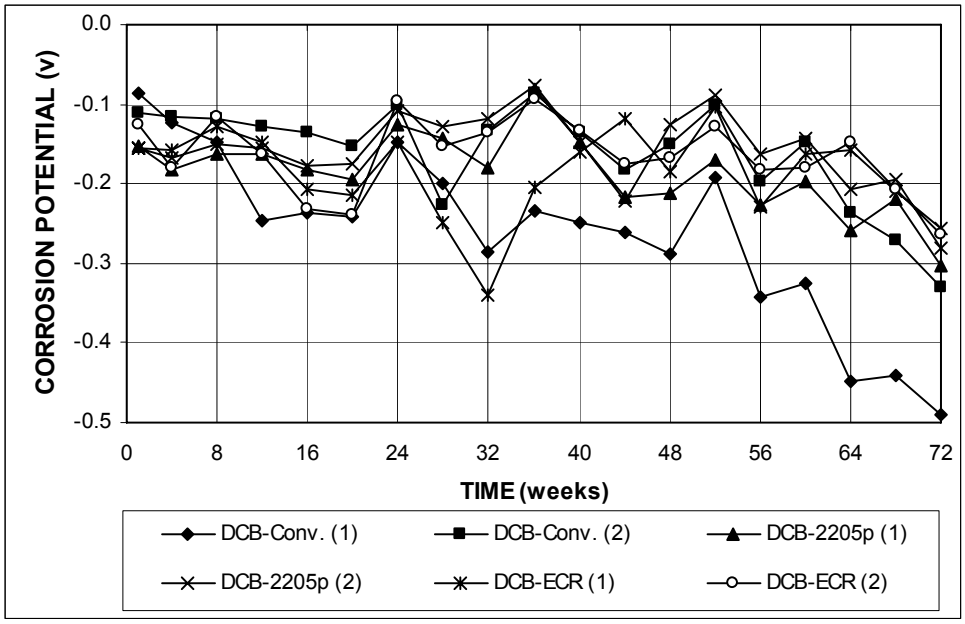

Figure 3.212 (a) – Average top mat corrosion potentials, with respect to a copper-copper sulfate electrode as measured in the field test for specimens with conventional steel, 2205p stainless steel, and ECR for the Doniphan County Bridge.

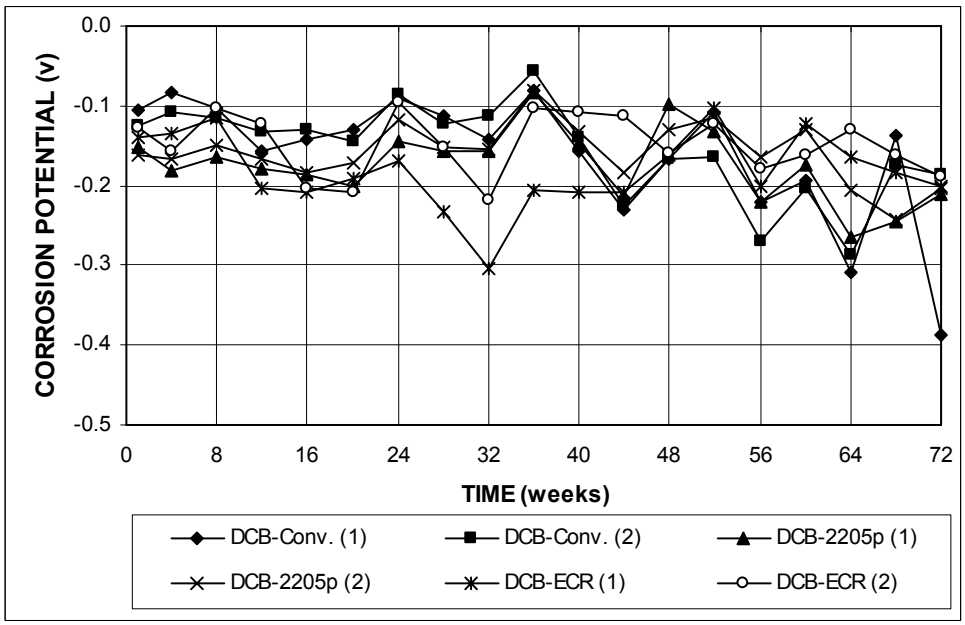

Figure 3.212 (b) – Average bottom mat corrosion potentials, with respect to a copper-copper sulfate electrode as measured in the field test for specimens with conventional steel, 2205p stainless steel, and ECR for the Doniphan County Bridge.

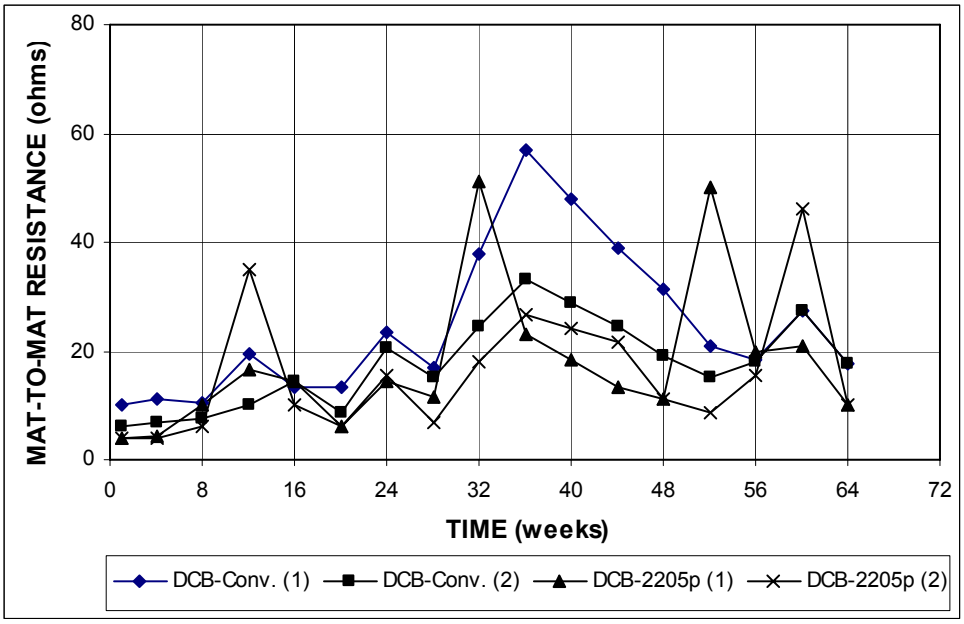

Figure 3.213 – Average mat-to-mat resistances as measured in the field test for specimens with conventional steel and 2205p stainless steel for the Doniphan County Bridge.

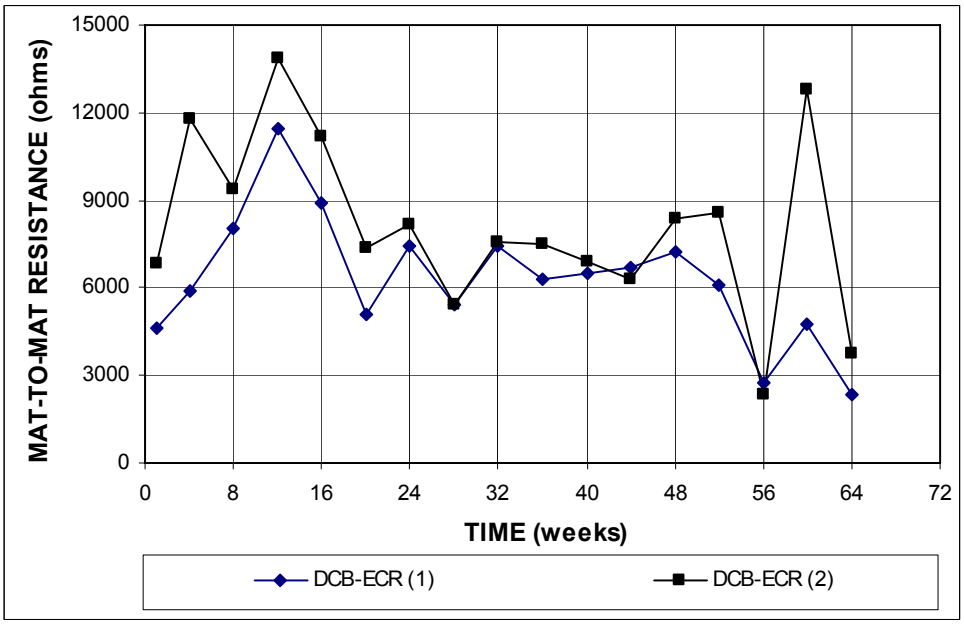

Figure 3.214 – Average mat-to-mat resistances as measured in the field test for specimens with ECR for the Doniphan County Bridge.

3.6.3.2 Mission Creek Bridge

The test results of specimens for the Mission Creek Bridge are presented in Figures 3.215 through 3.221. The total corrosion losses at week 48 are summarized in Table 3.30.

Figure 3.215 shows that specimens with conventional steel had the highest corrosion rates, with high values of 0.23 μm/yr for MCB-Conv. (1) and 0.34 μm/yr for MCB-Conv. (2), respectively. Specimens with ECR showed corrosion rates less than 0.003 μm/yr based on total area, and specimens with 2205p stainless steels had corrosion rates less than 0.001 μm/yr. As shown in Figure 3.126, no corrosion activity was observed for specimens with conventional ECR, with the exception of MCB-ECR (1) at week 20, which had a corrosion rate of 0.9 μm/yr based on exposed area.

Table 3.30 – Average corrosion losses (μm) as measured in the field test for specimens with conventional steel, 2205 pickled stainless steel, and ECR for the Mission Creek Bridge.

Steel Designation[a]	Age (weeks)	Test Bar				Average	Standard Deviation	Notes
		1	2	3	4			
MCB-Conv. (1)	48	β	0.06			0.03	0.04	
MCB-Conv. (2)	48	0.08	0.02			0.05	0.05	with cracks
MCB-2205p (1)	48	β	β			β	β	
MCB-2205p (2)	48	β	β			β	β	with cracks
MCB-ECR (1)	48	0.00	0.00	0.00	0.00	0.00	0.00	
MCB-ECR (1)*	48	0.00	0.00	0.00	0.00	0.00	0.00	
MCB-ECR (2)	48	β	0.00	0.00	0.00	β	β	with cracks
MCB-ECR (2)*	48	0.28	0.00	0.00	0.00	0.07	0.14	with cracks

[a] MCB = Mission Creek Bridge. Conv. = conventional steel.
2205p = 2205 pickled stainless steel used in the bridge decks. ECR = epoxy-coated reinforcement.

* Epoxy-coated bars, calculations based on exposed area of 16 3-mm ($^1/_8$-in.) diameter holes.

β Corrosion loss (absolute value) less than 0.005 mm.

Figure 3.217 shows that the conventional steel specimen with cracks [MCB-Conv. (2)] had the highest total corrosion loss of 0.05 μm at week 48, compared to values between 0.27 and 0.68 μm for conventional steel specimens with cracks in the field test (Section 3.1.3) at the same week. The conventional steel specimen without

cracks [MCB-Conv. (1)] had an average corrosion rate at week 48 of 0.03 μm, which is similar to the values between 0.001 and 0.024 for the conventional steel specimens without cracks in the field test (Section 3.1.3). The remaining specimens showed total corrosion losses of less than 0.005 μm based on total area, as indicated by the symbol β in Table 3.30. Based on exposed area, total corrosion losses of 0 and 0.14 μm were observed for MCB-ECR (1) and MCB-ECR (2), respectively, compared to values between 0.18 and 0.81 μm for ECR without cracks and between 0 and 1.06 μm for ECR with cracks in the field test (Section 3.1.3).

The average corrosion potentials of the top and bottom mats of steel with respect to a copper-copper sulfate electrode are shown in Figure 3.219. In the top mat, specimens with cracks generally showed more negative corrosion potentials than specimens without cracks, with the exception of MCB-2205p (2), which had corrosion potentials similar to those for MCB-2205p (1). MCB-Conv. (2) had the most negative corrosion potential in the top mat, with values between –0.350 and –0.590 V, followed by MCB-ECR (2), which had corrosion potentials more negative than –0.350 V after week 8. MCB-Conv. (1) showed active corrosion at week 48, with a corrosion potential of –0.380 V. Specimens with 2205p stainless steel and MCB-ECR (1) had corrosion potentials of the top mat above –0.250 V, indicating a low probability of corrosion. The bottom mat corrosion potentials for all steels remained above –0.200 V before week 32 and more positive than –0.300 V thereafter.

The average mat-to-mat resistances are shown in Figure 3.220 for specimens with conventional steel and 2205p stainless steel and in Figure 3.221 for specimens with ECR, respectively. For specimens with conventional steel and 2205p stainless steel, the mat-to-mat resistance remained below 20 ohms. For specimens with ECR, the average mat-to-mat resistances ranged between 600 and 1,200 ohms.

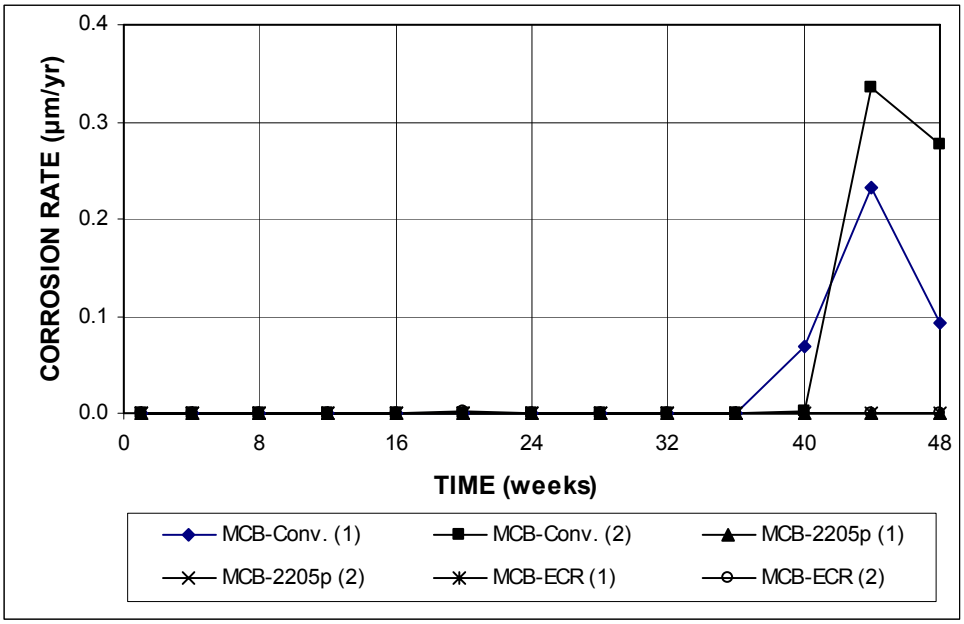

Figure 3.215 (a) – Average corrosion rates as measured in the field test for specimens with conventional steel, 2205p stainless steel, and ECR for the Mission Creek Bridge (ECR bars have 16 holes).

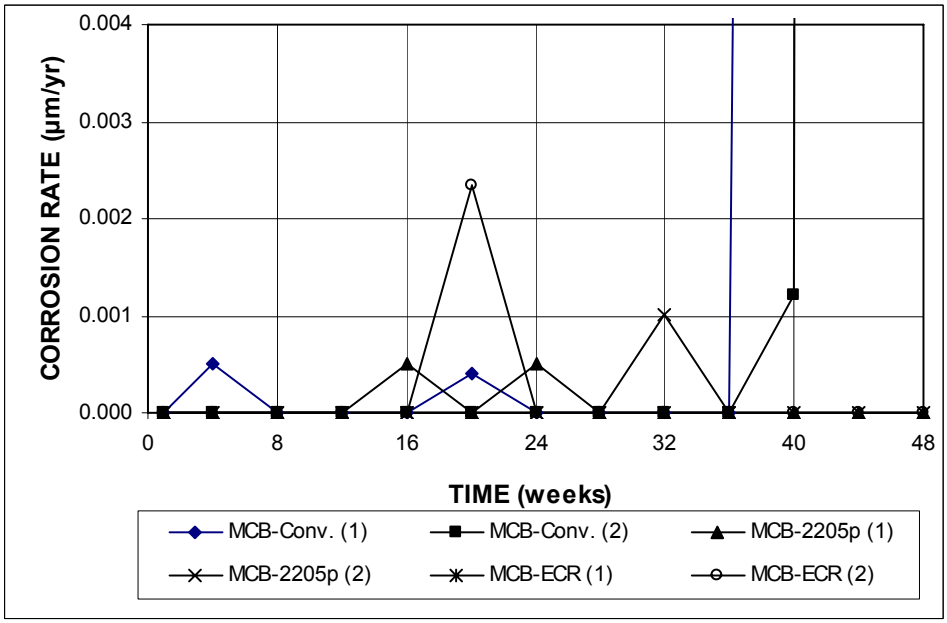

Figure 3.215 (b) – Average corrosion rates as measured in the field test for specimens with conventional steel, 2205p stainless steel, and ECR for the Mission Creek Bridge (ECR bars have 16 holes).

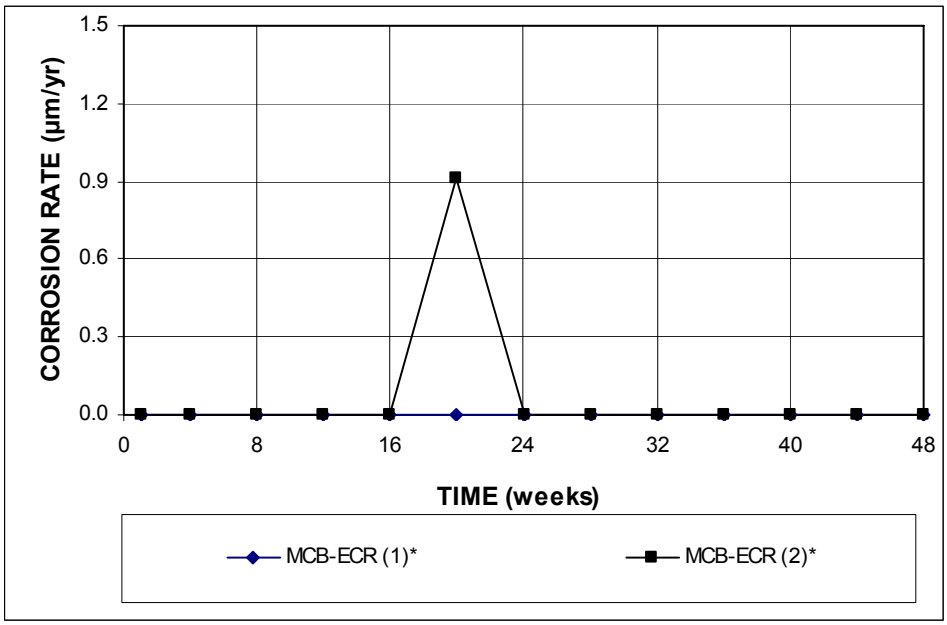

Figure 3.216 – Average corrosion rates as measured in the field test for specimens with ECR for the Mission Creek Bridge. * Based on exposed area (ECR bars have 16 holes).

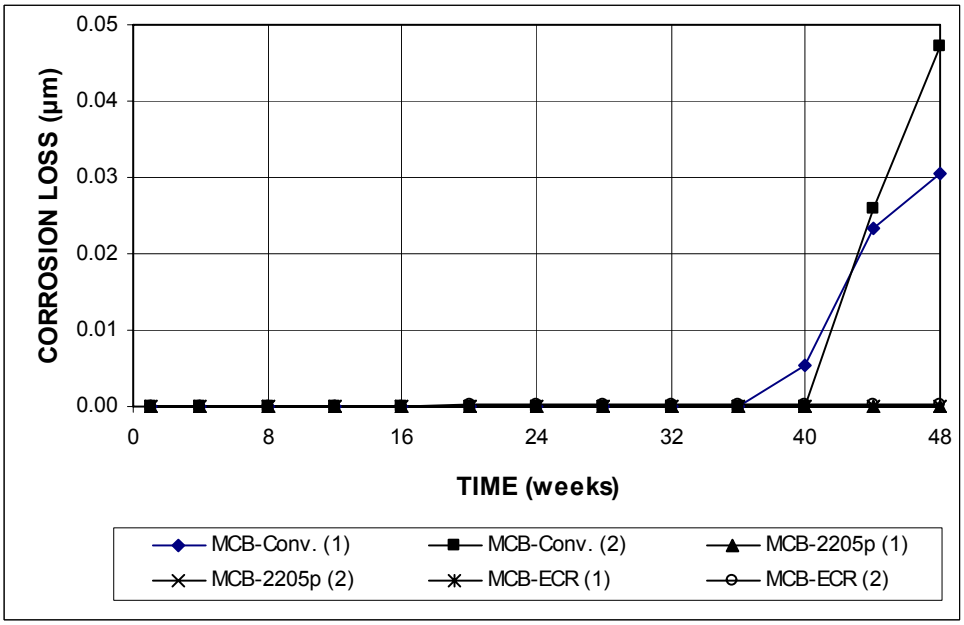

Figure 3.217 (a) – Average corrosion losses as measured in the field test for specimens with conventional steel, 2205p stainless steel, and ECR for the Mission Creek Bridge (ECR bars have 16 holes).

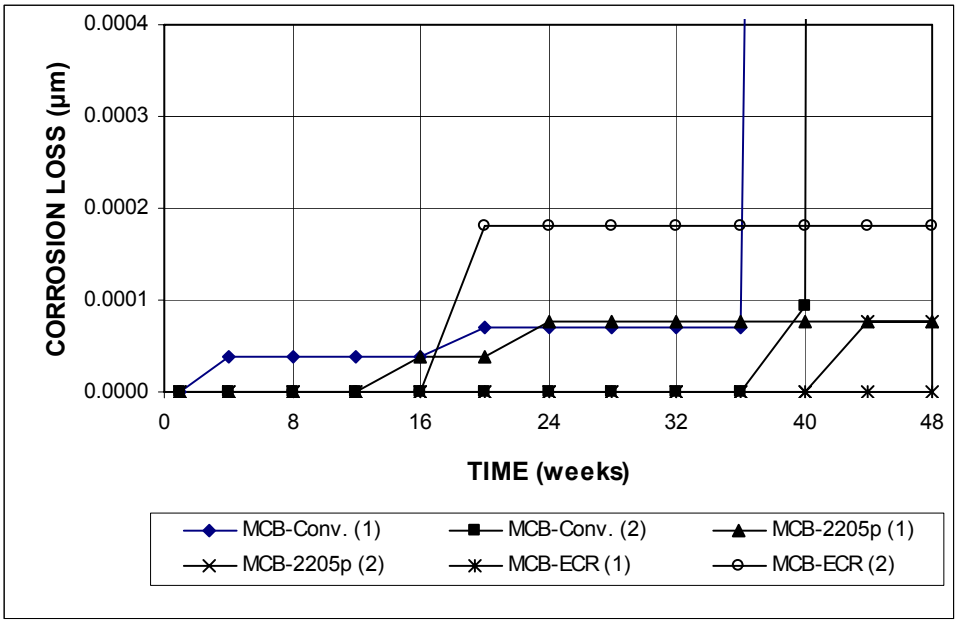

Figure 3.217 (b) – Average corrosion losses as measured in the field test for specimens with conventional steel, 2205p stainless steel, and ECR for the Mission Creek Bridge (ECR bars have 16 holes).

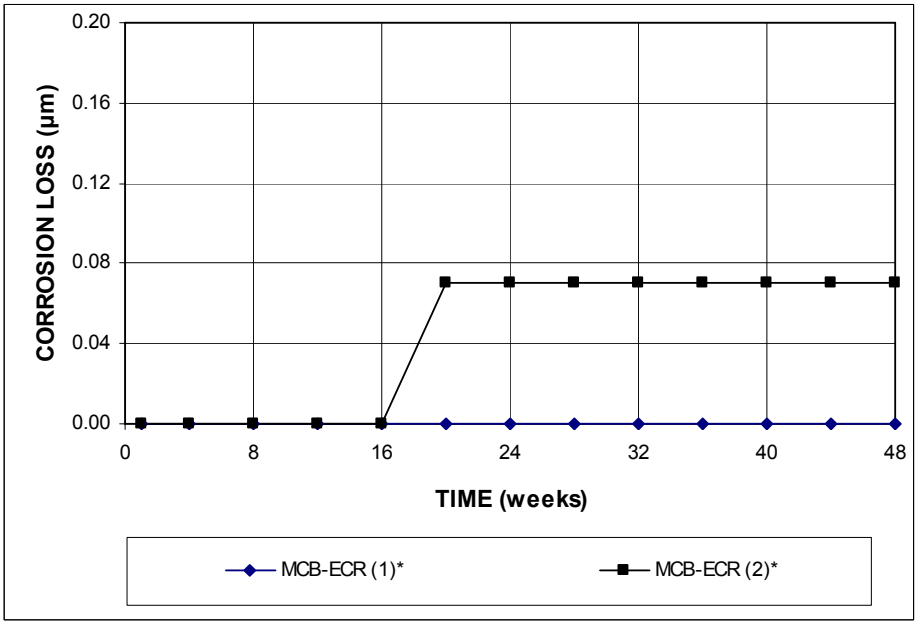

Figure 3.218 – Average corrosion losses as measured in the field test for specimens with ECR for the Mission Creek Bridge. * Based on exposed area (ECR bars have 16 holes).

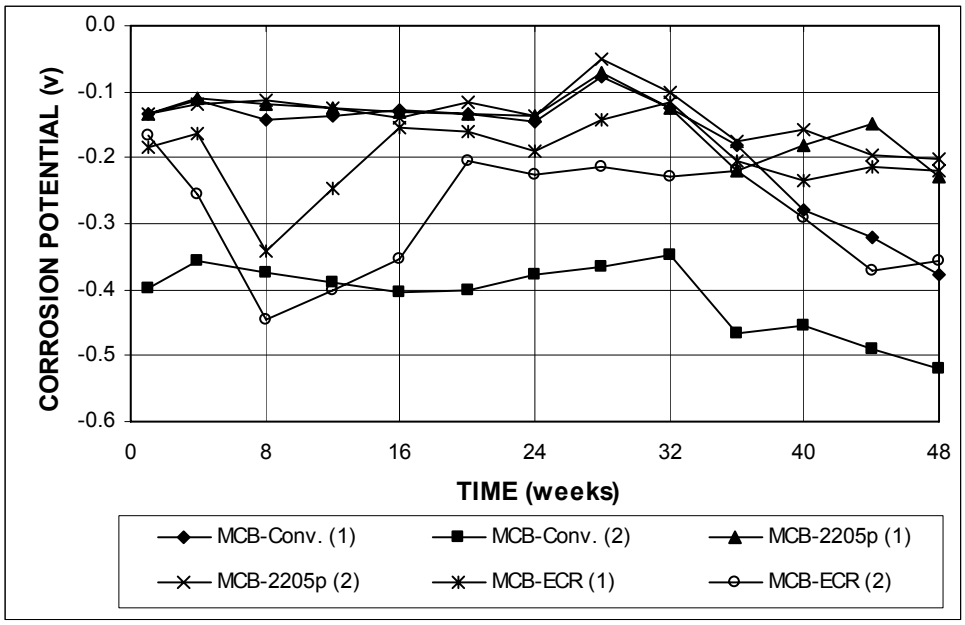

Figure 3.219 (a) – Average top mat corrosion potentials, with respect to a copper-copper sulfate electrode as measured in the field test for specimens with conventional steel, 2205p stainless steel, and ECR for the Mission Creek Bridge (ECR bars have 16 holes).

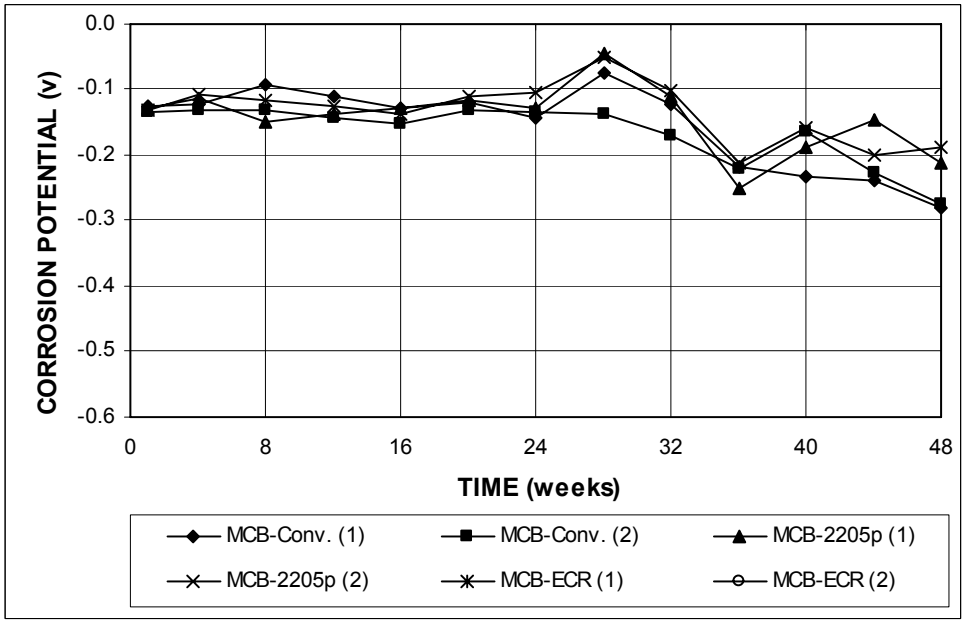

Figure 3.219 (b) – Average bottom mat corrosion potentials, with respect to a copper-copper sulfate electrode as measured in the field test for specimens with conventional steel, 2205p stainless steel, and ECR for the Mission Creek Bridge (ECR bars have 16 holes).

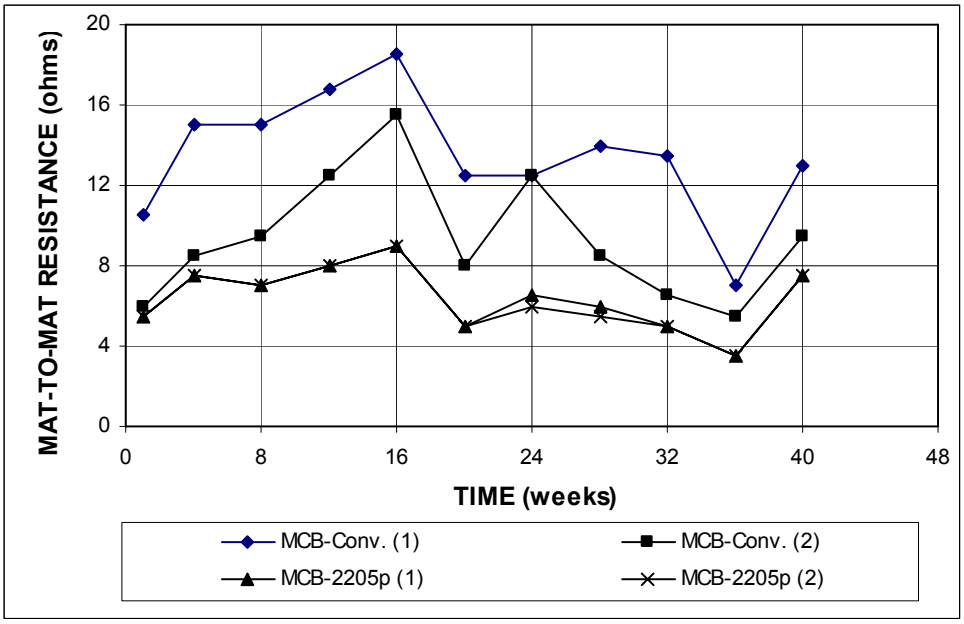

Figure 3.220 – Average mat-to-mat resistances as measured in the field test for specimens with conventional steel and 2205p stainless steel for the Mission Creek Bridge.

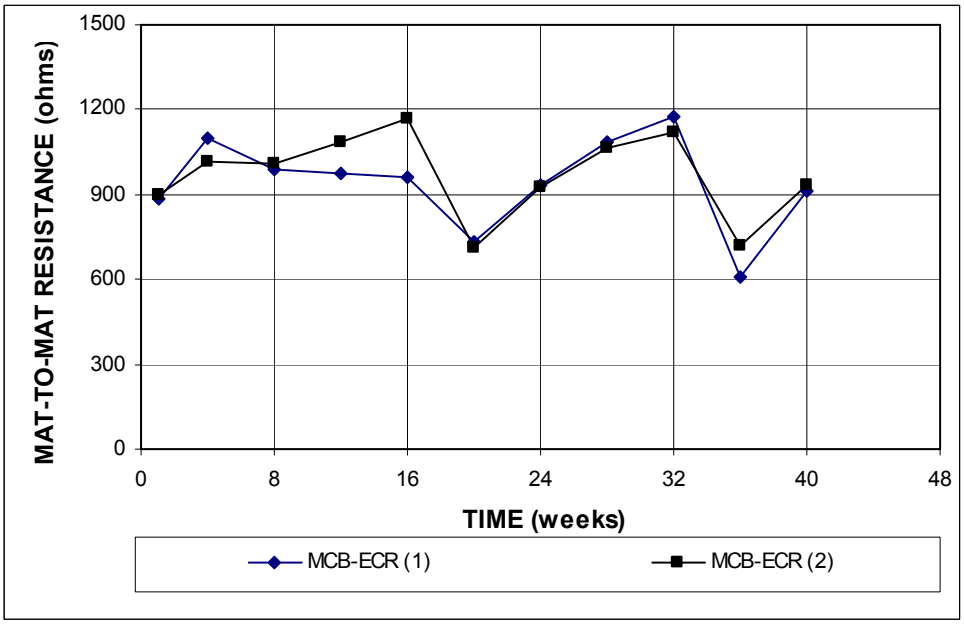

Figure 3.221 – Average mat-to-mat resistances as measured in the field test for specimens with ECR for the Mission Creek Bridge (ECR bars have 16 holes).

3.7 CATHODIC DISBONDMENT TEST

Three rounds of cathodic disbondment tests were performed in accordance with ASTM G 8 and ASTM A 775. The test specimens included conventional ECR, multiple coated reinforcement, ECR with the chromate pretreatment, two types of ECR with improved adhesion coatings developed by DuPont and Valspar, and ECR with a primer containing calcium nitrite. In addition, conventional epoxy-coated reinforcement from a previous batch was tested. According to ASTM A 775, four measurements were taken at 0°, 90°, 180°, and 270° and the values were averaged. The cathodic disbondment test results were recorded in terms of both the area of the disbonded coating (ASTM G 8) and the average coating disbondment radius of four measurements (ASTM A 775), respectively. Table 3.31 summarizes the individual and average results of the three rounds of cathodic disbondment tests. The table also identifies which coatings were applied at the same application plants.

As shown in Table 3.31, the average coating disbondment radius for three tests was above 4 mm (the maximum allowed in ASTM A 775) for conventional ECR (5.9 mm), conventional ECR from a previous batch (5.5 mm), and high adhesion Valspar bars (4.9 mm), indicating that these bars failed the coating disbondment requirement. Multiple coated reinforcement (1.7 mm), high adhesion DuPont bars (2.8 mm), ECR with the chromate pretreatment (1.0 mm), and ECR with a calcium nitrite primer (2.6 mm) met the coating disbondment requirement.

Table 3.31 also presents the area of disbonded coating in accordance with ASTM G 8. Conventional ECR and the conventional ECR from a previous batch exhibited the highest areas of disbonded coating, with average values of 1.78 and 1.68 cm^2, respectively. The high adhesion Valspar bars had an area of disbonded coating of 1.51 cm^2, followed by ECR with a calcium nitrite primer at 0.67 cm^2 and high

adhesion DuPont bars at 0.65 cm^2, respectively. Multiple coated reinforcement and ECR with the chromate pretreatment showed the lowest areas of disbonded coating, with average values of 0.27 and 0.20 cm^2, respectively.

Epoxy was applied to the conventional ECR and high adhesion Valspar bars by the same coating applicator (A), and both types of ECR failed the requirements in Annex A1 of ASTM A 775. The multiple coated bars and high adhesion DuPont bars were handled by the same coating applicator (C), and both types of ECR meet the coating requirements in ASTM A 775. Failure of the test criterion may be related to the manufacturing process, especially the surface preparation and coating application processes. The coating requirements in ASTM A 775 are qualification requirements for the epoxy coating itself and are not meant to be applied to production bars. In this study, the conventional epoxy-coated bars do not meet the cathodic disbondment requirement in ASTM A 775, although this does not appear to be affecting their behavior in the corrosion tests. As a result of these tests, it is recommended that cathodic disbondment requirements be strengthened in the quality control checks for production bars.

Table 3.31 – Cathodic disbondment test results

Type of Coating[a] (Application Plant ID[b])	No. of Test	Thickness (mils)	Coating Disbondment Radius[c] (mm)					Area of Disbonded Coating[d] (cm^2)	Visual Examination
			0°	90°	180°	270°	Average		
ECR (A)	1st		6.5	6.5	6	5.5	6.1	1.83	rust on exposured area, black color at surrounding area
	2nd		6.5	5	3.5	4	4.8	1.33	no rust
	3rd	9.8	6.5	6.5	7.5	6.5	6.8	2.19	little rust
	Average						5.9	1.78	
ECR+ (B)	1st	11.8	5.5	6.5	5.5	5	5.6	1.70	no rust
	2nd	10.8	5.5	4.5	4.5	5.5	5.0	1.61	no rust
	3rd	9.5	6.5	5.5	5.5	5.5	5.8	1.74	no rust
	Average						5.5	1.68	
MC (C)	1st		2.5	1.5	1	1	1.5	0.22	rust on exposured area
	2nd		2	1.5	1.5	3	2.0	0.35	rust on exposured area
	3rd	11.2	0.5	2.5	1.5	1.5	1.5	0.25	rust on exposured area
	Average						1.7	0.27	
ECR(DuPont) (C)	1st		4	3	3.5	3.5	3.5	0.93	no rust
	2nd		1.5	1	1.5	1	1.3	0.19	no rust
	3rd	8.8	3.5	4	3.5	4	3.8	0.83	no rust
	Average						2.8	0.65	
ECR(Valspar) (A)	1st		4.5	4	4.5	4	4.3	1.33	rust on exposured area
	2nd		6	4.5	5.5	4.5	5.1	1.67	no rust
	3rd	10.6	6.5	4.5	5.5	4.5	5.3	1.54	no rust
	Average						4.9	1.51	
ECR(Chromate) (D)	1st		0.5	1	0	0	0.4	0.06	rust on exposured area
	2nd		1	0.5	2	2.5	1.5	0.35	rust on exposured area
	3rd	11	1.5	0.5	0.5	1.5	1.0	0.19	no rust
	Average						1.0	0.20	
ECR(primer/ $Ca(NO_2)_2$) (E)	1st		1.5	2	2	2	1.9	0.58	no rust
	2nd		3.5	2.5	4.5	2.5	3.3	0.77	no rust
	3rd	8	3	2.5	2.5	2.5	2.6	0.67	no rust
	Average						2.6	0.67	

[a] ECR = conventional epoxy-coated reinforcement. ECR^+ = previous batch of conventional epoxy-coated reinforcment. MC = multiple coated reinforcement. ECR(DuPont) = ECR with high adhesion DuPont coatings. ECR(Valspar) = ECR with high adhesion Valspar coatings. ECR(Chromate) = ECR with the zinc and chromate pretreatment. ECR(primer/$Ca(NO_2)_2$) = ECR with a primer containing calcium nitrite.

[b] A = ABC coating, Waxahachie Texas. B = unknown. C = Western coating, Eugene Oregon. D = Harris, Alberta Canada. E = ABC coating, Wyoming Michigan.

[c] Coating disbonement radius is measured from the edge of a 3-mm ($^1/_8$-in) diameter hole.

[d] Area of disbonded coating is the total area after disbondment minus the original area of a 3-mm ($^1/_8$-in.) diameter hole.

3.8 SUMMARY OF RESULTS

This section presents a summary of the corrosion test results covered in Chapter 3.

In general, specimens in the ASTM G 109 and field tests show much lower total corrosion losses than those in the other tests. Compared to the other tests, ASTM G 109 and field tests provide a milder test environment, including a lower salt concentration and a less aggressive ponding and drying test cycle. In addition, frequent drying (leading to a lower moisture content in the concrete) further slows corrosion in the field test specimens. To date, only conventional steel specimens show significant corrosion in these two tests. Of specimens with epoxy-coated bars, all specimens in the ASTM G 109 test at week 60 and 92% of specimens (35 out of 38 specimens) in the field test at week 32 have total corrosion losses less than 0.005 μm based on the total area of the steel. The other 8% of the field test specimens with epoxy-coated bars have total corrosion losses of approximately 0.01 μm.

In the rapid macrocell test, mortar-wrapped specimens exhibited much lower corrosion activity than the corresponding bare bar specimens, as demonstrated in Sections 3.1, 3.3, and 3.5. The reasons include a lower concentration of chlorides at the anodes, additional passive protection provided by the cement hydration products, and a lower rate of diffusion of oxygen and moisture to the bars at the cathodes. In addition, a variation in the chloride content at the steel-mortar interface due to the non-homogeneous nature of chloride diffusion in mortar could result in a locally low chloride content at the exposed areas on ECR bar with holes. This point is supported by (1) the fact that both conventional ECR with four holes and ECR without holes (mortar-wrapped specimens) exhibited corrosion activity and (2) the corrosion potential measurements. Because variations in chloride content occur in structures in

the field, damage to the epoxy coating on a bar does not automatically mean that corrosion will occur at every point at which damage occurs.

Conventional steel exhibits the lowest corrosion resistance of the systems evaluated in this study. Conventional ECR has total corrosion losses equal to less than 5.6% of the corrosion loss of conventional steel based on total area.

A lower *w*/*c* ratio is effective in improving the corrosion protection of the steel in uncracked concrete, with the exception of conventional ECR cast in concrete with Rheocrete 222+, but provides no additional protection in cracked concrete.

Corrosion inhibitors can lower total corrosion losses in uncracked mortar or concrete. In cracked concrete, however, the use of corrosion inhibitors does not improve the corrosion protection of the steel.

In uncracked concrete (the SE test) with a *w*/*c* ratio of 0.45, the encapsulated calcium nitrite around drilled holes appears to provide protection for the first 45 weeks. When it is consumed, however, corrosion losses rapidly accumulate. For concrete with a *w*/*c* ratio of 0.35, however, ECR with a calcium nitrite primer performs better than conventional ECR; this is probably due to the low chloride penetration rate in concrete with a *w*/*c* ratio of 0.35, lowering the demand for the encapsulated calcium nitrite. In cracked concrete (the CB test), ECR with a primer containing encapsulated calcium nitrite does not show improvement in corrosion resistance when compared to conventional ECR at any *w*/*c* ratio.

Multiple coated reinforcement shows higher total corrosion losses than conventional ECR in concrete. Specimens with multiple coated bars have total corrosion losses between 5.3% and 17% of the corrosion loss for conventional ECR in the rapid macrocell test with bare bar specimens, and between 1.09 and 18.3 times the corrosion losses for conventional ECR in concrete. As shown by the top mat

corrosion potentials plots (Figures 3.104, 3.111, 3.116, and 3.122), zinc provides corrosion protection to the underlying steel. A full understanding of the performance of the multiple coated reinforcement will not be available until the tests are completed to determine the level of protection provided to the underlying steel.

The total corrosion losses for high adhesion ECR bars ranged between 8% and 98% of the corrosion loss of conventional ECR in the rapid macrocell test with bare bars and between 29% and 253% of the corrosion losses for conventional ECR in mortar or concrete.

No corrosion activity has been observed for the majority of the Doniphan County and Mission Creek bridge decks, with the exception of regions adjacent to the abutments, which is primarily due to the use of mild steel form ties.

2205p stainless steel in the accompanying bench-scale and field tests shows excellent performance. The results are consistent with the study by Balma et al. (2005).

ECR bars with the chromate pretreatment had the best quality of bonding between the epoxy and the substrate steel as measured by the cathodic disbondment test, followed by multiple coated reinforcement, ECR with a calcium nitrite primer, and high adhesion DuPont bars. Because conventional ECR and high adhesion Valspar bars do not meet the cathodic disbondment requirement in ASTM A 775, it is recommended that cathodic disbondment requirements be strengthened in the quality control checks for production bars.

The following sections summarize the detailed results for all the corrosion protection systems evaluated in this study.

3.8.1 Conventional Steel and Epoxy-Coated Reinforcement

Conventional steel and epoxy-coated reinforcement were evaluated as control specimens using the rapid macrocell, bench-scale, and field tests.

In the rapid macrocell test with bare bar specimens (Table 3.2), conventional steel had a total corrosion loss of 6.03 μm. Based on total area, ECR with four holes exhibited values of 0.34 μm, equal to 5.6% of the corrosion loss of conventional steel.

In the rapid macrocell tests with mortar-wrapped specimens (Table 3.3), conventional steel had a total corrosion loss of 4.82 μm. Based on total area, ECR with four holes exhibited a negative total corrosion loss less, indicating that macrocell corrosion losses were not observed for the reinforcing bar at the anode.

In the Southern Exposure test (Table 3.4), conventional steel cast in concrete with a *w/c* ratio of 0.35 had a total corrosion loss of –0.003 μm at week 40. By week 63, conventional steel with a *w*/*c* ratio of 0.35 had a total corrosion loss of 0.27 μm, equal to 45% of that observed for conventional steel (0.60 μm) in concrete with a *w*/*c* ratio of 0.45. Based on total area, conventional ECR with a *w/c* ratio of 0.45 and either four or 10 holes exhibited total corrosion losses of approximately 0.003 μm, equal to less than 3% of that for conventional steel. ECR with a *w/c* ratio of 0.35 and 10 holes had a corrosion loss equal to 82% of the corrosion loss of ECR with a *w*/*c* ratio of 0.45 and 10 holes.

In the cracked beam test (Table 3.5), conventional steel cast in concrete with a *w/c* ratio of 0.45 had a total corrosion loss of 5.23 μm, 1.69 times the corrosion loss of conventional steel cast in concrete with a *w/c* ratio of 0.35 (3.10 μm). ECR cast in concrete with a *w/c* ratio of 0.45 had total corrosion losses of 0.02 and 0.03 μm for ECR with four and 10 holes, respectively, equal to less than 1% of the corrosion loss of conventional steel. Conventional ECR with a *w/c* ratio of 0.35 and 10 holes had a

corrosion loss of 0.08 μm based on total area, 2.25 times the corrosion loss of conventional ECR with a *w*/*c* ratio of 0.45 and 10 holes.

In a previous study by Balma et al. (2005), ECR with four holes was evaluated in the rapid macrocell test with mortar-wrapped specimens and in the bench-scale tests. ECR with four holes was used as the anode and conventional steel as the cathode. Based on total area, the total corrosion losses were 0.39 μm for mortar-wrapped specimens at week 15, and 0.07 and 1.22 μm for the SE and CB test specimens at week 40, respectively. In the current study, conventional ECR had a negative total corrosion loss in the macrocell test with mortar-wrapped specimens. Conventional ECR in the current study had total corrosion losses of 0.003 and 0.024 μm, respectively, in the SE and CB tests, equal to 4.1% and 2.0% of those for specimens with ECR as the anode and uncoated steel as the cathode. The results demonstrate that uncoated steel at the cathode has a great effect on the corrosion performance of ECR. Epoxy-coated bars should be used throughout a bridge deck, rather than just as the top mat of steel.

In the ASTM G 109 test (Table 3.6), conventional steel exhibited a total corrosion loss equal to 1.0% of the corrosion loss of conventional steel in the SE test at week 60. Conventional ECR with four holes had a total corrosion loss equal to 35% of the corrosion loss of conventional ECR in the SE test. Conventional ECR with 10 holes had a total corrosion loss of 0.84 μm, compared with 0.76 μm for conventional ECR with 10 holes in the SE test.

In the field test (Tables 3.7 and 3.8), total corrosion losses less than 0.005 μm were observed for all specimens based on total area at week 32, with the exception of Conv. (2) with cracks, which had a loss of 0.29 μm.

3.8.2 Corrosion Inhibitors and Low Water-Cement Ratios

The rapid macrocell test with mortar-wrapped specimens, bench-scale tests, and a field test were used to evaluate the corrosion performance of three corrosion inhibitors, DCI, Rheocrete, and Hycrete, and ECR with a calcium nitrite primer at *w*/*c* ratios of both 0.45 and 0.35.

In the rapid macrocell test with mortar-wrapped specimens (Table 3.9), specimens cast in mortar with the corrosion inhibitor DCI-S had a negative total corrosion loss, indicating that macrocell corrosion losses were not observed for the reinforcing bars at the anode. Specimens cast in mortar with corrosion inhibitors Hycrete and Rheocrete showed no corrosion activity during the 15-week test period. ECR with a calcium nitrite primer exhibited a total corrosion loss of 0.003 μm based on total area. The poor performance of ECR with a calcium nitrite primer might be related to its appearance. On the as delivered ECR with a calcium nitrite primer, continuous damage was observed over a length of approximately two feet near the ends of the 20-foot long bars. Obvious delaminations and nonuniform coating colors were observed as well.

In the Southern Exposure test (Table 3.10), specimens with corrosion inhibitors DCI-S, Hycrete, or Rheocrete had total corrosion losses between 14% and 92% of that for conventional ECR without corrosion inhibitors. ECR with a calcium nitrite primer had total corrosion losses between 22% and 73% of the corrosion loss for conventional ECR. ECR with a primer containing calcium nitrite, however, exhibited higher total corrosion losses than conventional ECR by weeks 53 and 43, respectively, for specimens with four and 10 holes. Some specimens exhibited negative total corrosion losses at week 40, including ECR(Hycrete), ECR(Rheocrete), and ECR(Hycrete)-10h-35. Of the specimens with *w/c* ratios of 0.45 and 0.35, ECR(DCI)-

10h-35 had a total corrosion loss equal to 71% of the corrosion losses of the corresponding specimens with a *w/c* ratio of 0.45. ECR(Rheocrete)-10h-35 and ECR(primer/$Ca(NO_2)_2$)-10h-35, however, had total corrosion losses equal to 3.46 and 2.75 times, respectively, the corrosion losses of the corresponding specimens with a *w/c* ratio of 0.45.

In the cracked beam test (Table 3.11), specimens with corrosion inhibitors and a *w/c* ratio of 0.45 had total corrosion losses between 25% and 216% of that for conventional ECR. Specimens with corrosion inhibitors and a *w/c* ratio of 0.35 had total corrosion losses between 1.18 and 7.60 times those observed for the corresponding specimens with corrosion inhibitor and a *w/c* ratio of 0.45, and between 1.13 and 1.83 times those for conventional ECR without corrosion inhibitor and a *w/c* ratio of 0.35. The use of corrosion inhibitors or a lower *w/c* ratio does not appear to improve the corrosion protection of the steel in cracked concrete.

In the field test (Tables 3.12 and 3.13), based on total area, specimens with cracks and the corrosion inhibitor DCI-S [(ECR(DCI) (1) and ECR(DCI) (2)] exhibited total corrosion losses of approximately 0.01 μm and the remaining specimens with corrosion inhibitors had corrosion losses less than 0.005 μm.

3.8.3 Multiple Coated Reinforcement

Multiple coated bars were evaluated using the rapid macrocell, bench-scale, and field tests.

In the rapid macrocell test with bare bar specimens (Table 3.14), the multiple coated bars with only epoxy penetrated and with both the epoxy and zinc layers penetrated exhibited total corrosion losses of 17% and 5.3%, respectively of that for conventional ECR.

In the rapid macrocell test with mortar-wrapped specimens (Table 3.15), multiple coated bars with only the epoxy layer penetrated and both layers penetrated had total corrosion losses of 0.019 and –0.003 μm based on total area, compared to a loss of –0.003 μm for conventional ECR.

In the Southern Exposure test (Table 3.16), multiple coated bars with only the epoxy penetrated with four and 10 holes had total corrosion losses of 1.09 and 3.67 times, respectively, of those for the corresponding specimens with conventional ECR. For specimens with both layers penetrated with four and 10 holes, the total corrosion losses were 4.78 and 18.3 times, respectively, of the corrosion loss of the corresponding specimens with conventional ECR.

In the cracked beam test (Table 3.17), multiple coated bars with only the epoxy layer penetrated with four and 10 holes had total corrosion losses of 3.18 and 2.78 times, respectively, that for the corresponding specimens with conventional ECR. Multiple coated bars with both layers penetrated with four and 10 holes had total corrosion losses of 5.09 and 7.63 times, respectively, that for the corresponding specimens with conventional ECR.

In the ASTM G 109 test (Table 3.18), multiple coated bars with four holes had total corrosion losses of 3.87 and 2.87 times that of conventional ECR for specimens with only epoxy penetrated and both layers penetrated, respectively. For specimens with 10 holes, multiple coated bars with only epoxy and both layers penetrated exhibited total corrosion losses 35% and 10%, respectively, that for conventional ECR with 10 holes.

In the field test (Tables 3.19 and 3.20), all specimens with multiple coated bars exhibited total corrosion losses less than 0.005 μm based on total area.

3.8.4 ECR with Increased Adhesion

High adhesion ECR bars, including ECR with the chromate pretreatment to improve the adhesion between the epoxy and the steel and ECR with the high adhesion coatings produced by DuPont and Valspar, were evaluated using the rapid macrocell, bench-scale, and field tests.

In the rapid macrocell test with bare bar specimens (Table 3.21), the high adhesion ECR bars with four holes had total corrosion losses between 7.8% and 98% of the corrosion loss of conventional ECR.

In the rapid macrocell test with mortar-wrapped specimens, the high adhesion ECR bars with four holes showed no corrosion activity during the 15-week test period.

In the Southern Exposure test (Table 3.22), the high adhesion ECR bars with four holes had total corrosion losses between 29% and 92% of the corrosion loss of conventional ECR. The ECR(Chromate) and ECR(Valspar) specimens with four holes, however, exhibited higher total corrosion losses than conventional ECR by week 46. For specimens with 10 holes, ECR(Valspar) had a total corrosion loss 94% of that for conventional ECR. ECR(Chromate) and ECR(DuPont) with 10 holes had total corrosion losses, equal to 2.31 and 1.25 times, respectively, the loss for conventional ECR.

In the cracked beam test (Table 3.23), the high adhesion ECR bars with four holes had total corrosion losses between 1.66 and 2.53 times the loss for conventional ECR. The specimens with 10 holes exhibited total corrosion losses between 1.84 and 2.50 times the corrosion loss of conventional ECR.

In the field test (Tables 3.24 and 3.25), high adhesion ECR bars exhibited total corrosion losses less than 0.005 μm based on total area, with the exception of high adhesion Valspar bars with cracks [ECR(Valspar) (1)], which had a corrosion loss of

approximately 0.01 μm.

3.8.5 ECR with Increased Adhesion Epoxy Cast in Mortar or Concrete Containing Calcium Nitrite

Three types of high adhesion ECR bars cast with the corrosion inhibitor calcium nitrite (DCI-S) were evaluated using the rapid macrocell test with mortar-wrapped specimens and the Southern Exposure tests.

In the rapid macrocell test, the high adhesion ECR bars cast in mortar with DCI-S showed no corrosion activity during the 15-week test period.

In the Southern Exposure test (Table 3.26), high adhesion ECR bars cast in concrete with DCI-S had negative total corrosion losses, with values between –0.08 and –1.78 μm based on total area.

3.8.6 KDOT Bridge Projects

Corrosion potentials were measured at six month intervals for the two bridge decks constructed with 2205p stainless steel, the Doniphan County Bridge (DCB) and Mission Creek Bridge (MCB).

Three rounds of corrosion potential mapping have been performed for both bridge decks. No corrosion activity was observed for the majority of the bridge decks, with measured corrosion potentials more positive than –0.250 V over most of the bridges. Both bridges, however, showed corrosion potentials more negative than –0.350 V in regions close to the abutments, indicating active corrosion in these regions. This is probably due to the use of mild steel form ties in the abutments, as shown in Figure 3.215.

The Southern Exposure, cracked beam, and field tests were performed to study

the corrosion performance of 2205p stainless steel. Only 2205p stainless steel was evaluated in the SE and CB tests, while in the field test, 2205p stainless steel was tested along with conventional steel and ECR.

In the Southern Exposure test (Table 3.27), 2205p stainless steel had negative total corrosion losses, indicating that macrocell corrosion losses were not observed for the reinforcing bars at the anode. In the cracked beam test (Table 3.28), 2205p stainless had total corrosion losses less than 0.13% of the corrosion loss of conventional steel (Figure 3.23).

In the field test specimens for the Doniphan County Bridge (Table 3.29), the conventional steel specimens had total corrosion losses between 7.9% and 49% of those for conventional steel in the SE test (0.95 μm). Specimens with 2205p stainless steel exhibited total corrosion losses less than 0.005 μm. Specimens with conventional ECR showed total corrosion losses less than 0.006 μm, compared to a loss of 0.003 μm for conventional ECR in the SE test.

In the field test specimens for the Mission Creek Bridge (Table 3.30), the conventional steel specimens with and without cracks had total corrosion losses equal to 0.8% and 11%, respectively, of the corrosion loss for the corresponding specimens in the CB (6.32 μm) and SE (0.27 μm) tests. 2205p stainless steel and ECR specimens (with and without cracks) exhibited little corrosion, with total corrosion losses less than 0.005 μm.

CHAPTER 4

LINEAR POLARIZATION RESISTANCE TEST RESULTS

This chapter presents the linear polarization resistance (LPR) test results from this study. The test is used to measure the microcell corrosion rate of reinforcing bars in concrete for selected specimens in the Southern Exposure, cracked beam, and ASTM G 109 tests. The test program is summarized in Tables 2.7 through 2.9 in Chapter 2. One specimen of each type is selected for each corrosion protection system and the number of the specimen is given as "LPR Test Specimen No." in those tables. Both the top and bottom mat bars are tested every four weeks and the connected mat bars are tested every eight weeks.

Section 4.1 discusses the guidelines used to interpret microcell corrosion rate results from the LPR test. The microcell corrosion rates and total corrosion losses are shown in Section 4.2. The correlations between microcell corrosion rate and corrosion potential are presented in Section 4.3. Section 4.4 summarizes the results.

4.1 INTERPRETATION OF MICROCELL CORROSION RATE

The linear polarization resistance technique has been widely used to quantitatively determine the microcell corrosion rate of steel in concrete.

Berke (1987) used lollipop specimens with No. 10 (No. 3) reinforcing bars to study the effects of calcium nitrite on the corrosion performance of steel in concrete. The specimens were partially immersed in a 3% salt solution and corrosion performance was monitored using the linear polarization resistance test. The test results showed that for corrosion current densities less than 0.5 $\mu A/cm^2$, the reinforcing bars were passive and rust free after two years.

As presented earlier, in Chapter 1, the relationship between corrosion rate and corrosion current density for iron is given by

$$r = 11.59i \tag{4.1}$$

where r is corrosion rate in terms of μm/yr, and i is corrosion current density in $\mu A/cm^2$. For zinc, the coefficient in Eq. (4.1) changes from 11.59 to 14.99.

Clear (1989) made more than 5,000 measurements on more than 25 structures as well as numerous laboratory and outdoor exposure specimens using a 3LP (three-electrode linear polarization) device. Based on the results, Clear (1989) proposed guidelines for use in data interpretation (assuming constant corrosion rates with time), as shown in Table 4.1. The corrosion current densities were calculated by using a Stern-Geary constant B of 52 mV [Eq. (1.13)].

Table 4.1 – Guidelines for interpretation of LPR test results by Clear (1989) [+]

Corrosion Current Density [+]	**Corrosion Rate**	**Corrosion Level**
μA/cm²	**μm/yr**	
< 0.22	2.55	No corrosion damage expected
0.22 to 1.08	2.55 to 12.53	Corrosion damage possible in 10 to 15 years
1.08 to 10.76	12.53 to 124.82	Corrosion damage possible in 2 to 3 years
> 10.76	>124.82	Corrosion damage expected in 2 years or fewer

[+] Stern-Geary constant, B = 52 mV

Similar guidelines for data interpretation were developed by Broomfield (1997) based on laboratory and field investigations, as shown in Table 4.2. In the latter case, a guard ring (a second electrode concentric to the counter electrode) was introduced to confine the influence area of the counter electrode by actively confining the polarization current. A Stern-Geary constant B of 26 mV was used and this may explain the factor of two difference in interpretation at the low end. At the high end,

the difference between the two interpretations could be the result of (1) the use of a guard ring results in lower corrosion rates, or (2) the device used by Clear (1989) may have been used on more actively corroding structures and the interpretation range may therefore have been extended, as discussed by Broomfield (1997). By any measure, the corrosion rates shown for the three highest categories in Table 4.1 are very high.

Table 4.2 – Guidelines for interpretation of LPR test results by Broomfield (1997) [+]

Corrosion Current Density [+]	Corrosion Rate	Corrosion Level
μA/cm^2	μm/yr	
< 0.1	< 1.16	Passive condition
0.1 to 0.5	1.16 to 5.8	Low to moderate corrosion
0.5 to 1.0	5.8 to 11.6	Moderate to high corrosion
> 1.0	> 11.6	High corrosion

[+] Stern-Geary constant, B = 26 mV

In the current study, each bench-scale test specimen is tested in three ways, with the top, bottom, and connected mats. Even though the LPR test in this study was performed without the use of a guard ring, the polarized area is well-defined for the selected bench-scale test specimens, as shown in Table 2.27 in Chapter 2. A Stern-Geary constant B of 26 mV is used to calculate the corrosion current density [Eq. (1.13)] and microcell corrosion rate [Eq. (2.2)]. Therefore, the guidelines shown in Table 4.2 are more appropriate than those in Table 4.1 and will be used to interpret microcell corrosion rates from the LPR test in this study.

4.2 MICROCELL CORROSION

This section presents the LPR test results for bench-scale test specimens. For the specimens with epoxy-coated reinforcement, microcell corrosion rates and total

corrosion losses are expressed in terms of both the total and the exposed area of steel. It should be noted that for most test specimens, the LPR tests were performed every four weeks beginning in week 4. For some specimens, however, the LPR test started as late as week 16.

For each specimen, only the microcell corrosion rates in the top mat are reported in this section. This is due to the fact that the microcell corrosion rates in the bottom mat are usually one to two orders lower than those in the top mat. The corrosion rates and total corrosion losses based on total anodic area in contact with concrete are shown in Figures 4.1 through 4.34 for the different corrosion protection systems. The total corrosion losses are summarized in Table 4.3 for the SE and CB tests at week 40, and in Table 4.4 for the ASTM G 109 test at week 61, both based on total area and exposed area.

The guidelines developed by Broomfield (1997) were based on the laboratory and field investigations for conventional reinforcing steel, and, therefore, can be used to interpret the microcell corrosion rates for conventional steel. These guidelines, however, are not applicable for epoxy-coated reinforcement.

All microcell corrosion rate results and the corrosion potentials for the top, bottom, and connected mats are presented in Appendix E. In addition, Appendix E also presents individual comparisons between microcell corrosion rate and corrosion potential. As shown in Appendix E, the microcell corrosion rates in the connected mat are somewhere between the results of the top and bottom mats for the CB test specimens, but not necessarily for the SE and ASTM G 109 test specimens.

Table 4.3 – Total corrosion losses (μm) at week 40 based on microcell corrosion rates for the Southern Exposure and cracked beam tests based on the linear polarization resistance test

Steel Designation[a]	Based on Total Area		Based on Exposed Area	
	Southern Exposure Test	Cracked Beam Test	Southern Exposure Test	Cracked Beam Test
Control				
Conv.	3.26E-01	2.46E+01	-	-
Conv.-35	1.86E-01	3.22E+01	-	-
ECR	3.32E-04	1.51E-02	1.59E-01	7.25E+00
ECR-10h	7.01E-03	1.07E-01	1.35E+00	2.06E+01
ECR-10h-35	3.64E-03	2.25E-01	6.98E-01	4.31E+01
Corrosion Inhibitors				
ECR(DCI)	4.88E-04	2.09E-01	2.34E-01	1.01E+02
ECR(DCI)-10h	1.44E-03	2.28E-01	2.76E-01	4.37E+01
ECR(DCI)-10h-35	9.28E-04	8.39E-01	1.78E-01	1.61E+02
ECR(Rheocrete)	9.39E-04	4.12E-01	4.51E-01	1.98E+02
ECR(Rheocrete)-10h	5.31E-03	3.51E-01	1.02E+00	6.75E+01
ECR(Rheocrete)-10h-35	8.30E-03	1.90E-01	1.59E+00	3.65E+01
ECR(Hycrete)	2.12E-03	7.44E-02	1.02E+00	3.57E+01
ECR(Hycrete)-10h	2.14E-03	4.13E-01	4.10E-01	7.93E+01
ECR(Hycrete)-10h-35	1.65E-03	1.72E-01	3.17E-01	3.30E+01
ECR(primer/$Ca(NO_2)_2$)	1.44E-03	2.83E-01	6.89E-01	1.36E+02
ECR(primer/$Ca(NO_2)_2$)-10h	2.77E-03	1.68E-01	5.32E-01	3.23E+01
ECR(primer/$Ca(NO_2)_2$)-10h-35	5.48E-03	4.72E-01	1.05E+00	9.07E+01
Multiple Coated Bars				
MC(both layers penetrated)	1.39E-01	6.80E-01	6.68E+01	3.26E+02
MC(both layers penetrated)-10h	1.59E-01	1.00E+00	3.04E+01	1.93E+02
MC(only epoxy penetrated)	1.43E-01	9.32E-01	6.86E+01	4.47E+02
MC(only epoxy penetrated)-10h	5.69E-02	2.60E-01	1.09E+01	4.99E+01
Increased Adhesion				
ECR(Chromate)	1.22E-03	5.33E-01	5.83E-01	2.56E+02
ECR(Chromate)-10h	1.14E-02	3.91E-02	2.19E+00	7.51E+00
ECR(DuPont)	3.45E-03	1.21E-01	1.65E+00	5.79E+01
ECR(DuPont)-10h	1.66E-02	2.18E-01	3.18E+00	4.18E+01
ECR(Valspar)	2.58E-03	7.35E-01	1.24E+00	3.53E+02
ECR(Valspar)-10h	9.89E-03	3.72E-01	1.90E+00	7.15E+01
Increased Adhesion with Corrosion Inhibitor DCI				
ECR(Chromate)-DCI	2.97E-03		1.43E+00	
ECR(DuPont)-DCI	6.22E-04		2.98E-01	
ECR(Valspar)-DCI	1.57E-03		7.53E-01	

[a] Conv. = conventional steel. ECR = conventional epoxy-coated reinforcement.
ECR(Chromate) = ECR with the zinc chromate pretreatment.
ECR(DuPont) = high adhesion DuPont bars. ECR(Valspar) = high adhesion Valspar bars.
ECR(DCI) = conventional ECR in concrete with DCI inhibitor.
ECR(Rheocrete) = conventional ECR in concrete with Rheocrete inhibitor.
ECR(Hycrete) = conventional ECR in concrete with Hycrete inhibitor.
ECR(primer/$Ca(NO_2)_2$) = ECR with a primer containing calcium nitrite
MC(both layers penetrated) = multiple coated bars with both the zinc and epoxy layers penetrated.
MC(only epoxy penetrated) = mutiple coated bars with only the epoxy layer penetrated.
10h = epoxy-coated bars with 10 holes, otherwise four 3 mm ($^1/_8$ in.) diameter holes.
35 = concrete w/c=0.35, otherwise w/c=0.45.

Table 4.4 – Total corrosion losses (μm) at week 61 based on microcell corrosion rates for the ASTM G 109 test based on the linear polarization resistance test

Steel Designation[a]	Based on Total Area	Based on Exposed Area
	ASTM G 109 Test	ASTM G 109 Test
Control		
Conv.	7.89E-02	-
ECR	4.91E-04	2.16E-01
ECR-10h	9.28E-03	1.63E+00
Multiple Coated Bars		
MC(both layers penetrated)	7.88E-04	3.47E-01
MC(both layers penetrated)-10h	8.16E-03	1.44E+00
MC(only epoxy penetrated)	1.89E-03	8.31E-01
MC(only epoxy penetrated)-10h	9.75E-03	1.72E+00

[a] Conv. = conventional steel. ECR = conventional epoxy-coated reinforcement.
MC(both layers penetrated) = multiple coated bars with both the zinc and epoxy layers penetrated.
MC(only epoxy penetrated) = mutiple coated bars with only the epoxy layer penetrated.
10h = epoxy-coated bars with 10 holes, otherwise four 3 mm ($^1/_8$ in.) diameter holes.

4.2.1 Conventional Steel and Epoxy-Coated Reinforcement

This section describes the results from the LPR test for conventional steel and epoxy-coated reinforcement. The results, expressed in terms of corrosion rates and total corrosion losses, are shown in Figures 4.1 through 4.6.

Figures 4.1 and 4.2 show the microcell corrosion rates and total corrosion losses for the SE specimens. As shown in Figure 4.1(a), conventional steel in concrete with a *w*/*c* ratio of 0.45 (Conv.) exhibited the highest microcell corrosion rate, followed by the conventional steel in concrete with a *w*/*c* ratio of 0.35 (Conv.-35). The Conv. specimen showed moderate to high corrosion (see Table 4.2) by week 52 and high corrosion by week 60. The Conv.-35 specimen showed low to moderate corrosion by week 44. At the time of this writing, the highest microcell corrosion rates were 18.3 μm/yr for the Conv. specimen at week 68 and 2.05 μm/yr for the Conv.-35 specimen at week 56, respectively. As shown in Figure 4.1(b), conventional ECR with 10 holes (ECR-10h) showed the highest microcell corrosion among the

three ECR specimens, with a maximum value of 0.16 μm/yr at week 56, while the other two specimens exhibited negligible corrosion (less than 0.02 μm/yr) based on total area of steel.

The Conv. specimen had the highest total corrosion loss, followed by the Conv.-35 specimen, as shown in Figure 4.2(a). As shown in Table 4.3, the total corrosion losses at week 40 were 0.33 and 0.19 μm for the Conv. and Conv.-35 specimens, respectively. Of the three ECR specimens, shown in Figure 4.2(b), ECR-10h had the highest corrosion loss, followed by ECR-10h-35 and ECR with four holes. Based on total area, the total corrosion losses were 0.007 μm for ECR-10h, 0.004 μm for ECR-10h-35, and less than 0.001 μm for conventional ECR with four holes, as shown in Table 4.3. Based on exposed area, the respective values were 1.35, 0.70, and 0.16 μm.

Figures 4.3 and 4.4 show the microcell corrosion rates and total corrosion losses for the CB specimens. As described in Section 3.1.2.2, both the Conv. and Conv.-35 specimens exhibited high macrocell corrosion at the beginning of the test. In contrast, as shown in Figure 4.3(a), the Conv. and Conv.-35 specimens exhibited steady growth in microcell corrosion rate over time. The two specimens exhibit similar microcell corrosion rates. The highest microcell corrosion rates were 375 μm/yr at week 68 for the Conv. specimen and 126 μm/yr at week 56 for the Conv.-35 specimen. For conventional steel, the microcell corrosion behavior is different from the macrocell corrosion behavior. As shown in Figure 3.21(a) in Chapter 3, corrosion rates above 9 μm/yr during the initial weeks are observed for conventional steel because the cracks in the specimens provide a direct path for the chlorides to the steel. Then due to the formation of corrosion products, the average macrocell corrosion rates remained between 3 and 9 μm/yr.

As shown in Figure 4.3(b), the three ECR specimens had similar microcell corrosion rates, with values below 0.80 μm/yr.

Figure 4.4(a) shows that the Conv.-35 cracked beam specimen exhibited the highest corrosion loss (3.22 μm) at 40 weeks, followed by Conv. at 2.46 μm. As shown in Figure 4.4(b), ECR-10h-35 had the highest corrosion loss among the three ECR specimens, followed by ECR-10h and ECR with four holes. As shown in Table 4.3, based on total area, the total corrosion losses at week 40 were 0.23, 0.11, and 0.02 μm for ECR-10h-35, ECR-10h, and ECR with four holes, respectively. Based on exposed area, the respective values were 43.1, 20.6, and 7.25 μm.

Figures 4.5 and 4.6 show the microcell corrosion rates and total corrosion losses for the ASTM G 109 specimens (all had *w*/*c* ratio of 0.45). As shown in Figure 4.5, conventional steel exhibited the highest microcell corrosion rates, with microcell corrosion rates between 0.03 and 0.11 μm/yr based on total area. Conventional ECR with 10 holes exhibited higher microcell corrosion rates than conventional ECR with four holes, with a high value of approximately 0.03 μm/yr based on total area. As shown in Figure 5.6, conventional steel had the highest total corrosion loss, followed by ECR-10h and conventional ECR with four holes. The total corrosion losses at week 61 were 0.08 μm for conventional steel, followed by ECR-10h at 0.009 μm (1.63 μm based on exposed area) and conventional ECR with four holes at a value of less than 0.001 μm (0.22 μm based on exposed area), as shown in Table 4.4.

As shown in Table 4.4, conventional ECR exhibited total corrosion losses less than 7.1% of those for the corresponding conventional steel in the SE and CB tests. The use of a *w*/*c* ratio of 0.35 lowered the microcell corrosion by 40% in uncracked concrete (the SE test), but did not have an effect in cracked concrete (the CB test).

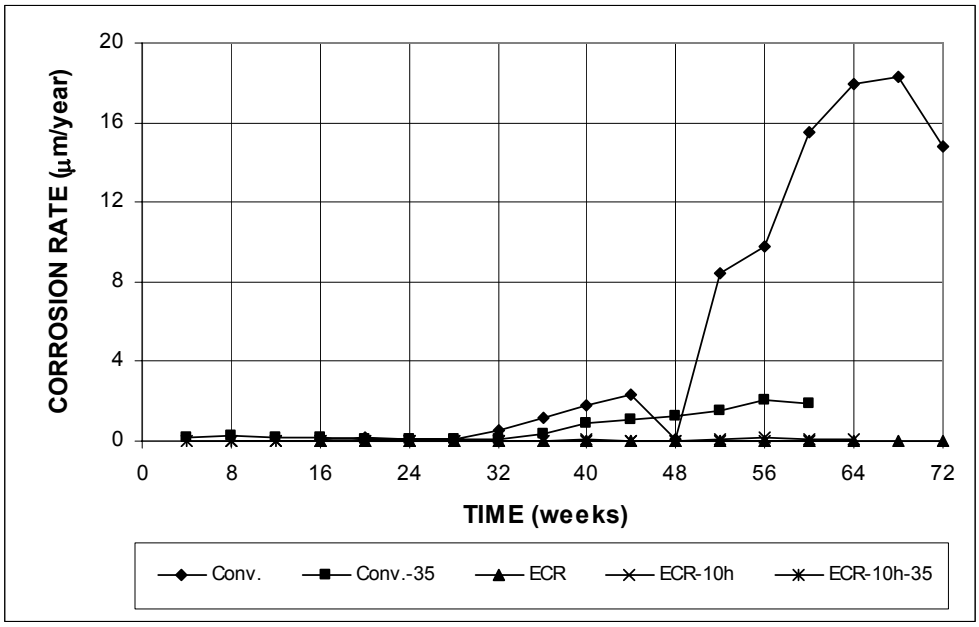

Figure 4.1 (a) – Microcell corrosion rates as measured using LPR in the Southern Exposure test for specimens with conventional steel and ECR (ECR have four holes and ECR-10h have 10 holes).

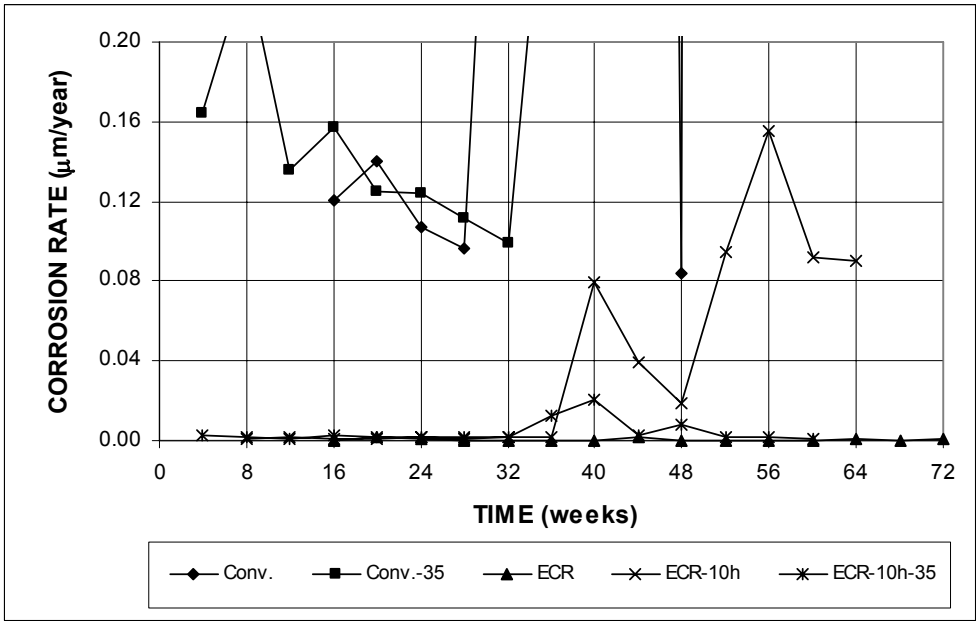

Figure 4.1 (b) – Microcell corrosion rates as measured using LPR in the Southern Exposure test for specimens with conventional steel and ECR (ECR have four holes and ECR-10h have 10 holes).

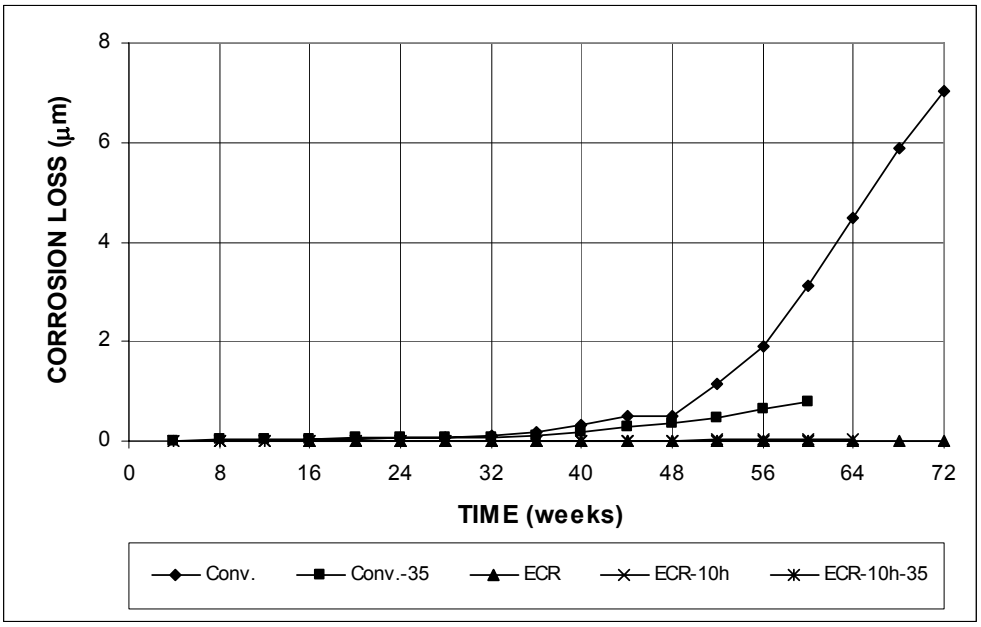

Figure 4.2 (a) – Microcell corrosion losses as measured using LPR in the Southern Exposure test for specimens with conventional steel and ECR (ECR have four holes and ECR-10h have 10 holes).

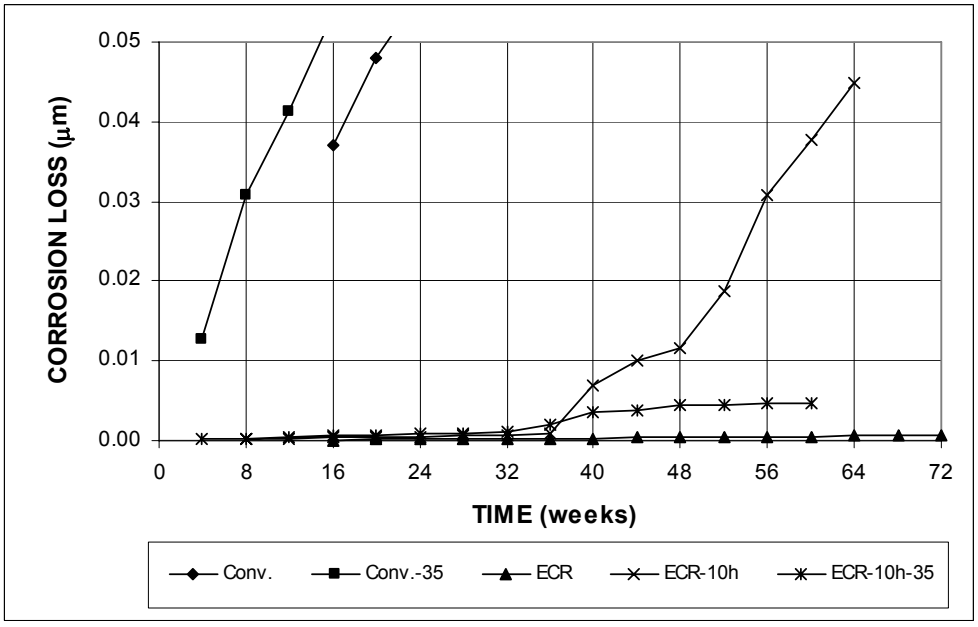

Figure 4.2 (b) – Microcell corrosion losses as measured using LPR in the Southern Exposure test for specimens with conventional steel and ECR (ECR have four holes and ECR-10h have 10 holes).

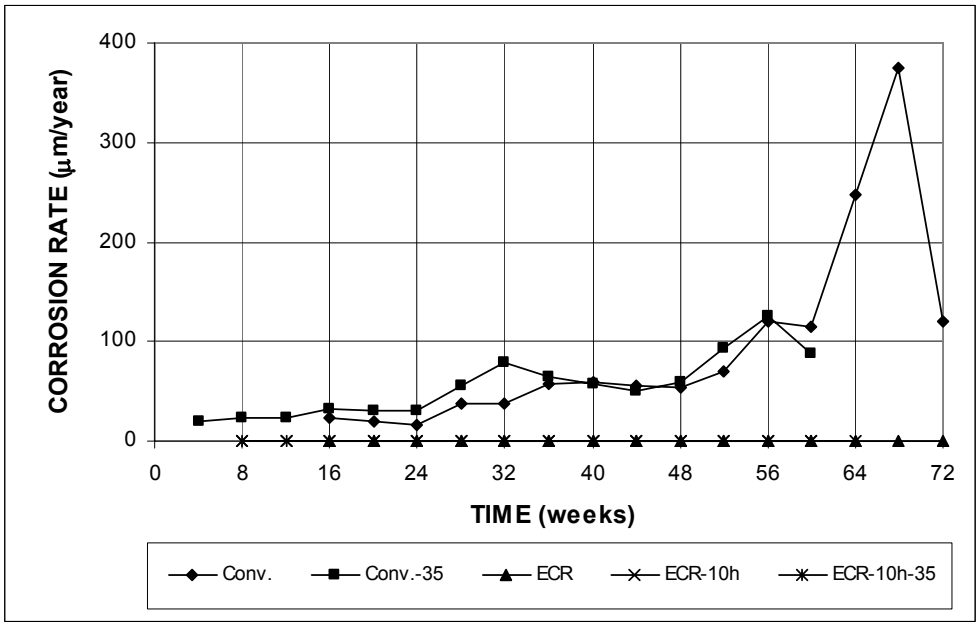

Figure 4.3 (a) – Microcell corrosion rates as measured using LPR in the cracked beam test for specimens with conventional steel and ECR (ECR have four holes and ECR-10h have 10 holes).

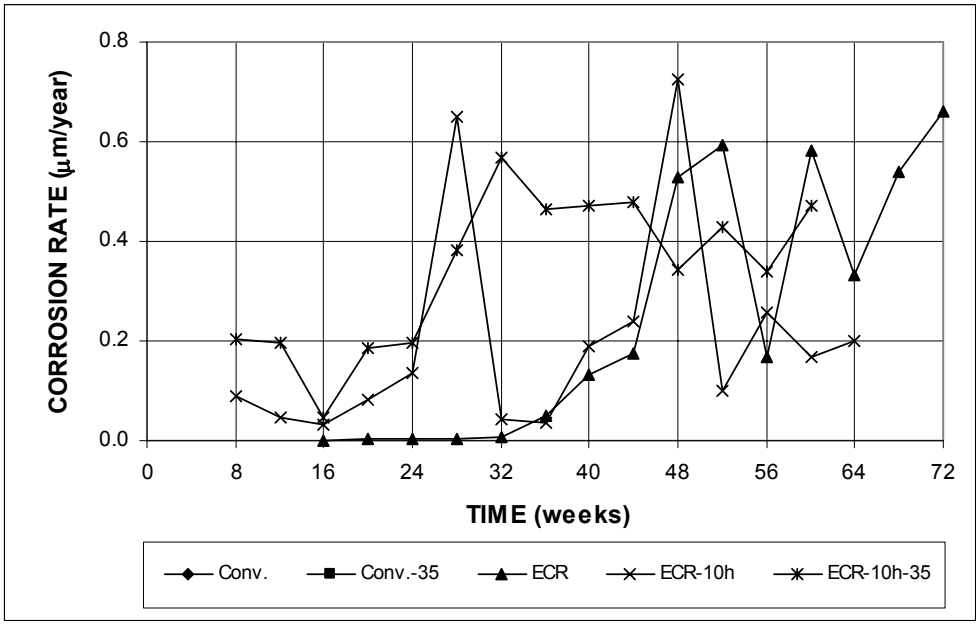

Figure 4.3 (b) – Microcell corrosion rates as measured using LPR in the cracked beam test for specimens with conventional steel and ECR (ECR have four holes and ECR-10h have 10 holes).

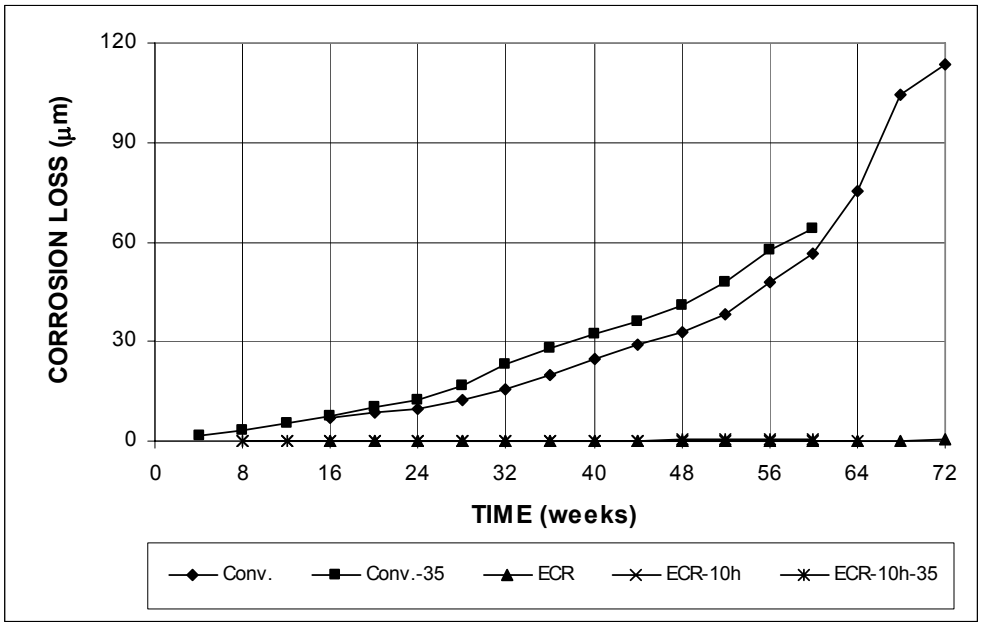

Figure 4.4 (a) – Microcell corrosion losses as measured using LPR in the cracked beam test for specimens with conventional steel and ECR (ECR have four holes and ECR-10h have 10 holes).

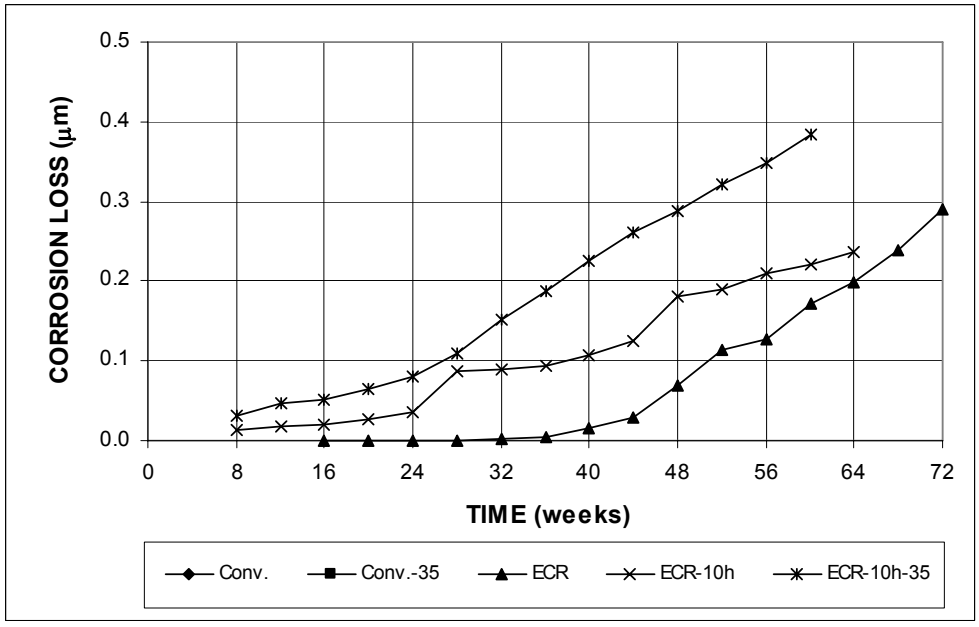

Figure 4.4 (b) – Microcell corrosion losses as measured using LPR in the cracked beam test for specimens with conventional steel and ECR (ECR have four holes and ECR-10h have 10 holes).

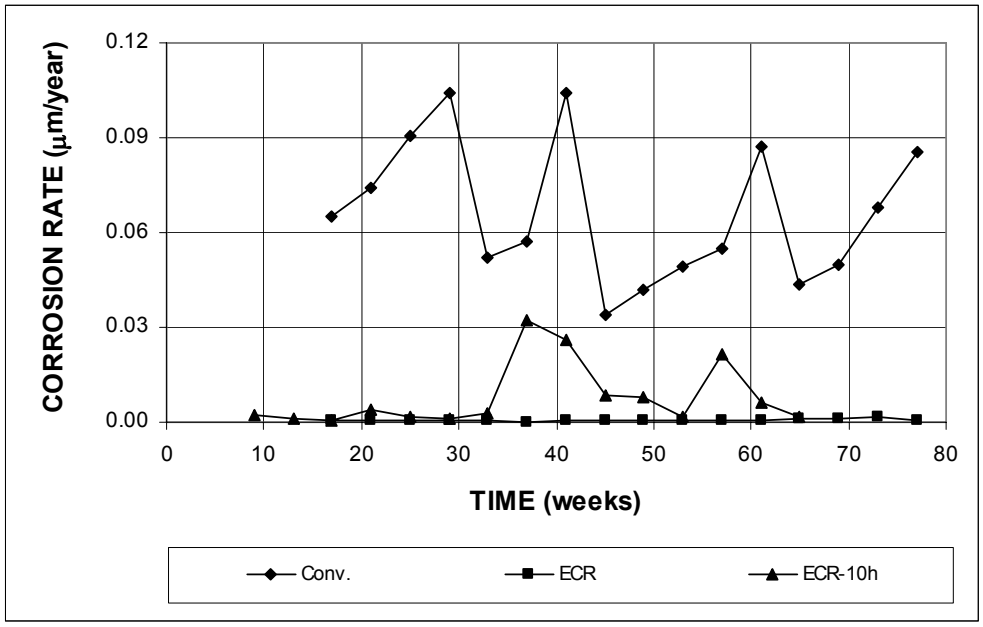

Figure 4.5 – Microcell corrosion rates as measured using LPR in the ASTM G 109 test for specimens with conventional steel and ECR (ECR have four holes and ECR-10h have 10 holes).

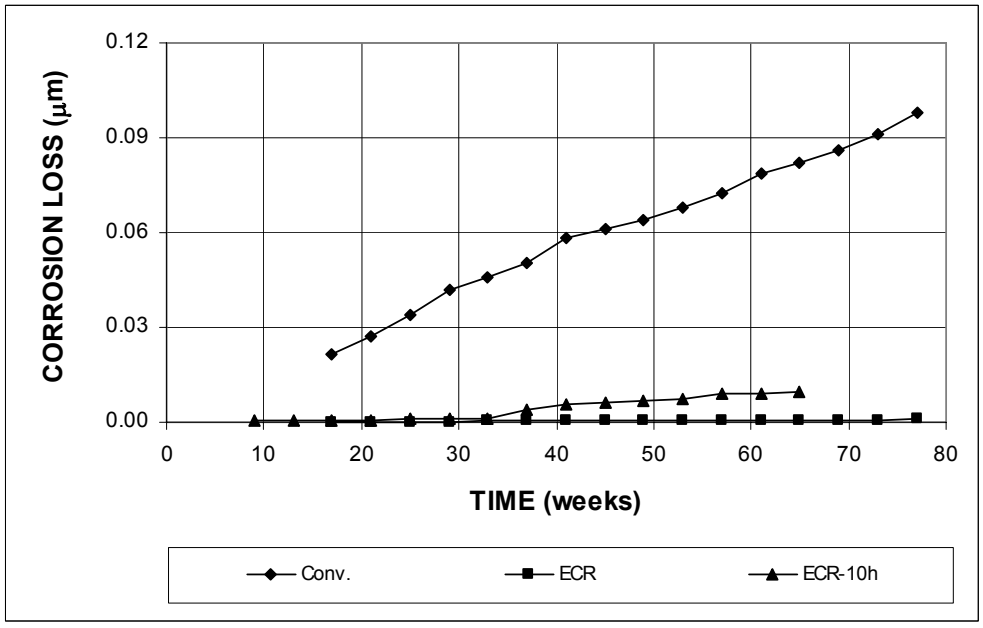

Figure 4.6 – Microcell corrosion losses as measured using LPR in the ASTM G 109 test for specimens with conventional steel and ECR (ECR have four holes and ECR-10h have 10 holes).

4.2.2 Corrosion Inhibitors and Low Water-Cement Ratios

This section presents the LPR test results for ECR in concrete with the corrosion inhibitors DCI, Rheocrete, and Hycrete, and ECR with a primer containing calcium nitrite. The bars were cast in concretes with *w*/*c* ratios of 0.45 and 0.35, and the results are shown in Figures 4.7 through 4.18. The total corrosion losses at week 40 are summarized in Table 4.3.

Figures 4.7 through 4.12 show the microcell corrosion rates and total corrosion losses based on total area for the SE specimens. All specimens in concrete with a *w*/*c* ratio of 0.45 and four holes exhibited similar corrosion rates, with values less than 0.01 μm/yr, as shown in Figure 4.7. Figure 4.8 shows that the specimens with 10 holes had microcell corrosion rates less than 0.16 μm/yr. Specimens ECR-10h and ECR(DCI)-10h exhibited microcell corrosion rates higher than 0.10 μm/yr, while the remaining three specimens had microcell corrosion rates less than 0.04 μm/yr, as shown in Figure 4.8. Figure 4.9 shows that all specimens in concrete with a *w/c* ratio of 0.35 and 10 holes had corrosion rates similar to those for ECR-10h-35, with microcell corrosion rates below 0.04 μm/yr.

For total corrosion losses, specimens with four holes and corrosion inhibitors had total corrosion losses higher than conventional ECR (Figure 4.10). Based on total area, these specimens had total corrosion losses less than 0.003 μm at week 40, as shown in Table 4.3. For specimens in concrete with a *w*/*c* ratio of 0.45 and with 10 holes (Figure 4.11), all specimens with corrosion inhibitors had total corrosion losses less than conventional ECR, with values below 0.006 μm at 40 weeks. After week 44, however, ECR(DCI)-10h had a total corrosion loss higher than conventional ECR. For specimens in concrete with a *w*/*c* ratio of 0.35 and 10 holes (Figure 4.12), ECR(Rheocrete)-10h-35 and ECR(primer/$Ca(NO_2)_2$)-10h-35 had total corrosion

losses high than conventional ECR with a *w*/*c* ratio of 0.35, with values of 0.008 and 0.006 μm at 40 weeks. ECR(Hycrete)-10h-35 and ECR(DCI)-10h-35 had total corrosion losses of less than 0.002 μm at week 40, as shown in Table 4.3.

Figures 4.13 through 4.18 show the microcell corrosion rates and total corrosion losses for the CB specimens. As shown in Figure 4.13, specimens with four holes had corrosion rates lower than 0.90 μm/yr based on total area, with the exception of ECR(Rheocrete) between weeks 36 and 40 and ECR(primer/$Ca(NO_2)_2$) at week 40, which showed microcell corrosion rates higher than 1.2 μm/yr. Figure 4.14 shows that specimens in concrete with a *w*/*c* ratio of 0.45 and 10 holes exhibited similar corrosion rates, with values less than 1.00 μm/yr, except for ECR(Rheocrete)-10h, which had a rate of 1.91 μm/yr at week 40. Figure 4.15 shows the corrosion rates for specimens in concrete with a *w/c* ratio of 0.35 and 10 holes. Based on total area, the ECR(DCI)-10h-35 specimen showed the highest microcell corrosion rates, with values as high as 1.42 μm/yr at week 12. The remaining specimens had microcell corrosion rates less than approximately 0.80 μm/yr, with the exception of ECR(Hycrete)-10h-35, which had a corrosion rate of 1.35 μm/yr at week 44.

For the total corrosion losses, shown in Figures 4.16 and 4.17, specimens in concrete with a *w*/*c* ratio of 0.45 and either four or 10 holes had total losses higher than conventional ECR, with values between 0.12 and 0.52 μm at 40 weeks. For specimens in concrete with a *w*/*c* ratio of 0.35 and 10 holes (Figure 4.18), ECR(DCI)-10h-35 and ECR(primer/$Ca(NO_2)_2$)-10h-35 had total corrosion losses higher than ECR-10h-35, with values of 0.84 and 0.47 μm at 40 weeks. The ECR(Rheocrete)-10h-35 and ECR(Hycrete)-10h-35 specimens had corrosion losses less than conventional ECR, with values of 0.19 and 0.17 μm at week 40.

As shown in Table 4.3, none of the corrosion inhibitors consistently reduced the

corrosion of reinforcing steel in concrete. In the SE test, in five out of nine cases, specimens showed improvement in corrosion protection compared to conventional ECR, with total corrosion loss between 20% and 76% of the loss for conventional ECR. The remaining specimens had total corrosion losses between 1.47 and 6.39 times the loss for conventional ECR. In the CB test, specimens with corrosion inhibitors Rheocrete and Hycrete in concrete with a *w*/*c* ratio of 0.35 and 10 holes exhibited better corrosion protection than conventional ECR, with corrosion losses of 85% and 77% of that observed for conventional ECR. The remaining specimens had total corrosion losses between 2.12 and 27.3 times the loss observed for conventional ECR.

ECR with a primer containing calcium nitrite did not show improvement in corrosion protection compared to conventional ECR, with the exception of specimens with a *w*/*c* ratio of 0.45 and 10 holes in the SE test, which had a total corrosion loss equal to 39% of the loss for conventional ECR. The remaining specimens exhibited total corrosion losses between 1.50 and 18.7 times those for conventional ECR in the SE and CB tests, respectively.

In uncracked concrete (the SE test) with corrosion inhibitors, the use of a *w*/*c* ratio of 0.35 improved the corrosion protection of reinforcing steel in concrete, except for ECR(Rheocrete). The total corrosion loss for ECR(Rheocrete)-10h-35 at 40 weeks was 1.56 times the value for ECR(Rheocrete)-10h, while in cracked concrete (the CB test), the use of a *w*/*c* ratio of 0.35 provided limited or no addition corrosion protection for reinforcing steel in concrete.

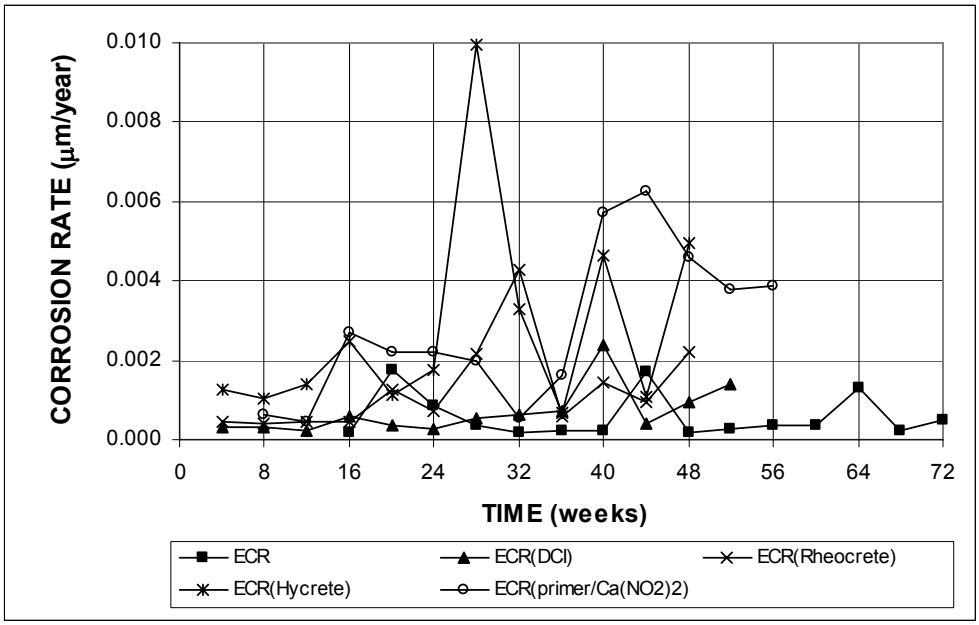

Figure 4.7 – Microcell corrosion rates as measured using LPR in the Southern Exposure test for specimens with ECR, ECR with a primer containing calcium nitrite, and ECR in concrete with corrosion inhibitors (ECR bars have four holes).

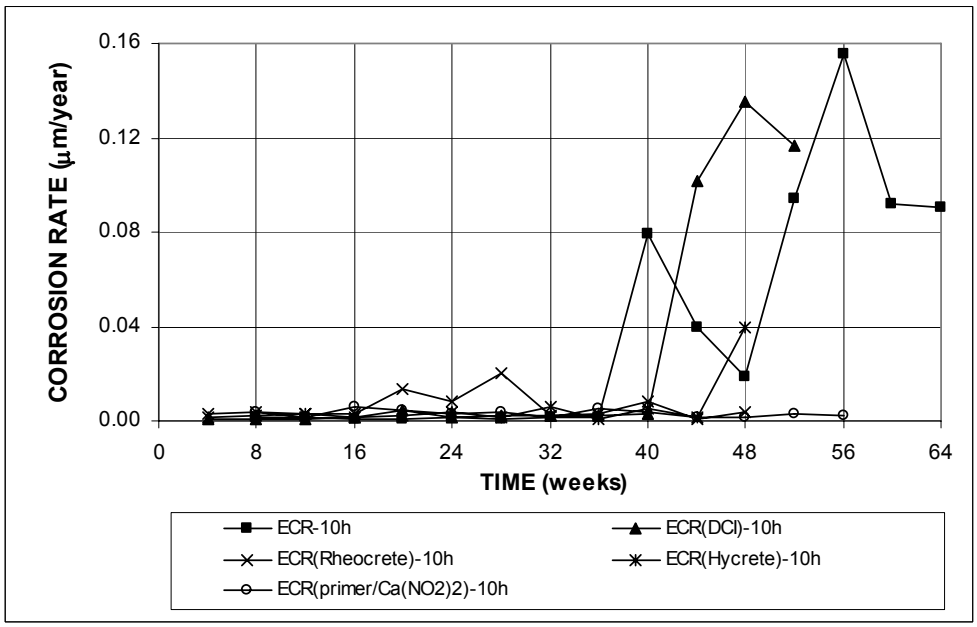

Figure 4.8 – Microcell corrosion rates as measured using LPR in the Southern Exposure test for specimens with ECR, ECR with a primer containing calcium nitrite, and ECR in concrete with corrosion inhibitors (ECR bars have 10 holes).

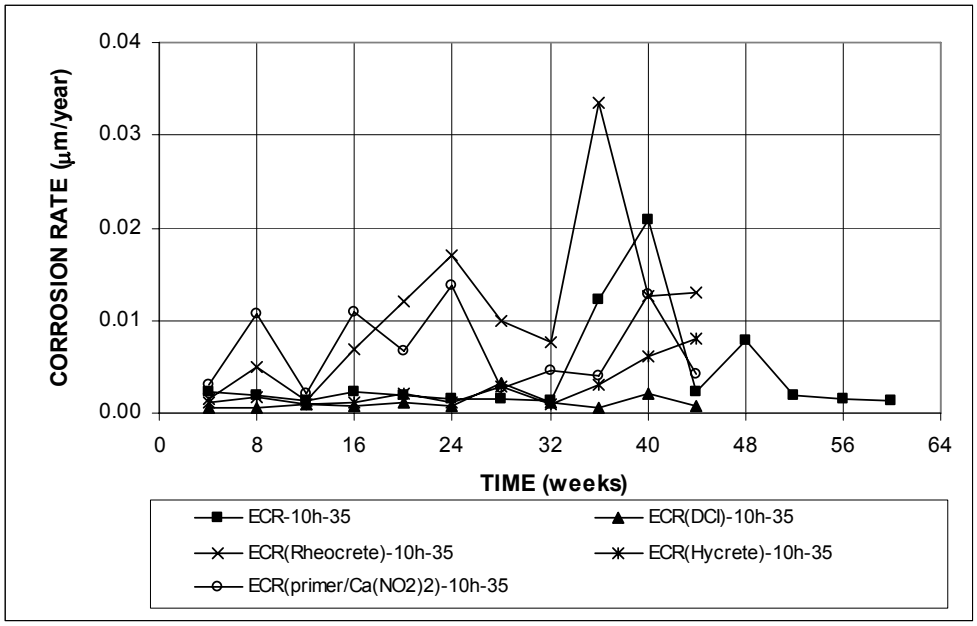

Figure 4.9 – Microcell corrosion rates as measured using LPR in the Southern Exposure test for specimens with ECR, ECR with a primer containing calcium nitrite, and ECR in concrete with corrosion inhibitors, water-cement ratio = 0.35 (ECR bars have 10 holes).

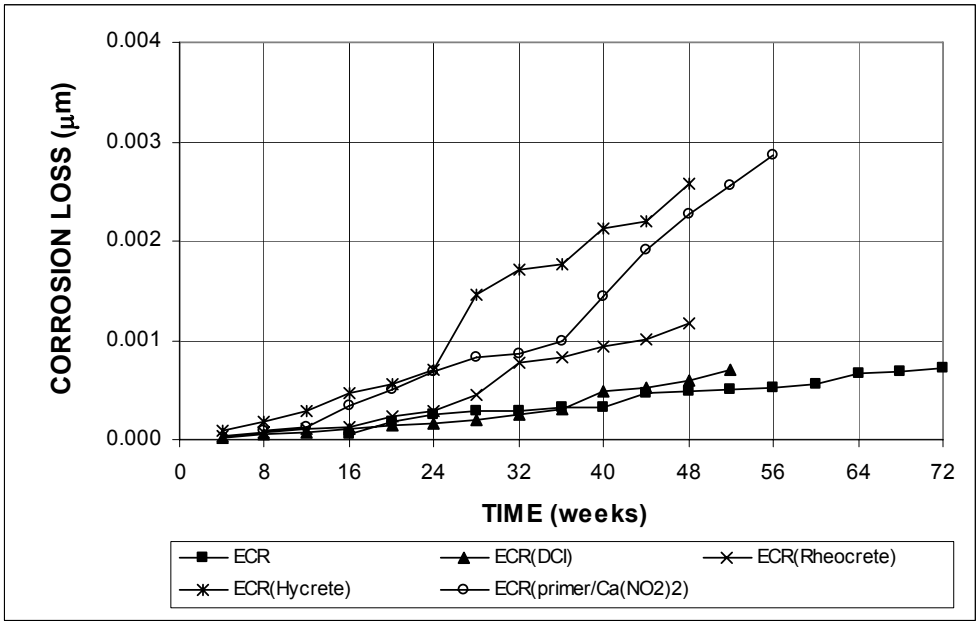

Figure 4.10 – Microcell corrosion losses as measured using LPR in the Southern Exposure test for specimens with ECR, ECR with a primer containing calcium nitrite, and ECR in concrete with corrosion inhibitors (ECR bars have four holes).

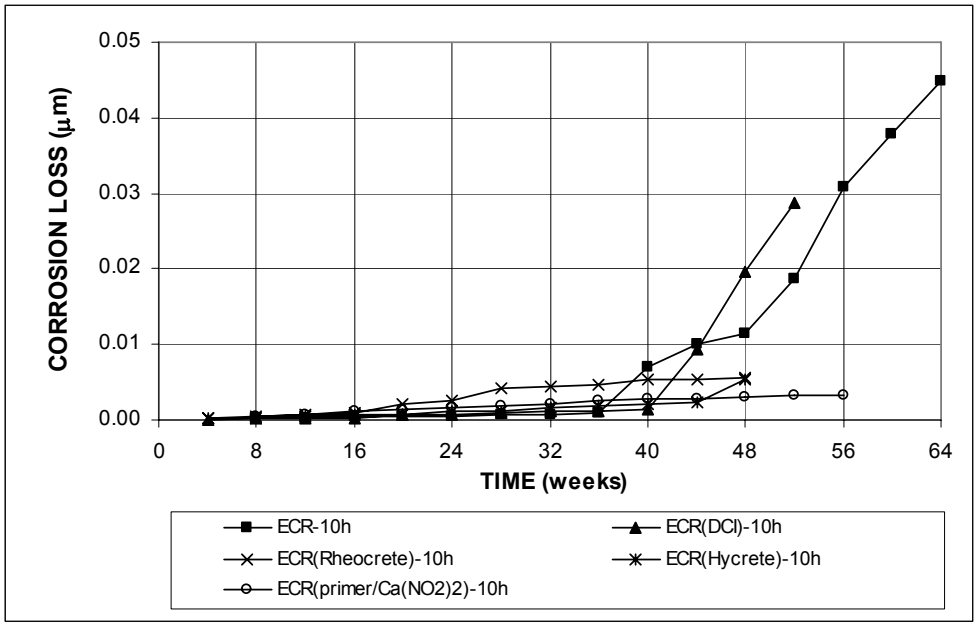

Figure 4.11 – Microcell corrosion losses as measured using LPR in the Southern Exposure test for specimens with ECR, ECR with a primer containing calcium nitrite, and ECR in concrete with corrosion inhibitors (ECR bars have 10 holes).

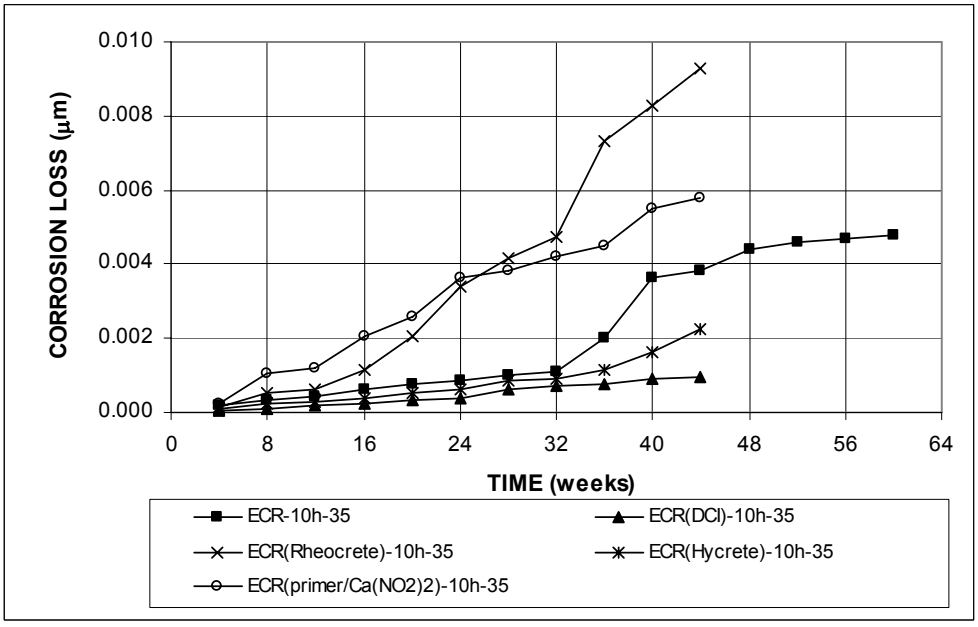

Figure 4.12 – Microcell corrosion losses as measured using LPR in the Southern Exposure test for specimens with ECR, ECR with a primer containing calcium nitrite, and ECR in concrete with corrosion inhibitors, water-cement ratio = 0.35 (ECR bars have 10 holes).

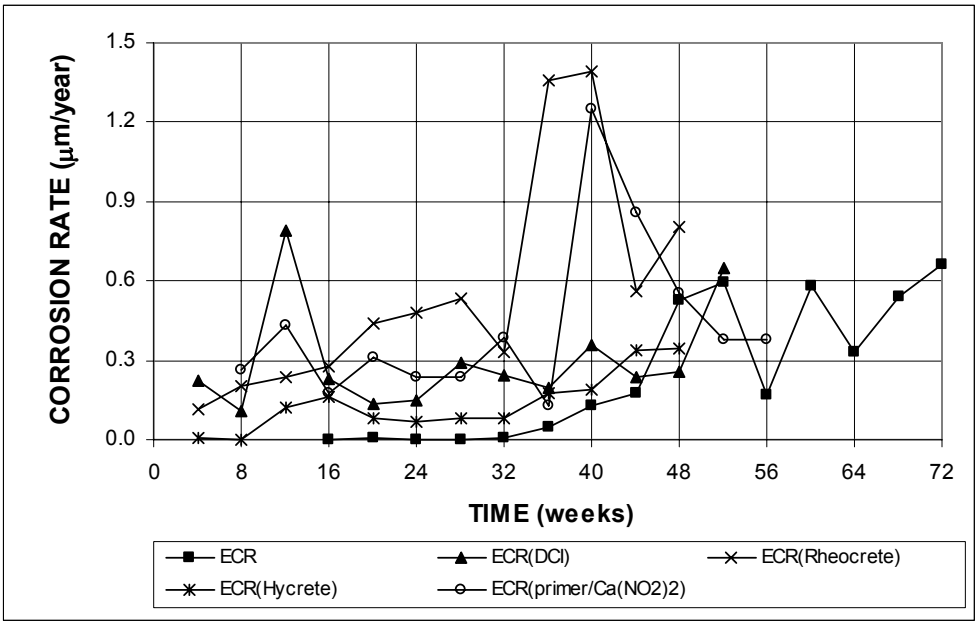

Figure 4.13 – Microcell corrosion rates as measured using LPR in the cracked beam test for specimens with ECR, ECR with a primer containing calcium nitrite, and ECR in concrete with corrosion inhibitors (ECR bars have four holes).

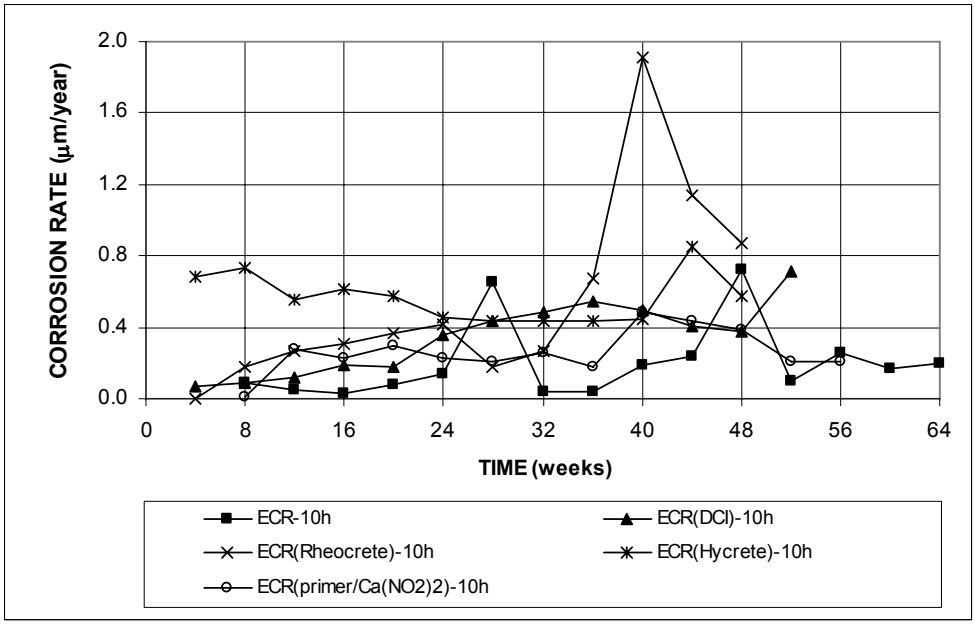

Figure 4.14 – Microcell corrosion rates as measured using LPR in the cracked beam test for specimens with ECR, ECR with a primer containing calcium nitrite, and ECR in concrete with corrosion inhibitors (ECR bars have 10 holes).

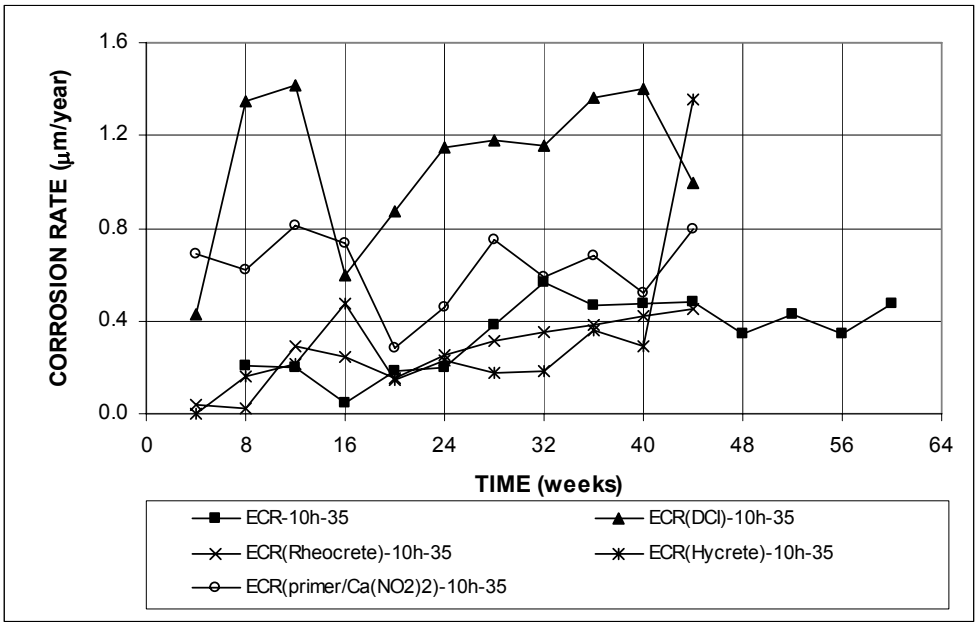

Figure 4.15 – Microcell corrosion rates as measured using LPR in the cracked beam test for specimens with ECR, ECR with a primer containing calcium nitrite, and ECR in concrete with corrosion inhibitors, water-cement ratio = 0.35 (ECR bars have 10 holes).

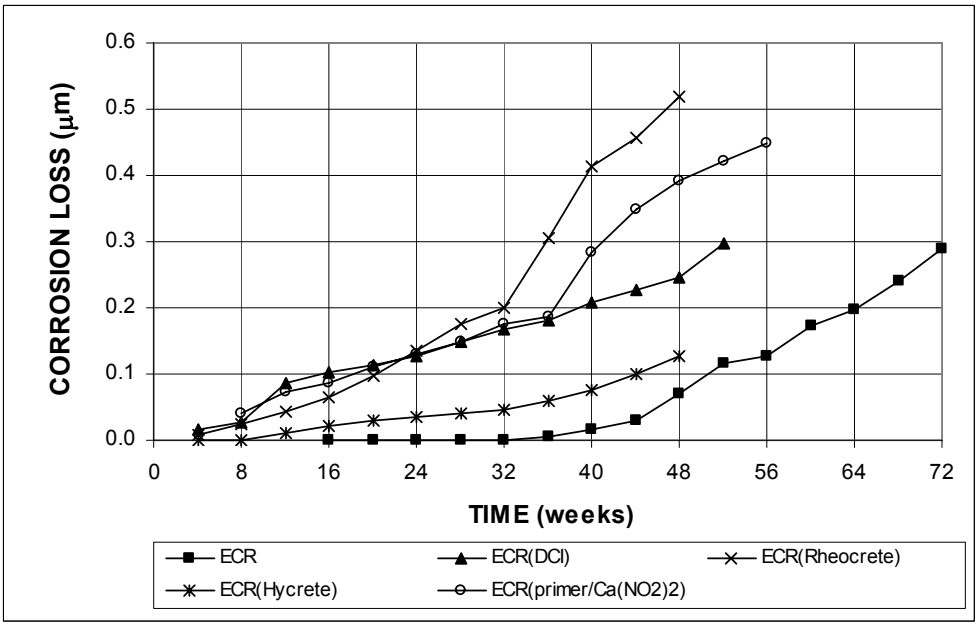

Figure 4.16 – Microcell corrosion losses as measured using LPR in the cracked beam test for specimens with ECR, ECR with a primer containing calcium nitrite, and ECR in concrete with corrosion inhibitors (ECR bars have four holes).

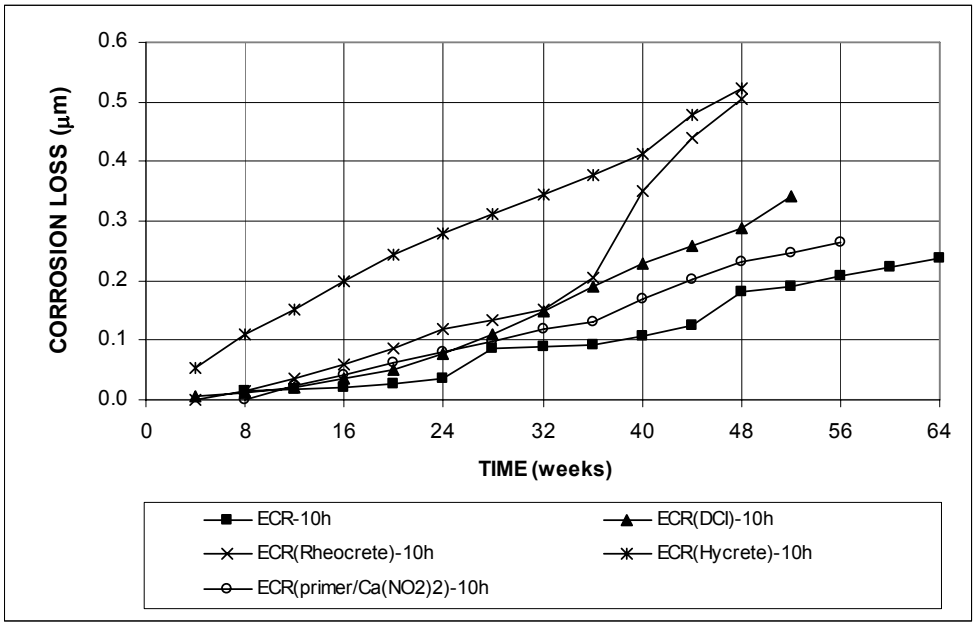

Figure 4.17 – Microcell corrosion losses as measured using LPR in the cracked beam test for specimens with ECR, ECR with a primer containing calcium nitrite, and ECR in concrete with corrosion inhibitors (ECR bars have 10 holes).

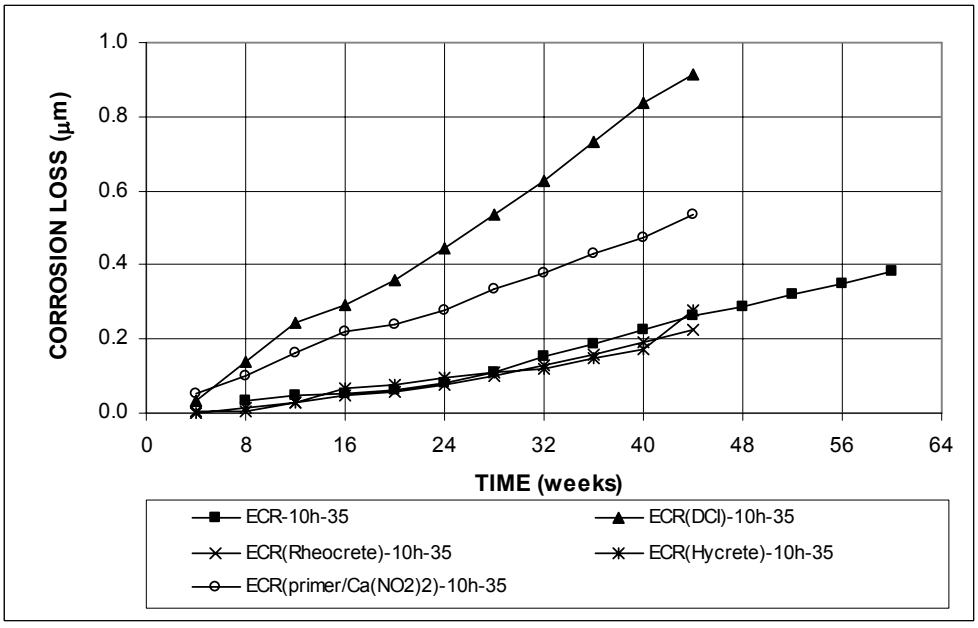

Figure 4.18 – Microcell corrosion losses as measured using LPR in the cracked beam test for specimens with ECR, ECR with a primer containing calcium nitrite, and ECR in concrete with corrosion inhibitors, water-cement ratio = 0.35 (ECR bars have 10 holes).

4.2.3 Multiple Coated Reinforcement

This section presents the results from the LPR test for the multiple coated bars with only the epoxy layer penetrated and with both the zinc and epoxy layers penetrated. The test results are shown in Figures 4.19 through 4.24 and the total corrosion losses are summarized in Tables 4.3 and 4.4.

Figures 4.19 and 4.20 show the microcell corrosion rates and the total corrosion losses for the SE specimens based on total area. As shown in Figure 4.19, specimens with multiple coated bars had much higher microcell corrosion rates than the specimens with conventional ECR, and exhibited corrosion rates between 0.15 and 0.51 μm/yr after week 32. Figure 4.20 shows that multiple coated bars had total corrosion losses based on total area of approximately 0.14 μm at 40 weeks, with the exception of multiple coated bars with 10 holes and only the epoxy penetrated, which had a loss of 0.06 μm at week 40. As shown in Table 4.3, multiple coated bars exhibited total microcell corrosion losses between 8 and 430 times those for conventional ECR in the SE test.

Figures 4.21 and 4.22 show the microcell corrosion rates and total corrosion losses for the CB specimens. The multiple coated bars had higher microcell corrosion rates than conventional ECR, as shown in Figures 4.21. The multiple coated bars had microcell corrosion rates less than 2.10 μm/yr based on total area. Figure 4.22 shows that multiple coated bars had total corrosion losses between 0.26 and 0.93 μm at 40 weeks, compared to values between 0.02 and 0.11 μm for conventional ECR. As shown in Table 4.3, multiple coated bars had total corrosion losses between 2.42 and 61.7 times those for conventional ECR in the CB test.

Figures 4.23 and 4.24 show the microcell corrosion rates and total corrosion losses for the ASTM G 109 specimens. As shown in Figure 4.23, the multiple coated bars showed corrosion rates similar to conventional ECR, with values of less than 0.015 μm/yr for specimens with four holes and 0.025 μm/yr for specimens with 10

holes, respectively. Figure 4.24 shows that multiple coated bars had total corrosion losses similar to those for conventional ECR. Total corrosion losses at week 61 were less than 0.002 μm for the multiple coated bars with four holes and between 0.008 and 0.010 μm for multiple coated bars with 10 holes, as shown in Table 4.4.

As shown in Table 4.3, multiple coated bars showed no improvement in corrosion protection compared to conventional ECR, with total corrosion losses between 2.42 and 430 times those for conventional ECR in the SE and CB tests. Based on the total corrosion losses at week 40 in the SE and CB tests, the comparison between the multiple coated bars with only the epoxy penetrated and with both layers penetrated produce mixed results.

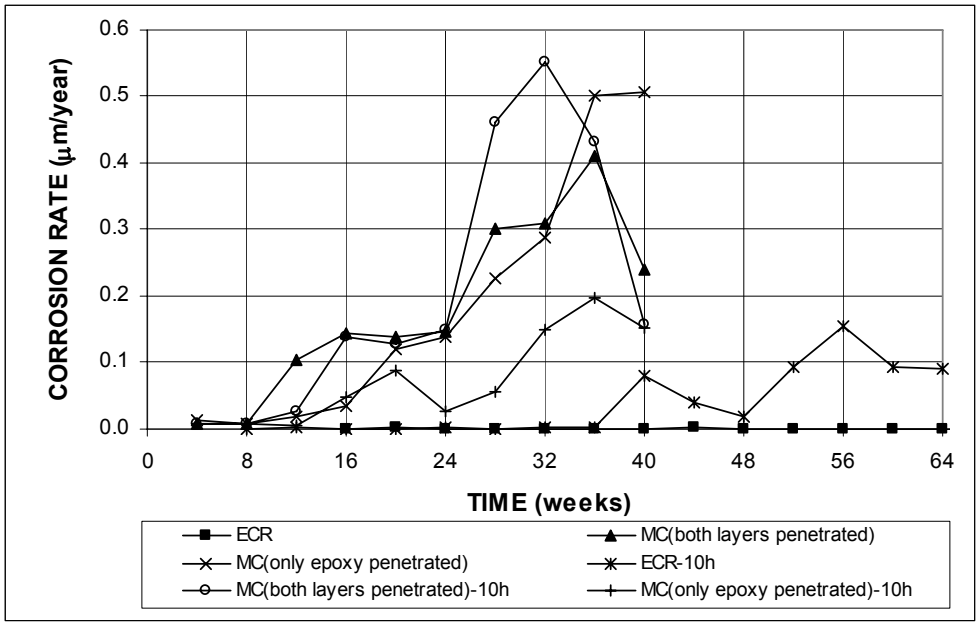

Figure 4.19 – Microcell corrosion rates as measured using LPR in the Southern Exposure test for specimens with ECR and multiple coated bars (ECR have four holes and ECR-10h have 10 holes).

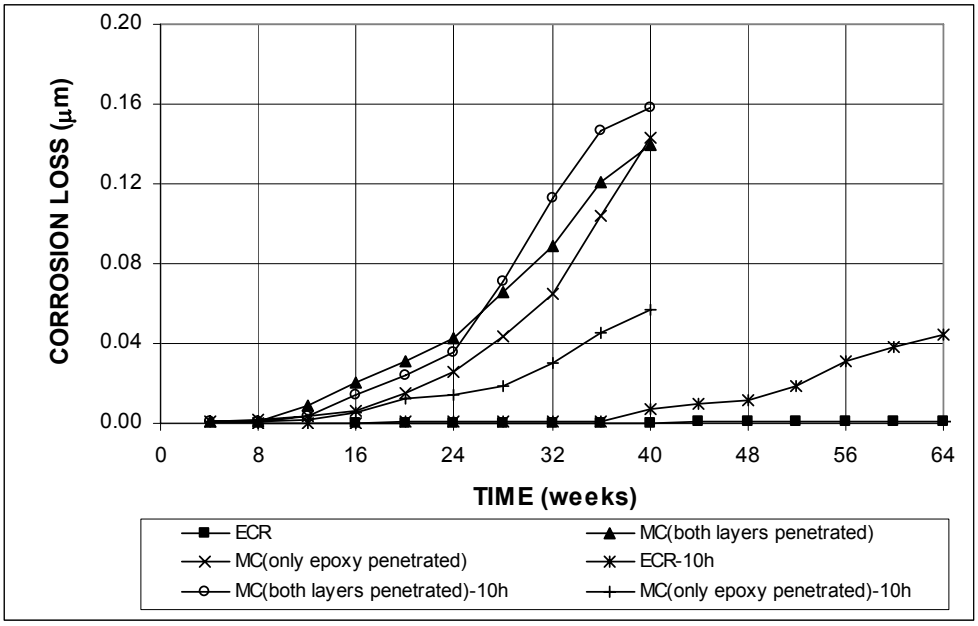

Figure 4.20 – Microcell corrosion losses as measured using LPR in the Southern Exposure test for specimens with ECR and multiple coated bars (ECR have four holes and ECR-10h have 10 holes).

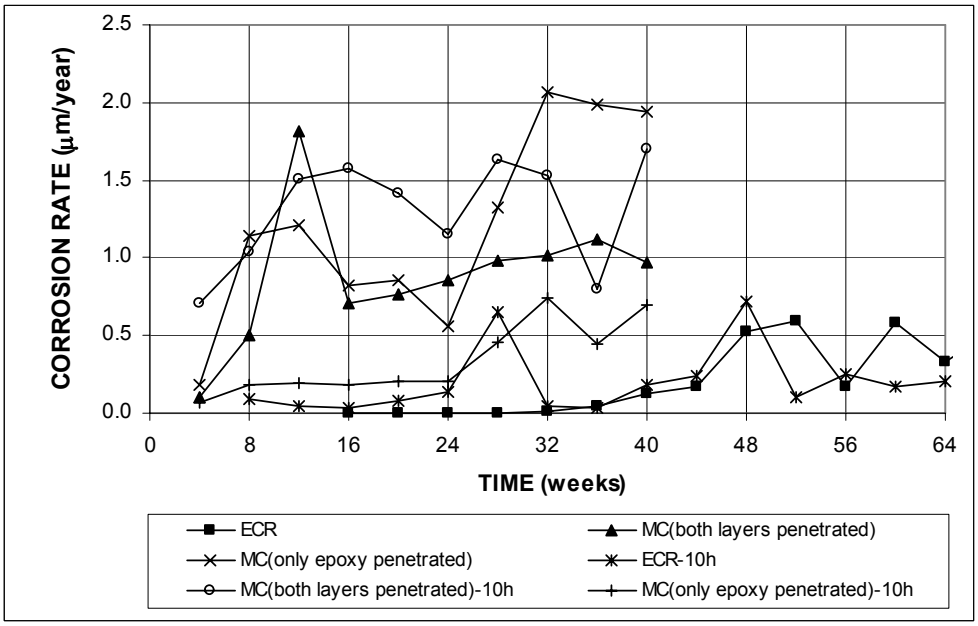

Figure 4.21 – Microcell corrosion rates as measured using LPR in the cracked beam test for specimens with ECR and multiple coated bars (ECR have four holes and ECR-10h have 10 holes).

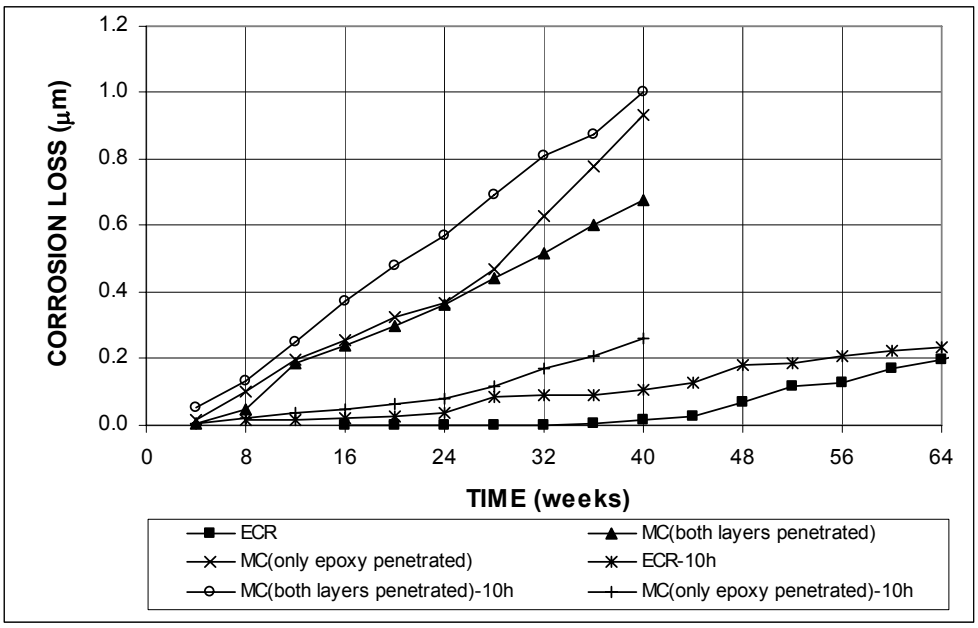

Figure 4.22 – Microcell corrosion losses as measured using LPR in the cracked beam test for specimens with ECR and multiple coated bars (ECR have four holes and ECR-10h have 10 holes).

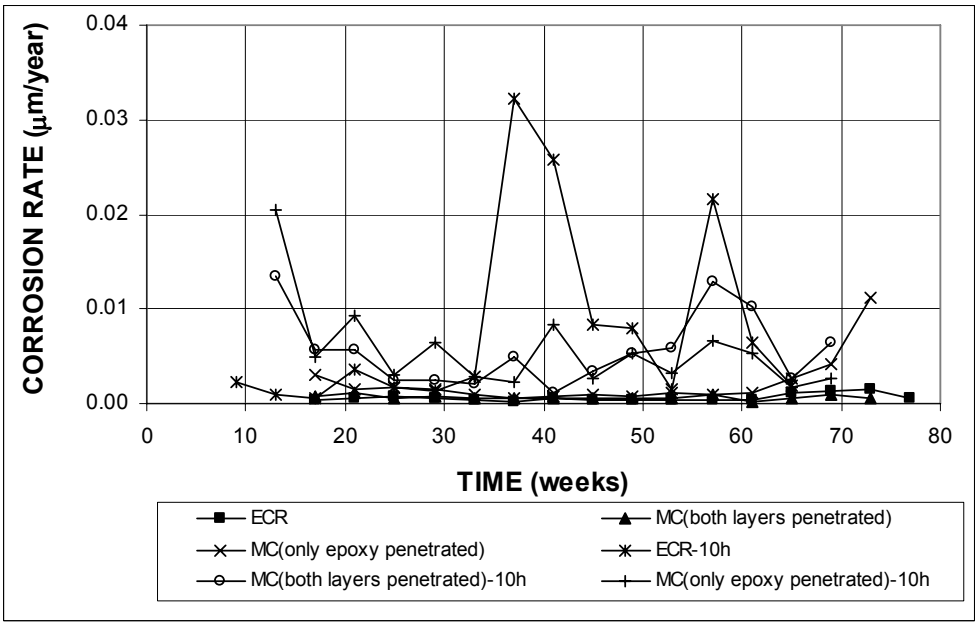

Figure 4.23 – Microcell corrosion rates as measured using LPR in the ASTM G 109 test for specimens with ECR and multiple coated bars (ECR have four holes and ECR-10h have 10 holes).

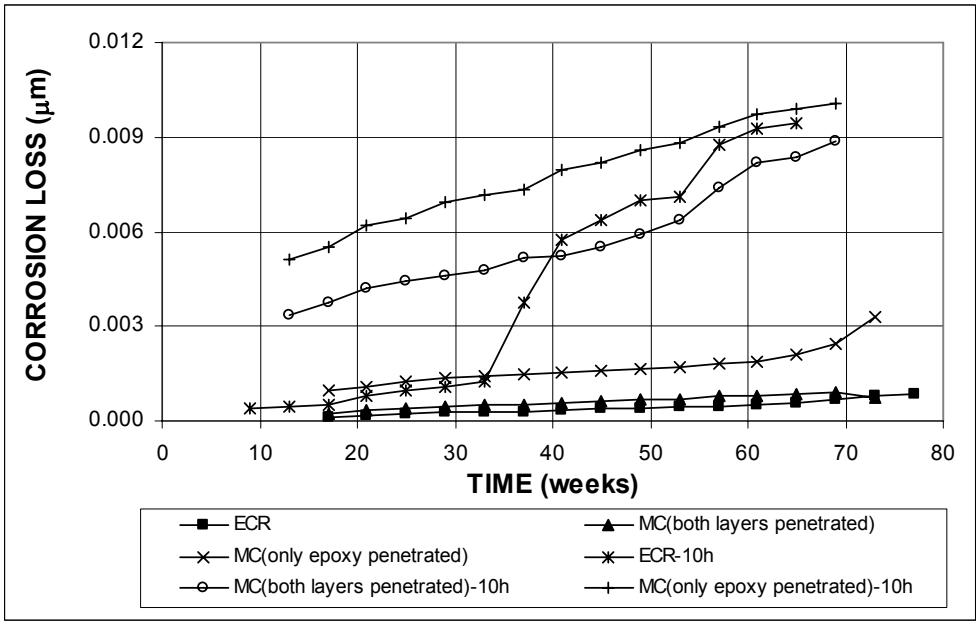

Figure 4.24 – Microcell corrosion losses as measured using LPR in the ASTM G 109 test for specimens with ECR and multiple coated bars (ECR have four holes and ECR-10h have 10 holes).

4.2.4 ECR with Increased Adhesion

This section presents the results from the LPR test for ECR with the zinc chromate pretreatment and the two types of ECR with improved adhesion epoxy developed by DuPont and Valspar. The results are shown in Figures 4.25 through 4.32.

The microcell corrosion rates and total corrosion losses for the SE specimens are shown in Figures 4.25 through 4.28. As shown in Figure 4.25, starting at week 40, the high adhesion ECR bars with four holes showed much higher microcell corrosion rates than conventional ECR. The corrosion rates based on total area for these specimens were less than 0.04 μm/yr, with the exception of the ECR(DuPont) and ECR(Valspar) specimens, which had microcell corrosion rates ranging from 0.05 to 0.12 μm/yr between weeks 52 and 60. The high adhesion ECR bars with 10 holes had microcell corrosion rates similar to those for ECR-10h, with values between 0.03 and

0.16 μm/yr, as shown in Figure 4.26. For total corrosion losses, the high adhesion ECR bars with four holes (Figure 4.27) had total losses between 0.001 and 0.004 μm at week 40, compared to a value of less than 0.001 μm for conventional ECR. Figure 4.28 shows that the high adhesion ECR bars with 10 holes had corrosion losses higher than conventional ECR before week 48 and similar values after that. At week 40, the high adhesion ECR bars had corrosion losses between 0.01 and 0.02 μm, compared to a value of less than 0.01 μm for conventional ECR, as shown in Table 4.3.

Microcell corrosion rates and total corrosion losses for the CB specimens are shown in Figures 4.29 through 4.32. As shown in Figure 4.29, the high adhesion ECR bars with four holes exhibited higher microcell corrosion rates than conventional ECR during the first 36 weeks and similar values after that. All specimens had microcell corrosion rates less than 1.30 μm/yr, with the exception of ECR(Valspar), which exhibited rates of 1.38 and 1.53 μm/yr, respectively, at week 28 and 32. Figure 4.30 shows that the high adhesion ECR bars with 10 holes had microcell corrosion rates similar to those for conventional ECR, with values below 1.10 μm/yr. For the total corrosion losses (Figures 4.31 and 4.32), high adhesion ECR bars showed higher total losses than conventional ECR, with the exception of ECR(Chromate)-10h. As shown in Table 4.3, high adhesion ECR bars with four holes had total corrosion losses between 0.01 and 0.74 μm at week 40, compared to a value of less than 0.005 μm for conventional ECR. For specimens with 10 holes, total corrosion losses were 0.04, 0.22, and 0.37 μm for ECR(Chromate)-10h, ECR(DuPont)-10h, and ECR(Valspar)-10h, respectively, compared to 0.11 μm for conventional ECR.

As shown in Table 4.3, high adhesion ECR bars did not show improvement in corrosion protection, with the exception of ECR(Chromate)-10h in the CB test, which had a total corrosion loss 36% of the loss observed for conventional ECR. The remaining specimens showed total corrosion losses between 1.41 and 48.6 times those observed for conventional ECR in the SE and CB tests.

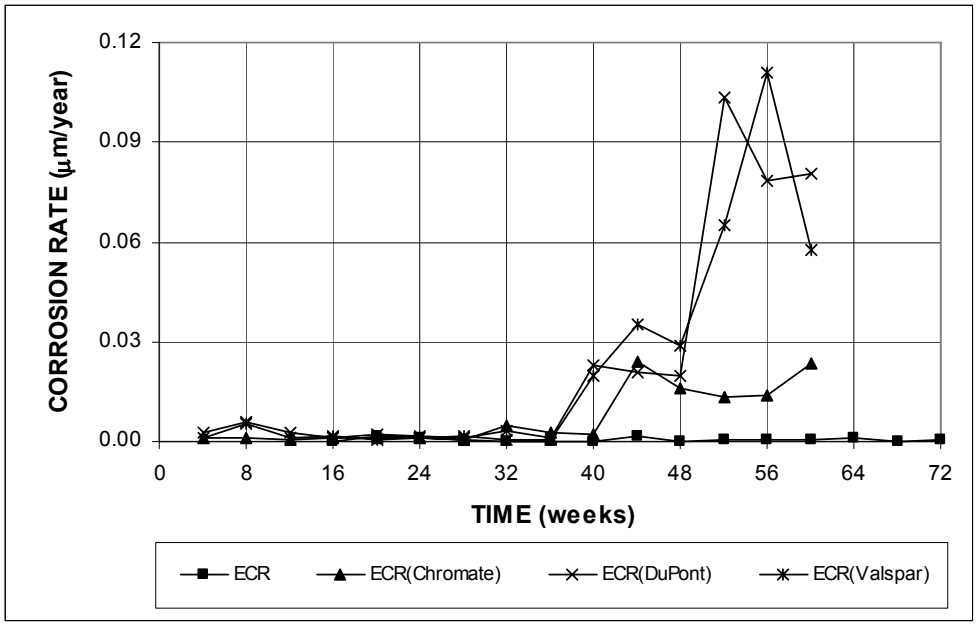

Figure 4.25 – Microcell corrosion rates as measured using LPR in the Southern Exposure test for specimens with ECR and ECR with increased adhesion (ECR bars have four holes).

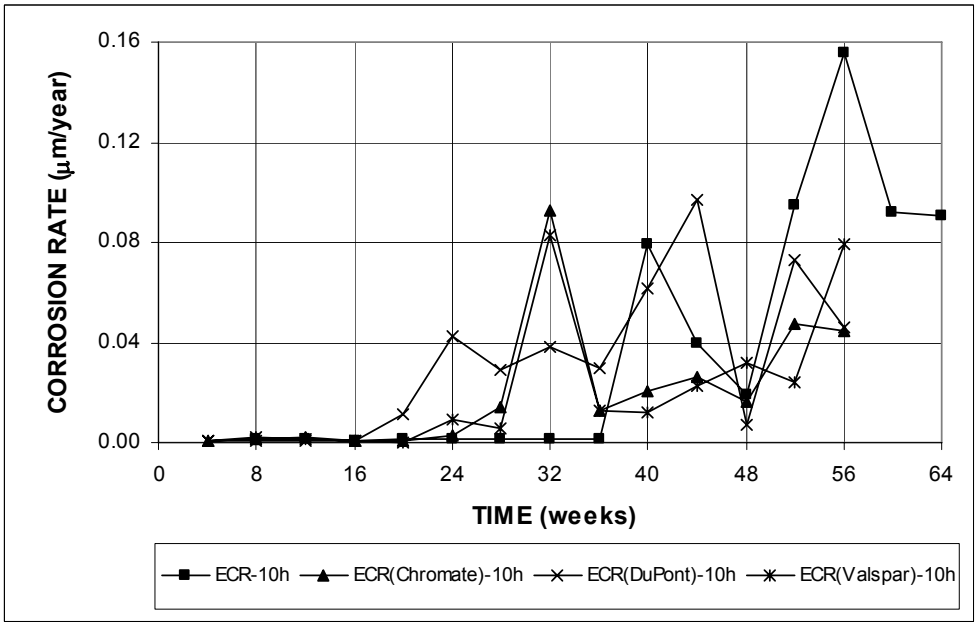

Figure 4.26 – Microcell corrosion rates as measured using LPR in the Southern Exposure test for specimens with ECR and ECR with increased adhesion (ECR bars have 10 holes).

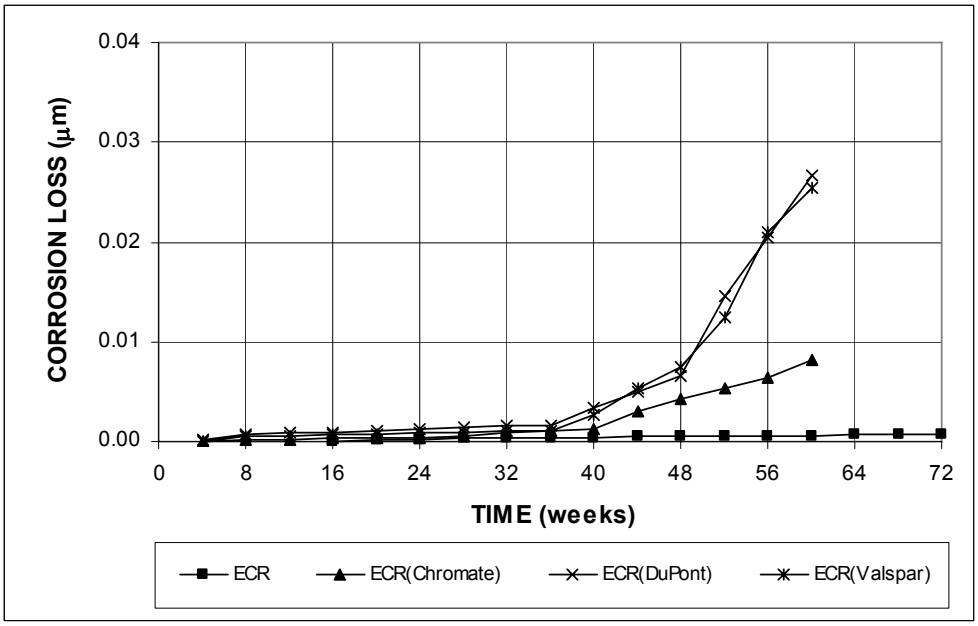

Figure 4.27 – Microcell corrosion losses as measured using LPR in the Southern Exposure test for specimens with ECR and ECR with increased adhesion (ECR bars have four holes).

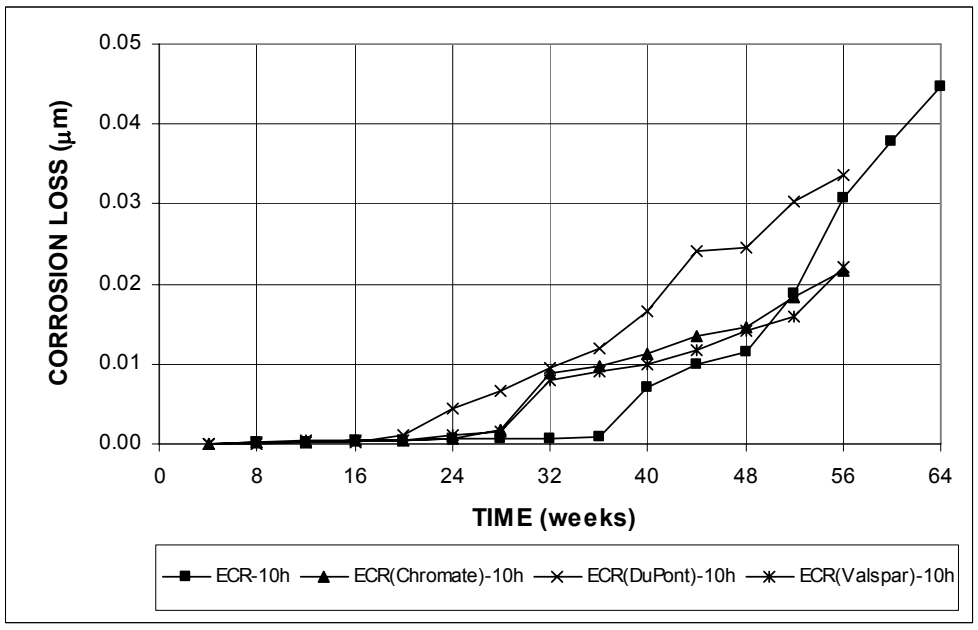

Figure 4.28 – Microcell corrosion losses as measured using LPR in the Southern Exposure test for specimens with ECR and ECR with increased adhesion (ECR bars have 10 holes).

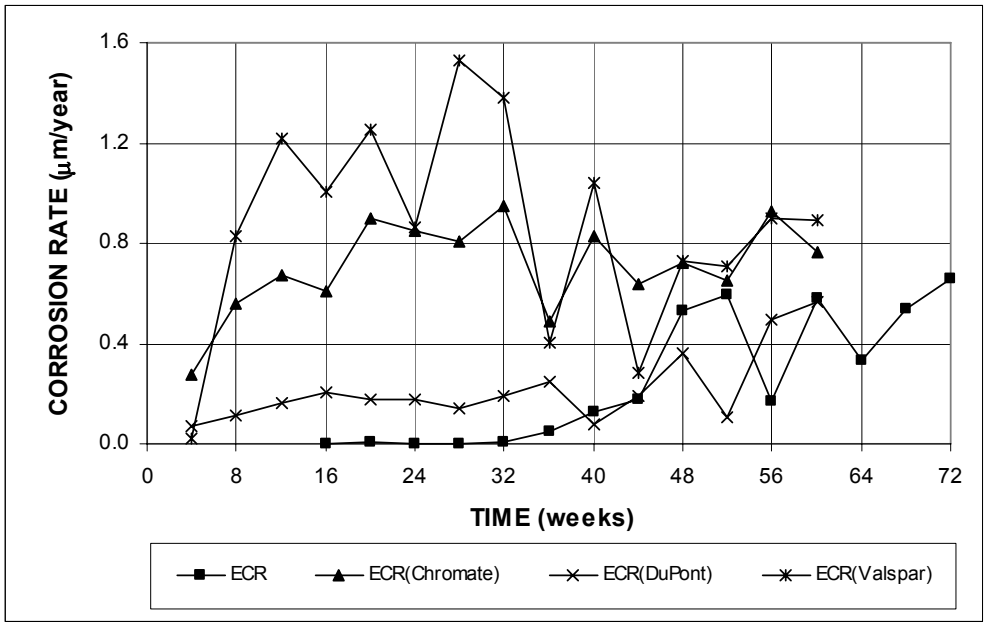

Figure 4.29 – Microcell corrosion rates as measured using LPR in the cracked beam test for specimens with ECR and ECR with increased adhesion (ECR bars with have holes).

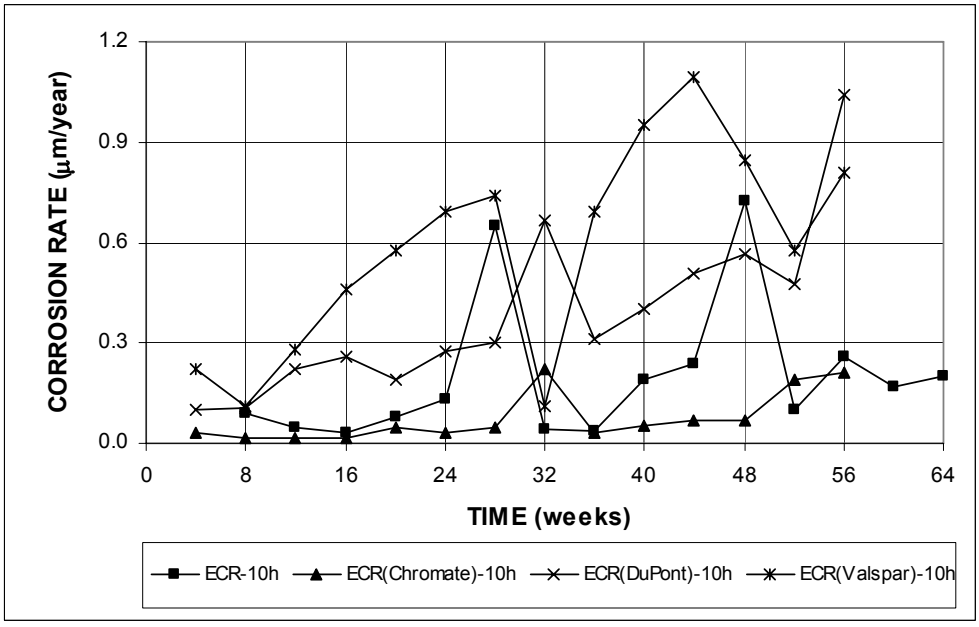

Figure 4.30 – Microcell corrosion rates as measured using LPR in the cracked beam test for specimens with ECR and ECR with increased adhesion (ECR bars have 10 holes).

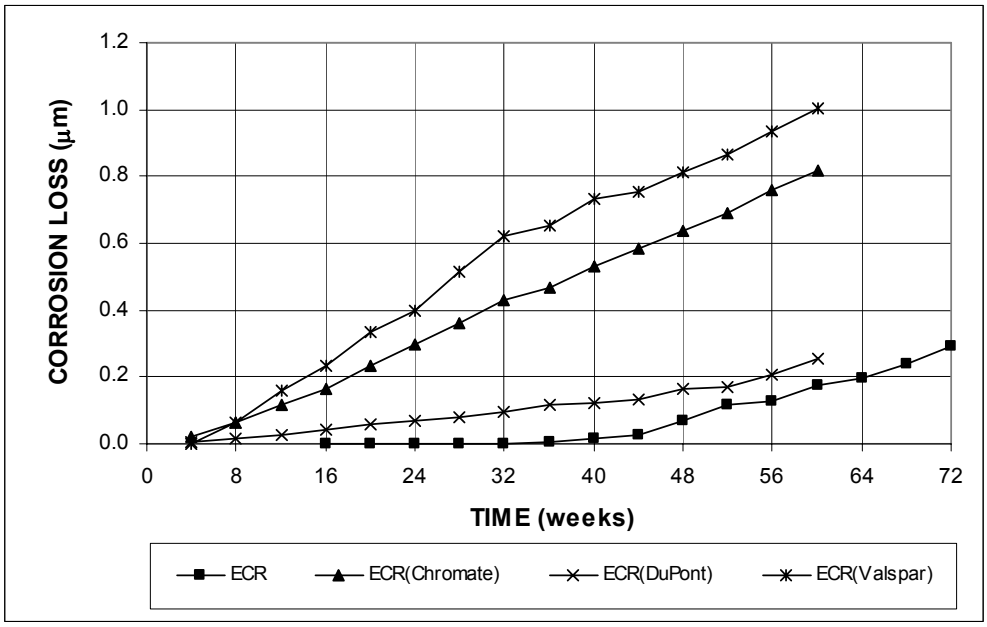

Figure 4.31 – Microcell corrosion losses as measured using LPR in the cracked beam test for specimens with ECR and ECR with increased adhesion (ECR bars have four holes).

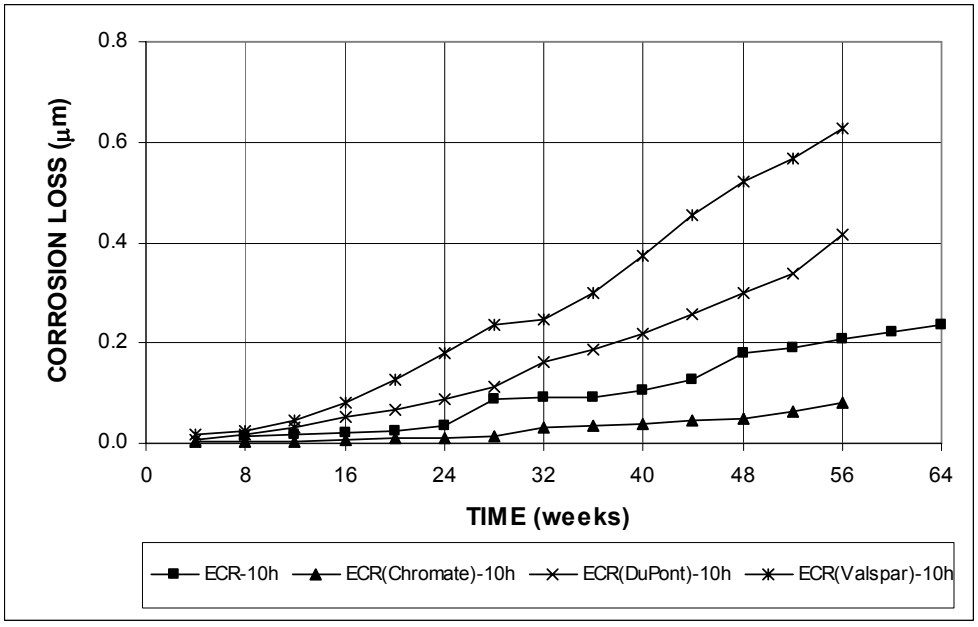

Figure 4.32 – Microcell corrosion losses as measured using LPR in the cracked beam test for specimens with ECR and ECR with increased adhesion (ECR bars have 10 holes).

4.2.5 ECR with Increased Adhesion Cast in Concrete Containing Calcium Nitrite

This section presents the results from the LPR test for SE specimens with ECR with increased adhesion cast in concrete with the corrosion inhibitor calcium nitrite (DCI-S). The results are shown in Figures 4.33 and 4.34. These corrosion protection systems were not evaluated using the CB test.

As shown in Figure 4.33, the high adhesion ECR bars cast in concrete with DCI-S had higher microcell corrosion rates than the ECR(DCI) specimen during the first 28 weeks and after that they had comparable results. All specimens had microcell corrosion rates less than 0.006 μm/yr, with the exception of ECR(Chromate)-DCI, which showed rates of approximately 0.01 μm/yr at weeks 20 and 40. For total corrosion losses (Figure 4.34), the high adhesion ECR bars cast in concrete with DCI-S had higher losses than conventional ECR with DCI-S. As shown in Table 4.3, the high adhesion ECR bars cast in concrete with DCI-S had total corrosion losses of less than 0.003 μm at week 40, with values that ranged between 1.27 and 6.08 times the value for conventional ECR cast in concrete with DCI-S. Compared to high adhesion ECR bars cast in concrete without DCI-S, the use of the corrosion inhibitor DCI-S reduced corrosion for ECR(DuPont) and ECR(Valspar), but not for ECR(Chromate).

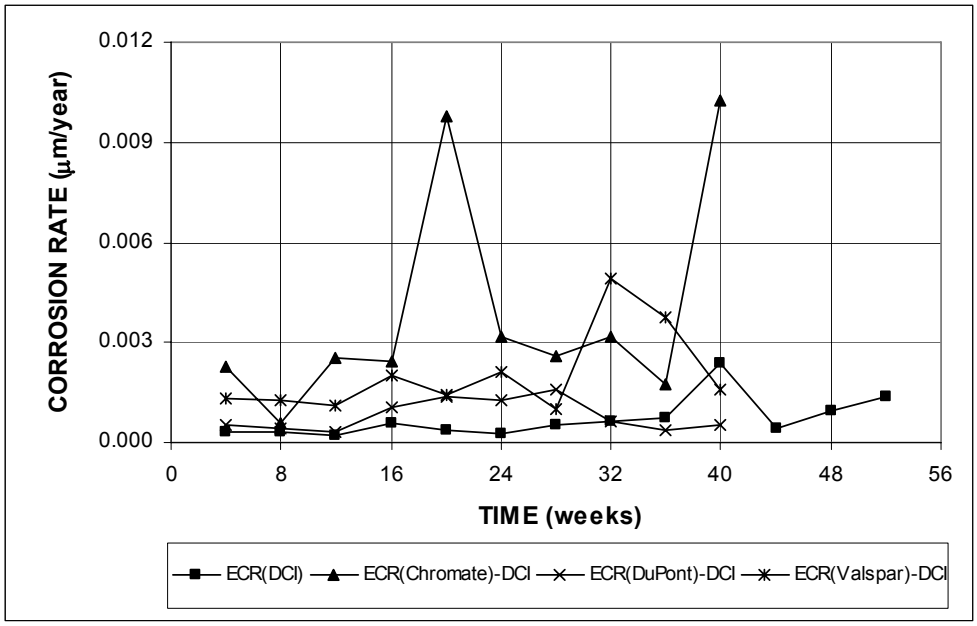

Figure 4.33 – Microcell corrosion rates as measured using LPR in the Southern Exposure test for specimens with ECR and ECR with increased adhesion cast in concrete with DCI (ECR bars have four holes).

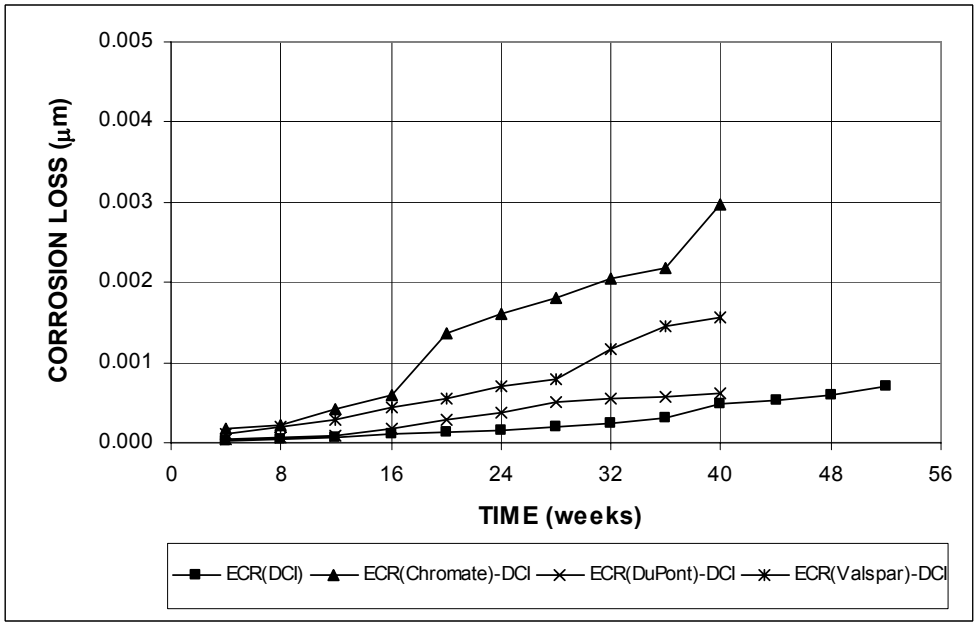

Figure 4.34 – Microcell corrosion losses as measured using LPR in the Southern Exposure test for specimens with ECR and ECR with increased adhesion cast in concrete with DCI (ECR bars have four holes).

4.3 MICROCELL CORROSION RATE VERSUS CORROSION POTENTIAL

This section presents the correlation between microcell corrosion rate and corrosion potential for the bench-scale test specimens described in Section 4.2. The microcell corrosion rate results from the linear polarization resistance (LPR) test are based on the total area of the steel in concrete. In general, if the coefficient of determination is greater than 0.70, a good linear relationship exists between the microcell corrosion rate and the corrosion potential.

Escalante (1990) investigated the corrosion performance of No. 13 (No. 4) conventional reinforcing bars using concrete cylinder specimens in simulated concrete pore solution with and without chlorides. The LPR test was performed to determine the microcell corrosion rate of the reinforcing bars, and corrosion potentials were measured with respect to a saturated calomel electrode. The results showed that the corrosion potential is inversely proportional to the microcell corrosion rate.

The linear polarization resistance test was used by Lambert and Page (1991) to monitor the corrosion performance of mild steel rods in concrete slabs [200 × 300 × 100 mm (7.87 × 11.81 × 3.94 in.)]. Their test results showed that a linear relationship exists between corrosion potential and the logarithm of the microcell corrosion rate, which signifies that the corrosion process of steel in concrete is subject to anodic control (an increase of corrosion rate with a shift of corrosion potential in the negative direction is characteristic of anodic control).

In a Strategic Highway Research Program (SHRP) study (Flis et al. 1993), the corrosion performance of conventional reinforcing bars in five bridges was investigated using the LPR test and corrosion potential measurements. The test results showed that at corrosion potentials more positive than –0.250 V (with respect to a

copper-copper sulfate electrode), which are characteristic of a passive state, corrosion rates were low and almost independent of corrosion potentials. In the active-passive transition region (a region includes both passive and active corrosion states), however, an increase in corrosion rate as measured in the LPR test was generally characterized by a shift of corrosion potentials in the negative direction.

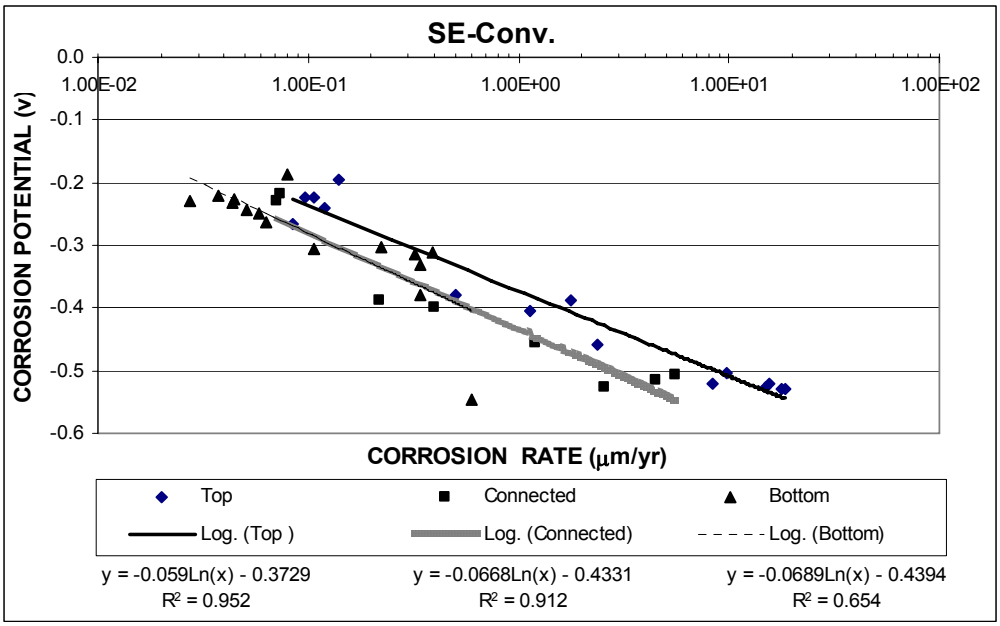

Figure 4.35 – Correlation between microcell corrosion rate and corrosion potential as measured in the LPR test for the Southern Exposure specimen with conventional steel

In this section, the degree of correlation between the microcell corrosion rate and the corrosion potential is investigated for the bench-scale specimens used in the LPR test. The coefficient of determination is used to evaluate the goodness of fit and the results are summarized in Tables 4.5 through 4.7 for the SE, CB, and ASTM G 109 tests, respectively. Microcell corrosion rates, corrosion potentials, and correlation results for individual specimens are shown in Appendix E. The correlations for each specimen are performed in three ways: top mat, connected mat, and bottom mat.

Figure 4.35 is a typical plot showing the correlations between microcell corrosion rate and corrosion potential for conventional steel in concrete with a *w*/*c* ratio of 0.45. As shown in Figure 4.35, the coefficients of determination are 0.952, 0.912, and 0.654 for the correlations for the top mat, connected mat, and bottom mat, respectively.

For the 30 SE specimens (Table 4.5), coefficients of determination above 0.70 were observed for 16 specimens in the top mat, 11 specimens in the connected mat, and five specimens in the bottom mat, indicating a strong correlation between microcell corrosion rate and corrosion potential in those cases. Coefficients of determination between 0 and 0.68 were observed for the remaining specimens. Compared to specimens cast in concrete with a *w*/*c* ratio of 0.45, specimens cast in concrete with a *w*/*c* ratio of 0.35 generally did not show a good correlation between the microcell corrosion rate and the corrosion potential.

For the 27 CB test specimens (Table 4.6), coefficients of determination above 0.70 were observed for just three specimens in the top and connected mats and one specimen in the bottom mat. Coefficients of determination between 0 and 0.68 were observed for the remaining specimens.

A good linear relationship is expected for specimens without cracks (SE test) in the active-passive transition region, as shown in Tables 4.5 and 4.6. In general, the Southern Exposure specimens show stronger correlations between microcell corrosion rate and corrosion potential than the cracked beam specimens. In the Southern Exposure test, conventional steel, conventional ECR, multiple coated bars, and high adhesion ECR bars show better correlations in the top mat than in the bottom mat. This is because the reinforcing bars in the top mat exhibited higher microcell corrosion than those in the bottom mat.

Table 4.5 – Coefficients of determination between microcell corrosion rate and corrosion potential for the Southern Exposure test

Steel Designation[a]	Top Mat	Connected Mat	Bottom Mat
Control			
Conv.	0.95	0.92	0.65
Conv.-35	0.86	0.73	0.29
ECR	0.72	0.04	0.67
ECR-10h	0.89	0.56	0.80
ECR-10h-35	0.89	0.84	0.45
Corrosion Inhibitors			
ECR(DCI)	0.22	0.13	0.12
ECR(DCI)-10h	0.74	0.85	0.23
ECR(DCI)-10h-35	0.04	0.03	0.03
ECR(Rheocrete)	0.34	0.91	0.03
ECR(Rheocrete)-10h	0.32	0.84	0.52
ECR(Rheocrete)-10h-35	0.07	0.17	0.05
ECR(Hycrete)	0.41	0.32	0.21
ECR(Hycrete)-10h	0.86	0.97	0.23
ECR(Hycrete)-10h-35	0.11	0.02	0.07
ECR(primer/$Ca(NO_2)_2$)	0.37	0.72	0.79
ECR(primer/$Ca(NO_2)_2$)-10h	0.80	0.67	0.79
ECR(primer/$Ca(NO_2)_2$)-10h-35	0.29	0.96	0.44
Multiple Coated Bars			
MC(both layers penetrated)	0.76	0.43	0.58
MC(both layers penetrated)-10h	0.74	0.85	0.01
MC(only epoxy penetrated)	0.57	0.44	0.21
MC(only epoxy penetrated)-10h	0.16	0.54	0.02
Increased Adhesion			
ECR(Chromate)	0.79	0.73	0.55
ECR(Chromate)-10h	0.74	0.66	0.08
ECR(DuPont)	0.87	0.33	0.73
ECR(DuPont)-10h	0.70	0.68	0.03
ECR(Valspar)	0.84	0.88	0.32
ECR(Valspar)-10h	0.77	0.91	0.34
Increased Adhesion with Corrosion Inhibitor DCI			
ECR(Chromate)-DCI	0.13	0.16	0.75
ECR(DuPont)-DCI	0.23	0.00	0.20
ECR(Valspar)-DCI	0.00	0.01	0.37

[a] Conv. = conventional steel. ECR = conventional epoxy-coated reinforcement.
ECR(Chromate) = ECR with the zinc chromate pretreatment.
ECR(DuPont) = high adhesion DuPont bars. ECR(Valspar) = high adhesion Valspar bars.
ECR(DCI) = conventional ECR in concrete with DCI inhibitor.
ECR(Rheocrete) = conventional ECR in concrete with Rheocrete inhibitor.
ECR(Hycrete) = conventional ECR in concrete with Hycrete inhibitor.
ECR(primer/$Ca(NO_2)_2$) = ECR with a primer containing calcium nitrite
MC(both layers penetrated) = multiple coated bars with both the zinc and epoxy layers penetrated.
MC(only epoxy penetrated) = mutiple coated bars with only the epoxy layer penetrated.
10h = epoxy-coated bars with 10 holes, otherwise four 3 mm ($^1/_8$ in.) diameter holes.
35 = concrete w/c=0.35, otherwise w/c=0.45.

Table 4.6 – Coefficients of determination between microcell corrosion rate and corrosion potential for the cracked beam test

Steel Designation[a]	Top Mat	Connected Mat	Bottom Mat
Control			
Conv.	0.01	0.57	0.38
Conv.-35	0.02	0.20	0.01
ECR	0.84	0.04	0.67
ECR-10h	0.22	0.00	0.53
ECR-10h-35	0.02	0.28	0.63
Corrosion Inhibitors			
ECR(DCI)	0.51	0.19	0.26
ECR(DCI)-10h	0.02	0.21	0.51
ECR(DCI)-10h-35	0.12	0.01	0.13
ECR(Rheocrete)	0.02	0.01	0.21
ECR(Rheocrete)-10h	0.56	0.50	0.05
ECR(Rheocrete)-10h-35	0.86	0.99	0.77
ECR(Hycrete)	0.91	0.91	0.20
ECR(Hycrete)-10h	0.20	0.26	0.01
ECR(Hycrete)-10h-35	0.57	0.13	0.40
ECR(primer/$Ca(NO_2)_2$)	0.41	0.03	0.30
ECR(primer/$Ca(NO_2)_2$)-10h	0.30	0.96	0.47
ECR(primer/$Ca(NO_2)_2$)-10h-35	0.13	0.49	0.06
Multiple Coated Bars			
MC(both layers penetrated)	0.08	0.01	0.01
MC(both layers penetrated)-10h	0.05	0.17	0.18
MC(only epoxy penetrated)	0.01	0.02	0.27
MC(only epoxy penetrated)-10h	0.40	0.20	0.61
Increased Adhesion			
ECR(Chromate)	0.29	0.27	0.25
ECR(Chromate)-10h	0.58	0.22	0.68
ECR(DuPont)	0.28	0.31	0.25
ECR(DuPont)-10h	0.01	0.02	0.00
ECR(Valspar)	0.10	0.46	0.46
ECR(Valspar)-10h	0.00	0.19	0.04

[a] Conv. = conventional steel. ECR = conventional epoxy-coated reinforcement.
ECR(Chromate) = ECR with the zinc chromate pretreatment.
ECR(DuPont) = high adhesion DuPont bars. ECR(Valspar) = high adhesion Valspar bars.
ECR(DCI) = conventional ECR in concrete with DCI inhibitor.
ECR(Rheocrete) = conventional ECR in concrete with Rheocrete inhibitor.
ECR(Hycrete) = conventional ECR in concrete with Hycrete inhibitor.
ECR(primer/$Ca(NO_2)_2$) = ECR with a primer containing calcium nitrite
MC(both layers penetrated) = multiple coated bars with both the zinc and epoxy layers penetrated.
MC(only epoxy penetrated) = mutiple coated bars with only the epoxy layer penetrated.
10h = epoxy-coated bars with 10 holes, otherwise four 3 mm ($^1/_8$ in.) diameter holes.
35 = concrete w/c=0.35, otherwise w/c=0.45.

Table 4.7 – Coefficients of determination between microcell corrosion rate and corrosion potential for the ASTM G 109 test

Steel Designation[a]	Top Mat	Connected Mat	Bottom Mat
Control			
Conv.	0.41	0.15	0.36
ECR	0.03	0.59	0.07
ECR-10h	0.58	0.64	0.53
Multiple Coated Bars			
MC(both layers penetrated)	0.02	0.26	0.17
MC(both layers penetrated)-10h	0.50	0.26	0.20
MC(only epoxy penetrated)	0.16	0.05	0.25
MC(only epoxy penetrated)-10h	0.60	0.10	0.67

[a] Conv. = conventional steel. ECR = conventional epoxy-coated reinforcement.
MC(both layers penetrated) = multiple coated bars with both the zinc and epoxy layers penetrated.
MC(only epoxy penetrated) = mutiple coated bars with only the epoxy layer penetrated.
10h = epoxy-coated bars with 10 holes, otherwise four 3 mm ($^1/_8$ in.) diameter holes.

As shown in Table 4.7 for the seven ASTM G 109 specimens, none had coefficients of determination above 0.70, indicating that a good correlation does not exist between microcell corrosion rate and corrosion potential. This is probably due to the fact that these specimens remained passive.

4.4 MICROCELL VERSUS MACROCELL CORROSION AND RELATIVE EFFECTIVENESS OF CORROSION PROTECTION SYSTEMS

This section compares the microcell and macrocell corrosion rates for bench-scale test specimens. Correlations were made between the microcell and macrocell corrosion losses for specimens in the Southern Exposure and cracked beam tests at week 40. Very little corrosion was observed for the ASTM G 109 test specimens and therefore, the comparison between the microcell and macrocell corrosion is not performed for specimens in the ASTM G 109 test. For the ECR specimens, total corrosion losses are based on the exposed area of the steel. The microcell corrosion rate results in the top mat are used because the macrocell corrosion rates represent the corrosion condition of reinforcing bars in the top mat of a bridge deck.

The microcell and macrocell total corrosion losses (based on exposed area for ECR specimens) are summarized in Table 4.8 for the SE and CB specimens. In the table, total corrosion losses are divided into two categories: specimens with *w*/*c* ratios of 0.45 and 0.35. For ECR specimens with a *w*/*c* ratio of 0.45, the average total corrosion losses for specimens with four and 10 holes are used to make comparisons to provide a more representative value for the behavior of specimens with concrete with a *w*/*c* ratio of 0.45 than is provided by the individual specimens with four or 10 holes alone.

A description of linear regression is given in Section 6.2 in Chapter 6, along with the two coefficients (correlation coefficient and coefficient of determination), which can be used to judge the strength of a linear relationship. In general, if the coefficient of determination is greater than 0.70, a good linear relationship exists between the microcell and macrocell corrosion.

Table 4.8 – Total corrosion losses (μm) at week 40 based on microcell and macrocell corrosion rates for the Southern Exposure and cracked beam tests. Losses based on total area for conventional steel and exposed area for epoxy-coated steel.

Steel Designation[a]	Southern Exposure Test		Cracked Beam Test	
	Microcell	Macrocell	Microcell	Macrocell
***w/c* = 0.45[b]**				
Conv.	3.26E-01	4.97E-02	2.46E+01	3.41E+00
ECR	7.53E-01	2.21E+00	1.39E+01	7.38E+00
ECR(DCI)	2.55E-01	5.98E-01	7.21E+01	3.01E+00
ECR(Rheocrete)	7.14E-01	3.06E-01	5.75E+01	1.38E+01
ECR(Hycrete)	7.35E-01	6.54E-01	1.33E+02	1.25E+01
ECR(primer/$Ca(NO_2)_2$)	6.10E-01	8.16E-01	8.40E+01	1.29E+01
MC(both layers penetrated)	4.86E+01	8.96E+00	2.59E+02	5.37E+01
MC(only epoxy penetrated)	3.76E+01	8.98E+00	2.01E+02	3.37E+01
ECR(Chromate)	1.39E+00	1.22E+00	1.32E+02	1.52E+01
ECR(DuPont)	2.42E+00	1.40E+00	4.98E+01	1.83E+01
ECR(Valspar)	1.57E+00	1.11E+00	2.12E+02	3.43E+01
ECR(Chromate)-DCI	1.43E+00	3.38E-01		
ECR(DuPont)-DCI	2.98E-01	1.27E-01		
ECR(Valspar)-DCI	7.53E-01	1.97E-01		
***w/c* = 0.35**				
Conv.-35	1.86E-01	1.30E-02	3.22E+01	2.91E+00
ECR-10h-35	6.98E-01	7.32E-01	4.31E+01	1.63E+01
ECR(DCI)-10h-35	1.78E-01	1.13E-01	1.61E+02	5.63E+01
ECR(Rheocrete)-10h-35	3.17E-01	2.67E-01	3.30E+01	4.63E+01
ECR(Hycrete)-10h-35	1.59E+00	7.46E-01	3.65E+01	1.13E+01
ECR(primer/$Ca(NO_2)_2$)-10h-35	1.05E+00	5.77E-01	9.07E+01	2.74E+01

[a] Conv. = conventional steel. ECR = conventional epoxy-coated reinforcement.
ECR(Chromate) = ECR with the zinc chromate pretreatment.
ECR(DuPont) = high adhesion DuPont bars. ECR(Valspar) = high adhesion Valspar bars.
ECR(DCI) = conventional ECR in concrete with DCI inhibitor.
ECR(Rheocrete) = conventional ECR in concrete with Rheocrete inhibitor.
ECR(Hycrete) = conventional ECR in concrete with Hycrete inhibitor.
ECR(primer/$Ca(NO_2)_2$) = ECR with a primer containing calcium nitrite
MC(both layers penetrated) = multiple coated bars with both the zinc and epoxy layers penetrated.
MC(only epoxy penetrated) = mutiple coated bars with only the epoxy layer penetrated.
35 = concrete w/c=0.35, otherwise *w/c* =0.45.

[b] Total corrosion losses for ECR specimens with a *w/c* ratio of 0.45 are average values of specimens with four and 10 holes.

4.4.1 Southern Exposure Test

The comparisons between the microcell and macrocell corrosion for the SE test specimens are shown in Figures 4.36 and 4.37. A total of 14 test series were evaluated

for specimens cast in concrete with a *w*/*c* ratio of 0.45 (Figure 4.36), including conventional steel, ECR, ECR in concrete with corrosion inhibitors DCI-S, Hycrete, and Rheocrete, ECR with a calcium nitrite primer, multiple coated bars with only the epoxy penetrated and both layers penetrated, three types of high adhesion ECR bars, and high adhesion ECR bars cast with DCI-S. As shown in Figure 4.36(a), multiple coated reinforcement showed much higher microcell and macrocell corrosion than the remaining types of corrosion protection systems. For the remaining corrosion protection systems, conventional ECR had the highest macrocell corrosion loss, as shown in Figure 4.36 (b). For microcell corrosion, the three high adhesion ECR bars and the ECR(Chromate) bars cast in concrete with calcium nitrite exhibited higher total corrosion losses than conventional ECR. The correlation coefficient r is 0.97, indicating a significant correlation between the microcell and macrocell corrosion based on the criteria in Table 6.1 in Chapter 6. The coefficient of determination r^2 is 0.95, which means that 95% of the total variation in the macrocell corrosion can be explained by a linear relationship between microcell and macrocell corrosion.

For specimens cast in concrete with a *w*/*c* ratio of 0.35, the comparison is based on test results for six series with conventional steel, ECR, ECR cast in concrete with corrosion inhibitors DCI-S, Hycrete, and Rheocrete, and ECR with a calcium nitrite primer. As shown in Figure 4.37, conventional ECR had a higher macrocell corrosion loss than specimens with corrosion inhibitors, with the exception of conventional ECR cast in concrete with Rheocrete, which had a loss slightly higher than conventional ECR. For microcell corrosion, conventional ECR cast in concrete with corrosion inhibitors DCI-S and Hycrete showed less total corrosion loss than conventional ECR. Values of 0.85 and 0.73 are obtained for the correlation coefficient r and coefficient of determination r^2, respectively, indicating that there is a good linear relationship between the microcell and macrocell corrosion for specimens

with a *w*/*c* ratio of 0.35.

4.4.2 Cracked Beam Test

The comparisons between the microcell and macrocell corrosion for the CB test specimens are shown in Figures 4.38 and 4.39. A total of 11 test series were evaluated for specimens cast in concrete with a *w*/*c* ratio of 0.45 (Figure 4.38), including conventional steel, ECR, ECR in concrete with corrosion inhibitors DCI-S, Hycrete, and Rheocrete, ECR with a calcium nitrite primer, multiple coated bars with only the epoxy penetrated and both layers penetrated, and three types of high adhesion ECR bars. Figure 4.38 shows the results for specimens cast in concrete with a *w*/*c* ratio of 0.45 in the CB test. As shown in Figure 4.38, conventional ECR cast in concrete with Hycrete and Rheocrete, ECR with a calcium nitrite primer, multiple coated reinforcement, and the three types of high adhesion ECR bars exhibited higher total corrosion losses than conventional ECR in both microcell and macrocell corrosion. Compared to conventional ECR alone, conventional ECR cast in concrete with DCI-S showed less total corrosion losses in the macrocell corrosion, but not in the microcell corrosion. The correlation coefficient *r* is 0.90 indicating that a significant correlation exists between the microcell and macrocell corrosion based on the criteria in Table 6.1. The coefficient of determination r^2, 0.80, which means that 80% of the total variation in the macrocell corrosion can be explained by the linear relationship between the microcell and macrocell corrosion.

For specimens cast in concrete with a *w*/*c* ratio of 0.35 in the CB test, the comparison is based on test results for six series with conventional steel, ECR, ECR cast in concrete with corrosion inhibitors DCI-S, Hycrete, and Rheocrete, and ECR with a calcium nitrite primer. For both microcell and macrocell corrosion, ECR(Rheocrete) exhibited less corrosion conventional ECR in terms of both

microcell and macrocell, as shown in Figure 4.39. ECR(DCI) and ECR(primer/$Ca(NO_2)_2$) showed higher total corrosion losses than conventional ECR in both microcell and macrocell corrosion. When compared to conventional ECR, ECR(Hycrete) showed a higher total corrosion loss in macrocell corrosion and a lower loss in microcell corrosion. Values of 0.69 and 0.47 are obtained for the correlation coefficient r and coefficient of determination r^2, respectively. These results indicate that a significant correlation does not exist between the microcell and macrocell corrosion for specimens with a *w*/*c* ratio of 0.35. The correlation, however, would be significant between microcell and macrocell corrosion if ECR(Rheocrete) is not included, as shown in Figure 4.40. In the latter case, the correlation coefficient and coefficient of determination are 0.98 and 0.97, respectively.

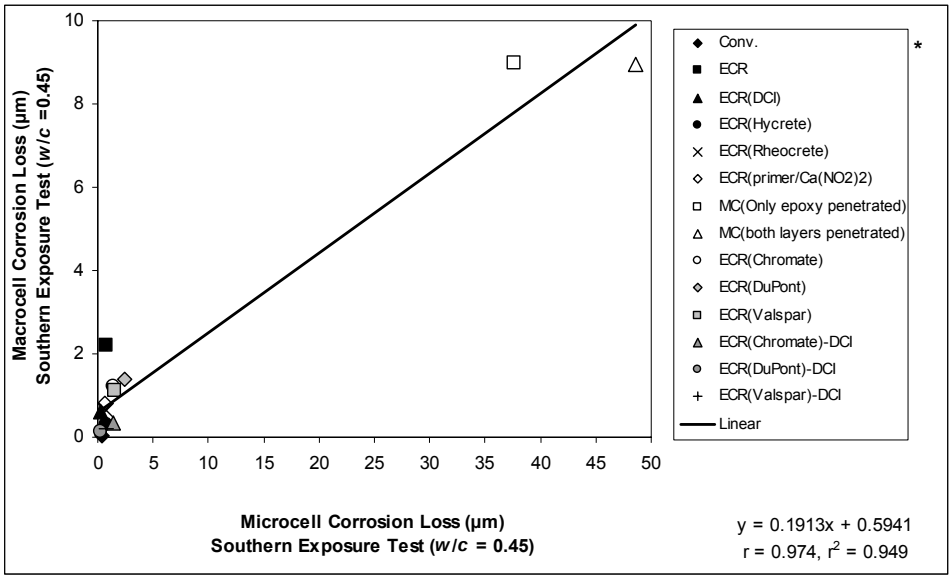

* Steel designations see Table 4.5.

Figure 4.36 (a) – Microcell vs. macrocell total corrosion losses at week 40, as measured in the Southern Exposure test for different corrosion protection systems, *w*/*c* = 0.45. Total corrosion losses for ECR specimens are average values of specimens with four and 10 holes. Losses based on total area for conventional steel and exposed area for epoxy-coated steel.

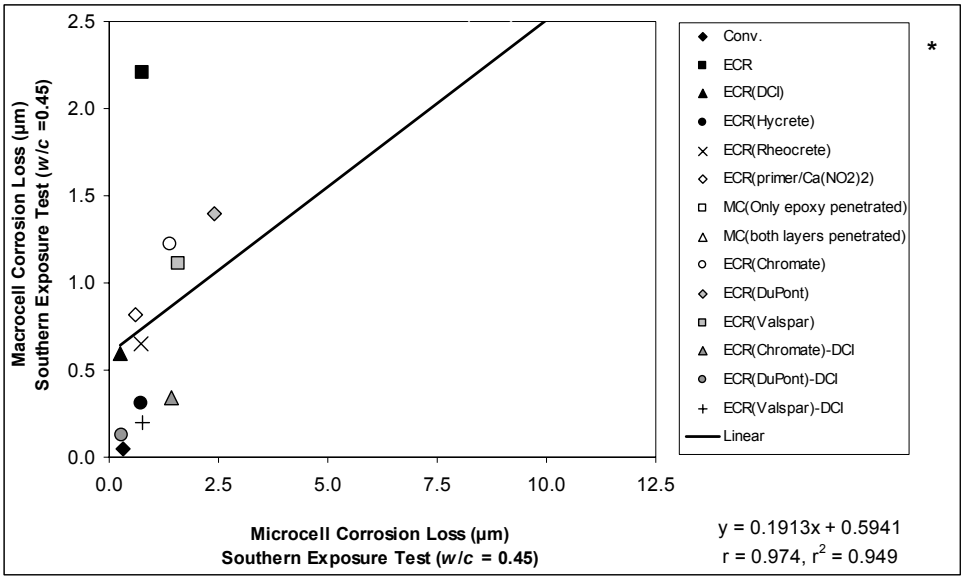

* Steel designations see Table 4.5.

Figure 4.36 (b) – Microcell vs. macrocell total corrosion losses at week 40, as measured in the Southern Exposure test for different corrosion protection systems, *w*/*c* = 0.45. Total corrosion losses for ECR specimens are average values of specimens with four and 10 holes. Losses based on total area for conventional steel and exposed area for epoxy-coated steel.

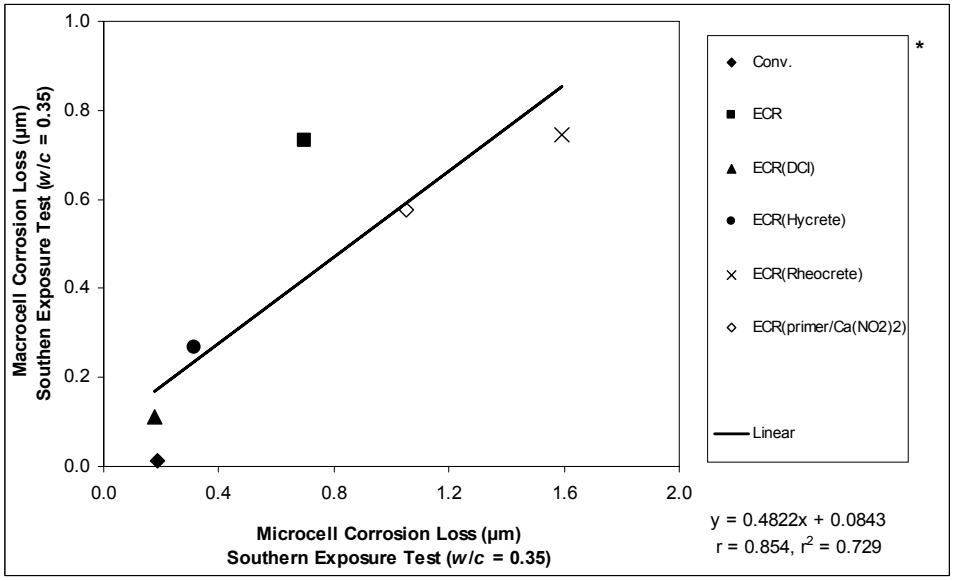

* Steel designations see Table 4.5.

Figure 4.37 – Microcell vs. macrocell corrosion losses at week 40, as measured in the Southern Exposure test for different corrosion protection systems, *w*/*c* = 0.35. Losses based on total area for conventional steel and exposed area for epoxy-coated steel.

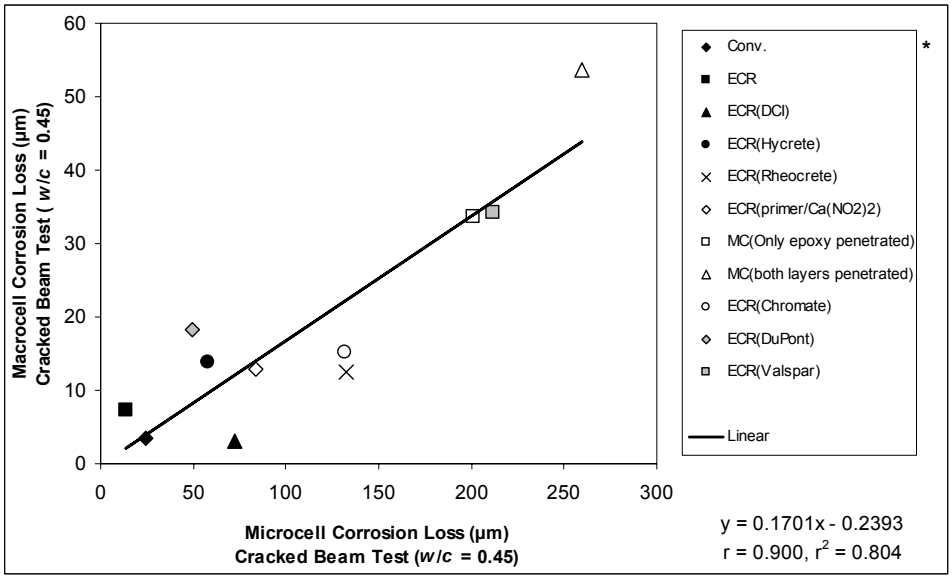

* Steel designation see Table 4.5.

Figure 4.38 – Microcell vs. macrocell corrosion losses at week 40, as measured in the cracked beam test for different corrosion protection systems, *w*/*c* = 0.45. Total corrosion losses for ECR specimens are average values of specimens with four and 10 holes. Losses based on total area for conventional steel and exposed area for epoxy-coated steel.

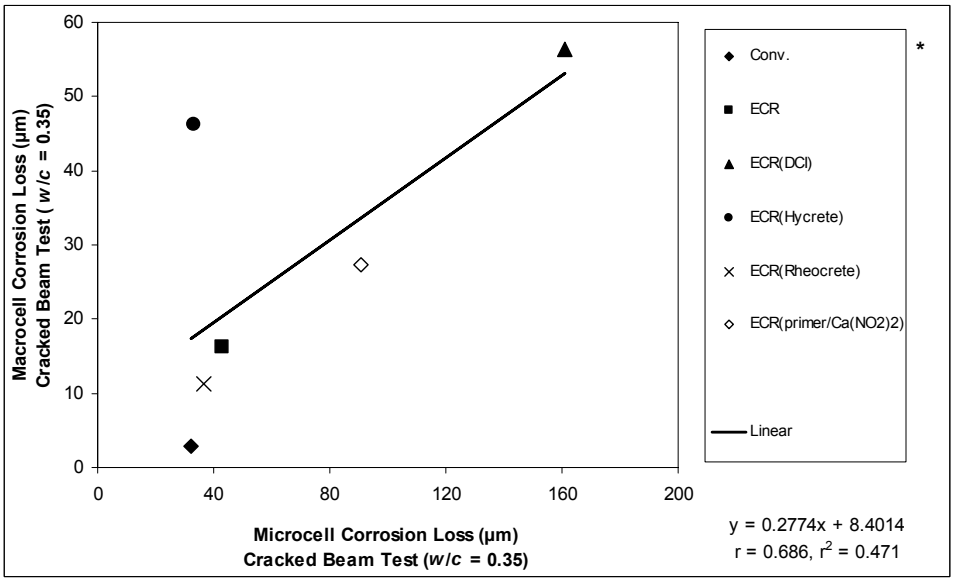

* Steel designation see Table 4.5.

Figure 4.39 – Microcell vs. macrocell corrosion losses at week 40, as measured in the cracked beam test for different corrosion protection systems, *w*/*c* = 0.35. Losses based on total area for conventional steel and exposed area for epoxy-coated steel.

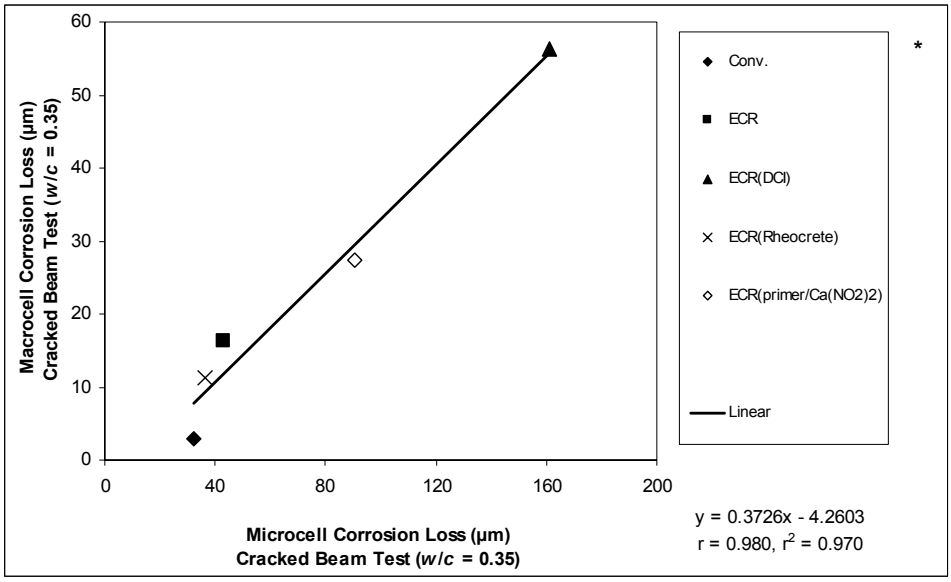

* Steel designation see Table 4.5.

Figure 4.40 – Microcell vs. macrocell corrosion losses at week 40, as measured in the cracked beam test for different corrosion protection systems, *w*/*c* = 0.35. Losses based on total area for conventional steel and exposed area for epoxy-coated steel. Data as shown in Figure 4.39, but with ECR(Hycrete) removed.

4.4.3 Relative Effectiveness of Corrosion Protection Systems

In this section, the different corrosion protection systems are compared using the results of the bench-scale tests. The relative effectiveness of these systems is presented based on both microcell and macrocell corrosion.

In the SE tests with a *w*/*c* ratio of 0.45 (Figure 4.36), conventional ECR cast in concrete with corrosion inhibitors DCI-S, Hycrete, and Rheocrete and ECR with a primer containing encapsulated calcium nitrite improves the corrosion protection of conventional ECR in concrete in terms of both microcell and macrocell corrosion. Multiple coated reinforcement shows the highest total corrosion losses in both microcell and macrocell corrosion, when compared to other corrosion protection systems. As shown in Figure 4.36(b), the three types of high adhesion ECR bars and ECR(Chromate) cast in concrete with DCI-S exhibit lower total corrosion losses than

conventional ECR in macrocell corrosion. However, these specimens show much higher losses than conventional ECR in microcell corrosion. The other two types of high adhesion ECR bars, ECR(DuPont) and ECR(Valspar) cast in concrete with the calcium nitrite inhibitor, show lower total corrosion losses than conventional ECR in both macrocell and microcell corrosion.

In the SE test with a *w*/*c* ratio of 0.35 (Figure 4.37), the use of corrosion inhibitor DCI-S and Hycrete improves corrosion performance of conventional ECR in both macrocell and microcell corrosion. Conventional ECR cast in concrete with Rheocrete shows higher total corrosion losses than conventional ECR alone, especially in microcell corrosion. ECR with a calcium nitrite primer produces mixed results, showing a higher corrosion loss than conventional ECR in microcell corrosion and provides significant help in macrocell corrosion.

In the CB test with a *w*/*c* ratio of 0.45 (Figure 4.38), none of the corrosion protection systems (including conventional ECR cast in concrete with corrosion inhibitors, ECR with a calcium nitrite primer, multiple coated reinforcement, and three types of high adhesion ECR bars) show better corrosion protection than conventional ECR, with the exception of ECR(DCI) in macrocell corrosion, which shows a lower total corrosion loss when compared to conventional ECR.

In the CB test with a *w*/*c* ratio of 0.35 (Figure 4.39), the use of Rheocrete does improve the corrosion performance of conventional ECR in concrete. The other two corrosion protection systems, ECR cast in concrete with DCI-S and ECR with a calcium nitrite primer, shows higher total corrosion losses than conventional ECR in both macrocell and microcell corrosion. When compared to conventional ECR, the use of the corrosion Hycrete shows slight improvement in microcell corrosion, but not in macrocell corrosion.

As shown in Table 4.8 and Figures 4.36 through 4.40, most damaged ECR bars exhibited similar but higher total corrosion losses based on exposed area than conventional steel based on total exposed area, in terms of both microcell and macrocell corrosion. In the SE test, conventional ECR cast in concrete with DCI-S at *w*/*c* ratios of 0.45 and 0.35, and high adhesion DuPont bars cast with DCI-S showed lower total corrosion losses based on exposed area than conventional steel based on total area in microcell corrosion. In the CB test, specimens that showed lower total corrosion losses were conventional ECR in microcell corrosion, and ECR cast in concrete with DCI-S in macrocell corrosion at a *w*/*c* ratio of 0.45. Multiple coated reinforcement exhibited the highest total corrosion losses based on exposed area, with values between 115 and 181 times the loss of conventional steel in the SE test and between 8.2 and 15.7 times the loss of conventional steel in the CB test based on total area. As will be discussed in Chapter 5, however, damaged epoxy-coated reinforcement can undergo much higher corrosion on small exposed areas than can uncoated conventional steel without causing concrete to crack, the usual condition that requires repair.

In general, the relative effectiveness of different corrosion protection systems is similar in both microcell and macrocell corrosion.

CHAPTER 5

ECONOMIC ANALYSIS

An economic analysis is performed to compare the cost effectiveness for bridge decks containing different corrosion protection systems following the procedures used by Kepler et al. (2000), Darwin et al. (2002), Balma et al. (2005), and Gong et al. (2006). The systems include conventional steel, epoxy-coated reinforcement (ECR), ECR cast in concrete with corrosion inhibitor DCI-S, Rheocrete, or Hycrete, ECR containing a calcium nitrite primer, multiple coated reinforcement, ECR with the chromate pretreatment, and two types of ECR with improved adhesion coatings produced by DuPont and Valspar. The bridge decks used in the comparison include a typical 230-mm (9 in.) bridge deck with a concrete cover of 76 mm (3 in.) over the top mat of reinforcing steel and a 191-mm (7.5 in.) concrete subdeck with a 38-mm (1.5 in.) silica fume concrete overlay. The total cost for a new bridge deck and subsequent repairs over a 75-year economic life are compared on a present-cost basis.

The service lives of bridge decks containing different steels are estimated based on the laboratory results for chloride thresholds and corrosion rates, along with the bridge deck surveys performed by Miller and Darwin (2000) and Lindquist, Darwin, and Browning (2005). The services lives of bridge decks containing ECR are also determined based on the experience of the Departments of Transportation in Kansas and South Dakota. Based on experience (Kepler et al. 2000), the second and subsequent repairs are assumed to be needed every 25 years.

5.1 SERVICE LIFE

Based on the laboratory test results, the service life of a concrete bridge deck

can be determined by estimating the time to corrosion initiation and the time to concrete cracking after corrosion initiation. The time to corrosion initiation is the time it takes for chlorides to penetrate the concrete cover and reach the chloride threshold at the depth of the reinforcing steel level, causing corrosion to occur. The time to concrete cracking is the time it takes for corrosion products to cause cracking and spalling of the concrete cover after corrosion initiation.

5.1.1 Time to Corrosion Initiation

The time to corrosion initiation can be determined based on the chloride threshold of a corrosion protection system and the chloride penetration rates at crack locations on bridge decks from surveys reported by Miller and Darwin (2000) and Lindquist et al. (2005).

Based on the laboratory test results, the chloride threshold is between 0.6 and 1.2 kg/m^3 (1.0 and 2.0 lb/yd^3) for conventional steel and epoxy-coated reinforcement with a damaged coating (including conventional ECR, ECR containing a calcium nitrite primer, multiple coated reinforcement, and the three types of ECR with increased adhesion). For concrete containing ECR cast with the corrosion inhibitor calcium nitrite (DCI-S), the chloride threshold depends on the dosage rate and is estimated to be in the range from 3.6 to 9.5 kg/m^3 (6.1 to 16.0 lb/yd^3) (Berke and Rosenberg 1989) for the DCI-S dosage rate from 10 to 30 L/m^3 (2 to 6 gal/yd^3). For concrete containing ECR cast with the corrosion inhibitors Rheocrete or Hycrete, the chloride threshold is assumed to be same as that of concrete containing ECR without a corrosion inhibitor. As discussed by Gong et al. (2006), both Rheocrete and Hycrete provide protection to reinforcing steel in concrete by forming a protective film at the steel surface and reducing the ingress of chlorides, oxygen, and water into concrete,

which cannot lengthen the time to corrosion initiation appreciably for the fully cracked concrete that is analyzed in this report. For the purposes of this analysis, the corrosion threshold of the zinc layer on the multiple coated (MC) bar is treated as the same as for steel.

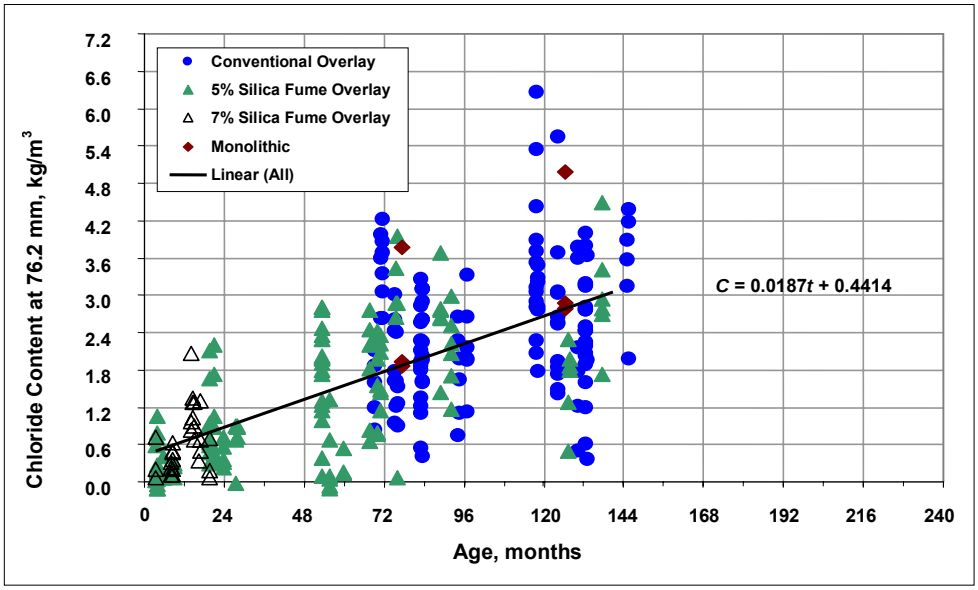

Figure 5.1 – Chloride content taken on cracks interpolated at depths of 76.2 mm (3 in.) versus placement age for bridges with an AADT greater than 7500

Based on the chloride thresholds, the times to corrosion initiation can be determined using the chloride data from bridge surveys reported by Miller and Darwin (2000) and Lindquist et al. (2005) to estimate chloride penetration rate. The chloride concentrations at crack locations are used in this report because significant cracking parallel to and directly above the reinforcing bars is observed in reinforced concrete bridge decks. Figure 5.1 shows the chloride concentration versus time at a depth of 76.2 mm (3 in.) for the bridges in the earlier studies with an annual average daily traffic (AADT) over 7500. The linear trend line between the chloride concentration and time can be described as

$$C = 0.0187t + 0.4414 \quad (5.1)$$

Where C is the water-soluble chloride concentration in terms of kg/m^3 and t is the time in terms of months.

Using the critical chloride thresholds and Eq. (5.1), the time to corrosion initiation can be estimated for the different corrosion protection systems. The results are shown in Table 5.1. As shown in the table, the time to corrosion initiation is presented as a range based on the range of the chloride thresholds.

Table 5.1 – Time to corrosion initiation for bridge decks with different corrosion protection systems (epoxy assumed to be damaged)

Steel Designation[a]	**Chloride Threshold kg/m^3 (lb/yd^3)**	**Time to Corrosion Initiation (years)**
Conv.	0.6 - 1.2 (1.0 - 2.0)	0.7 - 3.4
ECR	0.6 - 1.2 (1.0 - 2.0)	0.7 - 3.4
ECR(DCI)	3.6 - 9.5 (6.1 - 16.0)	14 - 40
ECR(Hycrete)	0.6 - 1.2 (1.0 - 2.0)	0.7 - 3.4
ECR(Rheocrete)	0.6 - 1.2 (1.0 - 2.0)	0.7 - 3.4
ECR(primer/Ca$(NO_2)_2$)	0.6 - 1.2 (1.0 - 2.0)	0.7 - 3.4
MC	0.6 - 1.2 (1.0 - 2.0)	0.7 - 3.4
ECR(Chromate)	0.6 - 1.2 (1.0 - 2.0)	0.7 - 3.4
ECR(DuPont)	0.6 - 1.2 (1.0 - 2.0)	0.7 - 3.4
ECR(Valspar)	0.6 - 1.2 (1.0 - 2.0)	0.7 - 3.4

[a] Conv. = conventional steel. ECR = conventional epoxy-coated reinforcement.
ECR(DCI) = ECR in concrete with DCI inhibitor.
ECR(Hycrete) = ECR in concrete with Hycrete inhibitor.
ECR(Rheocrete) = ECR in concrete with Rheocrete inhibitor.
MC = multiple coated bars.
ECR(primer/Ca$(NO_2)_2$) = ECR with a primer containing calcium nitrite.
ECR(Chromate) = ECR with the chromate pretreatment.
ECR(DuPont) = ECR with high adhesion DuPont coating.
ECR(Valspar) = ECR with high adhesion Valspar coating.

5.1.2 Time to Concrete Cracking

The time to concrete cracking after corrosion initiation is determined based on 1) the average corrosion rate of each corrosion protection system measured in the current study, and 2) the total corrosion loss that corresponds to the quantity of corrosion product that can cause the cracking and spalling of the concrete cover.

Average corrosion rates between weeks 50 and 70 were recommended by Balma et al. (2005) for use in an economic analysis because more stable corrosion behavior during this period was observed for bench-scale test specimens. In this report, corrosion rates between weeks 30 and 40 are used for all of the corrosion protection systems because week 40 is the shortest duration of any of the bench-scale tests described in this study. Because the steels are subjected to a more aggressive test environment in the laboratory than in actual structures, the corrosion rates used to calculate the time to concrete cracking are determined as half the average values of corrosion rates from the SE and CB tests in this study. The average corrosion rates for all coated specimens are based on the average values for the exposed area for ECR specimens with four and 10 holes in concrete with a *w*/*c* ratio of 0.45. The average corrosion rates used to calculate the time to concrete cracking are summarized in Table 5.2.

Table 5.2 – Corrosion rates used to calculate the time to concrete cracking [c]

Steel Designation[a]	Average Corrosion Rates (μm/yr)		Corrosion Rates[c] (μm/yr)
	SE Test[b]	CB Test[b]	
Conv.	0.54	6.59	1.78
ECR	0.78	7.81	2.15
ECR(DCI)	0.78	3.88	1.17
ECR(Hycrete)	0.07	9.95	2.50
ECR(Rheocrete)	0.53	20.88	5.35
ECR(primer/$Ca(NO_2)_2$)	0.99	9.98	2.74
MC(only epoxy penetrated)	4.46	34.46	9.73
MC(both layers penetrated)	13.62	65.33	19.74
ECR(Chromate)	2.31	21.28	5.90
ECR(DuPont)	1.64	25.75	6.85
ECR(Valspar)	1.25	18.93	5.04

[a] Conv. = conventional steel. ECR = conventional epoxy-coated reinforcement.
ECR(DCI) = ECR in concrete with DCI inhibitor.
ECR(Hycrete) = ECR in concrete with Hycrete inhibitor.
ECR(Rheocrete) = ECR in concrete with Rheocrete inhibitor.
ECR(primer/$Ca(NO_2)_2$) = ECR with a primer containing calcium nitrite.
MC(both layers penetrated) = multiple coated bars with both the zinc and epoxy layers penetrated.
MC(only epoxy penetrated) = mutiple coated bars with only the epoxy layer penetrated.
ECR(Chromate) = ECR with the chromate pretreatment.
ECR(DuPont) = ECR with high adhesion DuPont coating.
ECR(Valspar) = ECR with high adhesion Valspar coating.

[b] Average value of corrosion rates for specimens with four and 10 holes in concrete with a w/c ratio of 0.45.

[c] Corrosion rates used to calculate the time to concrete cracking, half of the average value of average corrosion rates from the Southern Exposure and cracked beam tests.

For conventional steel, the total corrosion loss that can result in a volume of corrosion products to crack concrete is estimated to be 25 μm (0.001 in.) (Pfeifer 2000), assuming that the corrosion loss is uniform along the length of a reinforcing bar. For localized corrosion, Torres-Acosta and Sagües (2004) used two types of specimens, cylinderical and prismatic beam concrete specimens, to estimate the amount of corrosion needed to crack concrete. The cylinderical specimen contained a dual-material pipe made of carbon steel pipe in the middle section and two polyvinyl chloride (PVC) pipes for the remainder. The prismatic specimen contained a dual-material reinforcing bar made of carbon steel at the center and Type 316L/N stainless

steel at both ends. For both specimens, the carbon steel section provided an anodic ring region and corrosion only occurred at this section. Based on their test results, Torres-Acosta and Sagües (2004) developed an equation to estimate the total corrosion loss needed to cause concrete cracking

$$x_{Crit} = 11\left(\frac{c}{\phi}\right)\left(\frac{c}{L}+1\right)^2 \tag{5.2}$$

where x_{Crit} is the critical corrosion loss needed to crack concrete in μm, c is concrete cover in mm, ϕ is reinforcing bar diameter in mm, and L is the length of anodic ring region in mm.

According to Eq. (5.2), for the ECR specimens with four holes tested in this report, the exposed steel at the drilled holes represent the anodic ring region defined by Torres-Acosta and Sagües (2004). The total corrosion loss needed to crack cover concrete is 1426 μm, based on a concrete cover of 25 mm (1 in.), a reinforcing bar diameter of 16 mm ($^5/_8$ in.), and an anodic ring with a length of 3.2 mm (0.15 in.). For this calculation, the length of anodic ring region equals the diameter of the drilled holes for epoxy-coated steel. The tensile stress caused by the increased volume of the corrosion products at the hole on one side of a bar, however, is estimated to be no more than half of that caused by the corrosion products over a ring shaped region. Therefore, twice the corrosion loss given by Eq. (4.2), 2852 μm, is required to crack the concrete cover of a Southern Exposure specimen. This conclusion was confirmed by Gong et al. (2006) using test results from Balma et al. (2005) and McDonald et al. (1998). Table 5.3 shows the time to first repair for bridge decks with different corrosion protection systems based on the above analysis. As shown in Table 5.3, bridge decks containing different epoxy-coated bars have service lives between 184 and 1247 years based on the above analysis – considerably longer than the 75-year economic life used for this analysis. The first time to repair, however, can be greatly

reduced by the adhesion loss between the epoxy coating and the steel, as indicated by Sagües et al. (1994).

To consider the effect of potential adhesion loss, the service life for bridge decks containing ECR has been estimated to be 30 years by the Kansas Department of Transportation and 40 years by the South Dakota Department of Transportation (Darwin et al. 2002). As shown in Table 5.3, the times to first repair of 30, 35, and 40 years are used to conduct the economic analysis in this report in addition to values of more than 75 years based on the calculated time to first repair, as performed by Balma et al. (2005) and Gong et al. (2006).

The combination of the time to corrosion initiation and time to concrete cracking gives the time to first repair, as shown in Table 5.3. The times to first repair based on both analysis and experience are used to conduct the economic analysis for the different corrosion protection systems.

Table 5.3 – Time to first repair based on the experience and analysis for different corrosion protection systems

Steel Designation[a]	Corrosion Inhibitor Dosage L/m^3 (gal/yd^3)	Time to Corrosion Initiation (years)	Corrosion Rates (μm/yr)	Total Corrosion Loss to Crack Concrete (μm)	Time to Concrete Cracking[b] (years)	Time to First Repair (years)
Conv.	-	0.7 3.4	1.78	25	14	15 17
ECR	-	0.7 3.4	2.15	2852	1328	30[c] 35[c] 40[c] >75
ECR(DCI)	10 - 30 (2 - 6)	14 40	1.17	2852	2446	30[c] 35[c] 40[c] >75
ECR(Hycrete)	5 - 10 (1 - 2)	0.7 3.4	2.50	2852	1139	30[c] 35[c] 40[c] >75
ECR(Rheocrete)	5 (1)	0.7 3.4	5.35	2852	533	30[c] 35[c] 40[c] >75
ECR(primer/ $Ca(NO_2)_2$)	-	0.7 3.4	2.74	2852	1039	30[c] 35[c] 40[c] >75
MC (only epoxy penetrated)	-	0.7 3.4	9.73	2852	293	30[c] 35[c] 40[c] >75
MC (both layers penetrated)	-	0.7 3.4	19.74	2852	145	30[c] 35[c] 40[c] >75
ECR(Chromate)	-	0.7 3.4	5.90	2852	483	30[c] 35[c] 40[c] >75
ECR(DuPont)	-	0.7 3.4	6.85	2852	416	30[c] 35[c] 40[c] >75
ECR(Valspar)	-	0.7 3.4	5.04	2852	565	30[c] 35[c] 40[c] >75

[a] Conv. = conventional steel. ECR = conventional epoxy-coated reinforcement.
ECR(DCI) = ECR in concrete with DCI inhibitor.
ECR(Hycrete) = ECR in concrete with Hycrete inhibitor.
ECR(Rheocrete) = ECR in concrete with Rheocrete inhibitor.
ECR(primer/$Ca(NO_2)_2$) = ECR with a primer containing calcium nitrite.
MC(both layers penetrated) = multiple coated bars with both the zinc and epoxy layers penetrated.
MC(only epoxy penetrated) = mutiple coated bars with only the epoxy layer penetrated.
ECR(DuPont) = ECR with high adhesion DuPont coating.
ECR(Valspar) = ECR with high adhesion Valspar coating.

[b] Time to concrete cracking after corrosion initiation.

[c] Time to first repair estimated by the Kansas and South Dakota Departments of Transportation, otherwise based on analysis.

5.2 COST EFFECTIVENESS

A prototype bridge deck with a thickness of 230 mm (9 in.), either monolithic or consisting of a 191-mm (7.5-in.) concrete subdeck and a 38-mm (1.5-in.) silica fume concrete overlay, is used to compare the cost effectiveness of different corrosion protection systems over a 75-year economic life. The total cost includes the cost of a new bridge deck and the subsequent repair costs every 25 years after the first repair.

The procedures for life cycle cost analysis used by Kepler et al. (2000), Darwin et al. (2002), Balma et al. (2005), and Gong et al. (2006) are used in this report and can be summarized as follows:

1. Determine the cost of a new bridge deck in terms of dollars per square meter by considering the in-place cost of concrete, steel, silica fume overlay, and corrosion inhibitors,
2. Determine the total repair costs, which include full-depth and partial-depth repairs, machine preparation, a 38-mm (1.5-in.) silica fume concrete overlay, and incidental costs,
3. Calculate the total cost over the 75-year economic life and compare the cost effectiveness based on the present value of the costs at discount rates of 2, 4, and 6%.

5.2.1 New Bridge Deck Costs

Based on average bids on KDOT projects from 2000 to 2003 (Balma et al. 2005), in-place costs equal \$475.30/m^3 (\$363.4/yd^3) for concrete and \$1148/m^3 (\$43.62/m^2) for silica fume overlay with a thickness of 38 mm (1.5 in.). The average density of reinforcing steel estimated by Kepler et al. (2000) is 143 kg/m^3 (241

lb/yd^3). The in-place cost of steel includes the cost of steel at the mill and the cost of fabrication, delivery, and placement. These costs can be obtained based on the data provided by manufacturers and fabricators in the years 2004 and 2005.

For conventional steel and ECR, the material costs are \$0.55/kg (\$0.25/lb) and \$0.68/kg (\$0.31/lb) at the mill, respectively. The costs of fabrication, delivery, and placement are \$1.30/kg (\$0.59/lb) for conventional steel and \$1.41/kg (\$0.64/lb) for epoxy-coated steel, giving an in-place cost of \$1.85/kg (\$0.84/lb) for conventional steel and \$2.09/kg (\$0.95/lb) for epoxy-coated steel, respectively. The in-place costs of ECR containing a calcium nitrite primer, multiple coated reinforcement, and any of the three types of ECR with increased adhesion are the same as those for ECR.

Prices of \$1.84/L (\$7/gal), \$4.21/L (\$16/gal), and \$3.94/L (\$15/gal) were provided by manufacturers for corrosion inhibitors DCI-S, Rheocrete, and Hycrete, respectively. The recommended dosage rates of 10-30 L/m^3 (2-6 gal/yd^3) for DCI-S, 5 L/m^3 (1 gal/yd^3) for Rheocrete, and 5-10 L/m^3 (1-2 gal/yd^3) for Hycrete, respectively, are used in the analysis summarized in Table 5.4.

Table 5.4 – In-place cost for different items in a new bridge deck

Items	**Corrosion Inhibitor Dosage**	**In-Place Costs**
	L/m^3 (gal/yd^3)	**(\$/m2)**
230-mm concrete deck		109.32
191-mm concrete subdeck + 38-mm silica fume overlay		134.39
Conventional steel		60.85
Epoxy-coated steel		68.74
DCI-S	10 (2)	4.23
	30 (6)	12.70
Hycrete	5 (1)	4.53
	10 (2)	9.06
Rheocrete	5 (1)	4.84
ECR containing a calcium nitrite		68.74
Multiple coated reinforcement		68.74
Three types of ECR with increased adhesion		68.74

All in-place material costs in terms of dollars per square meter are shown in Table 5.4, and the cost of a new bridge deck with different corrosion protection systems are summarized in Table 5.5. The cost of a new 230-mm (9-in.) bridge deck is \$170.17/m^2 for conventional steel and \$178.06/m^2 for conventional ECR. For bridge decks cast with corrosion inhibitor DCI-S or Hycrete, the cost depends on the dosage rate and is presented as a range. For new 230-mm (9-in.) bridge decks with ECR cast in concrete with corrosion inhibitors, the costs are between \$182.29/m^2 and \$190.76/m^2 for DCI-S, between \$182.59/m^2 and \$187.12/m^2 for Hycrete, and \$182.90/m^2 for Rheocrete. For a new 230-mm (9-in.) bridge deck reinforced with ECR containing a calcium nitrite primer, multiple coated reinforcement, or any of the three types of ECR with increased adhesion, the cost is the same as the deck containing conventional ECR.

For all of the corrosion protection systems, the cost of the 38-mm (1.5-in.) silica fume concrete overlay is \$25.07/m^2, when the cost of the subdeck is adjusted to account for its thickness of 191 mm (7.5 in.).

5.2.2 Repair Costs

Based on information from 27 bridge deck repair projects in Kansas for 1999 (Kepler et al. 2000), it is estimated that 22% of bridge decks receive partial-depth repairs and 6% receive full-depth repairs. As a standard repair practice in Kansas, a 38-mm (1.5-in.) silica fume overlay is also placed over the deck as part of the repair procedure.

The repair costs consist of the costs of full-depth and partial-depth repairs, machine preparation, a 38-mm (1.5-in.) silica fume overlay, and incidental costs, which can be determined based on the average low-bid costs reported by KDOT from 2000 to 2003 (Balma et al. 2005). The full-depth and partial-depth repair costs are

$380.30/m^2 and $125.77/m^2, respectively. Other costs are $13.13/m^2 for machine preparation, $43.61/m^2 for a 38-mm (1.5-in.) silica fume overlay, and $154.89/m^2 for incidental costs. Based on these costs, the average repair cost is $262.34/m^2, as shown below.

$$0.22 \times \frac{\$125.77}{m^2} + 0.06 \times \frac{\$380.30}{m^2} + \frac{\$13.10}{m^2} + \frac{\$43.60}{m^2} + \frac{\$154.89}{m^2} = \$262.34/m^2$$

5.2.3 Cost Effectiveness

The costs of bridge decks with different corrosion protection systems are compared based on the cost of a new bridge deck and the present value of the repair costs over the 75-year economic life. The present value of a repair cost is calculated at discount rates of 2, 4 and 6% and can be expressed as follows:

$$P = F \times (1+i)^{-n} \tag{4.3}$$

where P is the present value in $/m^2, F is the repair cost in $/m^2, i is the discount rate in %, and n is the time to repair in years.

The life cycle cost for different corrosion protection systems are summarized in Table 5.5 for monolithic decks and in Table 5.6 for silica fume overlay decks. As the time to first repair and the discount rate increase, the present costs for different corrosion protection systems decrease. The use of ECR with a primer containing calcium nitrite, multiple coated reinforcement, or any of the three types of ECR with increased adhesion provides the same cost as the use of conventional ECR.

The results show that a 230-mm (9-in.) bridge deck constructed with conventional steel is the highest cost option. The lowest cost option is a 230-mm (9-in.) concrete deck reinforced with conventional ECR. When the effect of adhesion loss is not considered, the 230-mm (9-in.) concrete deck reinforced with conventional

ECR has a present cost of $178.06/m^2. When a corrosion inhibitor is used, the lowest cost is $182.29/m^2 for a 230-mm (9-in.) bridge deck containing ECR with DCI-S at a dosage rate of 10 L/m^3 (2 gal/yd^3). The use of DCI-S at a dosage rate of 30 L/m^3 (6 gal/yd^3) increases the cost by $8.47/m^2. The other options are a bridge deck containing ECR with Rheocrete ($182.90/m^2), Hycrete at a lower bound of dosage rate ($182.59/m^2), and Hycrete at an upper bound of dosage rate ($187.12/m^2).

When the effect of adhesion loss is considered, the use of the 230-mm (9-in.) bridge deck containing conventional ECR (or the other ECR bars with the same cost) is the lowest cost option when the first repair occurs at 40 years. When a corrosion inhibitor is used, the lowest cost option is a bridge deck containing conventional ECR with DCI-S at the lower bound dosage rate, followed by the use of Hycrete at the lower bound dosage rate, Rheocrete, Hycrete at the upper bound dosage rate, and DCI-S at the upper bound dosage rate, respectively. For a 230-mm (9-in.) bridge deck reinforced with conventional ECR, at discount rates of 2%, 4%, and 6%, the costs are $369.29/m^2, $253.20/m^2, and $209.51/m^2, respectively, when the first repair occurs at 40 years. When a corrosion inhibitor is used, at the same time to first repair, the options are a bridge deck containing conventional ECR with DCI-S (between $213.74/m^2 and $381.99/m^2), Hycrete (between $214.04/m^2 and $378.35/m^2), and Rheocrete (between $214.35/m^2 and $374.13/m^2).

5.2.4 Summary

The lowest cost option is provided by any of the following (all have the same cost): 230-mm concrete decks reinforced with conventional ECR, ECR with a primer containing calcium nitrite, multiple coated reinforcement, or any of the three types of high adhesion ECR bars.

Table 5.5 – Economic analysis for bridge decks with different corrosion protection systems – monolithic decks

Option	Type of Deck	Type of Steel	Type of Corrosion Inhibitor	Cost of Deck ($/m^2)	Cost of Steel ($/m^2)	Cost of Corrosion Inhibitor ($/m^2)	Total Cost ($/m^2)	Cost of Repair 1 ($/m^2)	Time to Repair 1 (years)	Cost of Repair 2 ($/m^2)	Time to Repair 2 (years)	Cost of Repair 3 ($/m^2)	Time to Repair 3 (years)	Present Cost i = 2% ($/m^2)	Present Cost i = 4% ($/m^2)	Present Cost i = 6% ($/m^2)
1	230-mm	Conv.	–	109.32	60.85	–	170.17	262.34	14	262.34	39	262.34	64	564.05	399.81	319.54
2									17		42		67	541.33	374.32	295.58
3	230-mm	ECR	–	109.32	68.74	–	178.06	262.34	30	262.34	55			411.17	289.29	234.38
4									35		60			389.19	269.48	220.14
5									40		65			369.29	253.20	209.51
6									>75					178.06	178.06	178.06
7	230-mm	ECR(DCI)	DCI-S	109.32	68.74	4.23	182.29	262.34	30	262.34	55			415.40	293.52	238.61
8									35		60			393.42	273.71	224.37
9									40		65			373.52	257.43	213.74
10									>75					182.29	182.29	182.29
11						12.70	190.76	262.34	30	262.34	55			423.87	301.99	247.08
12									35		60			401.89	282.18	232.84
13									40		65			381.99	265.90	222.21
14									>75					190.76	190.76	190.76
15	230-mm	ECR(Hycrete)	Hycrete	109.32	68.74	4.53	182.59	262.34	30	262.34	55			415.70	293.82	238.91
16									35		60			393.72	274.01	224.67
17									40		65			373.82	257.73	214.04
18									>75					182.59	182.59	182.59
19						9.06	187.12	262.34	30	262.34	55			420.23	298.35	243.44
20									35		60			398.25	278.54	229.20
21									40		65			378.35	262.26	218.57
22									>75					187.12	187.12	187.12
23	230-mm	ECR(Rheocrete)	Rheocrete	109.32	68.74	4.84	182.90	262.34	30	262.34	55			416.01	294.13	239.22
24									35		60			394.03	274.32	224.98
25									40		65			374.13	258.04	214.35
26									>75					182.90	182.90	182.90
27	230-mm	ECR(primer/ $Ca(NO_2)_2$)	-	109.32	68.74	–	178.06	262.34	30	262.34	55			411.17	289.29	234.38
28									35		60			389.19	269.48	220.14
29									40		65			369.29	253.20	209.51
30									>75					178.06	178.06	178.06
31	230-mm	MC	-	109.32	68.74	–	178.06	262.34	30	262.34	55			411.17	289.29	234.38
32									35		60			389.19	269.48	220.14
33									40		65			369.29	253.20	209.51
34									>75					178.06	178.06	178.06
35	230-mm	ECR(Chromate)	–	109.32	68.74	–	178.06	262.34	30	262.34	55			411.17	289.29	234.38
36									35		60			389.19	269.48	220.14
37									40		65			369.29	253.20	209.51
38									>75					178.06	178.06	178.06
39	230-mm	ECR(DuPont)	–	109.32	68.74	–	178.06	262.34	30	262.34	55			411.17	289.29	234.38
40									35		60			389.19	269.48	220.14
41									40		65			369.29	253.20	209.51
42									>75					178.06	178.06	178.06
43	230-mm	ECR(Valspar)	–	109.32	68.74	–	178.06	262.34	30	262.34	55			411.17	289.29	234.38
44									35		60			389.19	269.48	220.14
45									40		65			369.29	253.20	209.51
46									>75					178.06	178.06	178.06

Table 5.6 – Economic analysis for bridge decks with different corrosion protection systems – silica fume overlay decks

Option	Type of Deck	Type of Steel	Type of Corrosion Inhibitor	Cost of Deck ($/m^2)	Cost of Steel ($/m^2)	Cost of Corrosion Inhibitor ($/m^2)	Total Cost ($/m^2)	Cost of Repair 1 ($/m^2)	Time to Repair 1 (years)	Cost of Repair 2 ($/m^2)	Time to Repair 2 (years)	Present Cost i = 2% ($/m^2)	Present Cost i = 4% ($/m^2)	Present Cost i = 6% ($/m^2)
47	191-mm + 38-mm SFO	ECR	–	134.39	68.74	–	203.13	262.34	30	262.34	55	436.24	314.36	259.45
48									35		60	414.26	294.55	245.21
49									40		65	394.36	278.27	234.58
50									>75			203.13	203.13	203.13
51	191-mm + 38-mm SFO	ECR(DCI)	DCI-S	134.39	68.74	4.23	207.36	262.34	30	262.34	55	440.47	318.59	263.68
52									35		60	418.49	298.78	249.44
53									40		65	398.59	282.50	238.81
54									>75			207.36	207.36	207.36
55						12.70	215.83	262.34	30	262.34	55	448.94	327.06	272.15
56									35		60	426.96	307.25	257.91
57									40		65	407.06	290.97	247.28
58									>75			215.83	215.83	215.83
59	191-mm + 38-mm SFO	ECR(Hycrete)	Hycrete	134.39	68.74	4.53	207.66	262.34	30	262.34	55	440.77	318.89	263.98
60									35		60	418.79	299.08	249.74
61									40		65	398.89	282.80	239.11
62									>75			207.66	207.66	207.66
63						9.06	212.19	262.34	30	262.34	55	445.30	323.42	268.51
64									35		60	423.32	303.61	254.27
65									40		65	403.42	287.33	243.64
66									>75			212.19	212.19	212.19
67	191-mm + 38-mm SFO	ECR(Rheocrete)	Rheocrete	134.39	68.74	4.84	207.97	262.34	30	262.34	55	441.08	319.20	264.29
68									35		60	419.10	299.39	250.05
69									40		65	399.20	283.11	239.42
70									>75			207.97	207.97	207.97
71	191-mm + 38-mm SFO	ECR(primer/ $Ca(NO_2)_2$)	-	134.39	68.74	–	203.13	262.34	30	262.34	55	436.24	314.36	259.45
72									35		60	414.26	294.55	245.21
73									40		65	394.36	278.27	234.58
74									>75			203.13	203.13	203.13
75	191-mm + 38-mm SFO	MC	-	134.39	68.74	–	203.13	262.34	30	262.34	55	436.24	314.36	259.45
76									35		60	414.26	294.55	245.21
77									40		65	394.36	278.27	234.58
78									>75			203.13	203.13	203.13
79	191-mm + 38-mm SFO	ECR(Chromate)	–	134.39	68.74	–	203.13	262.34	30	262.34	55	436.24	314.36	259.45
80									35		60	414.26	294.55	245.21
81									40		65	394.36	278.27	234.58
82									>75			203.13	203.13	203.13
83	191-mm + 38-mm SFO	ECR(DuPont)	–	134.39	68.74	–	203.13	262.34	30	262.34	55	436.24	314.36	259.45
84									35		60	414.26	294.55	245.21
85									40		65	394.36	278.27	234.58
86									>75			203.13	203.13	203.13
87	191-mm + 38-mm SFO	ECR(Valspar)	–	134.39	68.74	–	203.13	262.34	30	262.34	55	436.24	314.36	259.45
88									35		60	414.26	294.55	245.21
89									40		65	394.36	278.27	234.58
90									>75			203.13	203.13	203.13

CHAPTER 6

COMPARISON BETWEEN TEST METHODS

This chapter presents comparisons between the rapid macrocell test and the Southern Exposure (SE) or cracked beam (CB) test, and between the SE and CB tests. The comparisons are performed based on the results of a study by Balma et al. (2005).

Even though the tests in this report are not complete, comparisons were also performed based on the results at week 15 of the rapid macrocell test and week 40 of the SE and CB tests. In the current study, if conventional steel is included, a very good linear relationship can be obtained because conventional steel has a much higher corrosion rate and total corrosion loss than the epoxy-coated bars. The corrosion rates and total corrosion losses for epoxy-coated bars are very low and the scatter is high relative to the average values. As a result, without including the results for conventional steel, a linear relationship cannot be obtained based solely on specimens that contain epoxy-coated bars. The results obtained in the current study are, therefore, not used to compare test methods.

As noted in Chapter 1, Balma et al. (2005) used the rapid macrocell and bench-scale tests to evaluate the corrosion performance of different corrosion protection systems. The rapid macrocell test included three different specimen types: bare bar, lollipop, and mortar-wrapped. The lollipop specimen consisted of a 127-mm (5-in.) long bar with a depth of 76-mm (3-in.) embedded in a mortar cylinder, which had a diameter of 30-mm (1.2-in.) and depth of 102-mm (4-in.). The lollipop specimens were tested using the same test procedures as were the mortar-wrapped specimens in the current rapid macrocell test, except the solutions were not replaced at five week intervals as they were in the current study. The bench-scale tests included the SE, CB,

and ASTM G 109 tests. The corrosion protection systems evaluated in the study included conventional normalized steel, conventional Thermex-treated steel, microalloyed steel, MMFX microcomposite steel, epoxy-coated reinforcement (ECR), duplex steels (2101 and 2205, pickled and nonpickled), two corrosion inhibitors (DCI-S and Rheocrete 222+), and variations in the water-cement (*w/c*) ratio of mortar and concrete. The results at week 70 for the SE and CB tests were compared with the results at week 15 for the rapid macrocell test. The results for the SE test were also compared with the results for the CB test at week 70. The results for SE and CB tests at week 70 were selected because the corrosion behavior for specimens between weeks 50 and 70 is more stable than before and after.

This report presents comparisons based on the results at week 96 of the SE and CB tests and at week 15 of the rapid macrocell test. Balma et al. (2005) presented the same comparisons based on the results at week 70 for the SE and CB test. The two comparisons will be used to determine if SE and CB results at week 70 or 96 are more appropriate to evaluate corrosion performance for different corrosion protection systems.

The test programs for the rapid macrocell and bench-scale tests are shown in Tables C.1 through C.5 in Appendix C. The corrosion rate and total corrosion loss results are summarized in Tables C.6 through C.15 in Appendix C, which show the individual, average, and standard deviation for the test results of each corrosion protection system.

In addition, this chapter presents comparisons of coefficients of variation between corrosion rates and total corrosion losses, and between the results obtained with the rapid macrocell test and those obtained with the bench-scale tests. Levels of significance for comparisons are compared for the rapid macrocell test and the bench-

scale tests based on the Student's t-test.

Descriptions of the statistical difference between two samples and linear regression analysis are presented in Section 6.1 and 6.2, respectively. The correlations between the results in rapid macrocell test at week 15 and the results in the SE and CB tests at week 96 and between the SE and CB tests at week 96 are presented in Section 6.3. Comparisons based on coefficients of variation and levels of significance are covered in Section 6.4 and the results are summarized in Section 6.5.

6.1 STATISTICAL DIFFERENCE BETWEEN SAMPLES

The existence of a difference between the means of two populations can be evaluated using the Student's t-test when the sample sizes are small and the standard deviations of the two samples are unknown. In this study, the samples represent corrosion rates or total corrosion losses for two different types of steel. The level of significance in the difference in the performance of two steels can be determined using two-sample t-test procedures (Hayter 1996).

The corrosion rate or total corrosion loss data consist of a sample of n observations x_i (i = 1, …, n) from population A, with a sample mean $\bar{x}$ and a sample standard deviation s_x, and a sample of m observations y_j (j = 1, …, m) from population B, with a sample mean $\bar{y}$ and a sample standard deviation s_y. The populations A and B have means μ_A and μ_B, respectively. The difference in the population means $\mu_A - \mu_B$ is estimated by $\bar{x} - \bar{y}$, and the standard error is estimated by

$$s.e.(\bar{x} - \bar{y}) = \sqrt{\frac{s_x^2}{n} + \frac{s_y^2}{m}} \tag{6.1}$$

The standard error is an estimate of the standard deviation of the sampling distribution of means. The standard error is inversely proportional to the sample size.

The larger the sample size, the smaller the standard error.

For a two-sided hypothesis testing problem with the null hypothesis expressed as $H_0 : \mu_A - \mu_B = \delta$, the appropriate t-statistic is given by

$$t_{stat} = \frac{\overline{x} - \overline{y} - \delta}{\sqrt{\frac{s_x^2}{n} + \frac{s_y^2}{m}}} \tag{6.2}$$

To determine if the difference in the means of corrosion rates or total corrosion losses between two different types of steel is statistically significant, the value δ is set to zero. The value of t_{stat} is then compared to the value obtained from the t-distribution, t_{crit}, which depends on the level of significance α and the number of degrees of freedom of the t-distribution. The level of significance α represents the probability that the test will incorrectly identify a statistically significant difference in sample means when, in fact, there is no difference in μ_A and μ_B. The number of degrees of freedom v of the t-distribution is usually calculated from

$$v = \frac{(\frac{s_x^2}{n} + \frac{s_y^2}{m})^2}{\frac{s_x^4}{n^2(n-1)} + \frac{s_y^4}{m^2(m-1)}}. \tag{6.3}$$

At a certain significance level α, if the absolute value of t_{stat} is greater than t_{crit}, the null hypothesis H_0: $\mu_A = \mu_B$ is rejected and the difference in the means is considered statistically significant at that level. The confidence level $X\%$, which equals 1-α, measures the probability that the null hypothesis H_0: $\mu_A = \mu_B$ is accepted when it is true.

In this report, levels of significance are compared based on the results at week 96 of the SE and CB tests, and at week 15 of the rapid macrocell test. The t-test is performed at four different levels of significance, 0.20, 0.10, 0.05, and 0.02,

respectively. The results for the Student's t-test are shown in Tables C.16 through C.29 in Appendix C. These tables include the specimen types that are compared, the value of t_{stat}, and the values of t_{crit} for each level of significance. The values of t_{crit} were calculated in a Microsoft Excel spreadsheet. In the tables, a "Y" next to the t_{crit} value indicates that the difference in the means is statistically significant. The higher the level of significance, the higher the probability that the difference in the means is statistically significant.

6.2 LINEAR REGRESSION

A linear regression is used to determine a relationship between two variables. The most common form of linear regression is least squares fitting. Given a set of data (x_i, y_i) with n data points, the relationship can be described by a straight line, $y = ax + b$, where the slope a, the intercept with the y-axis b, and the linear correlation coefficient r can be determined as follows:

$$a = \frac{n\sum x_i y_i - \sum x_i \sum y_i}{n\sum (x_i)^2 - (\sum x_i)^2} \qquad b = \frac{\sum y_i - a\sum x_i}{n} \tag{6.4}$$

$$r = \frac{n\sum x_i y_i - \sum x_i \sum y_i}{\sqrt{\left[n\sum (x_i)^2 - (\sum x_i)^2\right]\left[n\sum (y_i)^2 - (\sum y_i)^2\right]}}. \tag{6.5}$$

The correlation coefficient r determines the strength and direction of the linear relationship between the two variables. A value of +1 or –1 indicates that there is a perfect linear relationship. A value close to zero means that there is no linear correlation between the two variables, and the distributions can be thought of as being independent of each other. A coefficient r greater than 0.8 generally indicates a strong correlation, whereas a r less than 0.5 generally indicates a weak correlation between variables. When the sample size is small, however, values of $|r| > 0.8$ may be obtained

when x and y are totally uncorrelated. Table 6.1 shows the probability of obtaining a value for $|r|$ when the data are uncorrelated (Kirkup 2002). If the probability of obtaining a given value of $|r|$ when the x-y data are uncorrelated is less than 0.05, then the correlation coefficient is considered significant.

Table 6.1 – Probabilities of obtaining calculated r values when the x-y data are uncorrelated

Number of data points *n*	**Correlation coefficient *r* calculated from *x* -*y* data**						
	0.50	**0.60**	**0.70**	**0.80**	**0.90**	**0.95**	**1.00**
3	0.667	0.590	0.506	0.410	0.287	0.202	0.000
4	0.500	0.400	0.300	0.200	0.100	0.050	0.000
5	0.391	0.285	0.188	0.105	0.037	0.013	0.000
6	0.313	0.208	0.122	0.056	0.014	0.004	0.000
7	0.253	0.154	0.080	0.031	0.006	0.001	0.000
8	0.207	0.116	0.053	0.017	0.002	<0.001	0.000
9	0.170	0.088	0.036	0.010	0.001	<0.001	0.000
≥10	0.141	0.067	0.024	0.005	<0.001	<0.001	0.000

The coefficient of determination, r^2 ($0 < r^2 < 1$), measures the strength of a linear relationship by representing the percent of the data that is the closest to the line of best fit. For example, if $r = 0.90$, then $r^2 = 0.81$, which means that 81% of the total variation in y can be explained by the linear relationship between x and y.

The residual Δy is defined as

$$\Delta y = y - \hat{y} \tag{6.6}$$

where y is the observed y-value, and $\hat{y}$ is the value calculated from the linear fitted model. The distribution of residuals is obtained by plotting residuals against the value of x, and it can be used to assess how well a linear model fits the data. If a linear model provides a good fit for the original data, the residual plot should show points scattered randomly within a horizontal band about the horizontal axis. An observable

pattern of the residual plot probably indicates that a better model is needed to describe the full range of the data.

If there are many large residuals, a different mathematical function to model the relationship may be appropriate. Data points that are outliers can be identified using residual plots. The standardized residual is defined as the residual divided by the error standard deviation σ_e, which is given by

$$\sigma_e = \sqrt{\frac{\sum (y_i - \hat{y}_i)^2}{n-2}} \tag{6.7}$$

where $\hat{y}$ is the value calculated from the linear fitted model, and n is the sample size. If the standardized residual is greater in absolute value than 3, a data point is considered to be a possible outlier (Hayter 1996).

6.3 CORRELATION BETWEEN TEST METHODS

This section presents the results of the comparisons between the rapid macrocell test and the Southern Exposure (SE) and cracked beam (CB) tests and between the SE and CB tests. Comparisons are made of the results at week 96 for the SE and CB tests and at week 15 for the rapid macrocell test. The corrosion rate and total corrosion loss results used for the comparisons are summarized in Tables C.6 through C.15 in Appendix C.

Three different types of specimens (bare bar, lollipop, and mortar-wrapped specimens) and two different NaCl concentrations in the anodic solution (1.6 m and 6.04 m) were used in the rapid macrocell test by Balma et al. (2005). The results of the SE and CB tests are compared with the results of the rapid macrocell test according to the types of specimens and NaCl concentrations used in the rapid macrocell test. As shown in Table 6.2, there are five comparisons between the rapid macrocell test and the SE or CB test. For each comparison, Table 6.2 lists the *w/c*

ratio used for the mortar or concrete in each test method, specimen types in the rapid macrocell test, the types of steel, and the number of reinforcing steels used for the comparisons.

Table 6.2 – Comparisons between the rapid macrocell test and the SE and CB tests

Comparison	SE or CB test	Rapid macrocell test	Types of steel	Number of reinforcing steels
1	*w/c* = 0.45	bare bar (1.6 m NaCl)	conventional, MMFX, microalloyed, and duplex steels	13
2	*w/c* = 0.45	bare bar (6.04 m NaCl)	conventional and duplex steels	7
3	*w/c* = 0.45, 0.35	lollipop (1.6 m NaCl) *w/c* = 0.45, 0.35	conventional steel with/without DCI or Rheocrete 222+	6
4	*w/c* = 0.45	mortar-wrapped (1.6 m NaCl) *w/c* = 0.50	conventional, MMFX, ECR, and duplex steels	11 (9)*

* First value is the number of steels used to compare the rapid macrocell test and the SE test. Second value, in parentheses, is the number of steels used to compare the rapid macrocell test and the CB test.

A linear regression is performed to determine if a linear relationship exists between the results (corrosion rates or total corrosion losses) of two different test methods. Analyses of correlation coefficient, coefficient of determination, and residual plots are used to evaluate the goodness of fit. Error bars for each data point are included to show the scatter of the test results. The magnitude of the error bars is +/- one standard deviation.

Residual plots are shown in Figures D.1 to D.9 in Appendix D, in which Δy is the residual, $\Delta y / \sigma_e$ is the standard residual, and x is the variable representing either corrosion rate or total corrosion loss. All of the plots show that the data points are scattered randomly within a horizontal band about the horizontal axis, with no observable patterns, indicating that linear regression lines are appropriate.

6.3.1 Rapid Macrocell Test Versus Southern Exposure Test

6.3.1.1 SE Test versus Rapid Macrocell Test with Bare Bar Specimens in 1.6 m ion NaCl

The SE test is compared with the rapid macrocell test with bare bar specimens in 1.6 m ion NaCl and simulated concrete pore solution. Concrete with a *w/c* ratio of 0.45 was used in the SE test, and a total of 13 test series were evaluated, including conventional, Thermex-treated, MMFX microcomposite, microalloyed, and duplex steels. Comparisons of corrosion rates and total corrosion losses are shown in Figures 6.1(a) and 6.1(b), respectively. Figure 6.1(a) shows that the correlation coefficient r is 0.64 for corrosion rates, indicating a significant correlation between the two test methods based on the criteria in Table 6.1. The coefficient of determination r^2, however, is only 0.41, which means that only 41% of the total variation in the SE test results can be explained by the linear relationship between the two test methods. For total corrosion losses, values of 0.86 and 0.75 are obtained for the correlation coefficient r and coefficient of determination r^2, respectively, as shown in Figure 6.1(b). These results show that there is a good linear relationship between the two test methods. Comparisons at week 70 show better correlations than those at week 96, with $r = 0.74$ and $r^2 = 0.54$ for corrosion rates, and $r = 0.93$ and $r^2 = 0.86$ for total corrosion losses, respectively.

As discussed by Balma et al. (2005), a comparison based on total corrosion losses is more effective than one based on corrosion rate because total corrosion losses take into consideration the corrosion rates throughout the test period and the corrosion rates usually vary from week to week.

6.3.1.2 SE Test versus Rapid Macrocell Test with Bare Bar Specimens in 6.04 m ion NaCl

The SE test is compared with the rapid macrocell test with bare bar specimens in 6.04 m ion NaCl and simulated concrete pore solution, and the results are shown in Figure 6.2. The comparisons are based on test results for seven series with conventional and duplex steels. In the SE test, all of the steels were evaluated in concrete with a *w/c* ratio of 0.45. The correlation coefficients *r* are 0.93 and 0.95 for corrosion rates and total corrosion losses, respectively, indicating that both correlations are significant based on Table 6.1. The coefficients of determination, 0.86 and 0.91 for corrosion rates and total corrosion losses, respectively, indicate that there is a strong linear relationship between the two test methods. The comparisons performed by Balma et al. (2005) at week 70 show similar correlations to those at week 96, with $r = 0.93$ and $r^2 = 0.86$ for corrosion rates, and $r = 0.95$ and $r^2 = 0.90$ for total corrosion losses, respectively.

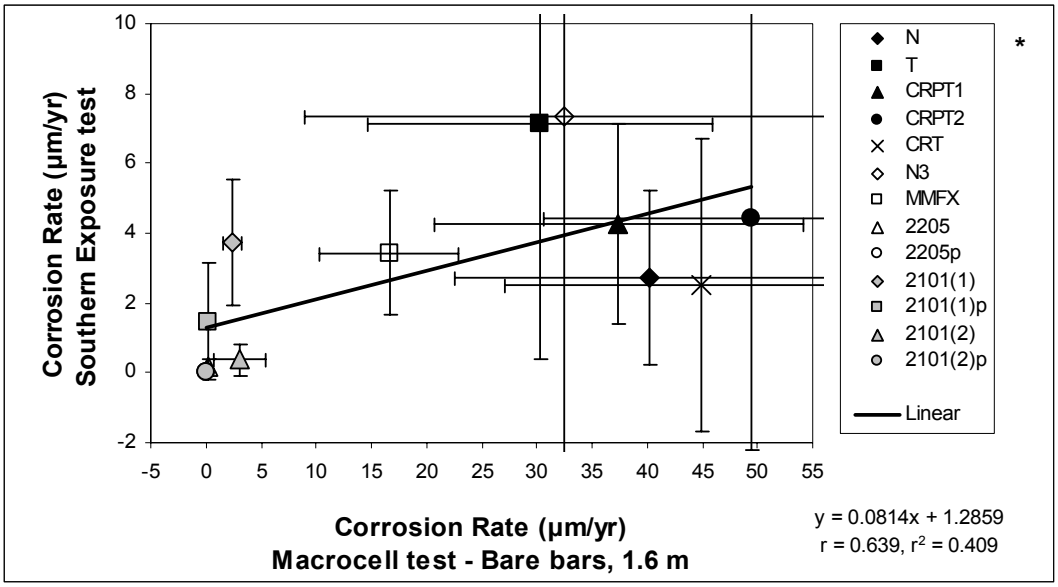

(a)

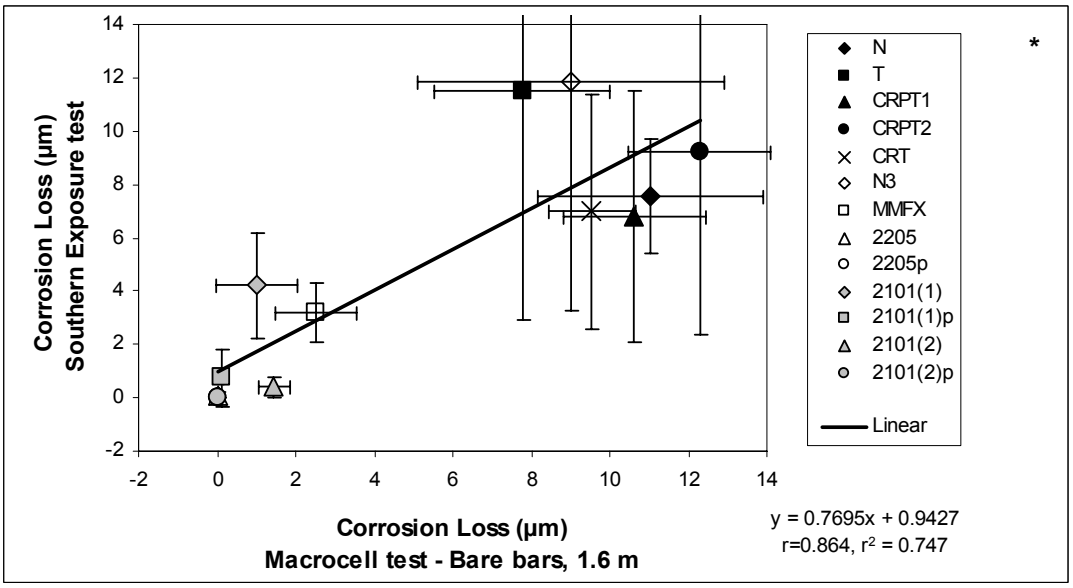

(b)

*** Steel type** → N and N3: conventional, normalized steel, T: Thermex-treated conventional steel, CRPT1: Thermex-treated microalloyed steel with a high phosphorus content (0.117%), CRPT2: Thermex-treated microalloyed steel with a high phosphorus content (0.100%), CRT: Thermex treated microalloyed steel with normal phosphorus content (0.017%), 2101(1) and 2101(2): duplex stainless steel (21% chromium, 1% nickel), 2205: duplex stainless steel (22% chromium, 5% nickel), p: pickled.

Figure 6.1 – (a) Corrosion rates and (b) total corrosion losses, Southern Exposure test (week 96) versus macrocell test with bare bars in 1.6 m ion NaCl and simulated concrete pore solution (week 15).

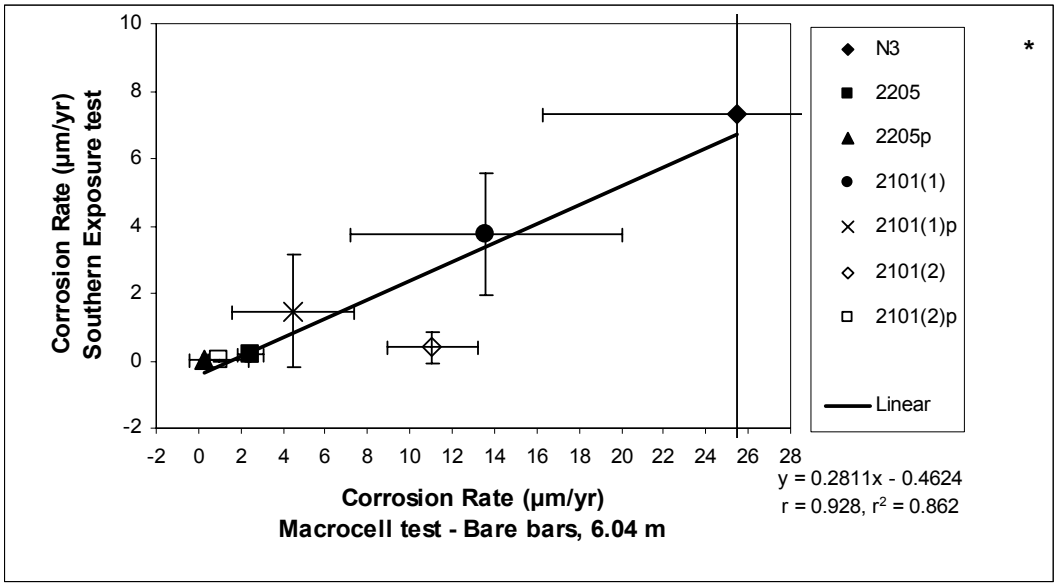

(a)

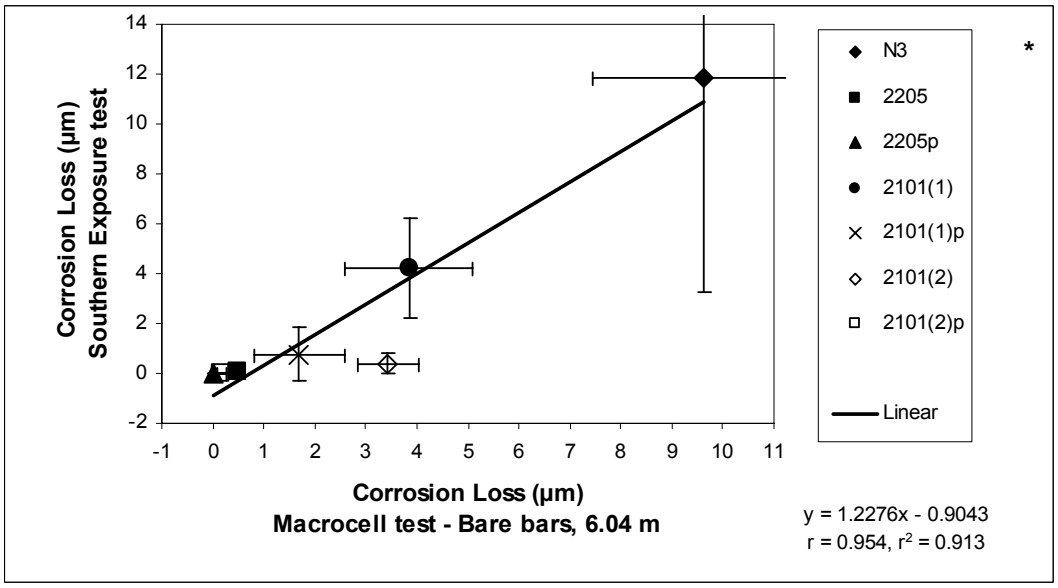

(b)

*** Steel type** → N3: conventional, normalized steel, 2101(1) and 2101(2): duplex stainless steel (21% chromium, 1% nickel), 2205: duplex stainless steel (22% chromium, 5% nickel), p: pickled.

Figure 6.2 – (a) Corrosion rates and (b) total corrosion losses, Southern Exposure test (week 96) versus macrocell test with bare bars in 6.04 m ion NaCl and simulated concrete pore solution (week 15).

6.3.1.3 SE Test versus Rapid Macrocell Test with Lollipop Specimens in 1.6 m ion NaCl

Figure 6.3 compares the results for the SE test and the rapid macrocell test with lollipop specimens in 1.6 m ion NaCl and simulated concrete pore solution. The comparisons are based on test results of six series with conventional steel, evaluated at *w/c* ratios of 0.45 and 0.35, with and without a corrosion inhibitor, DCI-S or Rheocrete 222+. The correlation coefficients *r* are 0.99 and 0.92 for corrosion rates and total corrosion losses, respectively, indicating that there is significant correlation between the two test methods. The coefficients of determination, 0.97 and 0.84 for corrosion rates and total corrosion losses, respectively, indicate that there is a strong linear relationship between the two test methods. The comparisons at week 70 show slightly weaker correlations than those at week 96, with $r = 0.98$ and $r^2 = 0.97$ for corrosion rates, and $r = 0.90$ and $r^2 = 0.80$ for total corrosion losses, respectively.

As shown in Figure 6.3, the conventional steel with a *w/c* ratio of 0.45 and no inhibitor exhibited much higher corrosion rates and total corrosion losses than the remaining reinforcing steels, and as a result it has a significant impact on the correlations.

6.3.1.4 SE Test versus Rapid Macrocell Test with Mortar-Wrapped Specimens in 1.6 m ion NaCl

Comparisons between the SE test and the rapid macrocell test with mortar-wrapped specimens in 1.6 m ion NaCl and simulated concrete pore solution are shown in Figure 6.4. The comparisons are based on test results of 11 series with conventional steel, MMFX microcomposite steel, combinations of conventional and MMFX steels, duplex steels, and epoxy-coated steel. The *w/c* ratios used in the SE

test and the rapid macrocell test with mortar-wrapped specimens are 0.45 and 0.50, respectively. The correlation coefficients r are 0.81 and 0.97 for corrosion rates and total corrosion losses, respectively, indicating that there is significant correlation between the two test methods based on Table 6.1. The coefficient of determination for corrosion rates is 0.65, indicating that only 65% of the total variation in the SE test results can be explained by the linear relationship between the two test methods. For total corrosion losses (r^2 = 0.94), a very good linear relationship exists between the SE test and the rapid macrocell test with mortar-wrapped specimens. The comparisons at week 70 show a stronger correlation for corrosion rates than those at week 96, with r = 0.87 and r^2 = 0.76, and approximately the same level of correlation for total corrosion losses, with r = 0.97 and r^2 = 0.95.

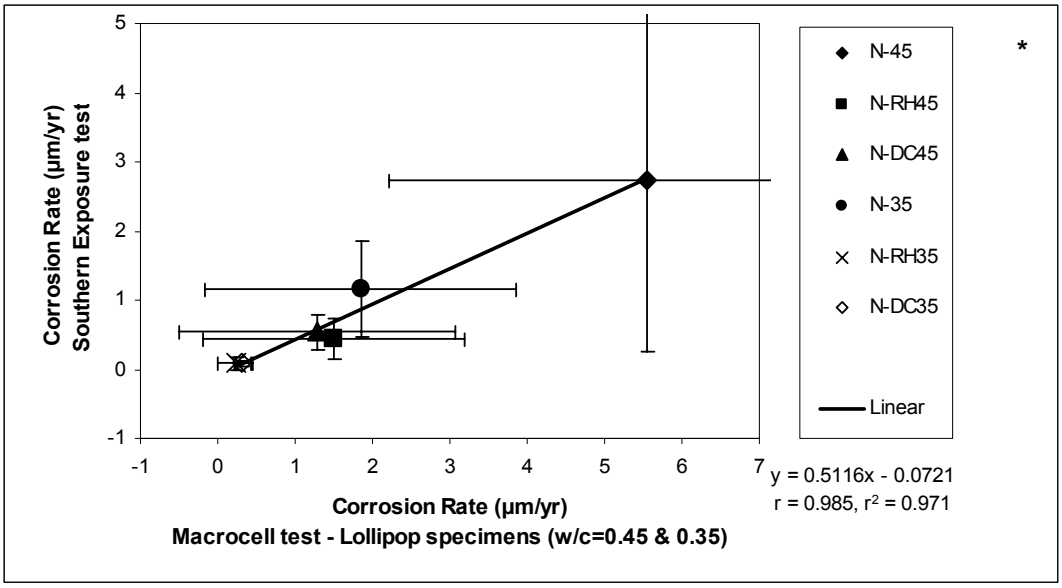

(a)

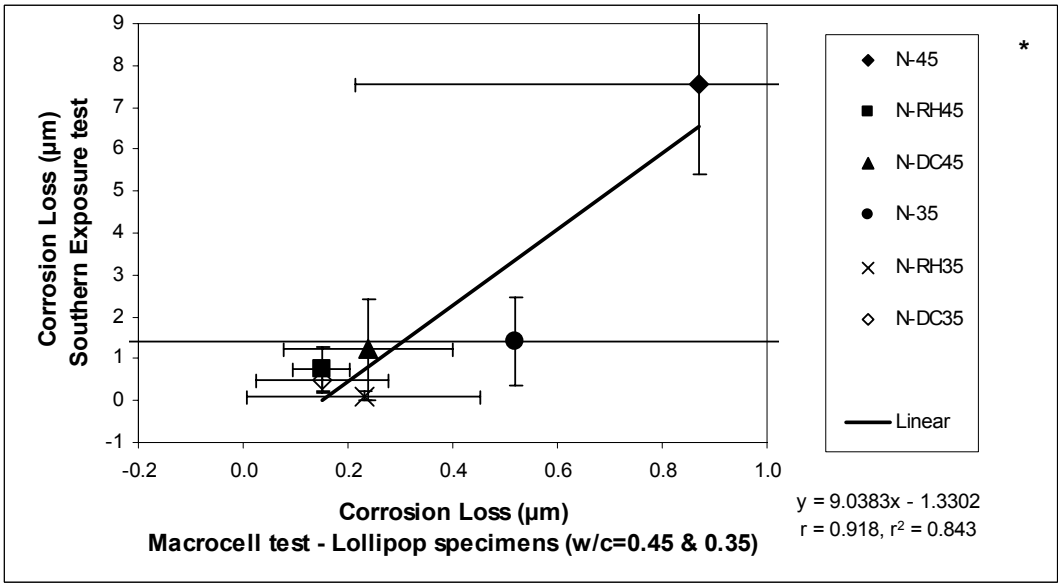

(b)

* A-B
A: steel type → N: conventional, normalized steel.
B: mix design → 45: *w/c* ratio of 0.45 and no inhibitor, RH45: *w/c* ratio of 0.45 and Rheocrete 222+, DC45: *w/c* ratio of 0.45 and DCI-S, 35: *w/c* ratio of 0.35 and no inhibitor, RH35: *w/c* ratio of 0.35 and Rheocrete 222+, DC35: *w/c* ratio of 0.35 and DCI-S.

Figure 6.3 – (a) Corrosion rates and (b) total corrosion losses, Southern Exposure test (week 96) versus macrocell test with lollipop specimens in 1.6 m ion NaCl and simulated concrete pore solution (week 15).

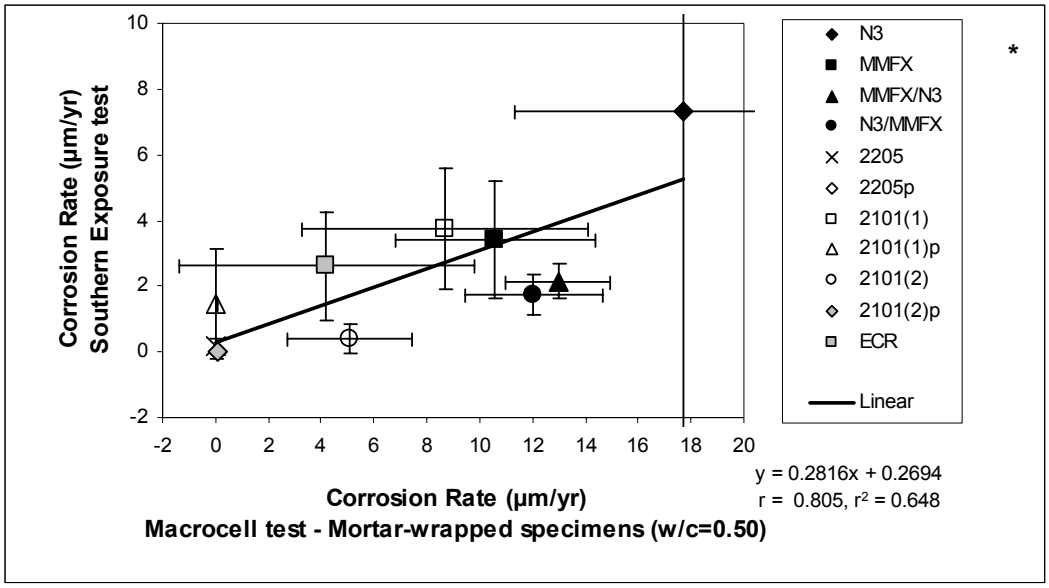

(a)

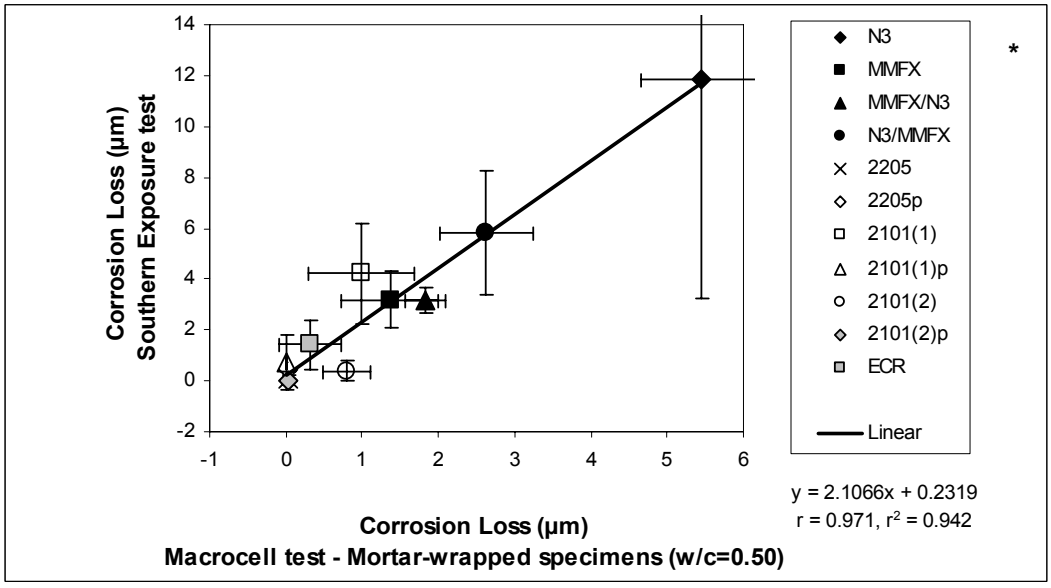

(b)

*** Steel type** → N3: conventional, normalized steel, MMFX: MMFX microcomposite steel, MMFX/N3: MMFX steel in the top mat and N3 steel in the bottom mat, N3/MMFX: N3 steel in the top mat and MMFX steel in the bottom mat, 2101(1) and 2101(2): duplex stainless steel (21% chromium, 1% nickel), 2205: duplex stainless steel (22% chromium, 5% nickel), ECR: epoxy-coated steel, p: pickled.

Figure 6.4 – (a) Corrosion rates and (b) total corrosion losses, Southern Exposure test (week 96) versus macrocell test with mortar-wrapped specimens in 1.6 m ion NaCl and simulated concrete pore solution.

6.3.1.5 Summary

Table 6.3 shows the coefficients of determination for the correlations between the macrocell test and the SE test at weeks 70 and 96. For corrosion rates, all of the correlations exhibit coefficients of determination at week 70 that are equal to or higher than those at week 96, as shown in Table 6.3. For total corrosion losses, the comparisons at week 70 show correlations similar to those at week 96, except for the comparisons between the SE test and rapid macrocell test with bare bar specimens in 1.6 m ion NaCl.

Table 6.3 – Coefficients of determination between the rapid macrocell test and the SE test at different ages

Comparison*	Steel	SE test at week 70+		SE test at week 96	
		Rate	Loss	Rate	Loss
1	conventional, MMFX, microalloyed, and duplex steels	0.54	0.86	0.41	0.75
2	conventional and duplex steels	0.86	0.90	0.86	0.91
3	conventional steel with/without DCI or Rheocrete 222+	0.97	0.80	0.97	0.84
4	conventional, MMFX, ECR, and duplex steels	0.76	0.95	0.65	0.94

* Comparison 1: SE test versus rapid macrocell test with bare bar specimens in 1.6 m ion NaCl
Comparison 2: SE test versus rapid macrocell test with bare bar specimens in 6.04 m ion NaCl
Comparison 3: SE test versus rapid macrocell test with lollipop specimens in 1.6 m ion NaCl
Comparison 4: SE test versus rapid macrocell test with mortar-wrapped specimens in 1.6 m ion NaCl

\+ Balma et al. (2005)

6.3.2 Rapid Macrocell Test Versus Cracked Beam Test

6.3.2.1 CB Test versus Rapid Macrocell Test with Bare Bar Specimens in 1.6 m ion NaCl

The CB test is compared with the rapid macrocell test with bare bar specimens in 1.6 m ion NaCl and simulated concrete pore solution. The correlations for corrosion rates and total corrosion losses are shown in Figures 6.5(a) and 6.5(b), respectively. Concrete with a *w/c* ratio of 0.45 was used for the CB test. The comparisons are based on test results for 13 series with conventional, thermex-treated,

MMFX, microalloyed, and duplex steels. As shown in Figure 6.5(a), the correlation coefficient r for corrosion rates is 0.48, indicating that the correlation between the two test methods is not significant. The coefficient of determination (r^2 = 0.23) indicates that there is not a linear relationship between the two test methods. The poor correlation at week 96 is not only because corrosion rates change from week to week, but also because some specimens in the CB test exhibit unusual behavior after week 70, as discussed by Balma et al. (2005). This behavior includes specimens [CRPT1, 2205, and 2201(1)p] with extremely high corrosion rates when compared to the other specimens in the same set and specimens (conventional and MMFX steels) that showed significant drops in corrosion rates as the result of more negative corrosion potentials in the bottom mat, indicating that chlorides had reached the bottom mat. As shown in Figure 6.5(b), values of 0.93 and 0.86 are obtained for the correlation coefficient r and coefficient of determination r^2, respectively, for total corrosion losses. These results show that the correlation for total corrosion losses is significant and there is a good linear relationship between the two test methods. The corrosion rates show a better correlation at week 70 than that at week 96, with r = 0.82 and r^2 = 0.67. The total corrosion losses show a correlation at week 70 similar to that at week 96, with r = 0.91 and r^2 = 0.84.

6.3.2.2 CB Test versus Rapid Macrocell Test with Bare Bar Specimens in 6.04 m ion NaCl

The CB test is compared with the rapid macrocell test with bare bar specimens in 6.04 m ion NaCl and simulated concrete pore solution, and the results are shown in Figure 6.6. The comparisons are based on test results for seven series with conventional and duplex steels. For corrosion rates, the correlation coefficient r and coefficient of determination r^2 are 0.45 and 0.20, respectively, indicating that a linear

relationship does not exist between the two test methods. As shown in Figure 6.6(b), however, the correlation coefficient (r = 0.96) and coefficient of determination (r^2 = 0.92) for total corrosion losses indicate that a very good linear relationship exists between the two test methods. The corrosion rates show a much stronger correlation at week 70 than that at week 96, with r = 0.87 and r^2 = 0.76. The total corrosion losses show a slightly weaker correlation at week 70 than that at week 96, with r = 0.95 and r^2 = 0.91.

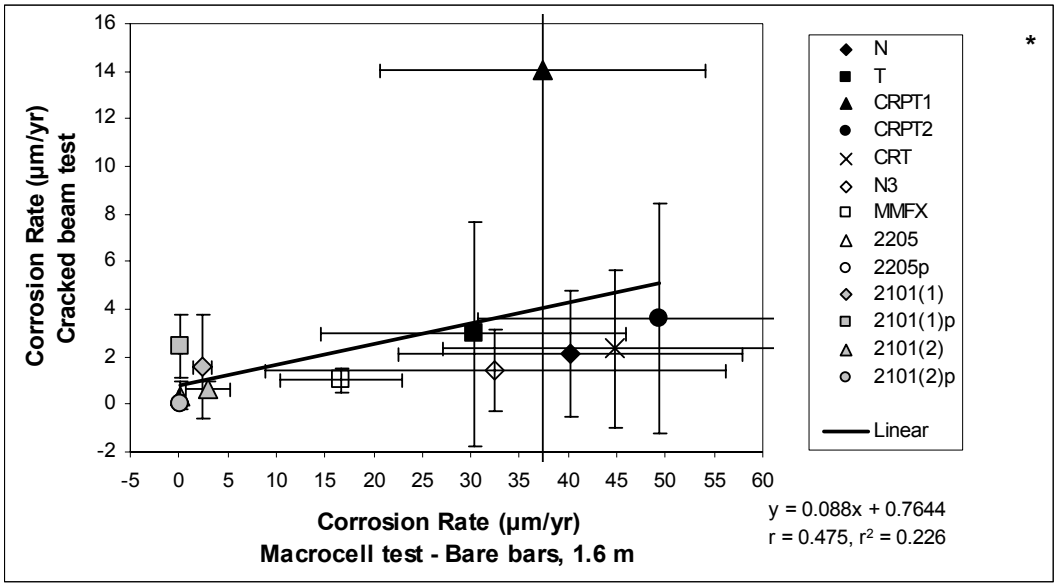

(a)

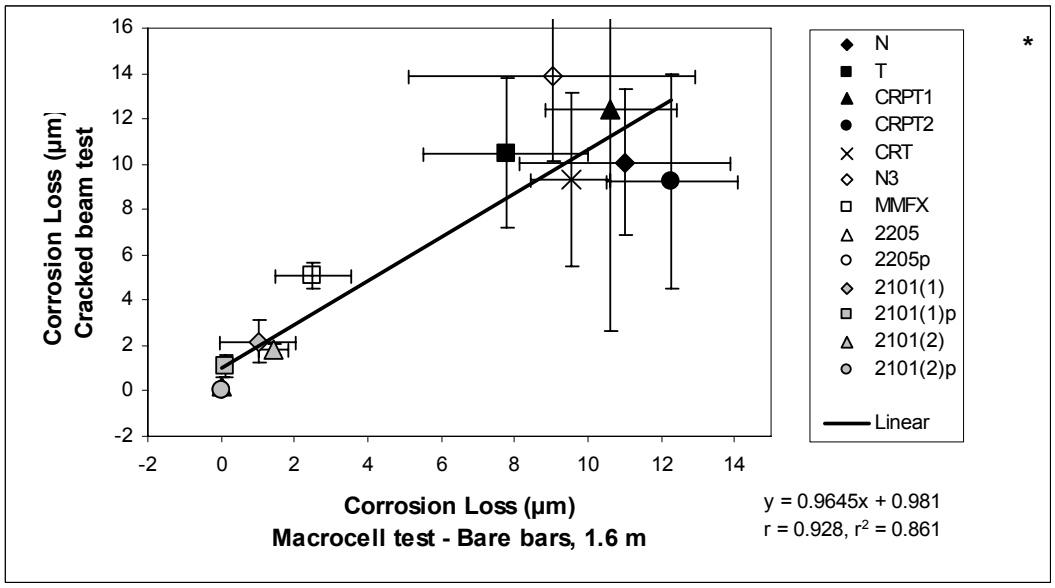

(b)

*** Steel type** → N and N3: conventional, normalized steel, T: Thermex-treated conventional steel, CRPT1: Thermex-treated microalloyed steel with a high phosphorus content (0.117%), CRPT2: Thermex-treated microalloyed steel with a high phosphorus content (0.100%), CRT: Thermex treated microalloyed steel with normal phosphorus content (0.017%), 2101(1) and 2101(2): duplex stainless steel (21% chromium, 1% nickel), 2205: duplex stainless steel (22% chromium, 5% nickel), p: pickled.

Figure 6.5 – (a) Corrosion rates and (b) total corrosion losses, cracked beam test (week 96) versus macrocell test with bare bars in 1.6 m ion NaCl and simulated concrete pore solution (week 15).

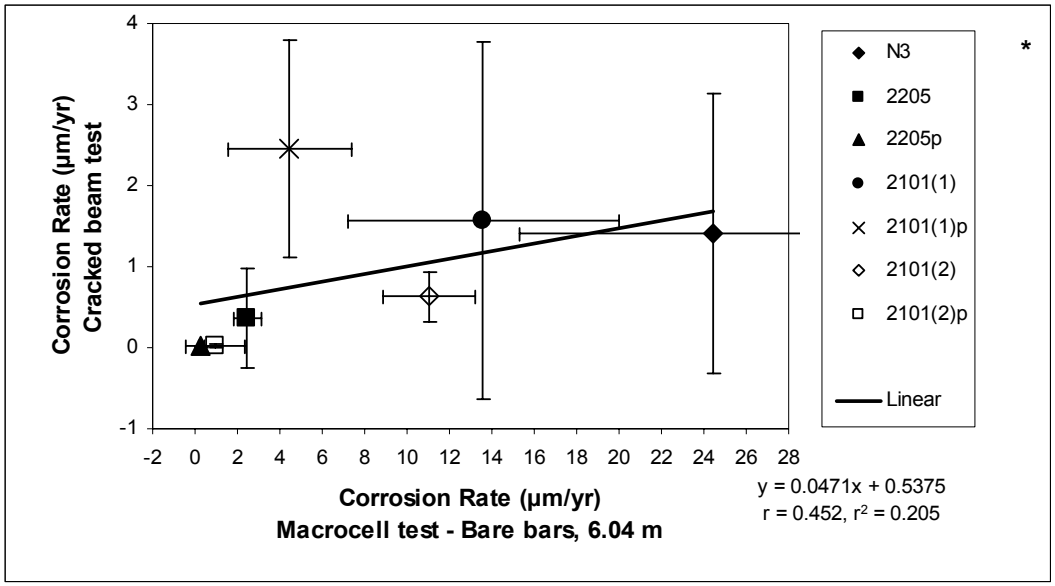

(a)

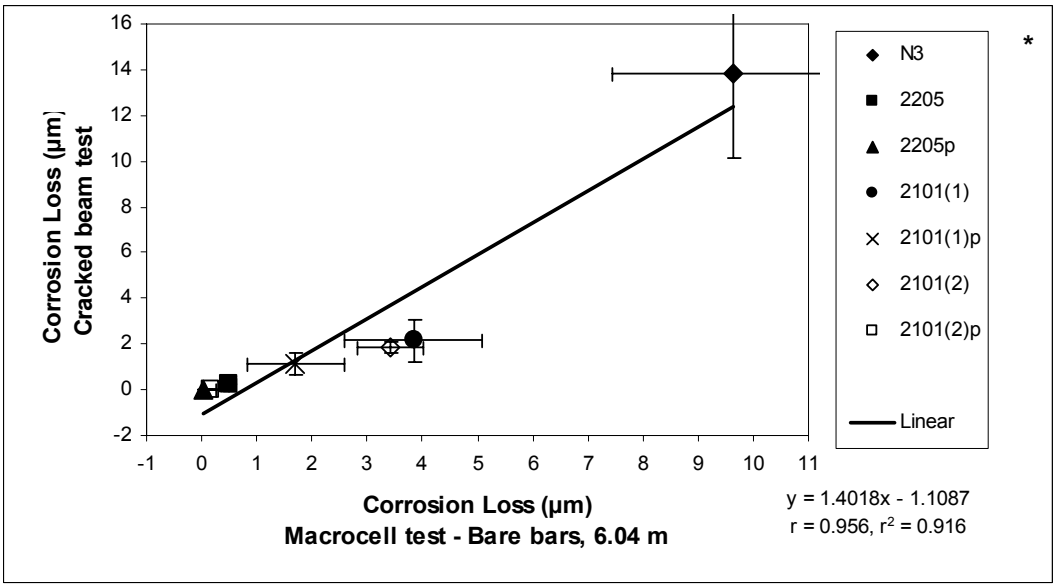

(b)

*** Steel type** → N3: conventional, normalized steel, 2101(1) and 2101(2): duplex stainless steel (21% chromium, 1% nickel), 2205: duplex stainless steel (22% chromium, 5% nickel), p: pickled.

Figure 6.6 – (a) Corrosion rates and (b) total corrosion losses, cracked beam test (week 96) versus macrocell test with bare bars in 6.04 m ion NaCl and simulated concrete pore solution (week 15).

6.3.2.3 CB Test versus Rapid Macrocell Test with Lollipop Specimens in 1.6 m ion NaCl

A comparison is made between the CB test and the rapid macrocell test with lollipop specimens in 1.6 m ion NaCl and simulated concrete pore solution. The comparisons are based on test results for six series with conventional steel, evaluated at *w/c* ratios of 0.45 and 0.35, with and without a corrosion inhibitor, DCI-S or Rheocrete 222+. In the CB test, the presence of cracks provides a direct path for chlorides to reach the reinforcing steel in concrete, causing corrosion to occur very rapidly. For this reason, as discussed by Balma et al. (2005), corrosion in the CB test is not sensitive to changes in concrete properties. As expected, a linear relationship does not exist between the two test methods. The coefficients of determination are 0.07 and 0.03 for corrosion rates and total corrosion losses, respectively, compared to the values of 0.04 and 0.01 for the correlations based on the results of the CB test at week 70.

6.3.2.4 CB Test versus Rapid Macrocell Test with Mortar-Wrapped Specimens in 1.6 m ion NaCl

Figure 6.7 shows the correlation between the CB test and the rapid macrocell test with mortar-wrapped specimens in 1.6 m ion NaCl and simulated concrete pore solution. The comparisons are based on test results for nine series with different types of steel, including conventional steel, MMFX microcomposite steel, combinations of conventional and MMFX steels, duplex steels, and epoxy-coated steel. The *w/c* ratios used in the CB test and the rapid macrocell test with mortar-wrapped specimens were 0.45 and 0.50, respectively. As shown in Figure 6.7(a), a linear relationship does not exist for corrosion rates obtained with the two test methods (r = 0.17 and r^2 = 0.03),

while it clearly does exist for total corrosion losses (r = 0.97 and r^2 = 0.95). The comparisons at week 70 show a far better correlation than at week 96 for corrosion rates, with r = 0.88 and r^2 = 0.77, and a slightly better correlation for total corrosion losses, with r = 0.98 and r^2 = 0.97, respectively.

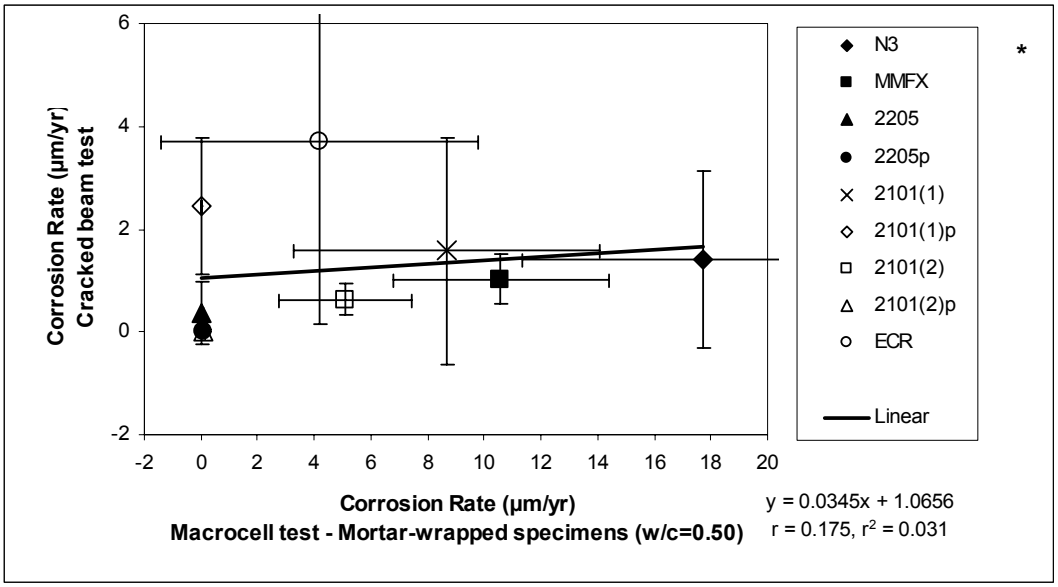

(a)

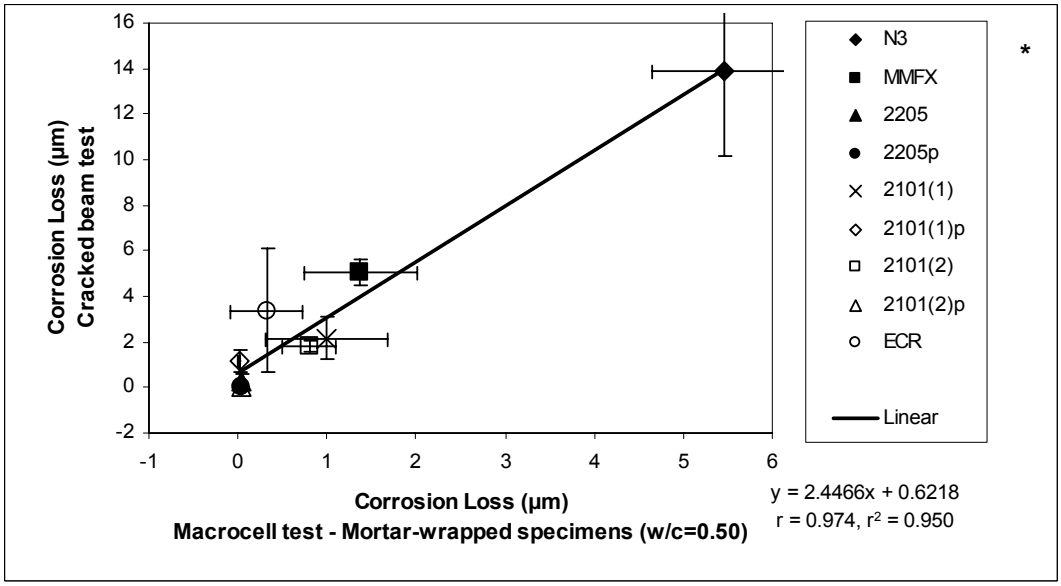

(b)

*** Steel type** → N3: conventional, normalized steel, MMFX: MMFX microcomposite steel, 2101(1) and 2101(2): duplex stainless steel (21% chromium, 1% nickel), 2205: duplex stainless steel (22% chromium, 5% nickel), ECR: epoxy-coated steel, p: pickled.

Figure 6.7 – (a) Corrosion rates and (b) total corrosion losses, cracked beam test (week 96) versus macrocell test with mortar-wrapped specimens in 1.6 m ion NaCl and simulated concrete pore solution (week 15).

6.3.2.5 Summary

Table 6.4 shows the coefficients of determination for the correlations between the macrocell test and the CB test at weeks 70 and 96. For corrosion rates, all of the correlations exhibit higher coefficients of determination at week 70 than at week 96, as shown in Table 6.4. For total corrosion losses, comparisons at week 96 show correlations similar to those at week 70.

Table 6.4 – Coefficients of determination between the rapid macrocell test and the CB test at different ages

Comparison	Steel	CB test at week 70[+]		CB test at week 96	
		Rate	Loss	Rate	Loss
1	conventional, MMFX, microalloyed, and duplex steels	0.67	0.84	0.23	0.86
2	conventional and duplex steels	0.76	0.91	0.20	0.96
3	conventional steel with/without DCI or Rheocrete 222+	0.04	0.01	0.07	0.03
4	conventional, MMFX, ECR, and duplex steels	0.77	0.97	0.03	0.95

[*] Comparison 1: CB test versus rapid macrocell test with bare bar specimens in 1.6 m ion NaCl
Comparison 2: CB test versus rapid macrocell test with bare bar specimens in 6.04 m ion NaCl
Comparison 3: CB test versus rapid macrocell test with lollipop specimens in 1.6 m ion NaCl
Comparison 4: CB test versus rapid macrocell test with mortar-wrapped specimens in 1.6 m ion NaCl

[+] Balma et al. (2005)

6.3.3 Southern Exposure Test Versus Cracked Beam Test

The SE test is compared with the CB test at week 96 and the results are shown in Figure 6.8. The comparisons are based on test results for 14 test series for different reinforcing steels, including conventional, Thermex-treated, microalloyed, MMFX microcomposite, duplex, and epoxy-coated steels. A *w/c* ratio of 0.45 was used for test specimens in both tests. As shown in Figure 6.8(a), a linear relationship between the two test methods does not exist for corrosion rates (r = 0.34 and r^2 = 0.12). For total corrosion losses, however, the correlation coefficient r = 0.93 and coefficient of determination r^2 = 0.87 indicate that the correlation is significant and a good linear relationship exists between the two test methods. The comparisons at week 70 by

Balma et al. (2005) show better correlations than those at week 96, with $r = 0.83$ and $r^2 = 0.69$ for corrosion rates, and $r = 0.96$ and $r^2 = 0.91$ for total corrosion losses, respectively.

A linear relationship cannot be obtained between the SE and CB tests at week 96 for specimens with conventional steel at *w/c* ratios of 0.45 and 0.35, with and without corrosion inhibitor DCI-S or Rheocrete 222+. As explained before, corrosion in the CB test is not sensitive to changes in concrete properties.

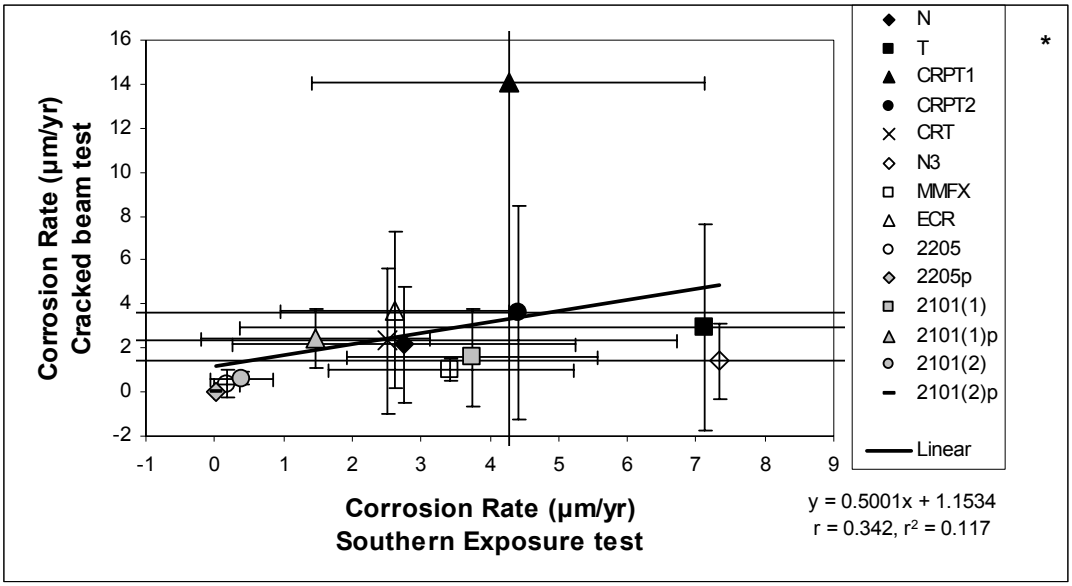

(a)

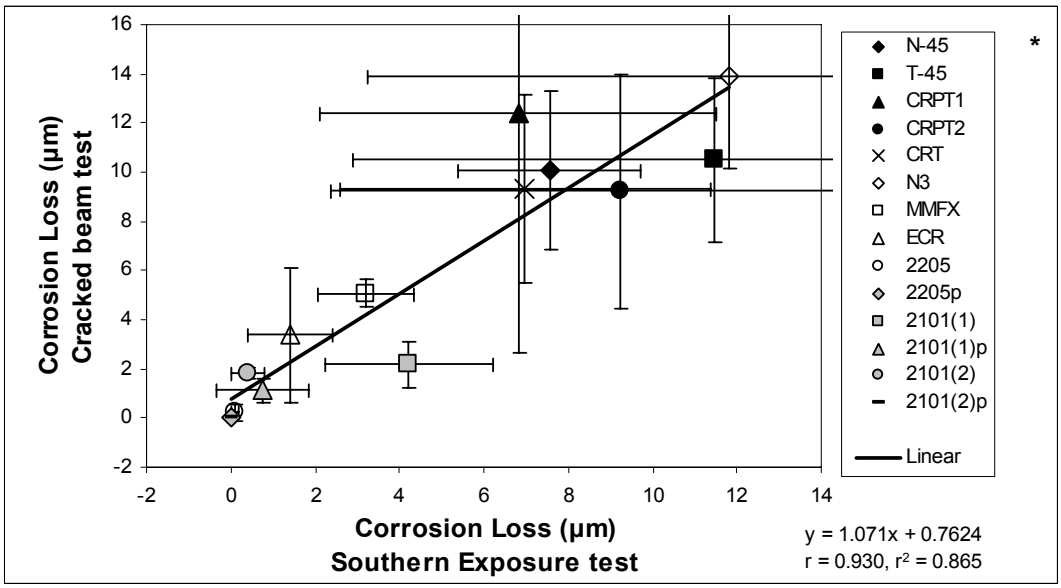

(b)

*** Steel type** → N and N3: conventional, normalized steel, T: Thermex-treated conventional steel, CRPT1: Thermex-treated microalloyed steel with a high phosphorus content (0.117%), CRPT2: Thermex-treated microalloyed steel with a high phosphorus content (0.100%), CRT: Thermex treated microalloyed steel with normal phosphorus content (0.017%), MMFX, MMFX microcomposite steel, ECR: epoxy-coated steel, 2101(1) and 2101(2): duplex stainless steel (21% chromium, 1% nickel), 2205: duplex stainless steel (22% chromium, 5% nickel), p: pickled.

Figure 6.8 – (a) Corrosion rates and (b) total corrosion losses, cracked beam test (week 96) versus Southern Exposure test (week 96) for specimens with different reinforcing steels.

6.4 COEFFICIENTS OF VARIATION

The coefficient of variation (*CV*) is defined as the sample standard deviation *s* divided by the sample average $\bar{x}$

$$CV = \frac{s}{\bar{x}}. \tag{6.8}$$

The coefficient of variation is a statistical measure of variability within a test. The lower the coefficient of variation, the lower the variability or the better the reliability.

Coefficients of variation are calculated for corrosion rates and total corrosion losses for the bench-scale tests at week 96 and for the rapid macrocell test at week 15. The individual, average, and standard deviation of the test results are summarized in Tables C.6 through C.10 for corrosion rates and Tables C.11 through C.15 for total corrosion losses, respectively, in Appendix C.

The coefficients of variation of corrosion rates and total corrosion losses for both the bench-scale and rapid macrocell tests are presented in Tables 6.5 through 6.9, which cover tests of corrosion inhibitors and different *w*/*c* ratios, conventional and microalloyed steels, MMFX microcomposite steels, ECR, and duplex stainless steels, respectively. Out of the 125 sets of test results, 84 (67% of the comparisons) exhibit a lower coefficient of variation for total corrosion losses than for the corresponding corrosion rates. This agrees with the conclusion by Balma et al. (2005) based on the results at week 70 for the bench-scale tests, in which 88 (70% of the comparisons) exhibit a lower coefficient of variation for total corrosion losses than for the corresponding corrosion rates. As discussed by Balma et al. (2005), higher variations in corrosion rates are expected due to the fact that corrosion rates usually vary from week to week due to the complexity of the corrosion process, while total corrosion losses increase gradually with time and the variations average out.

The coefficients of variation for the rapid macrocell test at week 15 are compared with those for the bench-scale tests at week 96 in Tables 6.10 through 6.16. The comparisons are made for the tests that showed a significant correlation (at least for total corrosion losses) in Section 6.2 – for example, the SE test and the rapid macrocell test with bare bar specimens in 1.6 m ion NaCl, shown in Figure 6.1. For corrosion rates, 50 out of 66 (76% of the comparisons) sets of tests exhibit a lower coefficient of variation in the rapid macrocell test than in the bench-scale tests. For total corrosion losses, the rapid macrocell test has a lower coefficient of variation than the corresponding bench-scale test in 42 sets of test results (64% of the comparisons). Based on the results at week 70 for the bench-scale tests (Balma et al. 2005), the rapid macrocell test has a lower coefficient of variation than the corresponding bench-scale test in 60% of the comparisons for corrosion rates and 52% of the comparisons for total corrosion losses. Overall, the comparisons show that the rapid macrocell test at week 15 has a lower variation than the bench-scale tests at week 96.

Table 6.5 – Comparison between coefficients of variation of corrosion rates and losses for specimens with corrosion inhibitors and different *w/c* ratios

Specimen designation*	Corrosion rate	Corrosion loss
"lollipop" Specimens in 1.6 m ion NaCl – 15 weeks		
M-N-45	0.60	0.76
M-N-RH45	1.13	0.37
M-N-DC45	1.39	0.69
M-N-35	1.09	1.55
M-N-RH35	0.98	0.98
M-N-DC-35	0.34	0.85
Southern Exposure test – 96 weeks		
SE-N-45	0.91	0.29
SE-N-RH45	0.69	0.72
SE-N-DC45	0.46	0.84
SE-N-35	0.59	0.76
SE-N-RH35	1.16	1.08
SE-N-DC35	0.47	0.55
SE-T-45	0.95	0.75
SE-T-RH45	0.87	0.77
SE-T-DC45	0.49	0.78
SE-T-35	1.73	0.34
SE-T-RH35	-	0.36
SE-T-DC35	0.92	0.84
Cracked beam test – 96 weeks		
CB-N-45	1.23	0.32
CB-N-RH45	0.95	0.22
CB-N-DC45	0.49	0.40
CB-N-35	0.46	0.13
CB-N-RH35	-	0.03
CB-N-DC35	1.07	0.43
CB-T-45	1.59	0.33
CB-T-RH45	0.95	0.35
CB-T-DC45	0.26	1.21
CB-T-35	0.36	0.20
CB-T-RH35	0.51	0.52
CB-T-DC35	0.41	0.16
ASTM G 109 test – 96 weeks		
G-N-45	1.52	0.71
G-N-RH45	1.36	0.36
G-N-DC45	0.58	0.80
G-N-35	0.12	0.39
G-N-RH35	0.25	0.15
G-N-DC35	0.57	0.55
G-T-45	1.19	1.36
G-T-RH45	1.45	0.49
G-T-DC45	1.67	0.80
G-T-35	1.00	0.96
G-T-RH35	-	0.71
G-T-DC35	-	0.66

* T - A - B

T: test → M: macrocell test, SE: Southern Exposure test, CB: cracked beam test, G: ASTM G 109 test

A: steel type → N: conventional, normalized steel, T: Thermex-treated conventional steel.

B: mix design → 45: *w/c* ratio of 0.45 and no inhibitor, RH45: *w/c* ratio of 0.45 and Rheocrete 222+, DC45: *w/c* ratio of 0.45 and DCI-S, 35: *w/c* ratio of 0.35 and no inhibitor, RH35: *w/c* ratio of 0.35 and Rheocrete 222+, DC35: *w/c* ratio of 0.35 and DCI-S.

Table 6.6 – Comparison between coefficients of variation of corrosion rates and losses for specimens with conventional normalized, conventional Thermex-treated, and microalloyed steels

Specimen designation*	Corrosion rate	Corrosion loss
Bare bars in 1.6 m ion NaCl – 15 weeks		
M-N	0.44	0.26
M-T	0.52	0.29
M-CRPT1	0.45	0.17
M-CRPT2	0.38	0.15
M-CRT	0.40	0.12
"Lollipop" specimens with caps in 1.6 m ion NaCl – 15 weeks		
M-Nc-50	0.60	0.56
M-Tc-50	0.44	0.63
M-CRPT1c-50	0.39	0.28
M-CRPT2c-50	0.32	0.34
M-CRTc-50	0.45	0.33
"Lollipop" specimens with caps in 1.6 m ion NaCl – 15 weeks		
M-N-50	0.46	0.40
M-T-50	0.43	0.50
M-CRPT1-50	0.65	0.61
M-CRPT2-50	0.47	0.49
M-CRT-50	0.50	0.55
Southern Exposure test – 96 weeks		
SE-N-45	0.91	0.29
SE-T-45	0.95	0.75
SE-CRPT1-45	0.67	0.69
SE-CRPT2-45	1.50	0.74
SE-CRT-45	1.67	0.63
SE-N/CRPT1-45	0.45	0.17
SE-CRPT1/N-45	0.52	0.33
Cracked beam test – 96 weeks		
CB-N-45	1.23	0.32
CB-T-45	1.59	0.33
CB-CRPT1-45	2.03	0.79
CB-CRPT2-45	1.34	0.51
CB-CRT-45	1.41	0.41
ASTM G 109 test – 96 weeks		
G-N-45	1.52	0.71
G-T-45	1.19	1.36
G-CRPT1-45	0.62	0.97
G-CRPT2-45	0.33	1.21
G-CRT-45	0.63	0.64

* T - A - B

T: test → M: macrocell test, SE: Southern Exposure test, CB: cracked beam test, G: ASTM G 109 test

A: steel type → N: conventional, normalized steel, T: Thermex-treated conventional steel, CRPT1: Thermex-treated microalloyed steel with a high phosphorus content (0.117%), CRPT2: Thermex-treated microalloyed steel with a high phosphorus content (0.100%), CRT: Thermex treated microalloyed steel with normal phosphorus content (0.017%), c: epoxy-filled caps on the end.

B: mix design → 50: *w/c* ratio of 0.50 and no inhibitor, 45: *w/c* ratio of 0.45 and no inhibitor.

Table 6.7 – Comparison between coefficients of variation of corrosion rates and losses for specimens with conventional and MMFX microcomposite steels

Specimen designation*	Corrosion rate	Corrosion loss
Bare bars in 1.6 m ion NaCl – 15 weeks		
M-N3	0.66	0.43
M-MMFX(1)	0.55	0.24
M-MMFX(2)	0.38	0.42
M-MMFXs	0.55	0.21
M-MMFXb	0.43	0.32
M-MMFX#19	0.21	0.35
Bare bars in 6.04 m ion NaCl – 15 weeks		
M-N3h	0.41	0.23
M-MMFXsh	0.23	0.32
Mortar-wrapped specimens in 1.6 m ion NaCl – 15 weeks		
M-N3-50	0.36	0.15
M-MMFX-50	0.36	0.46
M-MMFX/N3-50	0.15	0.14
M-N3/MMFX-50	0.21	0.23
Southern Exposure test – 96 weeks		
SE-N3-45	1.34	0.72
SE-MMFX-45	0.52	0.35
SE-MMFXb-45	0.57	0.25
SE-MMFX/N3-45	0.24	0.15
SE-N3/MMFX-45	0.35	0.41
Cracked beam test – 96 weeks		
CB-N3-45	2.45	0.55
CB-MMFX-45	0.96	0.22

* T - A - B

T: test → M: macrocell test, SE: Southern Exposure test, CB: cracked beam test

A: steel type → N, and N3: conventional, normalized steel, MMFX: MMFX microcomposite steel, s: sandblasted, b: bent bars in the anode or top mat, h: 6.04 m ion concentration.

B: mix design → 50: *w/c* ratio of 0.50 and no inhibitor, 45: *w/c* ratio of 0.45 and no inhibitor.

Table 6.8 – Comparison between coefficients of variation for corrosion rates and losses for specimens with conventional uncoated and epoxy-coated steel

Specimen designation*	Corrosion rate	Corrosion loss
Mortar-wrapped specimens in 1.6 m ion NaCl – 15 weeks		
M-N3-50	0.36	0.15
M-ECR-50	1.33	1.26
Southern Exposure test – 96 weeks		
SE-N3-45	1.34	0.72
SE-ECR-45	0.64	0.71
Cracked beam test – 96 weeks		
CB-N3-45	2.45	0.55
CB-ECR-45	0.96	0.81

* T - A - B
T: test → M: macrocell test, SE: Southern Exposure test, CB: cracked beam test
A: steel type → N3: conventional, normalized steel, ECR: epoxy-coated steel,
B: mix design → 50: *w/c* ratio of 0.50 and no inhibitor, 45: *w/c* ratio of 0.45 and no inhibitor.

Table 6.9 – Comparison between coefficients of variation for corrosion rates and losses for specimens with conventional and duplex stainless steels

Specimen designation*	Corrosion rate	Corrosion loss
Bare bars in 1.6 m ion NaCl – 15 weeks		
M-N3	0.66	0.43
M-2205	0.76	0.39
M-2205p	0.34	0.13
M-2101(1)	0.38	1.02
M-2101(1)p	1.05	0.71
M-2101(2)	0.75	0.28
M-2101(2)p	0.91	1.06
M-2101(2)s	2.00	1.05
Bare bars in 6.04 m ion NaCl – 15 weeks		
M-N3h	0.41	0.23
M-2205h	0.25	0.27
M-2205ph	0.45	0.49
M-2101(1)h	0.47	0.33
M-2101(1)ph	0.65	0.52
M-2101(2)h	0.19	0.18
M-2101(2)ph	1.47	0.59
M-2101(2)sh	0.92	0.89
Mortar-wrapped specimens in 1.6 m ion NaCl – 15 weeks		
M-N2-50	0.44	0.39
M-2205-50	0.89	0.26
M-2205p-50	1.14	0.38
M-2101(1)-50	0.62	0.70
M-2101(1)p-50	1.28	0.51
M-2101(2)-50	0.46	0.38
M-2101(2)p-50	0.68	0.28
Southern Exposure test – 96 weeks		
SE-N-45	0.91	0.29
SE-2205-45	1.47	1.33
SE-2205p-45	1.05	0.41
SE-2101(1)-45	0.49	0.47
SE-2101(1)p-45	1.14	1.44
SE-2101(2)-45	1.16	1.00
SE-2101(2)p-45	1.25	0.57
SE-N2/2205-45	0.63	0.31
SE-2205/N2-45	1.36	0.61
Cracked beam test – 96 weeks		
CB-N-45	1.23	0.32
CB-2205-45	1.66	1.41
CB-2205p-45	1.28	0.70
CB-2101(1)-45	1.40	0.42
CB-2101(1)p-45	0.55	0.43
CB-2101(2)-45	0.48	0.13
CB-2101(2)p-45	0.60	0.58

* T - A - B

T: test → M: macrocell test, SE: Southern Exposure test, CB: cracked beam test

A: steel type → N, N2, and N3: conventional, normalized steel, 2101(1) and 2101(2): duplex stainless steel (21% chromium, 1% nickel), 2205: duplex stainless steel (22% chromium, 5% nickel), p: pickled, s: sandblasted, h: 6.04 m ion concentration.

B: mix design → 50: *w/c* ratio of 0.50 and no inhibitor, 45: *w/c* ratio of 0.45 and no inhibitor.

Table 6.10 – Comparison between coefficients of variation for the macrocell test with bare bars in 1.6 m ion NaCl and simulated concrete pore solution and the Southern Exposure test

Steel type *	Corrosion rate		Corrosion loss	
	Macrocell – 15 weeks	SE – 96 weeks	Macrocell – 15 weeks	SE – 96 weeks
N	0.44	0.91	0.26	0.29
T	0.52	0.95	0.29	0.75
CRPT1	0.45	0.67	0.17	0.69
CRPT2	0.38	1.50	0.15	0.74
CRT	0.40	1.67	0.12	0.63
N3	0.66	1.34	0.43	0.72
MMFX	0.38	0.52	0.42	0.35
2205	0.76	1.47	0.39	1.33
2205p	0.34	1.05	0.13	0.41
2101(1)	0.38	0.49	1.02	0.47
2101(1)p	1.05	1.14	0.71	1.44
2101(2)	0.75	1.16	0.28	1.00
2101(2)p	0.91	1.25	1.06	0.57

*** Steel type** → N and N3: conventional, normalized steel, T: Thermex-treated conventional steel, CRPT1: Thermex-treated microalloyed steel with a high phosphorus content (0.117%), CRPT2: Thermex-treated microalloyed steel with a high phosphorus content (0.100%), CRT: Thermex treated microalloyed steel with normal phosphorus content (0.017%), MMFX: MMFX microcomposite steel, 2101(1) and 2101(2): duplex stainless steel (21% chromium, 1% nickel), 2205: duplex stainless steel (22% chromium, 5% nickel), p: pickled.

Table 6.11 – Comparison between coefficients of variation for the macrocell test with bare bars in 6.04 m ion NaCl and simulated concrete pore solution and the Southern Exposure test

Steel type *	Corrosion rate		Corrosion loss	
	Macrocell – 15 weeks	SE – 96 weeks	Macrocell – 15 weeks	SE – 96 weeks
N3	0.41	1.34	0.23	0.72
2205	0.25	1.47	0.27	1.33
2205p	0.45	1.05	0.49	0.41
2101(1)	0.47	0.49	0.33	0.47
2101(1)p	0.65	1.14	0.52	1.44
2101(2)	0.19	1.16	0.18	1.00
2101(2)p	1.47	1.25	0.59	0.57

*** Steel type** → N3: conventional, normalized steel, 2101(1) and 2101(2): duplex stainless steel (21% chromium, 1% nickel), 2205: duplex stainless steel (22% chromium, 5% nickel), p: pickled.

Table 6.12 – Comparison between coefficients of variation for the macrocell test with lollipop specimens in 1.6 m ion NaCl and simulated concrete pore solution and the Southern Exposure test

Steel type - Mix design *	Corrosion rate		Corrosion loss	
	Macrocell – 15 weeks	SE – 96 weeks	Macrocell – 15 weeks	SE – 96 weeks
N-45	0.60	0.91	0.76	0.29
N-RH45	1.13	0.69	0.37	0.72
N-DC45	1.39	0.46	0.69	0.84
N-35	1.09	0.59	1.55	0.76
N-RH35	0.98	1.16	0.98	1.08
N-DC35	0.34	0.47	0.85	0.55

* A-B
A: steel type → N: conventional, normalized steel.
B: mix design → 45: *w/c* ratio of 0.45 and no inhibitor, RH45: *w/c* ratio of 0.45 and Rheocrete 222+, DC45: *w/c* ratio of 0.45 and DCI-S, 35: *w/c* ratio of 0.35 and no inhibitor, RH35: *w/c* ratio of 0.35 and Rheocrete 222+, DC35: *w/c* ratio of 0.35 and DCI-S.

Table 6.13 – Comparison between coefficients of variation for the macrocell test with mortar-wrapped specimens in 1.6 m ion NaCl and simulated concrete pore solution and the Southern Exposure test.

Steel type *	Corrosion rate		Corrosion loss	
	Macrocell – 15 weeks	SE – 96 weeks	Macrocell – 15 weeks	SE – 96 weeks
N3	0.36	1.34	0.15	0.72
MMFX	0.36	0.52	0.46	0.35
MMFX/N3	0.15	0.24	0.14	0.15
N3/MMFX	0.21	0.35	0.23	0.41
2205	0.89	1.47	0.26	1.33
2205p	1.14	1.05	0.38	0.41
2101(1)	0.62	0.49	0.70	0.47
2101(1)p	1.28	1.14	0.51	1.44
2101(2)	0.46	1.16	0.38	1.00
2101(2)p	0.68	1.25	0.28	0.57
ECR	1.33	0.64	1.26	0.71

*** Steel type** → N3: conventional, normalized steel, MMFX: MMFX microcomposite steel, MMFX/N3: MMFX steel in the top mat and N3 steel in the bottom mat, N3/MMFX: N3 steel in the top mat and MMFX steel in the bottom mat, 2101(1) and 2101(2): duplex stainless steel (21% chromium, 1% nickel), 2205: duplex stainless steel (22% chromium, 5% nickel), ECR: epoxy-coated steel, p: pickled.

Table 6.14 – Comparison between coefficients of variation for the macrocell test with bare bars in 1.6 m ion NaCl and simulated concrete pore solution and the cracked beam test

Steel type *	Corrosion rate		Corrosion loss	
	Macrocell – 15 weeks	CB – 96 weeks	Macrocell – 15 weeks	CB – 96 weeks
N	0.44	1.23	0.26	0.32
T	0.52	1.59	0.29	0.33
CRPT1	0.45	2.03	0.17	0.79
CRPT2	0.38	1.34	0.15	0.51
CRT	0.40	1.41	0.12	0.41
N3	0.66	2.45	0.43	0.55
MMFX	0.38	0.96	0.42	0.22
2205	0.76	1.66	0.39	1.41
2205p	0.34	1.28	0.13	0.70
2101(1)	0.38	1.40	1.02	0.42
2101(1)p	1.05	0.55	0.71	0.43
2101(2)	0.75	0.48	0.28	0.13
2101(2)p	0.91	0.60	1.06	0.58

*** Steel type** → N and N3: conventional, normalized steel, T: Thermex-treated conventional steel, CRPT1: Thermex-treated microalloyed steel with a high phosphorus content (0.117%), CRPT2: Thermex-treated microalloyed steel with a high phosphorus content (0.100%), CRT: Thermex treated microalloyed steel with normal phosphorus content (0.017%), MMFX: MMFX microcomposite steel, 2101(1) and 2101(2): duplex stainless steel (21% chromium, 1% nickel), 2205: duplex stainless steel (22% chromium, 5% nickel), p: pickled.

Table 6.15 – Comparison between coefficients of variation for the macrocell test with bare bars in 6.04 m ion NaCl and simulated concrete pore solution and the cracked beam test

Steel type *	Corrosion rate		Corrosion loss	
	Macrocell – 15 weeks	CB – 96 weeks	Macrocell – 15 weeks	CB – 96 weeks
N3	0.41	2.45	0.23	0.55
2205	0.25	1.66	0.27	1.41
2205p	0.45	1.28	0.49	0.70
2101(1)	0.47	1.40	0.33	0.42
2101(1)p	0.65	0.55	0.52	0.43
2101(2)	0.19	0.48	0.18	0.13
2101(2)p	1.47	0.60	0.59	0.58

*** Steel type** → N3: conventional, normalized steel, 2101(1) and 2101(2): duplex stainless steel (21% chromium, 1% nickel), 2205: duplex stainless steel (22% chromium, 5% nickel), p: pickled.

Table 6.16 – Comparison between coefficients of variation for the macrocell test with mortar-wrapped specimens in 1.6 m ion NaCl and simulated concrete pore solution and the cracked beam test

Steel type *	Corrosion rate		Corrosion loss	
	Macrocell – 15 weeks	CB – 96 weeks	Macrocell – 15 weeks	CB – 96 weeks
N3	0.36	2.45	0.15	0.55
MMFX	0.36	0.96	0.46	0.22
2205	0.89	1.66	0.26	1.41
2205p	1.14	1.28	0.38	0.70
2101(1)	0.62	1.40	0.70	0.42
2101(1)p	1.28	0.55	0.51	0.43
2101(2)	0.46	0.48	0.38	0.13
2101(2)p	0.68	0.60	0.28	0.58
ECR	1.33	0.96	1.26	0.81

*** Steel type** → N3: conventional, normalized steel, 2101(1) and 2101(2): duplex stainless steel (21% chromium, 1% nickel), 2205: duplex stainless steel (22% chromium, 5% nickel), p: pickled.

6.5 LEVELS OF SIGNIFICANCE

In this section, the levels of significance for differences in corrosion performance are compared for corrosion rate and total corrosion losses between the rapid macrocell test at week 15 and the bench-scale tests at week 96. Comparison of the level of significance between two methods can be used to determine which test method is more capable of identifying a difference between two corrosion protection systems. The results of the Student's t-test are presented in Tables C.16 through C.29 in Appendix C. The comparisons are summarized in Tables 6.17 through 6.20. Most of the comparisons in this section are based on different steels (Tables 6.17, 6.18, and 6.20), while the remaining are based on conventional steel specimens with different corrosion inhibitors cast in concrete with *w*/*c* ratios of 0.45 and 0.35 (Table 6.19). In addition, the ratios of corrosion rate and total corrosion losses between pairs of steel or pairs of corrosion protection systems are summarized in those tables for both the rapid macrocell and bench-scale tests.

Tables 6.17 through 6.20 cover 45 comparisons between the rapid macrocell

and SE tests and 40 comparisons between the rapid macrocell and CB tests. The types of steel selected for comparisons were based on the fact that they showed some difference in corrosion performance (Balma et al. 2005). For pairs of steel or pairs of corrosion protection systems (Tables 6.17 through 6.20) used to make comparisons, it should be noted that one steel or corrosion protection system may show better corrosion performance than the other in the rapid macrocell test, but worse performance than the other in the SE or CB test. For corrosion rate, in six out of 45 cases for the SE test and 11 out of 40 cases for the CB test, the test results in the bench-scale test do not agree with those in the rapid macrocell test, which is primarily due to the fact that corrosion rates changed from week to week. For total corrosion losses, in four out of 45 cases for the SE test and five out of 40 cases for the CB test, the test results in the bench-scale tests disagree with those in the rapid macrocell test. In none of these nine cases for total corrosion losses, was the level of significance α 0.20 or lower, meaning that the systems being compared did not differ from each other significantly.

As shown in Tables 6.17 through 6.20, forty-five comparisons are made between different corrosion protection systems using the rapid macrocell and SE tests based on both corrosion rate and total corrosion losses. Out of the 45 comparisons for corrosion rate, in 33 cases, the levels of significance for the rapid macrocell test are higher (α is smaller) than those for the SE test, and in two cases, the macrocell and SE tests have the same level of significance. For total corrosion losses, in 16 cases, the levels of significance for the macrocell test are higher than those for the SE test, and in another 16 cases the macrocell and SE tests have the same level of significance. In one case for corrosion rate and five cases for total corrosion losses, the levels of significance for the macrocell test are lower than those for the SE test. According to

Balma et al. (2005), based on the results for the SE test at week 70, in four cases for both corrosion rate and total corrosion losses, the levels of significance for the macrocell test were higher than those for the SE test, and in 23 cases for corrosion rate and 25 cases for total corrosion losses, the macrocell and SE tests had the same level of significance.

There are a total of 40 comparisons between the rapid macrocell and CB tests. Out of the 40 comparisons for corrosion rate, in 25 cases the levels of significance for the rapid macrocell test are higher (α is lower) than those for the CB test, and in four cases the macrocell and CB tests have the same level of significance. For total corrosion losses, in 8 cases the levels of significance for the macrocell test are higher than those for the CB test, and in 22 cases the macrocell and CB tests have the same level of significance. In two cases for corrosion rate and one case for total corrosion losses, the levels of significance for the macrocell test are lower than for the CB test. According to Balma et al. (2005) based on the results of the CB test at week 70, in 16 cases for corrosion rate and one case for total corrosion losses, the levels of significance for the macrocell test are higher than for the SE test, and in 14 cases for corrosion rate and 28 cases for total corrosion losses, the macrocell and SE tests have the same level of significance.

Based on the results of the SE and CB tests at week 70, Balma et al. (2005) concluded that the rapid macrocell test yields results that are comparable to those obtained from the SE and CB tests. For most comparisons in this chapter, the levels of significance for the rapid macrocell test at week 15 are equal to or higher than those for the SE and CB tests at week 96, indicating that the rapid macrocell test is more capable of identifying a difference between two different corrosion protection systems.

Table 6.17 – Comparison of the levels of significance obtained from the Student's t-test for the rapid macrocell test with bare bars in 1.6 m ion NaCl and simulated concrete pore solution and the Southern Exposure and cracked beam tests

Corrosion rates

Type of steel*		Macrocell – 15 weeks		SE – 96 weeks		CB – 96 weeks	
		Level of Significance	Ratio[a]	Level of Significance	Ratio[a]	Level of Significance	Ratio[a]
N	N3	-	1.12	-	0.37	-	3.05
N	T	-	1.33	-	0.39	0.20	0.73
N	CRPT1	-	1.07	-	0.64	-	0.15
N	CRPT2	-	0.81	-	0.62	-	0.60
N	CRT	-	0.90	-	1.09	-	0.92
N3	MMFX	0.20	2.16	-	2.14	-	1.38
N3	2205	0.02	282.20	0.10	39.10	0.20	1.92
N3	2205p	0.02	388.02	0.05	1216.98	0.20	55.10
N3	2101(1)	0.02	15.00	-	1.96	-	0.45
N3	2101(1)p	0.02	206.94	-	5.01	-	0.29
N3	2101(2)	0.02	11.77	0.10	18.90	-	1.13
N3	2101(2)p	0.02	931.25	0.05	347.71	0.20	33.45
2205	2205p	-	1.38	-	31.13	-	28.65
2101(1)	2101(1)p	0.02	13.80	-	2.56	-	0.64
2101(2)	2101(2)p	0.05	79.13	0.20	18.39	0.02	29.71
2101(2)p	2205p	0.05	0.42	-	3.50	-	1.65

[a] Ratio of corroison rates between the two types of steel shown in column one and two.

Corrosion losses

Type of steel*		Macrocell – 15 weeks		SE – 96 weeks		CB – 96 weeks	
		Level of Significance	Ratio[b]	Level of Significance	Ratio[b]	Level of Significance	Ratio[b]
N	N3	-	1.22	-	0.64	0.20	1.46
N	T	0.10	1.42	-	0.66	-	1.00
N	CRPT1	-	1.04	-	1.11	-	0.80
N	CRPT2	-	0.90	-	0.82	-	1.08
N	CRT	-	1.16	-	1.08	-	1.07
N3	MMFX	0.02	4.40	0.10	3.68	0.05	2.69
N3	2205	0.02	240.32	0.02	117.92	0.02	28.86
N3	2205p	0.02	372.61	0.02	591.05	0.02	277.22
N3	2101(1)	0.02	8.90	0.10	2.81	0.02	3.12
N3	2101(1)p	0.02	88.78	0.02	15.81	0.02	6.03
N3	2101(2)	0.02	6.24	0.02	30.30	0.02	3.71
N3	2101(2)p	0.02	214.23	0.02	550.40	0.02	300.65
2205	2205p	0.20	1.55	-	5.01	-	9.61
2101(1)	2101(1)p	0.20	9.98	0.10	5.63	0.20	1.93
2101(2)	2101(2)p	0.02	34.36	0.20	18.17	0.02	81.10
2101(2)p	2205p	-	1.74	-	1.07	-	0.92

[b] Ratio of corroison losses between the two types of steel shown in column one and two.

*** Steel type** → N and N3: conventional, normalized steel, T: Thermex-treated conventional steel, CRPT1: Thermex-treated microalloyed steel with a high phosphorus content (0.117%), CRPT2: Thermex-treated microalloyed steel with a high phosphorus content (0.100%), CRT: Thermex treated microalloyed steel with normal phosphorus content (0.017%), 2101(1) and 2101(2): duplex stainless steel (21% chromium, 1% nickel), 2205: duplex stainless steel (22% chromium, 5% nickel), p: pickled.

Table 6.18 – Comparison of the levels of significance obtained from the Student's t-test for the rapid macrocell test with bare bars in 6.04 m ion NaCl and simulated concrete pore solution and the Southern Exposure and cracked beam tests

Corrosion rates

Type of steel*		Macrocell – 15 weeks		SE – 96 weeks		CB – 96 weeks	
		Level of Significance	Ratio[a]	Level of Significance	Ratio[a]	Level of Significance	Ratio[a]
N3	2205	0.02	10.30	0.10	39.10	0.20	1.92
N3	2205p	0.02	89.90	0.05	1216.98	0.20	55.10
N3	2101(1)	0.10	1.87	-	1.96	-	0.45
N3	2101(1)p	0.02	5.71	-	5.01	-	0.29
N3	2101(2)	0.05	2.31	0.10	18.90	-	1.13
N3	2101(2)p	0.02	26.56	0.05	347.71	0.20	33.45
2205	2205p	0.02	8.72	-	31.13	-	28.65
2101(1)	2101(1)p	0.05	3.05	-	2.56	-	0.64
2101(2)	2101(2)p	0.02	11.52	0.20	18.39	0.02	29.71
2101(2)p	2205p	-	3.38	-	3.50	-	1.65

[a] Ratio of corroison rates between the two types of steel shown in column one and two.

Corrosion losses

Type of steel*		Macrocell – 15 weeks		SE – 96 weeks		CB – 96 weeks	
		Level of Significance	Ratio[b]	Level of Significance	Ratio[b]	Level of Significance	Ratio[b]
N3	2205	0.02	19.59	0.02	117.92	0.02	28.86
N3	2205p	0.02	370.42	0.02	591.05	0.02	277.22
N3	2101(1)	0.02	2.51	0.10	2.81	0.02	3.12
N3	2101(1)p	0.02	5.67	0.02	15.81	0.02	6.03
N3	2101(2)	0.02	2.81	0.02	30.30	0.02	3.71
N3	2101(2)p	0.02	58.21	0.02	550.40	0.02	300.65
2205	2205p	0.02	18.91	-	5.01	-	9.61
2101(1)	2101(1)p	0.02	2.26	0.10	5.63	0.20	1.93
2101(2)	2101(2)p	0.02	20.71	0.20	18.17	0.02	81.10
2101(2)p	2205p	0.02	6.36	-	1.07	-	0.92

[b] Ratio of corroison losses between the two types of steel shown in column one and two.

*** Steel type** → N3: conventional, normalized steel, 2101(1) and 2101(2): duplex stainless steel (21% chromium, 1% nickel), 2205: duplex stainless steel (22% chromium, 5% nickel), p: pickled.

Table 6.19 – Comparison of the levels of significance obtained from the Student's t-test for the rapid macrocell test with lollipop specimens and the Southern Exposure test

Corrosion rates

Type of steel*		Macrocell – 15 weeks		SE – 96 weeks	
		Level of Significance	Ratio[a]	Level of Significance	Ratio[a]
N-45	N-RH45	0.10	3.70	0.20	6.26
N-45	N-DC45	0.05	4.32	0.10	5.08
N-45	N-35	0.10	3.00	0.20	2.37
N-35	N-RH35	0.20	8.12	0.20	13.97
N-35	N-DC35	0.20	5.83	0.20	12.13

[a] Ratio of corroison rates between the two corrosion protection systems shown in column one and two.

Corrosion losses

Type of steel*		Macrocell – 15 weeks		SE – 96 weeks	
		Level of Significance	Ratio[b]	Level of Significance	Ratio[b]
N-45	N-RH45	0.10	5.87	0.02	10.22
N-45	N-DC45	0.20	3.68	0.02	6.13
N-45	N-35	-	1.66	-	0.54
N-35	N-RH35	-	2.29	0.20	121.08
N-35	N-DC35	-	3.53	0.20	29.24

[b] Ratio of corroison losses between the two corrosion protection systems shown in column one and two.

* A-B
A: steel type → N: conventional, normalized steel.
B: mix design → 45: *w/c* ratio of 0.45 and no inhibitor, RH45: *w/c* ratio of 0.45 and Rheocrete 222+, DC45: *w/c* ratio of 0.45 and DCI-S, 35: *w/c* ratio of 0.35 and no inhibitor, RH35: *w/c* ratio of 0.35 and Rheocrete 222+, DC35: *w/c* ratio of 0.35 and DCI-S.

Table 6.20 – Comparison of the levels of significance obtained from the Student's t-test for the rapid macrocell test with mortar-wrapped specimens in 1.6 m ion NaCl and simulated concrete pore solution and the Southern Exposure and cracked beam tests

Corrosion rates

Type of steel*		Macrocell – 15 weeks		SE – 96 weeks		CB – 96 weeks	
		Level of Significance	Ratio[a]	Level of Significance	Ratio[a]	Level of Significance	Ratio[a]
N3	MMFX	0.05	1.67	-	2.14	-	1.38
N3	N3/MMFX	0.20	1.47	-	4.18	N/A	N/A
MMFX	MMFX/N3	-	0.82	0.20	1.60	N/A	N/A
N3	2205	0.02	612.50	0.10	39.10	0.20	1.92
N3	2205p	0.02	306.25	0.05	1216.98	0.20	55.10
N3	2101(1)	0.05	2.04	-	1.96	-	0.45
N3	2101(1)p	0.02	816.67	-	5.01	-	0.29
N3	2101(2)	0.02	3.47	0.10	18.90	-	1.13
N3	2101(2)p	0.02	167.05	0.05	347.71	0.20	33.45
N3	ECR	0.02	4.21	-	2.81	0.20	0.19
2205	2205p	-	0.50	-	31.13	-	28.65
2101(1)	2101(1)p	0.05	400.33	-	2.56	-	0.64
2101(2)	2101(2)p	0.02	48.18	0.20	18.39	0.02	29.71
2101(2)p	2205p	-	1.83	-	3.50	-	1.65

[a] Ratio of corroison rates between the two types of steel shown in column one and two.

Corrosion losses

Type of steel*		Macrocell – 15 weeks		SE – 96 weeks		CB – 96 weeks	
		Level of Significance	Ratio[b]	Level of Significance	Ratio[b]	Level of Significance	Ratio[b]
N3	MMFX	0.02	3.98	0.10	3.68	0.05	2.69
N3	N3/MMFX	0.02	2.08	0.20	2.03	N/A	N/A
MMFX	MMFX/N3	0.20	0.75	-	1.01	N/A	N/A
N3	2205	0.02	209.74	0.02	117.92	0.02	28.86
N3	2205p	0.02	208.99	0.02	591.05	0.02	277.22
N3	2101(1)	0.02	5.53	0.10	2.81	0.02	3.12
N3	2101(1)p	0.02	396.88	0.02	15.81	0.02	6.03
N3	2101(2)	0.02	6.79	0.02	30.30	0.02	3.71
N3	2101(2)p	0.02	193.23	0.02	550.40	0.02	300.65
N3	ECR	0.02	17.30	0.05	8.40	0.20	2.01
2205	2205p	-	1.00	-	5.01	-	9.61
2101(1)	2101(1)p	0.10	71.83	0.10	5.63	0.20	1.93
2101(2)	2101(2)p	0.02	28.47	0.20	18.17	0.02	81.10
2101(2)p	2205p	-	1.08	-	1.07	-	0.92

[b] Ratio of corroison losses between the two types of steel shown in column one and two.

*** Steel type** → N3: conventional, normalized steel, MMFX: MMFX microcomposite steel, MMFX/N3: MMFX steel in the top mat and N3 steel in the bottom mat, N3/MMFX: N3 steel in the top mat and MMFX steel in the bottom mat, 2101(1) and 2101(2): duplex stainless steel (21% chromium, 1% nickel), 2205: duplex stainless steel (22% chromium, 5% nickel), ECR: epoxy-coated steel, p: pickled.

6.6 DISCUSSION OF RESULTS

The results at week 15 of the rapid macrocell test are compared with the results at week 96 of the Southern Exposure (SE) test or the cracked beam (CB) test.

The total corrosion losses show strong correlations between the rapid macrocell test and the SE or CB test and between the SE and CB tests, except for specimens with conventional steel at *w*/*c* ratios of 0.45 and 0.35, with and without corrosion inhibitor DCI-S or Rheocrete 222+. As explained earlier, the CB test shows little effect of changes in concrete properties on the corrosion protection of steel in concrete, an observation that has ramifications beyond the discussions in this chapter.

A stronger linear relationship is generally observed for total corrosion losses than for corrosion rates because corrosion rates change from week to week, and also because total corrosion losses take into consideration corrosion rates throughout the test period.

Based on the comparisons in this report and the comparisons by Balma et al. (2005), total corrosion losses at week 70 have correlations with the rapid macrocell similar to those at week 96. The corrosion rates exhibit better correlations at week 70 than those at week 96, especially for the correlations between the rapid macrocell and CB tests, as discussed in Section 6.3.2.1.

The results of the SE test are also compared with the results of the CB test at week 96. There is not a good correlation for corrosion rates between the SE and CB tests, with a coefficient of determination of 0.12, compared with the value of 0.69 at week 70. Total corrosion losses show a good correlation between the two test methods, with a coefficient of determination of 0.87, similar to the value of 0.91 at week 70.

Based on the above information, the SE and CB results at week 70 or 96 are

both appropriate to evaluate corrosion performance for different corrosion protection systems because total corrosion losses showed similar correlations at both week 70 and 96.

Coefficients of variation for corrosion rates and total corrosion losses are compared for the rapid macrocell and bench-scale tests. Out of the 125 sets of test results, 67% of the comparisons at week 96 and 70% of the comparisons at week 70 exhibit lower coefficients of variation for total corrosion losses than for corrosion rates, indicating that corrosion rates are more scattered than total corrosion losses. Between the two test methods, 76% of corrosion rates and 64% of total corrosion losses exhibit lower coefficients of variation in the rapid macrocell test at week 15 than in the bench-scale tests at week 96, compared with 60% of corrosion rates and 52% of total corrosion losses at week 70. This indicates that the results in the bench-scale tests exhibit more scatter than those in the rapid macrocell test, especially at week 96.

The comparisons of results obtained using the Student's t-test show that, in general, the rapid macrocell test is more capable of identifying a difference between two corrosion protection systems than the SE and CB tests. In most cases, the results obtained using the rapid macrocell test agree with those for the bench-scale tests. For corrosion rate, the disagreement between the rapid macrocell and bench-scale tests are due mainly to the fact that corrosion rates changed from week to week. For total corrosion losses, in all nine cases for which these two methods disagree, the level of significance α was higher than 0.20, meaning that the systems being compared did not differ from each other significantly.

CHAPTER 7

CONCLUSIONS AND RECOMMENDATIONS

7.1 SUMMARY

This report presents the results of the evaluation of different corrosion protection systems for reinforcing steel in concrete. The corrosion protection systems evaluated in this study include:

- Conventional reinforcing steel,
- Conventional epoxy-coated reinforcement (ECR),
- Conventional ECR cast in concrete with corrosion inhibitor calcium nitrite (DCI-S), Rheocrete 222+, or Hycrete at *w/c* ratios of 0.45 and 0.35,
- ECR with a primer containing encapsulated calcium nitrite cast in concrete at *w/c* ratios of 0.45 and 0.35,
- Multiple coated reinforcement with a zinc layer underlying the conventional epoxy coating,
- ECR with increased adhesion, including ECR chemically pretreated with zinc chromate, and two types of ECR with high adhesion epoxy coatings produced by DuPont and Valspar,
- The three types of ECR with increased adhesion cast with the corrosion inhibitor calcium nitrite (DCI-S), and
- 2205 pickled stainless steel.

The corrosion protection systems described above were evaluated using the rapid macrocell tests with bare bar and mortar-wrapped specimens, three bench-scale tests, and a field test. The three bench-scale tests included the Southern Exposure

(SE), the cracked beam (CB), and the ASTM G 109 tests. Specimens with and without simulated cracks were used in the field test. An economic analysis was performed to find the most cost-effective corrosion protection system for reinforced concrete bridge decks.

Linear polarization resistance tests were used to determine microcell corrosion rates for selected bench-scale test specimens. The microcell corrosion rates were evaluated according to the guidelines developed by Broomfield (1997). Correlations were performed between microcell and macrocell corrosion, and between microcell corrosion rate and corrosion potential.

Three rounds of cathodic disbondment tests were performed to evaluate the quality of the bond between the epoxy and the underlying steel for different types of epoxy-coated reinforcement described above.

Corrosion potential mapping performed at six-month intervals, bench-scale tests (SE and CB tests), and field tests were used to evaluate the corrosion performance of 2205 pickled (2205p) stainless steel in two bridges, the Doniphan County Bridge (DCB) and Mission Creek Bridge (MCB).

Comparisons were also performed between the rapid macrocell test and the SE or CB test, and between the SE and CB tests based on the test results from a previous study by Balma et al. (2005). The corrosion protection systems evaluated in that study included conventional normalized steel, conventional Thermex-treated steel, microalloyed steel, MMFX microcomposite steel, epoxy-coated reinforcement (ECR), duplex steels (2101 and 2205, pickled and nonpickled), two corrosion inhibitors (DCI-S and Rheocrete 222+), and variations in the water-cement (*w/c*) ratio. The comparisons based on the results at week 70 of the SE and CB tests and at week 15 of the rapid macrocell tests were presented by Balma et al. (2005). This report presents

comparisons based on the results at week 96 of the SE and CB tests, and at week 15 of the rapid macrocell test. The coefficient of variation is used to compare the variability in corrosion rates and total corrosion losses for different test methods. In addition, levels of significance are compared between the rapid macrocell and bench-scale tests based on the results obtained from the Student's t-test.

7.2 CONCLUSIONS

The following conclusions are based on the results and observations presented in this report.

7.2.1 Evaluation of Corrosion Protection Systems

1. Much lower corrosion rates and total corrosion losses are observed in the ASTM G 109 and field tests than observed in the SE and CB tests. In these tests, only conventional steel shows significant corrosion, while the ECR specimens (all types) show little corrosion. This low corrosion activity is attributed to the low salt concentration of the ponding solution and less aggressive ponding and drying cycles when compared to the SE and CB tests. Regular drying, as occurs for the field test specimens, also slows corrosion.
2. Of the systems tested, conventional steel provides the least corrosion protection. In mortar or concrete (rapid macrocell, SE, and CB tests), conventional ECR exhibits total corrosion losses less than 5.6% of the corrosion loss of conventional steel based on total area.
3. In uncracked concrete (SE test) with a *w/c* ratio of 0.35, total corrosion losses are lower than observed at a *w/c* ratio of 0.45, with the exception of ECR cast in concrete with the corrosion inhibitor Rheocrete and ECR with a calcium nitrite

primer. In cracked concrete (CB test), a *w/c* ratio of 0.35 does not provide additional corrosion protection when the cracks provide a direct path for chlorides to reach the reinforcing bars.

4. In uncracked mortar and concrete (rapid macrocell and SE tests) containing corrosion inhibitors, total corrosion losses are lower than observed for concrete with the same *w/c* ratios but with no inhibitors. In cracked concrete (the CB test), the presence of corrosion inhibitors provides very limited or no additional protection to steel in concrete.
5. In the SE test in concrete with a *w*/*c* ratio of 0.45, the primer with encapsulated calcium nitrite seems to provide corrosion protection for reinforcing steel for a limited time; after it is consumed, corrosion rates increase rapidly. For concrete with a *w*/*c* ratio of 0.35, ECR with a calcium nitrite primer shows improvement in corrosion resistance when compared to conventional ECR, in all likelihood due to the low chloride penetration rate in concrete with *w*/*c* ratio of 0.35. In the CB test, ECR with a calcium nitrite primer exhibits higher total corrosion losses than conventional ECR.
6. Multiple coated reinforcement exhibits total corrosion losses between 1.09 and 18.3 times the losses for conventional ECR in the SE and CB tests. Corrosion potentials, however, show that the zinc provides protection to the underlying steel. A full evaluation of the system must wait until the end of the tests when the bars can be examined.
7. The three types of high adhesion ECR bars do not consistently exhibit improvement in corrosion protection when compared to conventional ECR.
8. Based on three rounds of corrosion potential mapping for both the Doniphan County Bridge and Mission Creek Bridge decks, no corrosion activity can be

observed for the majority of the bridge decks. Both bridges, however, show active corrosion at regions close to the abutments, primarily due to the use of mild steel form ties in the abutments.

9. 2205p stainless steel exhibits excellent corrosion performance, which is consistent with the test results from the previous study by Balma et al. (2005).
10. Based on three series of cathodic disbondment tests, the ECR with chromate pretreatment exhibits the best bonding between the epoxy and the underlying steel, followed by multiple coated reinforcement, ECR containing a calcium nitrite primer, and ECR with high adhesion DuPont coating, respectively. Conventional ECR and ECR with high adhesion Valspar coating show the worst bond quality consistently and fail the coating disbondment requirements outlined in ASTM A 775. Overall, however, performance in the cathodic disbondment test does not appear to affect the corrosion performance of the bars.
11. In general, the microcell corrosion rates in the connected mat are somewhere between the results of the top and bottom mats for the most CB test specimens, but not necessarily for the SE and ASTM G 109 test specimens. The microcell corrosion rates for the top mat are usually one to two orders higher than those in the bottom mat.
12. In general, the relative effectiveness of different corrosion protection systems is similar in macrocell and microcell corrosion. Based on exposed area, most damaged ECR bars exhibited higher total corrosion losses than conventional steel in terms of both microcell and macrocell corrosion. Total corrosion losses based on macrocell and microcell corrosion show a strong correlation. In the SE and CB tests with *w*/*c* ratios of 0.45 and 0.35, coefficients of determination

between 0.68 and 0.82 are observed for the correlations between macrocell and microcell corrosion, with the exception of the CB test with a *w*/*c* ratio of 0.35, which has a coefficient of determination of 0.47. However, a very good linear relationship (r^2 = 0.97) is observed between macrocell and microcell corrosion for the CB test with a *w*/*c* ratio of 0.35 if an outlier (ECR cast in concrete with the corrosion inhibitor Rheocrete) is not included.

13. Specimens in the SE test show better correlations between microcell corrosion rate and corrosion potential than those in the CB test.
14. An economic analysis shows that the lowest cost option is a 230-mm concrete deck reinforced with the following steels (all have the same cost): conventional ECR, ECR with a primer containing calcium nitrite, multiple coated reinforcement, or any of the three types of high adhesion ECR bars.

7.2.2 Comparisons Between Test Methods

1. In general, a stronger linear relationship is observed for total corrosion losses than for corrosion rates, primarily due to the fact that corrosion rates change from week to week and total corrosion losses take into consideration corrosion rates over time.
2. Total corrosion losses show strong correlations between the rapid macrocell test and the SE and CB tests and between the SE and CB tests (at 96 weeks) in all cases, except for conventional steel specimens cast in concrete with different *w*/*c* ratios (0.45 and 0.35) and corrosion inhibitors (DCI-S and Rheocrete 222+) in the CB test.
3. Total corrosion losses of the SE and CB tests at weeks 70 and 96 are both appropriate to evaluate corrosion performance for different corrosion protection

systems. Total corrosion losses show similar correlations between the results of the rapid macrocell test and those of the bench-scale tests at both 70 and 96 weeks.

4. Based on the SE and CB test results at both 70 and 96 weeks, corrosion rates are more scattered than total corrosion losses. The rapid macrocell test exhibits lower coefficients of variation than the bench-scale tests for both corrosion rates and total corrosion losses.
5. Based on the Student's t-test, the rapid macrocell test is more capable of identifying a difference between two corrosion protection systems than the SE or CB test.

7.3 RECOMMENDATIONS

1. Based on the economic analyses, a 230-mm concrete deck reinforced with any of the following steels (all have the same cost) is recommended: conventional ECR, ECR with a primer containing calcium nitrite, multiple coated reinforcement, or any of the three types of high adhesion ECR bars.
2. For the rapid macrocell test with mortar-wrapped specimens, a more aggressive test environment is recommended for epoxy-coated reinforcement, including the use of a higher salt concentration, ECR bars with more coating damage, and a longer test period, such as 30 weeks instead of 15 weeks.
3. In the current study, total corrosion losses for conventional ECR in the SE and CB tests are 4.1% and 2.0%, respectively, of the losses of conventional ECR from a previous study (Balma et al. 2005) containing ECR at the anode and conventional steel at the cathode. Therefore, it is recommended that epoxy-coated bars should be used throughout a structure, not just the steel that will

first come in contact with chlorides.

4. To more accurately predict the time to first repair for different corrosion protection systems, it is recommended that 1) the critical corrosion chloride thresholds be obtained for these systems based on bars without an epoxy coating, and 2) the long-term corrosion rates be based on values between weeks 50 and 70 in the SE and CB tests, values that are available only for conventional steel and epoxy-coated reinforcement at this writing.
5. To better determine the total corrosion loss required to crack cover concrete using the equation proposed by Torres-Acosta and Sagües (2005), the damaged area of the epoxy coating for epoxy-coated steel after concrete placement should be investigated in actual bridge decks.
6. Based on the fact that the conventional epoxy-coated bars do not meet the cathodic disbondment requirements in ASTM A 775, it is recommended that cathodic disbondment requirements be strengthened in the quality control checks for production bars.

REFERENCES

ACI Committee 318, *Building Code Requirements for Structural Concrete (ACI 318-05) and Commentary (ACI 318R-05)* (2005). American Concrete Institute, Farmington Hills, MI.

Allyn, M. and Frantz, G. C. (2001a). "Corrosion Tests with Concrete Containing Salts of Alkenyl-Succinic Acid," *ACI Materials Journal*, Vol. 98, No. 3, pp. 224-232.

Allyn, M. and Frantz, G. C. (2001b). "Strength and Durability of Concrete Containing Salts of Alkenyl-Succinic Acid," *ACI Materials Journal*, Vol. 98, No. 1, pp. 52-58.

Alonso, C., Andrade, C., Castellote, M., and Castro, P. (2000). "Chloride Threshold Values to Depassivate Reinforcing Bars Embedded in a Standard OPC Mortar," *Cement and Concrete Research*, Vol. 30, No. 7, pp. 1047-1055.

Andrade, C. and Alonso, C. (2001). "On-site Measurements of Corrosion Rate of Reinforcements," *Construction and Building Materials*, Vol. 15, No. 2-3, pp. 141-145.

Andrade, C. and González, J.A. (1978). "Quantitative Measurements of Corrosion Rate of Reinforcing Steels Embedded in Concrete Using Polarization Resistance Measurements," *Woerkstoffe und Korrosion*, Vol. 29, pp. 515-519.

ASTM A 775-04a (2004). "Standard Specification for Epoxy-Coated Steel Reinforcing Bars," *2005 Annual Book of ASTM Standards*, Vol. 01.04, American Society for Testing and Materials, West Conshohocken, PA.

ASTM A 934-04 (2004). "Standard Specification for Epoxy-Coated Prefabricated Steel Reinforcing Bars," *2005 Annual Book of ASTM Standards*, Vol. 01.04, American Society for Testing and Materials, West Conshohocken, PA.

ASTM A 955-03b (2003). "Standard Specification for Deformed and Plain Stainless Steel Bars for Concrete Reinforcement," *2004 Annual Book of ASTM Standards*, Vol. 01.04, American Society for Testing and Materials, West Conshohocken, PA.

ASTM C 876-91 (1991). "Standard Test Method for Half-Cell Potentials of Uncoated Reinforcing Steel in Concrete," *2005 Annual Book of ASTM Standards*, Vol. 03.02, American Society for Testing and Materials, West Conshohocken, PA.

ASTM G 8-96 (1996). "Standard Test Method for Cathodic Disbonding of Pipeline Coatings," *2003 Annual Book of ASTM Standards*, Vol. 06.02, American Society for Testing and Materials, West Conshohocken, PA.

ASTM G 59-97 (1997). "Standard Test Method for Conducting Potentiodynamic Polarization Resistance Measurements," *2003 Annual Book of ASTM Standards*, Vol. 03.02, American Society for Testing and Materials, West Conshohocken, PA.

ASTM G 109-99a (1999). "Standard Test Method for Determining the Effects of Chemical Admixtures on the Corrosion of Embedded Steel Reinforcement in Concrete Exposed to Chloride Environments," *2005 Annual Book of ASTM Standards*, Vol. 03.02, American Society for Testing and Materials, West Conshohocken, PA.

Balma, J., Darwin, D., Browning, J. P., and Locke, C. E. (2005). "Evaluation of Corrosion Protection Systems and Corrosion Testing Methods for Reinforcing Steel in Concrete," *SM Report* No. 76, The University of Kansas Center for Research, Inc., Lawrence, KS, 517 pp.

Berke, N.S. (1987). "The Effects of Calcium Nitrite and Mix Design on the Corrosion Resistance of Steel in Concrete (Part 2, Long-Term Results)," *Proc., Corrosion-87 Symposium on Corrosion of Metals in Concrete*, National Association of Corrosion Engineer, Houston, TX, pp. 134-144.

Berke, N. S., Pfeifer, D. W., and Weil, T. G. (1988). "Protection Against Chloride-Induced Corrosion," *Concrete International*, Vol. 10, No. 12, pp. 45-55.

Berke, N. S (1989). "A Review of Corrosion Inhibitors in Concrete," *Materials Performance*, Vol. 28, No. 10, pp. 41-44.

Berke, N. S. and Rosenberg, A. (1989). "Technical Review of Calcium Nitrite Corrosion Inhibitor in Concrete," *Transportation Research Record,* No. 1211, pp. 18-27.

Berke, N. S. (1991). "Corrosion Inhibitors in Concrete," *Concrete International*, Vol. 13, No. 7, pp. 24-27.

Berke, N. S. (1998). "Long-Term Corrosion Performance of Epoxy-Coated Steel and Calcium Nitrite," *NACE Corrosion 98*, Paper No. 652, National Association of Corrosion Engineers, Houston, TX.

Broomfield, J. P. (1997). *Corrosion of Steel in Concrete: Understanding, Investigation and Repair,* E & FN Spon, UK, 240 pp.

Burke, D. F. (1994). "Performance of Epoxy-Coated Rebar, Galvanized Rebar, and Plain Rebar with Calcium Nitrite in a Marine Environment," *Concrete Reinforcing Steel Institute,* Research Series – 2, 8 pp.

Callahan, M. R. (1989). "Deicing Salt Corrosion With and Without Inhibitors," *Transportation Research Record,* No. 1211, pp. 12-17.

Civjan, S. A., LaFave, J. M., Lovett, D., Sund, A. J., and Trybulski, J. (2003). "Performance Evaluation and Economic Analysis of Combinations of Durability Enhancing Admixture (Mineral and Chemical) in Structural Concrete for the Northeast U.S.A.," *TNETCR36,* The New England Transportation Consortium, Storrs, CT, 166 pp.

Clear, K. C. (1976). "Time-to-Corrosion of Reinforcing Steel in Concrete Slabs: V. 3, Performance After 830 Daily Salt Applications," *Publication* No. FHWA-RD-76-70, Federal Highway Administration, Washington, D.C., 64 pp.

Clear, K. C. (1981). "Time-to-Corrosion of Reinforcing Steel in Concrete Slabs: V. 4, Galvanized Reinforcing Steel," *Publication* No. FHWA-RD-82-028, Federal Highway Administration, Washington, D.C., 87 pp.

Kenneth C. Clear. (1989). "Measuring Rate of Corrosion of Steel in Field Concrete Structure," *Transportation Research Record*, No. 1211, pp. 28-38.

Clear, K. C. (1992). "Effectiveness of Epoxy-Coated Reinforcing Steel – Interim Report," Canadian Strategic Highway Research Program, Ottawa, ON, 79 pp.

Clear, K. C. (1994). "Effectiveness of Epoxy-Coated Reinforcing Steel – Final Report," Canadian Strategic Highway Research Program, Ottawa, ON, 128 pp.

Clemeña, G. G. and Virmani, Y. P. (2002). "Testing of Selected Metallic Reinforcing Bars for Extending the Service Life of Future Concrete Bridges: Testing in Outdoor Concrete Blocks", *VTRC 03-R6*, Virginia Transportation Research Council, 24 pp.

Clemeña, G. G. (2003). "Investigation of the Resistance of Several New Metallic Reinforcing Bars to Chloride-Induced Corrosion in Concrete," *VTRC 04-R7*, Virginia Transportation Research Council, 24 pp.

Cody, R. D., Cody, A. M., Spry, P. G., and Gan, G. (1996). "Concrete Deterioration by Deicing Salts: An Experimental Study," *Semisequicentennial Transportation Conference Proceedings*, Ames, IA.

Daigle, L., Lounis, A., and Cusson, D. (2004). "Numerical Prediction of Early-Age Cracking and Corrosion in High Performance Concrete Bridges – Case Study," *2004 Annual Conference of the Transportation Association of Canada*, Québec City, Québec, 20 pp.

Daniel, M. (2004). Lawrence Maintenance Office, Kansas Department of Transportation, Lawrence, KS. personal communication.

Darwin, D., Locke, C. E., Balma, J., and Kahrs, J. T. (1999). "Evaluation of Stainless Steel Clad Reinforcing Bars," *SL Report* 99-3, The University of Kansas Center for Research, Inc., Lawrence, KS, 43 pp.

Darwin, D., Locke, C. E., Browning, J. P., and Nguyen, T. V. (2002). "Mechanical and Corrosion Properties of a High-Strength, High Chromium Reinforcing Steel for Concrete," *SM Report* No. 66, The University of Kansas Center for Research, Inc., Lawrence, KS, 142 pp.

Detwiler, R.D., Kojundic, T., and Fidjestol, P. (1997). "Evaluation of Bridge Deck Overlays," *Concrete International*, Vol. 19, No. 8, pp. 43-45.

Escalante, E. (1990). "Effectiveness of Potential Measurements for Estimating Corrosion of Steel in Concrete," *Corrosion of Reinforcement in Concrete,* edited by Page, C.L. et al., Elsevier Applied Science, London, pp. 281-292.

Fazammehr, H. (1985). "Pore Solution Analysis of Sodium Chloride and Calcium Chloride Containing Cement Pastes," *Master of Science Thesis*, University of Oklahoma, Norman, OK, 101 pp.

Flis, J., Sehgal, A., Li, D., Kho, Y.-T., Sabotl, S., and Cady, P.D. (1993). "Condition Evaluation of Concrete Bridges Relative to Reinforcement Corrosion, Volume 2: Method for Measuring the Corrosion Rate of Reinforcing Steel," *SHRP-S-423*, National Research Council, Washington DC, 105 pp.

Funahashi, M. (1990). "Predicting Corrosion-Free Service Life of a Concrete Structure in a Chloride Environment," *ACI Materials Journal*, Vol. 87, No. 6, pp. 581-587.

Ge, B., Darwin, D., Locke, C. E., and Browning, J. P. (2004). "Evaluation of Corrosion Protection Systems and Testing Methods for Conventional Steel," *SM Report* No. 73, The University of Kansas Center for Research, Inc., Lawrence, KS, 213 pp.

Gaidis, J. M. and Rosenberg, A. M. (1987). "The Inhibition of Chloride-Induced Corrosion in Reinforced Concrete by Calcium Nitrite," *Cement, Concrete, and Aggregates*, Vol. 9, No. 1, pp. 30-33.

Glass, G. K. and Buenfeld, N. R. (1997). "The Presentation of the Chloride Threshold Level for Corrosion of Steel in Concrete," *Corrosion Science*, Vol. 39, No. 5, pp. 1001-1013.

Gong, L., Darwin, D., Browning, J. P., and Locke, C. E. (2002). "Evaluation of Mechanical and Corrosion Properties of MMFX Reinforcing Steel in Concrete," *SM Report* No. 70, The University of Kansas Center for Research, Inc, Lawrence, KS, 112 pp.

Gong, L., Darwin, D., Browning, J. P., and Locke, C. E. (2006). "Evaluation of Multiple Corrosion Protection Systems and Stainless Steel Clad Reinforcement for Reinforced Concrete," *SM Report* No. 82, The University of Kansas Center for Research, Inc, Lawrence, KS, 504 pp.

Griffith, A. and Laylor, H. M. (1999). "Epoxy Coated Reinforcement Study," *Report* No. OR-RD-99-25, Oregon Department of Transportation, Salem, OR, 36 pp.

Gu, P., and Beaudoin, J. J. (1998). "Obtaining Effective Half-Cell Potential Measurements in Reinforced Concrete Structures," *Construction Technology Updates,* No. 18, National Research Council of Canada, 4 pp.

Gu, P., Elliott, S., Beaudoin, J. J., and Arsenault, A. (1996). "Corrosion Resistance of Stainless Steel in Chloride-contaminated Concrete," *Cement and Concrete Research,* Vol. 26, No. 8, pp 1151-1156.

Hansson, C. M., Mammolitu, L. and Hope, B. B. (1998). "Corrosion Inhibitors in Concrete – Part I: The Principles," *Cement and Concrete Research,* Vol. 28, No. 2, pp 1775-1781.

Hausmann, D. A. (1967). "Steel Corrosion in Concrete," *Materials Protection*, Vol. 6, pp. 19-23.

Hope, B. B. and IP, A. K. C. (1987). "Chloride Corrosion Threshold in Concrete," *ACI Materials Journal*, Vol. 84, No. 4, pp. 306-314.

Hope, B. B. and IP, A. K. C. (1989). "Corrosion Inhibitors for Use in Concrete," *ACI Materials Journal*, Vol. 86, No. 6, pp. 602-608.

Jones, D. A. (1996). *Principles and Prevention of Corrosion,* Macmillan Publishing Company, New York, 572 pp.

Kahrs, J., Darwin, D., and Locke, C. E. (2001). "Evaluation of Corrosion Resistance of Type 304 Stainless Steel Clad Reinforcing Bars," *SM Report* No. 65, The University of Kansas Center for Research, Inc., Lawrence, KS, 76 pp.

Kansas Department of Transportation. (1990). *Standard Specifications for State Road and Bridge Construction*, Topeka, KS, 1154 pp.

Kansas Department of Transportation. (2001). *Snow & Ice Control & Other Motorist Services*, KDOT Maintenance Manual, Chapter 7, Topeka, KS, 38 pp.

Kepler, J. L., Darwin, D., and Locke, C. E. (2000). "Evaluation of Corrosion Protection Methods for Reinforced Concrete Structures," *SM Report* No. 58, The University of Kansas Center for Research, Inc., Lawrence, KS, 221 pp.

Kirkup, Les (2002). *Data Analysis with Excel: An Introduction for Physical Scientists*, Cambridge University Press, Cambridge, United Kingdom, 446 pp.

Lambert, P., Page, C. L., and Vassie, P. R. W. (1991). "Investigation of Reinforcement Corrosion. 2. Electrochemical Monitoring of Steel in Chloride-contaminated Concrete," *Materials and Structures*, Vol. 24, No. 143, pp. 351-358.

Lee, S. and Krauss, P. D. (2004). "Long-Term Performance of Epoxy-Coated Reinforcing Steel in Heavy Chloride-contaminated Concrete," *Publication* No. FHWA-RD-04-090, Federal Highway Administration, McLean, VA, 130 pp.

Lindquist, W.D., Darwin, D., Browning, J. P. (2005). "Cracking and Chloride Contents in Reinforced Concrete Bridge Decks," *SM Report* No. 78, The University of Kansas Center for Research, Inc., Lawrence, KS, 453 pp.

Liu, Y. and Weyers, R. E. (1998) "Modeling the Time-to-Corrosion Cracking in Chloride-contaminated Reinforced Concrete Structures," *ACI Materials Journals*, Vol. 95, No. 6, pp. 675-681.

Magee, J.H. (2005). Carpenter Technology Corp., Reading, PA, personal communication.

Mammolitu, L., Hansson, C. M., and Hope, B. B. (1999). "Corrosion Inhibitors in Concrete – Part II: Effect on Chloride Threshold Values for Corrosion of Steel in Synthetic Pore Solutions," *Cement and Concrete Research,* Vol. 29, No. 10, pp 1583-1589.

Mansfeld, F. (1981). "Recording and Analysis of AC Impedance Data for Corrosion Studies," *Corrosion*, Vol. 37, No. 5, pp. 301-307.

Marquardt, H. (1991). "Corrosion Measurements on Bridge Decks by Potential Mapping," *Structural Engineering International*, Vol. 1, No. 3, pp. 49-50.

Marquardt, H. (1998). "Locating Rebar Corrosion in Concrete Walls by Potential Measurements," *IABSE-Colloquium "Saving Buildings in Central and Eastern Europe"*, Berlin, June 4-5, 6 pp.

Martinez, S. L., Darwin, D., McCabe, S. L., and Locke, C. E. (1990). "Rapid Test for Corrosion Effects of Deicing Chemicals in Reinforced Concrete," *SL Report* No. 90-4, The University of Kansas Center for Research, Inc., Lawrence, KS, 61 pp.

McDonald, D. B., Sherman M. R., Pfeifer, D. W., and Virmani, Y. P. (1995). "Stainless Steel Reinforcing as Corrosion Protection," *Concrete International,* Vol. 17, No. 5, pp. 65-70.

McDonald, D. B., Pfeifer, D. W., and Sherman, M. R. (1998). "Corrosion Evaluation of Epoxy-Coated, Metallic-Clad and Solid Metallic Reinforcing Bars in Concrete," *Publication* No. FHWA-RD-98-153, Federal Highway Administration, McLean, VA, 127 pp.

Metha, P. K. and Monteiro, P. J. M. (1993) *Concrete Structure, Properties, and Materials*, Prentice Hall, Inc., Englewood Cliffs, NJ, 548 pp.

Nmai, C. K., Bury, M. A., and Farzam, H. (1994). "Corrosion Evaluation of a Sodium Thiocyanate-Based Admixture," *Concrete International*, Vol. 16, No. 4, pp. 22-25.

Nmai, C. K, Farrington, S. A., and Bobrowski, G. (1992). "Organic-Based Corrosion-Inhibiting Admixture for Reinforced Concrete," *Concrete International*, Vol. 14, No. 4, pp. 45-51.

Ost, B. and Monfore, G. E. (1974). "Penetration of Chloride into Concrete," *Materials Performance*, Vol. 13, No. 6, pp. 21-24.

Perenchio, W. F. (1992). "Corrosion of Reinforcing Bars in Concrete," *Annual Seminar*, Master Builders Technology, Cleveland, OH.

Pfeifer, D. W., and Scali, M. J. (1981). "Concrete Sealers for Protection of Bridge Structures," *National Cooperative Highway Research Board Program Report* 244, Transportation Research Board, National Research Council, Washington, D.C., 138 pp.

Pfeifer, D. W., Landgren, J. R., and Zoob, A. (1987). "Protective Systems for New Prestressed and Substructure Concrete," *Publication* No. FHWA-RD-86-193, Federal Highway Administration, McLean, VA, 127 pp.

Pfeifer, D. W. (2000), "High Performance Concrete and Reinforcing Steel with a 100-Year Service Life," *PCI Journal*, Vol. 45, No. 3, pp. 46-54.

Pike, R. G., Hay, R. E., Clifton, J. R., Beeghly, H. F., and Mathey, R. G. (1973), "Non-metallic Coatings for Concrete Reinforcing Bars," *Public Roads*, Vol. 37, No. 5, pp. 185-197.

Pyc, W. A., Zemajitis, J., Weyers, R. E., and Sprinkel, A. (1999), "Evaluating Corrosion-Inhibiting Admixtures," *Concrete International*, Vol. 21, No. 4, pp. 39-44.

Pyc, W. A., Sprinkel, A., Weyers, R. E., and Dillard, J. G. (2000), "Performance of Epoxy-Coated Reinforcing Steel," *Concrete International*, Vol. 22, No. 2, pp. 57-61.

Pyke, R. and Cohen, M. (1948). "Rate of Breakdown and Mechanism of Nitrite Inhibition of Steel Corrosion," *Electrochemical Society Journal*, Vol. 93, No. 3, pp. 63-78.

Rasheeduzzafar, Dakhil, F. H., Bader, M. A., and Khan, M. M. (1992). "Performance of Corrosion Resisting Steels in Chloride-Bearing Concrete," *ACI Materials Journal*, Vol. 89, No. 5, pp. 438-448.

Roberge, P. R. (2000). *Handbook of Corrosion Engineering*, McGraw Hill Companies, New York, 1139 pp.

Sagües, A. A. (1994). "Corrosion of Epoxy Coated Rebar in Florida Bridges," *WPI* No. 0510603, Final Report to Florida Department of Transportation, University of South Florida, Tampa, FL, 70 pp.

Scannell, W. T. and Clear, K. C. (1990). "Long-Term Outdoor Exposure Evaluation of Concrete Slabs Containing Epoxy-Coated Reinforcing Steel," *Transportation Research Record,* No. 1284*,* pp. 70-78.

Schmitt, T.R. and Darwin, D. (1995). "Cracking in Concrete Bridge Decks," *SM Report,* No. 39*,* The University of Kansas Center for Research, Inc., Lawrence, KS, 151 pp.

Schwensen, S. M., Darwin, D., and Locke, C. E. (1995). "Rapid Evaluation of Corrosion-Resistant Concrete Reinforcing Steel in the Presence of Deicers," *SL Report* No. 95-6, The University of Kansas Center for Research, Inc., Lawrence, KS, 90 pp.

Senecal, M. R., Darwin, D., and Locke, C. E., Jr. (1995). "Evaluation of Corrosion-Resistant Steel Reinforcing Bars," *SM Report* No. 40, The University of Kansas Center for Research, Inc., Lawrence, KS, 142 pp.

Sherman, M. R., McDonald, D. B., and Pfeifer, D. W. (1996). "Durability Aspects of Precast Prestressed Concrete Part 2: Chloride Permeability Study," *PCI Journal*, Vol. 41, No. 4, pp. 76-95.

Smith, J. L., Darwin, D., and Locke, C. E. (1995). "Corrosion-Resistant Steel Reinforcing Bars Initial Tests," *SL Report* No. 95-1, The University of Kansas Center for Research, Inc., Lawrence, KS, 43 pp.

Smith, F. N. and Tullman, M. (1999). "Using Stainless Steel as Long-Lasting Rebar Material," *Materials Performance*, Vol. 38, No. 5, pp. 72-76.

Smith, J. L. and Virmani, Y. P. (1996). "Performance of Epoxy Coated Rebars in Bridge Decks," *Publication* No. FHWA-RD-96-092, Federal Highway Administration, McLean, VA, 104 pp.

Smith, J. L. and Virmani, Y. P. (2000). "Materials and Methods for Corrosion Control of Reinforced and Prestressed Concrete Structures in New Construction," *Publication* No. FHWA-RD-00-081, Federal Highway Administration, McLean, VA, 82 pp.

South Dakota Department of Transportation. (1984). *Laboratory Performance on Corrosion Control Methods*, Interim Report, Research Program Division of Planning, Pierre, SD, 38 pp.

Steinbach, O.F., and King, C.V. (1950). *Experiments in Physical Chemistry*, American Book Company, New York, 250 pp.

Stern, M. and Weisert, E.D. (1958). "Experimental Observations on the relations between Polarization Resistance and Corrosion Rate," *Proceedings of the American Society for Testing Materials*, Vol. 59, pp. 1280-1290.

Torres-Acosta, A. A. and Sagües, A. A. (2004). "Concrete Cracking by Localized Steel Corrosion - Geometric Effects," *ACI Materials Journal*, Vol. 101, No. 6, pp. 501-507.

Tourney, P. and Berke, N. (1993). "A Call for Standardized Tests for Corrosion-Inhibiting Admixtures," *Concrete International*, Vol. 15, No. 4, pp. 57-62.

Trejo, D. and Monteiro, P. J. (2005). "Corrosion Performance of Conventional (ASTM A615) and Low-Alloy (ASTM A706) Reinforcing Bars Embedded in Concrete and Exposed to Chloride Environments," *Cement and Concrete Research*, Vol. 35, No. 3, pp. 562-571.

Trépanier S. M., Hope, B. B., and Hansson, C. M. (2001). "Corrosion inhibitors in concrete – Part III: Effect on Time to Chloride-Induced Corrosion Initiation and Subsequent Corrosion Rates of Steel in Mortar," *Cement and Concrete Research*, Vol. 31, No. 5, pp. 713-718.

Virmani, Y. P. (1990). "Effectiveness of Calcium Nitrite Admixtures as a Corrosion Inhibitor," *Public Roads*, Vol. 54, No. 1, pp. 171-182.

Virmani, Y. P., Clear, K. C., and Pasko, T. J. (1983). "Time-to-Corrosion of Reinforcing Steel in Concrete Slabs, Volume 5, Calcium Nitrite Admixture and Epoxy-Coated Reinforcing bars as Corrosion Protection Systems," *Publication* No. FHWA-RD-83-012, Federal Highway Administration, McLean, VA, 76 pp.

Weyers, R. E., Prowell, B. D., Sprinkel, M. M., and Vorster, M. (1993) "Concrete Bridge Protection, Repair, and Rehabilitation Relative to Reinforcement Corrosion: A Methods Application Manual," *Strategic Highway Research Program Report* No. SHRP-S-360, National Research Council, Washington, D.C., pp. 3, 44-45.

Weyers, R. E., Sprinkel, M. M., Pyc, W., Zemajtis, J., Liu, Y., and Mokarem, D. (1998). "Field Investigation of the Corrosion Protection Performance of Bridge Decks and Piles Constructed with Epoxy-Coated Reinforcing Steel in Virginia", *VTRC 98-R4*, Virginia Transportation Research Council, 38 pp.

Yeomans, S.R. (1994). "Performance of Black, Galbanized, and Epoxy-Coated Reinforcing Steels in Chloride-Contaminated Concrete," *Corrosion*, Vol. 50, No. 1, pp. 72-80.

Yonezawa, T., Ashworth, V., and Procter, R. P. M. (1988). "Study of the Pore Solution Composition and Chloride Effects in the Corrosion of Steel in Concrete," *Corrosion*, Vol. 44, No. 7, pp. 489-499.

Yunovich, M., Thompson, N. G., Balvanyos, T., and Lave, L. (2002). "Highway Bridges," Appendix D, *Corrosion Cost and Preventive Strategies in the United States*, by G. H. Koch, M. PO., H. Broongers, N. G. Thompson, Y. P. Virmani, and J. H. Payer, Report No. FHWA-RD-01-156, Federal Highway Administration, McLean, VA, 773 pp.

Zemajtis, J., Weyers, R. E., and Sprinkel, M. M. (1999). "Performance Evaluation of Corrosion Inhibitors and Galvanized Steel in Concrete Exposure Specimens", *VTRC 99-CR4*, Virginia Transportation Research Council, 67 pp.

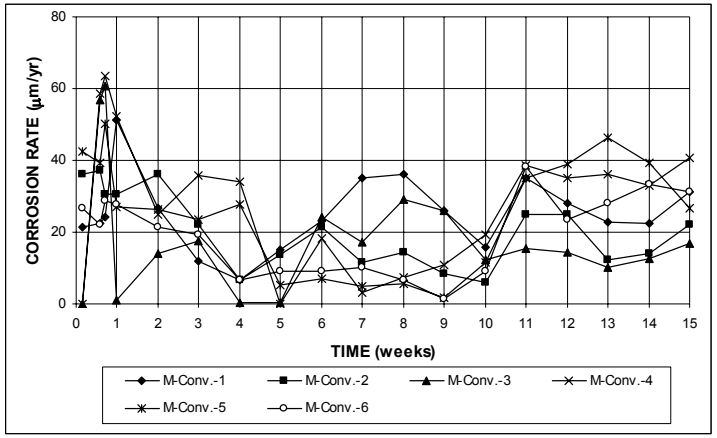

(a)

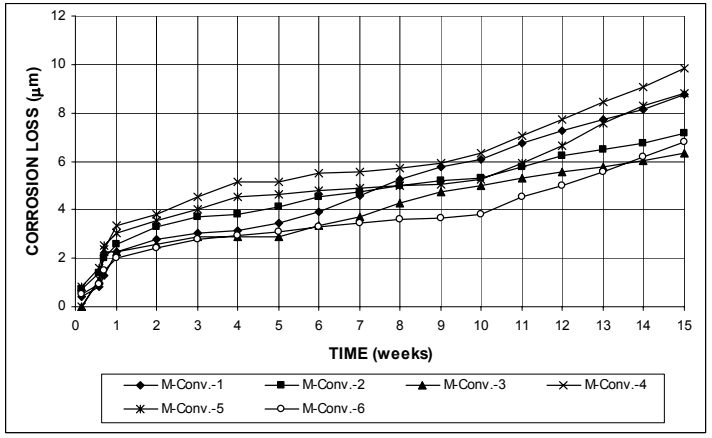

(b)

Figure A.1 – (a) Corrosion rates and (b) total corrosion losses as measured in the rapid macrocell test for bare bar specimens with conventional steel.

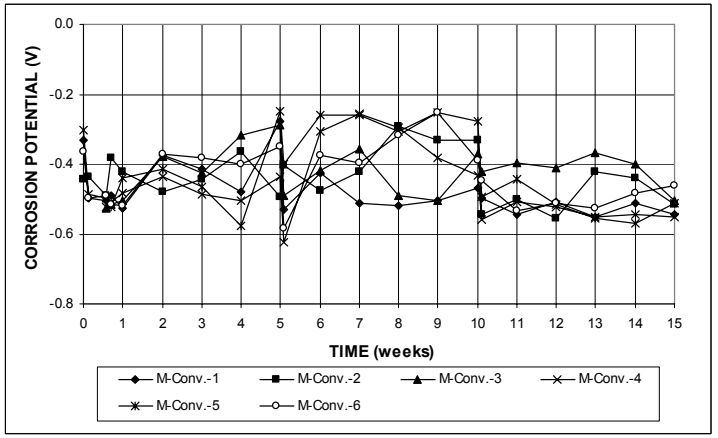

(a)

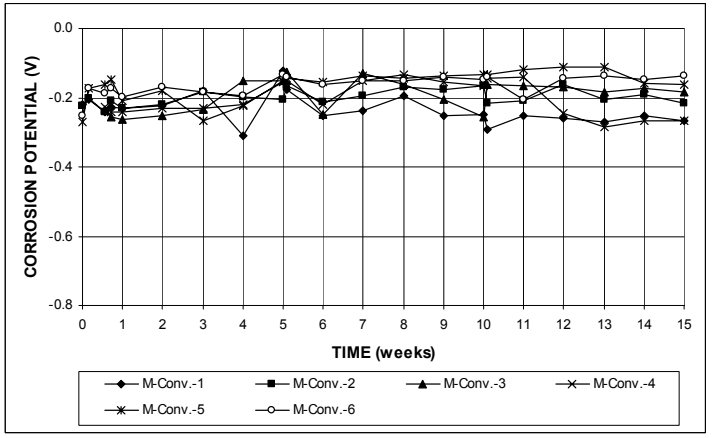

(b)

Figure A.2 – (a) Anode corrosion potentials and (b) cathode corrosion potentials with respect to saturated calomel electrode as measured in the rapid macrocell test for bare bar specimens with conventional steel.

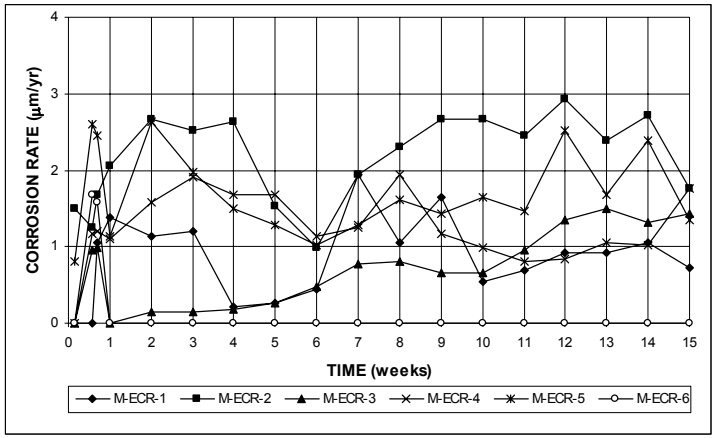

(a)

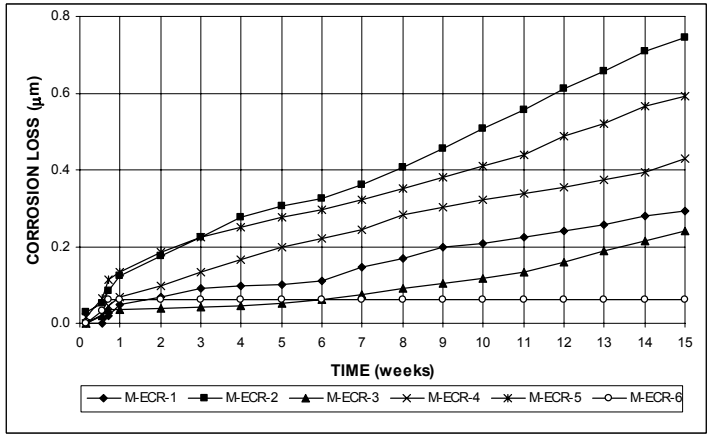

(b)

Figure A.3 – (a) Corrosion rates and (b) total corrosion losses based on the total area of the bar as measured in the rapid macrocell test for bare bar specimens with ECR (four 3-mm ($^1/_8$-in.) diameter holes).

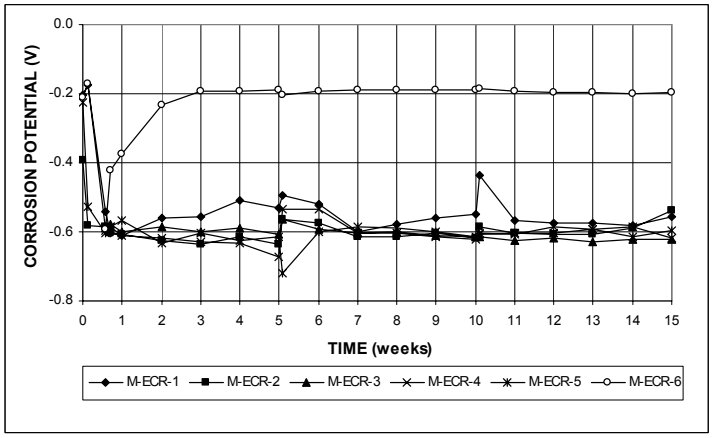

(a)

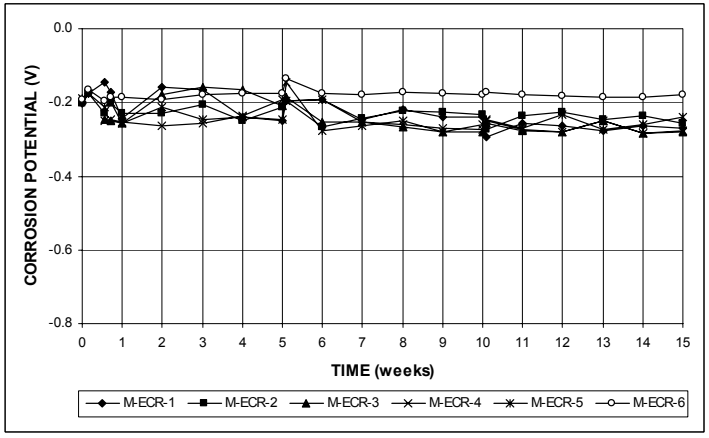

(b)

Figure A.4 – (a) Anode corrosion potentials and (b) cathode corrosion potentials with respect to saturated calomel electrode as measured in the rapid macrocell test for bare bar specimens with ECR (four 3-mm ($^1/_8$-in.) diameter holes).

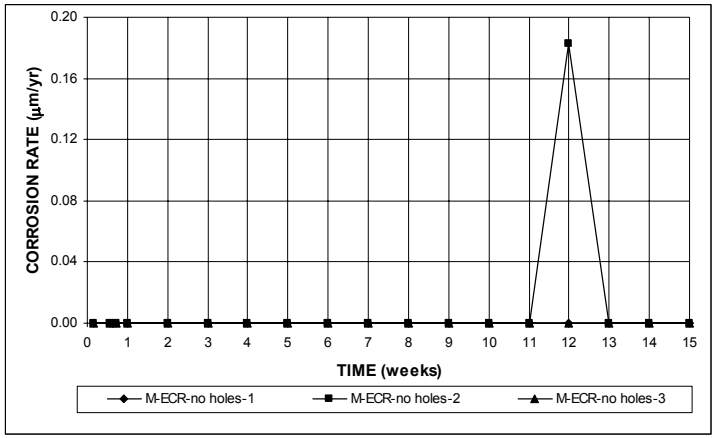

(a)

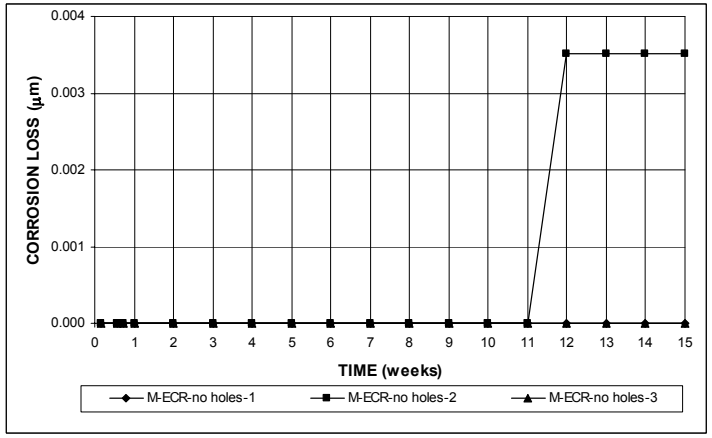

(b)

Figure A.5 – (a) Corrosion rates and (b) total corrosion losses of the bar as measured in the rapid macrocell test for bare bar specimens with ECR without holes.

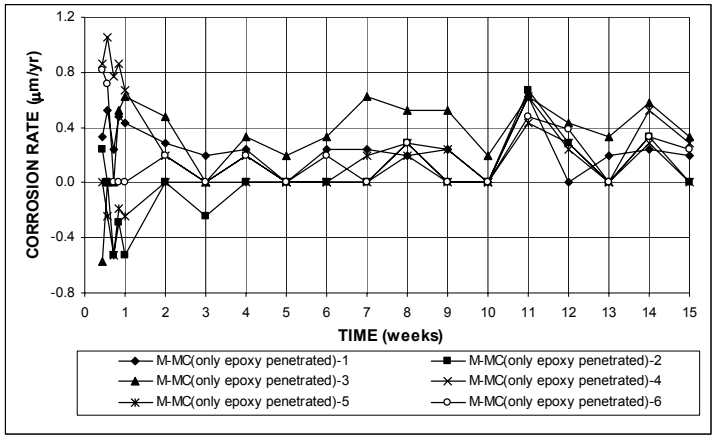

(a)

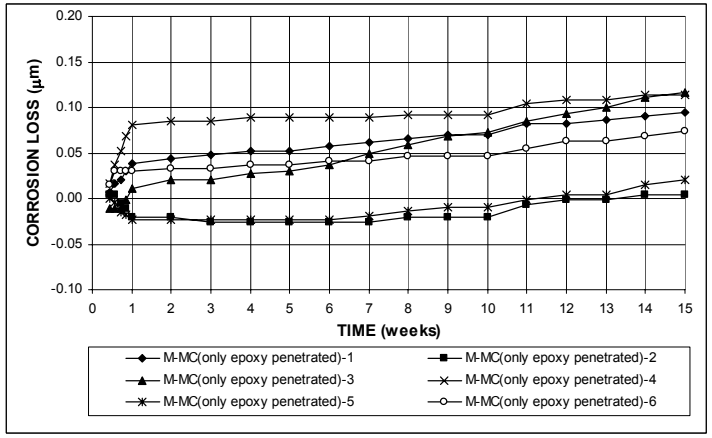

(b)

Figure A.6 – (a) Corrosion rates and (b) total corrosion losses based on the total area of the bar as measured in the rapid macrocell test for bare bar specimens with multiple coated bar (four 3-mm ($^1/_8$-in.) diameter holes, only epoxy penetrated).

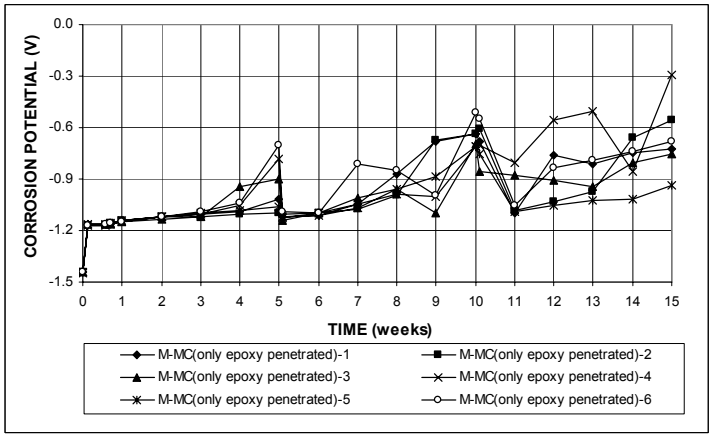

(a)

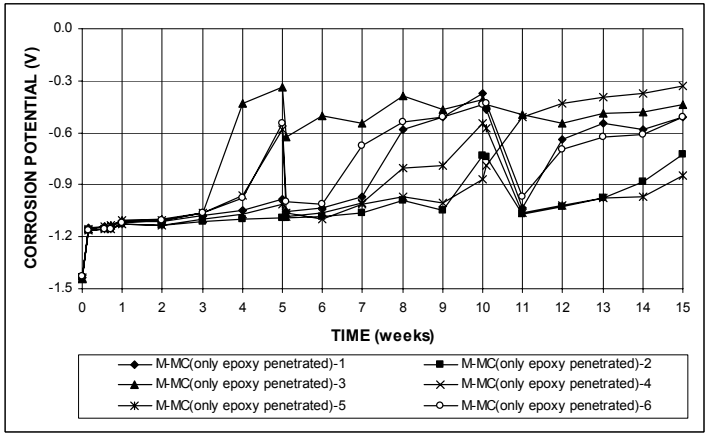

(b)

Figure A.7 – (a) Anode corrosion potentials and (b) cathode corrosion potentials with respect to saturated calomel electrode as measured in the rapid macrocell test for bare bar specimens with multiple coated bar (four 3-mm ($^1/_8$-in.) diameter holes, only epoxy penetrated).

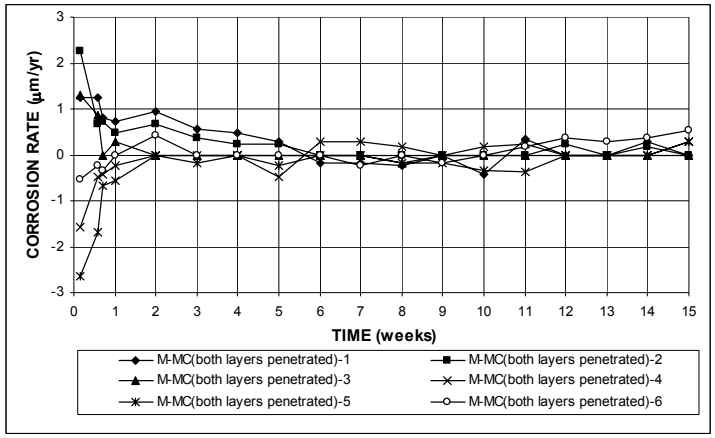

(a)

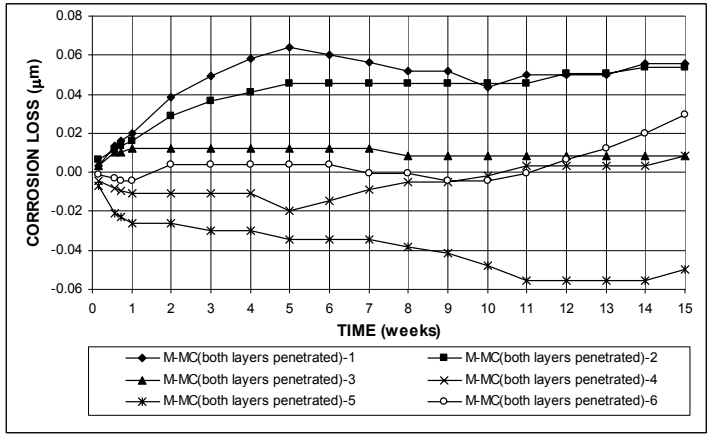

(b)

Figure A.8 – (a) Corrosion rates and (b) total corrosion losses based on the total area of the bar as measured in the rapid macrocell test for bare bar specimens with multiple coated bar (four 3-mm ($^1/_8$-in.) diameter holes, both layers penetrated).

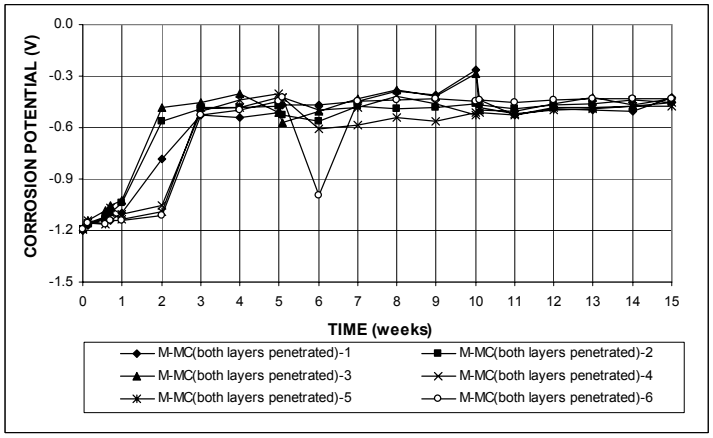

(a)

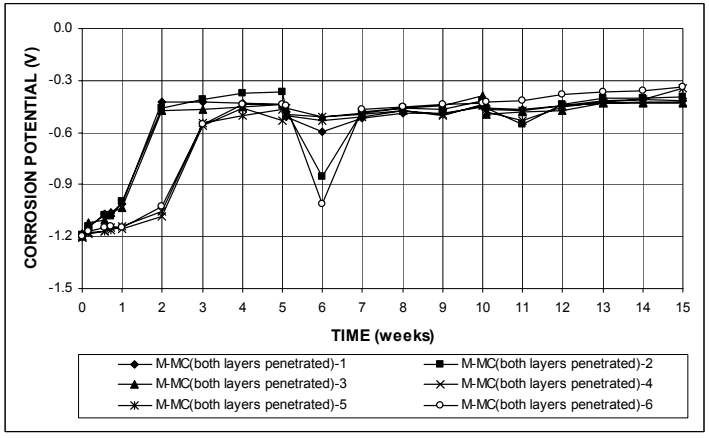

(b)

Figure A.9 – (a) Anode corrosion potentials and (b) cathode corrosion potentials with respect to saturated calomel electrode as measured in the rapid macrocell test for bare bar specimens with multiple coated bar (four 3-mm ($^1/_8$-in.) diameter holes, both layers penetrated).

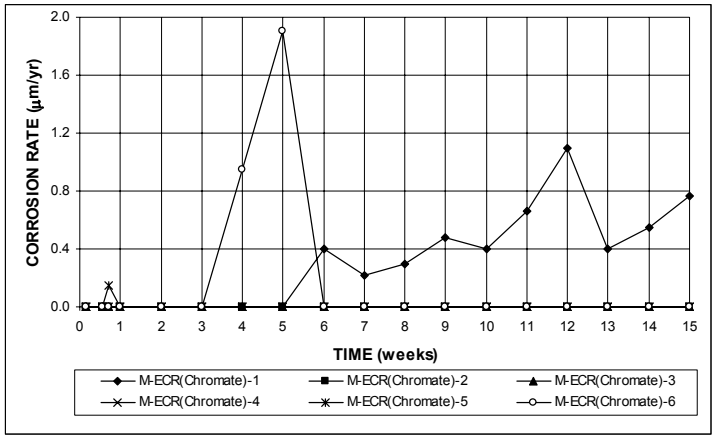

(a)

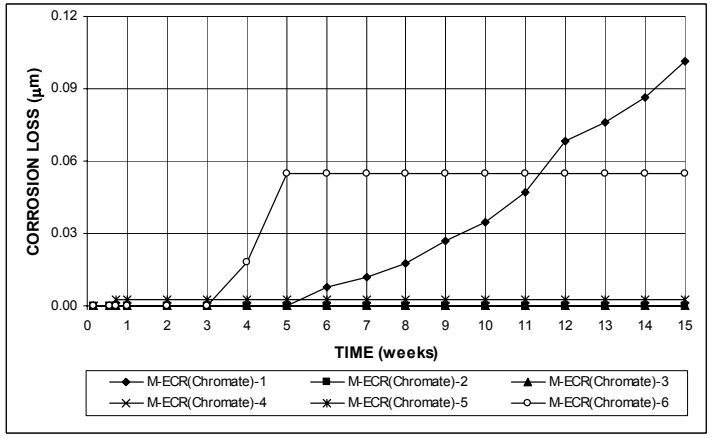

(b)

Figure A.10 – (a) Corrosion rates and (b) total corrosion losses based on the total area of the bar as measured in the rapid macrocell test for bare bar specimens with ECR with chromate pretreatment (four 3-mm ($^1/_8$-in.) diameter holes).

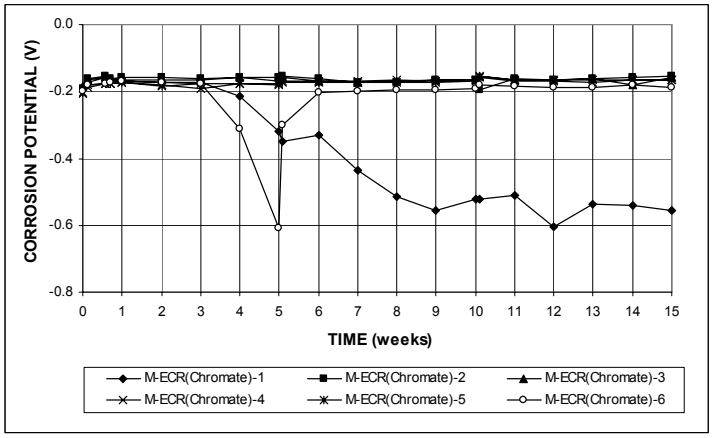

(a)

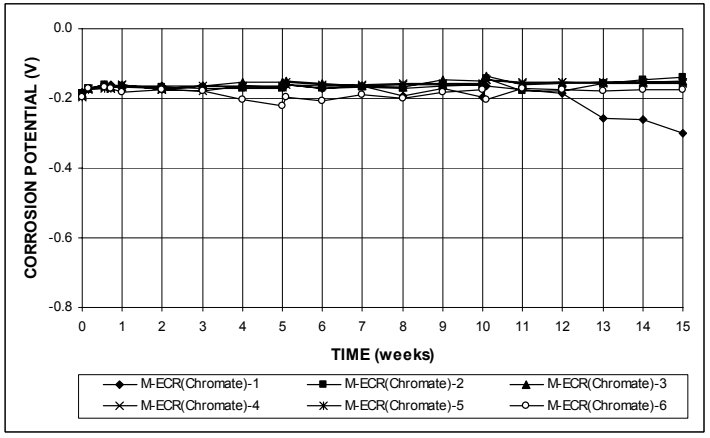

(b)

Figure A.11 – (a) Anode corrosion potentials and (b) cathode corrosion potentials with respect to saturated calomel electrode as measured in the rapid macrocell test for bare bar specimens with ECR with chromate pretreatment (four 3-mm ($^1/_8$-in.) diameter holes).

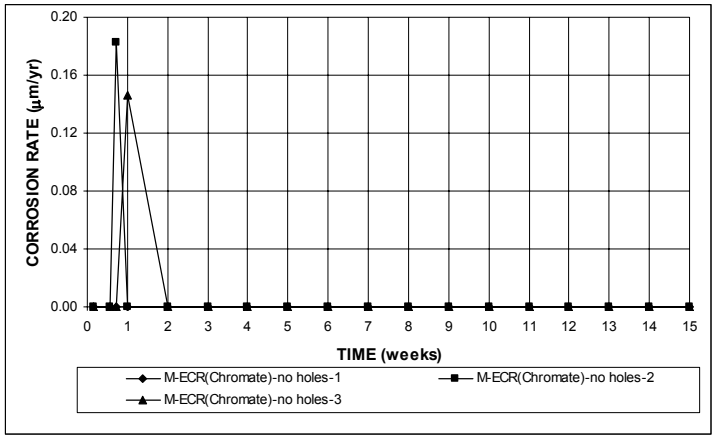

(a)

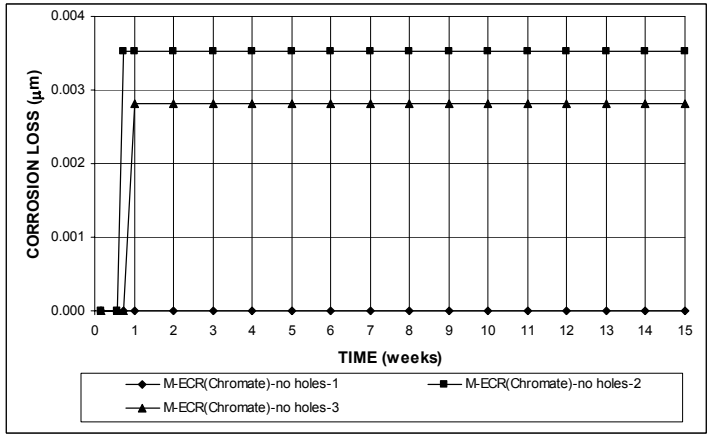

(b)

Figure A.12 – (a) Corrosion rates and (b) total corrosion losses as measured in the rapid macrocell test for bare bar specimens with ECR with chromate pretreatment without holes.

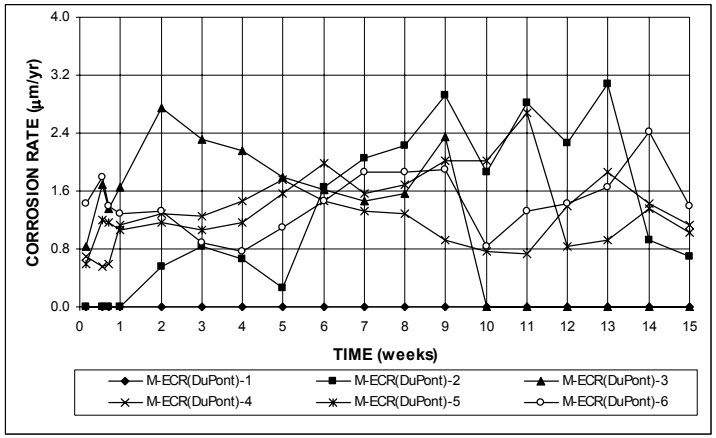

(a)

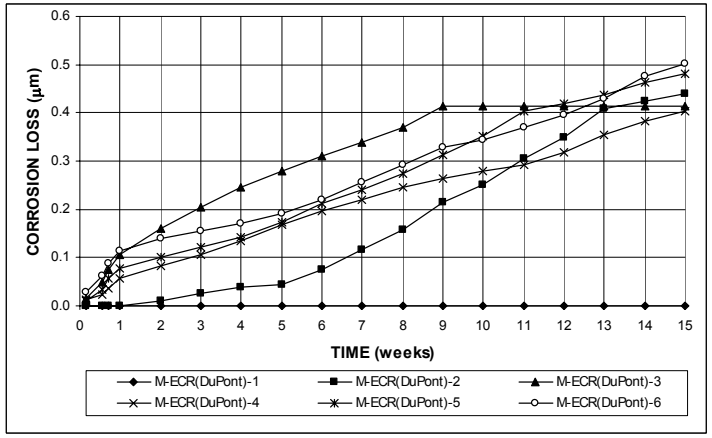

(b)

Figure A.13 – (a) Corrosion rates and (b) total corrosion losses based on the total area of the bar as measured in the rapid macrocell test for bare bar specimens with ECR with DuPont coating (four 3-mm ($^1/_8$-in.) diameter holes).

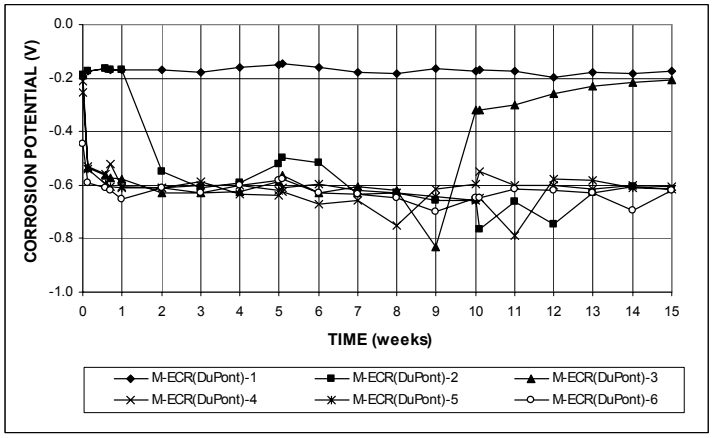

(a)

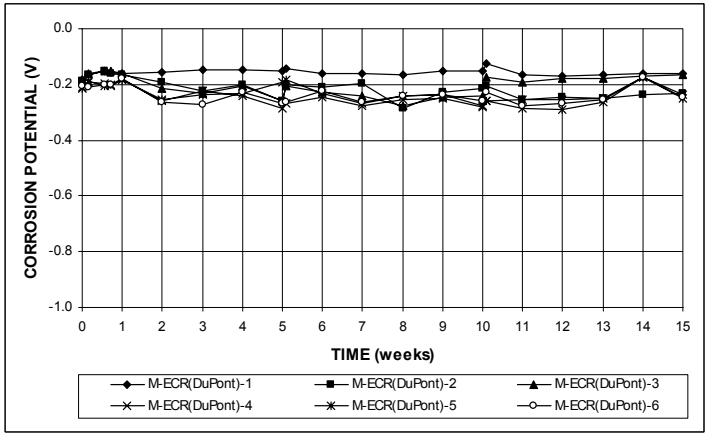

(b)

Figure A.14 – (a) Anode corrosion potentials and (b) cathode corrosion potentials with respect to saturated calomel electrode as measured in the rapid macrocell test for bare bar specimens with ECR with DuPont coating (four 3-mm ($^1/_8$-in.) diameter holes).

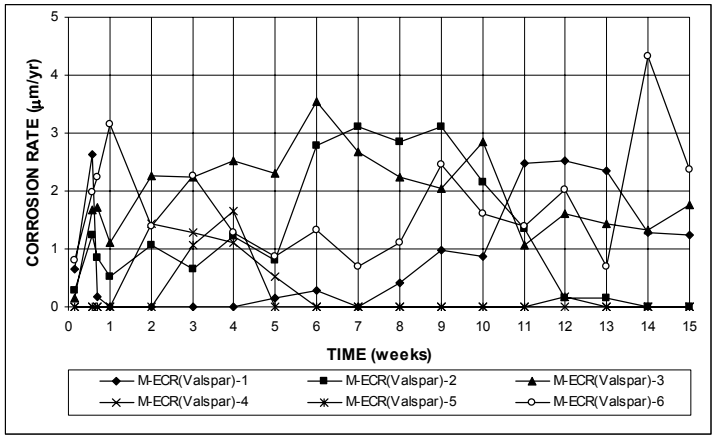

(a)

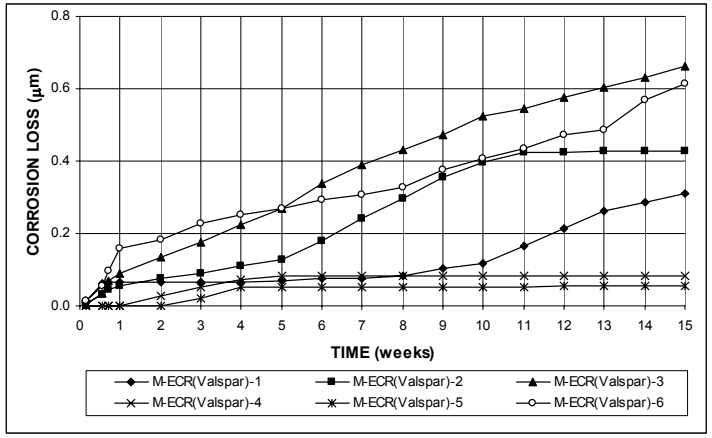

(b)

Figure A.15 – (a) Corrosion rates and (b) total corrosion losses based on the total area of the bar as measured in the rapid macrocell test for bare bar specimens with ECR with Valspar coating (four 3-mm ($^1/_8$-in.) diameter holes).

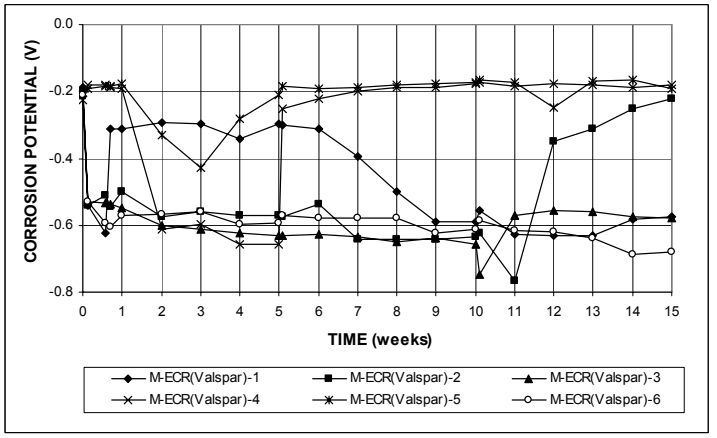

(a)

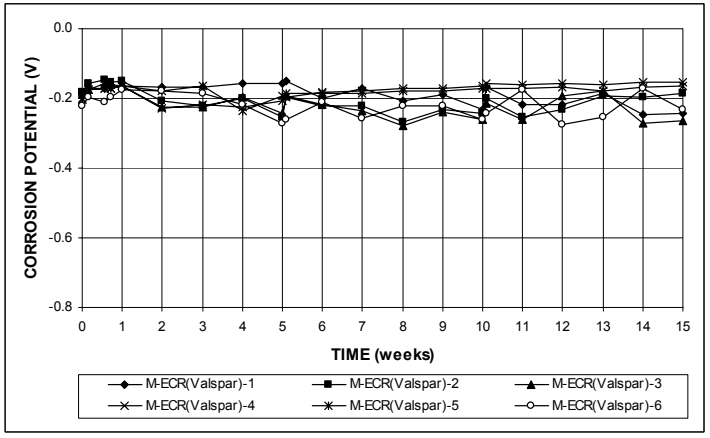

(b)

Figure A.16 – (a) Anode corrosion potentials and (b) cathode corrosion potentials with respect to saturated calomel electrode as measured in the rapid macrocell test for bare bar specimens with ECR with Valspar coating (four 3-mm ($^1/_8$-in.) diameter holes).

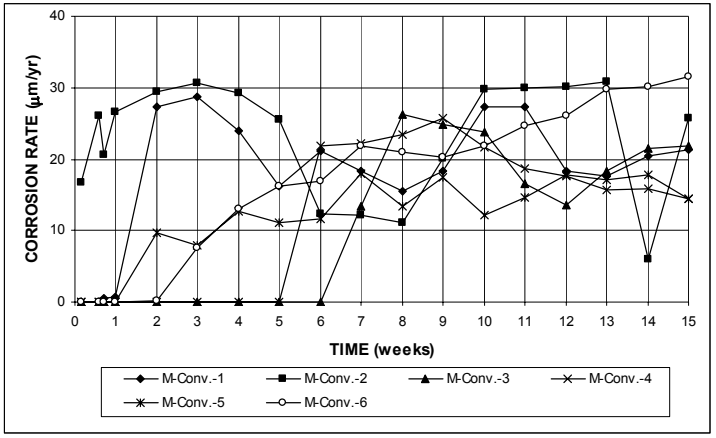

(a)

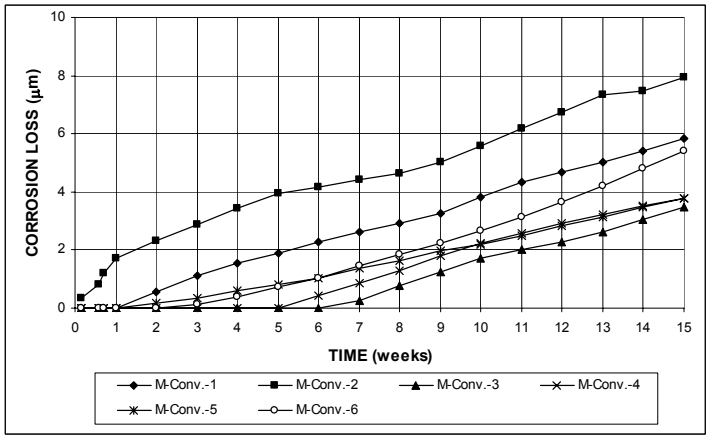

(b)

Figure A.17 – (a) Corrosion rates and (b) total corrosion losses as measured in the rapid macrocell test for mortar-wrapped specimens with conventional steel.

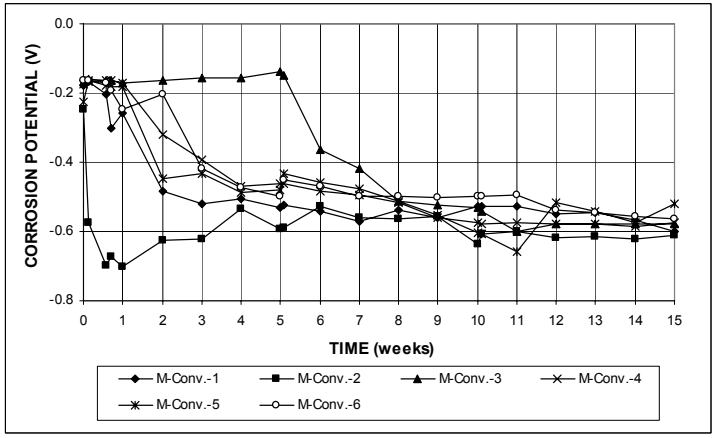

(a)

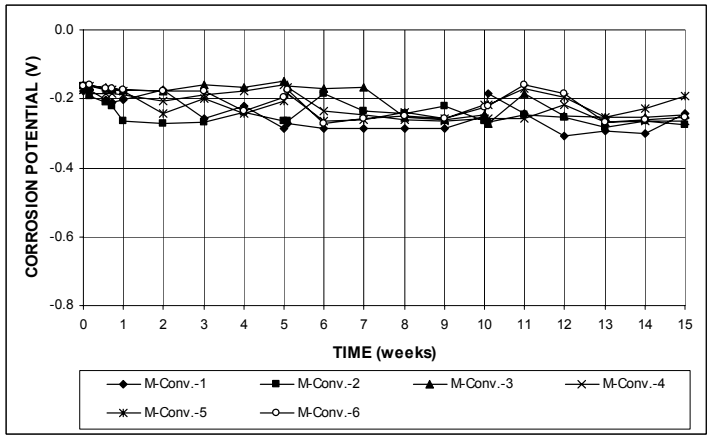

(b)

Figure A.18 – (a) Anode corrosion potentials and (b) cathode corrosion potentials with respect to saturated calomel electrode as measured in the rapid macrocell test for mortar-wrapped specimens with conventional steel.

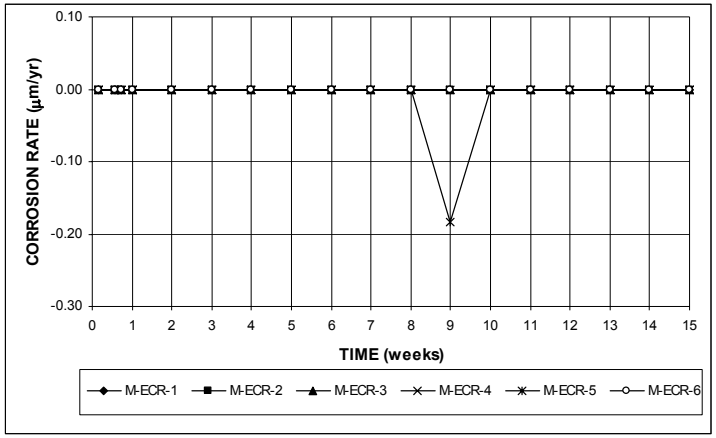

(a)

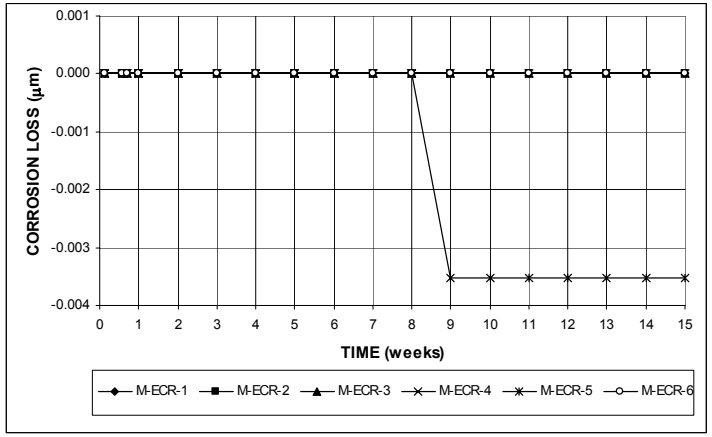

(b)

Figure A.19 – (a) Corrosion rates and (b) total corrosion losses based on the total area of the bar as measured in the rapid macrocell test for mortar-wrapped specimens with ECR (four 3-mm ($^1/_8$-in.) diameter holes).

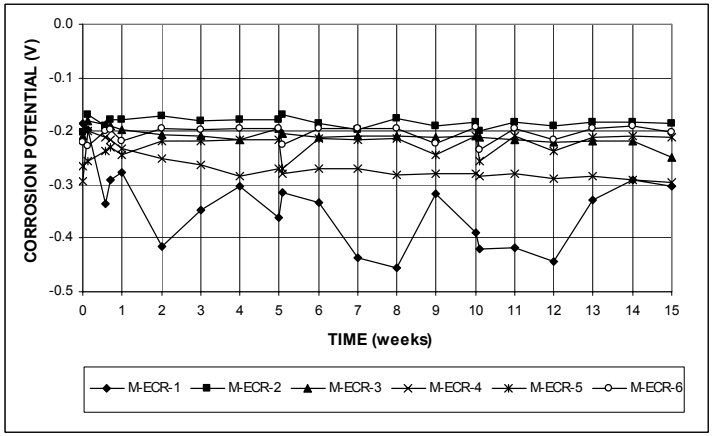

(a)

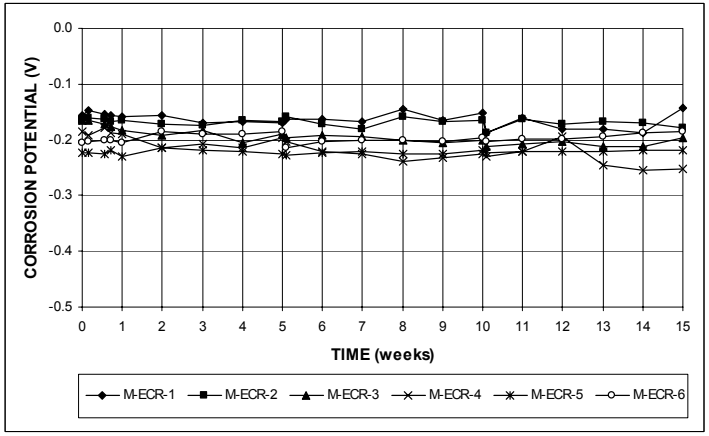

(b)

Figure A.20 – (a) Anode corrosion potentials and (b) cathode corrosion potentials with respect to saturated calomel electrode as measured in the rapid macrocell test for mortar-wrapped specimens with ECR (four 3-mm ($^1/_8$-in.) diameter holes).

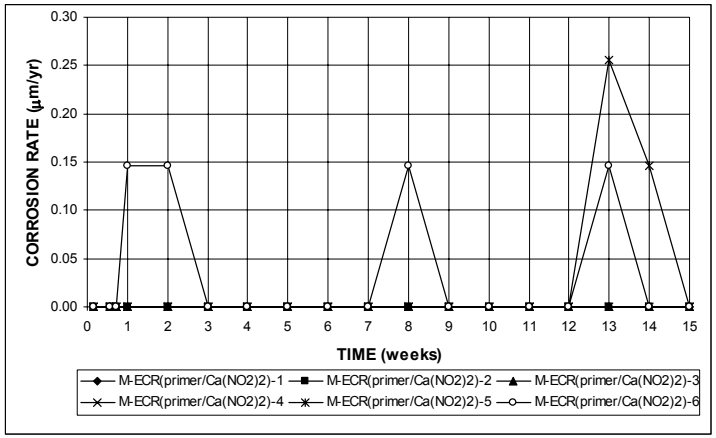

(a)

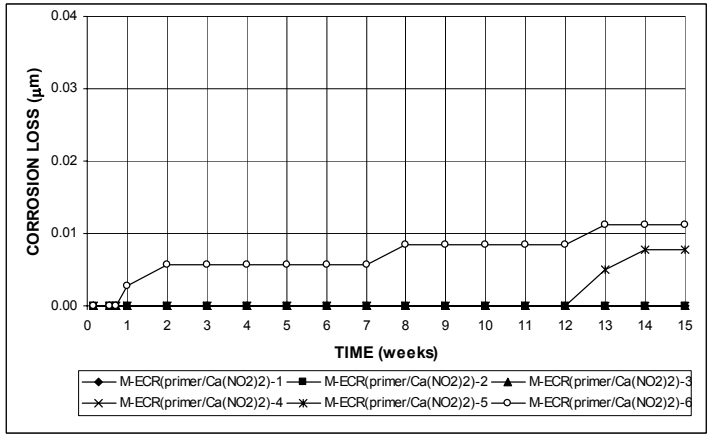

(b)

Figure A.21 – (a) Corrosion rates and (b) total corrosion losses based on the total area of the bar as measured in the rapid macrocell test for mortar-wrapped specimens with ECR with a primer containing calcium nitrite (four 3-mm ($^1/_8$-in.) diameter holes).

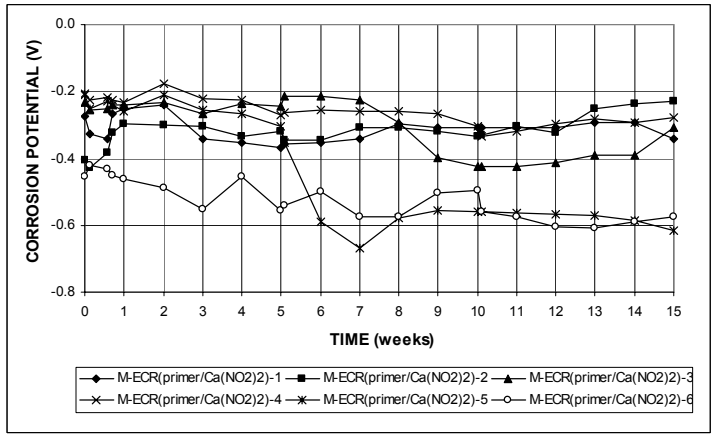

(a)

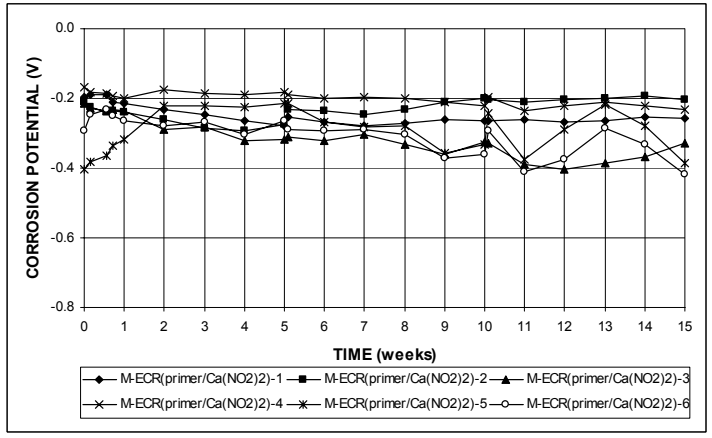

(b)

Figure A.22 – (a) Anode corrosion potentials and (b) cathode corrosion potentials with respect to saturated calomel electrode as measured in the rapid macrocell test for mortar-wrapped specimens with ECR with a primer containing calcium nitrite (four 3-mm ($^1/_8$-in.) diameter holes).

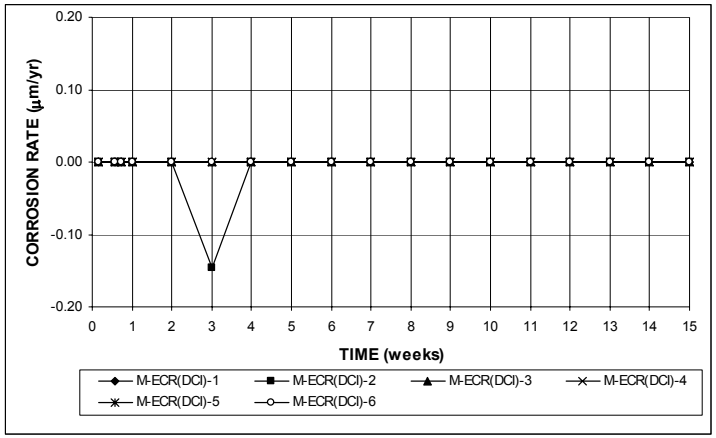

(a)

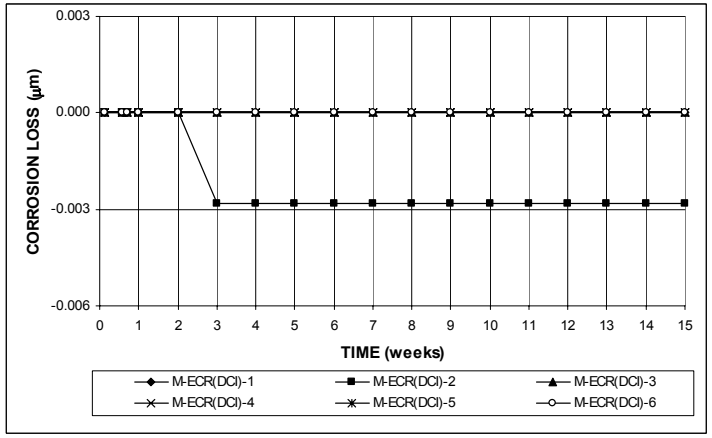

(b)

Figure A.23 – (a) Corrosion rates and (b) total corrosion losses based on the total area of the bar as measured in the rapid macrocell test for mortar-wrapped specimens with ECR in mortar with DCI (four 3-mm ($^1/_8$-in.) diameter holes).

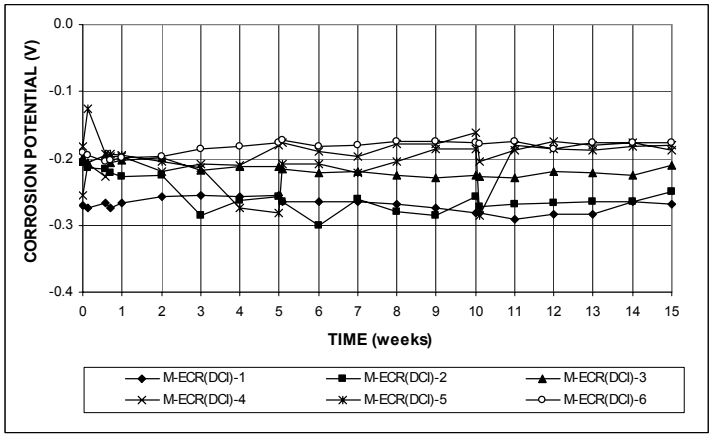

(a)

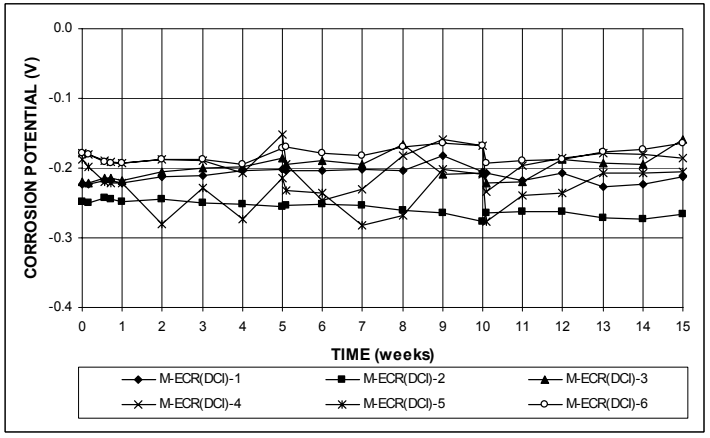

(b)

Figure A.24 – (a) Anode corrosion potentials and (b) cathode corrosion potentials with respect to saturated calomel electrode as measured in the rapid macrocell test for mortar-wrapped specimens with ECR in mortar with DCI (four 3-mm ($^1/_8$-in.) diameter holes).

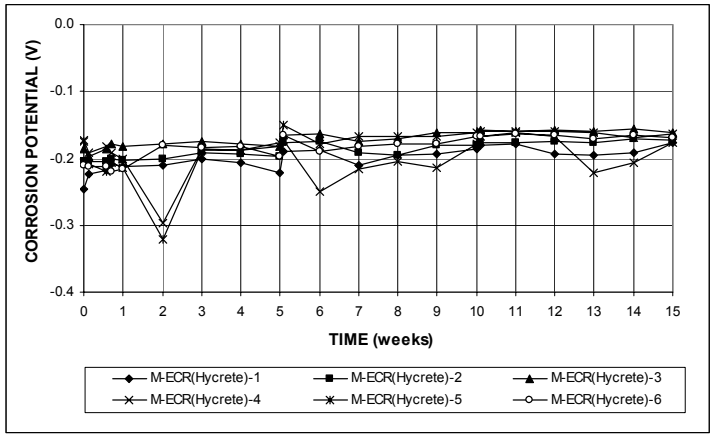

(a)

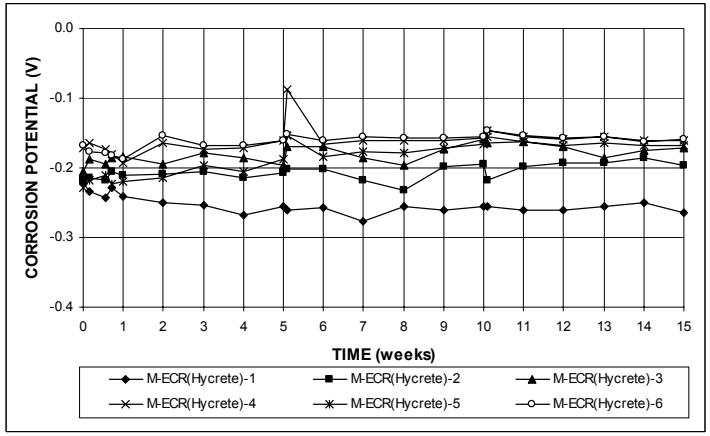

(b)

Figure A.25 – (a) Anode corrosion potentials and (b) cathode corrosion potentials with respect to saturated calomel electrode as measured in the rapid macrocell test for mortar-wrapped specimens with ECR in mortar with Hycrete (four 3-mm ($^1/_8$-in.) diameter holes).

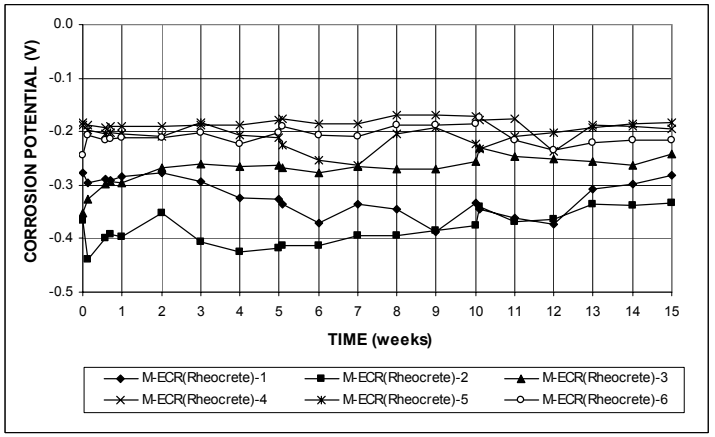

(a)

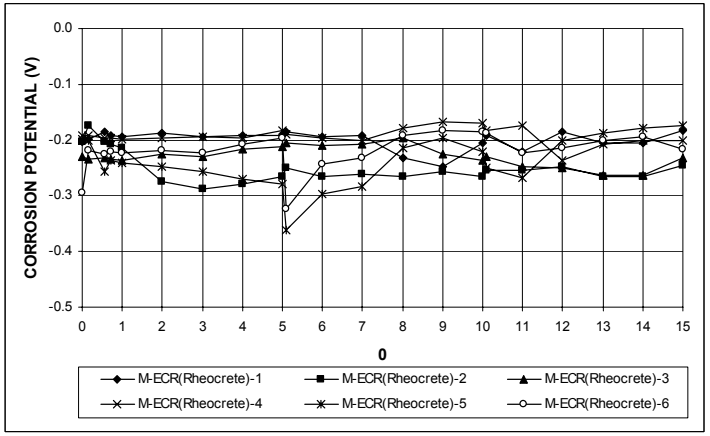

(b)

Figure A.26 – (a) Anode corrosion potentials and (b) cathode corrosion potentials with respect to saturated calomel electrode as measured in the rapid macrocell test for mortar-wrapped specimens with ECR in mortar with Rheocrete (four 3-mm ($^1/_8$-in.) diameter holes).

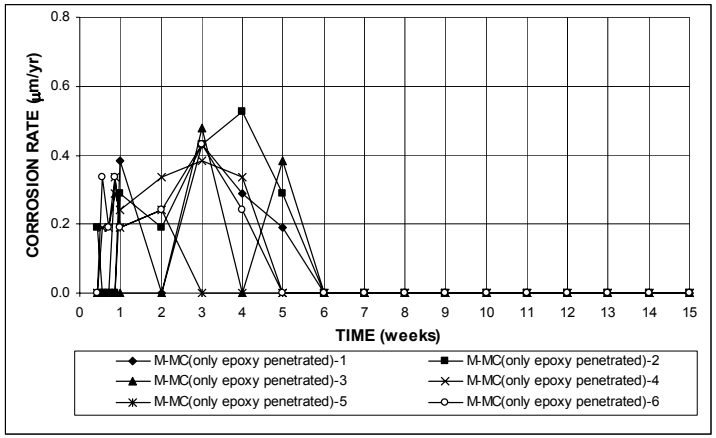

(a)

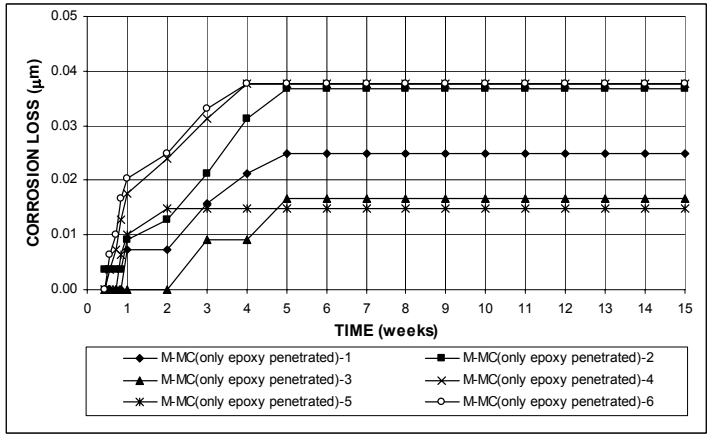

(b)

Figure A.27 – (a) Corrosion rates and (b) total corrosion losses based on the total area of the bar as measured in the rapid macrocell test for mortar-wrapped specimens with multiple coated bar (four 3-mm ($^1/_8$-in.) diameter holes, only epoxy penetrated).

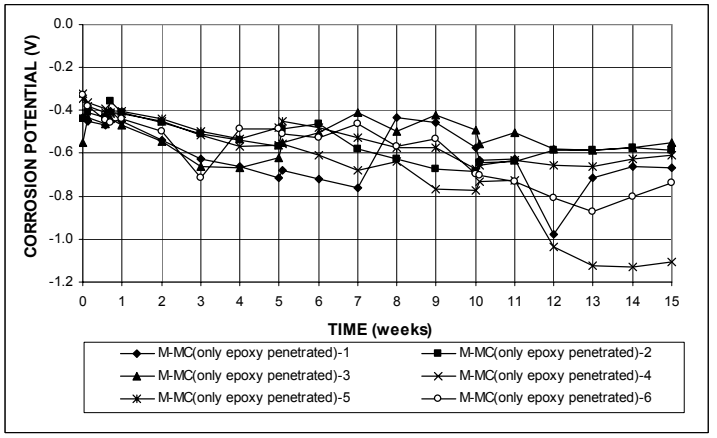

(a)

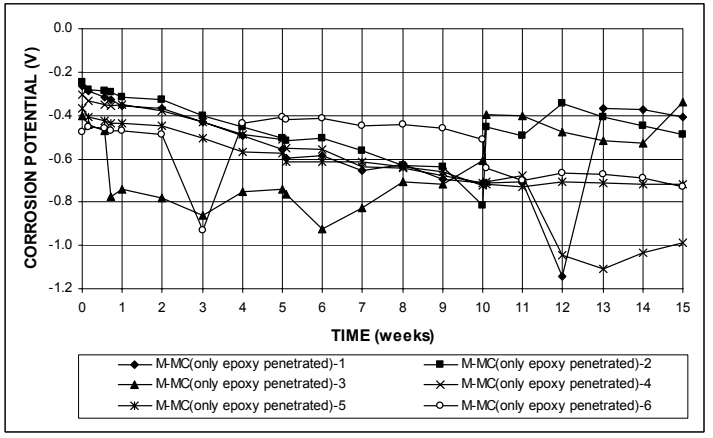

(b)

Figure A.28 – (a) Anode corrosion potentials and (b) cathode corrosion potentials with respect to saturated calomel electrode as measured in the rapid macrocell test for mortar-wrapped specimens with multiple coated bar (four 3-mm ($^1/_8$-in.) diameter holes, only epoxy penetrated).

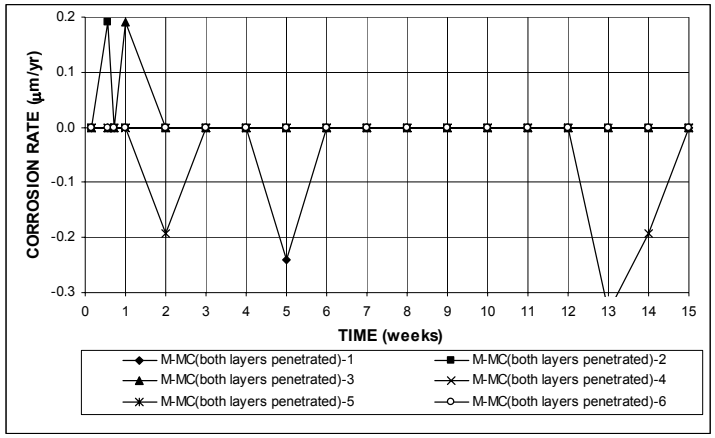

(a)

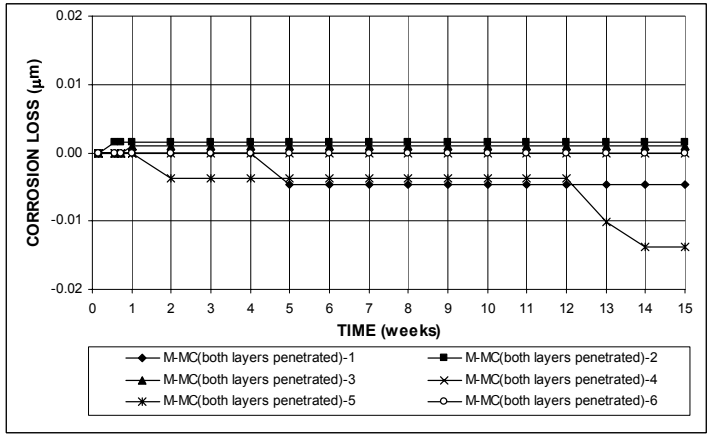

(b)

Figure A.29 – (a) Corrosion rates and (b) total corrosion losses based on the total area of the bar as measured in the rapid macrocell test for mortar-wrapped specimens with multiple coated bar (four 3-mm ($^1/_8$-in.) diameter holes, both layers penetrated).

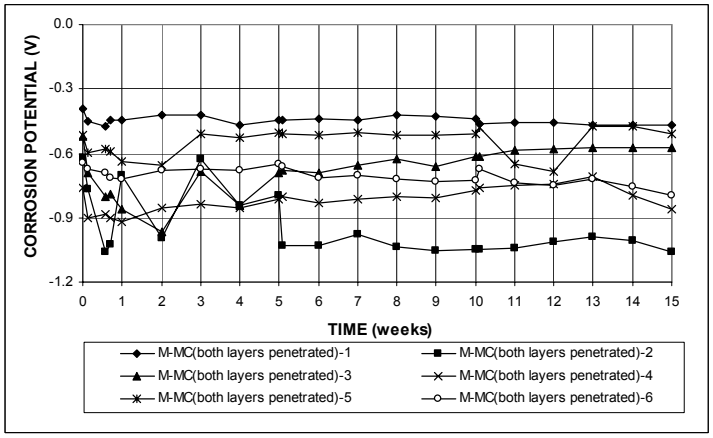

(a)

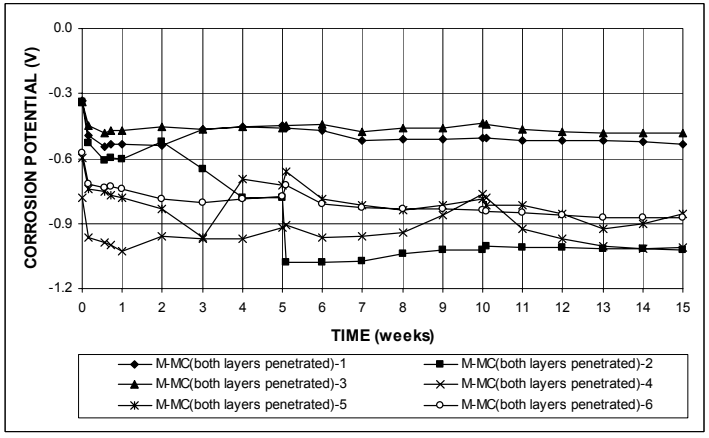

(b)

Figure A.30 – (a) Anode corrosion potentials and (b) cathode corrosion potentials with respect to saturated calomel electrode as measured in the rapid macrocell test for mortar-wrapped specimens with multiple coated bar (four 3-mm ($^1/_8$-in.) diameter holes, both layers penetrated).

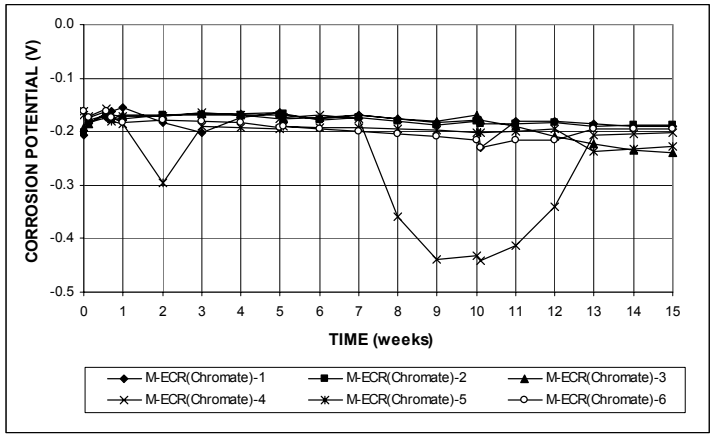

(a)

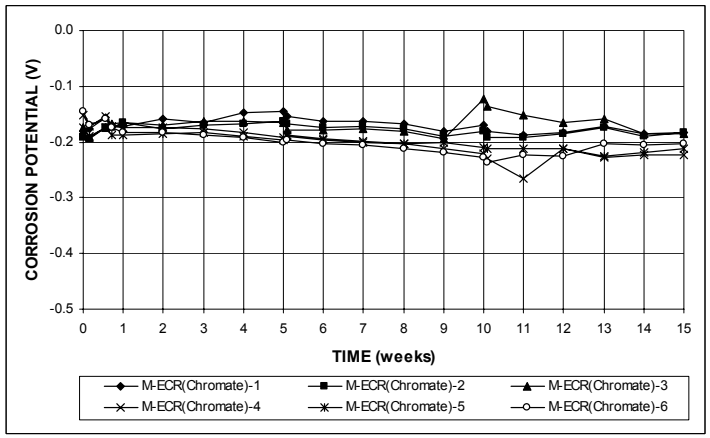

(b)

Figure A.31 – (a) Anode corrosion potentials and (b) cathode corrosion potentials with respect to saturated calomel electrode as measured in the rapid macrocell test for mortar-wrapped specimens with ECR with chromate pretreatment (four 3-mm ($^1/_8$-in.) diameter holes).

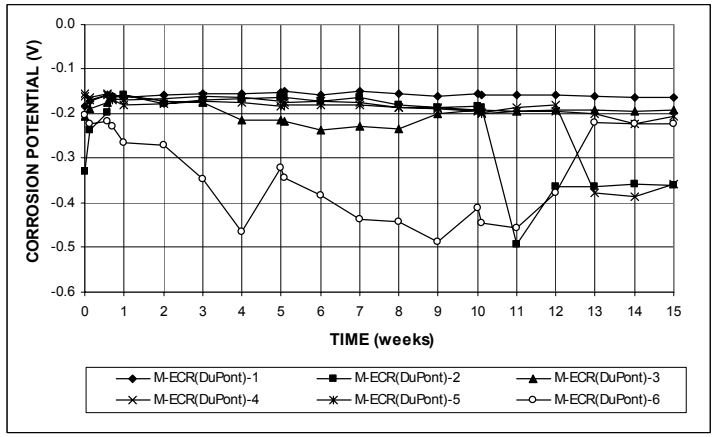

(a)

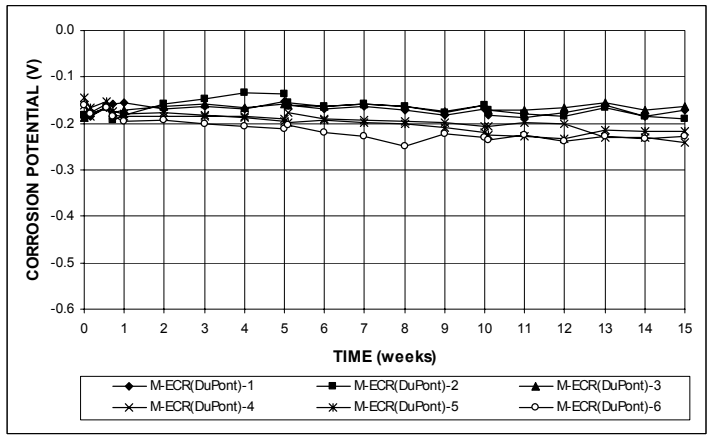

(b)

Figure A.32 – (a) Anode corrosion potentials and (b) cathode corrosion potentials with respect to saturated calomel electrode as measured in the rapid macrocell test for mortar-wrapped specimens with ECR with DuPont coating (four 3-mm ($^1/_8$-in.) diameter holes).

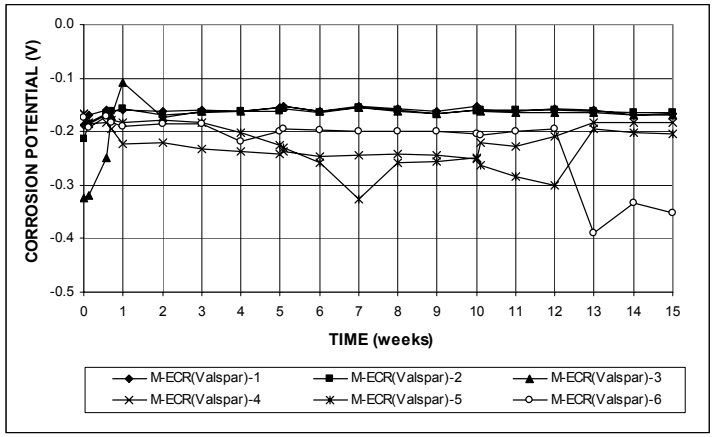

(a)

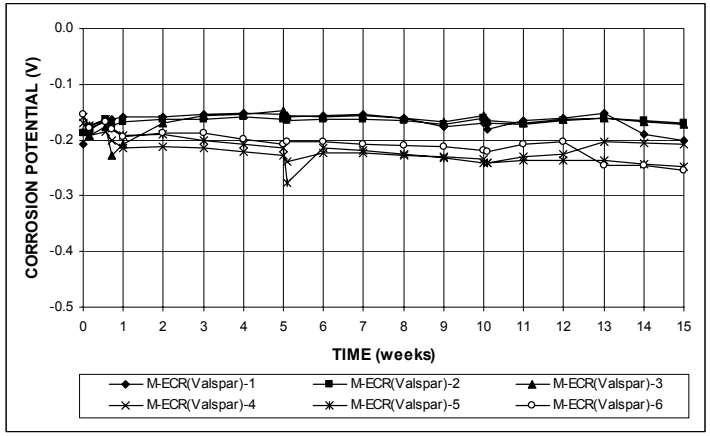

(b)

Figure A.33 – (a) Anode corrosion potentials and (b) cathode corrosion potentials with respect to saturated calomel electrode as measured in the rapid macrocell test for mortar-wrapped specimens with ECR with Valspar coating (four 3-mm ($^{1}/_{8}$-in.) diameter holes).

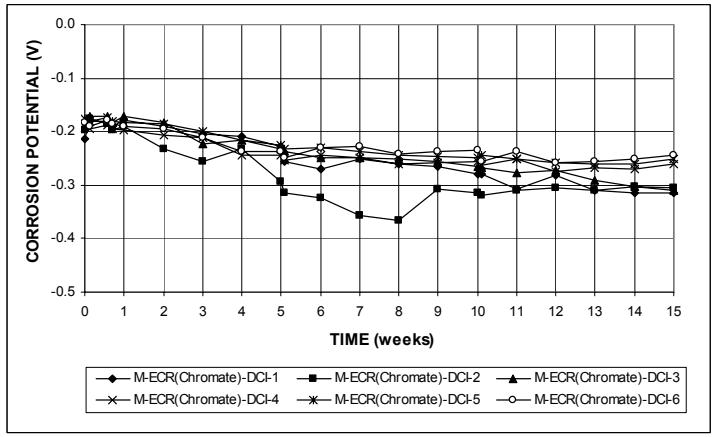

(a)

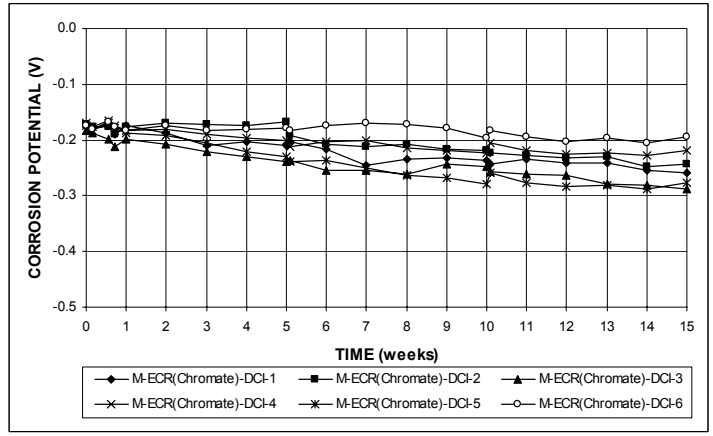

(b)

Figure A.34 – (a) Anode corrosion potentials and (b) cathode corrosion potentials with respect to saturated calomel electrode as measured in the rapid macrocell test for mortar-wrapped specimens with ECR with chromate pretreatment (four 3-mm ($^{1}/_{8}$-in.) diameter holes) in mortar with DCI.

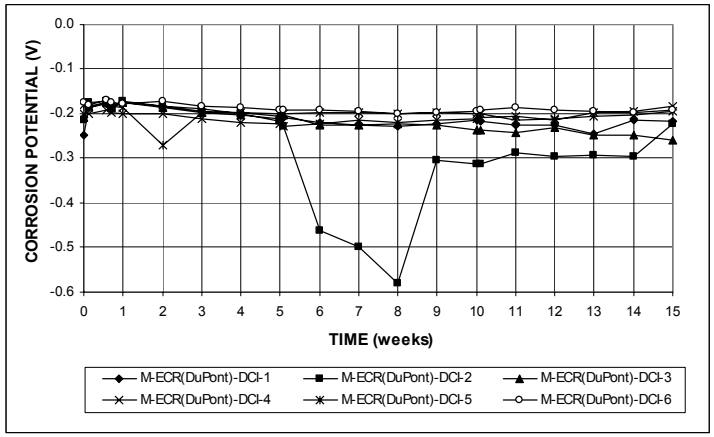

(a)

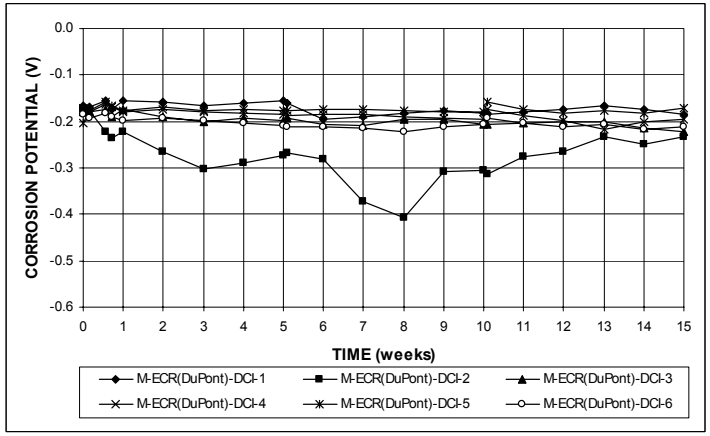

(b)

Figure A.35 – (a) Anode corrosion potentials and (b) cathode corrosion potentials with respect to saturated calomel electrode as measured in the rapid macrocell test for mortar-wrapped specimens with ECR with DuPont coating (four 3-mm ($^{1}/_{8}$-in.) diameter holes) in mortar with DCI.

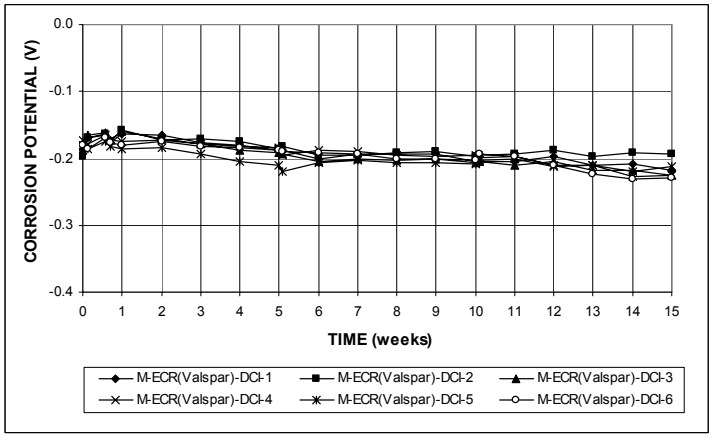

(a)

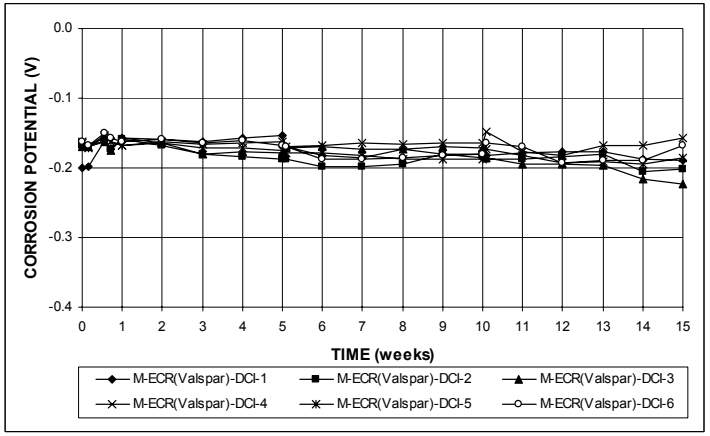

(b)

Figure A.36 – (a) Anode corrosion potentials and (b) cathode corrosion potentials with respect to saturated calomel electrode as measured in the rapid macrocell test for mortar-wrapped specimens with ECR with Valspar coating (four 3-mm ($^{1}/_{8}$-in.) diameter holes) in mortar with DCI.

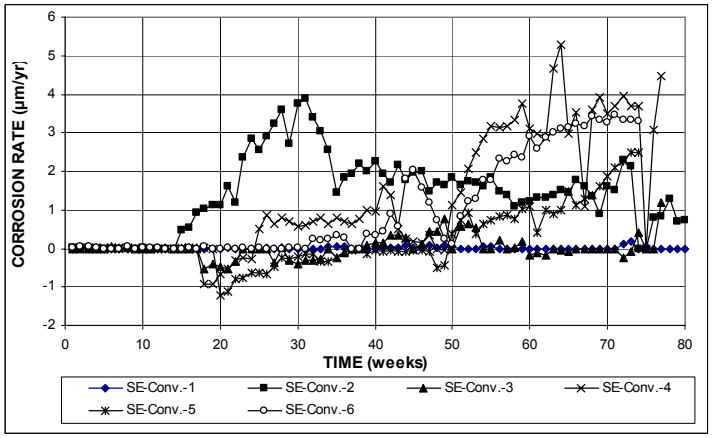

(a)

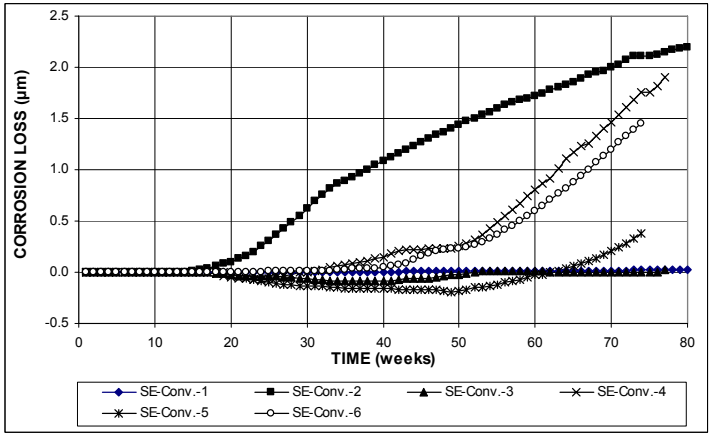

(b)

Figure A.37 – (a) Corrosion rates and (b) total corrosion losses as measured in the Southern Exposure test for specimens with conventional steel.

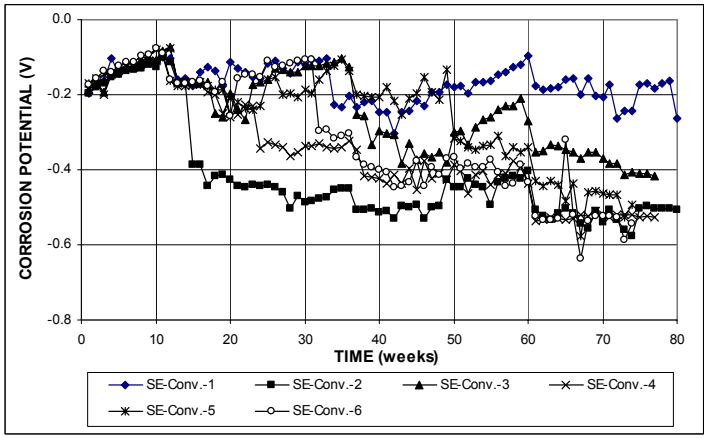

(a)

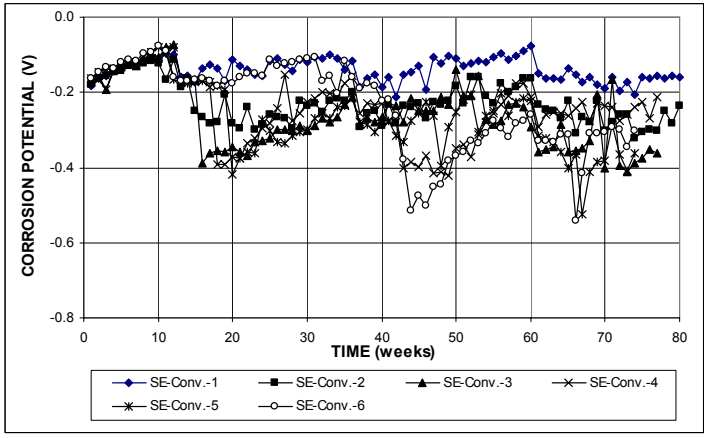

(b)

Figure A.38 – (a) Top mat corrosion potentials and (b) bottom mat corrosion potentials, with respect to copper-copper sulfate electrode as measured in the Southern Exposure test for specimens with conventional steel.

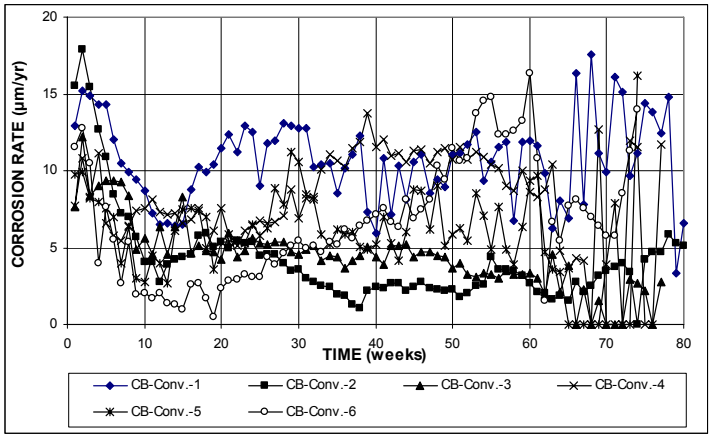

(a)

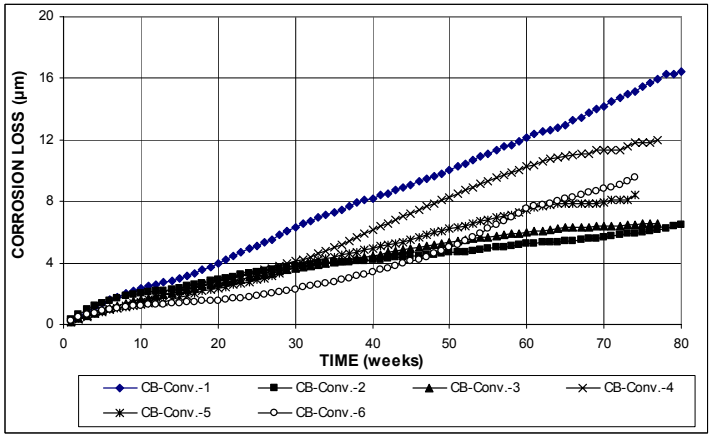

(b)

Figure A.39 – (a) Corrosion rates and (b) total corrosion losses as measured in the cracked beam test for specimens with conventional steel.

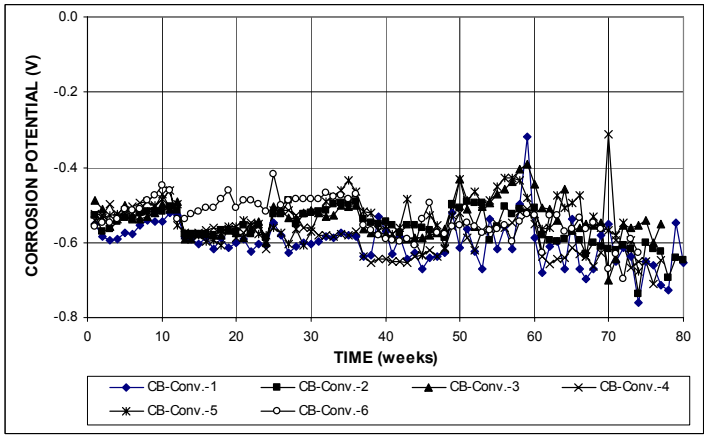

(a)

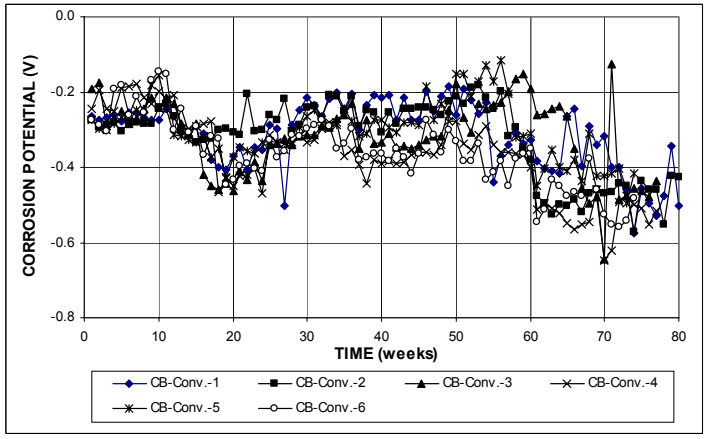

(b)

Figure A.40 – (a) Top mat corrosion potentials and (b) bottom mat corrosion potentials, with respect to copper-copper sulfate electrode as measured in the cracked beam test for specimens with conventional steel.

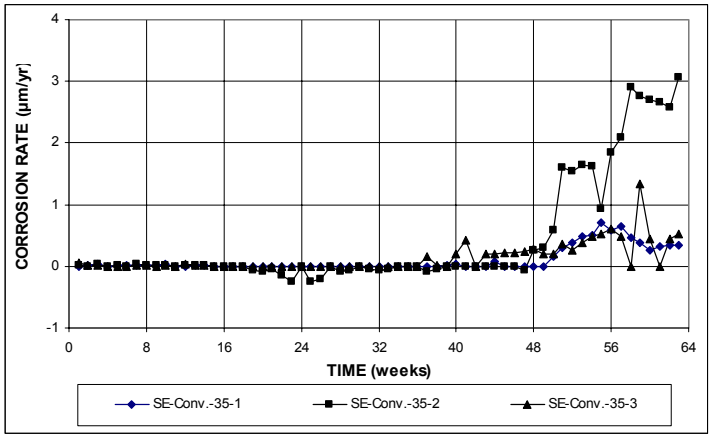

(a)

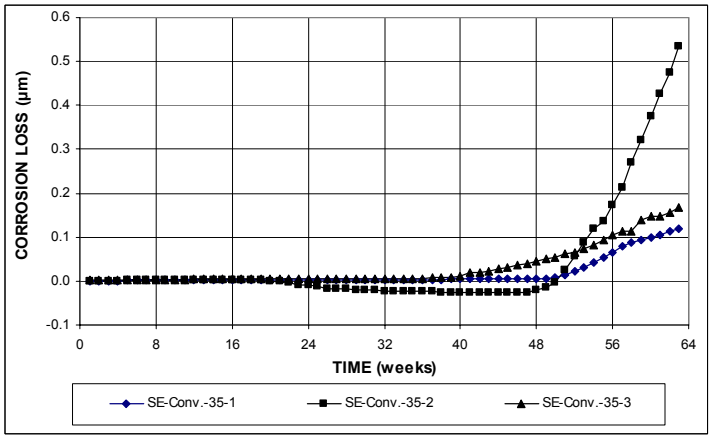

(b)

Figure A.41 – (a) Corrosion rates and (b) total corrosion losses as measured in the Southern Exposure test for specimens with conventional steel, a water-cement ratio of 0.35.

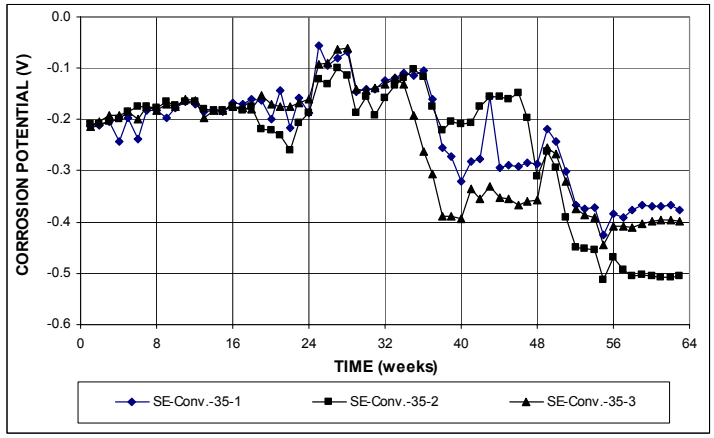

(a)

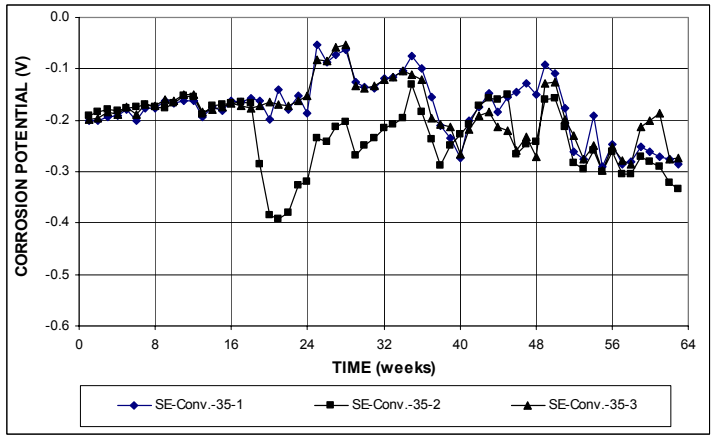

(b)

Figure A.42 – (a) Top mat corrosion potentials and (b) bottom mat corrosion potentials, with respect to copper-copper sulfate electrode as measured in the Southern Exposure test for specimens with conventional steel, a water-cement ratio of 0.35.

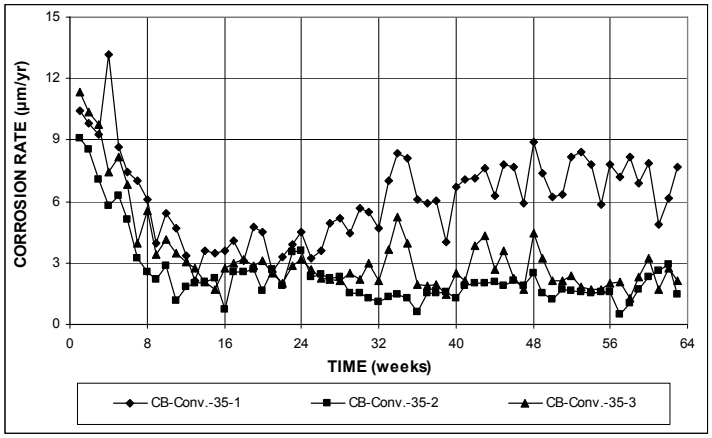

(a)

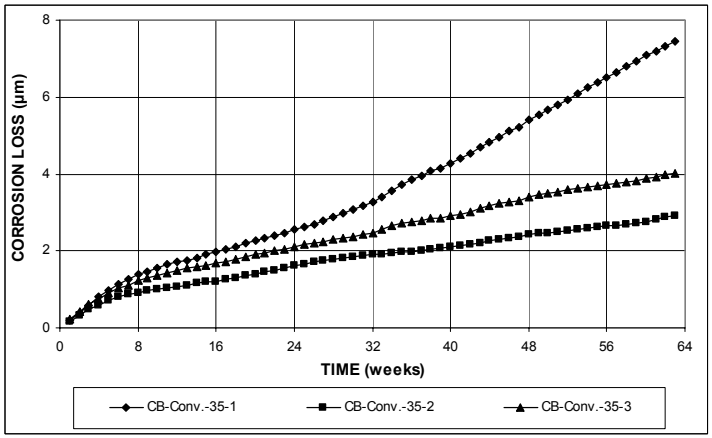

(b)

Figure A.43 – (a) Corrosion rates and (b) total corrosion losses as measured in the cracked beam test for specimens with conventional steel, a water-cement ratio of 0.35.

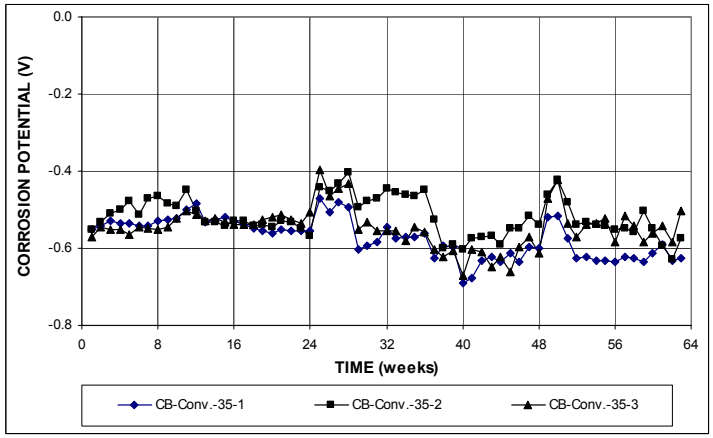

(a)

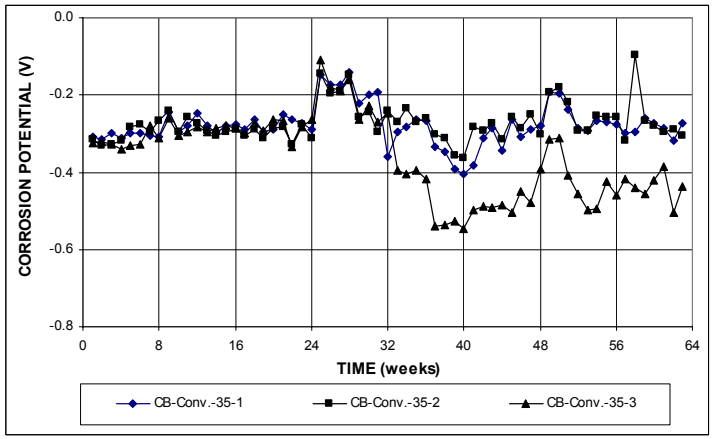

(b)

Figure A.44 – (a) Top mat corrosion potentials and (b) bottom mat corrosion potentials, with respect to copper-copper sulfate electrode as measured in the cracked beam test for specimens with conventional steel, a water-cement ratio of 0.35.

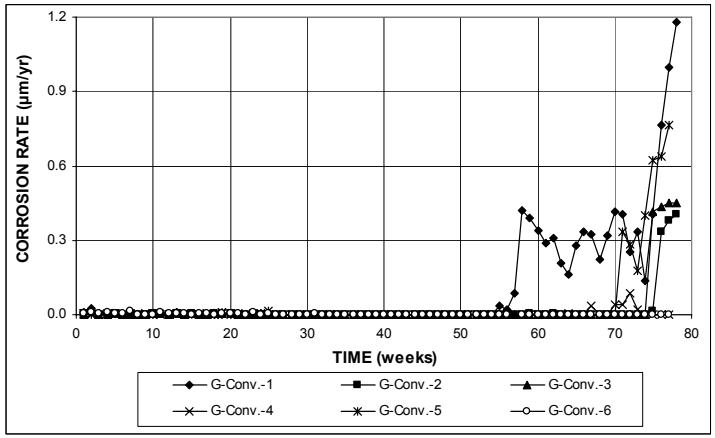

(a)

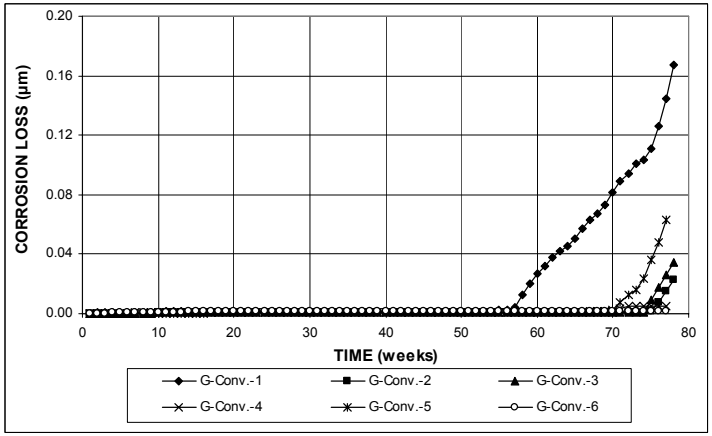

(b)

Figure A.45 – (a) Corrosion rates and (b) total corrosion losses as measured in the ASTM G 109 test for specimens with conventional steel.

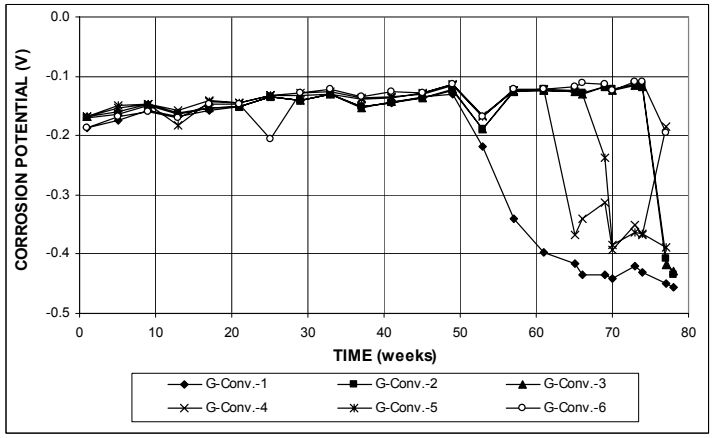

(a)

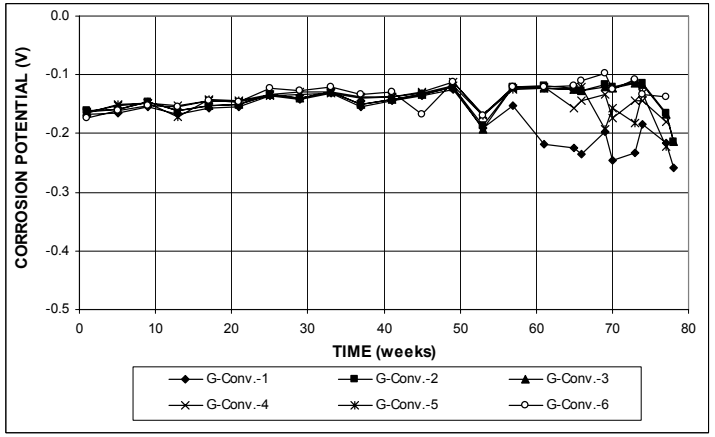

(b)

Figure A.46 – (a) Top mat corrosion potentials and (b) bottom mat corrosion potentials, with respect to copper-copper sulfate electrode as measured in the ASTM G 109 test for specimens with conventional steel.

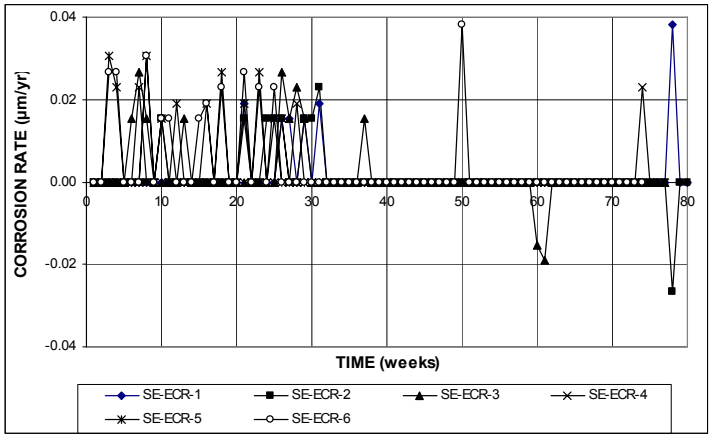

(a)

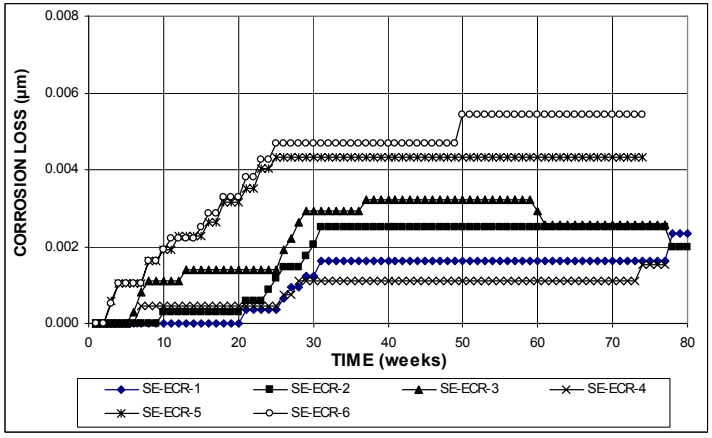

(b)

Figure A.47 – (a) Corrosion rates and (b) total corrosion losses based on total area of the bar as measured in the Southern Exposure test for specimens with ECR (four 3-mm ($^1/_8$-in.) diameter holes).

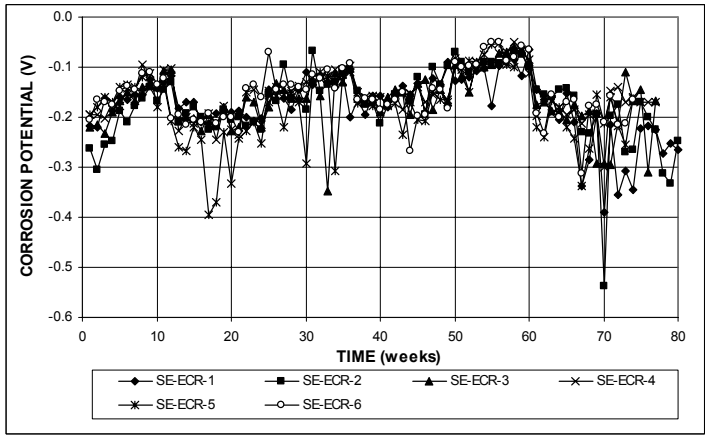

(a)

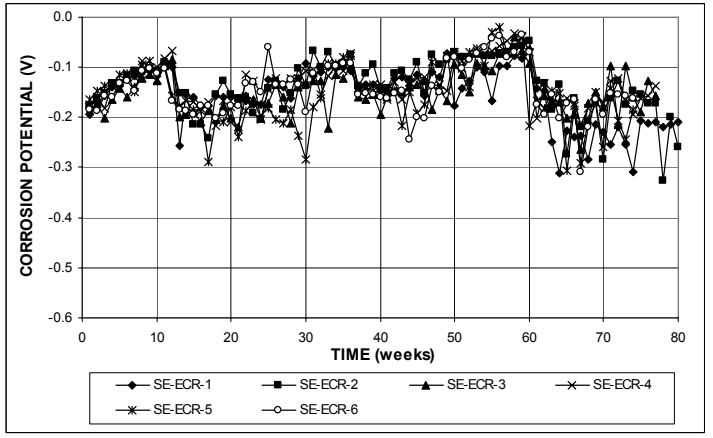

(b)

Figure A.48 – (a) Top mat corrosion potentials and (b) bottom mat corrosion potentials, with respect to copper-copper sulfate electrode as measured in the Southern Exposure test for specimens with ECR (four 3-mm ($^1/_8$-in.) diameter holes).

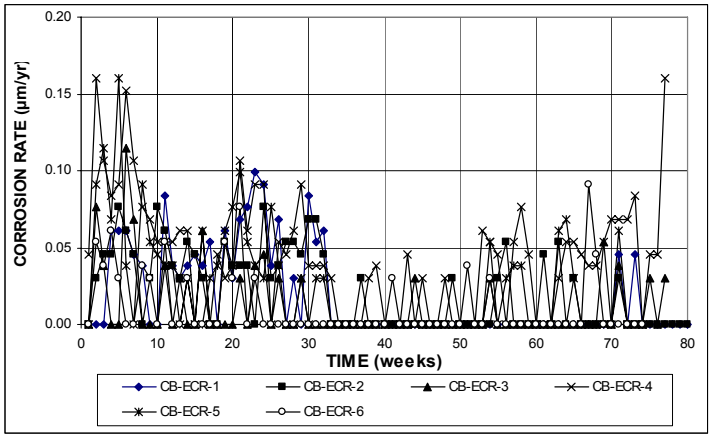

(a)

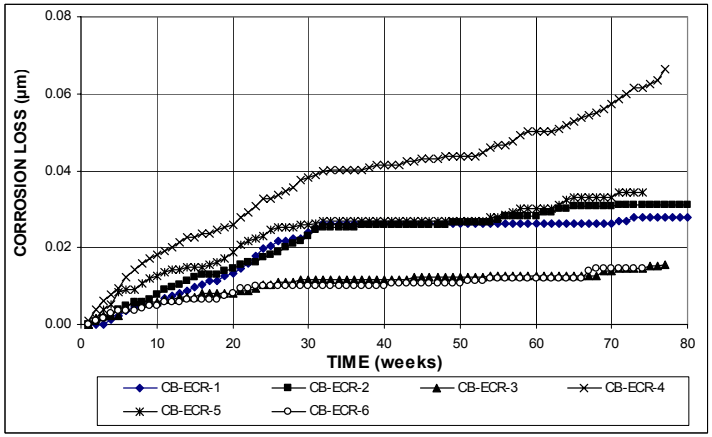

(b)

Figure A.49 – (a) Corrosion rates and (b) total corrosion losses based on total area of the bar as measured in the cracked beam test for specimens with ECR (four 3-mm ($^{1}/_{8}$-in.) diameter holes).

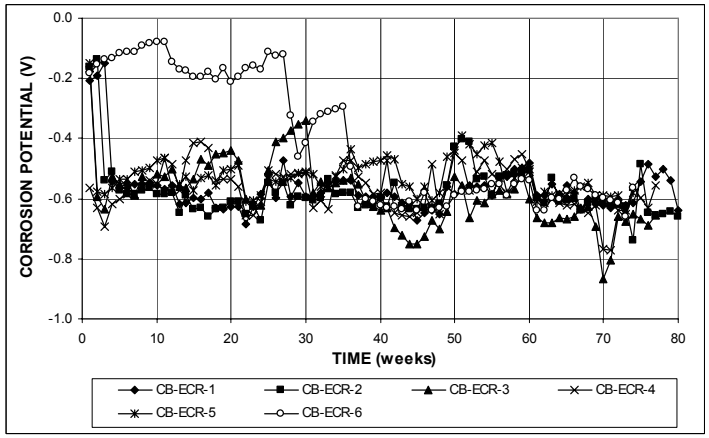

(a)

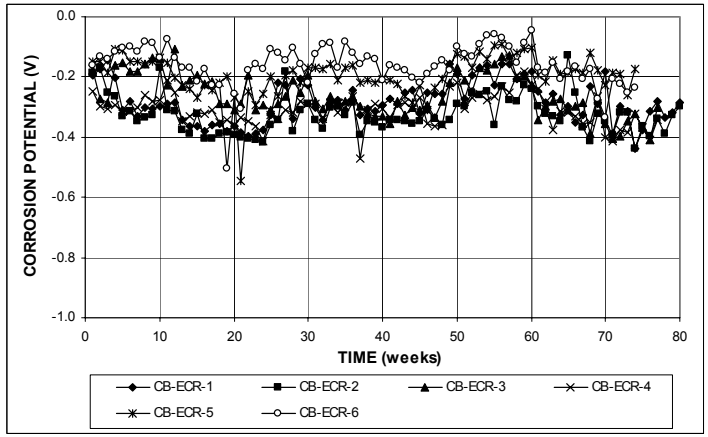

(b)

Figure A.50 – (a) Top mat corrosion potentials and (b) bottom mat corrosion potentials, with respect to copper-copper sulfate electrode as measured in the cracked beam test for specimens with ECR (four 3-mm ($^{1}/_{8}$-in.) diameter holes).

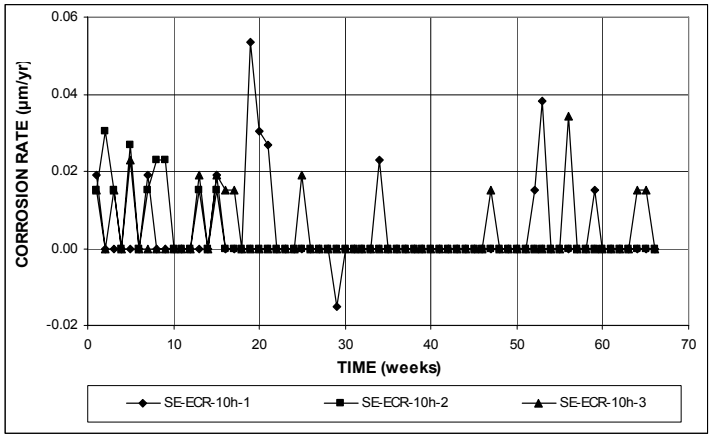

(a)

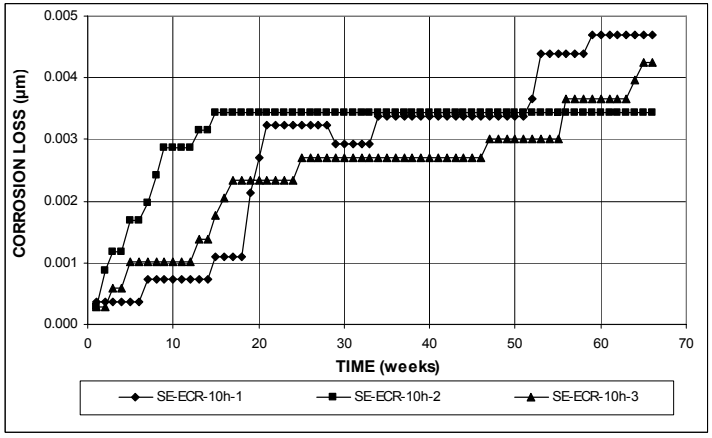

(b)

Figure A.51 – (a) Corrosion rates and (b) total corrosion losses based on total area of the bar as measured in the Southern Exposure test for specimens with ECR (ten 3-mm ($^1/_8$-in.) diameter holes).

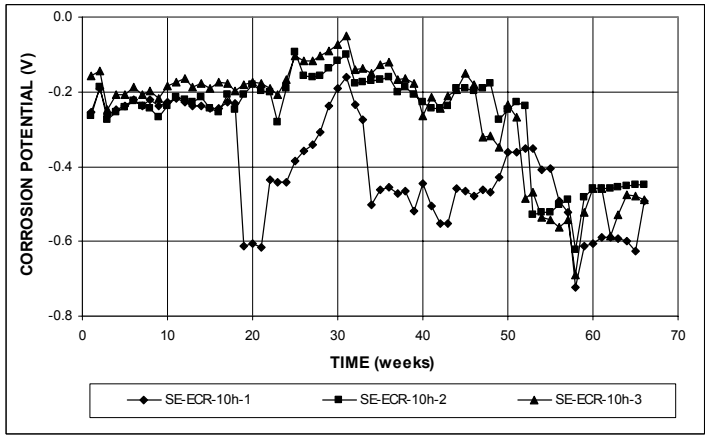

(a)

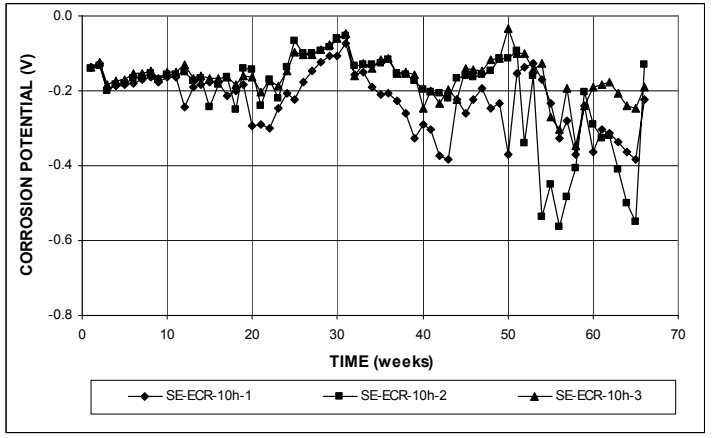

(b)

Figure A.52 – (a) Top mat corrosion potentials and (b) bottom mat corrosion potentials, with respect to copper-copper sulfate electrode as measured in the Southern Exposure test for specimens with ECR (ten 3-mm ($^1/_8$-in.) diameter holes).

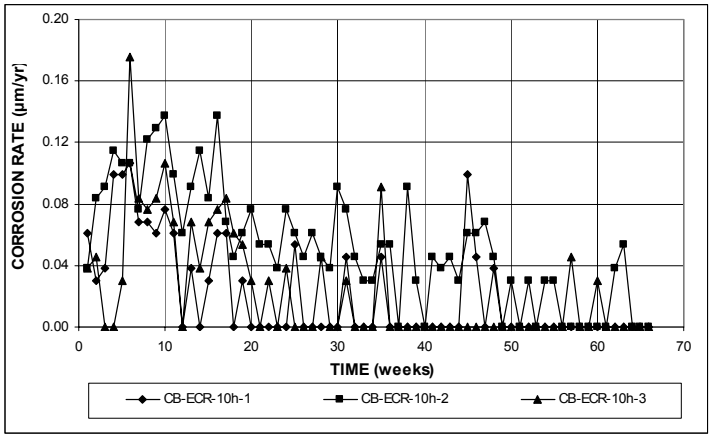

(a)

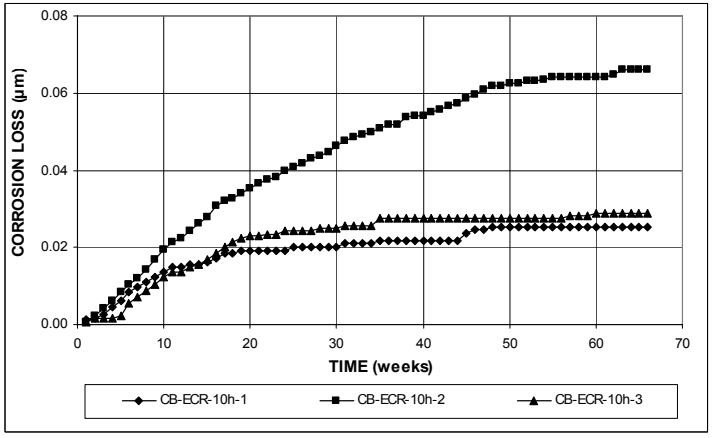

(b)

Figure A.53 – (a) Corrosion rates and (b) total corrosion losses based on total area of the bar as measured in the cracked beam test for specimens with ECR (ten 3-mm ($^1/_8$-in.) diameter holes).

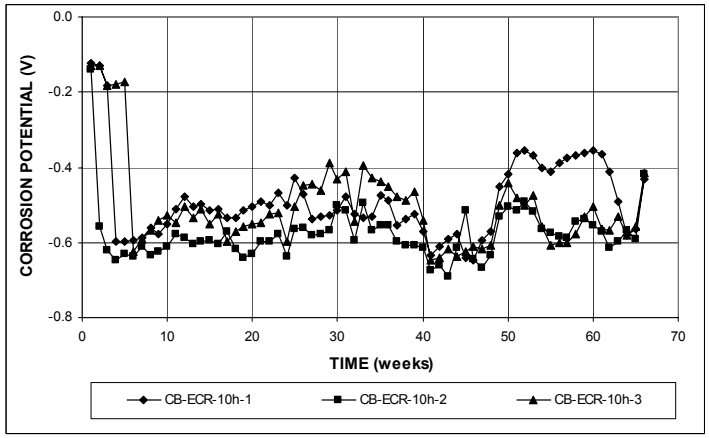

(a)

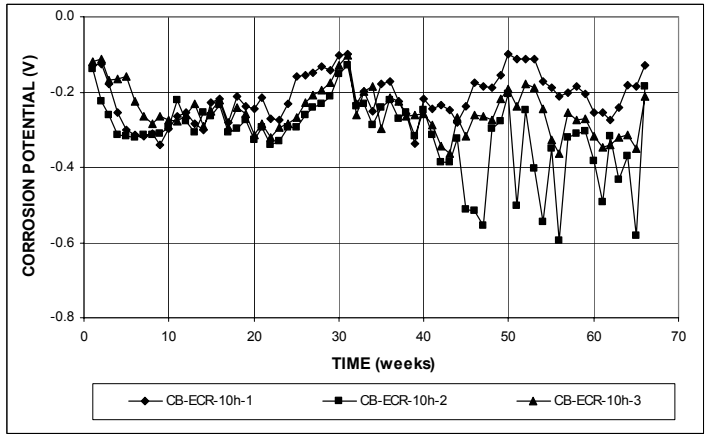

(b)

Figure A.54 – (a) Top mat corrosion potentials and (b) bottom mat corrosion potentials, with respect to copper-copper sulfate electrode as measured in the cracked beam test for specimens with ECR (ten 3-mm ($^1/_8$-in.) diameter holes).

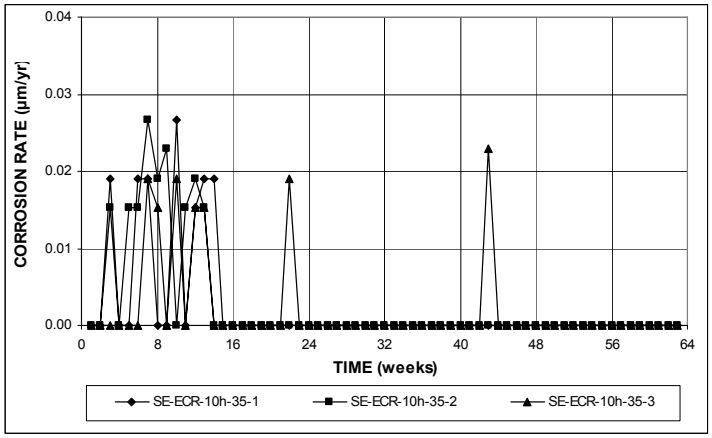

(a)

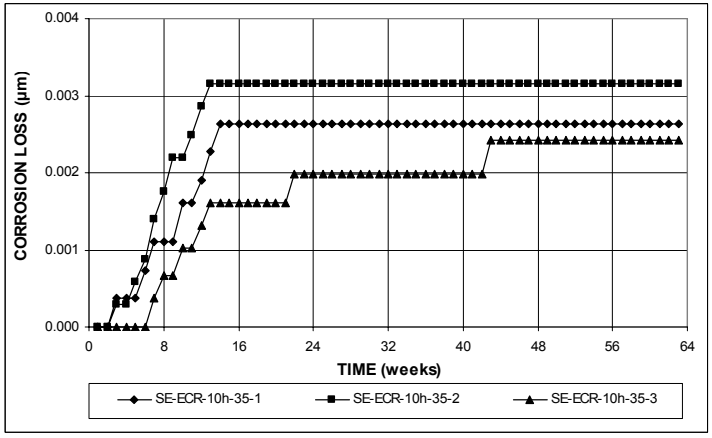

(b)

Figure A.55 – (a) Corrosion rates and (b) total corrosion losses based on total area of the bar as measured in the Southern Exposure test for specimens with ECR (ten 3-mm ($^1/_8$-in.) diameter holes), a water-cement ratio of 0.35.

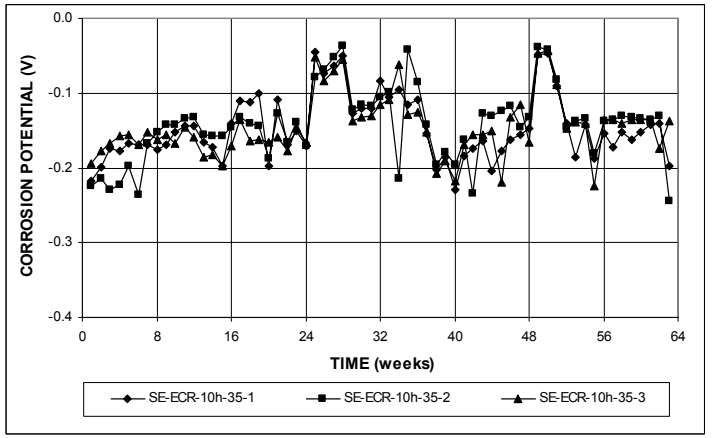

(a)

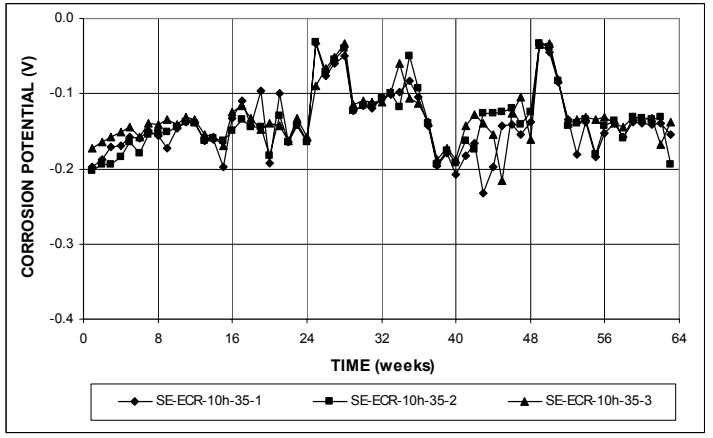

(b)

Figure A.56 – (a) Top mat corrosion potentials and (b) bottom mat corrosion potentials, with respect to copper-copper sulfate electrode as measured in the Southern Exposure test for specimens with ECR (ten 3-mm ($^1/_8$-in.) diameter holes), a water-cement ratio of 0.35.

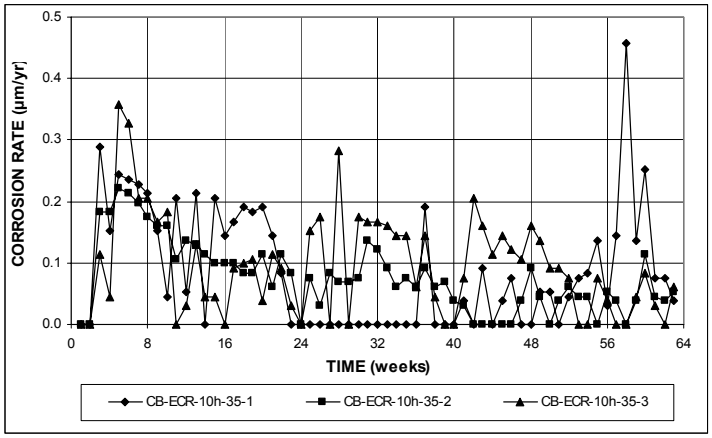

(a)

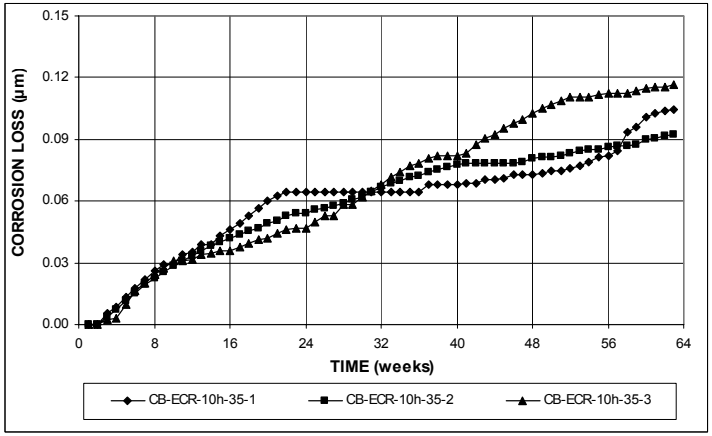

(b)

Figure A.57 – (a) Corrosion rates and (b) total corrosion losses based on total area of the bar as measured in the cracked beam test for specimens with ECR (ten 3-mm ($^1/_8$-in.) diameter holes), a water-cement ratio of 0.35.

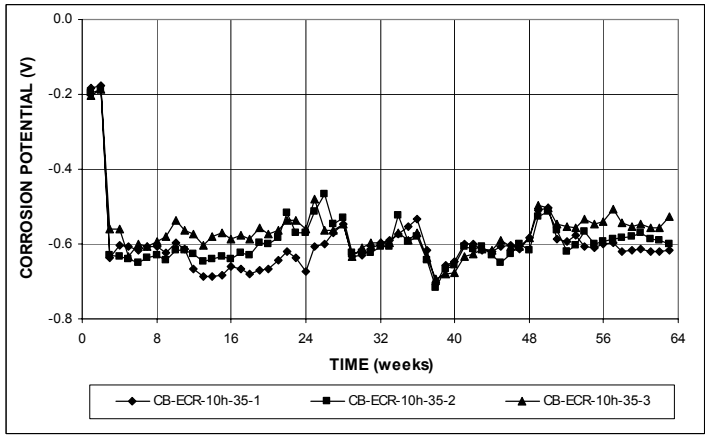

(a)

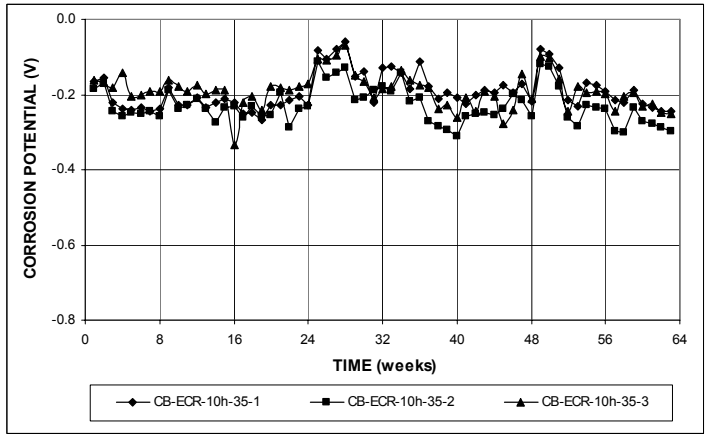

(b)

Figure A.58 – (a) Top mat corrosion potentials and (b) bottom mat corrosion potentials, with respect to copper-copper sulfate electrode as measured in the cracked beam test for specimens with ECR (ten 3-mm ($^1/_8$-in.) diameter holes), a water-cement ratio of 0.35.

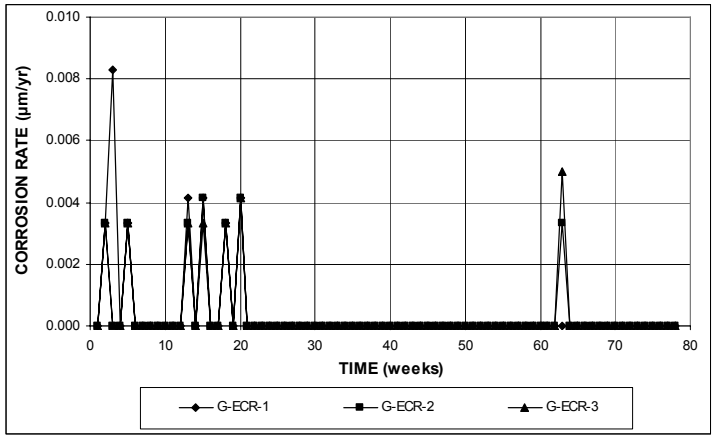

(a)

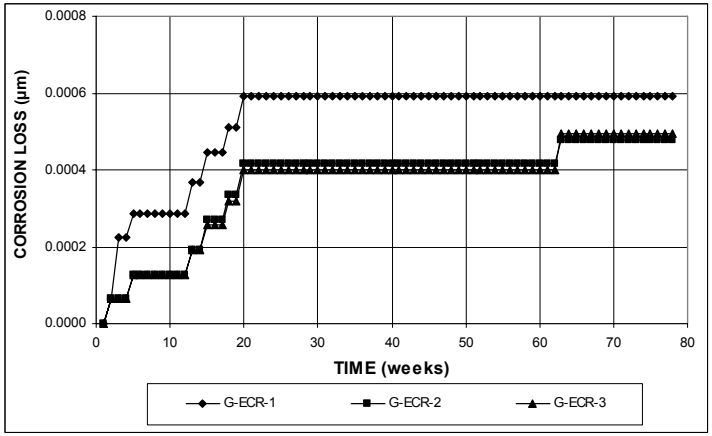

(b)

Figure A.59 – (a) Corrosion rates and (b) total corrosion losses based on total area of the bar as measured in the ASTM G 109 test for specimens with ECR (four 3-mm ($^1/_8$-in.) diameter holes).

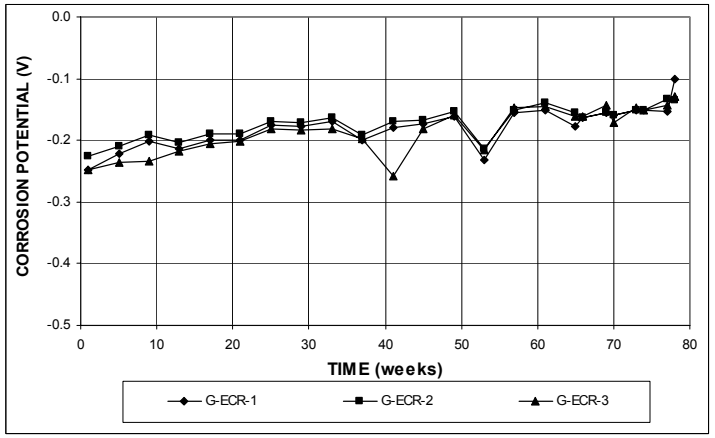

(a)

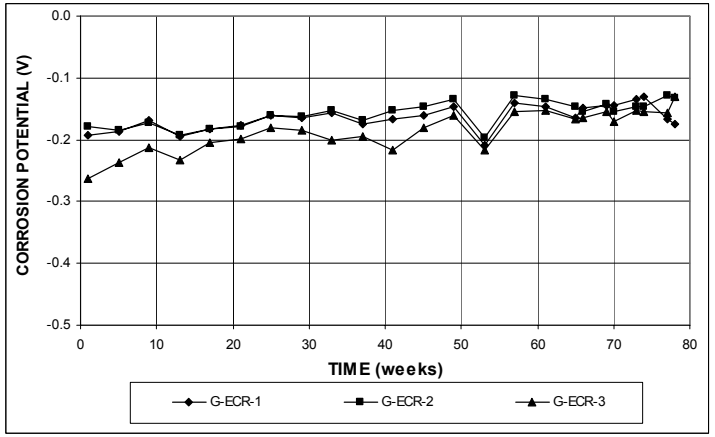

(b)

Figure A.60 – (a) Top mat corrosion potentials and (b) bottom mat corrosion potentials, with respect to copper-copper sulfate electrode as measured in the ASTM G 109 test for specimens with ECR (four 3-mm ($^1/_8$-in.) diameter holes).

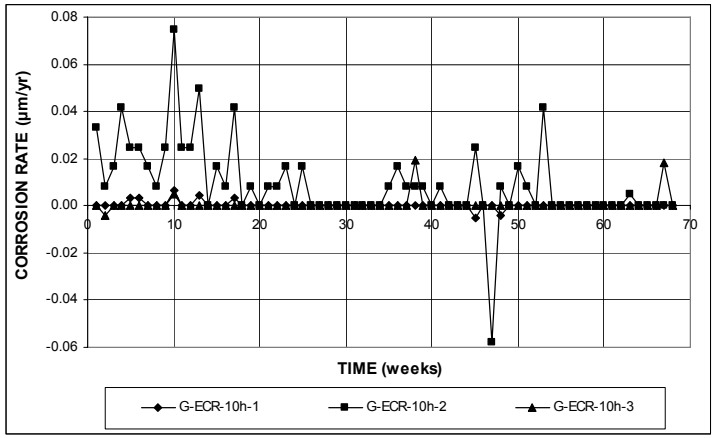

(a)

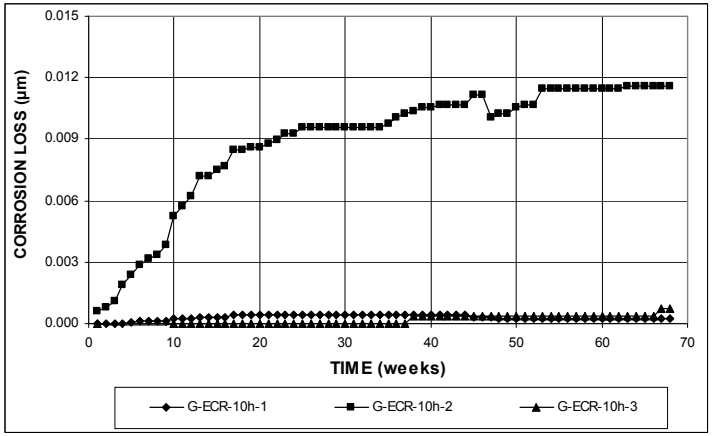

(b)

Figure A.61 – (a) Corrosion rates and (b) total corrosion losses based on total area of the bar as measured in the ASTM G 109 test for specimens with ECR (ten 3-mm ($^1/_8$-in.) diameter holes).

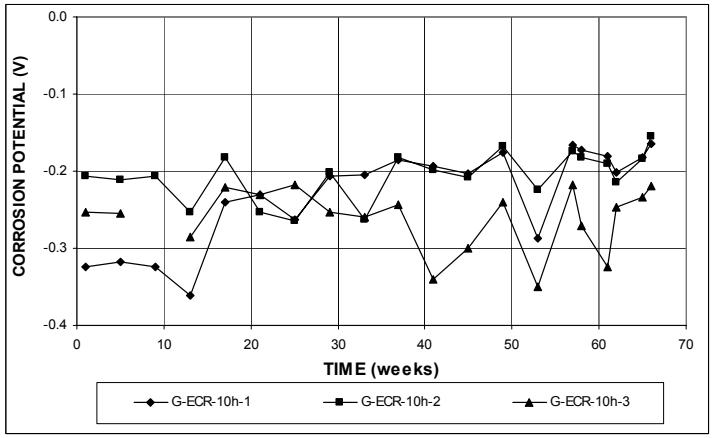

(a)

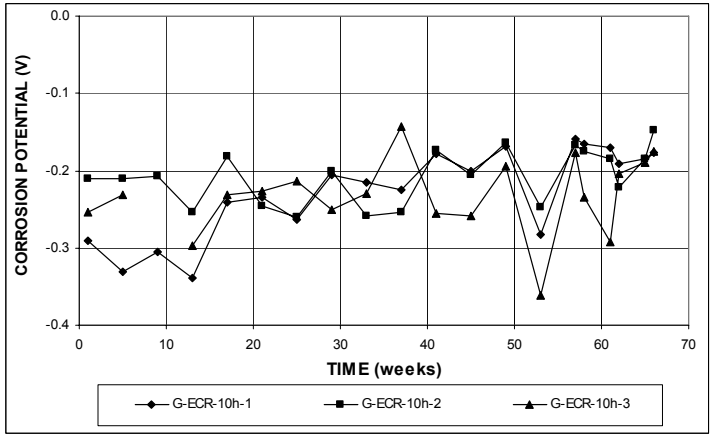

(b)

Figure A.62 – (a) Top mat corrosion potentials and (b) bottom mat corrosion potentials, with respect to copper-copper sulfate electrode as measured in the ASTM G 109 test for specimens with ECR (ten 3-mm ($^1/_8$-in.) diameter holes).

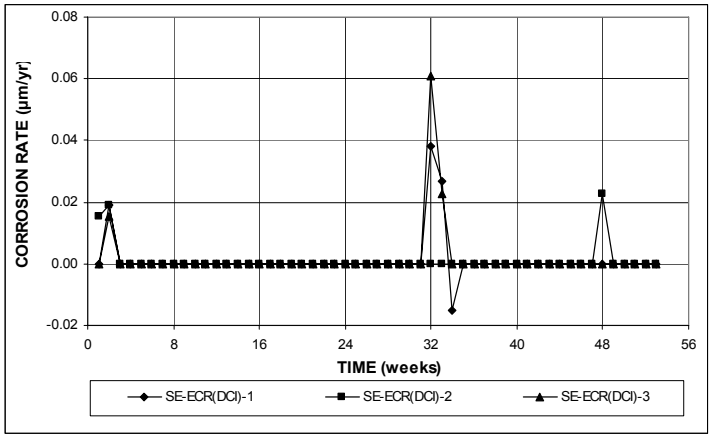

(a)

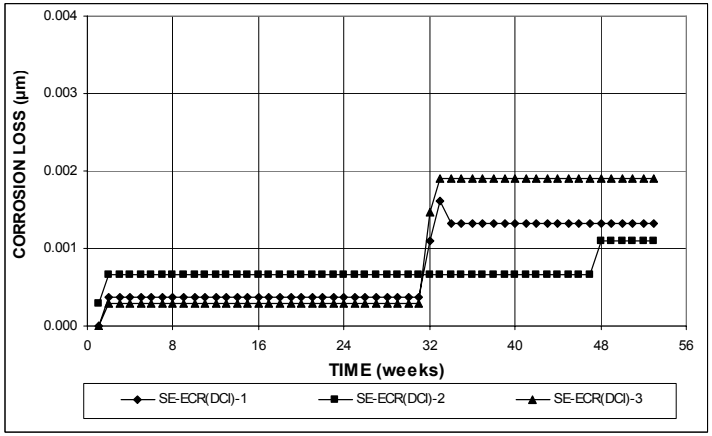

(b)

Figure A.63 – (a) Corrosion rates and (b) total corrosion losses based on total area of the bar as measured in the Southern Exposure test for specimens with ECR in concrete with DCI (four 3-mm ($^{1}/_{8}$-in.) diameter holes).

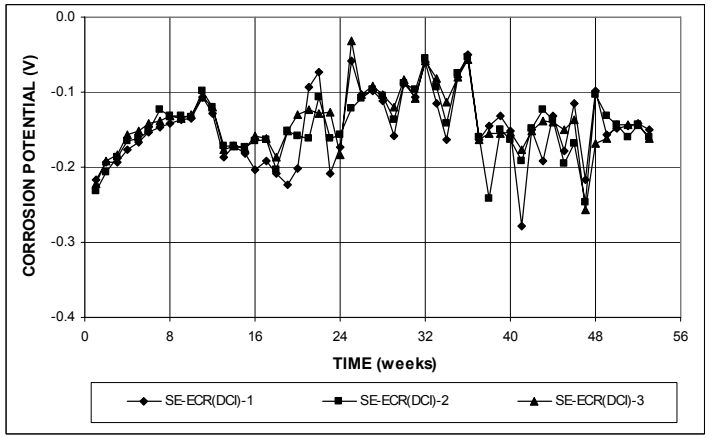

(a)

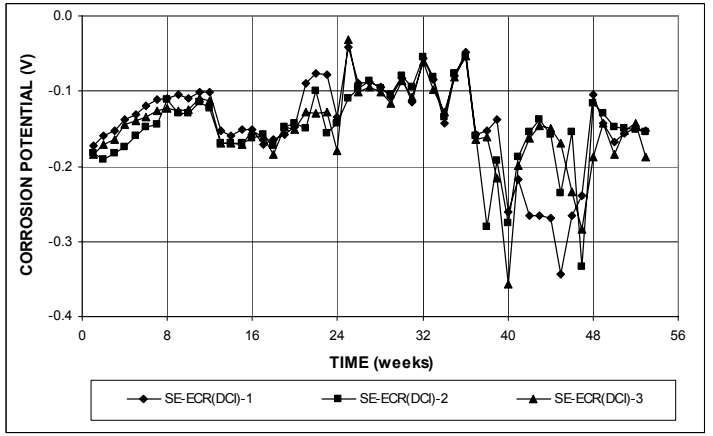

(b)

Figure A.64 – (a) Top mat corrosion potentials and (b) bottom mat corrosion potentials, with respect to copper-copper sulfate electrode as measured in the Southern Exposure test for specimens with ECR in concrete with DCI (four 3-mm ($^{1}/_{8}$-in.) diameter holes).

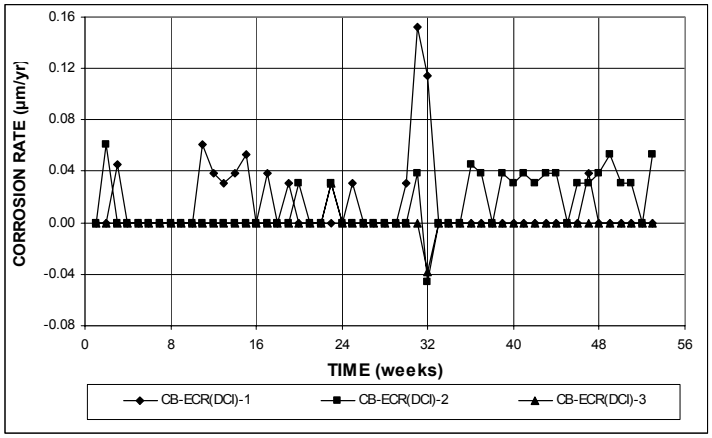

(a)

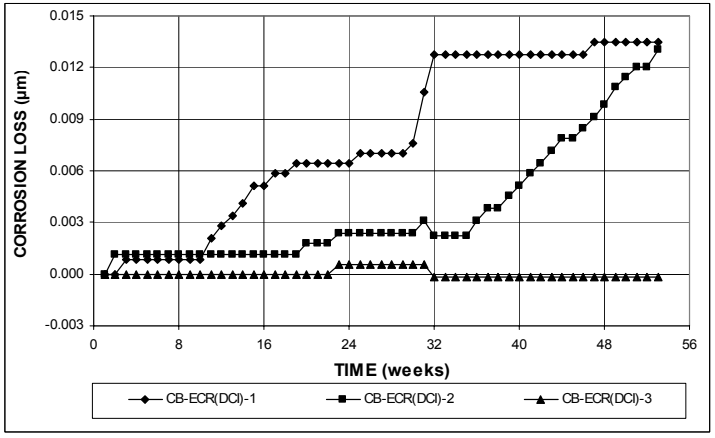

(b)

Figure A.65 – (a) Corrosion rates and (b) total corrosion losses based on total area of the bar as measured in the cracked beam test for specimens with ECR in concrete with DCI (four 3-mm ($^{1}/_{8}$-in.) diameter holes).

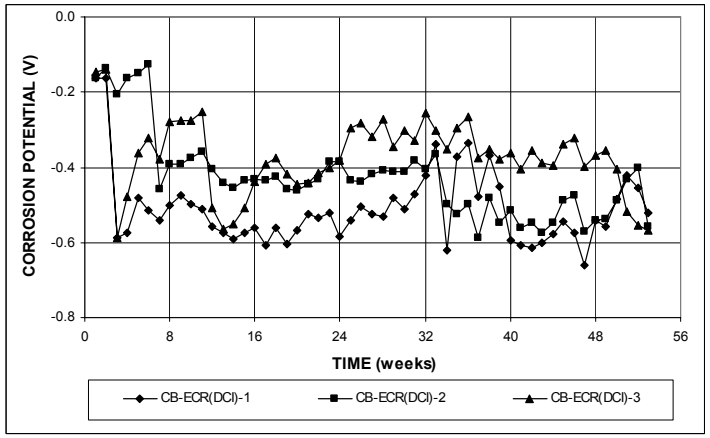

(a)

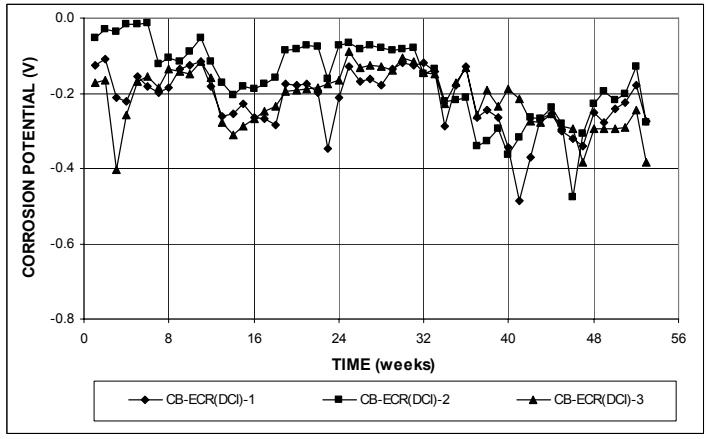

(b)

Figure A.66 – (a) Top mat corrosion potentials and (b) bottom mat corrosion potentials, with respect to copper-copper sulfate electrode as measured in the cracked beam test for specimens with ECR in concrete with DCI (four 3-mm ($^{1}/_{8}$-in.) diameter holes).

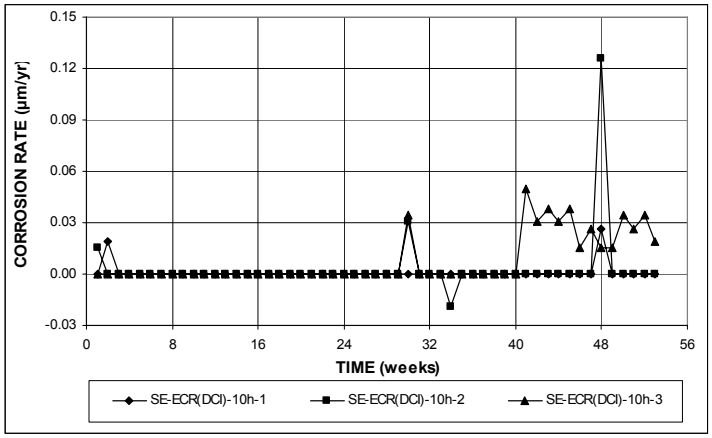

(a)

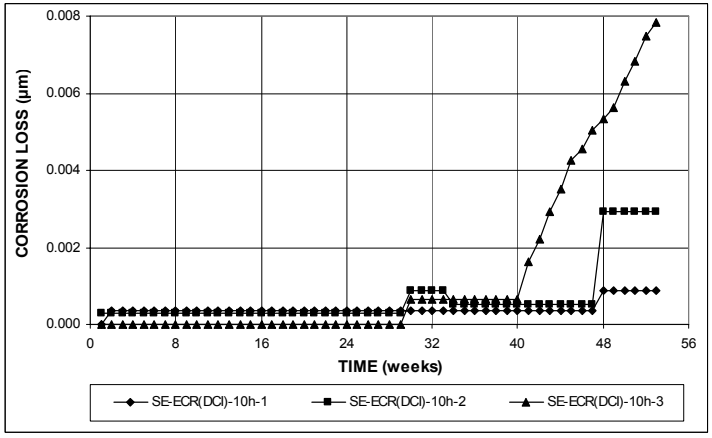

(b)

Figure A.67 – (a) Corrosion rates and (b) total corrosion losses based on total area of the bar as measured in the Southern Exposure test for specimens with ECR in concrete with DCI (ten 3-mm ($^1/_8$-in.) diameter holes).

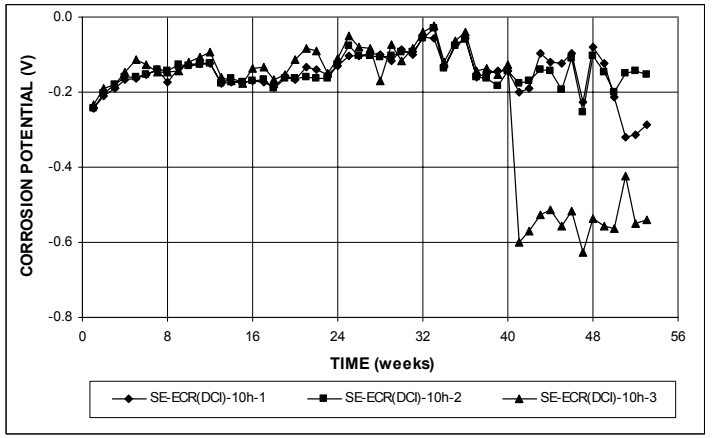

(a)

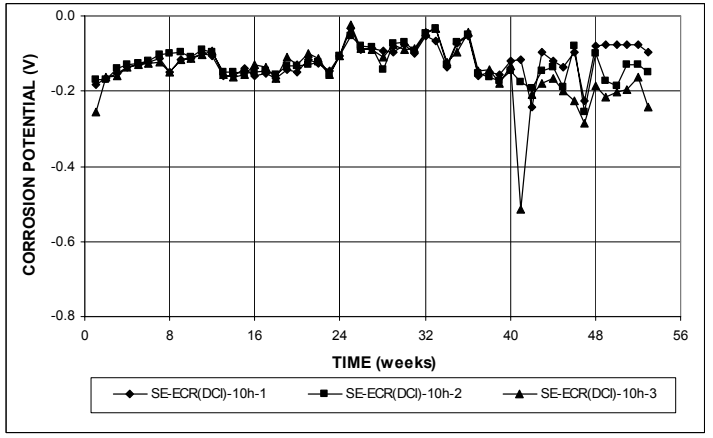

(b)

Figure A.68 – (a) Top mat corrosion potentials and (b) bottom mat corrosion potentials, with respect to copper-copper sulfate electrode as measured in the Southern Exposure test for specimens with ECR in concrete with DCI (ten 3-mm ($^1/_8$-in.) diameter holes).

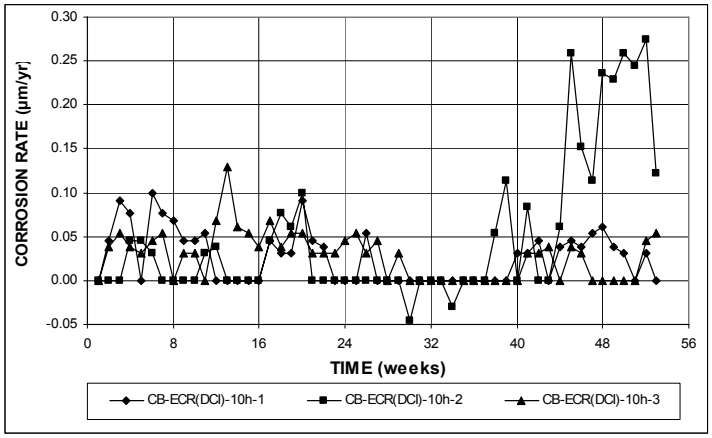

(a)

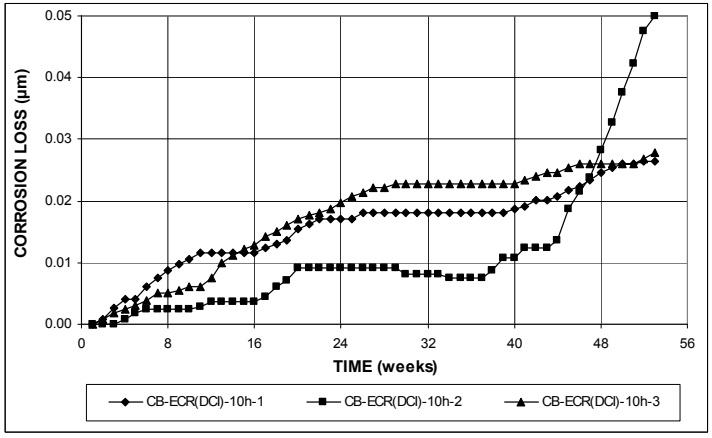

(b)

Figure A.69 – (a) Corrosion rates and (b) total corrosion losses based on total area of the bar as measured in the cracked beam test for specimens with ECR in concrete with DCI (ten 3-mm ($^1/_8$-in.) diameter holes).

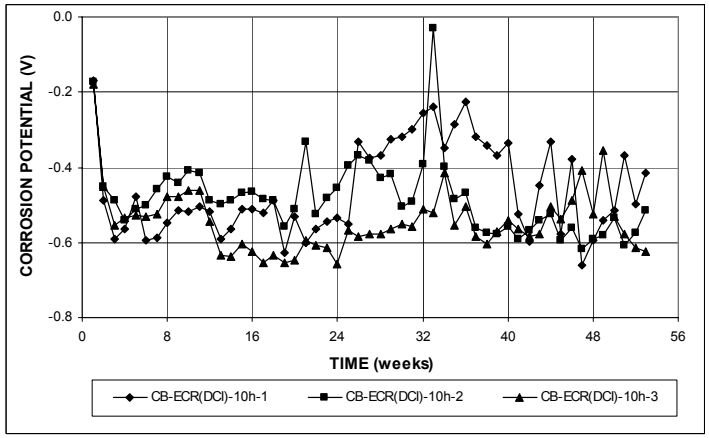

(a)

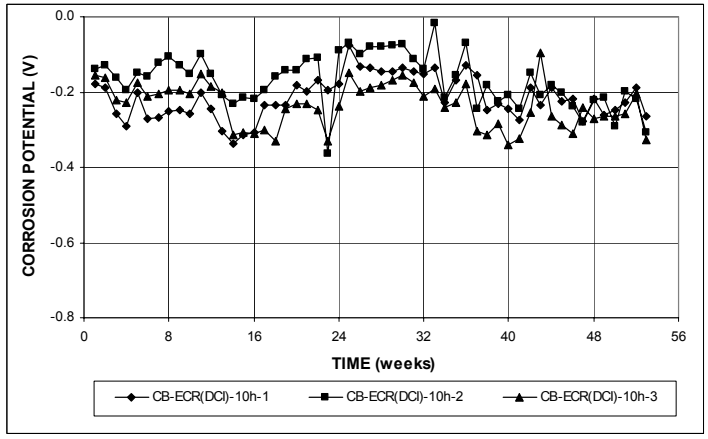

(b)

Figure A.70 – (a) Top mat corrosion potentials and (b) bottom mat corrosion potentials, with respect to copper-copper sulfate electrode as measured in the cracked beam test for specimens with ECR in concrete with DCI (ten 3-mm ($^1/_8$-in.) diameter holes).

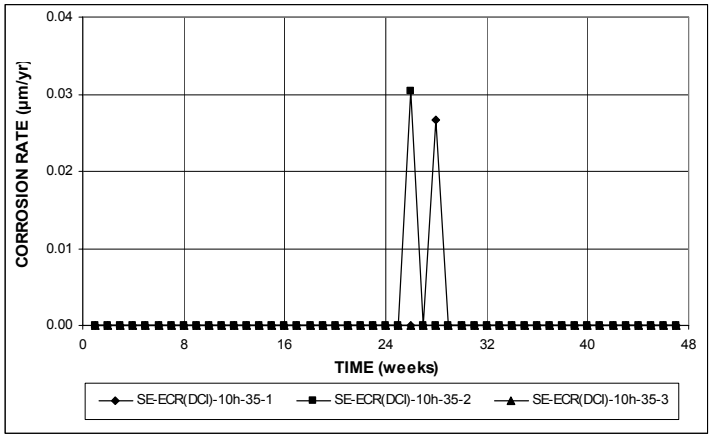

(a)

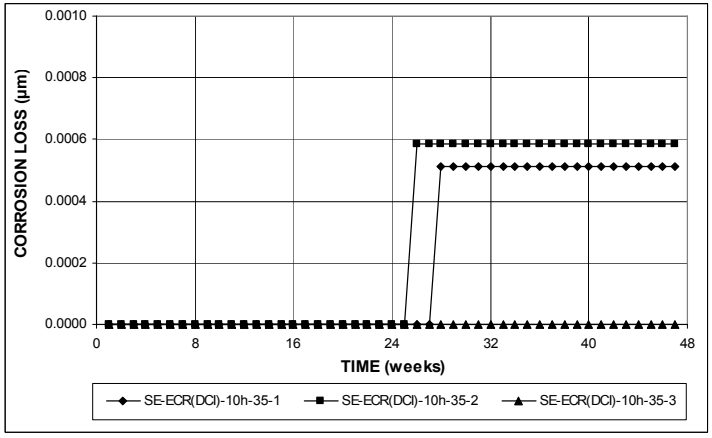

(b)

Figure A.71 – (a) Corrosion rates and (b) total corrosion losses based on total area of the bar as measured in the Southern Exposure test for specimens with ECR in concrete with DCI (ten 3-mm ($^{1}/_{8}$-in.) diameter holes), a water-cement ratio of 0.35.

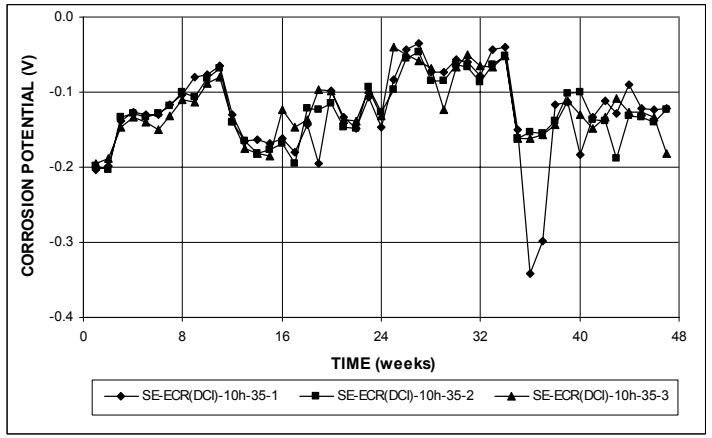

(a)

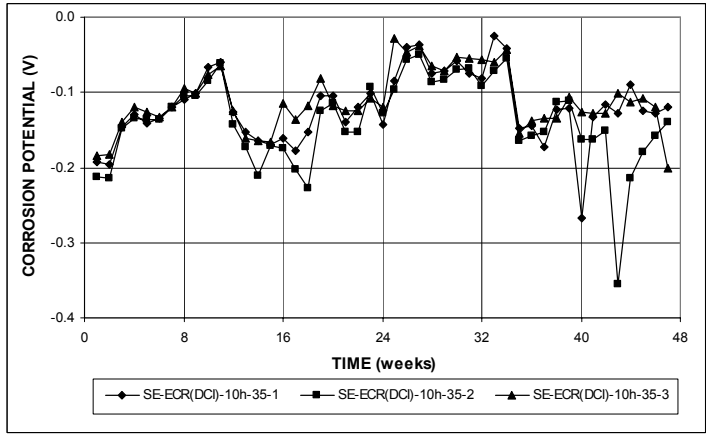

(b)

Figure A.72 – (a) Top mat corrosion potentials and (b) bottom mat corrosion potentials, with respect to copper-copper sulfate electrode as measured in the Southern Exposure test for specimens with ECR in concrete with DCI (ten 3-mm ($^{1}/_{8}$-in.) diameter holes), a water-cement ratio of 0.35.

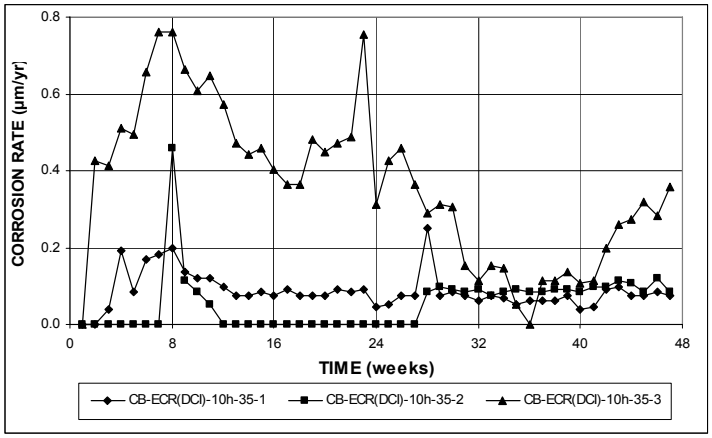

(a)

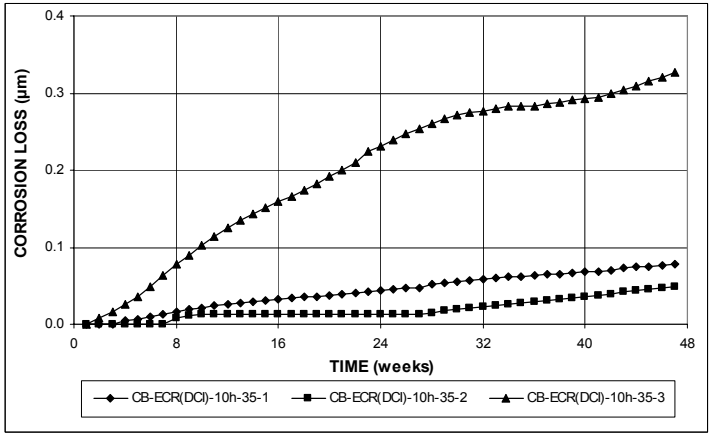

(b)

Figure A.73 – (a) Corrosion rates and (b) total corrosion losses based on total area of the bar as measured in the cracked beam test for specimens with ECR in concrete with DCI (ten 3-mm ($^1/_8$-in.) diameter holes), a water-cement ratio of 0.35.

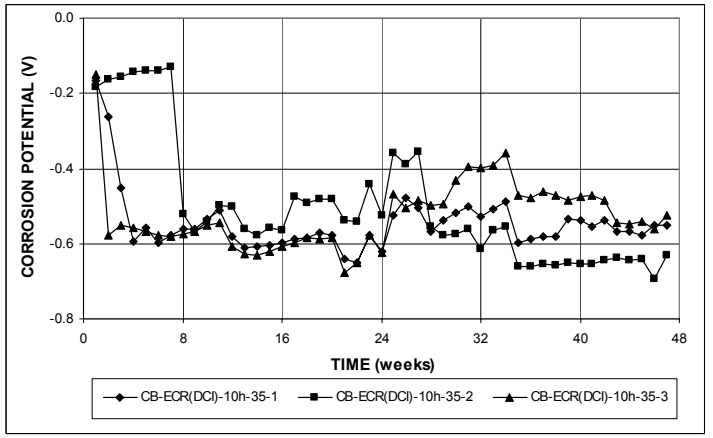

(a)

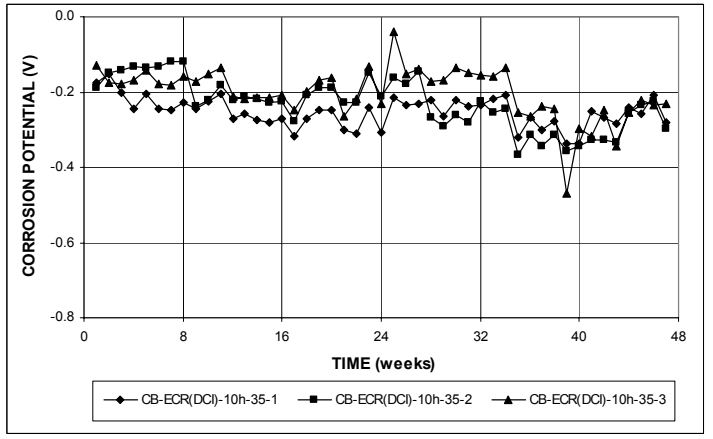

(b)

Figure A.74 – (a) Top mat corrosion potentials and (b) bottom mat corrosion potentials, with respect to copper-copper sulfate electrode as measured in the cracked beam test for specimens with ECR in concrete with DCI (ten 3-mm ($^1/_8$-in.) diameter holes), a water-cement ratio of 0.35.

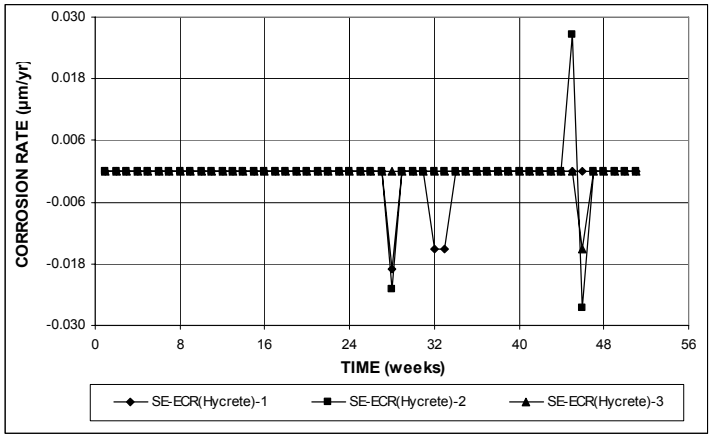

(a)

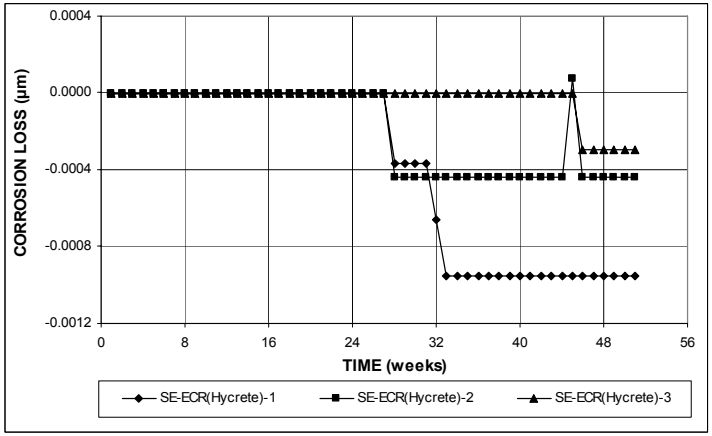

(b)

Figure A.75 – (a) Corrosion rates and (b) total corrosion losses based on total area of the bar as measured in the Southern Exposure test for specimens with ECR in concrete with Hycrete (four 3-mm ($^1/_8$-in.) diameter holes).

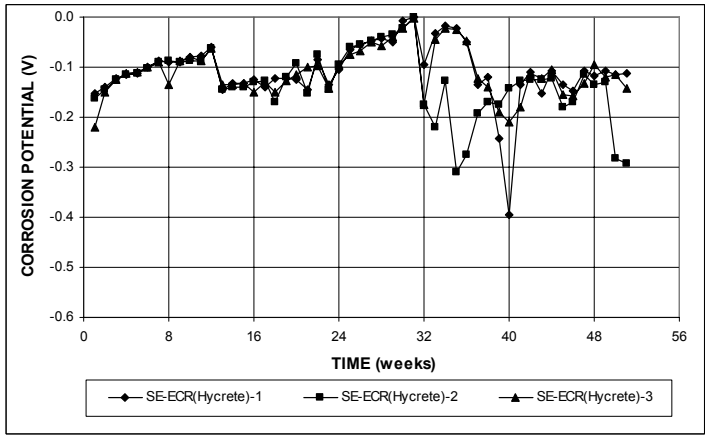

(a)

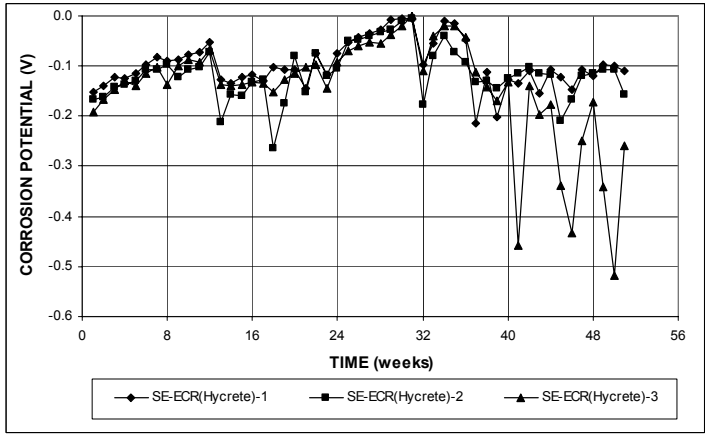

(b)

Figure A.76 – (a) Top mat corrosion potentials and (b) bottom mat corrosion potentials, with respect to copper-copper sulfate electrode as measured in the Southern Exposure test for specimens with ECR in concrete with Hycrete (four 3-mm ($^1/_8$-in.) diameter holes).

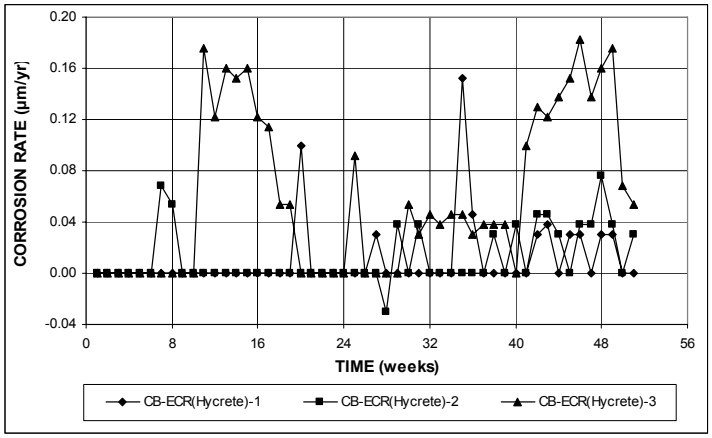

(a)

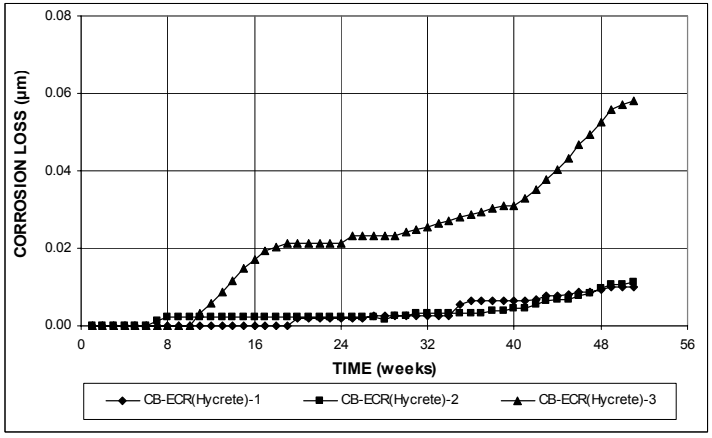

(b)

Figure A.77 – (a) Corrosion rates and (b) total corrosion losses based on total area of the bar as measured in the cracked beam test for specimens with ECR in concrete with Hycrete (four 3-mm ($^1/_8$-in.) diameter holes).

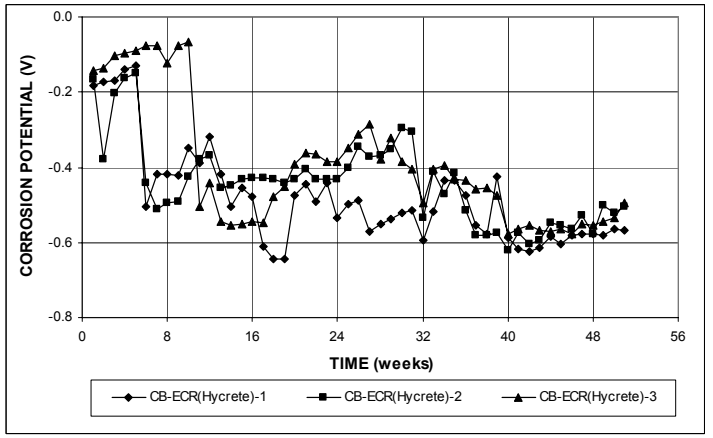

(a)

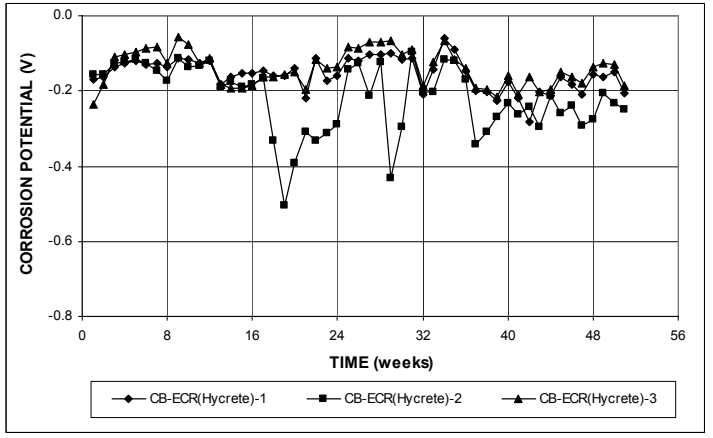

(b)

Figure A.78 – (a) Top mat corrosion potentials and (b) bottom mat corrosion potentials, with respect to copper-copper sulfate electrode as measured in the cracked beam test for specimens with ECR in concrete with Hycrete (four 3-mm ($^1/_8$-in.) diameter holes).

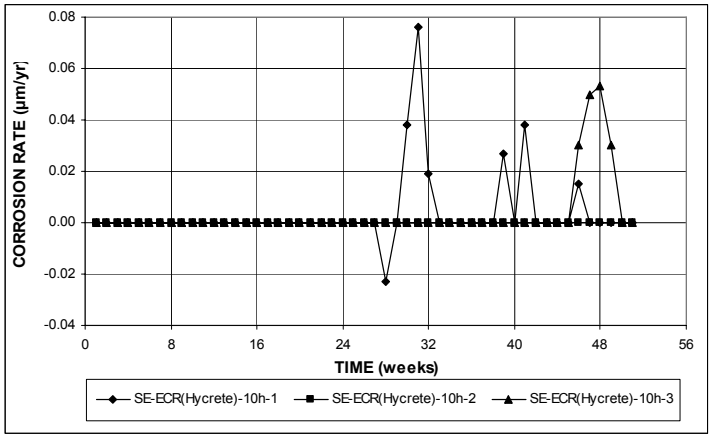

(a)

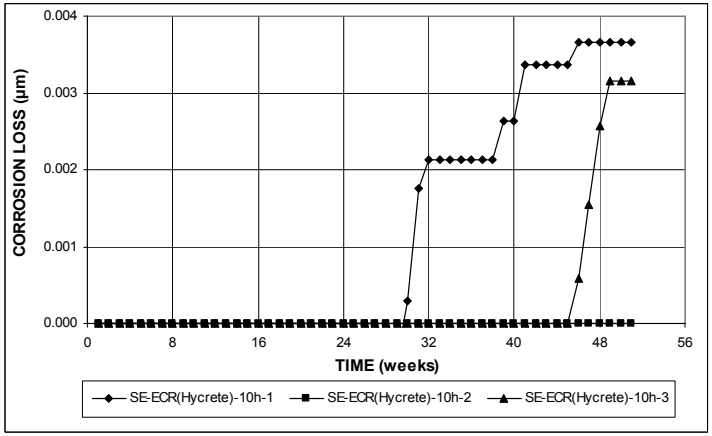

(b)

Figure A.79 – (a) Corrosion rates and (b) total corrosion losses based on total area of the bar as measured in the Southern Exposure test for specimens with ECR in concrete with Hycrete (ten 3-mm ($^1/_8$-in.) diameter holes).

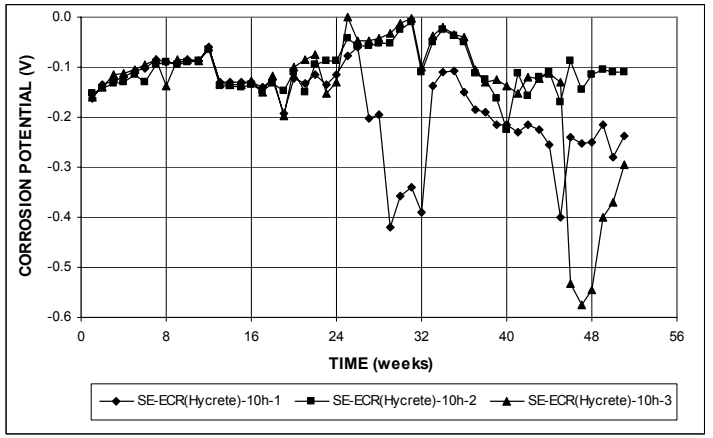

(a)

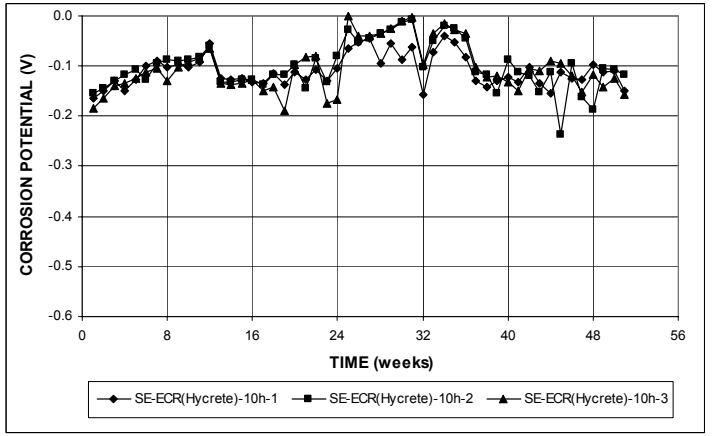

(b)

Figure A.80 – (a) Top mat corrosion potentials and (b) bottom mat corrosion potentials, with respect to copper-copper sulfate electrode as measured in the Southern Exposure test for specimens with ECR in concrete with Hycrete (ten 3-mm ($^1/_8$-in.) diameter holes).

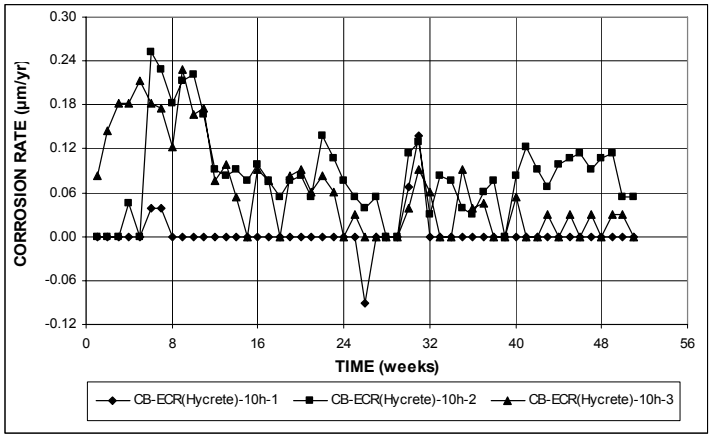

(a)

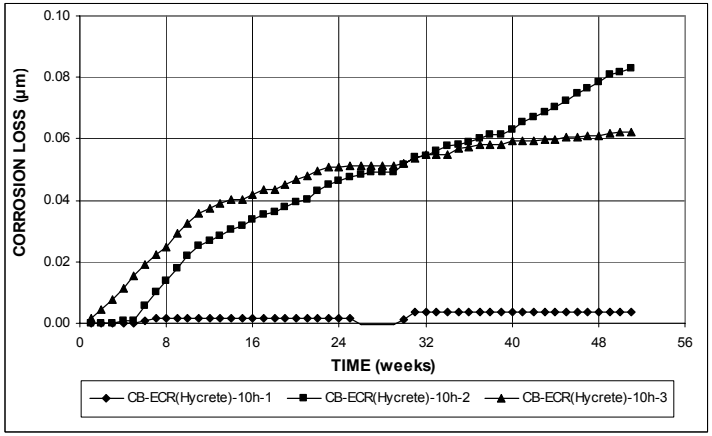

(b)

Figure A.81 – (a) Corrosion rates and (b) total corrosion losses based on total area of the bar as measured in the cracked beam test for specimens with ECR in concrete with Hycrete (ten 3-mm ($^{1}/_{8}$-in.) diameter holes).

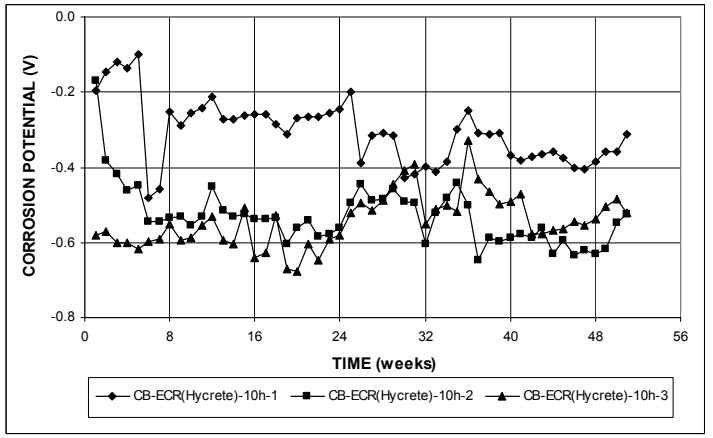

(a)

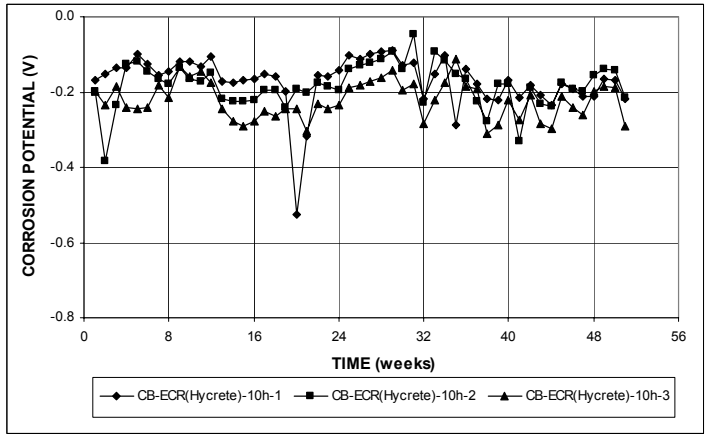

(b)

Figure A.82 – (a) Top mat corrosion potentials and (b) bottom mat corrosion potentials, with respect to copper-copper sulfate electrode as measured in the cracked beam test for specimens with ECR in concrete with Hycrete (ten 3-mm ($^{1}/_{8}$-in.) diameter holes).

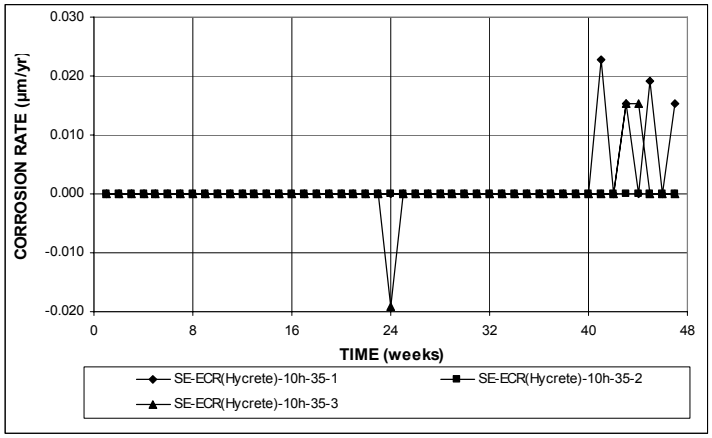

(a)

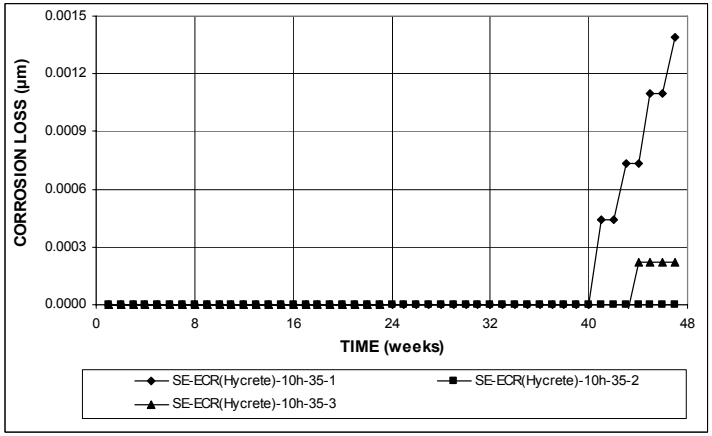

(b)

Figure A.83 – (a) Corrosion rates and (b) total corrosion losses based on total area of the bar as measured in the Southern Exposure test for specimens with ECR in concrete with Hycrete (ten 3-mm ($^1/_8$-in.) diameter holes), a water-cement ratio of 0.35.

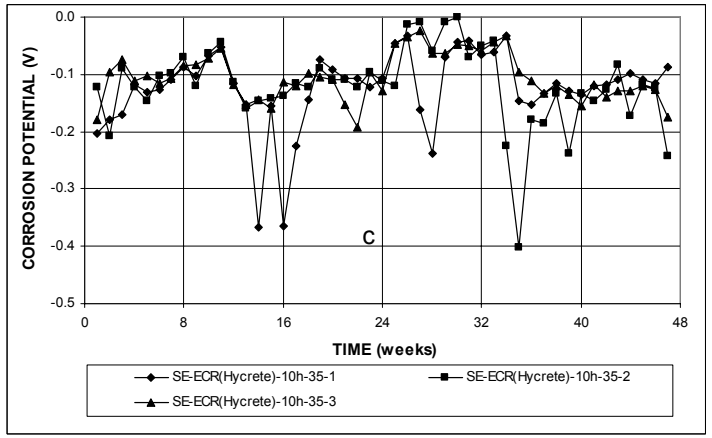

(a)

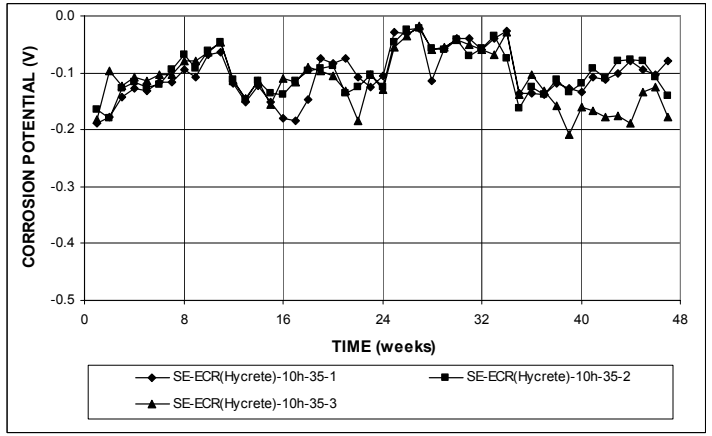

(b)

Figure A.84 – (a) Top mat corrosion potentials and (b) bottom mat corrosion potentials, with respect to copper-copper sulfate electrode as measured in the Southern Exposure test for specimens with ECR in concrete with Hycrete (ten 3-mm ($^1/_8$-in.) diameter holes), a water-cement ratio of 0.35.

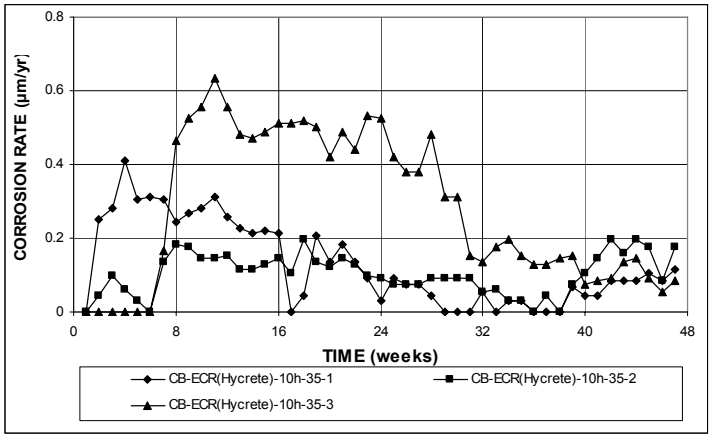

(a)

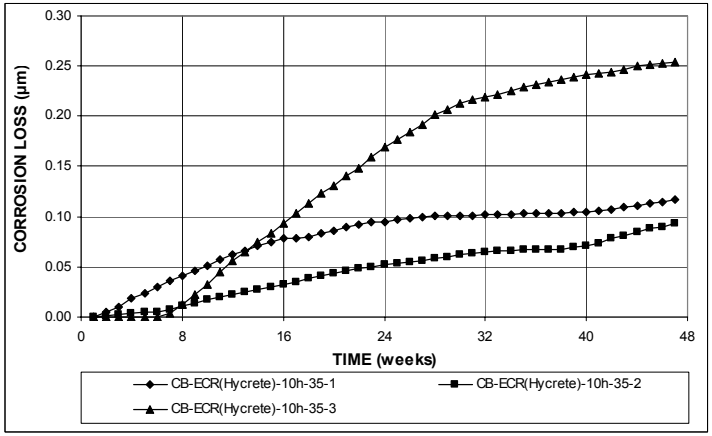

(b)

Figure A.85 – (a) Corrosion rates and (b) total corrosion losses based on total area of the bar as measured in the cracked beam test for specimens with ECR in concrete with Hycrete (ten 3-mm ($^1/_8$-in.) diameter holes), a water-cement ratio of 0.35.

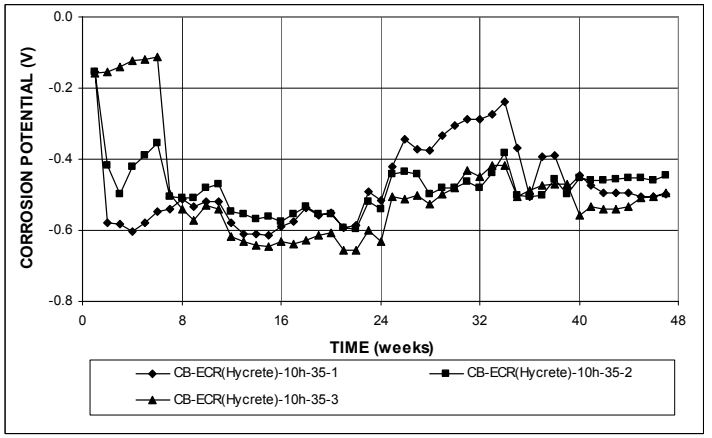

(a)

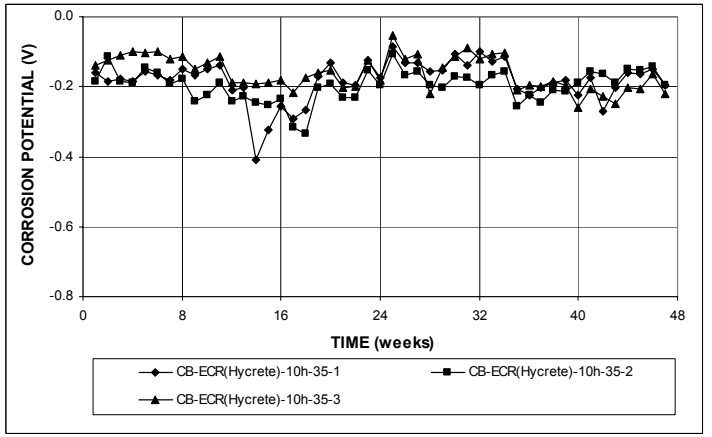

(b)

Figure A.86 – (a) Top mat corrosion potentials and (b) bottom mat corrosion potentials, with respect to copper-copper sulfate electrode as measured in the cracked beam test for specimens with ECR in concrete with Hycrete (ten 3-mm ($^1/_8$-in.) diameter holes), a water-cement ratio of 0.35.

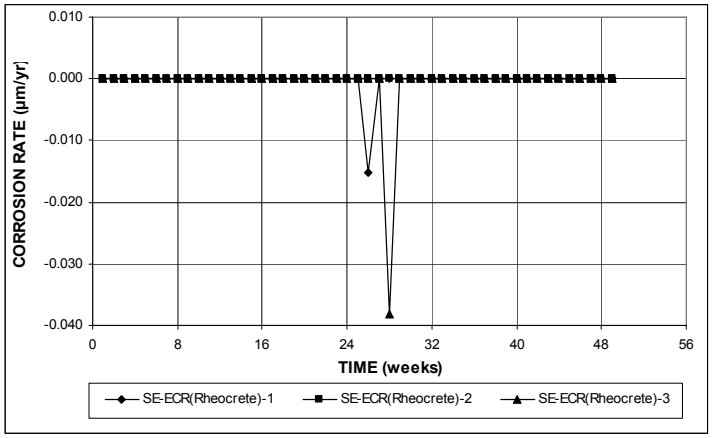

(a)

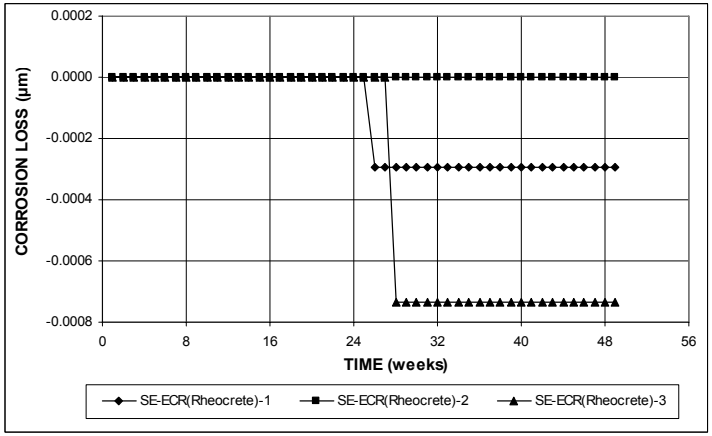

(b)

Figure A.87 – (a) Corrosion rates and (b) total corrosion losses based on total area of the bar as measured in the Southern Exposure test for specimens with ECR in concrete with Rheocrete (four 3-mm ($^1/_8$-in.) diameter holes).

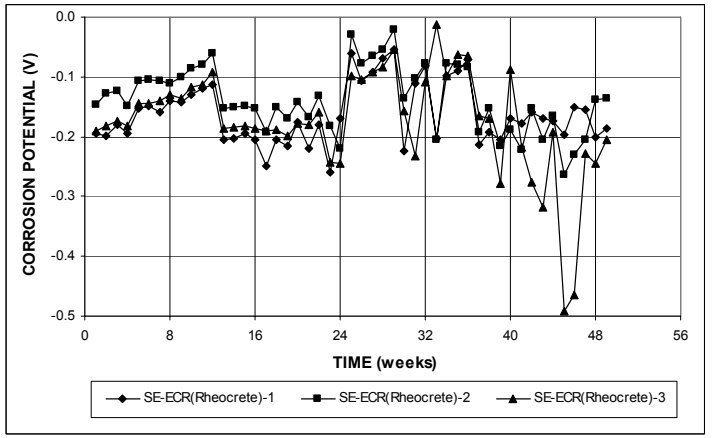

(a)

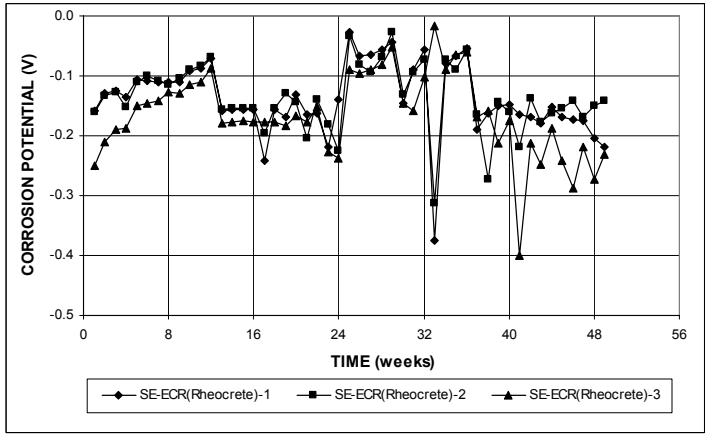

(b)

Figure A.88 – (a) Top mat corrosion potentials and (b) bottom mat corrosion potentials, with respect to copper-copper sulfate electrode as measured in the Southern Exposure test for specimens with ECR in concrete with Rheocrete (four 3-mm ($^1/_8$-in.) diameter holes).

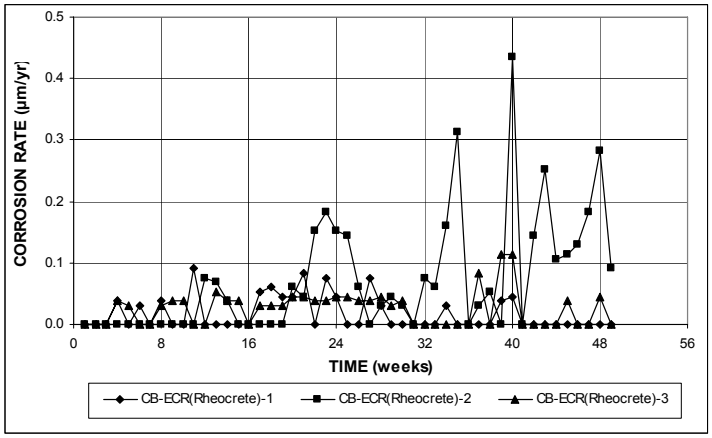

(a)

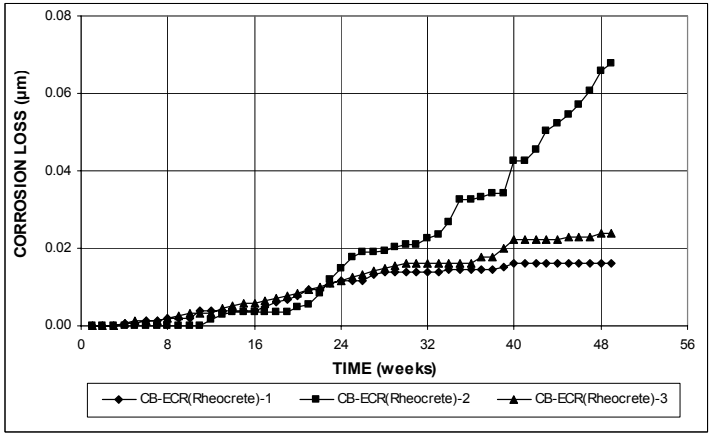

(b)

Figure A.89 – (a) Corrosion rates and (b) total corrosion losses based on total area of the bar as measured in the cracked beam test for specimens with ECR in concrete with Rheocrete (four 3-mm ($^1/_8$-in.) diameter holes).

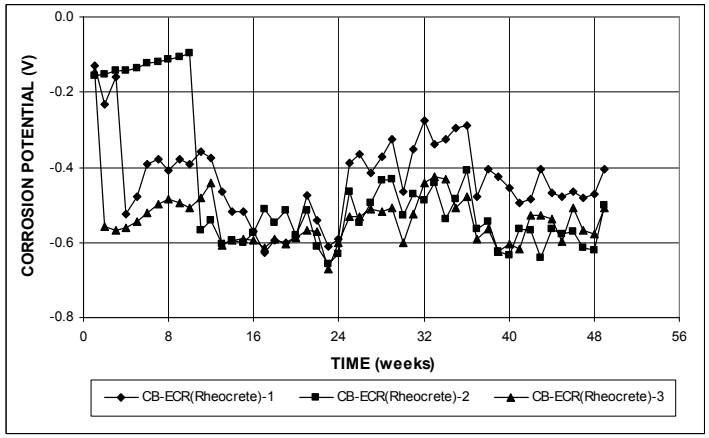

(a)

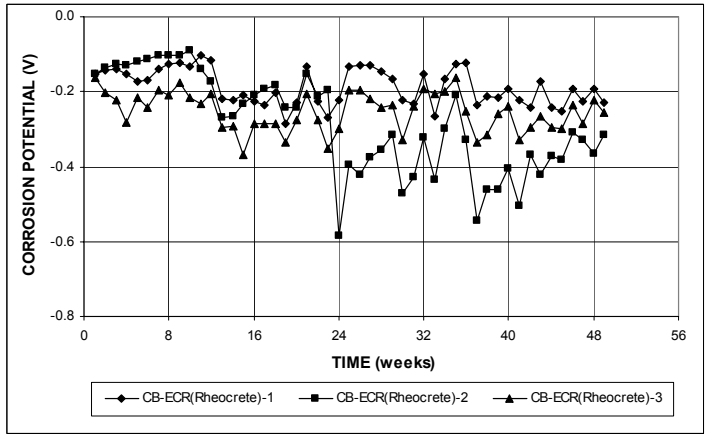

(b)

Figure A.90 – (a) Top mat corrosion potentials and (b) bottom mat corrosion potentials, with respect to copper-copper sulfate electrode as measured in the cracked beam test for specimens with ECR in concrete with Rheocrete (four 3-mm ($^1/_8$-in.) diameter holes).

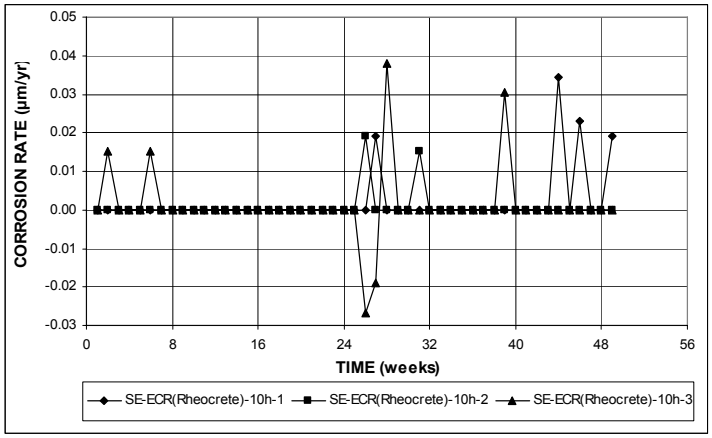

(a)

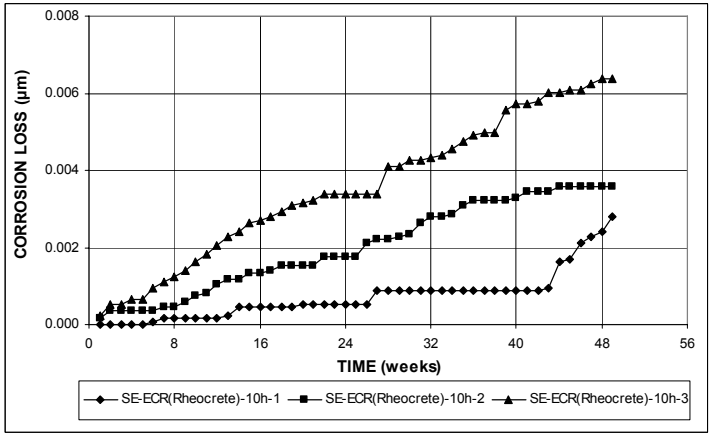

(b)

Figure A.91 – (a) Corrosion rates and (b) total corrosion losses based on total area of the bar as measured in the Southern Exposure test for specimens with ECR in concrete with Rheocrete (ten 3-mm ($^1/_8$-in.) diameter holes).

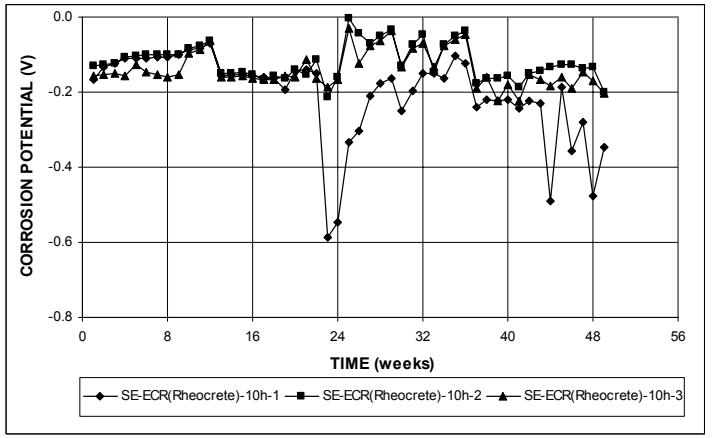

(a)

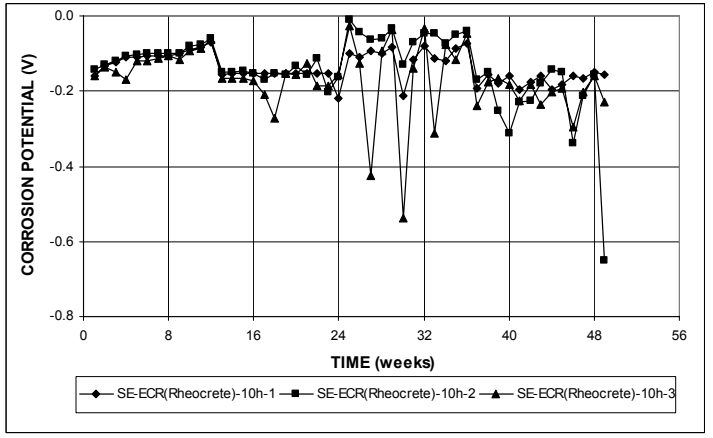

(b)

Figure A.92 – (a) Top mat corrosion potentials and (b) bottom mat corrosion potentials, with respect to copper-copper sulfate electrode as measured in the Southern Exposure test for specimens with ECR in concrete with Rheocrete (ten 3-mm ($^1/_8$-in.) diameter holes).

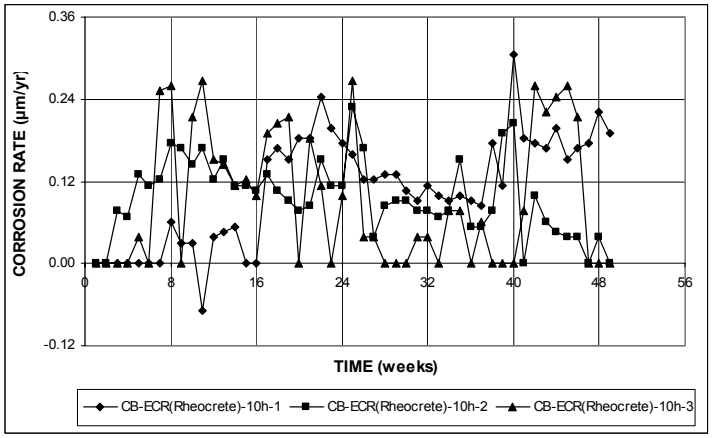

(a)

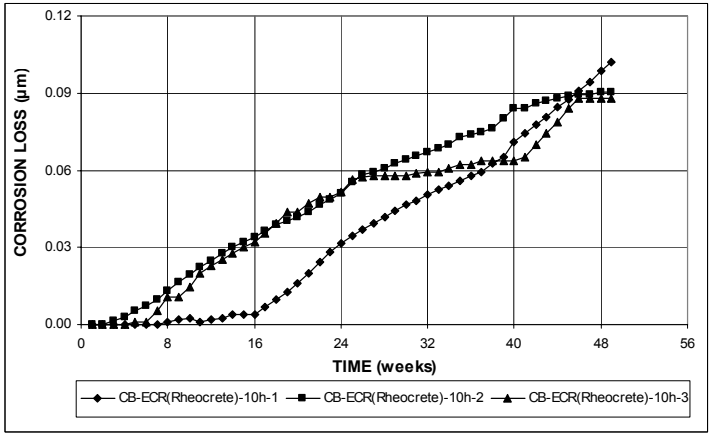

(b)

Figure A.93 – (a) Corrosion rates and (b) total corrosion losses based on total area of the bar as measured in the cracked beam test for specimens with ECR in concrete with Rheocrete (ten 3-mm ($^1/_8$-in.) diameter holes).

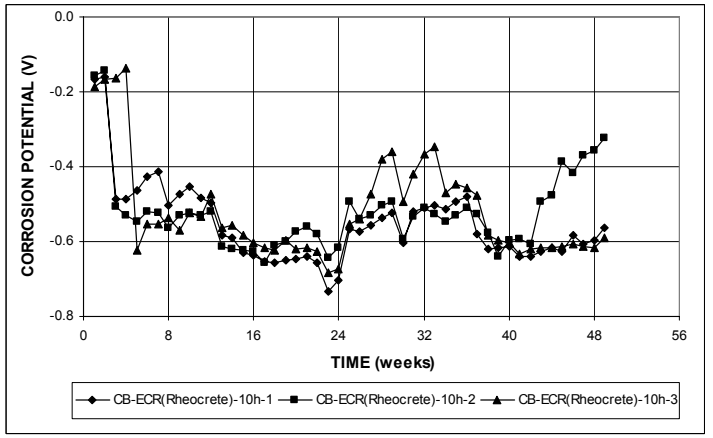

(a)

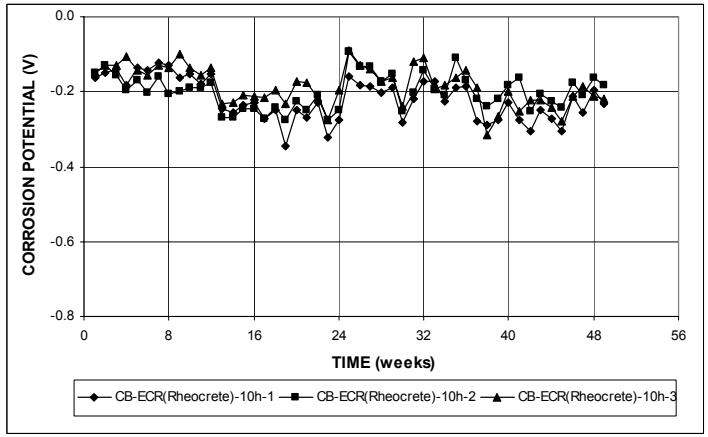

(b)

Figure A.94 – (a) Top mat corrosion potentials and (b) bottom mat corrosion potentials, with respect to copper-copper sulfate electrode as measured in the cracked beam test for specimens with ECR in concrete with Rheocrete (ten 3-mm($^1/_8$-in.) diameter holes).

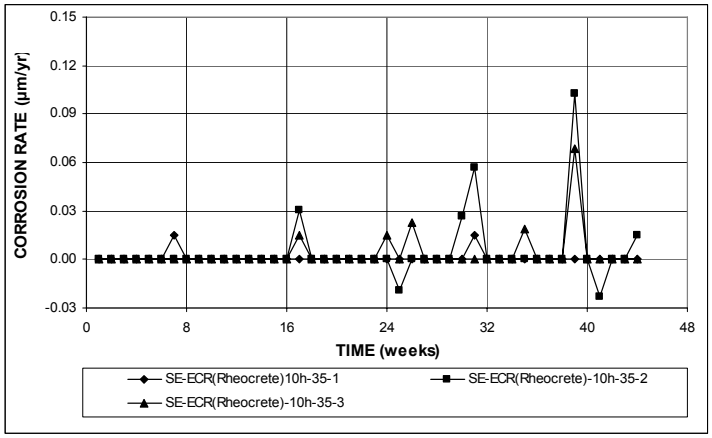

(a)

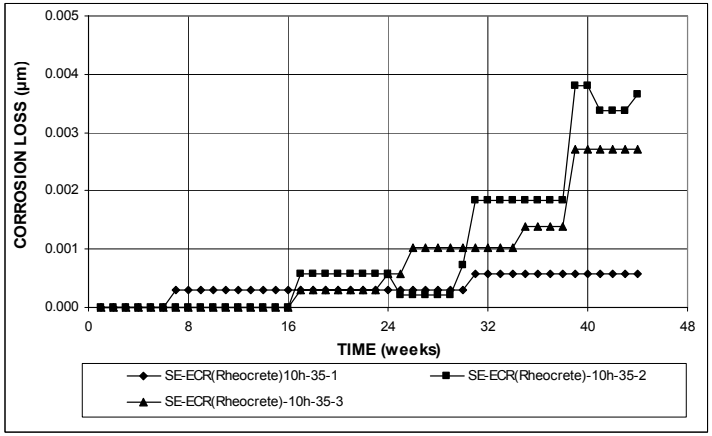

(b)

Figure A.95 – (a) Corrosion rates and (b) total corrosion losses based on total area of the bar as measured in the Southern Exposure test for specimens with ECR in concrete with Rheocrete (ten 3-mm ($^1/_8$-in.) diameter holes), a water-cement ratio of 0.35.

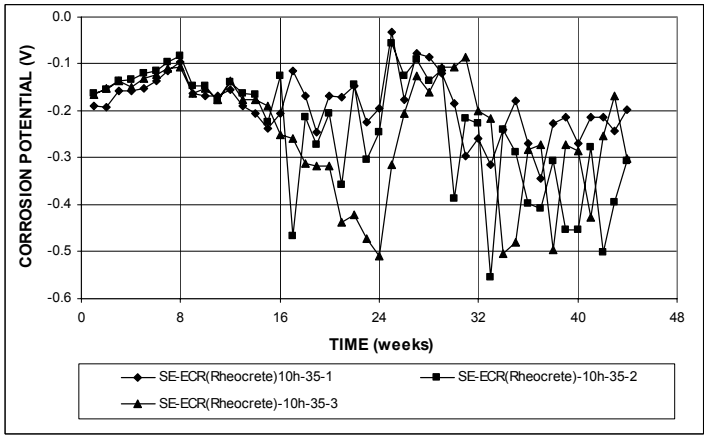

(a)

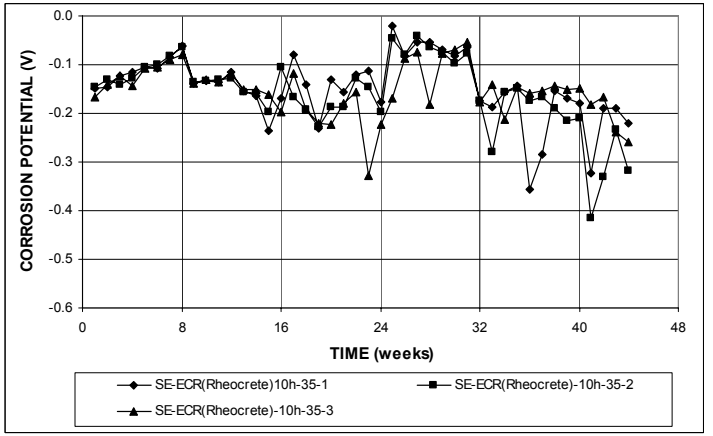

(b)

Figure A.96 – (a) Top mat corrosion potentials and (b) bottom mat corrosion potentials, with respect to copper-copper sulfate electrode as measured in the Southern Exposure test for specimens with ECR in concrete with Rheocrete (ten 3-mm ($^1/_8$-in.) diameter holes), a water-cement ratio of 0.35.

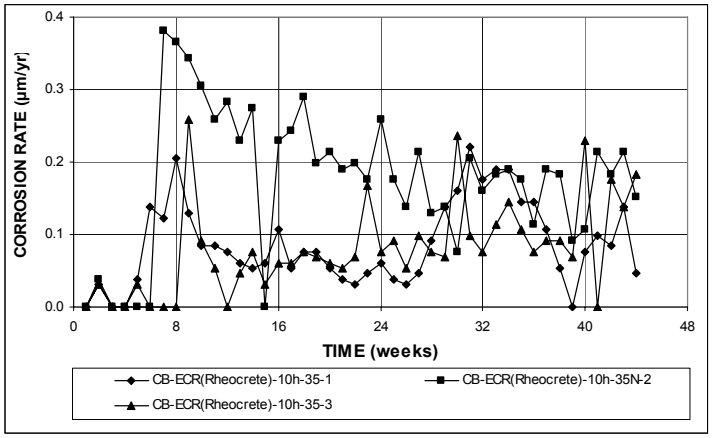

(a)

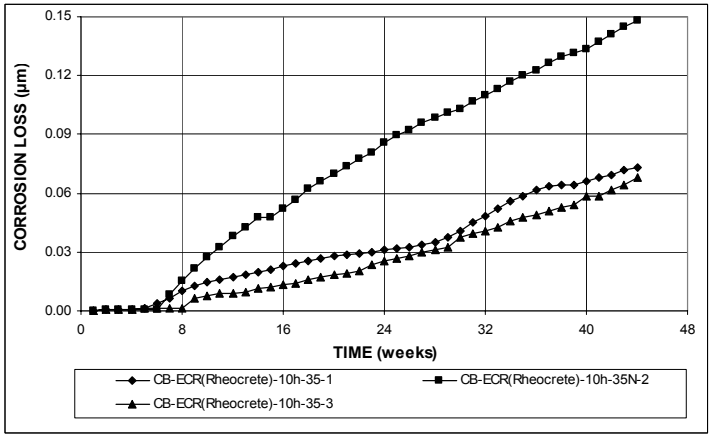

(b)

Figure A.97 – (a) Corrosion rates and (b) total corrosion losses based on total area of the bar as measured in the cracked beam test for specimens with ECR in concrete with Rheocrete (ten 3-mm ($^1/_8$-in.) diameter holes), a water-cement ratio of 0.35.

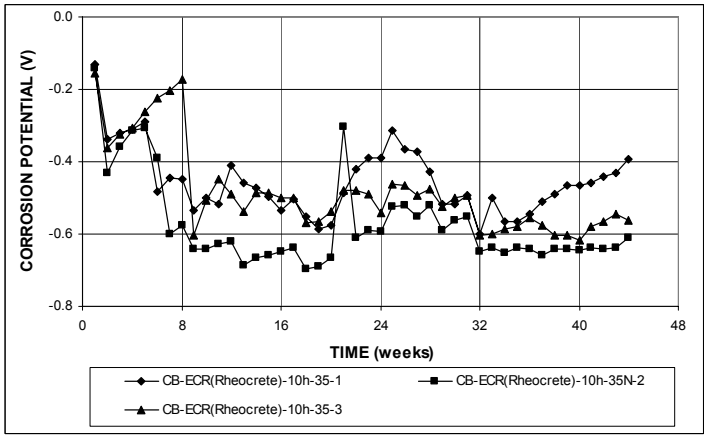

(a)

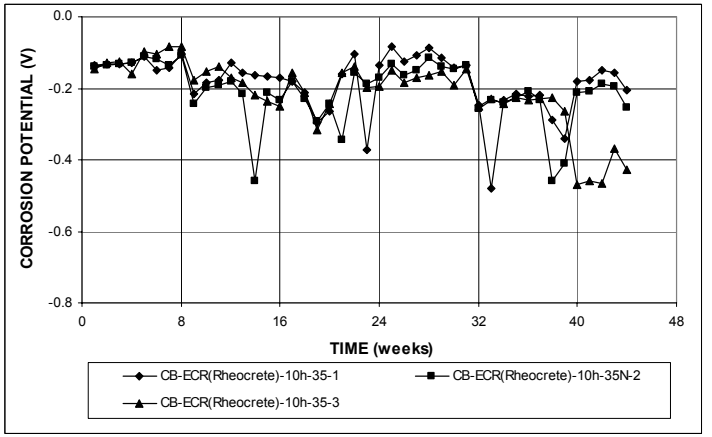

(b)

Figure A.98 – (a) Top mat corrosion potentials and (b) bottom mat corrosion potentials, with respect to copper-copper sulfate electrode as measured in the cracked beam test for specimens with ECR in concrete with Rheocrete (ten 3-mm ($^1/_8$-in.) diameter holes), a water-cement ratio of 0.35.

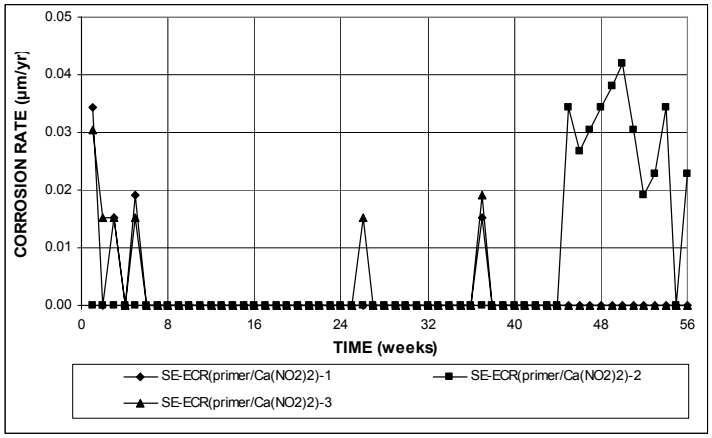

(a)

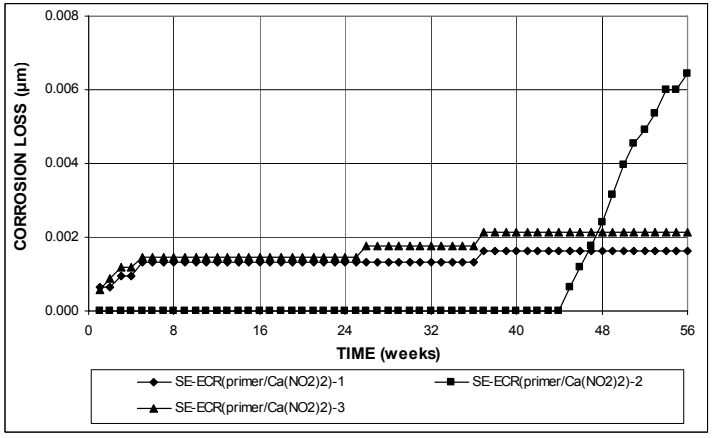

(b)

Figure A.99 – (a) Corrosion rates and (b) total corrosion losses based on total area of the bar as measured in the Southern Exposure test for specimens with ECR with a primer containing calcium nitrite (four 3-mm ($^1/_8$-in.) diameter holes).

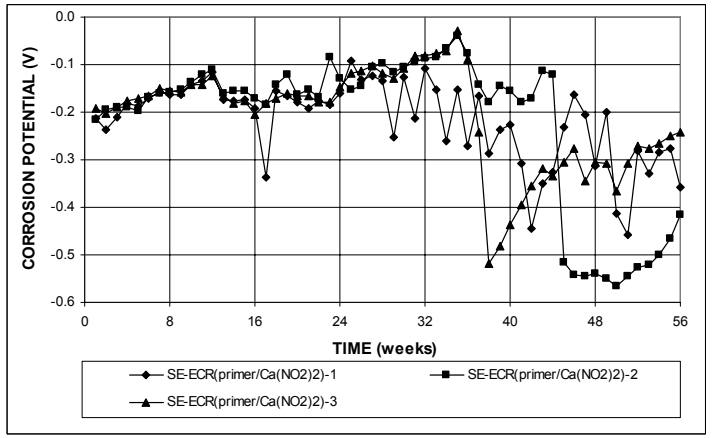

(a)

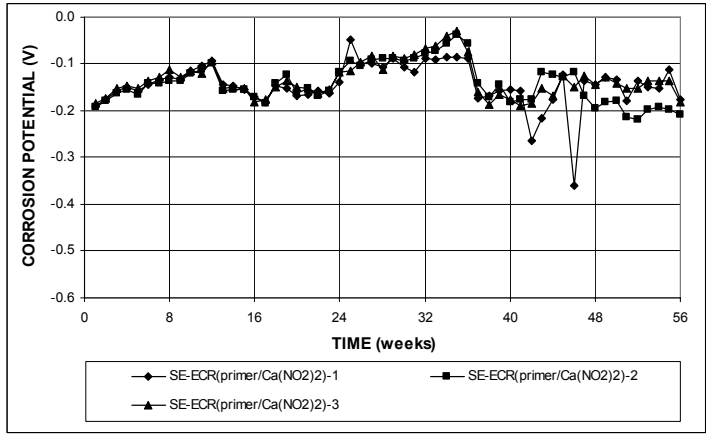

(b)

Figure A.100 – (a) Top mat corrosion potentials and (b) bottom mat corrosion potentials, with respect to copper-copper sulfate electrode as measured in the Southern Exposure test for specimens with ECR with a primer containing calcium nitrite (four 3-mm ($^1/_8$-in.) diameter holes).

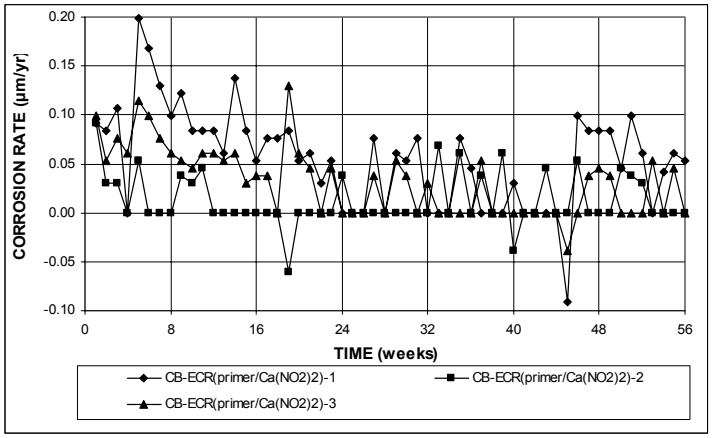

(a)

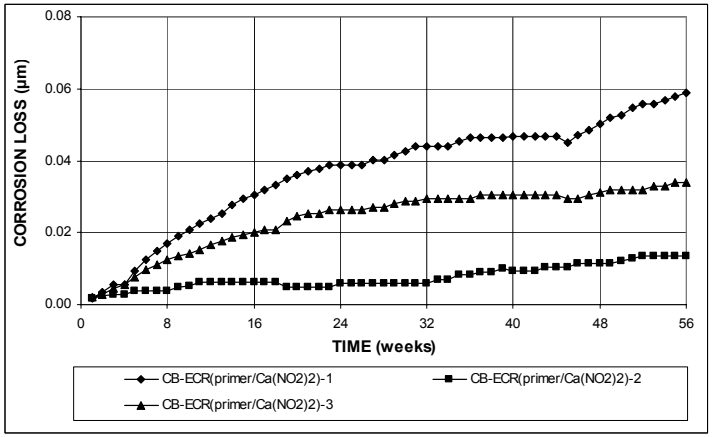

(b)

Figure A.101 – (a) Corrosion rates and (b) total corrosion losses based on total area of the bar as measured in the cracked beam test for specimens with ECR with a primer containing calcium nitrite (four 3-mm ($^1/_8$-in.) diameter holes).

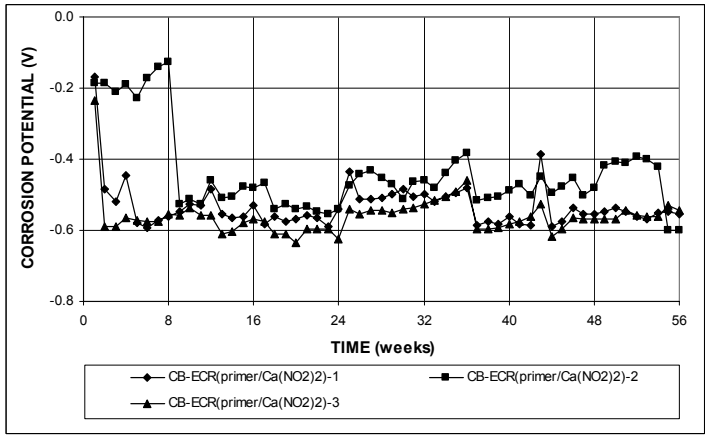

(a)

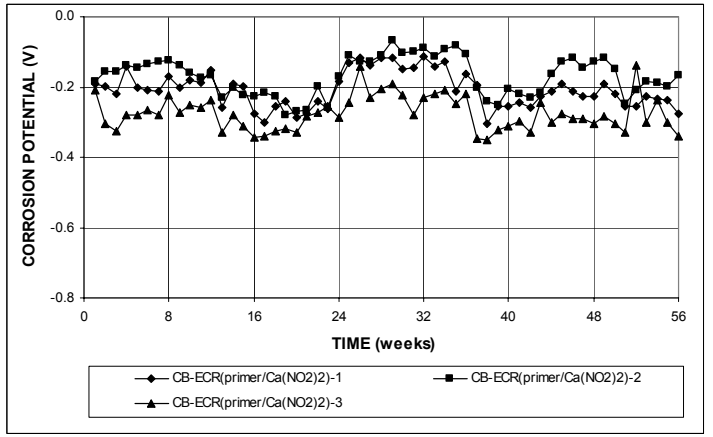

(b)

Figure A.102 – (a) Top mat corrosion potentials and (b) bottom mat corrosion potentials, with respect to copper-copper sulfate electrode as measured in the cracked beam test for specimens with ECR with a primer containing calcium nitrite (four 3-mm ($^1/_8$-in.) diameter holes).

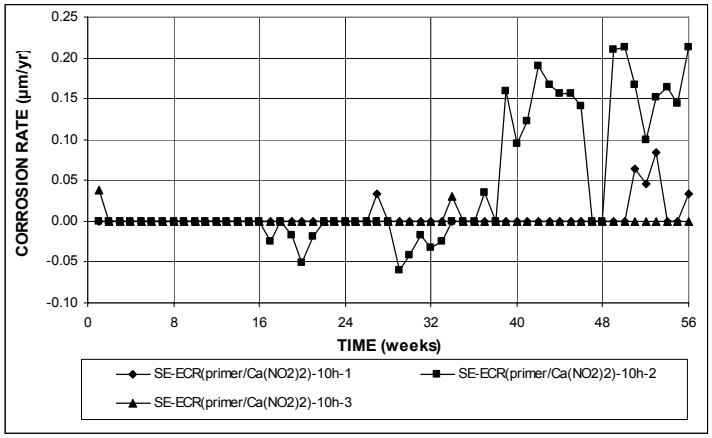

(a)

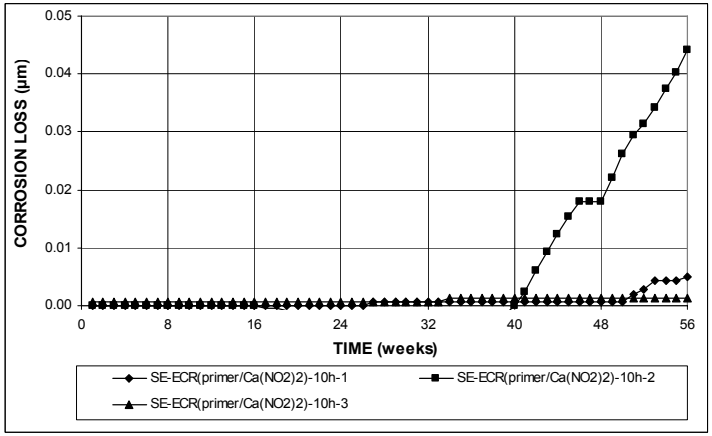

(b)

Figure A.103 – (a) Corrosion rates and (b) total corrosion losses based on total area of the bar as measured in the Southern Exposure test for specimens with ECR with a primer containing calcium nitrite (ten 3-mm ($^{1}/_{8}$-in.) diameter holes).

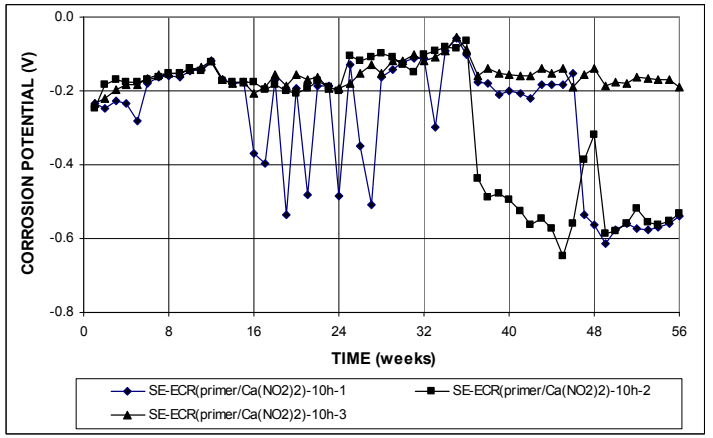

(a)

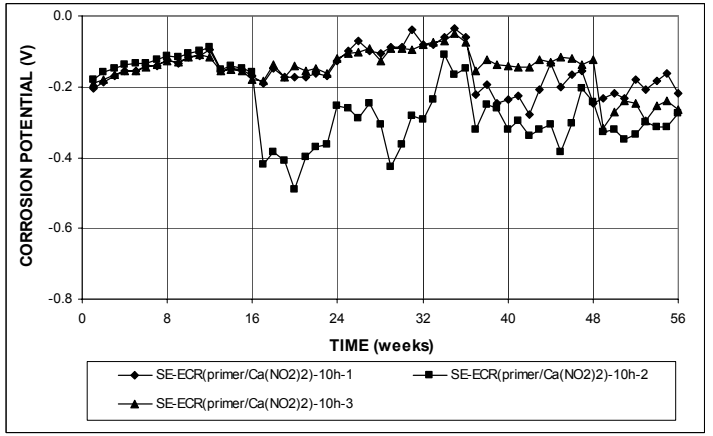

(b)

Figure A.104 – (a) Top mat corrosion potentials and (b) bottom mat corrosion potentials, with respect to copper-copper sulfate electrode as measured in the Southern Exposure test for specimens with ECR with a primer containing calcium nitrite (ten 3-mm ($^{1}/_{8}$-in.) diameter holes).

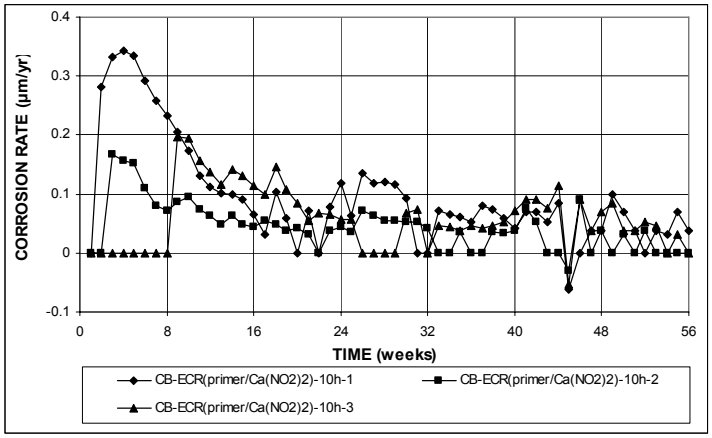

(a)

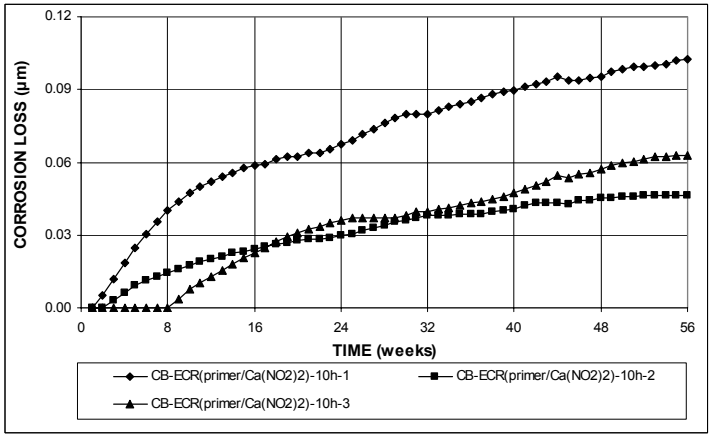

(b)

Figure A.105 – (a) Corrosion rates and (b) total corrosion losses based on total area of the bar as measured in the cracked beam test for specimens with ECR with a primer containing calcium nitrite (ten 3-mm ($^1/_8$-in.) diameter holes).

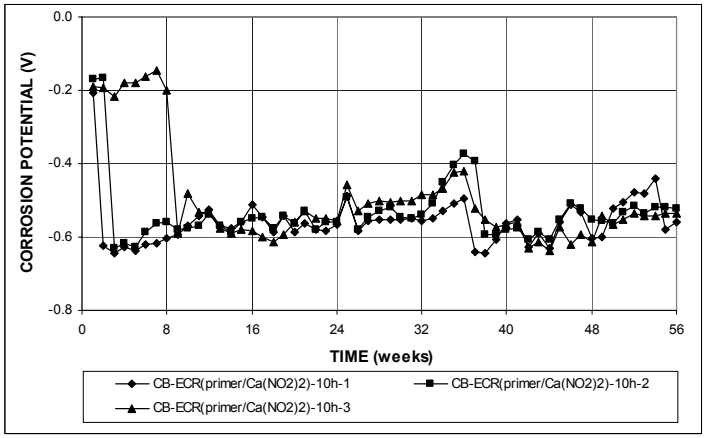

(a)

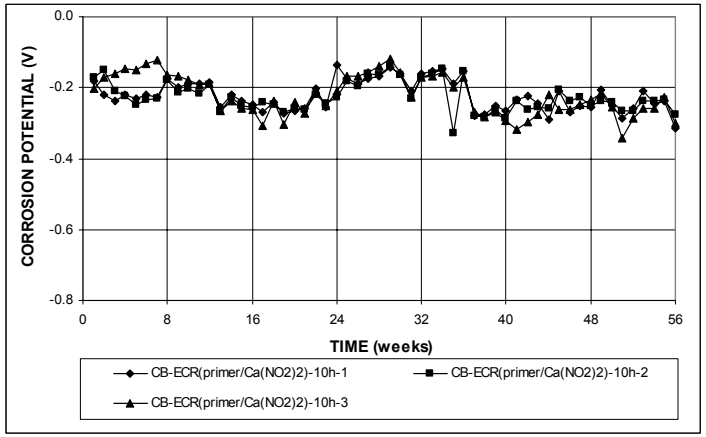

(b)

Figure A.106 – (a) Top mat corrosion potentials and (b) bottom mat corrosion potentials, with respect to copper-copper sulfate electrode as measured in the cracked beam test for specimens with ECR with a primer containing calcium nitrite (ten 3-mm ($^1/_8$-in.) diameter holes).

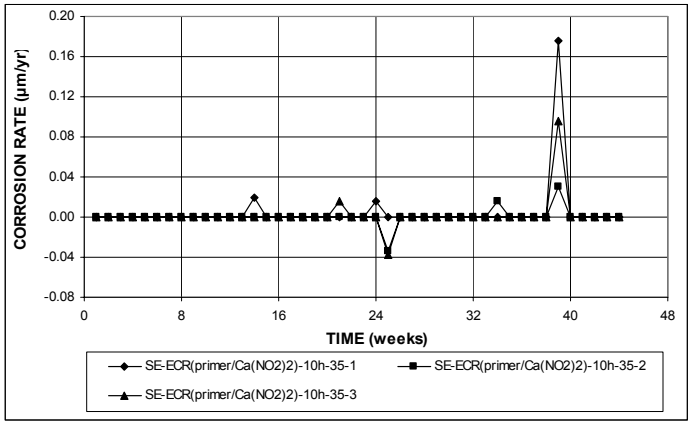

(a)

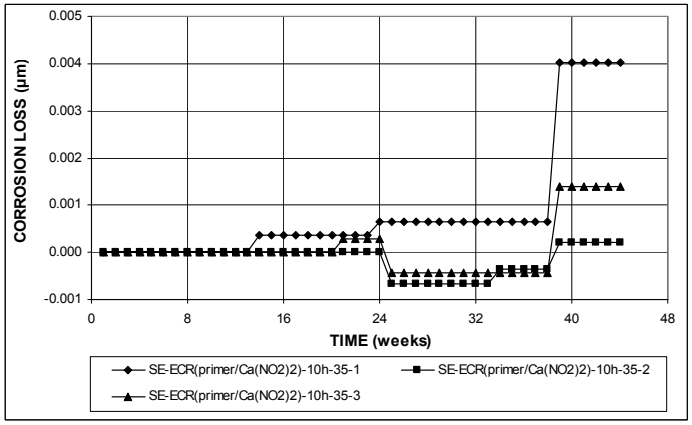

(b)

Figure A.107 – (a) Corrosion rates and (b) total corrosion losses based on total area of the bar as measured in the Southern Exposure test for specimens with ECR with a primer containing calcium nitrite (ten 3-mm ($^1/_8$-in.) diameter holes), a water-cement ratio of 0.35.

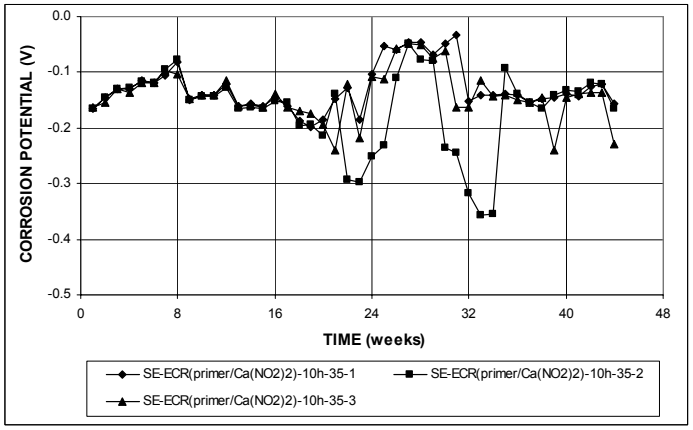

(a)

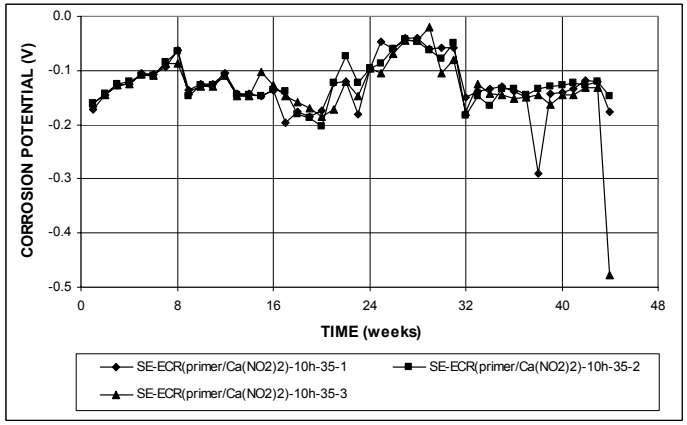

(b)

Figure A.108 – (a) Top mat corrosion potentials and (b) bottom mat corrosion potentials, with respect to copper-copper sulfate electrode as measured in the Southern Exposure test for specimens with ECR with a primer containing calcium nitrite (ten 3-mm ($^1/_8$-in.) diameter holes), a water-cement ratio of 0.35.

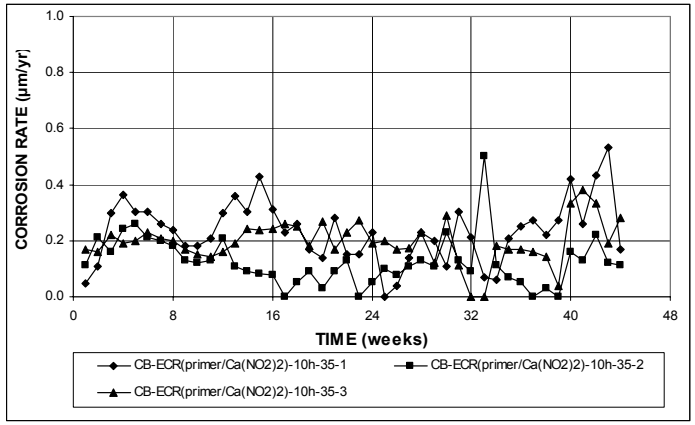

(a)

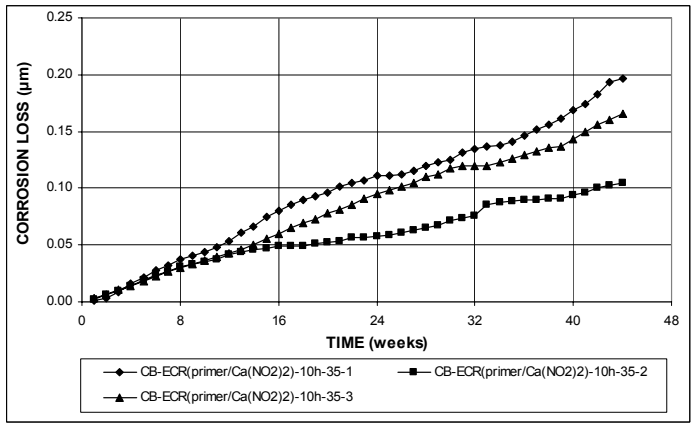

(b)

Figure A.109 – (a) Corrosion rates and (b) total corrosion losses based on total area of the bar as measured in the cracked beam test for specimens with ECR with a primer containing calcium nitrite (ten 3-mm ($^1/_8$-in.) diameter holes), a water-cement ratio of 0.35.

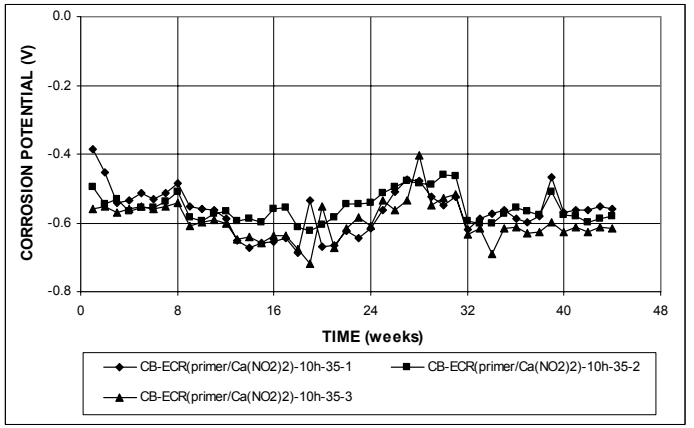

(a)

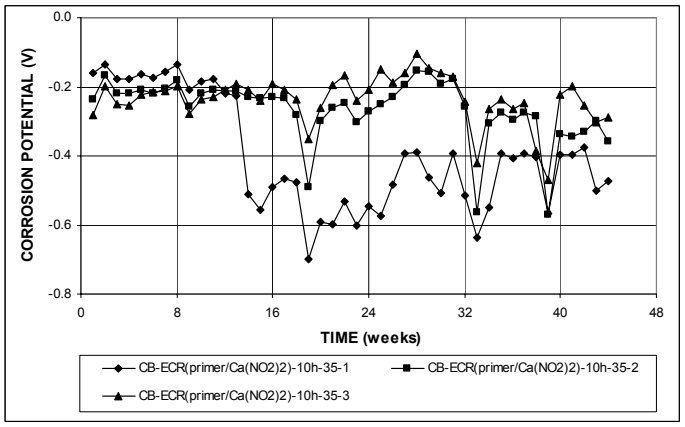

(b)

Figure A.110 – (a) Top mat corrosion potentials and (b) bottom mat corrosion potentials, with respect to copper-copper sulfate electrode as measured in the cracked beam test for specimens with ECR with a primer containing calcium nitrite (ten 3-mm ($^1/_8$-in.) diameter holes), a water-cement ratio of 0.35.

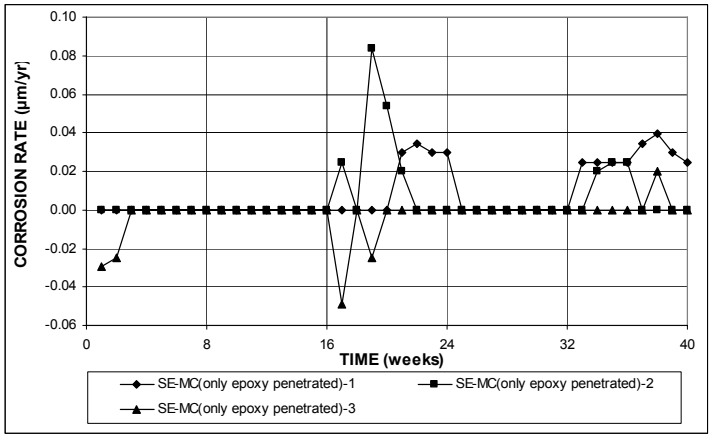

(a)

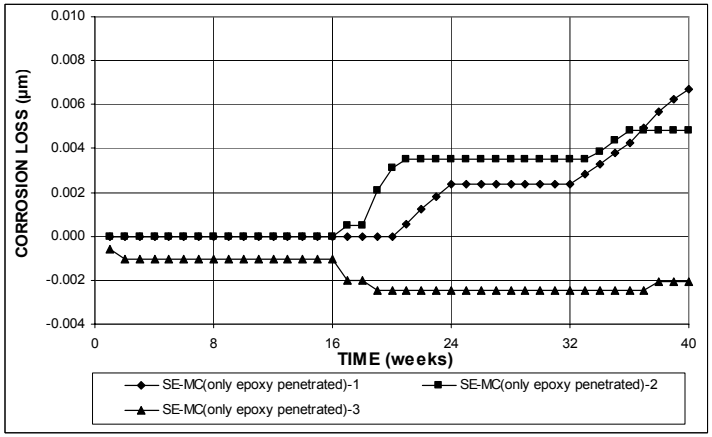

(b)

Figure A.111 – (a) Corrosion rates and (b) total corrosion losses based on total area of the bar as measured in the Southern Exposure test for specimens with multiple coated bar (four 3-mm ($^1/_8$-in.) diameter holes, only epoxy penetrated).

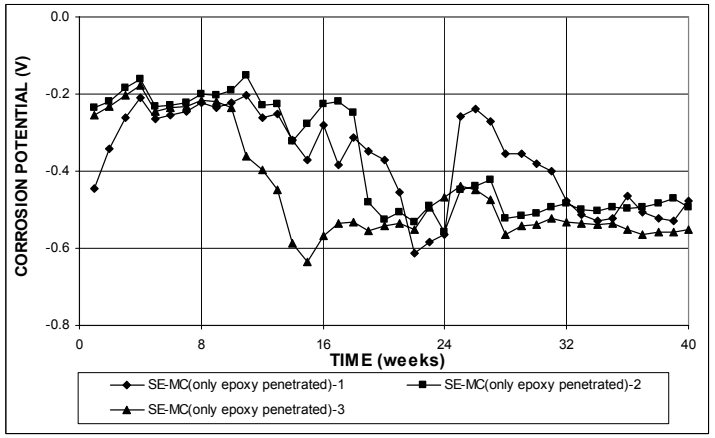

(a)

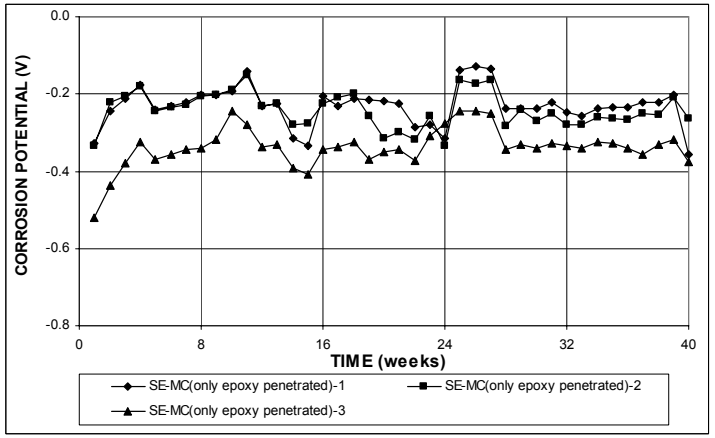

(b)

Figure A.112 – (a) Top mat corrosion potentials and (b) bottom mat corrosion potentials, with respect to copper-copper sulfate electrode as measured in the Southern Exposure test for specimens with ECR with multiple coated bar (four 3-mm ($^1/_8$-in.) diameter holes, only epoxy penetrated).

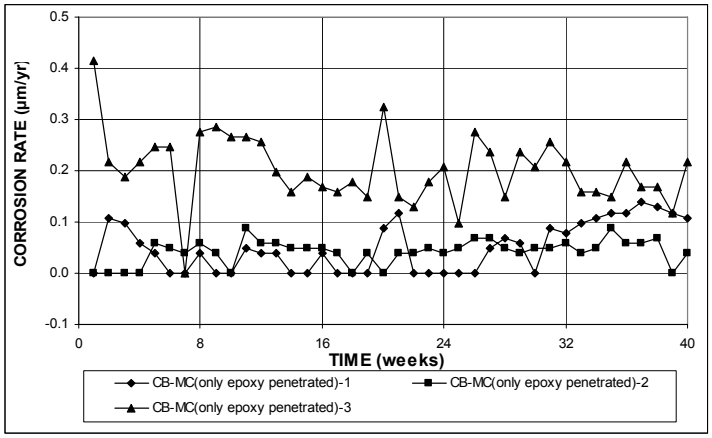

(a)

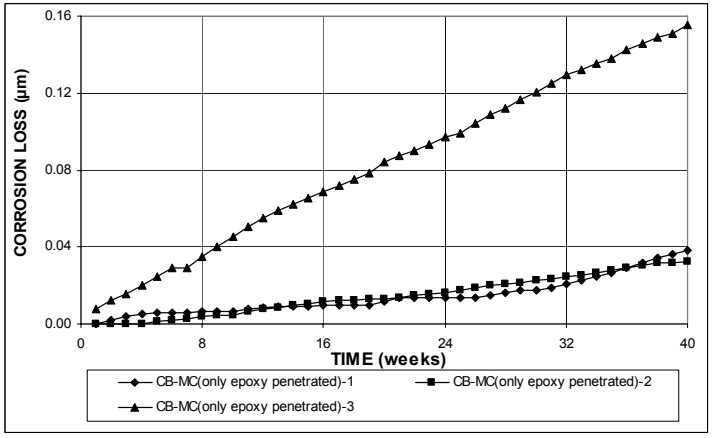

(b)

Figure A.113 – (a) Corrosion rates and (b) total corrosion losses based on total area of the bar as measured in the cracked beam test for specimens with multiple coated bar (four 3-mm ($^{1}/_{8}$-in.) diameter holes, only epoxy penetrated).

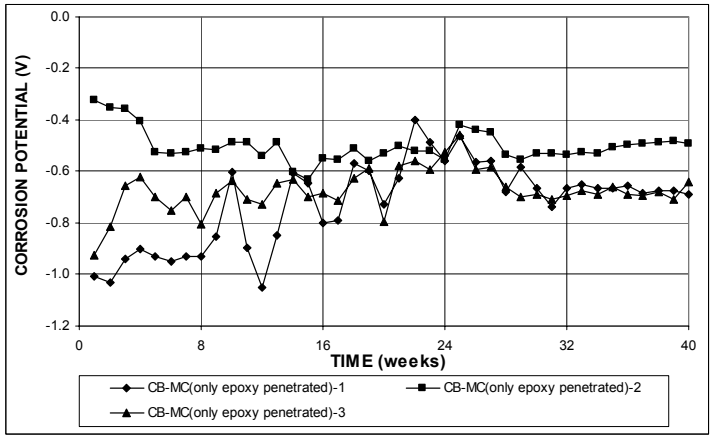

(a)

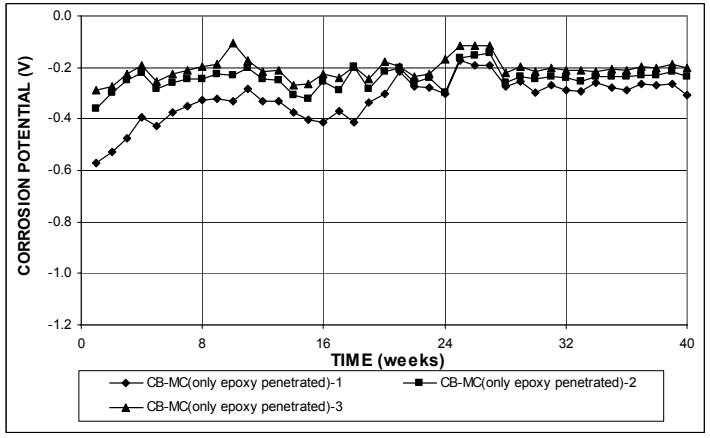

(b)

Figure A.114 – (a) Top mat corrosion potentials and (b) bottom mat corrosion potentials, with respect to copper-copper sulfate electrode as measured in the cracked beam test for specimens with ECR with multiple coated bar (four 3-mm ($^{1}/_{8}$-in.) diameter holes, only epoxy penetrated).

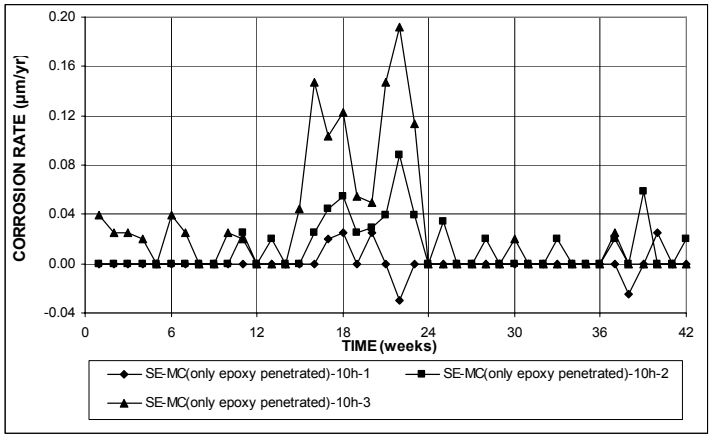

(a)

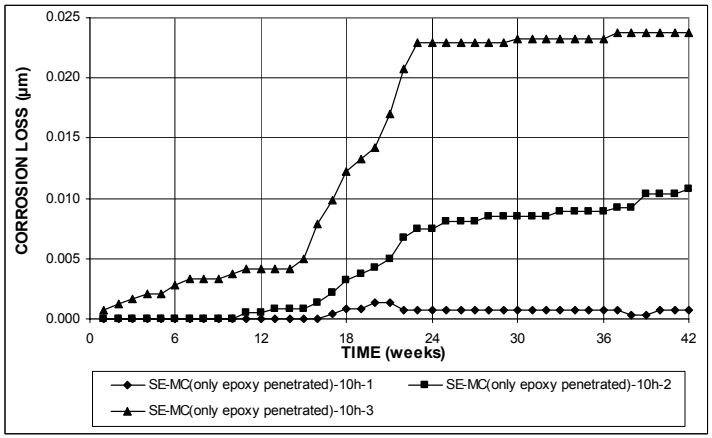

(b)

Figure A.115 – (a) Corrosion rates and (b) total corrosion losses based on total area of the bar as measured in the Southern Exposure test for specimens with multiple coated bar (ten 3-mm ($^1/_8$-in.) diameter holes, only epoxy penetrated).

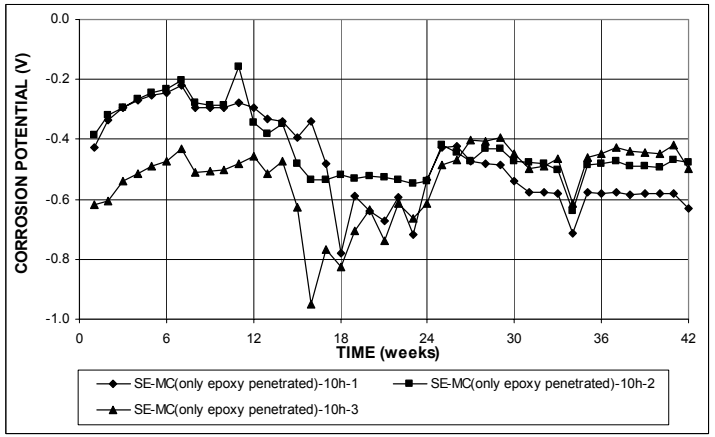

(a)

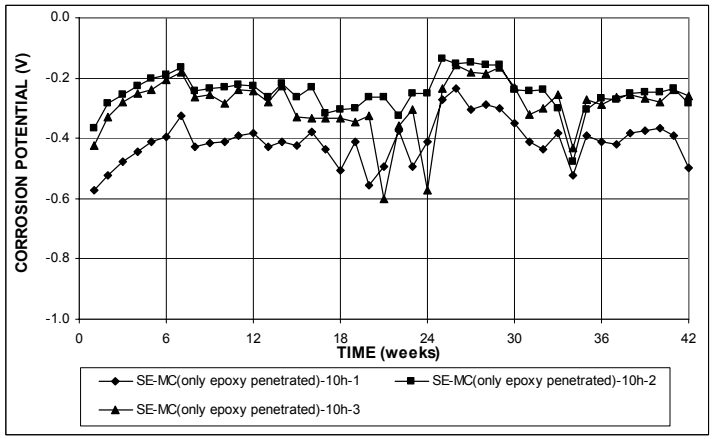

(b)

Figure A.116 – (a) Top mat corrosion potentials and (b) bottom mat corrosion potentials, with respect to copper-copper sulfate electrode as measured in the Southern Exposure test for specimens with ECR with multiple coated bar (ten 3-mm ($^1/_8$-in.) diameter holes, only epoxy penetrated).

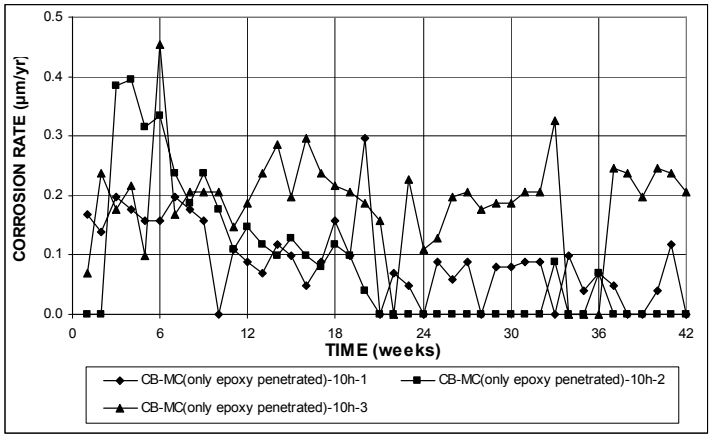

(a)

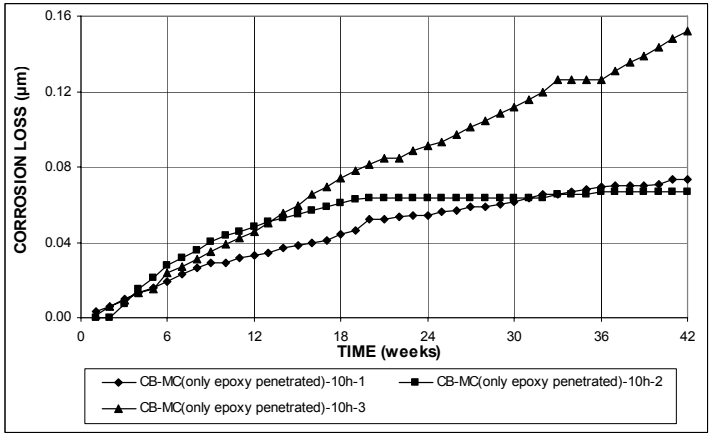

(b)

Figure A.117 – (a) Corrosion rates and (b) total corrosion losses based on total area of the bar as measured in the cracked beam test for specimens with multiple coated bar (ten 3-mm ($^1/_8$-in.) diameter holes, only epoxy penetrated).

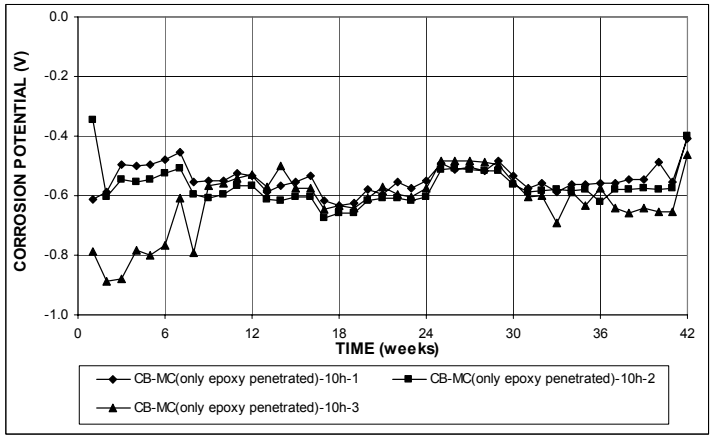

(a)

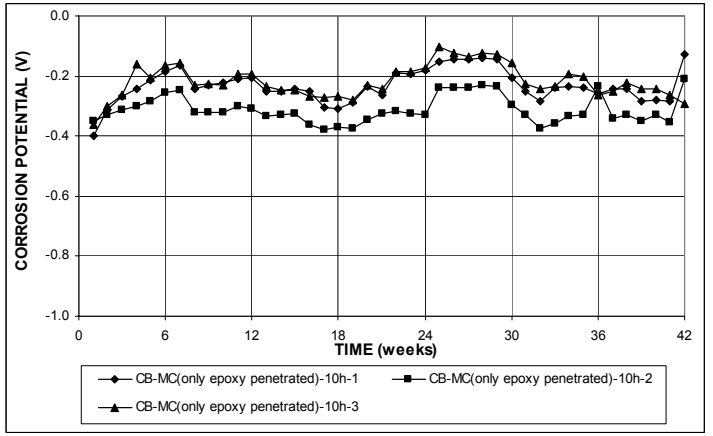

(b)

Figure A.118 – (a) Top mat corrosion potentials and (b) bottom mat corrosion potentials, with respect to copper-copper sulfate electrode as measured in the cracked beam test for specimens with ECR with multiple coated bar (ten 3-mm ($^1/_8$-in.) diameter holes, only epoxy penetrated).

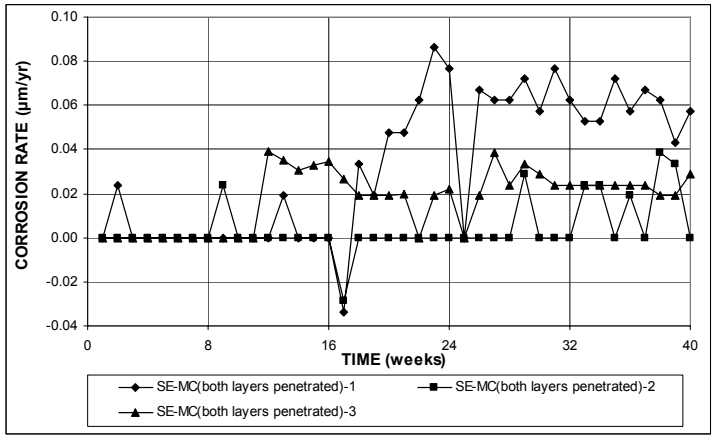

(a)

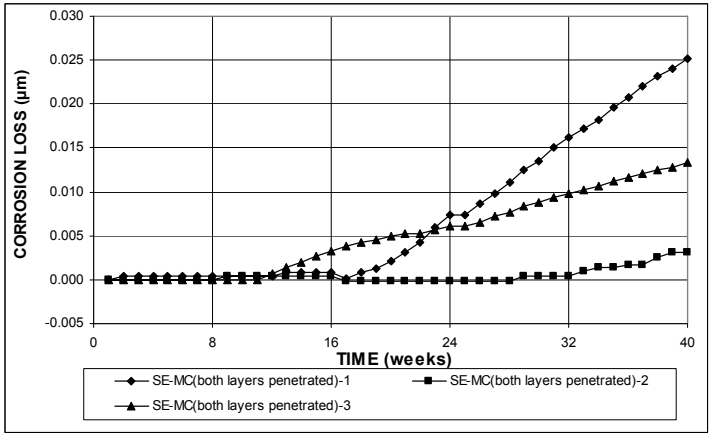

(b)

Figure A.119 – (a) Corrosion rates and (b) total corrosion losses based on total area of the bar as measured in the Southern Exposure test for specimens with multiple coated bar (four 3-mm ($^1/_8$-in.) diameter holes, both layers penetrated).

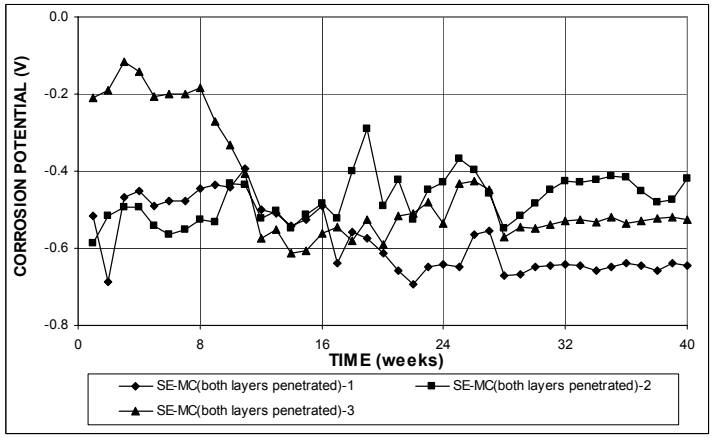

(a)

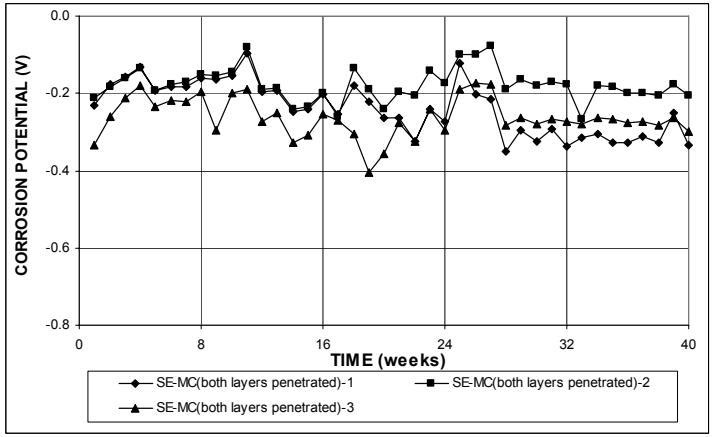

(b)

Figure A.120 – (a) Top mat corrosion potentials and (b) bottom mat corrosion potentials, with respect to copper-copper sulfate electrode as measured in the Southern Exposure test for specimens with ECR with multiple coated bar (four 3-mm ($^1/_8$-in.) diameter holes, both layers penetrated).

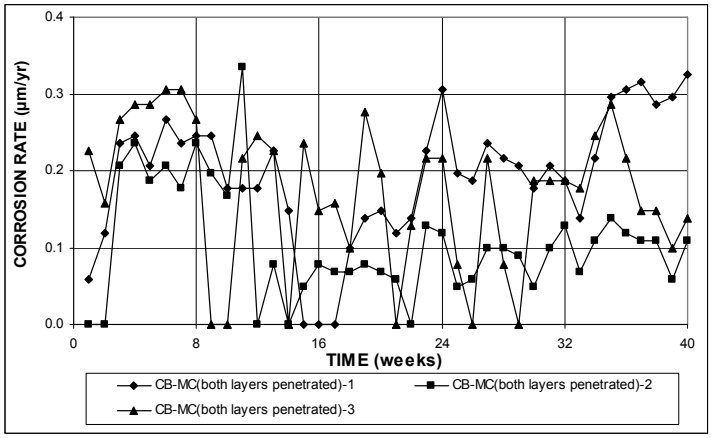

(a)

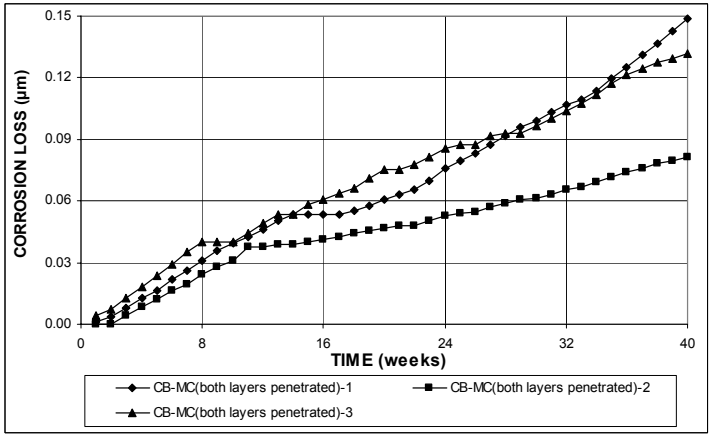

(b)

Figure A.121 – (a) Corrosion rates and (b) total corrosion losses based on total area of the bar as measured in the cracked beam test for specimens with multiple coated bar (four 3-mm ($^1/_8$-in.) diameter holes, both layers penetrated).

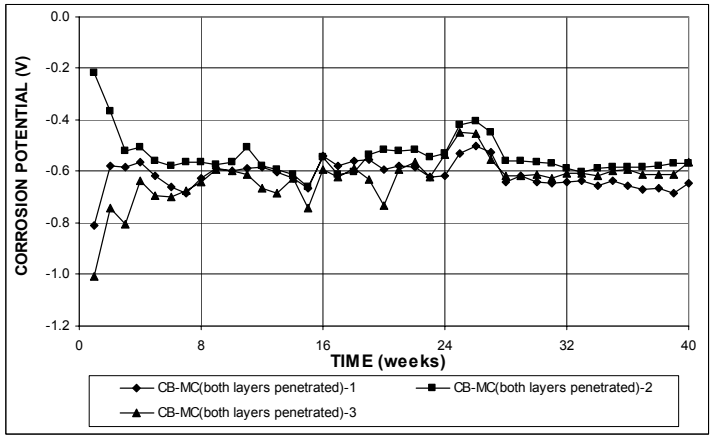

(a)

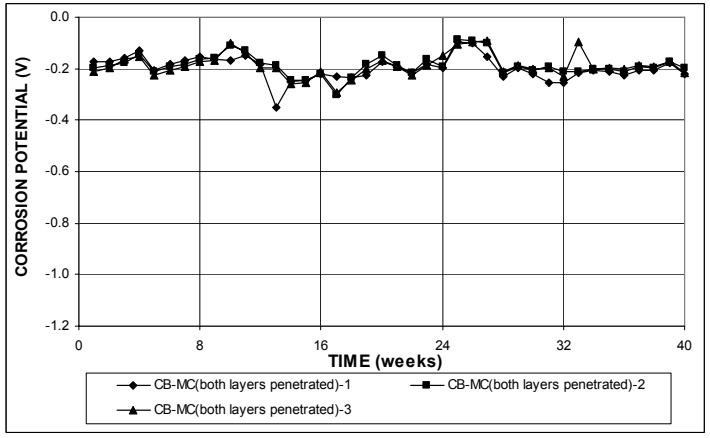

(b)

Figure A.122 – (a) Top mat corrosion potentials and (b) bottom mat corrosion potentials, with respect to copper-copper sulfate electrode as measured in the cracked beam test for specimens with ECR with multiple coated bar (four 3-mm ($^1/_8$-in.) diameter holes, both layers penetrated).

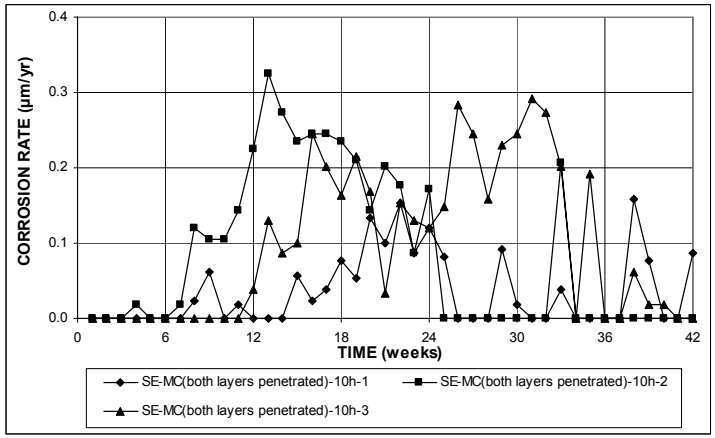

(a)

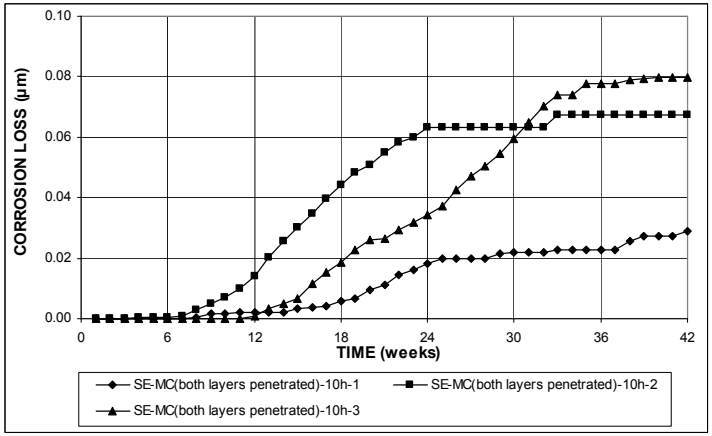

(b)

Figure A.123 – (a) Corrosion rates and (b) total corrosion losses based on total area of the bar as measured in the Southern Exposure test for specimens with multiple coated bar (ten 3-mm ($^1/_8$-in.) diameter holes, both layers penetrated).

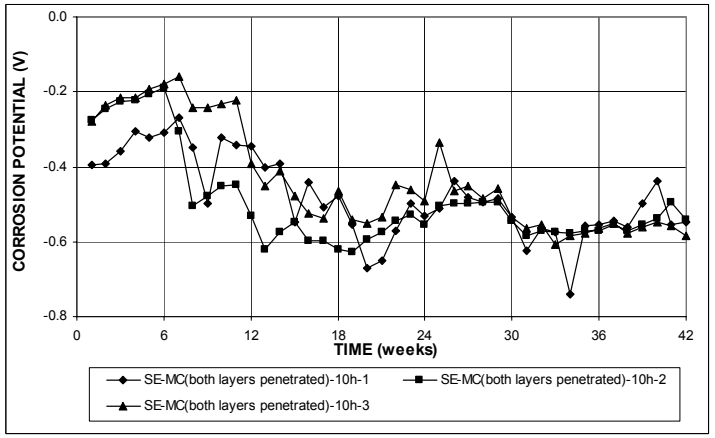

(a)

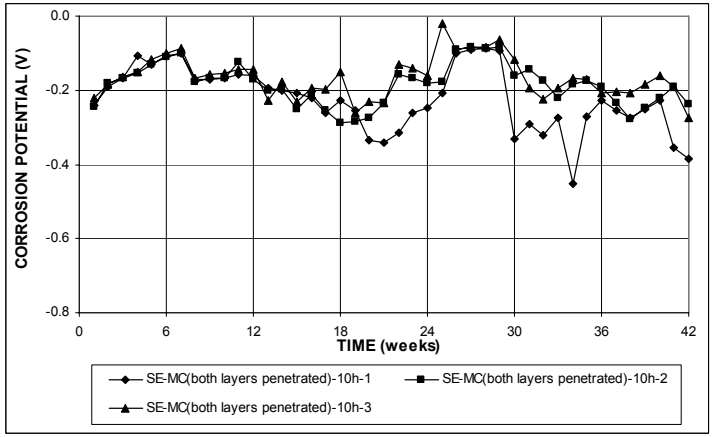

(b)

Figure A.124 – (a) Top mat corrosion potentials and (b) bottom mat corrosion potentials, with respect to copper-copper sulfate electrode as measured in the Southern Exposure test for specimens with ECR with multiple coated bar (ten 3-mm ($^1/_8$-in.) diameter holes, both layers penetrated).

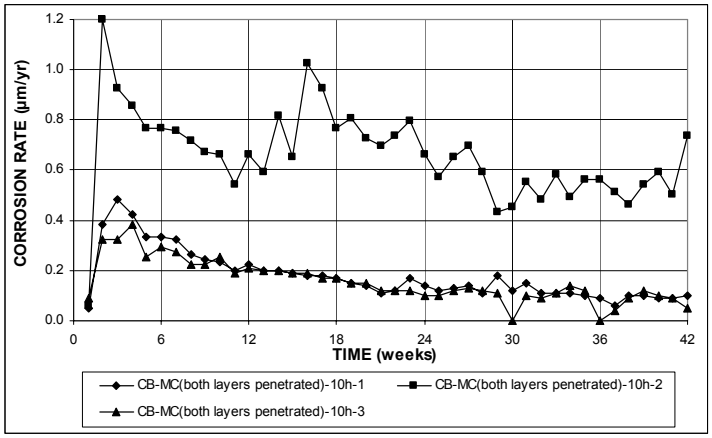

(a)

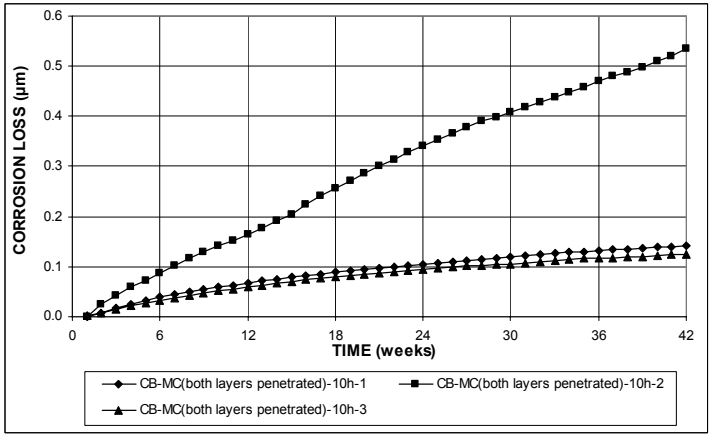

(b)

Figure A.125 – (a) Corrosion rates and (b) total corrosion losses based on total area of the bar as measured in the cracked beam test for specimens with multiple coated bar (ten 3-mm ($^1/_8$-in.) diameter holes, both layers penetrated).

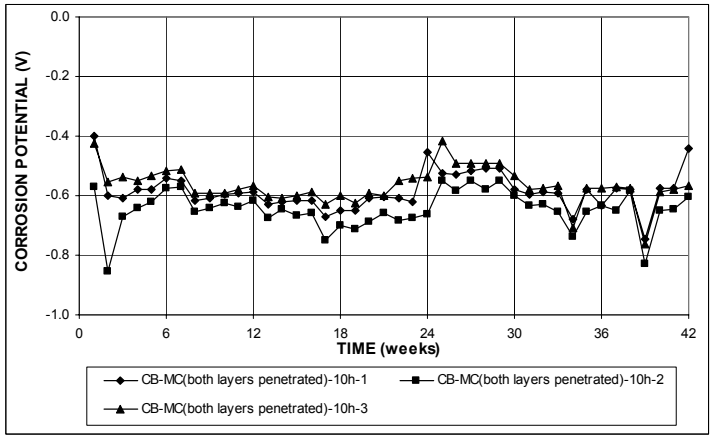

(a)

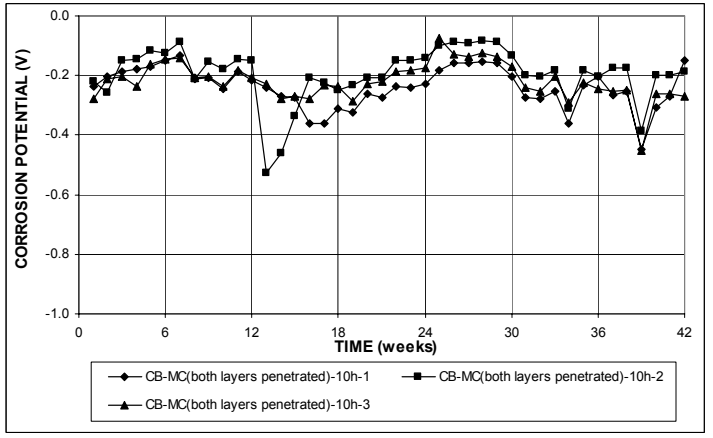

(b)

Figure A.126 – (a) Top mat corrosion potentials and (b) bottom mat corrosion potentials, with respect to copper-copper sulfate electrode as measured in the cracked beam test for specimens with ECR with multiple coated bar (ten 3-mm ($^1/_8$-in.) diameter holes, both layers penetrated).

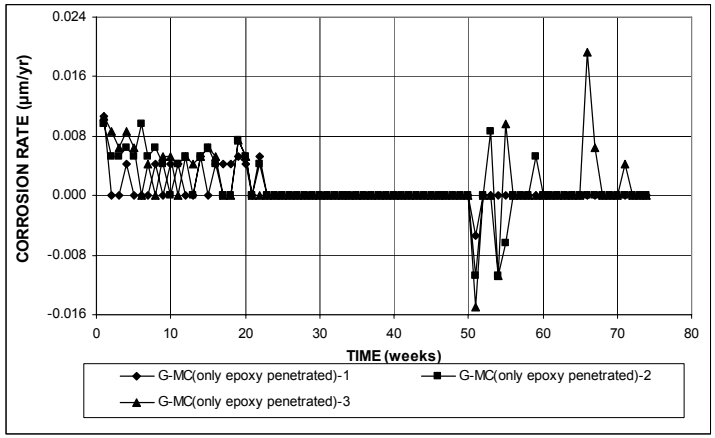

(a)

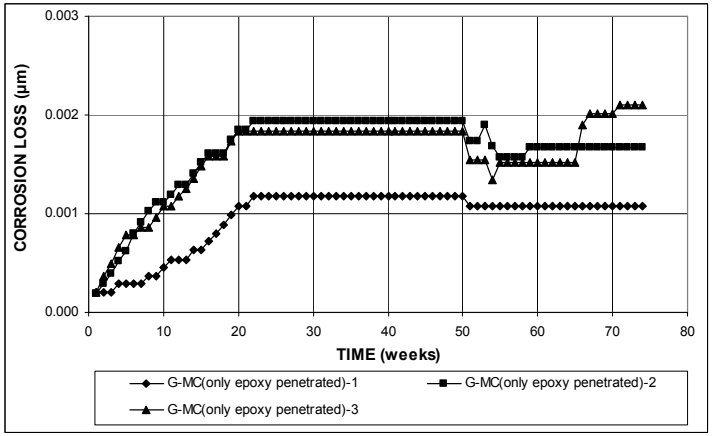

(b)

Figure A.127 – (a) Corrosion rates and (b) total corrosion losses based on total area of the bar as measured in the ASTM G 109 test for specimens with multiple coated bar (four 3-mm ($^1/_8$-in.) diameter holes, only epoxy penetrated).

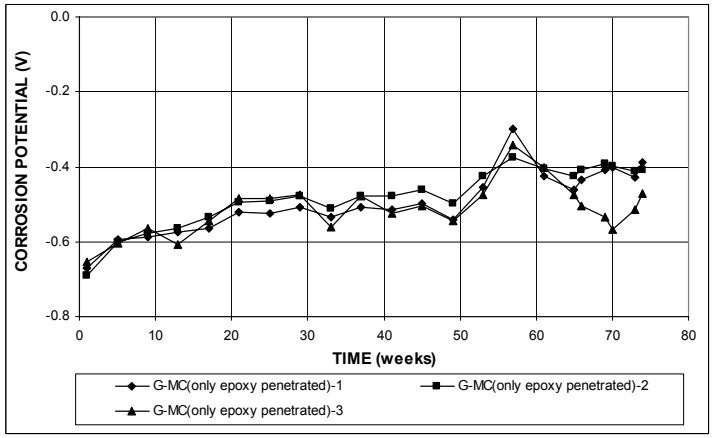

(a)

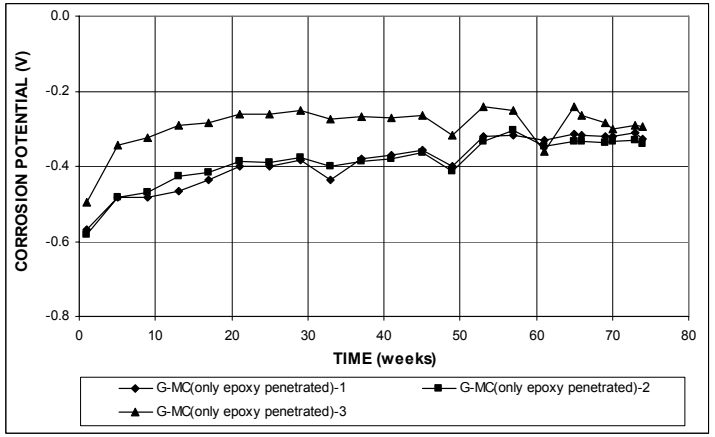

(b)

Figure A.128 – (a) Top mat corrosion potentials and (b) bottom mat corrosion potentials, with respect to copper-copper sulfate electrode as measured in the ASTM G 109 test for specimens with multiple coated bar (four 3-mm ($^1/_8$-in.) diameter holes, only epoxy penetrated).

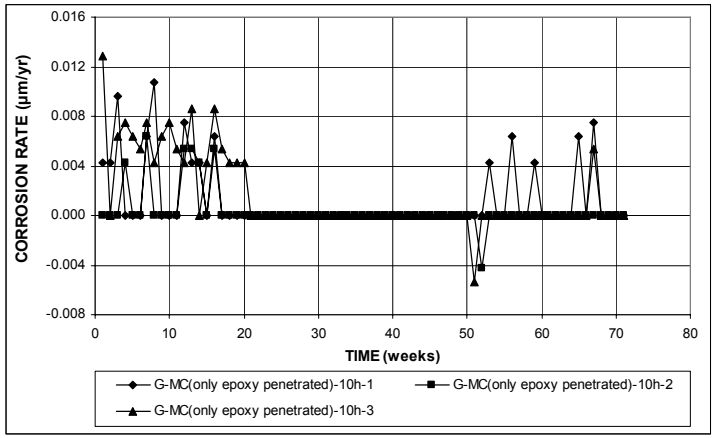

(a)

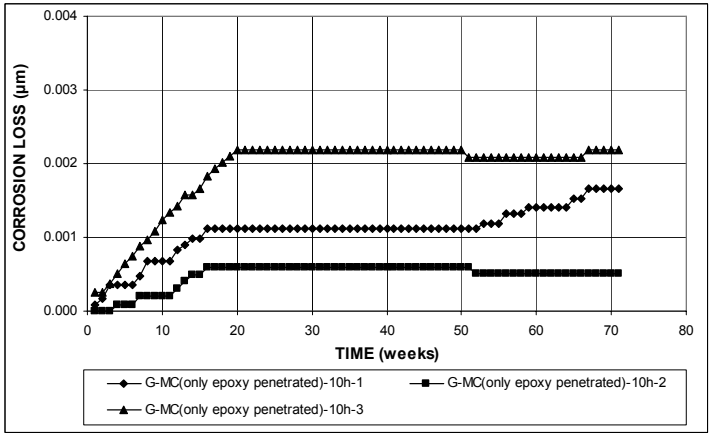

(b)

Figure A.129 – (a) Corrosion rates and (b) total corrosion losses based on total area of the bar as measured in the ASTM G 109 test for specimens with multiple coated bar (ten 3-mm ($^1/_8$-in.) diameter holes, only epoxy penetrated).

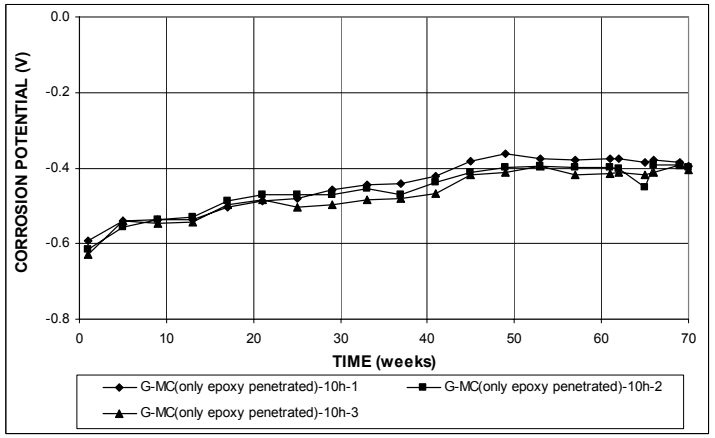

(a)

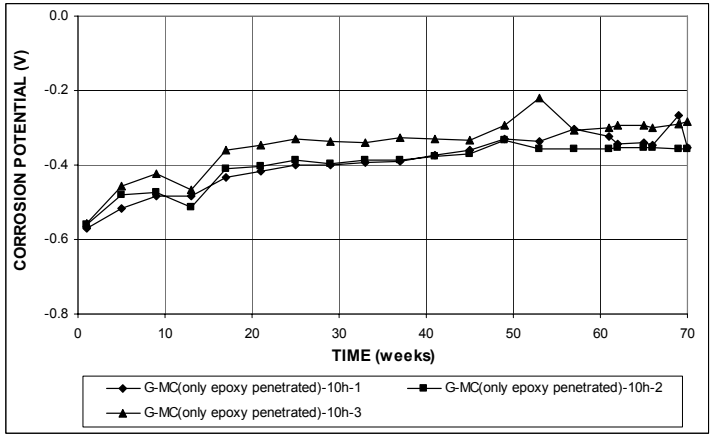

(b)

Figure A.130 – (a) Top mat corrosion potentials and (b) bottom mat corrosion potentials, with respect to copper-copper sulfate electrode as measured in the ASTM G 109 test for specimens with multiple coated bar (ten 3-mm ($^1/_8$-in.) diameter holes, only epoxy penetrated).

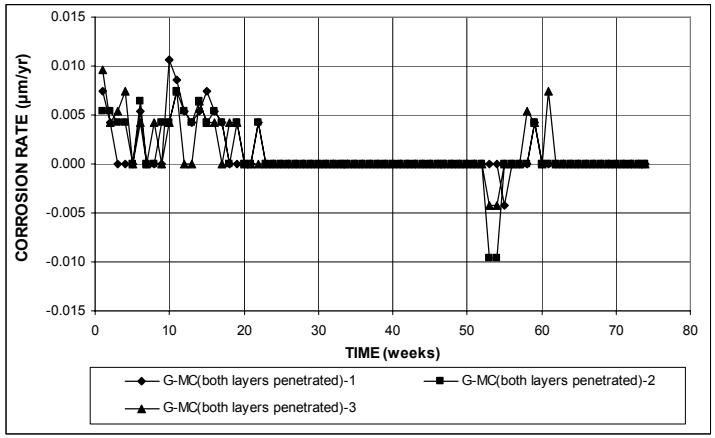

(a)

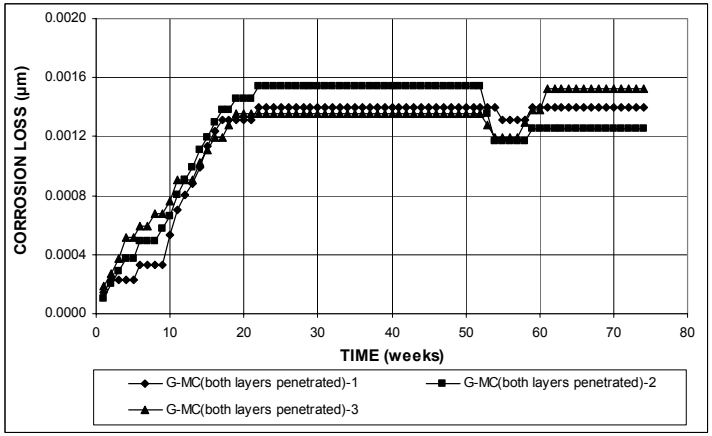

(b)

Figure A.131 – (a) Corrosion rates and (b) total corrosion losses based on total area of the bar as measured in the ASTM G 109 test for specimens with multiple coated bar (four 3-mm ($^1/_8$-in.) diameter holes, both layers penetrated).

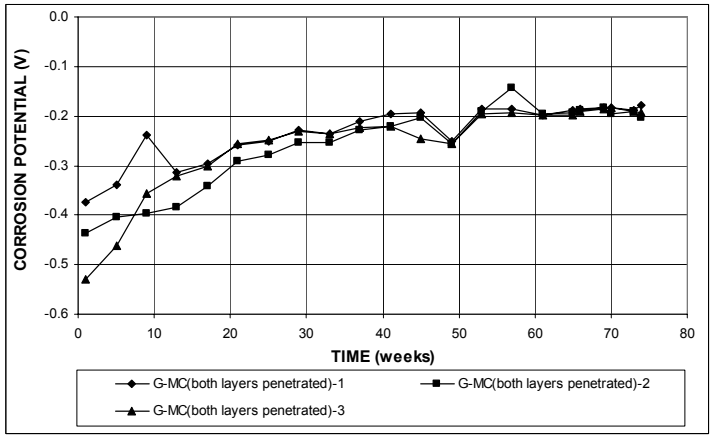

(a)

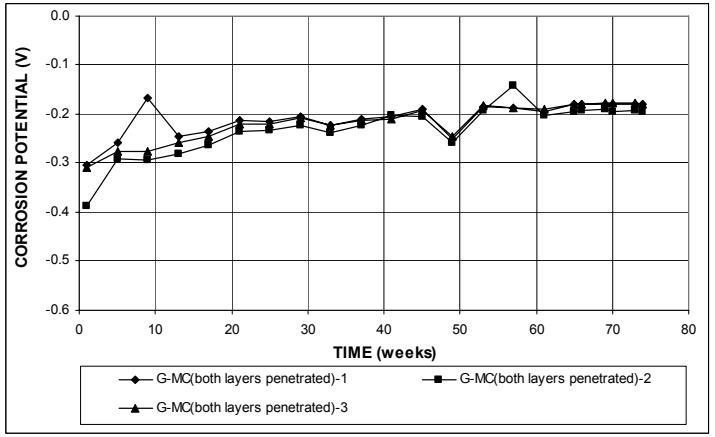

(b)

Figure A.132 – (a) Top mat corrosion potentials and (b) bottom mat corrosion potentials, with respect to copper-copper sulfate electrode as measured in the ASTM G 109 test for specimens with multiple coated bar (four 3-mm ($^1/_8$-in.) diameter holes, both layers penetrated).

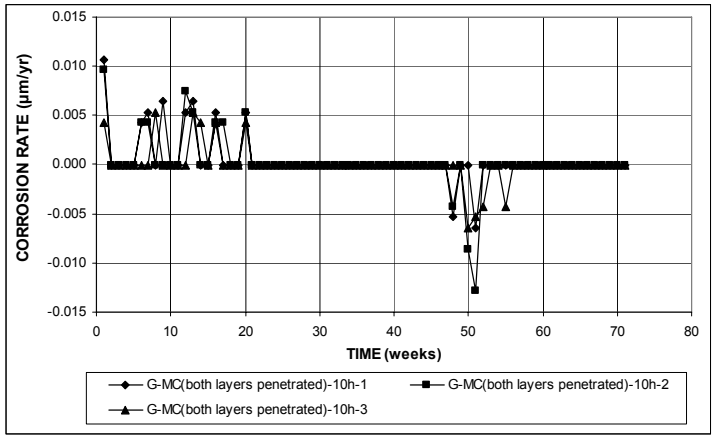

(a)

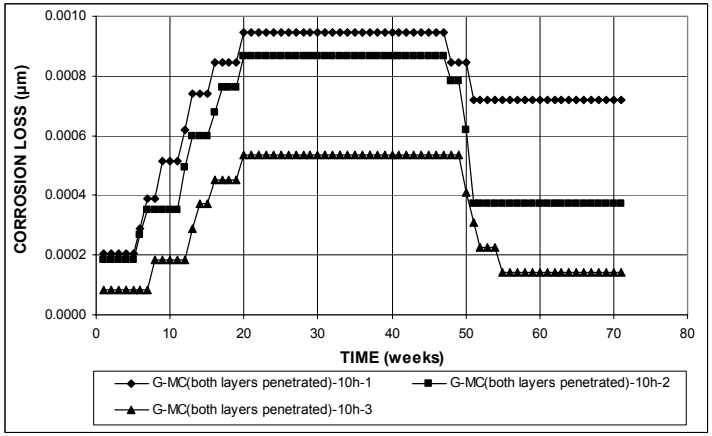

(b)

Figure A.133 – (a) Corrosion rates and (b) total corrosion losses based on total area of the bar as measured in the ASTM G 109 test for specimens with multiple coated bar (ten 3-mm ($^1/_8$-in.) diameter holes, both layers penetrated).

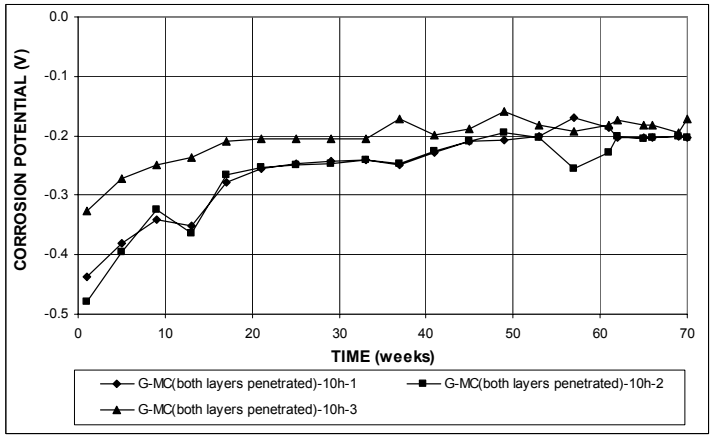

(a)

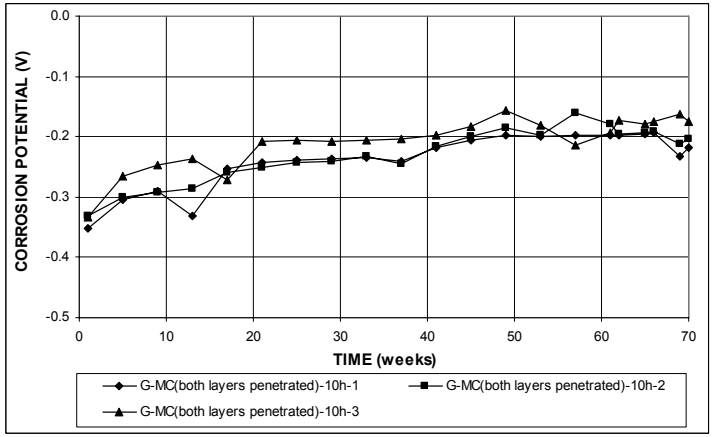

(b)

Figure A.134 – (a) Top mat corrosion potentials and (b) bottom mat corrosion potentials, with respect to copper-copper sulfate electrode as measured in the ASTM G 109 test for specimens with multiple coated bar (ten 3-mm ($^1/_8$-in.) diameter holes, both layers penetrated).

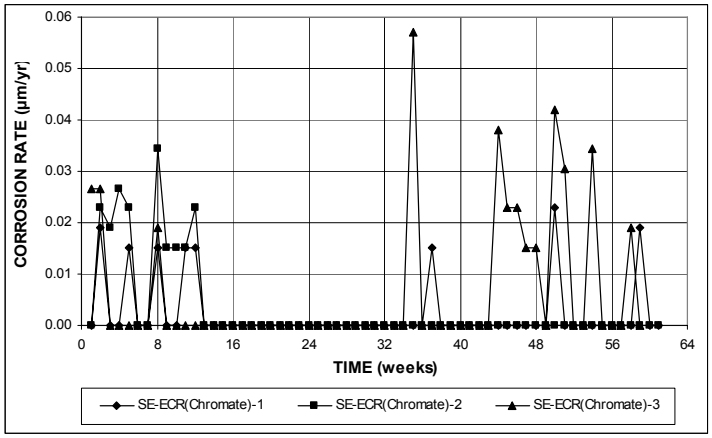

(a)

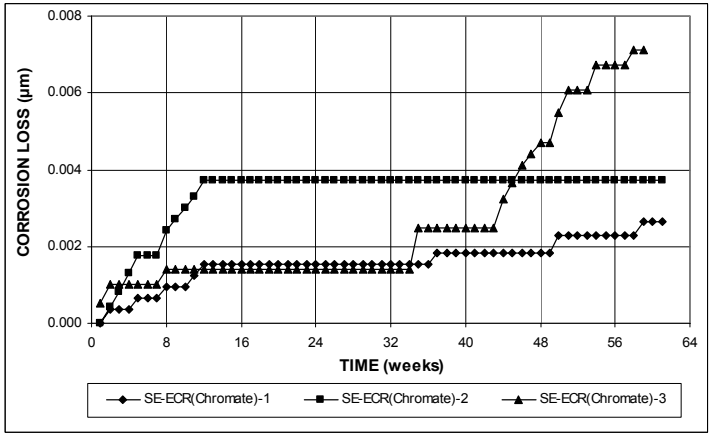

(b)

Figure A.135 – (a) Corrosion rates and (b) total corrosion losses based on total area of the bar as measured in the Southern Exposure test for specimens with ECR with chromate pretreatment (four 3-mm ($^1/_8$-in.) diameter holes).

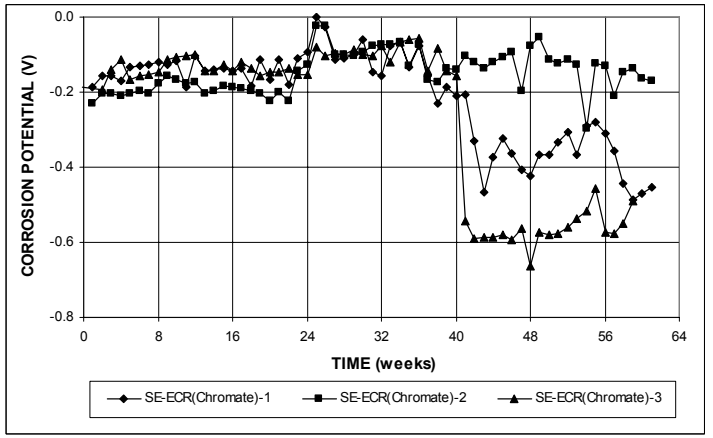

(a)

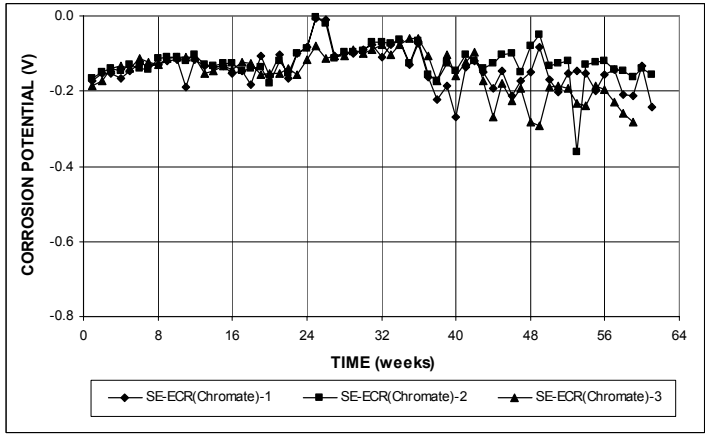

(b)

Figure A.136 – (a) Top mat corrosion potentials and (b) bottom mat corrosion potentials, with respect to copper-copper sulfate electrode as measured in the Southern Exposure test for specimens with ECR with chromate pretreatment (four 3-mm ($^1/_8$-in.) diameter holes).

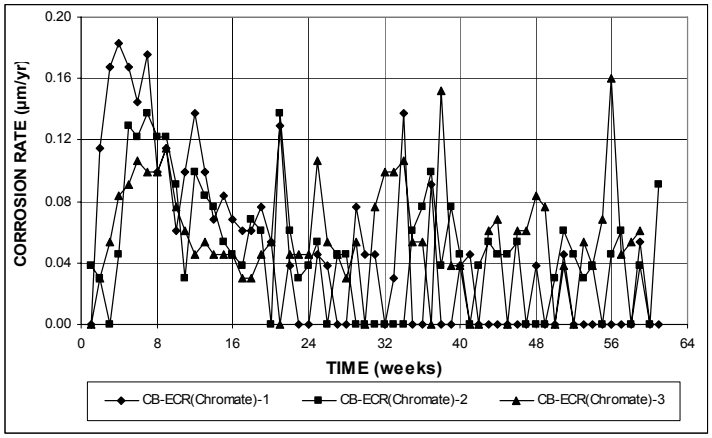

(a)

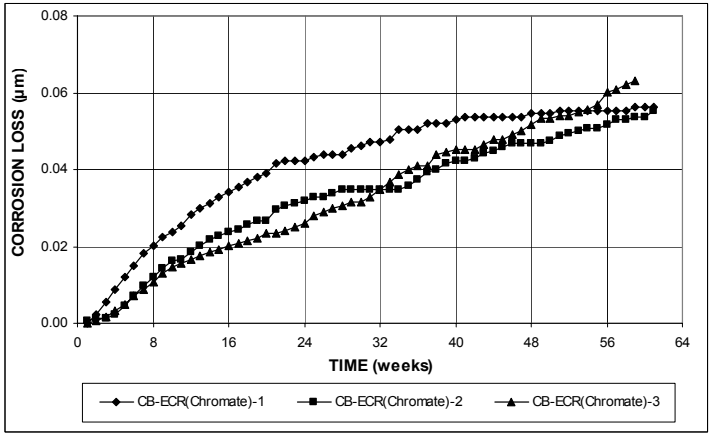

(b)

Figure A.137 – (a) Corrosion rates and (b) total corrosion losses based on total area of the bar as measured in the cracked beam test for specimens with ECR with chromate pretreatment (four 3-mm ($^{1}/_{8}$-in.) diameter holes).

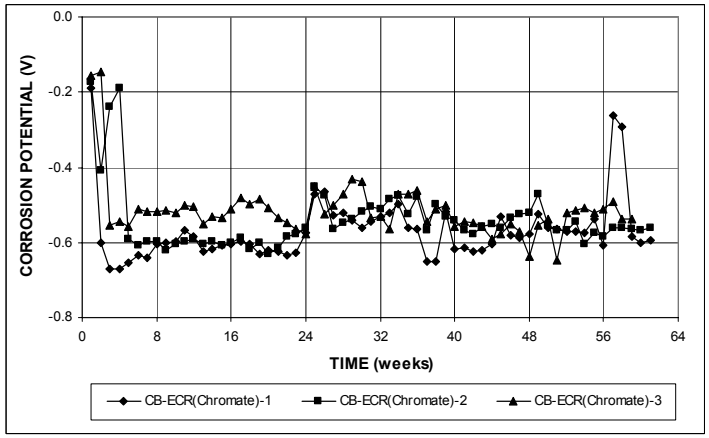

(a)

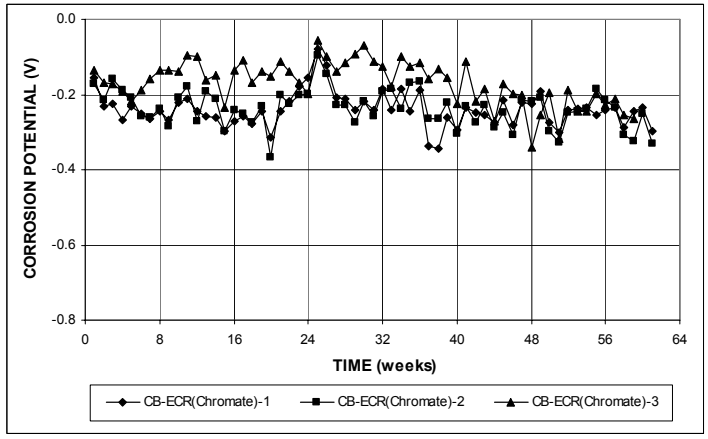

(b)

Figure A.138 – (a) Top mat corrosion potentials and (b) bottom mat corrosion potentials, with respect to copper-copper sulfate electrode as measured in the cracked beam test for specimens with ECR with chromate pretreatment (four 3-mm ($^{1}/_{8}$-in.) diameter holes).

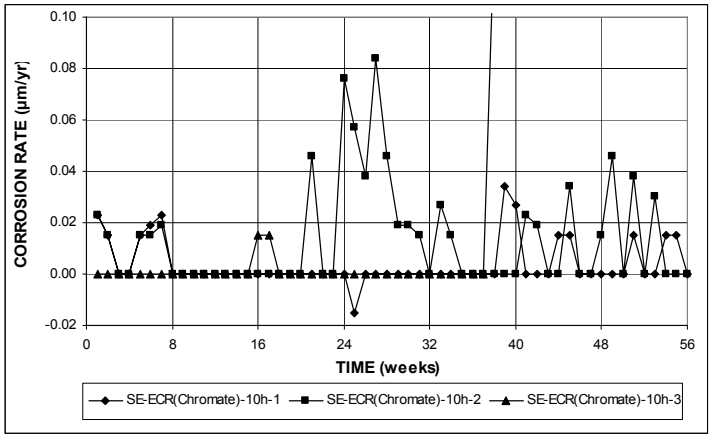

(a)

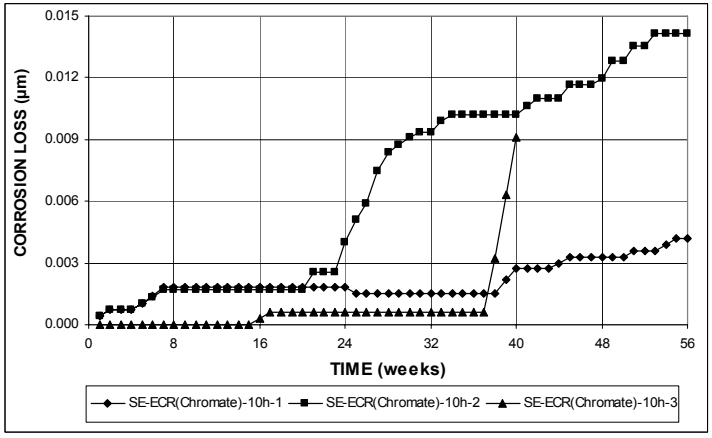

(b)

Figure A.139 – (a) Corrosion rates and (b) total corrosion losses based on total area of the bar as measured in the Southern Exposure test for specimens with ECR with chromate pretreatment (ten 3-mm ($^{1}/_{8}$-in.) diameter holes).

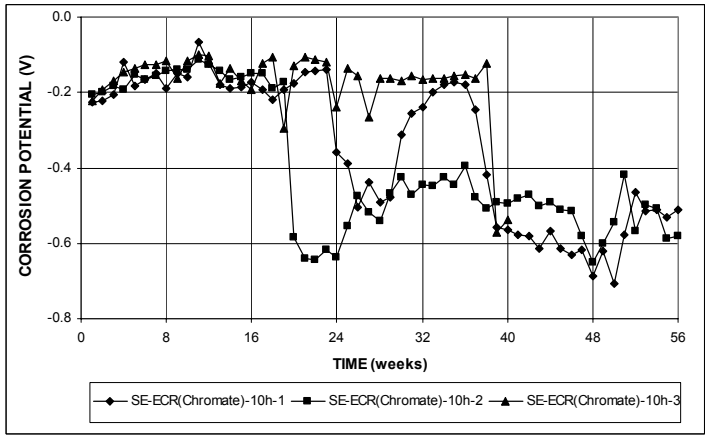

(a)

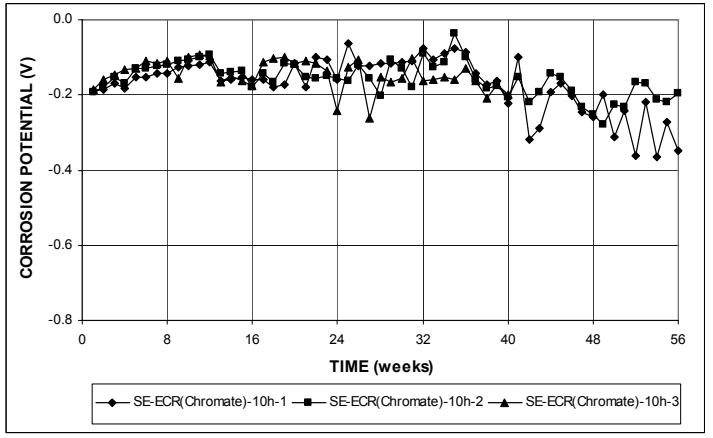

(b)

Figure A.140 – (a) Top mat corrosion potentials and (b) bottom mat corrosion potentials, with respect to copper-copper sulfate electrode as measured in the Southern Exposure test for specimens with ECR with chromate pretreatment (ten 3-mm ($^{1}/_{8}$-in.) diameter holes).

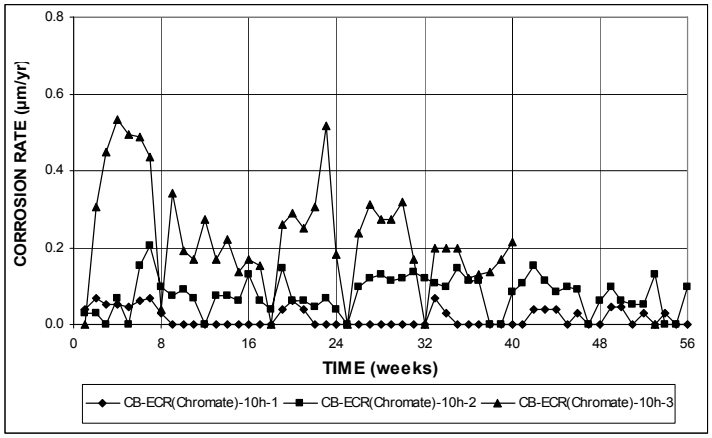

(a)

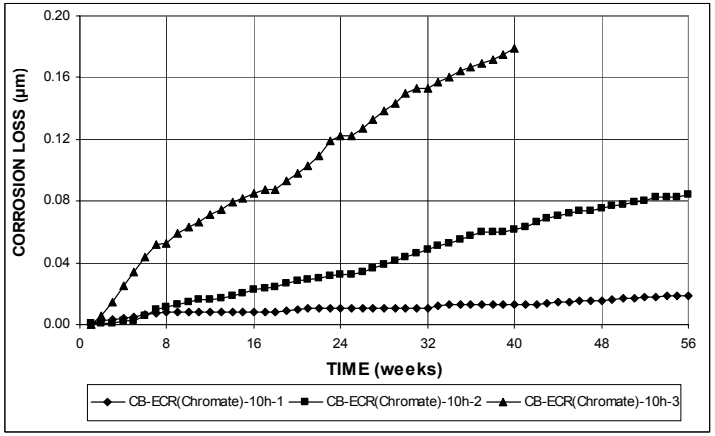

(b)

Figure A.141 – (a) Corrosion rates and (b) total corrosion losses based on total area of the bar as measured in the cracked beam test for specimens with ECR with chromate pretreatment (ten 3-mm ($^{1}/_{8}$-in.) diameter holes).

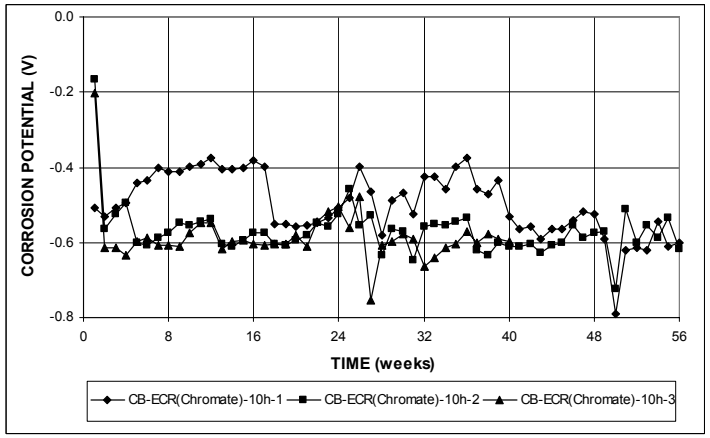

(a)

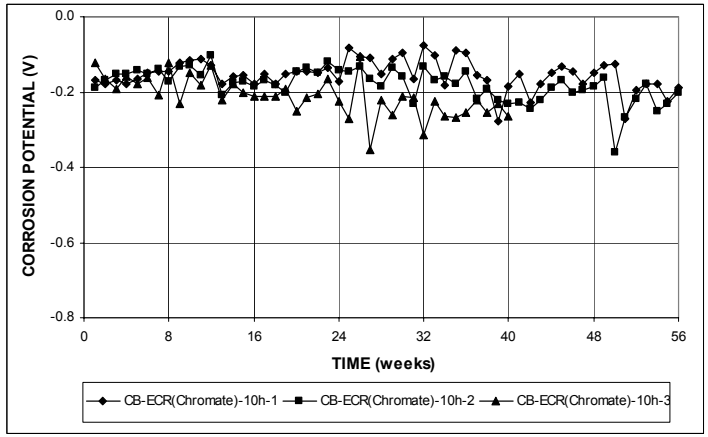

(b)

Figure A.142 – (a) Top mat corrosion potentials and (b) bottom mat corrosion potentials, with respect to copper-copper sulfate electrode as measured in the cracked beam test for specimens with ECR with chromate pretreatment (ten 3-mm ($^{1}/_{8}$-in.) diameter holes).

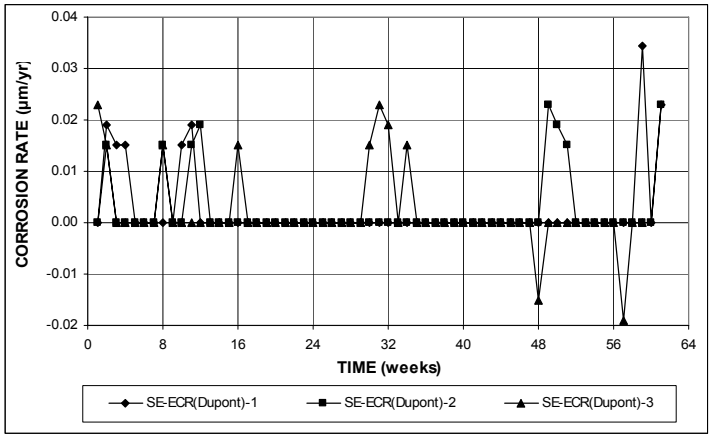

(a)

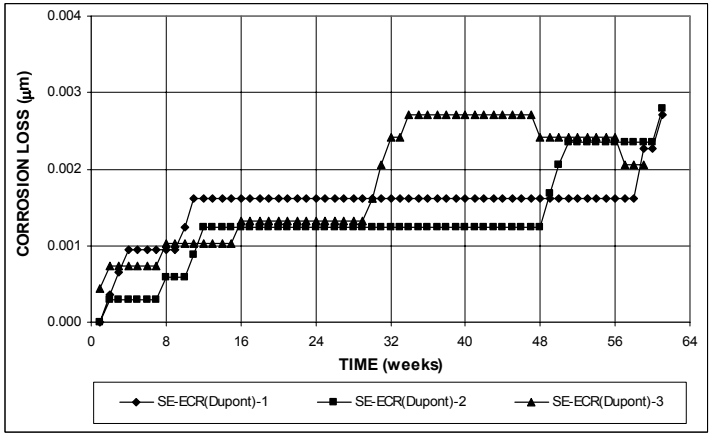

(b)

Figure A.143 – (a) Corrosion rates and (b) total corrosion losses based on total area of the bar as measured in the Southern Exposure test for specimens with ECR with DuPont coating (four 3-mm ($^1/_8$-in.) diameter holes).

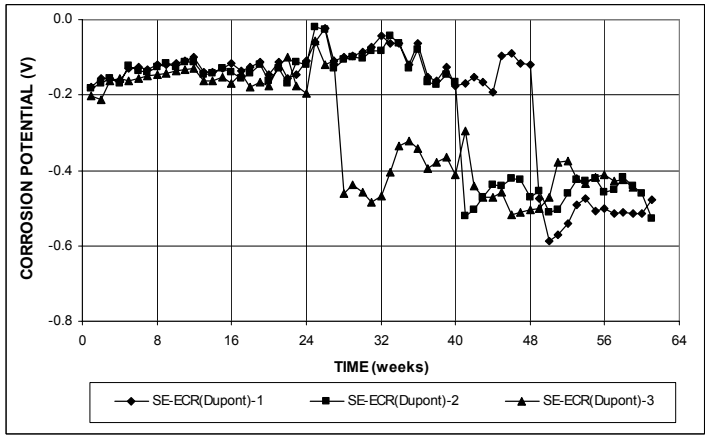

(a)

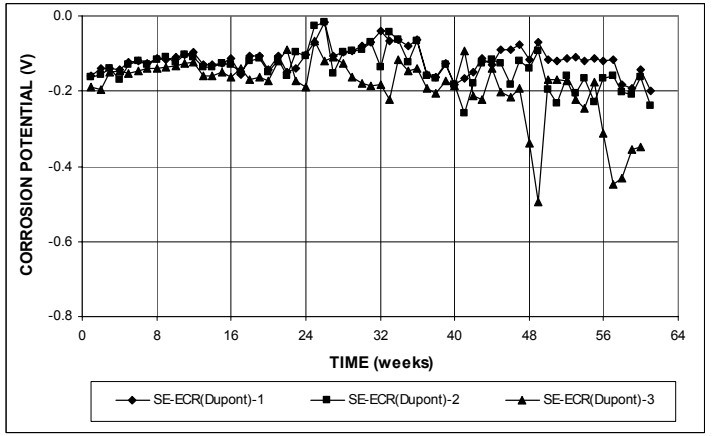

(b)

Figure A.144 – (a) Top mat corrosion potentials and (b) bottom mat corrosion potentials, with respect to copper-copper sulfate electrode as measured in the Southern Exposure test for specimens with ECR with DuPont coating (four 3-mm ($^1/_8$-in.) diameter holes).

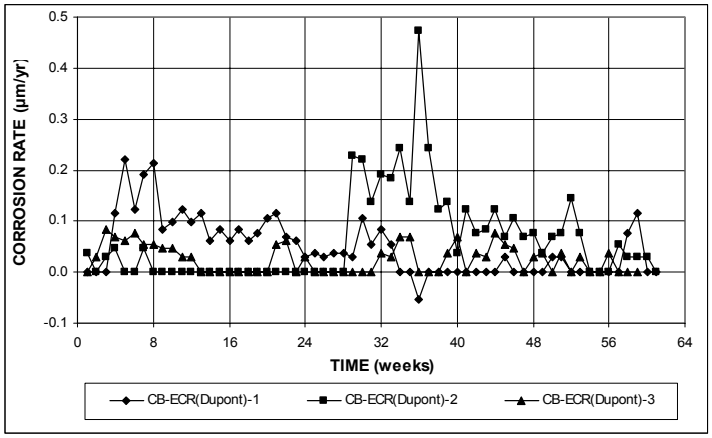

(a)

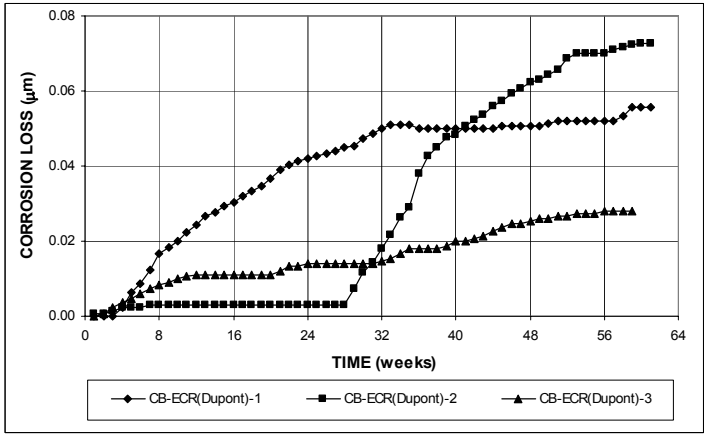

(b)

Figure A.145 – (a) Corrosion rates and (b) total corrosion losses based on total area of the bar as measured in the cracked beam test for specimens with ECR with DuPont coating (four 3-mm ($^{1}/_{8}$-in.) diameter holes).

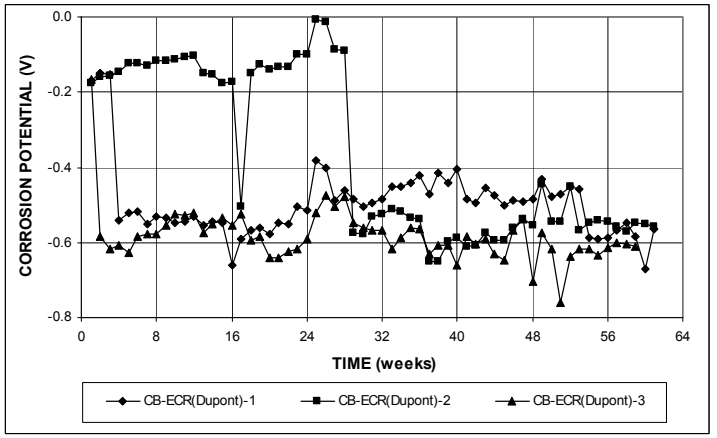

(a)

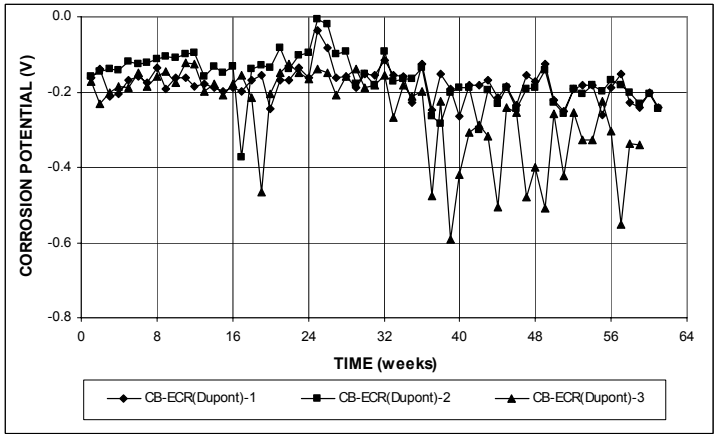

(b)

Figure A.146 – (a) Top mat corrosion potentials and (b) bottom mat corrosion potentials, with respect to copper-copper sulfate electrode as measured in the cracked beam test for specimens with ECR with DuPont coating (four 3-mm ($^{1}/_{8}$-in.) diameter holes).

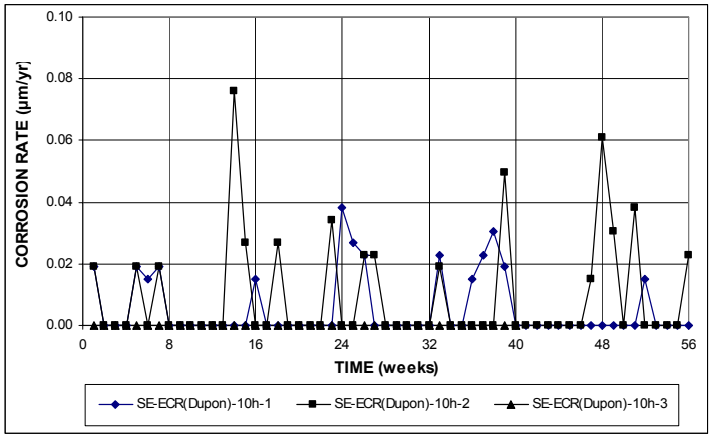

(a)

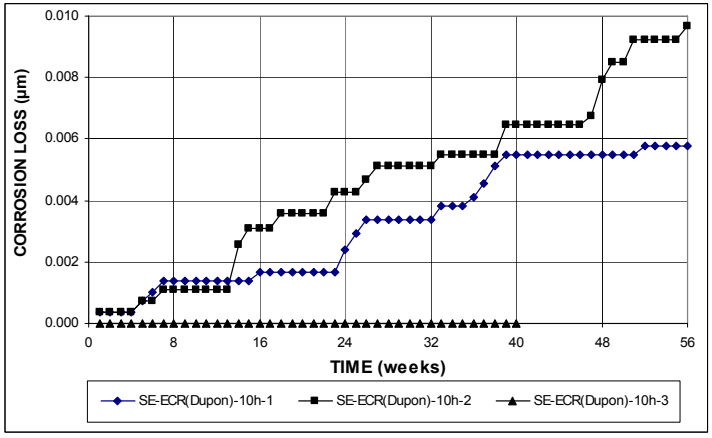

(b)

Figure A.147 – (a) Corrosion rates and (b) total corrosion losses based on total area of the bar as measured in the Southern Exposure test for specimens with ECR with DuPont coating (ten 3-mm ($^1/_8$-in.) diameter holes).

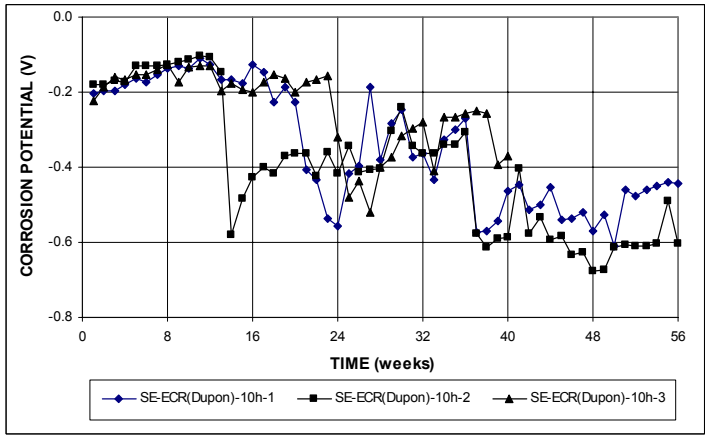

(a)

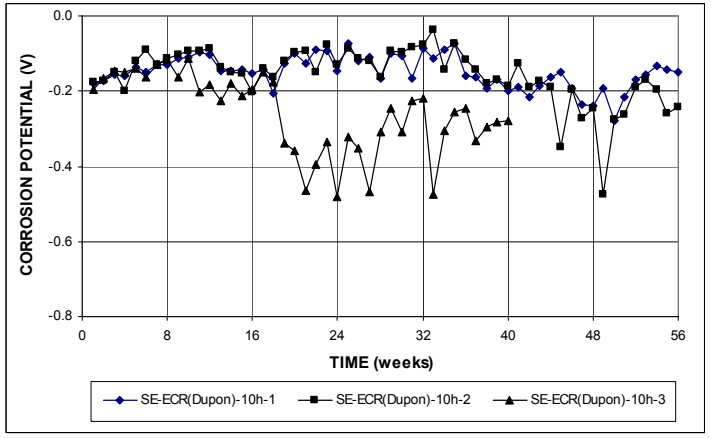

(b)

Figure A.148 – (a) Top mat corrosion potentials and (b) bottom mat corrosion potentials, with respect to copper-copper sulfate electrode as measured in the Southern Exposure test for specimens with ECR with DuPont coating (ten 3-mm ($^1/_8$-in.) diameter holes).

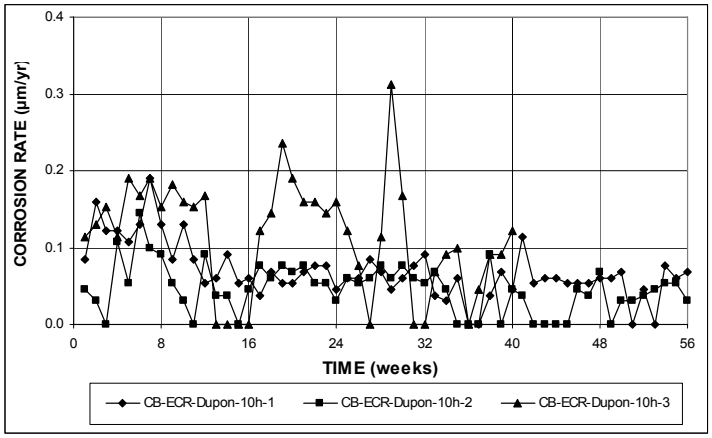

(a)

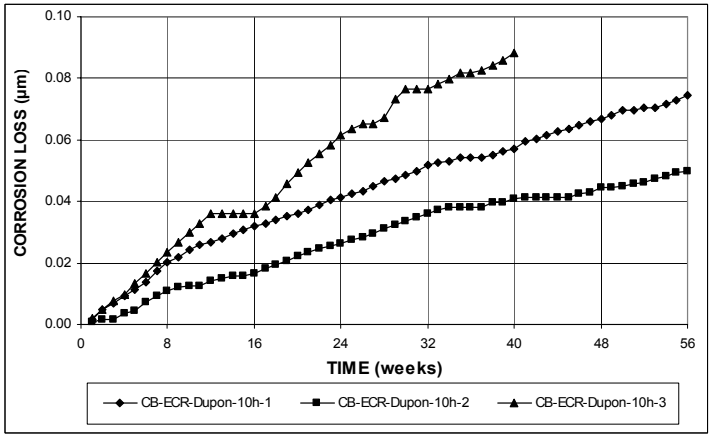

(b)

Figure A.149 – (a) Corrosion rates and (b) total corrosion losses based on total area of the bar as measured in the cracked beam test for specimens with ECR with DuPont coating (ten 3-mm ($^1/_8$-in.) diameter holes).

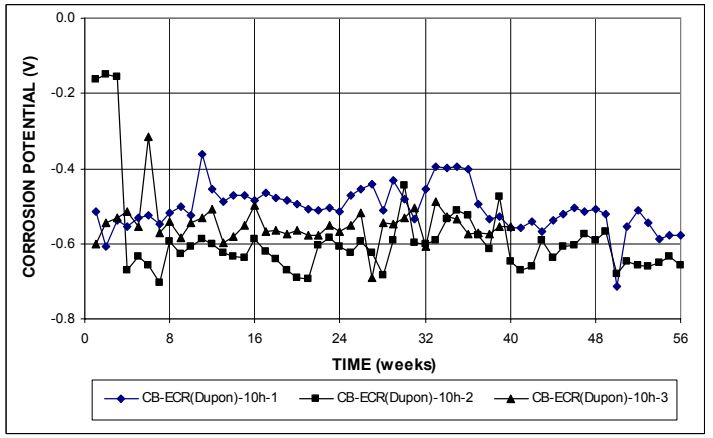

(a)

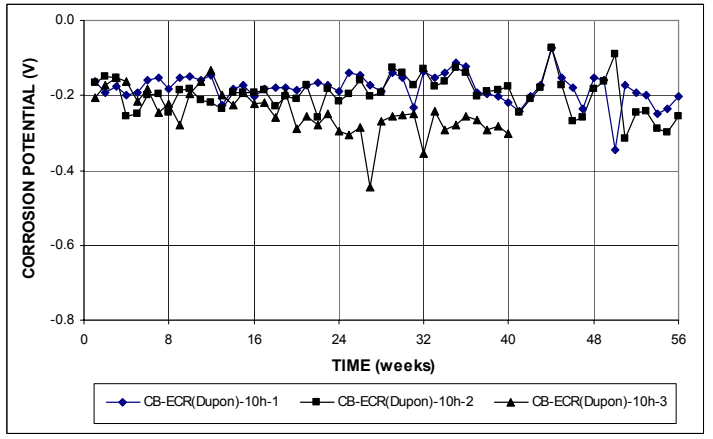

(b)

Figure A.150 – (a) Top mat corrosion potentials and (b) bottom mat corrosion potentials, with respect to copper-copper sulfate electrode as measured in the cracked beam test for specimens with ECR with DuPont coating (ten 3-mm ($^1/_8$-in.) diameter holes).

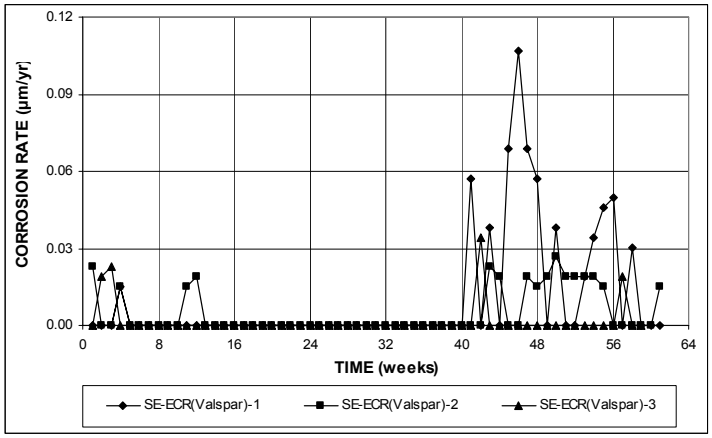

(a)

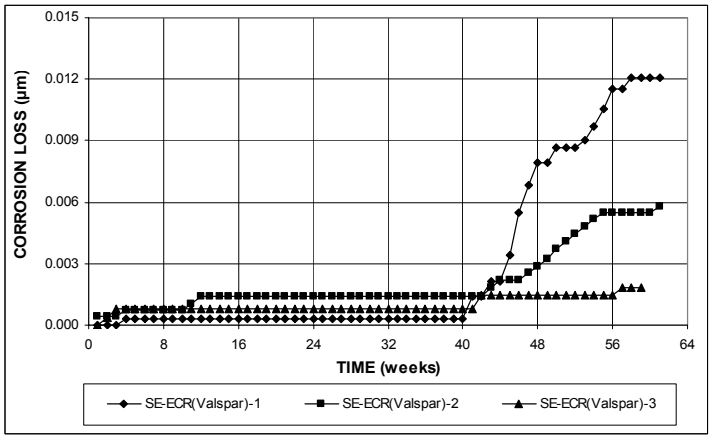

(b)

Figure A.151 – (a) Corrosion rates and (b) total corrosion losses based on total area of the bar as measured in the Southern Exposure test for specimens with ECR with Valspar coating (four 3-mm ($^1/_8$-in.) diameter holes).

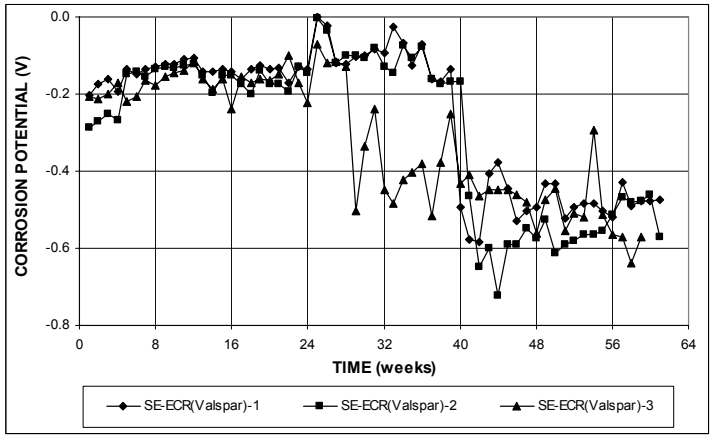

(a)

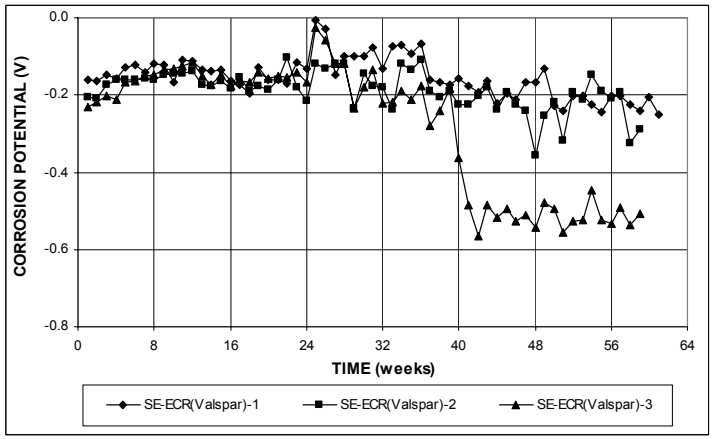

(b)

Figure A.152 – (a) Top mat corrosion potentials and (b) bottom mat corrosion potentials, with respect to copper-copper sulfate electrode as measured in the Southern Exposure test for specimens with ECR with Valspar coating (four 3-mm ($^1/_8$-in.) diameter holes).

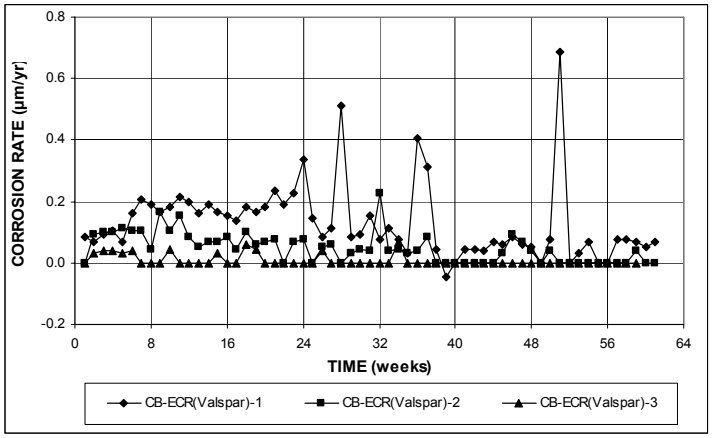

(a)

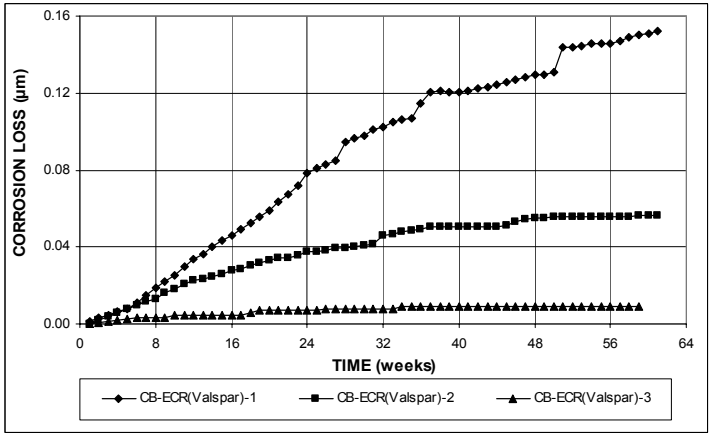

(b)

Figure A.153 – (a) Corrosion rates and (b) total corrosion losses based on total area of the bar as measured in the cracked beam test for specimens with ECR with Valspar coating (four 3-mm ($^1/_8$-in.) diameter holes).

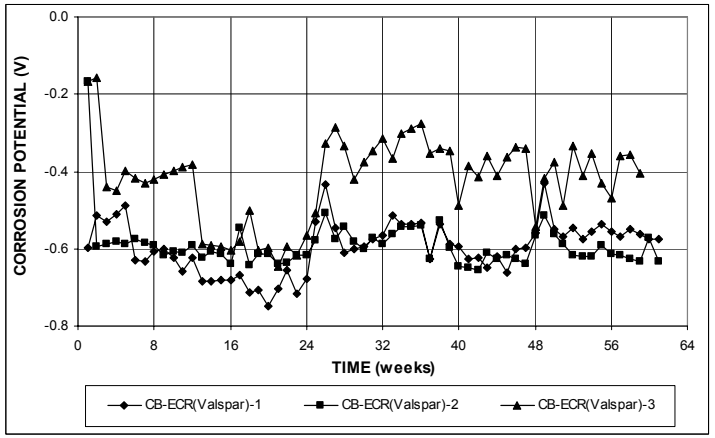

(a)

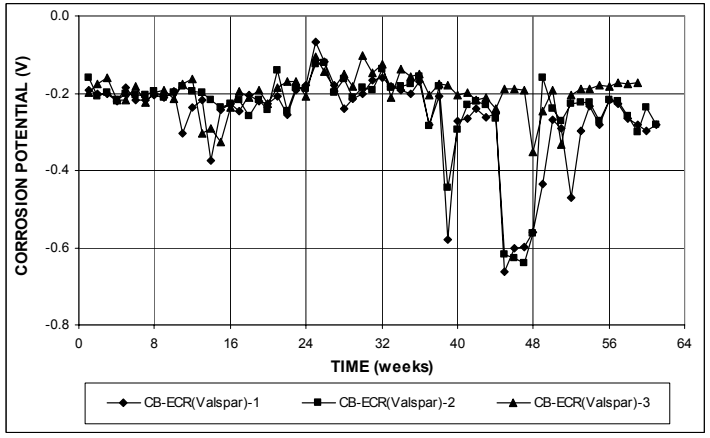

(b)

Figure A.154 – (a) Top mat corrosion potentials and (b) bottom mat corrosion potentials, with respect to copper-copper sulfate electrode as measured in the cracked beam test for specimens with ECR with Valspar coating (four 3-mm ($^1/_8$-in.) diameter holes).

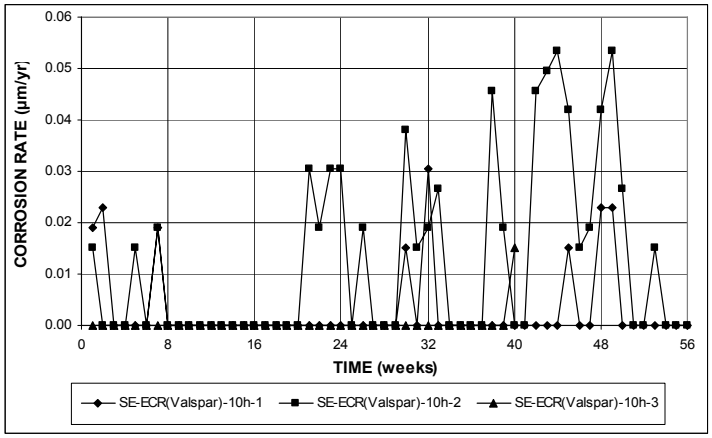

(a)

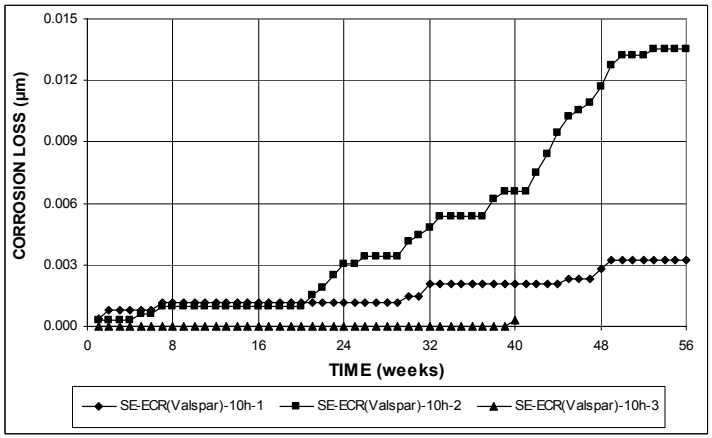

(b)

Figure A.155 – (a) Corrosion rates and (b) total corrosion losses based on total area of the bar as measured in the Southern Exposure test for specimens with ECR with Valspar coating (ten 3-mm ($^1/_8$-in.) diameter holes).

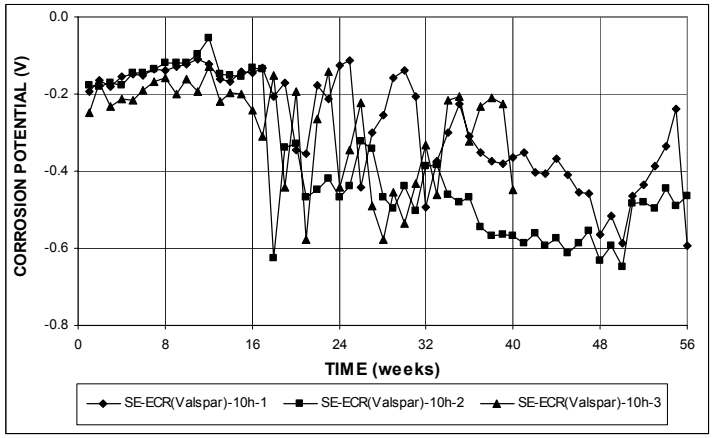

(a)

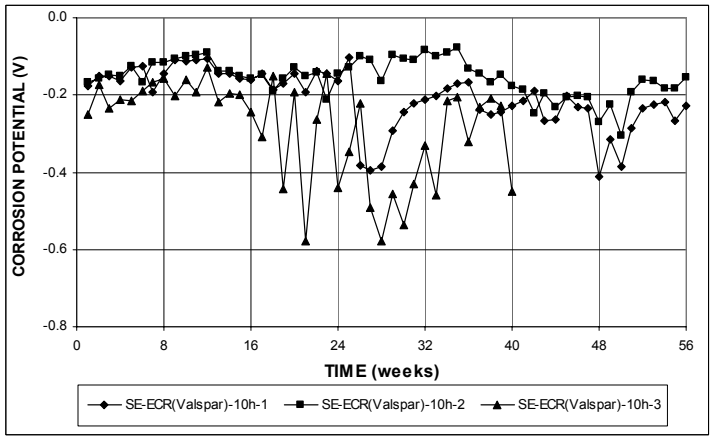

(b)

Figure A.156 – (a) Top mat corrosion potentials and (b) bottom mat corrosion potentials, with respect to copper-copper sulfate electrode as measured in the Southern Exposure test for specimens with ECR with Valspar coating (ten 3-mm ($^1/_8$-in.) diameter holes).

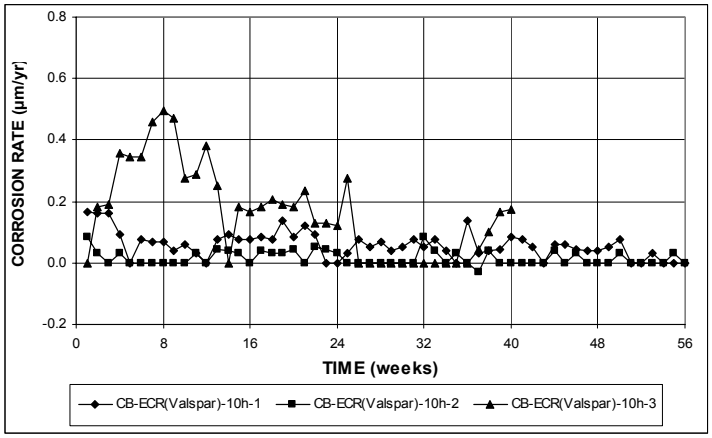

(a)

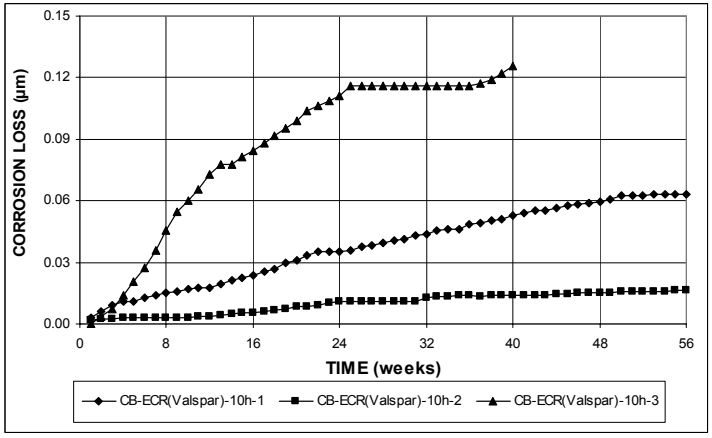

(b)

Figure A.157 – (a) Corrosion rates and (b) total corrosion losses based on total area of the bar as measured in the cracked beam test for specimens with ECR with Valspar coating (ten 3-mm ($^1/_8$-in.) diameter holes).

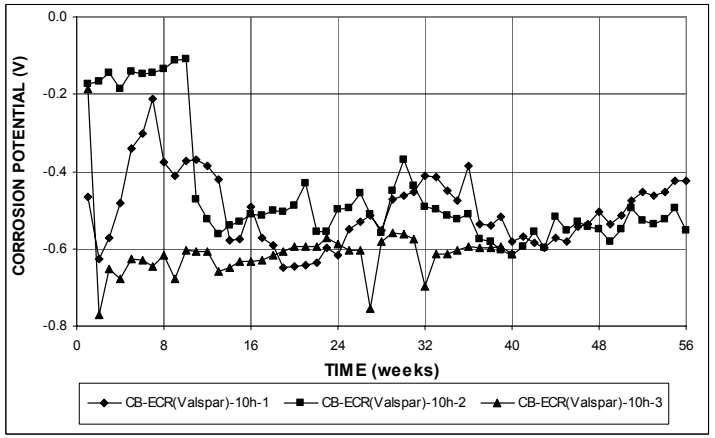

(a)

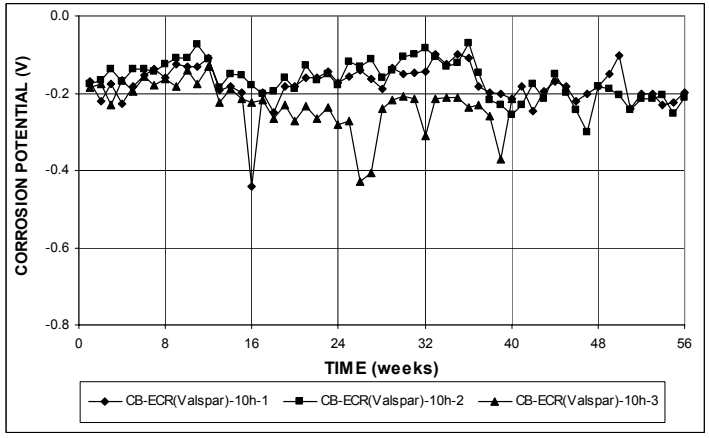

(b)

Figure A.158 – (a) Top mat corrosion potentials and (b) bottom mat corrosion potentials, with respect to copper-copper sulfate electrode as measured in the cracked beam test for specimens with ECR with Valspar coating (ten 3-mm ($^1/_8$-in.) diameter holes).

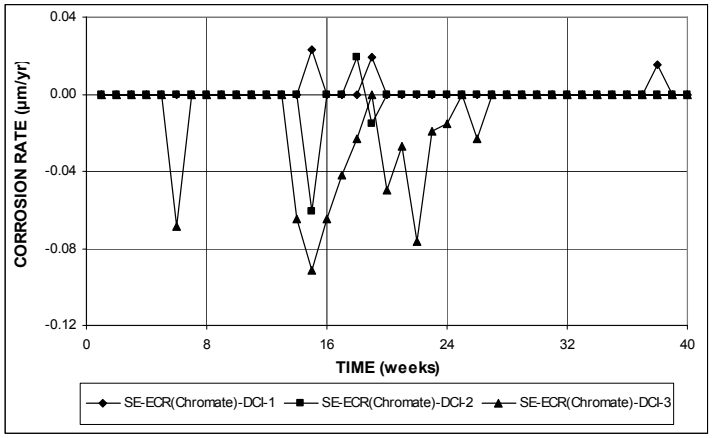

(a)

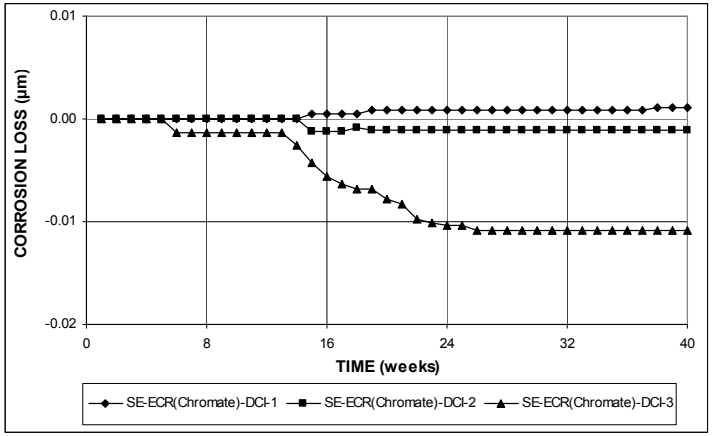

(b)

Figure A.159 – (a) Corrosion rates and (b) total corrosion losses based on total area of the bar as measured in the Southern Exposure test for specimens with ECR with chromate pretreatment (four 3-mm ($^1/_8$-in.) diameter holes) in concrete with DCI.

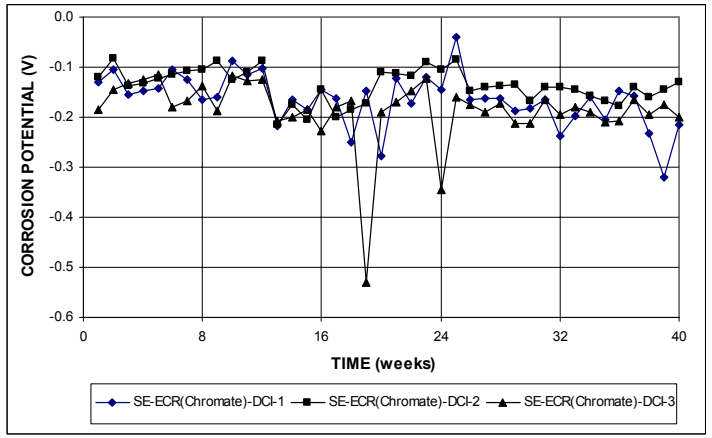

(a)

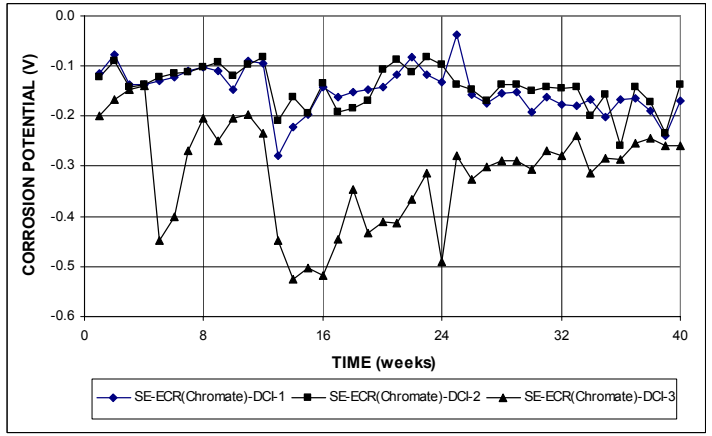

(b)

Figure A.160 – (a) Top mat corrosion potentials and (b) bottom mat corrosion potentials, with respect to copper-copper sulfate electrode as measured in the Southern Exposure test for specimens with ECR with chromate pretreatment (four 3-mm ($^1/_8$-in.) diameter holes) in concrete with DCI.

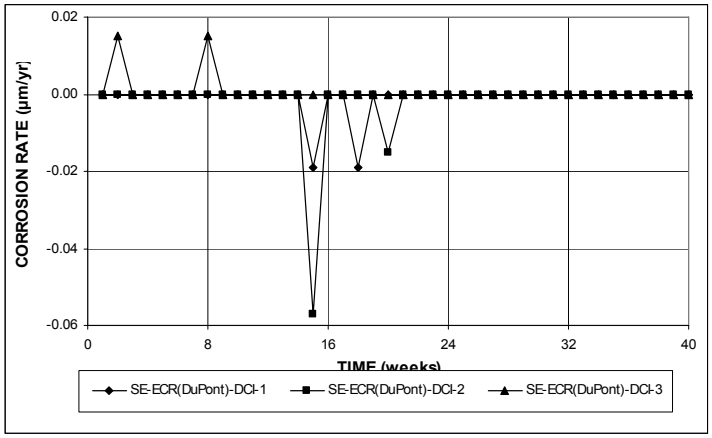

(a)

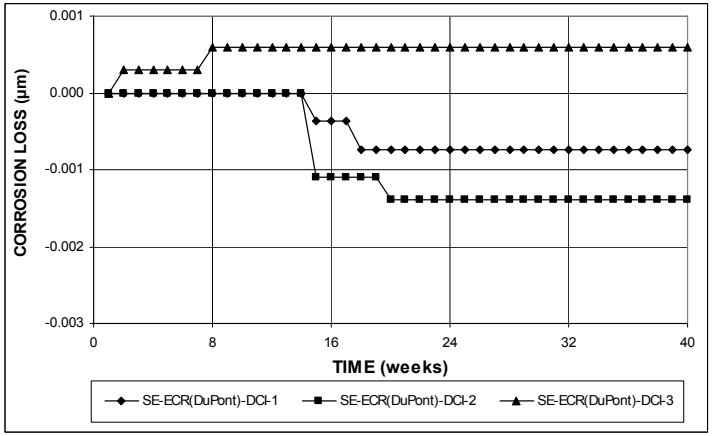

(b)

Figure A.161 – (a) Corrosion rates and (b) total corrosion losses based on total area of the bar as measured in the Southern Exposure test for specimens with ECR with DuPont coating (four 3-mm ($^1/_8$-in.) diameter holes) in concrete with DCI.

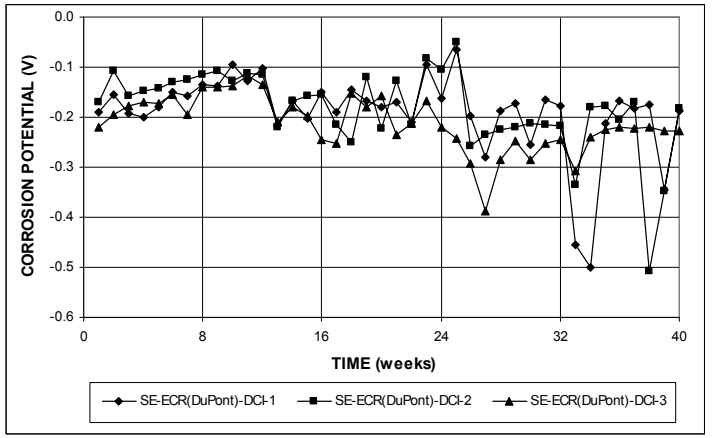

(a)

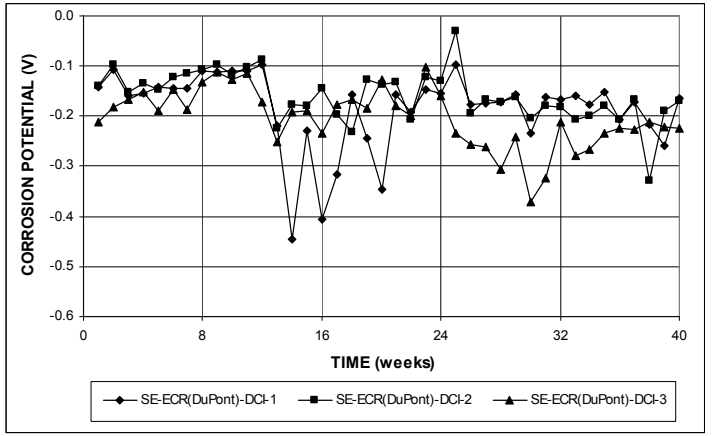

(b)

Figure A.162 – (a) Top mat corrosion potentials and (b) bottom mat corrosion potentials, with respect to copper-copper sulfate electrode as measured in the Southern Exposure test for specimens with ECR with DuPont coating (four 3-mm ($^1/_8$-in.) diameter holes) in concrete with DCI.

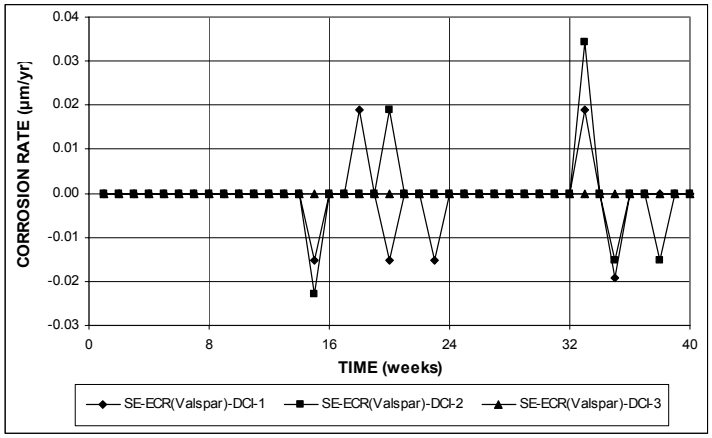

(a)

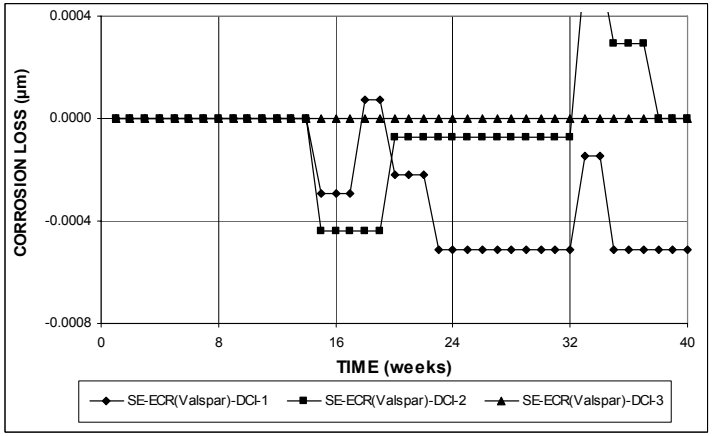

(b)

Figure A.163 – (a) Corrosion rates and (b) total corrosion losses based on total area of the bar as measured in the Southern Exposure test for specimens with ECR with Valspar coating (four 3-mm ($^1/_8$-in.) diameter holes) in concrete with DCI.

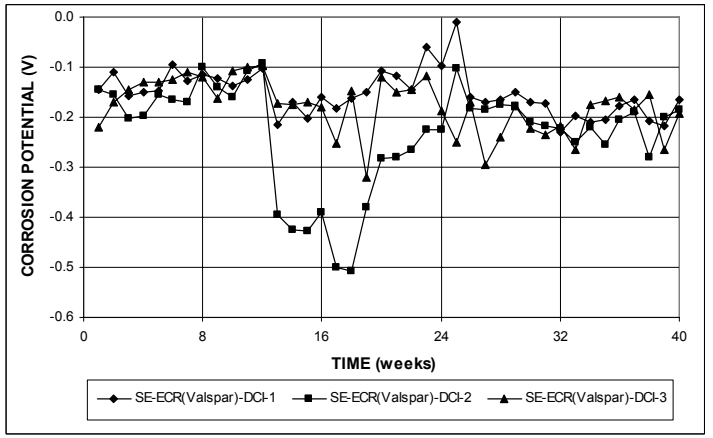

(a)

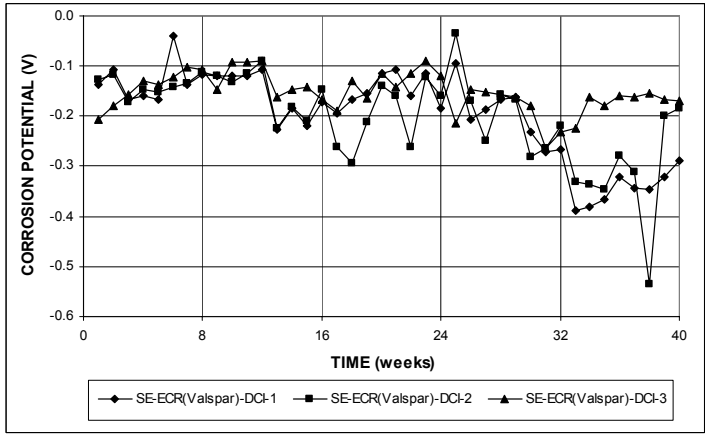

(b)

Figure A.164 – (a) Top mat corrosion potentials and (b) bottom mat corrosion potentials, with respect to copper-copper sulfate electrode as measured in the Southern Exposure test for specimens with ECR with Valspar coating (four 3-mm ($^1/_8$-in.) diameter holes) in concrete with DCI.

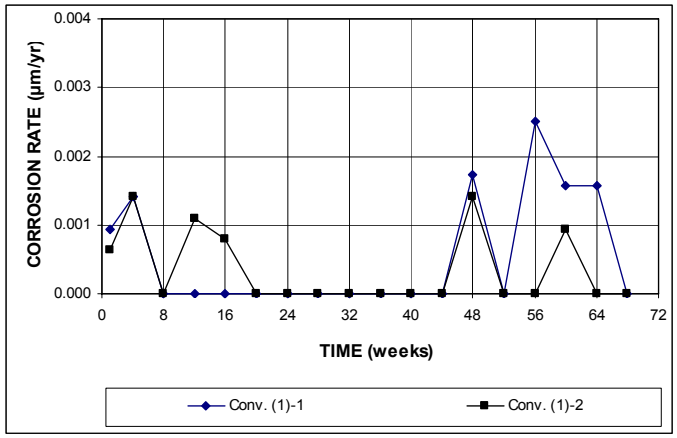

(a)

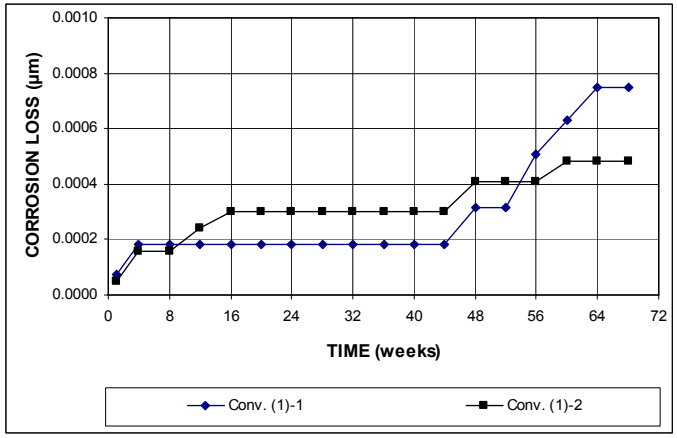

(b)

Figure A.165 – (a) Corrosion rates and (b) total corrosion losses as measured in the field test for specimens with conventional steel (without cracks, No. 1).

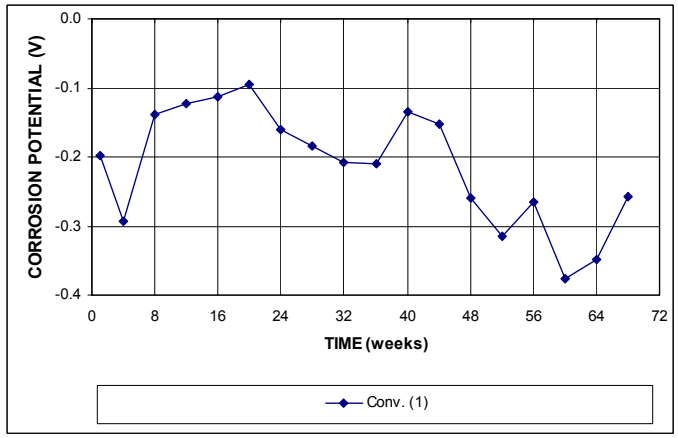

(a)

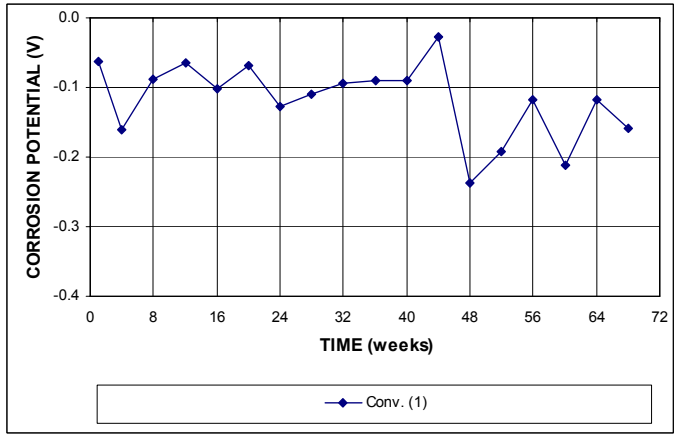

(b)

Figure A.166 – (a) Top mat corrosion potentials and (b) bottom mat corrosion potentials, with respect to copper-copper sulfate electrode as measured in the field test for specimens with conventional steel (without cracks, No. 1).

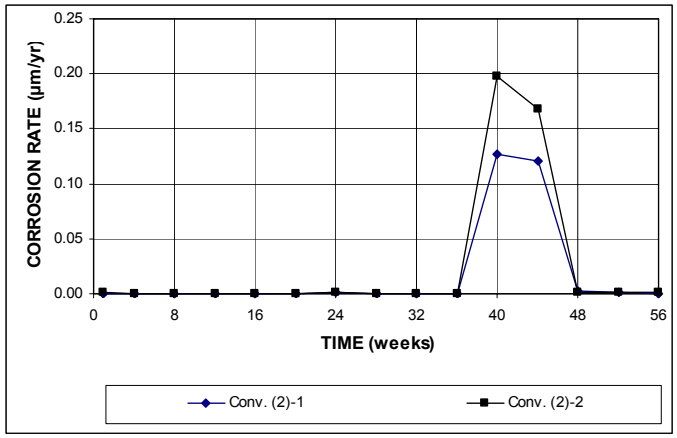

(a)

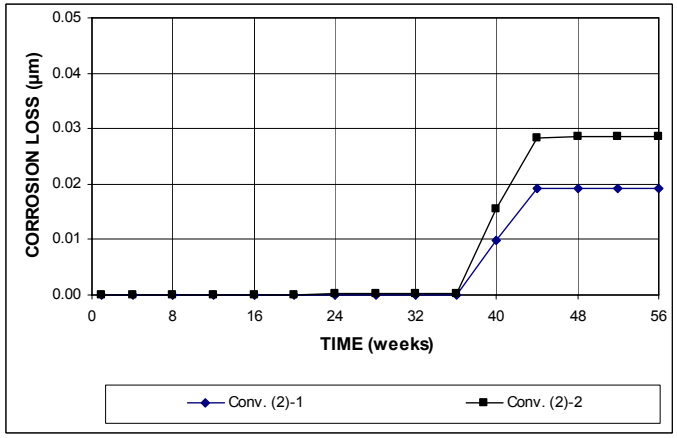

(b)

Figure A.167 – (a) Corrosion rates and (b) total corrosion losses as measured in the field test for specimens with conventional steel (without cracks, No. 2).

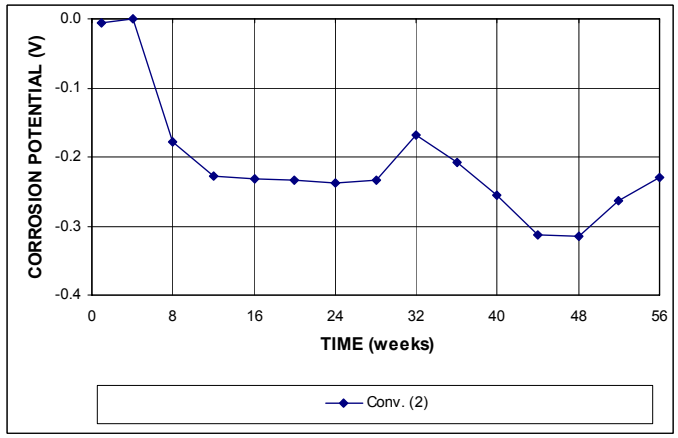

(a)

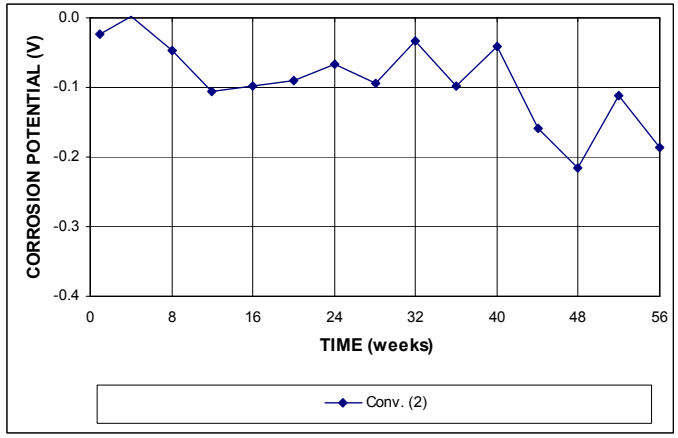

(b)

Figure A.168 – (a) Top mat corrosion potentials and (b) bottom mat corrosion potentials, with respect to copper-copper sulfate electrode as measured in the field test for specimens with conventional steel (without cracks, No. 2).

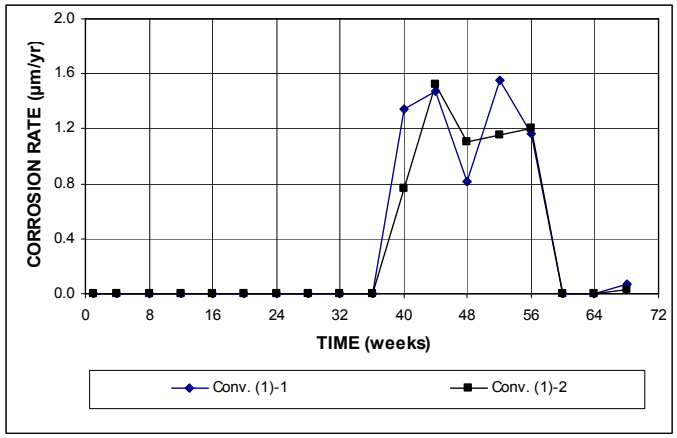

(a)

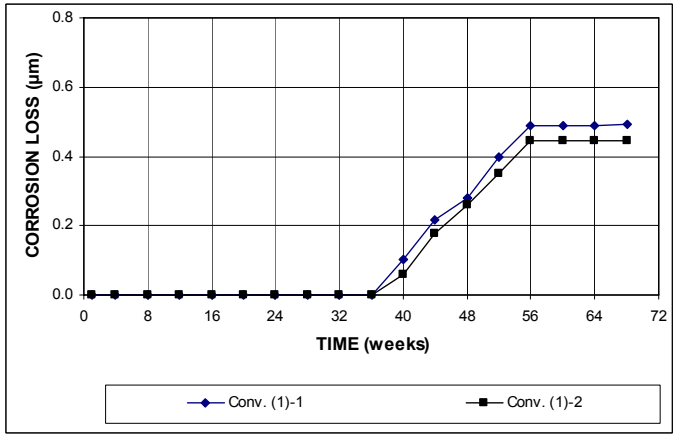

(b)

Figure A.169 – (a) Corrosion rates and (b) total corrosion losses as measured in the field test for specimens with conventional steel (with cracks, No. 1).

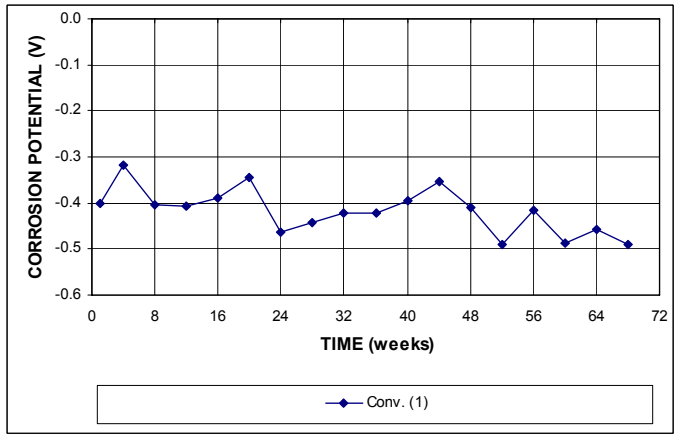

(a)

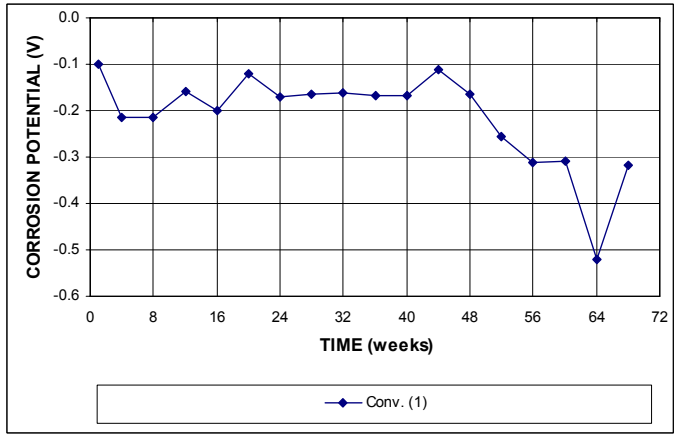

(b)

Figure A.170 – (a) Top mat corrosion potentials and (b) bottom mat corrosion potentials, with respect to copper-copper sulfate electrode as measured in the field test for specimens with conventional steel (with cracks, No. 1).

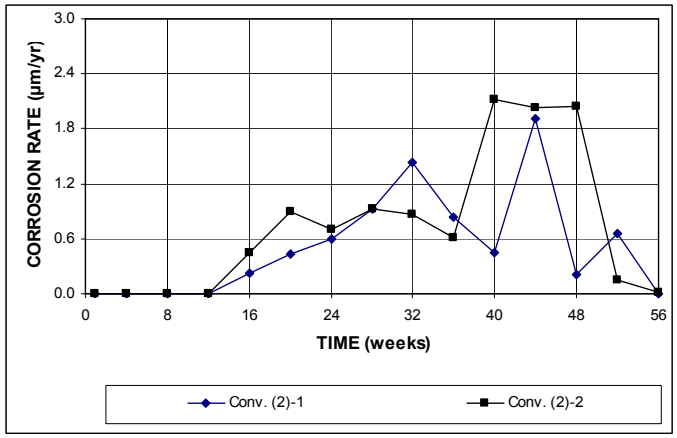

(a)

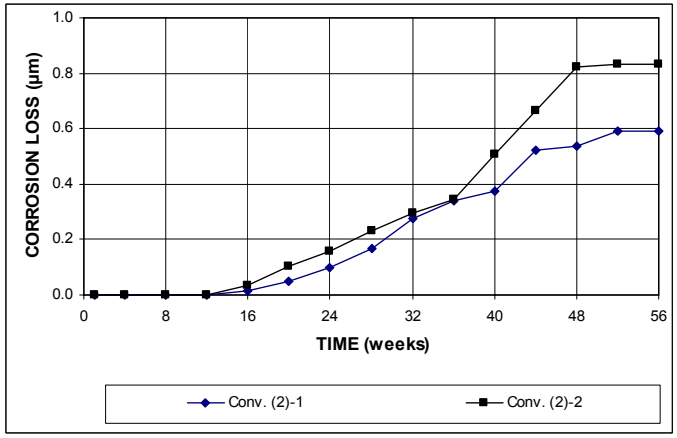

(b)

Figure A.171 – (a) Corrosion rates and (b) total corrosion losses as measured in the field test for specimens with conventional steel (with cracks, No. 2).

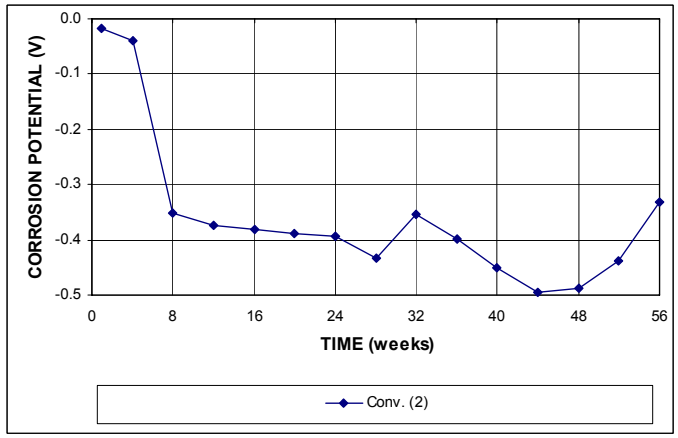

(a)

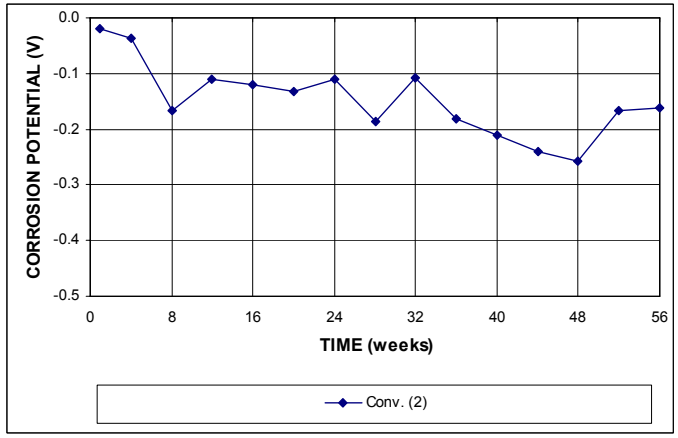

(b)

Figure A.172 – (a) Top mat corrosion potentials and (b) bottom mat corrosion potentials, with respect to copper-copper sulfate electrode as measured in the field test for specimens with conventional steel (with cracks, No. 2).

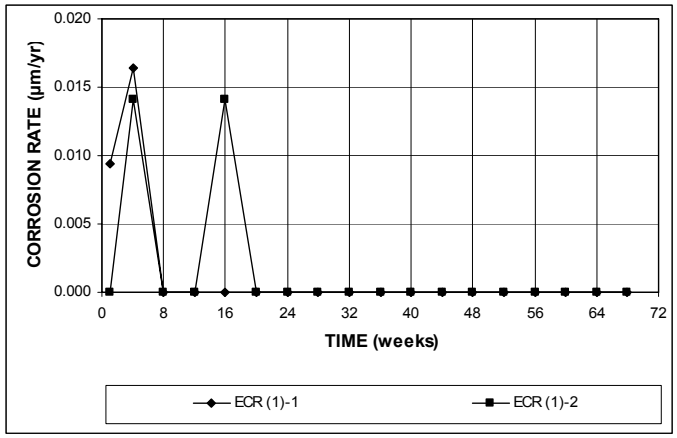

(a)

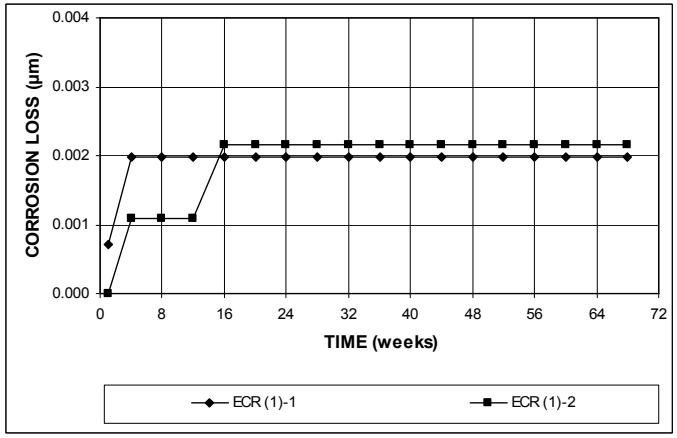

(b)

Figure A.173 – (a) Corrosion rates and (b) total corrosion losses base on total area of the bar as measured in the field test for specimens with ECR (without cracks, No. 1).

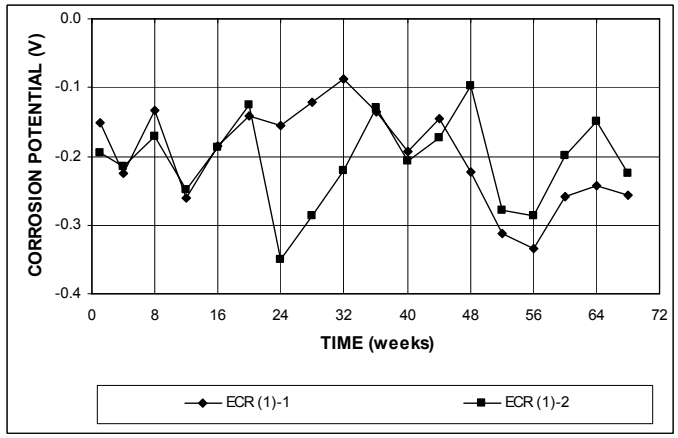

(a)

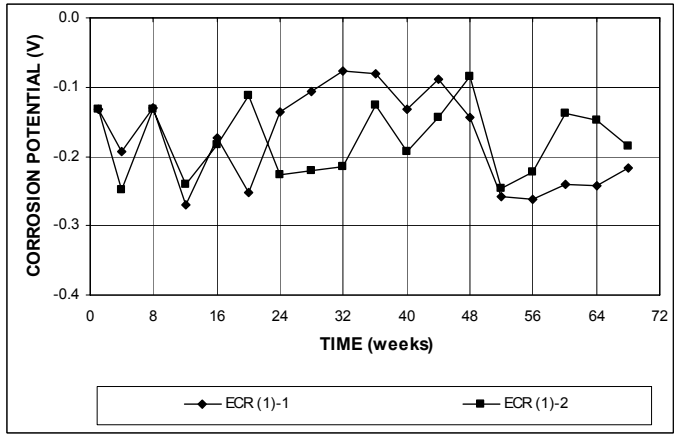

(b)

Figure A.174 – (a) Top mat corrosion potentials and (b) bottom mat corrosion potentials, with respect to copper-copper sulfate electrode as measured in the field test for specimens with ECR (without cracks, No. 1).

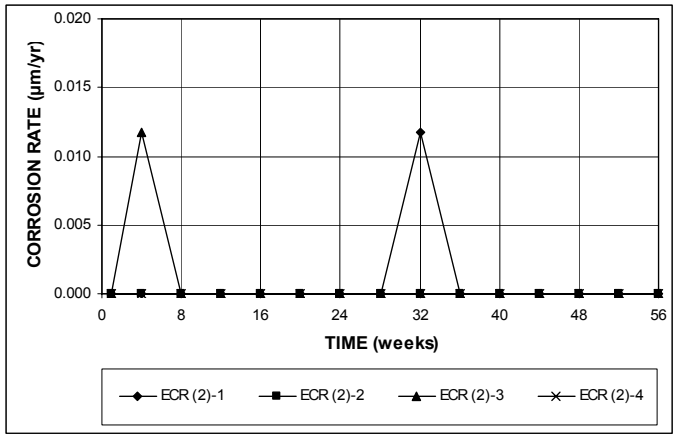

(a)

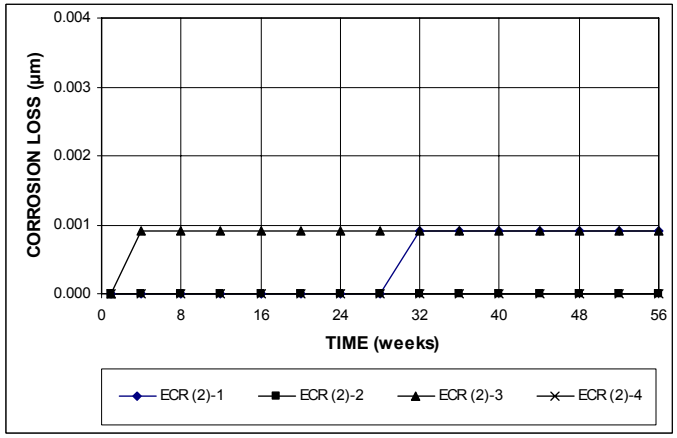

(b)

Figure A.175 – (a) Corrosion rates and (b) total corrosion losses base on total area of the bar as measured in the field test for specimens with ECR (without cracks, No. 2).

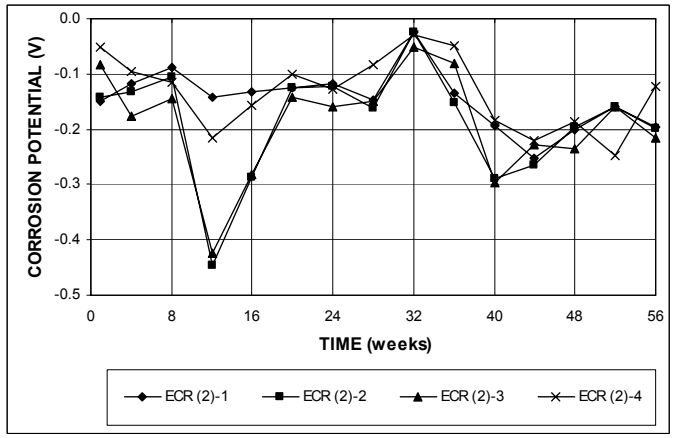

(a)

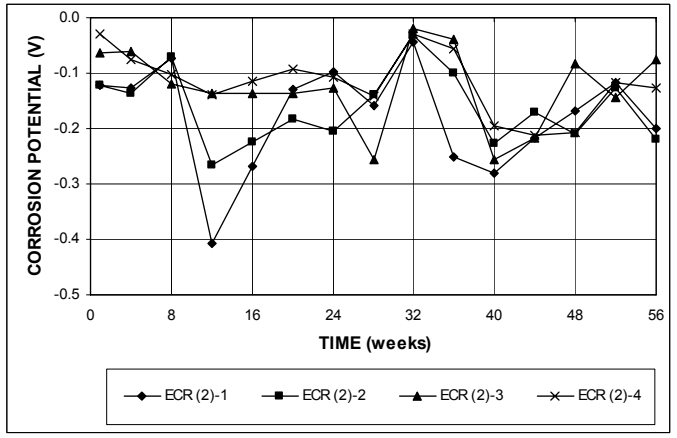

(b)

Figure A.176 – (a) Top mat corrosion potentials and (b) bottom mat corrosion potentials, with respect to copper-copper sulfate electrode as measured in the field test for specimens with ECR (without cracks, No. 2).

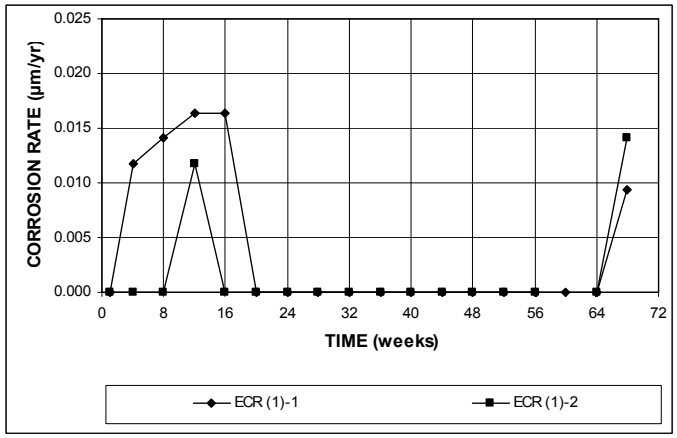

(a)

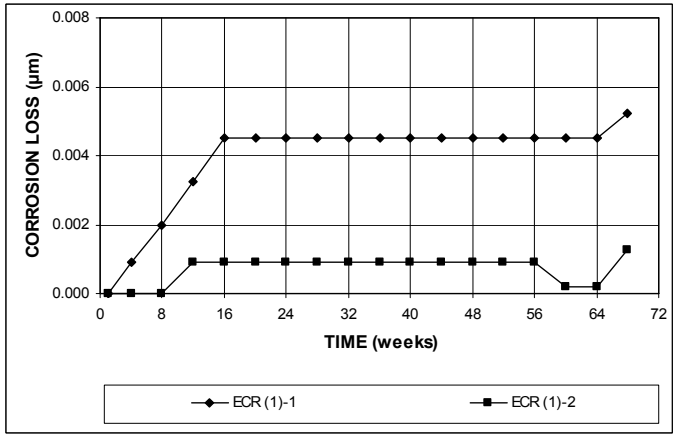

(b)

Figure A.177 – (a) Corrosion rates and (b) total corrosion losses base on total area of the bar as measured in the field test for specimens with ECR (with cracks, No. 1).

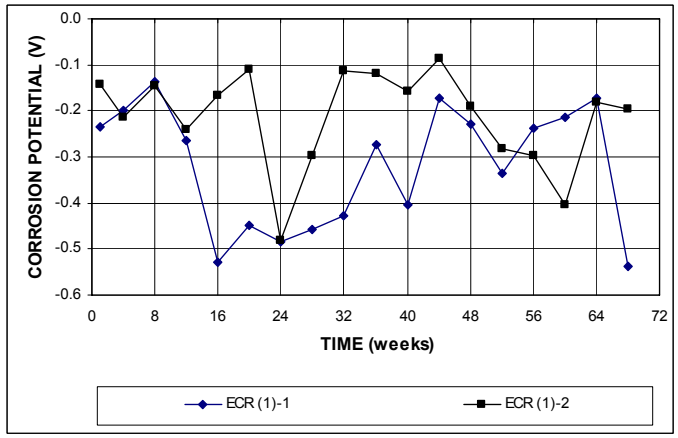

(a)

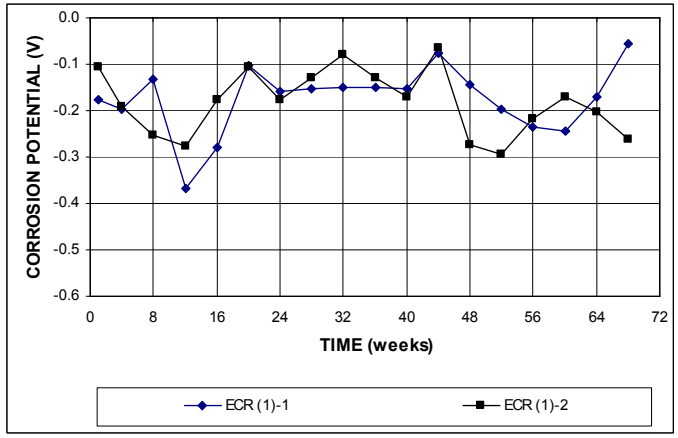

(b)

Figure A.178 – (a) Top mat corrosion potentials and (b) bottom mat corrosion potentials, with respect to copper-copper sulfate electrode as measured in the field test for specimens with ECR (with cracks, No. 1).

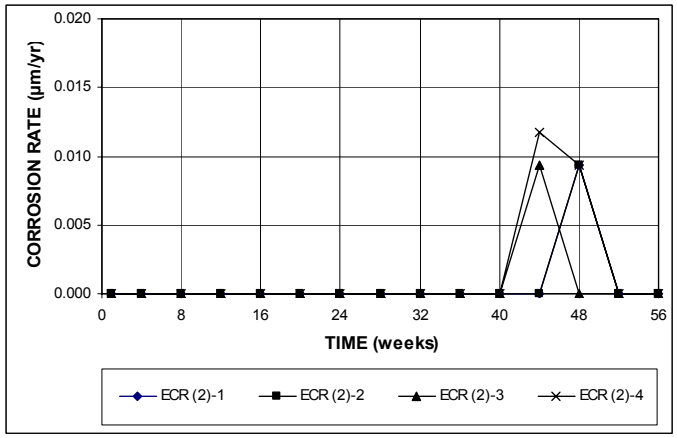

(a)

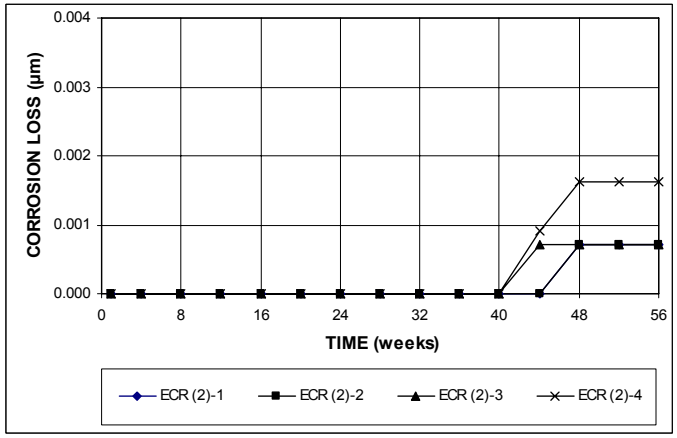

(b)

Figure A.179 – (a) Corrosion rates and (b) total corrosion losses base on total area of the bar as measured in the field test for specimens with ECR (with cracks, No. 2).

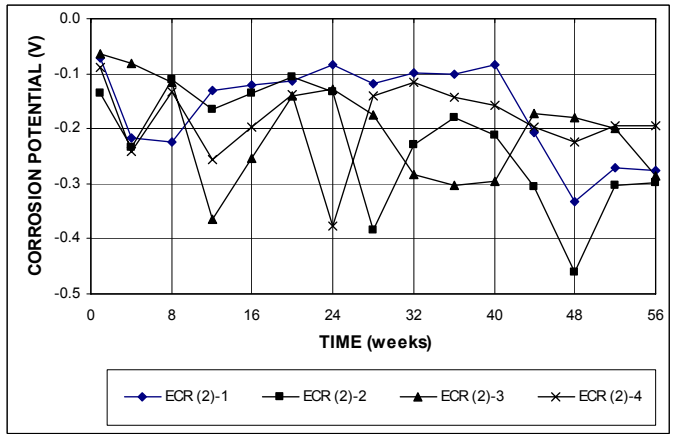

(a)

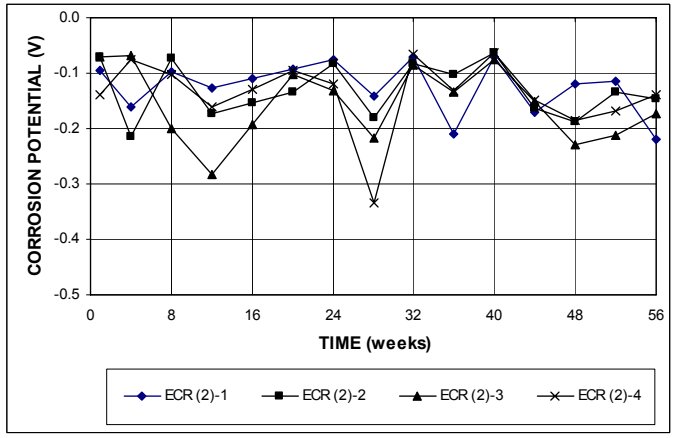

(b)

Figure A.180 – (a) Top mat corrosion potentials and (b) bottom mat corrosion potentials, with respect to copper-copper sulfate electrode as measured in the field test for specimens with ECR (with cracks, No. 2).

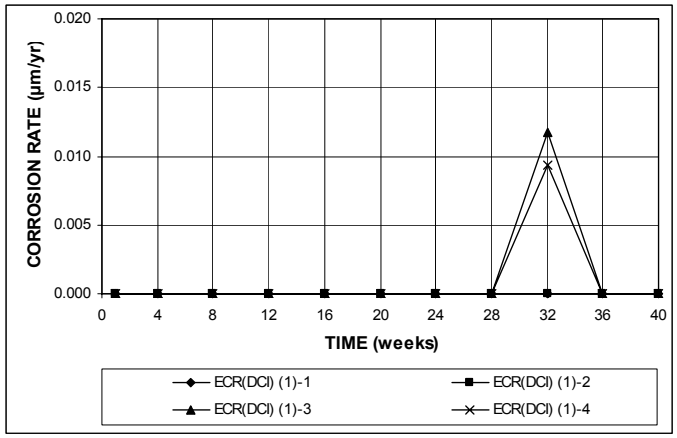

(a)

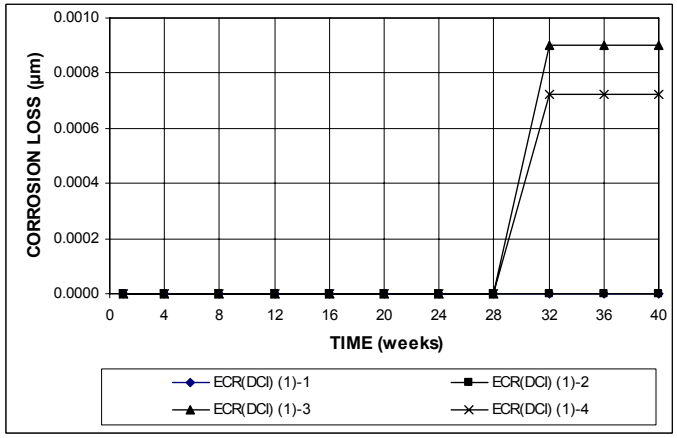

(b)

Figure A.181 – (a) Corrosion rates and (b) total corrosion losses base on total area of the bar as measured in the field test for specimens with ECR in concrete with DCI (without cracks, No. 1).

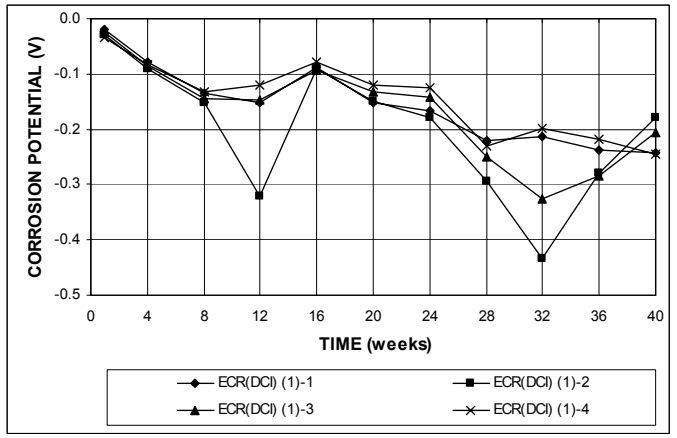

(a)

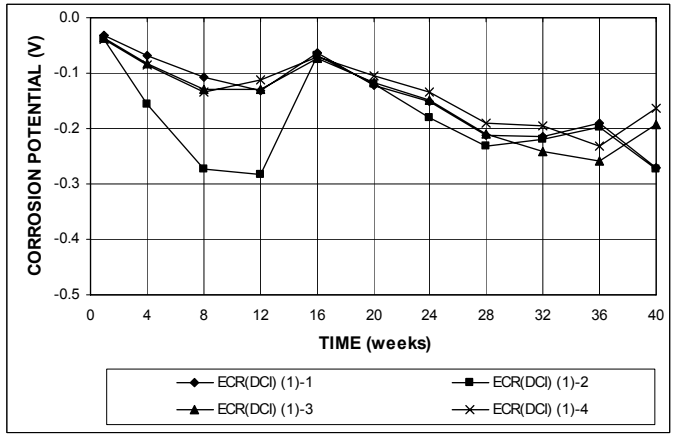

(b)

Figure A.182 – (a) Top mat corrosion potentials and (b) bottom mat corrosion potentials, with respect to copper-copper sulfate electrode as measured in the field test for specimens with ECR in concrete with DCI (without cracks, No. 1).

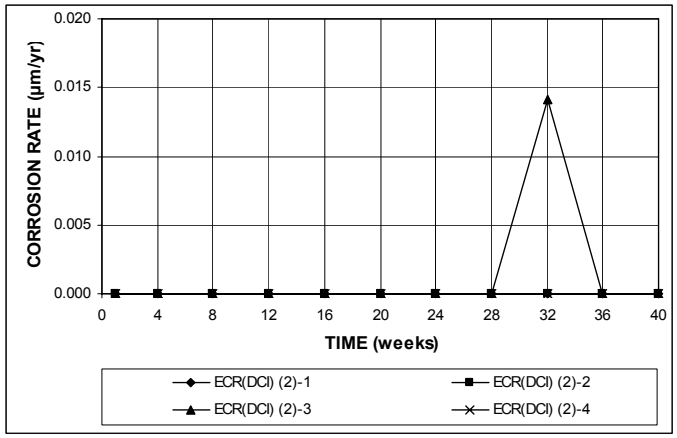

(a)

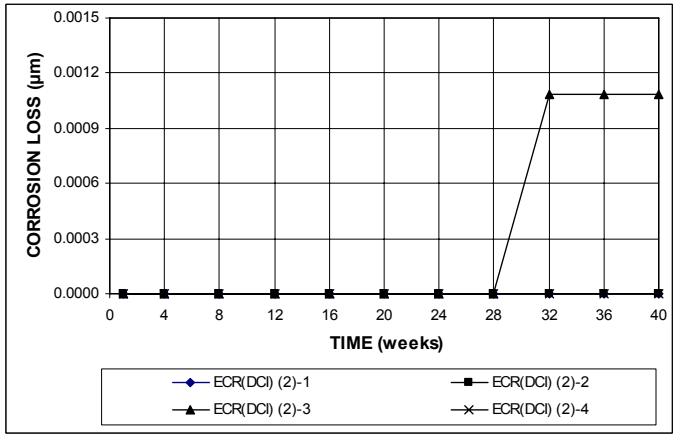

(b)

Figure A.183 – (a) Corrosion rates and (b) total corrosion losses base on total area of the bar as measured in the field test for specimens with ECR in concrete with DCI (without cracks, No. 2).

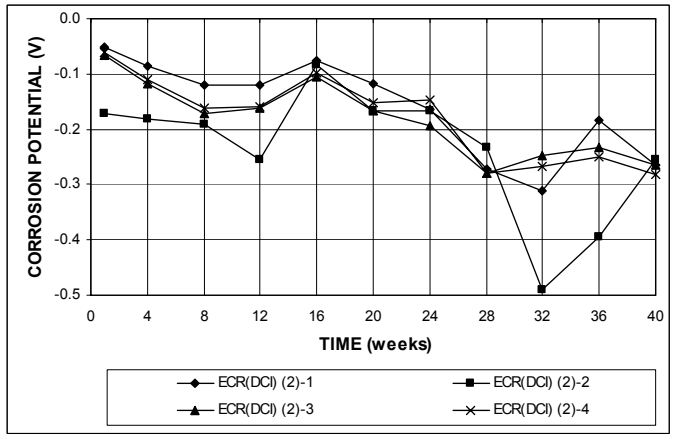

(a)

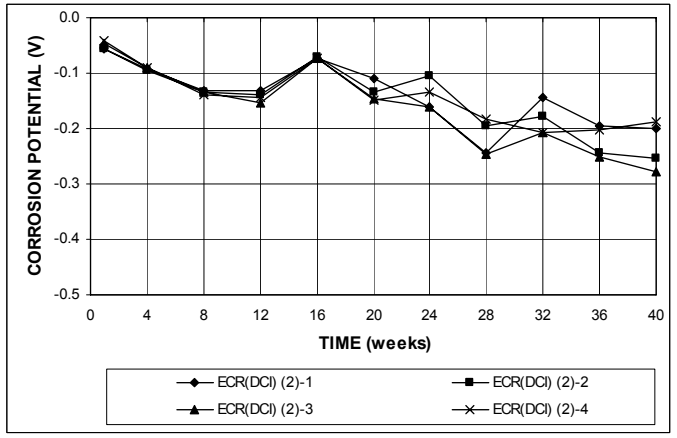

(b)

Figure A.184 – (a) Top mat corrosion potentials and (b) bottom mat corrosion potentials, with respect to copper-copper sulfate electrode as measured in the field test for specimens with ECR in concrete with DCI (without cracks, No. 2).

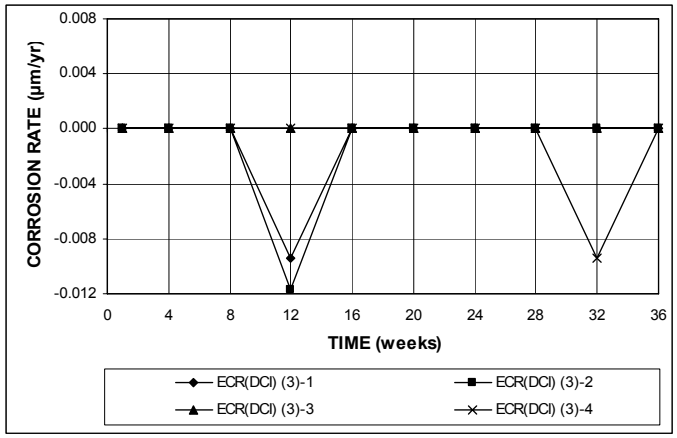

(a)

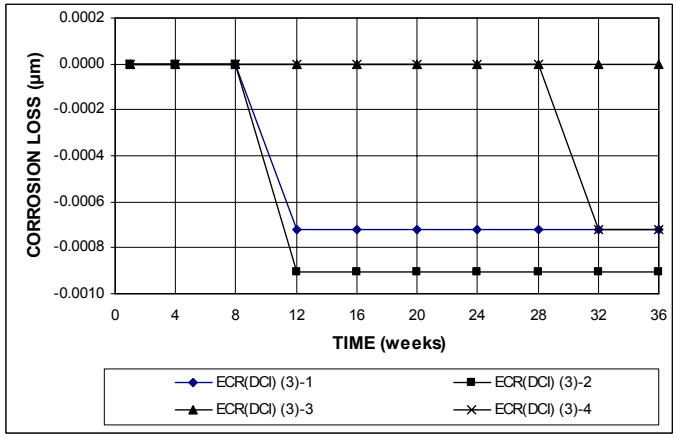

(b)

Figure A.185 – (a) Corrosion rates and (b) total corrosion losses base on total area of the bar as measured in the field test for specimens with ECR in concrete with DCI (without cracks, No. 3).

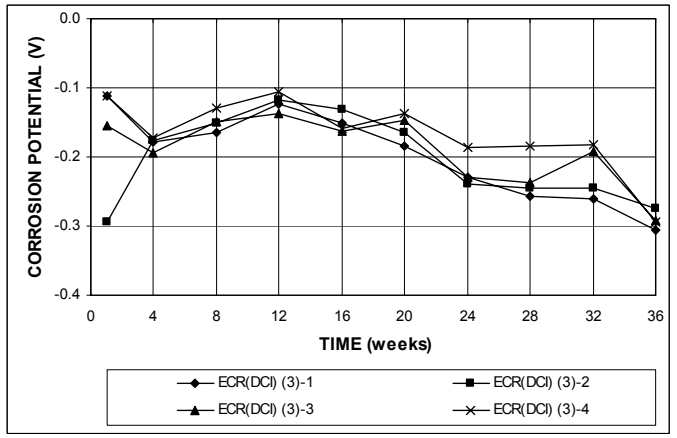

(a)

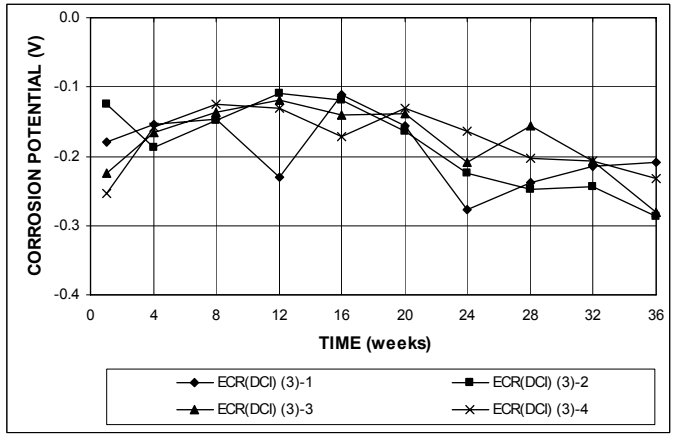

(b)

Figure A.186 – (a) Top mat corrosion potentials and (b) bottom mat corrosion potentials, with respect to copper-copper sulfate electrode as measured in the field test for specimens with ECR in concrete with DCI (without cracks, No. 3).

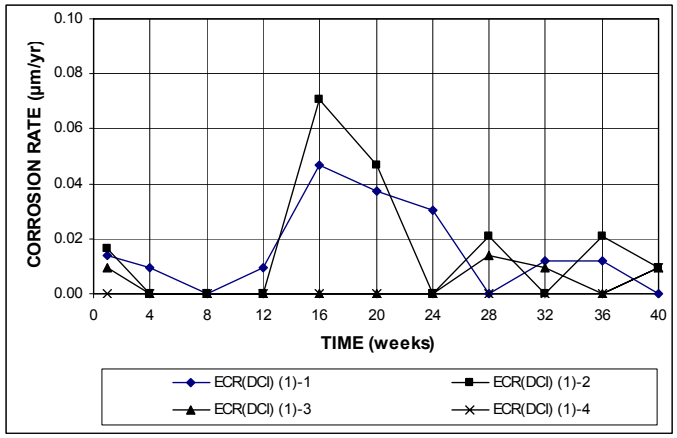

(a)

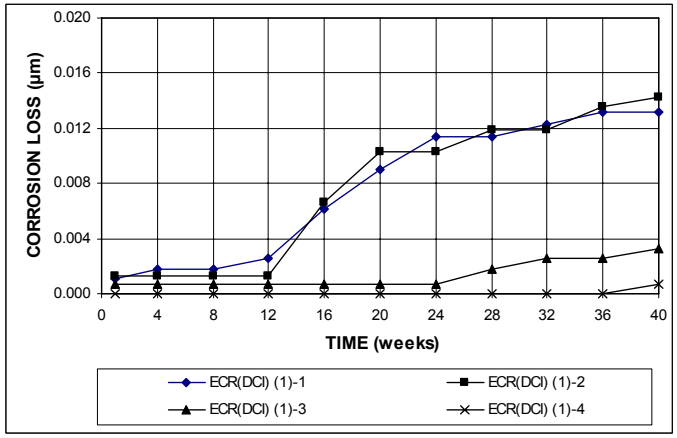

(b)

Figure A.187 – (a) Corrosion rates and (b) total corrosion losses base on total area of the bar as measured in the field test for specimens with ECR in concrete with DCI (with cracks, No. 1).

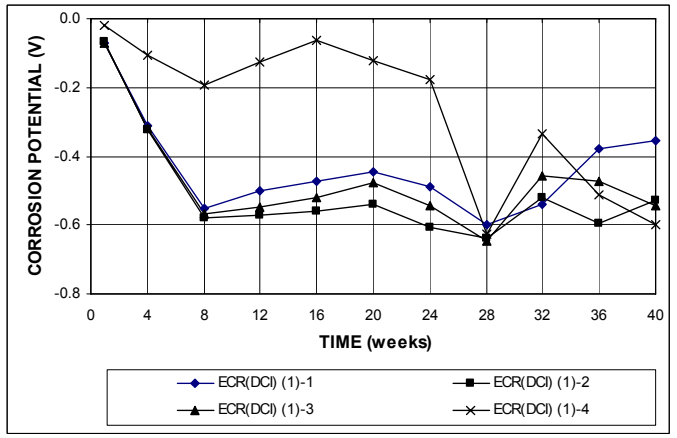

(a)

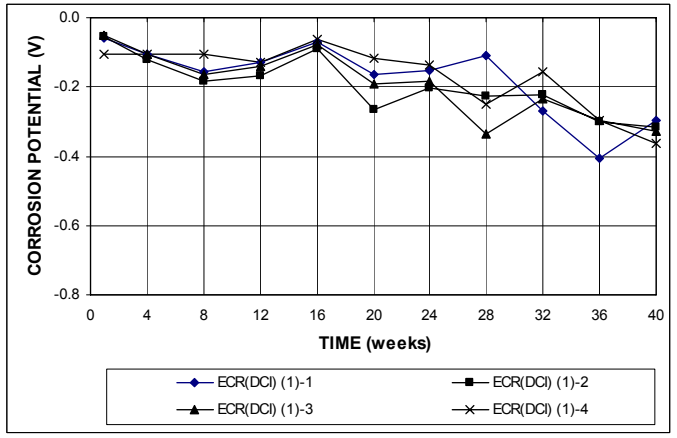

(b)

Figure A.188 – (a) Top mat corrosion potentials and (b) bottom mat corrosion potentials, with respect to copper-copper sulfate electrode as measured in the field test for specimens with ECR in concrete with DCI (with cracks, No. 1).

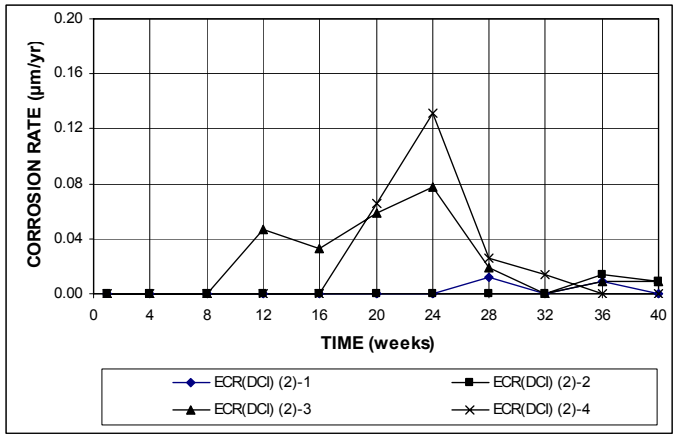

(a)

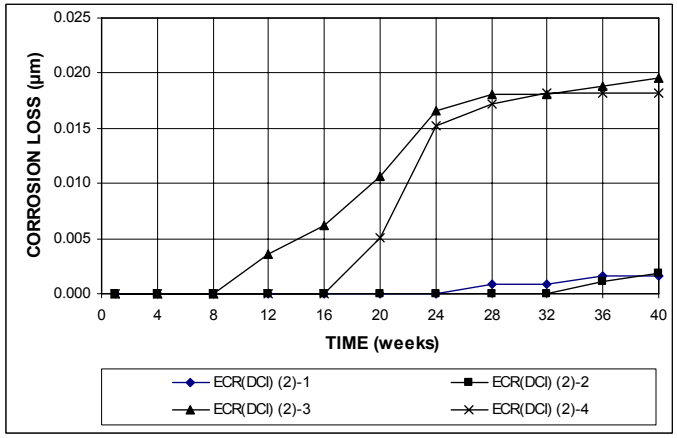

(b)

Figure A.189 – (a) Corrosion rates and (b) total corrosion losses base on total area of the bar as measured in the field test for specimens with ECR in concrete with DCI (with cracks, No. 2).

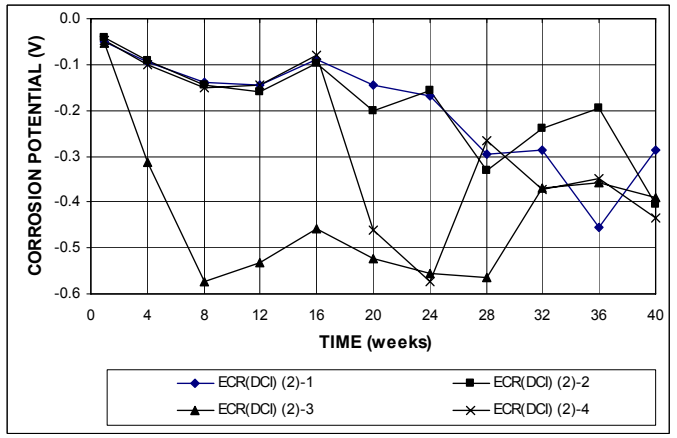

(a)

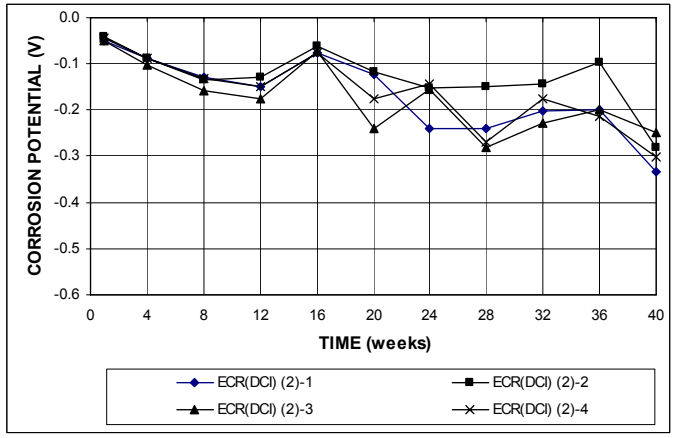

(b)

Figure A.190 – (a) Top mat corrosion potentials and (b) bottom mat corrosion potentials, with respect to copper-copper sulfate electrode as measured in the field test for specimens with ECR in concrete with DCI (with cracks, No. 2).

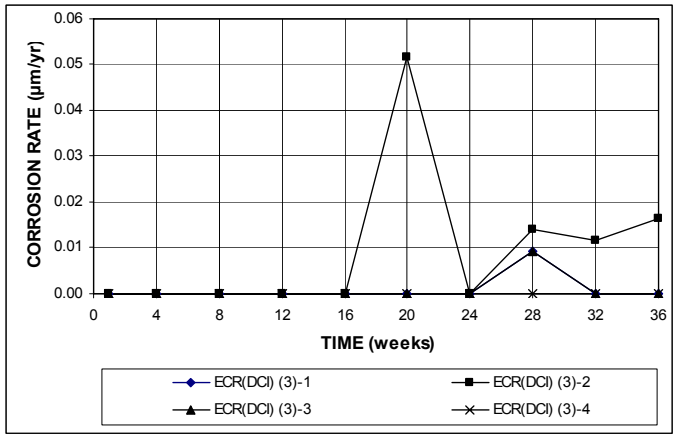

(a)

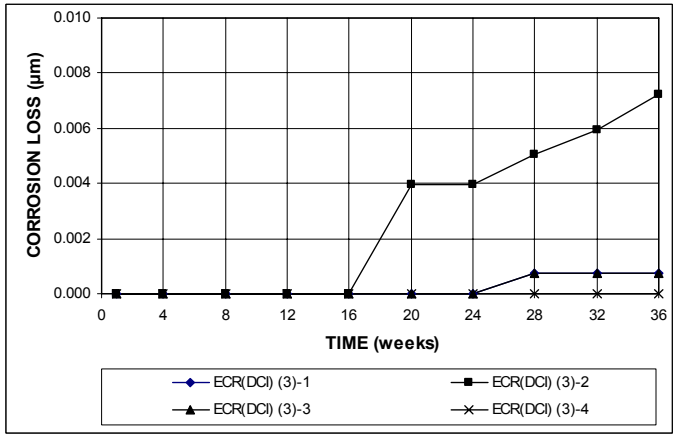

(b)

Figure A.191 – (a) Corrosion rates and (b) total corrosion losses base on total area of the bar as measured in the field test for specimens with ECR in concrete with DCI (with cracks, No. 3).

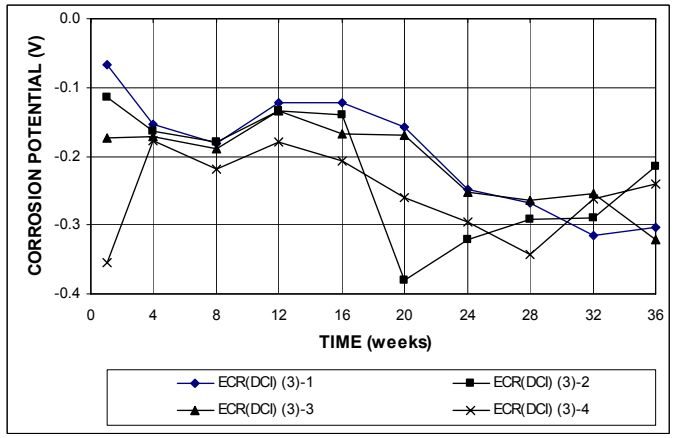

(a)

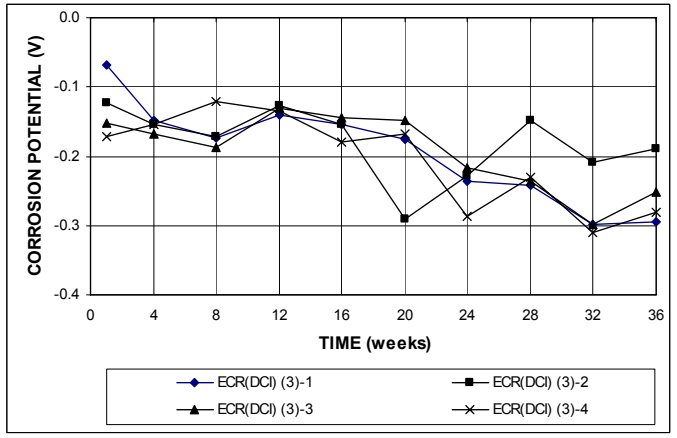

(b)

Figure A.192 – (a) Top mat corrosion potentials and (b) bottom mat corrosion potentials, with respect to copper-copper sulfate electrode as measured in the field test for specimens with ECR in concrete with DCI (with cracks, No. 3).

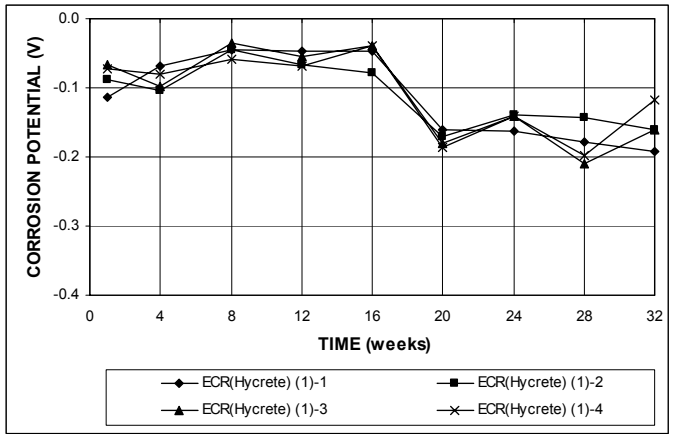

(a)

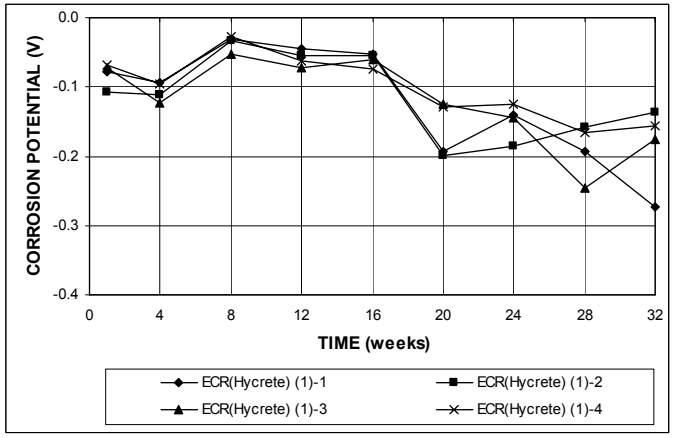

(b)

Figure A.193 – (a) Top mat corrosion potentials and (b) bottom mat corrosion potentials, with respect to copper-copper sulfate electrode as measured in the field test for specimens with ECR in concrete with Hycrete (without cracks, No. 1).

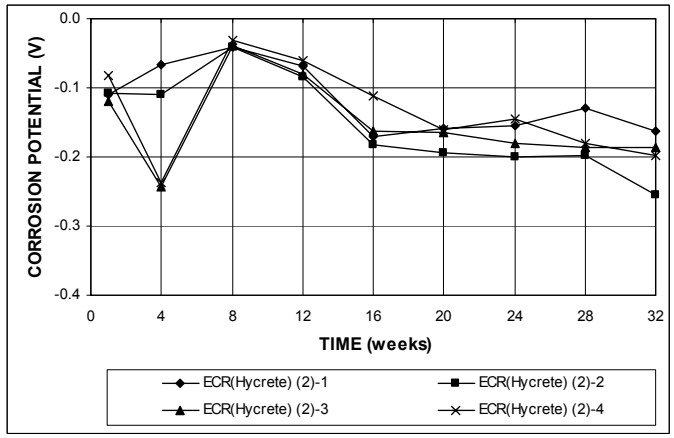

(a)

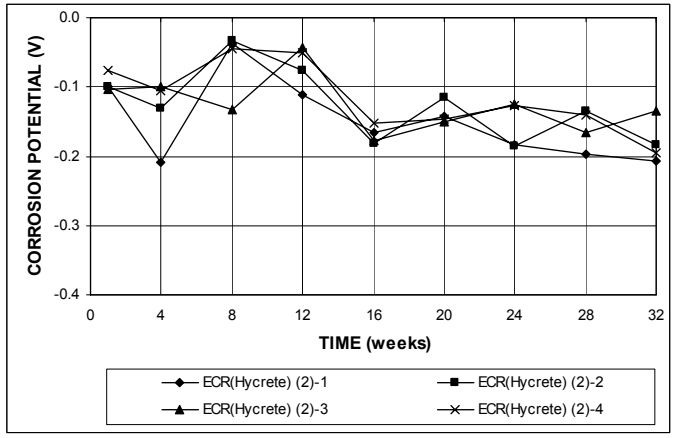

(b)

Figure A.194 – (a) Top mat corrosion potentials and (b) bottom mat corrosion potentials, with respect to copper-copper sulfate electrode as measured in the field test for specimens with ECR in concrete with Hycrete (without cracks, No. 2).

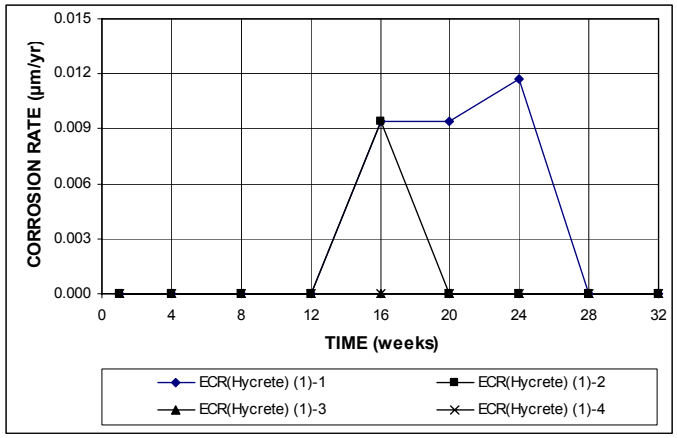

(a)

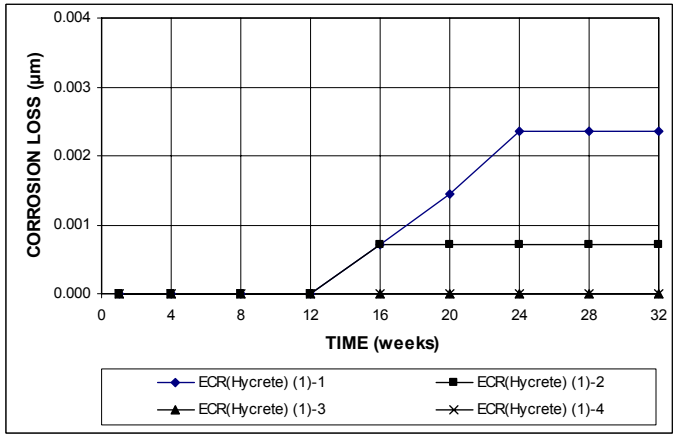

(b)

Figure A.195 – (a) Corrosion rates and (b) total corrosion losses base on total area of the bar as measured in the field test for specimens with ECR in concrete with Hycrete (with cracks, No. 1).

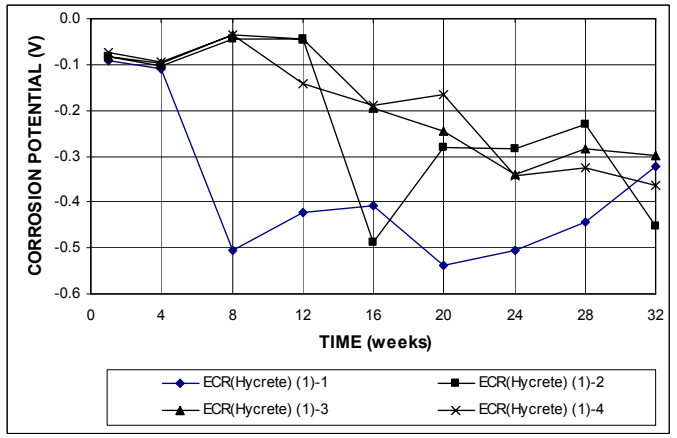

(a)

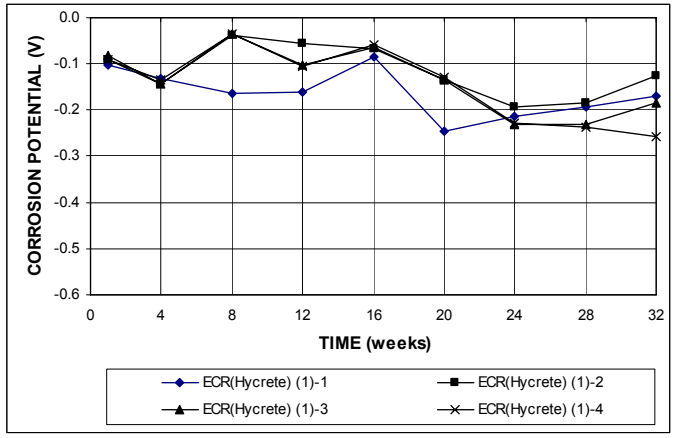

(b)

Figure A.196 – (a) Top mat corrosion potentials and (b) bottom mat corrosion potentials, with respect to copper-copper sulfate electrode as measured in the field test for specimens with ECR in concrete with Hycrete (with cracks, No. 1).

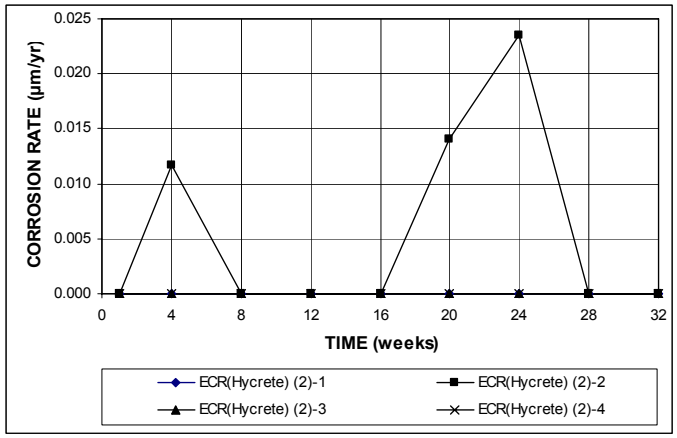

(a)

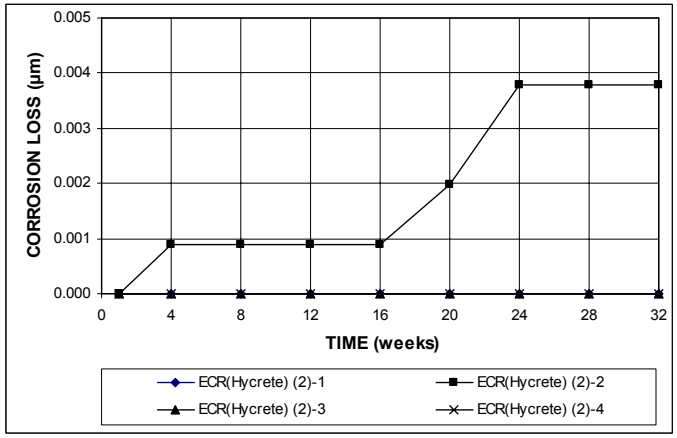

(b)

Figure A.197 – (a) Corrosion rates and (b) total corrosion losses base on total area of the bar as measured in the field test for specimens with ECR in concrete with Hycrete (with cracks, No. 2).

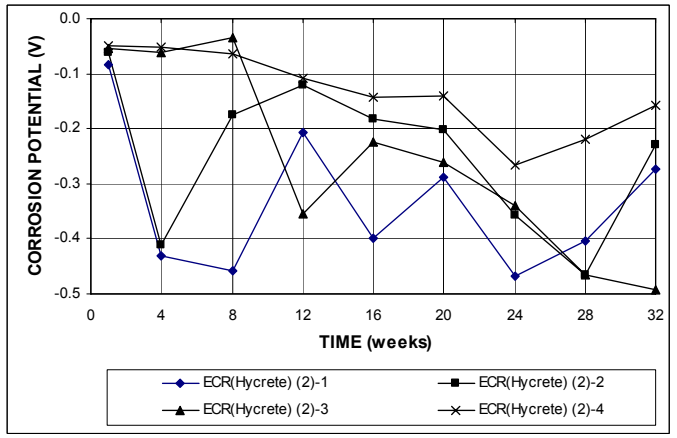

(a)

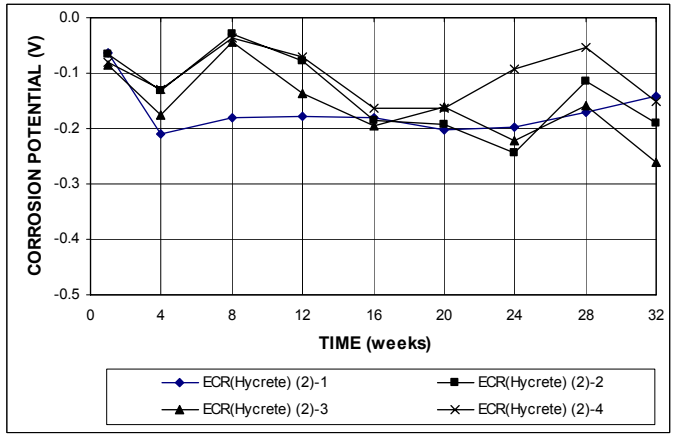

(b)

Figure A.198 – (a) Top mat corrosion potentials and (b) bottom mat corrosion potentials, with respect to copper-copper sulfate electrode as measured in the field test for specimens with ECR in concrete with Hycrete (with cracks, No. 2).

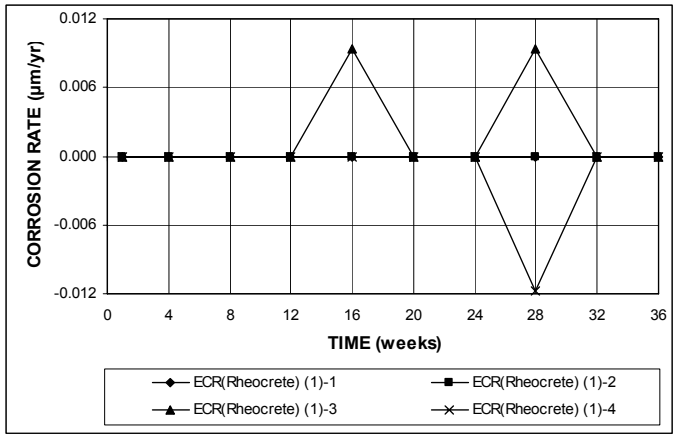

(a)

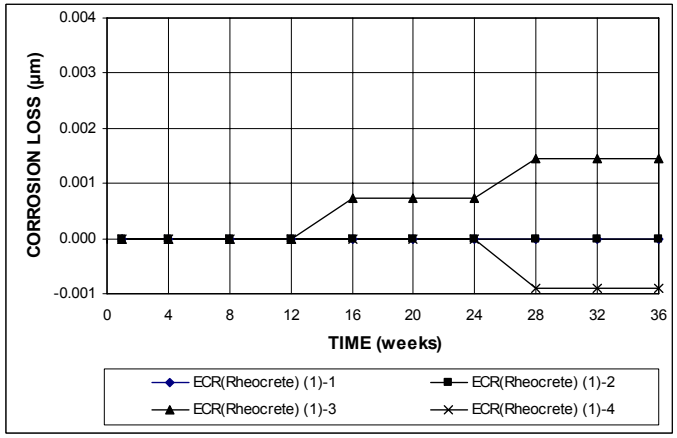

(b)

Figure A.199 – (a) Corrosion rates and (b) total corrosion losses base on total area of the bar as measured in the field test for specimens with ECR in concrete with Rheocrete (without cracks, No. 1).

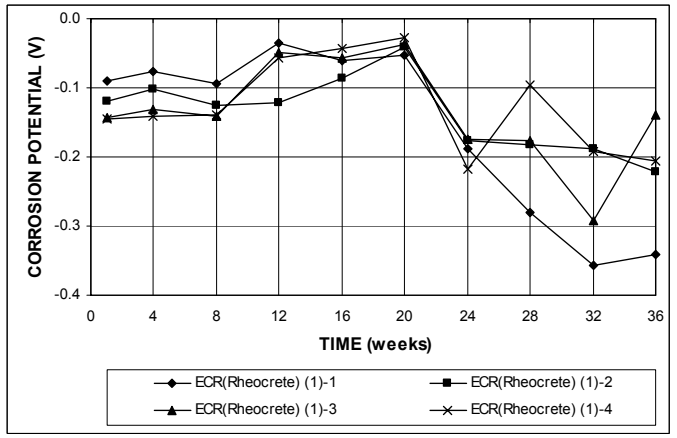

(a)

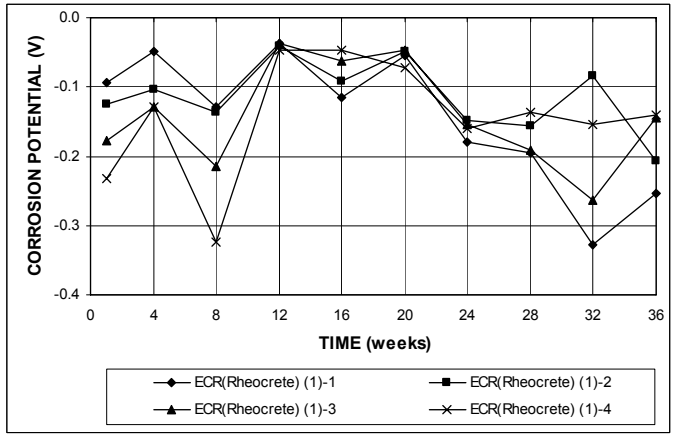

(b)

Figure A.200 – (a) Top mat corrosion potentials and (b) bottom mat corrosion potentials, with respect to copper-copper sulfate electrode as measured in the field test for specimens with ECR in concrete with Rheocrete (without cracks, No. 1).

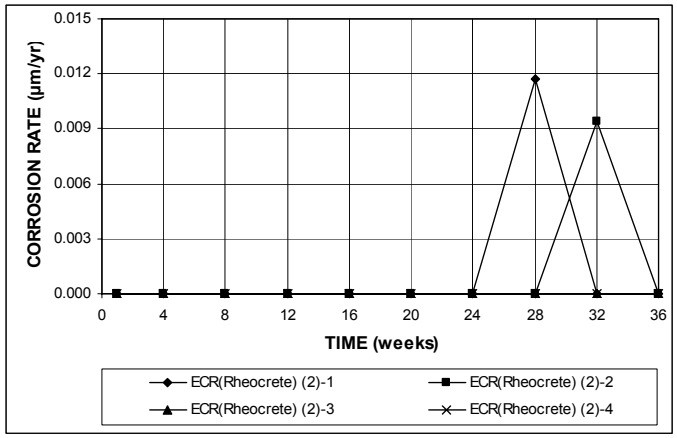

(a)

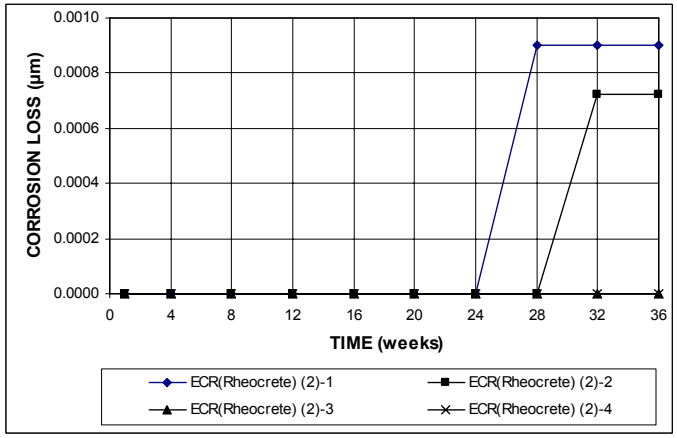

(b)

Figure A.201 – (a) Corrosion rates and (b) total corrosion losses base on total area of the bar as measured in the field test for specimens with ECR in concrete with Rheocrete (without cracks, No. 2).

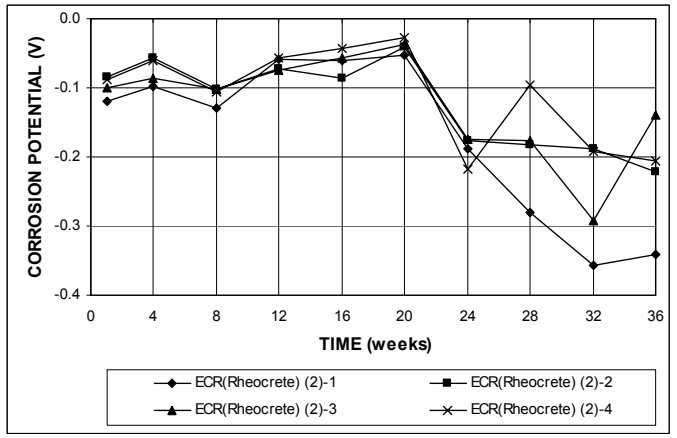

(a)

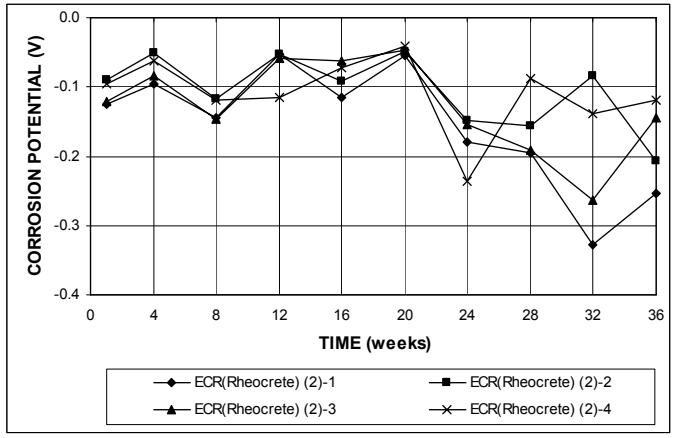

(b)

Figure A.202 – (a) Top mat corrosion potentials and (b) bottom mat corrosion potentials, with respect to copper-copper sulfate electrode as measured in the field test for specimens with ECR in concrete with Rheocrete (without cracks, No. 2).

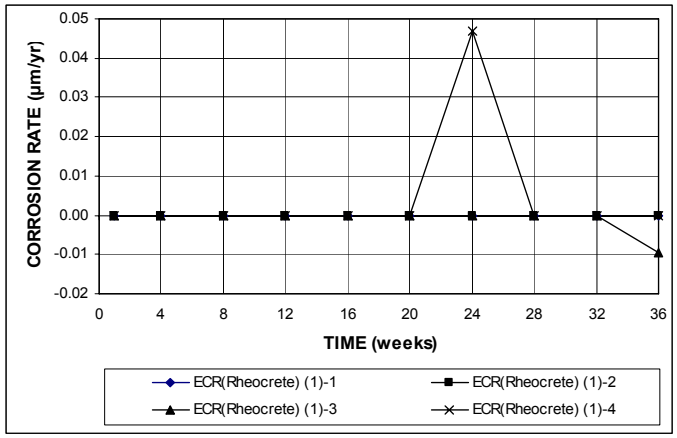

(a)

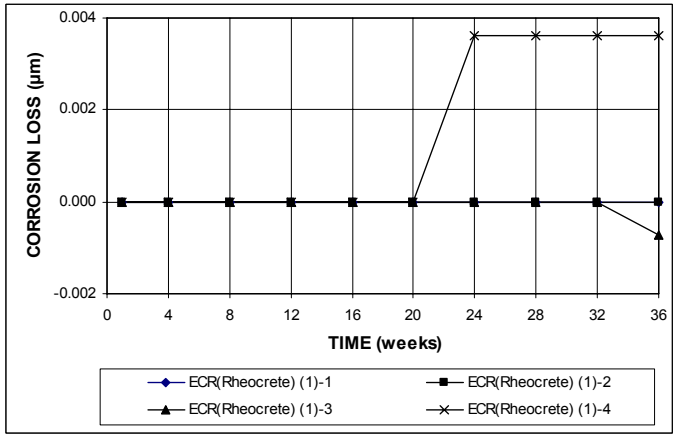

(b)

Figure A.203 – (a) Corrosion rates and (b) total corrosion losses base on total area of the bar as measured in the field test for specimens with ECR in concrete with Rheocrete (with cracks, No. 1).

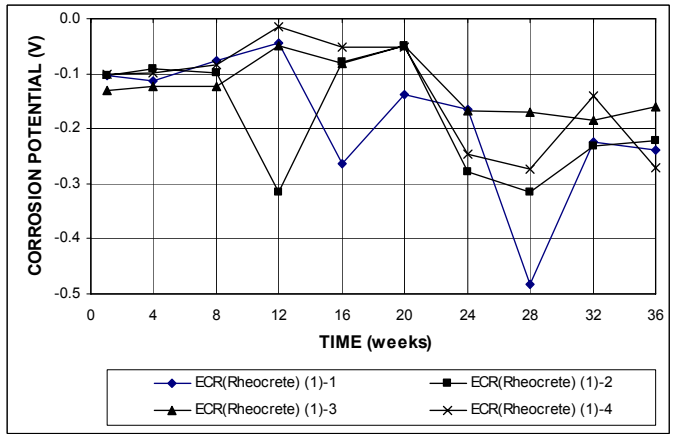

(a)

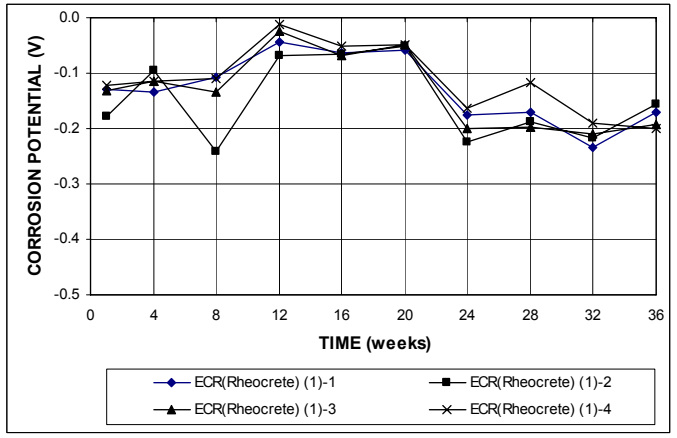

(b)

Figure A.204 – (a) Top mat corrosion potentials and (b) bottom mat corrosion potentials, with respect to copper-copper sulfate electrode as measured in the field test for specimens with ECR in concrete with Rheocrete (with cracks, No. 1).

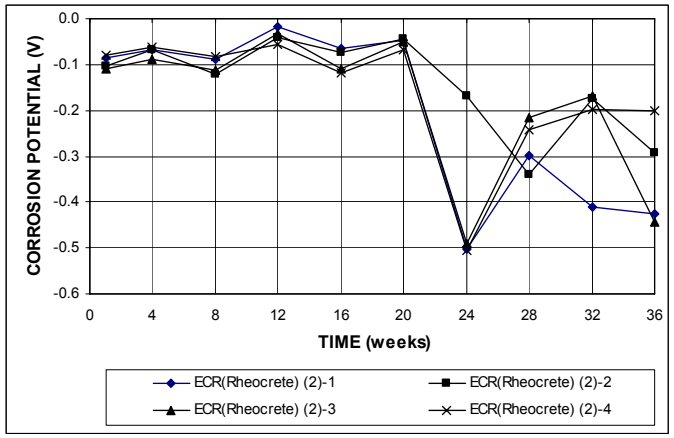

(a)

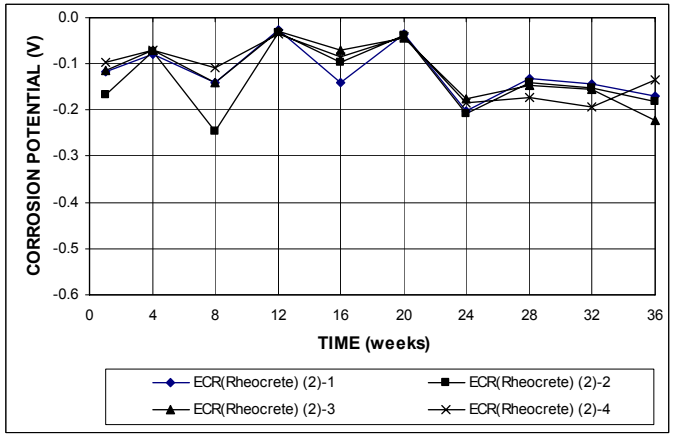

(b)

Figure A.205 – (a) Top mat corrosion potentials and (b) bottom mat corrosion potentials, with respect to copper-copper sulfate electrode as measured in the field test for specimens with ECR in concrete with Rheocrete (with cracks, No. 2).

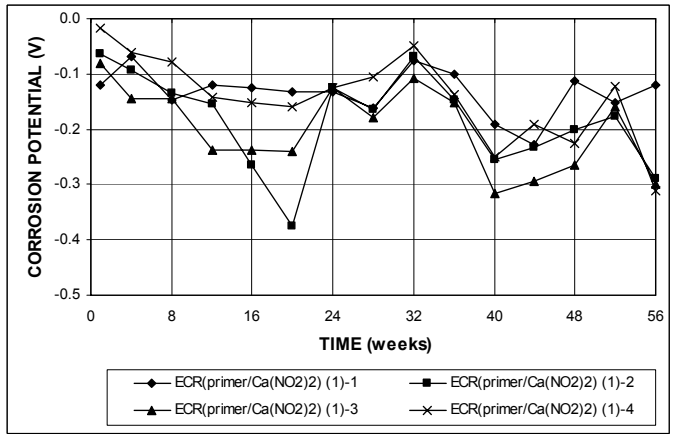

(a)

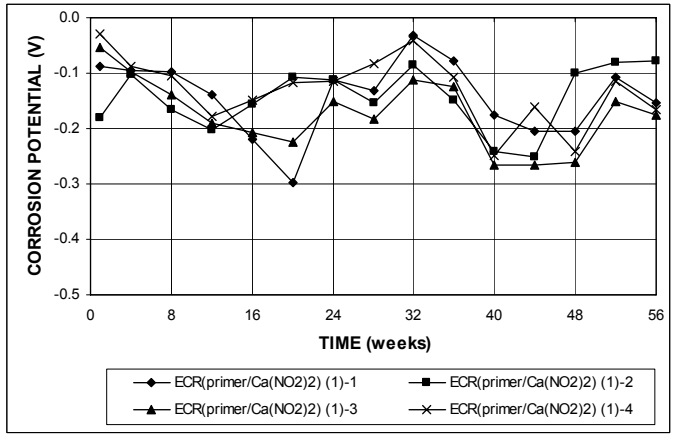

(b)

Figure A.206 – (a) Top mat corrosion potentials and (b) bottom mat corrosion potentials, with respect to copper-copper sulfate electrode as measured in the field test for specimens with ECR with a primer containing calcium nitrite (without cracks, No. 1).

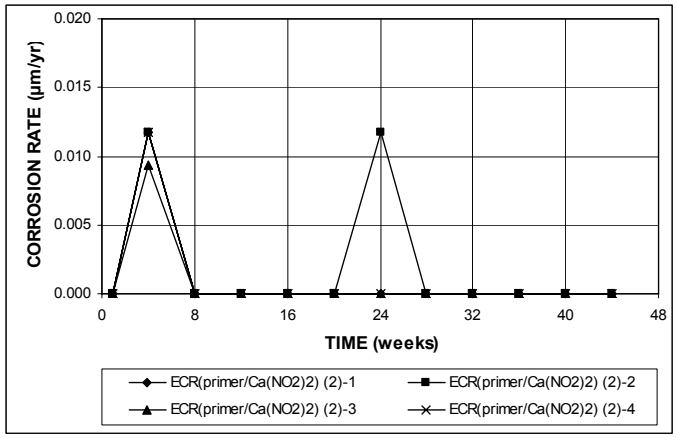

(a)

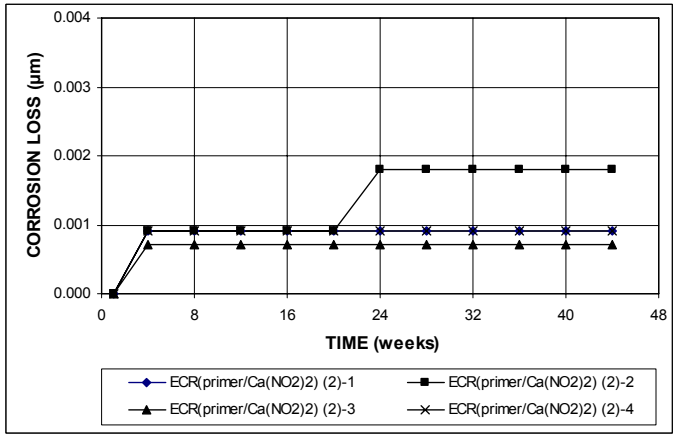

(b)

Figure A.207 – (a) Corrosion rates and (b) total corrosion losses base on total area of the bar as measured in the field test for specimens with ECR with a primer containing calcium nitrite (without cracks, No. 2).

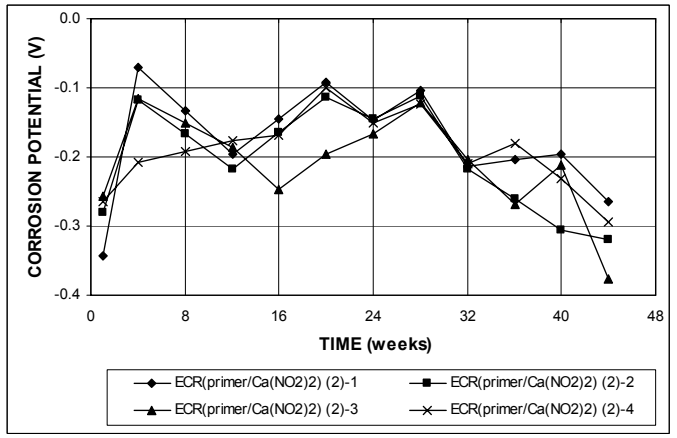

(a)

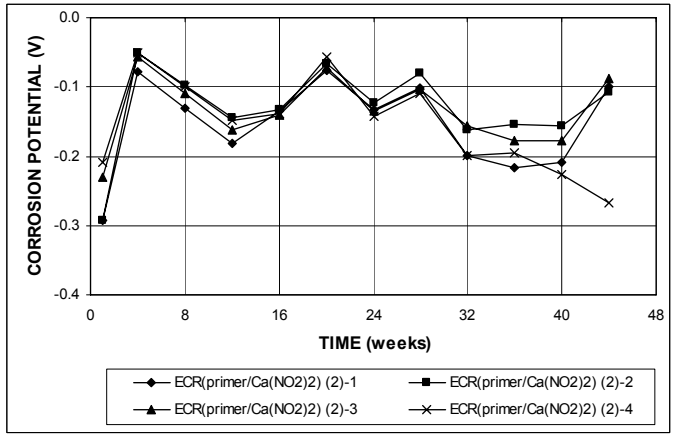

(b)

Figure A.208 – (a) Top mat corrosion potentials and (b) bottom mat corrosion potentials, with respect to copper-copper sulfate electrode as measured in the field test for specimens with ECR with a primer containing calcium nitrite (without cracks, No. 2).

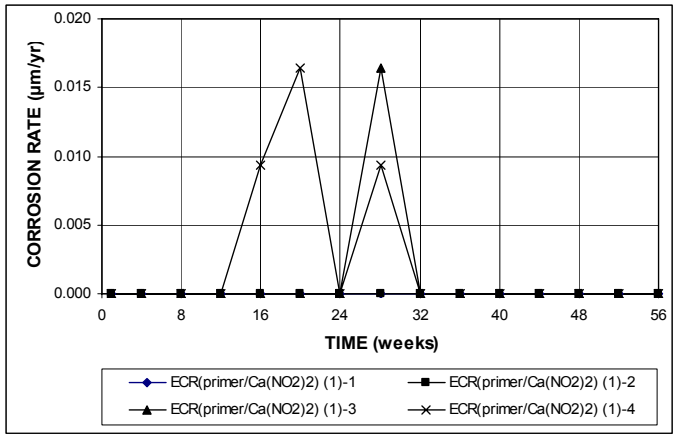

(a)

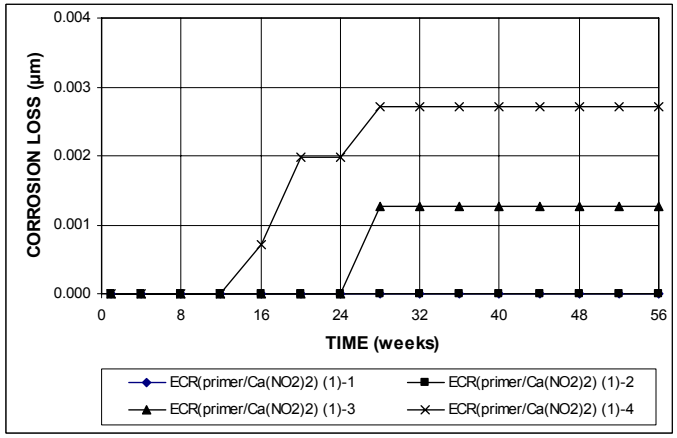

(b)

Figure A.209 – (a) Corrosion rates and (b) total corrosion losses base on total area of the bar as measured in the field test for specimens with ECR with a primer containing calcium nitrite (with cracks, No. 1).

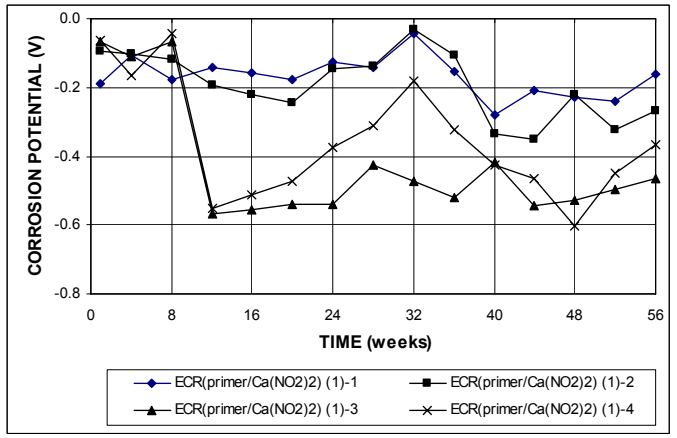

(a)

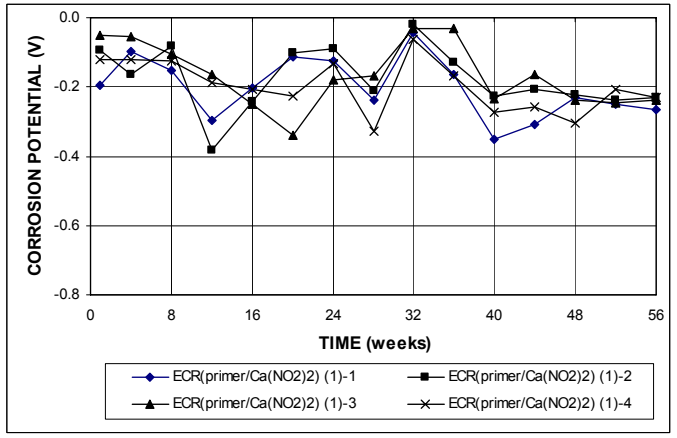

(b)

Figure A.210 – (a) Top mat corrosion potentials and (b) bottom mat corrosion potentials, with respect to copper-copper sulfate electrode as measured in the field test for specimens with ECR with a primer containing calcium nitrite (with cracks, No. 1).

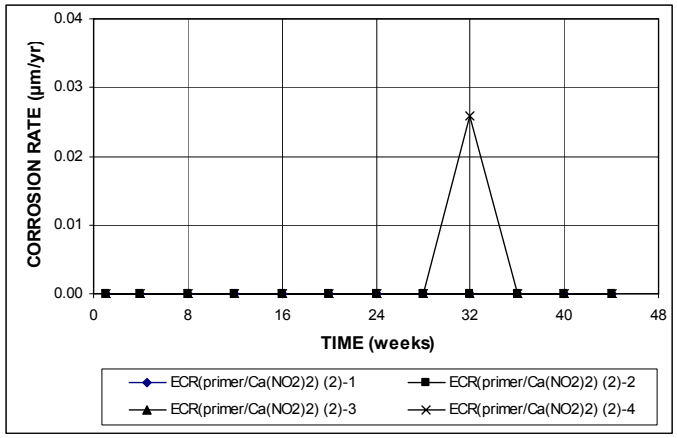

(a)

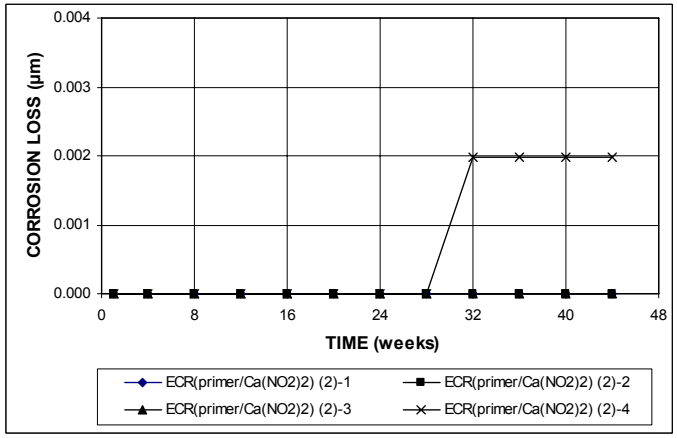

(b)

Figure A.211 – (a) Corrosion rates and (b) total corrosion losses base on total area of the bar as measured in the field test for specimens with ECR with a primer containing calcium nitrite (with cracks, No. 2).

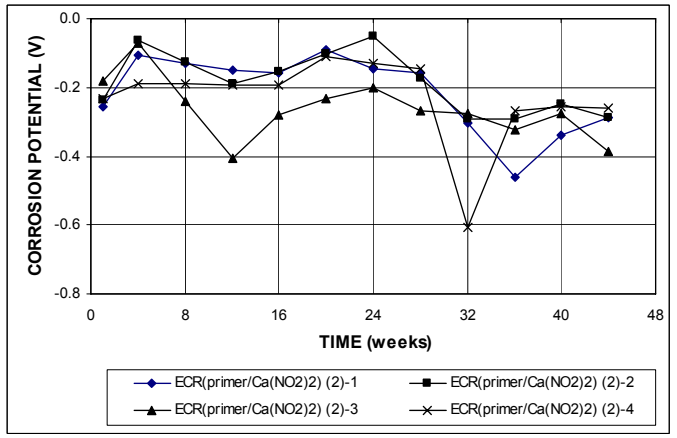

(a)

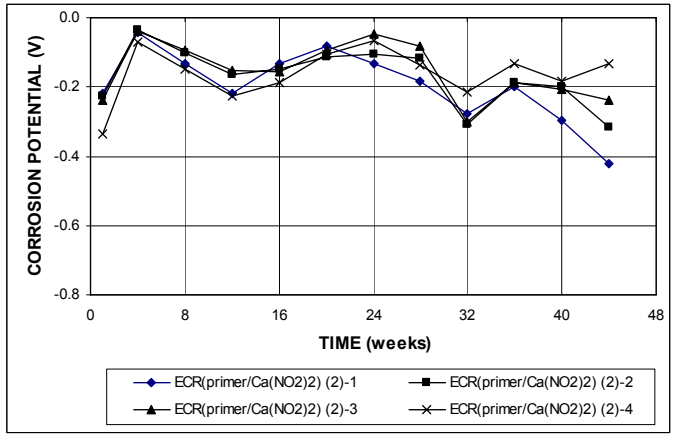

(b)

Figure A.212 – (a) Top mat corrosion potentials and (b) bottom mat corrosion potentials, with respect to copper-copper sulfate electrode as measured in the field test for specimens with ECR with a primer containing calcium nitrite (with cracks, No. 2).

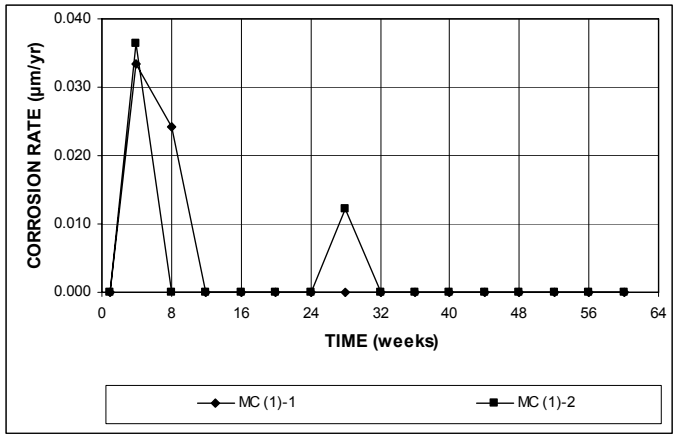

(a)

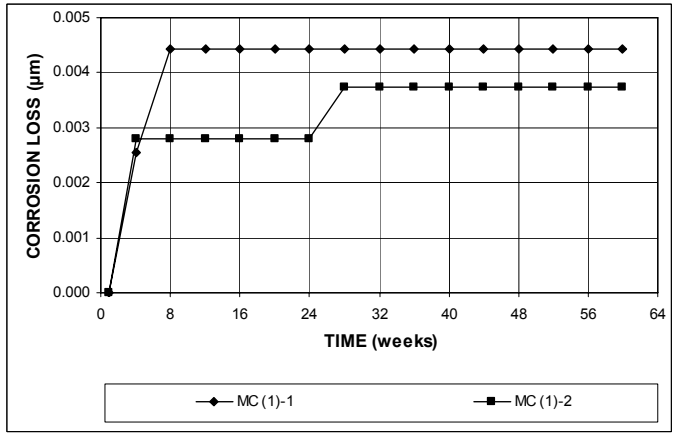

(b)

Figure A.213 – (a) Corrosion rates and (b) total corrosion losses base on total area of the bar as measured in the field test for specimens with multiple coated bars (without cracks, No. 1).

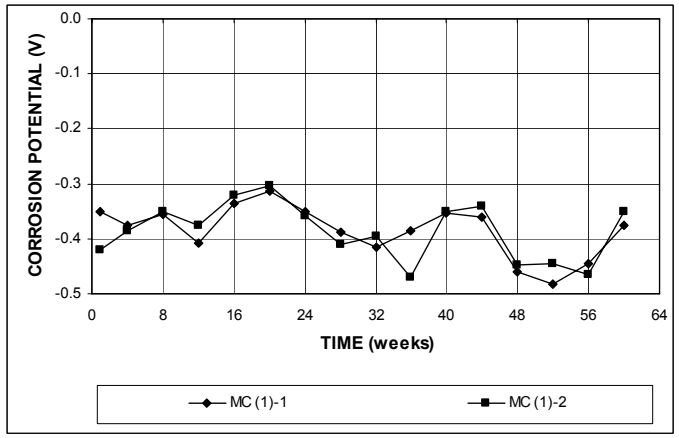

(a)

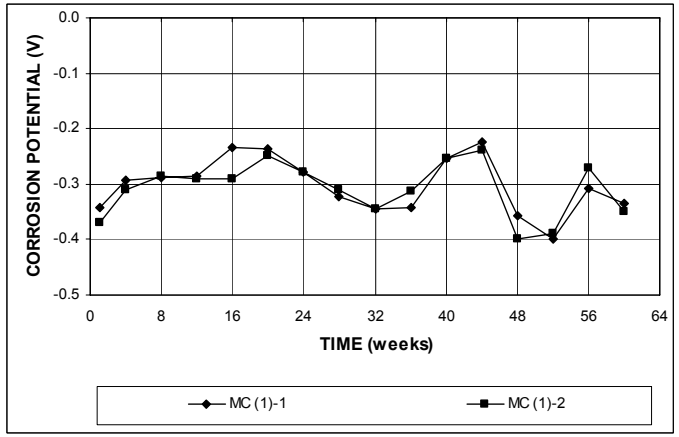

(b)

Figure A.214 – (a) Top mat corrosion potentials and (b) bottom mat corrosion potentials, with respect to copper-copper sulfate electrode as measured in the field test for specimens with multiple coated bars (without cracks, No. 1).

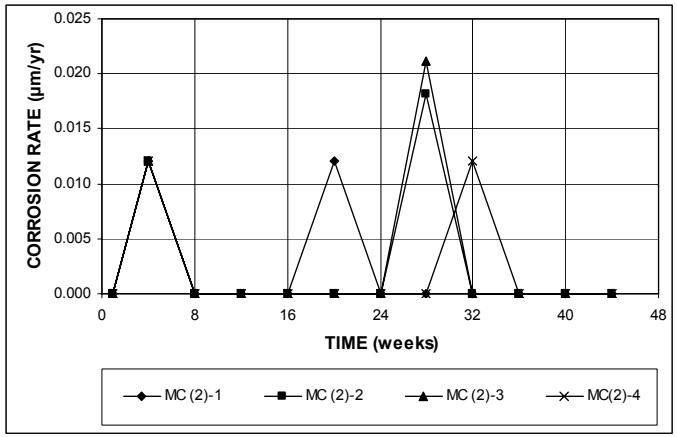

(a)

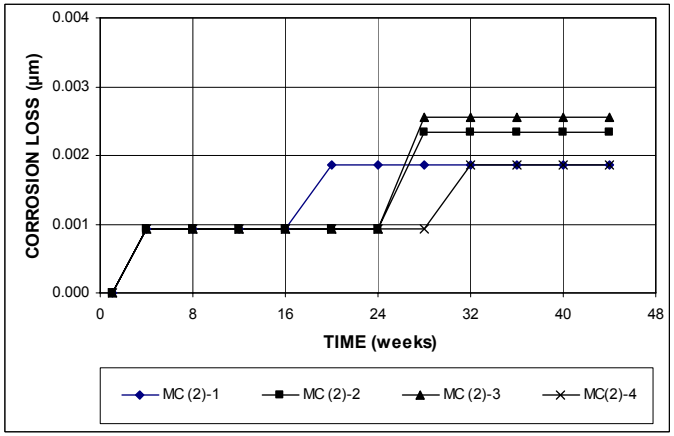

(b)

Figure A.215 – (a) Corrosion rates and (b) total corrosion losses base on total area of the bar as measured in the field test for specimens with multiple coated bars (without cracks, No. 2).

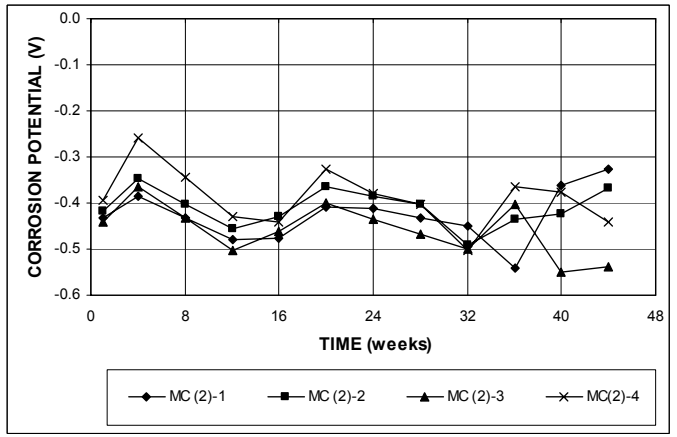

(a)

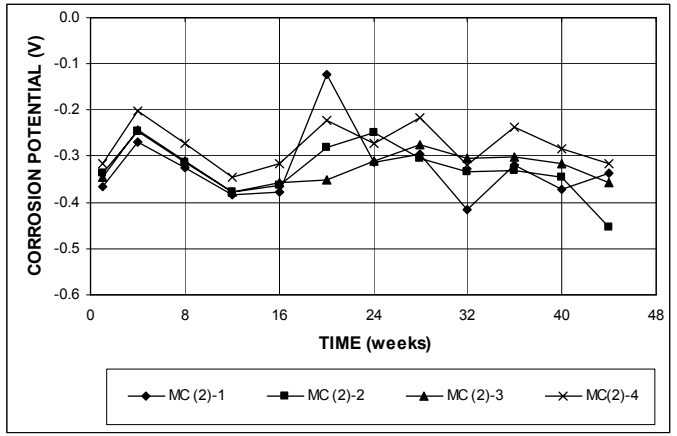

(b)

Figure A.216 – (a) Top mat corrosion potentials and (b) bottom mat corrosion potentials, with respect to copper-copper sulfate electrode as measured in the field test for specimens with multiple coated bars (without cracks, No. 2).

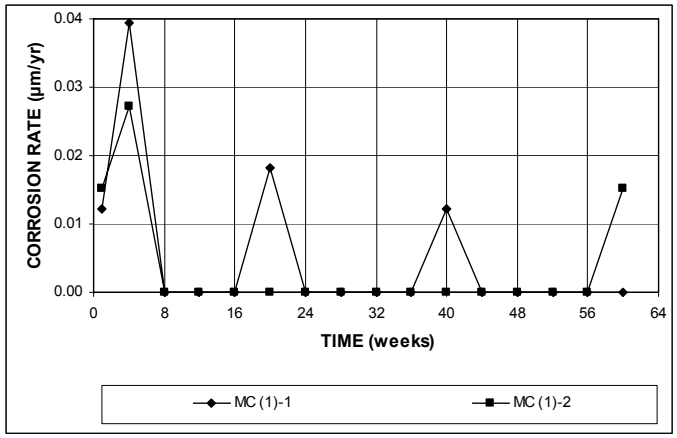

(a)

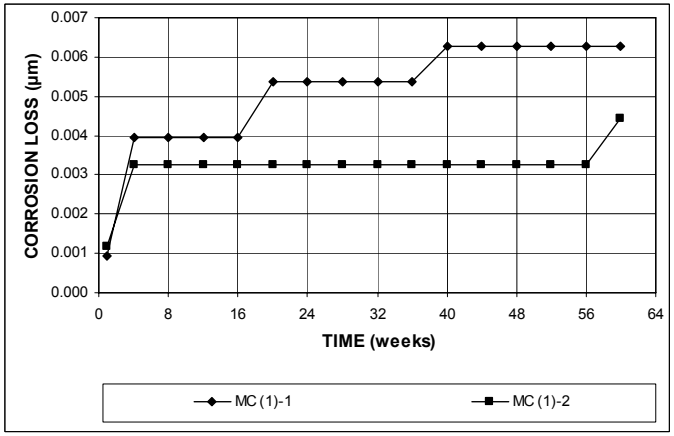

(b)

Figure A.217 – (a) Corrosion rates and (b) total corrosion losses base on total area of the bar as measured in the field test for specimens with multiple coated bars (with cracks, No. 1).

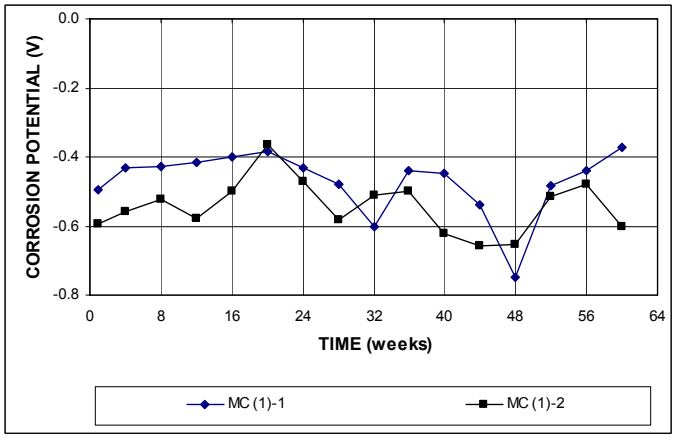

(a)

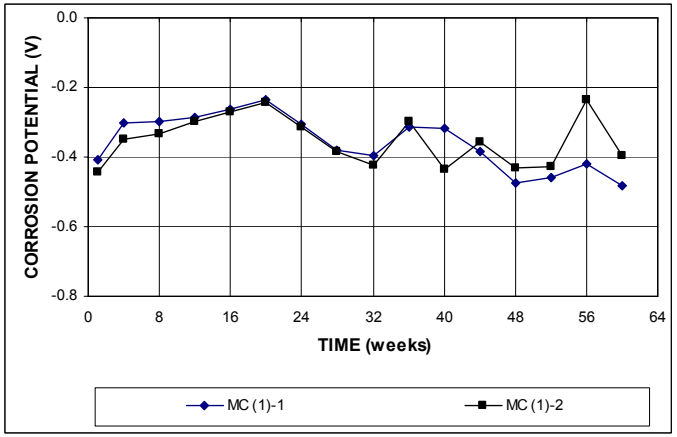

(b)

Figure A.218 – (a) Top mat corrosion potentials and (b) bottom mat corrosion potentials, with respect to copper-copper sulfate electrode as measured in the field test for specimens with multiple coated bars (with cracks, No. 1).

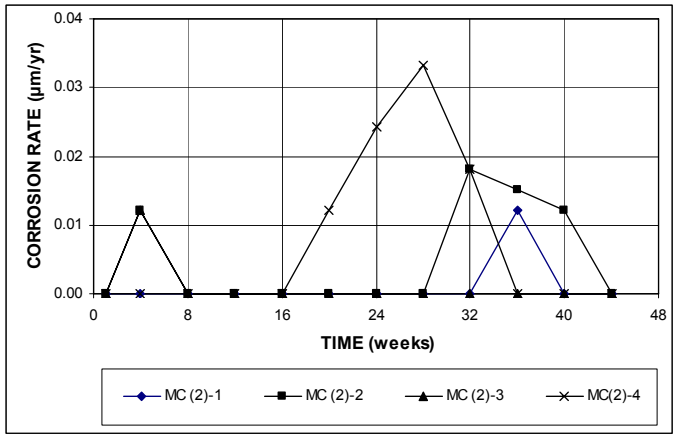

(a)

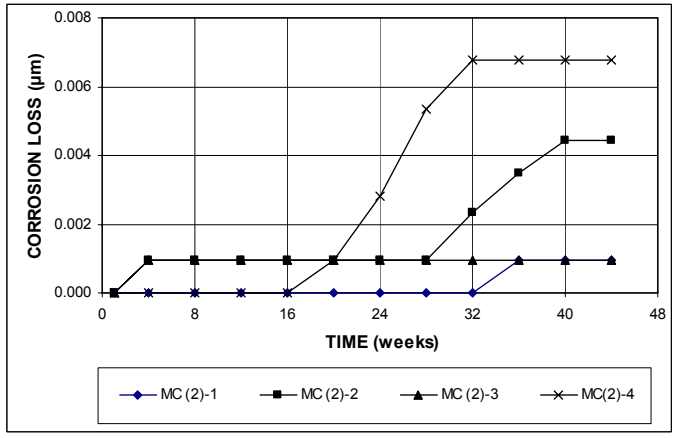

(b)

Figure A.219 – (a) Corrosion rates and (b) total corrosion losses base on total area of the bar as measured in the field test for specimens with multiple coated bars (with cracks, No. 2).

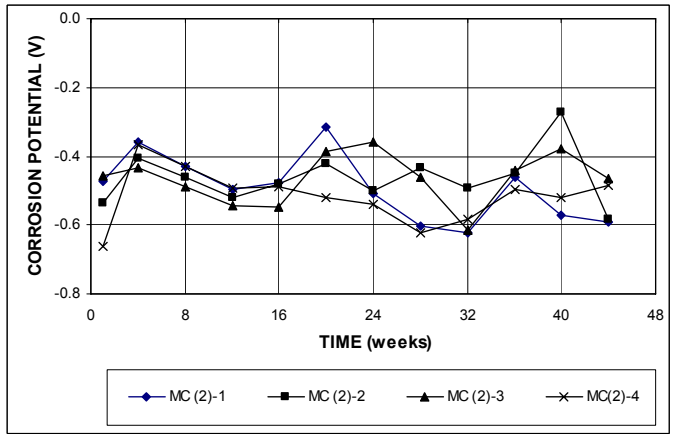

(a)

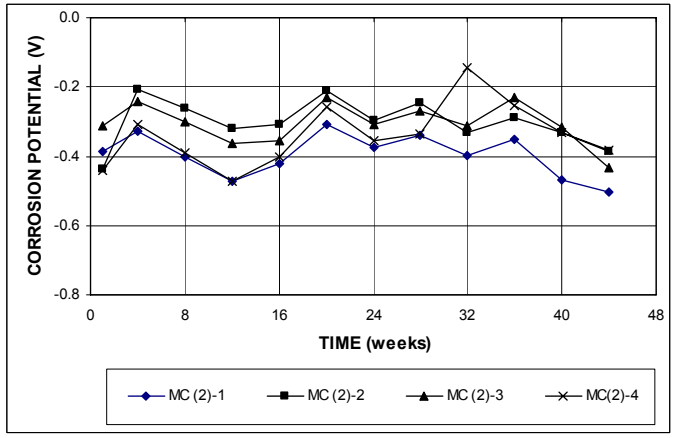

(b)

Figure A.220 – (a) Top mat corrosion potentials and (b) bottom mat corrosion potentials, with respect to copper-copper sulfate electrode as measured in the field test for specimens with multiple coated bars (with cracks, No. 2).

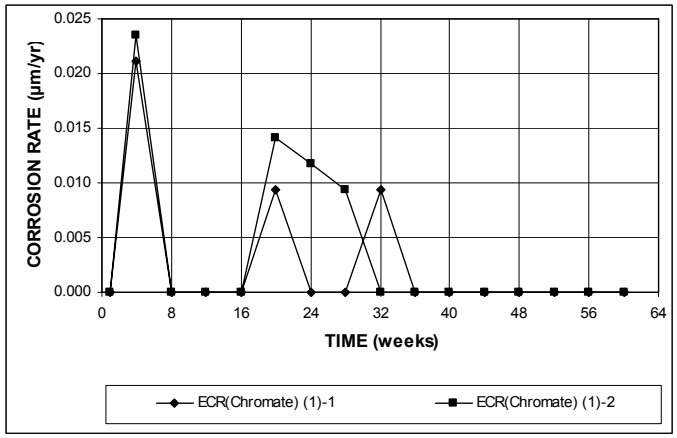

(a)

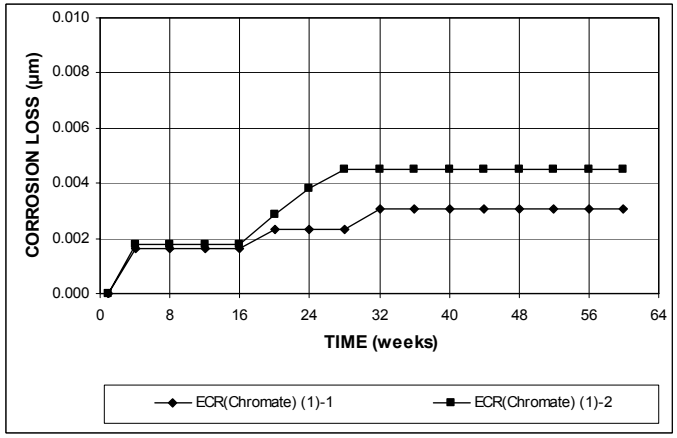

(b)

Figure A.221 – (a) Corrosion rates and (b) total corrosion losses base on total area of the bar as measured in the field test for specimens with ECR with chromate pretreatment (without cracks, No. 1).

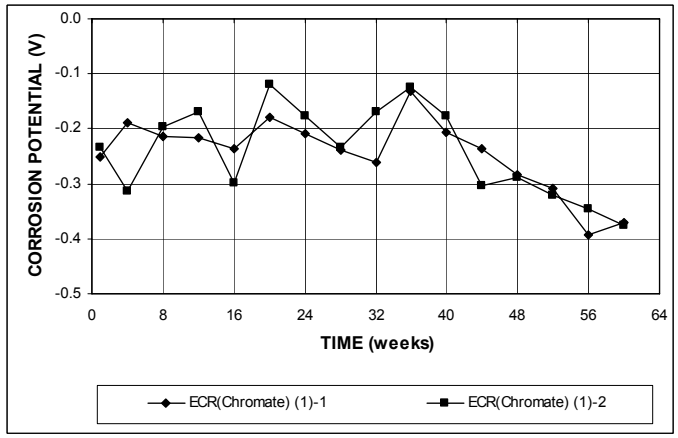

(a)

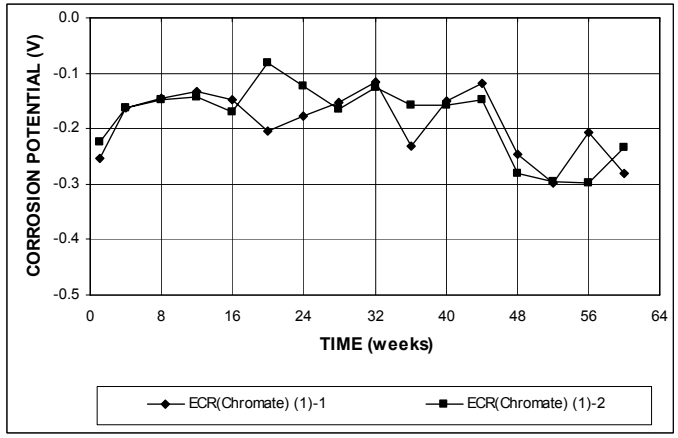

(b)

Figure A.222 – (a) Top mat corrosion potentials and (b) bottom mat corrosion potentials, with respect to copper-copper sulfate electrode as measured in the field test for specimens with ECR with chromate pretreatment (without cracks, No. 1).

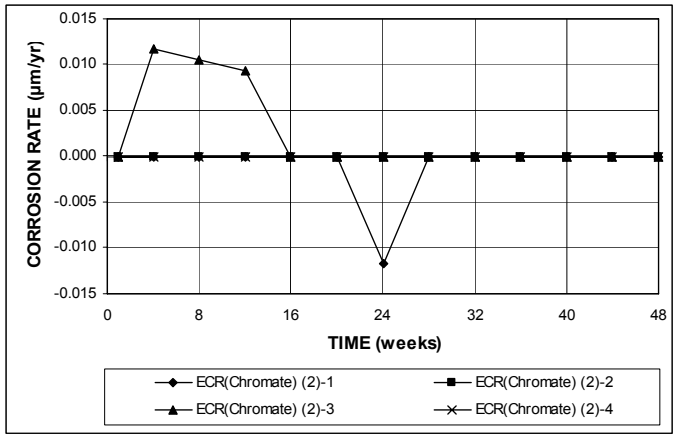

(a)

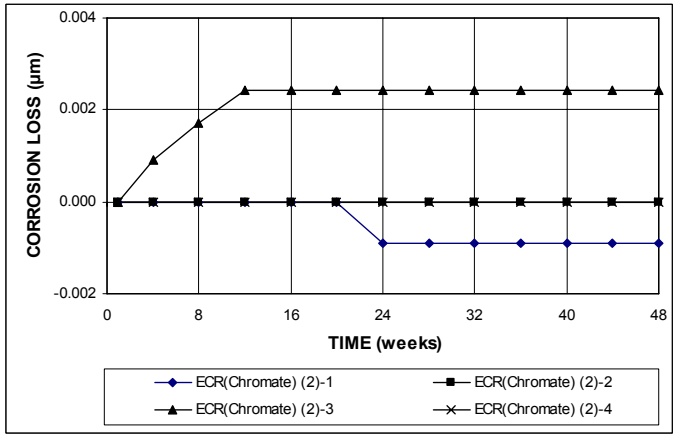

(b)

Figure A.223 – (a) Corrosion rates and (b) total corrosion losses base on total area of the bar as measured in the field test for specimens with ECR with chromate pretreatment (without cracks, No. 2).

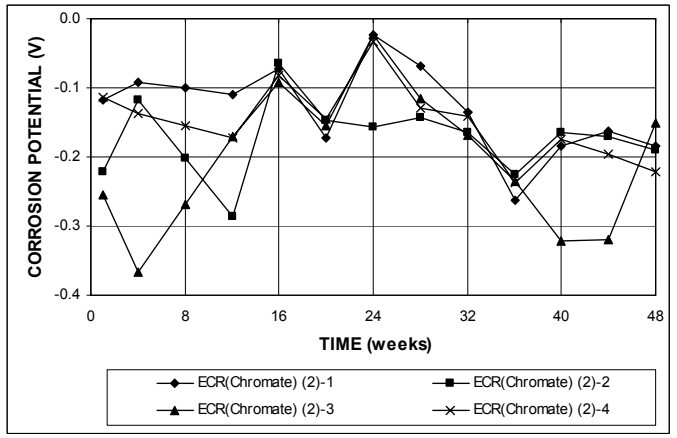

(a)

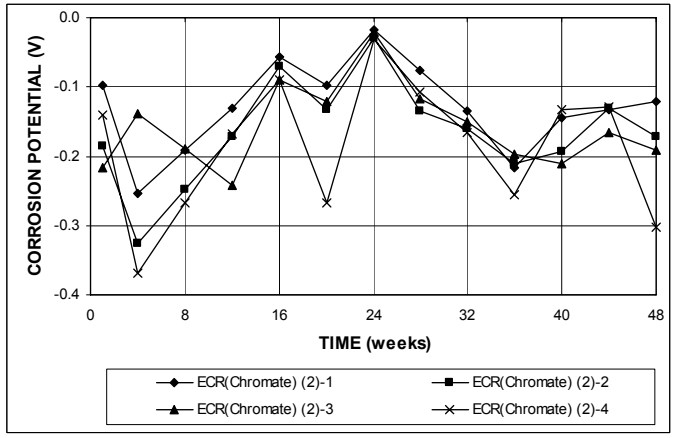

(b)

Figure A.224 – (a) Top mat corrosion potentials and (b) bottom mat corrosion potentials, with respect to copper-copper sulfate electrode as measured in the field test for specimens with ECR with chromate pretreatment (without cracks, No. 2).

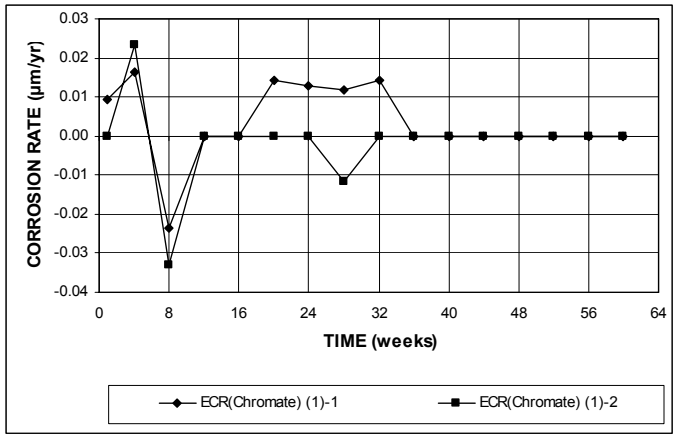

(a)

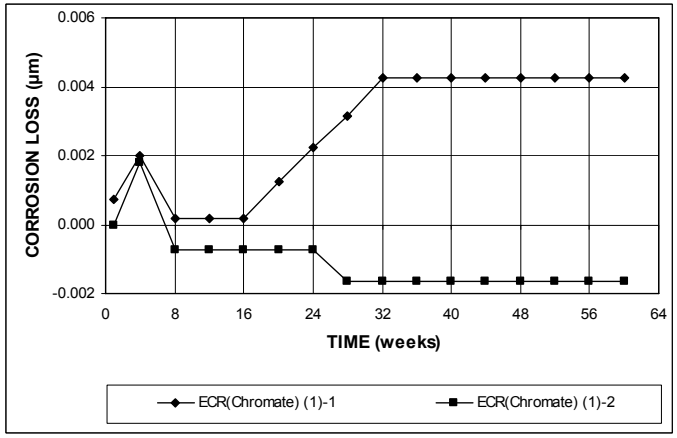

(b)

Figure A.225 – (a) Corrosion rates and (b) total corrosion losses base on total area of the bar as measured in the field test for specimens with ECR with chromate pretreatment (with cracks, No. 1).

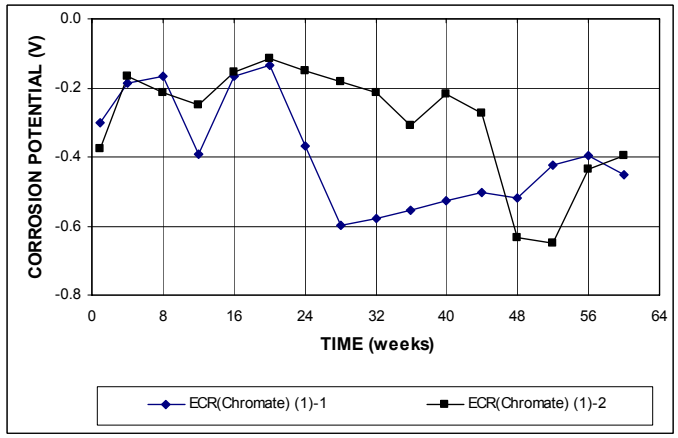

(a)

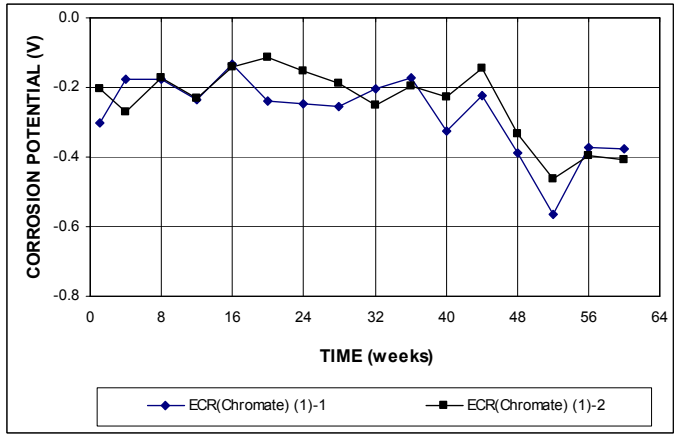

(b)

Figure A.226 – (a) Top mat corrosion potentials and (b) bottom mat corrosion potentials, with respect to copper-copper sulfate electrode as measured in the field test for specimens with ECR with chromate pretreatment (with cracks, No. 1).

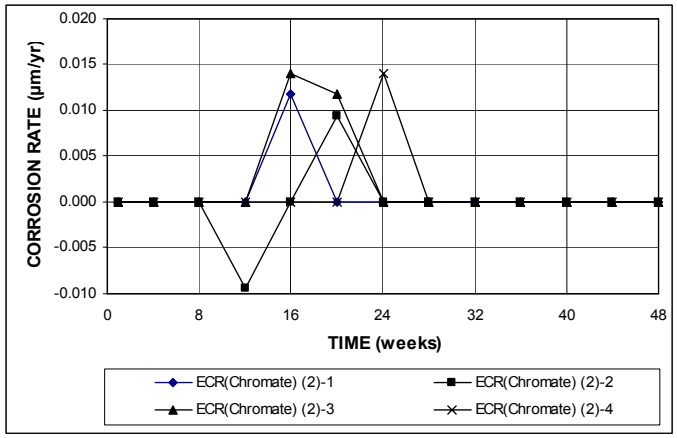

(a)

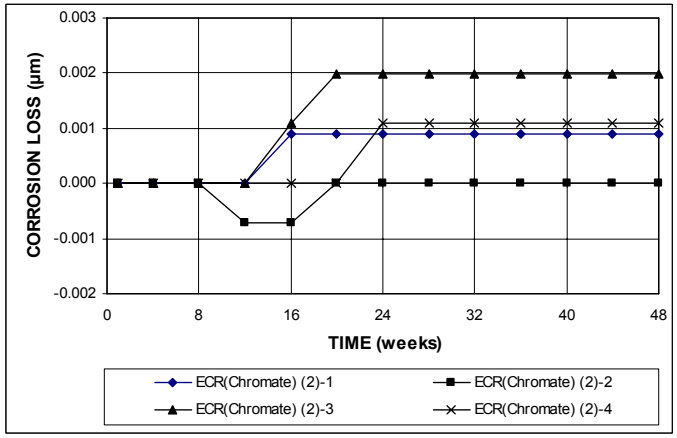

(b)

Figure A.227 – (a) Corrosion rates and (b) total corrosion losses base on total area of the bar as measured in the field test for specimens with ECR with chromate pretreatment (with cracks, No. 2).

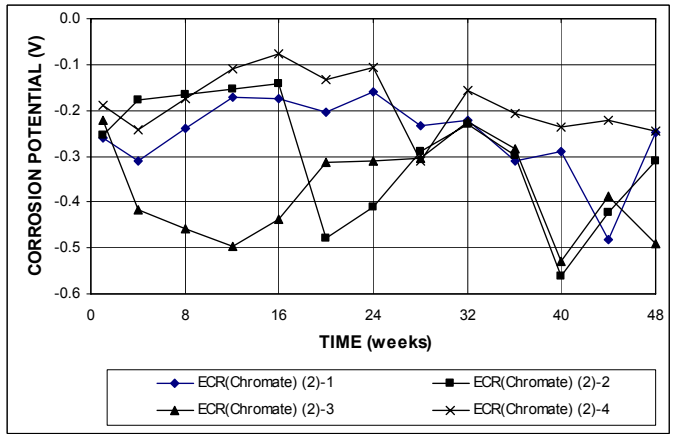

(a)

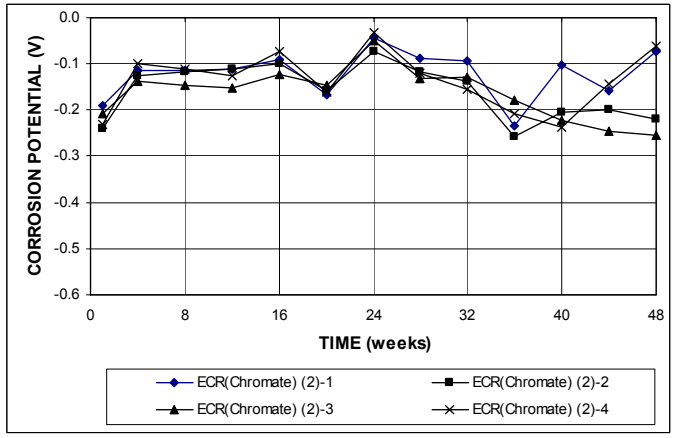

(b)

Figure A.228 – (a) Top mat corrosion potentials and (b) bottom mat corrosion potentials, with respect to copper-copper sulfate electrode as measured in the field test for specimens with ECR with chromate pretreatment (with cracks, No. 2).

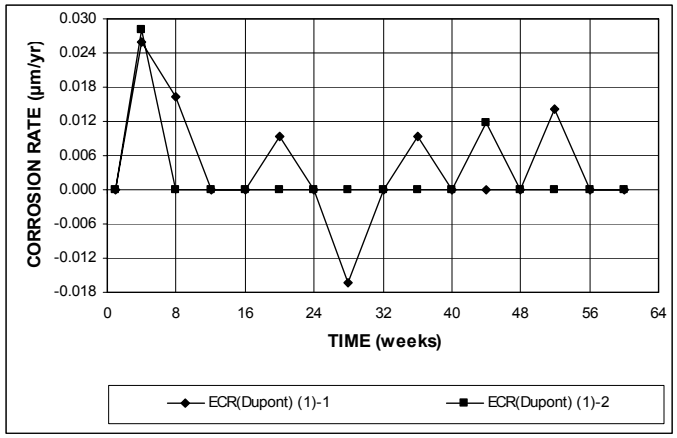

(a)

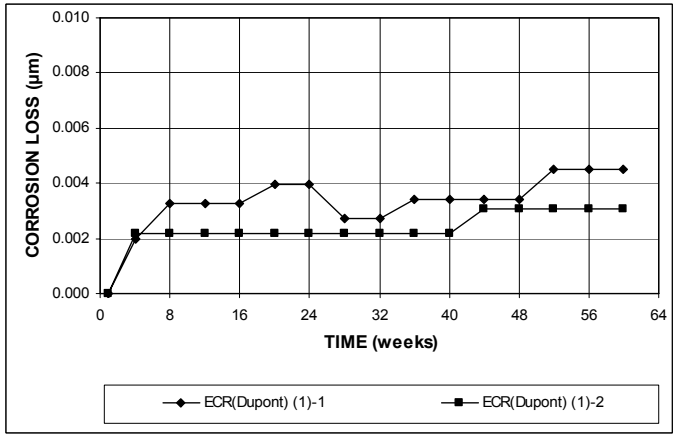

(b)

Figure A.229 – (a) Corrosion rates and (b) total corrosion losses base on total area of the bar as measured in the field test for specimens with ECR with DuPont coating (without cracks, No. 1).

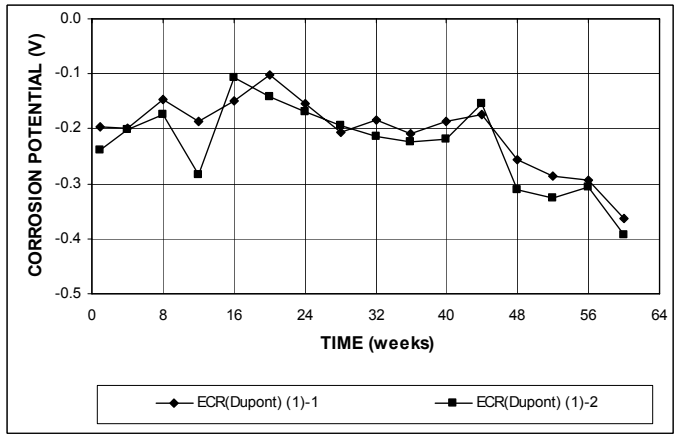

(a)

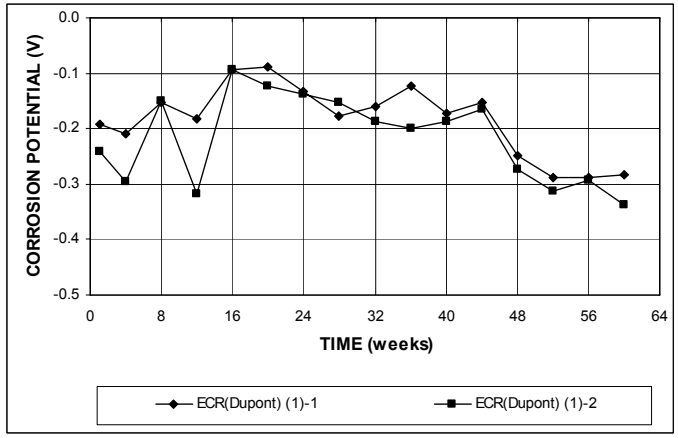

(b)

Figure A.230 – (a) Top mat corrosion potentials and (b) bottom mat corrosion potentials, with respect to copper-copper sulfate electrode as measured in the field test for specimens with ECR with DuPont coating (without cracks, No. 1).

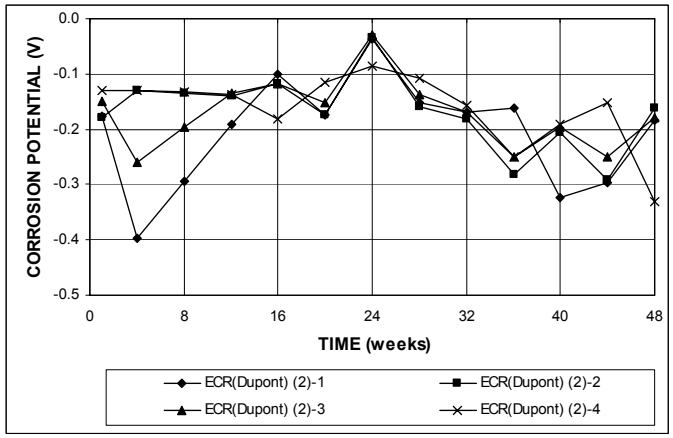

(a)

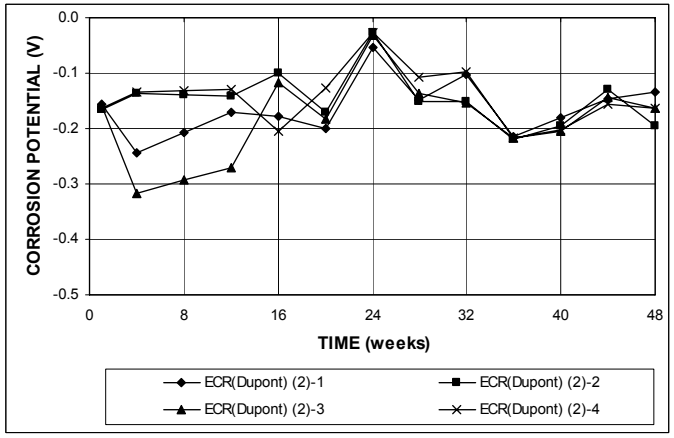

(b)

Figure A.231 – (a) Top mat corrosion potentials and (b) bottom mat corrosion potentials, with respect to copper-copper sulfate electrode as measured in the field test for specimens with ECR with DuPont coating (without cracks, No. 2).

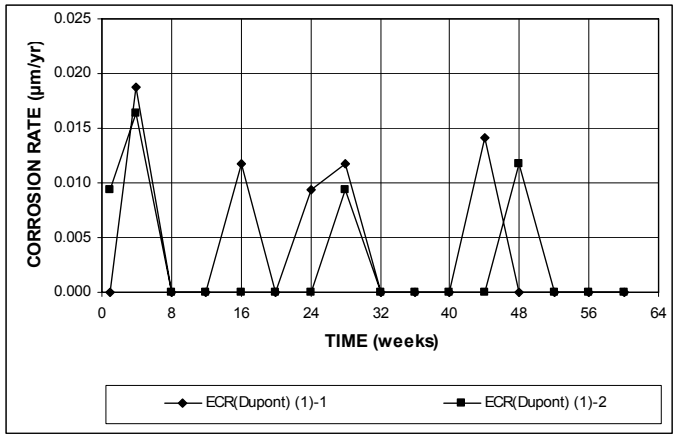

(a)

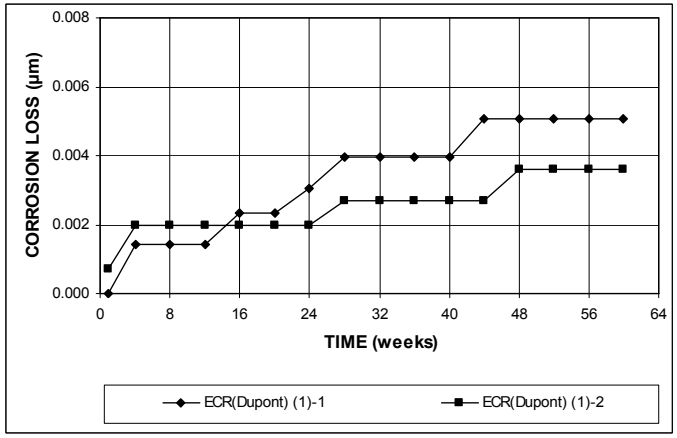

(b)

Figure A.232 – (a) Corrosion rates and (b) total corrosion losses base on total area of the bar as measured in the field test for specimens with ECR with DuPont coating (with cracks, No. 1).

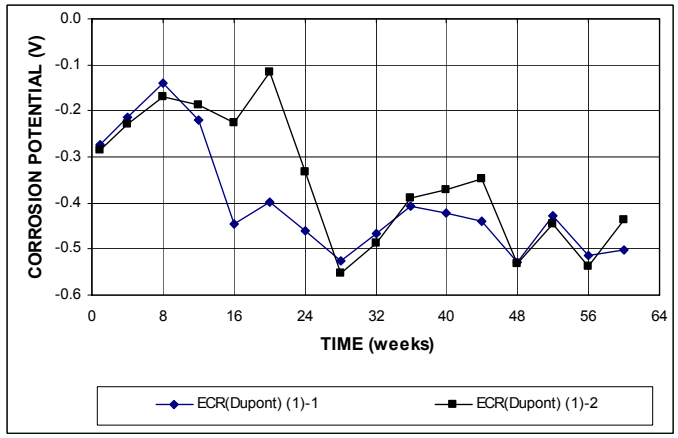

(a)

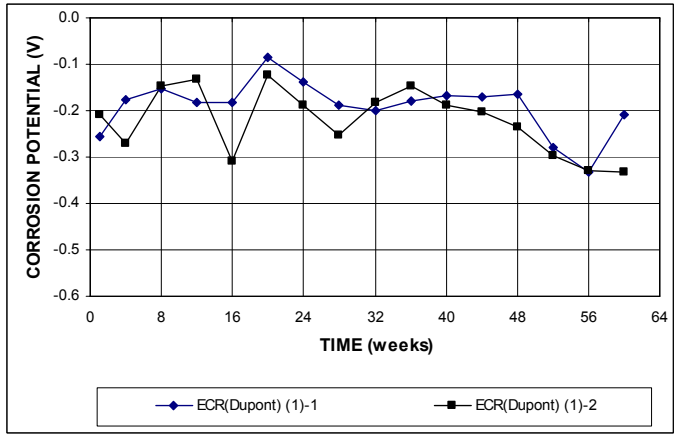

(b)

Figure A.233 – (a) Top mat corrosion potentials and (b) bottom mat corrosion potentials, with respect to copper-copper sulfate electrode as measured in the field test for specimens with ECR with DuPont coating (with cracks, No. 1).

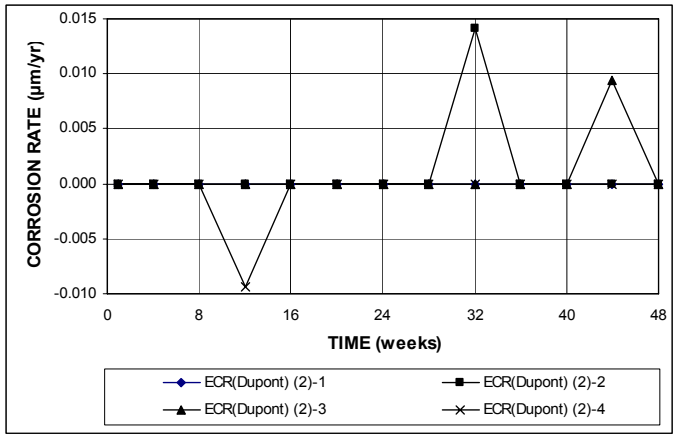

(a)

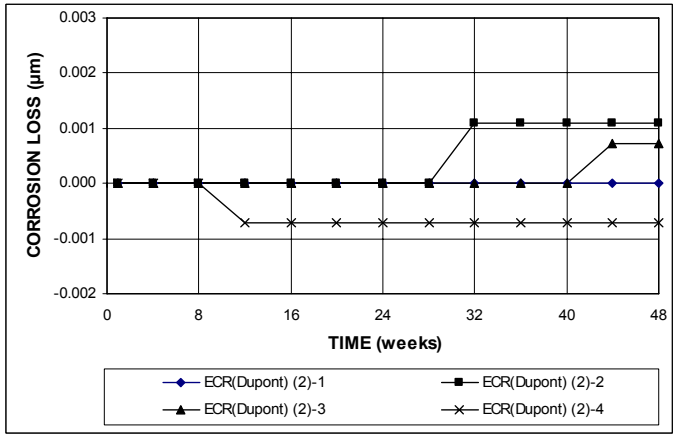

(b)

Figure A.234 – (a) Corrosion rates and (b) total corrosion losses base on total area of the bar as measured in the field test for specimens with ECR with DuPont coating (with cracks, No. 2).

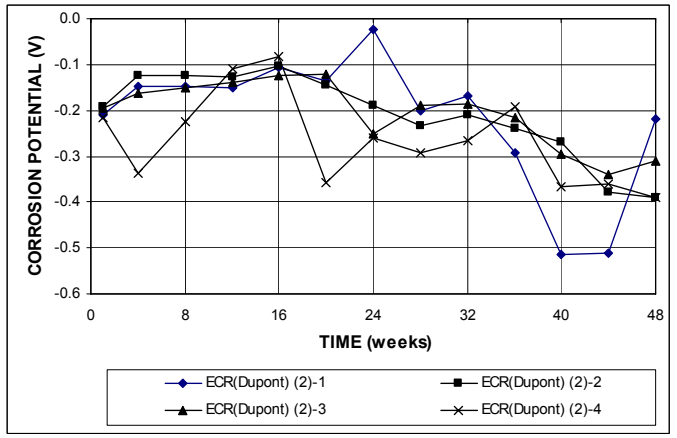

(a)

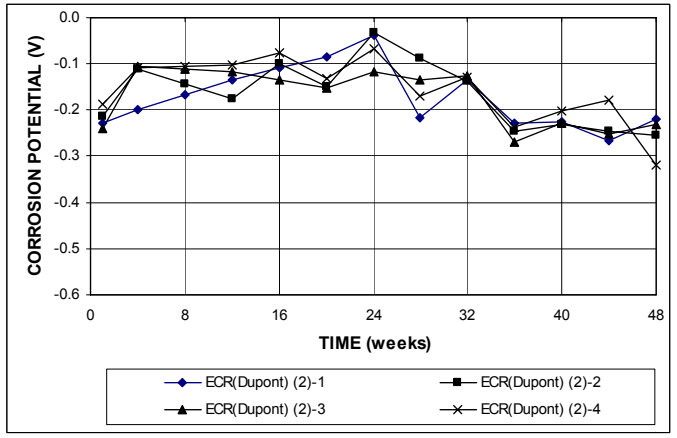

(b)

Figure A.235 – (a) Top mat corrosion potentials and (b) bottom mat corrosion potentials, with respect to copper-copper sulfate electrode as measured in the field test for specimens with ECR with DuPont coating (with cracks, No. 2).

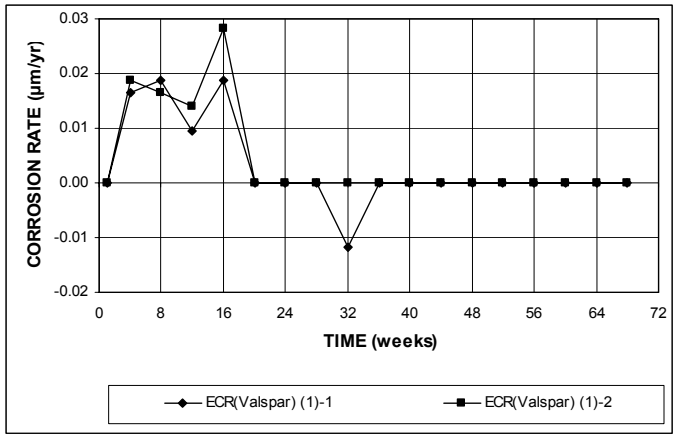

(a)

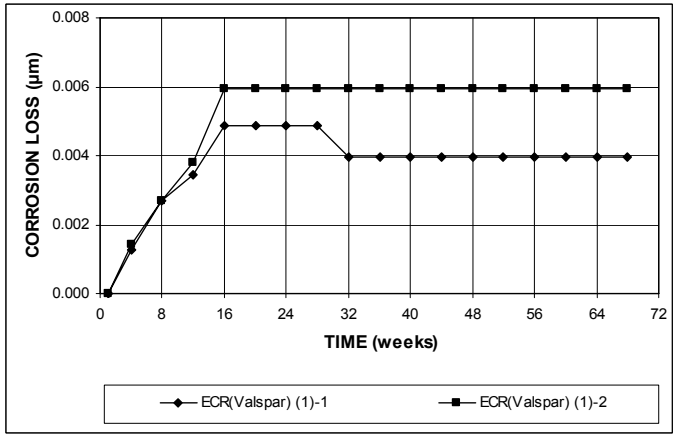

(b)

Figure A.236 – (a) Corrosion rates and (b) total corrosion losses base on total area of the bar as measured in the field test for specimens with ECR with Valspar coating (without cracks, No. 1).

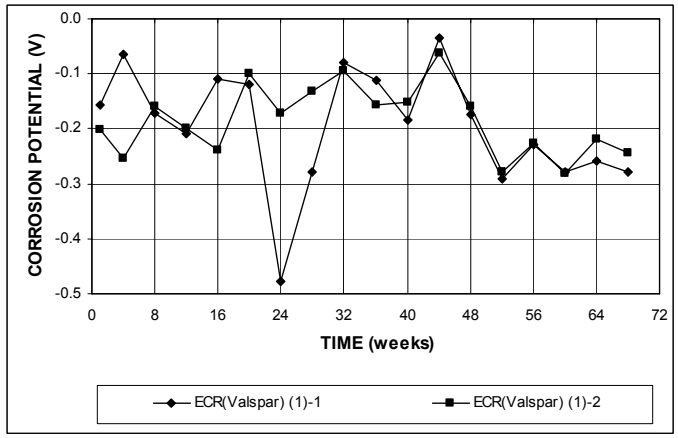

(a)

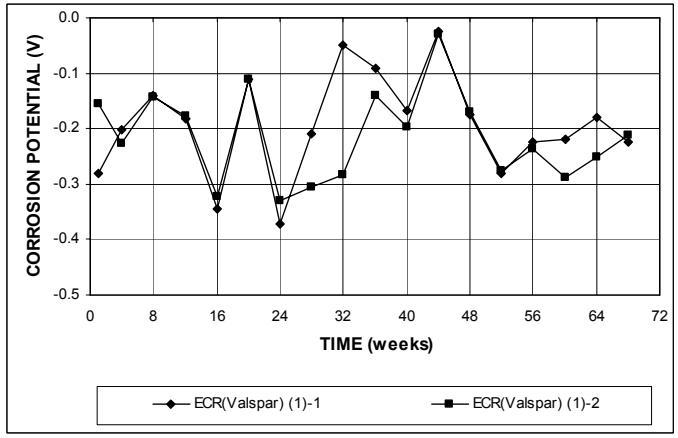

(b)

Figure A.237 – (a) Top mat corrosion potentials and (b) bottom mat corrosion potentials, with respect to copper-copper sulfate electrode as measured in the field test for specimens with ECR with Valspar coating (without cracks, No. 1).

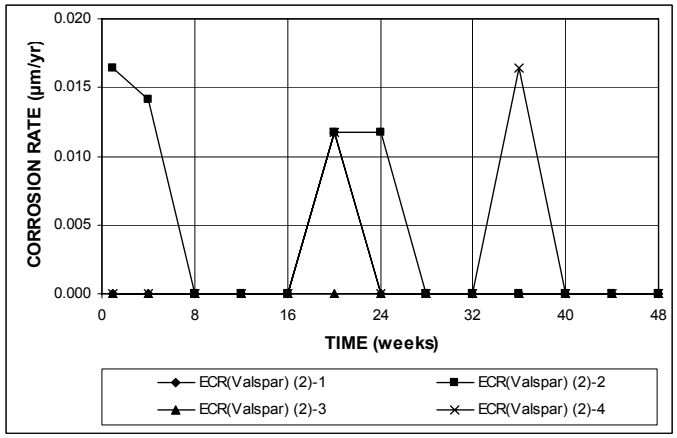

(a)

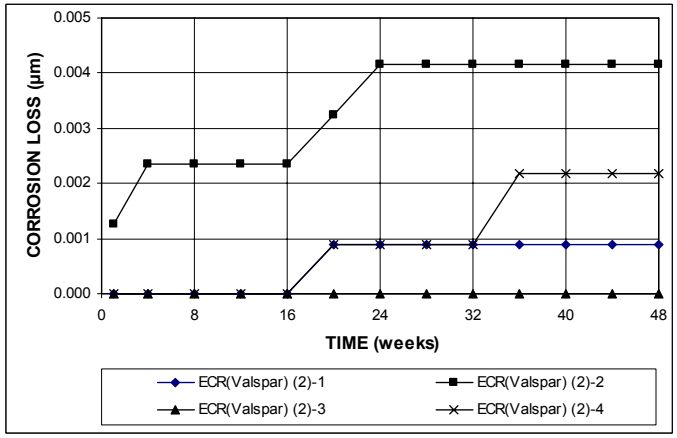

(b)

Figure A.238 – (a) Corrosion rates and (b) total corrosion losses base on total area of the bar as measured in the field test for specimens with ECR with Valspar coating (without cracks, No. 2).

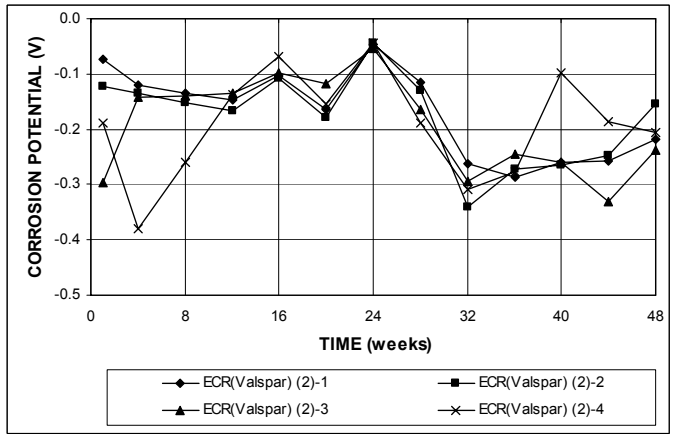

(a)

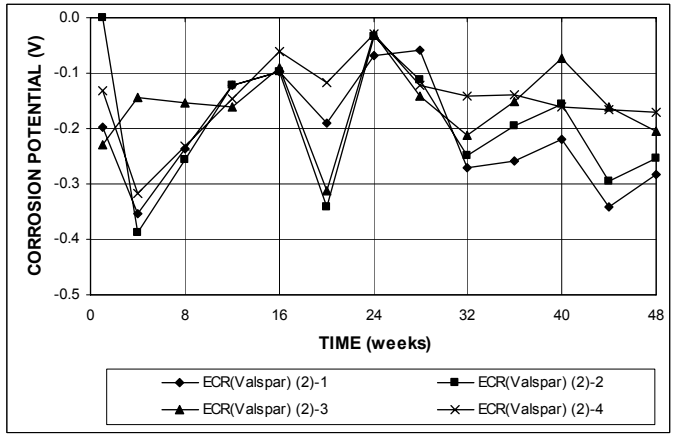

(b)

Figure A.239 – (a) Top mat corrosion potentials and (b) bottom mat corrosion potentials, with respect to copper-copper sulfate electrode as measured in the field test for specimens with ECR with Valspar coating (without cracks, No. 2).

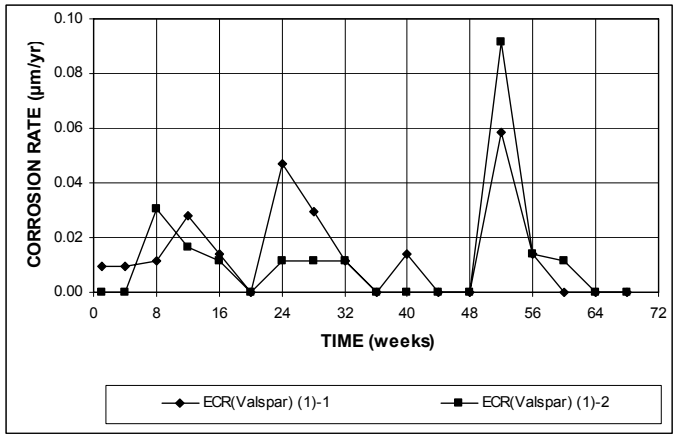

(a)

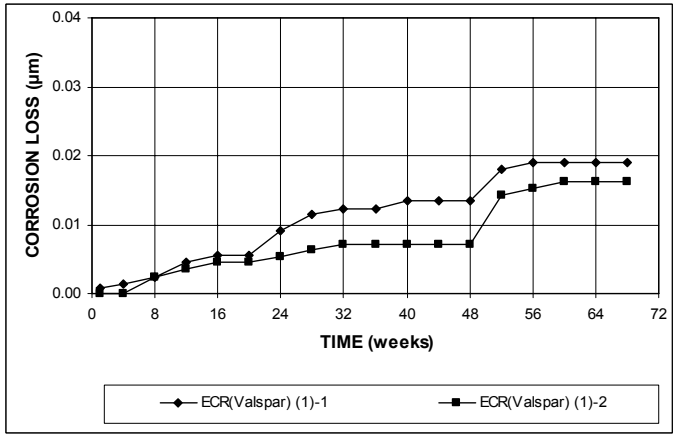

(b)

Figure A.240 – (a) Corrosion rates and (b) total corrosion losses base on total area of the bar as measured in the field test for specimens with ECR with Valspar coating (with cracks, No. 1).

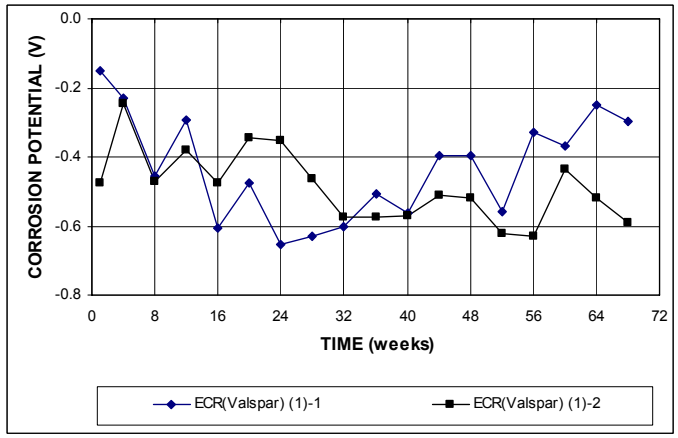

(a)

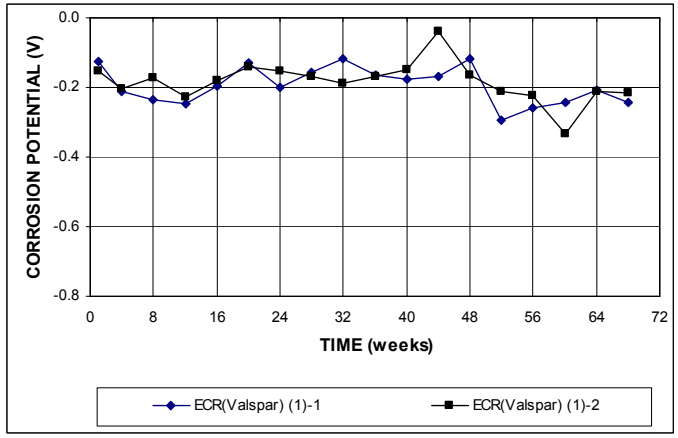

(b)

Figure A.241 – (a) Top mat corrosion potentials and (b) bottom mat corrosion potentials, with respect to copper-copper sulfate electrode as measured in the field test for specimens with ECR with Valspar coating (with cracks, No. 1).

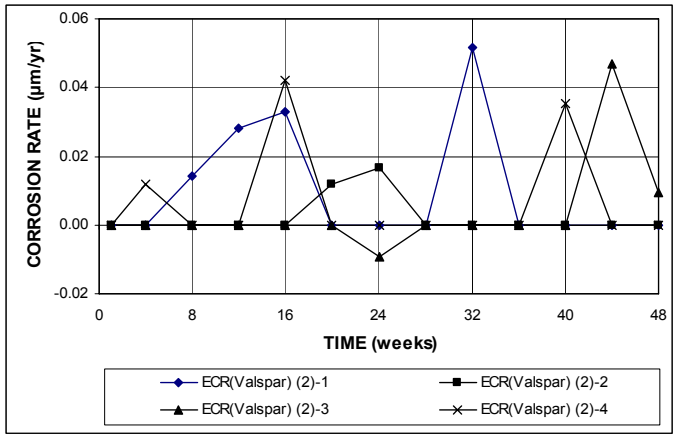

(a)

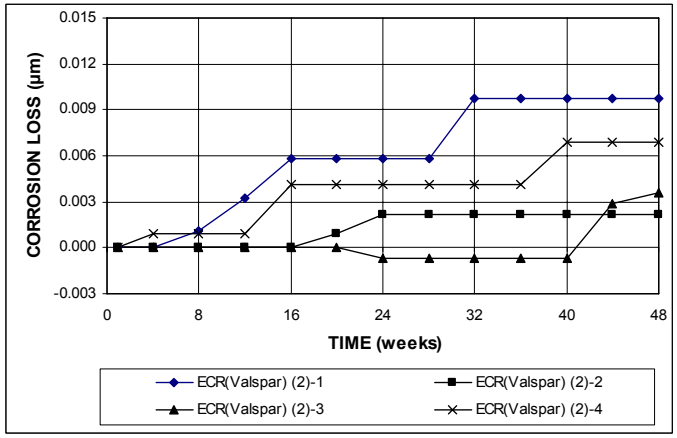

(b)

Figure A.242 – (a) Corrosion rates and (b) total corrosion losses base on total area of the bar as measured in the field test for specimens with ECR with Valspar coating (with cracks, No. 2).

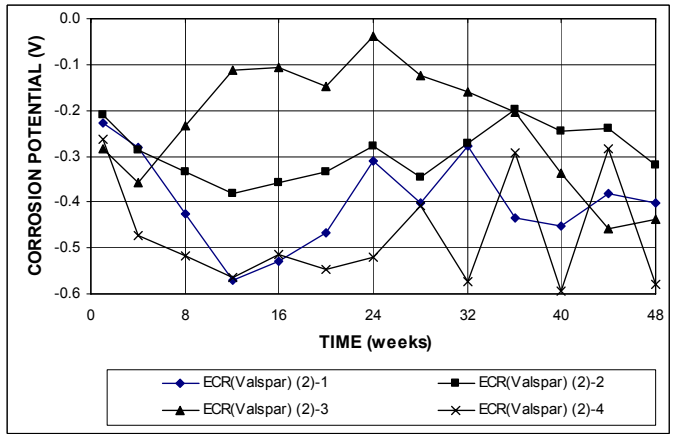

(a)

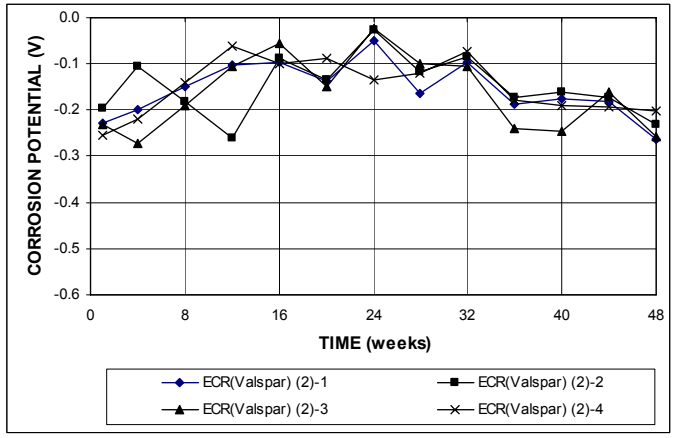

(b)

Figure A.243 – (a) Top mat corrosion potentials and (b) bottom mat corrosion potentials, with respect to copper-copper sulfate electrode as measured in the field test for specimens with ECR with Valspar coating (with cracks, No. 2).

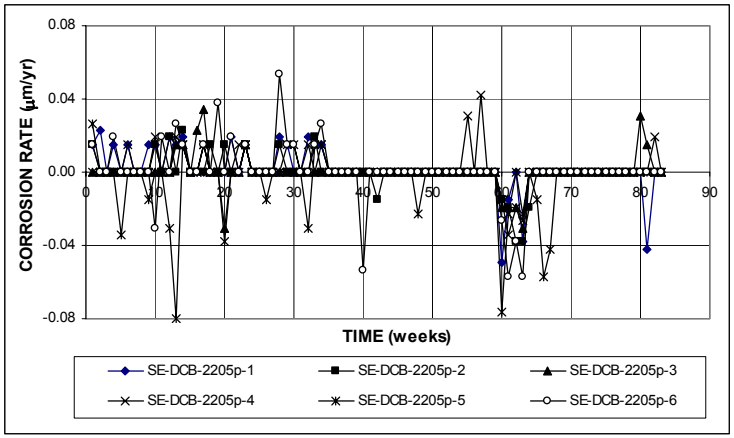

(a)

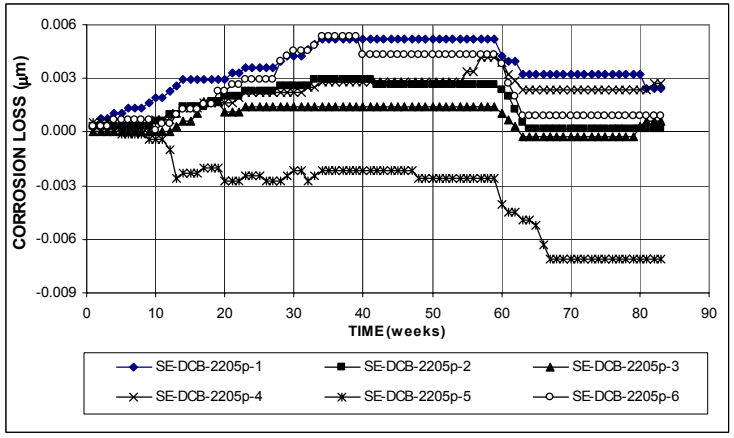

(b)

Figure A.244 – (a) Corrosion rates and (b) total corrosion losses as measured in the Southern Exposure test for specimens with 2205p stainless steel for Doniphan County Bridge.

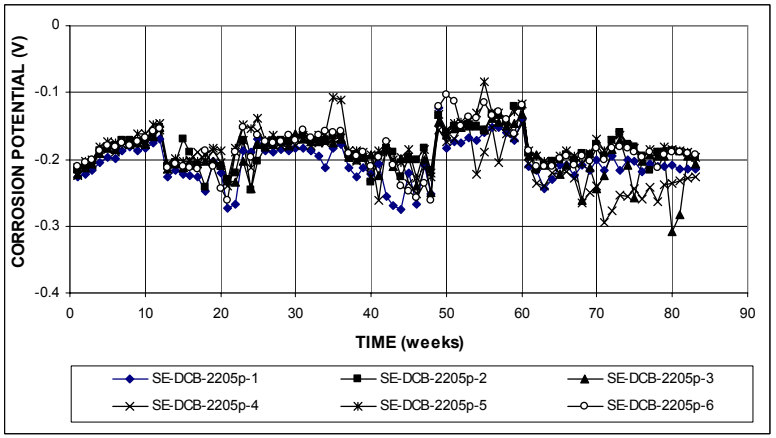

(a)

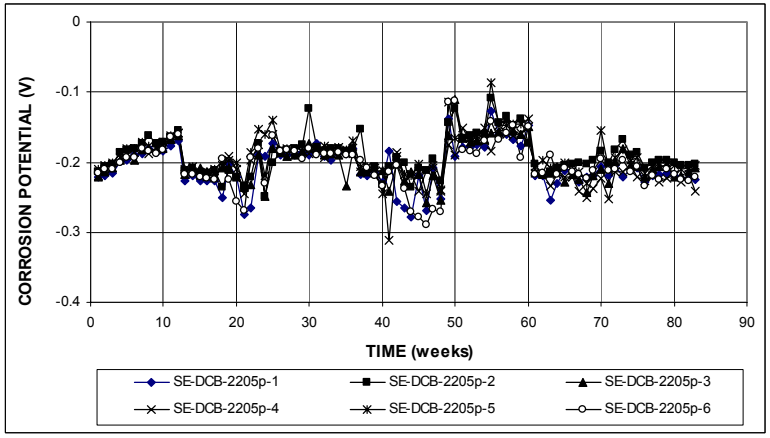

(b)

Figure A.245 – (a) Top mat corrosion potentials and (b) bottom mat corrosion potentials, with respect to copper-copper sulfate electrode as measured in the Southern Exposure test for specimens with 2205p stainless steel for Doniphan County Bridge.

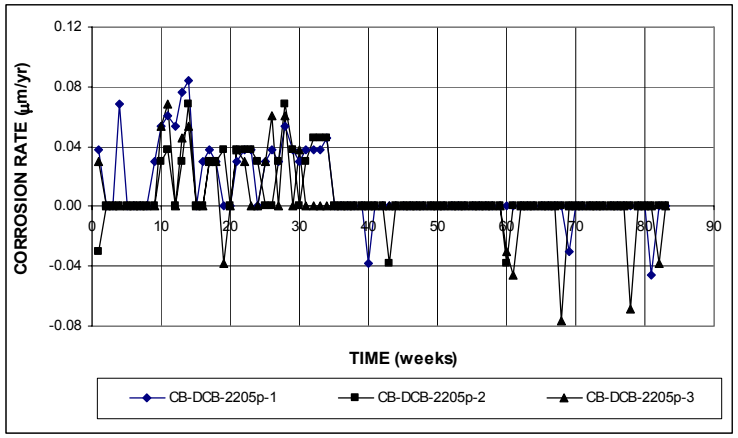

(a)

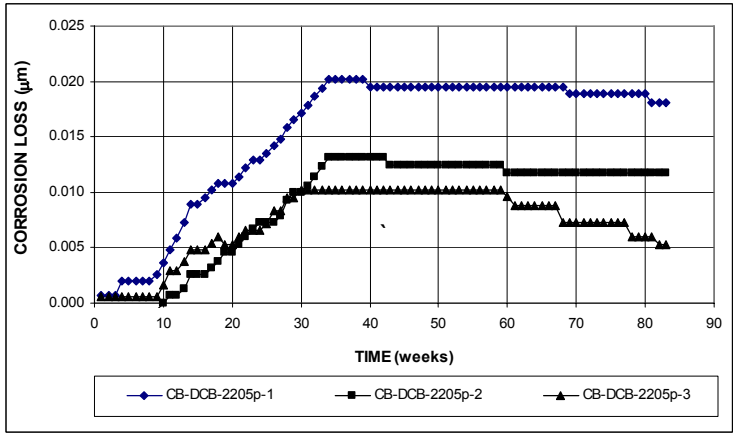

(b)

Figure A.246 – (a) Corrosion rates and (b) total corrosion losses as measured in the cracked beam test for specimens with 2205p stainless steel for Doniphan County Bridge.

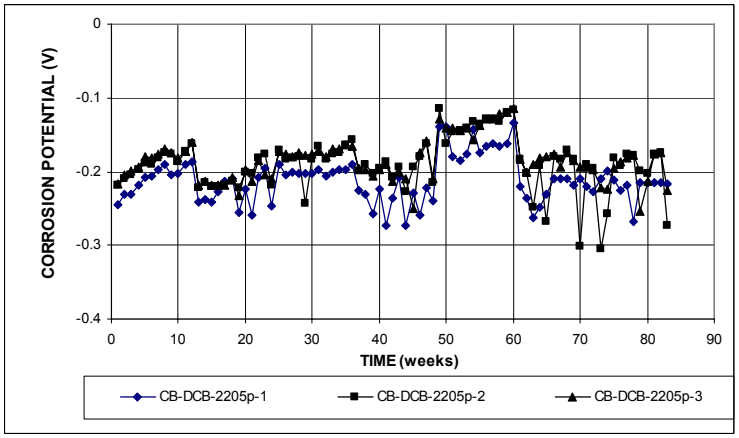

(a)

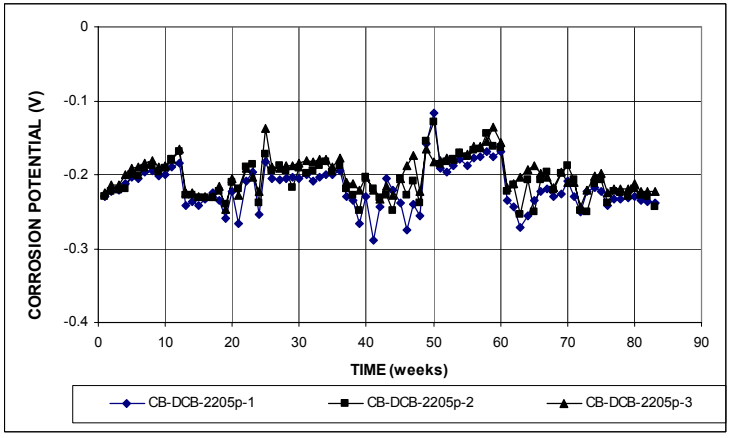

(b)

Figure A.247 – (a) Top mat corrosion potentials and (b) bottom mat corrosion potentials, with respect to copper-copper sulfate electrode as measured in the cracked beam test for specimens with 2205p stainless steel for Doniphan County Bridge.

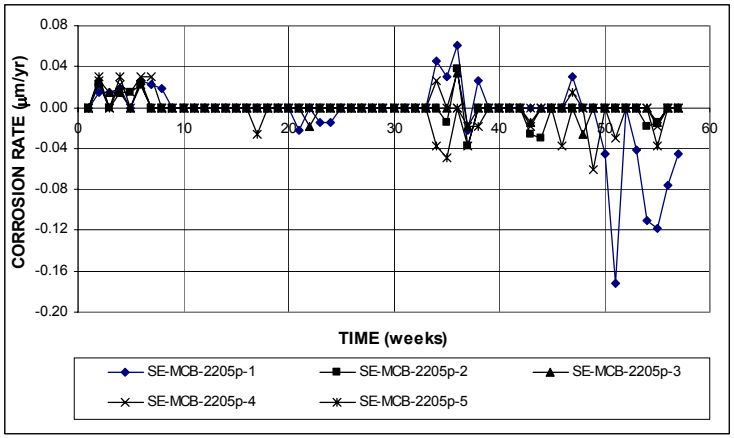

(a)

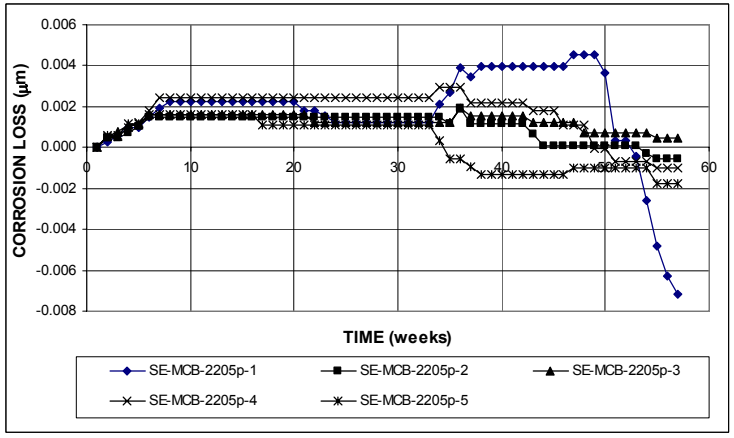

(b)

Figure A.248 – (a) Corrosion rates and (b) total corrosion losses as measured in the Southern Exposure test for specimens with 2205p stainless steel for Mission Creek Bridge.

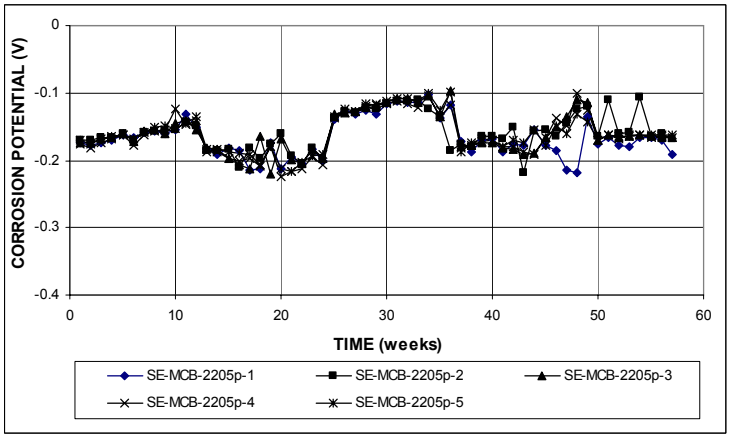

(a)

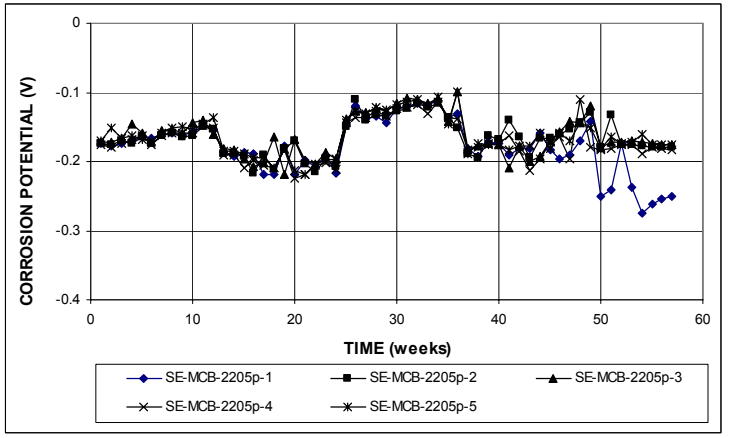

(b)

Figure A.249 – (a) Top mat corrosion potentials and (b) bottom mat corrosion potentials, with respect to copper-copper sulfate electrode as measured in the Southern Exposure test for specimens with 2205p stainless steel for Mission Creek Bridge.

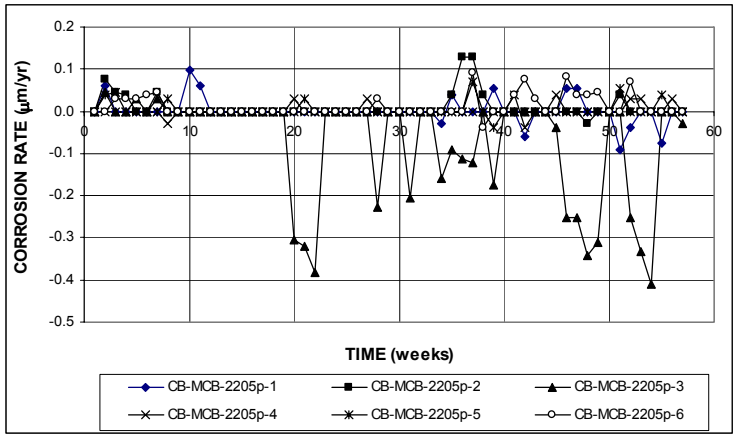

(a)

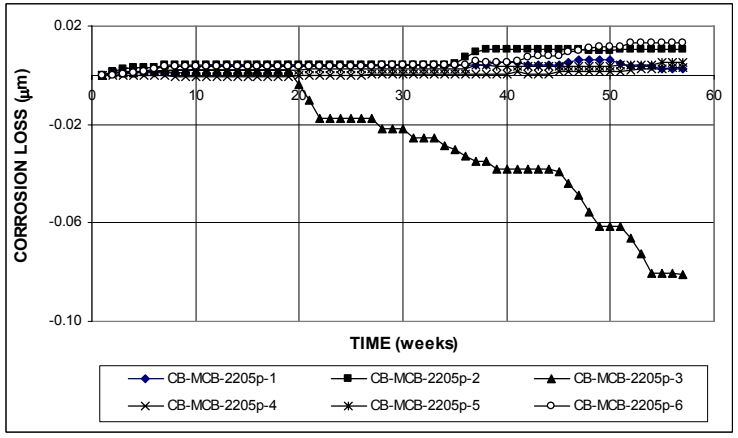

(b)

Figure A.250 – (a) Corrosion rates and (b) total corrosion losses as measured in the cracked beam test for specimens with 2205p stainless steel for Mission Creek Bridge.

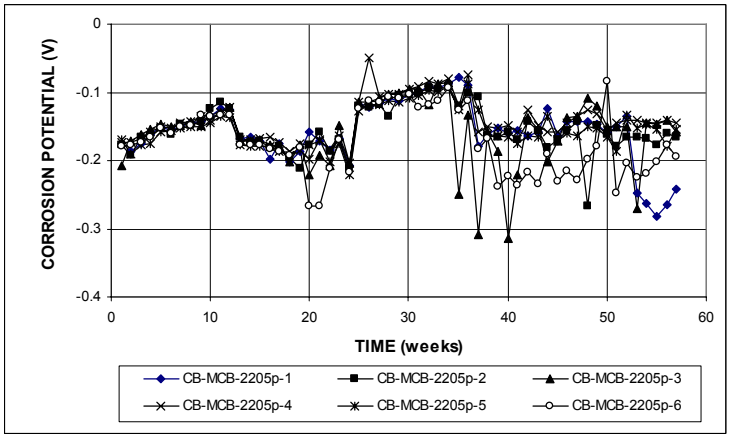

(a)

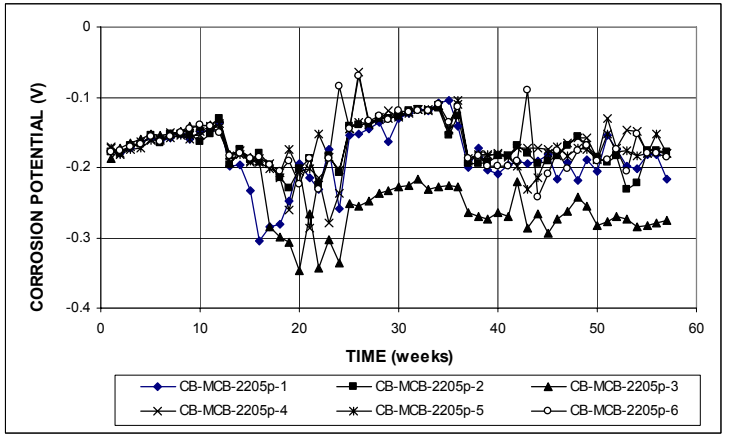

(b)

Figure A.251 – (a) Top mat corrosion potentials and (b) bottom mat corrosion potentials, with respect to copper-copper sulfate electrode as measured in the cracked beam test for specimens with 2205p stainless steel for Mission Creek Bridge.

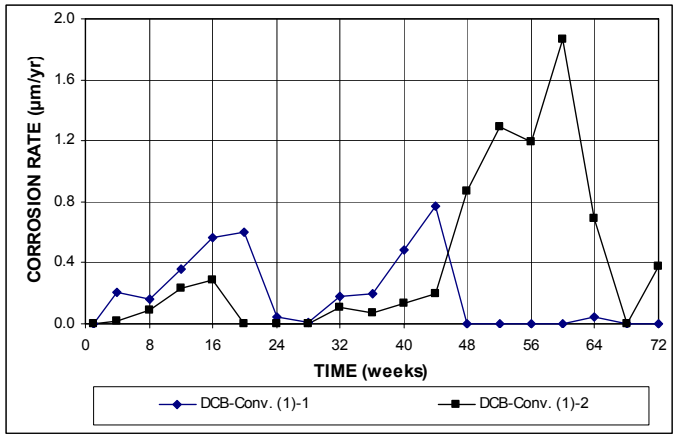

(a)

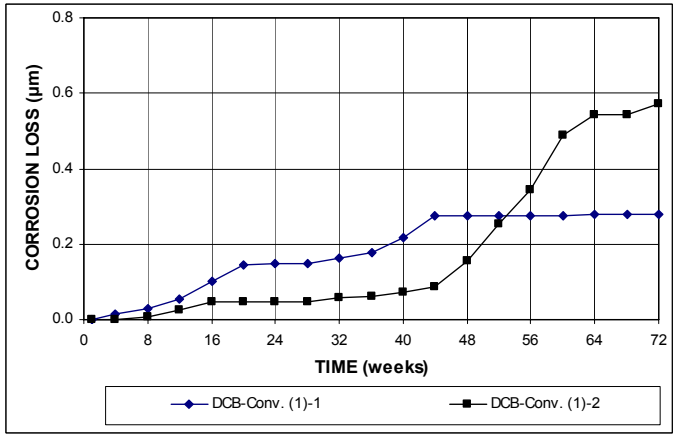

(b)

Figure A.252 – (a) Corrosion rates and (b) total corrosion losses as measured in the field test for specimens with conventional steel (No. 1) for Doniphan County Bridge.

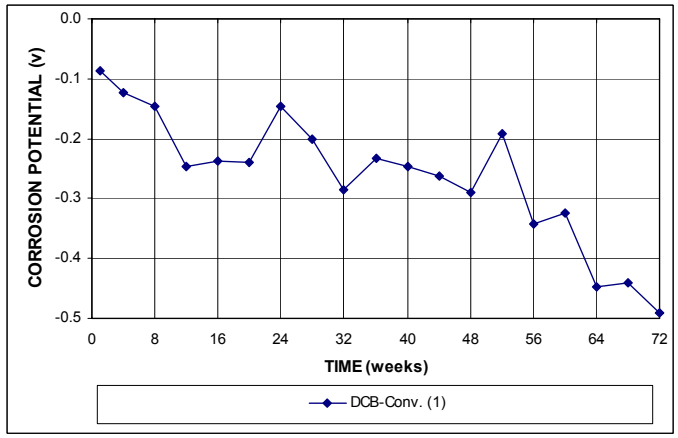

(a)

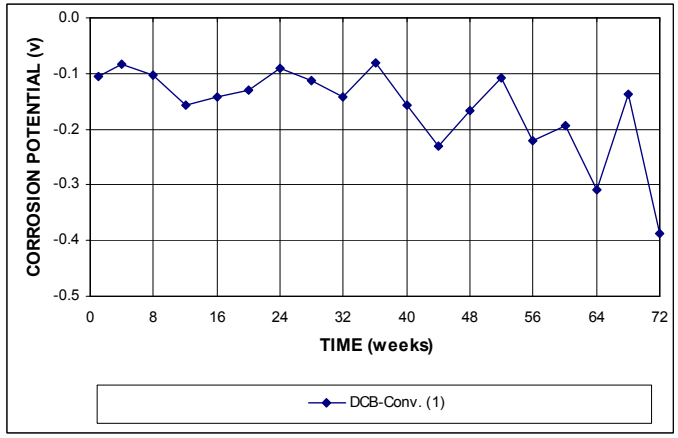

(b)

Figure A.253 – (a) Top mat corrosion potentials and (b) bottom mat corrosion potentials, with respect to copper-copper sulfate electrode as measured in the field test for specimens with conventional steel (No. 1) for Doniphan County Bridge

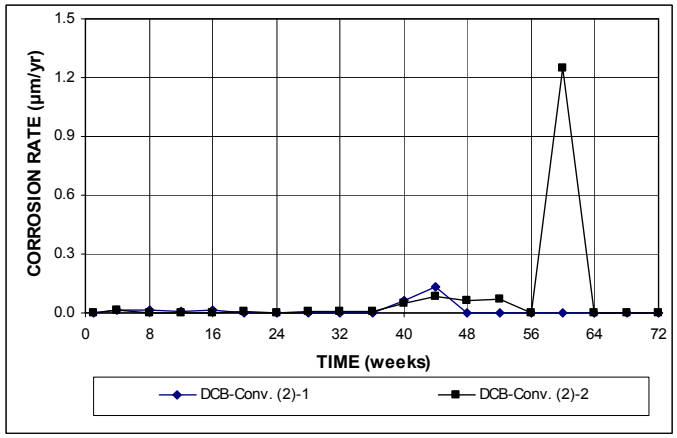

(a)

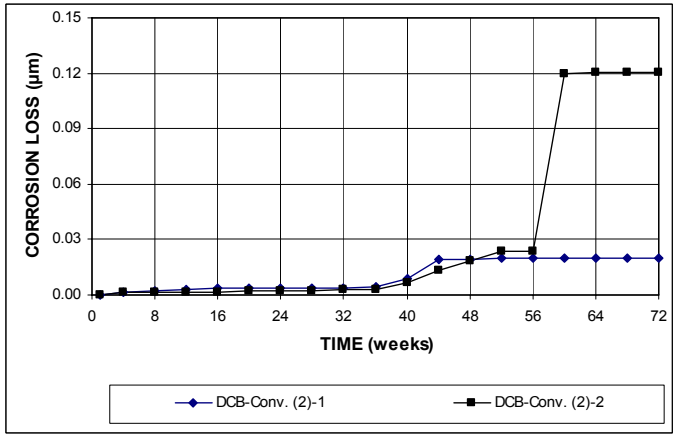

(b)

Figure A.254 – (a) Corrosion rates and (b) total corrosion losses as measured in the field test for specimens with conventional steel (No. 2) for Doniphan County Bridge.

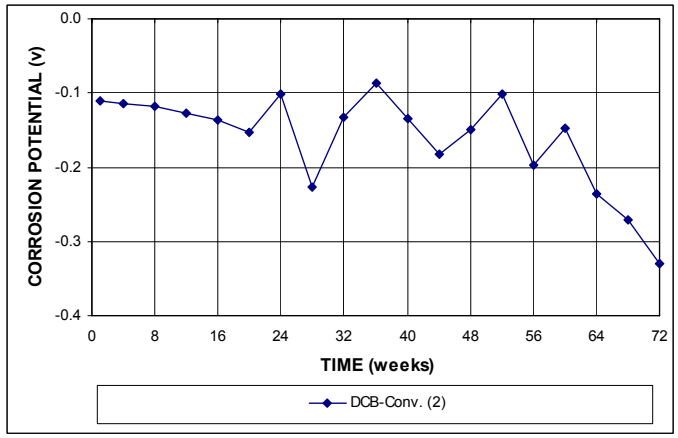

(a)

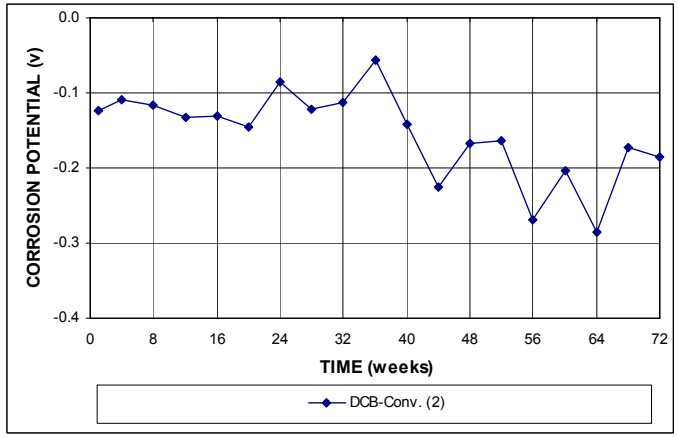

(b)

Figure A.255 – (a) Top mat corrosion potentials and (b) bottom mat corrosion potentials, with respect to copper-copper sulfate electrode as measured in the field test for specimens with conventional steel (No. 2) for Doniphan County Bridge

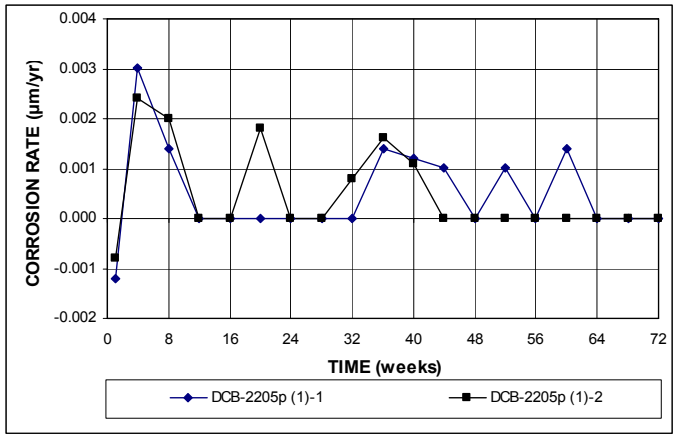

(a)

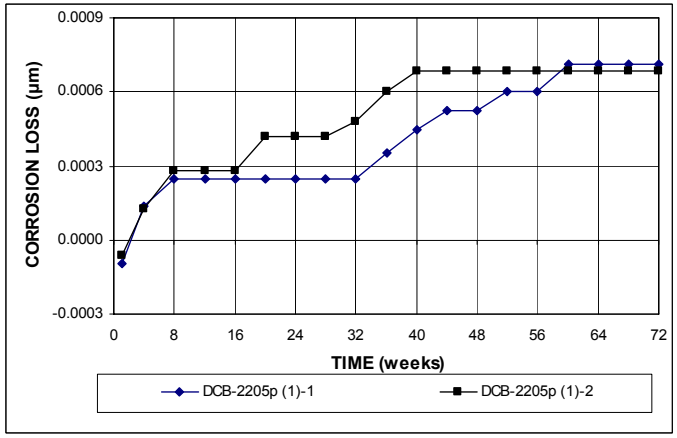

(b)

Figure A.256 – (a) Corrosion rates and (b) total corrosion losses as measured in the field test for specimens with 2205p stainless steel (No. 1) for Doniphan County Bridge.

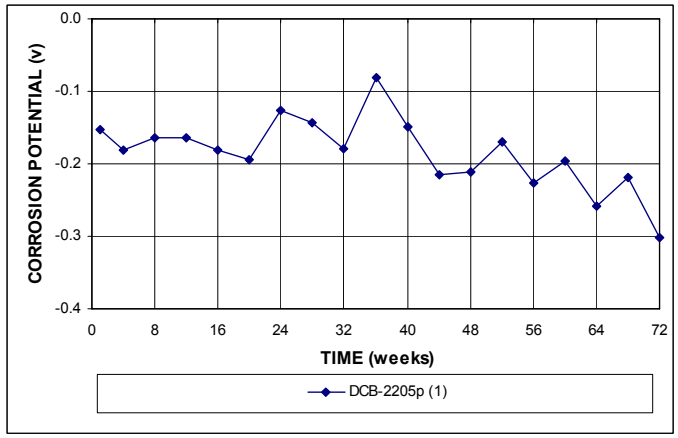

(a)

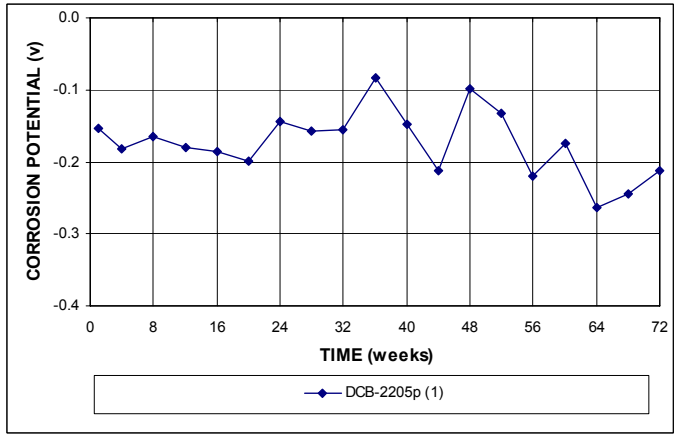

(b)

Figure A.257 – (a) Top mat corrosion potentials and (b) bottom mat corrosion potentials, with respect to copper-copper sulfate electrode as measured in the field test for specimens with 2205p stainless steel (No. 1) for Doniphan County Bridge

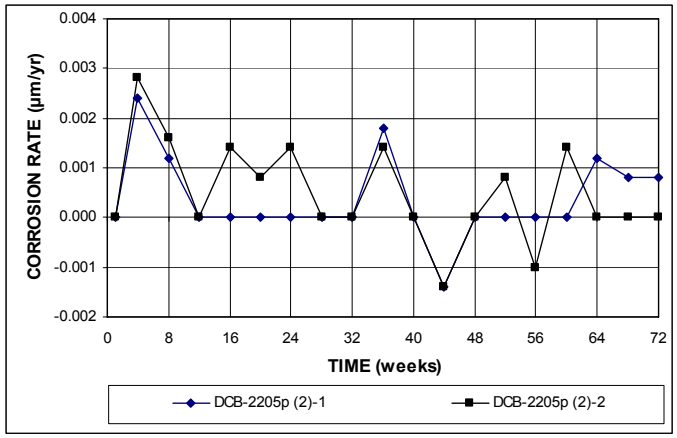

(a)

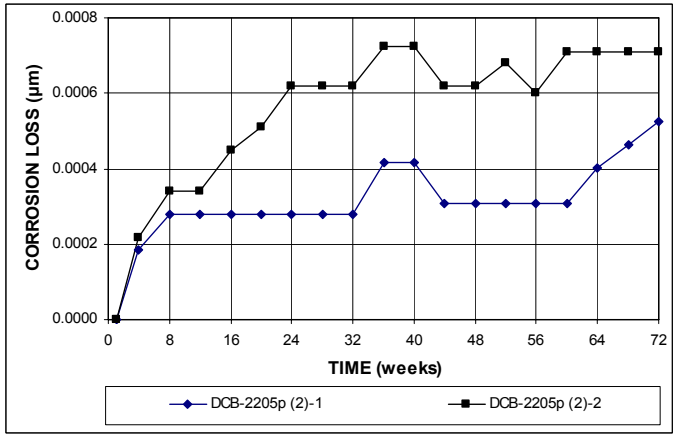

(b)

Figure A.258 – (a) Corrosion rates and (b) total corrosion losses as measured in the field test for specimens with 2205p stainless steel (No. 2) for Doniphan County Bridge.

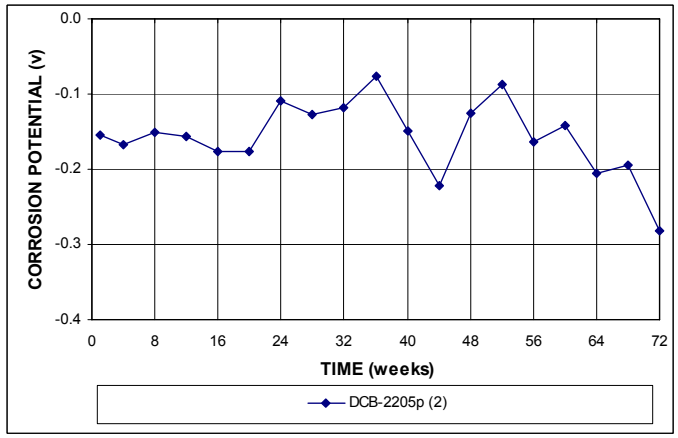

(a)

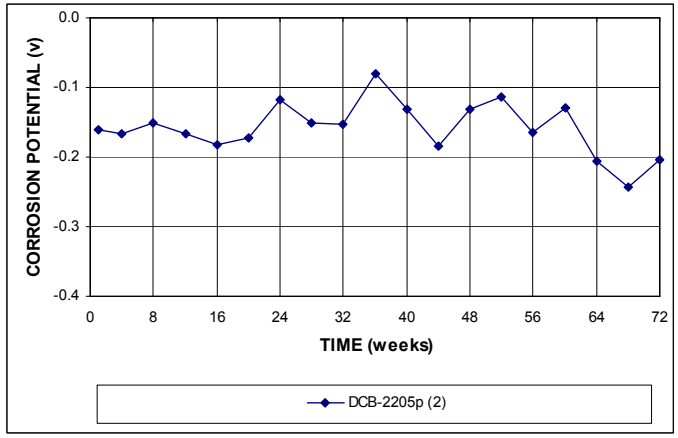

(b)

Figure A.259 – (a) Top mat corrosion potentials and (b) bottom mat corrosion potentials, with respect to copper-copper sulfate electrode as measured in the field test for specimens with 2205p stainless steel (No. 2) for Doniphan County Bridge

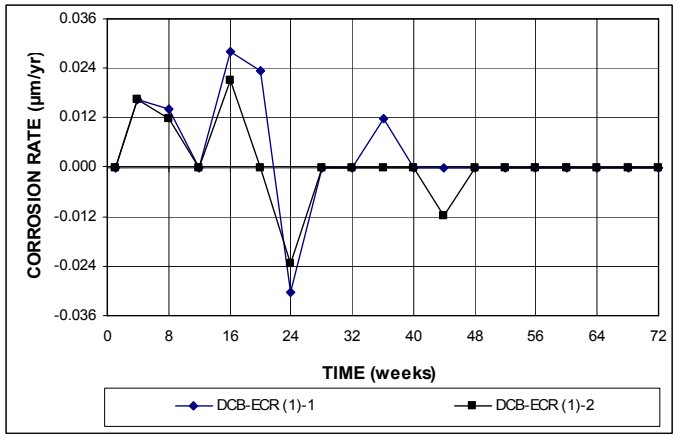

(a)

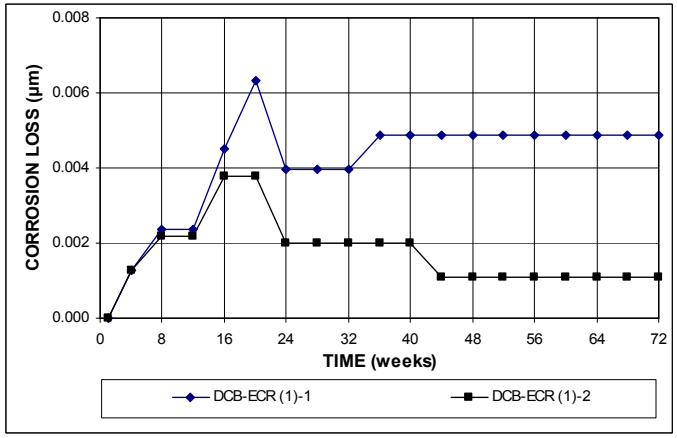

(b)

Figure A.260 – (a) Corrosion rates and (b) total corrosion losses as measured in the field test for specimens with ECR (No. 1) for Doniphan County Bridge.

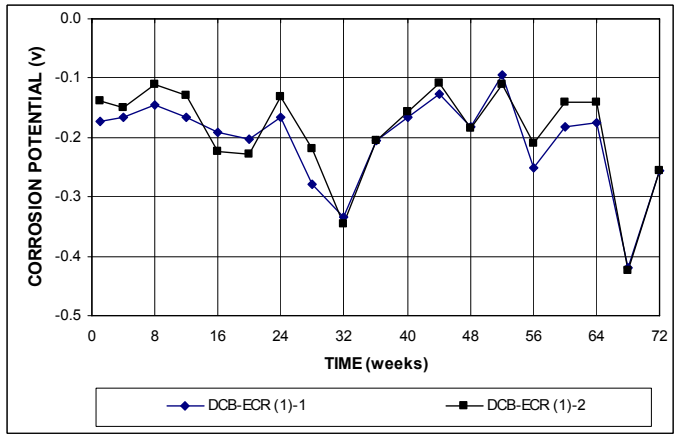

(a)

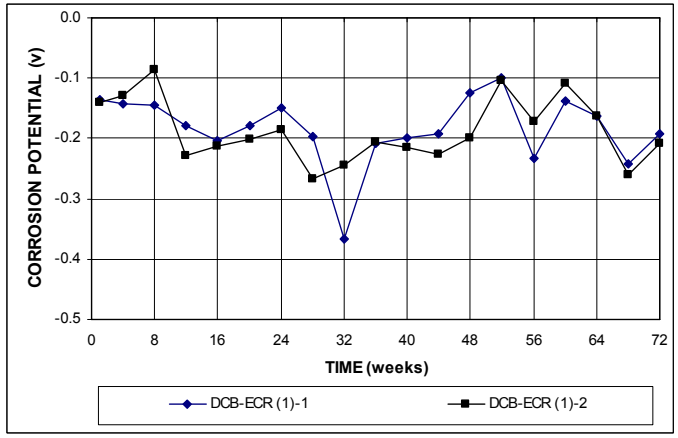

(b)

Figure A.261 – (a) Top mat corrosion potentials and (b) bottom mat corrosion potentials, with respect to copper-copper sulfate electrode as measured in the field test for specimens with ECR (No. 1) for Doniphan County Bridge

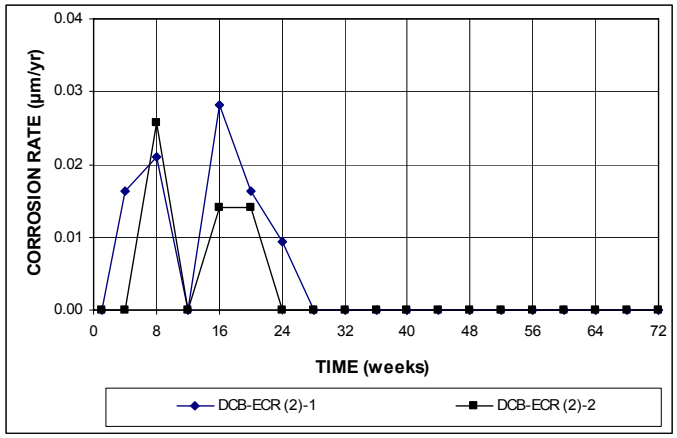

(a)

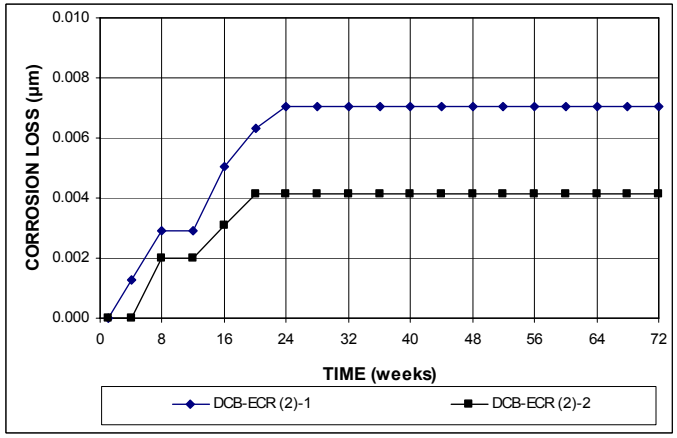

(b)

Figure A.262 – (a) Corrosion rates and (b) total corrosion losses as measured in the field test for specimens with ECR (No. 2) for Doniphan County Bridge.

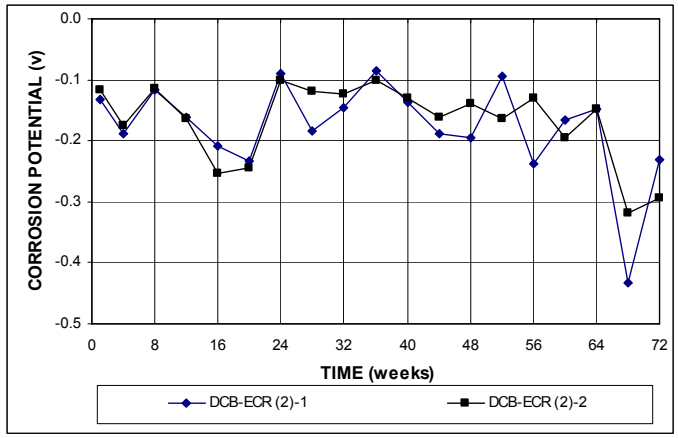

(a)

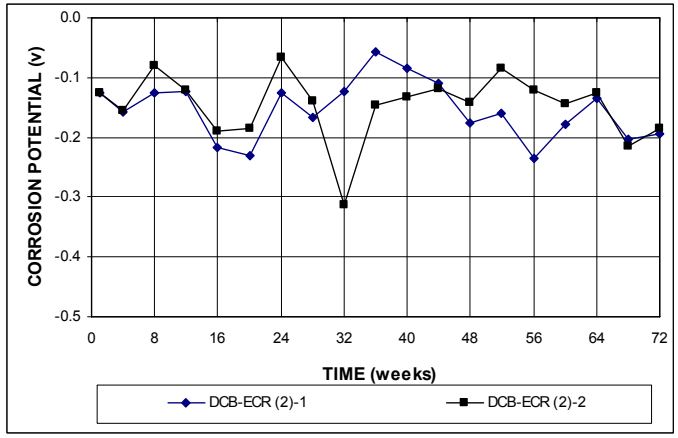

(b)

Figure A.263 – (a) Top mat corrosion potentials and (b) bottom mat corrosion potentials, with respect to copper-copper sulfate electrode as measured in the field test for specimens with ECR (No. 2) for Doniphan County Bridge

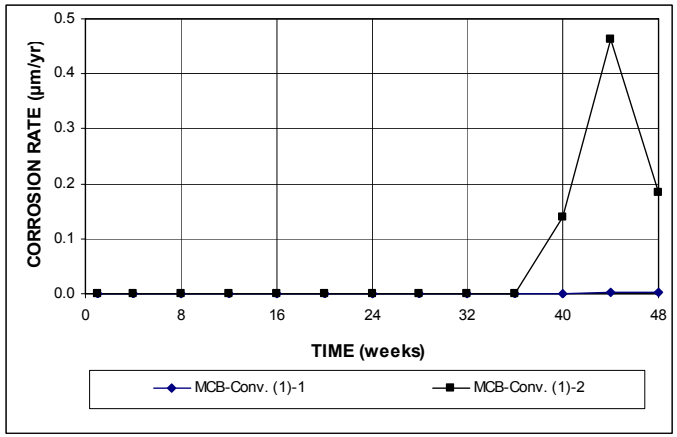

(a)

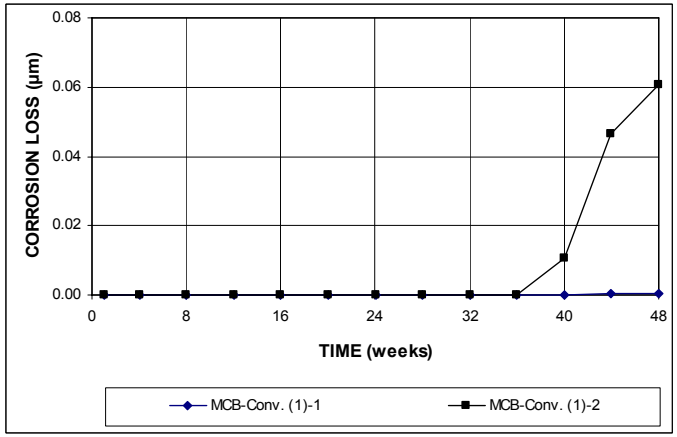

(b)

Figure A.264 – (a) Corrosion rates and (b) total corrosion losses as measured in the field test for specimens with conventional steel without cracks (No. 1) for Mission Creek Bridge.

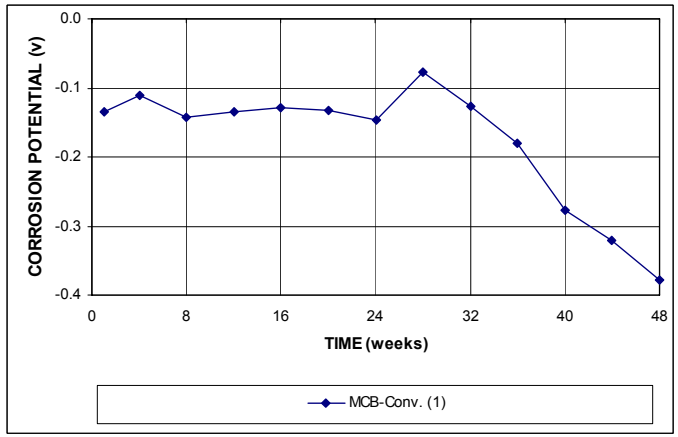

(a)

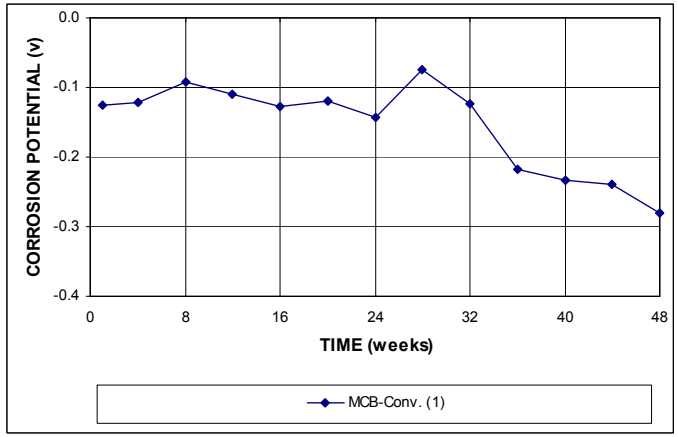

(b)

Figure A.265 – (a) Top mat corrosion potentials and (b) bottom mat corrosion potentials, with respect to copper-copper sulfate electrode as measured in the field test for specimens with conventional steel without cracks (No. 1) for Mission Creek Bridge

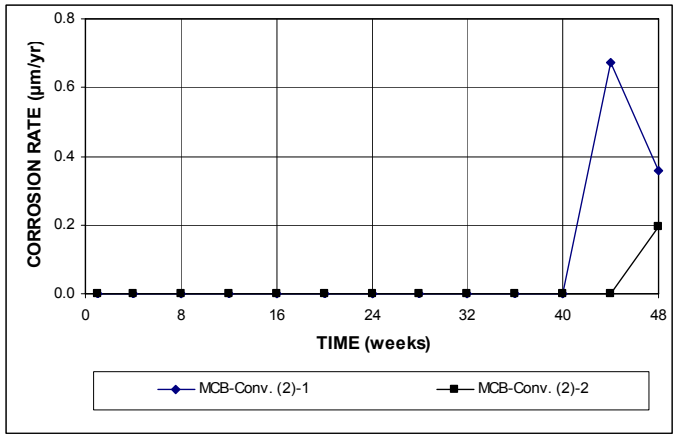

(a)

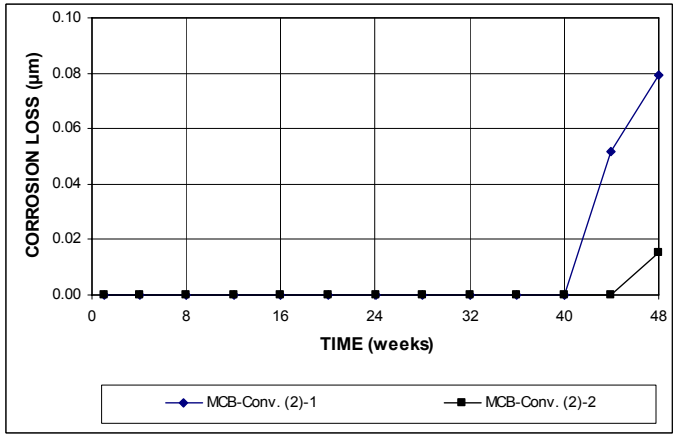

(b)

Figure A.266 – (a) Corrosion rates and (b) total corrosion losses as measured in the field test for specimens with conventional steel with cracks (No. 2) for Mission Creek Bridge.

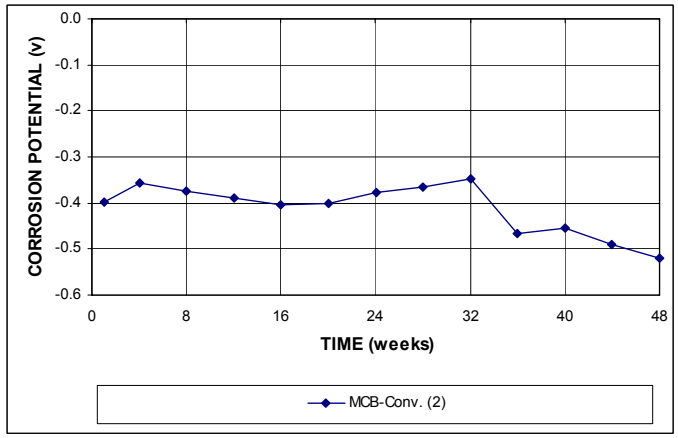

(a)

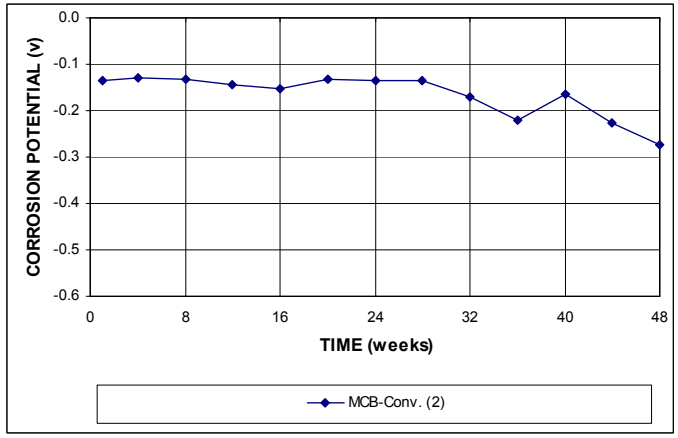

(b)

Figure A.267 – (a) Top mat corrosion potentials and (b) bottom mat corrosion potentials, with respect to copper-copper sulfate electrode as measured in the field test for specimens with conventional steel with cracks (No. 2) for Mission Creek Bridge

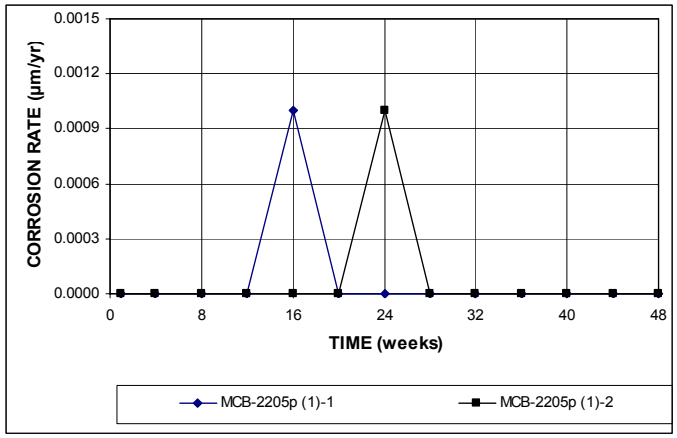

(a)

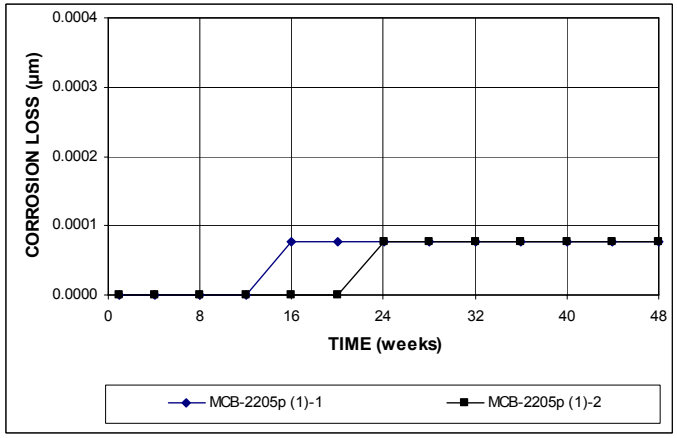

(b)

Figure A.268 – (a) Corrosion rates and (b) total corrosion losses as measured in the field test for specimens with 2205p stainless steel without cracks (No. 1) for Mission Creek Bridge.

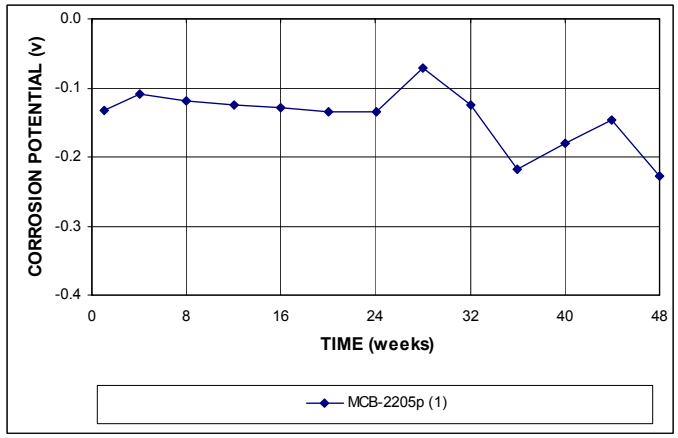

(a)

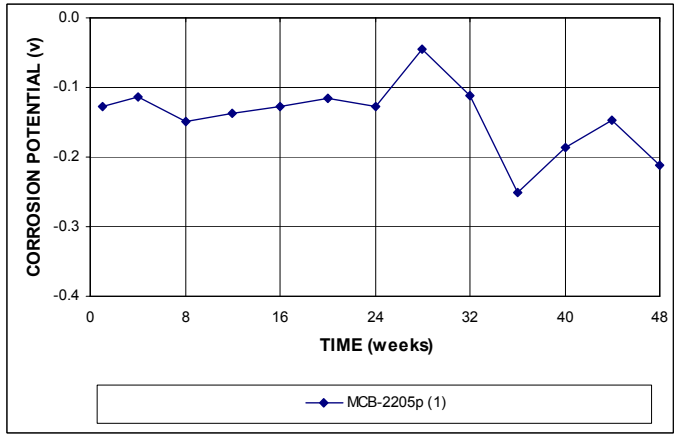

(b)

Figure A.269 – (a) Top mat corrosion potentials and (b) bottom mat corrosion potentials, with respect to copper-copper sulfate electrode as measured in the field test for specimens with 2205p stainless steel without cracks (No. 1) for Mission Creek Bridge

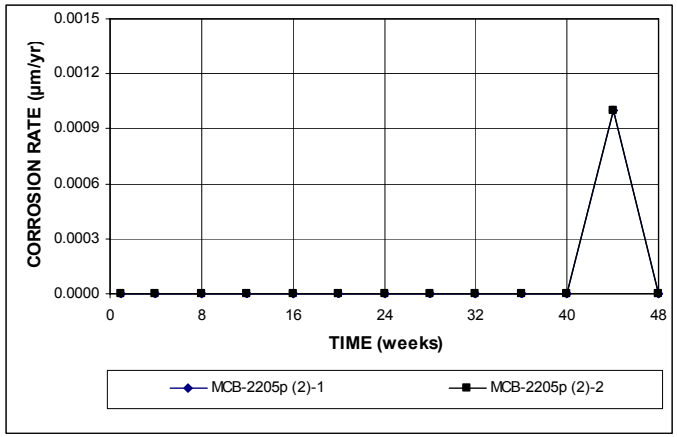

(a)

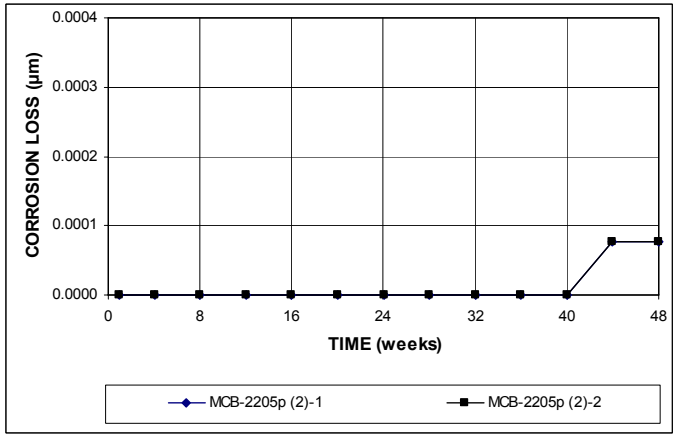

(b)

Figure A.270 – (a) Corrosion rates and (b) total corrosion losses as measured in the field test for specimens with 2205p stainless steel with cracks (No. 2) for Mission Creek Bridge.

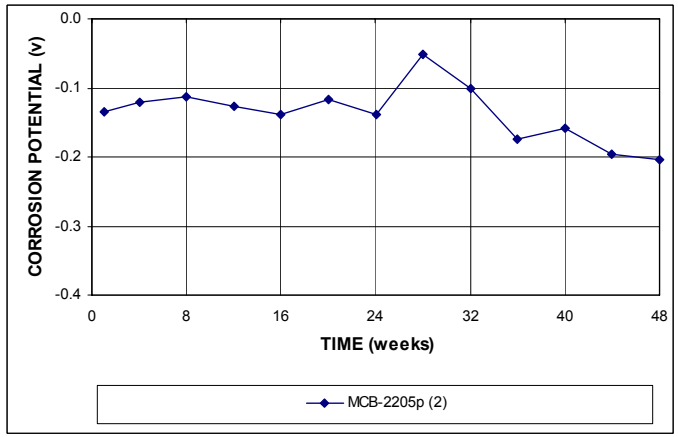

(a)

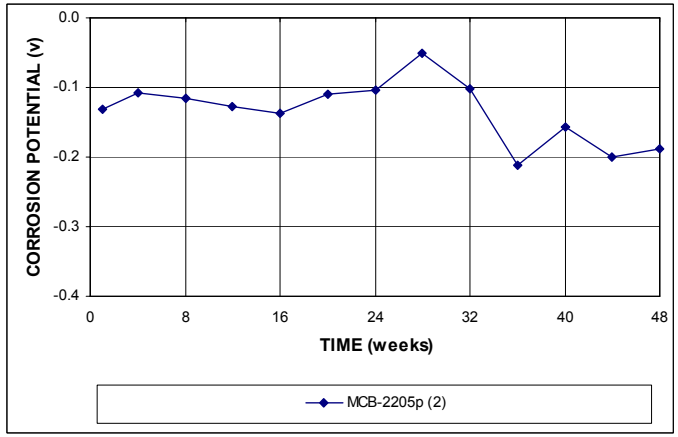

(b)

Figure A.271 – (a) Top mat corrosion potentials and (b) bottom mat corrosion potentials, with respect to copper-copper sulfate electrode as measured in the field test for specimens with 2205p stainless steel with cracks (No. 2) for Mission Creek Bridge

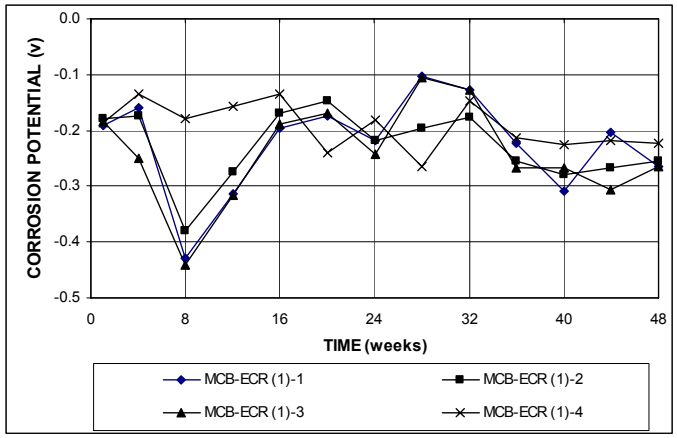

(a)

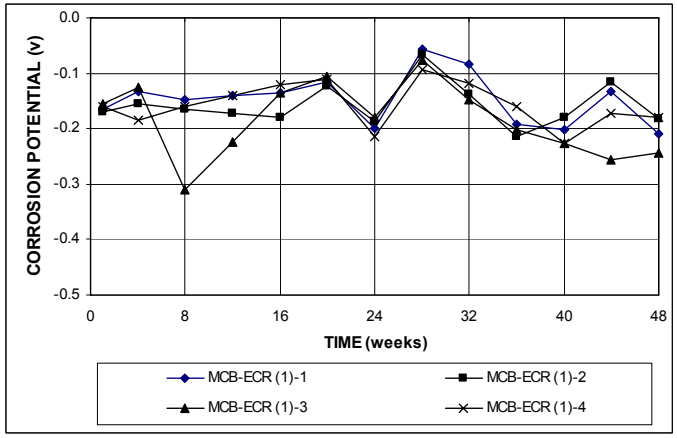

(b)

Figure A.272 – (a) Top mat corrosion potentials and (b) bottom mat corrosion potentials, with respect to copper-copper sulfate electrode as measured in the field test for specimens with ECR without cracks (No. 1) for Mission Creek Bridge

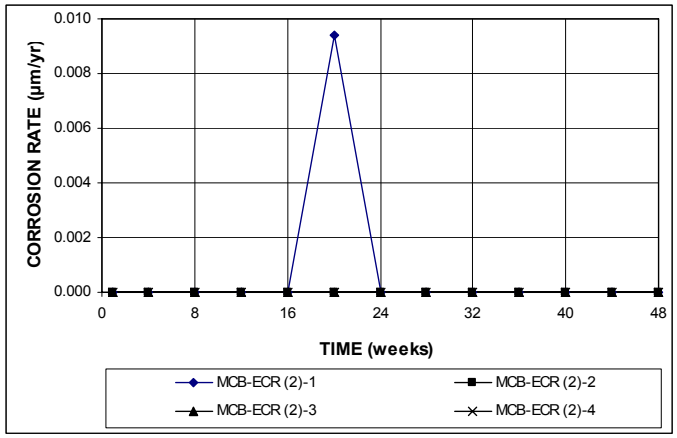

(a)

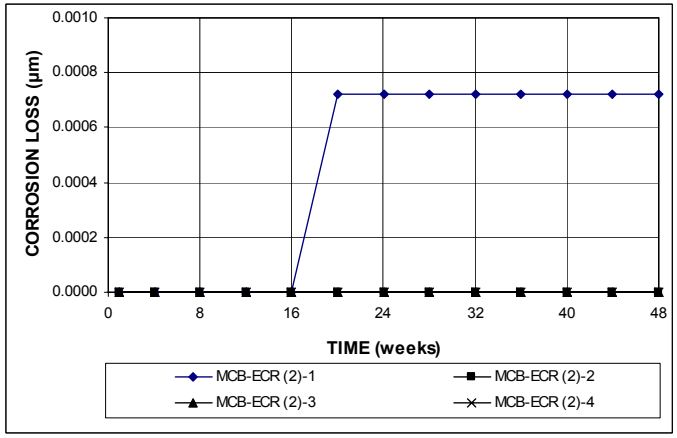

(b)

Figure A.273 – (a) Corrosion rates and (b) total corrosion losses based on total area of the steel as measured in the field test for specimens with ECR with cracks (No. 2) for Mission Creek Bridge.

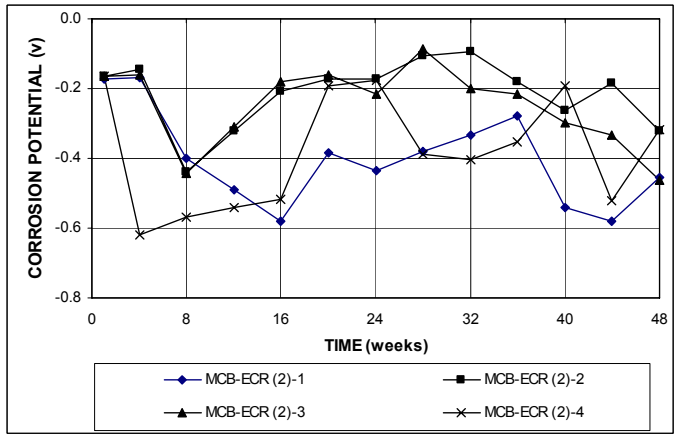

(a)

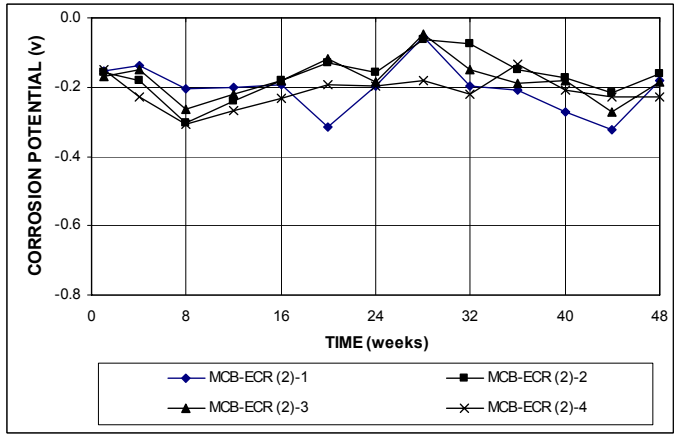

(b)

Figure A.274 – (a) Top mat corrosion potentials and (b) bottom mat corrosion potentials, with respect to copper-copper sulfate electrode as measured in the field test for specimens with ECR with cracks (No. 2) for Mission Creek Bridge

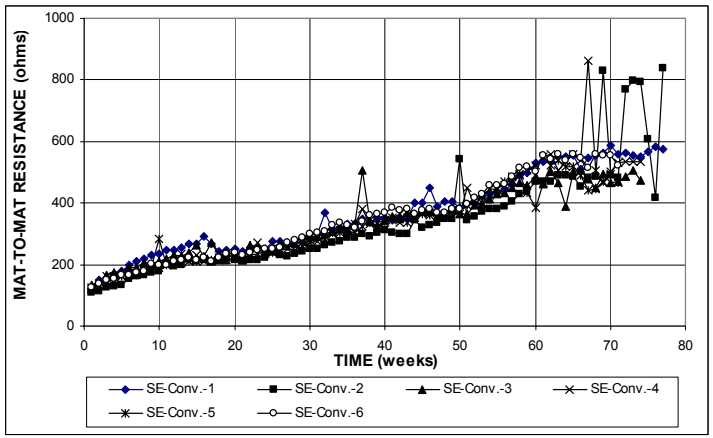

Figure B.1 – Mat-to-mat resistance as measured in the Southern Exposure test for specimens with conventional steel.

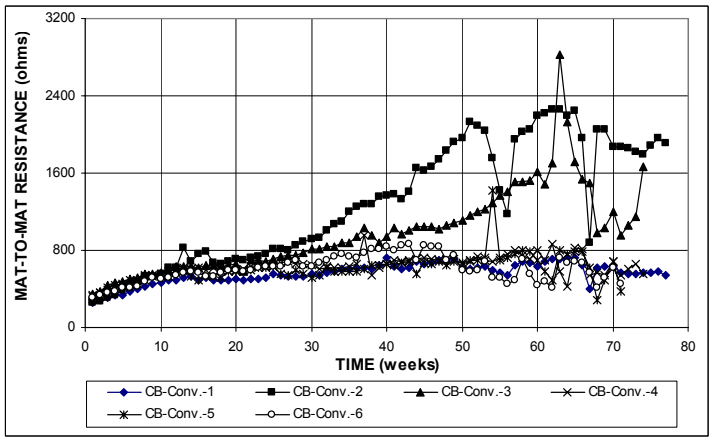

Figure B.2 – Mat-to-mat resistance as measured in the cracked beam test for specimens with conventional steel.

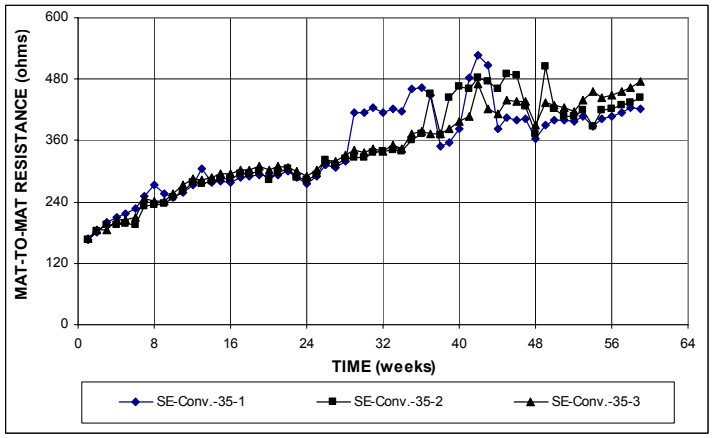

Figure B.3 – Mat-to-mat resistance as measured in the Southern Exposure test for specimens with conventional steel, a water-cement ratio of 0.35.

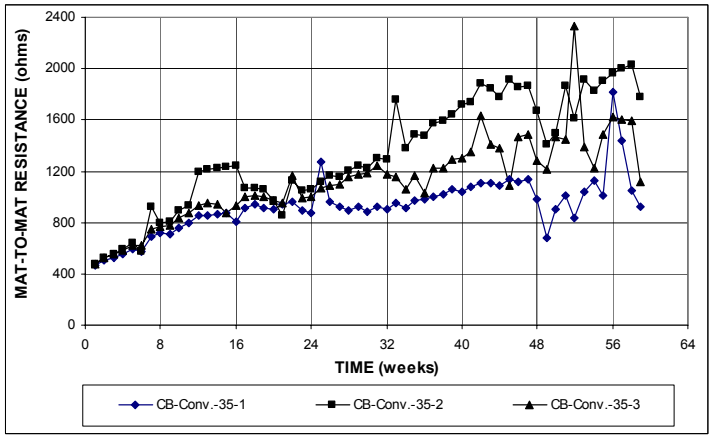

Figure B.4 – Mat-to-mat resistance as measured in the cracked beam test for specimens with conventional steel, a water-cement ratio of 0.35.

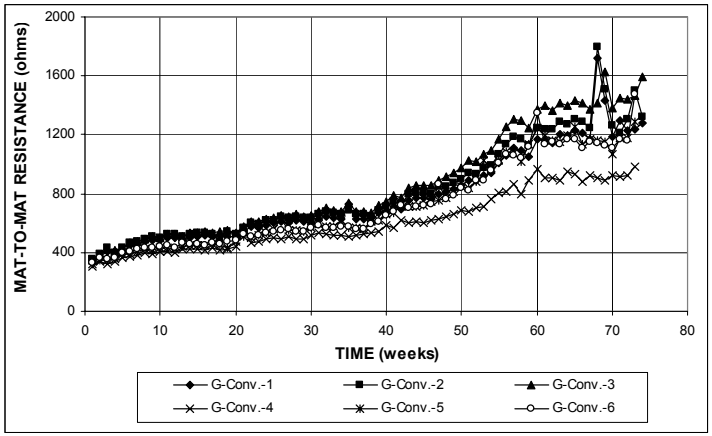

Figure B.5 – Mat-to-mat resistance as measured in the ASTM G 109 test for specimens with conventional steel.

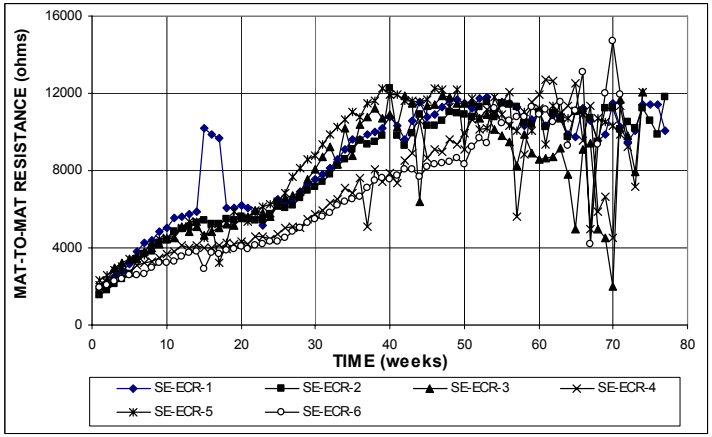

Figure B.6 – Mat-to-mat resistance as measured in the Southern Exposure test for specimens with ECR (four 3-mm ($^1/_8$-in.) diameter holes).

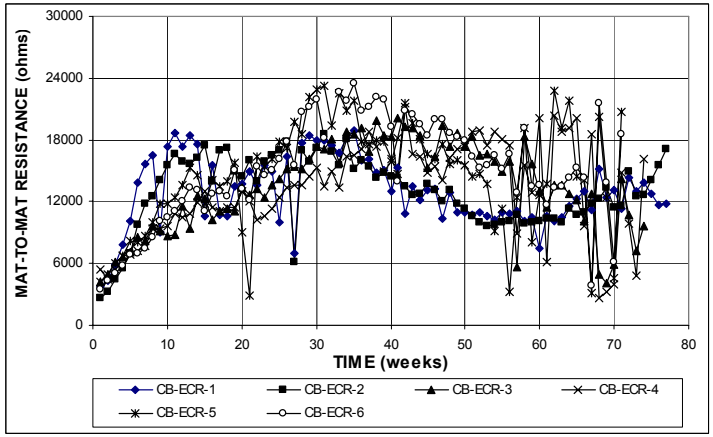

Figure B.7 – Mat-to-mat resistance as measured in the cracked beam test for specimens with ECR (four 3-mm ($^1/_8$-in.) diameter holes).

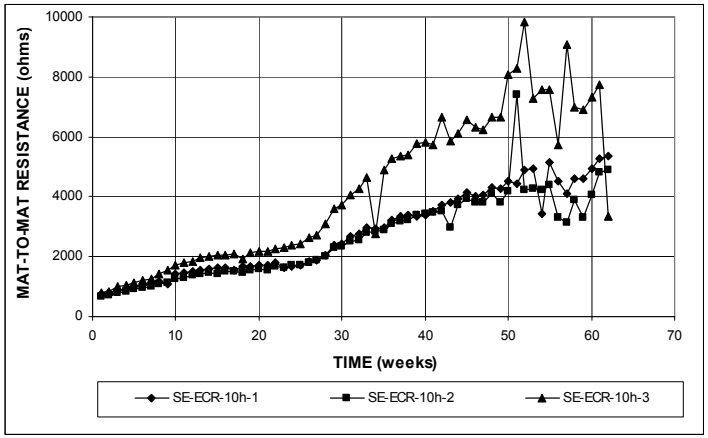

Figure B.8 – Mat-to-mat resistance as measured in the Southern Exposure test for specimens with ECR (ten 3-mm ($^1/_8$-in.) diameter holes).

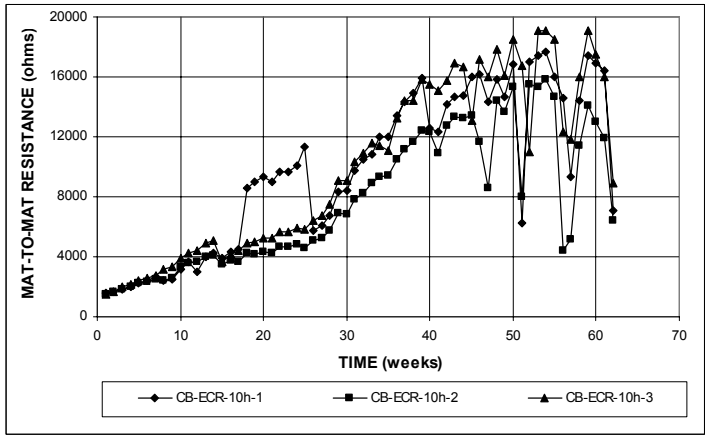

Figure B.9 – Mat-to-mat resistance as measured in the cracked beam test for specimens with ECR (ten 3-mm ($^1/_8$-in.) diameter holes).

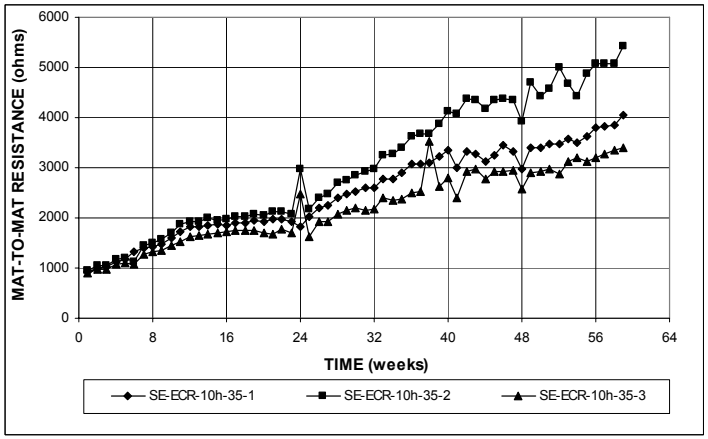

Figure B.10 – Mat-to-mat resistance as measured in the Southern Exposure test for specimens with ECR (ten 3-mm ($^1/_8$-in.) diameter holes), a water-cement ratio of 0.35.

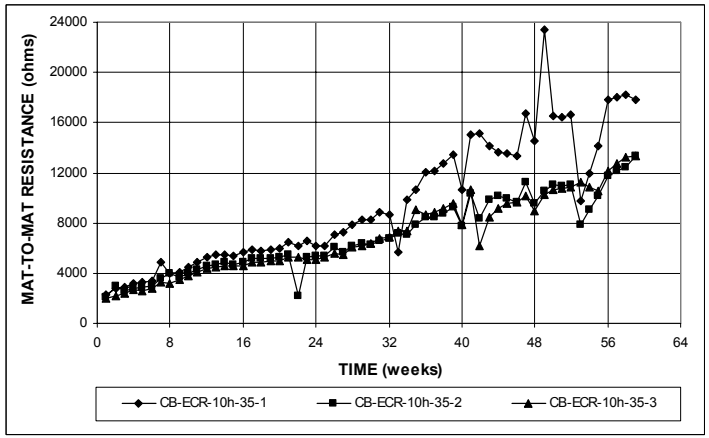

Figure B.11 – Mat-to-mat resistance as measured in the cracked beam test for specimens with ECR (ten 3-mm ($^1/_8$-in.) diameter holes), a water-cement ratio of 0.35.

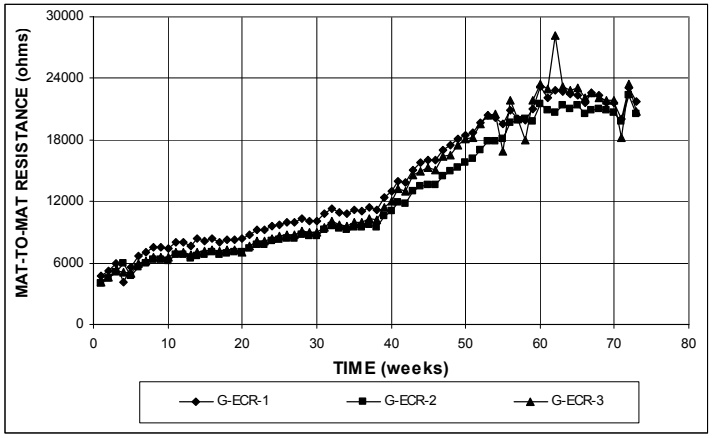

Figure B.12 – Mat-to-mat resistance as measured in the ASTM G 109 test for specimens with ECR (four 3-mm ($^1/_8$-in.) diameter holes).

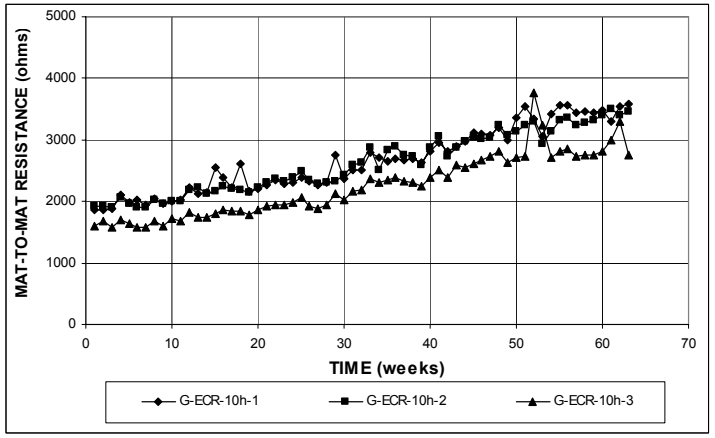

Figure B.13 – Mat-to-mat resistance as measured in the ASTM G 109 test for specimens with ECR (ten 3-mm ($^1/_8$-in.) diameter holes).

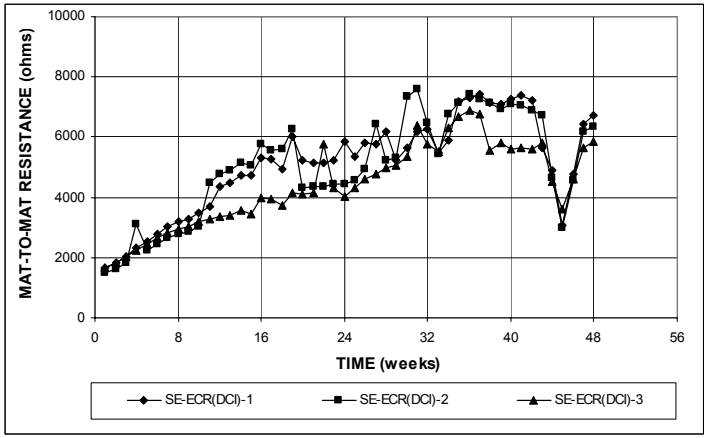

Figure B.14 – Mat-to-mat resistance as measured in the Southern Exposure test for specimens with ECR in concrete with DCI (four 3-mm ($^1/_8$-in.) diameter holes).

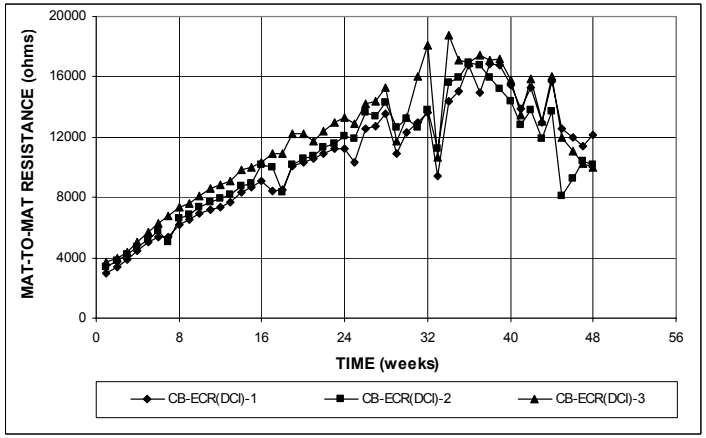

Figure B.15 – Mat-to-mat resistance as measured in the cracked beam test for specimens with ECR in concrete with DCI (four 3-mm ($^1/_8$-in.) diameter holes).

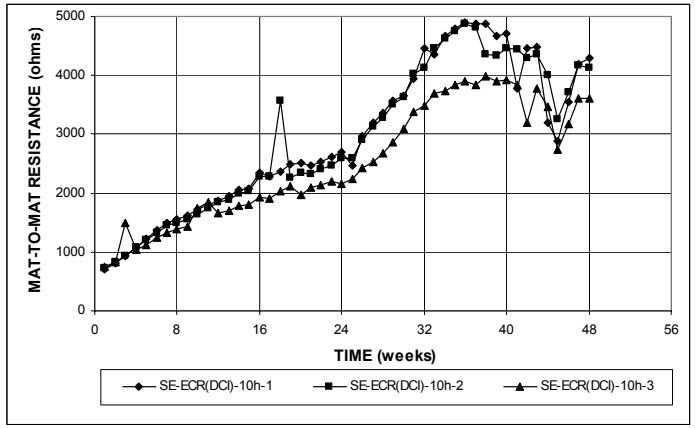

Figure B.16 – Mat-to-mat resistance as measured in the Southern Exposure test for specimens with ECR in concrete with DCI (ten 3-mm ($^1/_8$-in.) diameter holes).

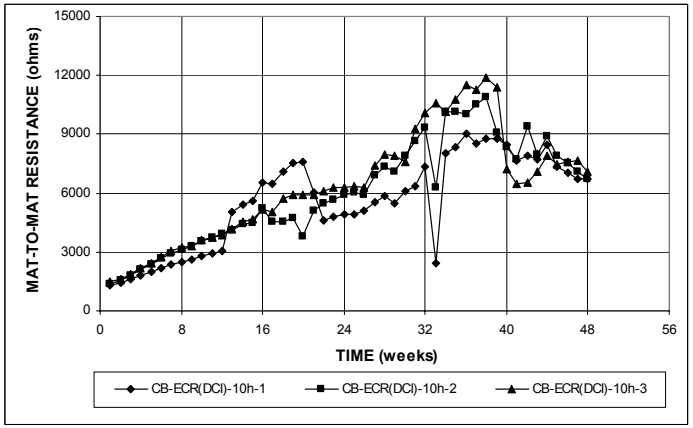

Figure B.17 – Mat-to-mat resistance as measured in the cracked beam test for specimens with ECR in concrete with DCI (ten 3-mm ($^1/_8$-in.) diameter holes).

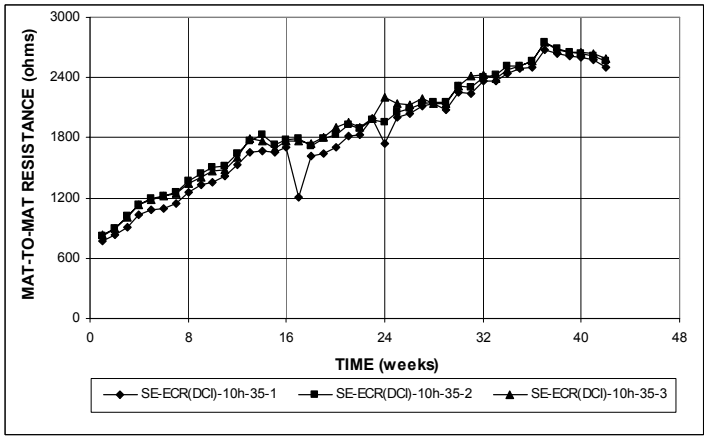

Figure B.18 – Mat-to-mat resistance as measured in the Southern Exposure test for specimens with ECR in concrete with DCI (ten 3-mm ($^1/_8$-in.) diameter holes), a water-cement ratio of 0.35.

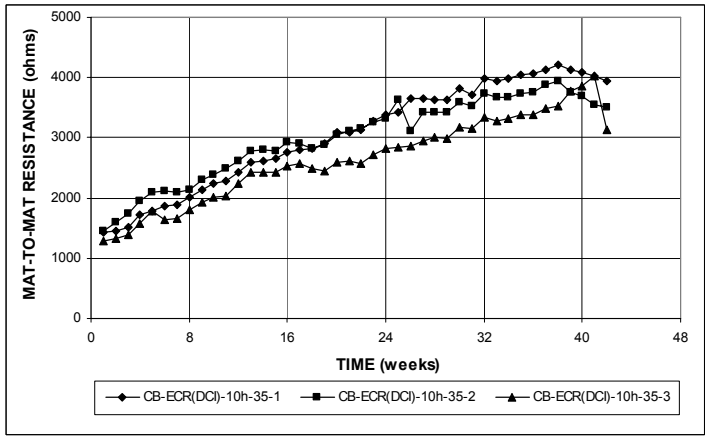

Figure B.19 – Mat-to-mat resistance as measured in the cracked beam test for specimens with ECR in concrete with DCI (ten 3-mm ($^1/_8$-in.) diameter holes), a water-cement ratio of 0.35.

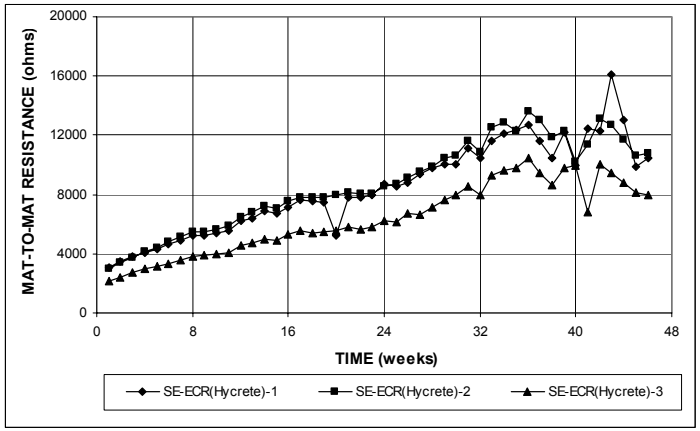

Figure B.20 – Mat-to-mat resistance as measured in the Southern Exposure test for specimens with ECR in concrete with Hycrete (four 3-mm ($^1/_8$-in.) diameter holes).

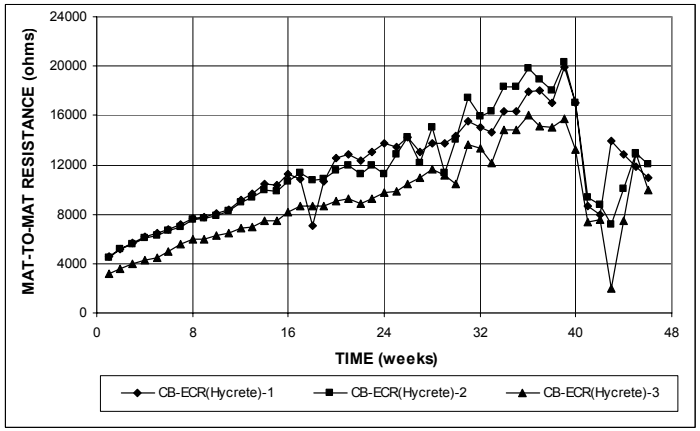

Figure B.21 – Mat-to-mat resistance as measured in the cracked beam test for specimens with ECR in concrete with Hycrete (four 3-mm ($^1/_8$-in.) diameter holes).

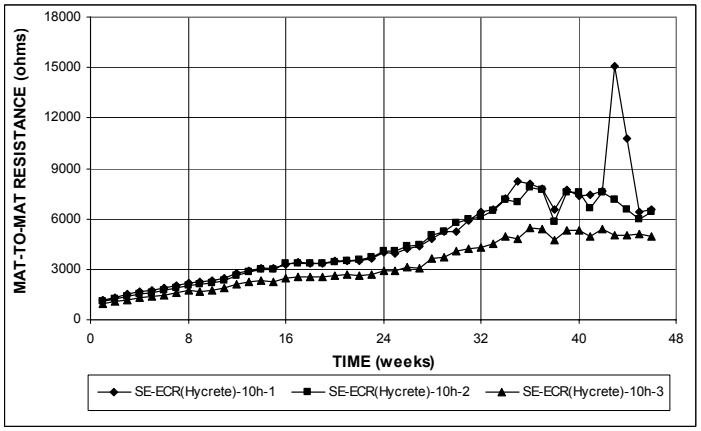

Figure B.22 – Mat-to-mat resistance as measured in the Southern Exposure test for specimens with ECR in concrete with Hycrete (ten 3-mm ($^1/_8$-in.) diameter holes).

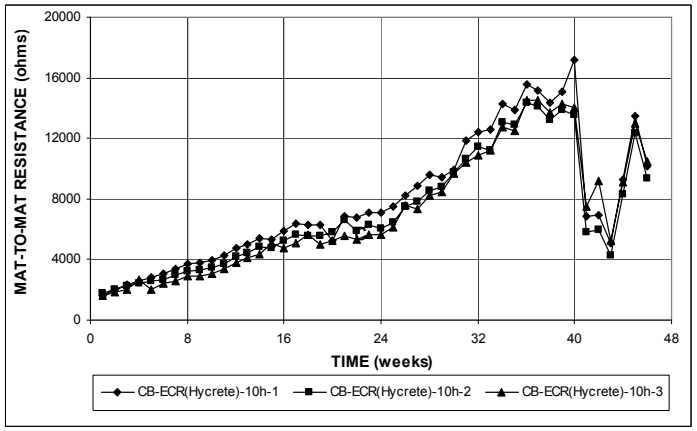

Figure B.23 – Mat-to-mat resistance as measured in the cracked beam test for specimens with ECR in concrete with Hycrete (ten 3-mm ($^1/_8$-in.) diameter holes).

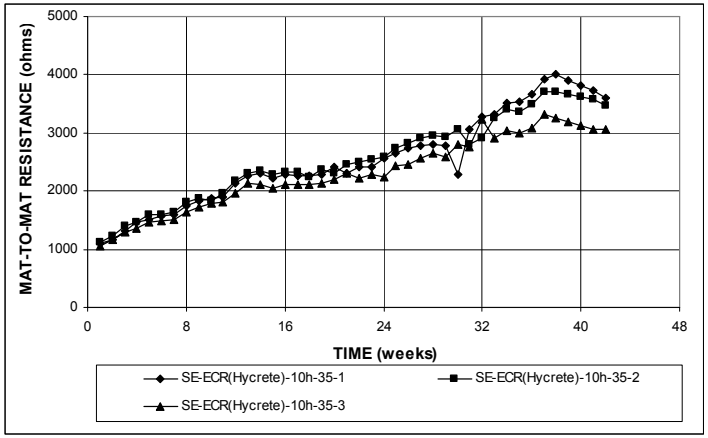

Figure B.24 – Mat-to-mat resistance as measured in the Southern Exposure test for specimens with ECR in concrete with Hycrete (ten 3-mm ($^1/_8$-in.) diameter holes), a water-cement ratio of 0.35.

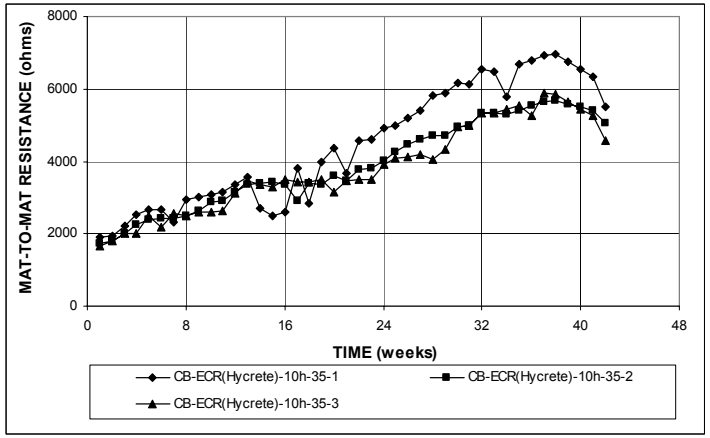

Figure B.25 – Mat-to-mat resistance as measured in the cracked beam test for specimens with ECR in concrete with Hycrete (ten 3-mm ($^1/_8$-in.) diameter holes), a water-cement ratio of 0.35.

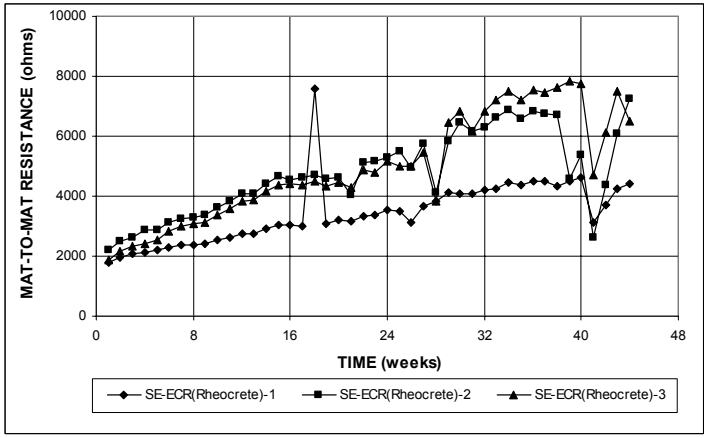

Figure B.26 – Mat-to-mat resistance as measured in the Southern Exposure test for specimens with ECR in concrete with Rheocrete (four 3-mm ($^1/_8$-in.) diameter holes).

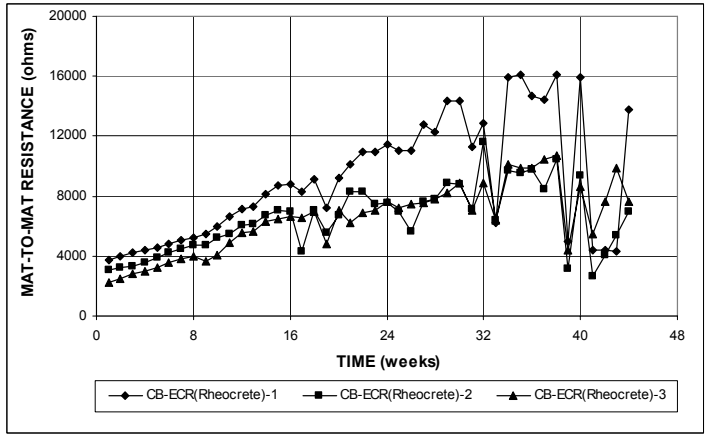

Figure B.27 – Mat-to-mat resistance as measured in the cracked beam test for specimens with ECR in concrete with Rheocrete (four 3-mm ($^1/_8$-in.) diameter holes).

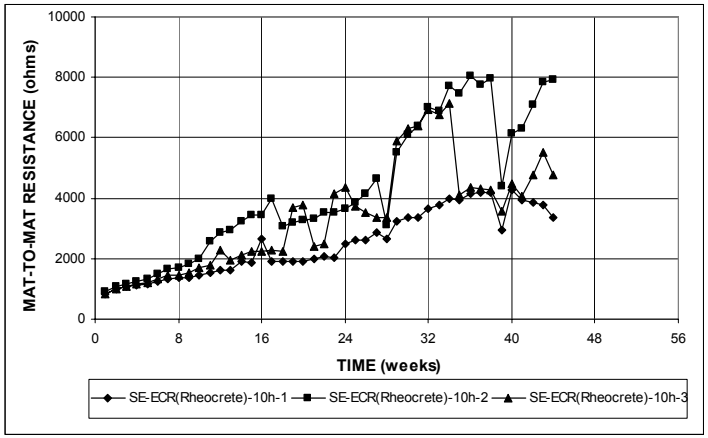

Figure B.28 – Mat-to-mat resistance as measured in the Southern Exposure test for specimens with ECR in concrete with Rheocrete (ten 3-mm ($^1/_8$-in.) diameter holes).

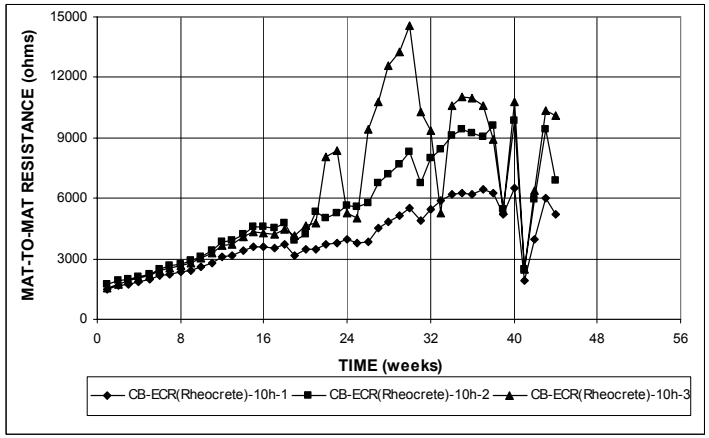

Figure B.29 – Mat-to-mat resistance as measured in the cracked beam test for specimens with ECR in concrete with Rheocrete (ten 3-mm ($^1/_8$-in.) diameter holes).

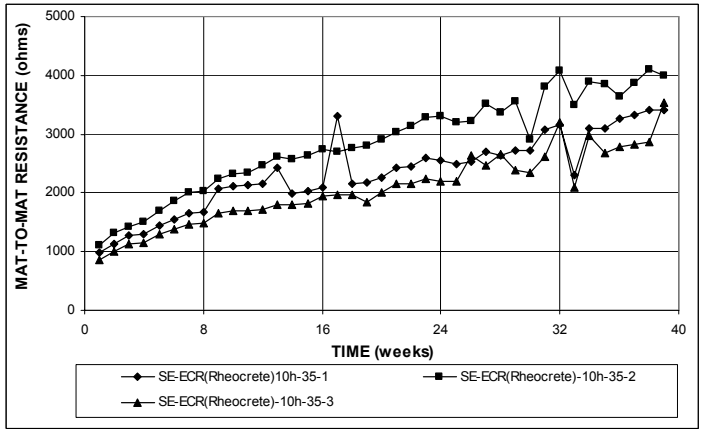

Figure B.30 – Mat-to-mat resistance as measured in the Southern Exposure test for specimens with ECR in concrete with Rheocrete (ten 3-mm ($^1/_8$-in.) diameter holes), a water-cement ratio of 0.35.

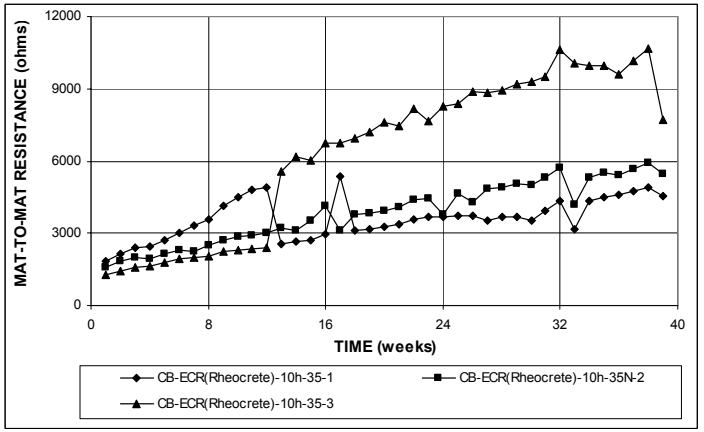

Figure B.31 – Mat-to-mat resistance as measured in the cracked beam test for specimens with ECR in concrete with Rheocrete (ten 3-mm ($^1/_8$-in.) diameter holes), a water-cement ratio of 0.35.

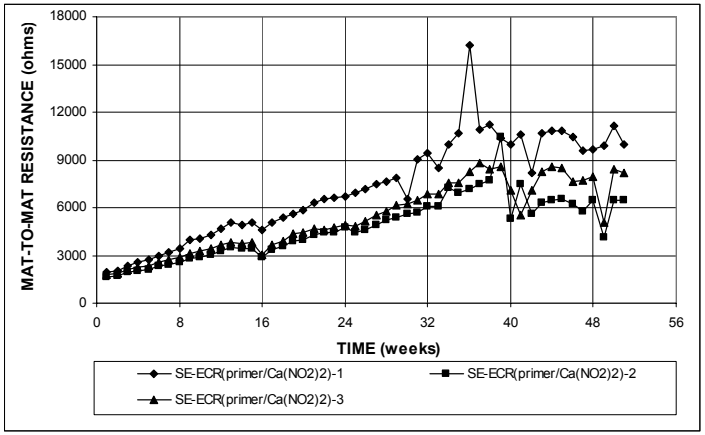

Figure B.32 – Mat-to-mat resistance as measured in the Southern Exposure test for specimens with ECR with primer containing calcium nitrite (four 3-mm ($^1/_8$-in.) diameter holes).

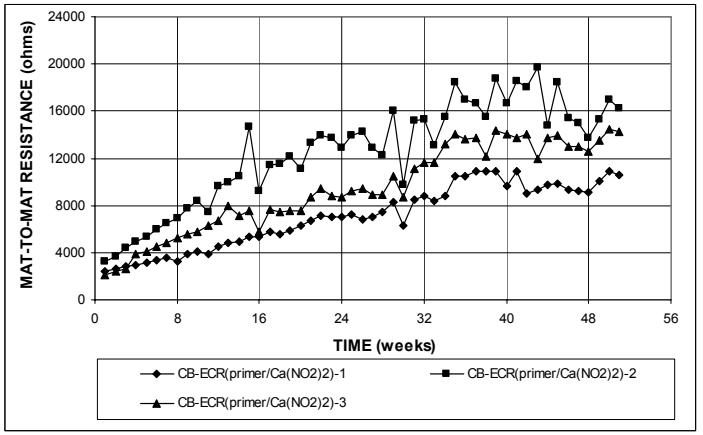

Figure B.33 – Mat-to-mat resistance as measured in the cracked beam test for specimens with ECR with primer containing calcium nitrite (four 3-mm ($^1/_8$-in.) diameter holes).

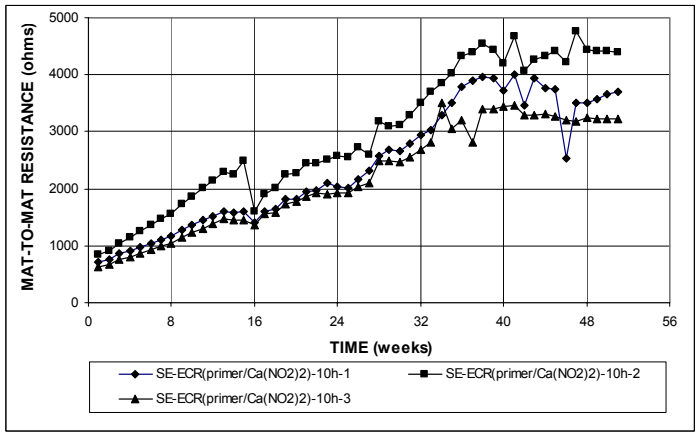

Figure B.34 – Mat-to-mat resistance as measured in the Southern Exposure test for specimens with ECR with primer containing calcium nitrite (ten 3-mm ($^1/_8$-in.) diameter holes).

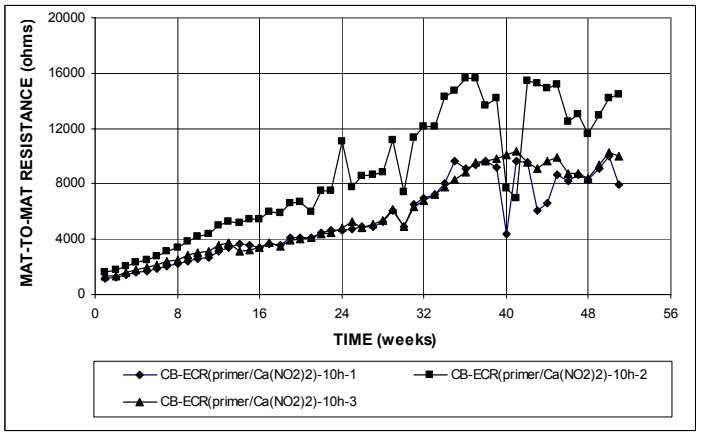

Figure B.35 – Mat-to-mat resistance as measured in the cracked beam test for specimens with ECR with primer containing calcium nitrite (ten 3-mm ($^1/_8$-in.) diameter holes).

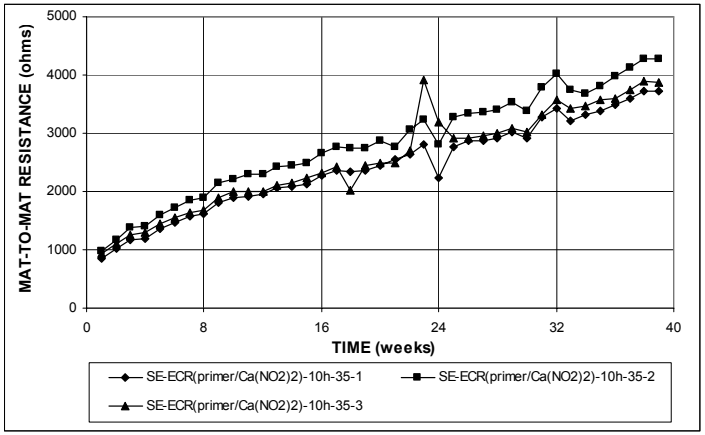

Figure B.36 – Mat-to-mat resistance as measured in the Southern Exposure test for specimens with ECR with primer containing calcium nitrite (ten 3-mm ($^1/_8$-in.) diameter holes), a water-cement ratio of 0.35.

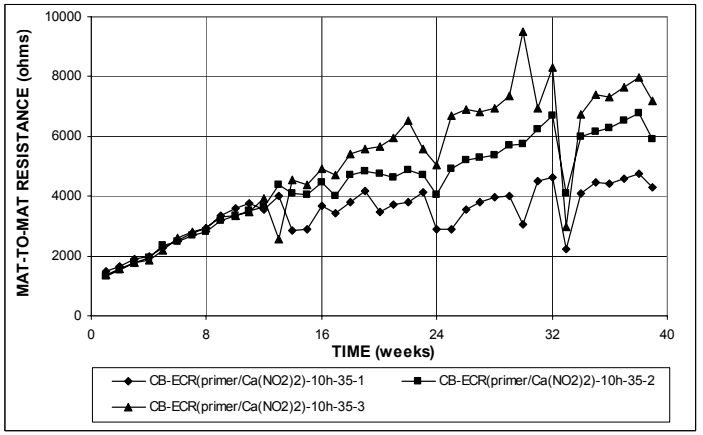

Figure B.37 – Mat-to-mat resistance as measured in the cracked beam test for specimens with ECR with primer containing calcium nitrite (ten 3-mm ($^1/_8$-in.) diameter holes), a water-cement ratio of 0.35.

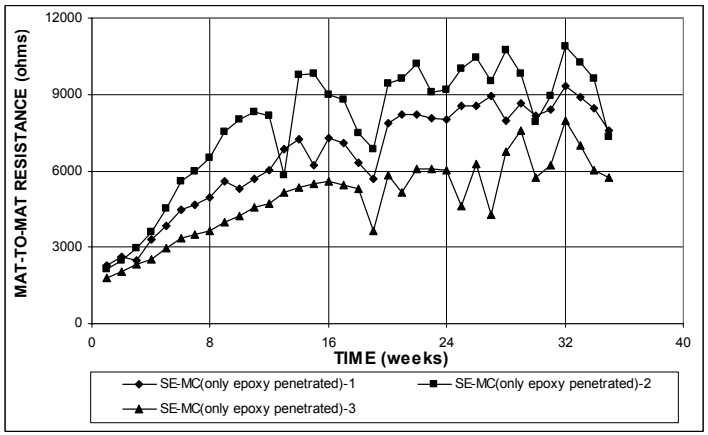

Figure B.38 – Mat-to-mat resistance as measured in the Southern Exposure test for specimens with multiple coated bar (four 3-mm ($^1/_8$-in.) diameter holes, only epoxy penetrated).

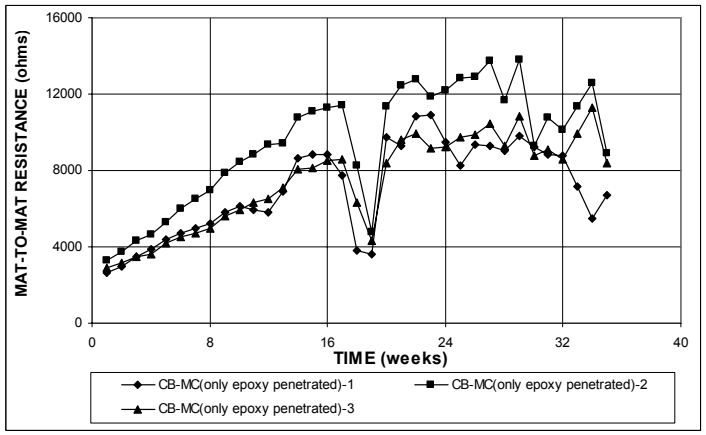

Figure B.39 – Mat-to-mat resistance as measured in the cracked beam test for specimens with multiple coated bar (four 3-mm ($^1/_8$-in.) diameter holes, only epoxy penetrated).

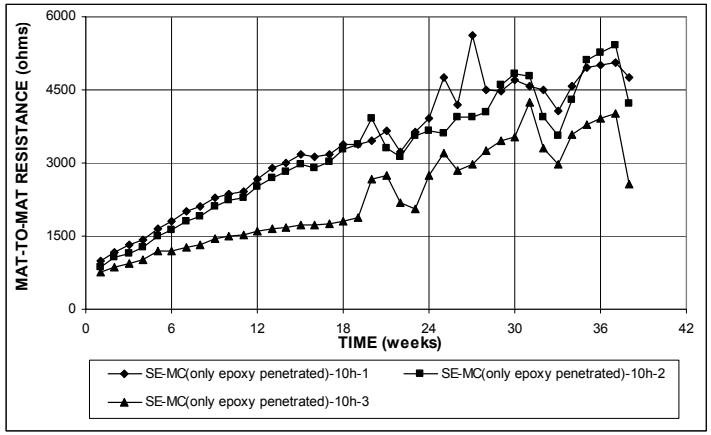

Figure B.40 – Mat-to-mat resistance as measured in the Southern Exposure test for specimens with multiple coated bar (ten 3-mm ($^1/_8$-in.) diameter holes, only epoxy penetrated).

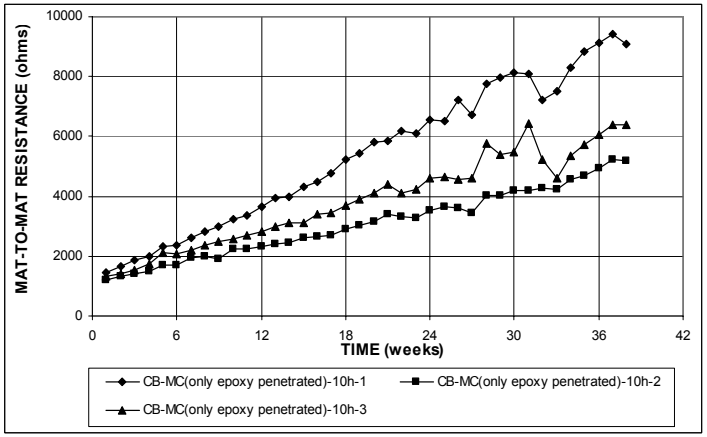

Figure B.41 – Mat-to-mat resistance as measured in the cracked beam test for specimens with multiple coated bar (ten 3-mm ($^1/_8$-in.) diameter holes, only epoxy penetrated).

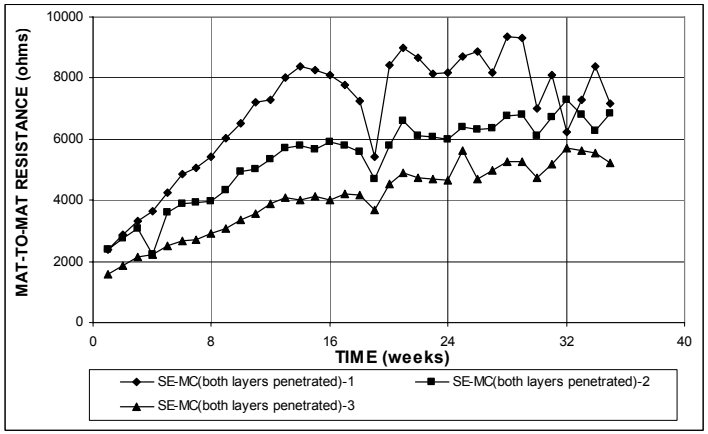

Figure B.42 – Mat-to-mat resistance as measured in the Southern Exposure test for specimens with multiple coated bar (four 3-mm ($^1/_8$-in.) diameter holes, both layers penetrated).

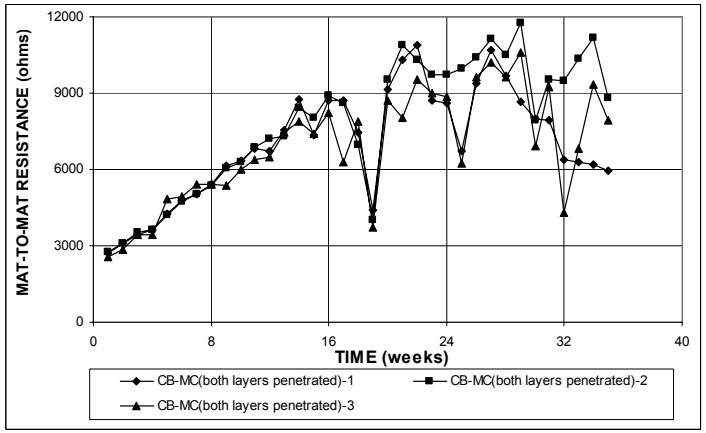

Figure B.43 – Mat-to-mat resistance as measured in the cracked beam test for specimens with multiple coated bar (four 3-mm ($^1/_8$-in.) diameter holes, both layers penetrated).

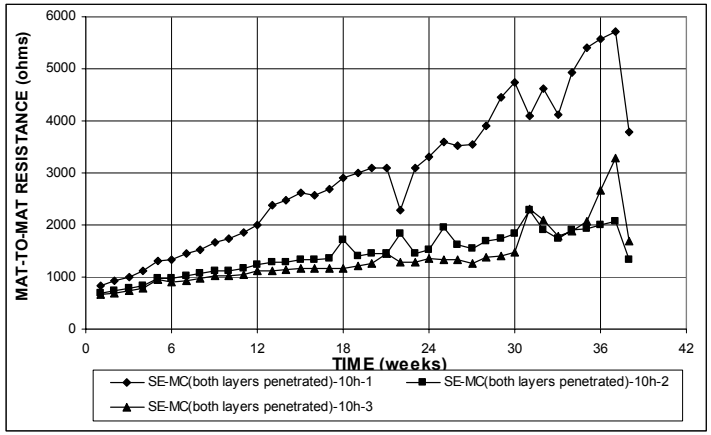

Figure B.44 – Mat-to-mat resistance as measured in the Southern Exposure test for specimens with multiple coated bar (ten 3-mm ($^1/_8$-in.) diameter holes, both layers penetrated).

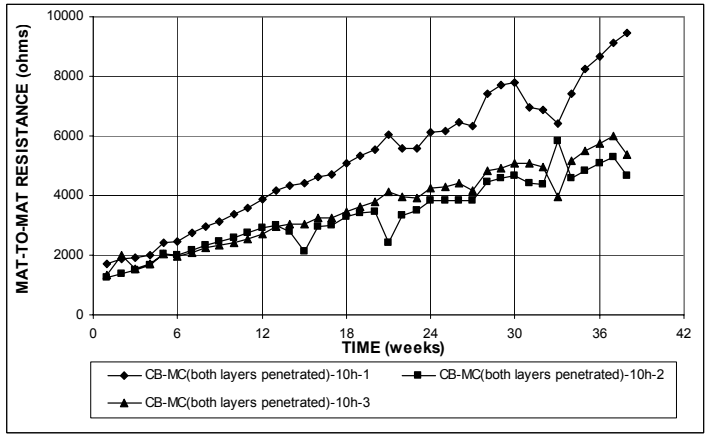

Figure B.45 – Mat-to-mat resistance as measured in the cracked beam test for specimens with multiple coated bar (ten 3-mm ($^1/_8$-in.) diameter holes, both layers penetrated).

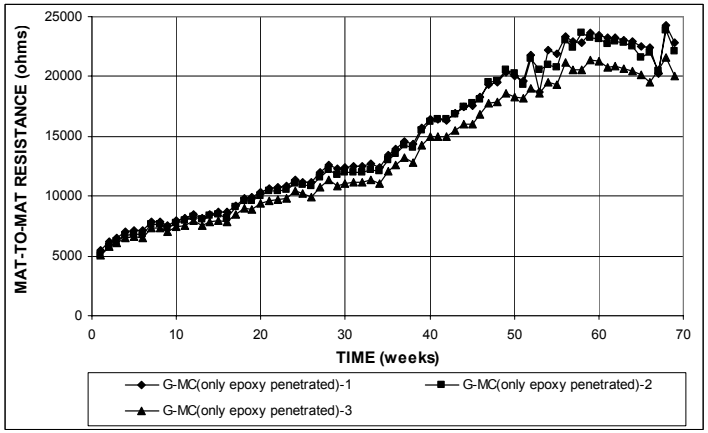

Figure B.46 – Mat-to-mat resistance as measured in the ASTM G 109 test for specimens with multiple coated bars (four 3-mm ($^1/_8$-in.) diameter holes, only epoxy penetrated).

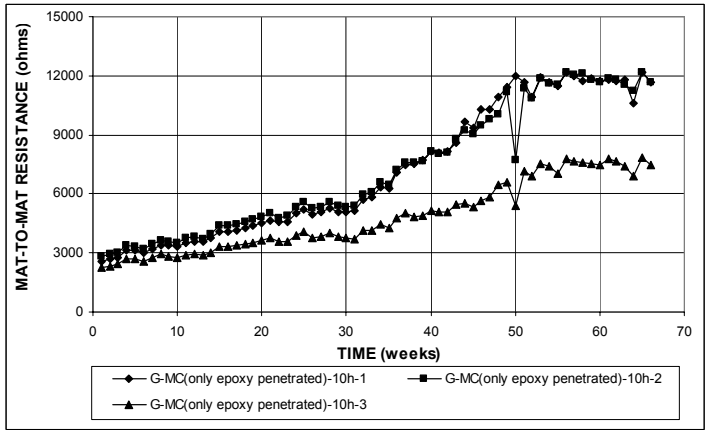

Figure B.47 – Mat-to-mat resistance as measured in the ASTM G 109 test for specimens with multiple coated bars (ten 3-mm ($^1/_8$-in.) diameter holes, only epoxy penetrated).

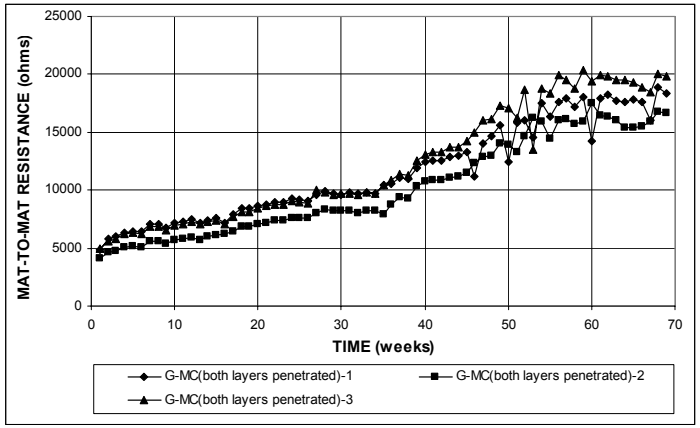

Figure B.48 – Mat-to-mat resistance as measured in the ASTM G 109 test for specimens with multiple coated bars (four 3-mm ($^1/_8$-in.) diameter holes, both layers penetrated).

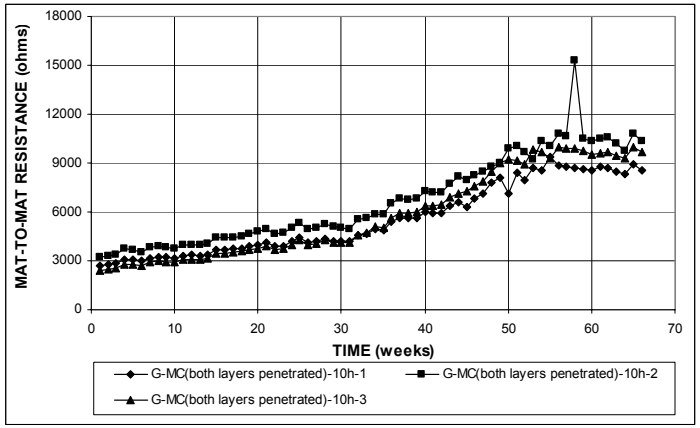

Figure B.49 – Mat-to-mat resistance as measured in the ASTM G 109 test for specimens with multiple coated bars (ten 3-mm ($^1/_8$-in.) diameter holes, both layers penetrated).

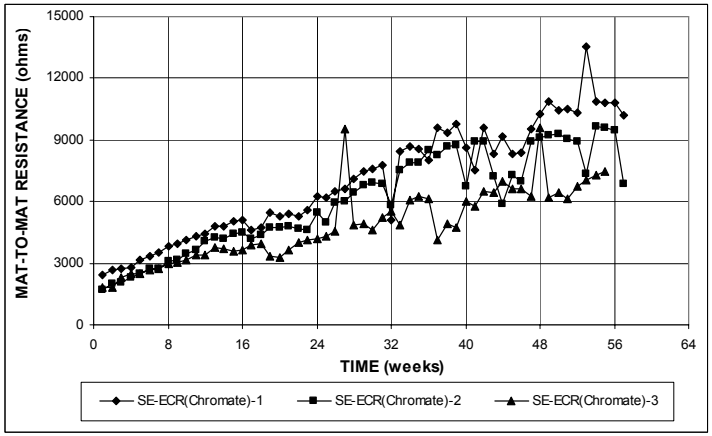

Figure B.50 – Mat-to-mat resistance as measured in the Southern Exposure test for specimens with chromate pretreatment (four 3-mm ($^1/_8$-in.) diameter holes).

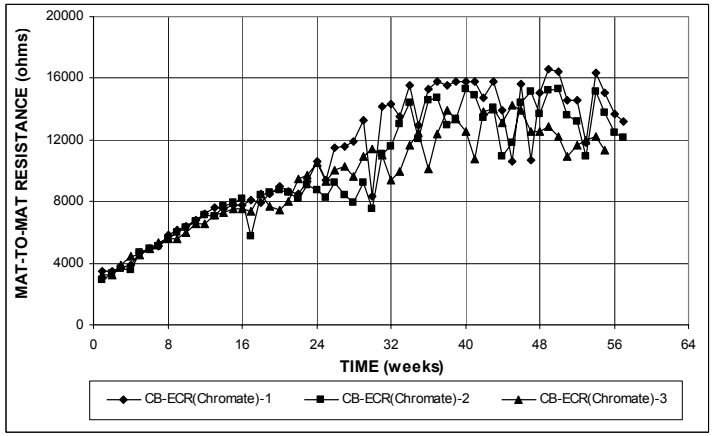

Figure B.51 – Mat-to-mat resistance as measured in the cracked beam test for specimens with chromate pretreatment (four 3-mm ($^1/_8$-in.) diameter holes).

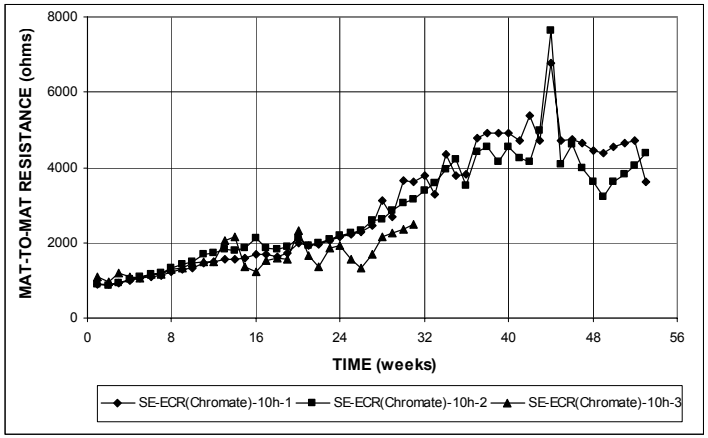

Figure B.52 – Mat-to-mat resistance as measured in the Southern Exposure test for specimens with chromate pretreatment (ten 3-mm ($^1/_8$-in.) diameter holes).

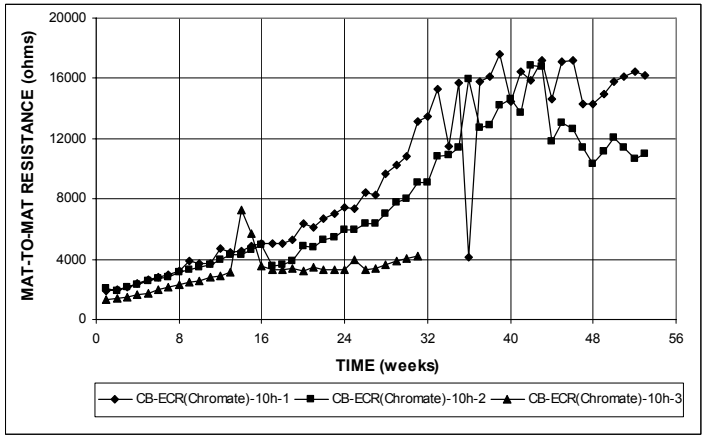

Figure B.53 – Mat-to-mat resistance as measured in the cracked beam test for specimens with chromate pretreatment (ten 3-mm ($^1/_8$-in.) diameter holes).

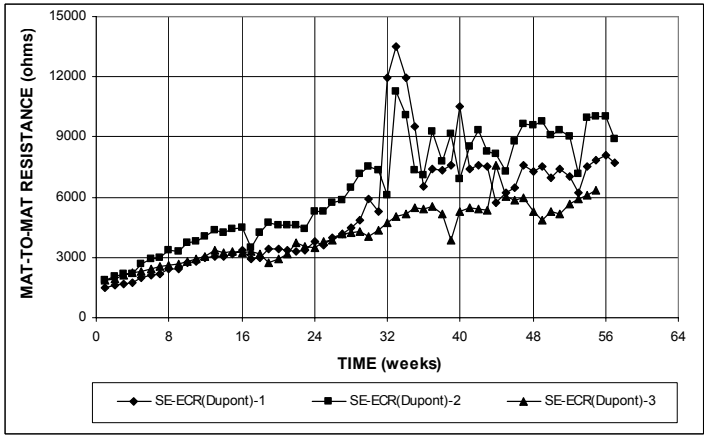

Figure B.54 – Mat-to-mat resistance as measured in the Southern Exposure test for specimens with DuPont coating (four 3-mm ($^1/_8$-in.) diameter holes).

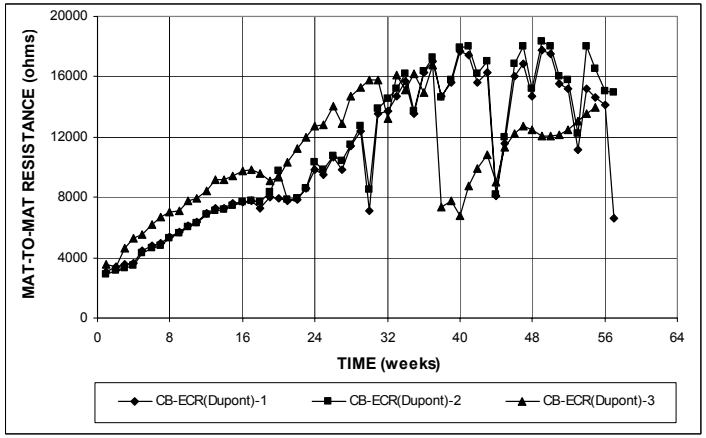

Figure B.55 – Mat-to-mat resistance as measured in the cracked beam test for specimens with DuPont coating (four 3-mm ($^1/_8$-in.) diameter holes).

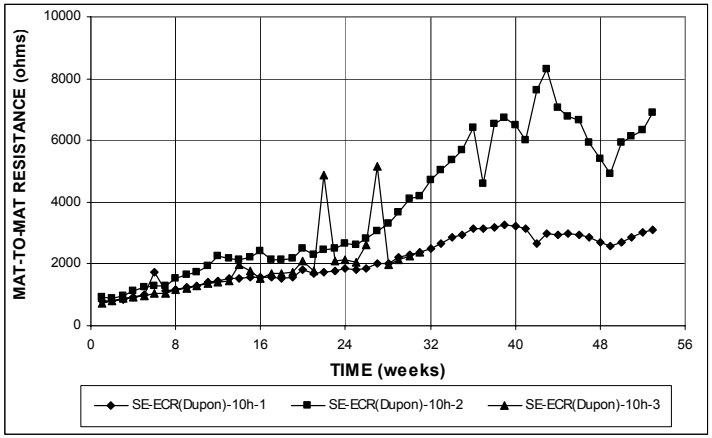

Figure B.56 – Mat-to-mat resistance as measured in the Southern Exposure test for specimens with DuPont coating (ten 3-mm ($^1/_8$-in.) diameter holes).

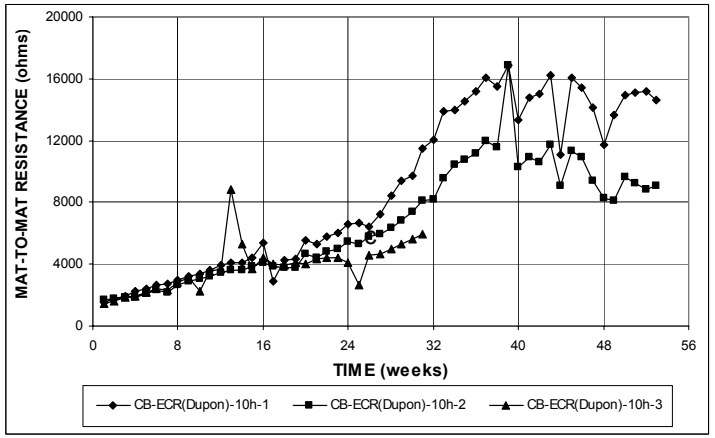

Figure B.57 – Mat-to-mat resistance as measured in the cracked beam test for specimens with DuPont coating (ten 3-mm ($^1/_8$-in.) diameter holes).

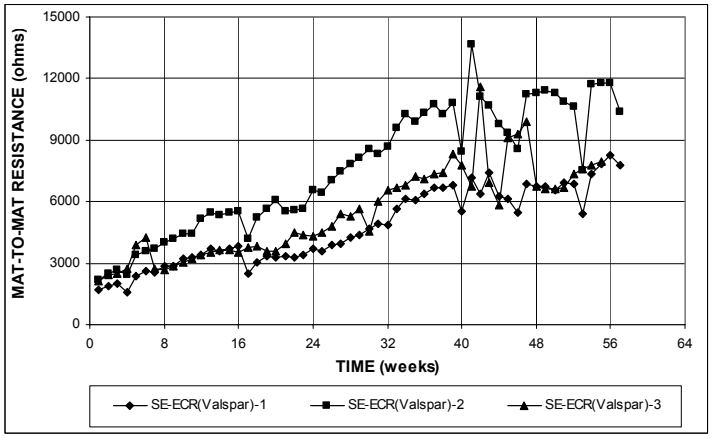

Figure B.58 – Mat-to-mat resistance as measured in the Southern Exposure test for specimens with Valspar coating (four 3-mm ($^1/_8$-in.) diameter holes).

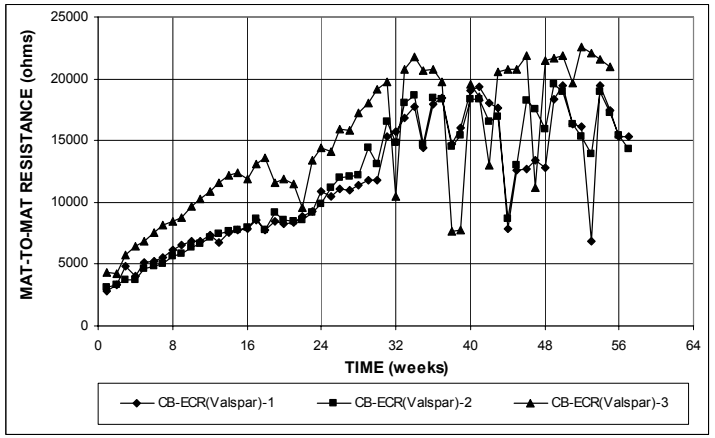

Figure B.59 – Mat-to-mat resistance as measured in the cracked beam test for specimens with Valspar coating (four 3-mm ($^1/_8$-in.) diameter holes).

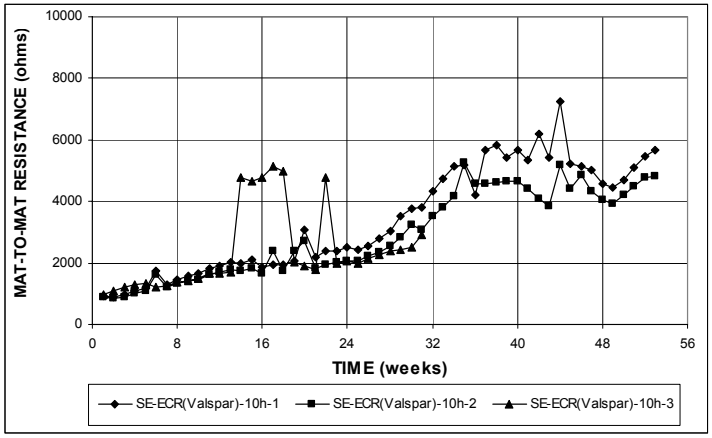

Figure B.60 – Mat-to-mat resistance as measured in the Southern Exposure test for specimens with Valspar coating (ten 3-mm ($^1/_8$-in.) diameter holes).

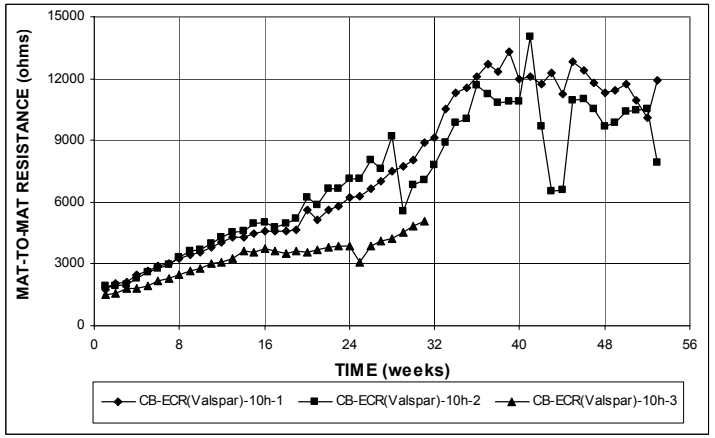

Figure B.61 – Mat-to-mat resistance as measured in the cracked beam test for specimens with Valspar coating (ten 3-mm ($^1/_8$-in.) diameter holes).

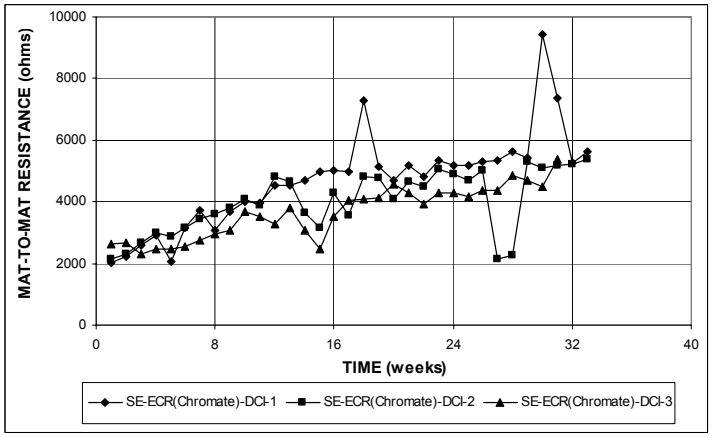

Figure B.62 – Mat-to-mat resistance as measured in the Southern Exposure test for specimens with chromate pretreatment in concrete with DCI (four 3-mm ($^1/_8$-in.) diameter holes).

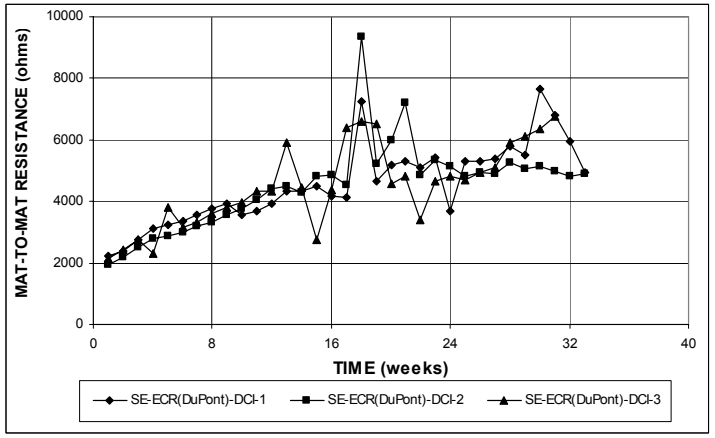

Figure B.63 – Mat-to-mat resistance as measured in the Southern Exposure test for specimens with DuPont coating in concrete with DCI (four 3-mm ($^1/_8$-in.) diameter holes).

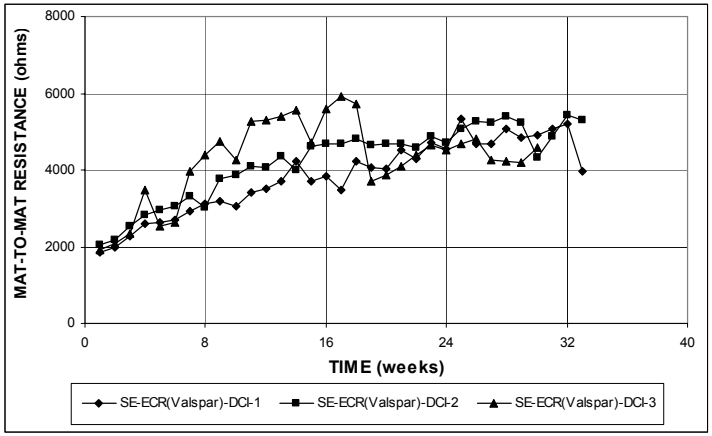

Figure B.64 – Mat-to-mat resistance as measured in the Southern Exposure test for specimens with Valspar coating in concrete with DCI (four 3-mm ($^{1}/_{8}$-in.) diameter holes).

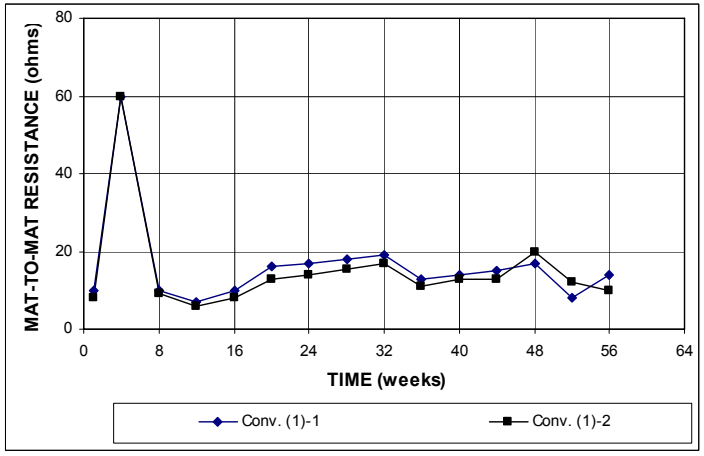

Figure B.65 – Mat-to-mat resistance as measured in the field test for specimens with conventional steel (without cracks, No. 1).

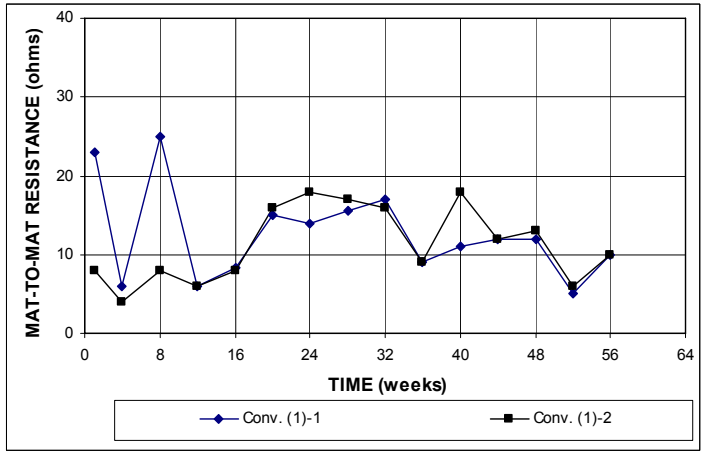

Figure B.66 – Mat-to-mat resistance as measured in the field test for specimens with conventional steel (with cracks, No.1).

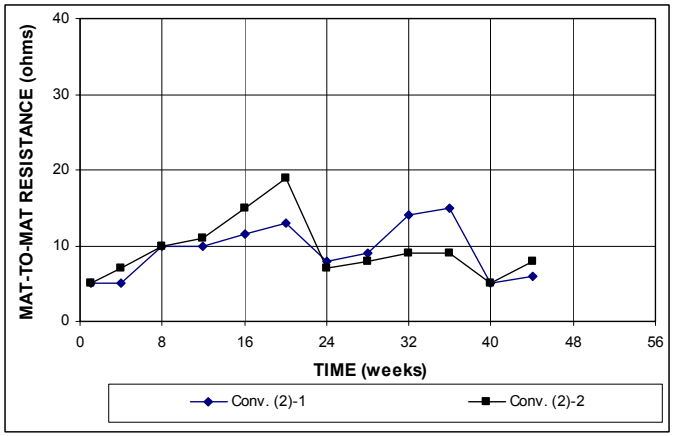

Figure B.67 – Mat-to-mat resistance as measured in the field test for specimens with conventional steel (without cracks, No. 2).

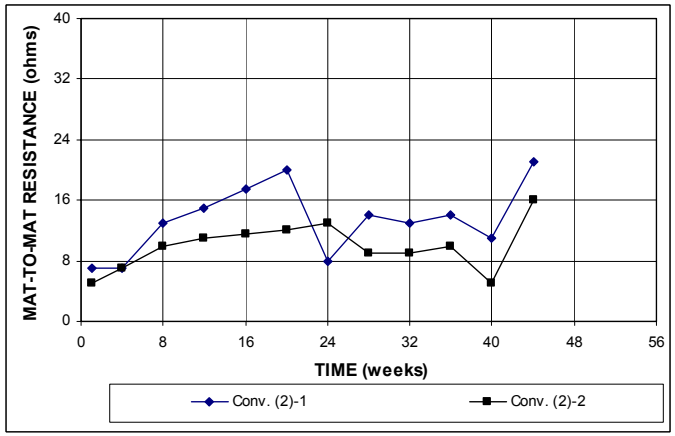

Figure B.68 – Mat-to-mat resistance as measured in the field test for specimens with conventional steel (with cracks, No. 2).

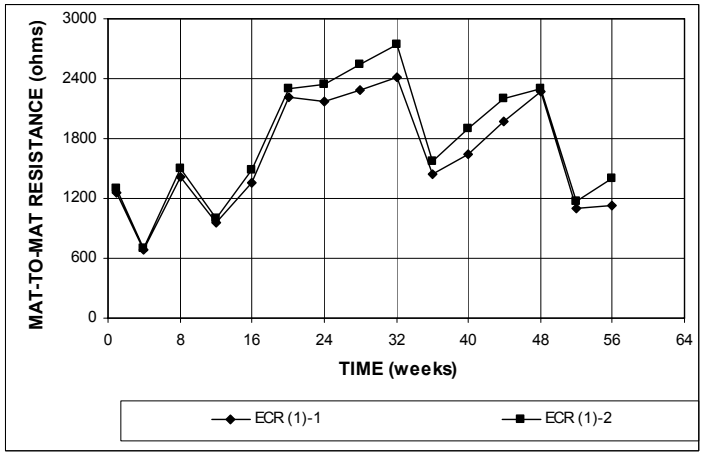

Figure B.69 – Mat-to-mat resistance as measured in the field test for specimens with ECR (without cracks, No. 1).

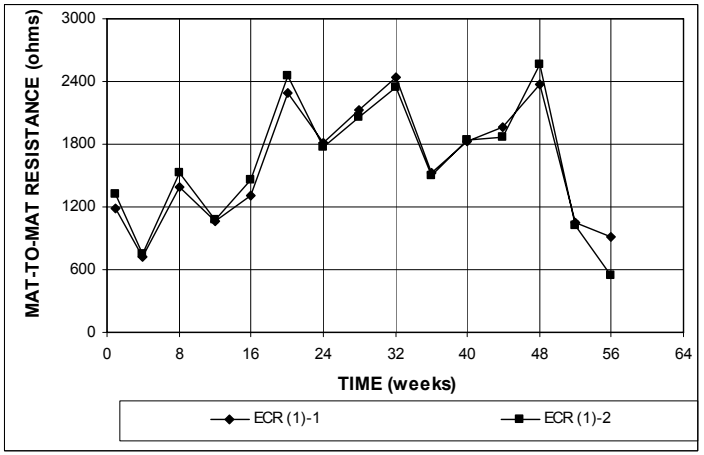

Figure B.70 – Mat-to-mat resistance as measured in the field test for specimens with ECR (with cracks, No.1).

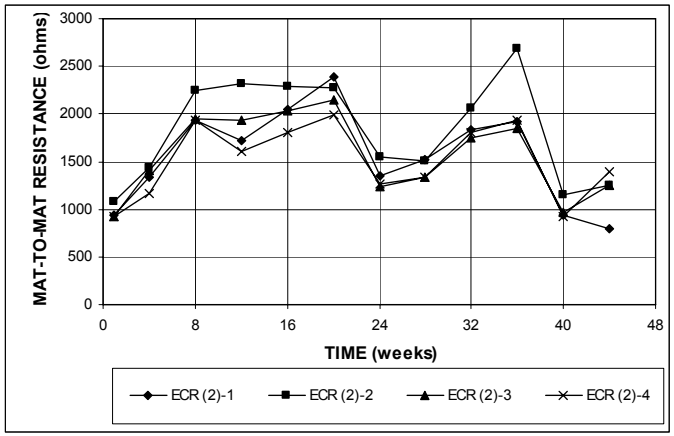

Figure B.71 – Mat-to-mat resistance as measured in the field test for specimens with ECR (without cracks, No. 2).

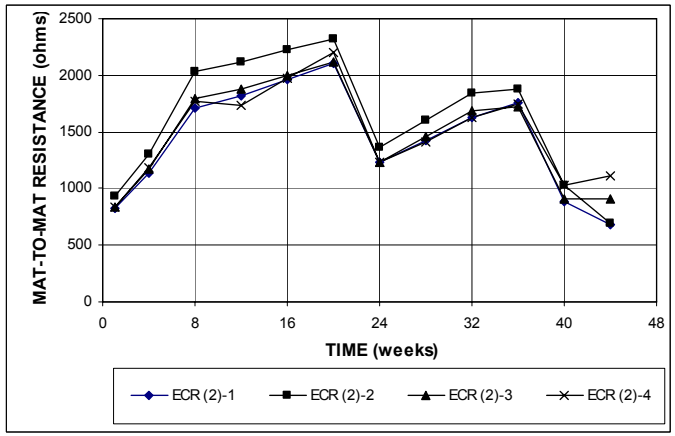

Figure B.72 – Mat-to-mat resistance as measured in the field test for specimens with ECR (with cracks, No. 2).

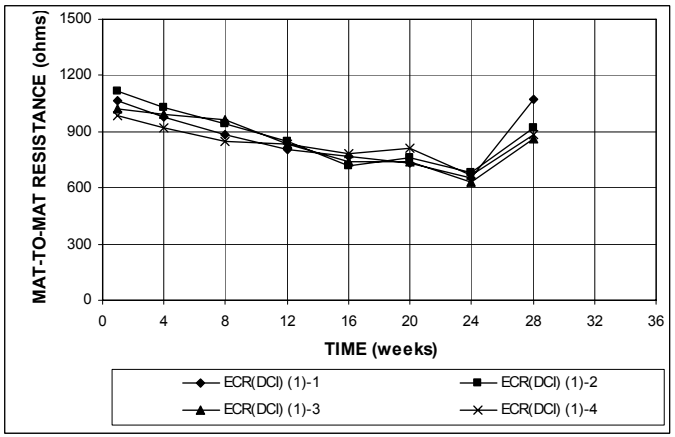

Figure B.73 – Mat-to-mat resistance as measured in the field test for specimens with ECR in concrete with DCI (without cracks, No. 1).

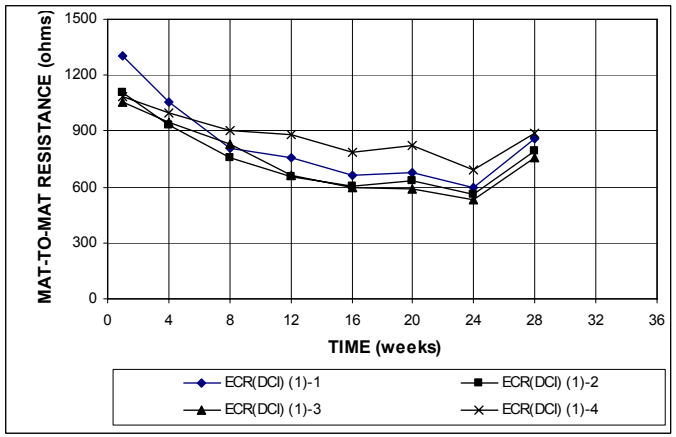

Figure B.74 – Mat-to-mat resistance as measured in the field test for specimens with ECR in concrete with DCI (with cracks, No.1).

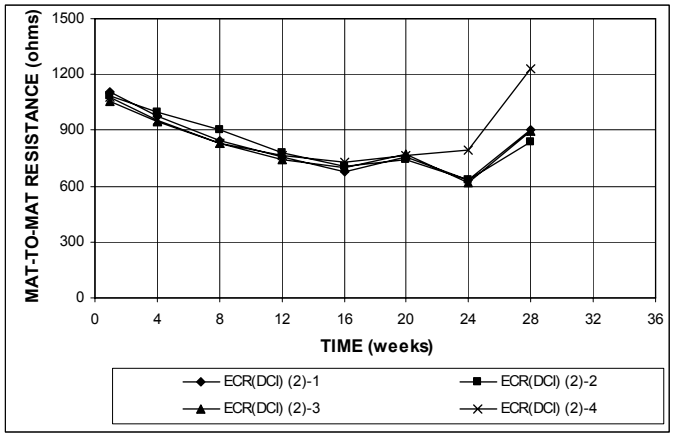

Figure B.75 – Mat-to-mat resistance as measured in the field test for specimens with ECR in concrete with DCI (without cracks, No. 2).

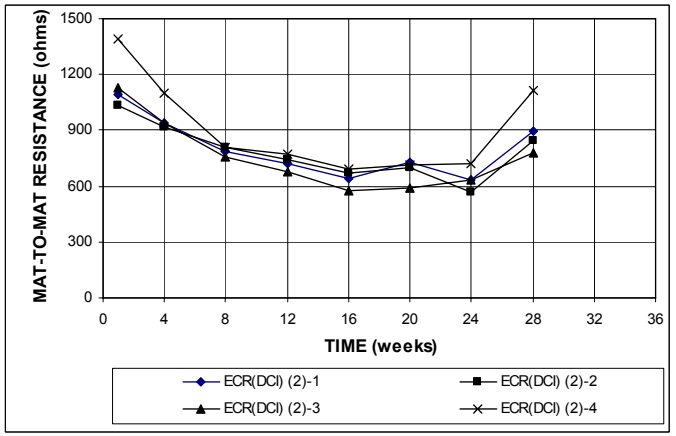

Figure B.76 – Mat-to-mat resistance as measured in the field test for specimens with ECR in concrete with DCI (with cracks, No. 2).

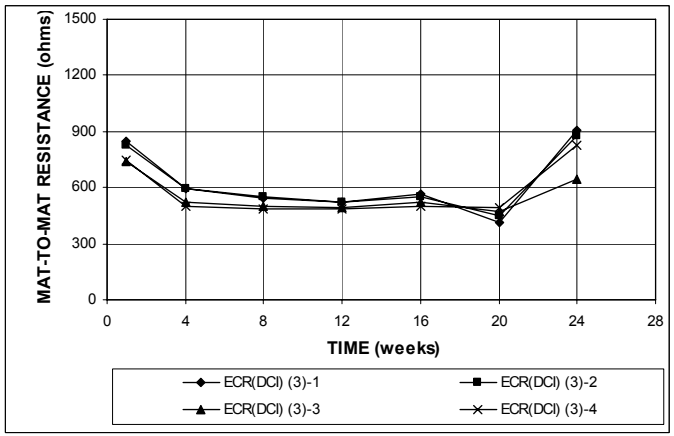

Figure B.77 – Mat-to-mat resistance as measured in the field test for specimens with ECR in concrete with DCI (without cracks, No. 3).

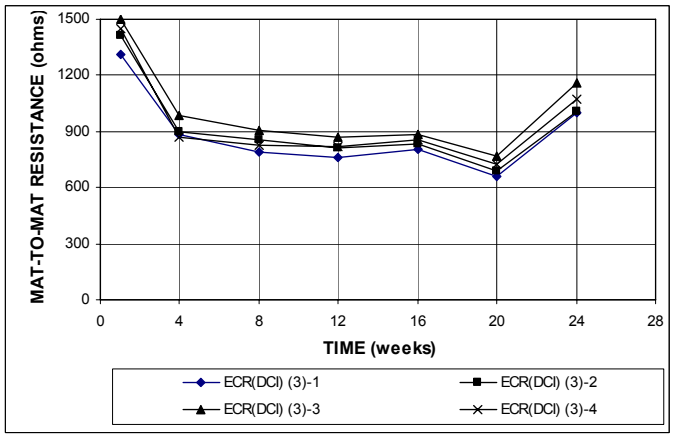

Figure B.78 – Mat-to-mat resistance as measured in the field test for specimens with ECR in concrete with DCI (with cracks, No.3).

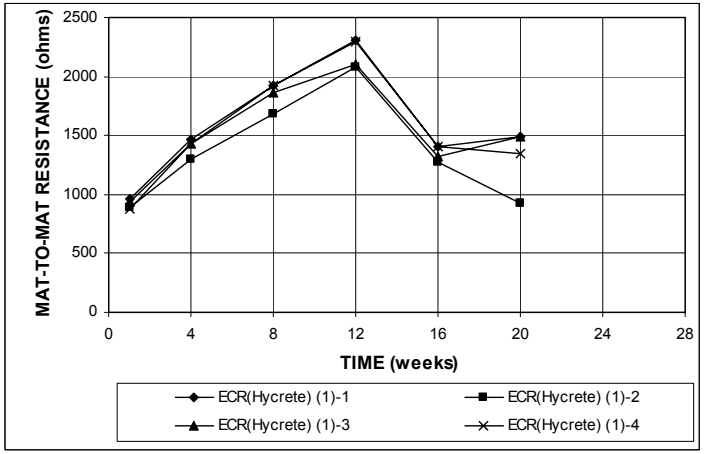

Figure B.79 – Mat-to-mat resistance as measured in the field test for specimens with ECR in concrete with Hycrete (without cracks, No. 1).

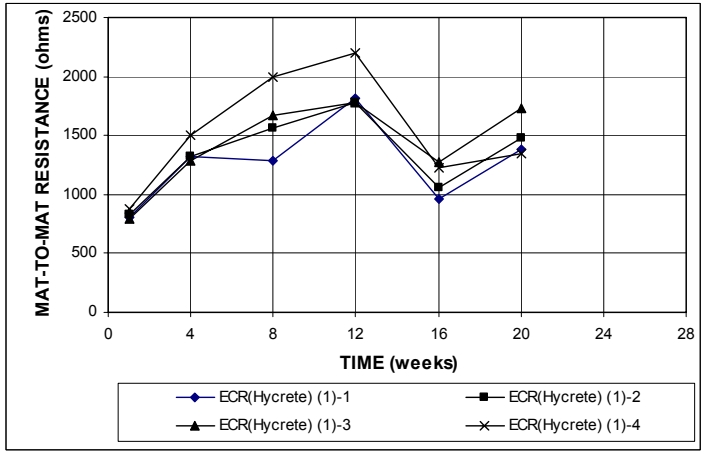

Figure B.80 – Mat-to-mat resistance as measured in the field test for specimens with ECR in concrete with Hycrete (with cracks, No.1).

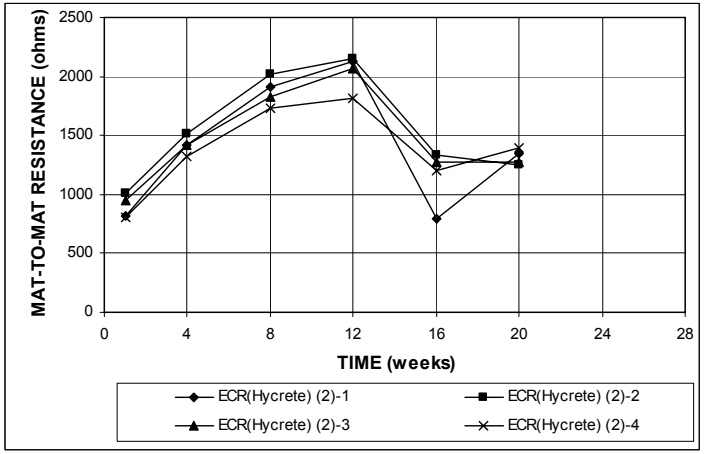

Figure B.81 – Mat-to-mat resistance as measured in the field test for specimens with ECR in concrete with Hycrete (without cracks, No. 2).

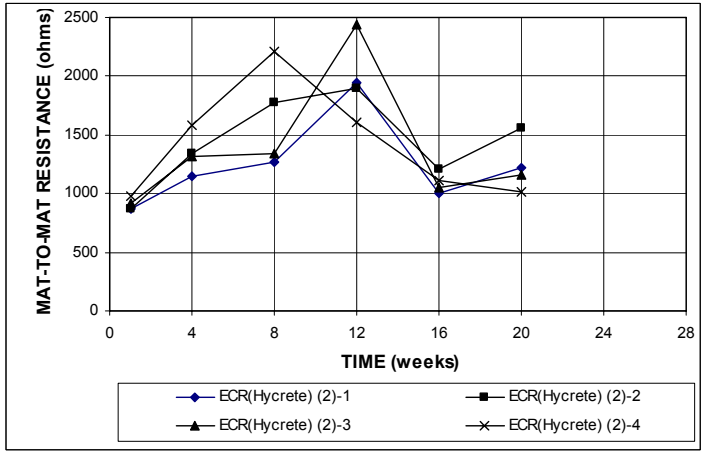

Figure B.82 – Mat-to-mat resistance as measured in the field test for specimens with ECR in concrete with Hycrete (with cracks, No. 2).

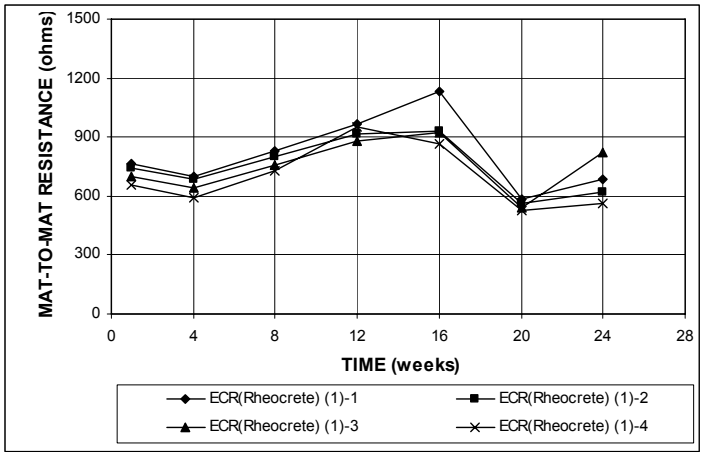

Figure B.83 – Mat-to-mat resistance as measured in the field test for specimens with ECR in concrete with Rheocrete (without cracks, No. 1).

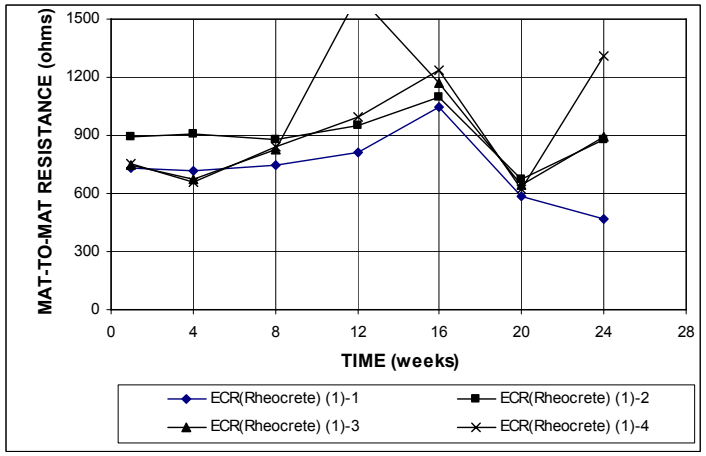

Figure B.84 – Mat-to-mat resistance as measured in the field test for specimens with ECR in concrete with Rheocrete (with cracks, No.1).

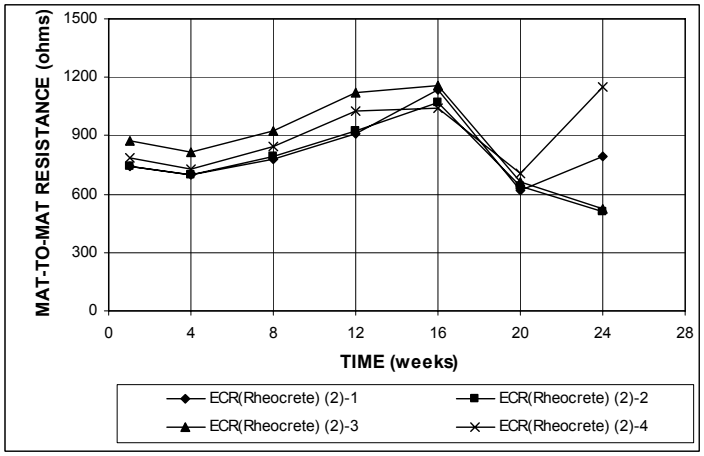

Figure B.85 – Mat-to-mat resistance as measured in the field test for specimens with ECR in concrete with Rheocrete (without cracks, No. 2).

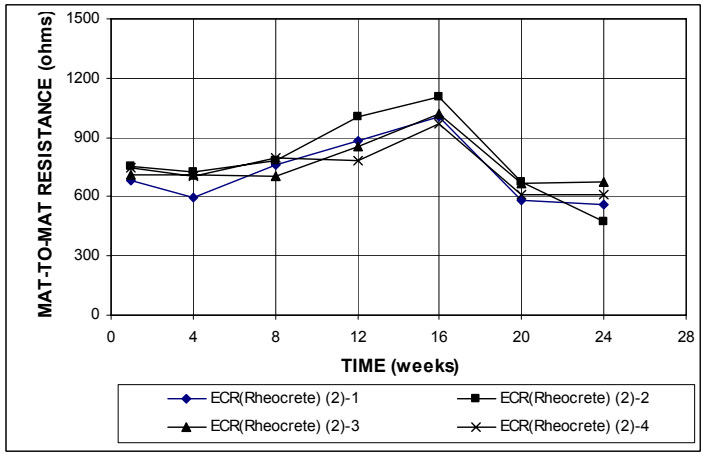

Figure B.86 – Mat-to-mat resistance as measured in the field test for specimens with ECR in concrete with Rheocrete (with cracks, No. 2).

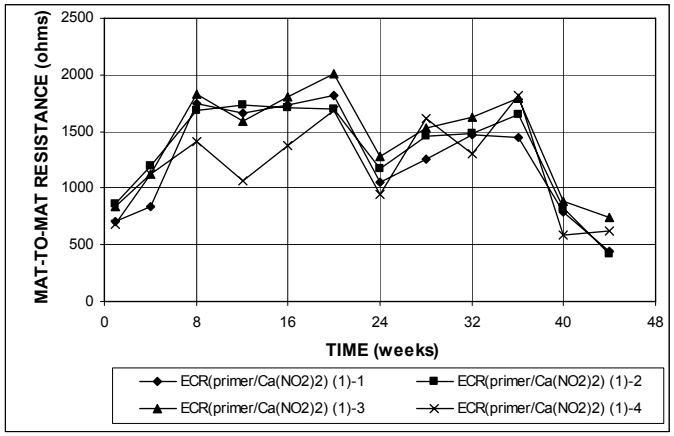

Figure B.87 – Mat-to-mat resistance as measured in the field test for specimens with ECR with a primer containing calcium nitrite (without cracks, No. 1).

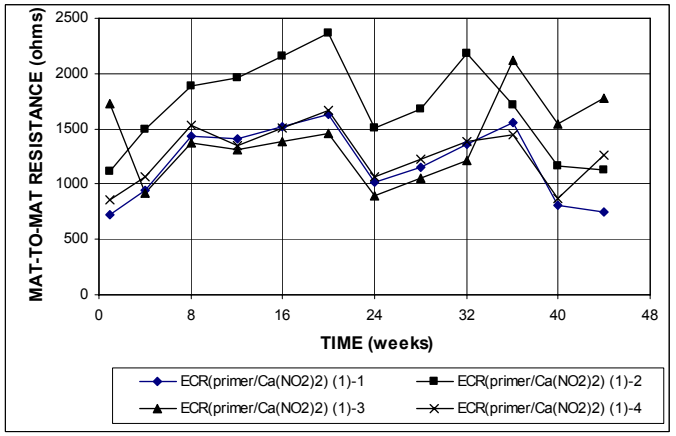

Figure B.88 – Mat-to-mat resistance as measured in the field test for specimens with ECR with a primer containing calcium nitrite (with cracks, No.1).

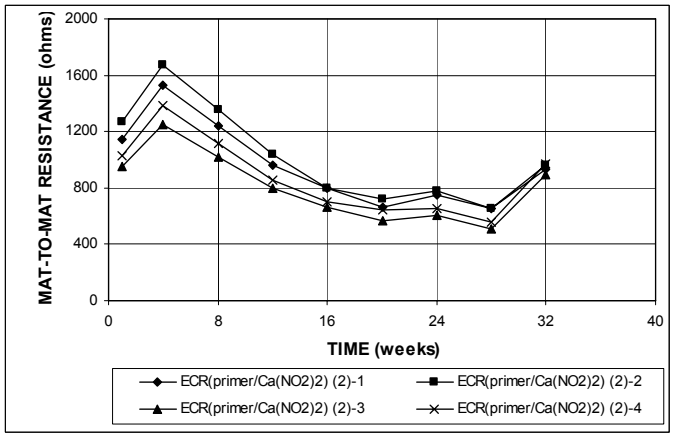

Figure B.89 – Mat-to-mat resistance as measured in the field test for specimens with ECR with a primer containing calcium nitrite (without cracks, No. 2).

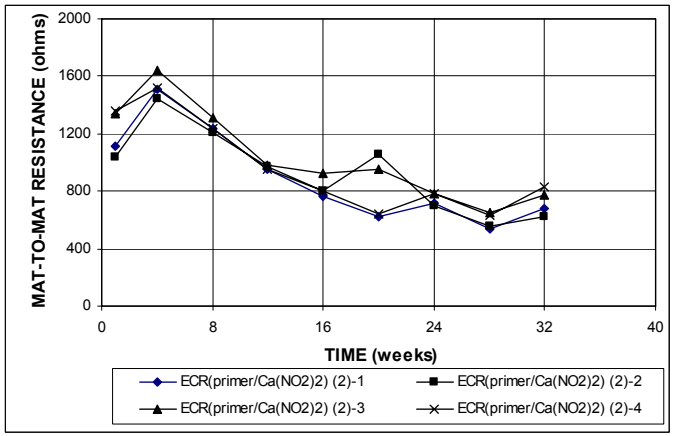

Figure B.90 – Mat-to-mat resistance as measured in the field test for specimens with ECR with a primer containing calcium nitrite (with cracks, No. 2).

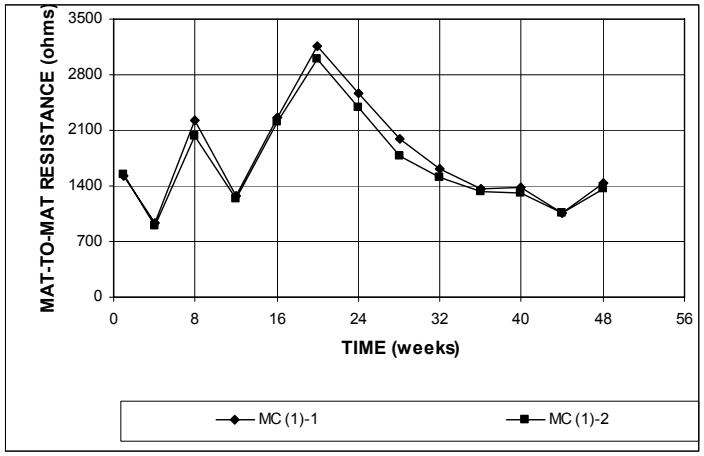

Figure B.91 – Mat-to-mat resistance as measured in the field test for specimens with multiple coated bars (without cracks, No. 1).

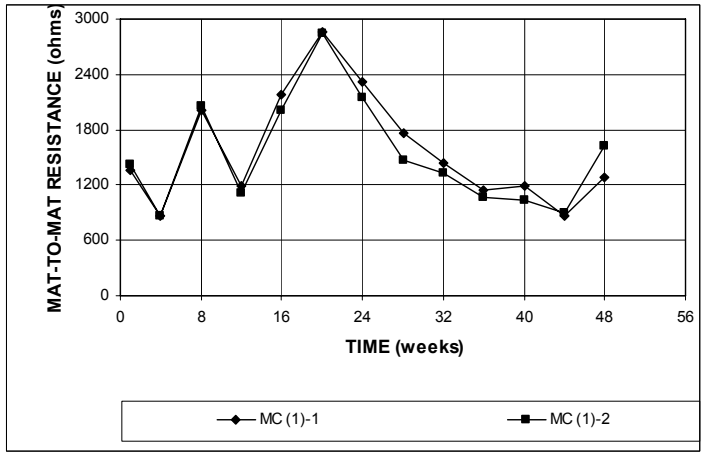

Figure B.92 – Mat-to-mat resistance as measured in the field test for specimens with multiple coated bars (with cracks, No.1).

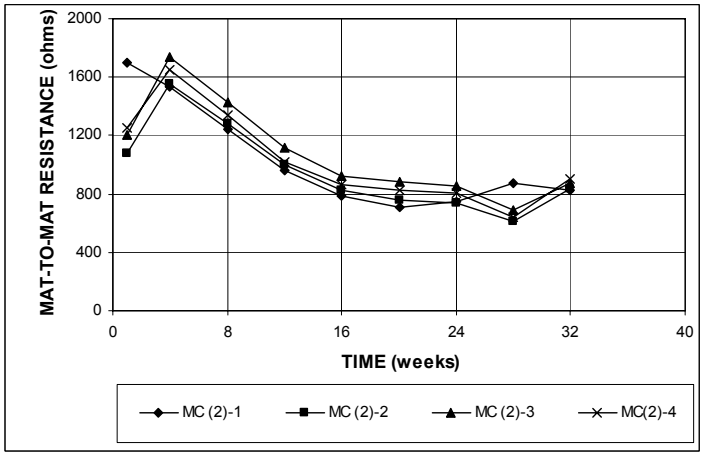

Figure B.93 – Mat-to-mat resistance as measured in the field test for specimens with multiple coated bars (without cracks, No. 2).

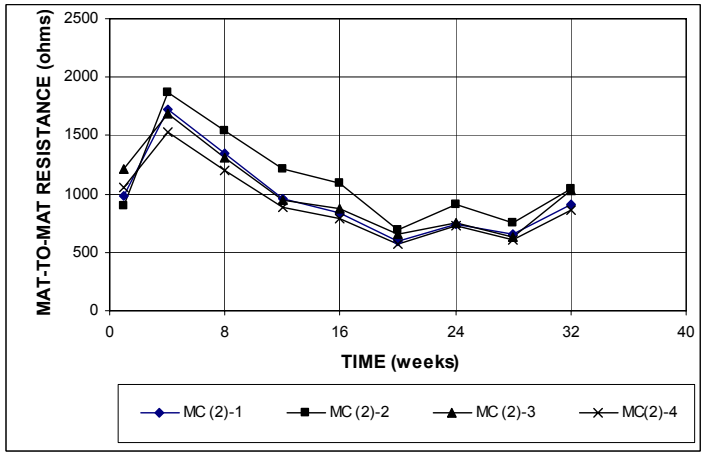

Figure B.94 – Mat-to-mat resistance as measured in the field test for specimens with multiple coated bars (with cracks, No. 2).

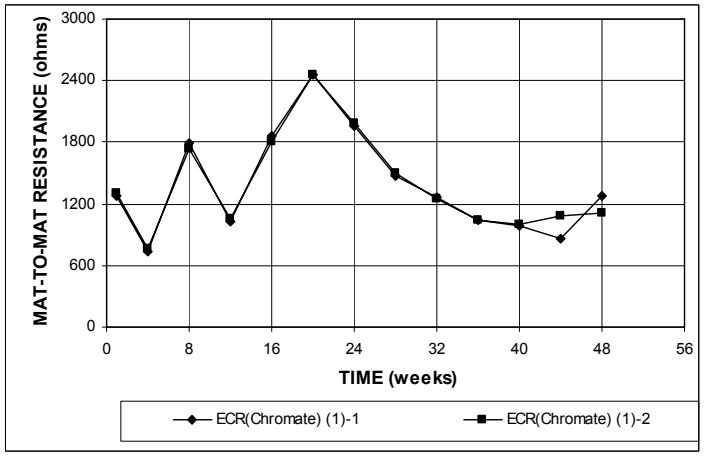

Figure B.95 – Mat-to-mat resistance as measured in the field test for specimens with ECR with chromate pretreatment (without cracks, No. 1).

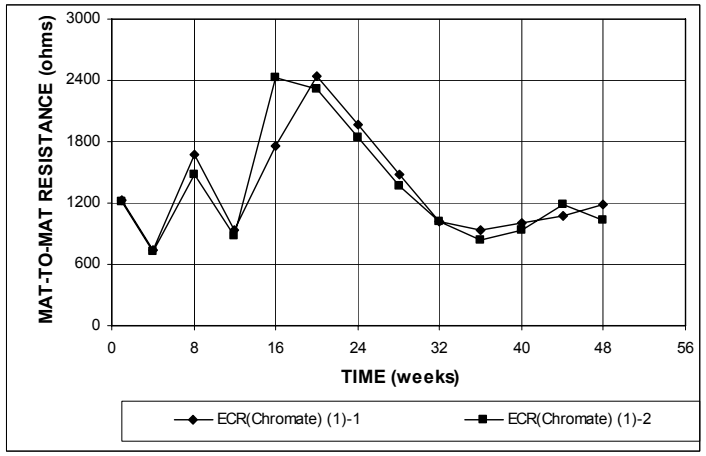

Figure B.96 – Mat-to-mat resistance as measured in the field test for specimens with ECR with chromate pretreatment (with cracks, No.1).

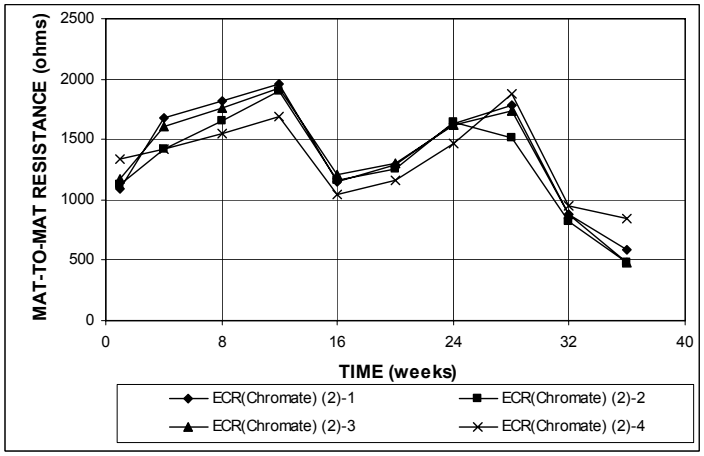

Figure B.97 – Mat-to-mat resistance as measured in the field test for specimens with ECR with chromate pretreatment (without cracks, No. 2).

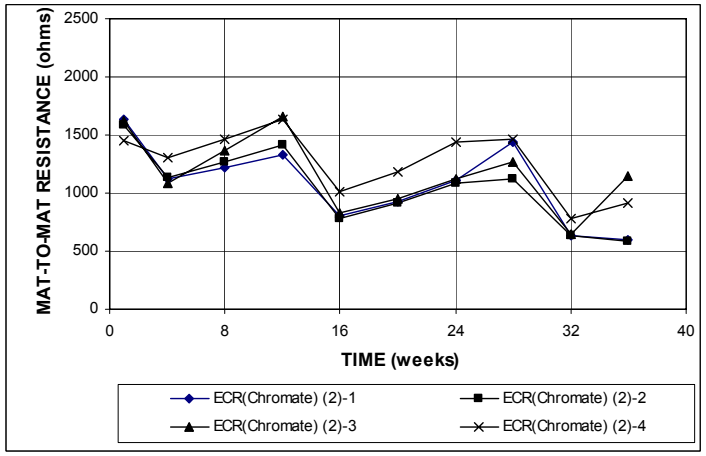

Figure B.98 – Mat-to-mat resistance as measured in the field test for specimens with ECR with chromate pretreatment (with cracks, No. 2).

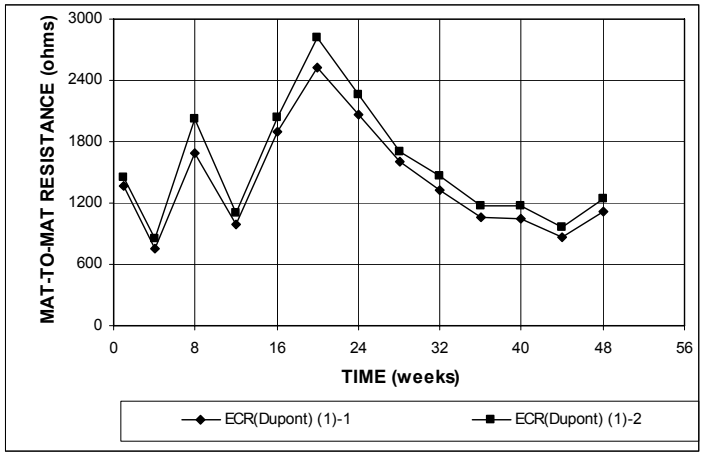

Figure B.99 – Mat-to-mat resistance as measured in the field test for specimens with ECR with DuPont coating (without cracks, No. 1).

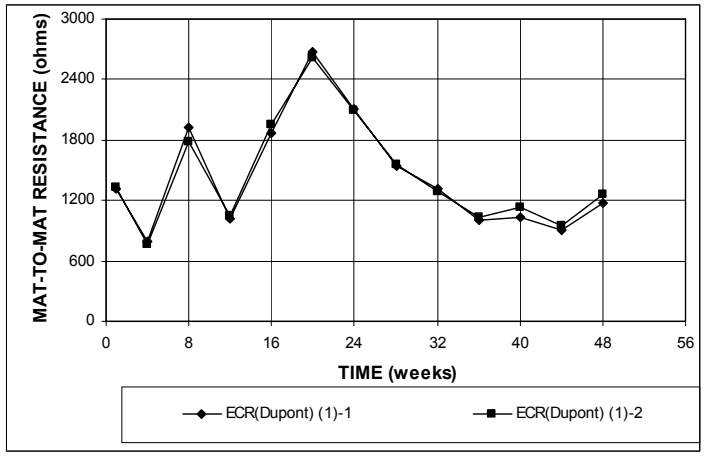

Figure B.100 – Mat-to-mat resistance as measured in the field test for specimens with ECR with DuPont coating (with cracks, No.1).

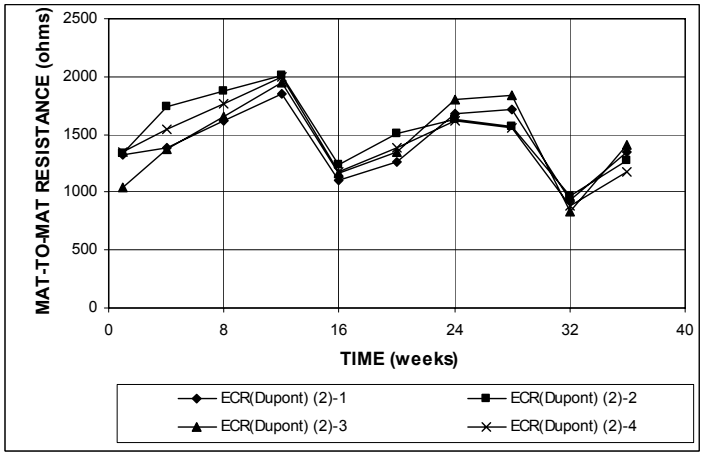

Figure B.101 – Mat-to-mat resistance as measured in the field test for specimens with ECR with DuPont coating (without cracks, No. 2).

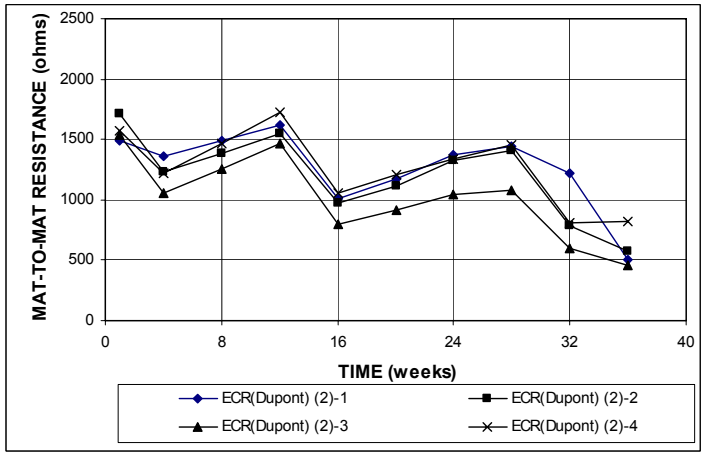

Figure B.102 – Mat-to-mat resistance as measured in the field test for specimens with ECR with DuPont coating (with cracks, No. 2).

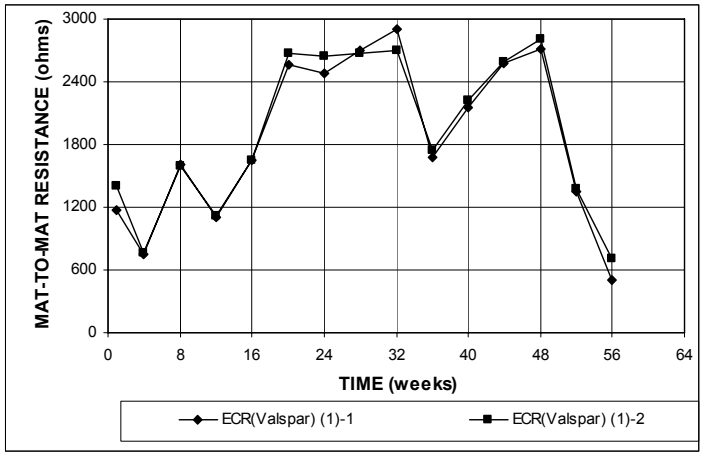

Figure B.103 – Mat-to-mat resistance as measured in the field test for specimens with ECR with Valspar coating (without cracks, No. 1).

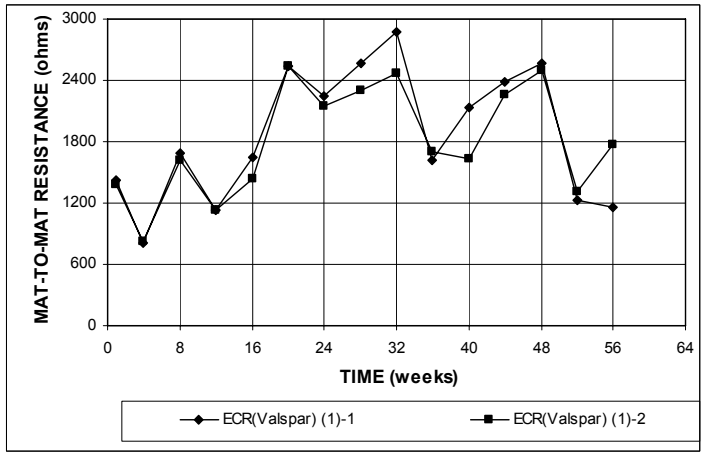

Figure B.104 – Mat-to-mat resistance as measured in the field test for specimens with ECR with Valspar coating (with cracks, No.1).

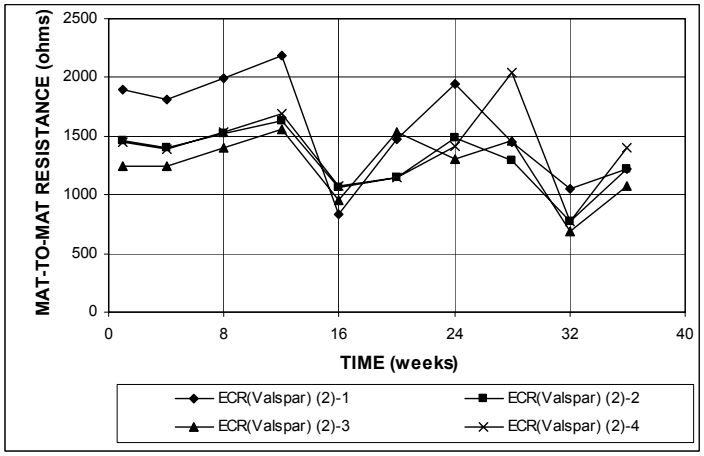

Figure B.105 – Mat-to-mat resistance as measured in the field test for specimens with ECR with Valspar coating (without cracks, No. 2).

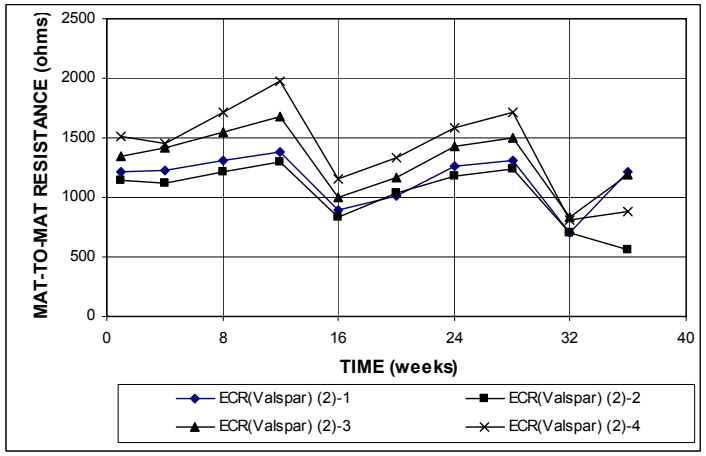

Figure B.106 – Mat-to-mat resistance as measured in the field test for specimens with ECR with Valspar coating (with cracks, No. 2).

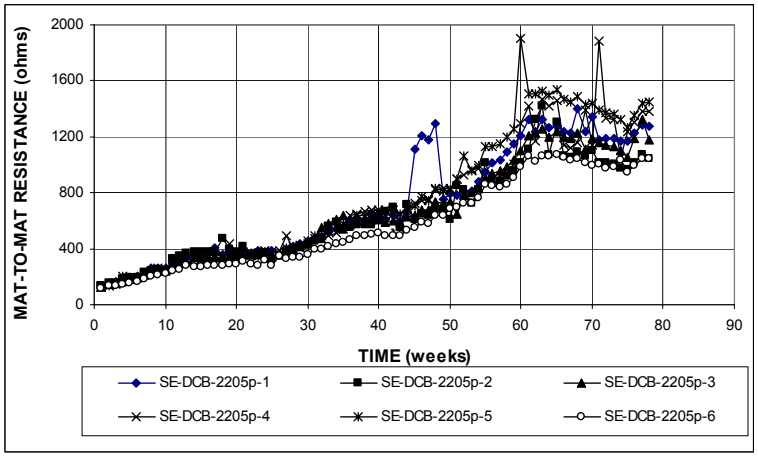

Figure B.107 – Mat-to-mat resistance as measured in the Southern Exposure test for specimens with 2205p stainless steel for Doniphan County Bridge.

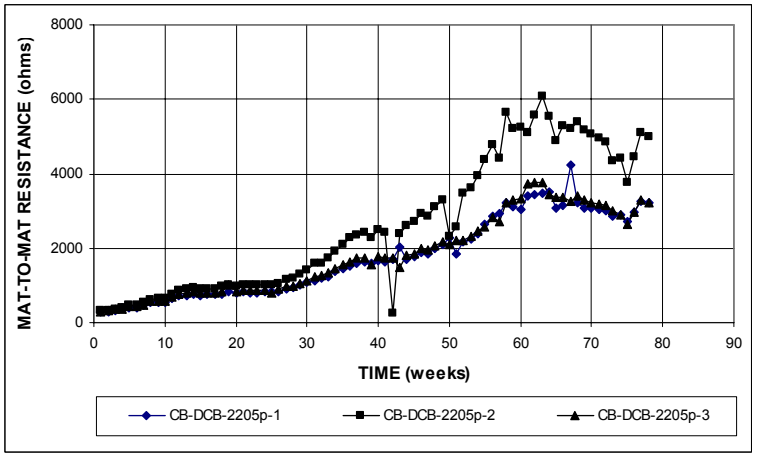

Figure B.108 – Mat-to-mat resistance as measured in the cracked beam test for specimens with 2205p stainless steel for Doniphan County Bridge.

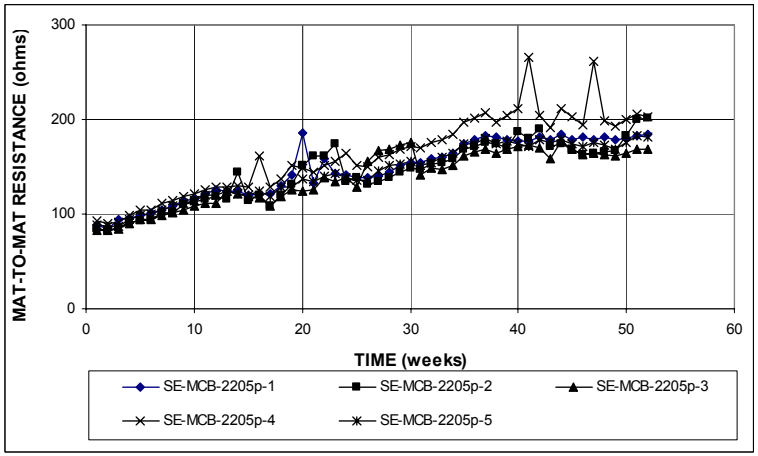

Figure B.109 – Mat-to-mat resistance as measured in the Southern Exposure test for specimens with 2205p stainless steel for Mission Creek Bridge.

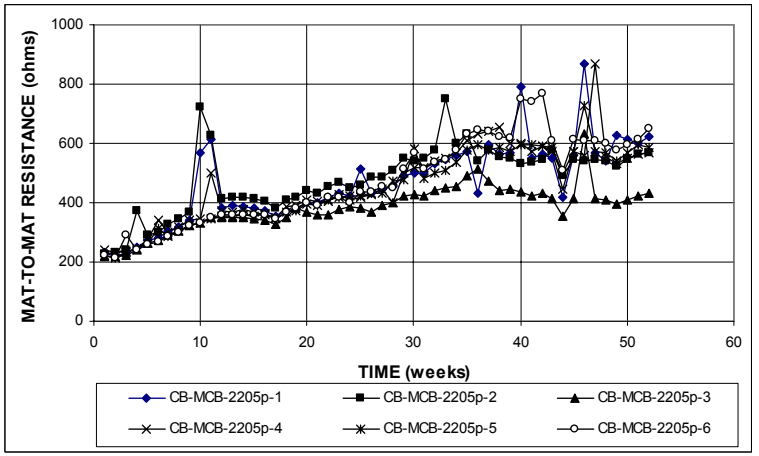

Figure B.110 – Mat-to-mat resistance as measured in the cracked beam test for specimens with 2205p stainless steel for Mission Creek Bridge.

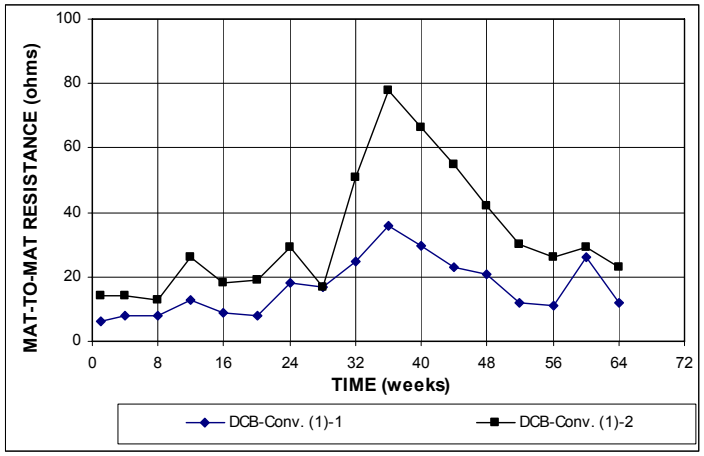

Figure B.111 – Mat-to-mat resistance as measured in field test for specimens with conventional steel (No. 1) for Doniphan County Bridge.

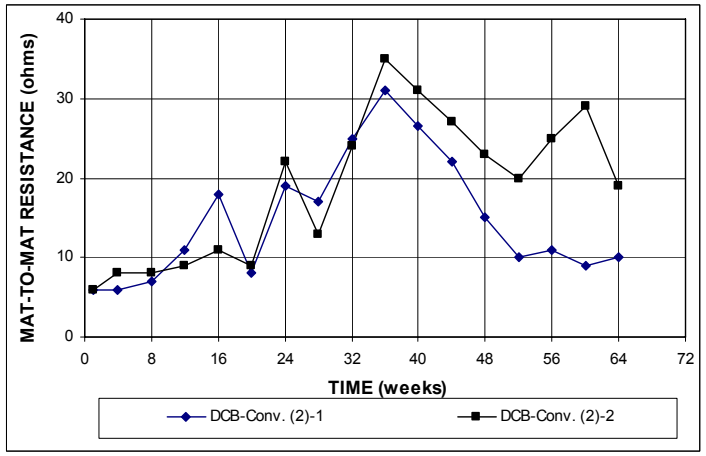

Figure B.112 – Mat-to-mat resistance as measured in the field test for specimens with conventional steel (No. 2) for Doniphan County Bridge.

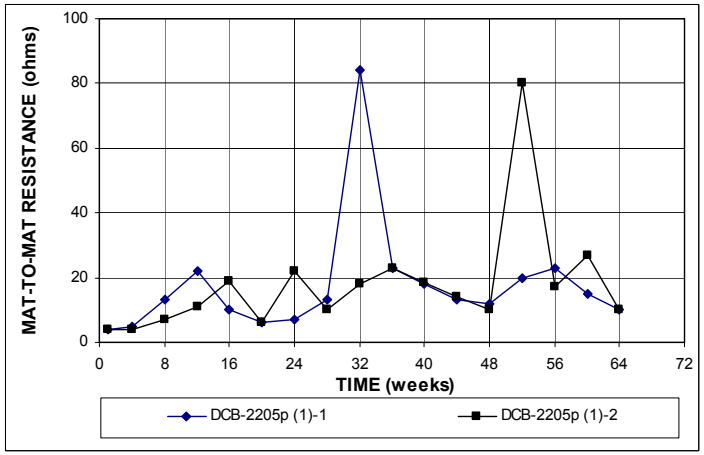

Figure B.113 – Mat-to-mat resistance as measured in the field test for specimens with 2205p stainless steel (No. 1) for Doniphan County Bridge.

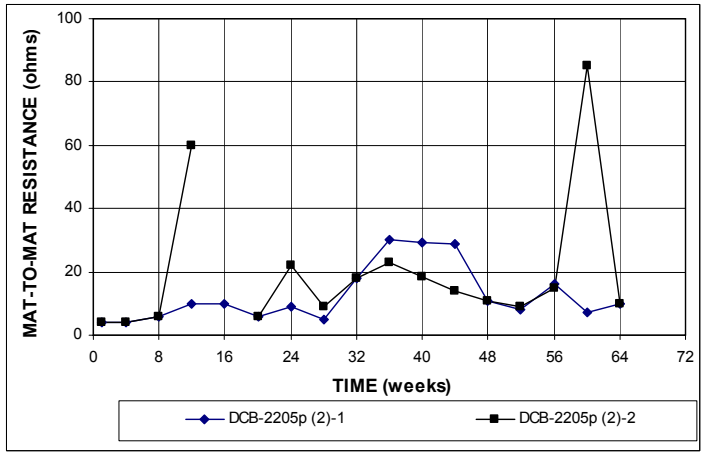

Figure B.114 – Mat-to-mat resistance as measured in the field test for specimens with 2205p stainless steel (No. 2) for Doniphan County Bridge.

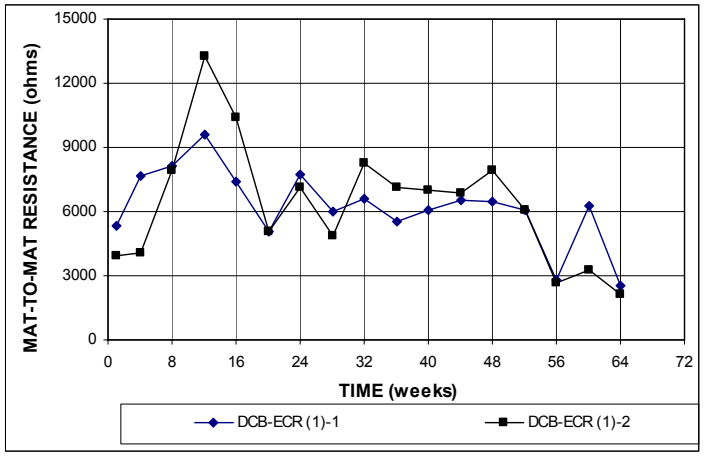

Figure B.115 – Mat-to-mat resistance as measured in field test for specimens with ECR (No. 1) for Doniphan County Bridge.

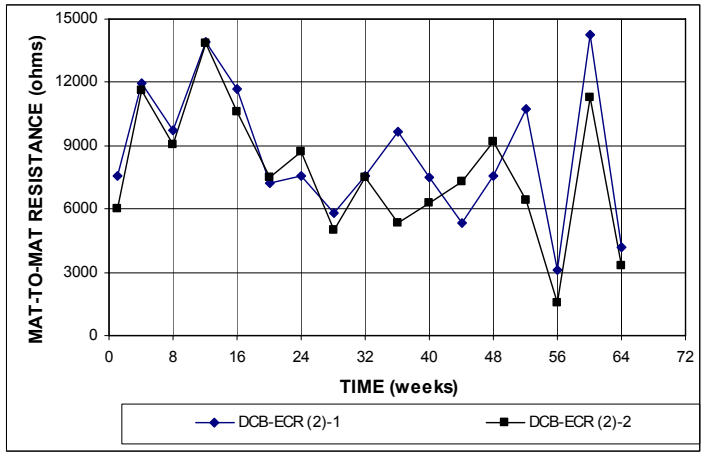

Figure B.116 – Mat-to-mat resistance as measured in the field test for specimens with ECR (No. 2) for Doniphan County Bridge.

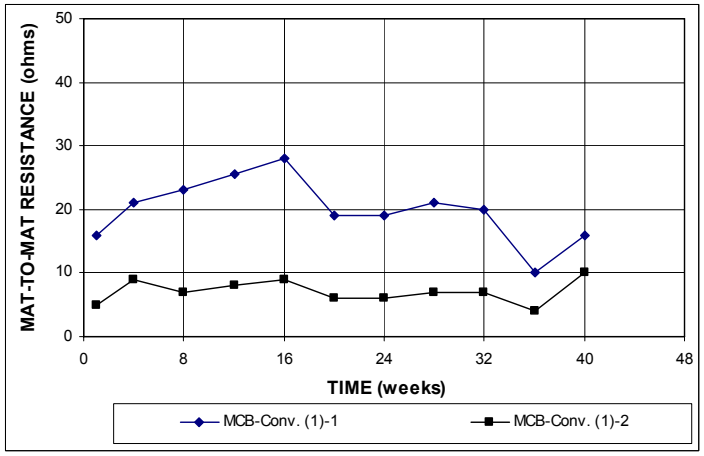

Figure B.117 – Mat-to-mat resistance as measured in the field test for specimens with conventional steel without cracks (No. 1) for Mission Creek Bridge.

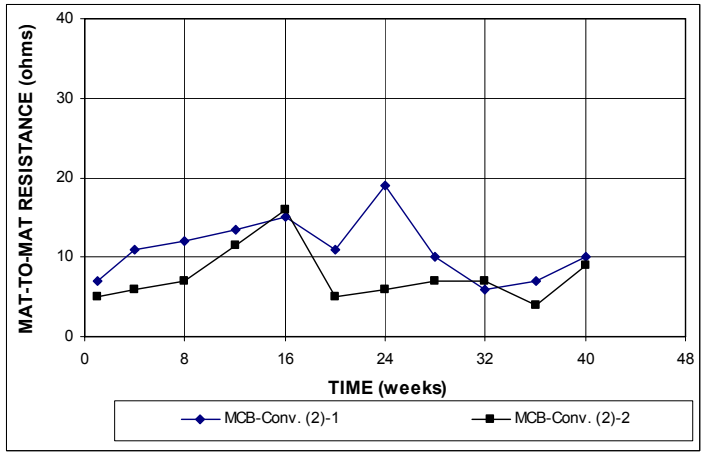

Figure B.118 – Mat-to-mat resistance as measured in the field test for specimens with conventional steel with cracks (No. 2) for Mission Creek Bridge.

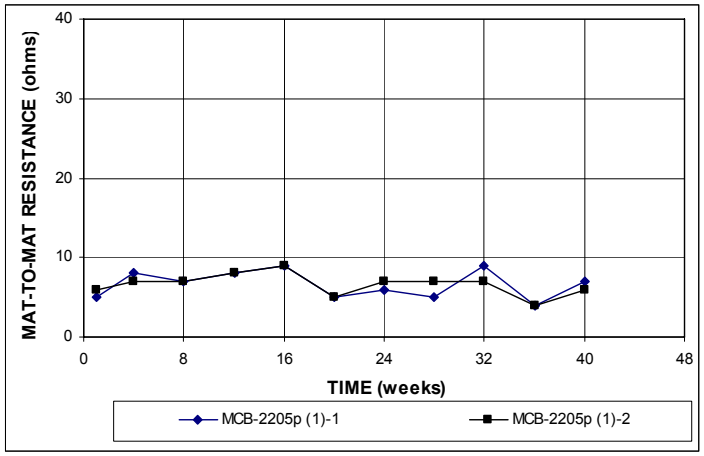

Figure B.119 – Mat-to-mat resistance as measured in the field test for specimens with 2205p stainless steel without cracks (No. 1) for Mission Creek Bridge.

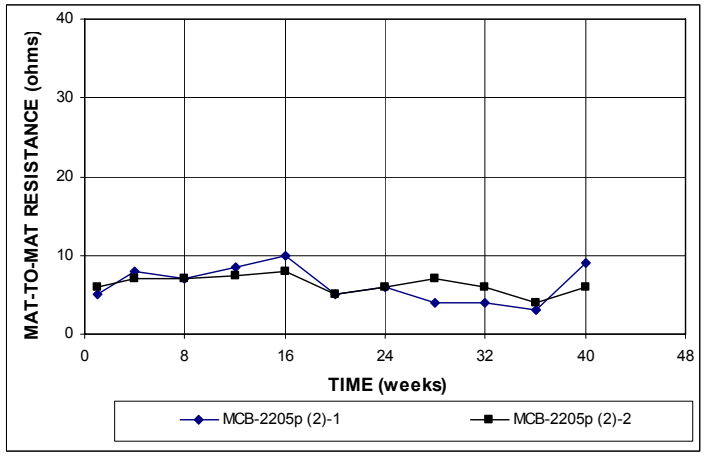

Figure B.120 – Mat-to-mat resistance as measured in the field test for specimens with 2205p stainless steel with cracks (No. 2) for Mission Creek Bridge.

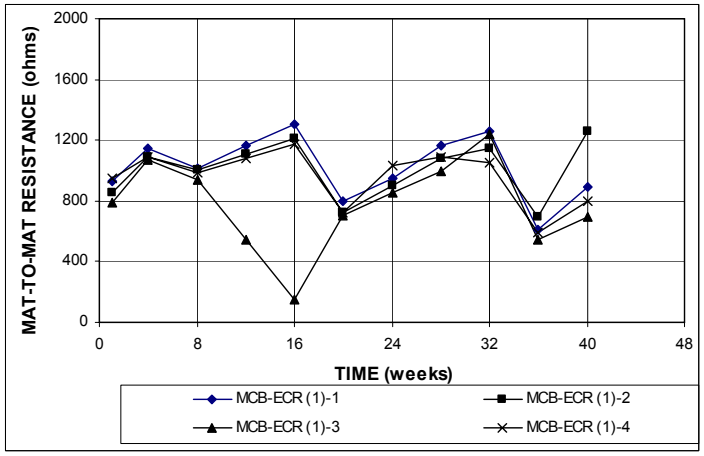

Figure B.121 – Mat-to-mat resistance as measured in the field test for specimens with ECR without cracks (No. 1) for Mission Creek Bridge.

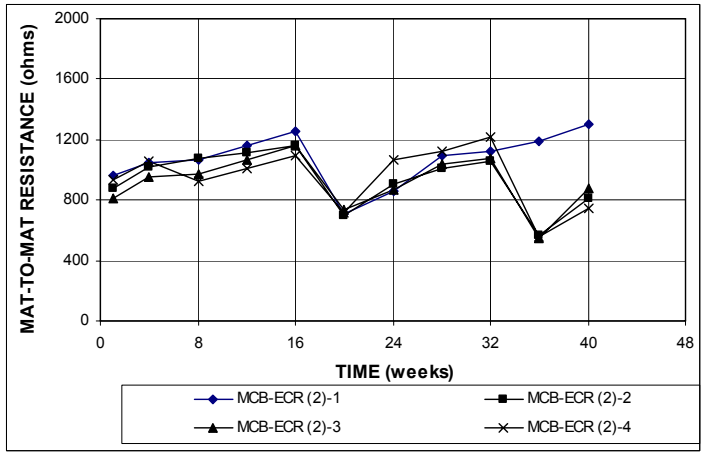

Figure B.122 – Mat-to-mat resistance as measured in the field test for specimens with ECR with cracks (No. 2) for Mission Creek Bridge.

APPENDIX C

Table C.1 – Test program for macrocell test with bare bar specimens

Specimen designation	NaCl ion concentration	Steel type	Number of tests
M-N	1.6 m	N	5
M-T	1.6 m	T	5
M-CRPT1	1.6 m	CRPT1	5
M-CRPT2	1.6 m	CRPT2	5
M-CRT	1.6 m	CRT	5
M-2101(1)	1.6 m	2101(1)	5
M-2101(1)p	1.6 m	2101(1)p	5
M-2101(2)	1.6 m	2101(2)	6
M-2101(2)p	1.6 m	2101(2)p	6
M-2101(2)s	1.6 m	2101(2)	6
M-2205	1.6 m	2205	5
M-2205p	1.6 m	2205p	5
M-N3	1.6 m	N3	6
M-MMFX(1)	1.6 m	MMFX	6
M-MMFX(2)	1.6 m	MMFX	6
M-MMFXb	1.6 m	MMFX	6
M-2101(1)h	6.04 m	2101(1)	5
M-2101(1)ph	6.04 m	2101(1)p	5
M-2101(2)h	6.04 m	2101(2)	6
M-2101(2)ph	6.04 m	2101(2)p	6
M-2101(2)sh	6.04 m	2101(2)s	6
M-2205h	6.04 m	2205	6
M-2205ph	6.04 m	2205p	5
M-N3h	6.04 m	N3	5
M-MMFXsh	6.04 m	MMFX	6

* M - A

M: macrocell test

A: steel type → N, N2, and N3: conventional normalized steel, T: conventional Thermex-treated steel, CRPT1: microalloyed steel with a high phosphorus content (0.117%), Thermex treated, CRPT2: microalloyed steel with a high phosphorus content (0.100%), Thermex treated, CRT: microalloyed steel with normal phosphorus content, Thermex treated, MMFX: MMFX-2 microcomposite steel, ECR: epoxy-coated steel, 2101(1) and 2101(2): Duplex stainless steel (21% chromium, 1% nickel), 2205: Duplex stainless steel (22% chromium, 5% nickel), p: pickled, s: sandblasted, b: bent bars at the anode, h: 6.04 m ion concentration.

Table C.2 – Test program for macrocell test with mortar specimens

Specimen designation	Type of specimen	NaCl ion concentration	Steel type	w/c ratio	Corrosion inhibitor	Number of tests
M-N-50	Lollipop	1.6 m	N	0.50	-	5
M-T-50	Lollipop	1.6 m	T	0.50	-	5
M-CRPT1-50	Lollipop	1.6 m	CRPT1	0.50	-	5
M-CRPT2-50	Lollipop	1.6 m	CRPT2	0.50	-	5
M-CRT-50	Lollipop	1.6 m	CRT	0.50	-	5
M-Nc-50	Lollipop	1.6 m	N	0.50	-	4
M-Tc-50	Lollipop	1.6 m	T	0.50	-	4
M-CPRT1c-50	Lollipop	1.6 m	CRPT1	0.50	-	4
M-CRPT2c-50	Lollipop	1.6 m	CRPT2	0.50	-	4
M-CRTc-50	Lollipop	1.6 m	CRT	0.50	-	4
M-N2-50	Mortar-wrapped	1.6 m	N2	0.50	-	5
M-2101(1)-50	Mortar-wrapped	1.6 m	2101(1)	0.50	-	4
M-2101(1)p-50	Mortar-wrapped	1.6 m	2101(1)p	0.50	-	4
M-2101(2)-50	Mortar-wrapped	1.6 m	2101(2)	0.50	-	6
M-2101(2)p-50	Mortar-wrapped	1.6 m	2101(2)p	0.50	-	6
M-2205-50	Mortar-wrapped	1.6 m	2205	0.50	-	6
M-2205p-50	Mortar-wrapped	1.6 m	2205p	0.50	-	6
M-N3-50	Mortar-wrapped	1.6 m	N3	0.50	-	6
M-MMFX-50	Mortar-wrapped	1.6 m	MMFX	0.50	-	6
M-MMFX/N3-50	Mortar-wrapped	1.6 m	MMFX/N3	0.50	-	3
M-N3/MMFX-50	Mortar-wrapped	1.6 m	N3/MMFX	0.50	-	3
M-ECR-50	Mortar-wrapped	1.6 m	ECR	0.50	-	6
M-N-45	Lollipop	1.6 m	N	0.45	-	5
M-N-RH45	Lollipop	1.6 m	N	0.45	Rheocrete 222+	5
M-N-DC45	Lollipop	1.6 m	N	0.45	DCI-S	5
M-N-35	Lollipop	1.6 m	N	0.35	-	5
M-N-RH35	Lollipop	1.6 m	N	0.35	Rheocrete 222+	5
M-N-DC35	Lollipop	1.6 m	N	0.35	DCI-S	5

* M – A - B

M: macrocell test

A: steel type → N, N2, and N3: conventional normalized steel, T: conventional Thermex-treated steel, CRPT1: microalloyed steel with a high phosphorus content (0.117%), Thermex treated, CRPT2: microalloyed steel with a high phosphorus content (0.100%), Thermex treated, CRT: microalloyed steel with normal phosphorus content, Thermex treated, MMFX: MMFX-2 microcomposite steel, ECR: epoxy-coated steel, 2101(1) and 2101(2): Duplex stainless steel (21% chromium, 1% nickel), 2205: Duplex stainless steel (22% chromium, 5% nickel), p: pickled, c: epoxy-coated caps on the end of the bar.

B: mix design → 50: *w/c* ratio of 0.50 and no inhibitor, 45: *w/c* ratio of 0.45 and no inhibitor, RH45: *w/c* ratio of 0.45 and Rheocrete 222+, DC45: *w/c* ratio of 0.45 and DCI-S, 35: *w/c* ratio of 0.35 and no inhibitor, RH35: *w/c* ratio of 0.35 and Rheocrete 222+, DC35: *w/c* ratio of 0.35 and DCI-S.

Table C.3 – Test program for the Southern Exposure test

Specimen designation	Steel type	w/c ratio	Corrosion inhibitor	Number of tests
SE-N-45	N	0.45	-	6
SE-T-45	T	0.45	-	6
SE-CRPT1-45	CRPT1	0.45	-	6
SE-CRPT2-45	CRPT2	0.45	-	6
SE-CRT-45	CRT	0.45	-	6
SE-N/CRPT1-45	N/CRPT1	0.45	-	6
SE-CRPT1/N/45	CRPT1/N	0.45	-	6
SE-2101(1)-45	2101(1)	0.45	-	6
SE-2101(1)p-45	2101(1)p	0.45	-	6
SE-2101(2)-45	2101(2)	0.45	-	6
SE-2101(2)p-45	2101(2)p	0.45	-	6
SE-2205-45	2205	0.45	-	6
SE-2205p-45	2205p	0.45	-	6
SE-2205/N2-45	2205/N2	0.45	-	3
SE-N2/2205-45	N2/2205	0.45	-	3
SE-N3-45	N3	0.45	-	6
SE-MMFX-45	MMFX	0.45	-	6
SE-MMFXb-45	MMFX	0.45	-	3
SE-MMFX/N3-45	MMFX/N3	0.45	-	3
SE-N3/MMFX-45	N3/MMFX	0.45	-	3
SE-ECR	ECR	0.45	-	6
SE-N-RH45	N	0.45	Rheocrete 222+	3
SE-N-DC45	N	0.45	DCI-S	3
SE-N-35	N	0.35	-	3
SE-N-RH35	N	0.35	Rheocrete 222+	3
SE-N-DC35	N	0.35	DCI-S	3
SE-T-RH45	T	0.45	Rheocrete 222+	3
SE-T-DC45	T	0.45	DCI-S	3
SE-T-35	T	0.35	-	3
SE-T-RH35	T	0.35	Rheocrete 222+	3
SE-T-DC35	T	0.35	DCI-S	3

* SE – A - B

SE: Southern Exposure test

A: steel type → N, N2, and N3: conventional normalized steel, T: conventional Thermex-treated steel, CRPT1: microalloyed steel with a high phosphorus content (0.117%), Thermex treated, CRPT2: microalloyed steel with a high phosphorus content (0.100%), Thermex treated, CRT: microalloyed steel with normal phosphorus content, Thermex treated, MMFX: MMFX-2 microcomposite steel, ECR: epoxy-coated steel, 2101(1) and 2101(2): Duplex stainless steel (21% chromium, 1% nickel), 2205: Duplex stainless steel (22% chromium, 5% nickel), p: pickled, b: bent bars on the top mat.

B: mix design → 45: *w/c* ratio of 0.45 and no inhibitor, RH45: *w/c* ratio of 0.45 and Rheocrete 222+, DC45: *w/c* ratio of 0.45 and DCI-S, 35: *w/c* ratio of 0.35 and no inhibitor, RH35: *w/c* ratio of 0.35 and Rheocrete 222+, DC35: *w/c* ratio of 0.35 and DCI-S.

Table C.4 – Test program for the cracked beam test

Specimen designation	Steel type	w/c ratio	Corrosion inhibitor	Number of tests
CB-N-45	N	0.45	-	6
CB-T-45	T	0.45	-	6
CB-CRPT1-45	CRPT1	0.45	-	6
CB-CRPT2-45	CRPT2	0.45	-	6
CB-CRT-45	CRT	0.45	-	6
CB-2101(1)-45	2101(1)	0.45	-	3
CB-2101(1)p-45	2101(1)p	0.45	-	3
CB-2101(2)-45	2101(2)	0.45	-	6
CB-2101(2)p-45	2101(2)p	0.45	-	6
CB-2205-45	2205	0.45	-	5
CB-2205p-45	2205p	0.45	-	5
CB-N3-45	N3	0.45	-	6
CB-MMFX-45	MMFX	0.45	-	6
CB-ECR	ECR	0.45	-	6
CB-N-RH45	N	0.45	Rheocrete 222+	3
CB-N-DC45	N	0.45	DCI-S	3
CB-N-35	N	0.35	-	3
CB-N-RH35	N	0.35	Rheocrete 222+	3
CB-N-DC35	N	0.35	DCI-S	3
CB-T-RH45	T	0.45	Rheocrete 222+	3
CB-T-DC45	T	0.45	DCI-S	3
CB-T-35	T	0.35	-	3
CB-T-RH35	T	0.35	Rheocrete 222+	3
CB-T-DC35	T	0.35	DCI-S	3

* CB – A - B

CB: Cracked beam test

A: steel type → N and N3: conventional normalized steel, T: conventional Thermex-treated steel, CRPT1: microalloyed steel with a high phosphorus content (0.117%), Thermex treated, CRPT2: microalloyed steel with a high phosphorus content (0.100%), Thermex treated, CRT: microalloyed steel with normal phosphorus content, Thermex treated, MMFX: MMFX-2 microcomposite steel, ECR: epoxy-coated steel, 2101(1) and 2101(2): Duplex stainless steel (21% chromium, 1% nickel), 2205: Duplex stainless steel (22% chromium, 5% nickel), p: pickled, b: bent bars on the top mat.

B: mix design → 45: *w/c* ratio of 0.45 and no inhibitor, RH45: *w/c* ratio of 0.45 and Rheocrete 222+, DC45: *w/c* ratio of 0.45 and DCI-S, 35: *w/c* ratio of 0.35 and no inhibitor, RH35: *w/c* ratio of 0.35 and Rheocrete 222+, DC35: *w/c* ratio of 0.35 and DCI-S.

Table C.5 – Test program for the ASTM G 109 test

Specimen designation	Steel type	w/c ratio	Corrosion inhibitor	Number of tests
G-N-45	N	0.45	-	6
G-T-45	T	0.45	-	6
G-CRPT1-45	CRPT1	0.45	-	6
G-CRPT2-45	CRPT2	0.45	-	6
G-CRT-45	CRT	0.45	-	6
G-N-RH45	N	0.45	Rheocrete 222+	3
G-N-DC45	N	0.45	DCI-S	3
G-N-35	N	0.35	-	3
G-N-RH35	N	0.35	Rheocrete 222+	3
G-N-DC35	N	0.35	DCI-S	3
G-T-RH45	T	0.45	Rheocrete 222+	3
G-T-DC45	T	0.45	DCI-S	3
G-T-35	T	0.35	-	3
G-T-RH35	T	0.35	Rheocrete 222+	3
G-T-DC35	T	0.35	DCI-S	3

* G – A - B

G: ASTM G 109 test

A: steel type → N, N2, and N3: conventional normalized steel, T: conventional, Thermex-treated steel, CRPT1: microalloyed steel with a high phosphorus content (0.117%), Thermex treated, CRPT2: microalloyed steel with a high phosphorus content (0.100%), Thermex treated, CRT: microalloyed steel with normal phosphorus content, Thermex treated, MMFX: MMFX-2 microcomposite steel, ECR: epoxy-coated steel, 2101(1) and 2101(2): Duplex stainless steel (21% chromium, 1% nickel), 2205: Duplex stainless steel (22% chromium, 5% nickel), p: pickled, b: bent bars on the top mat.

B: mix design → 45: *w/c* ratio of 0.45 and no inhibitor, RH45: *w/c* ratio of 0.45 and Rheocrete 222+, DC45: *w/c* ratio of 0.45 and DCI-S, 35: *w/c* ratio of 0.35 and no inhibitor, RH35: *w/c* ratio of 0.35 and Rheocrete 222+, DC35: *w/c* ratio of 0.35 and DCI-S.

Table C.6 – Average corrosion rates (μm/yr) at week 15 as measured in the rapid macrocell test with bare bar specimens (Balma et al. 2005)

Specimen designation	Steel type	Specimen						Average	Standard deviation
		1	2	3	4	5	6		
M-N	N	54.59	56.17	12.28	37.20	40.79		40.21	17.68
M-T	T	48.52	26.57	26.10	8.35	42.06		30.32	15.68
M-CRPT1	CRPT1	26.27	37.52	64.70	21.51	37.09		37.42	16.75
M-CRPT2	CRPT2	45.77	77.69	26.10	53.67	43.93		49.43	18.74
M-CRT	CRT	74.56	42.08	35.94	44.01	27.60		44.84	17.80
M-2101(1)	2101(1)	3.12	1.73	1.42	2.17	3.53		2.39	0.90
M-2101(1)p	2101(1)p	0.43	0.00	0.00	0.23	0.20		0.17	0.18
M-2101(2)	2101(2)	0.06	6.79	1.68	3.44	4.02	2.31	3.05	2.30
M-2101(2)p	2101(2)p	0.06	0.03	0.00	0.00	0.06	0.09	0.04	0.03
M-2101(2)s	2101(2)	0.49	0.12	0.14	8.03	59.42	2.49	11.78	23.53
M-2205	2205	0.12	0.29	0.09	0.03	0.12		0.13	0.10
M-2205p	2205p	0.09	0.06	0.14	0.09	0.09		0.09	0.03
M-N3	N3	52.60	0.26	67.77	40.17	32.43	22.08	35.88	23.61
M-MMFX(1)	MMFX	14.50	5.03	9.66	5.92	12.48	22.41	11.67	6.41
M-MMFX(2)	MMFX	11.74	8.71	22.83	12.68	21.29	22.42	16.61	6.26
M-MMFXs	MMFX	6.31	20.13	13.86	21.87	10.77	4.58	12.92	7.08
M-MMFXb	MMFX	8.09	16.38	6.44	6.48	8.54	7.26	8.87	3.78
M-MMFX#19	MMFX	35.42	27.66	31.59	19.24	34.61	26.44	29.16	6.05
M-2101(1)h	2101(1)	20.72	10.86	15.51	4.06	16.88		13.61	6.40
M-2101(1)ph	2101(1)p	2.63	3.03	2.08	9.13	5.40		4.46	2.91
M-2101(2)h	2101(2)	7.20	12.72	11.59	11.21	13.15	10.38	11.04	2.14
M-2101(2)ph	2101(2)p	3.47	0.23	0.00	0.00	1.82	0.23	0.96	1.41
M-2101(2)sh	2101(2)s	9.39	56.47	41.53	13.73	5.20	10.66	22.83	20.99
M-2205h	2205	2.40	1.24	2.69	2.80	2.92	2.77	2.47	0.63
M-2205ph	2205p	0.14	0.20	0.23	0.40	0.43		0.28	0.13
M-N3h	N3	33.87	37.80	12.17	24.51	18.96		25.46	10.52
M-MMFXsh	MMFX	53.02	30.81	50.13	34.49	49.94	36.62	42.50	9.59

* M - A

M: macrocell test

A: steel type → N, N2, and N3: conventional normalized steel, T: conventional, Thermex-treated steel, CRPT1: microalloyed steel with a high phosphorus content (0.117%), Thermex treated, CRPT2: microalloyed steel with a high phosphorus content (0.100%), Thermex treated, CRT: microalloyed steel with normal phosphorus content, Thermex treated, MMFX: MMFX-2 microcomposite steel, ECR: epoxy-coated steel, 2101(1) and 2101(2): Duplex stainless steel (21% chromium, 1% nickel), 2205: Duplex stainless steel (22% chromium, 5% nickel), p: pickled, s: sandblasted, b: bent bars at the anode, h: 6.04 m ion concentration

Table C.7 – Average corrosion rates (μm/yr) at week 15 as measured in the rapid macrocell test with mortar specimens (Balma et al. 2005)

Specimen designation	Steel type	Specimen						Average	Standard deviation
		1	2	3	4	5	6		
M-N-50	N	3.59	2.49	2.27	0.67	2.21		2.25	1.04
M-T-50	T	4.65	3.41	2.81	3.85	1.03		3.15	1.36
M-CRPT1-50	CRPT1	6.56	3.21	2.86	0.35	4.21		3.44	2.25
M-CRPT2-50	CRPT2	3.68	2.76	4.95	3.81	0.93		3.23	1.50
M-CRT-50	CRT	3.49	4.73	3.61	0.64	2.66		3.03	1.52
M-Nc-50	N	3.47	3.80	0.63	5.43			3.33	2.00
M-Tc-50	T	3.72	3.41	2.94	1.00			2.77	1.22
M-CPRT1c-50	CRPT1	4.37	7.66	5.04	3.05			5.03	1.94
M-CRPT2c-50	CRPT2	5.66	2.66	4.02	3.49			3.96	1.27
M-CRTc-50	CRT	4.46	4.79	3.84	9.41			5.63	2.55
M-N2-50	N2	17.43	19.02	24.83	5.49	14.65		16.28	7.09
M-2101(1)-50	2101(1)	9.13	13.06	11.56	0.95			8.68	5.40
M-2101(1)p-50	2101(1)p	0.00	0.00	0.03	0.06			0.02	0.03
M-2101(2)-50	2101(2)	5.52	4.91	5.81	3.76	8.87	1.76	5.11	2.36
M-2101(2)p-50	2101(2)p	0.09	0.03	0.12	0.03	0.17	0.20	0.11	0.07
M-2205-50	2205	0.06	0.03	0.00	0.03	0.06	0.00	0.03	0.03
M-2205p-50	2205p	0.09	0.00	0.00	0.12	0.14	0.00	0.06	0.07
M-N3-50	N3	11.21	9.16	26.07	19.31	21.15	19.31	17.70	6.36
M-MMFX-50	MMFX	8.87	17.37	10.12	9.54	11.68	5.98	10.59	3.81
M-MMFX/N3-50	MMFX/N3	15.20	11.44	12.28				12.98	1.97
M-N3/MMFX-50	N3/MMFX	15.03	10.58	10.55				12.05	2.58
M-ECR-50	ECR	0.03	14.57	0.61	5.12	4.91	0.00	4.20	5.60
M-N-45	N	8.32	7.21	0.08	4.75	7.37		5.54	3.33
M-N-RH45	N	4.32	1.15	0.32	0.08	1.62		1.50	1.69
M-N-DC45	N	0.16	0.08	0.12	1.90	4.16		1.28	1.78
M-N-35	N	3.37	4.51	0.00	1.19	0.16		1.85	2.01
M-N-RH35	N	0.21	0.06	0.08	0.61	0.18		0.23	0.22
M-N-DC35	N	0.48	0.24	0.32	0.20	0.36		0.32	0.11

* M – A - B

M: macrocell test

A: steel type → N, N2, and N3: conventional normalized steel, T: conventional Thermex-treated steel, CRPT1: microalloyed steel with a high phosphorus content (0.117%), Thermex treated, CRPT2: microalloyed steel with a high phosphorus content (0.100%), Thermex treated, CRT: microalloyed steel with normal phosphorus content, Thermex treated, MMFX: MMFX-2 microcomposite steel, ECR: epoxy-coated steel, 2101(1) and 2101(2): Duplex stainless steel (21% chromium, 1% nickel), 2205: Duplex stainless steel (22% chromium, 5% nickel), p: pickled, c: epoxy-coated caps on the end of the bar.

B: mix design → 50: *w/c* ratio of 0.50 and no inhibitor, 45: *w/c* ratio of 0.45 and no inhibitor, RH45: *w/c* ratio of 0.45 and Rheocrete 222+, DC45: *w/c* ratio of 0.45 and DCI-S, 35: *w/c* ratio of 0.35 and no inhibitor, RH35: *w/c* ratio of 0.35 and Rheocrete 222+, DC35: *w/c* ratio of 0.35 and DCI-S.

Table C.8 – Average corrosion rates (μm/yr) at week 96 as measured in the Southern Exposure test (Balma et al. 2005)

Specimen designation	Steel type	Specimen						Average	Standard deviation
		1	2	3	4	5	6		
SE-N-45	N	5.06	0.00	0.00	1.65	5.29	4.47	2.75	2.49
SE-T-45	T	12.49	5.28	1.28	17.79	0.34	5.61	7.13	6.76
SE-CRPT1-45	CRPT1	4.95	3.36	8.75	5.81	0.88	1.87	4.27	2.86
SE-CRPT2-45	CRPT2	6.65	0.87	17.02	0.02	1.13	0.83	4.42	6.62
SE-CRT-45	CRT	0.01	0.00	10.93	0.91	2.41	0.84	2.52	4.22
SE-N/CRPT1-45	N/CRPT1	4.69	5.64	3.11	9.05			5.62	2.51
SE-CRPT1/N/45	CRPT1/N	6.13	6.35	2.23	4.86	4.77	0.93	4.21	2.17
SE-2101(1)-45	2101(1)	1.70	4.34	5.19				3.74	1.82
SE-2101(1)p-45	2101(1)p	0.47	3.39	0.54				1.47	1.67
SE-2101(2)-45	2101(2)	0.01	0.36	0.00	0.48	1.10		0.39	0.45
SE-2101(2)p-45	2101(2)p	0.01	0.02	0.07	0.00	0.01		0.02	0.03
SE-2205-45	2205	0.26	0.03	0.64	0.01	0.00		0.19	0.28
SE-2205p-45	2205p	0.00	0.00	0.02	0.01	0.01		0.01	0.01
SE-2205/N2-45	2205/N2	0.05	0.00	0.25				0.10	0.13
SE-N2/2205-45	N2/2205	4.42	2.36	1.13				2.64	1.67
SE-N3-45	N3	0.00	24.83	0.00	0.00	11.34	7.88	7.34	9.84
SE-MMFX-45	MMFX	3.07		6.35	1.61	2.54	3.62	3.44	1.79
SE-MMFXb-45	MMFX	0.41	0.98	1.51				0.97	0.55
SE-MMFX/N3-45	MMFX/N3	1.70	2.03	2.72				2.15	0.52
SE-N3/MMFX-45	N3/MMFX	1.17	2.41	1.70				1.76	0.62
SE-ECR	ECR	3.17	5.66	2.16	1.73	0.93	2.03	2.61	1.66
SE-N-RH45	N	0.76	0.15	0.41				0.44	0.30
SE-N-DC45	N	0.29	0.55	0.79				0.54	0.25
SE-N-35	N	1.85	1.13	0.49				1.16	0.68
SE-N-RH35	N	0.06	0.00	0.19				0.08	0.10
SE-N-DC35	N	0.15	0.07	0.07				0.10	0.04
SE-T-RH45	T	0.04	0.96	0.60				0.53	0.47
SE-T-DC45	T	4.77	3.46	1.57				3.26	1.61
SE-T-35	T	0.00	0.03	0.00				0.01	0.02
SE-T-RH35	T	0.00	0.00	0.00				0.00	0.00
SE-T-DC35	T	0.01	0.01	0.00				0.01	0.01

* SE – A - B

SE: Southern Exposure test

A: steel type → N, N2, and N3: conventional normalized steel, T: conventional, Thermex-treated steel, CRPT1: microalloyed steel with a high phosphorus content (0.117%), Thermex treated, CRPT2: microalloyed steel with a high phosphorus content (0.100%), Thermex treated, CRT: microalloyed steel with normal phosphorus content, Thermex treated, MMFX: MMFX-2 microcomposite steel, ECR: epoxy-coated steel, 2101(1) and 2101(2): Duplex stainless steel (21% chromium, 1% nickel), 2205: Duplex stainless steel (22% chromium, 5% nickel), p: pickled, b: bent bars on the top mat.

B: mix design → 45: *w/c* ratio of 0.45 and no inhibitor, RH45: *w/c* ratio of 0.45 and Rheocrete 222+, DC45: *w/c* ratio of 0.45 and DCI-S, 35: *w/c* ratio of 0.35 and no inhibitor, RH35: *w/c* ratio of 0.35 and Rheocrete 222+, DC35: *w/c* ratio of 0.35 and DCI-S.

Table C.9 – Average corrosion rates (μm/yr) at week 96 as measured in the cracked beam test (Balma et al. 2005)

Specimen designation	Steel type	Specimen						Average	Standard deviation
		1	2	3	4	5	6		
CB-N-45	N	0.03	0.02	2.37	4.16	6.33	0.00	2.15	2.66
CB-T-45	T	0.06	1.67	1.09		11.29	0.67	2.96	4.70
CB-CRPT1-45	CRPT1	2.71	0.68	0.35	71.76	8.78	0.00	14.05	28.46
CB-CRPT2-45	CRPT2	0.64	1.58	0.14	7.99	0.00	11.34	3.61	4.84
CB-CRT-45	CRT	0.51	0.02	3.48	0.02		7.61	2.33	3.29
CB-2101(1)-45	2101(1)	4.11	0.45	0.15				1.57	2.21
CB-2101(1)p-45	2101(1)p	3.94	1.33	2.07				2.45	1.34
CB-2101(2)-45	2101(2)	0.39	0.43	0.42	1.06	0.83		0.63	0.30
CB-2101(2)p-45	2101(2)p	0.04	0.03	0.01	0.01	0.02		0.02	0.01
CB-2205-45	2205	0.10	1.45	0.23	0.04	0.02		0.37	0.61
CB-2205p-45	2205p	0.00	0.04	0.01	0.01	0.01		0.01	0.02
CB-N3-45	N3	0.00	0.00	0.00	0.00	4.24	0.00	0.71	1.73
CB-MMFX-45	MMFX	0.00	0.00	0.66	1.21	0.89	0.32	0.51	0.49
CB-ECR	ECR	10.65	2.94	3.33	2.96	1.82	0.56	3.71	3.55
CB-N-RH45	N	11.48	2.01	3.02				5.50	5.20
CB-N-DC45	N	1.98		0.96				1.47	0.73
CB-N-35	N	1.58	0.87	2.36				1.61	0.74
CB-N-RH35	N	0.00	0.00					0.00	0.00
CB-N-DC35	N	0.02	1.69	0.67				0.79	0.84
CB-T-RH45	T	2.25	3.97	0.02				2.08	1.98
CB-T-DC45	T	2.91	1.89	1.91				2.24	0.58
CB-T-35	T	2.65	3.28	1.52				2.48	0.89
CB-T-RH35	T	1.61	2.29	4.27				2.72	1.38
CB-T-DC35	T	0.83	0.93	0.38				0.72	0.29

* CB – A - B

CB: Cracked beam test

A: steel type → N and N3: conventional normalized steel, T: conventional Thermex-treated steel, CRPT1: microalloyed steel with a high phosphorus content (0.117%), Thermex treated, CRPT2: microalloyed steel with a high phosphorus content (0.100%), Thermex treated, CRT: microalloyed steel with normal phosphorus content, Thermex treated, MMFX: MMFX-2 microcomposite steel, ECR: epoxy-coated steel, 2101(1) and 2101(2): Duplex stainless steel (21% chromium, 1% nickel), 2205: Duplex stainless steel (22% chromium, 5% nickel), p: pickled, b: bent bars on the top mat.

B: mix design → 45: *w/c* ratio of 0.45 and no inhibitor, RH45: *w/c* ratio of 0.45 and Rheocrete 222+, DC45: *w/c* ratio of 0.45 and DCI-S, 35: *w/c* ratio of 0.35 and no inhibitor, RH35: *w/c* ratio of 0.35 and Rheocrete 222+, DC35: *w/c* ratio of 0.35 and DCI-S.

Table C.10 – Average corrosion rates (μm/yr) at week 96 as measured in the ASTM G 109 test (Balma et al. 2005)

Specimen designation	Steel type	Specimen						Average	Standard deviation
		1	2	3	4	5	6		
G-N-45	N	2.80	0.00	0.25				1.02	1.55
G-T-45	T	0.53	0.77	1.63	7.95	4.94	0.00	2.64	3.15
G-CRPT1-45	CRPT1	0.90	1.14	2.73	5.66	2.94	3.14	2.75	1.72
G-CRPT2-45	CRPT2	1.43	1.78	1.26	2.93	2.00	2.68	2.01	0.67
G-CRT-45	CRT	1.43	1.78	1.26	2.93	2.00	2.68	2.01	0.67
G-N-RH45	N	0.02	0.00	0.00				0.01	0.01
G-N-DC45	N	0.19	0.09	0.33				0.20	0.12
G-N-35	N	0.00	0.00	0.00				0.00	0.00
G-N-RH35	N	0.01	0.00	0.00				0.00	0.00
G-N-DC35	N	0.00	0.00	0.00				0.00	0.00
G-T-RH45	T	0.00	0.01	0.00				0.00	0.00
G-T-DC45	T	0.00	0.02	0.83				0.28	0.47
G-T-35	T	0.00	0.00	0.00				0.00	0.00
G-T-RH35	T	0.00	0.00	0.00				0.00	0.00
G-T-DC35	T	0.00	0.00	0.00				0.00	0.00

* G – A - B

G: ASTM G 109 test

A: steel type → N, N2, and N3: conventional normalized steel, T: conventional Thermex-treated steel, CRPT1: microalloyed steel with a high phosphorus content (0.117%), Thermex treated, CRPT2: microalloyed steel with a high phosphorus content (0.100%), Thermex treated, CRT: microalloyed steel with normal phosphorus content, Thermex treated, MMFX: MMFX-2 microcomposite steel, ECR: epoxy-coated steel, 2101(1) and 2101(2): Duplex stainless steel (21% chromium, 1% nickel), 2205: Duplex stainless steel (22% chromium, 5% nickel), p: pickled, b: bent bars on the top mat.

B: mix design → 45: *w/c* ratio of 0.45 and no inhibitor, RH45: *w/c* ratio of 0.45 and Rheocrete 222+, DC45: *w/c* ratio of 0.45 and DCI-S, 35: *w/c* ratio of 0.35 and no inhibitor, RH35: *w/c* ratio of 0.35 and Rheocrete 222+, DC35: *w/c* ratio of 0.35 and DCI-S.

Table C.11 – Average corrosion losses (μm) at week 15 as measured in the rapid macrocell test with bare bar specimens (Balma et al. 2005)

Specimen designation	Steel type	Specimen						Average	Standard deviation
		1	2	3	4	5	6		
M-N	N	14.11	13.89	7.56	9.28	10.32		11.03	2.88
M-T	T	7.84	9.38	8.05	4.02	9.56		7.77	2.23
M-CRPT1	CRPT1	8.86	11.98	10.41	8.99	12.92		10.63	1.80
M-CRPT2	CRPT2	11.61	14.85	10.48	13.39	11.10		12.29	1.80
M-CRT	CRT	8.63	8.45	9.70	11.22	9.68		9.53	1.11
M-2101(1)	2101(1)	0.67	0.69	0.32	0.55	2.85		1.01	1.04
M-2101(1)p	2101(1)p	0.17	0.05	0.01	0.17	0.12		0.10	0.07
M-2101(2)	2101(2)	1.40	1.57	1.29	0.81	1.58	2.04	1.45	0.40
M-2101(2)p	2101(2)p	0.04	0.01	0.02	0.03	0.02	0.13	0.04	0.04
M-2101(2)s	2101(2)	0.40	0.45	1.58	12.10	12.86	5.47	5.48	5.74
M-2205	2205	0.03	0.03	0.03	0.06	0.03		0.04	0.01
M-2205p	2205p	0.03	0.02	0.03	0.02	0.02		0.02	0.00
M-N3	N3	13.07	4.84	13.22	11.10	6.97	4.98	9.03	3.91
M-MMFX(1)	MMFX	7.26	4.78	6.20	4.90	3.64	6.66	5.57	1.36
M-MMFX(2)	MMFX	3.10	2.10	3.26	1.13	1.63	3.84	2.51	1.05
M-MMFXs	MMFX	1.96	2.63	3.23	3.29	2.86	2.14	2.69	0.55
M-MMFXb	MMFX	1.51	2.76	1.20	1.46	1.51	1.99	1.74	0.56
M-MMFX#19	MMFX	9.85	5.83	5.19	3.60	6.17	5.36	6.00	2.09
M-2101(1)h	2101(1)	3.85	3.48	4.38	2.03	5.46		3.84	1.26
M-2101(1)ph	2101(1)p	0.84	1.36	1.38	3.16	1.76		1.70	0.88
M-2101(2)h	2101(2)	2.28	3.83	3.80	3.78	3.24	3.64	3.43	0.60
M-2101(2)ph	2101(2)p	0.25	0.18	0.00	0.14	0.28	0.14	0.17	0.10
M-2101(2)sh	2101(2)s	7.61	15.81	19.87	2.41	2.24	3.12	8.51	7.60
M-2205h	2205	0.50	0.34	0.52	0.34	0.61	0.64	0.49	0.13
M-2205ph	2205p	0.02	0.03	0.02	0.02	0.05		0.03	0.01
M-N3h	N3	12.16	11.53	6.83	9.19	8.46		9.63	2.20
M-MMFXsh	MMFX	13.71	7.92	10.75	4.96	8.96	11.78	9.68	3.09

* M - A

M: macrocell test

A: steel type → N, N2, and N3: conventional normalized steel, T: conventional, Thermex-treated steel, CRPT1: microalloyed steel with a high phosphorus content (0.117%), Thermex treated, CRPT2: microalloyed steel with a high phosphorus content (0.100%), Thermex treated, CRT: microalloyed steel with normal phosphorus content, Thermex treated, MMFX: MMFX-2 microcomposite steel, ECR: epoxy-coated steel, 2101(1) and 2101(2): Duplex stainless steel (21% chromium, 1% nickel), 2205: Duplex stainless steel (22% chromium, 5% nickel), p: pickled, s: sandblasted, b: bent bars at the anode, h: 6.04 m ion concentration

Table C.12 – Average corrosion losses (μm) at week 15 as measured in the rapid macrocell test with mortar specimens (Balma et al. 2005)

Specimen designation	Steel type	Specimen						Average	Standard deviation
		1	2	3	4	5	6		
M-N-50	N	1.05	0.72	0.53	0.40	0.51		0.64	0.25
M-T-50	T	1.23	0.80	0.79	1.06	0.16		0.81	0.41
M-CRPT1-50	CRPT1	1.58	1.03	0.18	0.53	1.19		0.90	0.55
M-CRPT2-50	CRPT2	1.03	0.57	1.54	1.44	0.45		1.01	0.49
M-CRT-50	CRT	1.02	1.19	1.20	0.06	0.80		0.85	0.47
M-Nc-50	N	0.95	1.48	0.23	1.24			0.97	0.54
M-Tc-50	T	0.79	0.44	0.86	0.11			0.55	0.35
M-CPRT1c-50	CRPT1	0.92	1.52	1.06	0.84			1.08	0.30
M-CRPT2c-50	CRPT2	1.27	0.59	0.96	0.71			0.88	0.30
M-CRTc-50	CRT	1.14	0.97	0.54	1.28			0.98	0.32
M-N2-50	N2	4.04	2.95	2.22	3.75	6.21		3.84	1.51
M-2101(1)-50	2101(1)	0.76	1.95	0.93	0.32			0.99	0.69
M-2101(1)p-50	2101(1)p	0.01	0.00	0.02	0.02			0.01	0.01
M-2101(2)-50	2101(2)	1.15	0.51	0.77	0.54	1.21	0.64	0.80	0.31
M-2101(2)p-50	2101(2)p	0.02	0.02	0.03	0.02	0.04	0.03	0.03	0.01
M-2205-50	2205	0.03	0.03	0.02	0.02	0.03	0.02	0.03	0.01
M-2205p-50	2205p	0.04	0.03	0.02	0.02	0.02	0.02	0.03	0.01
M-N3-50	N3	5.54	5.08	7.01	5.21	4.79	5.12	5.46	0.80
M-MMFX-50	MMFX	2.18	0.56	1.88	0.99	1.68	0.93	1.37	0.63
M-MMFX/N3-50	MMFX/N3	1.60	1.75	2.11				1.82	0.26
M-N3/MMFX-50	N3/MMFX	3.33	2.21	2.35				2.63	0.61
M-ECR-50	ECR	0.02	1.03	0.08	0.51	0.23	0.03	0.32	0.40
M-N-45	N	0.65	1.76	0.03	0.65	1.24		0.87	0.66
M-N-RH45	N	0.22	0.09	0.16	0.10	0.17		0.15	0.05
M-N-DC45	N	0.18	0.05	0.28	0.18	0.48		0.24	0.16
M-N-35	N	0.41	1.94	0.07	0.13	0.05		0.52	0.81
M-N-RH35	N	0.21	0.06	0.08	0.61	0.18		0.23	0.22
M-N-DC35	N	0.13	0.36	0.05	0.05	0.14		0.15	0.13

* M – A - B

M: macrocell test

A: steel type → N, N2, and N3: conventional normalized steel, T: conventional Thermex-treated steel, CRPT1: microalloyed steel with a high phosphorus content (0.117%), Thermex treated, CRPT2: microalloyed steel with a high phosphorus content (0.100%), Thermex treated, CRT: microalloyed steel with normal phosphorus content, Thermex treated, MMFX: MMFX-2 microcomposite steel, ECR: epoxy-coated steel, 2101(1) and 2101(2): Duplex stainless steel (21% chromium, 1% nickel), 2205: Duplex stainless steel (22% chromium, 5% nickel), p: pickled, c: epoxy-coated caps on the end of the bar.

B: mix design → 50: *w/c* ratio of 0.50 and no inhibitor, 45: *w/c* ratio of 0.45 and no inhibitor, RH45: *w/c* ratio of 0.45 and Rheocrete 222+, DC45: *w/c* ratio of 0.45 and DCI-S, 35: *w/c* ratio of 0.35 and no inhibitor, RH35: *w/c* ratio of 0.35 and Rheocrete 222+, DC35: *w/c* ratio of 0.35 and DCI-S.

Table C.13 – Average corrosion losses (μm) at week 96 as measured in the Southern Exposure test (Balma et al. 2005)

Specimen designation	Steel type	Specimen						Average	Standard deviation
		1	2	3	4	5	6		
SE-N-45	N	10.25	9.47	7.96	4.31	6.36	7.02	7.56	2.16
SE-T-45	T	17.14	6.74	7.93	25.49	1.31	10.28	11.48	8.58
SE-CRPT1-45	CRPT1	6.90	4.75	13.70	11.01	2.01	2.54	6.82	4.70
SE-CRPT2-45	CRPT2	11.89	6.39	21.49	8.11	5.68	1.83	9.23	6.84
SE-CRT-45	CRT	10.68	8.67	12.13	1.90	6.77	1.71	6.98	4.40
SE-N/CRPT1-45	N/CRPT1	8.36	7.50	6.93	10.22			8.25	1.44
SE-CRPT1/N/45	CRPT1/N	9.80	9.10	5.14	6.90	11.12	13.81	9.31	3.07
SE-2101(1)-45	2101(1)	2.03	4.68	5.93				4.21	1.99
SE-2101(1)p-45	2101(1)p	0.11	1.99	0.14				0.75	1.08
SE-2101(2)-45	2101(2)	0.22	0.18	0.01	0.56	0.99		0.39	0.39
SE-2101(2)p-45	2101(2)p	0.01	0.02	0.02	0.01	0.04		0.02	0.01
SE-2205-45	2205	0.05	0.11	0.33	0.01	0.00		0.10	0.13
SE-2205p-45	2205p	0.02	0.03	0.03	0.01	0.01		0.02	0.01
SE-2205/N2-45	2205/N2	0.11	0.08	0.24				0.14	0.09
SE-N2/2205-45	N2/2205	4.74	5.54	8.48				6.25	1.96
SE-N3-45	N3	11.47	27.52	3.20	8.30	14.09	6.43	11.84	8.58
SE-MMFX-45	MMFX	4.67		4.13	2.22	2.90	2.18	3.22	1.13
SE-MMFXb-45	MMFX	5.30	3.61	6.09				5.00	1.27
SE-MMFX/N3-45	MMFX/N3	2.62	3.39	3.52				3.18	0.49
SE-N3/MMFX-45	N3/MMFX	3.26	6.22	8.05				5.84	2.41
SE-ECR	ECR	1.95	3.11	1.15	1.22	0.35	0.68	1.41	1.00
SE-N-RH45	N	1.35	0.36	0.51				0.74	0.54
SE-N-DC45	N	2.37	0.97	0.36				1.23	1.03
SE-N-35	N	11.47	27.52	3.20				14.06	12.37
SE-N-RH35	N	0.05	0.26	0.04				0.12	0.13
SE-N-DC35	N	0.19	0.55	0.70				0.48	0.26
SE-T-RH45	T	0.00	0.00	0.00				0.00	0.00
SE-T-DC45	T	7.12	2.32	1.85				3.76	2.92
SE-T-35	T	0.06	0.13	0.11				0.10	0.03
SE-T-RH35	T	0.09	0.04	0.07				0.07	0.02
SE-T-DC35	T	0.02	0.02	0.09				0.04	0.04

* SE – A - B

SE: Southern Exposure test

A: steel type → N, N2, and N3: conventional normalized steel, T: conventional, Thermex-treated steel, CRPT1: microalloyed steel with a high phosphorus content (0.117%), Thermex treated, CRPT2: microalloyed steel with a high phosphorus content (0.100%), Thermex treated, CRT: microalloyed steel with normal phosphorus content, Thermex treated, MMFX: MMFX-2 microcomposite steel, ECR: epoxy-coated steel, 2101(1) and 2101(2): Duplex stainless steel (21% chromium, 1% nickel), 2205: Duplex stainless steel (22% chromium, 5% nickel), p: pickled, b: bent bars on the top mat.

B: mix design → 45: *w/c* ratio of 0.45 and no inhibitor, RH45: *w/c* ratio of 0.45 and Rheocrete 222+, DC45: *w/c* ratio of 0.45 and DCI-S, 35: *w/c* ratio of 0.35 and no inhibitor, RH35: *w/c* ratio of 0.35 and Rheocrete 222+, DC35: *w/c* ratio of 0.35 and DCI-S.

Table C.14 – Average corrosion losses (μm) at week 96 as measured in the cracked beam test (Balma et al. 2005)

Specimen designation	Steel type	Specimen						Average	Standard deviation
		1	2	3	4	5	6		
CB-N-45	N	12.49	9.99	6.41	10.66	13.98	6.03	9.93	3.20
CB-T-45	T	12.06	8.41	9.58		14.18	5.58	9.96	3.31
CB-CRPT1-45	CRPT1	10.18	6.26	5.56	31.60	12.67	8.21	12.41	9.75
CB-CRPT2-45	CRPT2	7.73	6.63	4.41	16.76	6.53	13.28	9.22	4.74
CB-CRT-45	CRT	5.84	10.04	5.78	16.24	9.17	8.82	9.32	3.83
CB-2101(1)-45	2101(1)	2.96	2.40	1.16				2.17	0.92
CB-2101(1)p-45	2101(1)p	1.69	0.81	0.88				1.13	0.49
CB-2101(2)-45	2101(2)	1.72	1.48	1.83	2.05	2.06		1.83	0.24
CB-2101(2)p-45	2101(2)p	0.04	0.01	0.03	0.01	0.02		0.02	0.01
CB-2205-45	2205	0.13	0.82	0.12	0.07	0.03		0.24	0.33
CB-2205p-45	2205p	0.02	0.05	0.02	0.01	0.02		0.02	0.02
CB-N3-45	N3	13.62	8.14	6.17	3.24	4.86	4.67	6.78	3.73
CB-MMFX-45	MMFX	3.05	2.33	2.21	3.15	2.73	1.66	2.52	0.57
CB-ECR	ECR	8.01	2.32	3.70	4.51	0.70	0.95	3.37	2.72
CB-N-RH45	N	7.32	5.44	4.80				5.85	1.31
CB-N-DC45	N	9.55		5.32				7.43	2.99
CB-N-35	N	6.99	5.42	6.06				6.16	0.79
CB-N-RH35	N	4.31	4.53					4.42	0.15
CB-N-DC35	N	25.49	35.07	13.65				24.74	10.73
CB-T-RH45	T	5.49	5.68	2.79				4.65	1.61
CB-T-DC45	T	8.16	3.58	45.97				19.23	23.27
CB-T-35	T	5.95	6.12	4.13				5.40	1.10
CB-T-RH35	T	2.36	7.16	4.34				4.62	2.41
CB-T-DC35	T	2.54	3.11	3.53				3.06	0.50

* CB – A - B

CB: Cracked beam test

A: steel type → N and N3: conventional normalized steel, T: conventional Thermex-treated steel, CRPT1: microalloyed steel with a high phosphorus content (0.117%), Thermex treated, CRPT2: microalloyed steel with a high phosphorus content (0.100%), Thermex treated, CRT: microalloyed steel with normal phosphorus content, Thermex treated, MMFX: MMFX-2 microcomposite steel, ECR: epoxy-coated steel, 2101(1) and 2101(2): Duplex stainless steel (21% chromium, 1% nickel), 2205: Duplex stainless steel (22% chromium, 5% nickel), p: pickled, b: bent bars on the top mat.

B: mix design → 45: *w/c* ratio of 0.45 and no inhibitor, RH45 *w/c* ratio of 0.45 and Rheocrete 222+, DC45: *w/c* ratio of 0.45 and DCI-S, 35: *w/c* ratio of 0.35 and no inhibitor, RH35: *w/c* ratio of 0.35 and Rheocrete 222+, DC35: *w/c* ratio of 0.35 and DCI-S.

Table C.15 – Average corrosion losses (μm) at week 96 as measured in the ASTM G 109 test (Balma et al. 2005)

Specimen designation	Steel type	Specimen						Average	Standard deviation
		1	2	3	4	5	6		
G-N-45	N	4.60	1.72	1.30				2.54	1.80
G-T-45	T	0.13	0.05	1.27	10.97	2.97	2.67	3.01	4.09
G-CRPT1-45	CRPT1	1.03	1.18	1.05	10.53	4.23	4.86	3.81	3.71
G-CRPT2-45	CRPT2	1.33	1.61	1.85	11.65	2.94	0.93	3.38	4.11
G-CRT-45	CRT	1.43	1.78	1.26	2.93	2.00	2.68	2.01	0.67
G-N-RH45	N	0.00	0.00	0.00				0.00	0.00
G-N-DC45	N	0.16	0.16	0.57				0.30	0.24
G-N-35	N	0.02	0.05	0.04				0.04	0.01
G-N-RH35	N	0.01	0.01	0.01				0.01	0.00
G-N-DC35	N	0.03	0.02	0.01				0.02	0.01
G-T-RH45	T	0.00	0.01	0.00				0.01	0.00
G-T-DC45	T	0.01	0.14	0.12				0.09	0.07
G-T-35	T	0.17	0.01	0.06				0.08	0.08
G-T-RH35	T	0.01	0.01	0.04				0.02	0.01
G-T-DC35	T	0.02	0.02	0.00				0.01	0.01

* G – A - B

G: ASTM G 109 test

A: steel type → N, N2, and N3: conventional normalized steel, T: conventional Thermex-treated steel, CRPT1: microalloyed steel with a high phosphorus content (0.117%), Thermex treated, CRPT2: microalloyed steel with a high phosphorus content (0.100%), Thermex treated, CRT: microalloyed steel with normal phosphorus content, Thermex treated, MMFX: MMFX-2 microcomposite steel, ECR: epoxy-coated steel, 2101(1) and 2101(2): Duplex stainless steel (21% chromium, 1% nickel), 2205: Duplex stainless steel (22% chromium, 5% nickel), p: pickled, b: bent bars on the top mat.

B: mix design → 45: *w/c* ratio of 0.45 and no inhibitor, RH45: *w/c* ratio of 0.45 and Rheocrete 222+, DC45: *w/c* ratio of 0.45 and DCI-S, 35: *w/c* ratio of 0.35 and no inhibitor, RH35: *w/c* ratio of 0.35 and Rheocrete 222+, DC35: *w/c* ratio of 0.35 and DCI-S.

Table C.16 – Student's t-test for comparing the mean corrosion rates of specimens with different conventional steels

Specimens *		t_{stat}	t_{crit} X%:	80%	90%	95%	98%
			α:	0.20	0.10	0.05	0.02
Macrocell test with bare specimens							
M-N	M-N3	0.347		1.397 N	1.860 N	2.306 N	2.896 N
Macrocell test with mortar specimens							
M-N-50	M-N3-50	-5.861		1.476 Y	2.015 Y	2.571 Y	3.365 Y
M-N-50	M-N2-50	-4.382		1.533 Y	2.132 Y	2.776 Y	3.747 Y
M-N3-50	M-N2-50	0.346		1.397 N	1.860 N	2.306 N	2.896 N
Southern Exposure test							
SE-N-45	SE-N3-45	-1.109		1.476 N	2.015 N	2.571 N	3.365 N
Cracked beam test							
CB-N-45	CB-N3-45	1.117		1.397 N	1.860 N	2.306 N	2.896 N

t_{stat}: t-test statistic, t_{crit}: value of t calculated from Student's t-distribution, α: level of significance, X%: confidence level,
Y: statistically significant difference, i.e. null hypothesis rejected, N: not statistically significant difference, i.e. null hypothesis rejected.

* T - A - B

T: test → M: macrocell test, SE: Southern Exposure test, CB: cracked beam test

A: steel type → N, N2, and N3: conventional, normalized steel.

B: mix design → 50: *w/c* ratio of 0.50 and no inhibitor, 45: *w/c* ratio of 0.45 and no inhibitor.

Table C.17 – Student's t-test for comparing the mean corrosion losses of specimens with different conventional steels

Specimens *		t_{stat}	t_{crit} X%:	80%	90%	95%	98%
			α:	0.20	0.10	0.05	0.02
Macrocell test with bare specimens							
M-N	M-N3	0.976		1.397 N	1.860 N	2.306 N	2.896 N
Macrocell test with mortar specimens							
M-N-50	M-N3-50	-13.932		1.440 Y	1.943 Y	2.447 Y	3.143 Y
M-N-50	M-N2-50	-4.676		1.533 Y	2.132 Y	2.776 Y	3.747 Y
M-N3-50	M-N2-50	2.168		1.476 Y	2.015 Y	2.571 N	3.365 N
Southern Exposure test							
SE-N-45	SE-N3-45	-1.184		1.476 N	2.015 N	2.571 N	3.365 N
Cracked beam test							
CB-N-45	CB-N3-45	1.566		1.383 Y	1.833 N	2.262 N	2.821 N

t_{stat}: t-test statistic, t_{crit}: value of t calculated from Student's t-distribution, α: level of significance, X%: confidence level,
Y: statistically significant difference, i.e. null hypothesis rejected, N: not statistically significant difference, i.e. null hypothesis rejected.

* T - A - B

T: test → M: macrocell test, SE: Southern Exposure test, CB: cracked beam test

A: steel type → N, N2, and N3: conventional, normalized steel.

B: mix design → 50: *w/c* ratio of 0.50 and no inhibitor, 45: *w/c* ratio of 0.45 and no inhibitor.

Table C.18 – Student's t-test for comparing the mean corrosion rates of specimens with corrosion inhibitors and different *w/c* ratios

Specimens *		t_{stat}	t_{crit} X%:	80%	90%	95%	98%
			α:	0.20	0.10	0.05	0.02
Macrocell test with mortar specimens							
M-N-45	M-N-RH45	2.424		1.476 Y	2.015 Y	2.571 N	3.365 N
M-N-45	M-N-DC45	2.525		1.440 Y	1.943 Y	2.447 Y	3.143 N
M-N-45	M-N-35	2.129		1.440 Y	1.943 Y	2.447 N	3.143 N
M-N-35	M-N-RH35	1.792		1.533 Y	2.132 N	2.776 N	3.747 N
M-N-35	M-N-DC35	1.700		1.533 Y	2.132 N	2.776 N	3.747 N
Southern Exposure test							
SE-N-45	SE-N-RH45	2.233		1.476 Y	2.015 Y	2.571 N	3.365 N
SE-N-45	SE-N-DC45	2.145		1.476 Y	2.015 Y	2.571 N	3.365 N
SE-N-45	SE-N-35	1.455		1.440 Y	1.943 N	2.447 N	3.143 N
SE-N-35	SE-N-RH35	2.717		1.886 Y	2.920 N	4.303 N	6.965 N
SE-N-35	SE-N-DC35	2.706		1.886 Y	2.920 N	4.303 N	6.965 N
SE-T-45	SE-T-RH45	2.378		1.476 Y	2.015 Y	2.571 N	3.365 N
SE-T-45	SE-T-DC45	1.328		1.440 N	1.943 N	2.447 N	3.143 N
SE-T-45	SE-T-35	2.580		1.476 Y	2.015 Y	2.571 Y	3.365 N
SE-T-35	SE-T-RH35	1.000		1.886 N	2.920 N	4.303 N	6.965 N
SE-T-35	SE-T-DC35	0.267		1.886 N	2.920 N	4.303 N	6.965 N
Cracked beam test							
CB-N-45	CB-N-RH45	-1.049		1.886 N	2.920 N	4.303 N	6.965 N
CB-N-45	CB-N-DC45	0.568		1.476 N	2.015 N	2.571 N	3.365 N
CB-N-45	CB-N-35	0.468		1.440 N	1.943 N	2.447 N	3.143 N
CB-N-35	CB-N-RH35	3.744		1.886 Y	2.920 Y	4.303 N	6.965 N
CB-N-35	CB-N-DC35	1.255		1.638 N	2.353 N	3.182 N	4.541 N
CB-T-45	CB-T-RH45	0.368		1.476 N	2.015 N	2.571 N	3.365 N
CB-T-45	CB-T-DC45	0.338		1.533 N	2.132 N	2.776 N	3.747 N
CB-T-45	CB-T-35	0.218		1.533 N	2.132 N	2.776 N	3.747 N
CB-T-35	CB-T-RH35	-0.254		1.638 N	2.353 N	3.182 N	4.541 N
CB-T-35	CB-T-DC35	3.252		1.886 Y	2.920 Y	4.303 N	6.965 N
ASTM G 109 test							
G-N-45	G-N-RH45	1.129		1.886 N	2.920 N	4.303 N	6.965 N
G-N-45	G-N-DC45	0.911		1.886 N	2.920 N	4.303 N	6.965 N
G-N-45	G-N-35	1.136		1.886 N	2.920 N	4.303 N	6.965 N
G-N-35	G-N-RH35	-0.371		1.886 N	2.920 N	4.303 N	6.965 N
G-N-35	G-N-DC35	1.000		1.638 N	2.353 N	3.182 N	4.541 N
G-T-45	G-T-RH45	2.051		1.476 Y	2.015 Y	2.571 N	3.365 N
G-T-45	G-T-DC45	1.792		1.476 Y	2.015 N	2.571 N	3.365 N
G-T-45	G-T-35	2.052		1.476 Y	2.015 Y	2.571 N	3.365 N
G-T-35	G-T-RH35	1.732		1.886 N	2.920 N	4.303 N	6.965 N
G-T-35	G-T-DC35	1.732		1.886 N	2.920 N	4.303 N	6.965 N

t_{stat}: t-test statistic, t_{crit}: value of t calculated from Student's t-distribution, □: level of significance, X%: confidence level,

Y: statistically significant difference, i.e. null hypothesis rejected, N: not statistically significant difference, i.e. null hypothesis rejected.

* T - A - B

T: test → M: macrocell test, SE: Southern Exposure test, CB: cracked beam test, G: ASTM G 109 test

A: steel type → N: conventional, normalized steel, T: Thermex-treated conventional steel.

B: mix design → 45: *w/c* ratio of 0.45 and no inhibitor, RH45: *w/c* ratio of 0.45 and Rheocrete 222+, DC45: *w/c* ratio of 0.45 and DCI-S, 35: *w/c* ratio of 0.35 and no inhibitor, RH35: *w/c* ratio of 0.35 and Rheocrete 222+, DC35: *w/c* ratio of 0.35 and DCI-S.

Table C.19 – Student's t-test for comparing the mean corrosion losses of specimens with corrosion inhibitors and different *w/c* ratios

Specimens *		t_{stat}	t_{crit} X%:	80%	90%	95%	98%
			α:	0.20	0.10	0.05	0.02
Macrocell test with mortar specimens							
M-N-45	M-N-RH45	2.442		1.533 Y	2.132 Y	2.776 N	3.747 N
M-N-45	M-N-DC45	2.089		1.533 Y	2.132 N	2.776 N	3.747 N
M-N-45	M-N-35	0.741		1.415 N	1.895 N	2.365 N	2.998 N
M-N-35	M-N-RH35	0.785		1.533 N	2.132 N	2.776 N	3.747 N
M-N-35	M-N-DC35	1.023		1.533 N	2.132 N	2.776 N	3.747 N
Southern Exposure test							
SE-N-45	SE-N-RH45	7.294		1.440 Y	1.943 Y	2.447 Y	3.143 Y
SE-N-45	SE-N-DC45	5.947		1.440 Y	1.943 Y	2.447 Y	3.143 Y
SE-N-45	SE-N-35	-0.904		1.886 N	2.920 N	4.303 N	6.965 N
SE-N-35	SE-N-RH35	1.953		1.886 Y	2.920 N	4.303 N	6.965 N
SE-N-35	SE-N-DC35	1.902		1.886 Y	2.920 N	4.303 N	6.965 N
SE-T-45	SE-T-RH45	3.277		1.476 Y	2.015 Y	2.571 Y	3.365 N
SE-T-45	SE-T-DC45	1.986		1.440 Y	1.943 Y	2.447 N	3.143 N
SE-T-45	SE-T-35	3.248		1.476 Y	2.015 Y	2.571 Y	3.365 N
SE-T-35	SE-T-RH35	1.439		1.638 N	2.353 N	3.182 N	4.541 N
SE-T-35	SE-T-DC35	1.898		1.638 Y	2.353 N	3.182 N	4.541 N
Cracked beam test							
CB-N-45	CB-N-RH45	2.702		1.440 Y	1.943 Y	2.447 Y	3.143 N
CB-N-45	CB-N-DC45	1.003		3.078 N	6.314 N	12.706 N	31.821 N
CB-N-45	CB-N-35	2.724		1.440 Y	1.943 Y	2.447 Y	3.143 N
CB-N-35	CB-N-RH35	3.700		1.886 Y	2.920 Y	4.303 N	6.965 N
CB-N-35	CB-N-DC35	-2.991		1.886 Y	2.920 Y	4.303 N	6.965 N
CB-T-45	CB-T-RH45	3.033		1.476 Y	2.015 Y	2.571 Y	3.365 N
CB-T-45	CB-T-DC45	-0.686		1.886 N	2.920 N	4.303 N	6.965 N
CB-T-45	CB-T-35	2.829		1.476 Y	2.015 Y	2.571 Y	3.365 N
CB-T-35	CB-T-RH35	0.511		1.886 N	2.920 N	4.303 N	6.965 N
CB-T-35	CB-T-DC35	3.344		1.886 Y	2.920 Y	4.303 N	6.965 N
ASTM G 109 test							
G-N-45	G-N-RH45	2.443		1.886 Y	2.920 N	4.303 N	6.965 N
G-N-45	G-N-DC45	2.143		1.886 Y	2.920 N	4.303 N	6.965 N
G-N-45	G-N-35	2.411		1.886 Y	2.920 N	4.303 N	6.965 N
G-N-35	G-N-RH35	3.671		1.886 Y	2.920 Y	4.303 N	6.965 N
G-N-35	G-N-DC35	1.825		1.638 Y	2.353 N	3.182 N	4.541 N
G-T-45	G-T-RH45	1.799		1.476 Y	2.015 N	2.571 N	3.365 N
G-T-45	G-T-DC45	1.748		1.476 Y	2.015 N	2.571 N	3.365 N
G-T-45	G-T-35	1.752		1.476 Y	2.015 N	2.571 N	3.365 N
G-T-35	G-T-RH35	1.363		1.886 N	2.920 N	4.303 N	6.965 N
G-T-35	G-T-DC35	1.484		1.886 N	2.920 N	4.303 N	6.965 N

t_{stat}: t-test statistic, t_{crit}: value of t calculated from Student's t-distribution, α: level of significance, X%: confidence level,

Y: statistically significant difference, i.e. null hypothesis rejected, N: not statistically significant difference, i.e. null hypothesis rejected.

* T - A - B

T: test → M: macrocell test, SE: Southern Exposure test, CB: cracked beam test, G: ASTM G 109 test.

A: steel type → N: conventional, normalized steel, T: Thermex-treated conventional steel.

B: mix design → 45: *w/c* ratio of 0.45 and no inhibitor, RH45 *w/c* ratio of 0.45 and Rheocrete 222+, DC45: *w/c* ratio of 0.45 and DCI-S, 35: *w/c* ratio of 0.35 and no inhibitor, RH35: *w/c* ratio of 0.35 and Rheocrete 222+, DC35: *w/c* ratio of 0.35 and DCI-S.

Table C.20 – Student's t-test for comparing the mean corrosion rates of conventional normalized, conventional Thermex-treated, and microalloyed steels

Specimens *		t_{stat}	t_{crit}			
		X%:	80%	90%	95%	98%
		α:	0.20	0.10	0.05	0.02
Macrocell test with bare specimens						
M-N	M-T	0.935	1.415 N	1.895 N	2.365 N	2.998 N
M-N	M-CRPT1	0.256	1.415 N	1.895 N	2.365 N	2.998 N
M-N	M-CRPT2	-0.801	1.397 N	1.860 N	2.306 N	2.896 N
M-N	M-CRT	-0.413	1.397 N	1.860 N	2.306 N	2.896 N
Macrocell test with mortar specimens						
M-Nc-50	M-Tc-50	0.483	1.533 N	2.132 N	2.776 N	3.747 N
M-Nc-50	M-CRPT1c-50	-1.220	1.476 N	2.015 N	2.571 N	3.365 N
M-Nc-50	M-CRPT2c-50	-0.529	1.476 N	2.015 N	2.571 N	3.365 N
M-Nc-50	M-CRTc-50	-1.415	1.476 N	2.015 N	2.571 N	3.365 N
M-N-50	M-T-50	-1.178	1.415 N	1.895 N	2.365 N	2.998 N
M-N-50	M-CRPT1-50	-1.074	1.476 N	2.015 N	2.571 N	3.365 N
M-N-50	M-CRPT2-50	-1.199	1.415 N	1.895 N	2.365 N	2.998 N
M-N-50	M-CRT-50	-0.945	1.415 N	1.895 N	2.365 N	2.998 N
Southern Exposure test						
SE-N-45	SE-T-45	-1.491	1.440 Y	1.943 N	2.447 N	3.143 N
SE-N-45	SE-CRPT1-45	-0.984	1.383 N	1.833 N	2.262 N	2.821 N
SE-N-45	SE-CRPT2-45	-0.579	1.440 N	1.943 N	2.447 N	3.143 N
SE-N-45	SE-CRT-45	0.114	1.397 N	1.860 N	2.306 N	2.896 N
SE-N-45	SE-N/CRPT1-45	-1.779	1.440 Y	1.943 N	2.447 N	3.143 N
SE-CRPT1-45	SE-CRPT1/N-45	0.039	1.383 N	1.833 N	2.262 N	2.821 N
Cracked beam test						
CB-N-45	CB-T-45	-0.340	1.440 N	1.943 N	2.447 N	3.143 N
CB-N-45	CB-CRPT1-45	-1.019	1.476 N	2.015 N	2.571 N	3.365 N
CB-N-45	CB-CRPT2-45	-0.649	1.415 N	1.895 N	2.365 N	2.998 N
CB-N-45	CB-CRT-45	-0.096	1.415 N	1.895 N	2.365 N	2.998 N
ASTM G 109 test						
G-N-45	G-T-45	-1.035	1.440 N	1.943 N	2.447 N	3.143 N
G-N-45	G-CRPT1-45	-1.527	1.533 N	2.132 N	2.776 N	3.747 N
G-N-45	G-CRPT2-45	-1.066	1.886 N	2.920 N	4.303 N	6.965 N
G-N-45	G-CRT-45	-1.066	1.886 N	2.920 N	4.303 N	6.965 N

t_{stat}: t-test statistic, t_{crit}: value of t calculated from Student's t-distribution, α: level of significance, X%: confidence level,
Y: statistically significant difference, i.e. null hypothesis rejected, N: not statistically significant difference, i.e. null hypothesis rejected.

* T - A - B

T: test → M: macrocell test, SE: Southern Exposure test, CB: cracked beam test, G: ASTM G 109 test

A: steel type → N: conventional, normalized steel, T: Thermex-treated conventional steel, CRPT1: Thermex-treated microalloyed steel with a high phosphorus content (0.117%), CRPT2: Thermex-treated microalloyed steel with a high phosphorus content (0.100%), CRT: Thermex treated microalloyed steel with normal phosphorus content (0.017%), c: epoxy-filled caps on the end.

B: mix design → 50: *w/c* ratio of 0.50 and no inhibitor, 45: *w/c* ratio of 0.45 and no inhibitor.

Table C.21 – Student's t-test for comparing the mean corrosion losses of conventional normalized, conventional Thermex-treated, and microalloyed steels

Specimens *		t_{stat}	t_{crit} X%:	80%	90%	95%	98%
			α:	0.20	0.10	0.05	0.02
Macrocell test with bare specimens							
M-N	M-T	1.999		1.415 Y	1.895 Y	2.365 N	2.998 N
M-N	M-CRPT1	0.262		1.440 N	1.943 N	2.447 N	3.143 N
M-N	M-CRPT2	-0.824		1.440 N	1.943 N	2.447 N	3.143 N
M-N	M-CRT	1.084		1.476 N	2.015 N	2.571 N	3.365 N
Macrocell test with mortar specimens							
M-Nc-50	M-Tc-50	1.321		1.476 N	2.015 N	2.571 N	3.365 N
M-Nc-50	M-CRPT1c-50	-0.351		1.533 N	2.132 N	2.776 N	3.747 N
M-Nc-50	M-CRPT2c-50	0.296		1.533 N	2.132 N	2.776 N	3.747 N
M-Nc-50	M-CRTc-50	-0.027		1.533 N	2.132 N	2.776 N	3.747 N
M-N-50	M-T-50	-0.780		1.440 N	1.943 N	2.447 N	3.143 N
M-N-50	M-CRPT1-50	-0.972		1.476 N	2.015 N	2.571 N	3.365 N
M-N-50	M-CRPT2-50	-1.482		1.476 Y	2.015 N	2.571 N	3.365 N
M-N-50	M-CRT-50	-0.889		1.440 N	1.943 N	2.447 N	3.143 N
Southern Exposure test							
SE-N-45	SE-T-45	-1.085		1.476 N	2.015 N	2.571 N	3.365 N
SE-N-45	SE-CRPT1-45	0.352		1.415 N	1.895 N	2.365 N	2.998 N
SE-N-45	SE-CRPT2-45	-0.571		1.476 N	2.015 N	2.571 N	3.365 N
SE-N-45	SE-CRT-45	0.292		1.415 N	1.895 N	2.365 N	2.998 N
SE-N-45	SE-N/CRPT1-45	-0.607		1.415 N	1.895 N	2.365 N	2.998 N
SE-CRPT1-45	SE-CRPT1/N-45	-1.087		1.397 N	1.860 N	2.306 N	2.896 N
Cracked beam test							
CB-N-45	CB-T-45	-0.018		1.397 N	1.860 N	2.306 N	2.896 N
CB-N-45	CB-CRPT1-45	-0.593		1.440 N	1.943 N	2.447 N	3.143 N
CB-N-45	CB-CRPT2-45	0.301		1.397 N	1.860 N	2.306 N	2.896 N
CB-N-45	CB-CRT-45	0.301		1.383 N	1.833 N	2.262 N	2.821 N
ASTM G 109 test							
G-N-45	G-T-45	-0.240		1.440 N	1.943 N	2.447 N	3.143 N
G-N-45	G-CRPT1-45	-0.695		1.440 N	1.943 N	2.447 N	3.143 N
G-N-45	G-CRPT2-45	-0.430		1.440 N	1.943 N	2.447 N	3.143 N
G-N-45	G-CRT-45	0.488		1.886 N	2.920 N	4.303 N	6.965 N

t_{stat}: t-test statistic, t_{crit}: value of t calculated from Student's t-distribution, α: level of significance, X%: confidence level,
Y: statistically significant difference, i.e. null hypothesis rejected, N: not statistically significant difference, i.e. null hypothesis rejected.

* T - A - B

T: test → M: macrocell test, SE: Southern Exposure test, CB: cracked beam test, G: ASTM G 109 test.

A: steel type → N: conventional, normalized steel, T: Thermex-treated conventional steel, CRPT1: Thermex-treated microalloyed steel with a high phosphorus content (0.117%), CRPT2: Thermex-treated microalloyed steel with a high phosphorus content (0.100%), CRT: Thermex treated microalloyed steel with normal phosphorus content (0.017%), c: epoxy-filled caps on the end.

B: mix design → 50: *w/c* ratio of 0.50 and no inhibitor, 45: *w/c* ratio of 0.45 and no inhibitor.

Table C.22 – Student's t-test for comparing the mean corrosion rates of conventional and MMFX microcomposite steels

Specimens *		t_{stat}	t_{crit} X%:	80%	90%	95%	98%
			α:	0.20	0.10	0.05	0.02
Macrocell test with bare specimens in 1.6 m ion NaCl							
M-N3	M-MMFX(1)	2.425		1.476 Y	2.015 Y	2.571 N	3.365 N
M-N3	M-MMFX(2)	1.933		1.476 Y	2.015 N	2.571 N	3.365 N
M-MMFX(1)	M-MMFX(2)	-1.352		1.372 N	1.812 N	2.228 N	2.764 N
M-MMFX(2)	M-MMFXs	0.957		1.383 N	1.833 N	2.262 N	2.821 N
M-MMFX(2)	M-MMFXb	2.595		1.397 Y	1.860 Y	2.306 Y	2.896 N
M-MMFX(2)	M-MMFX#19	-3.532		1.372 Y	1.812 Y	2.228 Y	2.764 Y
Macrocell test with bare specimens in 6.04 m ion NaCl							
M-N3h	M-MMFXsh	-2.784		1.397 Y	1.860 Y	2.306 Y	2.896 N
Macrocell test with mortar specimens							
M-N3-50	M-MMFX-50	2.349		1.397 Y	1.860 Y	2.306 Y	2.896 N
M-N3-50	M-N3/MMFX-50	1.888		1.440 Y	1.943 N	2.447 N	3.143 N
M-MMFX-50	M-MMFX/N3-50	-1.236		1.440 N	1.943 N	2.447 N	3.143 N
Southern Exposure test							
SE-N3-45	SE-MMFX-45	0.953		1.476 N	2.015 N	2.571 N	3.365 N
SE-N3-45	SE-N3/MMFX-45	1.385		1.476 N	2.015 N	2.571 N	3.365 N
SE-MMFX-45	SE-MMFX/N3-45	1.509		1.476 Y	2.015 N	2.571 N	3.365 N
SE-MMFX-45	SE-MMFXb-45	2.869		1.476 Y	2.015 Y	2.571 Y	3.365 N
Cracked beam test							
CB-N3-45	CB-MMFX-45	0.266		1.476 N	2.015 N	2.571 N	3.365 N

t_{stat}: t-test statistic, t_{crit}: value of t calculated from Student's t-distribution, α: level of significance, X%: confidence level,

Y: statistically significant difference, i.e. null hypothesis rejected, N: not statistically significant difference, i.e. null hypothesis rejected.

* T - A - B

T: test → M: macrocell test, SE: Southern Exposure test, CB: cracked beam test

A: steel type → N, and N3: conventional, normalized steel, MMFX: MMFX microcomposite steel, s: sandblasted, b: bent bars in the anode or top mat, h: 6.04 m ion concentration.

B: mix design → 50: *w/c* ratio of 0.50 and no inhibitor, 45: *w/c* ratio of 0.45 and no inhibitor.

Table C.23 – Student's t-test for comparing the mean corrosion losses of conventional and MMFX microcomposite steels

Specimens *		t_{stat}	t_{crit}			
		X%:	**80%**	**90%**	**95%**	**98%**
		α:	**0.20**	**0.10**	**0.05**	**0.02**
Macrocell test with bare specimens in 1.6 m ion NaCl						
M-N3	M-MMFX(1)	2.046	1.440 Y	1.943 Y	2.447 N	3.143 N
M-N3	M-MMFX(2)	3.947	1.476 Y	2.015 Y	2.571 Y	3.365 Y
M-MMFX(1)	M-MMFX(2)	4.372	1.383 Y	1.833 Y	2.262 Y	2.821 Y
M-MMFX(2)	M-MMFXs	-0.367	1.415 N	1.895 N	2.365 N	2.998 N
M-MMFX(2)	M-MMFXb	1.582	1.415 Y	1.895 N	2.365 N	2.998 N
M-MMFX(2)	M-MMFX#19	-3.662	1.415 Y	1.895 Y	2.365 Y	2.998 Y
Macrocell test with bare specimens in 6.04 m ion NaCl						
M-N3h	M-MMFXsh	-0.029	1.397 N	1.860 N	2.306 N	2.896 N
Macrocell test with mortar specimens						
M-N3-50	M-MMFX-50	9.808	1.383 Y	1.833 Y	2.262 Y	2.821 Y
M-N3-50	M-N3/MMFX-50	5.900	1.476 Y	2.015 Y	2.571 Y	3.365 Y
M-MMFX-50	M-MMFX/N3-50	-1.498	1.440 Y	1.943 N	2.447 N	3.143 N
Southern Exposure test						
SE-N3-45	SE-MMFX-45	2.436	1.476 Y	2.015 Y	2.571 N	3.365 N
SE-N3-45	SE-N3/MMFX-45	1.590	1.440 Y	1.943 N	2.447 N	3.143 N
SE-MMFX-45	SE-MMFX/N3-45	0.068	1.476 N	2.015 N	2.571 N	3.365 N
SE-MMFX-45	SE-MMFXb-45	-2.003	1.638 Y	2.353 N	3.182 N	4.541 N
Cracked beam test						
CB-N3-45	CB-MMFX-45	2.762	1.476 Y	2.015 Y	2.571 Y	3.365 N

t_{stat}: t-test statistic, t_{crit}: value of t calculated from Student's t-distribution, α: level of significance, X%: confidence level,

Y: statistically significant difference, i.e. null hypothesis rejected, N: not statistically significant difference, i.e. null hypothesis rejected.

* T - A - B

T: test → M: macrocell test, SE: Southern Exposure test, CB: cracked beam test

A: steel type → N, and N3: conventional, normalized steel, MMFX: MMFX microcomposite steel, s: sandblasted, b: bent bars in the anode or top mat, h: 6.04 m ion concentration.

B: mix design → 50: *w/c* ratio of 0.50 and no inhibitor, 45: *w/c* ratio of 0.45 and no inhibitor.

Table C.24 – Student's t-test for comparing mean corrosion rates of conventional uncoated and epoxy-coated steel

Specimens *		t_{stat}	t_{crit} X%:	80%	90%	95%	98%
			α:	0.20	0.10	0.05	0.02
Macrocell test with mortar specimens							
M-N3-50	M-ECR-50[2]	3.902		1.383 Y	1.833 Y	2.262 Y	2.821 Y
Southern Exposure test							
SE-N3-45	SE-ECR-45[2]	1.161		1.476 N	2.015 N	2.571 N	3.365 N
Cracked beam test							
CB-N3-45	CB-ECR-45[2]	-1.865		1.415 Y	1.895 N	2.365 N	2.998 N

t_{stat}: t-test statistic, t_{crit}: value of t calculated from Student's t-distribution, α: level of significance, X%: confidence level,
Y: statistically significant difference, i.e. null hypothesis rejected, N: not statistically significant difference, i.e. null hypothesis rejected.

* T - A - B
T: test → M: macrocell test, SE: Southern Exposure test, CB: cracked beam test
A: steel type → N3: conventional, normalized steel, ECR: epoxy-coated rebar,
B: mix design → 50: *w/c* ratio of 0.50 and no inhibitor, 45: *w/c* ratio of 0.45 and no inhibitor.

[2] Corrosion rate based on total area of bar exposed to solution

Table C.25 – Student's t-test for comparing mean corrosion losses of conventional uncoated and epoxy-coated steel

Specimens *		t_{stat}	t_{crit} X%:	80%	90%	95%	98%
			α:	0.20	0.10	0.05	0.02
Macrocell test with mortar specimens							
M-N3-50	M-ECR-50[2]	14.106		1.415 Y	1.895 Y	2.365 Y	2.998 Y
Southern Exposure test							
SE-N3-45	SE-ECR-45[2]	2.958		1.476 Y	2.015 Y	2.571 Y	3.365 N
Cracked beam test							
CB-N3-45	CB-ECR-45[2]	1.811		1.383 Y	1.833 N	2.262 N	2.821 N

t_{stat}: t-test statistic, t_{crit}: value of t calculated from Student's t-distribution, α: level of significance, X%: confidence level,
Y: statistically significant difference, i.e. null hypothesis rejected, N: not statistically significant difference, i.e. null hypothesis rejected.

* T - A - B
T: test → M: macrocell test, SE: Southern Exposure test, CB: cracked beam test
A: steel type → N3: conventional, normalized steel, ECR: epoxy-coated rebar,
B: mix design → 50: *w/c* ratio of 0.50 and no inhibitor, 45: *w/c* ratio of 0.45 and no inhibitor.

[2] Corrosion loss based on total area of bar exposed to solution

Table C.26 – Student's t-test for comparing the mean corrosion rates of conventional and duplex stainless steels

Specimens *		t_{stat}	t_{crit}			
		X%:	**80%**	**90%**	**95%**	**98%**
		α:	**0.20**	**0.10**	**0.05**	**0.02**
Macrocell test with bare specimens in 1.6 m ion NaCl						
M-N3	M-2205	3.710	1.476 Y	2.015 Y	2.571 Y	3.365 Y
M-N3	M-2205p	3.714	1.476 Y	2.015 Y	2.571 Y	3.365 Y
M-N3	M-2101(1)	3.472	1.476 Y	2.015 Y	2.571 Y	3.365 Y
M-N3	M-2101(1)p	3.706	1.476 Y	2.015 Y	2.571 Y	3.365 Y
M-N3	M-2101(2)	3.391	1.476 Y	2.015 Y	2.571 Y	3.365 Y
M-N3	M-2101(2)p	3.720	1.476 Y	2.015 Y	2.571 Y	3.365 Y
M-N3	M-2101(2)s	1.771	1.372 Y	1.812 N	2.228 N	2.764 N
Macrocell test with bare specimens in 6.04 m ion NaCl						
M-N2h	M-2205h	4.878	1.533 Y	2.132 Y	2.776 Y	3.747 Y
M-N2h	M-2205ph	5.350	1.533 Y	2.132 Y	2.776 Y	3.747 Y
M-N2h	M-2101(1)h	2.152	1.440 Y	1.943 Y	2.447 N	3.143 N
M-N2h	M-2101(1)ph	4.302	1.533 Y	2.132 Y	2.776 Y	3.747 Y
M-N2h	M-2101(2)h	3.013	1.533 Y	2.132 Y	2.776 Y	3.747 N
M-N2h	M-2101(2)ph	5.168	1.533 Y	2.132 Y	2.776 Y	3.747 Y
M-N2h	M-2101(2)sh	0.269	1.415 N	1.895 N	2.365 N	2.998 N
Macrocell test with mortar specimens						
M-N-50	M-2205-50	5.129	1.533 Y	2.132 Y	2.776 Y	3.747 Y
M-N-50	M-2205p-50	5.119	1.533 Y	2.132 Y	2.776 Y	3.747 Y
M-N-50	M-2101(1)-50	1.827	1.440 Y	1.943 N	2.447 N	3.143 N
M-N-50	M-2101(1)p-50	5.131	1.533 Y	2.132 Y	2.776 Y	3.747 Y
M-N-50	M-2101(2)-50	3.374	1.533 Y	2.132 Y	2.776 Y	3.747 N
M-N-50	M-2101(2)p-50	5.104	1.533 Y	2.132 Y	2.776 Y	3.747 Y
Southern Exposure test						
SE-N-45	SE-2205-45	2.494	1.476 Y	2.015 Y	2.571 N	3.365 N
SE-N-45	SE-2205p-45	2.691	1.476 Y	2.015 Y	2.571 Y	3.365 N
SE-N-45	SE-2101(1)-45	-0.684	1.476 N	2.015 N	2.571 N	3.365 N
SE-N-45	SE-2101(1)p-45	0.913	1.476 N	2.015 N	2.571 N	3.365 N
SE-N-45	SE-2101(2)-45	2.272	1.476 Y	2.015 Y	2.571 N	3.365 N
SE-N-45	SE-2101(2)p-45	2.676	1.476 Y	2.015 Y	2.571 Y	3.365 N
SE-N-45	SE-N/2205-45	0.079	1.476 N	2.015 N	2.571 N	3.365 N
SE-2205-45	SE-2205/N-45	0.605	1.476 N	2.015 N	2.571 N	3.365 N
Cracked beam test						
CB-N-45	CB-2205-45	1.596	1.476 Y	2.015 N	2.571 N	3.365 N
CB-N-45	CB-2205p-45	1.972	1.476 Y	2.015 N	2.571 N	3.365 N
CB-N-45	CB-2101(1)-45	0.346	1.533 N	2.132 N	2.776 N	3.747 N
CB-N-45	CB-2101(1)p-45	-0.222	1.440 N	1.943 N	2.447 N	3.143 N
CB-N-45	CB-2101(2)-45	1.395	1.476 N	2.015 N	2.571 N	3.365 N
CB-N-45	CB-2101(2)p-45	1.965	1.476 Y	2.015 N	2.571 N	3.365 N

t_{stat}: t-test statistic, t_{crit}: value of t calculated from Student's t-distribution, α: level of significance, X%: confidence level,

Y: statistically significant difference, i.e. null hypothesis rejected, N: not statistically significant difference, i.e. null hypothesis rejected.

* T - A - B

T: test → M: macrocell test, SE: Southern Exposure test, CB: cracked beam test

A: steel type → N, N2, and N3: conventional, normalized steel, 2101(1) and 2101(2): duplex stainless steel (21% chromium, 1% nickel), 2205: duplex stainless steel (22% chromium, 5% nickel), p: pickled, s: sandblasted, h: 6.04 m ion concentration.

B: mix design → 50: *w/c* ratio of 0.50 and no inhibitor, 45: *w/c* ratio of 0.45 and no inhibitor.

Table C.27 – Student's t-test for comparing mean corrosion rates of pickled and non-pickled duplex steels

Specimens *		t_{stat}	t_{crit}			
		X%:	**80%**	**90%**	**95%**	**98%**
		α:	**0.20**	**0.10**	**0.05**	**0.02**
Macrocell test with bare specimens						
M-2205	M-2205p	0.759	1.533 N	2.132 N	2.776 N	3.747 N
M-2101(1)	M-2101(1)p	5.395	1.533 Y	2.132 Y	2.776 Y	3.747 Y
M-2101(2)	M-2101(2)p	3.204	1.476 Y	2.015 Y	2.571 Y	3.365 N
M-2205p	M-2101(2)p	2.682	1.397 Y	1.860 Y	2.306 Y	2.896 N
Macrocell test with bare specimens in 6.04 m ion NaCl						
M-2205h	M-2205ph	8.343	1.476 Y	2.015 Y	2.571 Y	3.365 Y
M-2101(1)h	M-2101(1)ph	2.913	1.476 Y	2.015 Y	2.571 Y	3.365 N
M-2101(2)h	M-2101(2)ph	9.650	1.397 Y	1.860 Y	2.306 Y	2.896 Y
M-2205ph	M-2101(2)ph	-1.168	1.476 N	2.015 N	2.571 N	3.365 N
Macrocell test with mortar specimens						
M-2205-50	M-2205p-50	-1.000	1.440 N	1.943 N	2.447 N	3.143 N
M-2101(1)-50	M-2101(1)p-50	3.207	1.638 Y	2.353 Y	3.182 Y	4.541 N
M-2101(2)-50	M-2101(2)p-50	5.184	1.476 Y	2.015 Y	2.571 Y	3.365 Y
M-2205p-50	M-2101(2)p-50	-1.206	1.383 N	1.833 N	2.262 N	2.821 N
Southern Exposure test						
SE-2205-45	SE-2205p-45	1.469	1.533 N	2.132 N	2.776 N	3.747 N
SE-2101(1)-45	SE-2101(1)p-45	1.600	1.638 N	2.353 N	3.182 N	4.541 N
SE-2101(2)-45	SE-2101(2)p-45	1.819	1.533 Y	2.132 N	2.776 N	3.747 N
SE-2205p-45	SE-2101(2)p-45	-1.239	1.533 N	2.132 N	2.776 N	3.747 N
Cracked beam test						
CB-2205-45	CB-2205p-45	1.299	1.533 N	2.132 N	2.776 N	3.747 N
CB-2101(1)-45	CB-2101(1)p-45	-0.587	1.638 N	2.353 N	3.182 N	4.541 N
CB-2101(2)-45	CB-2101(2)p-45	4.479	1.533 Y	2.132 Y	2.776 Y	3.747 Y
CB-2205p-45	CB-2101(2)p-45	-0.897	1.415 N	1.895 N	2.365 N	2.998 N

t_{stat}: t-test statistic, t_{crit}: value of t calculated from Student's t-distribution, α: level of significance, X%: confidence level,

Y: statistically significant difference, i.e. null hypothesis rejected, N: not statistically significant difference, i.e. null hypothesis rejected.

* T - A - B

T: test → M: macrocell test, SE: Southern Exposure test, CB: cracked beam test

A: steel type → 2101(1) and 2101(2): duplex stainless steel (21% chromium, 1% nickel), 2205: duplex stainless steel (22% chromium, 5% nickel), p: pickled, s: sandblasted, h: 6.04 m ion concentration.

B: mix design → 50: *w/c* ratio of 0.50 and no inhibitor, 45: *w/c* ratio of 0.45 and no inhibitor.

Table C.28 – Student's t-test for comparing the mean corrosion losses of conventional and duplex stainless steels

Specimens *		t_{stat}	t_{crit} X%:	80%	90%	95%	98%
			α:	0.20	0.10	0.05	0.02
Macrocell test with bare specimens in 1.6 m ion NaCl							
M-N3	M-2205	5.635		1.476 Y	2.015 Y	2.571 Y	3.365 Y
M-N3	M-2205p	5.644		1.476 Y	2.015 Y	2.571 Y	3.365 Y
M-N3	M-2101(1)	4.823		1.476 Y	2.015 Y	2.571 Y	3.365 Y
M-N3	M-2101(1)p	5.594		1.476 Y	2.015 Y	2.571 Y	3.365 Y
M-N3	M-2101(2)	4.726		1.476 Y	2.015 Y	2.571 Y	3.365 Y
M-N3	M-2101(2)p	5.632		1.476 Y	2.015 Y	2.571 Y	3.365 Y
M-N3	M-2101(2)s	1.253		1.397 N	1.860 N	2.306 N	2.896 N
Macrocell test with bare specimens in 6.04 m ion NaCl							
M-N2h	M-2205h	9.272		1.533 Y	2.132 Y	2.776 Y	3.747 Y
M-N2h	M-2205ph	9.759		1.533 Y	2.132 Y	2.776 Y	3.747 Y
M-N2h	M-2101(1)h	5.112		1.440 Y	1.943 Y	2.447 Y	3.143 Y
M-N2h	M-2101(1)ph	7.488		1.476 Y	2.015 Y	2.571 Y	3.365 Y
M-N2h	M-2101(2)h	6.116		1.533 Y	2.132 Y	2.776 Y	3.747 Y
M-N2h	M-2101(2)ph	9.610		1.533 Y	2.132 Y	2.776 Y	3.747 Y
M-N2h	M-2101(2)sh	0.345		1.440 N	1.943 N	2.447 N	3.143 N
Macrocell test with mortar specimens							
M-N-50	M-2205-50	5.653		1.533 Y	2.132 Y	2.776 Y	3.747 Y
M-N-50	M-2205p-50	5.653		1.533 Y	2.132 Y	2.776 Y	3.747 Y
M-N-50	M-2101(1)-50	3.762		1.476 Y	2.015 Y	2.571 Y	3.365 Y
M-N-50	M-2101(1)p-50	5.671		1.533 Y	2.132 Y	2.776 Y	3.747 Y
M-N-50	M-2101(2)-50	4.422		1.533 Y	2.132 Y	2.776 Y	3.747 Y
M-N-50	M-2101(2)p-50	5.650		1.533 Y	2.132 Y	2.776 Y	3.747 Y
Southern Exposure test							
SE-N-45	SE-2205-45	8.434		1.476 Y	2.015 Y	2.571 Y	3.365 Y
SE-N-45	SE-2205p-45	8.544		1.476 Y	2.015 Y	2.571 Y	3.365 Y
SE-N-45	SE-2101(1)-45	2.309		1.533 Y	2.132 Y	2.776 N	3.747 N
SE-N-45	SE-2101(1)p-45	6.307		1.440 Y	1.943 Y	2.447 Y	3.143 Y
SE-N-45	SE-2101(2)-45	7.971		1.476 Y	2.015 Y	2.571 Y	3.365 Y
SE-N-45	SE-2101(2)p-45	8.542		1.476 Y	2.015 Y	2.571 Y	3.365 Y
SE-N-45	SE-N/2205-45	0.908		1.533 N	2.132 N	2.776 N	3.747 N
SE-2205-45	SE-2205/N-45	-0.504		1.476 N	2.015 N	2.571 N	3.365 N
Cracked beam test							
CB-N-45	CB-2205-45	7.376		1.476 Y	2.015 Y	2.571 Y	3.365 Y
CB-N-45	CB-2205p-45	7.585		1.476 Y	2.015 Y	2.571 Y	3.365 Y
CB-N-45	CB-2101(1)-45	5.497		1.440 Y	1.943 Y	2.447 Y	3.143 Y
CB-N-45	CB-2101(1)p-45	6.591		1.476 Y	2.015 Y	2.571 Y	3.365 Y
CB-N-45	CB-2101(2)-45	6.181		1.476 Y	2.015 Y	2.571 Y	3.365 Y
CB-N-45	CB-2101(2)p-45	7.586		1.476 Y	2.015 Y	2.571 Y	3.365 Y

t_{stat}: t-test statistic, t_{crit}: value of t calculated from Student's t-distribution, α: level of significance, X%: confidence level,

Y: statistically significant difference, i.e. null hypothesis rejected, N: not statistically significant difference, i.e. null hypothesis rejected.

* T - A - B

T: test → M: macrocell test, SE: Southern Exposure test, CB: cracked beam test

A: steel type → N, N2, and N3: conventional, normalized steel, 2101(1) and 2101(2): duplex stainless steel (21% chromium, 1% nickel), 2205: duplex stainless steel (22% chromium, 5% nickel), p: pickled, s: sandblasted, h: 6.04 m ion concentration.

B: mix design → 50: *w/c* ratio of 0.50 and no inhibitor, 45: *w/c* ratio of 0.45 and no inhibitor.

Table C.29 – Student's t-test for comparing mean corrosion losses of pickled and non-pickled duplex steels

Specimens *		t_{stat}	t_{crit} X%:	80%	90%	95%	98%
			α:	0.20	0.10	0.05	0.02
Macrocell test with bare specimens							
M-2205	M-2205p	2.008		1.533 Y	2.132 N	2.776 N	3.747 N
M-2101(1)	M-2101(1)p	1.963		1.533 Y	2.132 N	2.776 N	3.747 N
M-2101(2)	M-2101(2)p	8.476		1.476 Y	2.015 Y	2.571 Y	3.365 Y
M-2205p	M-2101(2)p	-0.980		1.476 N	2.015 N	2.571 N	3.365 N
Macrocell test with bare specimens in 6.04 m ion NaCl							
M-2205h	M-2205ph	8.565		1.476 Y	2.015 Y	2.571 Y	3.365 Y
M-2101(1)h	M-2101(1)ph	3.124		1.415 Y	1.895 Y	2.365 Y	2.998 Y
M-2101(2)h	M-2101(2)ph	13.113		1.476 Y	2.015 Y	2.571 Y	3.365 Y
M-2205ph	M-2101(2)ph	-3.490		1.476 Y	2.015 Y	2.571 Y	3.365 Y
Macrocell test with mortar specimens							
M-2205-50	M-2205p-50	-0.019		1.397 N	1.860 N	2.306 N	2.896 N
M-2101(1)-50	M-2101(1)p-50	2.828		1.638 Y	2.353 Y	3.182 N	4.541 N
M-2101(2)-50	M-2101(2)p-50	6.169		1.476 Y	2.015 Y	2.571 Y	3.365 Y
M-2205p-50	M-2101(2)p-50	-0.409		1.383 N	1.833 N	2.262 N	2.821 N
Southern Exposure test							
SE-2205-45	SE-2205p-45	1.344		1.533 N	2.132 N	2.776 N	3.747 N
SE-2101(1)-45	SE-2101(1)p-45	2.651		1.638 Y	2.353 Y	3.182 N	4.541 N
SE-2101(2)-45	SE-2101(2)p-45	2.120		1.533 Y	2.132 N	2.776 N	3.747 N
SE-2205p-45	SE-2101(2)p-45	-0.224		1.440 N	1.943 N	2.447 N	3.143 N
Cracked beam test							
CB-2205-45	CB-2205p-45	1.419		1.533 N	2.132 N	2.776 N	3.747 N
CB-2101(1)-45	CB-2101(1)p-45	1.739		1.638 Y	2.353 N	3.182 N	4.541 N
CB-2101(2)-45	CB-2101(2)p-45	16.586		1.533 Y	2.132 Y	2.776 Y	3.747 Y
CB-2205p-45	CB-2101(2)p-45	0.197		1.415 N	1.895 N	2.365 N	2.998 N

t_{stat}: t-test statistic, t_{crit}: value of t calculated from Student's t-distribution, α: level of significance, X%: confidence level,

Y: statistically significant difference, i.e. null hypothesis rejected, N: not statistically significant difference, i.e. null hypothesis rejected.

* T - A - B

T: test → M: macrocell test, SE: Southern Exposure test, CB: cracked beam test

A: steel type → 2101(1) and 2101(2): duplex stainless steel (21% chromium, 1% nickel), 2205: duplex stainless steel (22% chromium, 5% nickel), p: pickled, s: sandblasted, h: 6.04 m ion concentration.

B: mix design → 50: *w/c* ratio of 0.50 and no inhibitor, 45: *w/c* ratio of 0.45 and no inhibitor.

APPENDIX D

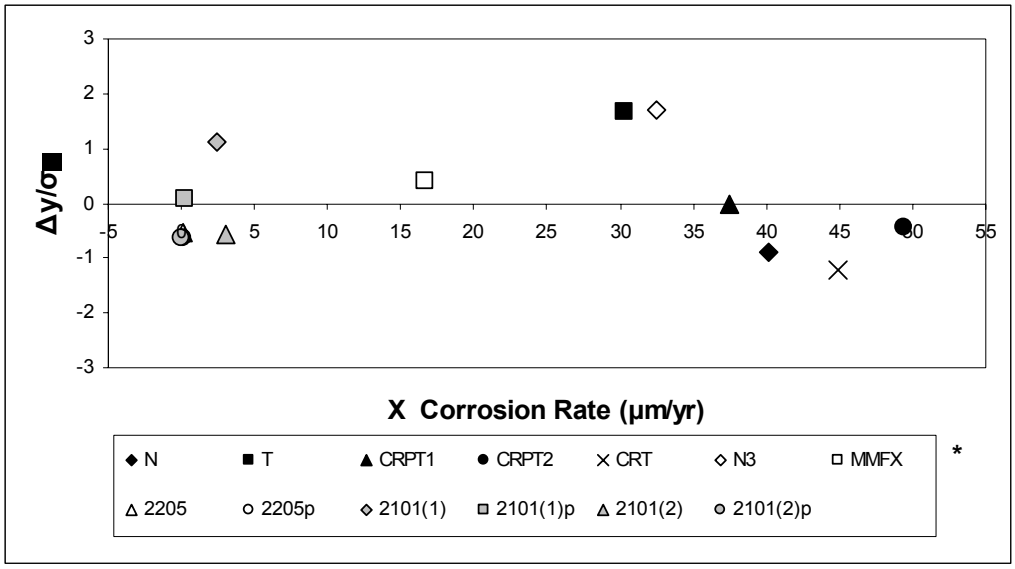

(a) Corrosion rates

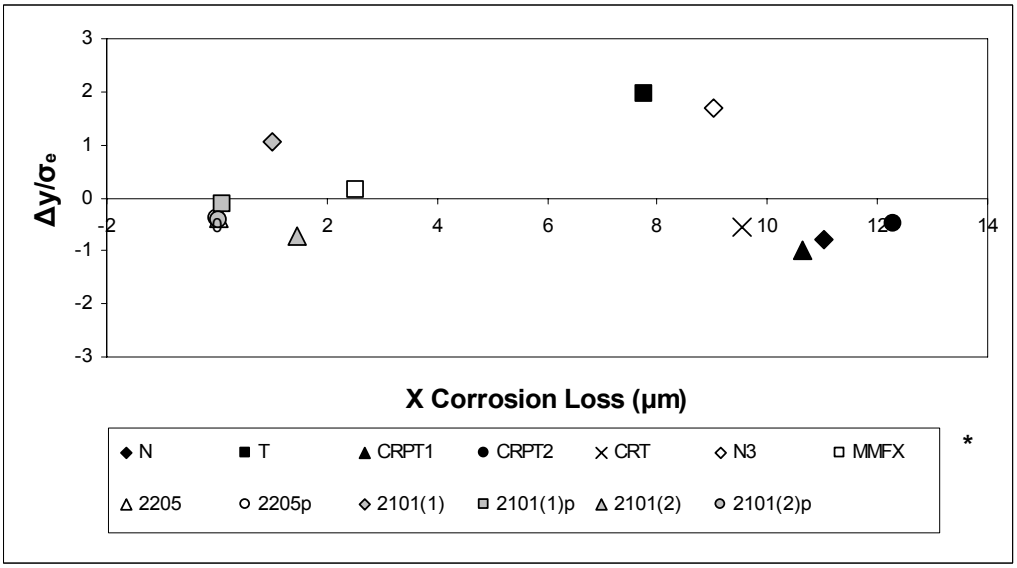

(b) Total corrosion losses

*** Steel type** → N and N3: conventional, normalized steel, T: Thermex-treated conventional steel, CRPT1: Thermex-treated microalloyed steel with a high phosphorus content (0.117%), CRPT2: Thermex-treated microalloyed steel with a high phosphorus content (0.100%), CRT: Thermex treated microalloyed steel with normal phosphorus content (0.017%), 2101(1) and 2101(2): duplex stainless steel (21% chromium, 1% nickel), 2205: duplex stainless steel (22% chromium, 5% nickel), p: pickled.

Figure D.1 – (a) Corrosion rates and (b) Total corrosion losses, distribution of standardized residuals for Southern Exposure test versus rapid macrocell test with bare bars in 1.6 m ion NaCl and simulated concrete pore solution.

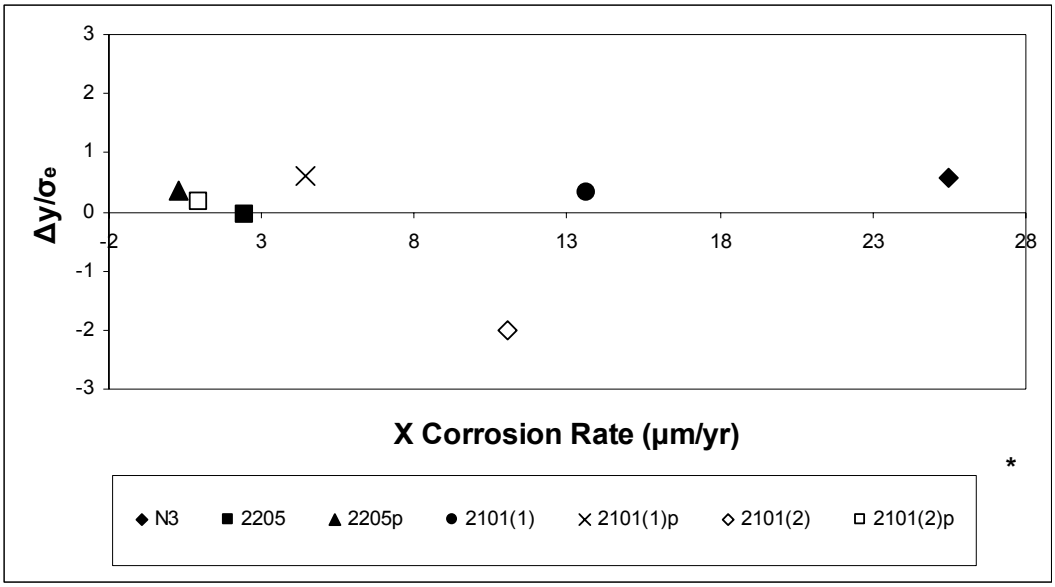

(a) Corrosion rates

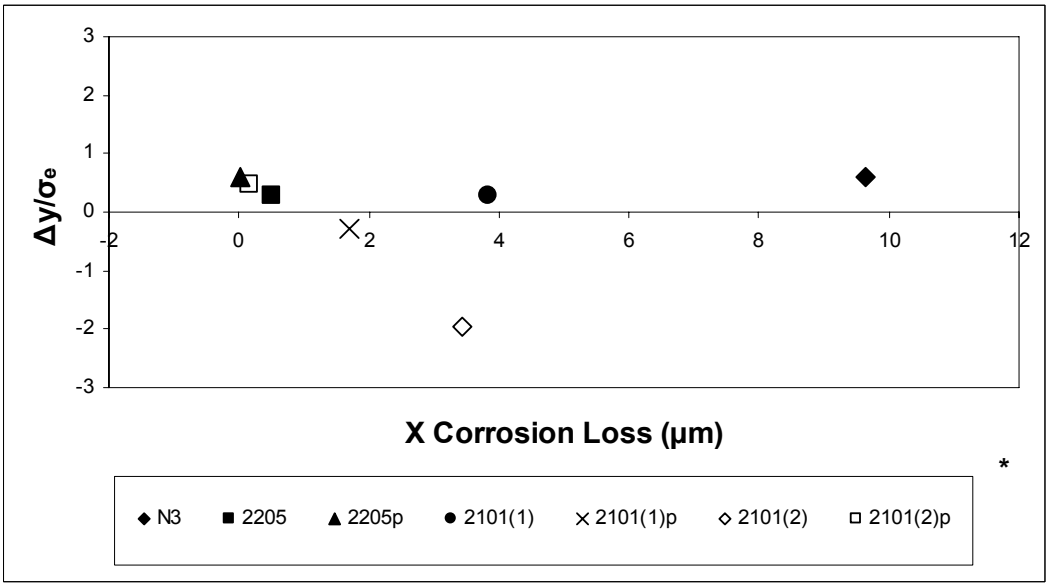

(b) Total corrosion losses

*** Steel type** → N3: conventional, normalized steel, 2101(1) and 2101(2): duplex stainless steel (21% chromium, 1% nickel), 2205: duplex stainless steel (22% chromium, 5% nickel), p: pickled.

Figure D.2 – (a) Corrosion rates and (b) Total corrosion losses, distribution of standardized residuals for Southern Exposure test versus rapid macrocell test with bare bars in 6.04 m ion NaCl and simulated concrete pore solution.

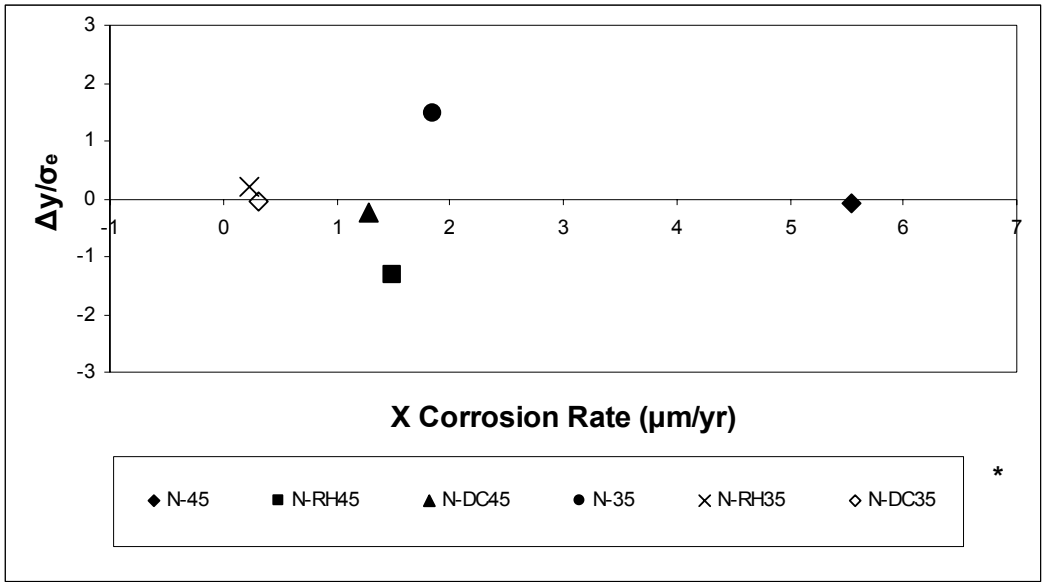

(a) Corrosion rates

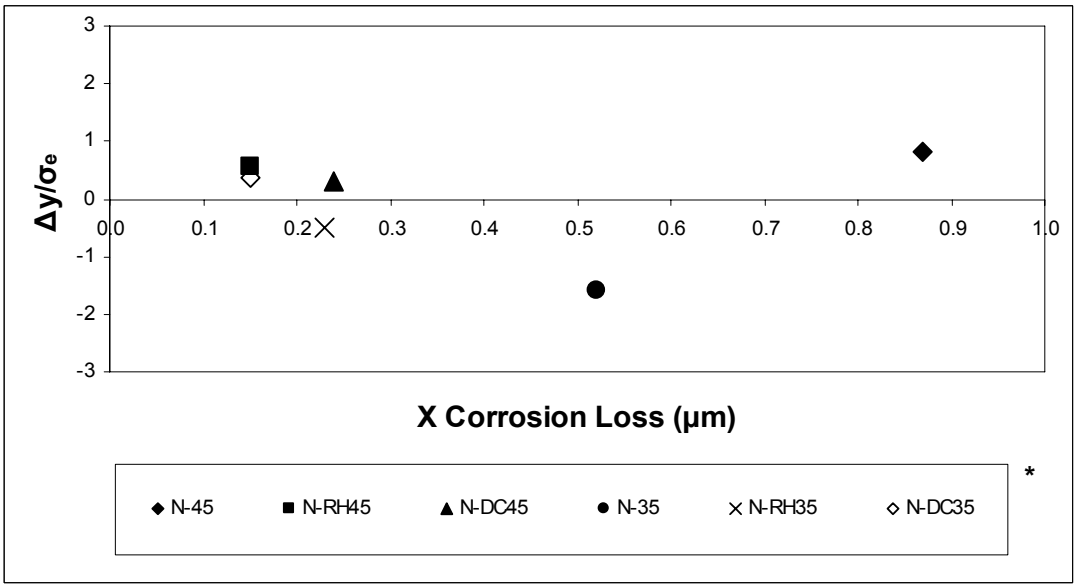

(b) Total corrosion losses

* A-B
A: steel type → N: conventional, normalized steel.
B: mix design → 45: *w/c* ratio of 0.45 and no inhibitor, RH45: *w/c* ratio of 0.45 and Rheocrete 222+, DC45: *w/c* ratio of 0.45 and DCI-S, 35: *w/c* ratio of 0.35 and no inhibitor, RH35: *w/c* ratio of 0.35 and Rheocrete 222+, DC35: *w/c* ratio of 0.35 and DCI-S.

Figure D.3 – (a) Corrosion rates and (b) Total corrosion losses, distribution of standardized residuals for Southern Exposure test versus rapid macrocell test with lollipop specimens in 1.6 m ion NaCl and simulated concrete pore solution.

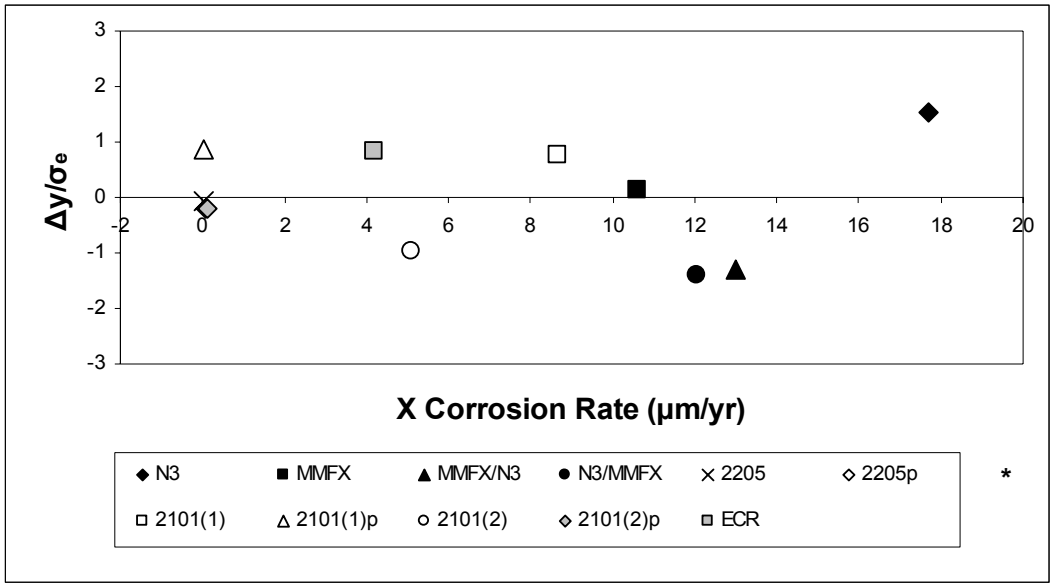

(a) Corrosion rates

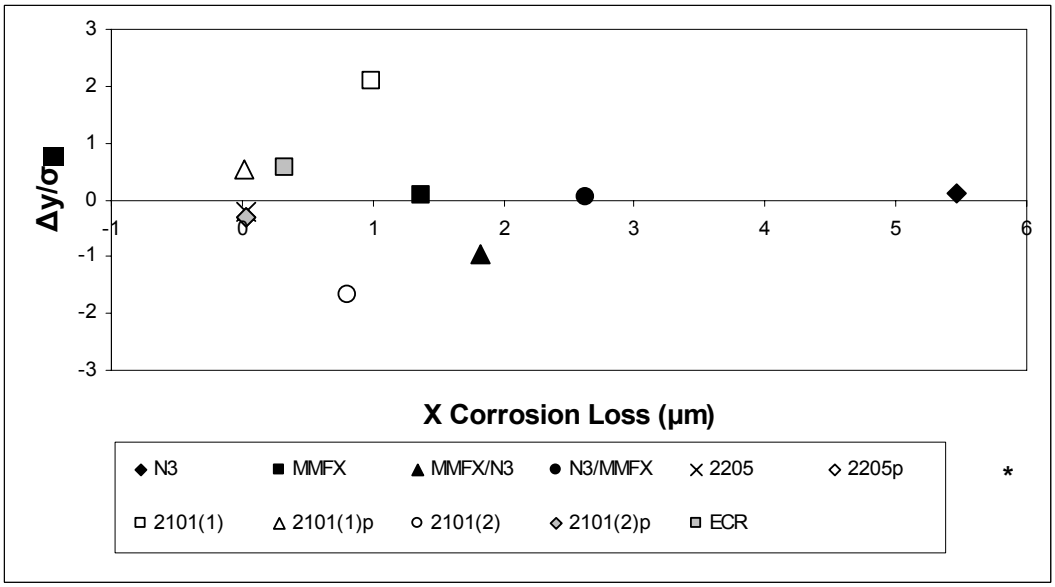

(b) Total corrosion losses

*** Steel type** → N3: conventional, normalized steel, MMFX: MMFX microcomposite steel, MMFX/N3: MMFX steel in the top mat and N3 steel in the bottom mat, N3/MMFX: N3 steel in the top mat and MMFX steel in the bottom mat, 2101(1) and 2101(2): duplex stainless steel (21% chromium, 1% nickel), 2205: duplex stainless steel (22% chromium, 5% nickel), ECR: epoxy-coated steel, p: pickled.

Figure D.4 – (a) Corrosion rates and (b) Total corrosion losses, distribution of standardized residuals for Southern Exposure test versus rapid macrocell test with mortar-wrapped specimens in 1.6 m ion NaCl and simulated concrete pore solution.

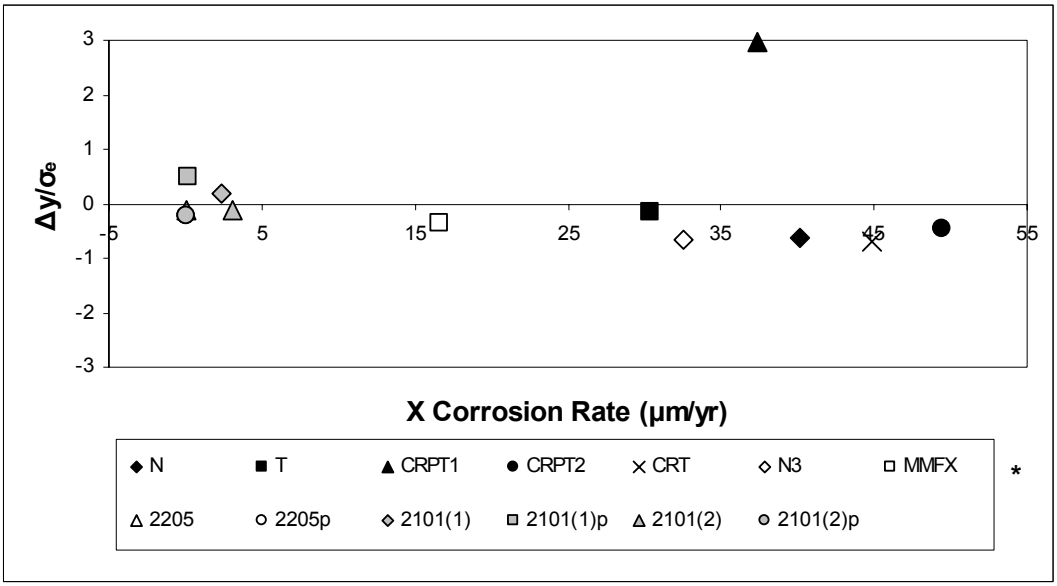

(a) Corrosion rates

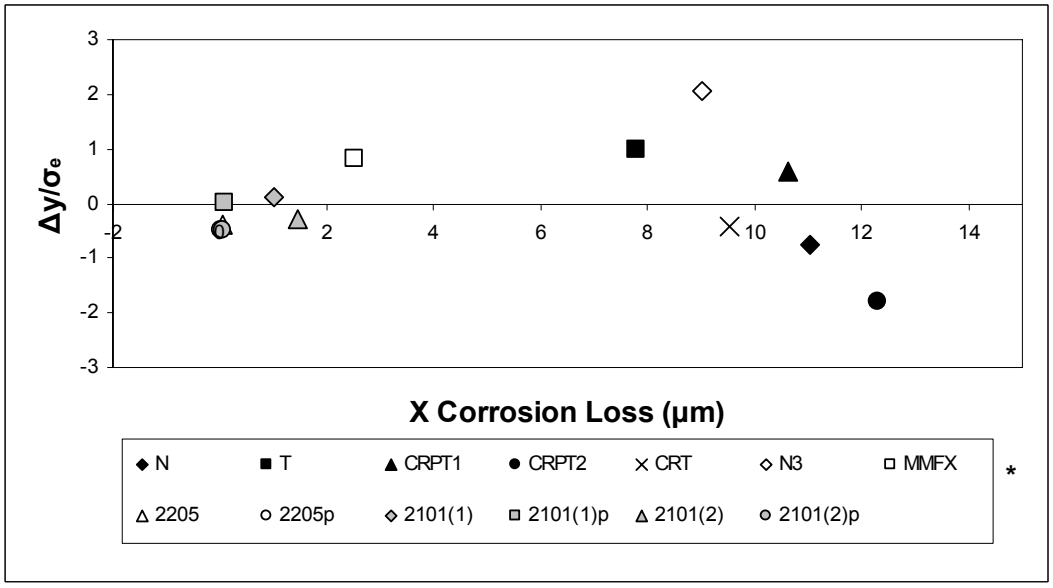

(b) Total corrosion losses

*** Steel type** → N and N3: conventional, normalized steel, T: Thermex-treated conventional steel, CRPT1: Thermex-treated microalloyed steel with a high phosphorus content (0.117%), CRPT2: Thermex-treated microalloyed steel with a high phosphorus content (0.100%), CRT: Thermex treated microalloyed steel with normal phosphorus content (0.017%), 2101(1) and 2101(2): duplex stainless steel (21% chromium, 1% nickel), 2205: duplex stainless steel (22% chromium, 5% nickel), p: pickled.

Figure D.5 – (a) Corrosion rates and (b) Total corrosion losses, distribution of standardized residuals for cracked beam test versus rapid macrocell test with bare bars in 1.6 m ion NaCl and simulated concrete pore solution.

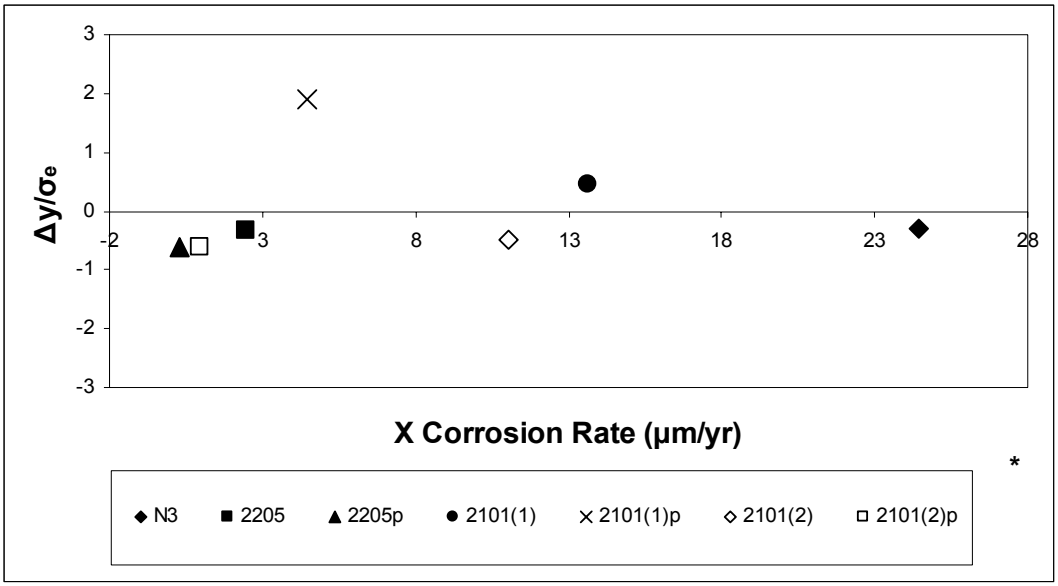

(a) Corrosion rates

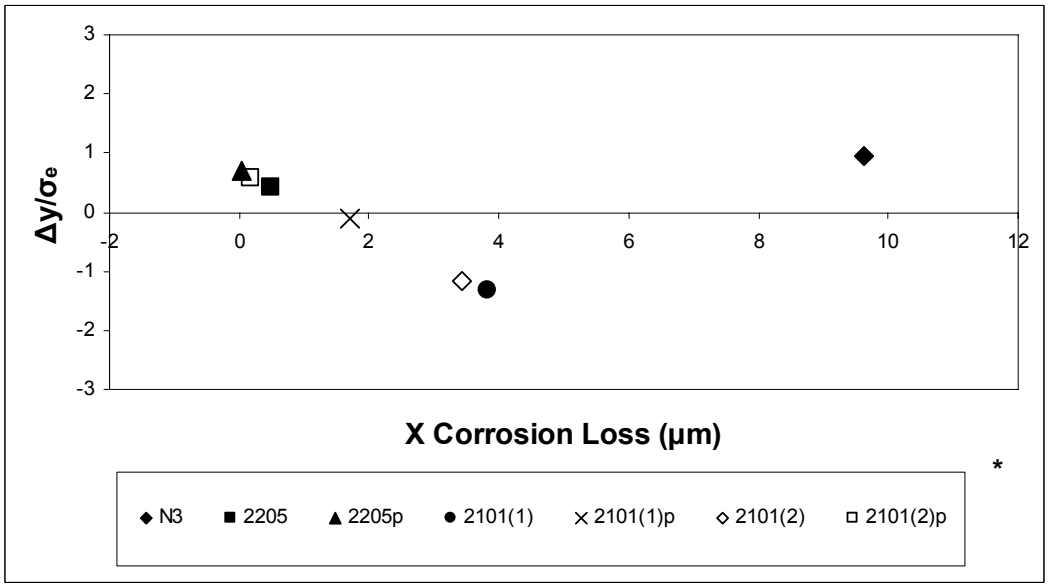

(b)

Total corrosion losses

*** Steel type** → N3: conventional, normalized steel, 2101(1) and 2101(2): duplex stainless steel (21% chromium, 1% nickel), 2205: duplex stainless steel (22% chromium, 5% nickel), p: pickled.

Figure D.6 – (a) Corrosion rates and (b) Total corrosion losses, distribution of standardized residuals for cracked beam test versus rapid macrocell test with bare bars in 6.04 m ion NaCl and simulated concrete pore solution.

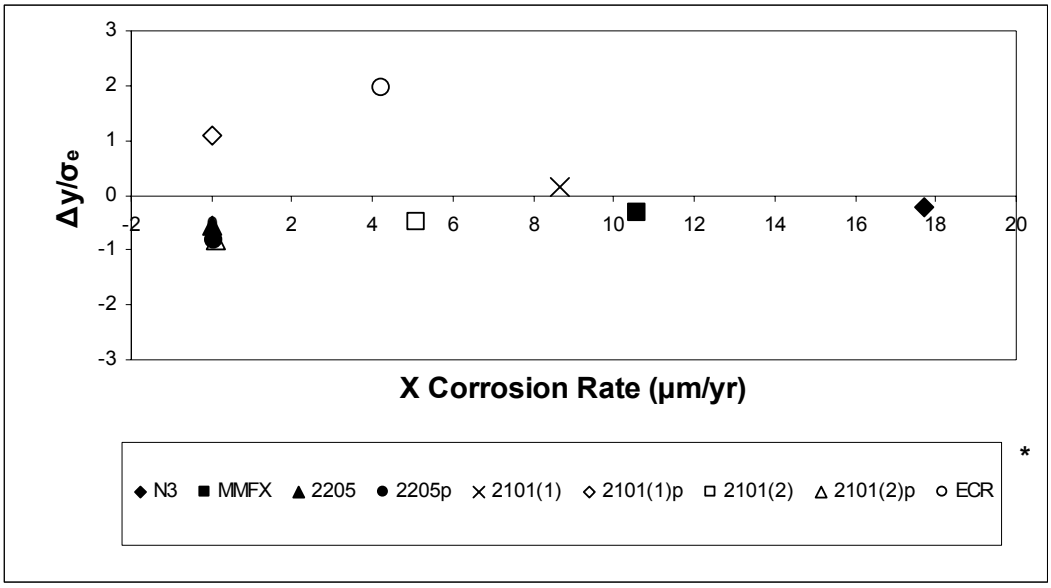

(a) Corrosion rates

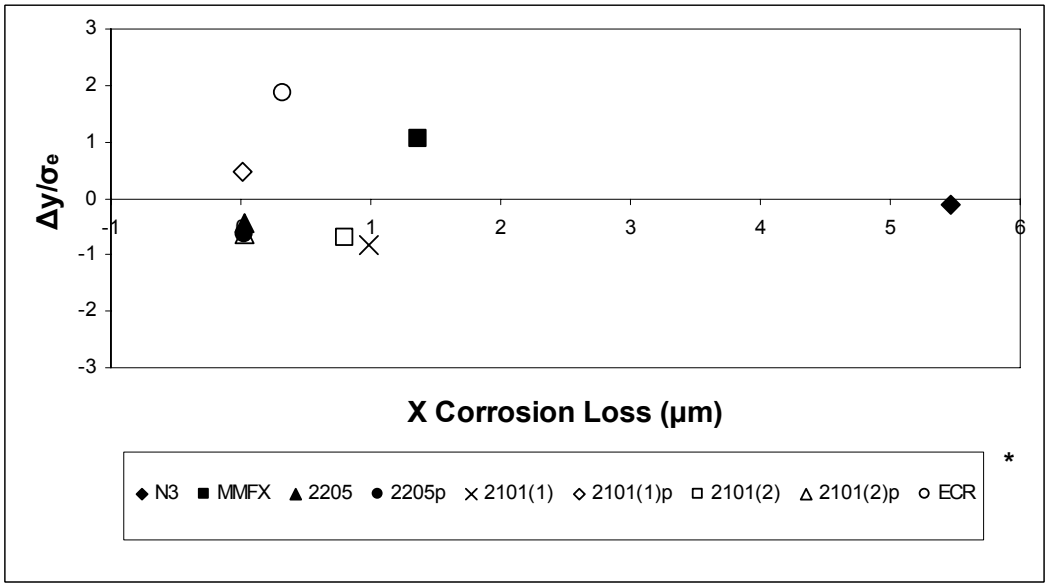

(b) Total corrosion losses

*** Steel type** → N3: conventional, normalized steel, MMFX: MMFX microcomposite steel, 2101(1) and 2101(2): duplex stainless steel (21% chromium, 1% nickel), 2205: duplex stainless steel (22% chromium, 5% nickel), ECR: epoxy-coated steel, p: pickled.

Figure D.7 – (a) Corrosion rates and (b) Total corrosion losses, distribution of standardized residuals for cracked beam test versus rapid macrocell test with mortar-wrapped specimens in 1.6 m ion NaCl and simulated concrete pore solution.

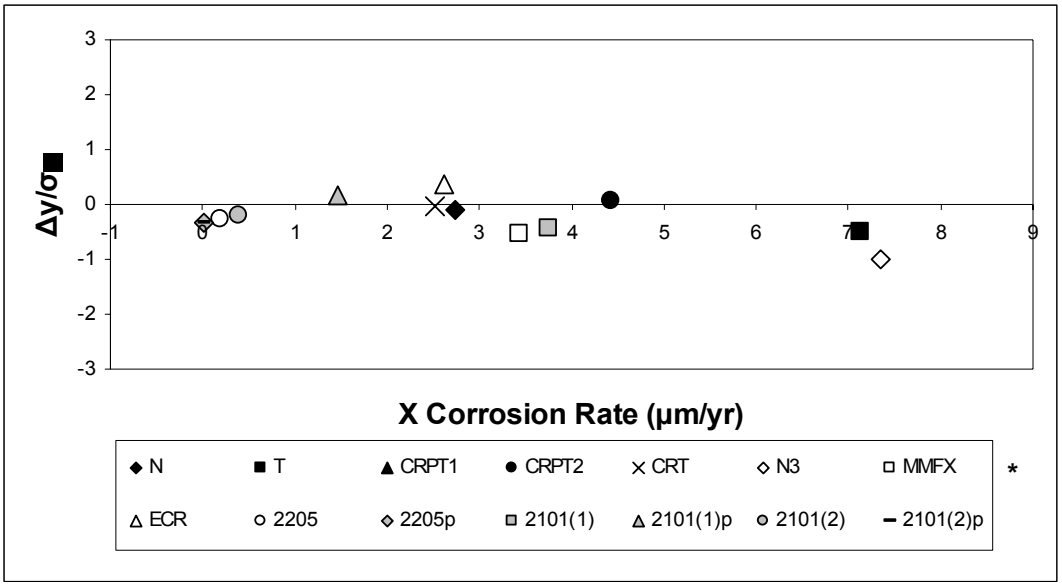

(a) Corrosion rates

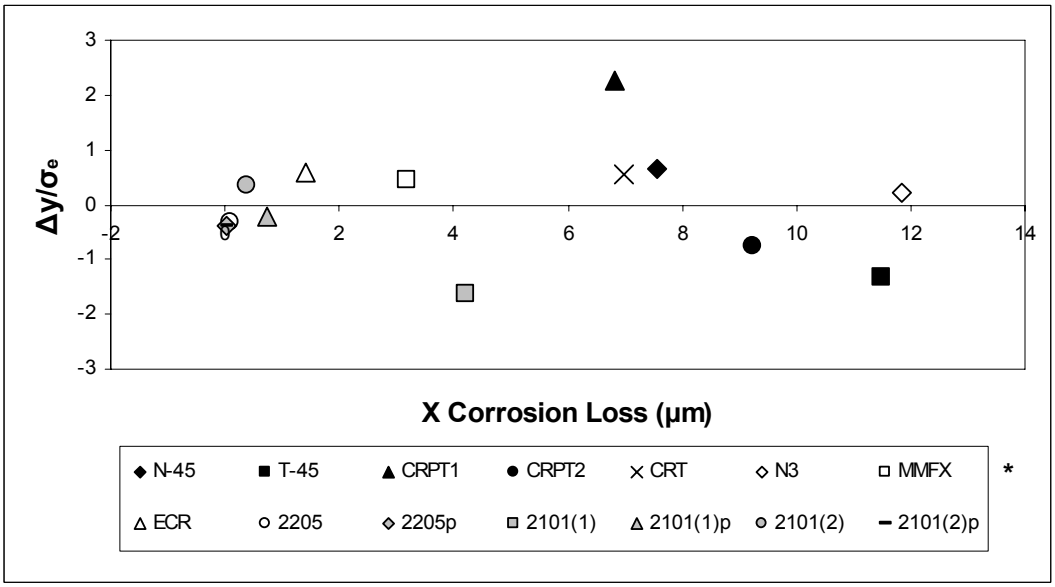

(b) Total corrosion losses

*** Steel type** → N and N3: conventional, normalized steel, T: Thermex-treated conventional steel, CRPT1: Thermex- treated microalloyed steel with a high phosphorus content (0.117%), CRPT2: Thermex-treated microalloyed steel with a high phosphorus content (0.100%), CRT: Thermex treated microalloyed steel with normal phosphorus content (0.017%), MMFX, MMFX microcomposite steel, ECR: epoxy-coated steel, 2101(1) and 2101(2): duplex stainless steel (21% chromium, 1% nickel), 2205: duplex stainless steel (22% chromium, 5% nickel), p: pickled.

Figure D.8 – (a) Corrosion rates and (b) Total corrosion losses, distribution of standardized residuals for cracked beam test versus Southern Exposure test for specimens with different reinforcing steel.

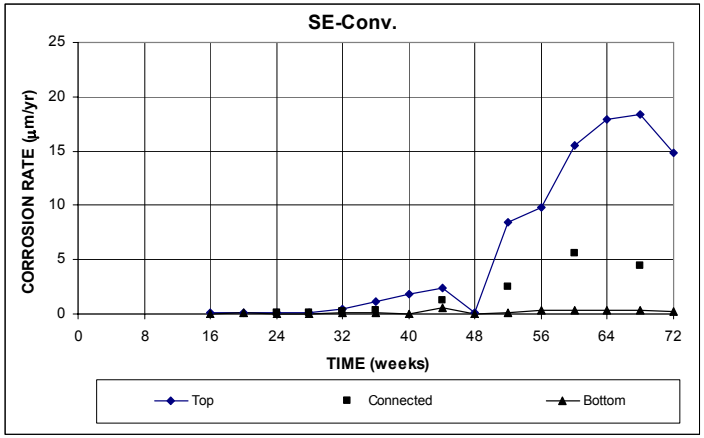

(a)

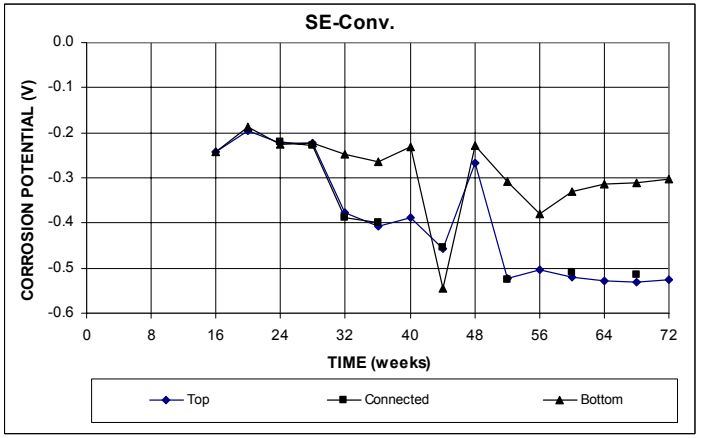

(b)

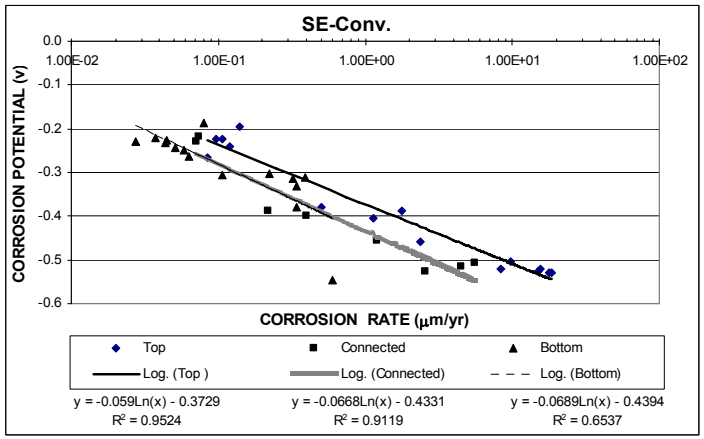

(b)

Figure E.1 – (a) Corrosion rate, (b) corrosion potential, and (c) correlation between microcell corrosion rate and corrosion potential as measured in the LPR test for the Southern Exposure specimen with conventional steel.

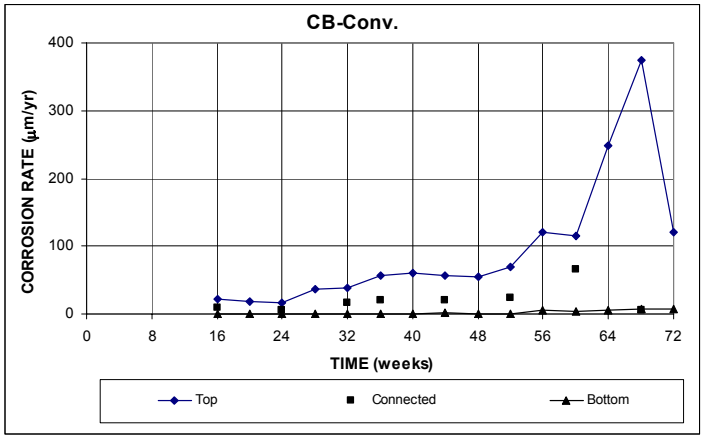

(a)

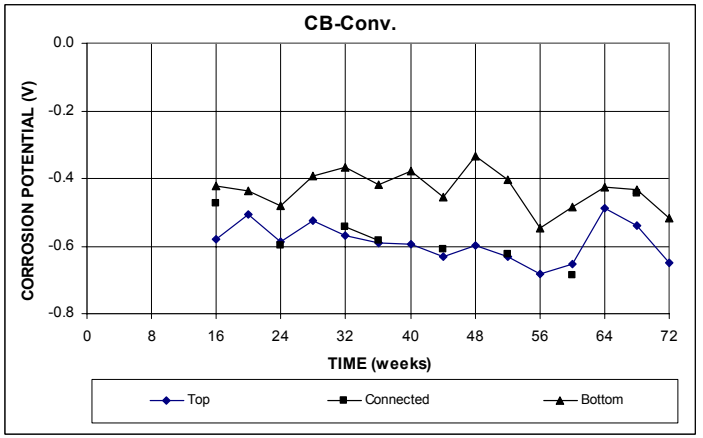

(b)

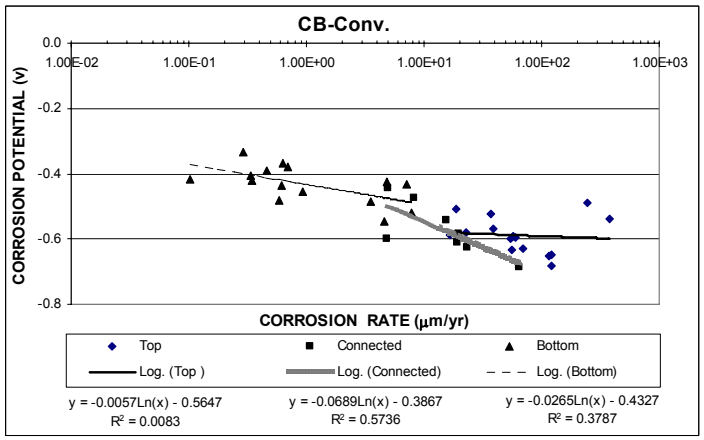

(c)

Figure E.2 – (a) Corrosion rate, (b) corrosion potential, and (c) correlation between microcell corrosion rate and corrosion potential as measured in the LPR test for the cracked beam specimen with conventional steel.

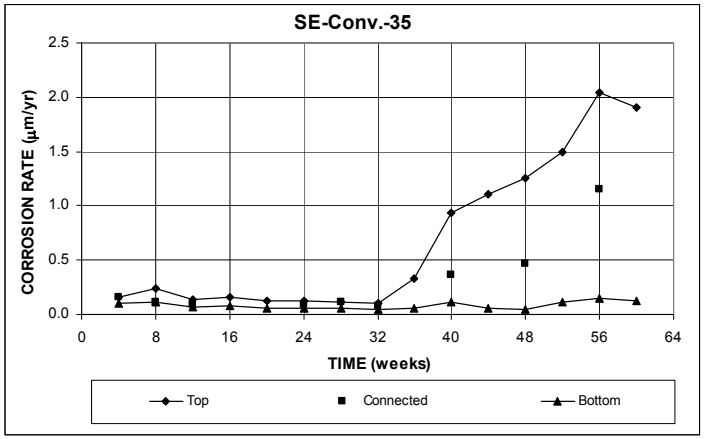

(a)

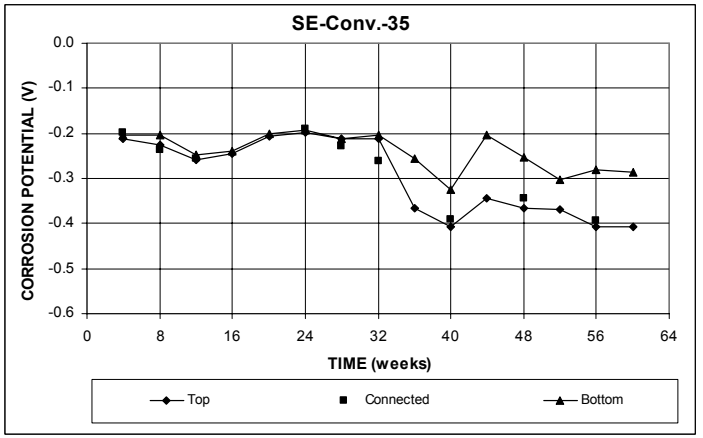

(b)

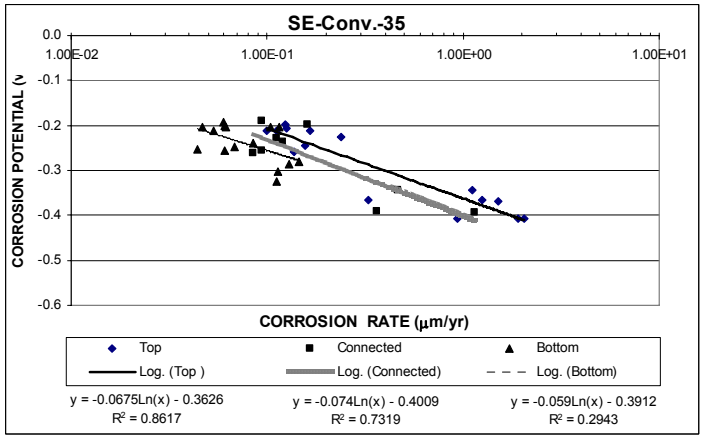

(c)

Figure E.3 – (a) Corrosion rate, (b) corrosion potential, and (c) correlation between microcell corrosion rate and corrosion potential as measured in the LPR test for the Southern Exposure specimen with conventional steel, a water-cement of 0.35.

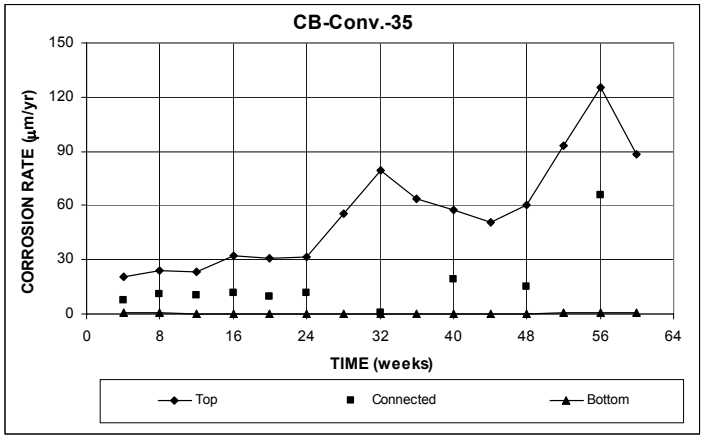

(a)

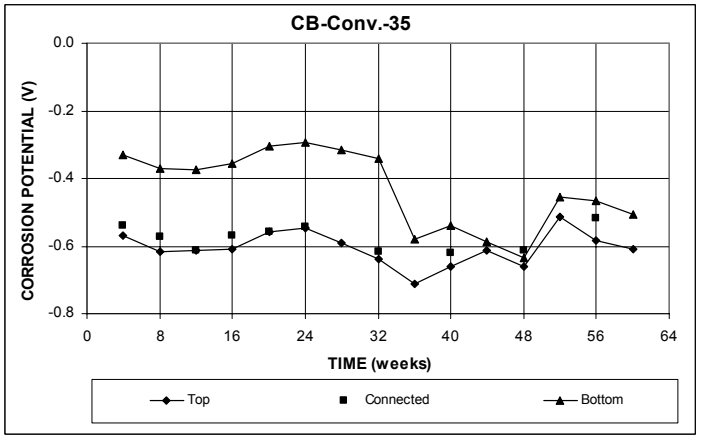

(b)

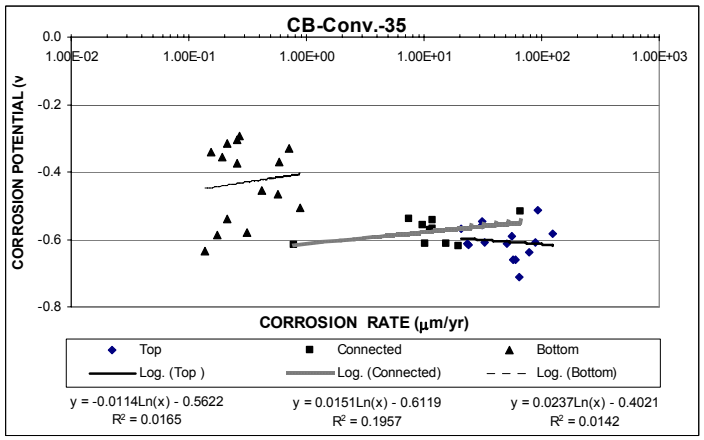

(c)

Figure E.4 – (a) Corrosion rate, (b) corrosion potential, and (c) correlation between microcell corrosion rate and corrosion potential as measured in the LPR test for the cracked beam specimen with conventional steel, a water-cement of 0.35.

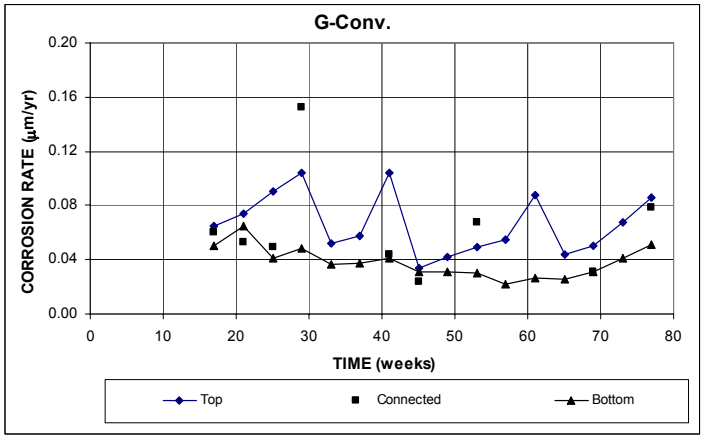

(a)

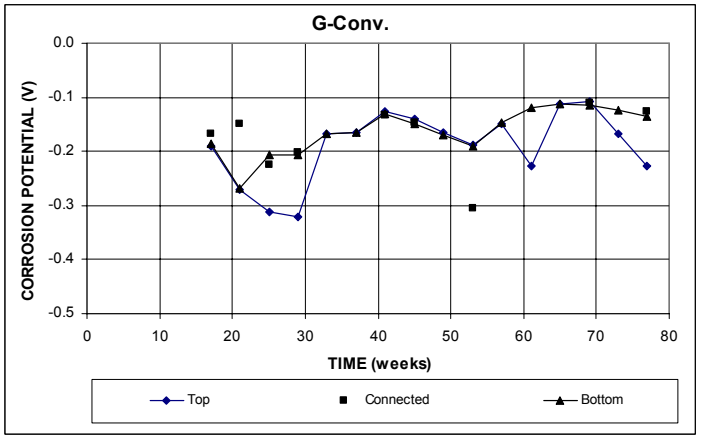

(b)

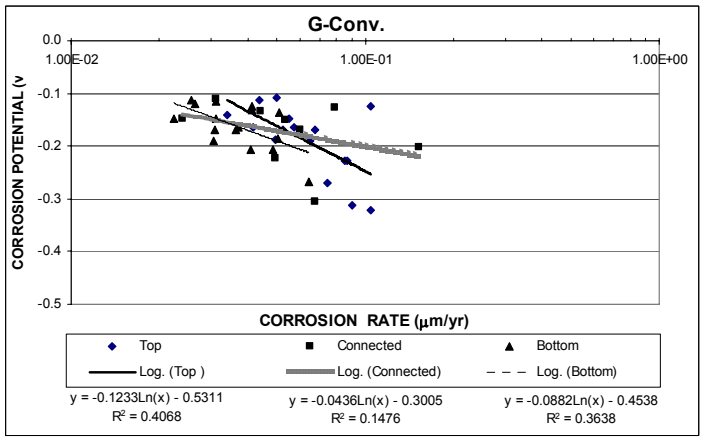

(c)

Figure E.5 – (a) Corrosion rate, (b) corrosion potential, and (c) correlation between microcell corrosion rate and corrosion potential as measured in the LPR test for the G 109 specimen with conventional steel.

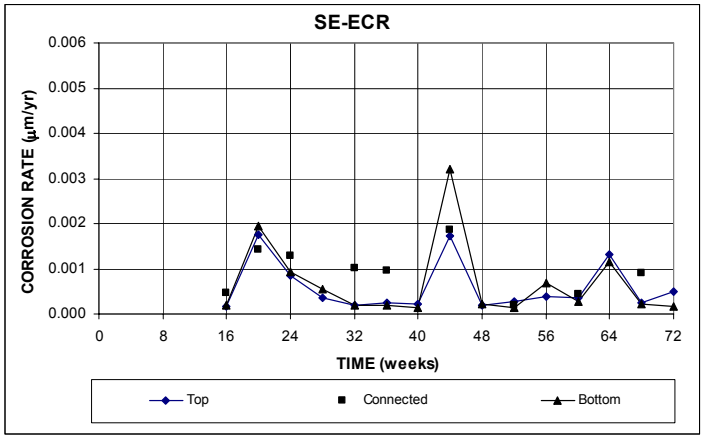

(a)

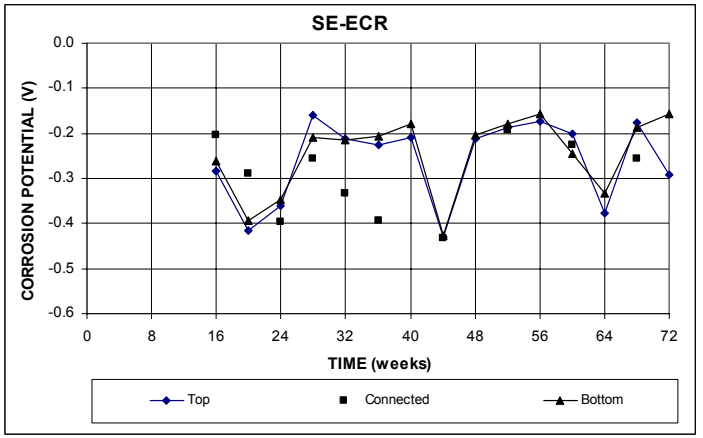

(b)

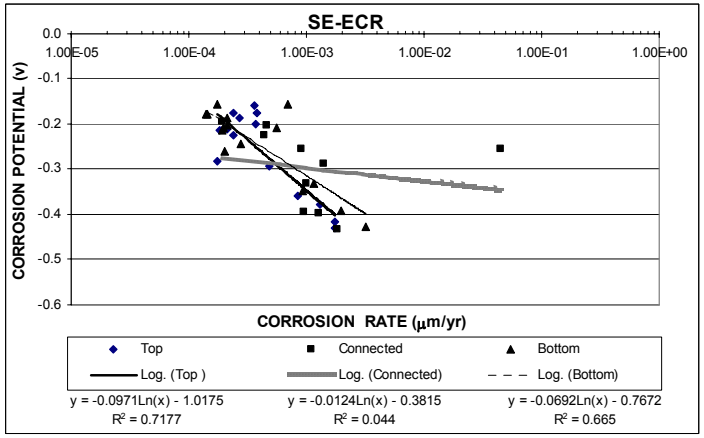

(c)

Figure E.6 – (a) Corrosion rate, (b) corrosion potential, and (c) correlation between microcell corrosion rate and corrosion potential as measured in the LPR test for the Southern Exposure specimen with ECR (four 3-mm ($^{1}/_{8}$-in.) diameter holes).

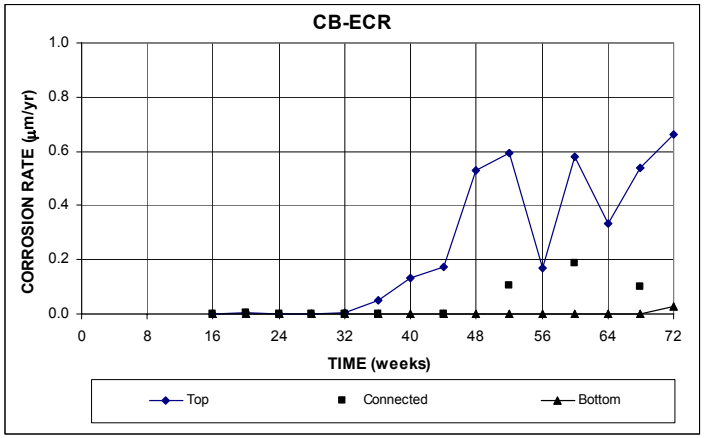

(a)

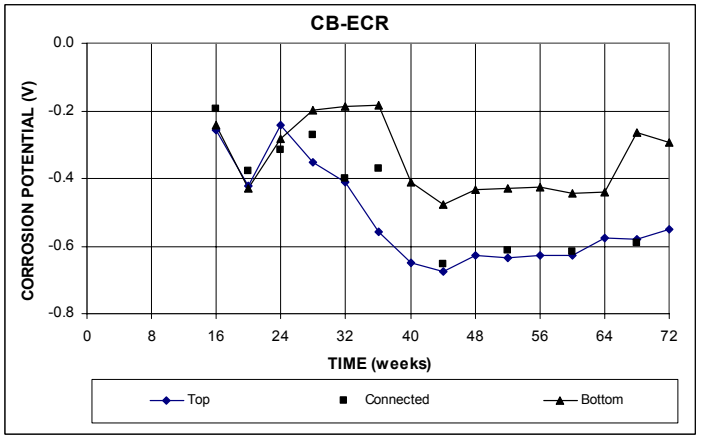

(b)

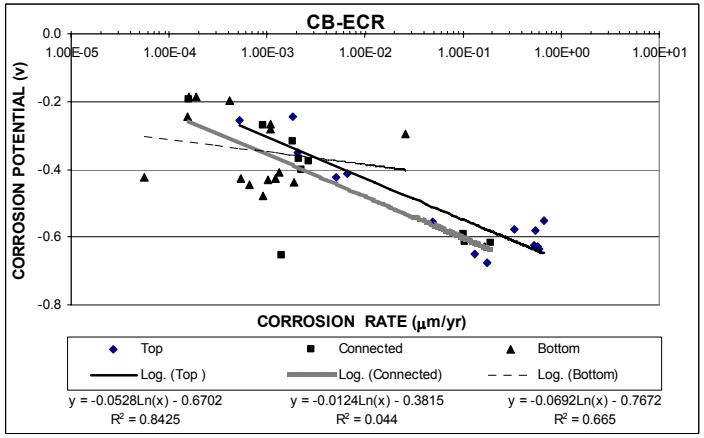

(c)

Figure E.7 – (a) Corrosion rate, (b) corrosion potential, and (c) correlation between microcell corrosion rate and corrosion potential as measured in the LPR test for the cracked beam specimen with ECR (four 3-mm ($^1/_8$-in.) diameter holes).

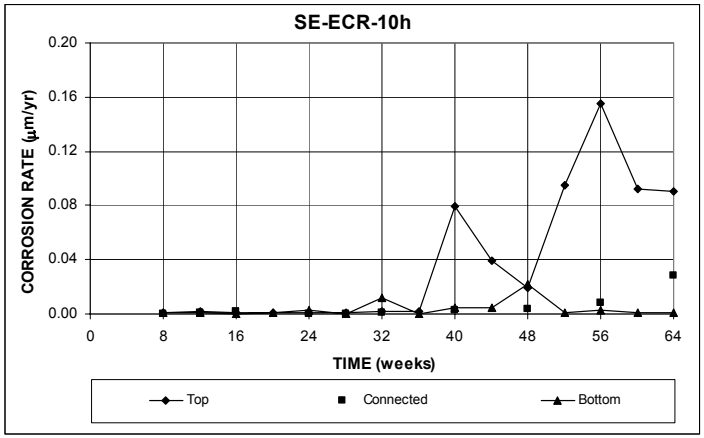

(a)

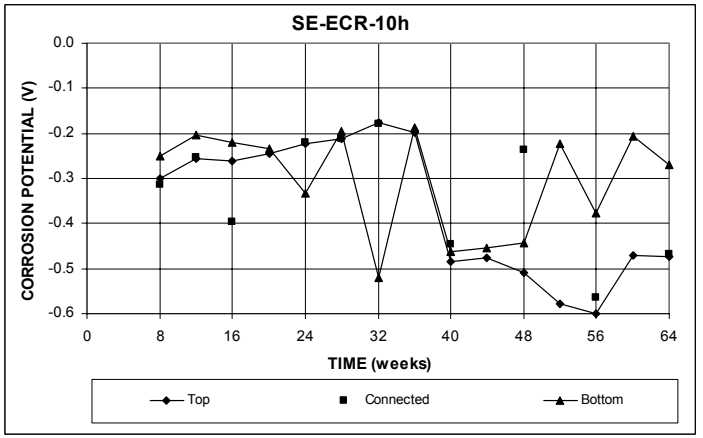

(b)

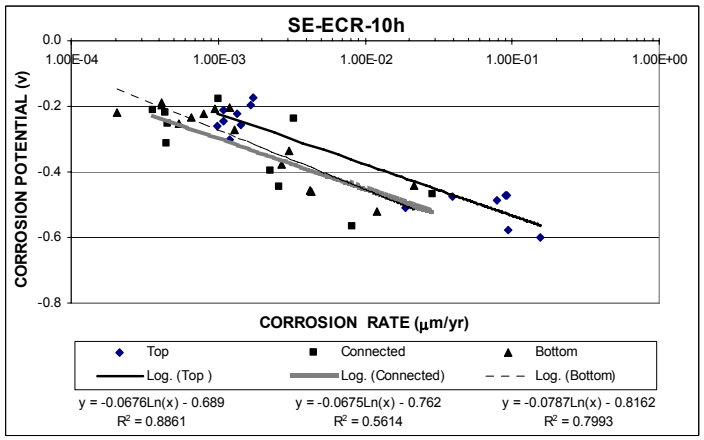

(c)

Figure E.8 – (a) Corrosion rate, (b) corrosion potential, and (c) correlation between microcell corrosion rate and corrosion potential as measured in the LPR test for the Southern Exposure specimen with ECR (ten 3-mm ($^{1}/_{8}$-in.) diameter holes).

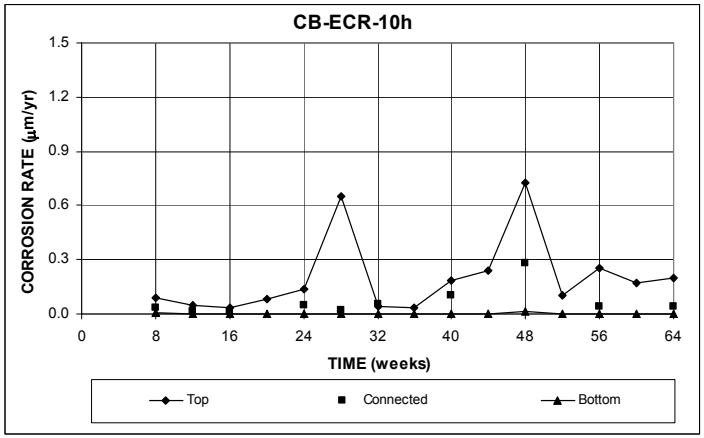

(a)

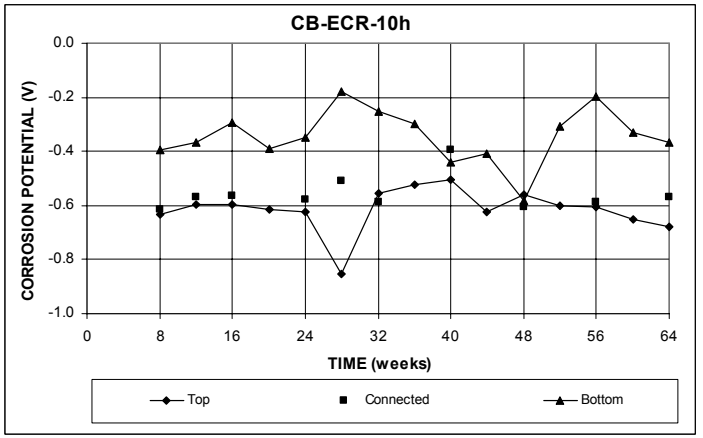

(b)

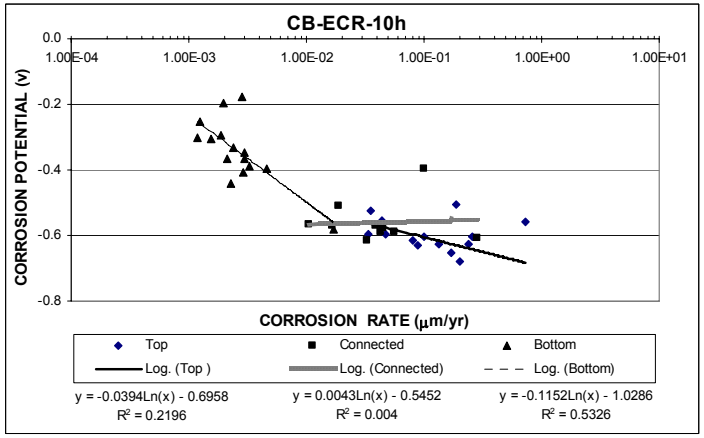

(c)

Figure E.9 – (a) Corrosion rate, (b) corrosion potential, and (c) correlation between microcell corrosion rate and corrosion potential as measured in the LPR test for the cracked beam specimen with ECR (ten 3-mm ($^{1}/_{8}$ -in.) diameter holes).

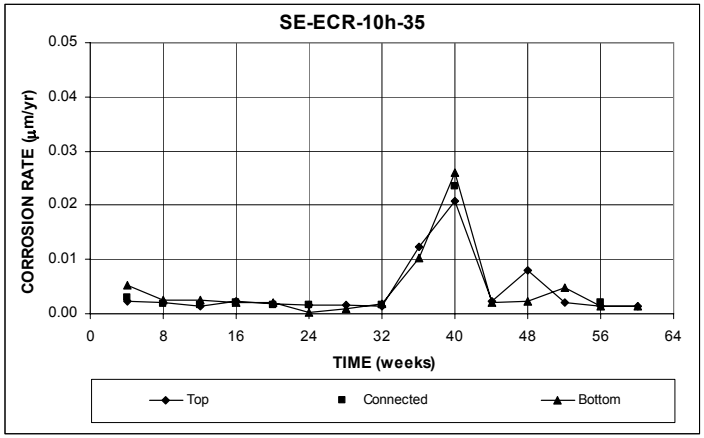

(a)

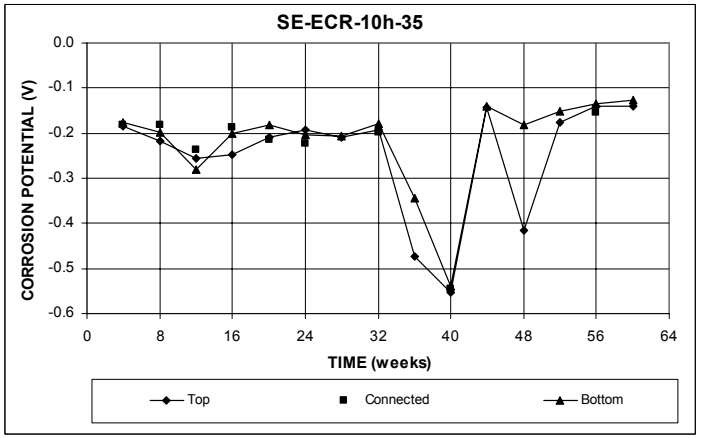

(b)

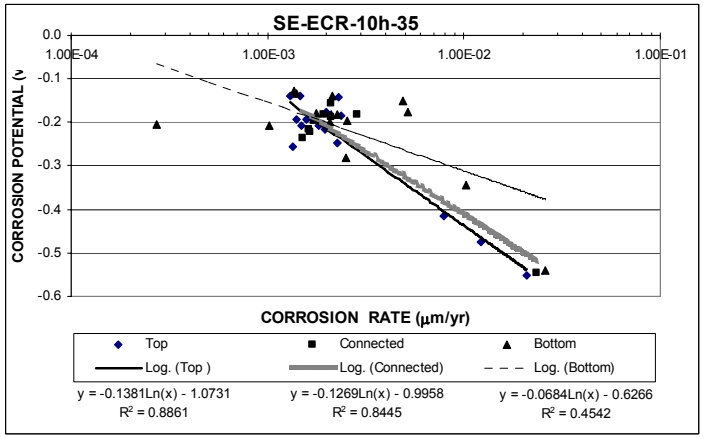

(c)

Figure E.10 – (a) Corrosion rate, (b) corrosion potential, and (c) correlation between microcell corrosion rate and corrosion potential as measured in the LPR test for the Southern Exposure specimen with ECR (ten 3-mm ($^1/_8$-in.) diameter holes), a water-cement ratio of 0.35.

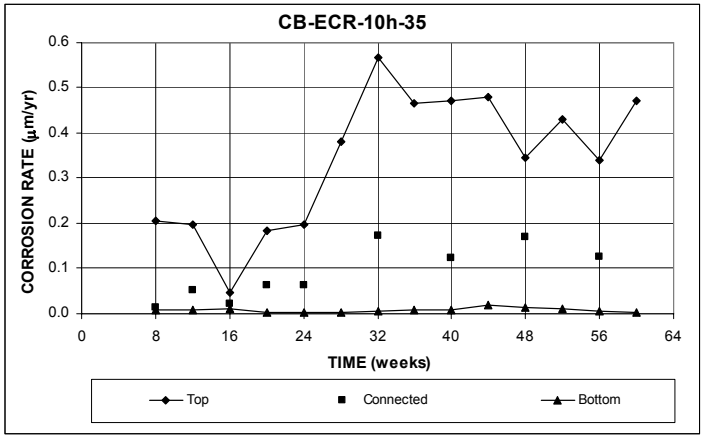

(a)

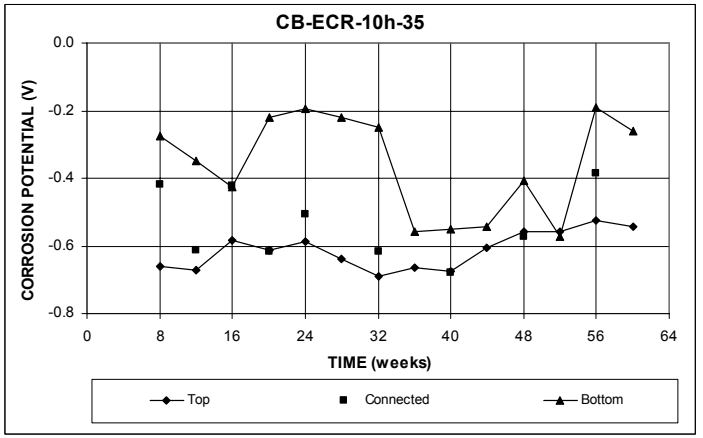

(b)

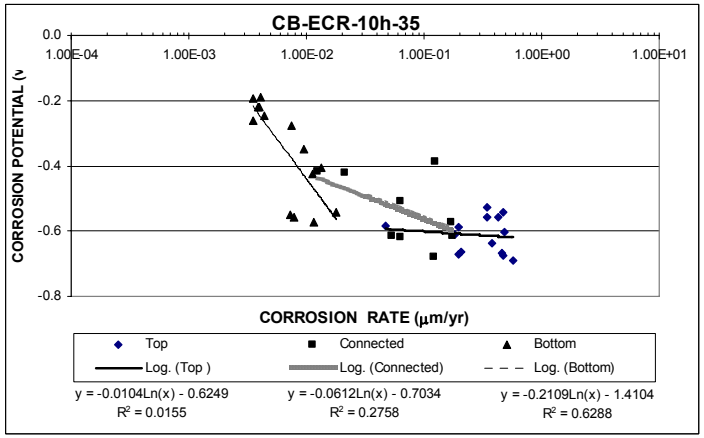

(c)

Figure E.11 – (a) Corrosion rate, (b) corrosion potential, and (c) correlation between microcell corrosion rate and corrosion potential as measured in the LPR test for the cracked beam specimen with ECR (ten 3-mm ($^1/_8$-in.) diameter holes), a water-cement ratio of 0.35.

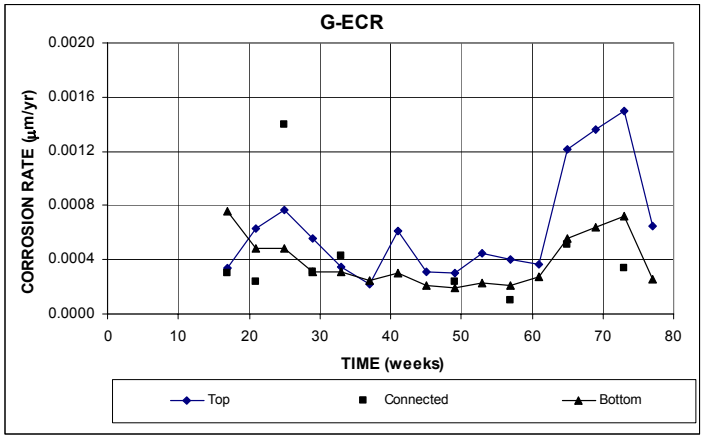

(a)

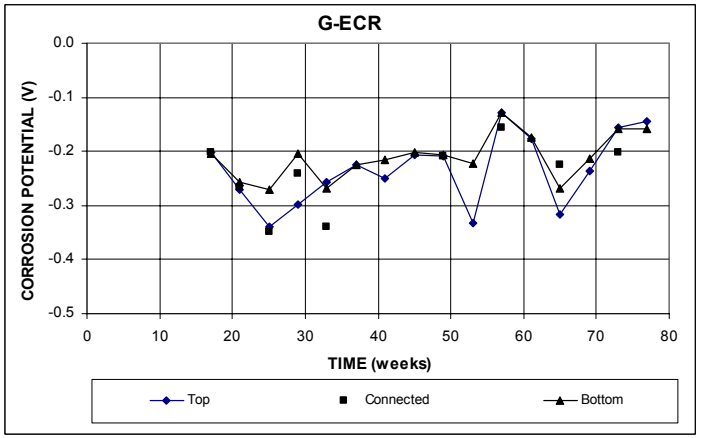

(b)

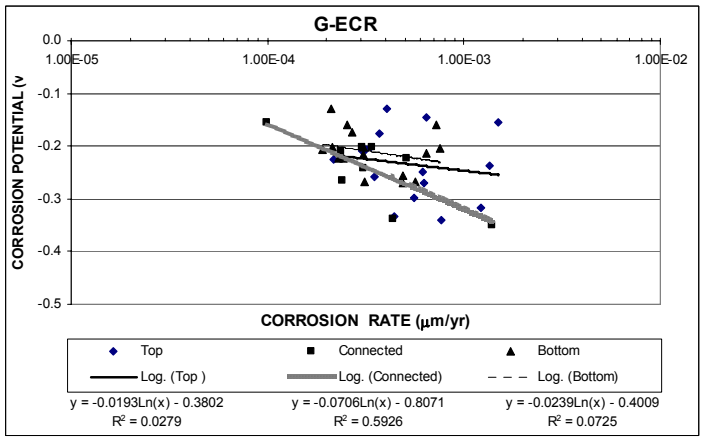

(c)

Figure E.12 – (a) Corrosion rate, (b) corrosion potential, and (c) correlation between microcell corrosion rate and corrosion potential as measured in the LPR test for the G 109 specimen with ECR (four 3-mm ($^{1}/_{8}$ -in.) diameter holes).

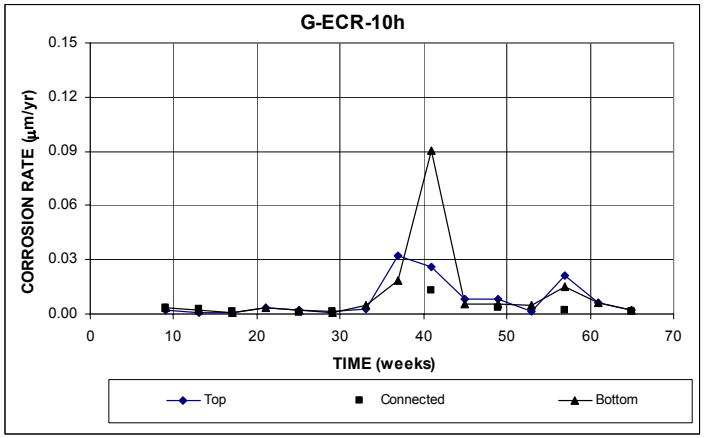

(a)

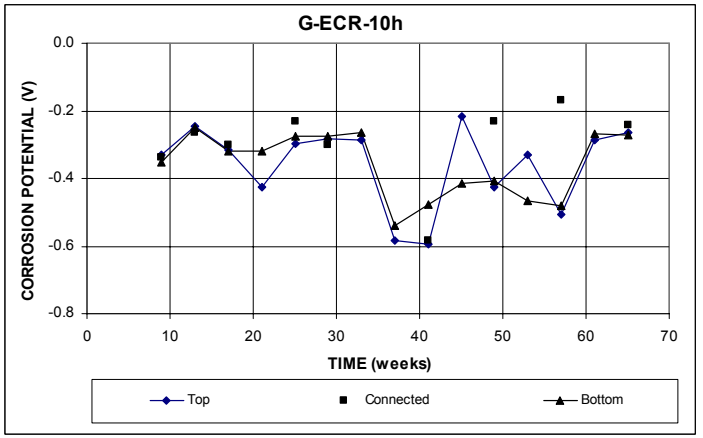

(b)

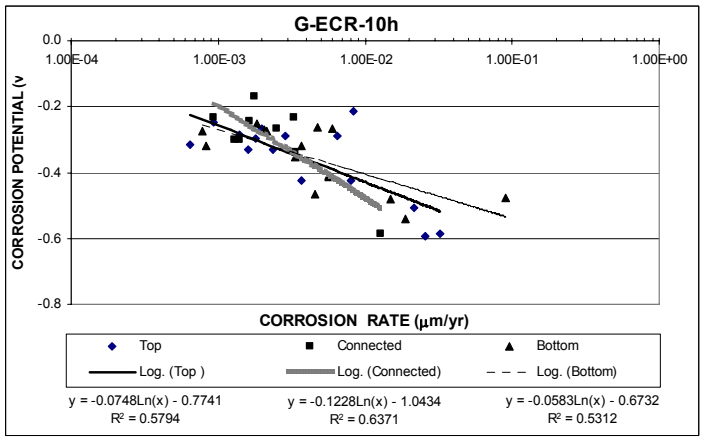

(c)

Figure E.13 – (a) Corrosion rate, (b) corrosion potential, and (c) correlation between microcell corrosion rate and corrosion potential as measured in the LPR test for the G 109 specimen with ECR (ten 3-mm ($^{1}/_{8}$ -in.) diameter holes).

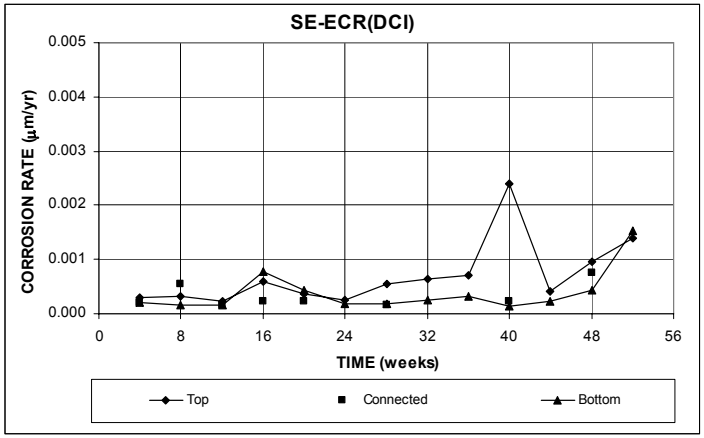

(a)

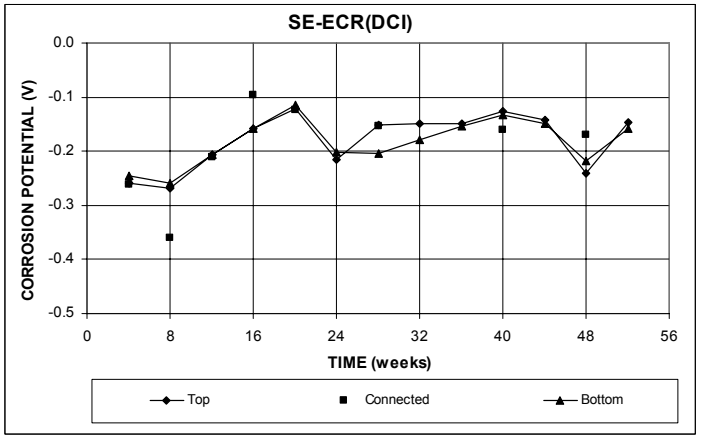

(b)

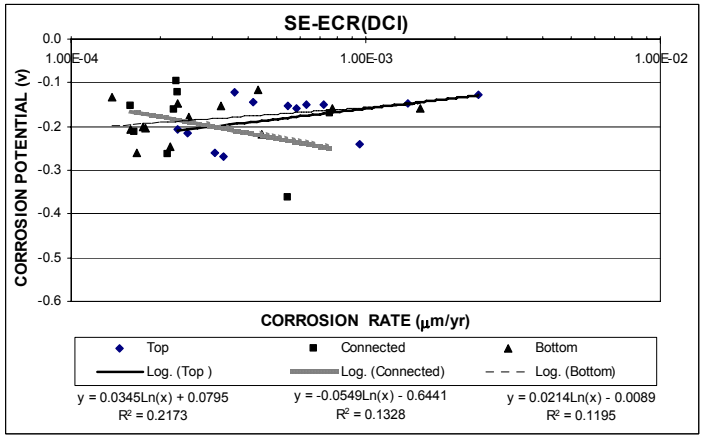

(c)

Figure E.14 – (a) Corrosion rate, (b) corrosion potential, and (c) correlation between microcell corrosion rate and corrosion potential as measured in the LPR test for the Southern Exposure specimen with ECR in concrete with DCI (four 3-mm ($^1/_8$-in.) diameter holes).

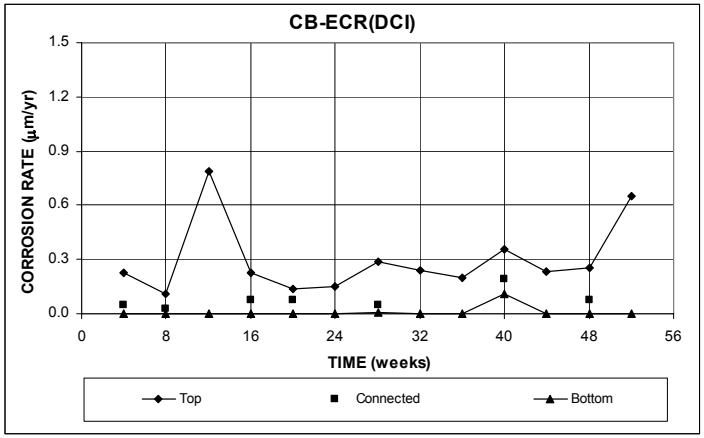

(a)

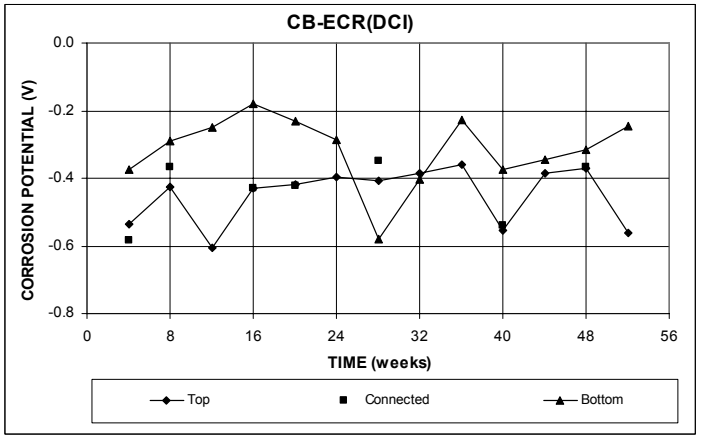

(b)

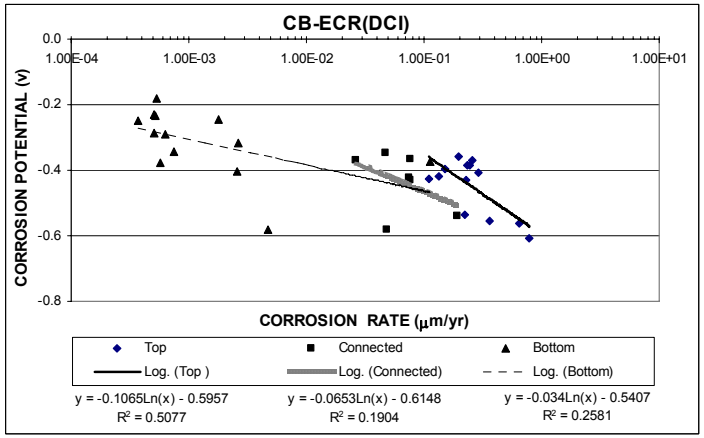

(c)

Figure E.15 – (a) Corrosion rate, (b) corrosion potential, and (c) correlation between microcell corrosion rate and corrosion potential as measured in the LPR test for the cracked beam specimen with ECR in concrete with DCI (four 3-mm ($^1/_8$ -in.) diameter holes).

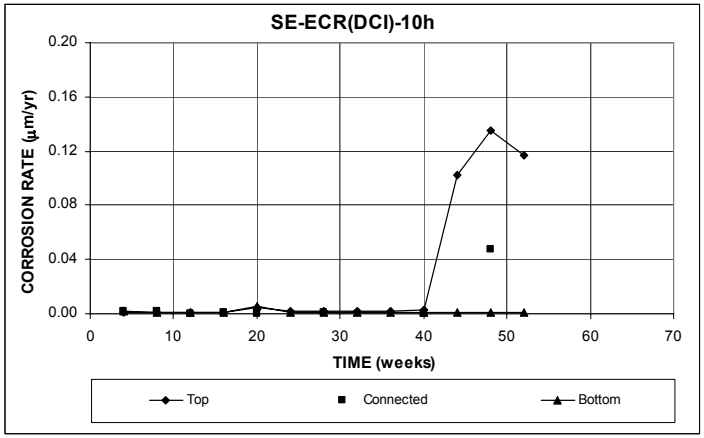

(a)

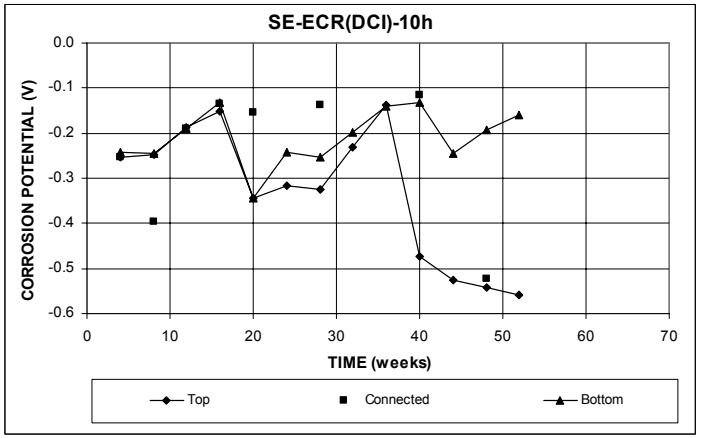

(b)

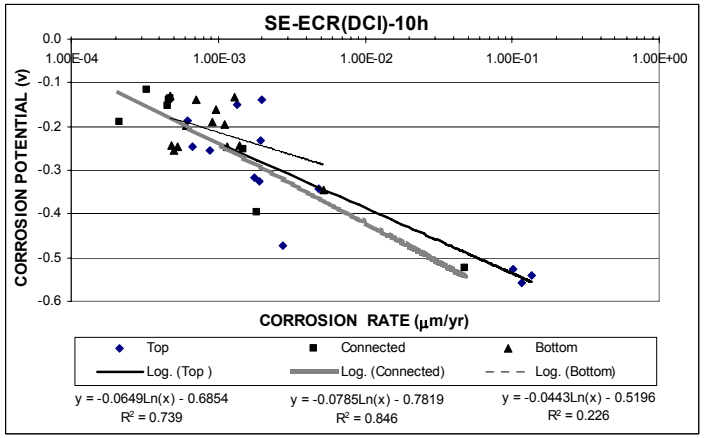

(c)

Figure E.16 – (a) Corrosion rate, (b) corrosion potential, and (c) correlation between microcell corrosion rate and corrosion potential as measured in the LPR test for the Southern Exposure specimen with ECR in concrete with DCI (ten 3-mm ($^{1}/_{8}$-in.) diameter holes).

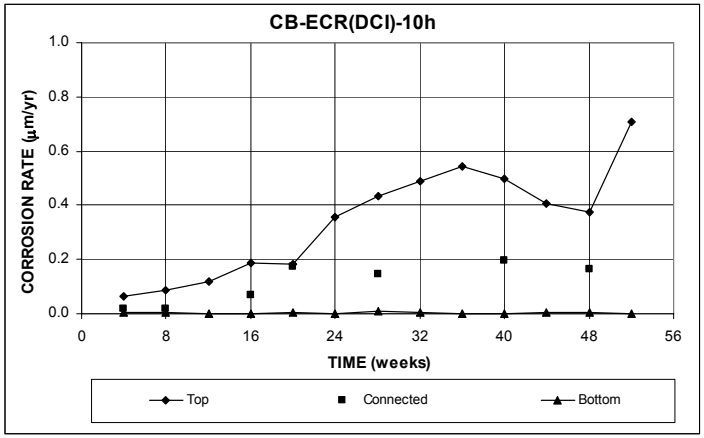

(a)

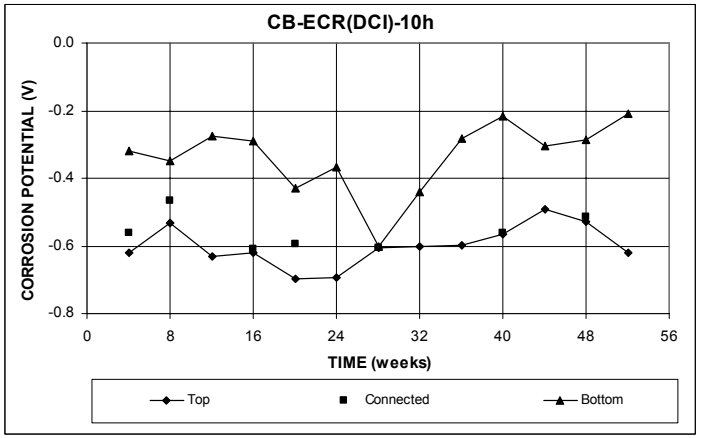

(b)

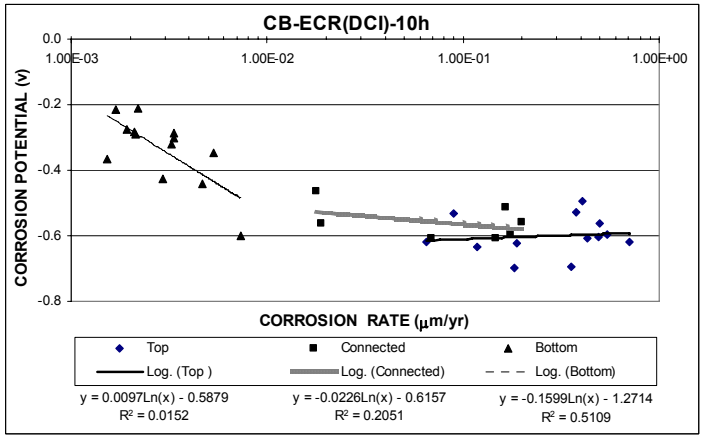

(c)

Figure E.17 – (a) Corrosion rate, (b) corrosion potential, and (c) correlation between microcell corrosion rate and corrosion potential as measured in the LPR test for the cracked beam specimen with ECR in concrete with DCI (ten 3-mm ($^1/_8$-in.) diameter holes).

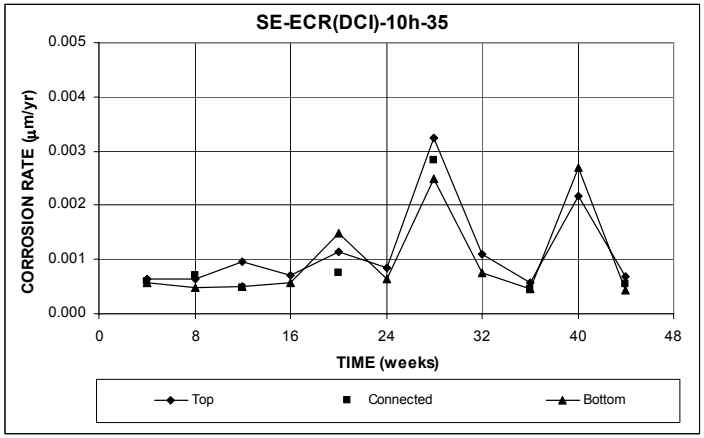

(a)

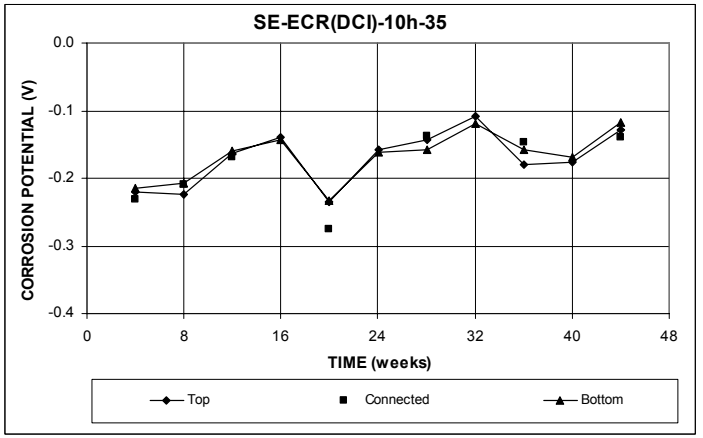

(b)

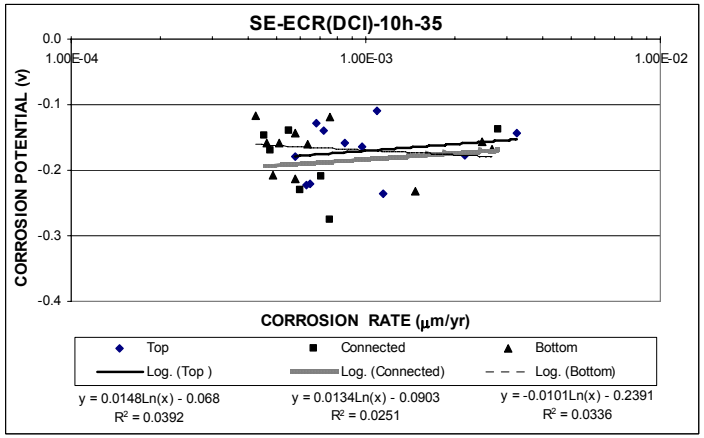

(c)

Figure E.18 – (a) Corrosion rate, (b) corrosion potential, and (c) correlation between microcell corrosion rate and corrosion potential as measured in the LPR test for the Southern Exposure specimen with ECR in concrete with DCI (ten 3-mm ($^{1}/_{8}$-in.) diameter holes), a water-cement ratio of 0.35.

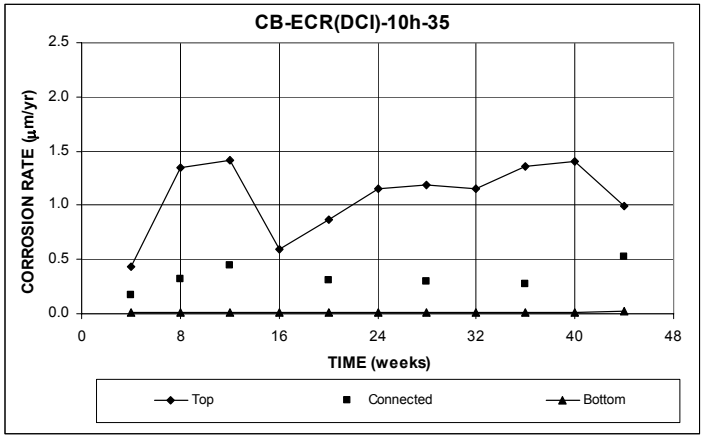

(a)

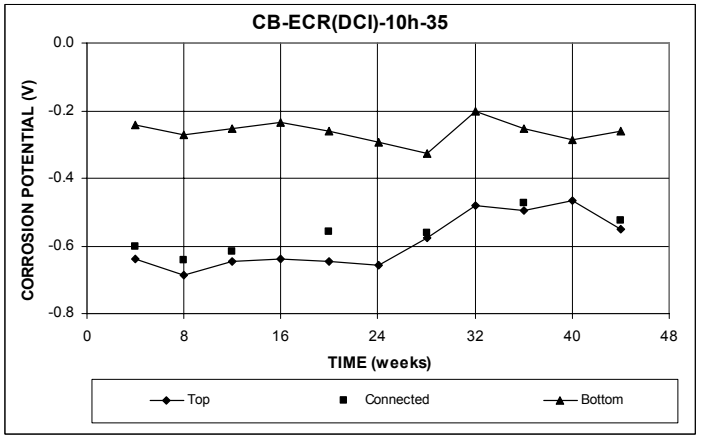

(b)

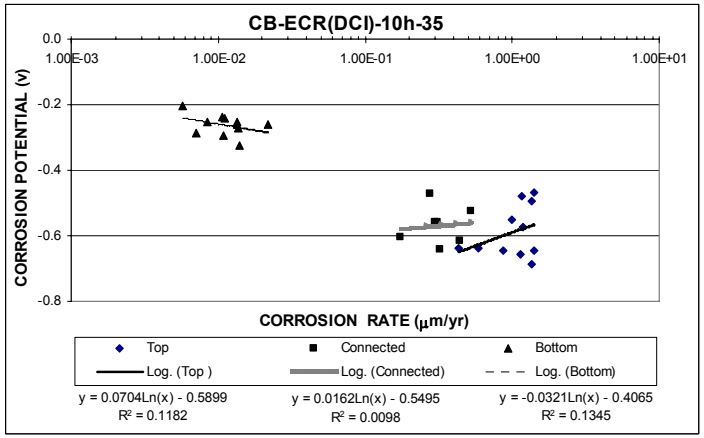

(c)

Figure E.19 – (a) Corrosion rate, (b) corrosion potential, and (c) correlation between microcell corrosion rate and corrosion potential as measured in the LPR test for the cracked beam specimen with ECR in concrete with DCI (ten 3-mm ($^1/_8$-in.) diameter holes), a water-cement ratio of 0.35.

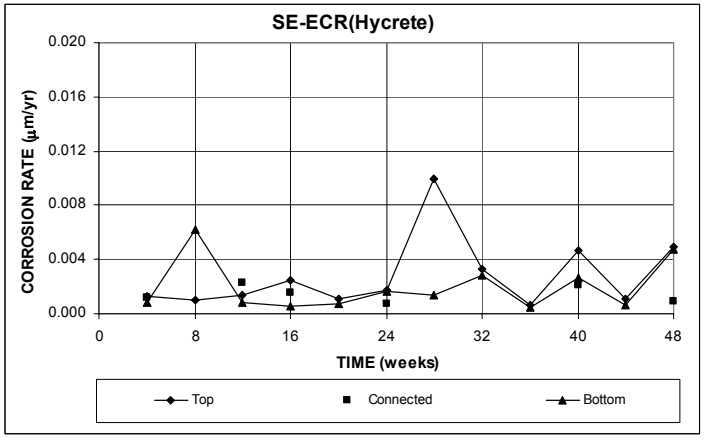

(a)

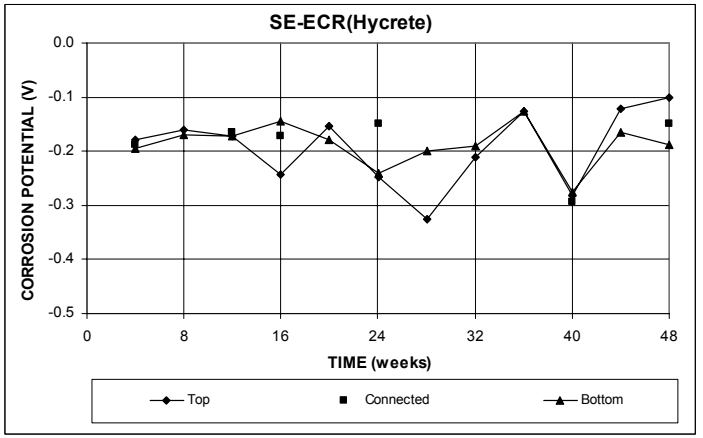

(b)

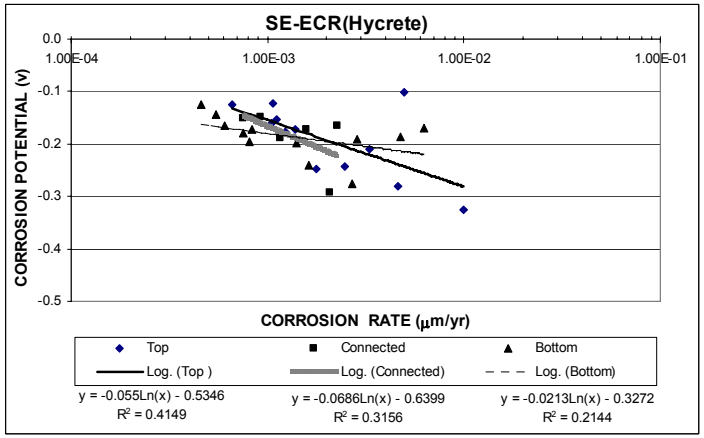

(c)

Figure E.20 – (a) Corrosion rate, (b) corrosion potential, and (c) correlation between microcell corrosion rate and corrosion potential as measured in the LPR test for the Southern Exposure specimen with ECR in concrete with Hycrete (four 3-mm ($^1/_8$-in.) diameter holes).

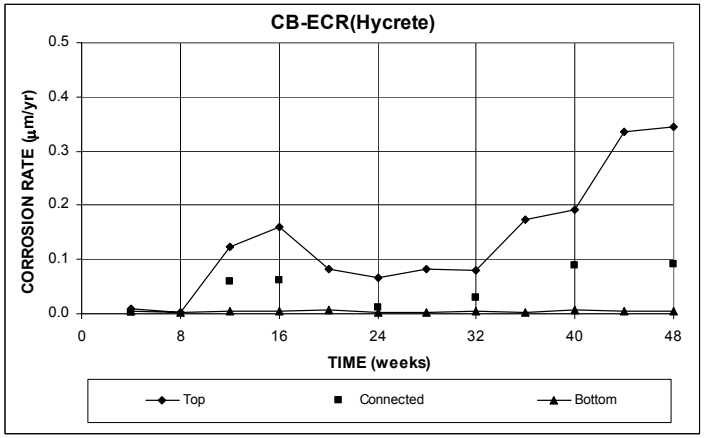

(a)

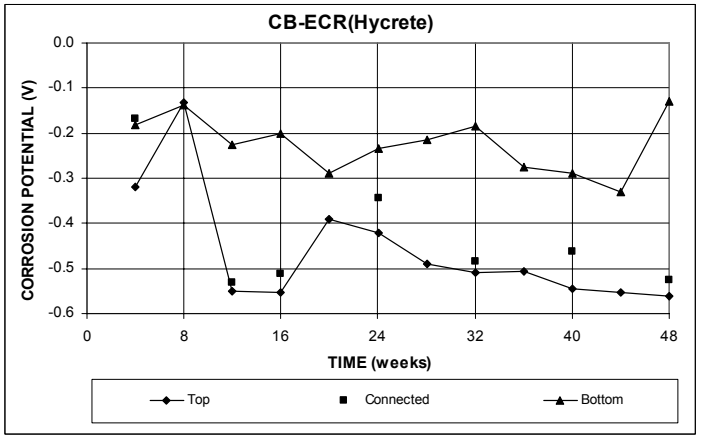

(b)

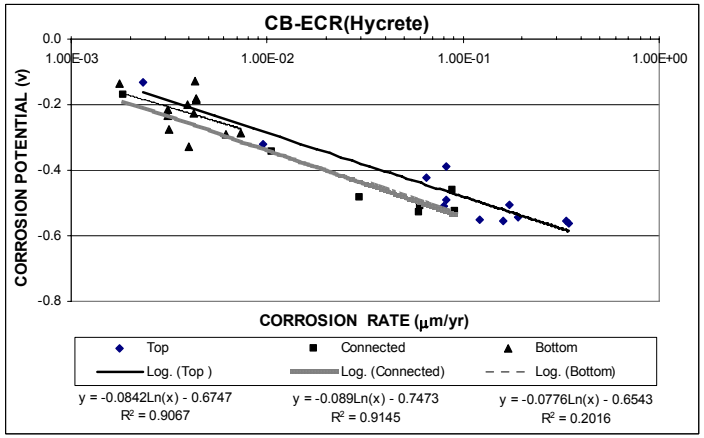

(c)

Figure E.21 – (a) Corrosion rate, (b) corrosion potential, and (c) correlation between microcell corrosion rate and corrosion potential as measured in the LPR test for the cracked beam specimen with ECR in concrete with Hycrete (four 3-mm ($^1/_8$-in.) diameter holes).

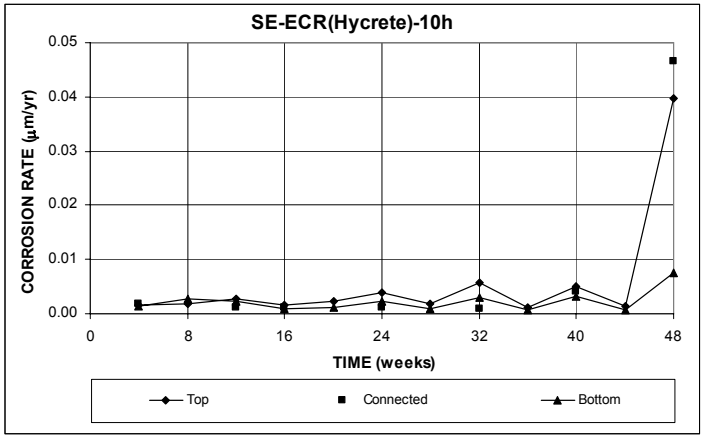

(a)

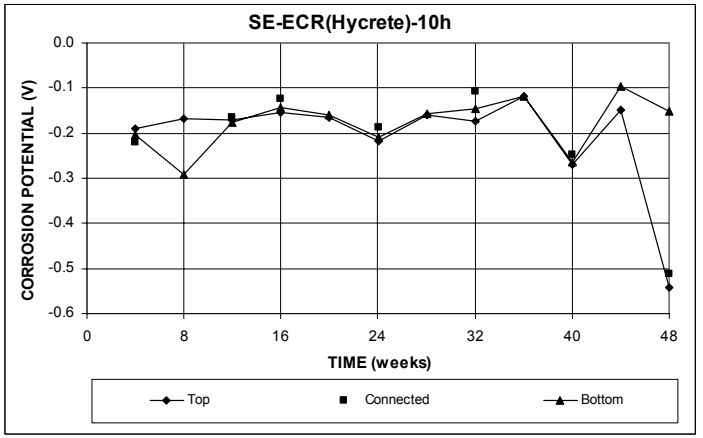

(b)

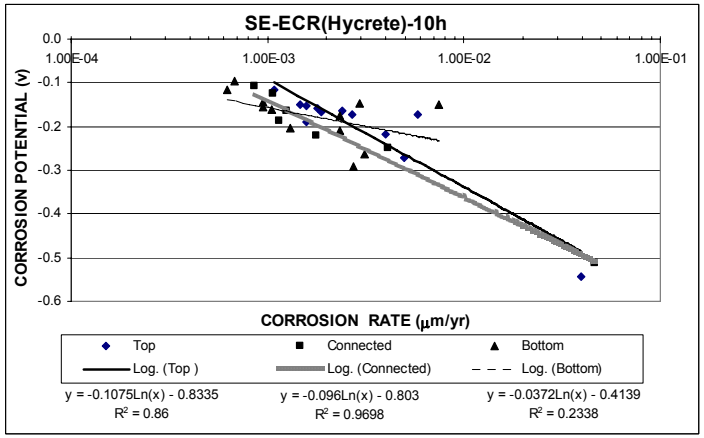

(c)

Figure E.22 – (a) Corrosion rate, (b) corrosion potential, and (c) correlation between microcell corrosion rate and corrosion potential as measured in the LPR test for the Southern Exposure specimen with ECR in concrete with Hycrete (ten 3-mm ($^1/_8$-in.) diameter holes).

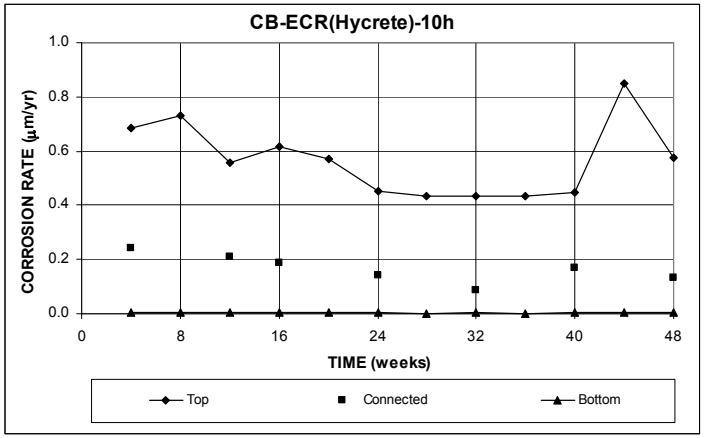

(a)

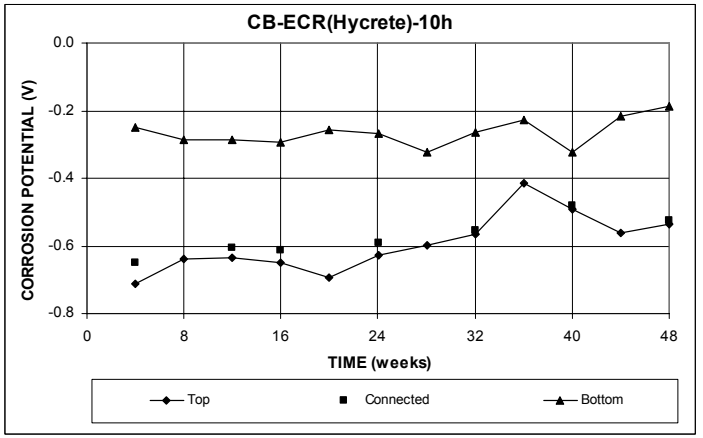

(b)

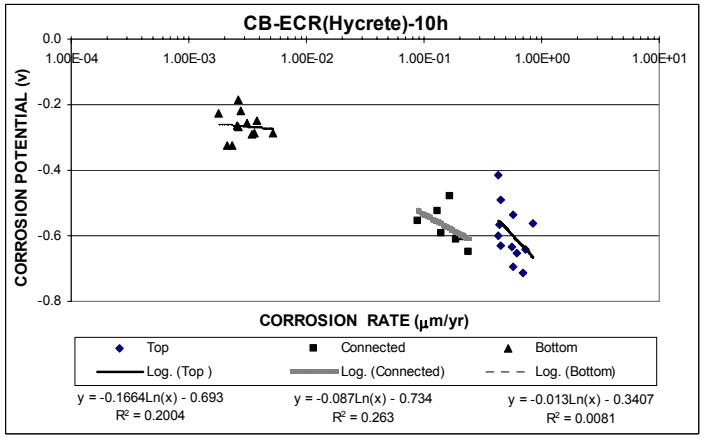

(c)

Figure E.23 – (a) Corrosion rate, (b) corrosion potential, and (c) correlation between microcell corrosion rate and corrosion potential as measured in the LPR test for the cracked beam specimen with ECR in concrete with Hycrete (ten 3-mm ($^1/_8$ -in.) diameter holes).

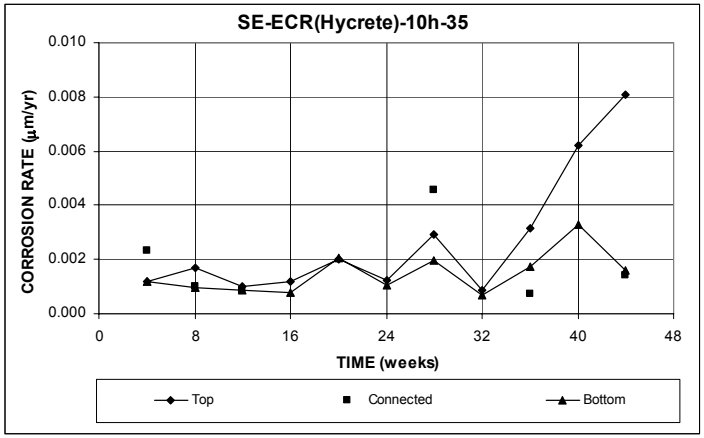

(a)

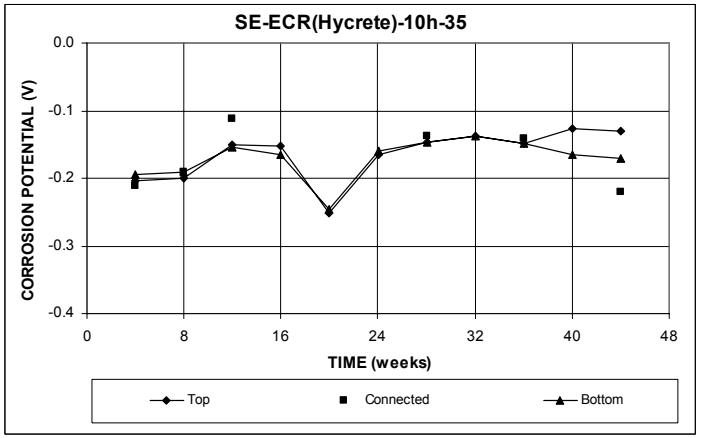

(b)

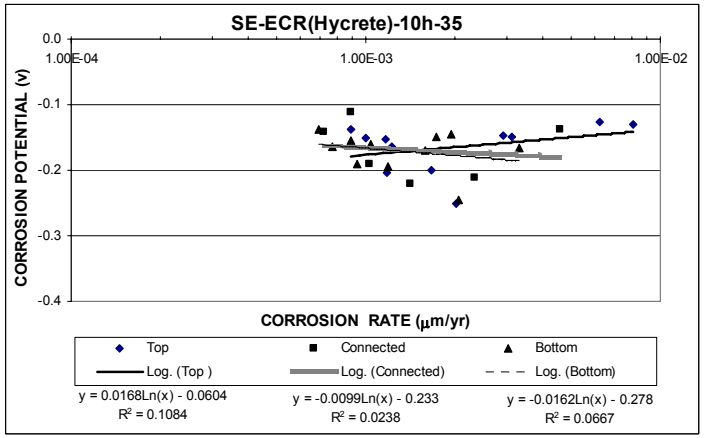

(c)

Figure E.24 – (a) Corrosion rate, (b) corrosion potential, and (c) correlation between microcell corrosion rate and corrosion potential as measured in the LPR test for the Southern Exposure specimen with ECR in concrete with Hycrete (ten 3-mm ($^{1}/_{8}$-in.) diameter holes), a water-cement ratio of 0.35.

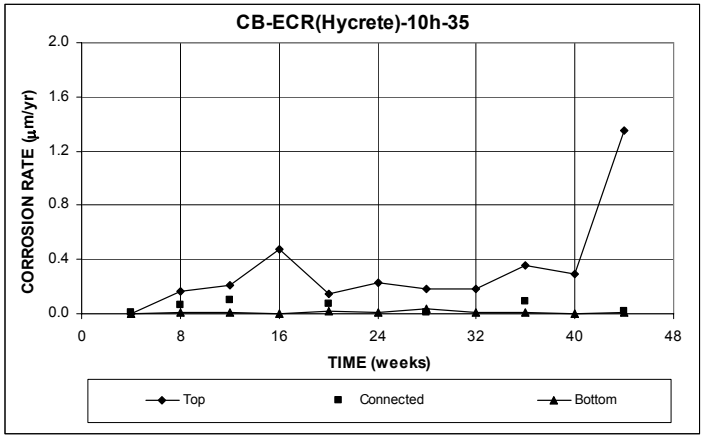

(a)

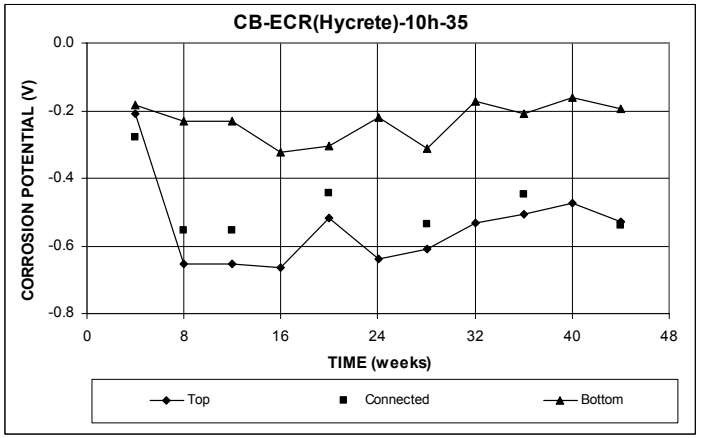

(b)

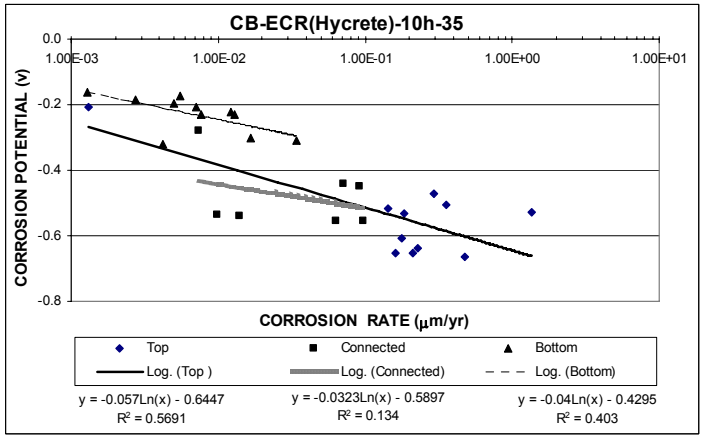

(c)

Figure E.25 – (a) Corrosion rate, (b) corrosion potential, and (c) correlation between microcell corrosion rate and corrosion potential as measured in the LPR test for the cracked beam specimen with ECR in concrete with Hycrete (ten 3-mm ($^1/_8$-in.) diameter holes), a water-cement ratio of 0.35.

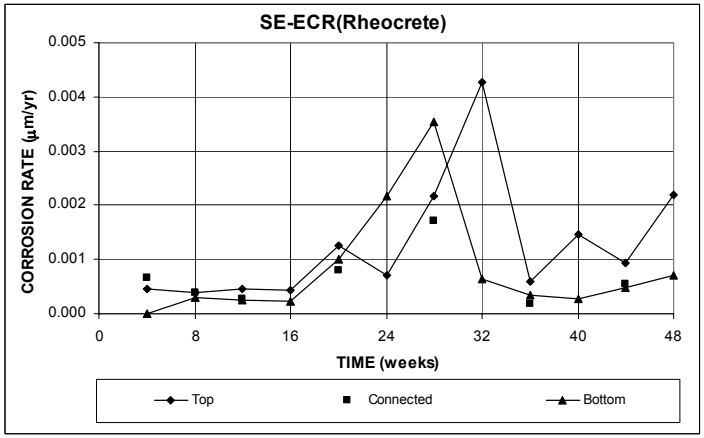

(a)

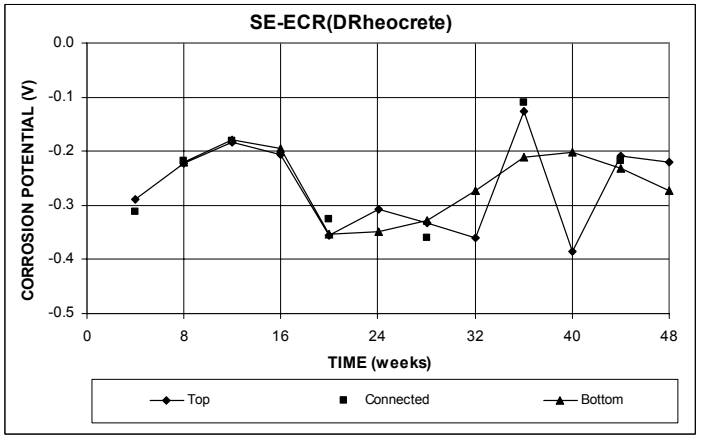

(b)

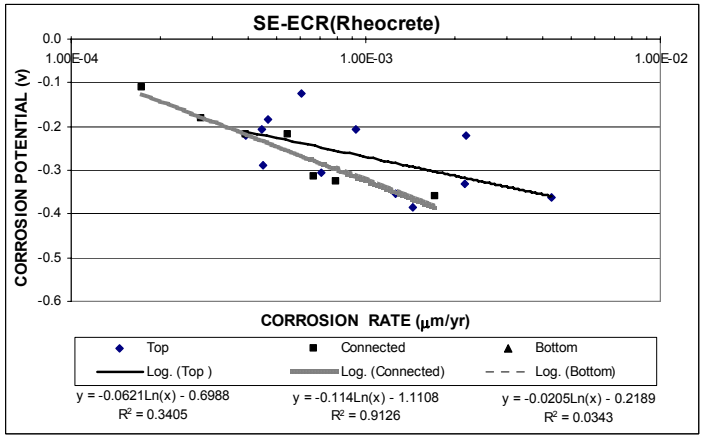

(c)

Figure E.26 – (a) Corrosion rate, (b) corrosion potential, and (c) correlation between microcell corrosion rate and corrosion potential as measured in the LPR test for the Southern Exposure specimen with ECR in concrete with Rheocrete (four 3-mm ($^1/_8$-in.) diameter holes).

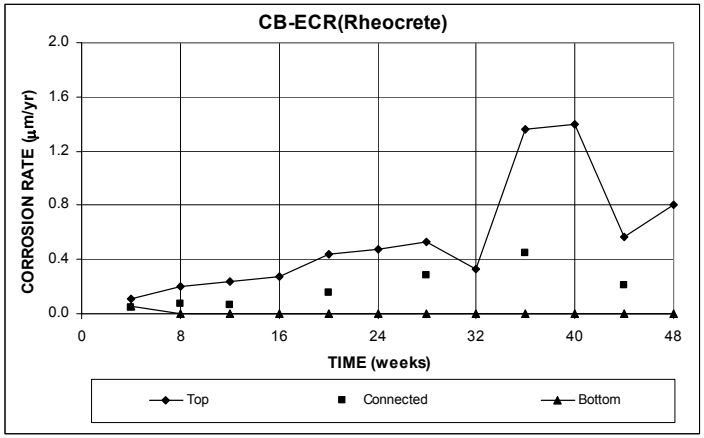

(a)

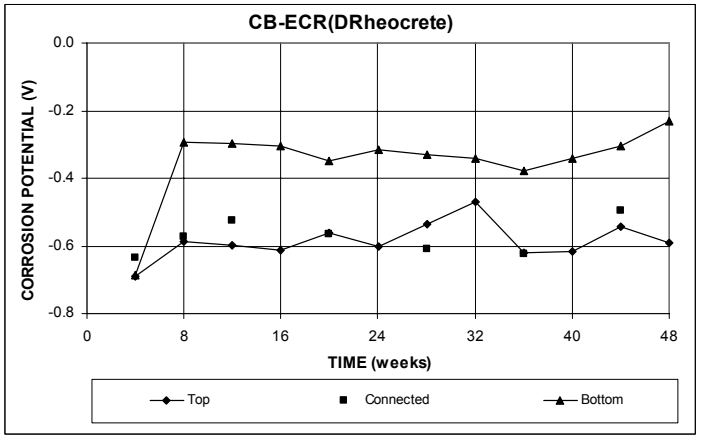

(b)

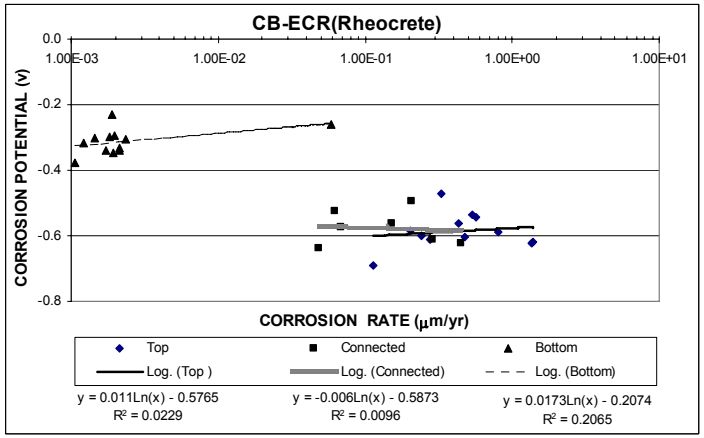

(c)

Figure E.27 – (a) Corrosion rate, (b) corrosion potential, and (c) correlation between microcell corrosion rate and corrosion potential as measured in the LPR test for the cracked beam specimen with ECR in concrete with Rheocrete (four 3-mm ($^{1}/_{8}$-in.) diameter holes).

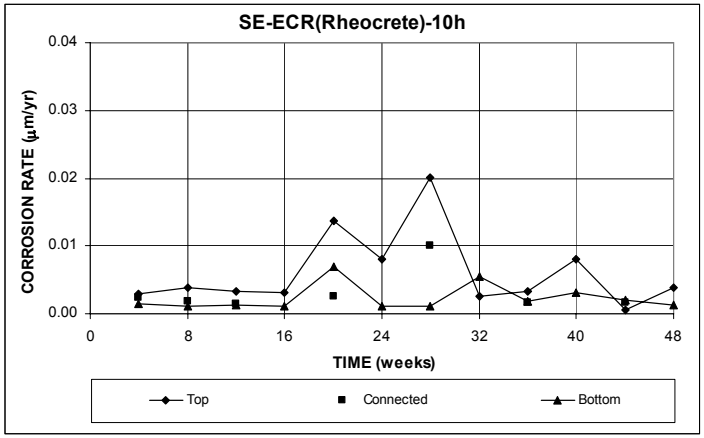

(a)

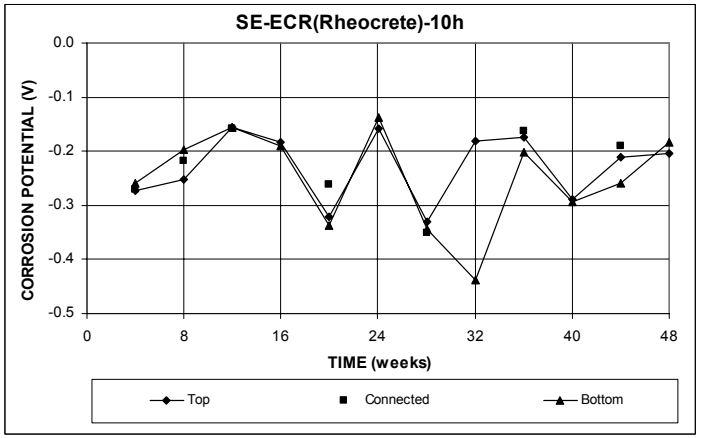

(b)

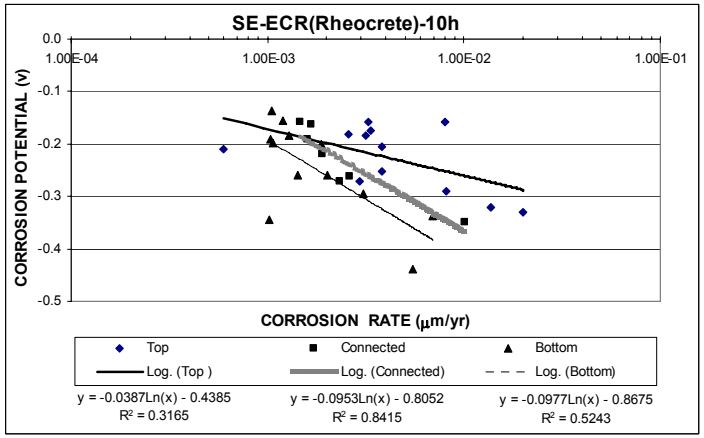

(c)

Figure E.28 – (a) Corrosion rate, (b) corrosion potential, and (c) correlation between microcell corrosion rate and corrosion potential, as measured in the LPR test for the Southern Exposure specimen with ECR in concrete with Rheocrete (ten 3-mm ($^1/_8$-in.) diameter holes).

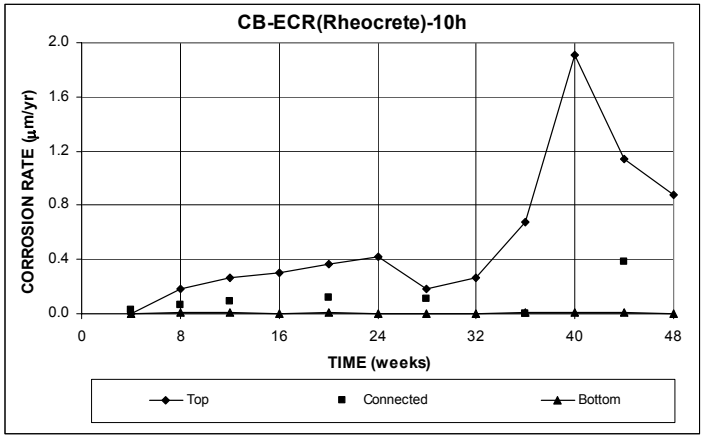

(a)

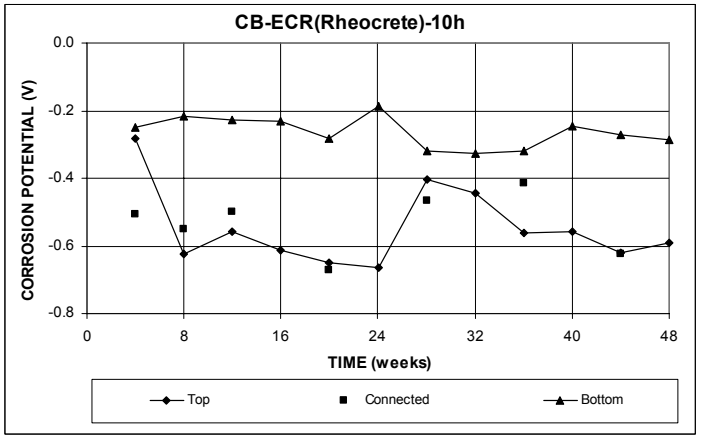

(b)

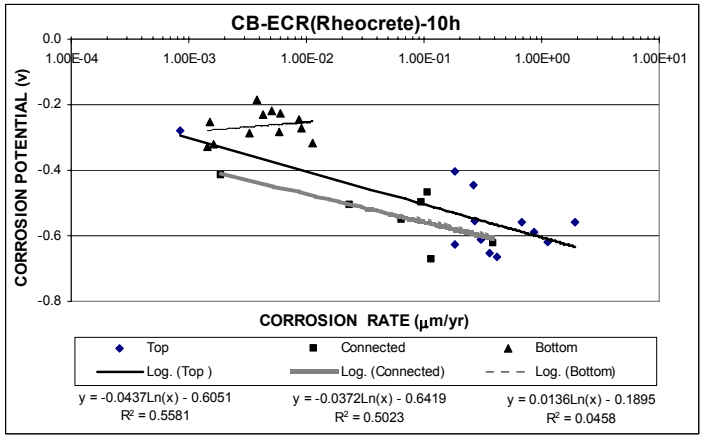

(c)

Figure E.29 – (a) Corrosion rate, (b) corrosion potential, and (c) correlation between microcell corrosion rate and corrosion potential as measured in the LPR test for the cracked beam specimen with ECR in concrete with Rheocrete (ten 3-mm ($^1/_8$-in.) diameter holes).

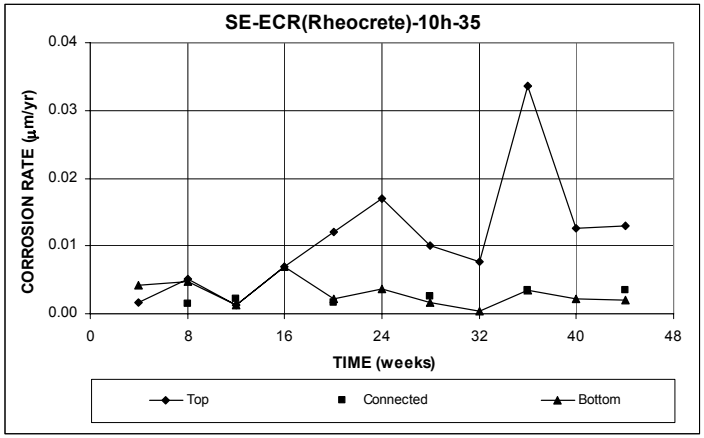

(a)

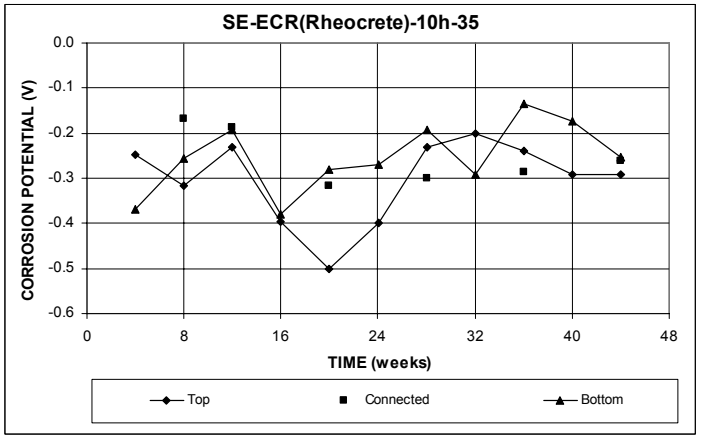

(b)

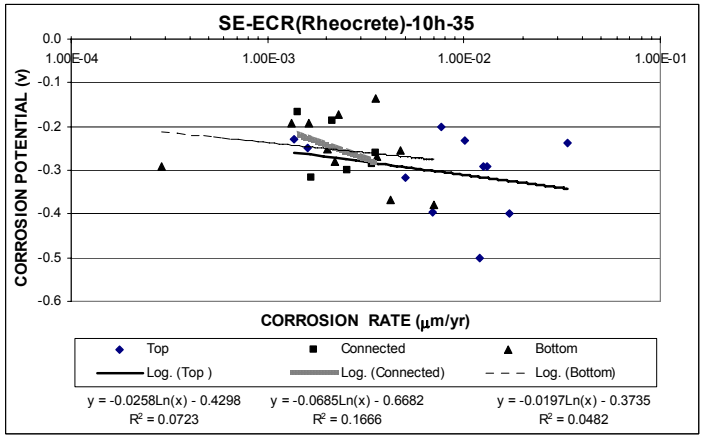

(c)

Figure E.30 – (a) Corrosion rate, (b) corrosion potential, and (c) correlation between microcell corrosion rate and corrosion potential as measured in the LPR test for the Southern Exposure specimen with ECR in concrete with Rheocrete (ten 3-mm ($^1/_8$-in.) diameter holes), a water-cement ratio of 0.35.

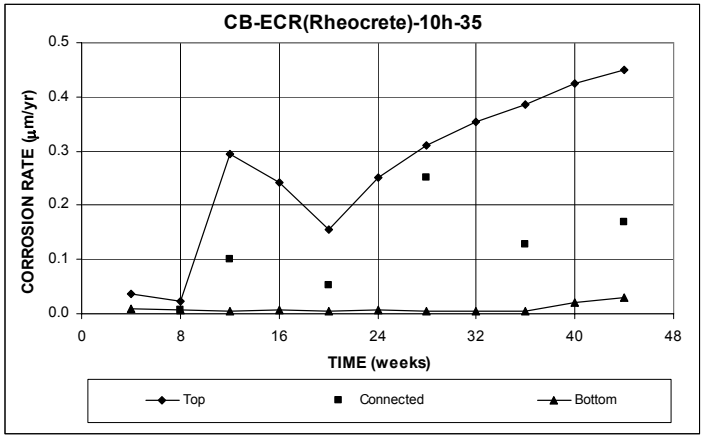

(a)

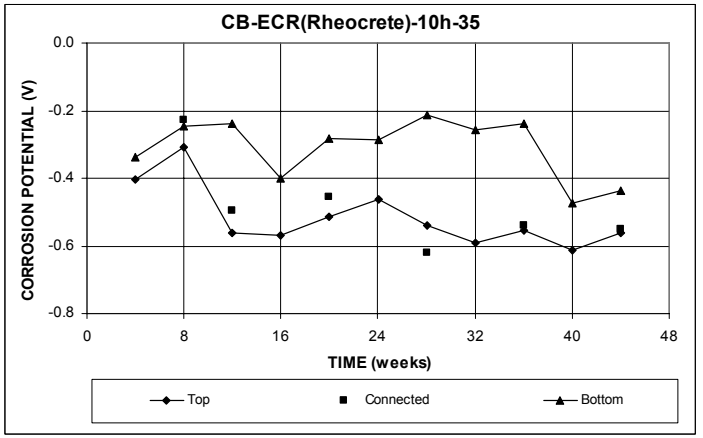

(b)

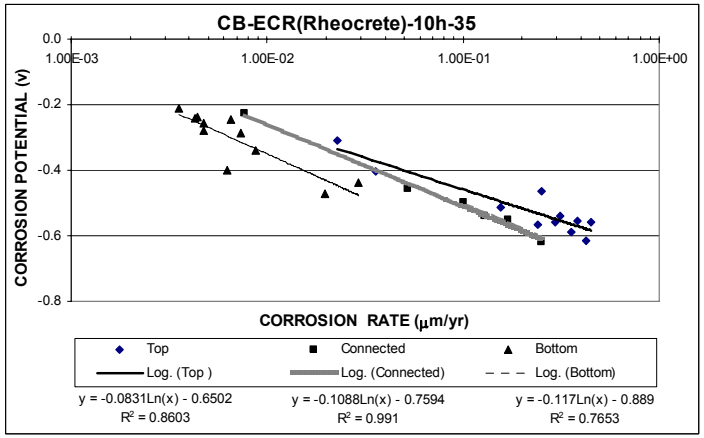

(c)

Figure E.31 – (a) Corrosion rate, (b) corrosion potential, and (c) correlation between microcell corrosion rate and corrosion potential as measured in the LPR test for the cracked beam specimen with ECR in concrete with Rheocrete (ten 3-mm ($^1/_8$-in.) diameter holes), a water-cement ratio of 0.35.

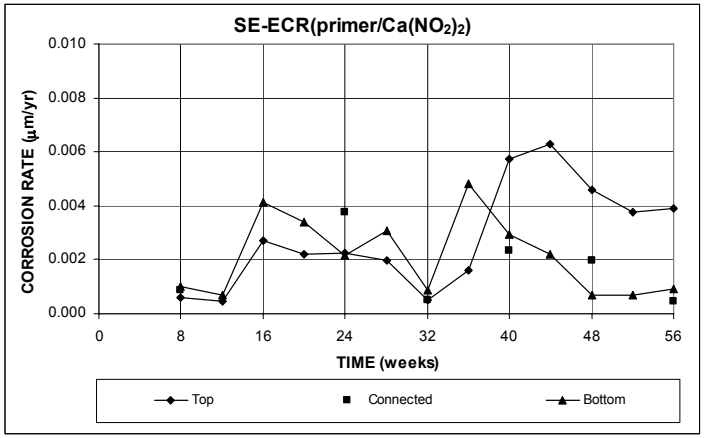

(a)

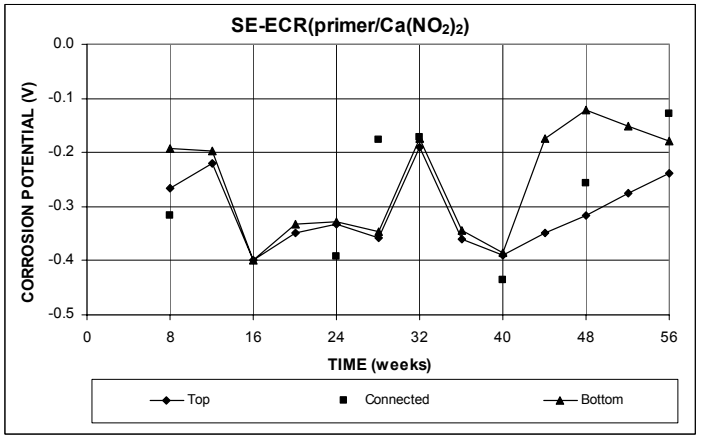

(b)

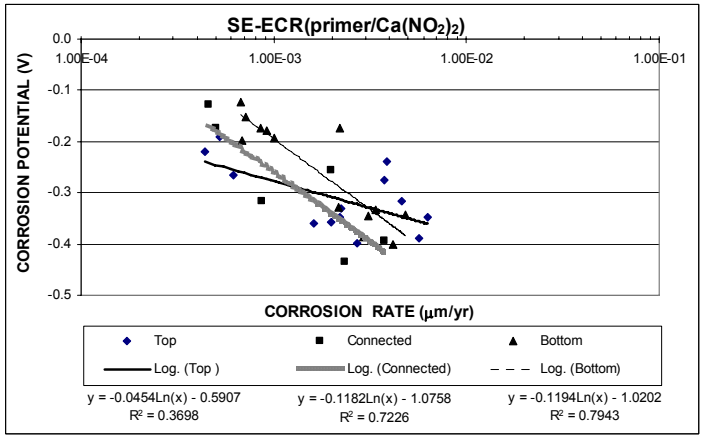

(c)

Figure E.32 – (a) Corrosion rate, (b) corrosion potential, and (c) correlation between microcell corrosion rate and corrosion potential as measured in the LPR test for the Southern Exposure specimen with ECR with primer containing calcium nitrite (four 3-mm ($^1/_8$-in.) diameter holes).

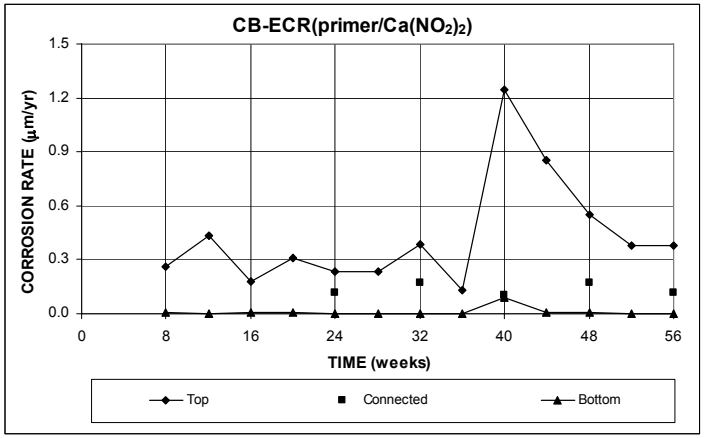

(a)

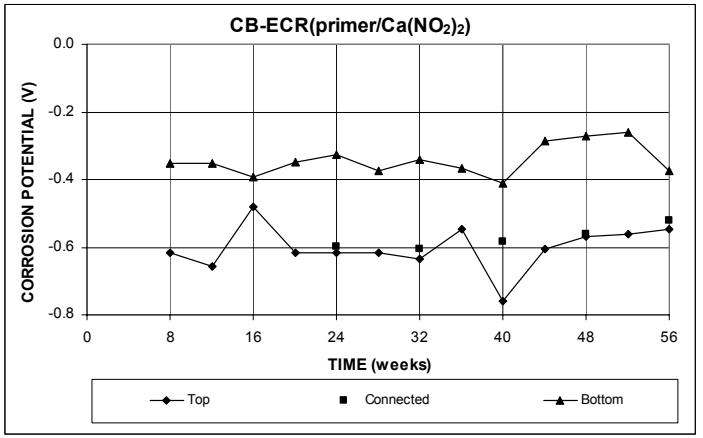

(b)

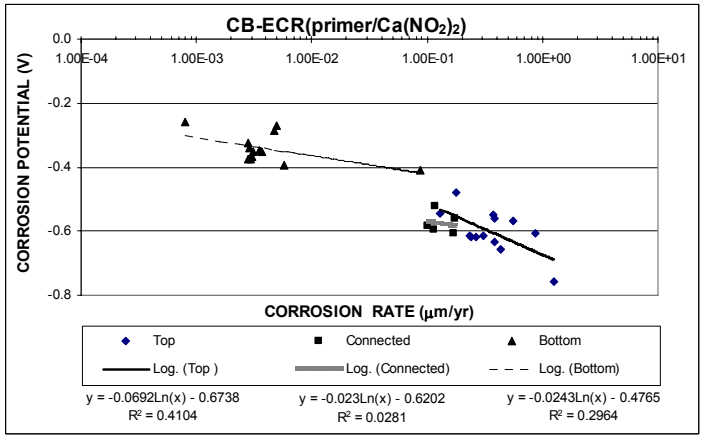

(c)

Figure E.33 – (a) Corrosion rate, (b) corrosion potential, and (c) correlation between microcell corrosion rate and corrosion potential as measured in the LPR test for the cracked beam specimen with ECR with primer containing calcium nitrite (four 3-mm ($^1/_8$ -in.) diameter holes).

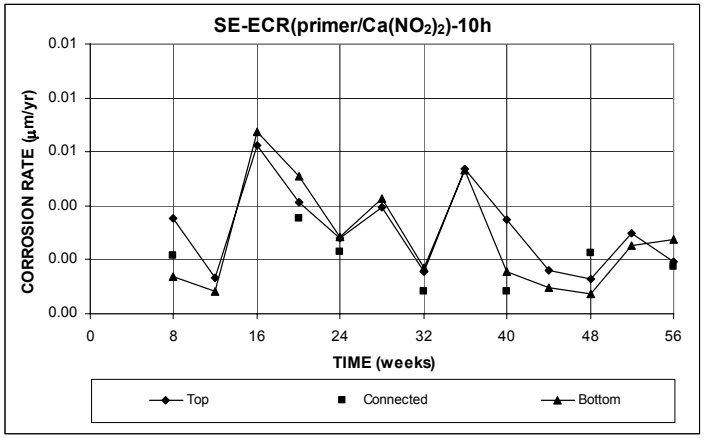

(a)

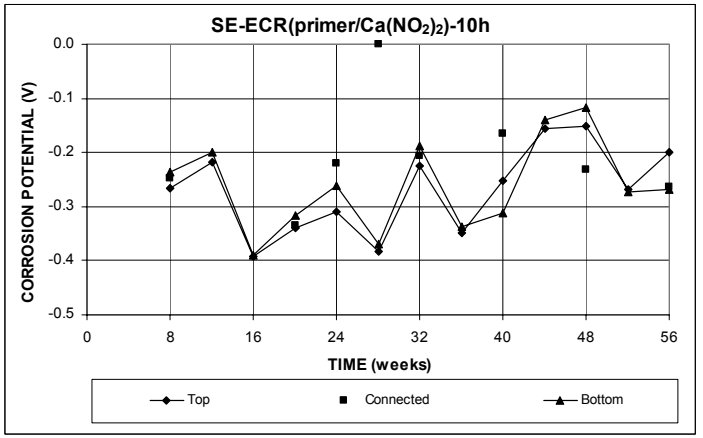

(b)

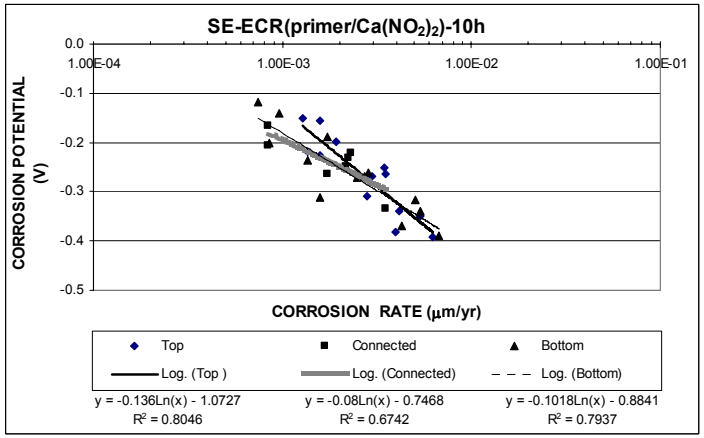

(c)

Figure E.34 – (a) Corrosion rate, (b) corrosion potential, and (c) correlation between microcell corrosion rate and corrosion potential as measured in the LPR test for the Southern Exposure specimen with ECR with primer containing calcium nitrite (ten 3-mm ($^{1}/_{8}$-in.) diameter holes).

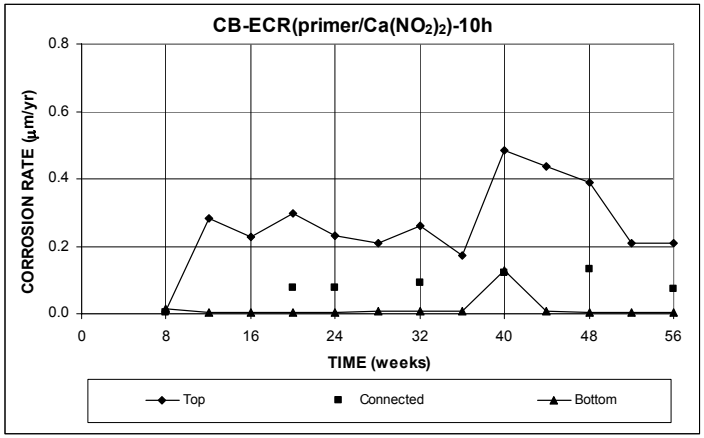

(a)

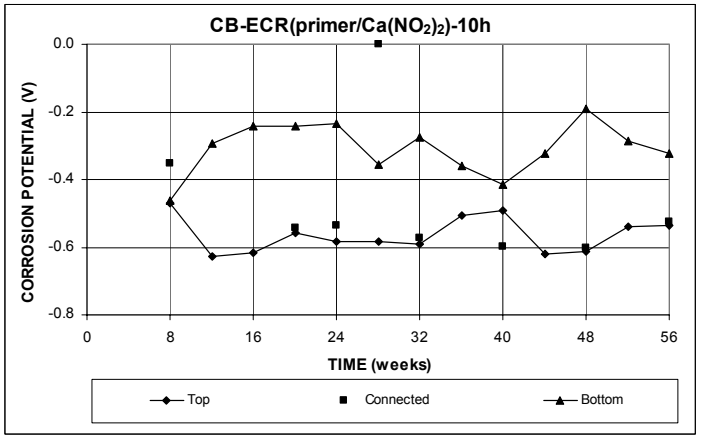

(b)

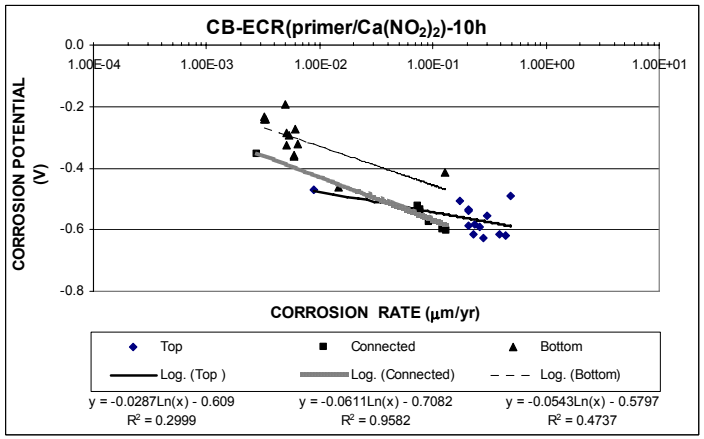

(c)

Figure E.35 – (a) Corrosion rate, (b) corrosion potential, and (c) correlation between microcell corrosion rate and corrosion potential as measured in the LPR test for the cracked beam specimen with ECR with primer containing calcium nitrite (ten 3-mm ($^{1}/_{8}$-in.) diameter holes).

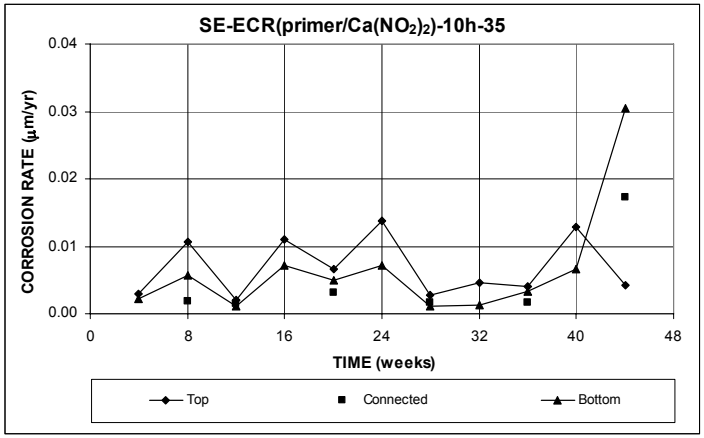

(a)

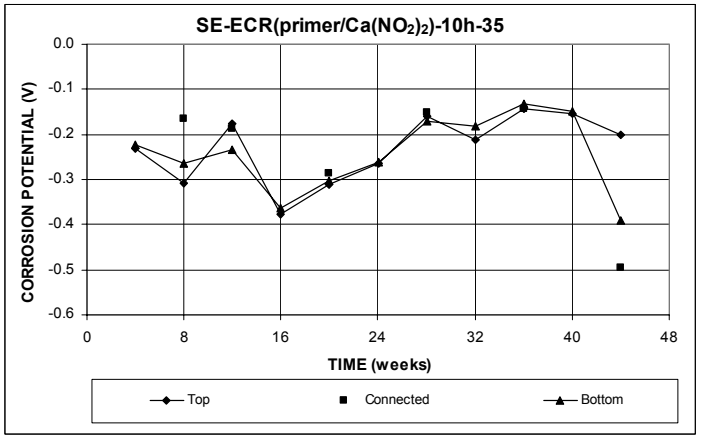

(b)

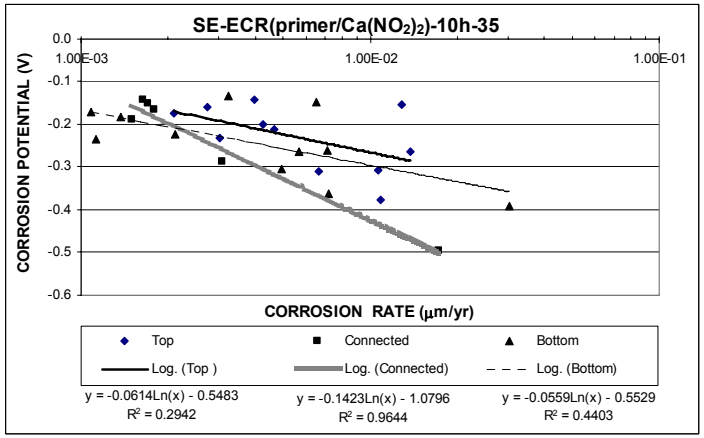

(c)

Figure E.36 – (a) Corrosion rate, (b) corrosion potential, and (c) correlation between microcell corrosion rate and corrosion potential as measured in the LPR test for the Southern Exposure specimen with ECR with primer containing calcium nitrite (ten 3-mm ($^1/_8$-in.) diameter holes), a water-cement ratio of 0.35.

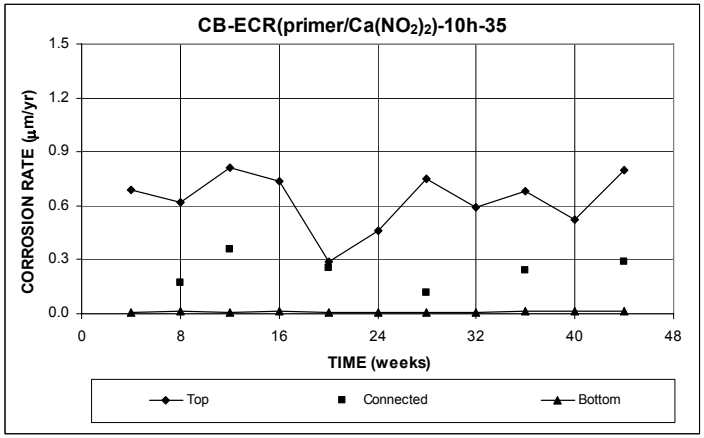

(a)

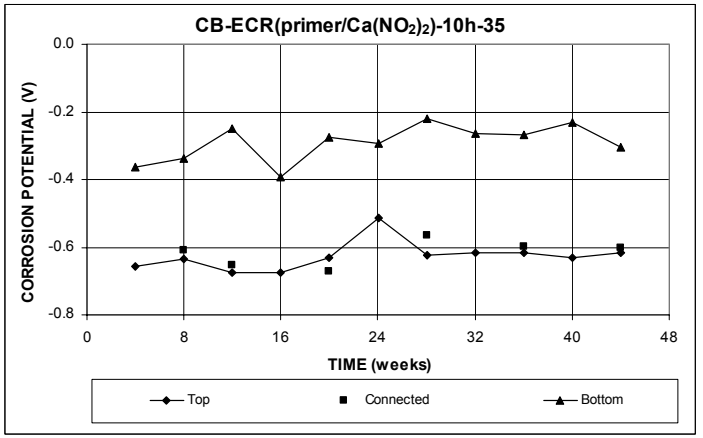

(b)

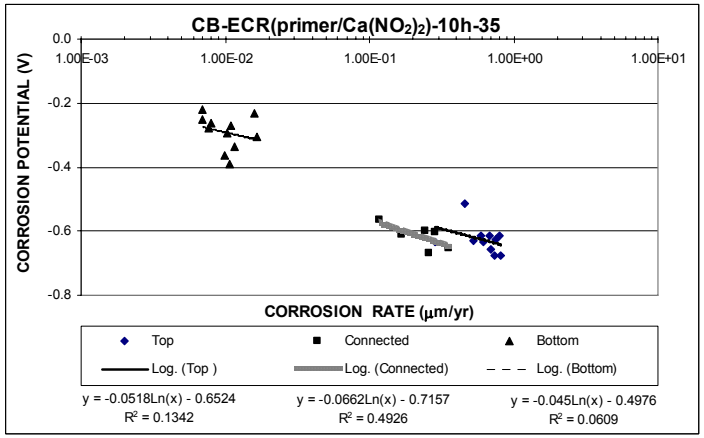

(c)

Figure E.37 – (a) Corrosion rate, (b) corrosion potential, and (c) correlation between microcell corrosion rate and corrosion potential, as measured in the LPR test for the cracked beam specimen with ECR with primer containing calcium nitrite (ten 3-mm ($^{1}/_{8}$-in.) diameter holes), a water-cement ratio of 0.35.

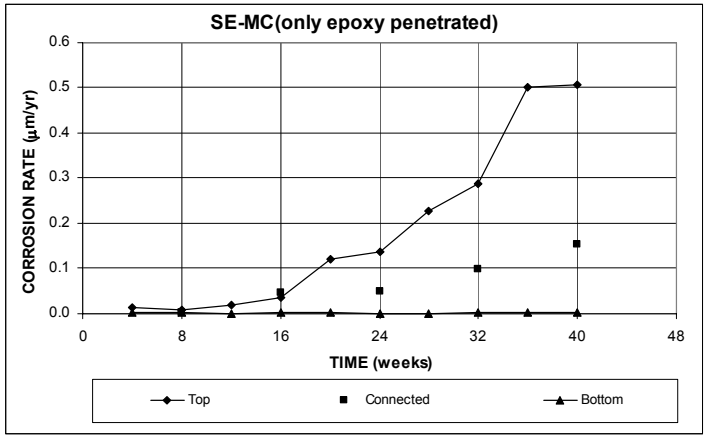

(a)

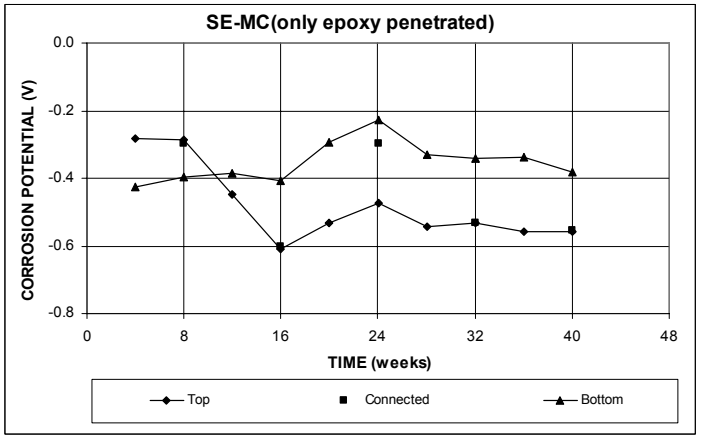

(b)

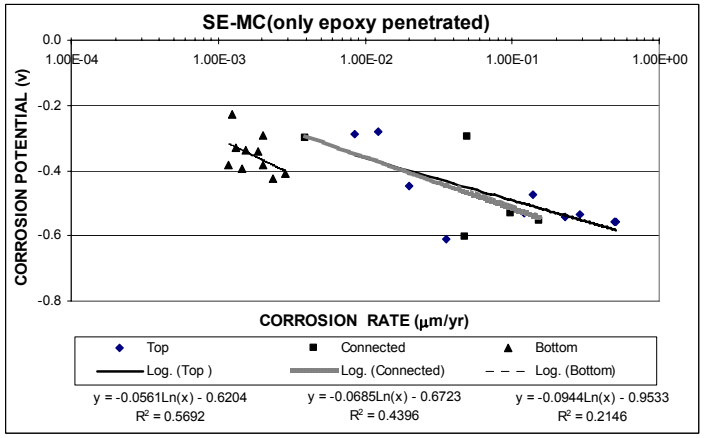

(c)

Figure E.38 – (a) Corrosion rate, (b) corrosion potential, and (c) correlation between microcell corrosion rate and corrosion potential as measured in the LPR test for the Southern Exposure specimen with multiple coated bar (four 3-mm ($^1/_8$ -in.) diameter holes, only epoxy penetrated).

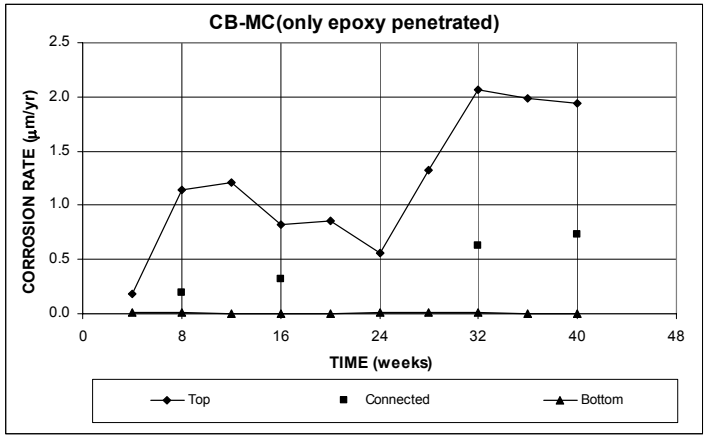

(a)

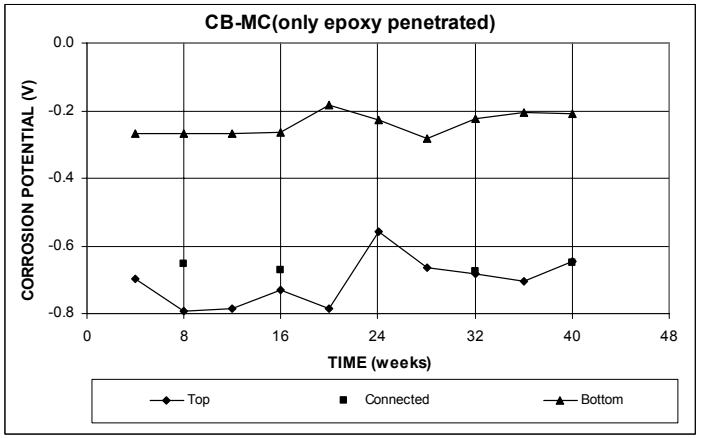

(b)

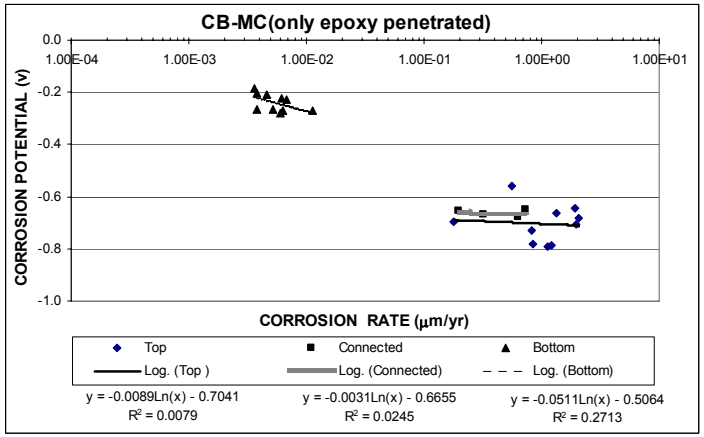

(c)

Figure E.39 – (a) Corrosion rate, (b) corrosion potential, and (c) correlation between microcell corrosion rate and corrosion potential as measured in the LPR test for the cracked beam specimen with multiple coated bar (four 3-mm ($^1/_8$ -in.) diameter holes, only epoxy penetrated).

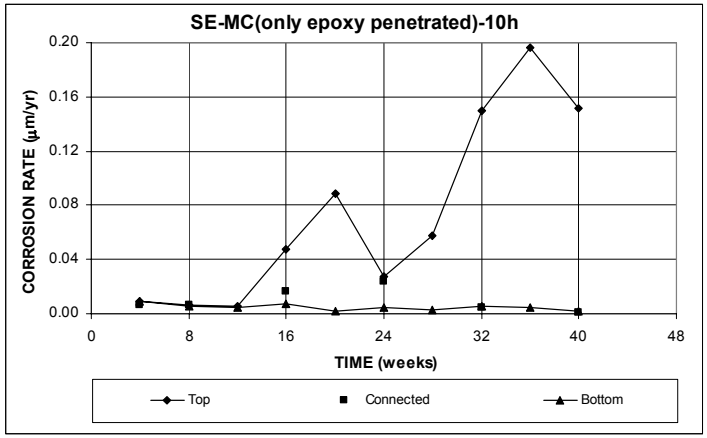

(a)

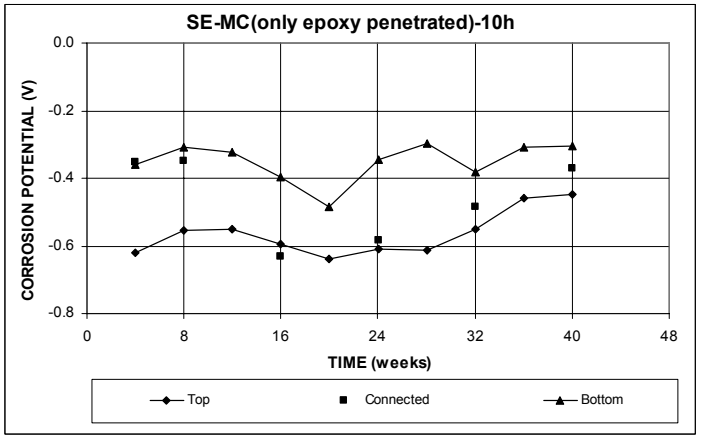

(b)

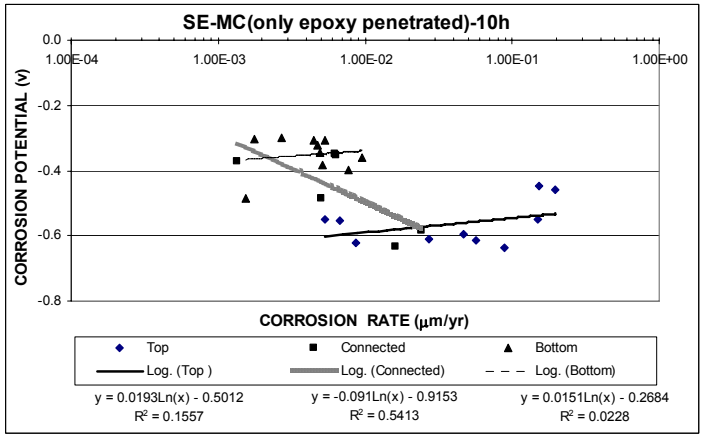

(c)

Figure E.40 – (a) Corrosion rate, (b) corrosion potential, and (c) correlation between microcell corrosion rate and corrosion potential as measured in the LPR test for the Southern Exposure specimen with multiple coated bar (ten 3-mm ($^1/_8$ -in.) diameter holes, only epoxy penetrated).

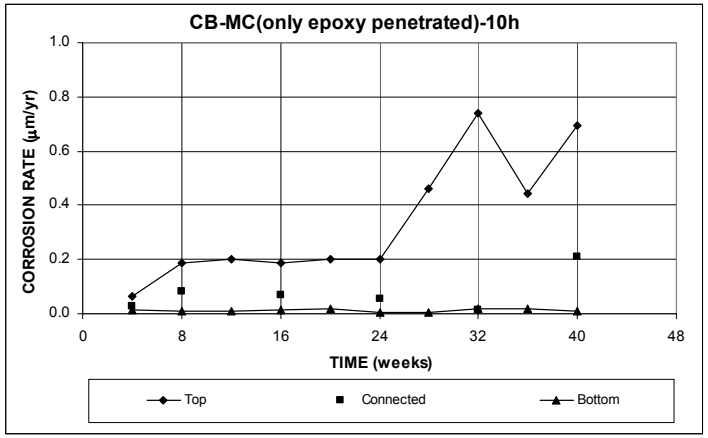

(a)

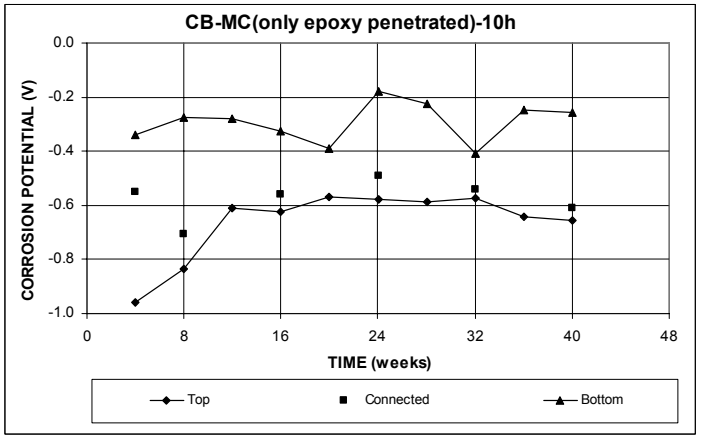

(b)

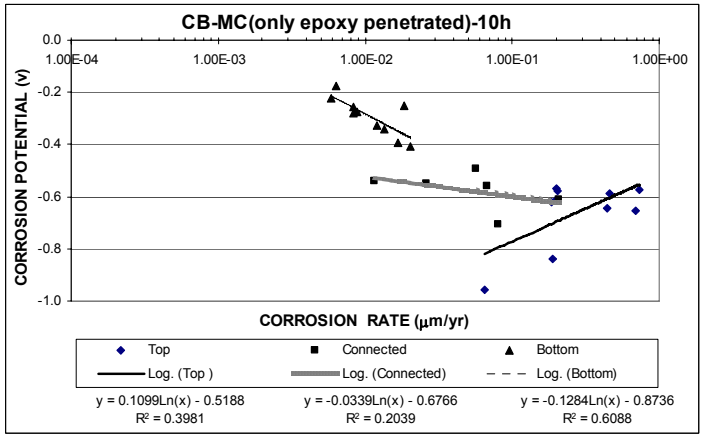

(c)

Figure E.41 – (a) Corrosion rate, (b) corrosion potential, and (c) correlation between microcell corrosion rate and corrosion potential as measured in the LPR test for the cracked beam specimen with multiple coated bar (ten 3-mm ($^1/_8$ -in.) diameter holes, only epoxy penetrated).

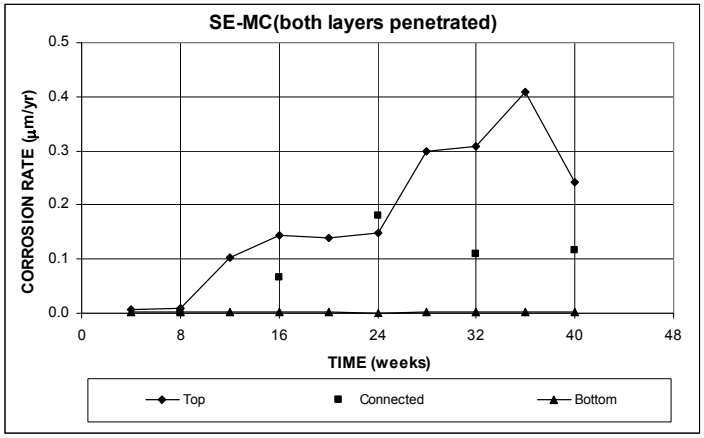

(a)

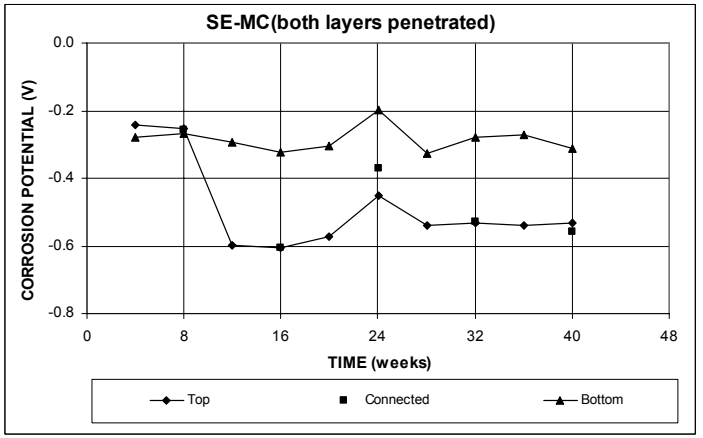

(b)

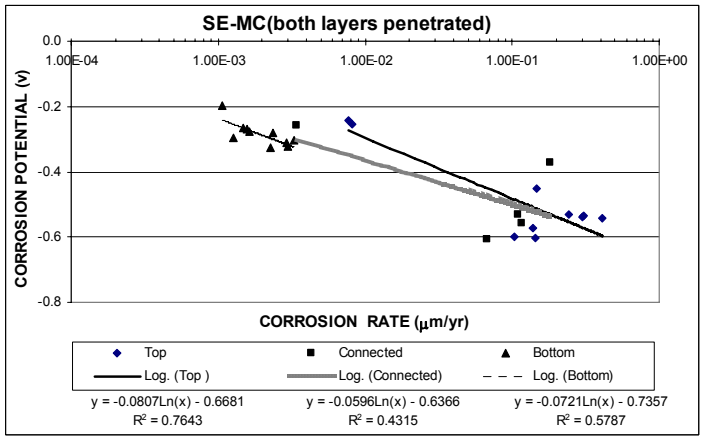

(c)

Figure E.42 – (a) Corrosion rate, (b) corrosion potential, and (c) correlation between microcell corrosion rate and corrosion potential as measured in the LPR test for the Southern Exposure specimen with multiple coated bar (four 3-mm ($^1/_8$ -in.) diameter holes, both layers penetrated).

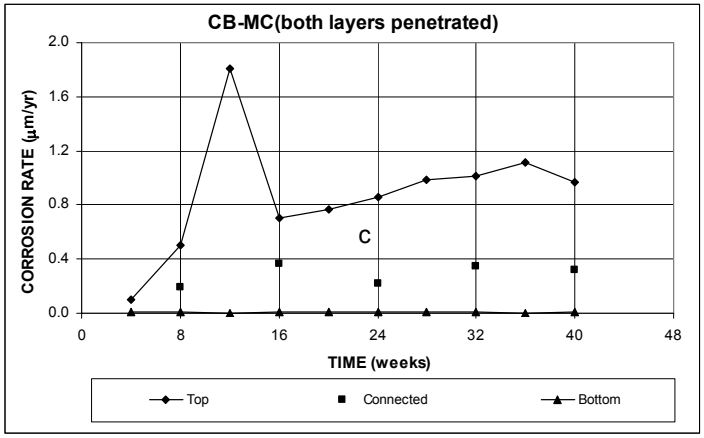

(a)

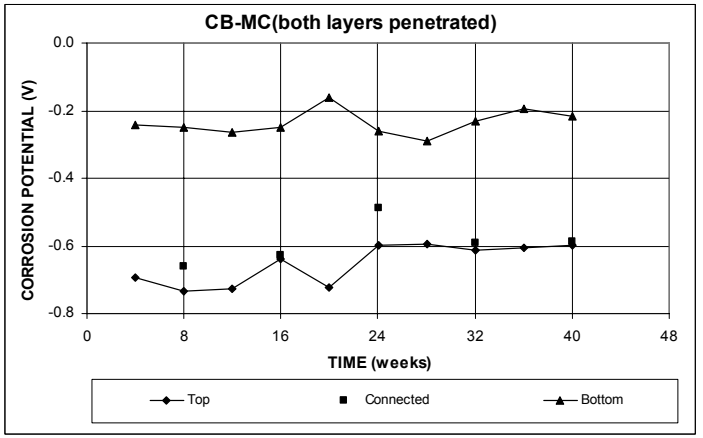

(b)

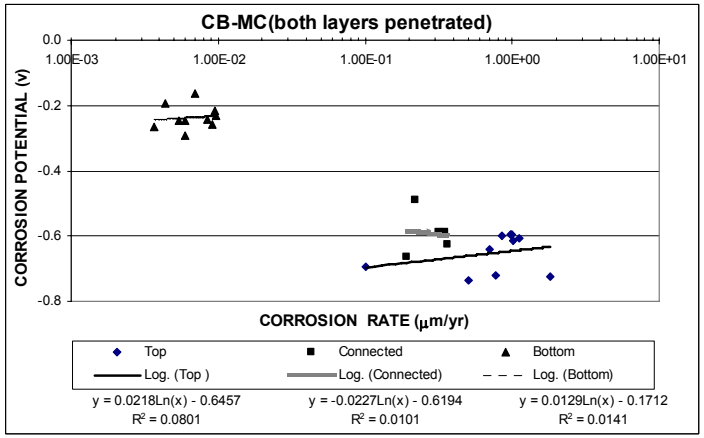

(c)

Figure E.43 – (a) Corrosion rate, (b) corrosion potential, and (c) correlation between microcell corrosion rate and corrosion potential as measured in the LPR test for the cracked beam specimen with multiple coated bar (four 3-mm ($^1/_8$ -in.) diameter holes, both layers penetrated).

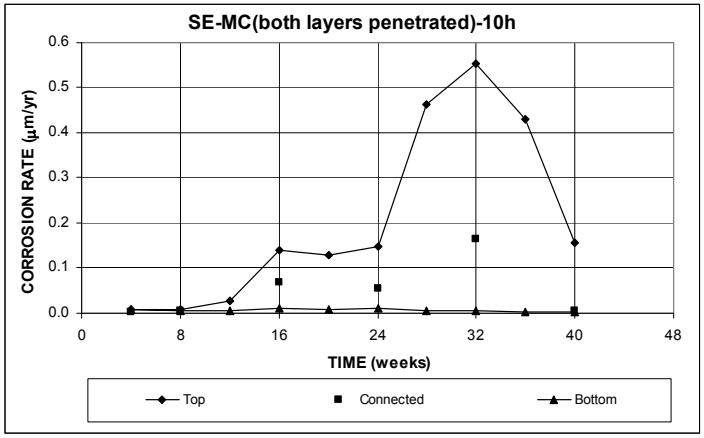

(a)

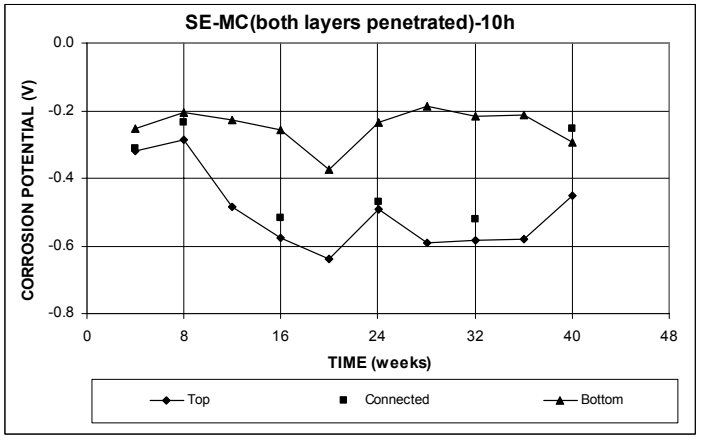

(b)

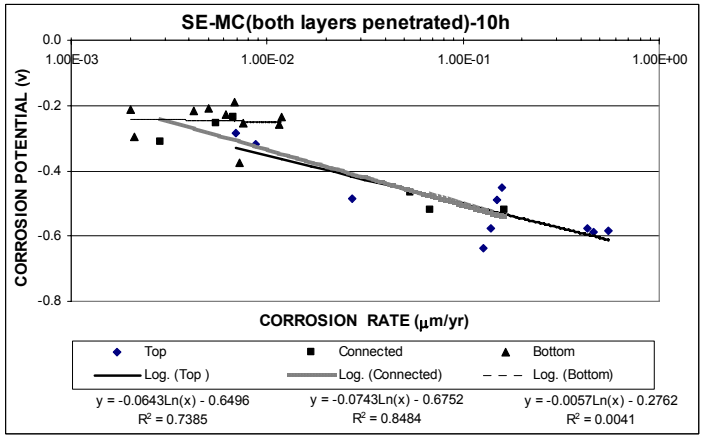

(c)

Figure E.44 – (a) Corrosion rate, (b) corrosion potential, and (c) correlation between microcell corrosion rate and corrosion potential as measured in the LPR test for the Southern Exposure specimen with multiple coated bar (ten 3-mm ($^{1}/_{8}$ -in.) diameter holes, both layers penetrated).

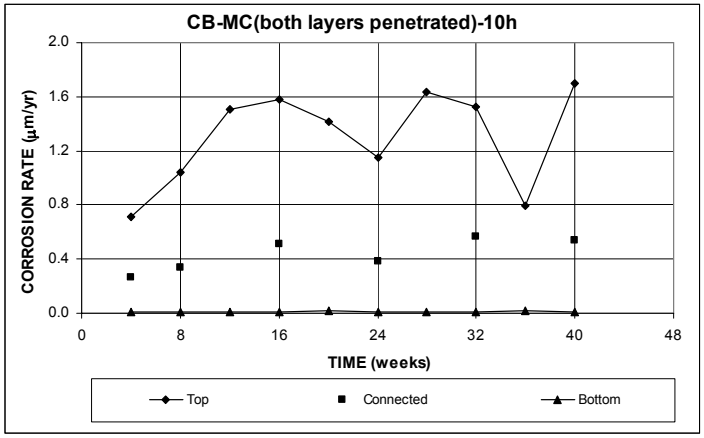

(a)

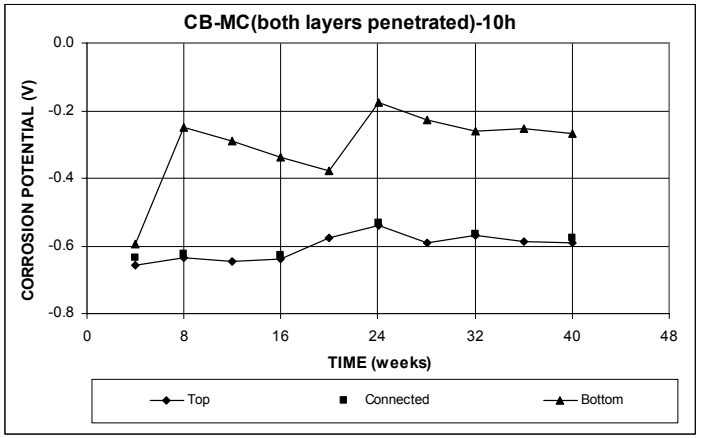

(b)

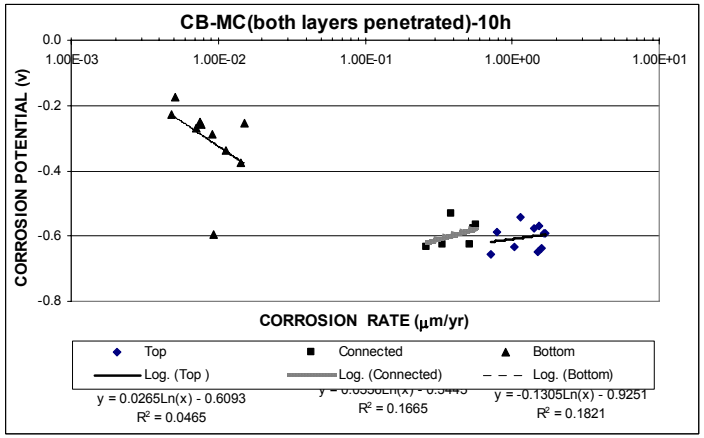

(c)

Figure E.45 – (a) Corrosion rate, (b) corrosion potential, and (c) correlation between microcell corrosion rate and corrosion potential as measured in the LPR test for the cracked beam specimen with multiple coated bar (ten 3-mm ($^1/_8$ -in.) diameter holes, both layers penetrated).

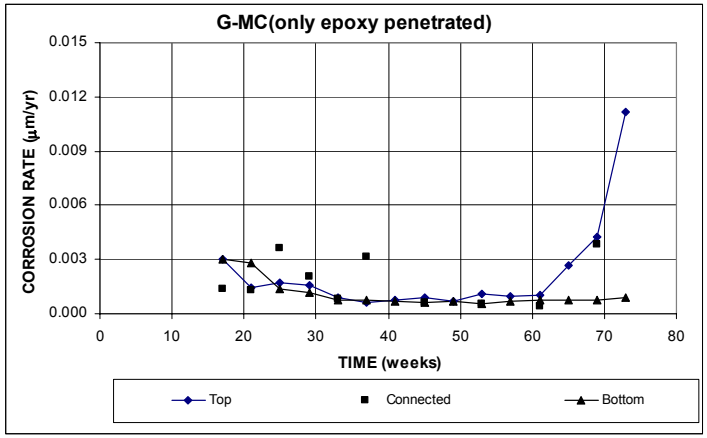

(a)

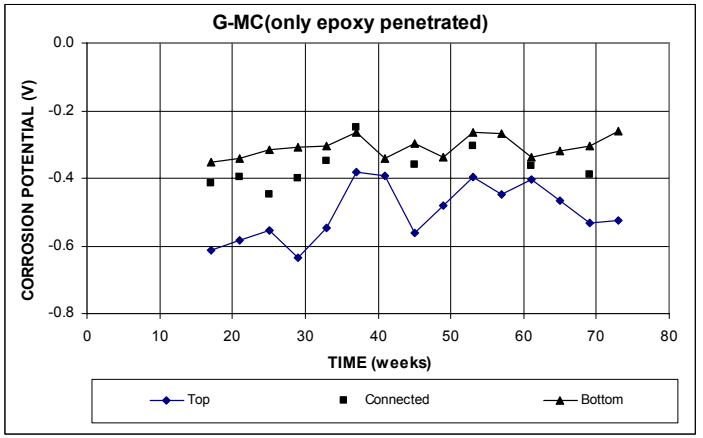

(b)

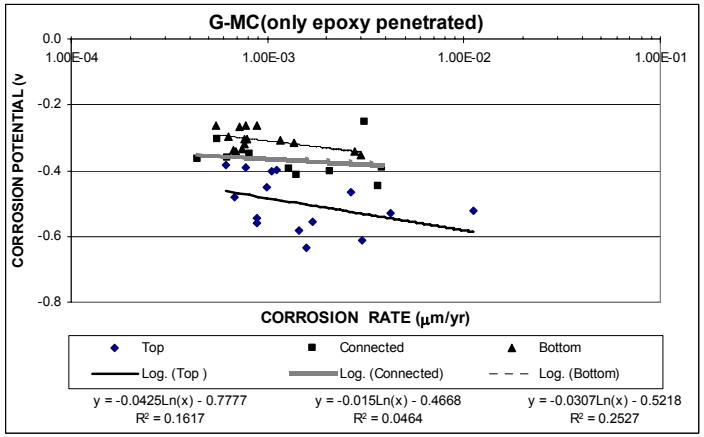

(c)

Figure E.46 – (a) Corrosion rate, (b) corrosion potential, and (c) correlation between microcell corrosion rate and corrosion potential as measured in the LPR test for the G 109 specimen with multiple coated bar (four 3-mm ($^1/_8$ -in.) diameter holes, only epoxy penetrated).

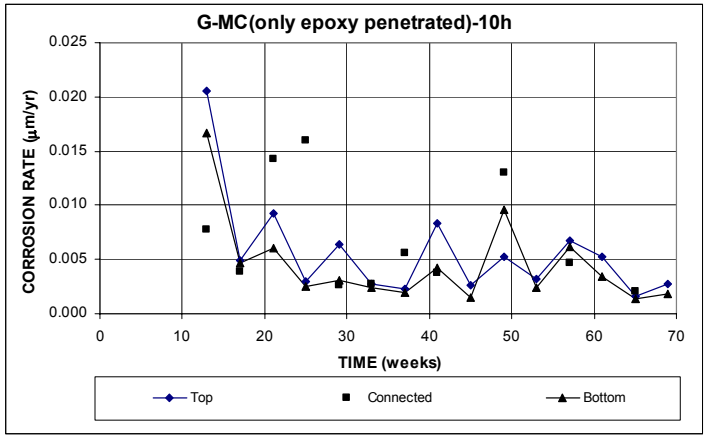

(a)

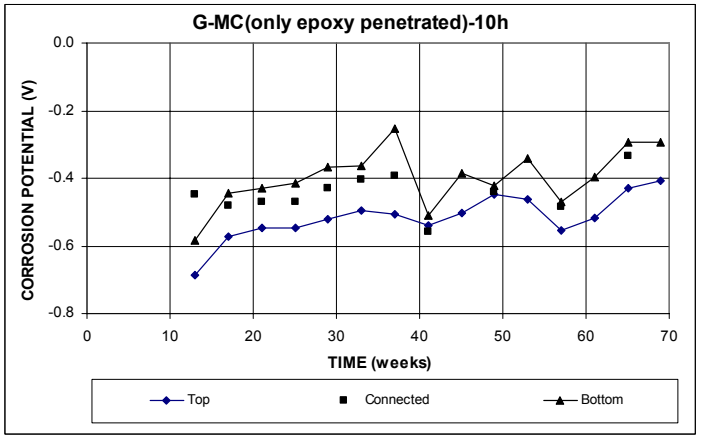

(b)

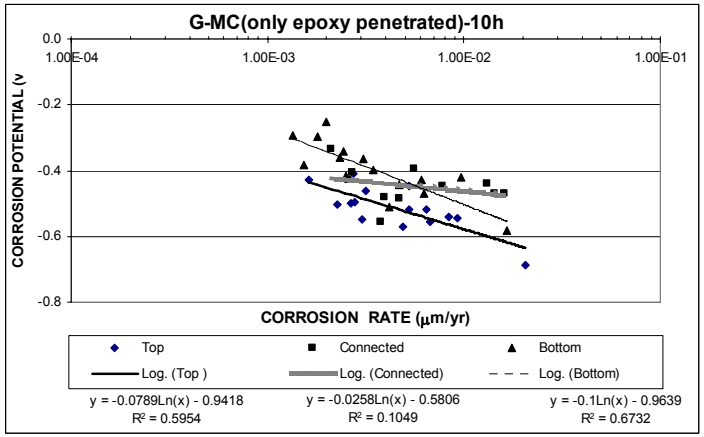

(c)

Figure E.47 – (a) Corrosion rate, (b) corrosion potential, and (c) correlation between microcell corrosion rate and corrosion potential as measured in the LPR test for the G 109 specimen with multiple coated bar (ten 3-mm ($^1/_8$ -in.) diameter holes, only epoxy penetrated).

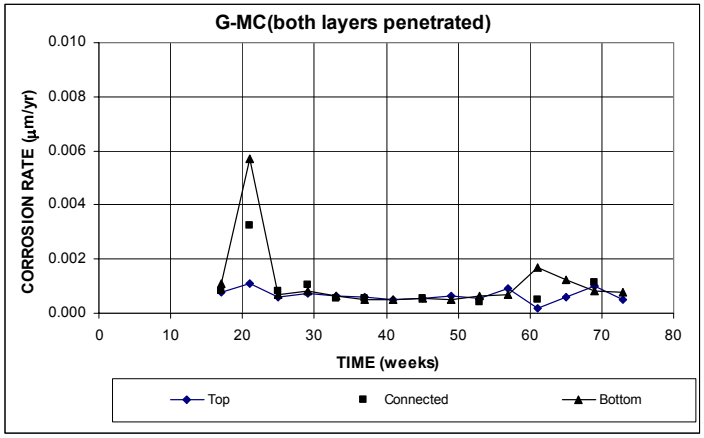

(a)

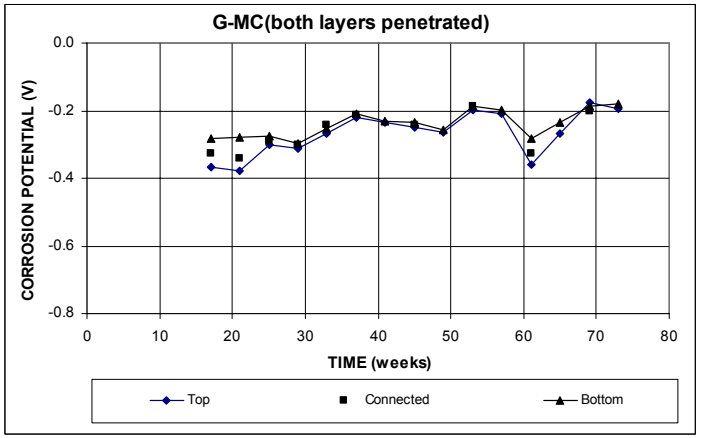

(b)

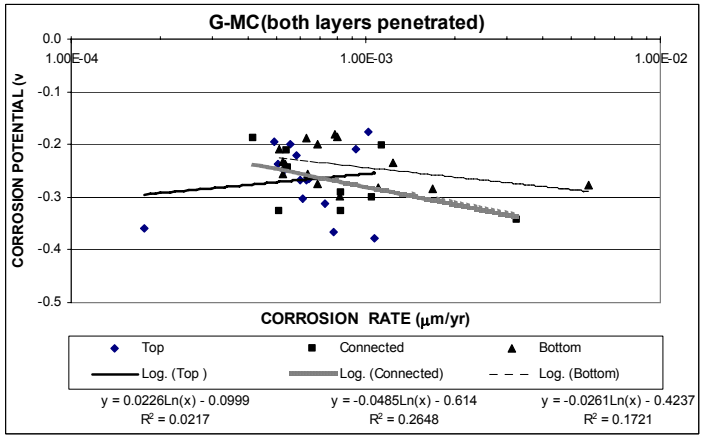

(c)

Figure E.48 – (a) Corrosion rate, (b) corrosion potential, and (c) correlation between microcell corrosion rate and corrosion potential as measured in the LPR test for the G 109 specimen with multiple coated bar (four 3-mm ($^1/_8$ -in.) diameter holes, both layers penetrated).

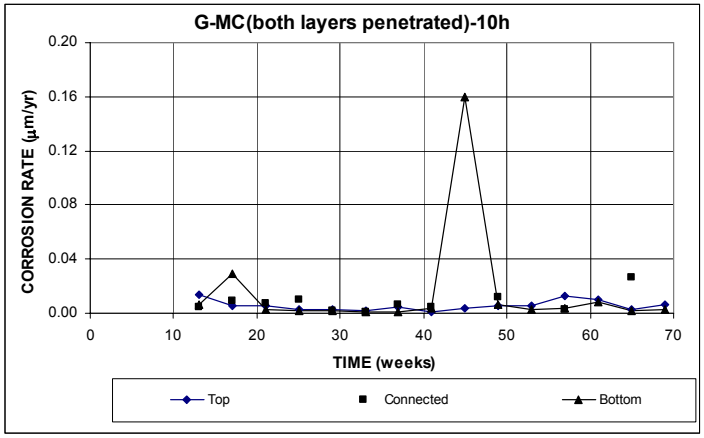

(a)

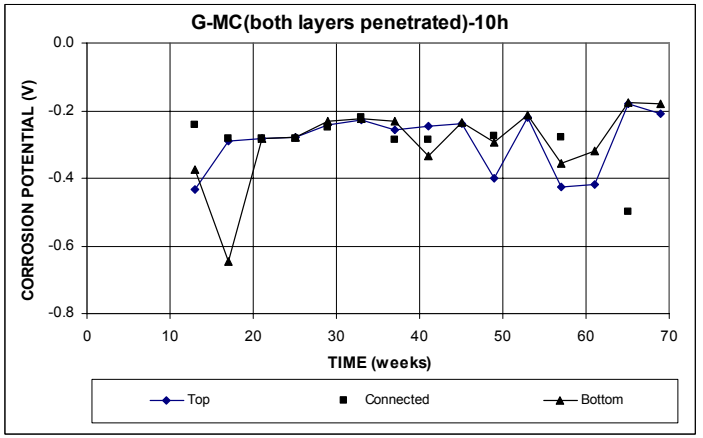

(b)

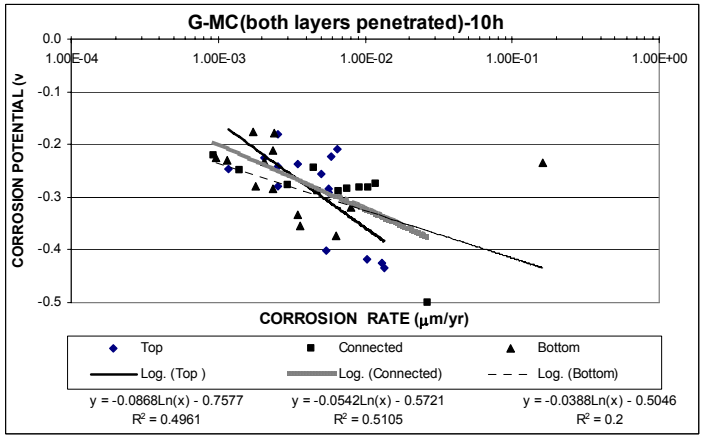

(c)

Figure E.49 – (a) Corrosion rate, (b) corrosion potential, and (c) correlation between microcell corrosion rate and corrosion potential as measured in the LPR test for the G 109 specimen with multiple coated bar (four 3-mm ($^1/_8$ -in.) diameter holes, both layers penetrated).

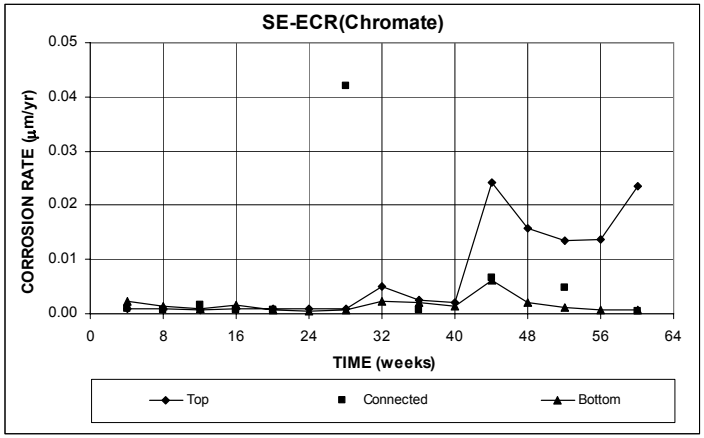

(a)

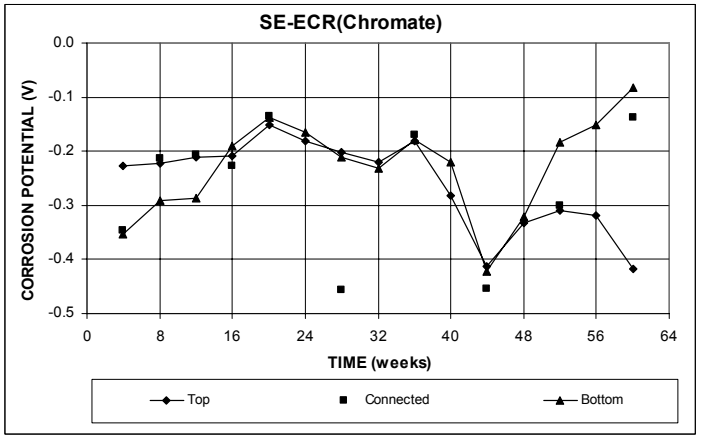

(b)

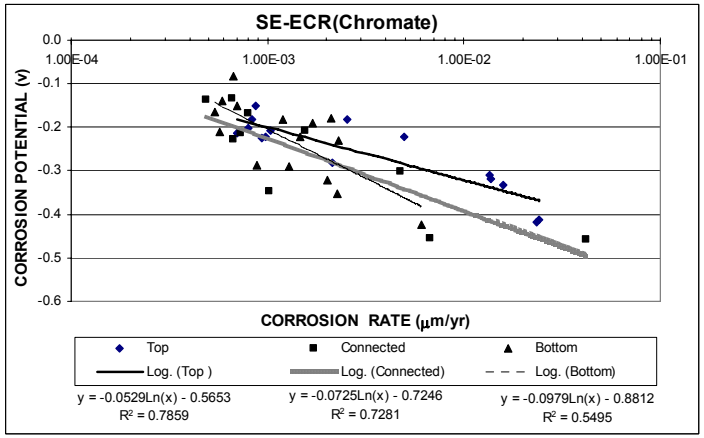

(c)

Figure E.50 – (a) Corrosion rate, (b) corrosion potential, and (c) correlation between microcell corrosion rate and corrosion potential as measured in the LPR test for the Southern Exposure specimen with ECR with chromate pretreatment (four 3-mm ($^1/_8$ -in.) diameter holes).

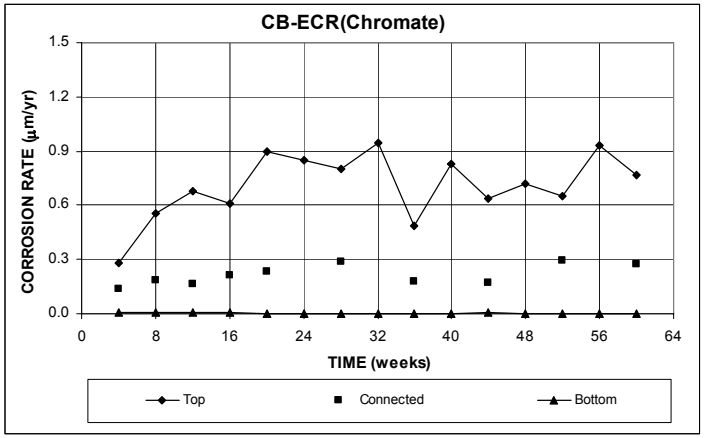

(a)

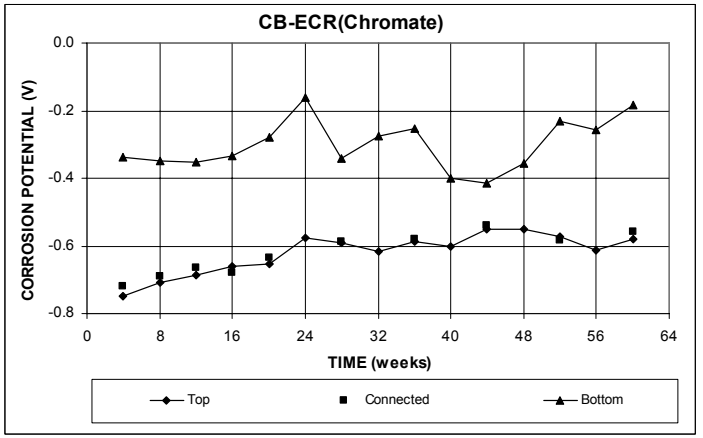

(b)

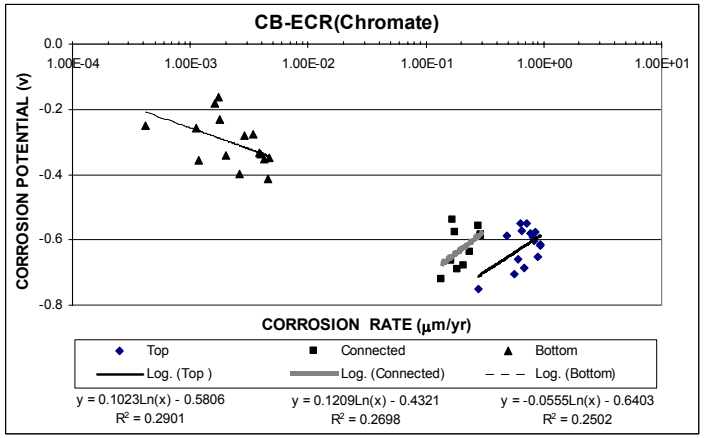

(c)

Figure E.51 – (a) Corrosion rate, (b) corrosion potential, and (c) correlation between microcell corrosion rate and corrosion potential as measured in the LPR test for the cracked beam specimen with ECR with chromate pretreatment (four 3-mm ($^1/_8$ -in.) diameter holes).

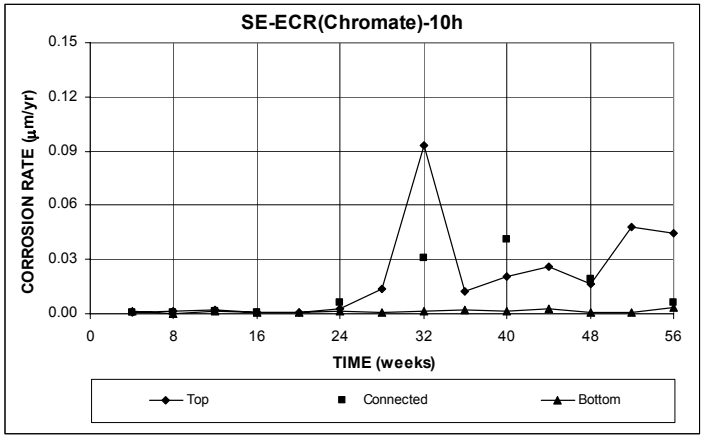

(a)

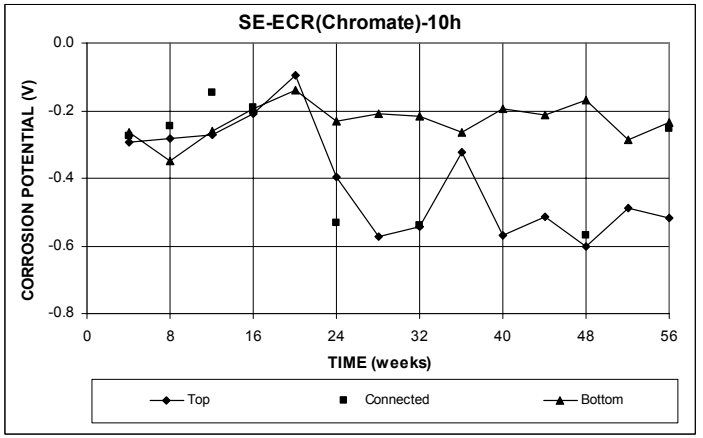

(b)

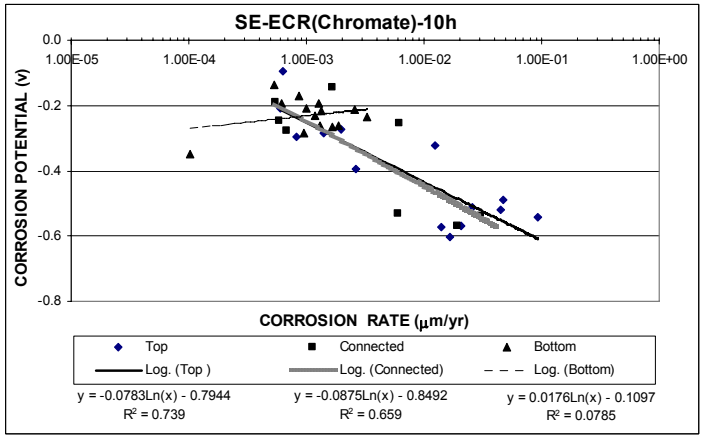

(c)

Figure E.52 – (a) Corrosion rate, (b) corrosion potential, and (c) correlation between microcell corrosion rate and corrosion potential as measured in the LPR test for the Southern Exposure specimen with ECR with chromate pretreatment (ten 3-mm ($^1/_8$ -in.) diameter holes).

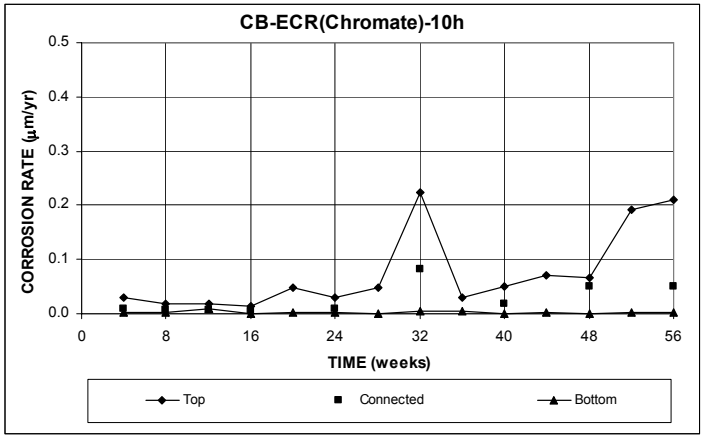

(a)

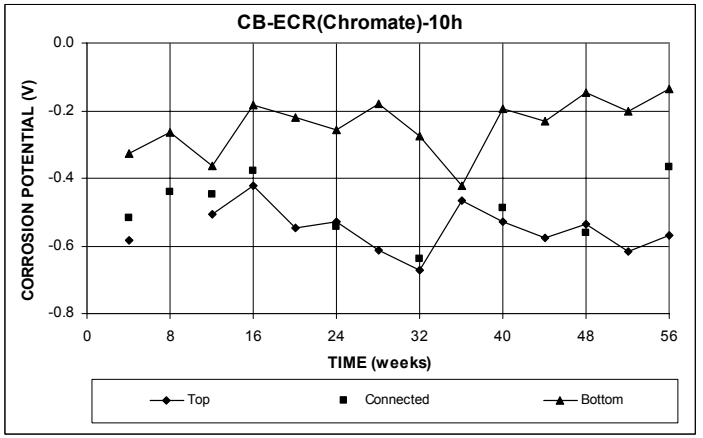

(b)

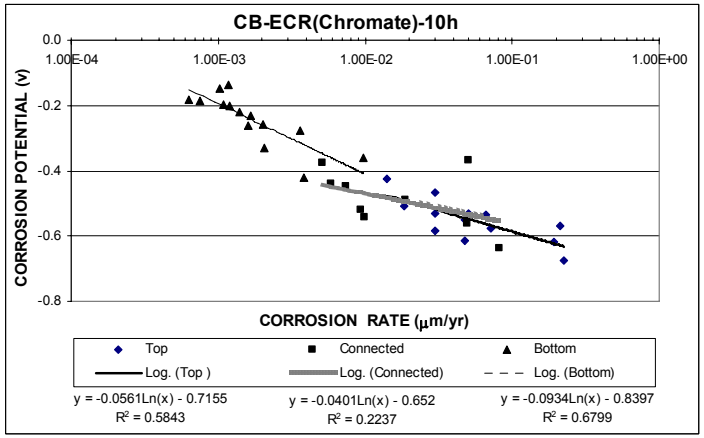

(c)

Figure E.53 – (a) Corrosion rate, (b) corrosion potential, and (c) correlation between microcell corrosion rate and corrosion potential as measured in the LPR test for the cracked beam specimen with ECR with chromate pretreatment (ten 3-mm ($^1/_8$ -in.) diameter holes).

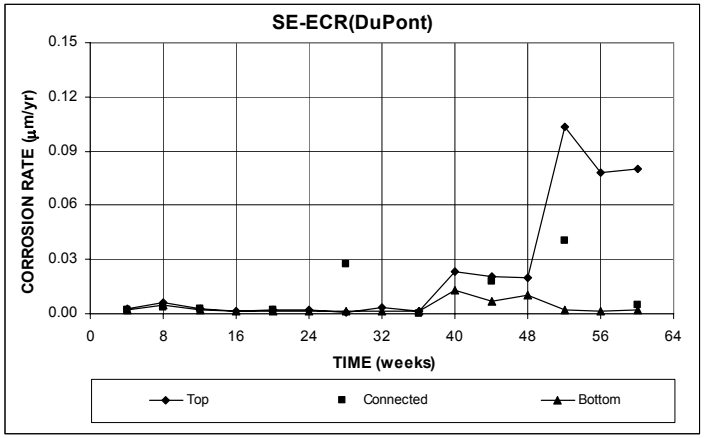

(a)

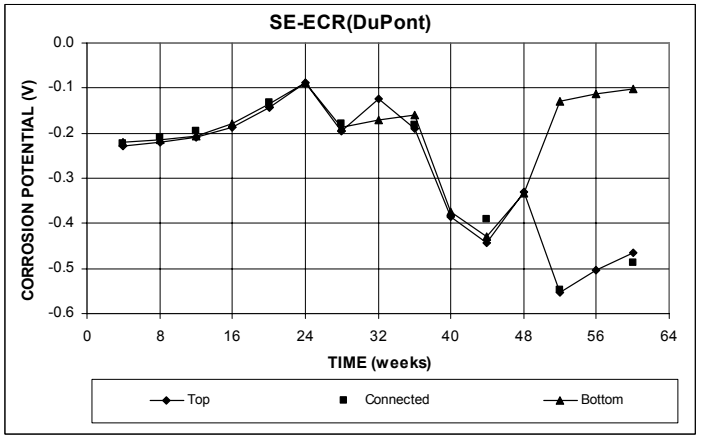

(b)

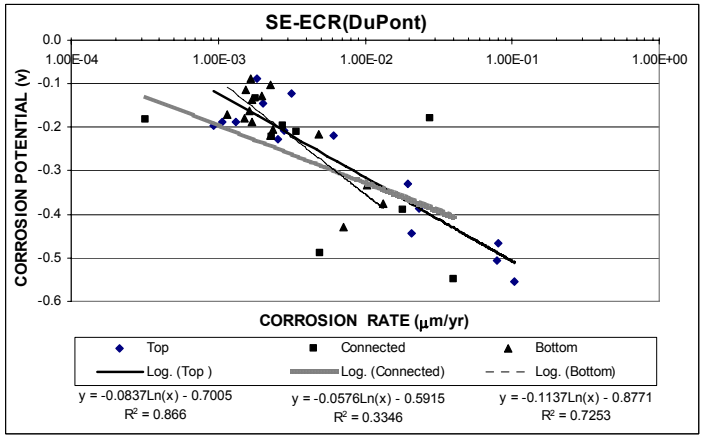

(c)

Figure E.54 – (a) Corrosion rate, (b) corrosion potential, and (c) correlation between microcell corrosion rate and corrosion potential as measured in the LPR test for the Southern Exposure specimen with ECR with DuPont Coating (four 3-mm ($^1/_8$ -in.) diameter holes).

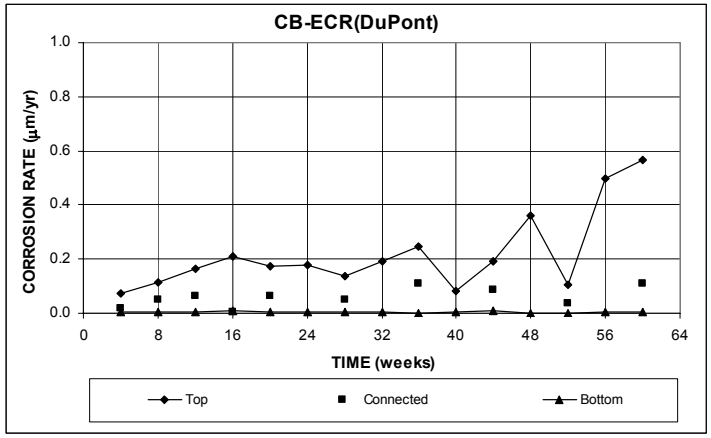

(a)

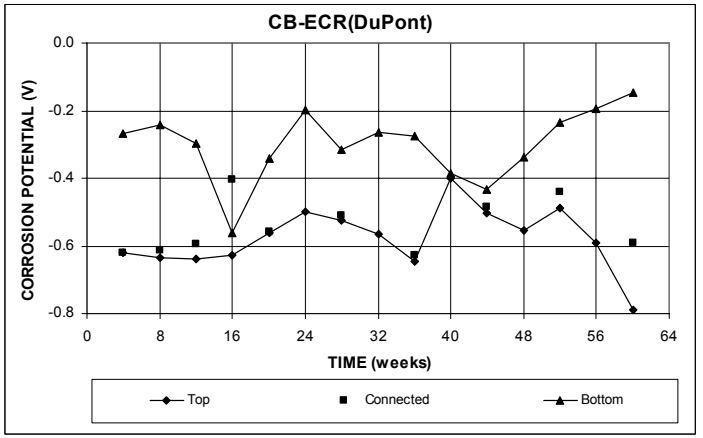

(b)

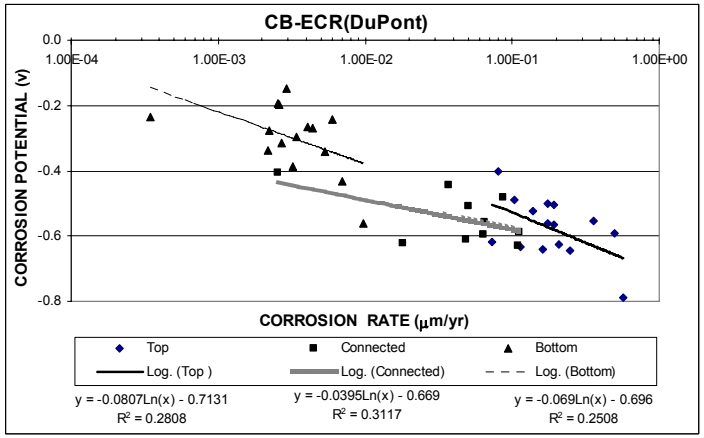

(c)

Figure E.55 – (a) Corrosion rate, (b) corrosion potential, and (c) correlation between microcell corrosion rate and corrosion potential as measured in the LPR test for the cracked beam specimen with ECR with DuPont Coating (four 3-mm ($^1/_8$ -in.) diameter holes).

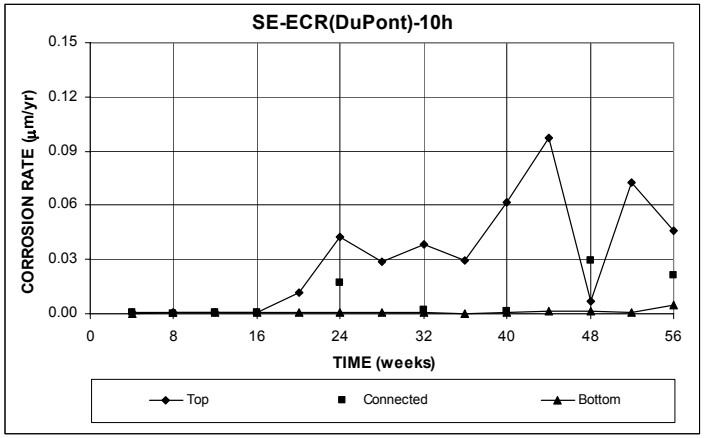

(a)

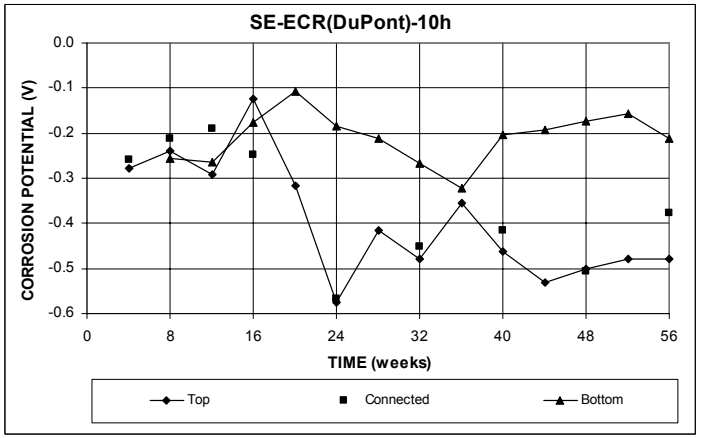

(b)

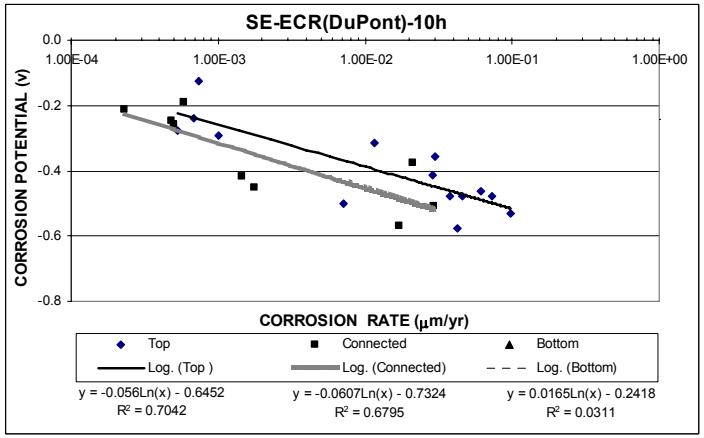

(c)

Figure E.56 – (a) Corrosion rate, (b) corrosion potential, and (c) correlation between microcell corrosion rate and corrosion potential as measured in the LPR test for the Southern Exposure specimen with ECR with DuPont Coating (ten 3-mm ($^{1}/_{8}$ -in.) diameter holes).

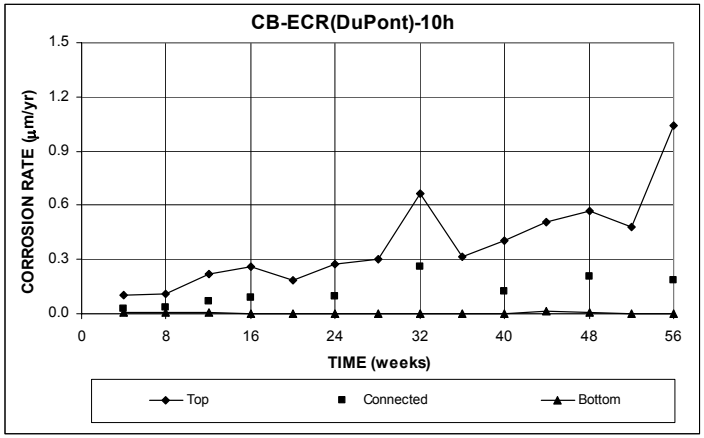

(a)

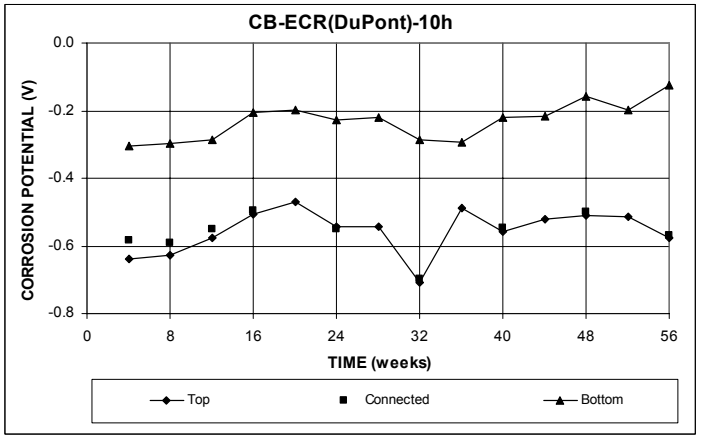

(b)

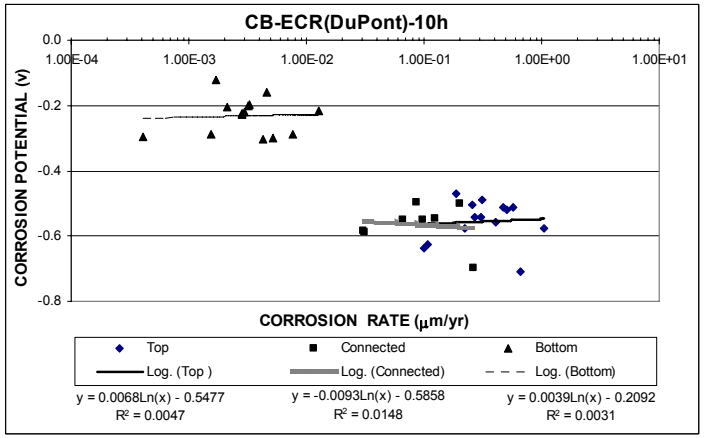

(c)

Figure E.57 – (a) Corrosion rate, (b) corrosion potential, and (c) correlation between microcell corrosion rate and corrosion potential as measured in the LPR test for the cracked beam specimen with ECR with DuPont Coating (ten 3-mm ($^1/_8$ -in.) diameter holes).

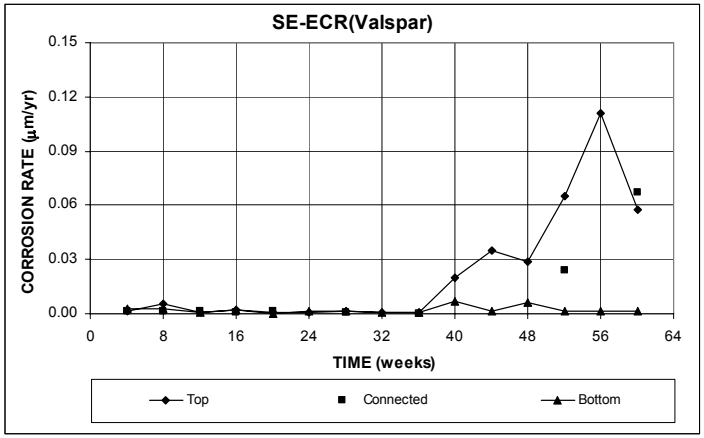

(a)

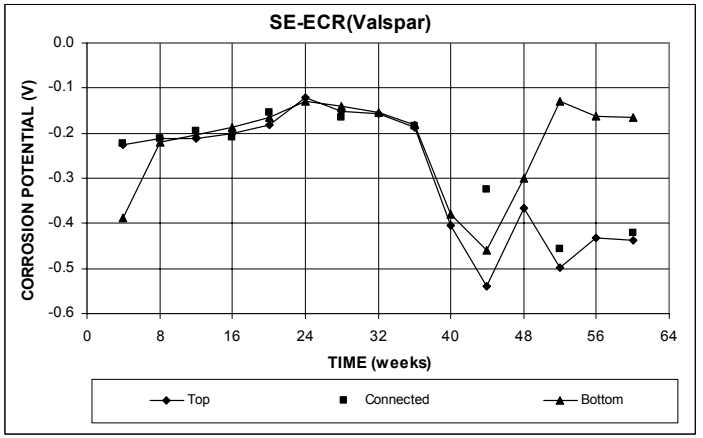

(b)

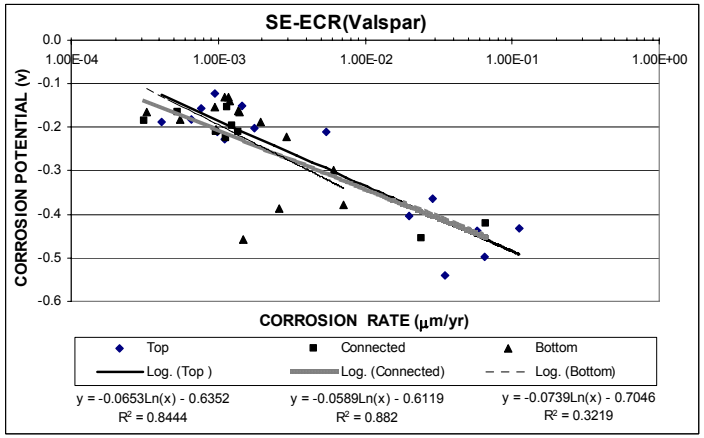

(c)

Figure E.58 – (a) Corrosion rate, (b) corrosion potential, and (c) correlation between microcell corrosion rate and corrosion potential as measured in the LPR test for the Southern Exposure specimen with ECR with Valspar Coating (four 3-mm ($^{1}/_{8}$ -in.) diameter holes).

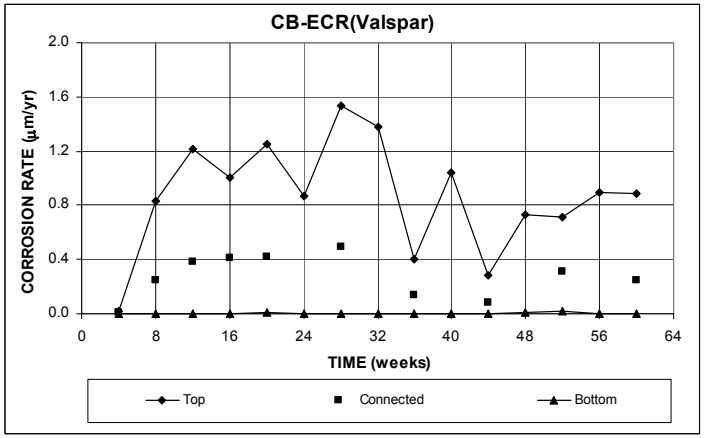

(a)

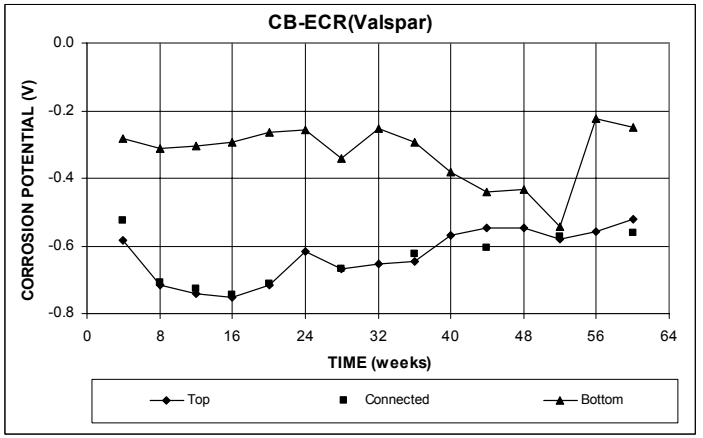

(b)

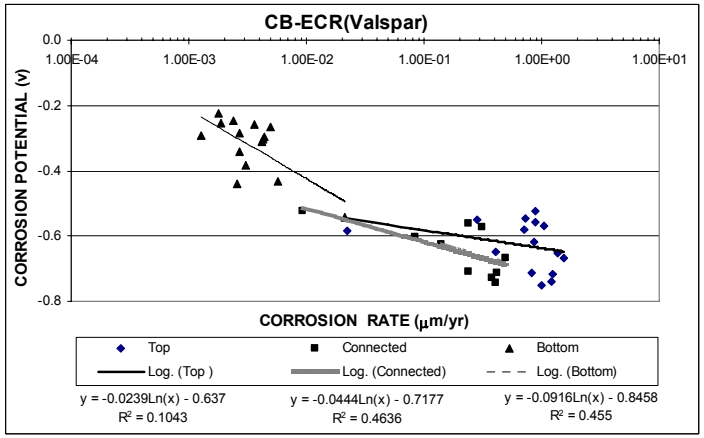

(c)

Figure E.59 – (a) Corrosion rate, (b) corrosion potential, and (c) correlation between microcell corrosion rate and corrosion potential as measured in the LPR test for the cracked beam specimen with ECR with Valspar Coating (four 3-mm ($^1/_8$ -in.) diameter holes).

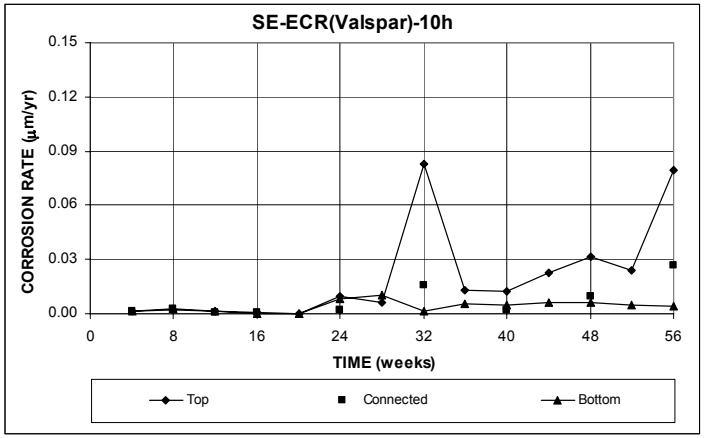

(a)

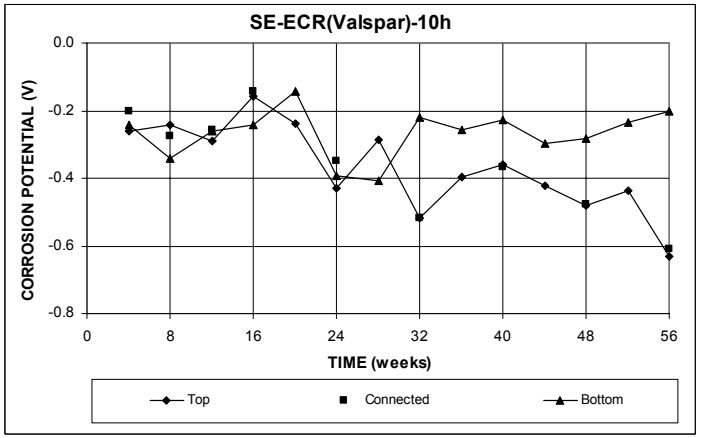

(b)

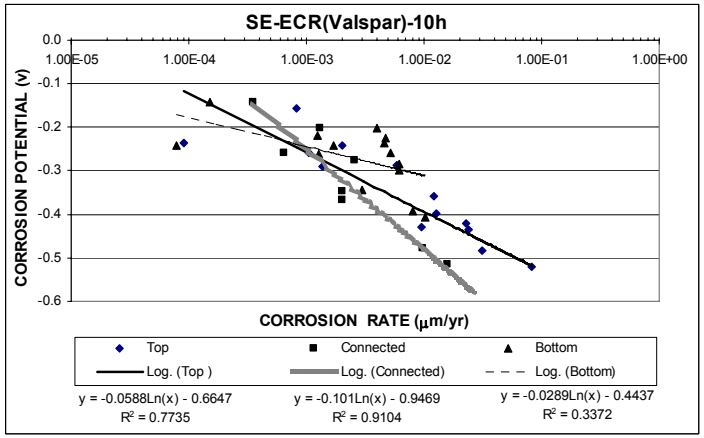

(c)

Figure E.60 – (a) Corrosion rate, (b) corrosion potential, and (c) correlation between microcell corrosion rate and corrosion potential as measured in the LPR test for the Southern Exposure specimen with ECR with Valspar Coating (ten 3-mm ($^1/_8$ -in.) diameter holes).

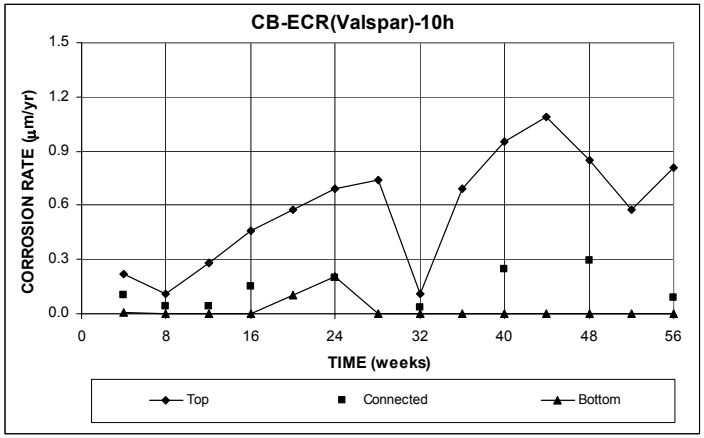

(a)

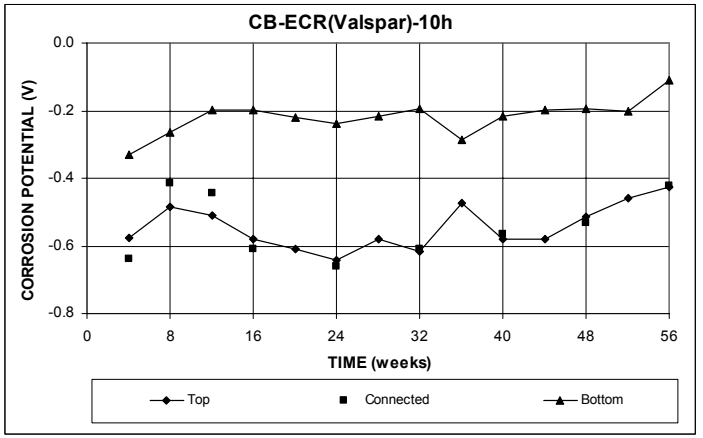

(b)

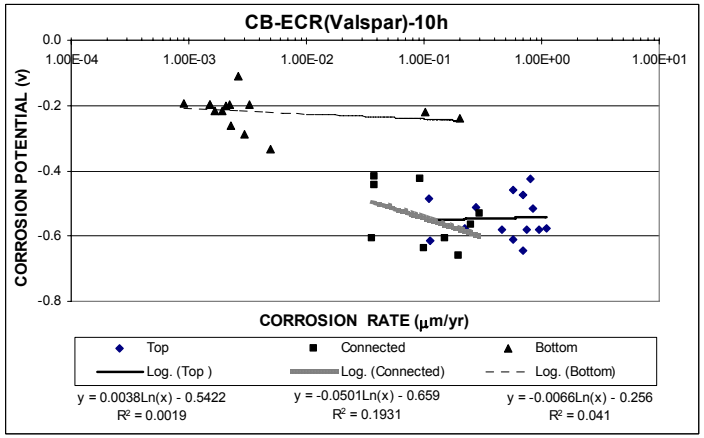

(c)

Figure E.61 – (a) Corrosion rate, (b) corrosion potential, and (c) correlation between microcell corrosion rate and corrosion potential as measured in the LPR test for the cracked beam specimen with ECR with Valspar Coating (ten 3-mm ($^1/_8$ -in.) diameter holes).

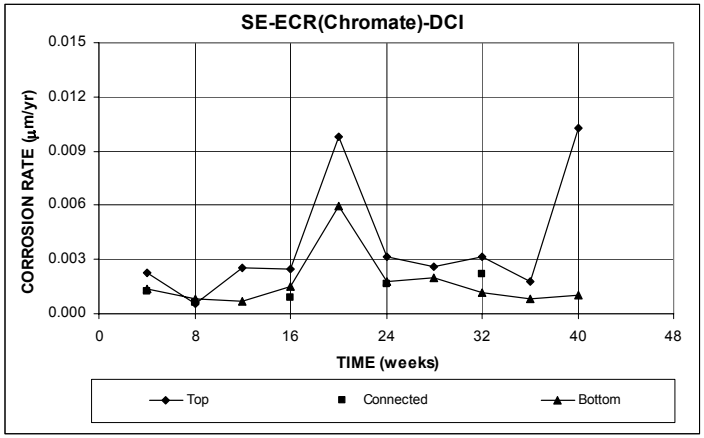

(a)

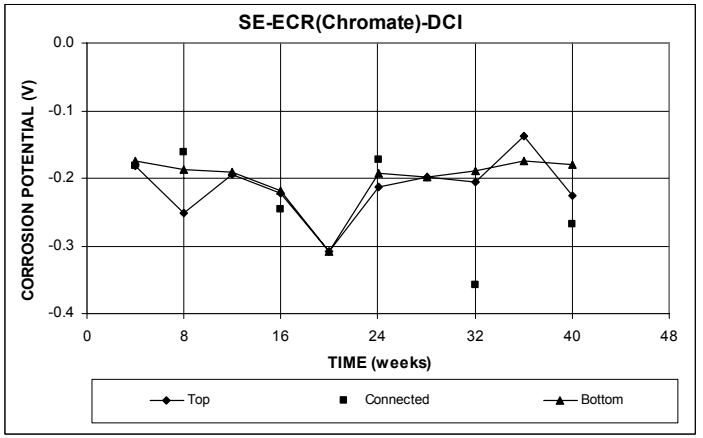

(b)

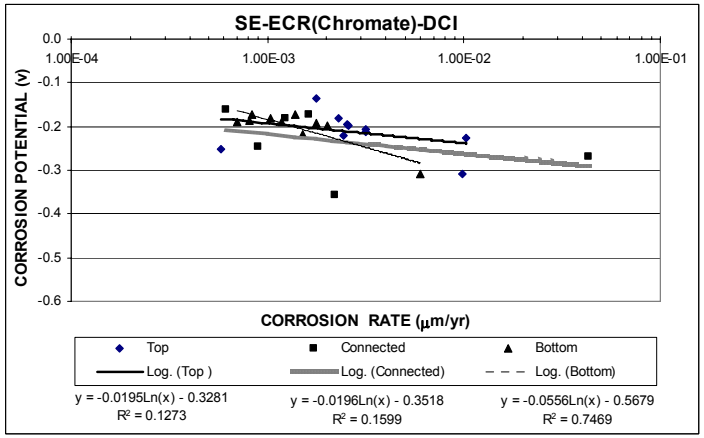

(c)

Figure E.62 – (a) Corrosion rate, (b) corrosion potential, and (c) correlation between microcell corrosion rate and corrosion potential as measured in the LPR test for the Southern Exposure specimen with ECR with chromate pretreatment (four 3-mm ($^1/_8$ -in.) diameter holes) in concrete with DCI.

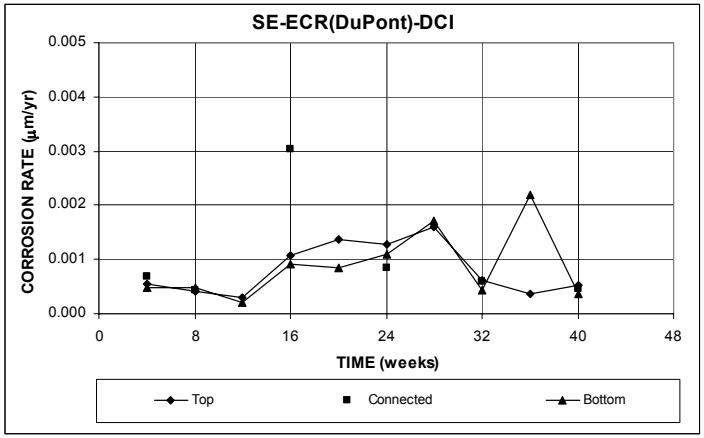

(a)

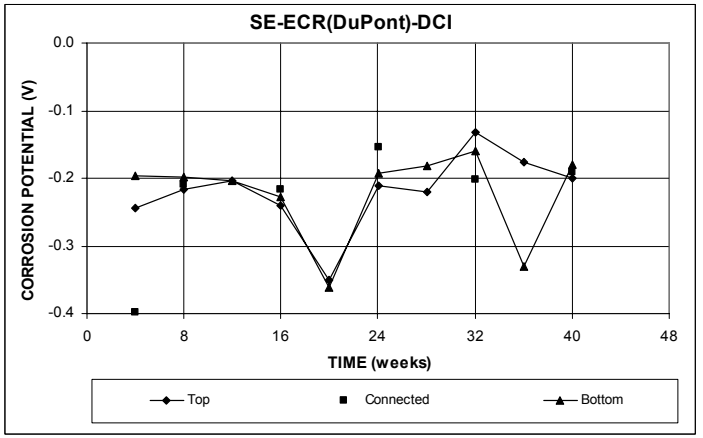

(b)

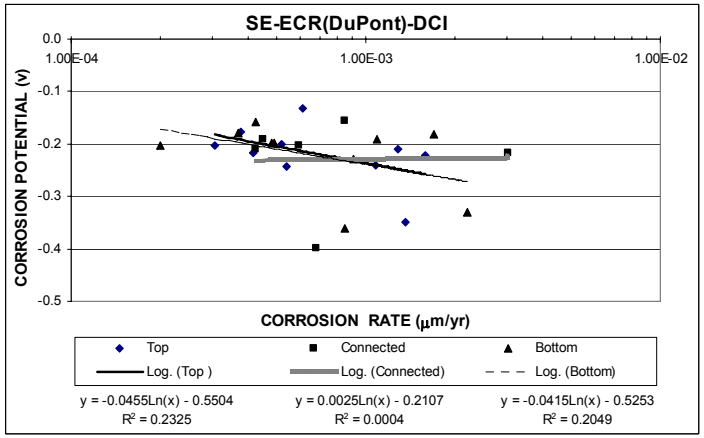

(c)

Figure E.63 – (a) Corrosion rate, (b) corrosion potential, and (c) correlation between microcell corrosion rate and corrosion potential as measured in the LPR test for the Southern Exposure specimen with ECR with DuPont coating (four 3-mm ($^1/_8$ -in.) diameter holes) in concrete with DCI.

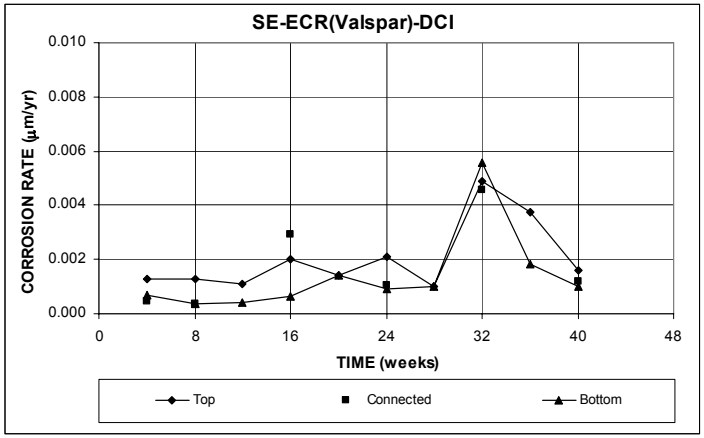

(a)

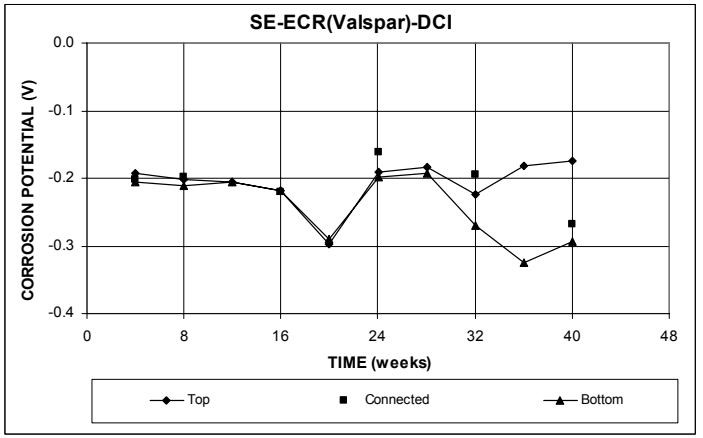

(b)

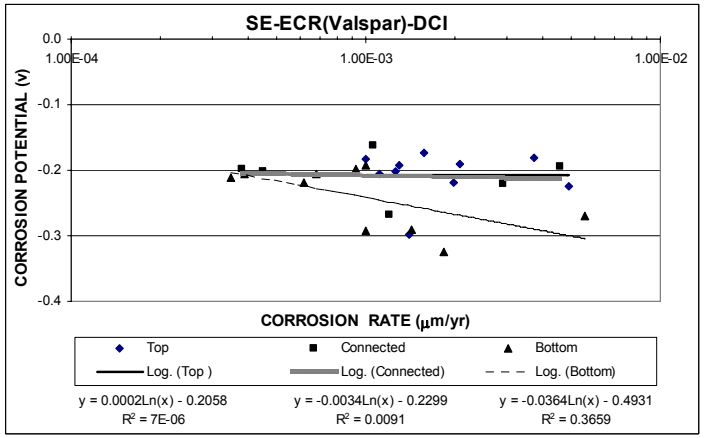

(c)

Figure E.64 – (a) Corrosion rate, (b) corrosion potential, and (c) correlation between microcell corrosion rate and corrosion potential as measured in the LPR test for the Southern Exposure specimen with ECR with DuPont coating (four 3-mm ($^1/_8$ -in.) diameter holes) in concrete with DCI.